

# PROCEEDINGS OF THE IRE®

Published Monthly by

The Institute of Radio Engineers, Inc.

VOLUME 46

January, 1958

NUMBER I

## EDITORIAL DEPARTMENT

Alfred N. Goldsmith,  
Editor Emeritus

D. G. Fink, Editor

E. K. Gannett,  
Managing Editor

Helene Frischauer,  
Associate Editor

## ADVERTISING DEPARTMENT

William C. Copp,  
Advertising Manager

Lillian Petranek,  
Assistant Advertising Manager

## EDITORIAL BOARD

D. G. Fink, Chairman

E. W. Herold, Vice-Chairman

E. K. Gannett

Ferdinand Hamburger, Jr.

T. A. Hunter

A. V. Loughren

W. N. Tuttle

George W. Bailey,  
Executive Secretary

Evelyn Benson, Assistant to the  
Executive Secretary

John B. Buckley, Chief Accountant

Laurence G. Cumming,  
Technical Secretary

Emily Sirjane, Office Manager

Authors are requested to submit three copies of manuscripts and illustrations to the Editorial Department, Institute of Radio Engineers, 1 East 79 St., New York 21, N. Y.

Responsibility for the contents of papers published in the PROCEEDINGS OF THE IRE rests upon the authors. Statements made in papers are not binding on the IRE for its members.

## CONTENTS

Poles and Zeros.....	1
Donald G. Fink, President, 1958.....	2
6319. Introduction to Radio Astronomy..... F. T. Haddock	3
6320. The Discovery and Identification by Karl Guthe Jansky of Electromagnetic Radiation of Extraterrestrial Origin in the Radio Spectrum..... C. M. Jansky, Jr.	13
6321. Early Radio Astronomy at Wheaton, Illinois..... Grote Reber	15
6322. The Telescope Program for the National Radio Astronomy Observatory at Green Bank, West Virginia..... R. M. Emberson and N. L. Ashton	23
6323. Noise Levels at the National Radio Astronomy Observatory..... J. W. Findlay	35
6324. Radio Astronomy at the Meudon Observatory..... E. J. Blum, J. F. Denisse, and J. L. Steinberg	39
6325. Considerations in High-Sensitivity Microwave Radiometry..... Peter D. Strum	43
6326. A Broad-Band Microwave Source Comparison Radiometer for Advanced Research in Radio Astronomy..... F. D. Drake and H. I. Ewen	53
6327. Present and Future Capabilities of Microwave Crystal Receivers..... C. T. McCoy	61
6328. A High Resolution Radio Telescope for Use at 3.5 M..... B. Y. Mills, A. G. Little, K. V. Sheridan, and O. A. Slee	67
6329. The Sydney 19.7-MC Radio Telescope..... C. A. Shain	85
6330. An Antenna Array for Studies in Meteor and Radio Astronomy at 13 Meters..... P. B. Gallagher	89
6331. Radio Telescope Antennas of Large Aperture..... John D. Kraus	92
6332. Radio Interferometry of Discrete Sources..... R. N. Bracewell	97
6333. Restoration in the Presence of Errors..... R. N. Bracewell	106
6334. Discussion of 10.7-CM Solar Radio Flux Measurements and an Estimation of the Accuracy of Observations..... W. J. Medd and A. E. Covington	112
6335. A Method of Calibrating Centimetric Radiometers Using a Standard Noise Source..... J. S. Hey and V. A. Hughes	119
6336. Measurements of Solar Radiation and Atmospheric Attenuation at 4.3-Millimeters Wavelength..... Robert J. Coates	122
6337. Scanning the Sun with a Highly Directional Array..... W. N. Christiansen and D. S. Mathewson	127
6338. A Dynamic Spectrum Analyzer for Solar Studies..... J. Goodman and M. Lebenbaum	132
6339. A Wide-Band Antenna System for Solar Noise Studies..... Henry Jasik	135
6340. The Radio Spectrum of Solar Activity..... A. Maxwell, G. Swarup, and A. R. Thompson	142
6341. Studies at the McMath-Hulbert Observatory of Radio Frequency Radiation at the Time of Solar Flares..... Helen W. Dodson	149
6342. A Swept-Frequency Interferometer for the Study of High-Intensity Solar Radiation at Meter Wavelengths..... J. P. Wild and K. V. Sheridan	160
6343. Radio Astronomy Polarization Measurements..... Marshall H. Cohen	172
6344. The Cornell Radio Polarimeter..... Marshall H. Cohen	183
6345. A Time-Sharing Polarimeter at 200 MC..... S. Suzuki and A. Tsuchiya	190
6346. A Polarimeter in the Microwave Region..... Kenji Akabane	194
6347. Critical Frequency, Refractive Index, and Cone of Escape in the Solar Corona..... R. N. Bracewell and C. V. Stableford	198
6348. Radio Sources and the Milky Way at 440 MC..... N. G. Roman and B. S. Yapple	199
6349. Flux Measurements of Cassiopeia A and Cygnus A between 18.5 MC and 107 MC..... H. W. Wells	205
6350. The Distribution of Cosmic Radio Background Radiation..... H. C. Ko	208



THE COVER—This view through a 200-inch optical telescope reveals a spiral nebula, containing about 100 billion stars, and a satellite nebula below it, six million light years from Earth. The seemingly solid center is in reality a vast collection of stars, while the curving arms consist of stars plus glowing clouds of hydrogen. Hydrogen clouds such as these are a major source of cosmic radiation at radio frequencies. The sketch below shows an 85-foot radio telescope now being built at the National Radio Astronomy Observatory, Green Bank, W. Va., to study microwave radiations from hydrogen clouds and other radio sources in our galaxy and other galaxies.

Spiral Nebula photo—Mount Wilson and Palomar Observatories  
Radio Telescope sketch—Blaw-Knox Co.

Copyright © 1958, by the Institute of Radio Engineers, Inc.

# PROCEEDINGS OF THE IRE

Published Monthly by

The Institute of Radio Engineers, Inc.

## BOARD OF DIRECTORS, 1957

\*J. T. Henderson, *President*

Yasujiro Niwa, *Vice-President*

\*W. R. G. Baker, *Treasurer*

\*Haraden Pratt, *Secretary*

\*D. G. Fink, *Editor*

\*J. D. Ryder, *Senior Past President*

\*A. V. Loughren,  
*Junior Past President*

### 1957

J. G. Brainerd (R3)

J. F. Byrne

J. J. Gershon (R5)

A. N. Goldsmith

A. W. Graf

W. R. Hewlett

R. L. McFarland (R1)

\*Ernst Weber

C. F. Wolcott (R7)

### 1957-1958

H. R. Hegbar (R4)

E. W. Herold

K. V. Newton (R6)

A. B. Oxley (R8)

F. A. Polkinghorn (R2)

J. R. Whinnery

### 1957-1959

D. E. Noble

Samuel Seely

\* *Members of Executive Committee*



Change of address (with 15 days advance notice) and letters regarding subscriptions and payments should be mailed to the Secretary of the IRE, 1 East 79 Street, New York 21, N. Y.

All rights of publication, including foreign language translations are reserved by the IRE. Abstracts of papers with mention of their source may be printed. Requests for republication should be addressed to The Institute of Radio Engineers.

(Continued)

6351. A Galactic Model for Production of Cosmic Rays and Radio Noise.....	<i>L. Marshall</i>	215
6352. Absorption Techniques as a Tool for 21-CM Research.....	<i>A. E. Lilley and E. F. McClain</i>	221
6353. Hydrogen Line Study of Stellar Associations and Clusters.....	<i>T. K. Menon</i>	230
6354. Extragalactic 21-CM Line Studies.....	<i>D. S. Heesch and N. H. Dieter</i>	234
6355. Excitation of the Hydrogen 21-CM Line.....	<i>George B. Field</i>	240
6356. Spectral Lines in Radio Astronomy.....	<i>A. H. Barrett</i>	250
6357. Measurements of Planetary Radiation at Centimeter Wavelengths.....	<i>C. H. Mayer, T. P. McCullough, and R. M. Sloanaker</i>	260
6358. Planetary and Solar Radio Emission at 11 Meters Wavelength.....	<i>John D. Kraus</i>	266
6359. Radio Emission from Comet 1956 h on 600 MC.....	<i>R. Coutrez, J. Hunaerts, and A. Koeckelenbergh</i>	274
6360. Lunar Thermal Radiation at 35 KMC.....	<i>John E. Gibson</i>	280
6361. Lunar Radio Echoes.....	<i>James H. Trexler</i>	286
6362. Radar Echoes from the Moon at a Wavelength of 10 CM.....	<i>B. S. Yapple, R. H. Bruton, K. J. Craig, and N. G. Roman</i>	293
6363. The Use of Radio Stars to Study Irregular Refraction of Radio Waves in the Ionosphere.....	<i>H. G. Booker</i>	298
6364. An Investigation of the Perturbations Imposed Upon Radio Waves Penetrating the Ionosphere.....	<i>Robert S. Lawrence</i>	315
6365. A Phase Tracking Interferometer.....	<i>Hays Penfield</i>	321
6366. Radio Astronomy Measurements at VHF and Microwaves.....	<i>J. Aarons, W. R. Barron, and J. P. Castelli</i>	325
6367. Some Measurements of High-Latitude Ionospheric Absorption Using Extraterrestrial Radio Waves.....	<i>C. G. Little and H. Leinbach</i>	334
6368. Cosmical Electrodynamics.....	<i>J. H. Piddington</i>	349
<b>Correspondence:</b>		
6369. The Effects on Radio Astronomical Observations Due to Longitudinal Propagation in the Presence of Field-Aligned Ionization.....	<i>S. Rush and L. Colin</i>	356
6370. Launching IGY Satellites.....	<i>William H. Finlay</i>	357
6371. Mobile Single-Sideband Equipment.....	<i>R. E. Morrow</i>	357
6372. Space-Charge Waves Along Magnetically-Focused Electron Beams.....	<i>W. W. Rigrod and J. Labus</i>	358
6373. A Plea for Maximum Utility in Government Contract Reports Covering Research and Development.....	<i>E. W. Herold</i>	360
6374. Properties of Ion Filled Waveguides.....	<i>L. D. Smullin and P. Chorney</i>	360
6375. On the Forward Characteristic of Semiconductor Diodes.....	<i>H. L. Armstrong</i>	361
6376. Poles and Zeros Squared.....	<i>A. Papoulis</i>	361
6377. Effect of Correlation on Combiner Diversity.....	<i>Karle S. Packard</i>	362
<b>Contributors</b> .....		364
<b>IRE News and Radio Notes:</b>		
Calendar of Coming Events.....		374
Activities of the IRE Sections and Professional Groups.....		377
Professional Group News.....		378
Obituary.....		379
Technical Committee Notes.....		379
<b>Books:</b>		
6378. "Solid State Physics," by A. J. Dekker.....	<i>Reviewed by Frank Herman</i>	379
6379. "The Science of Engineering Materials," ed. by J. E. Goldman.....	<i>Reviewed by L. T. DeVore</i>	379
6380. "Acoustical Engineering," by H. F. Olson.....	<i>Reviewed by B. B. Bauer</i>	380
Professional Groups.....		380
Sections and Subsections.....		381
Abstracts of IRE Transactions.....		383
6381. Abstracts and References.....		386

## ADVERTISING SECTION

Meetings with Exhibits.....	6A	Notes.....	28A	Membership.....	78A
IRE People.....	12A	Professional Group		Positions Open.....	110A
News—New Products.....	14A	Meetings.....	42A	Positions Wanted.....	116A
Industrial Engineering		Section Meetings.....	56A	Advertising Index.....	139A

## Poles and Zeros



**Star Noise.** This special issue brings together fifty papers on radio astronomy. It is the first publication to deal comprehensively with the engineering and equipment phases of this subject and it also presents new findings in astrophysics, for example, in connection with radio sources among the planets. Contributions have come from Australia, Japan, Canada, England, France, Belgium, Alaska, Hawaii, and the United States, and the list of authors includes a majority of the leading workers in this field. The Institute is highly honored that its PROCEEDINGS has been chosen as the vehicle for this massive report on the current state of this science.

Radio astronomy is 25 years old, to the month. The PROCEEDINGS in December, 1932 carried a report by the late Karl G. Jansky that he had observed for several months mysterious atmospheric noise at the Bell Laboratories station at Holmdel, N. J. Less than a year later, he identified the source as extraterrestrial, coming from the direction of the Milky Way, and in October, 1935 he reported that the local galaxy was in fact the source. It is seldom that credit for the discovery of a new branch of radio science can be narrowed down to one man, but there is no room for doubt that Jansky was the first to show that radio emissions from the stars could be certainly identified from among all the other random noises in the spectrum. His work is commemorated in this issue by his brother, IRE Past President C. M. Jansky, Jr. Following this early work, research in this field was carried out almost single-handedly for a decade by Grote Reber, whose recollections of his early experiments are also presented herein.

This issue has been 21 months in preparation. It was initially suggested independently by Editor Emeritus A. N. Goldsmith and D. C. Ports of the Professional Group on Antennas and Propagation. Special thanks go to Professor F. T. Haddock, head of the radio astronomy activities at the University of Michigan and a member of the PGAP Administrative Committee, who organized the issue and did yeoman service in procuring, reviewing and selecting the material. Delmer Ports and J. D. Kraus did much of the early planning and were most helpful to the staff in coordinating the project. Behind these men stands, of course, the PGAP itself. This issue is a monument to the vitality of the Professional

Group system and sets a high mark among all the special issues thus far published.

Readers will find big numbers to cope with in the pages that follow. The spread in power, for example, is a staggering  $10^{22}$ , from the  $10^{-16}$  watt to which a typical radio-astronomy receiver will respond, to the  $10^{36}$  watts radiated by the largest of the galactic transmitters within 300 million light years, which is roughly the distance to the farthest galaxies from which radio energy has been detected to date.

**A and R.** Among the miscellaneous inquiries which have recently confronted us is this: In the 12 postwar years to date, how many technical papers have been published throughout the world in the fields of electronics and the allied arts? Answer: Not less than 44,000. The authority for this staggering statistic lies in the back pages of each issue of the PROCEEDINGS, where we reprint the *Abstracts and References* compiled by the Radio Research Organization of the British Department of Scientific and Industrial Research. This organization 1) pores over some 200 technical journals in ten languages, 2) selects therefrom each month the titles and authors of over 300 papers and reviews, and 3) prepares definitive abstracts of the majority of the listed papers. Each listing is assigned its proper number in the Universal Decimal Classification and the whole collection is arranged in 19 parts, ranging from Acoustics and Audio Frequencies to Tubes and Thermionics. Once each year, the references are indexed alphabetically by author and subject; the index is reprinted as a separate part of the PROCEEDINGS in the May or June issue.

The record number of listings occurred in 1947, when the pent-up record of the war years was released in a flood of over 4,000 listed papers and reviews. Since 1951, when a low point was reached for some unaccountable reason, the list has grown each year, reaching 3,902 in 1956 and bidding fair to break the old record in the year just ended. Keeping track of such an outpouring is no mean task, and we are particularly indebted to the DSIR and the British publication, *Electronic and Radio Engineer* (which oldsters will recognize as the *Wireless Engineer*), for making possible republication of the abstracts in these pages.—D.G.F.



## Donald G. Fink

PRESIDENT, 1958

Donald G. Fink was born on November 8, 1911, at Englewood, N. J. He received the bachelor's degree in electrical engineering from the Massachusetts Institute of Technology in 1933, and the master's degree in electrical engineering from Columbia University in 1942.

During 1933-34 Mr. Fink was a research assistant in the M.I.T. departments of electrical engineering and geology. From 1934 to 1952 he was on the editorial staff of *Electronics*, becoming its editor-in-chief in November, 1946. Since 1952 he has been with the Philco Corporation as Director of Research.

Mr. Fink participated in the development of the loran system in 1941-43, when on leave to the Radiation Laboratory at M.I.T. In 1946, he was a civilian consultant on the staff of the Commander, Joint Task Force One, in charge of preparing damage reports on all electronic material and test facilities for the Bikini bomb tests.

He was a member of Panel 1 of the first National Television System Committee and editor of its *Proceedings*. He was also vice-chairman of the second National Television System Committee from 1950 to 1952, and chairman of Panel 12 and its

editorial committee.

He is a member of Tau Beta Pi, Sigma Xi and Eta Kappa Nu, and a fellow of the American Institute of Electrical Engineers and the Society of Motion Picture and Television Engineers. He is the editor of the recently published *Television Engineering Handbook*.

Mr. Fink became an Associate of the IRE in 1935, and rose through Senior Member grade in 1945 to become a Fellow in 1947. He was an IRE Director during 1949-51 and 1956-57, and Editor during 1956-57. He was a member of the editorial board from 1946 until 1957, the Membership Committee during 1942-48, the Television Committee during 1946-49, and the Television Systems Committee during 1949-57. He was chairman of the Membership Committee in 1946, the Television Committee during 1948-49, and the Joint Technical Advisory Committee in 1949.

He has been the recipient of the Medal of Freedom from the War Department in 1946, the Presidential Certificate of Merit in 1948, the Fall Meeting Plaque in 1951, and the Journal Award of the Society of Motion Picture and Television Engineers in 1956.

# Introduction to Radio Astronomy\*

F. T. HADDOCK†, MEMBER, IRE

In lieu of the usual "Scanning the Issue" page, the organizer of this special issue presents below, for the benefit of the general reader, a discussion of the contents of this issue. He has preceded the discussion by an excellent introduction which will orient the reader and will interpret for him the importance of radio astronomy to both astronomers and radio engineers.—*The Editor*

**Summary**—A general description of the nature of radio astronomy, its differences from optical astronomy, a review of the earliest beginnings of galactic and solar radio astronomy, and a listing of other important observational discoveries is given. A nearly complete bibliography of these early publications and of the principal review books and papers on Radio Astronomy is given.

Some practical aspects and instrumental developments of possible interest to radio engineers are pointed out. The papers in this issue of the PROCEEDINGS on Radio Astronomy are discussed generally and individually. A brief description of some new results on solar-burst spectra obtained at the Radio Astronomy Observatory at the University of Michigan is presented.

## INTRODUCTION

OUR CONCEPT of the Universe has been appreciably enlarged by radio observations in recent years. It has been found that radio waves are emitted from the Moon, Venus, Mars, Jupiter, and Saturn, from the Sun's gaseous atmosphere, from the debris of exploded stars, from neighboring galaxies of stars, from clusters of distant galaxies, from clouds of gas in the spiral arms of our Milky Way galaxy, from very distant Island Universes in collision, and from hundreds of invisible and unsuspected heavenly objects, popularly miscalled radio stars. Radio studies have taken the lead in mapping the structure of our own galaxy, and have revealed the fact that the Milky Way is a rather tightly wound spiral galaxy. The solar system is traveling along the inner edge of a spiral arm at a distance of 30,000 light years from the center of rotation of this disk of stars and gas. Many astronomers believe that some of the fainter radio sources are at distances beyond the range of present optical telescopes and that with the recent attainment of Doppler shift measurements on the radio hydrogen-line radiation from distant galaxies, cosmologists may soon be given a fresh and penetrating view into the depths of time and space.

Although cosmic ray and meteor studies have made valuable contributions, most of our knowledge of the Universe has been gained from electromagnetic light waves, falling on the earth through a window in the atmosphere about five octaves wide. Radio astronomy is now exploiting the existence of a second window through the atmosphere 12 octaves wide. Radio waves shorter than a few millimeters are absorbed by atmospheric oxygen and water vapor; whereas the ionospheric layers turn back radio waves longer than several decimeters [1]. Thus radio astronomy observations are made at frequencies used in television, fm radio, microwave relay links, rocket and satellite telemetering and control, and radar.

Light and radio waves are fundamentally the same except for their length. Radio waves are thousands of times longer than light waves; this large difference has two consequences of great importance to astronomy. First, the interaction of radio waves with interstellar gas, solar and planetary atmospheres,

and cosmic dust clouds complements that of light waves. Large regions of the Universe are forever inaccessible to optical study because of heavy obscuration by interstellar dust which, however, is transparent to radio waves. On the other hand, tenuous ionized gas-regions such as exist around the Sun as its corona, and surrounding super-giant blue stars as bright gaseous nebulas, and even enveloping all the stars in spiral galaxies, are transparent to light waves, but reflect, absorb, or emit radio waves. Thus radio methods offer new and powerful means of studying these gaseous regions and, at the same time, penetrating the obscuration due to cosmic dust without the least detectable effect. Second, the value of radio to astronomy is limited somewhat by the difficulty of obtaining high angular resolving power. Wave diffraction sets this instrumental limit as it does for optical telescopes, and since its blurring effect is proportional to wavelength, radio waves are very much harder to "focus sharply." For example, the most precise radio telescopes of today, operating on microwaves, are capable of producing angular resolution which is not quite as good as the unaided human eye with light waves. To compare with an optical telescope in resolution a radio antenna would need to be hundreds of miles in extent. However, position location is not the same as resolving power; if a radio source is much brighter than its surrounding background emission and its shape is assumed to be known, then its position can be located to a much smaller angular uncertainty than is indicated by the resolving power of the antenna.

With the largest optical telescopes it is practically impossible to obtain the ultimate instrumental resolution given by wave diffraction theory because of the inhomogeneities in the refractive index of the earth's atmosphere. When the atmosphere is very stable at the proper heights and stellar images are steady and sharp, the astronomer says that the "seeing" is good. Pronounced twinkling, or scintillation, and "dancing" of stellar images is poor "seeing." This "seeing" problem also exists in radio astronomy, with the additional complication, at the longer wavelengths, of ionospheric effects, including the Faraday rotation of the radio wave polarization, and occasional large absorption at decimeter wavelengths. Undoubtedly, "radio seeing" will also set a practical limit to the angular resolution obtainable at all wavelengths used in terrestrial radio astronomy.

For the above reasons and for the fact that stars are relatively poor radio emitters, the radio telescope presents to us a dustless and starless universe, populated largely by turbulent gas clouds.

## THE BEGINNINGS

It is very likely that the first attempt to measure the emission of radio waves from an extraterrestrial source was that of Sir Oliver Lodge [2], well-known radio pioneer, who in a lecture before the Royal Institution of Great Britain on June 1, 1894, only six years after Hertz discovered radio waves, stated, "I hope to try for long-wave radiation from the sun, filtering out the ordinary well-known waves by a blackboard

\* Original manuscript received by the IRE, December 10, 1957.

† University of Michigan, Ann Arbor, Mich.

certain fraction, which is relatively more intense in the microwave region, arises thermally from free electron collisions with positive ions in interstellar gas clouds [12, 13].

The first documented recognition of the reception of radio waves from the Sun was made in 1942 by Hey [14] in England and independently by Southworth [15] in New Jersey. Both wrote reports which had restricted circulation because of the war and were not published until later. Reber [16] in Wheaton, Ill., independently discovered and identified solar radiation at 160 mc in the following year and was the first to publish the evidence. He devoted only a few lines to the Sun in this paper on galactic radiation.

Southworth used radar receivers and paraboloids in a deliberate attempt to detect radio emission from the Sun. He was successful on June 29, at 10,000 mc and at 3000 mc a week or two later. He correctly attributed this emission to thermally generated radiation. He has recently given a good detailed account of this work [17] and of his early association with Jansky at the Bell Telephone Laboratories in New Jersey. These measurements initiated the study of the radio undisturbed or "quiet" Sun. Now we will describe the discovery of radio bursts, the second main class of solar radio emission.

Undoubtedly there have been many unpublished observations of high hissing noise levels arising before or after radio fadeouts, but the first publication was in 1936 when Arakawa [18] noted that, "High noise accompanied these sudden fadeings (4–20-mc band), especially on local circuits. The effect must be related to solar activities, since they occur only on daylight routes." And two years later Heightman [19] wrote, "At such times (when fadeouts occur) the writer has often observed the reception of a peculiar radiation, mostly on frequencies over 20 mc, which on a receiver takes the form of a smooth though loud hissing sound. This is presumably caused by the arrival of charged particles from the Sun on the aerial."

During this period scientists [20] were studying the association of short-wave radio fadeouts with solar flares (chromospheric eruptions), terrestrial magnetic pulses, enhanced atmospheric static, and sudden increases in noise level mentioned above. It appears that the question of the origin of this enhanced noise attracted the least attention. In 1939 one paper appeared in Japan by Nakagami and Miya [21] which described an experiment made near 15 mc to measure the angle of arrival of noise "like that from a grinder" attaining a level of 40 db above the background just before and shortly after a fadeout. They found that this noise occurred only during the day and that its direction of arrival was from high elevations, but they did not note the significance of the corresponding elevation of the Sun. They concluded that this noise probably originated in or near the *E* layer.

On February 26–28, 1942, a number of British Army radars, operating at frequencies between 55 and 80 mc, suffered severe interference. This was investigated by Hey and was described in restricted reports in 1942 and 1945. He had found that the direction of arrival of the interference was from the Sun and that during this period there was a large sunspot group on the disk of the Sun. Hey concluded that it was difficult to imagine any other explanation than that the radiation originated at the Sun in association with the sunspot activity.

In January, 1946, Hey [22] published a letter in *Nature*, briefly describing the 1942 event and, in a postscript, F. J. M. Stratton described the solar flares and geomagnetic effects associated with the solar event. Appleton and Hey [22, 23] pointed out that the previously reported noise from the Sun was many times greater than that to be expected from the Sun as a black-body radiator. The relationship between the intense solar radio noise and sunspot activity was substantiated in Sydney by Pawsey, Payne-Scott, and McCready [24] in 1946.

Ryle and Vonberg [25] in England first published interferometric measurements made to obtain the size of a radio

emitting region. They used two antennas spaced 140 wavelengths apart to give a multilobed pattern analogous to Michelson's method for measuring stellar diameters. An emitting source on the Sun during July, 1946, was found to be less than 10 minutes arc, less than  $\frac{1}{3}$  the diameter of the Sun. In 1947, McCready, Pawsey, and Payne-Scott [26] published results obtained earlier in February, 1946, giving similar results on the source size but using a cliff interferometer which consists of only one antenna 250 feet above the ocean and utilizing the reflected ray to produce a multilobed pattern at low angles of elevation, analogous to Lloyd's mirror interferometer.

The polarization of the intense radio emission from sunspot regions was first detected and found to be circularly polarized during July, 1946. Observations were conducted by three independent groups [25, 27, 28] in England and Australia.

Since then both the basic thermal component from the "quiet" Sun and the nonthermal intense bursts from the active Sun have been subjected to detailed study at various frequencies from a few mc to a few 100,000 mc.

#### HIGHLIGHTS OF OTHER OBSERVATIONAL DISCOVERIES

In 1946 and 1947, Hey and Stewart [28] in England first used radar equipment to study meteors. They gave the first definite proof that most transient echoes from the *E*-layer region were from meteors. With Parsons [29] they made the first radar measurement of meteor velocities.

Dicke and Beringer [30] in 1945 made the first measurement of the thermal radio emission of the Moon. They used the chopper-type microwave radiometer, at 24,000 mc, which Dicke [31] had developed at the M.I.T. Radiation Laboratory in order to measure thermal microwaves from atmospheric oxygen and water vapor. Piddington and Minnett [32] in Sydney made the first extended series of observations of the lunar emission at various phases in 1949.

Radar echoes from the Moon were first obtained in 1946 by scientists at the U. S. Army Signal Corps Laboratory [33] at 111.5 mc, and a little later by Bay [34] in Hungary at 120 mc using a novel electrochemical integrator.

An outstanding discovery was made in 1951 by Ewen and Purcell [35] at Harvard University by the detection of the 1420-mc line radiation from the ground state of atomic hydrogen, which occurs as gas largely in the spiral arms of the Milky Way. The detection was shortly confirmed by Muller and Oort [36] in Leiden and by Christiansen and Hindman [37] in Sydney.

The possibility that this radio spectral line might be detected from the galaxy was first pointed out by van de Hulst in a Leiden Observatory talk in April, 1944, and was published the following year [38]. His talk was stimulated by a recent paper in the *Astrophysical Journal* by Reber on "Cosmic Static." The importance of this line is realized when it is pointed out that atomic hydrogen in the ground state constitutes the major fraction of interstellar matter and is undetectable by optical methods. It has also made possible the radio measurement of velocities by means of the Doppler shift. This has been extremely valuable. In 1955, Lilley and McClain [39] at the U. S. Naval Research Laboratory reported the "red-shift" of a distant radio source by observing in absorption the 1420-mc hydrogen line Doppler-shifted to 1340 mc. This indicated a line-of-sight recession of 16,830 km in good agreement with the optical determination.

An unexpected discovery was made in 1955, by Burke and Franklin [40] at the Department of Terrestrial Magnetism in Washington, D. C. when they detected bursts of radio emission from the planet Jupiter at 22 mc. When Shain [41] in Sydney was notified of this, he was able to identify Jovian bursts on his galactic radiation records at 18 mc back to 1950, and found that a source of emission was localized on Jupiter.

In 1956 and 1957, Mayer, McCullough and Sloanaker [42]

at the U. S. Naval Research Laboratory detected for the first time microwave emission, at 10,000 mc, from Venus, Jupiter, and Mars and the partial polarization of radiation from the Crab Nebula [43]. In 1956, Kraus [44] at Ohio State University reported the detection of Jupiter-type bursts from Venus at 27 mc. To date, attempts by others to confirm this have not been successful. In 1957, Drake and Ewen [45] at Harvard at 8000 mc confirmed the detection of the thermal emission from Jupiter and detected for the first time radio emission from the planet Saturn. In the spring of 1957 there appeared a bright naked-eye comet denoted Arend-Roland, 1956h. Many radio astronomers attempted to detect radio emission from it; most were unsuccessful. However, scientists in Belgium at 600 mc, and in Bonn, Germany, at 1420 mc claimed possible success [46].

No attempt has been made above to cover all the important observational results nor any of the theoretical work. Little has been mentioned of solar-terrestrial relationships, and, as with this entire issue, next to nothing has been given on meteors, principally because the meteor work warrants separate treatment and has been studied by people not otherwise engaged in radio astronomy, with the important exceptions of the Manchester group under Lovell, and, in the past, by the group under Hey. For an adequate survey of radio astronomy, including the neglected topics, the reader is referred to the following selected bibliography of books and monographs [47-54], technical review papers [55-73] and popular articles, which are usually well-illustrated [74-86]. A nearly complete bibliography of radio astronomy has been compiled by Martha Stahr Carpenter [87] of Cornell University. The research staff of the Radiophysics Laboratory [88] in Sydney has compiled a bibliography with short abstracts for the period 1954-1956.

#### THE IMPORTANCE OF RADIO ASTRONOMY TO ENGINEERING

The history of technology shows clearly that our engineering and technical progress depends more and more on the results of research that has been motivated by curiosity about the nature of our physical world. A popularly cited example is the technology of nuclear power which is based on the results of over fifty years of research in pure physics. It is not possible to predict if a new field of engineering will arise from results of radio astronomy investigations, but we already have several applications.

In 1943, Southworth [89] applied for a patent, which was later granted, claiming a method of artificial vision for scanning a terrain in overcast weather for object location, for scene identification, etc., using reflected radio waves emitted by the Sun.

The direct use of radio waves from the Sun for all-weather navigation [90] is an attractive application for ships. The Collins Radio Company [91] has developed, under a U. S. Navy Contract, a radio sextant for tracking the Sun all day. It utilizes the radiation from the Sun near a wavelength of one centimeter and a fire-control radar-type scanning antenna with a modified Dicke-type receiver. An experimental version [92] was tested by the U. S. Navy a number of years ago. It works through heavy overcast with an accuracy somewhat better than can be obtained in clear weather with the standard optical sextant. With improved sensitivity, it should be practical to track radio "stars" 24 hours a day under overcast skies, as predicted by the writer [93] shortly after the detection of centimeter wave radio sources.

With the advent of large gain antennas and sensitive low-noise receivers, the use of radio sources for antenna and receiver calibrations will become both more practical and necessary. Specially designed antennas of modest size at micro-wavelengths can provide matched transmission line terminations with equivalent noise temperatures near absolute zero.

These may be useful in making noise level measurements of low-noise receivers, masers, etc. With larger antennas of known gain, the brighter radio sources can potentially provide absolute noise level increments for international standardization. Conversely, absolute antenna gain can be measured by using a calibrated receiver, or by using a standard gain antenna and a calibrated attenuator with an uncalibrated receiver. At present, the absolute flux density at the earth from the brighter radio sources is known to accuracy of about 20 to 50 per cent, but some effort and much importance is being given to the determination of the absolute energy spectrum of radio sources. The Sun and radio sources have been widely used by radio astronomers to measure relative antenna patterns. At meter wavelengths the energy from the Sun is frequently variable and the galactic background emission level is well above absolute zero. Therefore the above remarks apply principally to centimeter wavelengths; at millimeter wavelengths the signal-to-noise ratio on radio sources is small and atmospheric absorption is troublesome, although the Sun and the Moon are relatively easy to detect.

The directional pointing of antenna beams of sensitive radars can be calibrated on extraterrestrial radio sources, after due correction for total refraction through the earth's atmosphere. Perhaps more important is the determination of this total refraction of waves from a radio source or moon echo. This can be determined with the use of a calibrated antenna system or interferometer. Knowledge of total refraction and its vagaries at different frequencies is important in radio guidance, detections, and tracking systems involving high flying objects, satellites, etc.

The present results of radio astronomy provide us with a fairly good estimate of the minimum radio noise levels that can be expected on earth and in outer space over the radio astronomy frequency spectrum. Depending on the frequency band, naturally generated noise originates principally from the Earth, its atmosphere, the Sun, the Milky Way, or various discrete radio sources. Less accurate estimates can be made of occasional large increases in noise level caused by radio bursts from the Sun, Jupiter, and, perhaps, Venus and Saturn. With the large antennas and low-noise receivers now being built or planned for various applications, it is becoming increasingly valuable to know the probability of radio noise outbursts and the level of the steady background emission from the various astronomical objects.

The study of solar radio radiation is becoming increasingly important in the prediction of radio propagation conditions involving the ionosphere. As noted in the introduction there is an association between increased radio noise from the Sun and sudden ionospheric disturbances, or radio communication fadeouts. At present it is not possible to predict the occurrence of a solar flare or a fadeout, but recent evidence [94] suggests that the characteristics and timing of radio solar bursts with respect to solar flares make it possible to predict whether or not a geomagnetic storm will follow within a few days. These storms are associated with [95] earth current changes, auroras, and anomalous ionospheric phenomena, called ionospheric storms, which can seriously disrupt radio communications, especially in high latitudes. Since these radio "blackouts" can last several days their prediction is greatly desired by communication people.

The day-to-day variations in solar activity affect the ion density of all layers in the ionosphere, and hence the choice for optimum frequency for communications that involve the ionosphere. The sunspot number, or area, is the most commonly used index of solar activity, although the daily level of radio flux around 3000 mc is very closely correlated with sunspot area and appears to be a better solar index for some applications. For instance, it can be measured precisely and continuously in any weather. In 1957, Denisse and Kundu [96] found a close and linear relation between 3000-mc solar flux

and the ionizing flux of the *E* layer. The correlation is better than when using sunspots in place of the radio solar flux.

#### THE CONTRIBUTION OF RADIO ASTRONOMY TO INSTRUMENTATION

On the instrumental side, radio astronomers have developed to a high state certain specialized antenna and receiving systems. An outstanding innovation by Hanbury Brown and Twiss [97] is the conception, development, and use of a new type of radio and optical interferometer for measuring the diameter of radio sources or, in an optical analog, optical stars. Their instrument detects the signals from two spaced antennas, or telescopes, independently, and then correlates the low-frequency detector outputs. The system has proved to be largely free of the effects of atmospheric and ionospheric seeing. This is expected since the relative phases are lost and only the correlation in their intensity fluctuations is measured. This is radically different from the familiar Michelson interferometer. It can be used with a very great separation between antennas. They have measured the optical diameter of the star Sirius [98] to be  $0.0068 \pm 0.0005$  second of arc, in good agreement with an astronomical estimate. This post-detection interferometer has two weaknesses however. It requires a good signal-to-noise ratio and, consequently, it can only be used on the brighter objects, and since phase information is lost it cannot be used to determine an unsymmetrical component in the brightness distribution across the object, as can be accomplished with a predetection radio interferometer.

Many different and effective techniques have been developed to measure the size, position, brightness, radio spectrum, distribution, and polarization of radio sources in the sky and on the Sun. They have been well described in the literature and several outstanding developments are represented in this issue of the PROCEEDINGS [99]. Radio astronomy has stimulated the conception, the design, and the construction of many large, high-gain reflector-type antennas [100]. One of the first high-gain antennas is the 50-foot precision paraboloid at the U. S. Naval Research Laboratory. It was used in three investigations described in this issue [101]. The largest steerable antenna known in the world is the 250-foot paraboloid [102] in Manchester, England.

Although low-noise receivers are being developed for many applications, it is in radio astronomy that high stability of the receiver gain, pass band, and noise figure can be exploited because of the frequent possibility of long-time integration of the receiver output to obtain greater sensitivity. An example of good radiometer stability has recently been announced by Drake and Ewen [45]. Their 8000-mc receiver has an hourly drift rate in noise level equivalent to  $0.1^\circ\text{K}$  antenna temperature change.

Trexler [103], at the U. S. Naval Research Laboratory, has reported the transmission and reception of voice modulated 200-mc signals reflected from the Moon, without appreciable change in fidelity. The writer can attest that he could not detect any change in quality of the voice transmissions after their flight to the Moon and back, as recorded on magnetic tape. However, the background noise level during recording was high and fidelity was not easy to judge. In any case, it appears that the Moon offers unusual broadcast possibilities. This prospect is not particularly appreciated by radio astronomers since the Sun and man-made interference already preclude daytime observing for certain programs, and the exclusion of moon-lighted nights would leave them not much better off, for observing time, than the optical astronomers.

After this attempt to point up some practical aspects of radio astronomy and its potential importance to technology, it is well to mention that astronomers, and many other "non-applied" scientists, feel that the principal value of engineering is its ability to contribute to man's quest for knowledge of his surroundings.

#### COMMENTS ON PAPERS IN THIS ISSUE

Among the papers selected for this issue are a number describing antennas and receivers of advanced or novel design, a number giving recent observational results of astronomical or geophysical interest, and a few of more direct practical value; three or four papers on theoretical aspects of radio generation, and two papers describing the newly established U. S. National Radio Astronomy Observatory in Green Bank, W. Va. Since about 80 per cent of the contents of this issue are from U. S. scientists with the balance from groups in Australia, Belgium, Canada, England, France, and Japan, the issue does not give a representative view of the over-all field. There is nothing from the two large and active groups in England at Cambridge and Manchester Universities, the influential Leiden Observatory group in Holland, nor from the rapidly growing centers in Germany and the U.S.S.R. On the other hand there are several papers of outstanding instrumental interest from the large group in Australia (papers by Mills, *et al.*, Shain, Christiansen and Mathewson, and Wild and Sheridan) and two papers from Japan on their speciality (by Suzuki and Tsuchiya, and Akabane) of radio polarimeters for solar burst analysis. There is a review paper from the large and growing center in Paris (by Blum, Denisse, and Steinberg) which may serve to introduce many U. S. readers to a pioneering group in radio astronomy which is not so well known here as are the groups in English-speaking countries.

The emphasis in this issue on the U. S. effort is natural partly because there has been an awakening interest here in radio astronomy. Many U. S. universities are now in the process of planning or setting up programs in this field. The stimulation of such activity was an important motive behind the creation of the National Radio Astronomy Observatory which will make available large radio telescopes and isolated sites to universities which would not otherwise go in for radio astronomy. It is believed that this country has begun to contribute its share to the development of basic discoveries, many of which were made here, but followed up principally in England and Australia.

The papers by C. M. Jansky, Jr., on his brother's discovery of extraterrestrial radio waves, and by Reber, describing his lonely follow-up of Jansky's work, bring out the fact that radio astronomy research began here and remained here for a decade. But after World War II, England and Australia largely took it over and developed it to the point where optical astronomers could no longer ignore its potential value. Reber's paper is a gem. In down-to-earth language he presents a vivid picture of his persistent, and often frustrating, efforts to detect radio waves from the Milky Way at frequencies where techniques were still in an experimental state of development.

Emberson and Ashton describe the activities and plans of Associated Universities, Inc. in setting up and operating the U. S. National Radio Astronomy Observatory, with National Science Foundation support. Ashton is the design engineer for their 140-foot steerable precision reflector which is now planned to be in operation in 2 or 3 years. Although it is not as large as the 250-foot paraboloid in Manchester, England, it should be usable at wavelengths which are 5 or 10 times shorter. In the following paper, Findlay describes the unwanted noise levels in Green Bank, W. Va., the location of the National Radio Astronomy Observatory.

Drake and Ewen describe the development of an outstanding broad-band microwave radiometer and observations made with it. They have detected radio emission from the planet Saturn and from planetary nebulas for the first time, using a 28-foot reflector. Strum presents the design considerations that arose in the development of this radiometer which can detect input noise level changes of a few hundredths of a degree Kelvin. McCoy considers the possibility of developing low-noise crystal mixers for millimeter wavelengths. He concludes that it will be possible to obtain low receiver noise

figures which do not increase noticeably with frequency from 10 kmc to 50 or 100 kmc. This is an exciting prospect which in practice may compete for some time with masers in future millimeter-wave astronomy.

Mills, *et al.*, present the design and performance details of their large synthetic pencil-beam antenna at 3.5 meters, commonly called a "Mills Cross." This antenna-receiver system has an effective beam width of less than one degree and is being used to complete the largest catalog of radio sources extant. Many interesting results have been found with this instrument. Shain, of the same laboratory, describes a similar installation at 15 meters wavelength with which he has obtained a map of galactic background emission which shows clearly the regions where the background is reduced by absorption due to interstellar ionized clouds of hydrogen in the spiral arms of the Milky Way.

Kraus writes about a very large fixed reflector antenna of novel design now under construction by his radio astronomy group at Ohio State University. He plans to conduct surveys of the sky for radio sources in the depths of space at several frequencies simultaneously. The antenna beam will be reflected by a flat, tiltable sheet in order to cover a wide range of elevation angles.

The next two papers, by Bracewell, apply information theory analysis to the efficient reduction of data and planning of the observing programs. The first paper considers the information content of interferometer records, and the second evaluates the loss of data due to noise and to the finite antenna beamwidth.

The next fourteen papers all pertain to the Sun. The papers by Medd and Covington and by Hey and Hughes deal with the calibration of absolute solar radio flux at 10 cm. The valuable feature here is that both have obtained the same absolute flux value from the Sun on June 30, 1954. On this date the Sun was eclipsed by the Moon and it was in a very undisturbed state. The N.R.L. eclipse expedition to Sweden also obtained excellent solar measurements on this day at the same wavelength and have deduced the relative brightness distribution across the solar disk from the measured eclipse curve [104].

The paper by Coates is the first detailed report in radio astronomy of observations at a wavelength less than 8 mm. The technique, the atmospheric measurements, and the solar results are all of interest. He gives evidence of excess radiation from sunspot regions. Christiansen and Mathewsen describe the evolution of an instrument for obtaining high angular resolution for solar studies. They are principally interested in measuring the size, shape, and intensity of sunspot radiation near 20-cm wavelength [105].

The next three papers describe the receiver, the antenna system, and some observational results of dynamic spectra of solar bursts over the frequency range of 100 to 600 mc. This type of solar investigation was initiated and developed by Wild and his colleagues in Australia at frequencies from 40-240 mc, and was a major advance over that of recording solar radiation at a number of single frequencies. Goodman and Lebenbaum describe the three mechanically tuned superheterodyne receivers and the output display. Jasik developed the antenna feed system for use with a 28-foot paraboloid reflector. The feed consists of four confocal broad-band antennas for simultaneous operation at the reflector focus. This development is an advance in the utilization of a paraboloidal reflector. Maxwell and Goldstein describe their site, equipment, and operation. They show photographs of their records, illustrating several types of solar bursts.

The Sun has been observed at the University of Michigan with similar equipment since August 28, 1957. As each receiver sweeps almost over an octave, giving complete coverage of the 100- to 580-mc frequency band every 0.3 second, the output is displayed as an intensity modulated line on a precision cathode-ray tube. This is photographed on a slowly moving

(1 cm/min) 35-mm film, producing a frequency-time record with solar intensity appearing as variations in photographic density. The combination of the film characteristic and the logarithmic response of the receiver permits the recording of a wide range of signal intensities in considerable detail. On September 3, at about 12:15:10 U.T., three simultaneous bursts were recorded with "U-Type" spectra (as found by Maxwell), having a duration of a few seconds, with their low-frequency "reversing" points at 130 mc, 250 mc, and 375 mc. Between 130 mc and 125 mc there existed a continuous interfering signal which could have masked a few megacycles of the low-frequency limit of the "fundamental" frequency burst; the lowest frequencies could also have been attenuated in the Sun, as suggested by Wild, Murry, and Rowe when they presented evidence of the second harmonic. Maxwell has reported evidence of two simultaneous "U-Type" bursts in a 2 to 3 frequency ratio but without evidence of a "fundamental" frequency. Classical Type III burst groups (fast drift bursts) associated with flare onsets have been recorded, however, with an unexpected broad-band, burst-free, continuum emission beginning 3 to 4 minutes after the Type III event and lasting from 1½ to 2½ hours, with a pronounced low frequency cut-off (above 300 mc), but showing a tendency to drift to somewhat lower frequencies. It is believed that this continuum emission is distinct from that associated with Type I noise storms observed at lower frequencies. It is similar in character, and in following a Type III event, and in duration to the emission found by Boisshot and called Type IV. Denisse has suggested that Type IV emission is due to synchrotron radiation, on the basis of its source being large and greatly elevated in the solar corona (4 or 5  $R_{\odot}$ ). This spectral type has also been noted by Maxwell, *et al.*, in their paper in this issue. Fig. 3 is a photographic record of the outstanding event of September 12, 1957. It shows a typical Wild Type III fast burst group beginning at 15:15 U.T. at all frequencies. Then one minute later there begins a Type II slow drift from high to low frequencies. The fine detail showing its composition as many fast bursts similar to the Type III bursts has not been reported before. After this burst there appears a general brightening of the entire high-frequency band, entirely free of detailed structure, lasting 150 minutes. The September 13, 1957, record shows also a Type III burst group again preceding a high frequency "smooth" emission, this time lasting 90 minutes.

Dodson reviews some results of attempting to correlate optical flares on the Sun with radio bursts, ionospheric disturbances, and geomagnetic storms. A valuable finding is a description of a radio event associated with optical flares which indicates the probable occurrence of a geomagnetic storm within a few days, described earlier in this paper.

Wild and Sheridan describe the recent development of a sweep-frequency interferometer for studying meter-wave solar bursts and noise storms. This instrument measures the size and position of the emitting region on the Sun and its dynamic spectrum simultaneously, or it can measure the burst polarization characteristics and spectrum. The output records are complex but contain much information. It appears that appreciable effort is required to reduce the data completely.

The next four papers deal with the measurement of the polarization characteristics of solar radio emission. Cohen presents a general review of the problem and then describes the Cornell University meter wave equipment. Suzuki and Tsuchiya, and Akabane describe meter wave and microwave polarimeters, which have been developed in Japan. The short paper by Bracewell and Stableford is a theoretical one which will be of value in interpreting records of solar radio emission.

The three papers by Roman and Yaplee, by Wells, and by Ko report measurements and discussions of spectra of radio sources and cosmic background radiation. Marshall presents a theory of galactic radio emission involving synchrotron emission from high energy interstellar electrons being deviated by

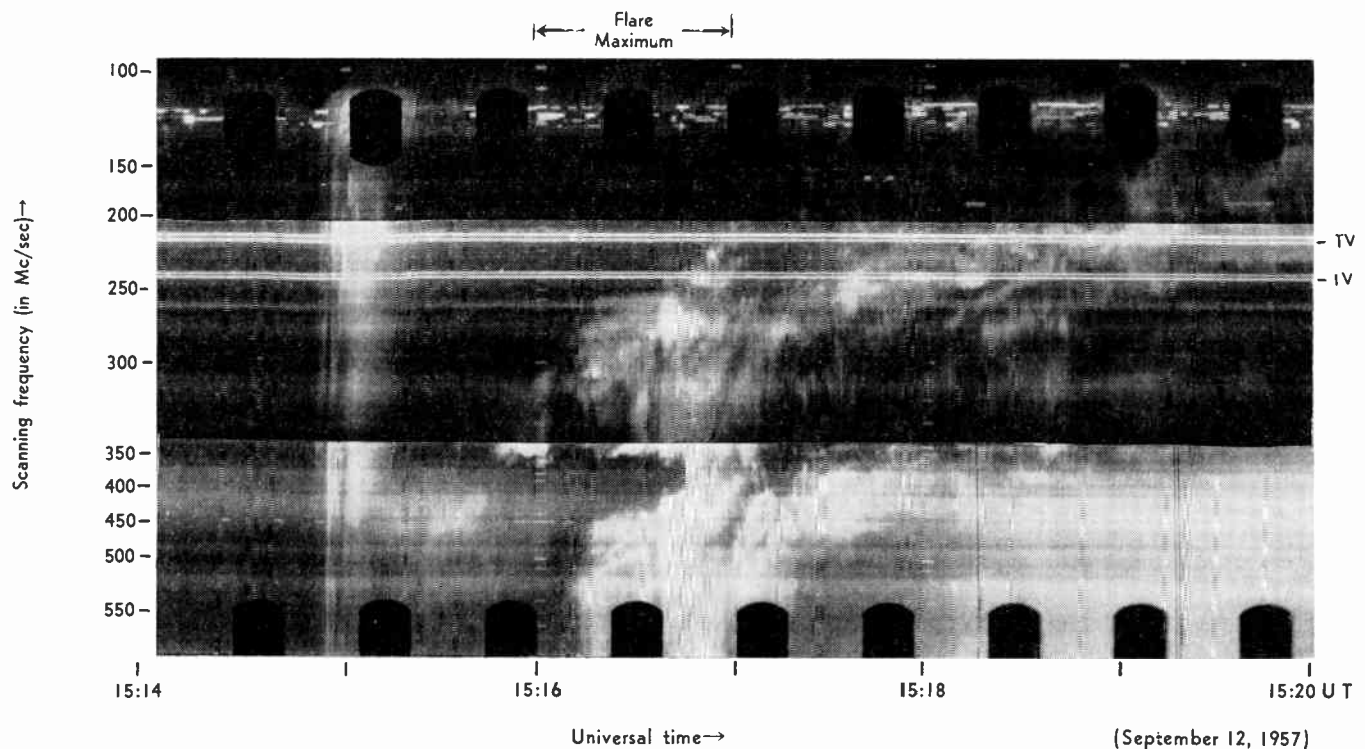


Fig. 3—A log-intensity modulated display, recorded at the University of Michigan, of dynamic spectra of an unusual solar radio burst complex at the time of a solar flare. Frequency increases vertically downwards and time increases to the right. The horizontal bright lines, both solid and broken, are man-made signals. The broad horizontal banded structure is due to receiver gain and noise level variations, and to the combining of three different receiver outputs. The fine uniform vertical lines are the individual scan lines. The vertical columns of dashes are the frequency and time markers. The Type III, fast drift, bursts begin on all frequencies near 15:15 U.T.; the Type II, slow drift, burst begins shortly afterwards on the higher frequencies and drifts downward in frequency. The detailed structure of this slow drift event appears to be composed of individual fast drift bursts of restricted frequency range. The broad-band, featureless, brightening at the higher frequencies following the Type II burst lasted 150 minutes. This is believed to be the new Type IV burst.

galactic magnetic field.

The next five papers deal with radio spectral line radiation, in contrast with the continuum radiation which we have been considering; the first four are concerned with the 21-cm line from atomic hydrogen. The paper by Barrett is a tutorial paper on radio spectroscopy for the radio astronomer; he describes some radio spectral lines that warrant future investigation. Lilley and McClain review the techniques of measurement of the 21-cm line in absorption when viewed against a background of bright continuum emission from a radio source or sources, and discuss the potentialities of this technique. Menon has reported a very interesting astronomical study, using the 21-cm radiation from gaseous regions surrounding clusters and associations of stars within our galaxy. Heeschen and Dieter describe some results and many fascinating possibilities of measuring the 21-cm line radiation from external galaxies and clusters of galaxies. The theoretical paper by Field discusses the various mechanisms in outer space which can affect the excitation temperature of the hydrogen line. He has been interested in the possibility of detecting very dilute hydrogen gas in the regions between external galaxies, an important cosmological problem. Since there is nothing in this issue on the spiral arm structure of our galaxy as revealed by the 21-cm line studies, the reader is referred to a recent publication [106] on this topic which shows a map of the spiral arms.

Mayer, McCullough, and Sloanaker give an account of their recent detection and measurement of microwave emission from the planets Venus, Mars, and Jupiter. Drake and Ewen, as mentioned earlier, confirmed these detections and also detected Saturn. It is believed that this emission is thermal planetary radiation. This work has opened up a new approach to the study of planetary surfaces. At the other end of the

radio astronomy spectrum, Kraus reports the measurements of nonthermal bursts of radiation on 11 meters from Jupiter and the first detection of bursts from Venus. This type of emission is not the same as that observed at microwaves and is probably generated in the atmosphere or ionosphere of the planet. Although the physical cause of excitation may reside in or on the solid part of the planet. The report of radio bursts from Venus has not yet been confirmed by other observers.

Coutrez, Hunaerts, and Koeckelenbergh present evidence of the detection of 600-mc radiation from the recent naked-eye comet, Arend-Roiand, visible in the spring of 1957. A few observers have claimed the possible detection of this cometary radiation on different radio frequencies. However, a greater number have tried without success to detect this comet.

The next three papers deal with the Moon. Gibson has made a careful series of measurements of the thermal radiation from the moon at 8.5-mm wavelength. Observations like these shed light on the thermal and radio characteristics of the outer few feet or inches of the Moon's crust. Trexler reports the radar detection of the Moon using a 220-foot paraboloid scooped out of the ground and paved. His results show clearly that the lunar echo is from a small localized region at the center of the lunar disk, less than 200 miles in diameter. As mentioned earlier, Trexler demonstrated the potentialities of using the Moon in a radio communications link to obtain hemispherical coverage of the earth at high frequencies. Yaplee, *et al.*, also find that lunar echoes are returned from a localized central region, but at a wavelength of 10 cm, in contrast to the 150 cm used by Trexler. Yaplee, *et al.*, have made an effort toward measuring the precise distance to the Moon. They use a Cesium clock to get sufficient frequency control, and expect to obtain a distance measurement with an uncertainty of 500-1000 feet.

Booker has reviewed the work on radio source scintillations made at meter wavelengths and gives a theoretical discussion of the observations. Lawrence and Penfield, in separate papers, describe an observational investigation of phase and amplitude scintillations of radio sources due to the ionosphere, and the two-element interferometer and receivers developed for these measurements. Aarons, Barron, and Castelli describe vhf and microwave scintillations of radio sources. The latter

study has received little attention outside of France and should be of interest to both radio engineers and astronomers.

Little and Leinbach report the first detailed account of high latitude ionospheric absorption using radio sources. This report is the fruit of several years of investigation.

Piddington has written an interesting theoretical paper on various processes possibly involved in cosmic radio generation.

## REFERENCES

- [1] G. Reber and G. R. Ellis recently have been able to observe the radio galaxy at wavelengths of several hundred meters through occasional "holes" in the ionosphere; see "Cosmic radio-frequency radiation near one megacycle," *J. Geophys. Res.*, vol. 61, pp. 1-10; March, 1956.
- [2] O. J. Lodge, "Signalling through space without wires," (lecture of June 1, 1894) *The Electrician*, London, 2nd ed., 1897; 3rd ed., 1900.
- [3] K. G. Jansky, "Directional studies of atmospherics at high frequencies," *Proc. IRE*, vol. 20, pp. 1920-1932; December, 1932.  
 —, "Radio waves from outside the solar system," *Nature*, vol. 132, p. 66; July 8, 1933.  
 —, "Electrical disturbance of extraterrestrial origin," *Proc. IRE*, vol. 21, pp. 1387-1398; October, 1933.  
 —, "Electrical phenomena that apparently are of interstellar origin," *Popular Astronomy*, vol. 41, pp. 548-555; December, 1933.  
 —, "A note on the source of interstellar interference," *Proc. IRE*, vol. 23, pp. 1158-1164; October, 1935.  
 —, "Minimum noise levels obtained on short-wave radio receiving systems," *Proc. IRE*, vol. 25, pp. 1517-1530; December, 1937.
- C. M. Jansky, Jr., "The beginnings of radio astronomy," *Amer. Scientist*, vol. 45, pp. 5-12; January, 1957.
- , "The discovery and identification by Karl Guthe Jansky of electromagnetic radiation of extraterrestrial origin in the radio spectrum," this issue, p. 13.
- [4] H. T. Friis and C. B. Feldman, "A multiple unit steerable antenna for short-wave reception," *Proc. IRE*, vol. 25, pp. 841-917; July, 1937.
- [5] G. Reber, "Cosmic static," *Astrophys. J.*, vol. 91, pp. 621-624; June, 1940.  
 —, "Cosmic static," *Proc. IRE*, vol. 30, pp. 367-378; August, 1942.  
 —, "Early radio astronomy at Wheaton, Illinois," this issue, p. 15.
- [6] H. A. Kramers, "On the theory of X-ray absorption and of the continuous X-ray spectrum," *Phil. Mag.*, vol. 46, pp. 836-871; November, 1923.
- [7] J. S. Hey, S. J. Parsons, and J. W. Phillips, "Fluctuations in cosmic radiation at radio frequencies," *Nature*, vol. 158, p. 234; August 17, 1946.
- [8] J. G. Bolton and G. J. Stanley, "Variable source of radio frequency radiation in the constellation of Cygnus," *Nature*, vol. 161, pp. 312-313; February 28, 1948.
- [9] J. G. Bolton, G. J. Stanley, and O. B. Slee, "Positions of three discrete sources of galactic radio-frequency radiation," *Nature*, vol. 164, pp. 101-102; July 16, 1949.
- [10] W. Baade and R. Minkowski, "Identification of the radio sources in Cassiopeia, Cygnus A, and Puppis A," *Astrophys. J.*, vol. 119, pp. 206-214; January, 1954.  
 —, "On the identification of radio sources," *Astrophys. J.*, vol. 119, pp. 215-231; January, 1954.
- [11] G. Westerhout and J. H. Oort, "A comparison of the intensity distribution of radio-frequency radiation with a model of the galactic system," *Bull. Astron. Inst. Neth.*, vol. 11, pp. 232-333; August 26, 1951.
- [12] P. A. G. Sheuer and M. Ryle, "An investigation of the H II regions by a radio method," *Monthly Notices Roy. Astron. Soc.*, vol. 113, pp. 3-17; 1953.
- [13] F. T. Haddock, C. H. Mayer, and R. M. Sloanaker, "Radio observations of ionized hydrogen nebulae and other discrete sources at a wave-length of 9.4 cm.," *Nature*, vol. 174, pp. 176-179; July 24, 1954.  
 F. T. Haddock, "Hydrogen Emission Nebulae as Radio Sources," International Astronomical Union, H. C. van de Hulst, Ed., Cambridge University Press, Cambridge, Eng., pp. 192-196; 1957.
- [14] J. S. Hey, "Solar radiations in the 4-6 meter radio wave-length band," *Nature*, vol. 157, pp. 47-48; 1946.
- [15] G. C. Southworth, "Microwave radiation from the sun," *J. Franklin Inst.*, vol. 239, pp. 285-297; 1945.
- [16] G. Reber, "Cosmic static," *Astrophys. J.*, vol. 100, pp. 279-287; November, 1944.
- [17] G. C. Southworth, "Early history of radio astronomy," *Sci. Monthly*, vol. 82, pp. 55-66; 1956.
- [18] D. Arakawa, "Abnormal attenuation in short radio wave propagation," *Rep. Radio Res. Japan*, vol. 6, pp. 31-38; May, 1936.
- [19] D. W. Heightman, "The uhf: a review of conditions in 1937," *Wireless World*, vol. 42, pp. 356-357; April 12, 1938.
- [20] J. H. Dellinger, "A new cosmic phenomenon," *Science*, vol. 82, p. 351; October 11, 1935.  
 —, "Sudden disturbances of the ionosphere," *J. Res. NBS*, vol. 19, pp. 111-141; August, 1937.  
 H. W. Newton and H. J. Barton, "Bright solar eruptions and radio fades during the years 1935-1936," *Monthly Notices Roy. Astron. Soc.*, vol. 97, pp. 594-611; 1937.
- [21] M. Nakagami and K. Miya, "Incident angle of short-waves and high-frequency noise during Dellinger effect," *Electrotech. J. Japan*, vol. 3, p. 216; 1939.
- [22] J. S. Hey, "Solar radiations in the 4-6 metre radio wave-length band," *Nature*, vol. 157, pp. 47-48; January 12, 1946.
- [23] E. V. Appleton, "Departure of long-wave solar radiation from black-body intensity," *Nature*, vol. 156, pp. 534-535; November 3, 1945.  
 E. V. Appleton and J. S. Hey, "Solar noise—I," *Phil. Mag.*, vol. 37, pp. 73-84; February, 1946.
- [24] J. L. Pawsey, R. Payne-Scott, and L. L. McCready, "Radio-frequency energy from the sun," *Nature*, vol. 157, pp. 158-159; February 9, 1946.
- [25] M. Ryle and D. D. Vonberg, "Solar radiation on 175 mc/sec," *Nature*, vol. 158, pp. 339-340; September 7, 1946.
- [26] L. L. McCready, J. L. Pawsey, and R. Payne-Scott, "Solar radiation at radio frequencies and its relation to sunspots," *Proc. Roy. Soc.*, vol. A190, pp. 357-375; August 12, 1947.
- [27] D. F. Martyn, "Polarization of solar radio frequency emissions," *Nature*, vol. 158, p. 308; August 31, 1946.  
 E. V. Appleton and J. S. Hey, "Circular polarization of solar radio noise," *Nature*, vol. 158, p. 339; September 7, 1946.

- [28] J. S. Hey and G. S. Stewart, "Derivation of meteor stream radiants by radio reflection methods," *Nature*, vol. 158, pp. 481-484; October 5, 1946.
- , "Radar observations of meteors," *Proc. Phys. Soc.*, vol. 59, pp. 858-883; 1947.
- [29] J. S. Hey, S. J. Parsons, and G. S. Stewart, "Radar observations of the Giacobinid meteor shower," *Monthly Notices Roy. Astron. Soc.*, vol. 107, pp. 176-183; 1947.
- [30] R. H. Dicke and R. Beringer, "Microwave radiation from the sun and moon," *Astrophys. J.*, vol. 102, pp. 375-376; May, 1946.
- [31] R. H. Dicke, "The measurement of thermal radiation at microwave frequencies," *Rev. Sci. Instr.*, vol. 17, pp. 268-275; July, 1946.
- [32] J. H. Piddington and H. C. Minnett, "Microwave thermal radiation from the moon," *Aust. J. Sci. Res.*, vol. A2, pp. 63-77; 1949.
- [33] J. Mofensen, "Radar echoes from the moon," *Electronics*, vol. 19, pp. 92-98; April, 1946.
- H. D. Webb, "Project Diana—Army radar contacts the moon," *Sky and Telescope*, vol. 5, pp. 3-6; April, 1946.
- J. H. De Witt and E. K. Stodola, "Detection of radio signals reflected from the moon," *Proc. IRE*, vol. 37, pp. 229-242; March, 1949.
- [34] Z. Bay, "Reflections of microwaves from the moon," *Hung. Acta Phys.*, vol. 1, pp. 1-22; April, 1946.
- [35] H. I. Ewen and E. M. Purcell, "Radiation from hyperfine levels of interstellar hydrogen," *Phys. Rev.*, vol. 83, p. 881; August 15, 1951.
- , "Radiation from galactic hydrogen at 1420 mc/sec," *Nature*, vol. 168, pp. 356-358; September 1, 1951.
- [36] C. A. Muller and J. H. Oort, "The interstellar hydrogen line at 1420 mc/sec and an estimate of galactic rotation," *Nature*, vol. 168, p. 358; 1951.
- [37] J. L. Pawsey, note to *Nature*, vol. 168, p. 358; 1951.
- [38] H. C. van de Hulst, "Radio waves from space" (in Dutch), *Ned. Tijdschr. Natuurk.*, vol. 11, pp. 210-221; 1945.
- [39] A. E. Lilley and E. F. McClain, "The hydrogen line red shift of radio source Cygnus-A," *Astrophys. J.*, vol. 123, pp. 172-175; January, 1956.
- [40] B. F. Burke and K. L. Franklin, "Observations of a variable radio source associated with the planet Jupiter," *J. Geophys. Res.*, vol. 60, pp. 213-217; 1955.
- [41] C. A. Shain, "Location on Jupiter of a source of radio noise," *Nature*, vol. 176, pp. 836-837; October 29, 1955.
- [42] C. H. Mayer, T. P. McCullough, and R. M. Sloanaker, "Measurements of planetary radiation at centimeter wavelengths," this issue, p. 254.
- [43] C. H. Mayer, T. P. McCullough, and R. M. Sloanaker, "Evidence for polarized radio radiation from the Crab Nebula," *Astrophys. J.*, vol. 126, pp. 468-470; September, 1957.
- [44] J. D. Kraus, "Impulsive radio signals from the planet Venus," *Nature*, vol. 178, pp. 33-34; July 7, 1956.
- , "Planetary and solar radio emission at 11 meters wavelength," this issue, p. 266.
- [45] F. D. Drake and H. I. Ewen, "A broad-band microwave source comparison radiometer for advanced research in radio astronomy," this issue, p. 53.
- [46] R. Coutrez, J. Hunaerts, and A. Koeckelenbergh, "Radio emission from comet 1956h on 600 mc," this issue, p. 274.
- H. G. Muller, W. Priester, and G. Fischer, "Radioemission des kometen 1956h," (in German), *Naturwiss.*, vol. 14, pp. 392-393; 1957.
- [47] M. Nicolet, "Bruits solaires et cosmiques," *Inst. Roy. Meteor. Belgique, Memoires*, vol. 35, 107 pp.; 1949.
- [48] B. Lovell and J. A. Clegg, "Radio Astronomy," Chapman and Hall, London, Eng., 238 pages; 1952.
- [49] I. S. Shklovsky, "Radio Astronomy" (in Russian), Moscow, 215 pp.; 1953; 2nd ed., 295 pp.; 1955.
- [50] A. C. B. Lovell, ed., "Radio Astronomy," occasional notes, *Roy. Astron. Soc.*, vol. 3, pp. 33-79; 1954.
- [51] J. L. Pawsey and R. N. Bracewell, "Radio Astronomy," Clarendon Press, Oxford, Eng., 361 pp.; 1955.
- [52] "Radio Astronomy" (in Russian), Fifth Conference on Questions of Cosmology, Moscow, 567 pp.; 1956.
- [53] R. Coutrez, "Radioastronomie," Monographies 5, Observatoire Royal de Belgique, Bruxelles, 383 pp.; 1956.
- [54] H. C. van de Hulst, (Ed.) "Radio Astronomy," International Astronomical Union, Symposium No. 4, Cambridge University Press, 409 pp.; 1957.
- [55] C. J. Bakker and H. C. van de Hulst, "Radio waves from space" (in Dutch), *Ned. Tijdschr. Natuurk.*, vol. 11, pp. 201-221; December, 1945.
- [56] G. Reber and J. L. Greenstein, "Radio-frequency investigations of astronomical interest," *The Observatory*, vol. 67, pp. 15-26; February, 1947.
- [57] J. W. Herbstreit, "Cosmic Radio Noise," in "Advances in Electronics," L. Marton, Ed., vol. 1, Academic Press, New York, N. Y., pp. 347-380; 1948.
- [58] G. Reber, "Galactic radio waves," *Sky and Telescope*, vol. 8, pp. 139-141; April, 1949.
- [59] J. S. Hey, "Reports on the progress of radio astronomy," *Monthly Notices Roy. Astron. Soc.*, vol. 109, pp. 179-214; 1949.
- [60] O. Struve, "Progress in radio astronomy," *Sky and Telescope*, vol. 9, pp. 27-30; December, 1949; and pp. 55-56; January, 1950.
- [61] M. Ryle, "Radio Astronomy," *Rep. Prog. Phys., London*, vol. 13, pp. 184-246; 1950.
- [62] J. L. Pawsey, "Solar radio-frequency radiation," *Proc. IEE*, pt. III, vol. 97, pp. 290-308; 1950.
- [63] A. C. B. Lovell, "The new science of radio astronomy," *Nature*, vol. 167, pp. 94-97; January 20, 1951.
- [64] J. S. Hey, "Radio astronomy," *Science Prog.*, No. 155, pp. 427-448; July, 1951.
- [65] O. Struve, "Galactic exploration by radio," *Sky and Telescope*, vol. 11, pp. 214-217; July, 1952.
- [66] R. Hanbury Brown, "A symposium on radio astronomy at Jodrell Bank," *Observatory*, vol. 73, pp. 185-192; October, 1953.
- [67] J. L. Pawsey, "Radio astronomy in Australia," *Roy. Astron. Soc. Canada*, vol. 47, pp. 137-152; July-August, 1953.
- [68] J. L. Pawsey and S. F. Smerd, "Solar radio emission," in "The Sun," G. P. Kuiper, Ed., University of Chicago Press, Chicago, Ill., ch. 7, pp. 466-531; 1953.
- J. P. Wild, "Techniques of observation of radio-frequency radiation from the sun," *Ibid.*, ch. 9, sec. 10, pp. 676-692.
- J. P. Wild, "Table of solar radio instruments," *Ibid.*, Appendix, Table 2, pp. 734-737.
- [69] "Washington conference on radio astronomy—1954," *J. Geophys. Res.*, vol. 59, pp. 149-201; March, 1954.
- [70] J. A. Roberts, "Radio astronomy," *Res.*, vol. 7, pp. 388-399; October, 1954.
- [71] J. P. Wild, "Observational radio astronomy," in "Advances in Electronics and Electron Physics," L. Martin, Ed., Academic Press, vol. 7, ch. 5; 1955.
- [72] "Radioastronomy" in "Vistas in Astronomy," A. Beer, Ed., Pergamon Press, London, Eng., vol. 1, ch. 6, pp. 519-616; 1955.
- [73] A. C. B. Lovell, "Radio astronomy and the Jodrell Bank telescope," *Proc. IEE*, pt. B, vol. 103, pp. 711-721; November, 1956.
- [74] G. Reber, "Radio astronomy," *Sci. Amer.*, vol. 181, pp. 34-41; September, 1949.
- [75] H. I. Ewen, "Radio waves from interstellar hydrogen," *Sci. Amer.*, vol. 189, pp. 42-46; December, 1953.
- [76] J. D. Kraus, "Radio telescopes," *Sci. Amer.*, vol. 192, pp. 36-43; March, 1955.
- [77] J. P. Wild, "Radio waves from the sun," *Sci. Amer.*, vol. 192, pp. 40-44; June, 1955.
- [78] B. J. Bok, "New science of radio astronomy," *Sci. Monthly*, vol. 80, pp. 333-345; June, 1955.
- [79] J. D. Kraus, "The radio sky," *Sci. Amer.*, vol. 195, pp. 32-37; July, 1956.
- [80] J. Pfeiffer, "The Changing Universe," Random House, New York, N. Y., 243 pp.; 1956. This is a popularization of radio astronomy by a science writer.
- [81] R. Minkowski, "Colliding galaxies," *Sci. Amer.*, vol. 195, pp. 125-134; September, 1956.
- [82] A. R. Sandage, "The red-shift," *Sci. Amer.*, vol. 195, pp. 170-182; September, 1956.
- [83] M. Ryle, "Radio galaxies," *Sci. Amer.*, vol. 195, pp. 204-220; September, 1956.
- [84] B. J. Bok, "A National Radio Observatory," *Sci. Amer.*, vol. 195, pp. 56-64; October, 1956.
- [85] G. S. Hawkins, "The development of radio astronomy," *Amer. Scientist*, vol. 45, pp. 13-27; January, 1957.
- [86] A. E. Lilley, "The absorption of radio waves in space," *Sci. Amer.*, vol. 197, pp. 48-55; July, 1957.
- [87] M. S. Carpenter, "Bibliography of Extraterrestrial Radio Noise," School of Electrical Engineering, Cornell University, Ithaca, N. Y., Radio Astronomy Rep. Nos. 11, 12, 13, and 15, 346 pp.; 1950-1957.
- [88] "Radio Astronomy Bibliography, 1954-1956," Division of Radiophysics, Commonwealth Scientific and Industrial Research Organization, Sydney, Australia, 292 pp.; August, 1957.
- [89] G. C. Southworth, "System for and method of utilizing microwave radiation from the sun," U. S. Patent No. 2,458,654; filed December 27, 1943.
- [90] J. S. Kelly and R. G. Stiles, "Radiometry and all-weather navigation," *Amer. Soc. Navig. Eng.*, vol. 63, pp. 381-385; 1951.

- [91] G. R. Marner, "Radiosostante," *Boll. Uffic. Cons. Auton. Porto di Genova*, anno 48, no. 9; September, 1954.  
D. O. McCoy, "An all-weather radio sextant," 1955 IRE CONVENTION RECORD, pt. 5, pp. 92-101.
- [92] For a photograph of the ship-board installation, see Southworth [17], p. 63.
- [93] "Radio Sextant," *Time*, vol. 64, p. 45; July 19, 1954.
- [94] H. W. Dodson, "Studies at the McMath-Hulbert Observatory of radio frequency radiation at the time of a solar flare," this issue, p. 149.
- [95] M. A. Ellison, "The sun and its influence," Routledge and Kegan Paul Ltd., London, Eng., 221 pp.; 1955.  
L. Harang, "The Aurorae," John Wiley and Sons, Inc., New York, N. Y., pp. 147-157; 1951.
- [96] E. J. Blum, J. F. Denisse, and J. L. Steinberg, "Radio astronomy at the Meudon Observatory," this issue, p. 39.
- [97] R. Hanbury Brown and R. Q. Twiss, "A new type of interferometer for use in radio astronomy," *Phil. Mag.*, vol. 45, pp. 663-682; July, 1954.  
—, "Correlation between photons in two coherent beams of light," *Nature*, vol. 177, pp. 27-29; January 7, 1956.
- [98] R. Hanbury Brown and R. Q. Twiss, "A test of a new type of stellar interferometer on Sirius," *Nature*, vol. 178, pp. 1046-1048; November 10, 1956.
- , "The question of correlation between photons in coherent light rays," *Nature*, vol. 178, pp. 1447-1448; December 29, 1956.  
E. M. Purcell, *Ibid.*, pp. 1449-1450.
- [99] See [51, 61, 68, 71].
- [100] See [50, 76, 83, 84, 86], and articles in this issue by R. M. Emberson and N. L. Ashton; J. D. Kraus; and J. H. Trexler.
- [101] See articles in this issue by N. G. Roman and B. S. Yaplee; C. H. Mayer, T. P. McCullough, and R. M. Sloanaker; and B. S. Yaplee, *et al.*
- [102] See [73] and [84]; a large color photograph of this antenna is in *Life*, vol. 43, p. 29; July 15, 1957.
- [103] J. H. Trexler, "Lunar radio echoes," this issue, p. 286.
- [104] C. H. Mayer, R. M. Sloanaker, and J. P. Hagen, "Observation of the Solar Eclipse of 30 June, 1954, at 9.4 cm Wave-length," IAU, Symposium No. 4, Cambridge University Press, pp. 269-272; 1957. F. T. Haddock, "The Radial Brightness Distribution of the Sun at 9.4 cm," *ibid.*, pp. 273-278.
- [105] W. N. Christiansen, D. S. Mathewson, and J. L. Pawsey, "Radio pictures of the sun," *Nature*, vol. 180, pp. 944-946; November 9, 1957.
- [106] F. J. Kerr, J. V. Hindman, and M. S. Carpenter, "The large scale structure of the galaxy," *Nature*, vol. 180, pp. 677-679; October 5, 1957.



# The Discovery and Identification by Karl Guthe Jansky of Electromagnetic Radiation of Extraterrestrial Origin in the Radio Spectrum\*

C. M. JANSKY, JR.†, FELLOW, IRE

Karl Jansky's discovery of 25 years ago was a remarkable scientific achievement, not only because it signalled the birth of radio astronomy, but because it was one of the relatively few instances where a new branch of radio science was founded by one man alone. We are privileged to present in the following pages a unique account of this work written by Jansky's brother, who is himself an eminent radio engineer.—*The Editor.*

**Summary**—December, 1957, marks the 25th anniversary of the completion of Karl Guthe Jansky's field studies which proved that electromagnetic waves in the radio spectrum of extraterrestrial origin were reaching the earth. April, 1958 will mark the 25th anniversary of the date on which this basic discovery was disclosed in full to the scientific world. This paper describes briefly the steps which led to Jansky's basic discovery, some of the important results of later studies in radio astronomy, and the relationship between pure and applied science illustrated by the basic discovery and subsequent work in this field.

IT IS well known that light waves and radio waves are one and the same thing except for a difference in wavelength. Both types of waves travel at a velocity of 186,000 miles per second (approximately 300,000 km per second). The wavelengths to which the human eye is sensitive extend from approximately 4 ten-millionths of a meter for violet light to 7.2 ten-millionths of a meter for red light. In contrast, the range of radio wavelengths may be defined very roughly as extending from 0.25 centimeter to 20,000 meters. The entire range of wavelengths having the property of light and radio waves is referred to as the electromagnetic spectrum. Its boundaries lie below the radio band in one direction and above the visible light band in the other.

Associated with each wavelength is the frequency of the source which generates it. This relationship is approximately: frequency in kilocycles per second equals 300,000 divided by wavelength in meters. Thus 300-meters wavelength in the radio band equals approximately 1000 kc (a frequency and wavelength in the standard broadcast band), and 3 meters correspond to a frequency of 100,000 kc, that is, 100 mc (a frequency in the fm broadcast band). Light waves are usually referred to by their wavelength rather than the frequency of the source.

Until 1932, man's study of the stars, planets, sun, moon, and, in fact, all objects and space removed more than a relatively few miles from the earth—that is, the study of astronomy—was limited to what could be seen or photographed in the visible spectrum (except that

special techniques and devices extended this study slightly below and slightly above the visible spectrum). Up to 1932 it was not known that electromagnetic waves in the radio portion of the electromagnetic spectrum were reaching the earth from outer stellar space. The first man to detect and identify such radio waves was Karl Guthe Jansky. Utilizing data accumulated over a period of time in excess of one year, he determined that the electromagnetic waves he was receiving on 14.6 meters (20.53 mc) at Holmdel, N. J. came from a direction corresponding to the center of the galaxy of which our solar system is a part. This discovery opened a whole new window for studying the stars and the space between them. Today this radio window extending from about 0.25 centimeter to 20 meters is 50 to 100 times as wide as the visible spectrum window.

Distances in the universe are so great that earth-bound units of measurement are of little value. Astronomers use as a unit of distance the "light year." Since light travels 186,000 miles per second, a light year in miles is  $186,000 \times 60 \times 60 \times 24 \times 365$ , or very nearly 5.9 trillion miles.

The United States federal debt (1957) is approximately 279 billion dollars. To state that this debt has reached "astronomical" figures is literally true, as the federal debt expressed in cents is approximately 5 times the number of miles in the astronomical unit of distance, namely the "light year." The distance from the center of the Milky Way, that is, the center of our galaxy, to the earth is approximately 30,000 light years.

Today radio astronomers are studying radio waves from the sun and from certain of the planets. Radio maps or pictures of the heavens as they look at specific radio wavelengths have been prepared. There are many concentrated sources of radio waves in the sky at points where optical telescopes cannot detect the presence of stars. Some of these may be so distant as to be beyond the range of optical telescopes. There are huge masses of hydrogen in outer stellar space. The study of these by radio telescopes is yielding information on the rate of rotation of our own and other galaxies around their centers.

\* Original manuscript received by the IRE, November 8, 1957.

† Chairman of the Board, Jansky & Bailey, Inc., Washington, D. C.

A very strong radio source is the apparent collision of two galaxies estimated distant from the earth 300,000,000 light years. This is a reasonably distant radio transmitter. The radio waves now reaching the earth from this source were generated 300 million years ago at a time when, according to geologists, dinosaurs roamed the planet.

The story of Karl Jansky's work from 1928 to 1932, which led to the discovery that furnished the foundation for the Science of Radio Astronomy, contains many lessons for those whose life work is in the field of either pure or applied science, and particularly for students and young people who hope to become scientists. After receiving his degree at the University of Wisconsin in 1927, Karl Jansky joined the staff of Bell Telephone Laboratories. He was stationed at the company's field laboratory in New Jersey. Here he was assigned a project involving the study of static and interfering noises which were affecting the operation of Bell System transoceanic radiotelephone circuits. While some of his work was done on long wavelengths of the order of 4000 meters, of particular concern to radio astronomy are his studies on 14.6 meters (20.53 mc). These required instrumentation and it is important to note that in the late 1920's and early 1930's adequate instrumentation for his project, and particularly for wavelengths as short as 14.6 meters, involved many new and unsolved problems.

About March, 1929, Karl Jansky began the design and construction of a 14.6-meter rotatable, directional antenna system and the development of the associated receiving apparatus. Due to interruptions, it was not until the fall of 1930 that this installation with its recording equipment was in good working order. Next came the long period of time devoted to the unimpressive, prosaic and laborious taking of data, that is, data on the characteristics and intensity of static received on 14.6 meters as a function of two variables: 1) time and 2) direction.

In his paper<sup>1</sup> Karl Jansky described his equipment and classified into three distinct groups the types of static he was receiving on 14.6 meters. The first group he described as static from local thunderstorms and the second as static from thunderstorms some distance away. Then he stated, "The third group is composed of a very steady hiss static, the origin of which is not yet known." While he speculated on the possible source of this new type of static, it is important to note his comment that "the data as yet only cover observations taken over a few months and more observations are necessary before any hard and fast deductions can be drawn."

By the end of December, 1932, Karl Jansky had available data taken throughout an entire calendar year on the hiss static described in the paper referred to above.

In his paper on this data<sup>2</sup> he set forth with reasonable accuracy, considering the limitations of his antenna, the point of origin of the extraterrestrial hiss static he was receiving:

"In conclusion, data have been presented which show the existence of electromagnetic waves in the earth's atmosphere which apparently come from a direction that is fixed in space. The data obtained give for the coordinates of this direction a right ascension of 18 hours and a declination of  $-10$  degrees."

It is difficult to overestimate the importance of Karl Jansky's deductions and the attendant circumstances. A very practical scientific project having as its objective the improvement of transoceanic radiotelephone service had brought forth a major fundamental discovery in the field of pure science.

There exists no definitive boundary between pure and applied science. The discovery of extraterrestrial noise came as a result of a research program originally directed to a very practical end. Today (1957) radio astronomy is making possible the development of radio sextants which will enable the navigators of ships and aircraft to take celestial bearings without regard to visibility conditions. This is an excellent illustration of the fact that a practical scientific study may lead to discoveries in the field of pure science; conversely, research in pure science may yield highly practical results.

Karl Jansky was only twenty-seven years of age when he delivered his classic paper.<sup>2</sup> Unfortunately, he did not live to see the remarkable developments which have taken place in recent years in the science built upon his discovery.

Today, the frontiers of radio astronomy are being pushed back by the efforts of workers in many nations—Great Britain, The Netherlands, Australia, the United States, Canada, Russia, France, Japan, Norway, Sweden, and others. As workers in one country develop new instrumentation and acquire new knowledge, that information is conveyed to fellow workers in other countries. Meetings held in one nation are attended by scientists from others. The emphasis is not primarily on competition but upon mutual understanding and cooperative effort directed toward a common objective—the acquisition of more and more knowledge of the universe in which we live.

December, 1957 marks the 25th anniversary of the completion of the field studies which proved that electromagnetic waves in the radio spectrum of extraterrestrial origin were reaching the earth. April, 1958 will mark the 25th anniversary of the date on which this basic discovery was disclosed in full to the scientific world. The man who made this discovery was a United States scientist.

Some time after Karl Jansky presented his paper in 1932, his superiors transferred his activities to other fields. He would have preferred to continue his work in radio astronomy.

<sup>1</sup> K. Jansky, "Directional studies of atmospherics at high frequencies," presented at International Scientific Radio Union, Washington, D. C.; April, 1933.

<sup>2</sup> K. Jansky, "Electrical disturbances apparently of extraterrestrial origin," presented at the International Scientific Radio Union, Washington, D. C.; April, 1933.

Except for the interest and work of a second United States scientist, Grote Reber, for approximately ten years little attention was paid to Karl Jansky's discovery. Then, it was not primarily in the United States that major activity in the field of radio astronomy developed. Therefore, while there are many competent scientists in the United States doing outstanding work

in this field, unfortunately this nation has been relatively slow in developing radio astronomy facilities comparable to those in other nations. Also, while without question the importance of Karl Jansky's work is recognized by many United States scientists, there is even greater appreciation of his work abroad than at home.

## Early Radio Astronomy at Wheaton, Illinois\*

GROTE REBER†

Although Karl Jansky discovered the existence of radio emissions from outer space as early as 1932, a decade passed before the scientific world began to take interest in it. During that barren period one man, and one man alone, compelled by a great love of science and research, carried forward Jansky's initial work. That same man now recounts for us in his own words the pioneering experiments he conducted during his lonely vigil of the heavens.—  
*The Editor.*

**Summary**—A history is given of radio astronomy experiments conducted by the author from 1936 through 1947. A description of the parabolic reflector and equipment design is presented along with reasons for the choice of successive operating frequencies of 3300, 910, 160, and 480 mc. The results are reviewed in light of more recent knowledge. Published articles covering the scientific details will be found in the footnotes.

### INTRODUCTION

MY INTEREST in radio astronomy began after reading the original articles by Karl Jansky.<sup>1,2</sup> For some years previous I had been an ardent radio amateur and considerable of a DX addict, holding the call sign W9GFZ. After contacting over sixty countries and making WAC,<sup>3</sup> there did not appear to be any more worlds to conquer.

It is interesting to see how the mystifying peculiarities of short-wave communications of 1930 gradually have been resolved into an orderly whole. The solar activity minimum of the early thirties must have brought with it abnormally low-critical frequencies. Many a winter night was spent fishing for DX at 7 mc when nothing could be heard between midnight and dawn. It is now clear that the MUF over all of North America was well below 7 mc for several hours. An hour after

sunset when the west coast stations disappeared 14 mc went dead. These years would have been a very fine time for low-frequency radio astronomy. The now appreciated long quiescence of the sun during the latter half of the seventeenth century<sup>4</sup> would have been even better!

One further recollection is that on these quiet nights it was always possible to make the receiver quieter by taking off the antenna. This receiver uses a regenerative detector and one rf stage. The detector and rf stage are tuned separately so that the latter may be gradually tuned across the former. When this was done with the antenna off, no appreciable change could be heard in the sound of rushing water. When the same thing was done with the antenna on, the rushing sound increased several times in loudness at the resonant frequency of the rf stage. Whether or not this difference was due to cosmic static or merely to some vaguery of the receiver is not readily resolved at present. Near the next solar activity minimum it might be interesting to try the old receiver out again with a similar antenna, which was an inverted "L" 40 feet high and 200 feet long. The above experiences were at 225 West Wesley Street, about 70 yards from 212 West Seminary Avenue where the rest of the observations were conducted. All this property now belongs to the Illinois Bell Telephone Company.

\* Original manuscript received by the IRE, November 5, 1957.

† Wailuku, Maui, Hawaii.

<sup>1</sup> K. G. Jansky, "Directional studies of atmospherics at high frequencies," *PROC. IRE*, vol. 20, pp. 1920-1932; December, 1932.

<sup>2</sup> K. G. Jansky, "Electrical disturbances apparently of extra-terrestrial origin," *PROC. IRE*, vol. 21, pp. 1387-1398; October, 1933.

<sup>3</sup> Worked all continents.

<sup>4</sup> D. J. Schove, "The sunspot cycle 649 BC to AD 2000," *J. Geophys. Res.*, vol. 60, pp. 127-146; June, 1955.

### ORGANIZED EXPERIMENTS

In my estimation it was obvious that K. G. Jansky had made a fundamental and very important discovery. Furthermore, he had exploited it to the limit of his equipment facilities. If greater progress were to be made, it would be necessary to construct new and different equipment especially designed to measure the cosmic static. Two fundamental problems presented themselves. These were, are, and will continue to be: How does the cosmic static, at any given frequency, change in intensity with position in the sky; and how does cosmic static, at any given position in the sky, change in intensity with frequency? To solve these problems would require an antenna which could be tuned over a wide frequency range, provide a narrow acceptance pattern in mutually perpendicular planes, and be capable of pointing to all visible places in the sky.

About this time I had completed a modicum of academic learning. Two features stood out as pertinent. First, geometrical optics demonstrates that the angular resolving power of a device is proportional to its aperture in wavelengths. Consequently, for a given physical size aperture, the angular resolving power is proportional to frequency. Obviously a high frequency was indicated. Secondly, Planck's black body radiation law shows that for radio frequencies at any probable temperature, the intensity per unit frequency bandwidth of radiant energy is proportional to the square of the frequency. Again, a high frequency was indicated. Thus, on the face of the prevailing ignorance, a very high frequency should be used since much better resolution would be secured and very much more energy would be available for measurement. Some frequency in the decimeter region was indicated.

### RADIO TELESCOPE

Consideration of the antenna problem showed that any type of wire network would be exceedingly complicated since several hundred minute dipoles would be needed. The only feasible antenna would be a parabolic reflector or mirror. By changing the simple focal device it would be possible to tune the mirror over a very wide frequency range. About this time Barrow<sup>5</sup> published some experiments on circular waveguides. The patterns of these apertures seemed just the thing for looking into a mirror. Thus I conceived the idea of using a single dipole inside a short length of waveguide at the focus of the mirror. It turned out to be a very satisfactory, simple arrangement providing good shielding against radiation other than from the desired direction. The focal point of the mirror was placed in the aperture plane of the waveguide.

If optical practice were to be followed, the mirror should be on an equatorial mounting. This would have

<sup>5</sup> W. L. Barrow, "Transmission of electromagnetic waves in hollow tubes of metal," *Proc. IRE*, vol. 24, pp. 1298-1328; October, 1936.

been very complicated and exceedingly expensive. Even an alt-azimuth mounting would be prohibitive in cost and could not have been used profitably in the confined location available. Therefore, a meridian transit mount was decided upon. The mirror was to be as large as possible consistent with available funds. One inquiry was made for a purchased framework of steel. The American Bridge Company offered a design which consisted of a circular billboard 50 feet in diameter and 10 feet thick with a horizontal axis through the center mounted upon two vertical pillars 30 feet high. The billboard was to have a four leg parapet 35 feet high on one side with counterweights and locking mechanism on the other side. Since the mirror skin and supports plus turning motors were extras, I adjudged their offering price of 7000 dollars, erected, to be excessive! This was in 1936. Not many years later I wished I had been more of a speculator. In any case, I decided to design the mirror and do the job myself.

The mounting had been decided upon. Only one more problem remained, distortion of the surface by bending. This could be reduced greatly by using a deep framework. Various materials were considered. From an academic point of view, the best material for preventing bending is the one with the highest ratio of modulus of elasticity to density and not the highest ratio of strength to weight. Of the common materials, steel and aluminum are about equal. However, although much inferior, wood was decided upon because of cheapness and ease of working. Even with wood, the bending on a mirror 30 feet in diameter could be made negligible by using a deep framework. Most of the wooden members were 2 inches  $\times$  4 inches cross section and from 6 to 20 feet long. All joints were fastened by steel gusset plates of various widths and  $\frac{1}{8}$  inch thick. The bolts were  $\frac{1}{2}$  inch in diameter. All pieces were given two coats of paint before assembly and two coats afterwards. The framework was given added coats every couple of years. When disassembled in 1947, all pieces were found to be dry, solid, and as good as when put together. With reasonable care, it could have lasted indefinitely. The skin was 26-gauge galvanized iron in 45 pieces of pie; nine on the inside and 36 on the outside. These were supported on 72 radial wooden rafters cut to a parabolic curve. The sheet metal was not preformed but was allowed to drape snugly over the rafters and was fastened with a flat head brass wood screw at every lineal foot. The joints were overlapped about 2 inches and fastened with bolts every foot of lineal joint. All joints were spaced half way between rafters. The over-all diameter of skin was 31 feet 5 inches. Since the focal length was 20 feet, a relatively flat mirror was required. This, in conjunction with the multiple joint skin, allowed a good smooth surface to be secured. The major roughness was due to the bolt heads. The exact accuracy was unknown. However, the mirror platform was flat to plus or minus an eighth

of an inch in all positions as found by measurement, so the skin had a commensurate parabolic accuracy. All the wooden pieces, including the lattice parapet, were cut, drilled, and painted by me personally. Part time assistance of two men was secured on the foundations, metal parts, and erecting the structure, with the exception of the skin which I personally put together piece by piece. The entire job was completed in four months; from June to September, 1937. The over-all weight was less than two tons. This mirror usually emitted snapping, popping, and banging sounds every morning and evening. The rising and setting sun caused unequal expansion in the skin and the various pieces would slip over one another until equilibrium was attained, no matter how tightly the joining bolts were pulled up. When parked in a vertical position, great volumes of water poured through the center hole during a rain storm. This caused rumors among the local inhabitants that the machine was for collecting water and for controlling the weather. The center hole, 2 feet in diameter, was included, just in case it would be desirable to use the mirror for centimeter waves with an elliptical secondary mirror at prime focus. A similar opening was built into the carriage, so that a very long focal length could be secured if the receiver were placed below the bottom of the carriage. This Gregorian scheme was never used. The lower parts of the machine provided an enticing structure for all the children of the neighborhood to climb upon. However, they were prevented from getting on top by the overhanging nature of the skin.

When working at the focal point, the mirror was tipped far south to an elevation of about  $10^\circ$ . The structure had a peculiar attraction for private flyers who would examine it from many directions and distances in their putt-putt airplanes. More than once, when one of these flyers would approach down the beam from the south, I had the sensation that a motorcycle was coming up out of the ground right through the center back of the mirror. Obviously, the mirror also had good acoustical properties.

This radio telescope was acquired by the National Bureau of Standards in 1947 and was erected on a turntable at their field station near Sterling, Va. About 1952, it was disassembled and the parts sent to Boulder, Colorado. Recently, the National Bureau of Standards has made the antenna available to the National Radio Astronomy Observatory on an indefinite loan basis for exhibition and demonstration purposes.

#### ELECTRONIC APPARATUS AND TESTS AT 9 CM

The shortest possible wavelength in the middle 1930's was on the order of 10 cm. An RCA type 103A end plate magnetron was acquired for general testing. This tube could be operated from 2500 to 5000 mc, depending upon the electrode voltages and magnetic field applied. The frequency limits really were due to the resonance of the internal anode structure which

had a natural period of about 3300 mc. At optimum, nearly  $\frac{1}{2}$  w could be put into a small lamp bulb. Audio modulation was applied in the end plate circuit.

Quite a variety of crystal detectors were experimented with. All could be made to work, more or less. However, a clear amber piece of zinc sulfide, known as sphalerite, was by far the best since it was sensitive all over, no matter where the cat whisker was placed. The rest of the receiver consisted of a four-stage audio amplifier using 6F5 triodes giving a gain of the order of 100 db. It was peculiarly free from microphonics and was very reliable. Using this equipment, a variety of experiments<sup>6,7</sup> were conducted on cavity resonators, etc. For close work, a 0-200 microammeter was used directly in the crystal circuit. The magnetron was tried as a detector in place of the crystal, but was found to be worthless because of very great shot noise voltage. Two other attempts were made to improve upon the crystal detector.

One was a special small diode entirely made of tungsten and pyrex. The spacing from anode to cathode was carefully adjusted to about 0.005 inch and the physical structure so arranged that the anode became part of a tunable line or cavity. Energy was fed into a cavity by a small dipole and hairpin loop. In spite of all efforts, this device was markedly poorer than the crystal. The significance of electron transit time was only beginning to be appreciated.

Next, an elaborate Barkhausen tube<sup>8</sup> was constructed on the theory that the virtual cathode beyond the grid could be made to come as close as desired to the anode and thus cut down on the electron transit time loss. The tunable system consisted of lecher wires three half-waves long. Sliding shorting-bars at each end provided outside adjustment. The tube seals were at the voltage nodes at third points and thus reduced capacity effects. A glass bellows allowed for unequal expansion between the glass envelope and the tungsten lecher bars. The anodes were small semicylinders at the voltage peak in the center of the system. The Barkhausen grid and the internal filament were placed in the exact center of the two anodes. Considerable effort was expended in getting this device, with all the minute parts, put together properly. Unfortunately, it was all for naught since the sensitivity was no better than the diode. Considerable shot-noise voltage, produced by stray electrons finding their way to the anodes, created a terrific racket and it was necessary to fall back on the crystal detector. This vacuum tube construction work was done by the glass experts at the University of Chicago.

During the spring and summer of 1938, a considerable number of observations were made at 3300 mc

<sup>6</sup> Grote Reber, "Electric resonance chambers," *Communications*, vol. 18, pp. 5-25; December, 1938.

<sup>7</sup> Grote Reber, "Electromagnetic horns," *Communications*, vol. 19, pp. 13-15; February, 1939.

<sup>8</sup> H. E. Hollmann, "The retarding-field tube as a detector for any carrier frequency," *PROC. IRE*, vol. 22, pp. 630-656; May, 1934.

mostly during the day. The crystal detector in its cavity, a short length of waveguide horn, and the audio amplifier were mounted just behind the mirror focal point. The antenna was parallel to the celestial equator. Various parts of the Milky Way, Sun, Moon, Jupiter, Venus, Mars, and several of the bright stars, such as Sirius, Vega, Antares, etc., were all examined. The output of the audio amplifier was passed through a copper-oxide rectifier and displayed on a microammeter. Observations were made visually of the meter indication and were tabulated, sometimes at minute intervals, sometimes at longer intervals, such as an hour. Some small irregular fluctuations were encountered, but no repeatable results were secured which might be construed to be of celestial origin. All this was rather dampening to the enthusiasm. Admittedly, the sensitivity of the system was quite poor. However, the frequency was 160 times as great as Jansky used and the presumed black body radiation intensity should be 26,000 times as great. If anything could be deduced from these efforts, it seemed to be that the relation between celestial radiation intensity and frequency did not conform to Planck's law.

#### ELECTRONIC APPARATUS AND TESTS AT 33 CM

Consideration showed that it would be best to lower frequency a bit and build more conventional electronic apparatus using triode tubes with the aim of greatly increasing the sensitivity. A couple of years prior to this, RCA had brought out the type 955 acorn triode. These commercial tubes were of different internal construction and of considerably inferior performance to the experimental tubes described by Thompson and Rose.<sup>9</sup> The early 955's also were better than the later versions. These early type tubes had a smaller diameter cylinder and a hemispherical top, compared to the flat top of the later tubes. A pair of tubes were connected in a push-pull arrangement with the grid pins soldered together, since this circuit determined the highest operating frequency. The plate and cathode leads were tuned by lecher systems. The former determined the frequency and the latter the strength of oscillation. A pair of the early tubes could be made to oscillate up to nearly 1000 mc. In 1938, these early tubes were still abundant and several oscillators were made for testing receivers, etc. Only about fifty volts were required on the anodes.

About this time, RCA brought out the type 953 acorn diode with the anode lead coming out of the top. An adjustable cylindrical resonator was constructed which could be used with either the 953 or the above described tungsten diode. These diodes and crystals were all tested for sensitivity and were found to be about equal at 910 mc and some two orders of magnitude poorer than the regenerative detector. Also, it was now observed that

the tungsten diode had a faint rattle sound associated with it which increased in strength as the filament temperature was increased. This rattle was not present in the 953 with its low-temperature cathode. Apparently, the rattle was due to minute bits of tungsten boiling off the white hot filament. This is typical of the kind of thing which may be overlooked when no comparative observations are possible.

A new cavity resonator with an iris was constructed, for use at the focal point of the mirror, out of a steel drum container for 100 pounds of white lead. The dimensions of this drum determined the operating frequency of 910 mc. A half-wave dipole was placed a quarter-wave length from the back of the cavity. A half-wave lecher wire went from the center of dipole through a hole in the rear of cavity and was coupled by a small loop to the filament tuner of the push-pull detector. Thus, the entire antenna system resonated in a three half-wave mode. The detector and audio amplifier were placed in a small drum attached to rear of cavity. The entire arrangement was supported in circular bands, so the drum could be turned on its axis to change the plane of polarization received, since it was thought that there might be some variation with the plane of polarization of the still to be found celestial energy.

During the autumn of 1938 and during the following winter, a variety of observations, both by day and by night and with various polarizations, were made at 910 mc. All the same objects were examined again without any positive results. In a measure, it was disappointing. However, since I am a rather stubborn Dutchman, this had the effect of whetting my appetite for more. Here was a circumstance where the frequency had dropped nearly two octaves and the sensitivity had improved by two orders of magnitude and still nothing resulted. Perhaps the actual relation between intensity of the celestial radiation and frequency was opposite from Planck's law.

All this old equipment is still in existence and it might be interesting to set it up again and measure just what absolute sensitivity was achieved, both at 3300 and at 910 mc.

#### ELECTRONIC APPARATUS AND TESTS AT 187 CM

By then, autumn 1938, it was perfectly clear that a further great increase in sensitivity was necessary and that attempting to operate at exceedingly high frequencies was wrong. The resolution would have to be whatever it came out, for better or for worse. Concurrent with these experiences, I had been following in the literature various articles on the input resistance of triodes by Ferris, wide-band amplifiers by Percival, and trying to understand a rather deep book about random fluctuations by Moullin. Also I had been gaining experience in the radio receiver industry. It was clear that a big jump in sensitivity could be made by changing from a crystal to a regenerative detector. Another big jump

<sup>9</sup> B. J. Thompson, "Vacuum tubes of small dimensions for use at extremely high frequencies," *PROC. IRE*, vol. 21, pp. 1707-1721; December, 1933.

would be to a superheterodyne receiver. Also, a superhet with an rf stage was much better and two rf stages still better. The tunable feature of a superhet seemed of little value. What was important was the rf stages. Also, it seemed that a wide bandwidth should be used, which again ruled against a superhet. Finally, I decided upon a multistage tuned radio-frequency amplifier with as wide a bandwidth and as high a frequency as feasible.

RCA brought out the 954 acorn pentode in 1935; the first ones were exceedingly poor, having many internal shorts. However, by purchasing new tubes from the autumn 1938 production, instead of dealer stock, some respectable samples were secured. About this time a small bulletin<sup>10</sup> was issued by the National Bureau of Standards which described a multistage amplifier using 954 tubes with coaxial line resonators. It was tunable from about 100 to 300 mc and over-all gain data was included. This bulletin was of much assistance in determining a suitable design. The wide range tunable feature seemed of no particular value and tended to introduce feedback. Also, the gain dropped rapidly above 200 mc. A frequency somewhere near 150 mc appeared suitable since it already was clear that a low-internal random fluctuation voltage only could be secured if the first-stage gain was fairly high, such as eight or more.

The idea of a cavity resonator at the focus of a mirror still seemed good compared to an open dipole, and I decided to continue using a cavity. This relatively low frequency would require a large but light cavity, which should be cheap and with as little welding as possible. Inquiry disclosed that aluminum sheet 1/16 inch thick could be secured in pieces 6 feet wide and 12 feet long. One piece could be formed into a cylinder about 4 feet in diameter and 6 feet long. ALCOA fabricated this resonator, including various size irises for the aperture, at a very nominal price. In essence, the operating frequency of 162 mc was determined by the size of a drum which could easily be made from a standard size sheet of aluminum.

The NBS design was revised<sup>11</sup> to provide capacity tuning over a range of 150 to 170 mc and the whole assembly of copper water pipe and copper plate was brazed into one piece by the local blacksmith. After fitting the by-pass capacitors and connections, an over-all trial was made and the entire five stages worked immediately. Furthermore, the, by then, well-known thermal fluctuation voltage easily could be found when the first tuned circuit was tuned through resonance; this was very encouraging. No signal generator was available to measure the sensitivity, but obviously it was good. This amplifier was then attached to the back of the large aluminum drum. The antenna was quite similar

to that used at 910 mc but with additional fine-tuning adjustments.

Before hoisting this cumbersome assembly atop the parapet of the mirror, some ground tests were made. These provided quite a shock, since all kinds of man-made electrical disturbances now could be heard which before were not known to exist. The main one was caused by automobile ignition sparking. However, this trouble mostly disappeared after 10:00 P.M.; this was reassuring. Thus on the first Saturday when help could be obtained, the whole assembly was placed atop the mirror and trials were started. This was in the early spring of 1939.

During the day, no worthwhile results could be secured because of the multitude of automobiles in continual operation. This disturbance leaked into the drum from the back around the edge of the mirror. Cars at the front side and in front of the mirror could hardly be detected. Thus, the shielding action of drum really was effective. The output of the receiver came down a coaxial microphone cable as a small dc voltage. About three-quarters of this voltage was bucked out by a battery and the remainder was fed into a dc amplifier. The display was a microammeter. About two hours were required for equipment warmup. After 10:00 P.M., disturbances quieted down and observations were made in earnest. Data were taken by manually recording the meter indication every minute. Continual aural monitoring was employed to delete those times when interference was present. This data was then plotted as meter reading vs time.

During the night, good smooth flat reproducible plots were secured, but nothing could be found which moved along in sidereal time. In early March, the plane of the galaxy to the south still crossed the meridian after sunrise. While the auto disturbances did not become really bad until about 10:00 A.M., the amplifier was subject to gain variations when the sun came up. This was found to be due to unequal thermal expansions which caused some of the resonators on the interstage couplers to become out of tune compared to the others. On cloudy mornings the trouble was absent and some plots were secured which seemed to show excess energy when the plane of the galaxy crossed the meridian. These occasions were few since the cloudy morning had to appear on a weekend when I was not at work in the city. By early April, the plane of the galaxy was crossing the meridian during hours of darkness and good reproducible plots were secured every night when observations were made. It was now apparent that cosmic static from the Milky Way had really been found and that it was of substantial strength, especially to the south. As the months went by, the more northerly parts of the galaxy became available. However, the cosmic static became weaker and dropped nearly to the limit of the system sensitivity at a declination of 20° north. These results confirmed Jansky in a general way.

<sup>10</sup> F. W. J. Dunmore, "A unicontrol radio receiver for ultra-high frequencies," *PROC. IRE*, vol. 24, pp. 837-849; June, 1936; and *J. Res. NBS*, vol. 15, Res. Paper RP856; 1935.

<sup>11</sup> G. Reber W9GFZ and E. H. Conklin, "UHF receivers," *Radio*, no. 225, pp. 112-161; January, 1938; no. 235, pp. 17-177; January, 1939; no. 236, front cover; February, 1939.

During the summer of 1939, a variety of celestial objects were examined but nothing convincing could be found, except from the Milky Way. Particular effort was made to find the sun but it was lost under compound equipment difficulties. Only thickly clouded days were possible for observation since thermal effects were induced by scattered clouds. Also, it developed that the 953 diode had another internal trouble. The velocity potential of the diode was in series with the signal voltage. This velocity potential is dependent upon cathode temperature and effective spacing between anode and cathode. During quiet periods, the velocity potential was stable. However, when a strong auto ignition disturbance was imposed, there was a small internal rearrangement of active areas on the cathode. Thus, the diode velocity potential would be different after, compared to before, a strong burst of ignition sparking. Consequently, a shift in the dc zero level occurred irregularly up and down after each objectionable vehicle went by. Several 953's and 955's were tried but to no avail. A 200,000-ohm diode load resistor was used at the time. The solution seemed to be to move everything out to the country, which then was not feasible. These preliminary results<sup>12,13</sup> were published in 1940. The intensity was guessed at by noting the effect of resistance shunts across the first tuned circuit; no calibrated signal generator was available then. In any case, the observed intensity was far below that encountered by Jansky. Obviously, the source of cosmic static was some new and unknown phenomenon.

The above success further whetted my appetite on the basis of, "If a little is good, more is better." A survey of the sky was contemplated; this would mean collecting a lot of data. Obviously, an automatic recorder was a primary necessity. Thus, a General Radio dc amplifier and Esterline Angus 5-ma recorder were purchased early in 1940. Also, new power supplies with entire ac operation and automatic regulation were built to replace the old dc system with its manual voltage adjustments. The new steady power supply had a great effect on receiver stability and resulted in effective long-term sensitivity. A few all night vigils were made with this automatic apparatus to gain confidence in its operation and to gain experience in how interference manifested itself.

In addition, a decent signal generator was imperative, if any quantitative measures were to be secured. Since one could not be purchased, I built my own signal generator rather as a copy of a Hazeltine machine designed for the old low-frequency television band. My design uses a WE 316A tube, with a tuning range of 140 to 200 mc, a reference output level of 1 v across 10 ohms, and an inductive attenuator to 120 db. No detect-

able leakage could be found. The case is all brazed copper pipe and plate by the same blacksmith mentioned above and the cover is sealed water tight using lead foil gaskets.

Finally by 1941, things seemed to be in order for starting a survey of the sky. Preliminary results were published the following year<sup>14</sup> with an analysis of the theoretical conditions governing receiver sensitivity. Later studies merely have confirmed these early investigations. Even today, explorers of the Milky Way at wavelengths less than a few meters do not receive any net celestial energy, but in fact merely measure changes in the net rate at which their equipment dissipates energy into the sidereal universe via the antenna beam. Further efforts to detect the sun failed, as mentioned above.

Returning now to the theory, it is worth mentioning that a significant improvement in signal to ripple ratio of 3 db may be secured by using a push-pull full-wave rectifier instead of the common half-wave type which loses half of the random fluctuation peaks. This is not particularly important on wide bandwidths, but I have found it to be worthwhile at low frequencies, where only a few kilocycles of bandwidth may be secured due to crowded channels.

#### IMPROVED APPARATUS AND TESTS AT 187 CM

Before much data had been accumulated, a greatly improved receiver was designed on the basis of the above and other<sup>15</sup> equipment studies. The type 954 tube was still the best tube available in 1941. Improvement in sensitivity only seemed possible by increasing the bandwidth or lengthening the integration time. Since auto ignition disturbance was so severe, it was desirable that the integration time should remain short, in order that the auto disturbance might quickly clear when an offending car had passed. Thus I decided to widen the bandwidth to the maximum feasible. Wide-band couplers of the Y type were designed using coaxial elements. The load resistance turned out to be about 7000 ohms for an 8-mc bandwidth, with some impedance step down from plate to grid. Again the whole affair was brazed into one piece. Because of the circuit complexity, considerable time was required to align everything. It would have been nearly impossible without the signal generator. Finally, a five-stage receiver emerged having a gain of about 90 db over the frequency band of 156 to 164 mc, compared to only 0.16-mc bandwidth of the earlier design. To maintain bandwidth, the diode load resistor was reduced to 15,000 ohms. This had the effect of reducing and stabilizing the velocity potential. The wide bandwidth eliminated the detuning caused by the temperature effects and the resistor on each grid did

<sup>12</sup> Grote Reber, "Cosmic static," *PROC. IRE*, vol. 28, pp. 68-71; February, 1940.

<sup>13</sup> Grote Reber, "Cosmic static," *Astrophys. J.*, vol. 91, pp. 621-632; June, 1940.

<sup>14</sup> Grote Reber, "Cosmic static," *PROC. IRE*, vol. 30, pp. 367-378; August, 1942.

<sup>15</sup> Grote Reber, "Filter networks for uhf amplifiers," *Electronic Indus.*, vol. 3, pp. 86-198; April, 1944.

wonders for holding the stage gain constant. This receiver is nearly impervious to mechanical and electrical shock. The traces became sharp and clear; sensitivity and stability were sufficient to read to 0.001 of total output voltage during a run of several hours. It was operated for several thousand hours, merely by replacing a 954 from time to time. The antenna system was broad-banded by removing the front iris, so that the drum had full aperture toward the mirror, and by replacing the wire dipole inside with two aluminum cones, also made by ALCOA, having a 15° angle of rotation.

Now that really worthwhile electronic equipment was at hand, a complete survey of the sky was undertaken early in 1943. Data also could be secured during the day, except that the traces were quite rough due to auto disturbances. For some reason, the sun was not tried until September. A relatively high-gain setting was used, corresponding to the weaker parts of the galaxy then under observation. On the very first try the quiet sun put the pen hard against the pin at full scale for half an hour near meridian transit. Two further day's tries were required before proper on scale readings were obtained. The observations continued daily up to the middle of 1944 before a complete coverage of the available Milky Way was secured. During these years, the sun was at low activity and the solar traces were all very much alike and uninteresting. The results<sup>16</sup> were published in 1944 and included a polar diagram of the antenna pattern taken on the strong source in Cassiopeia. At the time, it was not realized that at the center of these contour circles there was actually a minute object of very high surface brightness. If the solar data reported should change into units of temperature, then the sun could be represented by a disk one-half a degree in diameter at a temperature of slightly less than a million degrees. This had no meaning at the time.

The first man-made electronic interference appeared during this survey. It was caused by badly adjusted iff transceivers in aeroplanes. The squitter could be heard for many miles when the plane crossed the antenna acceptance pattern. The ignition systems in commercial planes were shielded sufficiently well so that no sparking could be detected. A few small private planes were heard, but these rarely operated at night.

#### APPARATUS AND TESTS AT 62½ CM

When it became apparent, toward the end of 1943, that the situation was fairly well in hand at 160 mc, I cast about to see what could be done at higher frequencies to improve the resolution. An increase of two to one would be the least acceptable and three to one would be more interesting and significant. Cosmic static, clearly now, had an inverse intensity vs frequency relation.

<sup>16</sup> Grote Reber, "Cosmic static," *Astrophys. J.*, vol. 100, pp. 279-287; November, 1944.

Consequently, the effective sensitivity should be at least equal to, and preferably surpass, that achieved at 160 mc. The use of a rather anemic commercial signal generator covering a frequency range from 400 to 550 mc also became available. Therefore, I decided on a new operating frequency of 480 mc.

The only tube offering any hope as an rf amplifier, to which I had access, was the RCA orbital beam type A5588A. A four-stage amplifier providing a gain of over 100 db on a bandwidth of 10 mc was constructed in 1944. These tubes certainly would amplify but that is all that can be said for them. The secondary emitter had a life of only 50 hours or so and the internal fluctuation voltage was exceedingly high.

A re-examination of the antenna focal apparatus was made to improve its efficiency<sup>17</sup> and broad-band characteristics. The drum had desirable properties of shielding which should be retained, but it was cumbersome and tended to be rather sharply resonant. The concept of its operation was that the field radiated from a virtual image point in the aperture plane which was made coincident with the focal point of the mirror. The drum acted more or less like an ellipse which transformed this virtual image point back to the antenna. I decided it would be best to do away with this image transformation and place the tips of a cone antenna directly at the focal point of mirror. Since the field from a cone antenna is nominally radial, a hemispherical shield should be provided over the back half of cones with a radius of about one-half wavelength. Several models were built and tested.<sup>18</sup>

A couple of months observations were made during the spring of 1945 using the four-stage amplifier and the new focal point apparatus. The results were very poor since the Milky Way could not be detected, nor even the quiet sun. On one day only the sun was detected when it was radiating in a steady but enhanced manner. The significance of this was not realized at the time. Just how poor this equipment was, could easily be guessed by the fact that auto ignition disturbance rarely was detected. Since these electron multiplier tubes cost thirty dollars each and could be seen to rapidly die in a few hours, the cost of observation averaged several dollars an hour. In fact, the best part of the life of a new tube was used up in getting the set aligned. Thus, not only were the results practically nil, but operation was very uneconomical.

#### IMPROVED APPARATUS AND NEW TESTS AT 62½ CM

Even before the four-stage amplifier was finished, it was clear that it would be rather ineffective. By using special dispensation, I secured some GE 446B lighthouse tubes in the summer of 1945. These had markedly

<sup>17</sup> Grote Reber, "Reflector efficiency," *Electronic Indus.*, vol. 3, pp. 101-216; July, 1944.

<sup>18</sup> Grote Reber, "Antenna focal devices for parabolic mirrors," *Proc. IRE*, vol. 35, pp. 731-734; July, 1947.

less gain but were an immense improvement in life, stability, simplicity, and particularly low-internal fluctuation voltage. A new six-stage amplifier with a 6-mc bandwidth was built using these high grade triodes.

Observations commenced in the summer of 1946. Success was immediate on both the Milky Way and the sun. Also, automobile ignition sparking now was very objectionable during the day. The galactic radiation was markedly weaker than at 160 mc, as was expected. However, the quiet sun was much stronger. Again the gain was set much higher than need be, so that the quiet sun held the pen at full scale for a quarter-hour on the initial try. There seems to be no way of guessing these matters in advance, especially with such an unknown phenomenon. In fact, it seemed that perhaps the sun was a black body radiator but the temperature would have had to be nearer a million degrees than the optical value of six thousand degrees.

Most daytime observations were still unattended since I continued to work in the city. Examination of the solar records showed several cases where automobile ignition interference was abnormally strong and persistent during a half hour or so near solar transit. Why the cars should pick this time to be particularly objectionable seemed quite mysterious. In time, a similar circumstance occurred on a weekend when I was present. Listening observations and pointing the antenna beam away from and towards the sun quickly unravelled the situation. The sun was, in fact, emitting hiss-type transients which rose to great amplitude and fell again in a second or less. These occurred repeatedly and in an overlapping manner, so that for a couple of minutes at a time the pen would remain hard at full scale. Apparently there were many small independent sources of intense transient solar radio waves such as I had never encountered before.<sup>19</sup> The phenomenon became more frequent by the spring of 1947. Also the background intensity rose and fell with irregular periods of a week or more.<sup>20</sup> Obviously, circumstances in the sun were far different now than in 1943 and 1944. Also, as expected, much more detail was found in the structure of the Milky Way.<sup>21</sup> The Cygnus region was divided into two loops. One of these turned out to be the now well-known colliding galaxies source of minute dimensions, as was previously suspected.<sup>22</sup> The other is known as Cygnus-X and seems to be behind a dust cloud. One of the loops in Taurus later was identified as the Crab Nebula. A long slender source in Virgo now is suspected to be the resultant of local galactic clustering, that is, clustering of galaxies in the neighborhood of the Milky Way. These were the last set of observations completed at Wheaton, Ill.

<sup>19</sup> Grote Reber, "Solar radiation at 480 mc," *Nature*, vol. 158, p. 945; December, 1946.

<sup>20</sup> Grote Reber, "Solar intensity at 480 mc," *Proc. IRE*, vol. 36, p. 88; January, 1948.

<sup>21</sup> Grote Reber, "Cosmic static," *Proc. IRE*, vol. 36, pp. 1215-1218; October, 1948.

<sup>22</sup> G. Reber and J. L. Greenstein, "Radio frequency investigations of astronomical interest," *Observatory*, February, 1947.

#### EQUIPMENT FOR USE AT 21 CM

During the autumn of 1945, I met H. C. van de Hulst. He explained his theoretical work on neutral hydrogen and asked for my estimate of the possibility of detecting it. Since I did not know anything about the matter, I could not guess. Neither could he guess whether or not the line would appear in emission or in absorption. At the time I had only the unsatisfactory experience with A5588A tubes at 480 mc. If the line were to be observed in absorption, the matter would be practically hopeless; if in emission, then there might be some possibility. In any case, before trying more microwave experiments, it seemed best to have the lighthouse tubes going at 480 mc. By the autumn of 1946, this had been accomplished.

Consideration was then possible for work at 1420 mc. First, there was no test equipment. To remedy this, I built another signal generator covering the range of 1200 to 1600 mc. The oscillator was modified from the transmitter section of an ABJ type iff equipment and it uses a 2C43 tube with an inductive attenuator. Experiment quickly showed that none of the GE lighthouse tubes would be satisfactory amplifiers at 1420 mc. About this time Sylvania brought out a better version known as the 5768 rocket tube which was similar to some European tubes. A prototype stage was tested and found satisfactory. The necessary movable selectivity was to be obtained by an echo box bought on the surplus market; it has a bandwidth of about 50 kc. It was intended to construct a multistage amplifier using the Sylvania tubes and insert the echo box in the chain. Provided that the amplifier was good enough to detect the continuum, it seemed likely that a fairly strong absorption line might be detected. If the line were to appear in emission, then so much the better. The entire setup was never completed because operations were closed at Wheaton, Ill., during the early summer of 1947. In view of present day knowledge, it seems likely that the experiment would have been successful.

#### ADDENDA

The above was written in Australia during August and September, 1957 from memory and without recourse to log books, etc., located in Wheaton and Hawaii. Thus, there may be some slight error in minor facts, for example, the date when certain tubes became available, etc.

Two errors are worth correcting. The data<sup>19</sup> purporting to show results from Andromeda Nebula were really chance drifts in the early equipment. Selected charts secured much later can be used to prove its existence. Equally good charts are available to deny it. The detectability of this object was on the edge of equipment capabilities as already explained.<sup>21</sup> If all the data had been combined statistically, as is common practice today, the Andromeda Nebula certainly would have appeared. This process is really one of greatly lengthening the integration time.

Using fluctuation voltage it is possible<sup>14</sup> to deduce the size of the elementary charges causing this voltage. When the result was published, a value corresponding to three electrons was given. This was an error caused by an incorrect and much too low value of capacity. Afterwards, the mistake was found and the proper value of electron charge secured in agreement with other methods.

These old experiments at Wheaton were quite thrilling at the time. My present experiments<sup>23</sup> at the other end of the spectrum in Tasmania using cosmic static at kilometer wavelengths fully equal the old in the realm of the unexpected.

Much remains to be done.

<sup>23</sup> Grote Reber, "Between the atmospherics," *J. Geophys. Res.* (in press).

## The Telescope Program for the National Radio Astronomy Observatory at Green Bank, West Virginia\*

R. M. EMBERSON†, SENIOR MEMBER, IRE, AND N. L. ASHTON‡

**Summary**—A brief account is given of the initiation of the feasibility study on the establishment and operation of the National Radio Astronomy Observatory at Green Bank, West Virginia. The principal research facilities will be the radio telescopes, and a series of such telescopes have been proposed. The desired performance characteristics are reviewed. A 140-foot steerable paraboloid on an equatorial mount has been designed. The steps leading to this design are described, as well as the general features of the designed and the expected operating performance. The National Radio Astronomy Observatory is being sponsored by the National Science Foundation.

### INTRODUCTION

IN January, 1954, a conference<sup>1</sup> on radio astronomy was held in Washington, D. C., jointly sponsored by the National Science Foundation, the California Institute of Technology, and the Department of Terrestrial Magnetism of the Carnegie Institution of Washington. Participants included both United States scientists and engineers, as well as numerous distinguished foreign visitors. The conference made clear to the US participants that the lead in radio astronomy had been taken by other countries, this despite such noteworthy contributions as Karl Jansky's initial discovery,<sup>2</sup> G. Reber's pioneering work,<sup>3</sup> the tremendous advances in our

electronics techniques, particularly those related to radar and radio communications, and the first observation of the 1420-mc radiation of interstellar hydrogen by Ewen and Purcell.<sup>4</sup> The conference also indicated that US radio astronomy would fall behind further and further if steps were not taken to provide observing facilities comparable to those planned or being built in other countries.

The equipment requirements of radio astronomers are of three general classes: the antenna system; the receiver and data processing equipment; and the ancillary power supplies, time and frequency standards and similar items. In most instances, the antenna is, by far, the most costly part of the observing equipment. Because of the cost and other factors most US radio astronomers have been working with antennas that are smaller and less effective than those of foreign scientists, who, soon after World War II, gained support of their respective governments for the construction of large radio astronomy equipment. The smaller size, or gain of an antenna, can be compensated for in part through better electronics—a receiver with a better noise figure and extreme stability to permit integration of the very weak celestial signals over longer periods of time; but for angular resolution and the avoidance of confusion, which is important to astronomers, there is no substitute for aperture size. Hence, the conclusion from the January, 1954, conference was that larger and more effective antennas were needed in the United States. How to obtain them was another question. The suggestion was made that several institutions might join together

\* Original manuscript received by the IRE, November 8, 1957. This work was supported by the National Science Foundation.

† Associated Universities, Inc., New York, N. Y.

‡ University of Iowa, Iowa City, Iowa.

<sup>1</sup> "Proceedings of conference on radio astronomy, January 4-6, 1954," *J. Geophys. Res.*, vol. 59, p. 140; March, 1954. See also "Radio Astronomy Conference," *Science*, vol. 119, p. 588; April 30, 1954.

<sup>2</sup> K. Jansky, "Directional studies of atmospherics at high frequencies," *PROC. IRE*, vol. 20, pp. 1920-1932; December, 1932.

—, "Electrical disturbances apparently of extraterrestrial origin," *PROC. IRE*, vol. 21, pp. 1387-1398; October, 1933.

<sup>3</sup> G. Reber, "Cosmic static," *PROC. IRE*, vol. 28, pp. 68-70; February, 1940.

—, *Astrophys. J.*, vol. 91, pp. 621-632; June, 1940.

<sup>4</sup> H. I. Ewen and E. M. Purcell, *Nature*, vol. 168, p. 356; 1951.

in the construction of a large antenna, larger than any single institution could afford. In the spring of 1954, there were conversations between representatives of Harvard, Massachusetts Institute of Technology, and the Naval Research Laboratory on a proposal to construct a large steerable paraboloid. This would be a general purpose research tool, applicable to astronomical problems as well as to more immediately utilitarian studies, such as scatter propagation. The enthusiasm of the scientists and engineers was dampened by the high estimated cost of a large paraboloid. But the conversations continued, and a parallel was found in the research reactor and large accelerators at the Brookhaven National Laboratory. This laboratory was established and is operated by Associated Universities, Inc.<sup>5</sup> under a contract with the Atomic Energy Commission. The research facilities there are enjoyed by visiting scientists as well as by those on the permanent staff. Why not establish a radio astronomy observatory along the same general pattern?

After further conferences, the National Science Foundation made a grant to Associated Universities, Inc. for a study on the feasibility of establishing and operating a radio astronomy observatory. The study included a search for a suitable site, plans for the site development, several investigations contributing to the design and construction of large antennas, and a plan for the organization and operation of the proposed observatory.<sup>6</sup> More recently, the National Science Foundation has contracted with Associated Universities, Inc. to establish and operate a National Radio Astronomy Observatory at Green Bank, West Virginia.

In the remainder of this article, the portion of the feasibility study and of subsequent contract activities related to large antennas will be discussed. To help in understanding decisions that have been made, it is desirable to recognize that what an engineer regards as an antenna system is a telescope to the astronomer, and the astronomer routinely deals with signals that the communication engineer would regard as a small amount of noise. The term "telescope" will be employed in deference to the nomenclature of the astronomers, and we will regard it as an instrument for research, even though the tonnage of materials involved are about the same as for a destroyer.

The nature of the signals studied by radio astronomers is described in other articles in this issue of the PROCEEDINGS.<sup>7</sup> Let us note briefly here that the signals are weak as judged by radio communications or radar

standards. All wavelengths transmitted by the earth's atmosphere are represented (e.g., from less than 1-cm wavelength to more than 10 meters). There are some frequencies of particular astronomical importance because of relatively strong bright-line radiations associated with natural atomic and molecular processes, (e.g., the 21-cm radiation of the hydrogen atom). The typical celestial radiation is unmodulated white noise, and in some cases may be polarized. The signals come from many sources—from the sun, from the center of our Milky Way system or galaxy, from unique objects such as the Crab Nebula, from external galaxies, and from sources of such low visual luminosity that no optical identification has been possible. All that precedes is concerned with radio astronomy in the passive or receiving-only phase, wherein the transmitters are natural phenomena and not under the control of the experimenter. The active or radar phase of radio astronomy is limited to the solar system, and there is no sharp line of demarcation between these studies and those of the upper atmosphere that stem from geophysical and radio communications interests. Throughout this paper the discussion will generally be directed to the passive phase of radio astronomy, but most of what is said is equally applicable to the active phase.

#### GENERAL DISCUSSION

At the outset, the Advisory Committee<sup>8</sup> for the feasibility study pointed out that the observing requirements in the microwave region required a telescope with both high gain and high resolution. At meter wavelengths and longer, high resolution was the dominant requirement because of the more satisfactory status of the receiver art for such radiations. It was also noted that resolution at the longer wavelengths was a linear affair, e.g., a simple array or Mills Cross,<sup>9</sup> whereas the high-gain, high-resolution telescope for microwaves would involve a paraboloid, or something equivalent, and the cost would vary as the square or some higher power of the aperture. Thus a concept for the telescopes at Green Bank was formed early, namely, that the relatively expensive paraboloids would be part of the permanent equipment, whereas arrays would be regarded as expendable equipment and tailored to fit the particular needs of each observing program. This concept recognizes that a paraboloid is inherently a broad-band de-

<sup>5</sup> Associated Universities, Inc. is a nonprofit corporation chartered by the Board of Regents of the State of New York; the corporation is sponsored by nine universities: Columbia, Cornell, Harvard, Johns Hopkins, Massachusetts Institute of Technology, Pennsylvania, Princeton, Rochester, and Yale.

<sup>6</sup> B. J. Bok, "A national radio observatory," *Sci. Amer.*, vol. 195, pp. 56-64; October, 1956.

<sup>7</sup> L. V. Berkner, "National radio observatory site," *Sky and Telescope*, vol. 15, p. 398; July, 1956.

<sup>8</sup> J. W. Findlay, "Noise levels at a radio astronomy observatory," this issue, p. 35.

<sup>8</sup> The feasibility study started early in 1955, with an Advisory Committee under the chairmanship of J. P. Hagen, Naval Research Laboratory, and composed of B. J. Bok, Harvard College Observatory; A. J. Deutsch, Mt. Wilson and Palomar Observatories; H. I. Ewen, Harvard College Observatory; L. Goldberg, University of Michigan; W. E. Gordon, Cornell University; F. T. Haddock, University of Michigan; J. D. Kraus, Ohio State University; A. B. Meinel, University of Chicago; M. A. Tuve, Carnegie Institution of Washington; H. E. Wells, Carnegie Institution of Washington; and J. B. Weisner, Massachusetts Institute of Technology. When Dr. Hagen was made the head of Vanguard, he resigned his position on the Advisory Committee, and Dr. Bok served as chairman until he left to become the director of the Australian National Observatory.

<sup>9</sup> B. Y. Mills, A. G. Little, K. V. Sheridan, and O. B. Slee, "A high resolution radio telescope for use at 3.5 cm," this issue, p. 67.

vice, limited at one extreme when the aperture is the same order of magnitude as the longest wavelength to be observed, and at the other extreme when the irregularities of the paraboloid surface (openings, if a mesh; deviation from the best-fitting true paraboloid) are a significant fraction of the shortest wavelength.

There have been numerous theoretical studies on the short-wavelength limitations of paraboloid surfaces.<sup>10</sup> Experimental evidence and the theoretical predictions are in general agreement, Friis<sup>11</sup> and his colleagues having shown with the Homdel 60-foot paraboloid that surface deviations of 1/16th the observed wavelength have significance if utmost gain is the objective. From the experimental point of view, the radio astronomer does not have a free choice of what wavelength will be observed. There are practical factors of interference from man-made sources. If these devices are intentional transmitters, they generally radiate in fixed bands which the radio astronomer will try to avoid. The astronomers are also limited by the transparency of the earth's atmosphere. And, finally, the celestial radiations have a continuum plus certain bright lines (sometimes these may be observed as absorption lines,<sup>12</sup> similar to the Fraunhofer lines in the solar spectrum). As previously mentioned, one of the most important of these "bright lines" is the 21-cm radiation from atomic hydrogen, because hydrogen is a fundamental building block of the universe and the most abundant element found not only throughout our Milky Way system, but in other galaxies as well. Because of the great importance of this hydrogen radiation, any general purpose radio telescope must be capable of working effectively at 21 cm.<sup>13</sup> Thus it is seen that, independent of the diameter, a paraboloid for a radio astronomy telescope must meet a surface tolerance of  $\pm \frac{1}{2}$  inch to be ideal for 21-cm work; of course, the paraboloid would have value if the surface irregularities were greater than 1/16th the wavelength, but the over-all antenna gain would suffer. Furthermore, if the irregularities were systematic in character because of the manufacturing process, curious

effects might be introduced into some experiments, such as polarization measurements.

With the minimum acceptable specification for the surface tolerance essentially predetermined, there remains for selection only the diameter and focal length (or f/d ratio). Of these, the f/d ratio is the easier to fix. The choice depends primarily on the rf feed that will be placed at the focus to "illuminate"<sup>14</sup> the paraboloid. Here some compromises are necessary, although there is general agreement that the f/d ratio should be less than 0.5 and greater than 0.25. A ratio of 0.5 would have certain advantages if multiple feeds or clusters are employed at the focus. But the consensus is that an f/d ratio of 0.40 to 0.45 is best for horn-type feeds, which will be employed for work at 21-cm and shorter wavelengths.

The diameter of the paraboloid may not be freely chosen. As already mentioned, the cost of a radio telescope varies as some power, greater than two, of the diameter; and because of the predetermined surface specification, the structural problems of the telescope are important factors. Early in the feasibility study for the radio astronomy observatory, structural engineers were asked to estimate at what size a conventional steerable paraboloid, such as the Jodrell Bank telescope, would be limited by the strength of the materials available for its construction. The answer to this question is not unique, depending on what assumptions are made. To illustrate, consider a simpler structure, namely, a tower. It is perhaps technically feasible to construct a tower 29,000 feet tall and meeting quite strict specifications for rigidity. The completed structure might closely resemble Mount Everest and would be fantastically costly. If an equally extreme design were adopted for a telescope, a truly enormous aperture might be obtained; but if more or less conventional designs are visualized, apertures of two to three thousand feet should be possible before the physical characteristics of the structural materials would be limiting. There was unanimous agreement that the cost of such a telescope would be beyond the budget available for the initial establishment of the observatory.

The above considerations gave rise to numerous suggestions for unconventional or exotic designs—huge bowls carved in the surface of the earth; a floating sphere with the paraboloid set into the upper portion; phased panels arranged to be equivalent to an optical zone or Fresnel lens. These suggestions were rejected as being unproven and, hence, too great a gamble for inclusion in the early planning stages for the observatory or as being limited in applicability to general research problems. Even the so-called conventional approach offers very many solutions, depending on the detailed choices made by the designer. As the studies pro-

<sup>10</sup> S. Silver, Ed., "Microwave Antenna Theory and Design," Mass. Inst. Tech. Rad. Lab. Ser., vol. 12, McGraw-Hill Book Co., Inc., New York, N. Y.; 1949.

R. C. Spencer, "Multiple Feed High-Gain Antennas for Radio Astronomy," paper presented at IAU conference; May 27, 1955.

D. J. Cheng, "Study of Phase Error and Tolerance Effects in Microwave Reflectors," Syracuse Univ. Res. Inst., Syracuse, N. Y., Contract No. AF 30(602)-924; December 31, 1955.

<sup>11</sup> J. Robieux, "Influence of the Manufacturing Precision of an Antenna on its Performance," Compagnie Generale de T.S.F., Paris, France, Contract No. AF 61(514)-737C; May 27, 1955.

A. B. Crawford, H. T. Friis, and W. C. Jahes, Jr., "A 60-foot diameter parabolic antenna for propagation studies," *Bell Sys. Tech. J.*, vol. 35, pp. 1199-1205; September, 1956.

J. Ruze, "Physical Limitations on Antennas," Mass. Inst. Tech., Res. Lab. Electronics, Cambridge, Mass., Tech. Rep. No. 248; 1952.

<sup>12</sup> A. E. Lilley, "The absorption of radio waves in space," *Sci. Amer.*, vol. 197, pp. 48-55; July, 1957.

<sup>13</sup> The giant 250-foot telescope of the University of Manchester, nearing completion at Jodrell Bank, was conceived by Prof. Lovell before the hydrogen radiation had been observed: a redesign of the reflector has been accomplished while the telescope was being constructed in order that 21-cm observations might be undertaken.

<sup>14</sup> In the discussion of antenna patterns, the usual custom is adopted for a transmitting system rather than for a passive receiving-only system.

ceeded, it became evident that there was no uniquely best design for a radio telescope, even if the problem were narrowed by closely specifying the diameter and other performance characteristics.

At the same time that the preceding studies were undertaken, an investigation was made of the feasibility of housing very large telescopes in a radome, thereby relieving the telescope of most climatic disturbances, particularly winds and solar heating. Two types of radomes were considered: those made of flexible material and supported by air;<sup>15</sup> and those made of rigid, self-supporting surface panels.<sup>16</sup> Both types have been employed to house military radars. In theory, the air supported type is more attractive, because the absence of any thick struts or braces would eliminate many possible secondary sources that might introduce spurious signals or distorted polarization effects. It is important to note here that a military radar operates at essentially a fixed wavelength and the characteristics of a rigid radome may be selected so as to minimize the possible diffraction and interference effects; radio astronomy, on the other hand, is interested in wavelengths from 1 cm to 10 m and it is not possible to "broad band" the structural radome design for this large portion of the spectrum. On the other hand, the air supported fabric for a radome could be kept thin, compared even to a 3-cm wavelength and could be made very homogeneous; acceptable dielectric and absorption constants were predicted from measurements made on the materials used in the military radomes.<sup>17</sup> A tentative design was made for a radome large enough to house a 500- or 600-foot telescope. In order that the radome would not burst when the barometric pressure fell (or that the fabric would not droop on the telescope when the barometric pressure rose), automatic fans or blowers would be necessary to move air in or out of the radome. These and related technical problems could be solved, but no assurance could be obtained on the life of the radome fabric exposed continuously to climatic factors. Five or ten years is a long time by military standards: many equipments are obsolete in shorter times. But by astronomical standards, a radome life of 25 years seemed to be minimal. The presently available radome materials cannot promise such durability, even with careful annual maintenance at a considerable cost. The combination of maintenance cost and capital outlay amortized over a few years is prohibitive. Accordingly, a fundamental decision was made to design all telescopes to

stand in the open. This decision was made with full recognition that observations requiring the utmost performance of the telescope would have to wait for favorable observing conditions, *e.g.*, little or no wind, overcast sky or at night, to minimize thermal effects.

The 250-foot telescope at Jodrell Bank, which was well started in 1955, elicited the suggestion that a larger telescope be considered for the observatory at Green Bank. Accordingly, a study was undertaken,<sup>18</sup> not for the immediate purpose of designing and constructing the larger telescope, but primarily to learn what structural problems would be involved. A diameter of 600 feet was assumed for the paraboloid, with the added stipulations that the telescope be effective for 21-cm work and that structural materials be employed economically, in the hope that the cost might be held down. The results of the study were that the cost would exceed \$10 million and that the performance specifications could not be met unless either enormous quantities of materials were employed (the Mount Everest solution), or compensating devices were incorporated. The latter solution appeared more feasible and was explored to determine the nature of the compensation that would be needed. An altazimuth mount, similar to that of the Jodrell Bank telescope, had been adopted for the 600-foot study, and this proved to be an advantage when compensations were added because gravity deformations were single-valued functions of the altitude angle.

By this point in the feasibility study for the radio astronomy observatory, a telescope program had been formulated, as follows:

- 1) A small telescope (10- or 20-foot aperture) mounted on the roof of the laboratory building to be available for testing electronic components undergoing alignment or repair, and otherwise to be available for observation;
- 2) An intermediate telescope, perhaps similar to the 60-foot telescope at Harvard's Agassiz Station;<sup>19</sup>
- 3) A 140-foot telescope, to be a precision instrument, comparable in precision at its size to the 50-foot telescope at the Naval Research Laboratory;
- 4) A 300-foot telescope, to be a precursor for a larger telescope;
- 5) A 600-foot telescope, perhaps the largest completely steerable paraboloid to be built;
- 6) Provision for arrays and for mobile equipment brought by visiting astronomers.

More recently, the telescope program has been modified to include more than one of the intermediate telescopes, item 2). Some consideration is being given to abandoning the fourth and fifth items in favor of a very much larger telescope, increased gain and resolution being

<sup>15</sup> W. Bird, "Design and Fabrication of Experimental Radome and Associated Equipment," Cornell Aeronaut. Lab., Ithaca, N. Y., 1954. See also *Life*, May 9, 1949 and January 4, 1954.

<sup>16</sup> R. B. Fuller, "Industrial logistics and design strategy," *Penn. Triangle, Army-Navy-Air Force J.*, vol. 2, October, 1954. See also private communications and presentations, IAU conference; March 25, 1955.

<sup>17</sup> L. C. Van Atta, private communication:

Material	Dielectric Constant	Loss (at 3000 mc)
S-82D Fiberglass	4.57	0.039
S-84D Nylon	3.50	0.041.

<sup>18</sup> J. Feld, "Feasibility Study of 600-foot Diameter Radio Astronomy Reflector," private communication; July 20, 1955.

<sup>19</sup> D. S. Heesch, "Harvard's new radio telescope," *Sky and Telescope*, vol. 15, pp. 388-389; July, 1956.

bought at the expense of steerability or sky coverage.

The 140-foot telescope is the most challenging problem of the present program. The specifications for this instrument were drafted in 1955 and are reproduced as follows, along with revisions that seemed desirable as the design studies proceeded.

- 1) Focal length/diameter ratio, 0.35 to 0.5, with the larger value preferred;
- 2) Surface tolerance,  $\pm \frac{3}{8}$  inch over the entire aperture and  $\pm \frac{1}{4}$  inch over the inner half aperture;
- 3) Surface material, to be electrically equivalent to a continuous sheet with the largest dimension of any opening not more than  $\frac{1}{4}$  inch;
- 4) RF feed support, capable of a 500-pound load held to  $\frac{1}{8}$  inch of correct position;
- 5) Rigidity and drive and control system to be capable of an accuracy of 5 per cent of the beamwidth at half power for 10-cm radiation, or about 30" of arc. Design for normal use in winds to 30 mph and with slight reduction of accuracy in winds to 45 mph. In addition to a polar axis tracking rate, both axes will have a variable scanning rate, from 10' to 4° per minute of time, and a maximum slew rate of 30° per minute of time.

By the fall of 1955, it seemed desirable to amend the specifications, the paraboloid tolerance over the entire surface being reduced to  $\pm \frac{1}{4}$  inch and the angular precision of the instrument set at 5 per cent of the half-power beamwidth for 3-cm radiation or 10" of arc. About a year later, further revisions were made. The precision desired for the paraboloid surface was redefined, as follows: For wind speeds up to 16 mph, the root-mean-square deviation from the best paraboloid shall be no more than  $\pm \frac{1}{4}$  inch for all positions of the paraboloid. Under a no-wind condition and for zenith distances of less than 60°, the surface accuracy should be as much better than  $\pm \frac{1}{4}$  inch as can be obtained without appreciably increasing the cost of the reflector. The paraboloid surface shall be adjustable by means of rear-mounted studs or other means. The number of rigid panels that make up the surface shall be kept as small as is consistent with the surface tolerances demanded of the panels. The specifications for the rigidity of the mount and for the drive and control system were modified to include conditions of no wind and of 16 mph; it appeared that at Green Bank the winds would be less than 16 mph for at least 80 per cent of the time.

Wind Condition	Zero Wind	16-mph Wind
Absolute pointing accuracy	$\pm 30''$	$\pm 40''$
Relative pointing accuracy*	$\pm 10''$	$\pm 20''$
Tracking accuracy over 15 minute time	$\pm 10''$	$\pm 20''$
Tracking accuracy over 1 hour or more	$\pm 20''$	$\pm 40''$

\* Relative pointing accuracy is defined as the accuracy with which the telescope can be moved from one point to another point, assuming the subtended angle between points is under 30° and that both points are 30° or more above the horizon.

Concerning over-all rigidity, it was specified that the entire structure be designed to act as a simple elastic body for all expected gravity or wind loads, in addition to the general understanding that such deflections or deformations be kept as small as might be consistent with an economical employment of structural members.

The specifications for the support of the rf feed were modified to accommodate anticipated requirements for more complex and, hence, more bulky and heavier equipment to be held at or behind the focus; to provide for a load of 1000 pounds; and to be supported by a tripod or tetrapod mount, the mounting base or plate to be not less than 4 feet behind the focus. Deflections due to gravity, as the telescope is moved about the sky, should be not more than  $\frac{1}{8}$  inch laterally from the axis of the paraboloid. A tolerance of 1/16 inch is desirable if it can be achieved at no great additional expense. The focal length shall be 60 feet, making the f/d ratio about 0.43.

After some preliminary exercises that proved that no one had had experience in building anything similar to the proposed telescope but that were, perhaps of educational value, a decision was made for AUI to develop a design for the telescope in which we had confidence. Three independent design studies were initiated. The first was undertaken by Husband, the man primarily responsible for the construction of the 250-foot telescope at Jodrell Bank. The second was undertaken by D. S. Kennedy & Co. of Cohasset, Mass., the firm with the most large-reflector experience in the United States. A third study was undertaken by Feld. It is important to note that his design development was on a different basis than the first two. They were free to choose any combination of features that would produce an efficient design promising the desired performance. The Feld 140-foot study was to develop further some of the concepts of the 600-foot study, thereby providing experience with essentially a quarter-scale model and all to be competitive, dollar-wise, with the two other designs.

The main features of the Husband design are shown in Fig. 1. This design was independently conceived but, nevertheless, strongly resembles a design for a 220-foot telescope proposed by Grote Reber in 1948, Fig. 2 (p. 29). Reber was too far ahead of US science and technology. In his own words, ". . . for the most part the attitude was that I was harmless and if no interest was shown in what I was saying, I would go away quietly." The Reber-Husband concept supports each point of the reflector by structural elements that carry the load directly to the ground. The large horizontal cylinder, which rotates on rollers as well as on axial bearings, gives great depth and, hence, rigidity to the reflector. Rotation from horizon-to-horizon through the zenith is possible. The cylinder is mounted on a huge bridge or carriage that can rotate about a vertical axis; a small part of the load is carried on a central bearing and the remainder is carried by wheels rolling on circular rails or tracks. This altazimuth mount permits complete

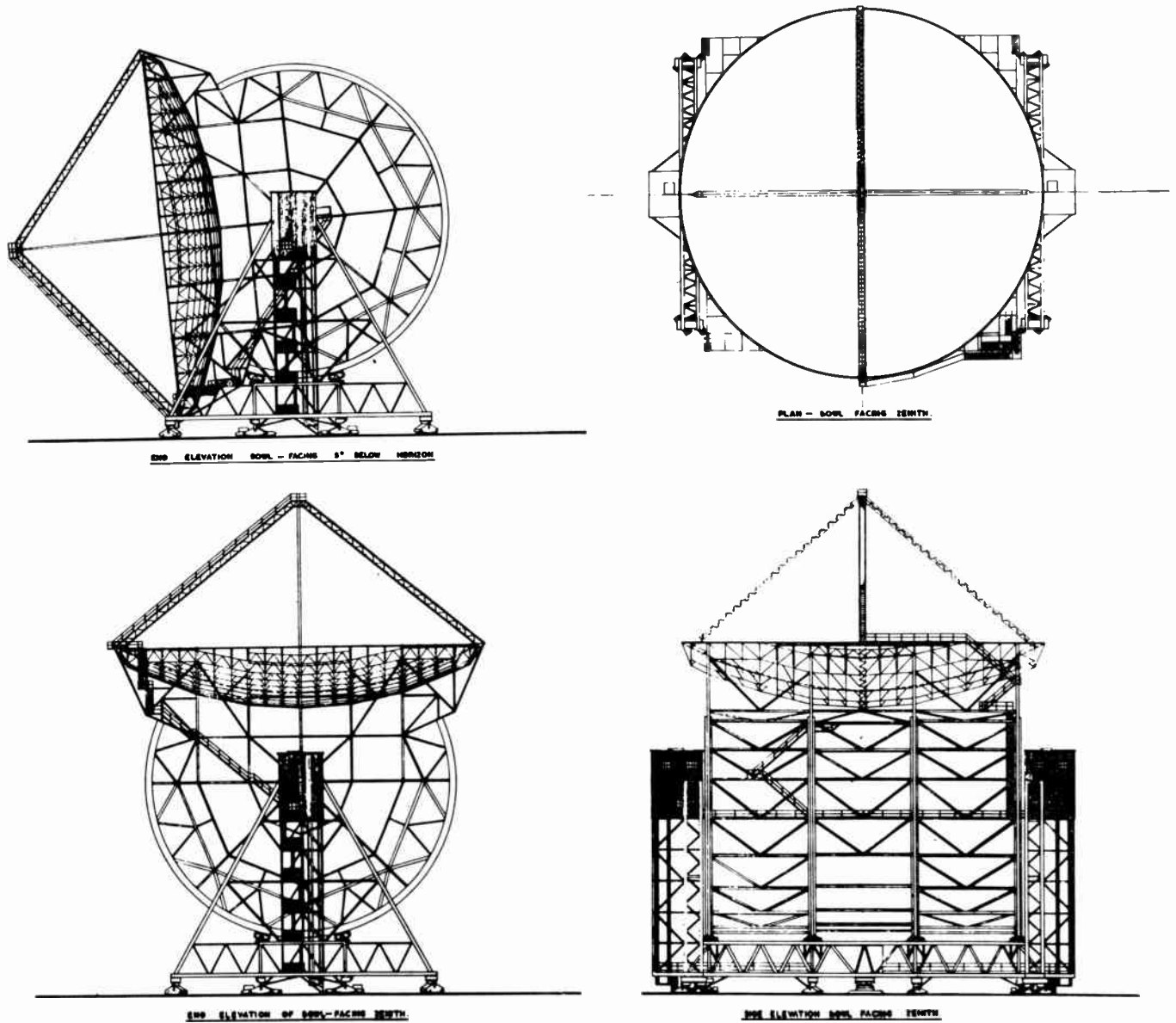


Fig. 1—Drawing by Husband & Company of Sheffield, Eng. for the proposed 140-foot altazimuth telescope design. The two end elevations show the reflector pointed to the zenith and horizon. The front elevation again shows the reflector pointing to the zenith. The plan view shows the quadruple support for the antenna feed.

coverage of the sky. In order to track a celestial object, *i.e.*, to point the telescope constantly in one direction in space by compensating for the rotation of the earth, it is necessary that there be simultaneous motions about both the altitude and azimuth axes. This coordinate conversion from altitude and azimuth (or elevation and bearing, for those trained in other services) to the astronomers' hour angle and declination (most easily understood as the celestial counterparts of terrestrial longitude and latitude) will be discussed in more detail later.

Fig. 3 and Fig. 4 show the principal features of the Kennedy design. The base of the telescope is a vertical cylinder or silo. A huge D-shaped turret rotates on top of the silo, thereby providing azimuth motion. The reflector may rotate about an axis that approximately

coincides with the upper straight edge of the D-shaped turret. This altitude motion is limited to about  $90^\circ$ , from horizon to zenith. But the D turret may be rotated through  $360^\circ$  and, hence, complete sky coverage is available.

The Feld design is novel, as shown in Fig. 5, in that the parabolic reflector is a thin shell, so thin compared to the diameter as to be similar to an egg shell. The reflector is supported by a massive ring girder. The tendency of the shell to turn the ring inside out is counteracted by stressed cables from the lower edge of the ring to a central work station where adjustment of the tension in each cable would be possible. The ring girder is supported on two diametrically opposed shafts, and a cross truss, quite independent of the parabolic shell, ties

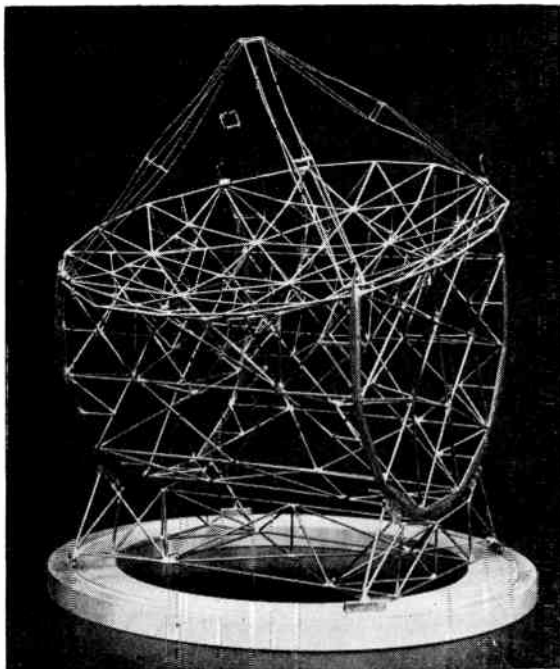


Fig. 2—Revolutionary concept of 220-foot radio telescope designed by Grote Reber.

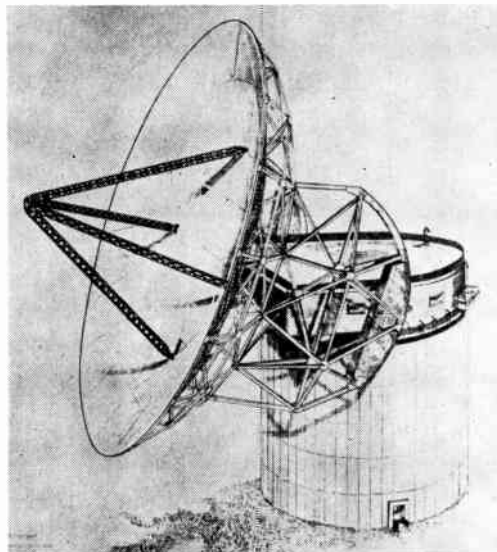


Fig. 4—Rear elevation of Kennedy design, showing truss structure of the reflector.

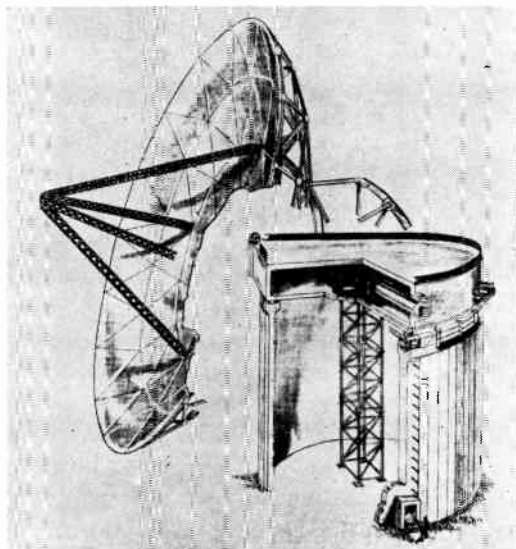


Fig. 3—General side elevation of 140-foot altazimuth telescope proposed by D. S. Kennedy Company of Cohasset, Mass.

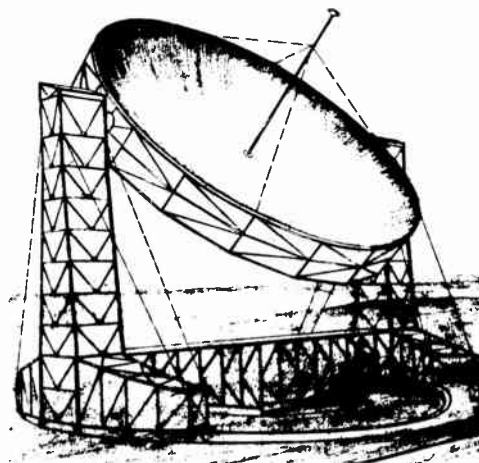


Fig. 5—General view of the 140-foot altazimuth radio telescope design proposed by Dr. Jacob Feld of New York, N. Y.

these shafts together. Rotation through  $360^\circ$  on these shafts permits the reflector to point from horizon to horizon and also, when the reflector is in the inverted position, brings the paraboloid focus down for easy access, a desirable feature if frequent changes or adjustment of the rf feed and other focal region components are necessary. A bridge and tower system, similar in appearance to the 250-foot telescope, provides azimuth rotation through  $360^\circ$ . In this instance, most of the gravity load is carried on the central bearing and the wheels and circular tracks are to take care of wind loads.

These three designs, dissimilar as they appear, have

one thing in common: all are altazimuth mounts. In retrospect, this coincidence is not surprising. The designers were given desired performance specifications and asked to provide a telescope to give that performance. Each approached the problem from a structural point of view and each adopted the altazimuth mount as the simplest and most economical structure. Whether or not the altazimuth concept for a telescope is the cheapest when drive and control as well as structure are considered is another matter. Numerous factors are involved. Reference has already been made to the fact that astronomers usually employ a celestial coordinate system of hour angle and declination. Hour angle is measured east or west of the local meridian plane, just as longitude on the earth is measured east or west of the Greenwich meridian. Declination is measured north or south of the equator plane. Most astronomical optical telescopes are equatorially mounted: there is a polar axis parallel to the earth about which hour angle is

generated, and there is a declination axis perpendicular to the polar axis about which declination is generated. The preference for an equatorial mount is dictated by the observational requirement that the telescope be capable of pointing continuously and precisely at any chosen celestial object.

If only approximate celestial tracking is required, the equatorial mount is simplicity itself. If great precision is desired, the drive and control for an equatorial mount becomes more complicated. The sidereal rate is correct only for a star or other very distant celestial object. If observations are being made of some member of the solar system, a corrected rate is necessary for the polar axis rotation; the correction is very large for the moon because it makes one revolution around the earth in about a month; the correction for the sun is smaller because its apparent movement through the sky requires one year. During the course of several hours of observation of a member of the solar system, the corrected polar axis rate may be regarded as constant, but it will, of course, vary appreciably from date to date. All members of the solar system revolve in planes that usually are close to but not coincident with the earth's equator plane. Hence, there are northward and southward motions that require small positive or negative declination rates for the telescope. Any refractive effects of the earth's atmosphere will introduce small deviations between the apparent rates of a celestial object and those predicted from an ephemeris. These atmospheric deviations are largest for celestial objects near the horizon and become smaller the closer an object approaches the zenith. Hence, small variable corrections may be necessary for both the polar and declination rates. Finally, any systematic errors of the telescope—errors in the drive gears or bending of the telescope due to gravity loads—will enter into the most precise angular measurements. Of course, an observer may carefully calibrate the telescope deflections and then apply any necessary corrections to the polar and declination drives. It is also important to note that all of the relatively small corrections discussed above need be applied to the drives of the equatorial telescope only when utmost precision is desired. It is equally important to observe that this precision can be obtained only if the basic drives are inherently stable and repeatable and, hence, within the precision tolerances given, free of large random errors.

All that has been said concerning the drives for an equatorial mount applies to an altazimuth mount. In addition, the altazimuth mount requires some means of conversion from azimuth and altitude to hour angle and declination. A moment of consideration of the path of a celestial object as it rises in the east, passes across the meridian, and sets in the west, makes it clear that the corresponding azimuth motion is always in one direction but the rate varies slowly, being a maximum as the object crosses the meridian and being symmetrical with respect to the meridian. The maximum value is not the same for all celestial objects but depends on the zenith

distance at the moment of crossing the meridian. If the object should pass through the zenith, a momentary infinite azimuth rate would be required of the telescope. This mechanical impossibility is avoided by the establishment of a small zone about the zenith of  $3^\circ$  or  $5^\circ$  radius, through which the telescope is not expected to track automatically. The altitude motion of a celestial object that traverses the sky also changes slowly, depending on the zenith distance of the object. The altitude rate has its maximum upward value when the object is on the eastern horizon; the rate becomes zero as the object crosses the meridian; the rate is maximum downward when the object is at the western horizon.

Provided zenith passage difficulty is avoided, azimuth and altitude rates are slowly and smoothly varying functions of hour angle and declination. But in order that the instantaneous position of the telescope as well as the azimuth and altitude rates be determined with the precision given in the telescope specifications, it is necessary that the coordinate conversion device, whether electrical, mechanical, or a combination, be inherently stable and repeatable within the specific tolerances.

A basic study<sup>20</sup> was made of the drive and control system for a 140-foot radio telescope. Various firms that manufacture drive and control equipment were consulted on many aspects of the problem. These explorations were not exhaustive, but it became clear that at least one technically feasible solution existed for each part of an altazimuth drive and control system. These solutions automatically include an equatorial system.

A cost study<sup>21</sup> on a uniform basis was made of equatorial and altazimuth telescopes. From this it became evident that the cost of coordinate conversion, by itself, was a function of the precision desired and not directly controlled by the size and other design details of the telescope. It also became clear that an equatorial mount was structurally quite easy for a small reflector. But as the reflector size increased, the equatorial mount became relatively difficult and more expensive, compared to an altazimuth mount, because of the large counterweights or equivalent devices required that, in turn, demanded larger and stronger bearings and other parts of the structure. This study could not demonstrate that for a 140-foot reflector one type of telescope would be much cheaper than the other. It was summarized by Roderick<sup>22</sup> that the 140-foot size was unfortunate because it was in the middle of the "gray" area and thus not determinate. From Tasmania, G. Reber<sup>23</sup> wrote: "The

<sup>20</sup> J. O. Silvey and D. V. Stallard, "A Study of Position Measurement and Control System for a Proposed 140-Foot Radio Telescope," M.I.T. Servomech. Lab., Cambridge, Mass., private communication; May 1, 1956.

<sup>21</sup> T. C. Kavanagh, private communication; January 4, 1957. Background information and estimates were kindly provided by J. Feld, H. C. Husband, D. S. Kennedy, and others.

<sup>22</sup> J. W. Roderick, private communication; Prof. Roderick is a consultant to the radio telescope design study that is being conducted by the CSIRO, Sydney, Australia. Thanks are due to Dr. E. G. Bowen and his colleagues for a profitable exchange of information.

<sup>23</sup> G. Reber, private letter; October 7, 1956.

140-foot figure seems to have been arrived at as some kind of compromise. It is a peculiarly unfortunate one. Over the years I have been investigating various aspects of large mirror design. It is quite clear that everything up to about 100 feet should be made equatorial. At 200 feet this is impossible. Only an altazimuth mount is feasible. Within this range 100 to 200 feet the problem is indeterminate and much time and effort may be expended trying to find a best solution. . . ."

Other factors should be considered in deciding between an equatorial or altazimuth mount for a radio telescope. With an altazimuth telescope, one edge of the reflector is always up (except for the unique situation when the reflector is pointing to the zenith). This single aspect with respect to gravity will simplify any corrections that might be necessary due to gravity deformations, *e.g.*, bending of the support of the rf feed at the focus, sagging of the reflector, or bending of the supporting structure, because the compensating devices will need be controlled by the altitude angle only. On the other hand, if a reflector is equatorially mounted, the reflector essentially rolls on its rim in the course of tracking a celestial object from the eastern horizon across the meridian to the western horizon. Thus any compensating devices for an equatorial telescope must be controlled by two coordinates, hour angle and declination. Similarly, if observing corrections are necessary for atmospheric refraction, for spurious signals scattered by the ground, or for any other cause dependent on the altitude angle, such corrections are simpler for an altazimuth instrument. On the other hand, because an equatorially mounted reflector rolls on its rim, the reflector does maintain a fixed position with respect to directions in the sky. This characteristic could be observationally important if polarization or similar phenomena were being studied that are characterized by fixed position angles in the sky. Admittedly, this latter factor would vanish if both the rf feed at the focus and the surface of the paraboloid were symmetrical in all directions with respect to the axis of the paraboloid, but seldom would this be true.

Finally, in addition to the factors already enumerated, it was necessary to recognize the bias of the astronomers in favor of an equatorial mount. It is only fair to say that in some instances the bias is intuitive, whereas for others it results from unhappy experiences with electronic and electrical equipment; whatever the reason, the consequence is that these astronomers prefer structural complexity to electronic or electrical complexity. The merits of these arguments will be disputed by many readers of the PROCEEDINGS; but because astronomers will be using the telescope, a decision was made in the late fall of 1956, to table further consideration of altazimuth mounts and to concentrate on an equatorial telescope.

D. S. Kennedy & Co. completed the equatorial 60-foot telescope at the Agassiz Station of the Harvard College Observatory and equatorial proposals were

made by both Feld and Husband. In all cases, the astronomers and engineers advising AUI were not satisfied. Accordingly, at the time the decision was made to concentrate on an equatorial telescope, a decision was also made to start a new design. Also, it was decided to develop this design with the *ad hoc* group of scientists and engineers reviewing the work at frequent steps rather than upon completion, thereby insuring that the best suggestions from a large group could be considered for incorporation. Ashton<sup>24</sup> agreed to undertake the design work under the unusual condition of almost continuous review by an official advisory group.<sup>25</sup> The remainder of this article will be concerned with the equatorial design for a 140-foot radio telescope that is the result of this joint effort.

The decision for an equatorial telescope placed a major share of the design problems on the structure. These will be discussed in detail elsewhere.<sup>26</sup> The readers of the PROCEEDINGS will be interested in the broader aspects of the structural concepts and of their relation to the drive and control and other problems. The specifications given earlier apply. In addition, a solid surface for the reflector was specified in order to minimize difficulties at short wavelengths and with phenomena involving polarization.

The general features of the design are shown in Fig. 6–Fig. 9, which are photographs of a model constructed for test purposes. The foundation will be made of concrete. The polar shaft rotates on two bearings that are adjustable to permit alignment of the polar axis of the telescope with the axis of the earth. A yoke and a drive gear of 42-foot radius are attached to the north, or upper, end of the polar shaft. At the upper ends of the yoke are two bearings for the declination shaft; these are movable to permit adjustment of the declination axis to be perpendicular to the polar axis. Steel is contemplated for all metal up to the declination axis. The reflector, supporting structure and 35-foot radius wheel for the declination gear, are made of aluminum.

The foundation stands about 40 feet high, not including the subsurface portion that extends down to the rock strata 30 feet below the existing ground level. The large volume inside the foundation will be utilized for the control and observing station and for housing transformers, motors, pumps and similar ancillary equipment. The telescope proper will weigh approximately 2000 tons. In addition, for the survival condition of a

<sup>24</sup> N. L. Ashton, 820 Park Road, Iowa City, Iowa; Prof. Ashton designed the 50-foot parabolic reflector that was built for the Naval Research Laboratory by the Collins Radio Company.

<sup>25</sup> This *ad hoc* advising group consists of T. C. Kavanagh, chairman, P. P. Bijlaard, N. A. Christensen, A. M. Freudenthal, J. O. Silvey, D. Lindorff, E. J. Poitras, B. H. Rule, F. T. Haddock, E. F. McClain, and H. E. Tatel. J. G. Bolton, who was serving on the *ad hoc* group and also on the IAU Advisory Committee for the entire project, resigned early in 1957, because of the press of his own radio astronomy affairs. Although there have been sharp differences of opinion on many points, resolution has been possible and the group has worked effectively and efficiently with Ashton.

<sup>26</sup> N. L. Ashton, in preparation.

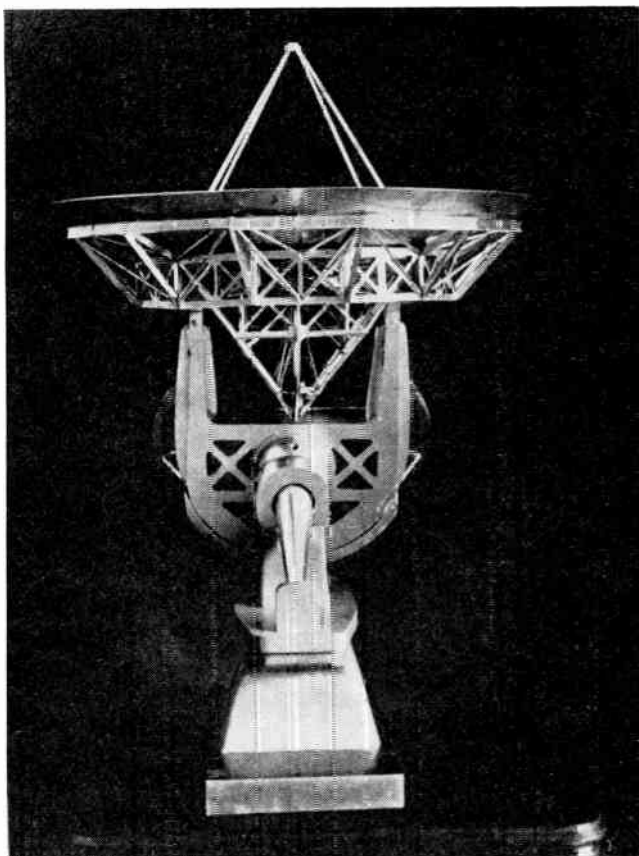


Fig. 6—Photograph of a model (about 1:60) of the 140-foot telescope, built for wind tunnel tests.

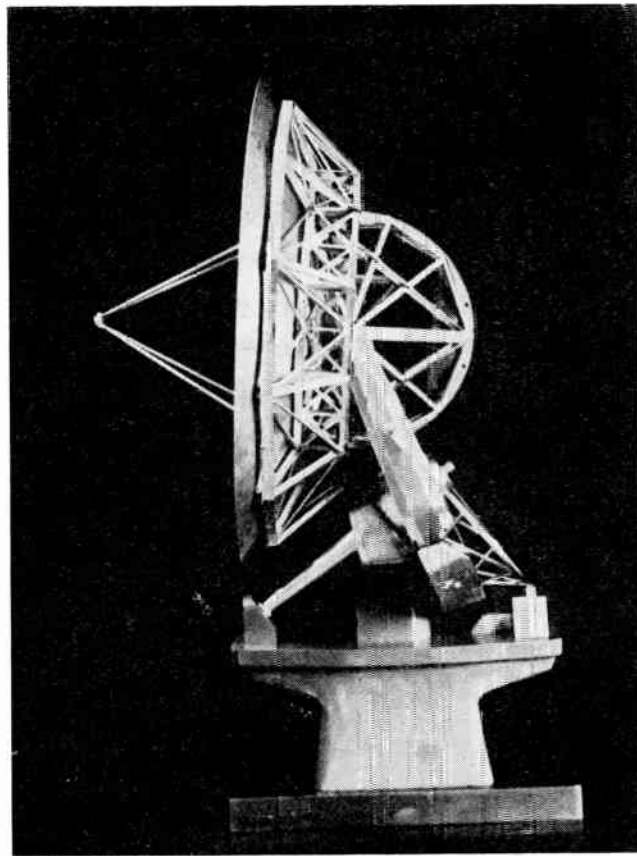


Fig. 7—Another photograph of the model; note the tilted (side view) polar shaft, which will be adjusted to be parallel to the axis of the earth.

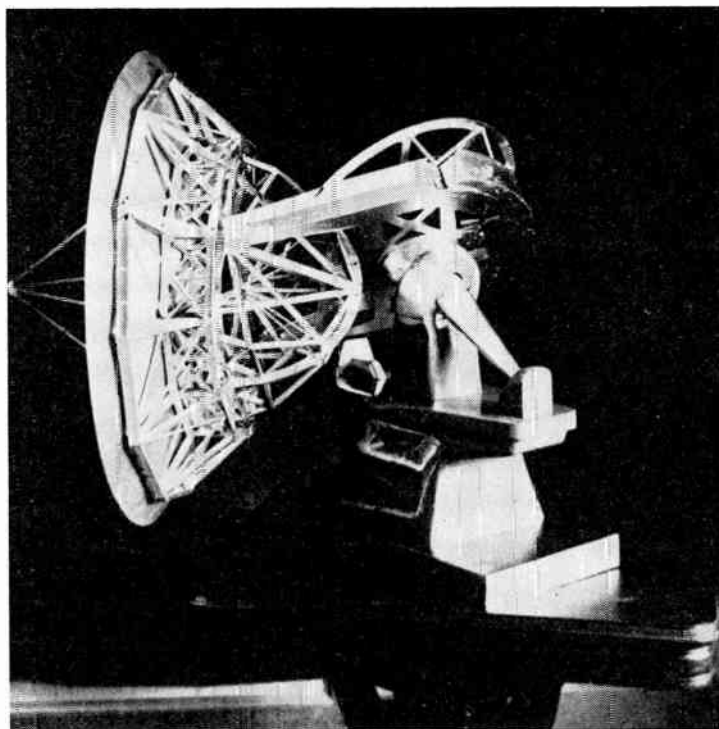


Fig. 8—The end view shows the general configuration of the yoke, declination axis, and reflector.

120-knot wind, the overturning moment in the east-west direction is 16,670-foot kip<sup>27</sup> and in the north-south direction, is 17,880-foot kip. The foundation has been conservatively designed to withstand these forces and torques. The foundation tower has a 51×52-foot cross section at ground level that decreases to 45×34 feet just beneath the gussets that support the top platform, which measures 95×39 feet. A nominal wall thickness of 3 feet has been adopted throughout. Approximately 2850 cubic yards of concrete will be needed.

The polar shaft is mounted on two oil pad bearings,<sup>28</sup> similar in concept to those employed successfully on the 200-inch Palomar telescope. The bearing on the upper, or north, end of the polar shaft is formed around a segment of a sphere of 11-foot radius. The center of gravity of the telescope can be kept near the center of the sphere. The bearing at the lower, or south, end of the polar shaft is only 5 feet in diameter. This lower or tail bearing can be adjusted in position, thereby moving the polar axis about the center of the upper bearing and thus permitting the alignment of the polar axis. The tail bearing will also counteract wind torques. These bearings present some difficult fabrication and erection problems because the surfaces must be smooth and accurate to within a few thousandths of an inch.

The yoke at the north end of the polar shaft is not set perpendicular to the shaft. In a preliminary design for the telescope the yoke was slightly longer than in the present design and the angle between the yoke and polar shaft was 51°, the complement of the latitude of the observatory site. With this arrangement, when the telescope was in the meridian, the yoke arms would be vertical and the reflector could be turned from the south horizon through the zenith to the north horizon, thereby providing complete coverage of the sky. Persuasive arguments were made by some members of the advisory group that significant savings in the cost of the telescope could be achieved if the complete sky coverage was sacrificed. Insofar as purely celestial objects are concerned, any object below the pole can be observed above the pole twelve hours later. Thus the subpolar region of the sky would be of interest only in association with transitory phenomena and geophysical phenomena, such as the aurora, that never complete a circumpolar circuit. After much deliberation, the sky coverage was reduced, corresponding approximately to that of the 200-inch Palomar telescope. In retrospect, this reduction in sky coverage will result in only a small saving, perhaps of the order of one per cent of the total cost of the telescope; really large savings could be made only if the sky coverage were drastically reduced, which is, of course, unacceptable for a general purpose instrument.

The yoke consists of two arms, 64 feet long and with a cross section in the shape of a simple Greek cross that

measures 12×12 feet 6 inches at the base and tapers to 8×9 feet at the top. The lower end of the yoke is appropriately cross-braced. Concrete counterweights are placed in the lower part of the yoke and also in the central portion of the polar shaft.

Attached to the yoke and set perpendicular to the polar shaft is a segment of a wheel of 42-foot radius. The decision to adopt a large radius wheel is in sharp contrast to the designs for the Harvard 60-foot telescope and the 25-m telescopes at Dwingeloo, the Netherlands, and at Bonn, Germany. Large radius wheels were adopted in design studies made independently by Feld, Husband, Kennedy, Reber, Tuve, and Tatel. While it is true that precision gears are routinely made with smaller radii, the consensus was that comparable angular precision could be obtained with a large radius and by this solution problems of gear tooth loading could be much simplified. The main polar axis gear will have 618 teeth of 3½-inch circular pitch and with a 12-inch face. Safety brakes will be applied to the rim of the wheel, thereby further reducing the loading on the gear teeth when the telescope is subjected to very high winds or other unusual conditions.

The declination bearings are standard Torrington self-aligning spherical roller bearings. These bearings are designed to take both radial and end thrust. Either bearing alone can carry the entire load of the reflector and back-up structure under the most severe conditions envisioned. The telescope will be stowed with the telescope pointing in the meridian plane and fairly close to the zenith and, in use, the telescope may be frequently scanned across a few preferred regions of the sky. As a consequence, the loading and use of the bearings will be anything but uniform. No difficulties are anticipated, however, in view of the conservative loads incorporated in the design.

The thermal differential between the steel yoke and the aluminum reflector is accommodated at the declination axis. A steel tube connects the bearings at the top of the yoke arms. Exterior to and concentric with this steel tube is an aluminum tube. The midpoints of these tubes are fastened together by a suitable coupling. The ends of the aluminum tubes are radially adjustable with respect to the steel tube. This adjustability is desired because the reflector is fastened to the aluminum tube and it is necessary that the reflector be aligned so that its axis is perpendicular to the declination axis.

The reflector is rotated about the declination axis by means of a 35-foot radius gear. There was some doubt about the long-term suitability of any available aluminum alloys for the gear teeth, so inserts of bronze have been specified. Bronze has a thermal expansion coefficient sufficiently close to that of aluminum so that no difficulties are anticipated. The declination main gear will have 360 teeth of 3½-inch circular pitch and with a 9-inch face.

The reflector surface is made of ¼-inch aluminum plate made up in 72 panels. These panels, roughly 20

<sup>27</sup> One kip = 1000 pounds.

<sup>28</sup> These bearings have been designed by the Friction and Lubrication Section of the Research Laboratory of the Franklin Institute, Philadelphia, Pa.

feet long and 10 feet wide, are in three groups of 36, 24, and 12, all in any one group being identical. The panels are designed with a sufficient depth of structure behind the surface plate so as to be inherently stiff or rigid to within less than  $\frac{1}{4}$  inch, even for loads (such as from winds) in excess of those due to gravity. Each panel is supported at only four points. Two, at the innermost end of the panel, are matched with cantilevered mounts at the end of the panel on the next inner ring. The other two support points are located at about two thirds the length of the panel, measured from the inner end. This support method was adopted to insure that the ends of the panels would meet in a truly tangential manner and without cusps or other discontinuities in the surface. It is thus seen that the actual reflector surface is supported by the heavy back structure, which fastens to the declination shaft and gear, at only 148 places, including 4 for a special circular panel at the vertex. These 148 connections have been made manually adjustable. Thus the panels may be made to conform to a paraboloid with a precision limited only by the accuracy of the individual panels, the precision of the surface testing procedure, and the patience of the operators. The entire reflector, including back structure and gear wheel, will weigh about 516,000 pounds. The back structure without the panels will weigh 407,000 pounds. An erection procedure similar to that employed by Hooghoudt<sup>29</sup> for the Dwingeloo 25-m telescope is therefore feasible. The back structure will be assembled on the ground, pointing to the zenith and supported at the two declination bearing journals. Standard techniques, requiring transits, tapes, and stadia rods, may be employed to adjust the 148 shoes, where the panels will be fastened, to the predicted paraboloid with a tolerance of perhaps 1/16 inch. If the structure is then lifted and placed on the telescope without mishap, the panels can be raised and placed in position and the reflector should be correct to within the 1/16-inch tolerance of the mounting shoes and the deviations of the individual panels.

Several techniques have been suggested for surveying the surface of the paraboloid. If the telescope is pointed to the zenith, standard transit and tape methods may be employed. Standard surveying techniques are not easily applied for other aspects away from the zenith and become impossible when the telescope is turned to point near the horizon. Whatever method is adopted should, of course, have an intrinsic precision better than the tolerance set for the paraboloid surface; a precision of  $\frac{1}{8}$  inch or less is therefore desired for the survey procedure. Modified survey techniques have been suggested, including some requiring the use of invar wires and strain gauges; such methods perhaps could be made to be satisfactory if sufficient development efforts were devoted to them. Stereophotography, which has been used with great success for mapping and more recently for studying the instantaneous reaction of bridges and

similar structures to moving loads, could be made to work. The desired precision of  $\frac{1}{8}$  inch would require, however, the use of the very finest cameras mounted on fixed 70-foot piers, the very careful measurement of the plates in a comparator, and the lengthy and tedious reduction of these data that could, of course, be speeded up if the reduction were programmed for a high-speed computer. The consensus was that this would not be an ideal solution for the survey problem, both because of the limitations imposed by the fixed piers and because of the large effort (and, hence, time) required to obtain the result.

An ideal survey method, in addition to providing the desired precision, should be applicable for any position of the reflector and should give results quickly in order to facilitate on-the-spot adjustment of the surface panels. Also, the survey method should interfere as little as possible with the normal observational use of the telescope. Various optical schemes have been suggested. Some would check on a finite number of fiducial points, *e.g.*, a point at each of the 148 attachment shoes; these usually depend upon the precise measurement of angles with the assumption that the radial distance from the vertex has not changed significantly. Such techniques would be acceptable for a survey of the inner portion of the reflector but are marginal for the outer ring. Another optical technique involves distance measurement, *e.g.*, from a position near the focus to a mirror located in the reflector surface. The method employs a light beam that is modulated at a frequency that can be handled with routine electronic techniques and the distance measurement, or differential measurement which involves the equivalent of a phase shift determination. An interesting development of this principle is commercially available in the "geodimeter."<sup>30</sup> The models now on the market were designed for precision surveys over longer distances than the focal length of the paraboloid and, while the percentage accuracy is very good, the absolute accuracy does not meet our requirements. A new model now under development may have the necessary precision, but the time required to check only 148 points on the paraboloid would probably be excessive.

Various sonar schemes have been suggested, but upon more careful investigation none have been promising. Various radar schemes have been considered, including those employing pulse techniques as well as phase sensitive schemes essentially equivalent to the geodimeter. Of these, several suggestions by Pedersen<sup>31</sup> have much merit and promise.

The support of the rf feed is not a structural part of the reflector. Divergent views were obtained on the best type of support. A central mast with suitable guys would have certain advantages and could be employed for

<sup>30</sup> Svenska Aktiebolaget Gasaccumulator, "AGA Geodimeter," Stockholm, Sweden; 1956. U. S. representative: Berg, Hedstrom & Co., Inc., 1170 Broadway, New York, N. Y.

<sup>31</sup> Norman Pedersen, private communication, Russell Sage Laboratory, Rensselaer Polytechnic Inst., Troy, N. Y.

<sup>29</sup> G. B. Hooghoudt, private communication.

supporting dipole feeds and special types of inverted horns. Bipods with guys, tripods, and quadripods appear generally to offer more flexibility. A quadripod will be built for the 140-foot telescope; this decision was based on consideration of stability, symmetry, and adaptability to a variety of feeds and receiver components. If desired at a later date, another type of feed support may be easily substituted.

A great deal of thought was given to the side-lobe and back-lobe effects of the feed support. In general practice, side lobes may be 20 db down from the central beam and back lobes may be 30 to 40 db down. For many installations, *e.g.*, in an aircraft or part way up the mast of a ship, there are so many other nearby objects to increase spurious side lobes that attempts to refine the feed support and reduce the inherent side lobes and back lobes

are not warranted. This situation does not pertain to large radio astronomy telescopes. If the 140-foot telescope will have 20-db side lobes, these will have appreciable directive gain. It is therefore desirable to reduce the side lobes and back lobes to levels below those usually accepted. Studies of this problem have been planned, the results of which will be reported later.

#### ACKNOWLEDGMENT

Many individuals have contributed to the work reported herein, including those named in the text and references, and J. W. Findlay and D. S. Heeschen of the AUI staff. All share credit for bringing the radio telescope program to its present status, and we express our thanks and appreciation to them and to the NSF staff members associated with the work.

# Noise Levels at the National Radio Astronomy Observatory\*

J. W. FINDLAY†

*Summary*—The measurements which have been made of the field strengths of radio signals received at the Green Bank site of the National Radio Astronomy Observatory are described. The site is relatively free from interference and the measures which are being adopted to preserve its radio quietness are discussed.

#### INTRODUCTION

THE PURPOSE of this paper is to discuss briefly the levels of man-made noise which exist at the location which has been chosen as the site of the National Radio Astronomy Observatory.

The smallest radio signals which can be detected in radio astronomy are at present determined mainly by the noise figures, stability, and bandwidths of receivers and by the sizes of the antenna systems used. In the future, however, it is reasonable to foresee that the use in receivers of low noise crystals, traveling wave tubes, or masers, and the development of larger antennas, will bring about the state of affairs in which the limit of usefulness of a radio telescope will be set by the noise at the observing site. Part of this noise comes from man-made sources. A part which will also become more important as better receivers are developed, comes from radiation from the ground and surrounding objects entering the receiving system of the radio telescope. This latter source of noise is not considered in the present paper,

since current receiver techniques are not yet so good as to make it a limiting factor in the performance of a radio telescope. However, fairly soon it will be an important factor to consider in the design of future radio telescopes. The present paper discusses first, the approximate levels of the smallest signals which have been detected so far in radio astronomy, next, the levels of noise at the site of the National Radio Astronomy Observatory are described, and last, the measures which have been taken to reduce to a minimum any future deterioration of the site are discussed.

#### THE SIGNALS RECEIVED IN RADIO ASTRONOMY

A survey of the results of various observers over a wide range of frequencies allows of an order of magnitude to be stated for the lower limit of the flux density which is detectable with present day techniques and instruments. This minimum detectable flux is about  $10^{-25}$  watts per square meter in 1 cps bandwidth. This is, of course, a figure which is right only to an order of magnitude, but it generally describes the results for frequencies from about 50 mc up to 10 kmc. Improvements of an order of magnitude at least are to be expected when results from larger antennas and from new receiver techniques are available.

However, the present figure illustrates the magnitude of the problem of avoiding interference from man-made

\* Original manuscript received by the IRE, November 11, 1957.

† Associated Universities, Inc., New York, N. Y.

sources. A transmitter which radiates isotropically  $1 \mu\text{v}$  per cycle per second of bandwidth gives this minimum detectable flux at a free space range of nearly 1,000,000 km.

Every available technique for shielding the radio astronomy antennas by suitable choice of site and for reducing the side lobes and back lobes of the antennas must be employed. Sources of interference which are acceptable in communication systems may require much further screening and suppression if they exist near a radio astronomy site.

#### LEVELS OF MAN-MADE NOISE AT GREEN BANK

The choice of Green Bank, W. Va., as the site of the National Radio Astronomy Observatory was made partly as a result of the low levels of radio signals received in that area. During the site selection process, measurements of field strengths of radio signals were made at a number of possible sites. These measurements were made by Jansky and Bailey, Inc., of Washington, D. C., using the equipment outlined in Table I. The results of

TABLE I  
EQUIPMENT USED FOR FIELD STRENGTH SURVEYS

Frequency range	Equipment used	Antenna used	Minimum detectable field strengths
120 kc-18 mc	RCA 308A Field Intensity Meter	3 loop antennas	20 $\mu\text{v}$ /meter
20 mc-400 mc	AN/URM-47	Resonant dipole	1 $\mu\text{v}$ /meter to 10 $\mu\text{v}$ /meter
375 mc-1000 mc	Stoddart Field Intensity Meter NM50A	Resonant dipole	40 $\mu\text{v}$ /meter to 200 $\mu\text{v}$ /meter
1.0 kmc-10.75 kmc	AN/URM-42	Cone antenna	400 $\mu\text{v}$ /meter to 2000 $\mu\text{v}$ /meter

these measurements for Green Bank, in October, 1955, in the frequency range from 20 mc to 10 kmc are shown in Fig. 1.

It will be realized readily that the signals recorded in Fig. 1 are very large compared with the low levels at which radio astronomy measurements are made. Nevertheless, the primary purpose of the survey, which was to insure that the site chosen suffered a minimum of interference from signals generated at a considerable distance from the observatory, was very adequately fulfilled.

Other measurements have been made at Green Bank since the site has been occupied. Locke and Argyll from the Dominion Observatory of Canada, made measurements at Green Bank in March, 1957. The results of their survey are given in Fig. 2. These measurements were made with equipment which was capable of detecting a signal level approximately 20 db lower than the earlier survey. This increase in sensitivity was acquired by using an antenna of about 10 db gain and since this gain

was not very accurately known the increased sensitivity of the equipment was achieved at some loss of absolute accuracy in the results.

An attempt was made in June, 1957, to detect radiation from the overhead power lines in the neighborhood of the radio telescope sites. A group of engineers from the Westinghouse Electric Corp., Baltimore, joined with representatives of the Monongahela Power Co. in making measurement near various typical overhead lines. The lines tested were carrying either 7200-v single-phase or 13,200-v three-phase current on wooden poles about 25 feet from the ground. Receiving equipment covering the frequency ranges 950 mc-2040 mc and 7.3 kmc-11.26 kmc was operated about 5 feet above the ground below the lines with a directional antenna pointed toward the lines. The minimum detectable field strengths were about 50 microvolts per meter at 1200 mc and 500 microvolts per meter at 11 kmc. No noise above these limiting fields was detected, except in the special case when an arc was intentionally drawn from a 7200-volt line to earth. This produced a small signal, just audible in the receiver noise, at frequencies near 1150 mc.

The results of the foregoing experiments cannot, of course, determine the limiting noise levels at the Green Bank site. However, all the evidence so far goes to support the view that the site chosen is very free from electrical noise. Now that the site is occupied, more measurements will be made using the techniques of radio astronomy to study more closely the noise levels and to determine, if possible, the sources of any noise that is found.

#### THE PROTECTION OF GREEN BANK FROM FUTURE INTERFERENCE

A number of steps have been taken to insure that the observatory site will be protected as far as possible against any future increase in the levels of radio noise. Indeed, it is hoped that a continued program of interference reduction will result in the site becoming more quiet to match the probable improvements of radio astronomical techniques.

A total area of land of about 2700 acres is being acquired for the observatory site. This quite large area will give very adequate facilities for large antenna systems, and it has the additional advantage of allowing particularly sensitive instruments to be located well within the perimeter of land under the control of the observatory, and thus be isolated from local noise.

Starting from the perimeter, and working outwards, restrictive covenants are being acquired on the land of adjacent land owners. These covenants are an agreement that no electrical equipment will be operated on the land that causes interference to the instruments at the observatory. The actual land area which will be covered by these covenants is not yet determined, but it is certain that very valuable additional protection against interference will be obtained in this way.

An important factor in deciding on the site for the ob-

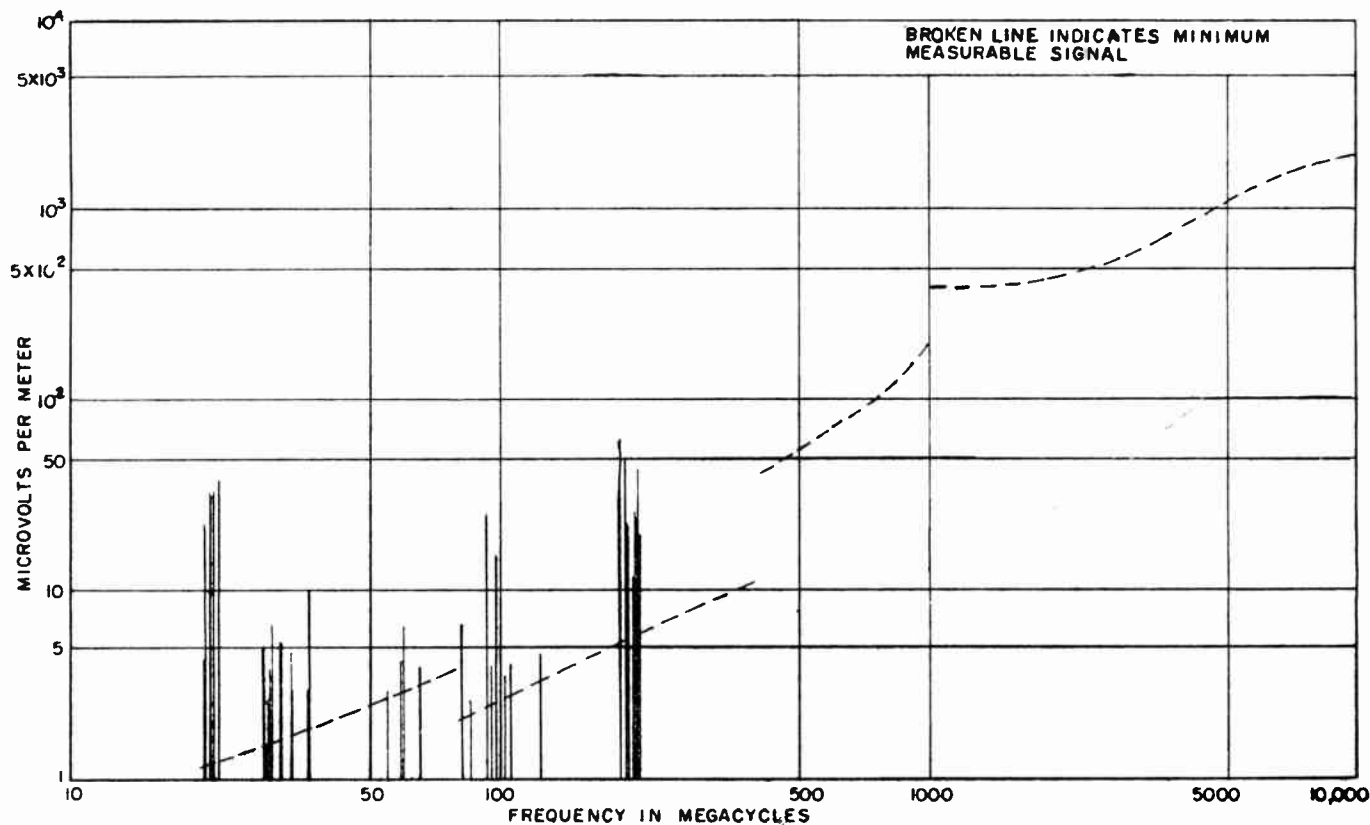


Fig. 1—Measured field strengths of radio signals received at Green Bank on a weekday in October, 1955.

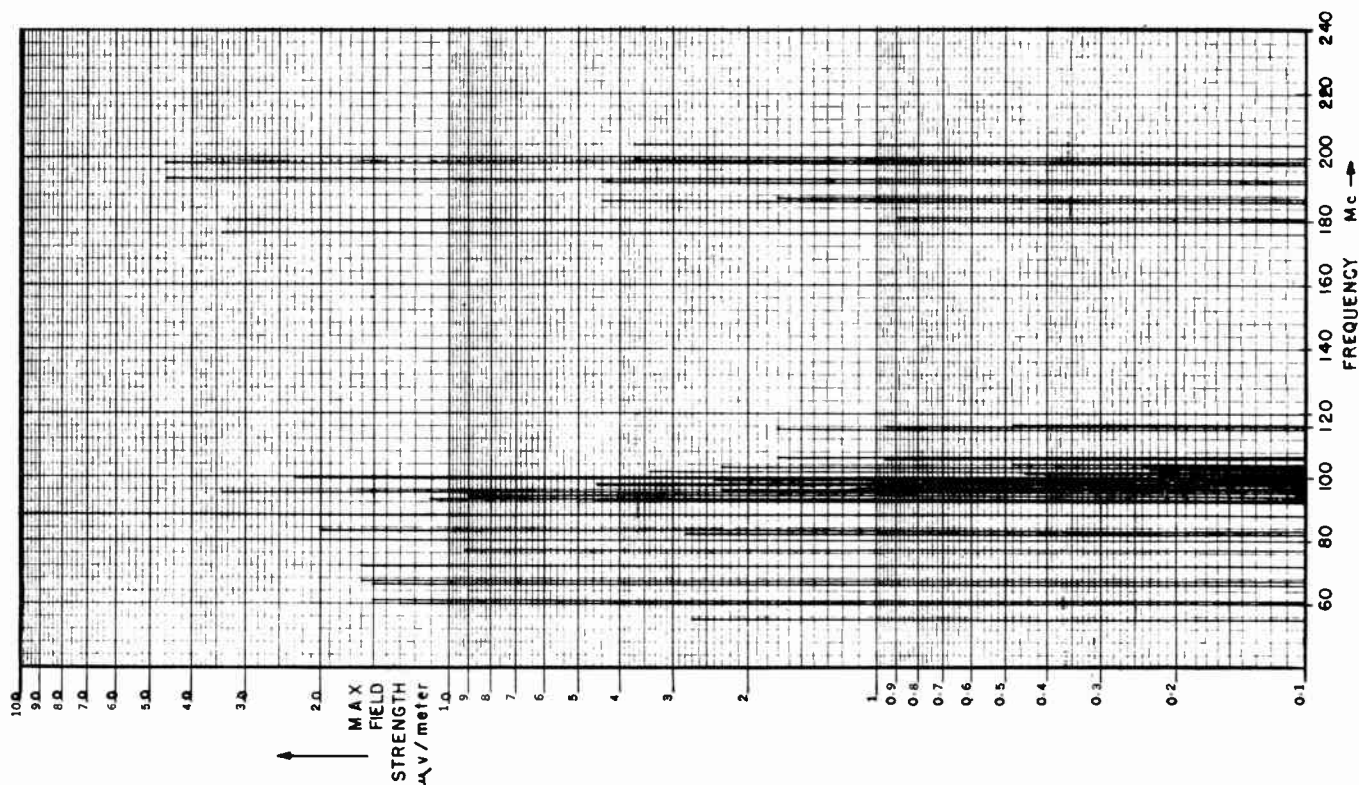


Fig. 2—Approximate field strengths of radio signals received at Green Bank in March, 1957.

servatory was that the State of West Virginia was prepared to introduce legislation for the protection of the site from interference. A bill, known by short title as the "Radio Astronomy Zoning Act," was passed on August 9, 1956, by the State of West Virginia. This bill restricts the operation, within 10 miles from the observatory, of any unlicensed electrical equipment which generates interfering field strengths greater than certain prescribed limits.

The site of the observatory lies in a flat valley, at an elevation of about 2700 feet, surrounded by ranges of mountains rising about 2000 feet above the level valley floor. This topography was chosen since it provides the best possible screening of the antennas from radiation which might reach them from distant radio transmitters. Although some such radiation does exist, as is evidenced by Fig. 1 and Fig. 2, its effect in obscuring considerable parts of the frequency spectrum is not serious. However, to insure that the present situation should not deteriorate in the future, specific measures to limit the increase of licensed radio radiation into the valley are essential. Submissions, therefore, have been made to the Federal Communications Commission for the limitation of radiation from licensed radio transmitters. These submissions, which were presented by Dr. Lloyd V. Berkner, President of Associated Universities, Inc., and by Dr. Alan T. Waterman, Director of the National Science Foundation, were based on the primary importance to the United States of good fundamental research in radio astronomy. Protection of two kinds was requested. First, the existence of the radiation from neutral hydrogen at a frequency of 1420 mc provides the only presently known line radiation in radio astronomy. This radiation may be observed directly, or absorption of radio waves of the same frequency can be studied. The atoms responsible for the emission or absorption may be in motion relative to the observers on the earth, and so the frequency observed may differ by a Doppler shift from 1420 mc. There is, therefore, a very good case for clearing that part of the frequency spectrum near 1420 mc from all transmissions. The FCC was asked to consider clearing the frequency range from 1400–1427 mc over the whole of the United States.

The second kind of protection which was requested was specific to the observatory at Green Bank. Since it is intended that the National Radio Astronomy Ob-

servatory should be a center for research open to qualified scientists from all institutions, an attempt should be made to accord it particular protection.

Accordingly, the following requests were made to the FCC:

- 1) Flag all new applications which are made by operators within 50 miles of Green Bank, except mobile operations. Consult with a group of scientists designated by AUI at Green Bank on any interference problem which might arise from the new applications and work out each problem on a case-by-case basis. This same group should review interference problems created by existing uses, and reach solutions if possible.
- 2) Exchange where possible tv channels 53 and 54 with other uhf tv channels so that as far as possible no tv transmitter operates on channels 53 and 54 within 150 miles of Green Bank. (The frequency concerned here is 700–712 mc, the half-frequency of the hydrogen line.)
- 3) Adopt the same procedure as in 2) for tv channel 14. (The frequency concerned here is 472–476 mc, the one-third frequency of the hydrogen line.)
- 4) Require any tv station in channels 14, 53, and 54 which remain within 150 miles of Green Bank to attenuate their harmonics to 80 db below carrier level.

These requests follow the pattern of extending the protection of the hydrogen line frequency, by asking in 2), 3), and 4) for a restriction of radiation of the subharmonics of the line from stations near to Green Bank, and also suggest in 1) a means by which the effects of interference from licensed operators near Green Bank can be reduced to a minimum.

The measures which have so far been taken for protecting the Green Bank site will, it is hoped, result in the maintenance, and possibly the improvement, of an already good site for radio astronomy in the United States of America.

#### ACKNOWLEDGMENT

We gratefully acknowledge the work of all who have assisted in making the measurements of radio interference at Green Bank, and particularly Jansky & Bailey, Inc., Dr. Locke and E. Argyll, the Westinghouse Electric Corp., and the Monongahela Power Co.



# Radio Astronomy at the Meudon Observatory\*

E. J. BLUM†, J. F. DENISSE†, AND J. L. STEINBERG†

**Summary**—This paper describes the principal instruments used for radio astronomical observations at the Nançay field station. They are a variable spacing interferometer made of two 7.5-meter mirrors movable on rail tracks, several radio-telescopes and interferometers for solar research at 3-cm wavelength, and a 32-antenna interferometer operating on the wavelength of 177 cm. The second part of the paper gives some new results concerning the sources of solar radio emission and a phenomenon of scintillation at 3-cm wavelength apparently caused by the troposphere.

## THE NANÇAY OBSERVATORY

THE Nançay radio astronomy field station is located 120 miles south of Paris in a region, up to now, free from man-made interference. A building (Fig. 1) housing 15 persons, including rooms, dormitory, and workshops, was erected on a section of flat land about one mile long in both the east-west and the north-south directions. It has been designed to meet the requirements for the first few years of operation of the station. Other buildings are being built now. Electrical power is distributed through the land by underground armored cables. Observing sites in the station are connected by telephone and by special network for distribution of time signals, both solar and sidereal.

The field station includes principally two levelled platforms, 50 meters wide. The first, which is now in use, is oriented east-west, with a total length of 1750 meters; the second, nearing completion, is north-south. Along these platforms, every 50 meters, special plugs provide ac power. Other areas of smaller extent are also provided with facilities for observations.

### *The Variable Spacing Interferometer (Fig. 1)*

In the northern part of the platform that runs east-west, a special rail-track of 6-meters gauge and 1500 meters long has been built. On this track, antennas used for different purposes can be moved easily. During 1957, a second rail-track, oriented north-south will be completed; it intersects the first one near its center.

The variable spacing interferometer built on this T-shaped track uses two parabolic antennas, 7.5 meters in diameter, of German origin (Giant Wurzburg). They are equatorially mounted; motion in right ascension is achieved by 3 electrical motors coupled by differential gear boxes. Speeds of rotation are 15 minutes, 6° and 36° per minute. The same system is used for declination drive with only two motors. Position angles are indicated by selsyns with an accuracy of about 1 minute of arc. The mechanical stiffness of the mount is sufficient to maintain a pointing accuracy of the same order. This

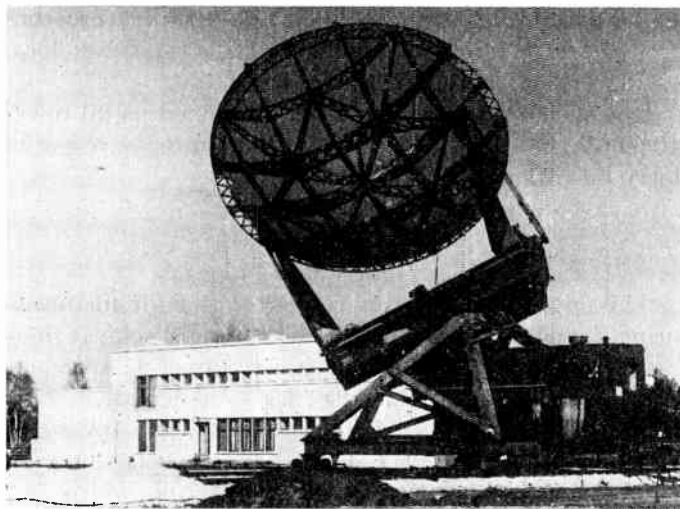


Fig. 1—One mirror of the variable spacing interferometer.

instrument is going to be used first on fixed frequencies near the 1420-mc hydrogen line for galactic and solar studies.

### *The 3-CM Wavelength Equipments*

Several equipments are operated on 3 cm essentially for solar studies. Size, intensity, brightness distribution of bright solar regions can be investigated with an interferometer operating on 9350 mc.<sup>1</sup> The two parabolic antennas are 2 meters in diameter, equatorially mounted, and separated by 60 meters. The base line is oriented east-west and the antennas are automatically driven to follow the sun. The resolving power of this instrument is about 1.5 minute of arc near the meridian and as the angular separation between the interference fringes varies with the diurnal motion of the sun, this apparatus can be used as a variable spacing interferometer for brightness distribution studies. Owing to the large distance between each antenna and the main receiver, separate mixers and IF preamplifiers mounted close to the antennas are used. The local oscillator wave is generated at the electric center of the base line and transmitted through waveguide to each mixer. The 60-mc IF signals are transmitted by coaxial cables to the main receiver, where their frequency is converted to 10 mc and the bandwidth is reduced to 400 kc, to prevent smearing of the fringes. A three-section waveguide filter is used to eliminate one of the input sidebands.

A 4-antenna interferometer with unequal spacing, already described in the literature,<sup>2</sup> also is used on a 3-cm

\* Original manuscript received by the IRE, November 6, 1957.

† Observatoire de Meudon, Service de Radioastronomie, Paris, France.

<sup>1</sup> I. Alon, M. R. Kundu, and J. L. Steinberg, *Compt. Rend. Acad. Sci.*, vol. 244, p. 1726; March, 1957.

<sup>2</sup> J. Arsac, *Rev. Opt.*, vol. 35, pp. 65, 136, 396; June, 1956.

wavelength for solar studies. The effects of the earth atmosphere on microwave propagation have been studied, since 1954, with conventional equipment. The reflectors are surplus searchlight mirrors of 1.5-meter diameter, whose vertical axis of rotation has been tilted to be parallel to the earth's axis. A temperature controlled box fixed on the mount contains the mixer, local oscillator, and IF preamplifier.

One such antenna is mounted on a fixed metal tower 10 feet high. A similar equipment is mounted on a special lorry movable on the rail tracks.

### *The 32-Antenna Interferometer (Fig. 2)*

This high resolution instrument was built for measuring the positions and intensities of bright solar regions radiating in the meter range. It consists of 32 antennas erected on an east-west base; its total length is 1550 meters. This array, working on the frequency 169 mc, is analogous to a diffracting grating and its polar diagram in right ascension has several lobes of width 3.8 minutes of arc between half-power points, separated from one another by  $2^\circ$ . This angular separation is large enough to insure that only one individual lobe is pointed on the sun. Each elementary antenna is a parabolic mirror 5 meters in diameter and is illuminated by a dipole and a reflector; it can be rotated around a horizontal axis mounted on a concrete base.

Each elementary antenna is connected, by electrically equal lengths of transmission line, to the main receiver which is in a cabin near the geometrical center of the array. Coaxial cables of a type developed by the French Post Office are used throughout; losses are 25 db for 800 meters length at 169 mc. Thus, the received signals must be preamplified near the elementary antennas. Adjacent pairs of antennas deliver their signals to one of 16 preamplifiers used in the system. Each preamplifier is housed in a weather proofed container. The preamplifier gain is 50 db, the bandwidth is 7 mc, and the noise figure is 5 db. The circuit involves two cascode stages, 2 amplifiers, and the output stage. The stability of the phase rotation across the over-all bandwidth of 2.5 mc of the complete instrument has been carefully tested for any abnormal phase rotation which would badly distort the polar diagram of the array. Single tuned amplifier stages are used throughout. Stabilized supply voltages and gain control voltages are fed to these preamplifiers from the central cabin through neoprene insulated cables. Each preamplifier embodies a noise diode and the observer can check each individual amplifier noise figure and gain from the central cabin. The coaxial cables, whose total length is about 4 km, are deeply buried 80 cm, so that variations in attenuation due to changes in temperature are avoided. With the branching system adopted, the total electrical length from any elementary antenna to the receiver can be held constant within 0.1 wavelength (including the amplifiers).

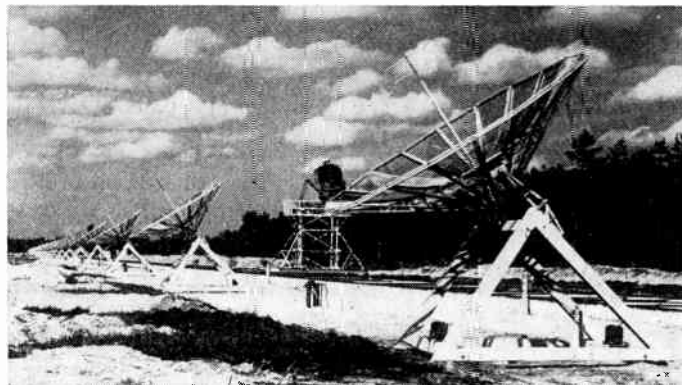


Fig. 2—General view of the 32-antenna interferometer; one of the 3-cm radio telescopes is seen on the rail track.

Signals are recorded, both on electronic servorecorders with linear response and a time constant of one second and on fast recorders with a logarithmic scale and a time constant less than  $1/50$  second.

The total collecting area of this interferometer is 640 square meters. The north-south branch of this interferometer is going to be built in 1957–1958.

The most powerful radio sources, including Hydra A in consideration of its small apparent diameter, are currently used to test the polar diagram and the sensitivity of this equipment.

The Nançay field station is sponsored jointly by the Paris Observatory and the École Normale Supérieure; the maintenance of the station, building of the equipment, observations, and associated researches are carried out by about 20 persons from the Meudon Observatory.

### SOME RECENT RESULTS

Most of the recent observations have been carried out at the Nançay field station with the 32-antenna interferometer and with the 3-cm equipment which has been described above.

The main part of the work for the last two years has been concerned with studies of the solar activity on both meter and centimeter wavelengths; numerous observations were devoted also to the study of atmospheric effects on solar radiation observed at 3-cm wavelength; besides occasional observations of lesser importance, a general survey of the radio sources is now in progress with the large interferometer.

### *Solar Observations*

As is well known, the solar activity in the meter wavelength range is mainly characterized by the occurrence of highly fluctuating sources (called *R* centers) of very intense radio emission labelled in the literature as noise storms or enhanced radiation. The highly fluctuating character of these sources, which are always accompanied by type I bursts, make their study rather difficult and, in spite of very ingenious investigations carried out in Australia, little is known about this outstanding phenomenon.

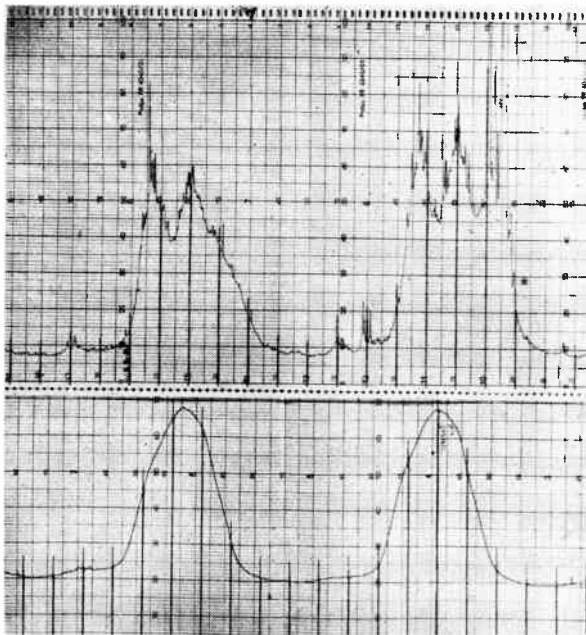


Fig. 3—Drift curves of the sun; above: moderately active; below: quiet.

The large interferometer allows the sun to be scanned each day during 2 hours around local noon with a resolving power of 3.8 minutes of arc. The location of solar radio centers of activity is given with an accuracy of a fraction of a minute and the diameters of sources as small as one minute can be measured.

Daily observations have been carried out since May, 1956. From the drift curves (see Fig. 3) obtained each day and reduced, the location and diameter of the *R* centers are deduced and plotted on a diagram that shows the one dimensional evolution of the sources of activity across the sun's disk (see Fig. 4).<sup>3,4</sup>

The radio centers generally last for several days, but their displacements from day to day are highly irregular and it is often rather difficult to relate without ambiguity a given *R* center with an optical spot. From their mean speed of rotation and their position when they appear on the limb, one can measure the heights of the *R* centers that are found highly variable with a mean value around 400,000 km above the sun's surface. Incidentally, this height is much larger than the critical frequency height calculated from standard data on the solar corona. Diameter of radio centers can vary from one day to another, ranging from less than one minute to 6 minutes, rarely more.

Very often, for periods of several weeks, no center of radio emission is observed, in spite of the occurrence of large and active optical spots; then one radio center flares up, soon followed by several others widely separated in heliographic longitude, showing some kind of collective property that does not seem to have any optical counterpart (see Fig. 4).

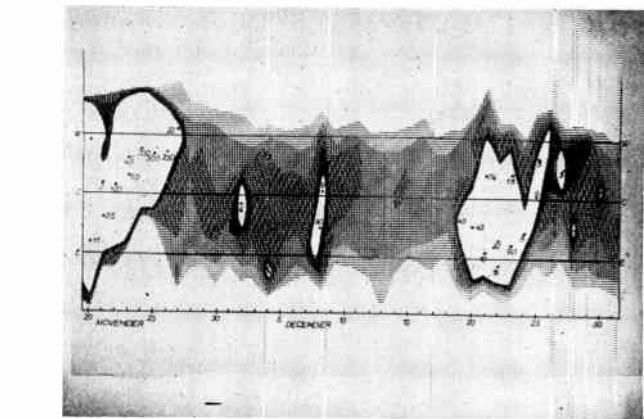


Fig. 4—Diagram showing daily position in right ascension of the *R* centers; E-W is the horizontal diameter of the optical disk. Peaks amplitudes are indicated in  $10^{-22} \text{ W m}^{-2} (\text{cps})^{-1}$ .

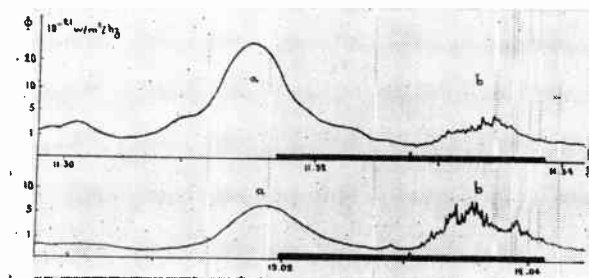


Fig. 5—Drift curves of the sun on November 20, 1956, showing: a) a type IV burst (storm phase), b) an *R* center.

rated in heliographic longitude, showing some kind of collective property that does not seem to have any optical counterpart (see Fig. 4).

In the course of this investigation a new type of solar radio emission was clearly identified.<sup>5</sup> The 200-mc observations of Dodson, Hedeman, and Owren have indicated that outbursts of radioemission associated with solar flares can be separated into two distinct phases. In the first or *main* phase the noise level rises suddenly and lasts for about 10 minutes; in the second, or *storm* phase which starts soon afterwards, the level rises much more gradually and stays very high for hours. The radiation of the storm phase is circularly polarized and was believed to be identical to the noise storms.

Observations with the large interferometer disclosed new information on the storm phase which indicates that it is an entirely new type of solar radio emission. Fig. 5 shows drift curves obtained on the sun with an ordinary *R* center and an outburst (storm phase) together on the disk. The difference between the two types of radiation is striking: the outburst (called type IV by Boischoth<sup>5</sup>) is completely free of type I bursts characteristic of noise storms. Furthermore, the diameter of the quiet type IV source is larger than the diameter of the *R* centers; it can reach about 10 minutes of arc between half-power points. Sometimes, especially at the begin-

<sup>3</sup> E. J. Blum, A. Boischoth, and M. Ginat, *Compt. Rend. Acad. Sci.*, vol. 243, p. 19; July, 1956.

<sup>4</sup> Y. Avignon, E. J. Blum, A. Boischoth, R. Charvin, M. Ginat, and P. Simon, *Compt. Rend. Acad. Sci.*, vol. 244, p. 1460; March, 1957.

<sup>5</sup> A. Boischoth, *Compt. Rend. Acad. Sci.*, vol. 244, p. 1326; March, 1957.

ning rapid motions of the order of 500 km are observed. All of these properties make the source of the storm phase an object distinct from the  $R$  centers or, at least, a very extreme case. It is interesting to speculate about the possibility that this emission is due to synchrotron radiation emitted by fast electrons produced along with the cosmic rays that are known to be associated with certain flares; this suggestion is supported by the very high intensity of the emission that precludes a thermal origin, and the smoothness and large size of the source that is likely to be produced by a microscopic process.

Other observations are progressing with the two antenna 3-cm interferometer; diameters of localized regions of steady emission which account for the slowly varying component were found of the order of 5 minutes of arc, and valuable results were also obtained on the outbursts<sup>1</sup> (Fig. 6).

#### Solar Scintillations in the 3-CM Wavelength Region

Several experiments are concerned with the study of solar scintillations that were discovered to exist on a wavelength of 3 cm.<sup>6</sup> This phenomenon has a twofold interest. As such, it limits the seeing for radio astronomical observations, especially at low elevations, but it is also a powerful tool for studying atmospheric inhomogeneities probably responsible for the anomalous radio propagation within or beyond the horizon.

The first studies were devised<sup>7,8</sup> to assess the atmospheric origin of the scintillations. Comparing records of the sun's radiation obtained with two different radiometers, it was found that identical patterns of scintillations are obtained as long as the two antennas are not separated by more than about 100 meters; the correlation becomes weak when the receivers are more than 200 meters apart (see Fig. 7). The correlation coefficient between the two records is roughly given by:  $\rho(D) = e^{-(D/170)^2}$ , where  $D$  in meters is the distance between the two lines of sight of the radiometers.

The amplitudes and pseudoperiods of the scintillations increase with the zenithal distance; their occurrence is strongly related to the existence on the sun of localized regions of steady emission whose diameter is about equal to 5 minutes of arc. The whole disk of the quiet sun appears to be too large in diameter to produce scintillations. On the contrary, some radio outbursts of the very narrow diameter of the order of 1 minute of arc, give rise to large increases in scintillations.

Experiments to find the origin of the scintillations and height of the turbulent layers were performed along two lines; in one series of experiments comparisons were made of scintillations observed on 3 cm and 33 cm. The same kind of scintillations were observed on both wave-

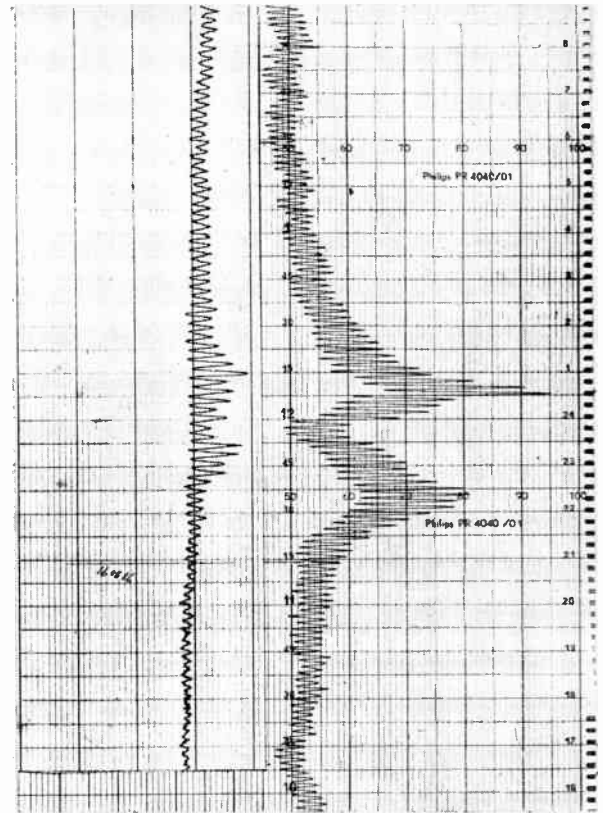


Fig. 6—Interferometric records of 3-cm double bursts showing different fringe visibility; the burst on the left has the smallest diameter.

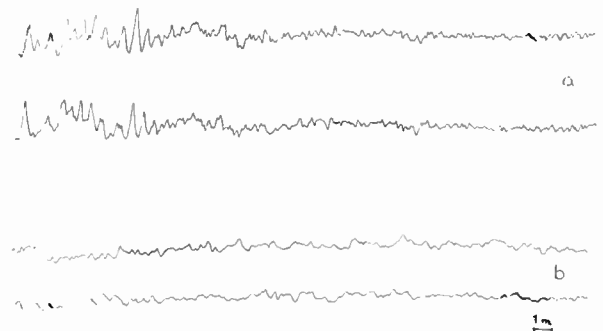


Fig. 7—Simultaneous record of solar scintillations with two antennas at distance  $D$ : a)  $D=60$  m; good correlation ( $\rho=0.88$ ), b)  $D=460$  m; no correlation ( $\rho=0.05$ ).

lengths, but they were rather weaker on the longer wave showing that the phenomenon was very probably not of ionospheric origin. In another series of observations one component of the wind existing in the turbulent layer was estimated by measuring time lags existing between two records obtained simultaneously with different antennas. Some results are given in Fig. 8 where the measured winds are compared with the corresponding component of the winds measured by the Trappes Meteorological Station situated 200 km northwest of Nançay. It is quite noticeable that the radio winds and the winds measured of the height of the tropopause are always of the same sense and also of comparable magnitude. These results suggest that the observed scintillations take

<sup>6</sup> I. Kazès and J. L. Steinberg, *Compt. Rend. Acad. Sci.*, vol. 240, p. 493; January, 1955.

<sup>7</sup> I. Kazès, *Compt. Rend. Acad. Sci.*, vol. 245, p. 636; August, 1957.

<sup>8</sup> I. Kazès and J. L. Steinberg, *Compt. Rend. Acad. Sci.*, vol. 245, p. 782; August, 1957.

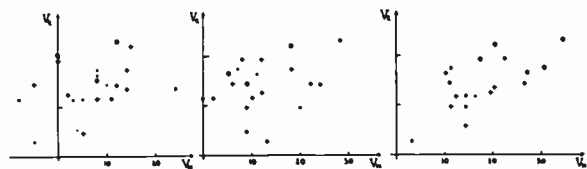


Fig. 8—Comparison of speed  $V_r$  (m/s) of radio winds measured on direction: •: N-S, ○: S-N, +: N-O, -: S-E, with the same component  $V_m$  of meteorological winds measured at different heights, from left to right: 500–1500 m, 5000–6000 m, tropopause (9000–13,000 m).

place in the low atmosphere in a region close to the tropopause.

Besides the topics outlined here, the Meudon Observatory Group is also actively engaged in research concerned with solar-terrestrial relationships, absolute measurements, galactic structure, theoretical studies, etc.

Work on solar terrestrial relationship is mainly due to Simon. He has first confirmed and extended<sup>9</sup> the findings by Denisse of a definite relation between the occurrence of solar enhanced radiation on meter wavelengths and the increase of geomagnetic activity. He was able to demonstrate furthermore a very close control of the solar radio noise on the geomagnetic perturbations following the onset of the brightest chromospheric flares.<sup>10</sup>

Along different lines, Kundu and Denisse<sup>11</sup> found a

<sup>9</sup> P. Simon, *Ann. Astrophys.*, vol. 19, p. 122; May–June, 1956.

<sup>10</sup> P. Simon, *Ann. Géophys.*, vol. 12, p. 167; July–September, 1956.

<sup>11</sup> J. F. Denisse and M. R. Kundu, *Compt. Rend. Acad. Sci.*, vol. 244, p. 45; January, 1957.

close and linear relation between the 10-cm solar radiation and the ionizing flux of the  $E$  layer as measured by the index  $(f_oE)^4/\cos Z$ . This relation shows that the  $E$ -layer ionization is more closely related to the 10-cm solar radiation than to the sunspots themselves or to the coronal green line intensity. This result stresses the interest of the 10-cm solar radiation as an index of solar activity.

Observations by Le Roux led to a complete mapping of the sky brightness on the wavelength 33 cm.<sup>12,13</sup> On the same wavelength absolute measurements were also carried out on the brightest radio sources and on the sky.<sup>13</sup>

Theoretical works are concerned with the physics of plasma,<sup>14–17</sup> the theory of ionospheric interaction (Luxembourg effect),<sup>18</sup> and the studies by Arzac of antenna performances and design and image formation in radio astronomy.<sup>19,20</sup>

<sup>12</sup> J. F. Denisse, E. Le Roux, and J. L. Steinberg, *Compt. Rend. Acad. Sci.*, vol. 240, p. 278; June, 1955.

<sup>13</sup> J. F. Denisse, J. Lequeux, and E. Le Roux, *Compt. Rend. Acad. Sci.*, vol. 244, p. 3030; April, 1957.

<sup>14</sup> M. Bayet, J. L. Delcroix, and J. F. Denisse, *J. Phys. Radium*, vol. 16, p. 274; November, 1955.

<sup>15</sup> M. Bayet, J. L. Delcroix, and J. F. Denisse, *J. Phys. Radium*, vol. 17, p. 923; December, 1956.

<sup>16</sup> M. Bayet, J. L. Delcroix, and J. F. Denisse, *J. Phys. Radium*, vol. 17, p. 1005; December, 1956.

<sup>17</sup> M. Bayet, J. L. Delcroix, and J. F. Denisse, *Compt. Rend. Acad. Sci.*, vol. 244, p. 171; January, 1957.

<sup>18</sup> M. Bayet, J. L. Delcroix, and J. F. Denisse, *Ann. Télécom.*, 1957, to be published.

<sup>19</sup> J. Arzac, *Optica Acta*, vol. 3, p. 55; June, 1956.

<sup>20</sup> J. Arzac, *Aust. J. Phys.*, vol. 10, p. 16; June, 1957.

## Considerations in High-Sensitivity Microwave Radiometry\*

PETER D. STRUM†, SENIOR MEMBER, IRE

**Summary**—This paper discusses considerations in high-sensitivity microwave radiometry, especially as applied to systems having temperature thresholds significantly less than 1°K. Many considerations that have been ignored in previous analyses are shown to be prominent. The influences of the background radiation from space, atmospheric oxygen, atmospheric water vapor, and earth-bound radiators are shown to set a threshold level. Fluctuations in gain and temperature of the antenna, the waveguide system, the comparison source, the noise balancer, the receiver, and other amplifying components are shown to set another threshold. Impedance-modulation effects set still another threshold. The intrinsic internal receiver noise establishes an irreducible threshold. Continuous nonswitched types of radiometers usually are not suited for high-sensitivity appli-

cations because the present state of the art in gain stability is not adequate. The square-wave switched system is most likely to yield satisfactory results. In these systems the optimum performance is obtained when the magnitude of the signal within the system is minimized at approximately the level at which measurements will be made. This result establishes the requirement for noise balancing which may be either continuously adjusted or adjusted once for each measurement.

### INTRODUCTION

THE observation of radio sources at microwave frequencies requires a high degree of sensitivity. Nonthermal radio sources have a noise spectrum that compensates approximately for changes in antenna gain for a given aperture size. For this reason there is

\* Original manuscript received by the IRE, November 11, 1957.

† Ewen Knight Corp., Needham, Mass.

little to recommend any particular frequency band for detection of nonthermal sources other than the practical requirements of avoiding interference from the generally cluttered radar bands and the necessity for remaining below about 10 kmc for optimum freedom from oxygen and water vapor effects. It will be shown later that for highest sensitivity it is necessary to maximize the pre-detection bandwidth. Here again practical considerations lead to a choice of operating frequency.

The first switched form of microwave radiometer was designed by Dicke.<sup>1</sup> Since that time, improved techniques have become available to permit increased bandwidth and to permit improved over-all stabilization. This paper will discuss these improvements and the effects that they have had on enhancing the importance of some of the other effects.

### DESCRIPTION OF SYSTEMS

A block diagram characteristic of most radiometer systems is shown in Fig. 1 with an expression for the differential temperature threshold. The symbols in the expression are connected by lines to the components that contribute chiefly to them. This expression is

$$\frac{\Delta T}{290} = \left\{ \gamma_1 \rho + \beta \sigma \left[ \frac{(F_e - 1) \gamma_2}{\sqrt{B}} \right] \right\} \alpha \mu \frac{\phi}{\sqrt{\tau}} k \quad (1)$$

where

- $\Delta T$  = the threshold differential temperature,
- $\gamma_1$  = a gain fluctuation factor related to  $\rho$ ,
- $\rho$  = an impedance modulation factor,
- $\beta$  = a background radiation factor,
- $\sigma$  = a radiation factor due to antenna side lobes,
- $F_e$  = effective system noise figure,
- $\gamma_2$  = another gain fluctuation factor,
- $B$  = bandwidth just prior to detection,
- $\alpha$  = a detection constant,
- $\mu$  = a modulation factor,
- $\phi$  = a filtering factor,
- $\tau$  = the output integration time constant,
- $k$  = the operator's criterion of detectability.

This expression for the differential sensitivity contains twelve factors as compared with the usual three or four treated in previous theoretical analyses.<sup>2-4</sup> These factors can be divided into four major categories: those accounting for internal system noise, those accounting for antenna and other effects, those accounting for impedance modulation, and those accounting for gain fluctuations. The last three categories have seldom been discussed.

<sup>1</sup> R. H. Dicke, "The measurement of thermal radiation at microwave frequencies," *Rev. Sci. Instr.*, vol. 17, pp. 268-275; July, 1946.

<sup>2</sup> S. J. Goldstein, Jr., "A comparison of two radiometer circuits," *PROC. IRE*, vol. 43, pp. 1663-1666; November, 1955. This comparison was shown to be in error by D. G. Tucker and M. H. Graham in their correspondence in *PROC. IRE*, vol. 45, pp. 365-366; March, 1957.

<sup>3</sup> J. Galejs, "Comparison of subtraction-type and multiplier-type radiometers," *PROC. IRE*, vol. 45, pp. 1420-1422; October, 1957.

<sup>4</sup> W. Selove, "A dc comparison radiometer," *Rev. Sci. Instr.*, vol. 25, pp. 120-122; February, 1954.

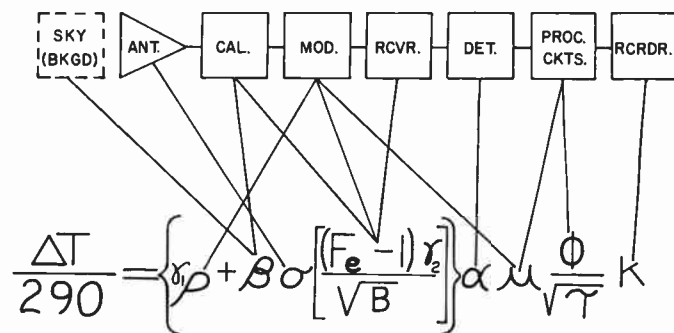


Fig. 1—Block diagram of typical system and the threshold equation showing the influence of the components on the factors in the equation.

Prior to the detailed analysis, a systematic nomenclature is suggested. The major categories are:

- 1) The continuous, or total-power, radiometer with or without dc offset,
- 2) The continuous band-comparison radiometer,
- 3) The continuous two-receiver radiometer,
- 4) The switched source-comparison radiometer,
- 5) The switched band-comparison radiometer,
- 6) The noise-compensated source-comparison radiometer,
- 7) The automatic-null source-comparison radiometer.

Although the continuous, or total-power, radiometer will be shown to have the ultimate sensitivity on the basis of internal receiver noise, the noise-compensated and automatic-null source-comparison radiometers will be shown to have the ultimate sensitivity in the presence of gain fluctuations.

The analysis of the threshold level will be divided into four parts, as indicated above.

### Threshold Due to Internal Noise

For this discussion the following parameters can be considered unimportant:  $\gamma_1$ ,  $\rho$ ,  $\beta$ ,  $\sigma$ , and  $\gamma_2$ . This leaves

$$\left. \frac{\Delta T}{290} \right|_{\text{int}} = \frac{(F_e - 1) \alpha \mu \phi k}{\sqrt{B \tau}} \quad (2)$$

to account for internal receiver noise and the effects of the output processing circuitry.

First, consider the effective noise figure,  $F_e$ . This component is made up of the internal noise of the receiver plus contributions of loss and excess noise in the waveguide, the calibrator, and the modulator. The effective noise figure of the receiver coincides with the standard definition of average noise figure,<sup>5</sup> except for the important case of superheterodyne utilizing direct conversion and having equal signal and image responses. For this case the effective noise figure is one half (3 db less than) the noise figure as given by the

<sup>5</sup> "Standards on electron devices: methods of measuring noise," *PROC. IRE*, vol. 41, pp. 890-896; July, 1953.

standard definition.<sup>6</sup> This reduction in effective noise figure results from the fact that the receiver, under the standard definition of noise figure, is presumed to have one useful pass band, whereas noise from a radio source will enter two equal-width and equal-amplitude pass bands, thus doubling the signal power. It is erroneous to treat this condition as a doubling of the bandwidth instead of a doubling of the power, because the action of the conversion process literally "folds" one of the input bands over on top of the other in such a way that twice as much power is contained in the width of a single band at the output of the converter with no consequent increase in internal noise. Furthermore, the bandwidth, as used in the sensitivity expression, implies the bandwidth that limits the number of samples per second of the signal that reaches the detector. This is determined usually by the predetection amplifier bandwidth only.

The noise figure of a waveguide, calibrator, or modulator can be determined on the basis that each is a passive dissipative element. Analysis of a lossy pad shows the noise figure of such a network to be

$$F = 1 + \frac{T_i}{290} (L - 1) \quad (3)$$

where  $L$  is the loss in the pad due to resistive elements at a temperature  $T_i$ , the thermal or internal temperature. It is seen that reduction of either the temperature to 0°K or the loss to unity will reduce the noise figure of this type of component to 0 db. In fact a reduction of  $T_i$  to a very low value would permit an increase of  $L$  while maintaining  $F$  within reasonable bounds. The inadvisability of such a procedure, however, is shown by<sup>7</sup>

$$F = F_1 + (F_2 - 1)L_1 \quad (4)$$

where  $F_1$  is the noise figure of the first component,  $F_2$  is the noise figure of the subsequent system, and  $L_1$  is the loss of the first component. The loss, therefore, enhances the influence of subsequent components directly.

The calibrator (or noise balancer) may have a contribution to its noise temperature as a result of the deliberate injection of excess noise from a noise generator. Such an injection usually is accomplished by means of a directional coupler on the waveguide between the antenna and the input to the modulator. In some cases an attenuator is inserted between the noise generator and the directional coupler. The excess noise from such an injection system must be stable to the order of magnitude set by the desired threshold level. This means that the coupling factor of the directional coupler and the attenuation of the variable attenuator must be stable as a function of orientation, temperature, and the like. These effects will be discussed under the discussion of gain variations.

The noise figure of a calibrator including the excess noise from a noise generator is

$$F = 1 + \frac{T_i}{290} (L - 1) + \frac{C}{L_A} \left( \frac{T_G}{290} - 1 \right) \quad (5)$$

where  $C$  is the coupling factor of the directional coupler (a ratio less than unity),  $T_G$  is the noise temperature of the noise generator, and  $L_A$  is the loss in the attenuator (a ratio larger than unity).

As mentioned above, the bandwidth  $B$ , is the bandwidth of the circuits just prior to the detector, assuming that these are the narrowest circuits up to that point. Precisely, the noise bandwidth is defined by

$$B = \frac{1}{g_0} \int_0^\infty g(f) df \quad (6)$$

where  $g_0$  is the maximum power gain,  $g(f)$  is the gain-frequency function, and  $f$  is the frequency. In most cases the noise bandwidth coincides with the half-power bandwidth.

In considering the effects of the factor  $\alpha$ , one must consider the influence of the type of detector. A systematic set of detector nomenclature should help to remove some of the misunderstanding that has existed in the past. First of all, the usual detector types are the linear, the square law, and the general law. Enough confusion exists with regard to the linear detector to require further elaboration. Linear detectors can be classified as average detectors, peak-envelope detectors, or peak-peak detectors. The average detector is the one usually assumed in theoretical descriptions of the linear detector when it is assumed that the detector consists of a simplified diode having a constant forward resistance and a constant back resistance and no output capacitor. Most authors have assumed the use of an average detector in their analyses of the linear detector.<sup>8,9</sup> They have even included the detection efficiency of such a detector ( $1/\pi$ ) as an inherent part of their result. The peak-envelope detector has an output network with a time constant sufficiently long that there is insignificant reduction of voltage between cycles of the center frequency,  $f_0$ , yet sufficiently short that none of the envelope frequency components are removed. For this form of detector, the output voltage would be just the envelope of the input voltage, not 0.32 of the envelope. The peak-peak detector, on the other hand, has an RC network at its output, having a time constant sufficiently long that the output voltage cannot follow the envelope of the input voltage. In this case, the output voltage will "ride up" on the envelope by an amount determined by the detection efficiency and the output time constant. Such a detector is a nonlinear filter and

<sup>6</sup> P. D. Strum, "A note on noise temperature," IRE TRANS., vol. MTT-4, pp. 145-151; July, 1956.

<sup>7</sup> H. T. Friis, "Noise figures of radio receivers," PROC. IRE, vol. 32, pp. 419-422; July, 1944.

<sup>8</sup> S. O. Rice, "Mathematical analysis of random noise," *Bell Sys. Tech. J.*, vol. 23, pp. 282-332; July, 1944, and vol. 24, pp. 46-156; January, 1945.

<sup>9</sup> J. L. Lawson and G. E. Uhlenbeck, "Threshold Signals," *Mass. Inst. Tech. Rad. Lab. Ser.*, vol. 24, McGraw-Hill Book Co., Inc., New York, N. Y., pp. 59-63; 1950.

has not been analyzed. An intuitive analysis would indicate that such a detector has a poorer signal-to-noise ratio than the other types because a large number of samples are removed from the averaging process. A more important reason for the inadvisability of using this form of detector would be the fact that an interfering signal of short duration would be "stretched." The general-law detector will not be discussed, because its behavior always approaches that of the square-law detector at low snr.

In the Appendix, square-law and linear detectors are shown to be almost equivalent on a signal-to-noise ratio basis, but there remains one significant difference. The linear detector exhibits the property of modulating the amplitude of the small signal if the larger signal varies. This is not the case for the square-law detector. The factor  $\alpha$  is 1.0 for square-law detectors and 1.05 for average or peak-envelope detectors.

The modulation and filtering factors,  $\mu$  and  $\phi$ , are determined on the basis of the modulation and the post-detection filtering processes. The modulation factor,  $\mu$ , is unity when signal plus noise is continuously compared at the output with a noise-free comparison voltage. Considerations of gain fluctuation in a later section will show that this mode of operation is unsuited for high-sensitivity radiometry. The usual form of modulation is a switching function that permits the input from the antenna to be connected to the receiver half of the time and the input from a stable comparison source to be connected to the receiver the other half of the time. In such a system the snr resulting from internal receiving system noise must suffer because the signal is not being continuously observed. The degradation from unity (increase in  $\mu$ ) depends upon the modulation form, the types of output filters, and the type of coherent detector. Table I shows the results of a waveform and filtering analysis. The filter factor  $\phi$  is the product of several filter factors,  $\phi'$ ,  $\phi''$  . . . .

Filter factor  $\phi'$  takes into account the filter between the detector and the synchronous detector, and filter factor  $\phi''$  takes into account the effect of the final low-pass filter. If rectangular modulation other than square wave is used and an ordinary synchronous detector is used, the modulation factor  $\mu$  must be multiplied by a modulation factor  $\mu'$  accounting for the duty ratio as follows:

$$\mu' = |\sin \delta \pi| \quad (7)$$

where  $\delta$  is the duty ratio. If more sophisticated forms of rectangular modulation and demodulation are used, such as narrow gating at the output, analysis becomes more involved and is beyond the scope of the present considerations. For most radiometry applications such a form of modulation and demodulation is unsuited because the effective observation time is reduced.

The time constant,  $\tau$ , has the usual definition and is equal to the product RC when a single RC network is used at the output. A single RC network does not have optimum ratio of noise bandwidth to circuit bandwidth, where the circuit bandwidth is related to the time constant. A critically damped, or other form of more sophisticated filter, would be more suited for optimizing the rate of rise of a signal while maintaining a constant noise background.

The detectability criterion,  $k$ , is strongly affected by the type of output presentation and the demands of the operator. Certain of these considerations are discussed by Lawson and Uhlenbeck.<sup>10</sup> For the usual analog recording, in which the residual background forms a drift-free "wiggly" record having an rms magnitude as given by (1) or (2), a wide variety of requirements can be established as a function of the personal requirements of the operator. In analyzing an analog tracing, the usual points of reference are the peaks of the trace rather than the actual trace itself. Frequently the operator requires that the displacement of the mean value of the trace be of the order of the peak-to-peak value for a high percentage of the time. Fig. 2 is a plot of  $k$ . It is seen that the required  $k$  can rise sharply as a function of the percentage of the time that the average values are separated by the required amount. It has been the experience of the author that a minimum detectable signal for most operators requires a  $k$  of about 2.5 to 4.0. In any given trace analysis the determination of the rms fluctuation would require a detailed statistical analysis.

A technique that has been established by many radio astronomers involves the use of many tracings of essentially the same measurement. If the many tracings are analyzed statistically, the threshold level can be reduced by a factor of the order of  $N^{-1/2}$ , where  $N$  is the number of tracings. This is similar to the radar situation in which traces are repeated one over the other on an oscilloscope.<sup>11</sup>

TABLE I

TABLE OF MODULATION/FILTERING FACTORS,\*  $\mu\phi'$  AND  $\phi''$ 

Type of modulation and/or filtering	Relative threshold power		
	rms†	ave	peak
$\mu\phi'$			
Continuous comparison	1	1	1
Noise-free comparison	$\sqrt{2}$	$\sqrt{2}$	$\sqrt{2}$
Equal-noise comparison			
Switched comparison			
Square-wave, audio filter	$\pi/\sqrt{2}$	2	$\pi/\sqrt{2}$
Square-wave, no filter	2	2	‡
Sine-wave, audio filter	$2\sqrt{2}$	$\pi$	$2\sqrt{2}$
$\phi''$			
Ideal low-pass filter		$1/\sqrt{\pi}$	
1-RC filter		$1/\sqrt{\pi}$	

\*  $\mu\phi = \mu\phi'\phi''$ .

† RMS is seldom considered; few output devices respond to the rms value of a wave.

‡ Not a suitable mode of operation.

<sup>10</sup> Lawson and Uhlenbeck, *op. cit.*, pp. 161-165.

<sup>11</sup> *Ibid.*, p. 163.

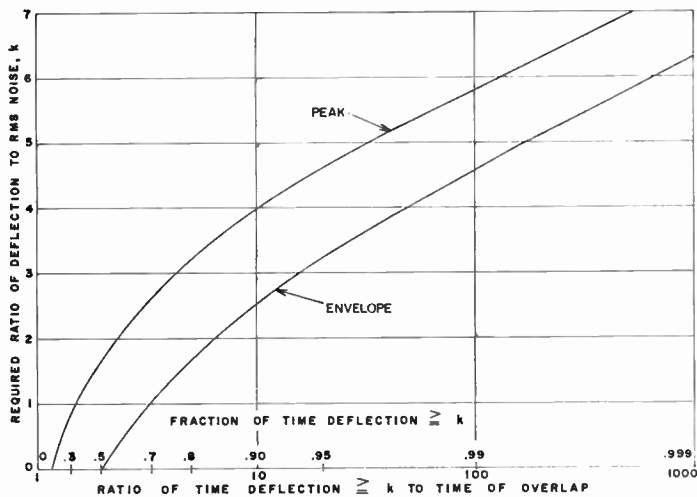


Fig. 2—The criterion of detectability of a signal on a single analog trace.

On the other hand, if one chose to digitize the output, the individual samples would have a Gaussian distribution. Therefore, one would require a number of samples from the same region to decide on a probable average value. The number required will depend upon the frequency distribution of the noise fluctuations and the desired accuracy. The digital output, for single readings, will have a larger degree of uncertainty than the analog recording would have for the same instrumental time constant. The analog recording permits the operator to do a bit of "eye integration." Eye integration can be one of the most useful tools in the interpretation of analog recordings.

*Threshold Due to Antenna and Other Effects*

In this section the threshold established by the characteristics of the antenna, the atmosphere, and the ambient and outer space will be discussed. Fig. 3 shows a typical antenna pattern showing the influence of the source, the atmosphere, and the ground. For this case the angular size of the signal source is smaller than the main beam of the antenna, a condition that frequently exists, except for large antennas observing large targets, such as the sun or the moon. The lower part of Fig. 3 shows the profile of the temperature contributions from the three regions. To obtain the total antenna temperature it is necessary to integrate the entire solid angle surrounding the antenna and divide by  $4\pi$ , which is the integral of gain over the full sphere. Symbolically this can be represented by

$$T_a = \frac{\int_s T(\theta, \phi) G(\theta, \phi) dS}{\int_s G(\theta, \phi) dS} \tag{8}$$

where

$dS$  = the solid angle given by  $\sin \theta \cdot d\theta d\phi$ .

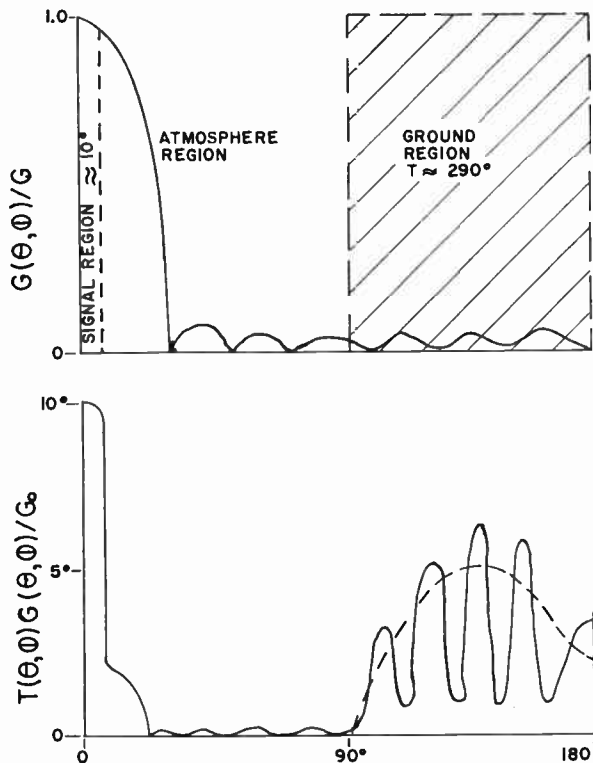


Fig. 3—A typical two-dimensional antenna pattern showing the effects of the source, the atmosphere, and the ground on antenna temperature.

As seen in Fig. 3, a typical situation might have contributions from the back lobes that are of the order of or larger than the contribution from the source. Under conditions where the back lobes are small and the source is weak the atmospheric contribution in the main beam, due to high-temperature absorption, may become large. The noise temperature from such a contribution can be computed as follows:

$$T_{BB} = T_{at}(L_{WV}L_{OX} - 1) \tag{9}$$

where

- $T_{BB}$  = the apparent background temperature in the main beam,
- $L_{WV}$  = the loss attributable to water vapor,
- $L_{OX}$  = the loss attributable to atmospheric oxygen,
- $T_{at}$  = the temperature of the atmosphere.

Such an expression is a simplification because there will not be a uniform distribution of temperature or absorption. The situation does not change radically, however, if one assumes  $T_{at}$  of about 250° to 290° and uses the experimentally determined values of absorption for the frequency of operation. At the lower microwave frequencies the absorption is significantly less than at frequencies above, say, 5 kmc. The contribution from atmospheric absorption at 10 kmc might be as large as tens of degrees.

The preceding discussion has dealt with the static approximation for the various antenna temperature components. Another consideration is the variability of these components and the spectrum of the variabilities.

For instance, if the antenna of Fig. 3 is rotated to track a source across the sky, the back lobes will continuously increase and decrease their contribution to the apparent temperature. In some instances this variability is of such magnitude as to obliterate the contribution from a small source. Another variable component is the atmospheric absorption. The absorbing regions are in a continual change. This turbulence causes both the loss and the temperature, and consequently the apparent temperature, to be a function of time. The rate of change will be dependent upon meteorological conditions.

The random component caused by the changing interception of the back lobes and the ground virtually can be eliminated by fixing the antenna position and permitting the source to drift through the antenna beam. This mode of operation, however, limits the available integration time. A choice must be made between tracking with the consequent increase in back-lobe variability and locking the antenna with the consequent reduction in integration time. Fixing the antenna position will have no effect on the turbulence of the atmosphere.

The antenna, to some degree, can deal with the problem of man-made interference. If sufficiently high-gain and low-back lobes are used, angular discrimination against man-made interference can be achieved.

In dealing with scatter propagation Schott showed that the usefulness of increasing the size of an antenna is determined by the apparent angular size of the scattering region, when viewed from the receiving site.<sup>12</sup> Inasmuch as a plane wave front from a small diameter radio source will be "wrinkled" by inhomogeneities of the atmosphere, there is an upper limit in apparent temperature of a source determined by the apparent angular size when viewed through the atmosphere.

Another way of looking at this phenomenon is with regard to the phase correlation of the rays incident on the antenna. Studies have shown that a typical half-width of the space-phase correlation is about 200 feet at 10 kmc.<sup>13</sup> This means that the ultimate sensitivity at 10 kmc as a function of antenna size will not be achieved until antennas of about 200-foot diameter are used. When the antenna beamwidth is reduced below the apparent angular size (or the aperture is made large with respect to the space-phase correlation width) no increase in apparent temperature occurs, but improved resolution is available. Others have dealt with calibration of the antenna.<sup>14,15</sup> Until such a calibration is made only relative source temperatures can be measured.

<sup>12</sup> F. W. Schott, "On the response of a directive antenna to incoherent radiation," *PROC. IRE*, vol. 39, pp. 677-680; June, 1951.

<sup>13</sup> E. J. Blum, J. F. Denisse, and J. L. Steinberg, "Radio astronomy at the Meudon Observatory," this issue, p. 39.

<sup>14</sup> J. Aarons, "Antenna and receiver measurements by solar and cosmic noise," *PROC. IRE*, vol. 42, pp. 810-815; May, 1954.

<sup>15</sup> R. N. Whitehurst, F. H. Mitchell, and J. Copeland, "A calibration procedure for microwave radiometers," *PROC. IRE*, vol. 45, pp. 1410-1411; October, 1957. This procedure calls for the difficult operation of intercepting the main beam only with absorbing material. A minimum separation of antenna and absorbing material would be of the order of tens of aperture diameters.

### Threshold Due to Spurious Modulation

A perfect modulator would yield at its output an available power proportional to the effective temperature of the source at each position. Physically achievable modulators usually yield an additional output component resulting from impedance variations. Such a situation is not too serious if these variations are systematically predictable. That is, the errors due to impedance modulation can be "calibrated out." If the impedance modulation varies in an unsystematic way, a threshold level is introduced that is relatively independent of the other characteristics of the system.

Impedance modulation can have varying degrees of influence on the output power of the system depending upon the configuration of the mixer or amplifier at the input of the receiver. For instance, Dicke<sup>16</sup> indicated a means of reducing the effect in a balanced mixer.

An analysis based on the variation of the output impedance of a resistive pad with a variable impedance at the input has been found to yield an approximate maximum bound for this effect. This result is given by

$$\rho_{\max} \cong \left[ \frac{S_1 S_2 (F_e + 1) + F_e - 1}{S_1 S_2 (F_e - 1) + F_e + 1} - 1 \right] \left( F_e + \frac{T_a}{290} - 1 \right) \quad (10)$$

where  $S_1$  and  $S_2$  are the standing-wave ratios in the two positions of the modulator. This factor vanishes under two conditions, where  $S_1$  equals  $S_2$  or any other condition in which  $S_1$  yields an output noise voltage equal to that resulting from  $S_2$ . In the latter case, the impedances in the two positions might be complex conjugates if the input network of the receiver is purely resistive.

One means of reducing the spurious modulation is by the use of a unidirectional device, either directly as the modulator or following the modulator. Laboratory results of this application were reported by Mayer.<sup>17</sup>

### Threshold Due to Gain Fluctuations

The importance of gain fluctuations was described by Dicke.<sup>18</sup> In fact one of his significant contributions was the use of modulation to reduce the effect of gain fluctuations. Most gain fluctuations of the systematic type can be reduced to a low level. That is, such things as drifts in supply voltages and changes in ambient temperature, vibration, orientation, are amenable to engineering solution. The difficulty is that, for extremely high sensitivities, the engineering labor becomes prohibitive. Besides the effort required, there would be an irreducible minimum in the gain fluctuation that would result from spontaneous changes within circuit elements. For high sensitivity the approach must be to re-

<sup>16</sup> R. H. Dicke, *op. cit.*, pp. 271-272.

<sup>17</sup> C. H. Mayer, "Improved microwave noise measurements using ferrites," *IRE TRANS.*, vol. MTT-4, pp. 24-28; January, 1956.

<sup>18</sup> R. H. Dicke, *op. cit.*, pp. 270-271.

duce systematic gain fluctuation to a reasonable extent and then use modulation to reduce the effects further. Fig. 4 shows an approximate form of the probability density and spectrum of gain fluctuations, assuming that the fluctuations are random. The spectrum is a rapidly decreasing function of frequency. Therefore, one should choose a frequency for modulation,  $f_a$ , higher than the maximum significant component in the gain-fluctuation spectrum. Frequencies that are related integrally or fractionally to the power-line frequency are generally unsuited for modulation. This results from the fact that wave shapes synchronized to the power-line frequency are generated continually and would cause interference unless extreme caution were exercised in reducing ground currents and partially filtered components in the dc power supplies.

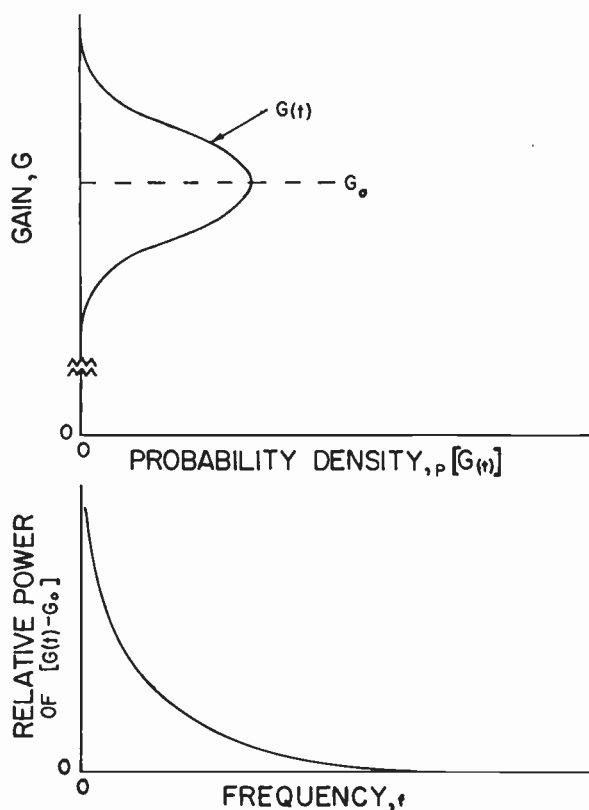


Fig. 4—Approximate probability density and spectrum of random gain fluctuations.

The gain variability factor,  $\gamma$ , can be defined by

$$\gamma = 1 + \frac{[G(t) - G_0]_{rms}}{G_0} \quad (11)$$

where

$G(t)$  = the gain as a function of time,

$G_0$  = the average gain over a long period,

subscript rms = the root mean square value.

The gain fluctuation factor as defined by (11) can be divided into individual factors inasmuch as certain components may contribute larger fluctuations than

others. If the receiving system is divided into two sections, the first having noise figure  $F_1$ , gain  $G_{01}$ , and fluctuating gain  $G_1(t)$  and the second having a noise figure  $F_2$  and an average gain  $G_{02}$ , the individual factor is

$$\gamma' = 1 + \frac{[(T_a/290) + (F_1 - 1)] \frac{[G_1(t) - G_{01}]_{rms}}{G_{01}}}{[(T_a/290) + (F_1 - 1)] + (F_2 - 1)/G_{01}} \quad (12)$$

where  $\gamma'$  is the gain-fluctuation factor for the second section.

If a modulation frequency,  $f_a$ , is chosen so that the contribution from all components within the receiver is small, there still remains an important influence. This influence results from inequalities of the two sources. For instance, if one uses the Dicke system in which the comparison source is at about 290°K and the antenna temperature is only a few degrees, an offset, or signal, of the order of 290° will always be present. If such an offset is then subtracted out by means of a dc voltage at the output as in the case of a continuous comparison radiometer, there will remain a spurious signal given by

$$\Delta T_G = |T_{c1} - T_{c2}| (\gamma - 1) \quad (13)$$

where

$\Delta T_G$  = the threshold rms temperature fluctuation as determined by gain fluctuations,

$T_{c1}$  and  $T_{c2}$  = the temperatures of the comparison sources (one being the antenna and the other being a local comparison source),

$\gamma$  = the over-all gain fluctuation factor.

This result shows that it is desirable to make the antenna temperature and the comparison-source temperature as nearly equal as possible in the region of the sky where the measurement is to take place. The addition of noise to the cooler source will accomplish this result. Noise can be injected from a noise generator coupled through an adjustable attenuator and a directional coupler. Such a connection can eliminate the effects of gain variation on the threshold. (It should be noted that gain variations will always modulate the signal.)

If a servomechanism were included to control an adjustable attenuator, the system signal would remain at or near zero.<sup>19</sup> One could then read the position of the adjustable attenuator and determine the apparent temperature of the antenna. For many observations this is an unnecessary complexity. If a stable noise source, stable attenuator, and stable directional coupler are used, many useful astronomical observations can be made by means of adjusting the balance just prior to making an observation.<sup>20</sup> In this case it is desirable to examine the threshold due to instabilities of the direc-

<sup>19</sup> K. E. Machin, M. Ryle, and D. D. Vonberg, "The design of an equipment for measuring small radio-frequency noise powers," *Proc. IEE*, vol. 99, pt. III, pp. 127-134; May, 1952.

<sup>20</sup> F. D. Drake and H. I. Ewen, "A broad-band microwave source comparison radiometer for advanced research in radio astronomy," this issue, p. 53.

tional coupler and the attenuator. This can be shown to be

$$\Delta T = \Delta A T_{\text{bal}} \quad (14)$$

$\Delta T$  = the temperature threshold,

$\Delta A$  = the change of attenuation in power ratio,

$T_{\text{bal}}$  = the temperature corresponding to the added noise power.

This shows that for small balancing noise powers, larger attenuation changes can be tolerated than for large balancing noise powers. This result furthermore indicates that it is desirable to have the coupling factor of the directional coupler as small as possible (assuming the coupler is more stable than the attenuator) to obtain the available balancing noise power. This also suggests that the attenuation in the adjustable attenuator can be very small, in which region most attenuators have a small rate of change of attenuation per unit of physical change. It should be pointed out that, if the noise balancing power is added to the antenna line, the excess noise should be added to the other excess noises of the system to obtain the over-all effective excess noise,  $F_e - 1$ .

The temperature of the comparison source must be stabilized to the degree required by the sensitivity threshold. The implication is that the comparison source must be automatically stabilized, or it must be insulated in such a way that the rate of change of temperature as a function of ambient temperature changes will be sufficiently low to permit useful observations. Techniques for stabilizing comparison sources include temperature controlled refrigeration and heating, change-of-state operations (such as the melting of ice or the boiling of water), and reducing the temperature of the source to nearly absolute zero. Mayer *et al.* have made observations using an auxiliary antenna oriented so as to have a low antenna temperature,<sup>21</sup> but this method suffers from practical limitations for very high-sensitivity work.

An area that has been ignored generally when gain fluctuations are being considered has been the post-detector amplification. In a high-sensitivity system this amplification may become substantial. For instance, a typical situation may be one in which the dc and ac components of noise at the output of the detector are of the order of 0.1 volt. If a threshold of the order of 0.01°K is required in a system having an equivalent over-all noise temperature of 4000°K (as discussed by Drake and Ewen),<sup>20</sup> the equivalent signal voltage at the input of the post-detection amplifiers will be about  $\frac{1}{4} \mu\text{v}$ . A continuous-comparison radiometer operating at such a level would require a higher degree of stability than is normally available with dc amplifiers. In fact, this level requires the utmost care in the design of an ac amplifier. Microphonics and equivalent input noise of the audio amplifier must be equivalent to an input voltage less than about 0.1  $\mu\text{v}$ . Also the synchronous detec-

tor following the audio amplifier will have an inherent drift. To overcome this threshold the signal voltage must be amplified to a level several times greater than the inherent instabilities of the synchronous detector. This level may be of the order of millivolts, thus requiring a gain of about 80 db. To prevent overloading of the vacuum tubes in the amplifier the background noise must be drastically reduced by reducing the bandwidth. The bandwidth reduction required is approximately the same order as the required power gain; for example, the bandwidth reduction factor must be about  $10^{-8}$ .

After synchronous detection, the signal (of the order of millivolts and higher) can easily be handled by the amplifiers in standard analog recorders. Here again, however, a significant gain is required, because a few millivolts must be raised to a few volts.

Excluding the gain of the antenna, the tabulation of a typical system gain distribution would be as follows:

Antenna	40 to 60 db
Receiver	70 to 90 db
Audio amplifier	60 to 80 db
Recorder	40 to 60 db.

#### PRESENT AND FUTURE SYSTEMS

The present state of the art is exemplified by the radiometers described by Drake and Ewen.<sup>20</sup> In their receiver the low noise figure and large bandwidth were obtained by using low-noise traveling-wave tubes of a recent design. To obtain the low-threshold levels, they used integration times of the order of tens or hundreds of seconds. It is not likely that the integration time for useful observations can be extended much further, nor can the bandwidth be greatly increased without introducing the problem of interference. Much is expected, by the radio astronomer at this time, of the solid-state maser amplifier.<sup>22</sup> With such amplifiers the internal noise of the receiver can be reduced to the equivalent of a few degrees, probably less than 10°K. If one immediately compares this with the 4000°K of the typical traveling-wave tube receiver, it would seem that tremendous strides could be made in reducing the threshold level. There are two serious limits to the reduction. The irreducible obstacle seems to be the effect of the environment in which the antenna is immersed. Other factors such as waveguide attenuation, modulator losses, and the like set an upper limit for the equivalent system noise at the present time of the order of 100°K. Another detail is that the bandwidths of present-day masers are of the order of hundreds of kilocycles, whereas bandwidths of the order of hundreds of megacycles would be required if significant improvement is to be achieved.

In any event, when the maser becomes available the situation will be reversed from the usual in that the

<sup>22</sup> See for example, J. P. Wittke, "Molecular amplification and generation of microwaves," *PROC. IRE*, vol. 45, pp. 291-316; March, 1957. Also see footnotes.

<sup>21</sup> Mayer *et al.*, this issue, p. 254.

excess system noise will be almost totally contributed by components other than the receiver. For ultimate threshold reduction a perfect antenna, having a small beam and no back lobes and no losses between its aperture and the input of the maser, would be required.

Fig. 5 shows the variation in background and receiver noise in equivalent °K. The figure includes portions of the spectrum outside the microwave region to show the trends. At the high-frequency end of the spectrum the atmospheric effects are becoming important to such an extent that high-sensitivity radiometry becomes impossible.

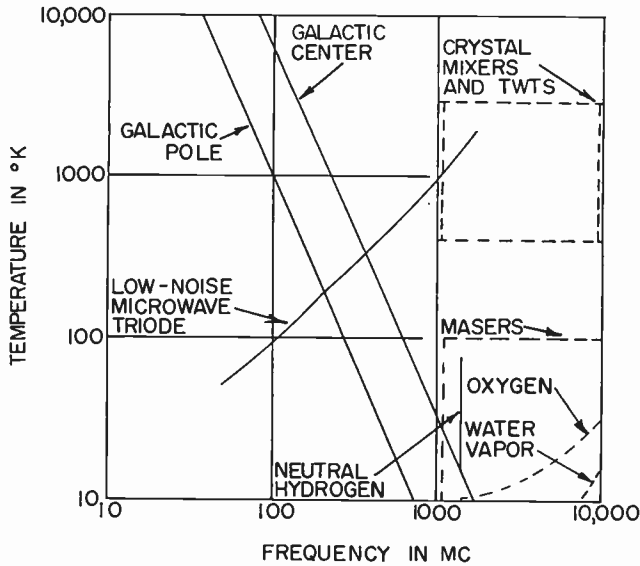


Fig. 5—Background and receiver noise vs frequency.

CONCLUSION

The usual threshold-sensitivity equations become inadequate when microwave radiometers are pushed towards their ultimate threshold level. The number of factors requiring consideration are increased from about four to about twelve. Present-day techniques permit threshold levels, several orders of magnitude lower than those in the early days of radiometry and future possibilities, seem to promise reductions in the threshold level of one or two more orders of magnitude. To push to these new reduced levels will require the utmost care and reconsideration of most of the details of radiometer design. When such new radiometers become available they will be limited by their environment much as the present Mt. Palomar optical telescope.

APPENDIX

The detector is the predominant nonlinear element in a radiometer. An analysis of the signal-to-noise performance is, therefore, in order.

First consider a square-law detector. The output snr of significance is the ratio of the average output voltage,  $\bar{E}$ , to the rms deviations (from  $\bar{E}$ ) of the output voltage,

$E_{rms}$ . The square-law detector yields an output voltage proportional to input power or input mean-square voltage. That is, for the noise of the receiving system only

$$\begin{aligned} \bar{E}_1 &= a\bar{e}_r^2 \\ &= a'P_R B_1 \end{aligned}$$

where  $a$  and  $a'$  are detection constants,  $\bar{e}_r^2$  is the mean-square receiver-noise voltage,  $P_R$  is the power density (in watts per cps) of the receiver noise, and  $B_1$  is the bandwidth of the circuits preceding the detector. If a signal is added and is of the same random nature as the receiver noise,

$$\begin{aligned} \bar{E}_2 &= a(\bar{e}_r^2 + \bar{e}_s^2) \\ &= a'B_1(P_R + P_s) \end{aligned}$$

where  $\bar{e}_s^2$  is mean-square signal voltage and  $P_s$  is signal-power density. The deflection, or difference in average value, will then be

$$\begin{aligned} D &= \bar{E}_2 - \bar{E}_1 \\ &= a\bar{e}_s^2 \end{aligned}$$

The deviation of the output voltage (from  $\bar{E}$ ) has been shown to be equal to the average voltage;<sup>8</sup> therefore,

$$E_{rms} = a(\bar{e}_r^2 + \bar{e}_s^2)$$

for continuous comparison, or

$$E_{rms} = a\left(\bar{e}_r^2 + \frac{\bar{e}_s^2}{2}\right)$$

for square-wave switched comparison. In either case

$$E_{rms} \cong a\bar{e}_r^2$$

when

$$\bar{e}_s^2 \ll \bar{e}_r^2.$$

The output snr is, therefore,

$$\frac{D}{E_{rms}} \cong \frac{\bar{e}_s^2}{\bar{e}_r^2}$$

Next consider a linear detector, either average or peak-envelope. Again the output snr of significance is the ratio of the average output voltage to the rms deviations of the output voltage. A linear detector yields an output voltage proportional to the input voltage. For receiving system noise only,

$$\bar{E}_1' = \eta \sqrt{\frac{\pi}{2} \bar{e}_r^2}$$

where  $\eta$  is the detection efficiency ( $\eta=1$  for a perfect peak-envelope detector and  $\eta=1/\pi$  for a half-wave average detector). If a signal is added and is of the same random nature as the receiver noise,

$$\bar{E}_2' = \eta \sqrt{\frac{\pi}{2} (\bar{e}_r^2 + \bar{e}_s^2)}$$

The deflection, or difference in average value, is then

$$\begin{aligned} D' &= \bar{E}_2' - \bar{E}_1' \\ &= \eta \sqrt{\frac{\pi}{2}} (\sqrt{\bar{e}_r^2 + \bar{e}_s^2} - \sqrt{\bar{e}_r^2}) \\ &= \bar{E}_1' \left( \sqrt{1 + \frac{\bar{e}_s^2}{\bar{e}_r^2}} - 1 \right). \end{aligned}$$

For small signals

$$D' \cong \bar{E}_1' \frac{\bar{e}_s^2}{2\bar{e}_r^2}$$

showing the square-law relationship for small signals in a perfectly linear detector. Rearranging this relationship gives

$$\begin{aligned} D' &\cong \eta \sqrt{\frac{\pi}{2}} \frac{\bar{e}_s^2}{2\sqrt{\bar{e}_r^2}} \\ &\cong \eta^2 \frac{\pi}{4} \frac{\bar{e}_s^2}{\bar{E}_1'} \end{aligned}$$

When this is compared with the relation for  $D$  for the square-law case an important difference is apparent. The output deflection for the linear detector is inversely proportional to the system noise voltage; for the square-law detector it is independent.

The rms deviation of the output voltage has been shown to be<sup>8</sup>

$$\begin{aligned} E_{rms}' &= \eta \sqrt{2 - \frac{\pi}{2}} \sqrt{\bar{e}_r^2 + \bar{e}_s^2} \\ &\cong \eta \sqrt{2 - \frac{\pi}{2}} \sqrt{\bar{e}_r^2} \end{aligned}$$

when

$$\bar{e}_s^2 \ll \bar{e}_r^2.$$

The output snr is, therefore,

$$\begin{aligned} \frac{D'}{E_{rms}'} &\cong \frac{\sqrt{\pi/2} (\bar{e}_s^2/2\bar{e}_r^2)}{\sqrt{2 - \pi/2} \sqrt{\bar{e}_r^2}} \\ &= 0.95 \bar{e}_s^2/\bar{e}_r^2. \end{aligned}$$

These results show a slightly better signal-to-noise performance for the square-law detector, but the difference is negligible in comparison with most other variables.

As a function of input snr, Fig. 6 shows the ratio of the average output voltage to the rms deviation from the average for both detector types. At high-signal levels the linear detector gives superior performance.

Probability densities of several important features of a random noise signal that has been passed through a narrow band-pass filter are shown in Fig. 7. The random

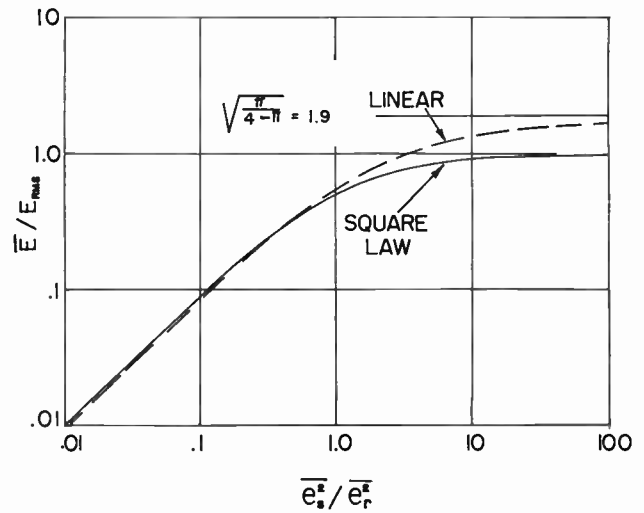


Fig. 6—Ratio of average output voltage to rms deviation from the average vs input snr for linear and square-law detectors.

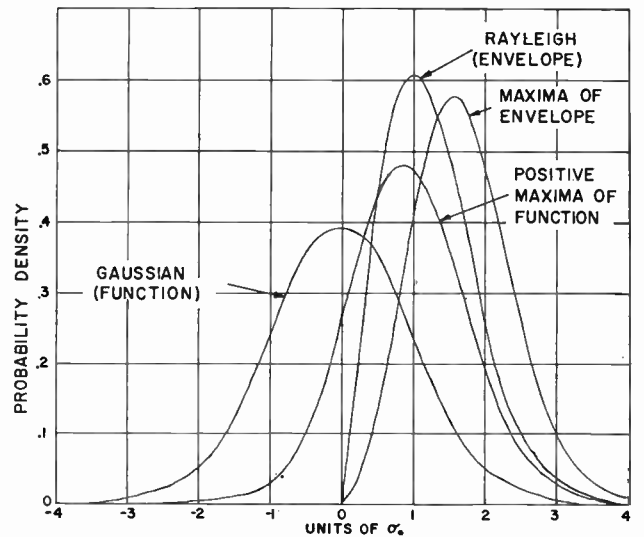


Fig. 7—Probability densities of several features of random noise that has been passed through a narrow band-pass filter.

(Gaussian) function is the noise voltage prior to detection. The positive peaks of this voltage have a similar probability density shifted to the positive side, but some positive peaks appear at negative voltages. These two curves apply to the interpretation of the output record (in determining  $k$ ) as well as to the detection of noise voltage. The Gaussian wave envelope has a Rayleigh distribution, and the peaks of the envelope have a modified distribution shifted towards higher values.

After rectification the distributions depend on the law of the detector. Fig. 8 shows the probability densities for the linear and the square-law detectors. Appropriate dc and rms deviations are marked on the figure. The difference between these distributions permits identification of the approximate detection law by observing the voltage on an oscilloscope (provided the bandwidth of the viewing circuits is greater than that of the predetection noise).

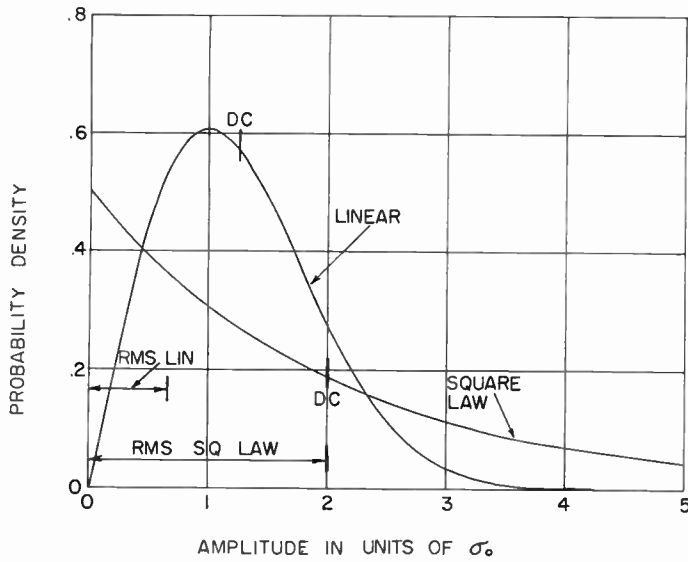


Fig. 8—Probability densities of detected output voltage for linear and square-law detectors.

The spectra of these powers and voltages are given in Fig. 9. The essential characteristics of these spectra are approximately independent (for our purposes, which dictate an invariant principal component of noise) of the type of detector. Bandwidths  $B_1$ ,  $B_2$ , and  $B_3$  represent respectively the predetection, audio-filter, and final-filter bandwidths.

From the figure it is apparent that the choice of the audio frequency,  $f_a$ , for modulation is independent of these spectra out to the vicinity of  $f_a = B_1$ . There the available over-all power is reduced, but snr is not affected. It is seen that the successive filters improve snr successively.

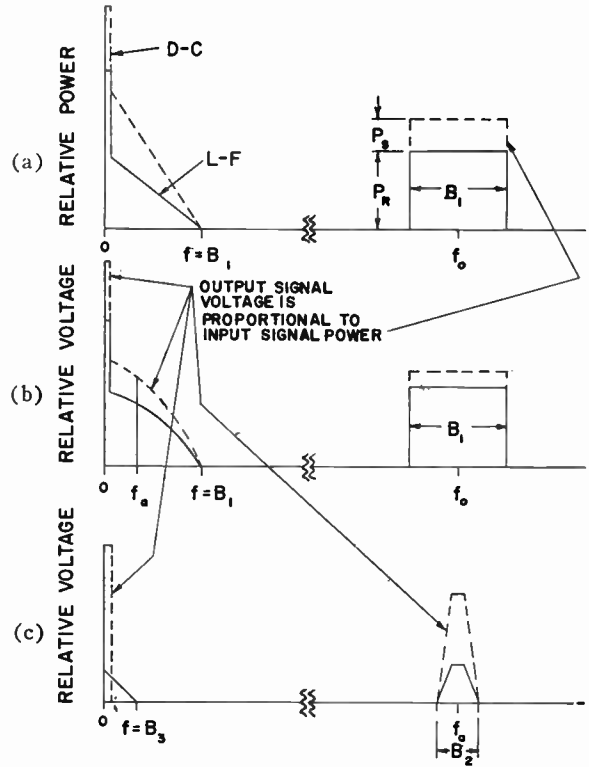


Fig. 9—Approximate power and voltage spectra.

ACKNOWLEDGMENT

The author wishes to thank the many members of the staff of the Ewen Knight Corporation for stimulating discussions that led to several of the results reported here. In particular H. I. Ewen and F. D. Drake brought their knowledge and experience in the field of radio astronomy to bear on the details of the analysis.

# A Broad-Band Microwave Source Comparison Radiometer for Advanced Research in Radio Astronomy\*

F. D. DRAKE†, MEMBER, IRE AND H. I. EWEN†, SENIOR MEMBER, IRE

**Summary**—A sensitive microwave radiometer system operating at short centimeter wavelengths has been developed which will allow large extensions of the known spectra of a large number of radio sources; facilitate the measurement of source polarization; give information on galactic structure and the sources of galactic radio emission; provide new data on the physical structure of planetary nebulas; and provide a means of measuring more accurately planetary temperatures, and the precise position of the brighter radio sources.

A traveling-wave tube radiometer operating at 8000 mc with a bandwidth of 1000 mc and sensitivities of the order of 0.01°K is

described. The radiometer is more than one order of magnitude more sensitive than other existing radiometers operating at 8000 mc. The very serious effects of gain fluctuations, acting on small residual signals, when trying to achieve very high sensitivities, are discussed. A means of eliminating such effects by introducing compensating noise has been found successful. Radio observations with this radiometer in conjunction with a 28-foot parabolic reflector have shown that: 1) The predicted sensitivity is achieved. 2) Zero-level stability is extremely high. 3) It has been possible to detect in detail the distribution of radio brightness at this wavelength in the vicinity of the galactic plane. 4) Radiation from the planets Jupiter and Saturn has been detected, this being the first detection of Saturn as a radio source. 5) Radiation from two planetary nebulas has been detected, this being the first detection of these objects as radio sources.

\* Original manuscript received by the IRE, November 8, 1957.  
 † Harvard College Observatory, Cambridge, Mass., and Ewen Knight Corp., Needham Heights, Mass.

## INTRODUCTION

RADIO observations of celestial sources at centimeter wavelengths have been impeded by two causes.

- 1) The radio brightness of radio sources, in general, decreases rapidly with decreasing wavelength;
- 2) The sensitivities of available radiometers decrease as one goes to shorter wavelengths.

These two causes in combination have largely discouraged attempts to observe the sky extensively at the short centimeter wavelengths, even though shorter wavelengths allow one to achieve more narrow antenna beams with a given antenna dimension.

It has been known for several years that these wavelengths may provide information vital to the solution of many outstanding astronomical problems. Among the astronomical problems which now may be more effectively attacked at short centimeter wavelengths, one may list:

- 1) The spectra of discrete radio sources.—Spectra information now will be greatly extended with respect to available information.<sup>1-5</sup> These spectra provide important clues with regard to the mechanism of radio emission operating in a radio source.
- 2) The polarization of radio sources.—These measurements are facilitated at short wavelengths because the earth's ionosphere affects the polarization of the radiation to a much smaller degree at these frequencies than at lower frequencies.<sup>6</sup>
- 3) The origin of the radiation in the vicinity of the galactic plane.—An accurate knowledge of this radiation, evaluated in conjunction with longer wavelength data, will determine whether the radiation is of thermal or nonthermal origin.
- 4) Galactic structure as determined from the distribution of regions of ionized hydrogen.—Clouds of ionized hydrogen are thermal emitters, which dominate the radio sky at short centimeter wavelengths.
- 5) The physical structure of planetary nebulas.—These objects, whose position in the picture of cosmic evolution is still poorly understood, are difficult to study

<sup>1</sup> F. T. Haddock, C. H. Mayer, and R. M. Sloanaker, "Radio observations of ionized hydrogen nebulae and other discrete sources at a wave-length of 9.4 cm," *Nature*, vol. 174, pp. 176-177; July 24, 1954.

<sup>2</sup> F. T. Haddock and T. P. McCullough, Jr., "Extension of radio source spectra to a wavelength of 3 centimeters," *Astron. J.*, vol. 60, pp. 161-162; June, 1955.

<sup>3</sup> V. M. Plechikov and V. A. Razin, "Results of measures of the intensity of radio emission of discrete sources at wavelengths of 3.2 and 9.7 cm," *Proc. Fifth Conf. on Questions of Cosmogony, Academy of Sciences of the USSR, Moscow*, pp. 430-435; 1956.

<sup>4</sup> N. L. Kaydanovsky and N. S. Kardashev, "Results of observations of discrete sources of cosmic radio emission at a wavelength of 3.2 cm," *Proc. Fifth Conf. on Questions of Cosmogony, Academy of Sciences of the USSR, Moscow*, pp. 436-437; 1956.

<sup>5</sup> N. G. Roman and F. T. Haddock, "A model for nonthermal radio source spectra," *Astrophys. J.*, vol. 124, pp. 35-42; July, 1956.

<sup>6</sup> C. H. Meyer, T. P. McCullough, and R. M. Sloanaker, "Evidence for polarized radio radiation from the Crab Nebula," *Astrophys. J.*, vol. 126, pp. 468-470; September, 1957.

photographically with high precision, but some aspects of these objects may be studied with a microwave radiometer of sufficient sensitivity.

6) The temperatures of the planets.—The extensive work already done at the Naval Research Laboratory, Washington, D. C., at 3-cm wavelength, indicates the value of such observations, since temperatures obtained by radio techniques differ markedly, in some cases, from temperatures determined by other means.

7) The precise determination of the positions of radio sources.—The narrow antenna beams obtainable at short wavelengths facilitate position determinations both by decreasing the confusion produced by having several sources in the beam antenna simultaneously, and by providing a radiometer response that is more sensitive to changes in antenna pointing. Furthermore, at short wavelengths one may observe sources of small optical size, such as Venus, thereby providing an accurate calibration of antenna pointing error.

## CONSIDERATIONS IN RECEIVER DESIGN

The receiving system to be described was specifically designed for the measurement of very low-level thermal noise powers associated with antenna temperatures produced by faint celestial sources of small angular size.

The "signal" produced by these sources has a noise-like character similar to the thermal and shot noise of the receiving system. The design criteria for the system then involve distinguishing a small change in the noise power output level of the receiver when the signal noise is introduced at the terminals of the antenna.

The minimum detectable signal of this system represents a change in the output-power level of the receiver of one part in 400,000 or a detectable antenna temperature change of 0.01°K in the presence of an equivalent 4000°K-system noise.

The minimum detectable signal is determined by fluctuations in the receiver output level in the absence of a signal. These output-level fluctuations are produced by spurious gain fluctuations within the active circuits of the receiver and by the statistical fluctuations in a noise-like waveform.

The normal method that has been used to reduce gain fluctuations and other spurious effects is to modulate the signal at a frequency at which the amplitude of such effects is negligible. The amplitude of the signal may then be determined by means of a coherent detector driven at the modulation frequency.<sup>7</sup>

Dicke's original description<sup>7</sup> of such a radiometer involved a 30-cps modulation of the signal by means of mechanically switching the receiver input between the antenna terminals and a resistive load at "room" temperature. Comparison was obtained then between the thermal noise presented at the terminals of the antenna

<sup>7</sup> R. H. Dicke, "The measurement of thermal radiation at microwave frequencies," *Rev. Sci. Instr.*, vol. 17, pp. 268-275; July 1946.

and the thermal noise of the resistor. Various other methods of modulation have been employed; however, each involves the fundamental concept of sequencing "signal" and "comparison" information through active amplifier circuits in a modulation pattern which in most cases can be represented by a square wave. Each cycle of the square wave contains one-half period of signal information followed by a half-period of comparison information.

In many systems this simple modulation scheme of switching to a resistive comparison load has been sufficient to reduce the effect of gain fluctuations below the level of statistical noise fluctuations. The receiving system described in this paper involves the successful application of further techniques to reduce the effect of gain fluctuations. Such techniques become increasingly significant for systems with low statistical noise fluctuations.

Theoretically, the fluctuations in the output-noise level of the receiver produced by the statistical nature of the noise waveform can be reduced to any desired degree by increasing the integration time after detection (narrowing the post detection bandwidth).

Expressed in equivalent temperature units the rms value of these fluctuations  $\overline{\Delta T}$  is

$$\overline{\Delta T} = \text{Equivalent system noise} / \sqrt{B\tau}, \quad (1)$$

where the equivalent system noise can be obtained from the noise figure  $F$  of the system by the expression

$$(F - 1)T_0. \quad (2)$$

$T_0$  is the reference ambient temperature, 290°K. In (1) above:

$B$  = the predetection bandwidth, and

$\tau$  = the time constant of the integration network after the detector.

Presumably we can increase  $\tau$  or  $B$  and thereby reduce  $\overline{\Delta T}$  to any desired value. There is, of course, a practical limitation to the maximum value of  $\tau$ , which is introduced by the amount of available observing time; this maximum value may be determined either by a change in source position as a function of time or a time dependent change in the amplitude of the power received by the antenna. An increase in  $B$  may be limited by the bandwidth of the signal, the current state of equipment development, man-made interference "noise," and many other factors.

To date, instrumentation at short wavelengths has consisted of superheterodyne receivers. The sensitivity of such systems has been limited by the relatively narrow bandwidths that can be easily achieved. Existing superheterodyne receivers provide a maximum sensitivity of the order of 0.5°K, with a five-second integration time. The introduction of traveling-wave tubes at short centimeter wavelengths has offered the possibility of achieving, at the cost of a slight increase in noise figure,

extremely wide bandwidths, of the order of 3 kmc at a frequency of 8 kmc. In actual application, it was found desirable to limit the bandwidth to about 1 kmc in order to avoid interference. The sensitivity of such a system, in theory, can be more than an order of magnitude greater than that given by existing superheterodyne receivers.

In order to test the efficacy of traveling-wave tube radiometers in radio astronomy application, such a radiometer was built and then was tested by actual observation of celestial sources.

### TRAVELING-WAVE TUBE RADIOMETER

A simplified block diagram of the basic receiving system is shown in Fig. 1. The receiver is basically a trf type consisting of three cascaded traveling-wave tube amplifiers. The center frequency of the interstage filters is 8000 mc and the bandwidth of each filter is 1000 mc.

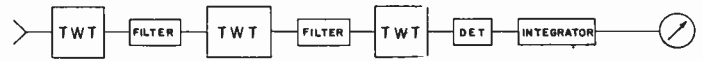


Fig. 1—Block diagram of basic receiving system employing traveling-wave tubes.

The measured system noise figure is 11½ db, providing an over-all equivalent system noise of about 4000°K. With an integration time of 100 seconds the value of  $\overline{\Delta T}$  from (1) is about 0.01°K. Hence, the fluctuations in the output power level of the receiver due to the statistical nature of the noise waveform are very small indeed.

Now let us direct our attention to the effect of gain fluctuations. With an equivalent system noise of 4000°K a gain change of ±1 per cent would produce a ±40°K change in the receiver output. To reduce this effect to 0.01°K would require stabilizing the gain of the receiver to one part in 400,000 or 0.00025 per cent. An easier approach would be to modulate the signal by comparison to a resistive load<sup>7</sup> as described above.

Fig. 2 is a simplified block diagram of the receiver modified by inserting a ferrite switch at the input to the first twt. Modulation of the signal is obtained by switching between the antenna terminals and a resistive load at "room temperature."

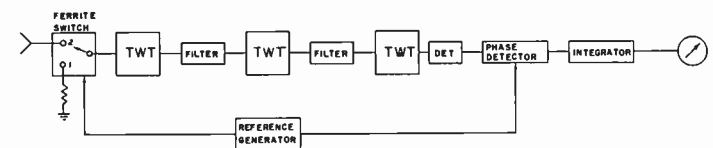


Fig. 2—Block diagram of receiving system with addition of comparison switching circuits.

The general expression for the minimum detectable signal is then:

$$\overline{\Delta T} = K \left[ \frac{(F - 1)T_0}{\sqrt{B\tau}} + \left( \frac{G(t) - G_0}{G_0} \right) (\Delta T_c + T_A) \right] \quad (3)$$

where

$K$  = a constant introduced here to simplify the expression by eliminating other effects not discussed in this paper,<sup>8</sup>

$F$  = the system noise figure,

$T_0$  = the reference ambient temperature, 290°K,

$B$  = the predetection bandwidth (1000 mc),

$\tau$  = the time constant of the integration network,

$G(t)$  = the gain of the receiving system at time  $t$ ,

$G_0$  = the average value of  $G(t)$  during the period of observation,

$\Delta T_c = T_{e2} - T_{e1}$ ,

$T_{e1}$  = temperature "observed" by the receiver with the switch connected to the resistive load,

$T_{e2}$  = temperature "observed" by the receiver with the switch connected to the antenna terminals, and with no radio source in the antenna beam,

$T_A$  = effective antenna temperature, "signal" produced by a radio source.

This expression for  $\Delta T$  may be divided into two parts.

- 1) The effect of statistical noise fluctuations:

$$\overline{\Delta T} = K \left( \frac{(F-1)T_0}{\sqrt{B\tau}} \right). \quad (4)$$

- 2) The effect of gain variations:

$$\overline{\Delta T} = K \left[ \left( \frac{G(t) - G_0}{G_0} \right) (\Delta T_c + T_A) \right]. \quad (5)$$

The first part obtains a value of 0.01°K as described above. For a 1 per cent variation in gain, the second part obtains a value of 2.9°K, if we assume to a first approximation that with no signal:

$$T_{e1} = 290^\circ\text{K}$$

$$T_{e2} = 0^\circ\text{K}.$$

It is evident from (5) that gain fluctuations limit the minimum detectable signal by an amount equal to the percentage of the gain change multiplied by the noise unbalance at the input terminals of the receiver, in the absence of a signal. To achieve a sensitivity of 0.01°K, it is then necessary to balance the noise temperatures  $T_{e1}$  and  $T_{e2}$  to better than 1°K, if gain fluctuations are no greater than 1 per cent.

Various methods have been proposed to achieve condition  $T_{e1} = T_{e2}$ . For this particular system the most convenient one was to introduce additional noise at input terminal 2 and increase  $T_{e2}$  until balance was obtained.

Fig. 3 is a block diagram of the receiver in the "noise compensated" form. The addition of noise to terminal 2 was achieved by inserting a fractional amount of the noise power available from an argon gas discharge noise source into the side arm of a directional coupler. The main arm of the coupler was inserted in the antenna transmission line between terminal 2 of the receiver and

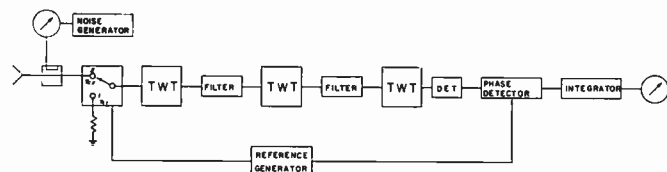


Fig. 3—Block diagram of receiving system with the addition of "noise compensating" circuits.

the antenna terminals. The addition of a variable attenuator between the noise generator and the coupler provided an easy means for adjustment of the amount of noise added to terminal 2.

The addition of approximately 300°K of equivalent noise power to the input of the receiver does, of course, increase the over-all system noise from 4000°K to 4300°K. However, this produces a negligible effect on  $\overline{\Delta T}$  as given by (4) when one considers the fact that this addition of 300°K of noise improves system sensitivity from 2.9°K to approximately 0.01°K. An effective sensitivity of 0.01°K was achieved in practice, thus providing a receiver more than one order of magnitude more sensitive than existing receivers at this frequency.

To improve further the sensitivity of such a system and, in fact, to determine the ultimate limitations on the sensitivity of the system described herein, we must analyze in greater detail the dependence of the terms in (3) on time and antenna position.

$T_{e2}$  may be represented by the expression:

$$T_{e2} = T_B + T_T + T_{\alpha 2} + T_I$$

where individual component contributions to  $T_{e2}$  exclusive of the noise compensating component are:

$T_B$  = the equivalent black body temperature of the galactic background radiation field "observed" by the antenna,

$T_T$  = temperature due to tropospheric effects,

$T_{\alpha 2}$  = temperature due to losses in the ferrite switch and side lobe contributions of the feed system and reflector,

$T_I$  = effective temperature due to man-made interference.

At a frequency of 8000 mc:

$T_B$  is less than 1°K. However, it is a function of antenna position. For fixed antennas it is a function of time as a consequence of the earth's diurnal rotation.

$T_T$  will depend primarily on the water vapor and oxygen content of the atmosphere in the solid angle of the antenna main beam. It will, therefore, be dependent on time as well as antenna position. The absolute magnitude of this effect might be as high as 30°K.

$T_{\alpha 2}$  will depend on the geometrical configuration of the antenna system and topographic and reflecting properties of the antenna surroundings. It will depend primarily on position, and even for a well-designed antenna pointing toward the zenith this effect might be as large as 20°K.

<sup>8</sup> P. D. Strum, "Considerations in high-sensitivity microwave radiometry," this issue, p. 43.

$T_I$  will, of course, depend on time, position of the antenna, and physical proximity of sources of man-made noise.

The problem for the future is simply expressed as the determination of the function  $T_{e2}(t, \theta, \phi)$  for each system.

If we include the noise compensation required for balance, then:

$$T_{e2} = \frac{T_{NG}}{(A_1 + A_2)} + T_B + T_T + T_{\alpha 2} + T_I$$

where

$T_{NG}$  = effective noise generator temperature,  
 $A_1 + A_2$  = attenuation of the variable attenuator plus the coupler.

The first term of  $T_{e2}$  can be made time dependent only, with a long thermal time constant, by application of known techniques to temperature stabilize components.

$T_{e1}$  can be represented by the expression:

$$T_{e1} = T_0 + T\alpha_1,$$

where

$T_0$  = ambient temperature of the load, and  
 $T\alpha_1$  = temperature component produced by losses in the ferrite switch when connected to position 1.

If  $T_0$  varies appreciably with time, the resistive element can be placed in an oven and stabilized to 0.01°K during the time of observation.  $T\alpha_1$  will be dependent only on time and its thermal time constant can be increased by various techniques.

Many of the effects discussed above can be easily controlled if the desired system sensitivity is no greater than 0.01°K, as was the case in the development of the radiometer described here. However, one of the purposes of this more detailed discussion is to point out the problems that will be associated with radiometers employing very low internal noise amplifiers. With a solid state Maser, for instance, the term  $F - 1/\sqrt{B\tau}$  in (3) will be reduced by a factor of 1000 at microwave frequencies. Fluctuations in the output-power level of the receiver will no longer be determined by the statistical fluctuations of the noise waveform. This fluctuation, presently the weak link in radiometer systems, will become the strongest link and the heretofore *negligible* effects represented by the second term

$$K \left[ \left( \frac{G(t) - G_0}{G_0} \right) (\Delta T_c + T_A) \right]$$

will completely determine receiver performance. The receiver reported here is in the "twilight" zone between yesterday and tomorrow in radiometer development.

#### ASTRONOMICAL OBSERVATIONS

The radiometer has been operated in conjunction

with an equatorially-mounted 28-foot paraboloid with a solid aluminum surface for the purpose of making actual tests on celestial sources of radiation. The beam-width to half-power points is 18' of arc. Because the receiver has been in a developmental status and under constant revision, precise calibration has not been attempted nor has the antenna gain been carefully measured. The results to date are, therefore, of a preliminary nature and stated antenna temperatures may be in error by a factor of two.

Fig. 4 is a reproduction of the radiometer response as the radio source Cassiopeia A was allowed to drift through the antenna beam. Such a "drift curve" should resemble a rectilinear plot of the antenna beam pattern, if the radio source is much smaller than the size of the antenna beam, as is the case here. The time constant in this case was 80 seconds, and the peak antenna temperature recorded for this source was about 2°K. The theoretical rms fluctuation amplitude at the radiometer output should be about 0.02°K under these conditions. The observed amplitude as recorded is approximately equivalent to this predicted value.

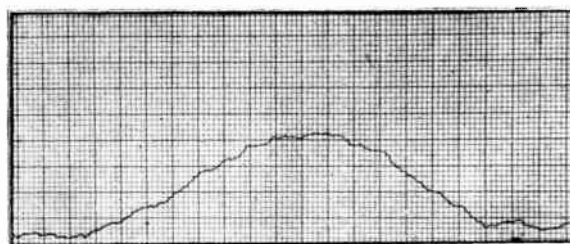


Fig. 4—Radiometer response as the strong radio source Cassiopeia A drifted through the antenna beam. Maximum antenna temperature = 2°K. Receiver time constant = 80 seconds.

Fig. 5 is a "drift curve" of the radio source associated with the galactic nebulosity M17. The time constant for this record was 80 seconds, and the peak radiometer deflection was about 3°K. The antenna was driven around the polar axis at a speed slightly greater than that of the earth's rotation, so that, although only about 10 minutes of right ascension displacement are shown by the tracing, about two and one-half hours were required for the observation. The most remarkable quality of this tracing from an instrumentation standpoint, besides the high sensitivity obtained, is the high stability of the zero-intensity level, which drifted at a rate of only 0.1°K per hour. The small rate of zero-level drift is quite encouraging to radio astronomers, who have long found a lack of zero-level stability to be a major obstacle in obtaining optimum observational data. The zero-level drift existing in this and other figures may be attributed to drift in the temperature of the resistive load against which antenna temperatures are compared. Oven stabilization of the resistive load was not included during this series of tests.

The source labelled A in Fig. 5 is associated with the emission nebula M17. The source labelled B in Fig. 5 lies very near the position of the galactic plane as found by

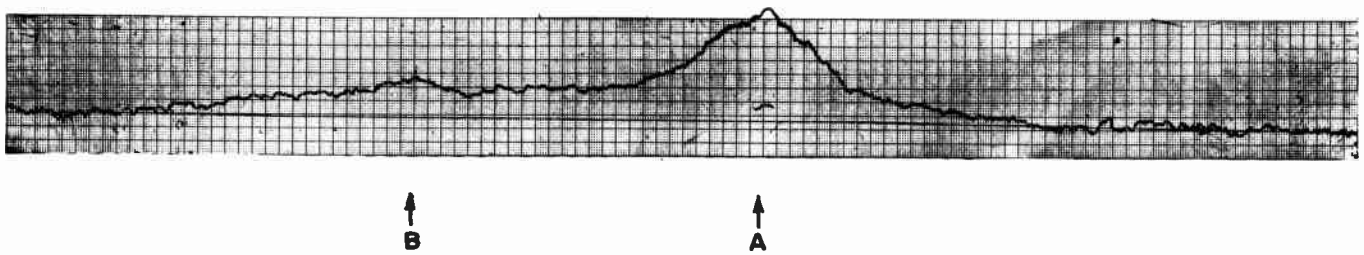


Fig. 5—Radiometer response as the region of the nebula M17 passed through the antenna beam. Maximum antenna temperature =  $3^{\circ}\text{K}$ . Time constant = 80 seconds. Source *A* is the radio source associated with M17, Source *B* lies near the galactic plane.

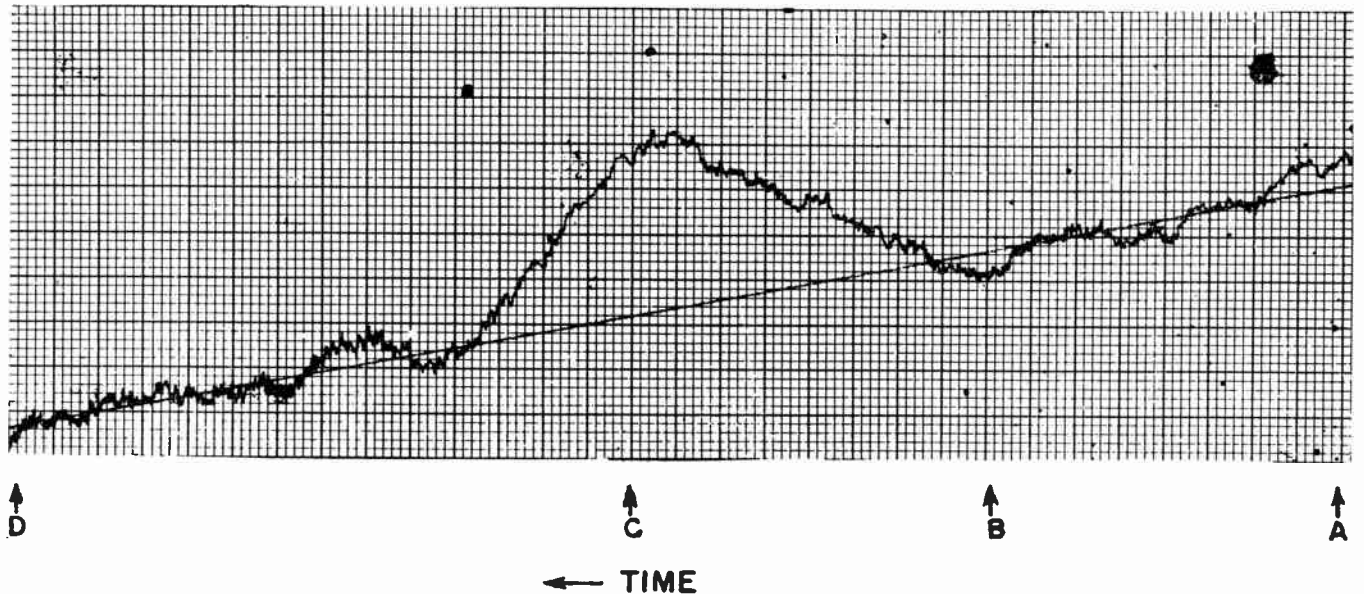


Fig. 6—Radiometer measure of radio emission from Jupiter. Maximum antenna temperature  $0.15^{\circ}\text{K}$ . Time constant = 320 seconds. Between *A* and *B*, the antenna pointed  $\frac{1}{2}^{\circ}$  east of Jupiter; between *B* and *C*, the antenna pointed at the planet; between *C* and *D*, the antenna pointed  $\frac{1}{2}^{\circ}$  west of Jupiter.

radio investigations at longer wavelengths. Since, optically, there is no emission nebula that might be responsible for this source, it appears quite likely that this source actually is the galactic plane. The narrow width of the response to this source then indicates that the galactic plane appears quite narrow at centimeter wavelengths, possibly being only a few minutes of arc in width, as has been predicted by astronomical theorists. To the left and right of source *B*, one may observe an extended source of radio emission, which is probably associated with galactic nebulosities, such as Index Catalog 4701, close to the galactic plane.<sup>1,9</sup> This tracing probably marks the first observation at these wavelengths of faint emission in the vicinity of and at the position of the galactic plane.

Fig. 6 is an observation of thermal radio emission from the planet Jupiter. The time constant was 320 seconds, giving a theoretical sensitivity in this case of  $0.010^{\circ}\text{K}$ . Referring to Fig. 6, the antenna was positioned  $\frac{1}{2}^{\circ}$  east of Jupiter at point *A* on the scan and

then allowed to track this position to establish a radiometer zero level, with Jupiter just outside the beam pattern. At *B*, the antenna was pointed directly at Jupiter and allowed to track the planet. During this portion of the scan, the radiometer output should describe an exponential curve asymptotic to the antenna temperature produced by the planet. At *C*, the antenna was pointed  $\frac{1}{2}^{\circ}$  west of Jupiter, and again allowed to track. During this portion of the scan, the radiometer output should describe another exponential until the zero level is again reached. The radiometer response does follow the predicted path and indicates a peak antenna temperature due to the planet of  $0.15^{\circ}\text{K}$ . If it is assumed that the gain of the antenna is one half that of a perfect antenna, a black body temperature slightly greater than  $200^{\circ}\text{K}$  is indicated.

Fig. 7 is a radiometer measurement of the emission from the planet Saturn, taken in the same manner as the Jupiter observation. The antenna tracked east of the planet from *A* to *B*, pointed at the planet from *B* to *C*, and west of the planet following *C*. The antenna temperature due to the planet as measured by this scan is  $0.04^{\circ}\text{K}$ , corresponding to a flux of about  $4 \times (10^{-26})$

<sup>9</sup> F. T. Haddock, C. H. Mayer, and R. M. Sloanaker, "Radio emission from the Orion Nebula and other sources at  $\lambda 9.4 \text{ cm}$ ," *Astrophys. J.*, vol. 119, pp. 456-459; March, 1954.

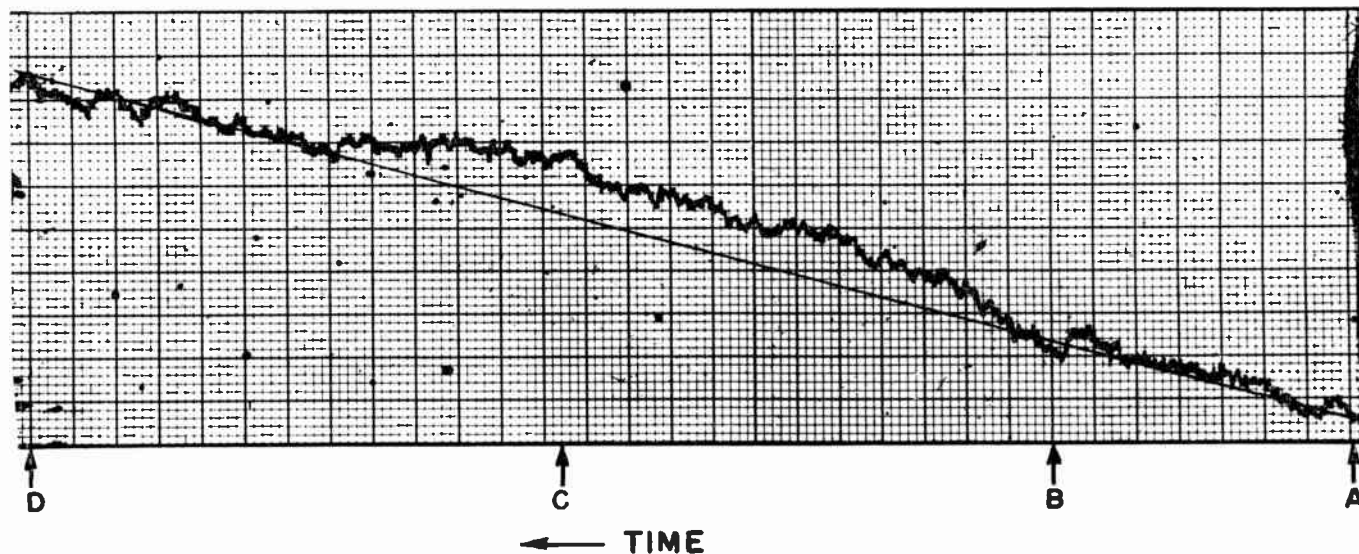


Fig. 7—Radiometer measure of radio emission from Saturn. Maximum antenna temperature  $0.04^{\circ}\text{K}$ . Time constant = 320 seconds. Between A and B, the antenna pointed  $\frac{1}{2}^{\circ}$  east of Saturn; between B and C, the antenna pointed at the planet; between C and D, the antenna pointed  $\frac{1}{2}^{\circ}$  west of Saturn.

watt  $\text{m}^{-2}(\text{cps})^{-1}$  or  $5.5 \times (10^{-16})$  watts of power detected at the antenna terminals. This is probably the smallest antenna temperature detected to date with a microwave radiometer. In this case, one may not determine a black body temperature for the planet without first knowing whether the well-known rings are contributing to the radio emission. If the particles making up the rings are much smaller than the 3.75-cm receiver wavelength, or are very cold, the particles will contribute very little emission at this wavelength. Since we do not have a reliable measure of the size of the ring particles or their temperature, it is possible to invert the argument, accepting the planetary temperature given by other means,<sup>10</sup> and determine whether or not the rings are present radiowise. To eliminate calibration errors as much as possible, the predicted ratio of the antenna temperature of Jupiter to that of Saturn was computed for both cases; *i.e.*, with and without the presence of the rings. Since the observations of Jupiter and Saturn were made in quick succession, taking the ratio of the observed antenna temperatures from these observations should eliminate systematic calibration errors. From published data for the date of the observations, July 24, 1957, the ratio of the antenna temperature Jupiter to Saturn should be 4.7 if the rings are transparent, and about 3.0 if the rings are opaque. The observed ratio is 4.3, indicating that the rings are not radio sources at 8000 mc, which may mean that they principally consist of particles smaller than 3.75 cm in diameter, or are at a temperature less than about  $20^{\circ}\text{K}$ .

A "drift curve" of the planetary nebula NGC 7293 (the "Helix" Nebula) is shown in Fig. 8. This represents the first radio observation of a planetary nebula.

This tracing was made in the same manner as the tracings of Cassiopeia A and the region of M17, with an 80-second time constant, and indicates a maximum antenna temperature for the nebula of  $0.25^{\circ}\text{K}$ . It is desirable with weak signals to take a mean of several observa-



Fig. 8—Radiometer response as the planetary nebula NGC 7293 passed through the antenna beam. Maximum antenna temperature =  $0.25^{\circ}\text{K}$ . Time constant = 80 seconds.

tions, as this allows one to make a statistical analysis of the data to derive a measure of its reliability. Five observations of NGC 7293 have been combined to obtain a mean curve. The resultant curve and the probable errors derived for the experimental points are shown in Fig. 9. The mean probable error is  $0.022^{\circ}\text{K}$ . The actual scatter among the points themselves suggests that the actual probable error is somewhat smaller than this. This can occur because the observer must draw an arbitrary zero level through each tracing of the radio source before deriving antenna temperatures from the tracing, and this zero will always be slightly in error. The effect is to introduce no error in the relative positions of the derived experimental points, but to enhance the probable errors derived in a straightforward way from the observational data. It is fortunate that this is the case, as one can be sure that the derived probable errors are too large, and hence the data are actually more reliable than the probable errors indicate. In this case, the actual scatter among the points indicates that the true probable error is of the order of  $0.010^{\circ}\text{K}$ .

<sup>10</sup> C. W. Allen, "Astrophysical Quantities," University of London, London, Eng., 1956.

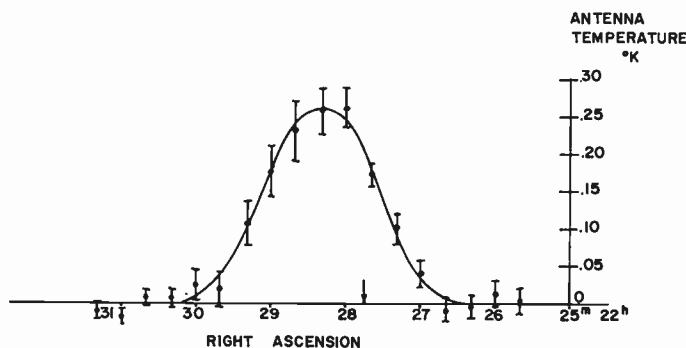


Fig. 9—Mean of 5 observations of NGC 7293, with probable errors of the observed points indicated. The mean probable error is  $0.022^{\circ}\text{K}$ ; the arrow indicates the optical center of the nebula.

From the published optical data,<sup>11-13</sup> the expected antenna temperature for the nebula was computed. The uncertainties in the optical data make it possible for this temperature to be in error by at least a factor of five. In the case of NGC 7293, assuming the antenna gain to be half that of an ideal antenna, the predicted antenna temperature is  $0.16^{\circ}\text{K}$ , which is in excellent agreement with the observed antenna temperature of  $0.26^{\circ}\text{K}$  from Fig. 9. The data of Fig. 9 show a response to the nebular signal which is broadened about  $6'$  of arc over the response from a point source. This is to be expected, as this nebula is about  $15'$  of arc in diameter, and has faint optical extensions extending at least as far as  $10'$  of arc from the center of the nebula. The arrow in Fig. 9 indicates the optical center of the nebula, and it is seen that the center of the radio emission as determined from the present observations deviates appreciably from the optical center, and actually lies very near the edge of the nebula. The difference between the two centers seems too large to be attributable to instrumental errors and is probably real. It is of interest to note that the center of radio emission apparently deviates from the optical center in the same direction as faint extensions of the nebula, recently observed on large-scale, high quality, photographs. Further radio and optical studies of this nebula are clearly indicated.

Fig. 10 is a reproduction of a drift curve of the planetary nebula NGC 6853 (the "Dumbbell" Nebula). A time constant of 80 seconds was used, and a maximum antenna temperature of  $0.10^{\circ}\text{K}$  is indicated. Four such observations have been combined to give the results shown in Fig. 11. The mean probable error from the data is  $0.017^{\circ}\text{K}$ , although, as before, the scatter of the points among themselves suggests that the true probable error is of the order of  $0.008^{\circ}\text{K}$ , which is representative of the extremely high-receiver sensitivity. The antenna temperature predicted from the optical data is

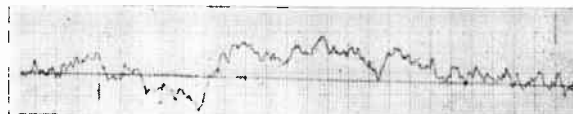


Fig. 10—Radiometer response as the planetary nebula NGC 6853 passed through the antenna beam. Maximum antenna temperature =  $0.10^{\circ}\text{K}$ . Time constant = 80 seconds.

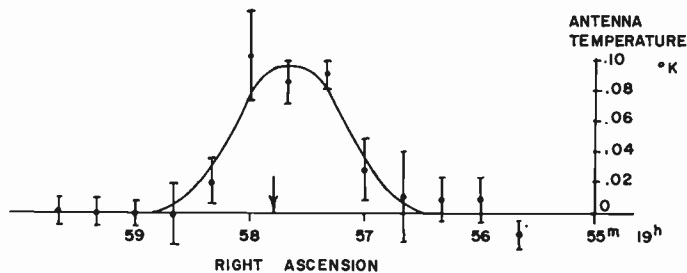


Fig. 11—Mean of 4 observations of NGC 6853, with probable errors of the observed points indicated. The mean probable error is  $0.017^{\circ}\text{K}$ ; the arrow indicates the optical center of the nebula.

$0.07^{\circ}\text{K}$ , which is in remarkable agreement with the observed temperature of  $0.09^{\circ}\text{K}$ . In this case, the optical position of the nebula, as indicated by the arrow in Fig. 11, is in close agreement with the radio position. This was expected since the dimensions of this nebula are roughly  $6' \times 8'$ .

#### CONCLUSION

The traveling-wave tube radiometer described in this report fulfills the theoretical sensitivity deduced from its electronic characteristics. The inherent high stability achieved is of great value to radio astronomers. This high sensitivity and stability was achieved by careful consideration and treatment of circuit components which do not affect the simple theoretical considerations of circuit sensitivity.

Astronomical results indicate that one may readily observe the temperature of the planets with a radiometer of the type described. For the first time, it is possible with ease and reasonable speed to make a detailed study of galactic radiation at 3- to 4-cm wavelengths. Preliminary observations described here suggest that much important data will accrue from such a study. The radio observations of planetary nebulas, achieved for the first time through the use of this radiometer, have established a new field for the application of radio astronomy. The first results reported here indicate that such radio information will greatly improve the accuracy to which some parameters of the nebulas are known, and may bring to light important aspects of these objects which have not been observable until now.

#### ACKNOWLEDGMENT

The authors are grateful to Peter D. Strum, Harry E. Adams, and A. William Gruhn of the Ewen Knight Corp. for the extensive, unprecedented engineering development required to achieve the optimum equipment performance described here.

<sup>11</sup> D. H. Menzel and L. H. Aller, "Physical processes in gaseous nebulas. XII. The electron densities of some bright planetary nebulas," *Astrophys. J.*, vol. 93, pp. 195-201; January, 1941.

<sup>12</sup> T. Page and J. L. Greenstein, "Ionized hydrogen regions in planetary nebulas," *Astrophys. J.*, vol. 114, pp. 98-105; July, 1951.

<sup>13</sup> I. S. Shklovsky, "A new scale of distances to planetary nebulas," *Astron. J. Soviet Union*, vol. 33, pp. 222-235; 1956.

# Present and Future Capabilities of Microwave Crystal Receivers\*

C. T. McCOY†

**Summary**—The lower limits of receiver noise are explained in terms of the fundamental physical constants of vacuum tubes and microwave crystal rectifiers.

With negative-grid vacuum tubes, the receiver noise, expressed in absolute temperature units, can be about 30°K at 10 mc but increases to about 1000°K at 1000 mc. For crystal superheterodyne at all frequencies below 10,000 mc, the receiver noise can be down to 600°K, limited only by the crystal mixer. Above 10,000 mc the crystal rectifier parasitic elements—spreading resistance and barrier capacity—cause the receiver noise to increase rapidly to values of approximately 7000°K at 70,000 mc.

For the future, high mobility semiconductors and new rectifier geometry promise substantial reduction of the parasitics. Also, a cooling mechanism promises limitless reduction in noise; a receiver noise of 150°K for all frequencies below 100,000 mc seems feasible.

## I. INTRODUCTION AND BACKGROUND

THERE are many military and commercial receiver applications in which the environment is sufficiently controlled or selected so that the weakest detectable signal is determined solely by the equivalent thermal-type noise at the input of the receiver. A reduction in receiver noise would permit either an equivalent reduction in transmitter power or an increase in range, or both.

This paper reviews the present-day fundamental limitations of this receiver noise in the frequency range from 10 to 100,000 mc. The two types of receivers covered are the negative-grid vacuum-tube amplifier and the crystal superheterodyne, because both are capable of realizing approximately the lowest receiver noise of today and of the future.

The complete treatment of low-noise amplifiers and crystal mixers is extremely complicated, as anyone will agree who has read literature on the subject.<sup>1,2</sup> To evaluate the present state of the low-noise art, as well as its future prospects, the major noise contributions should be boiled down to a few basic parameters. This paper attempts to accomplish this, without excessive loss of rigor, by considering the amplifier noise as only that coming from the first triode stage, and the crystal-converter noise as only that in a simple broad-band (signal and image-matched) design. Optimized operating and design parameters always are assumed.

\* Original manuscript received by the IRE, August 2, 1957; revised manuscript received, November 3, 1957.

† Philco Corp., Philadelphia, Pa.

‡ G. E. Valley and H. Wallman, "Vacuum Tube Amplifiers," M.I.T. Rad. Lab. Ser., McGraw-Hill Book Co., Inc., New York, N. Y., vol. 18; 1948.

§ H. C. Torrey and C. A. Whitmer, "Crystal Rectifiers," M.I.T. Rad. Lab. Ser., McGraw-Hill Book Co., Inc., New York, N. Y., vol. 15; 1948.

The vacuum-tube noise parameters have been scattered throughout literature for some time. The relationship between crystal-mixer noise and a few fundamental crystal-physics parameters, with expectations for the future, is only now appearing in literature, but without the conceptual simplification presented here.

## II. DISCUSSION AND ANALYSIS

### A. Receiver Noise

Friis' standard noise-figure definitions and relationships<sup>3</sup> are used throughout this paper, though antenna noise is separated from receiver noise. Further, it is found convenient to quote the magnitude of noise in various terms, such as: 1) a power  $P$  in watts; 2) an absolute noise temperature  $T$  in degrees Kelvin; 3) a normalized (to 290°K) temperature ratio  $\tau$ ; or 4) in decibels, db, by taking 10 times the common log of  $\tau$ .

For example, the noise contributions to the over-all receiver-noise sensitivity  $\tau_s$  of a broad-band microwave crystal superheterodyne receiver is given by<sup>4-6</sup>

$$\tau_s = (F_x - 2) + L_x(F_{IF} - 1) + 2\tau_a \quad (1)$$

where

$(F_x - 2)$  = the excess mixer noise figure,

$L_x$  = mixer conversion loss, and

$(F_{IF} - 1)$  = the excess IF noise figure, and  $\tau_a$  the normalized antenna temperature, all in dimensionless units of temperature ratio.<sup>7</sup>

All similar noise formulas will be in these units. A

<sup>3</sup> H. T. Friis, "Noise figures of radio receivers," PROC. IRE, vol. 32, pp. 419-422; July, 1944.

<sup>4</sup> P. D. Strum, "A note on noise temperature," IRE TRANS., vol. MTT-4, pp. 145-151; July, 1956.

<sup>5</sup> The term "noise sensitivity" and the symbol  $\tau_s$  are identical to "operating noise figure" and  $F_{op}$ , respectively, in footnotes 4 and 6. The author believes the sensitivity term has the advantages of being more self-explanatory, shorter, and less apt to be confused with the standard term "noise figure." The symbol  $F_{op}$  can be confused with "optimum noise figure."

<sup>6</sup> D. O. North and H. T. Friis, "Discussion on noise figures of radio receivers," PROC. IRE, vol. 33, pp. 125-127; February, 1945.

<sup>7</sup> The corresponding narrow-band (*i.e.*, image-blocked) receiver-noise sensitivity  $\tau_s$  is given by

$$\tau_s = (F_x - 1) + L_x(F_{IF} - 1) + \tau_a \quad (1a)$$

Narrow-band mixer-noise figure  $F_x$  and conversion loss  $L_x$  approximately is equal, but not identical (footnote 11), to its respective broad-band counterpart. Whether broad-band or narrow-band receiving inherently is more sensitive depends on the relative magnitudes of the receiver noise and the antenna noise. For radio astronomy, when the desired signal is an increment in the antenna-noise background, and when this background noise is small compared to the receiver noise, the effect of the increment will be twice as great (3 db better) in the broad-band receiver.

typical microwave-receiver noise figure of 7.5 db has noise composition, in the normalized temperature ratio units of (1), of:

$$5.6 = (4.2 - 2) + 3.5(1.4 - 1) + 2. \quad (2)$$

If each of the terms of (1) is multiplied by the normalizing temperature  $T_0$  of 290°K, inherent in the definition of a noise figure, (1) and (2) can be re-expressed as

$$T_s = T_x + T_{IF} + 2T_a, \quad (3)$$

$$1625^\circ\text{K} = 638^\circ\text{K} + 407^\circ\text{K} + 580^\circ\text{K}. \quad (4)$$

The sum of the first two terms on the right side of the above equation represents the receiver noise<sup>8</sup> and they may be given the normalized noise temperature symbol of  $\tau_r$ , or in terms of the absolute temperature by  $T_r$ . It may be noted that when the normalized antenna temperature  $\tau_a$  is unity, the over-all receiver-noise sensitivity  $\tau_s$  is identical in definition to the standard receiver-noise figure  $F_r$ . Both the receiver-noise figure and the receiver-noise sensitivity refer the total noise to the input of the receiver. The former includes a standard 290°K antenna noise and the latter, the actual operating antenna noise. The parameters  $\tau_x$ ,  $\tau_r$ ,  $\tau_{IF}$ , and  $\tau_a$  are convenient for identifying the noise sources and comparing their magnitude. To simplify nomenclature without loss of clarity, the generic name of these terms will be called "noise." The dimension—in db, ratio, or degrees Kelvin—will indicate the form clearly. The lowest possible sensitivity noise  $T_s$  would of course be 0°K, with no noise contribution from either receiver  $T_r$  or antenna  $T_a$ . This represents infinite sensitivity, which is represented more clearly in db units, namely,

$$\tau_s = 0 = -\infty \text{ db}.$$

### B. The Vacuum Tube Amplifier in the 10 to 1000-MC Range

If the bandwidth is sufficiently narrow and low-loss networks are employed, the excess noise figure ( $F-1$ ) of a vacuum-tube amplifier will be determined both in theory and practice solely by tube parameters as expressed in<sup>9-11</sup>

$$F - 1 = \tau_v \left[ \frac{g_e}{g_m} \right]^{1/2} \quad (5)$$

where  $\tau_v$  has a value of approximately 6 for present-day oxide cathodes. The ratio of electronic input conductance to transconductance of the tube is  $g_e/g_m$ . Electronic

<sup>8</sup> This more properly is called "excess receiver noise."

<sup>9</sup> An approximation derivable from formulas of footnotes 10 and 11.

<sup>10</sup> L. J. Giacoletto and H. Johnson, "UHF triode design in terms of operating parameters and electrode spacings," *Proc. IRE*, vol. 41, pp. 51-58; January, 1953.

<sup>11</sup> Valley and Wallman, *op. cit.*, pp. 563, 638-640.

input conductance is proportional to the square of the frequency because of electron transit time between cathode and grid. Thus, the minimum excess noise for vacuum tubes is proportional to frequency. Other than frequency (and a compromise with amplification factor to achieve adequate gain), the minimum ratio of  $g_e/g_m$  is determined solely by the practicalities involved in minimizing cathode-grid spacing and maximizing cathode-emission current density.

The best low-noise vacuum tubes of today, such as the GL 6229 and 417A, have the typical value of  $g_e/g_m$  of 0.02 at 100 mc. Using these values and a  $\tau_v$  of 6, the frequency dependency of the excess amplifier noise ( $F_r - 1$ ) is shown by the solid line in Fig. 1. The 416B with ex-

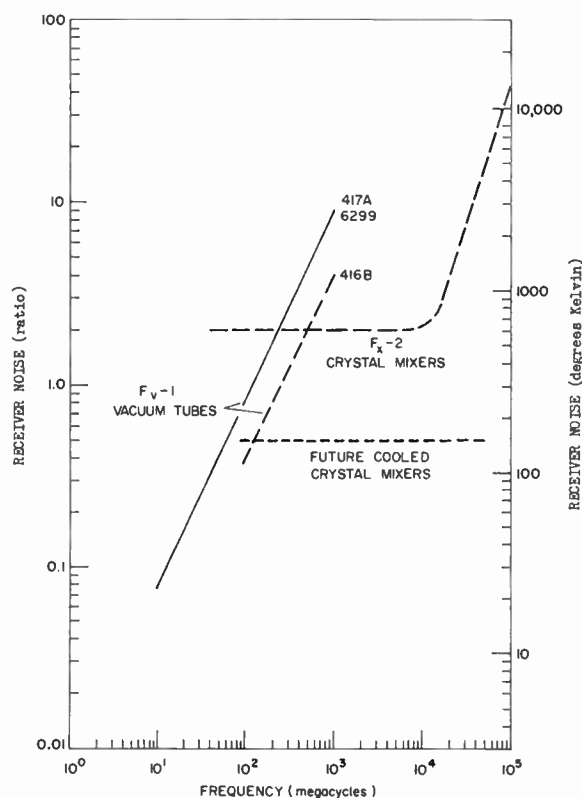


Fig. 1—Receiver noise vs frequency.

ceptionally close-grid cathode spacing achieves excess noise ( $F_v - 1$ ), as shown by the dotted straight line, but has not been suitable for the low vhf because of its internal construction.

For a vacuum-tube receiver, the noise due to the receiver alone,  $T_r$ , would be the  $F_v - 1$  curves of Fig. 1, which can be seen to have values (in absolute temperature) of about 30°K at 10 mc; these curves rise with frequency to about 1000°K at 1000 mc. The over-all noise sensitivity  $T_s$  would be obtained by adding on the antenna temperature  $T_a$ .

### C. Crystal-Mixer Noise in 500 to 10,000-MC Range

Discussed here are the essential physical dependences of crystal-mixer noise figure  $F_x$ , conversion loss  $L_x$ , and

noise temperature<sup>12</sup>  $t_x$ . For a broad-band crystal-mixer superheterodyne receiver, the over-all noise sensitivity  $\tau_s$  can be derived by<sup>13</sup>

$$\tau_s = (L_x t_x - 2) + L_x(F_{IF} - 1) + 2\tau_a \quad (6)$$

which is the same as (1), with  $F_x$  being replaced by the equivalent  $L_x t_x$  product. Omitting the antenna noise contribution, the receiver noise  $\tau_r$  dependency is

$$\tau_r = (L_x t_x - 2) + L_x(F_{IF} - 1). \quad (7)$$

Usually, any combination of a sufficiently good IF tube and/or a low enough frequency can be chosen to make the IF contributing term much smaller than that of the mixer. The dependencies of  $L_x$  and  $t_x$  on crystal rectifier physics will be explained now.

1) *Conversion Loss*: Conversion is derived solely by the action of the local oscillator on the barrier resistance,<sup>14-16</sup> in the equivalent circuit of the crystal rectifier shown in Fig. 2. To small rf signals, the converter essentially acts<sup>17</sup> as the passive resistive network of Fig. 3. Conversion loss is calculable readily from this network, which is calculable from the circuit of Fig. 2, which in turn is calculable from local oscillator and bias parameters plus the physics parameters of the rectifier soon to be discussed. When the rf source (antenna) is matched identically to the converter at both signal and image frequencies, the converter is of the broad-band type, in contrast to a narrow-band designation for an "open" or "short" termination of the image.

One important characteristic of the broad-band mixing is that the conversion loss  $L_0$ <sup>18</sup> is the same from either the signal or image terminal to IF. Another, is that broad-band conversion loss  $L_0$  never can be less than 2, for exactly as much signal energy is converted to and absorbed in the image terminal as in the IF. Despite this loss, the broad-band converter noise almost is as low<sup>16</sup> as the narrow band; is far simpler to design and test; is the one implied in present-day commercial and military crystal specifications; and therefore, is discussed in this paper.

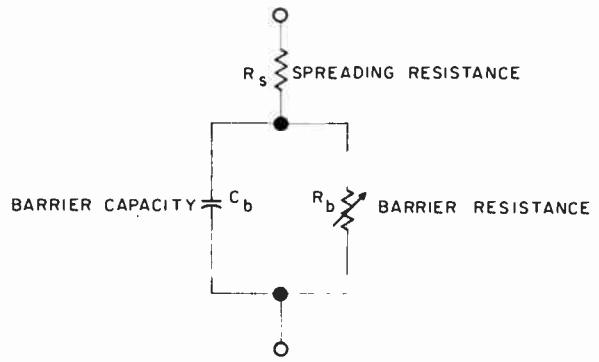


Fig. 2—Equivalent circuit of a crystal diode.

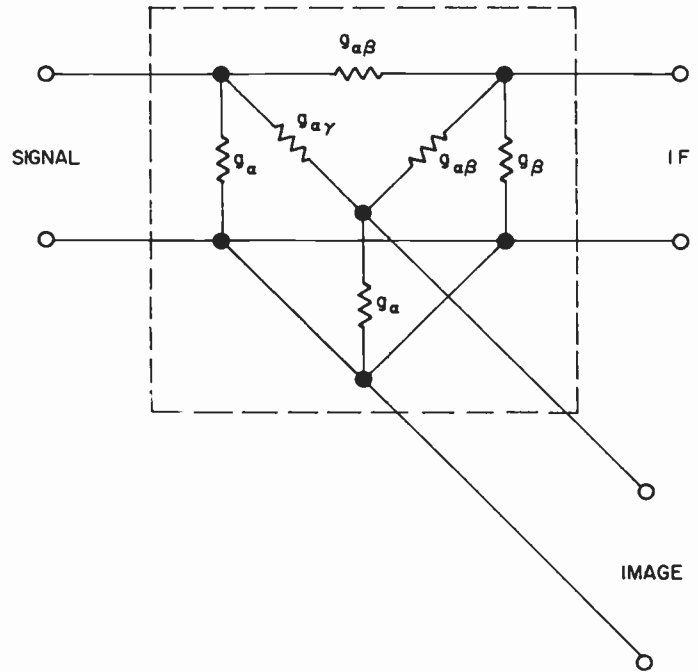


Fig. 3—Equivalent circuit of a crystal mixer.

All crystal rectifiers of any design or semiconductor have the same limit in resistance variability, namely, the maximum value of the coefficient  $\alpha$  in the forward current-voltage ( $I-V$ ) equation of the barrier:

$$I = A[e^{\alpha V} - 1]. \quad (8)$$

The maximum value for  $\alpha$  is<sup>19</sup>

$$\alpha = \frac{q}{KT} \cong 40 \text{ volt}^{-1} \quad (9)$$

for  $T = 290^\circ\text{K}$

where

- $q$  = the charge of the electron,
- $K$  = Boltzmann's constant, and
- $T$  = the temperature of the semiconductor.

The best possible conversion loss  $L_0$  (broad-band) due to barrier resistance alone has been calculated as a function of the local oscillator drive  $V$ , and is shown by

<sup>19</sup> Torrey and Whitmer, *op. cit.*, p. 82.

<sup>12</sup> This refers in standard Friis terminology to the noise of the IF output resistance of the mixer. The noise contributions to over-all receiver-noise sensitivity as given in (1)-(3) are different and given the notation  $\tau$  in this paper. Section (II-C 2) introduces a third noise temperature,  $l$ . All have the same basic meanings and dimensionless units.

<sup>13</sup> Torrey and Whitmer, *op. cit.*, chs. 3 and 5.

<sup>14</sup> Torrey and Whitmer, *op. cit.*, Secs. 5.11 and 5.12.

<sup>15</sup> G. C. Messenger and C. T. McCoy, "Theory and operation of crystal diodes as mixers," *PROC. IRE*, vol. 45, pp. 1269-1283; September, 1957.

<sup>16</sup> C. T. McCoy, "Principles of low noise receiver design," *Conv. Rec. of Second Microwave Crystal Rectifier Symposium, Hexagon, U. S. Signal Corps Eng. Labs., Fort Monmouth, N. J.; February 27-29, 1956, and Electronic Industries & Tele-Tech*, vol. 16, pp. 54-57, 152-154; November, and pp. 64, 65, 142, 144, 146; December, 1957.

<sup>17</sup> This simplification excludes harmonic image terminals that footnote 11 shows to be as effective as the fundamental image terminal under certain conditions. However, for best design the harmonic image terminals are shorted out, leaving an effective conversion network as shown in Fig. 3.

<sup>18</sup> The subscript 0 means broad-band conversion, the subscript  $x$  does not specify the type.

the solid line in Fig. 4. It can be seen that the line asymptotically approaches the minimum theoretical value of 2. The spreading resistance  $R_s$  and barrier capacity  $C_b$ , called parasitic elements, increase the conversion loss over that attainable by barrier alone. These elements can be minimized only, never completely eliminated. Least parasitic degradation comes from dividing it equally between the two elements as shown by the dotted and dashed curves in Fig. 4, which represent the performance of the 1N263 germanium mixer diode at 9300 mc. A conversion loss  $L_0$  of 3.3, as represented by the minimum of the upper curve of Fig. 4, has been achieved in practice, and is only a few tenths of a decibel worse than that achievable by barrier resistance alone.

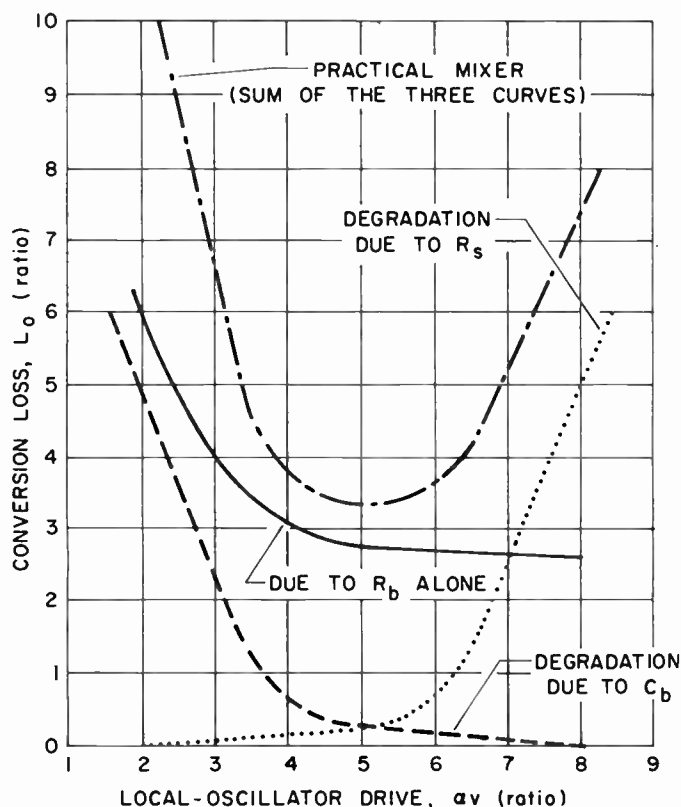


Fig. 4—Conversion loss vs local oscillator drive.

2) *Noise Temperature*: The total series resistance ( $R_s + R_b$ ) of Fig. 2 at any instant of time in a local oscillator cycle has a noise temperature  $t$  comprised of a complicated combination of thermal noise in the spreading resistance, shot noise in the barrier, and  $1/f$ -type semiconductor noise. The proportions vary over the local oscillator excitation cycle but the average is denoted by  $\bar{i}$ , which means the time-average noise temperature of the rectifier resistance of Fig. 2. Circuit theory<sup>4,20</sup> shows that  $\bar{i}$  will also be the noise temperature of each of the conductances of Fig. 3; from this can be calculated the relation

$$F_x - 2 = L_0 t_x - 2 = \bar{i}(L_0 - 2). \quad (10)$$

At room temperature, the shot noise of the barrier resistance in the forward conduction region has a minimum theoretical value of about  $\frac{1}{2}$  and the spreading resistance thermal noise is unity, of course.<sup>21</sup> The  $1/f$ -type-semiconductor noise contribution to  $\bar{i}$  is not yet completely resolved. It increases rapidly with local oscillator drive ( $V$  of Fig. 4), but decreases with reduction of spreading resistance. The lowest possible  $\bar{i}$  would have no  $1/f$ -type noise contribution and, therefore, would have a room temperature value somewhere between  $\frac{1}{2}$  and 1. In practice, for the best present-day microwave diodes, such as 1N263 in germanium and 1N23E in silicon, the local oscillator drive can be kept small and mostly within the forward conductivity region of the barrier; this results in a time-average crystal noise temperature  $\bar{i}$  of under 1.5 at a frequency of 30 mc. The conversion loss  $L_0$  of 3.3 previously mentioned was obtained with these same operating conditions.

3) *Crystal-Mixer Noise Contribution*: As discussed previously, the lowest present-day crystal-mixer noise contribution ( $L_x t_x - 2$ )—or its equivalent  $\bar{i}(L_0 - 2)$ —to the receiver-noise temperature  $\tau_r$  in (7) is about 2 in normalized units, or 580°K in absolute temperature units. At low IF frequencies for moderately narrow bandwidths (10 mc or less), good low-noise vacuum tubes can make the IF noise term  $L_x (F_{IF} - 1)$  appreciably less than this. Thus for all rf frequencies from vhf to 10,000 mc, present-day crystal-mixer superheterodyne receivers can have a receiver noise  $T_r$  of about 600°K. This is illustrated by the flat portion of the  $(F_x - 2)$  mixer noise curve in Fig. 1.

A word needs to be said on the choice of IF frequency for minimizing receiver noise in (7). The IF term increases almost linearly with frequency, as was explained in Section II-B. The mixer term due to the average crystal noise temperature  $\bar{i}$  in (10) decreases with frequency in a complicated manner. The portion of  $\bar{i}$  as a result of shot and thermal noise is flat with frequency. The remainder due to the semiconductor noise causes the frequency dependency. Literature<sup>15,22</sup> has estimated the semiconductor noise portion of  $\bar{i}$  to be  $(\bar{i} - 1)$  or  $(\bar{i} - \frac{1}{2})$ . The experimental data are not conclusive because of measurement problems and continual improvement of mixer diodes. As crystal-physics development reduces the parasitic elements, the  $1/f$ -semiconductor noise contribution to  $\bar{i}$  is reduced; therefore, the mixer noise  $\bar{i}(L_0 - 2)$  should become less and less frequency dependent. The optimum IF for lowest receiver noise depends on the relative magnitudes of the mixer and IF noise, and the quality of the mixer diode. The better the mixer diode, the lower the optimum IF

<sup>20</sup> W. L. Pritchard, "Notes on a crystal mixer performance," IRE TRANS., vol. MTT-3, pp. 37-39; January, 1955.

<sup>21</sup> Torrey and Whitmer, *op. cit.*, p. 183.

<sup>22</sup> P. D. Strum, "Some aspects of mixer crystal performance," PROC. IRE, vol. 41, pp. 875-889; July, 1953.

will be for minimum receiver noise. IF bandwidth requirements often necessitate a frequency higher than the low-noise optimum. For present-day mixer crystals of the 1N263 or 1N23E class and vacuum tubes of the 417B class, the optimum IF for receiver noise reduction probably is less than the commonly accepted 30 mc.

#### D. Crystal Superheterodyne for Above 10,000 MC

At frequencies appreciably higher than 10,000 mc, the spreading resistance and barrier capacity parasitics are the cause for rapid increase in both conversion loss and noise temperature.

Referring to Fig. 4, for the conditions of equal increase in conversion loss due to the parasitics—spreading resistance and barrier capacity—the actual conversion loss  $L_0$  can be approximated,<sup>15</sup> neglecting higher-order frequency terms, by

$$L_0 = L_b(1 + 2\omega C_b R_s) \quad (11)$$

where

$L_b$  = the loss due to barrier alone, and

$\omega$  = the rf radian frequency.

Fig. 4, representing the 1N263 germanium performance at 9300 mc, which also is typical of the best silicon, shows the second term in the parentheses to be about 0.25. For a barrier  $L_b$  of 2.7, the proportionality relation of (11) would predict a conversion loss  $L_0$  of about 8 (or 9 db) at 70,000 mc. This substantially agrees with the millimeter crystal performance reported.<sup>23</sup>

The more the conversion loss is degraded because of parasitics, the larger the local oscillator drive ( $V$  in Fig. 4) needed for optimizing. This, of course, increases the time-average crystal temperature  $\bar{i}$ . Thus, referring to (10) and (11), the reason is obvious for the rapid increase in mixer noise ( $F_x - 2$ ) with frequency; therefore, receiver noise  $T_r$  increases from a value of about 600°K at 10,000 mc to the high values for the millimeter wavelength indicated in Fig. 1.

#### E. Prospects for the Future

An explanation now of the basic physical dependencies of the crystal-diode parasitics will indicate how they can be reduced greatly. This would extend the flat portion of the mixer noise ( $F_x - 2$ ) curve of Fig. 1 to much higher frequencies. Also to be pointed out are the possible benefits of reduced temperatures<sup>24</sup> (that is, "cooling") on conversion loss  $L_0$  and the time-average crystal temperature  $\bar{i}$ .

The minimum value of the product of crystal-diode spreading resistance  $R_s$  and barrier capacity  $C_b$  has been

shown,<sup>15,24</sup> theoretically and experimentally, to be determined by the proportionality

$$R_s C_b \propto a \left[ \frac{\epsilon^{1/2}}{N^{1/2} b} \right] \quad (12)$$

where

$a$  = the radius of the whisker wire-semiconductor contact;

$\epsilon$  = the dielectric constant;

$N$  = the carrier concentration, and

$b$  = the mobility.

The bracket term represents fundamental physical constants with a calculable minimum theoretical value for any semiconductor. This minimum value for both germanium and silicon almost has been achieved so that with an approximate 4-micron contact radius for  $a$  the value of 0.25 for X-band conversion loss degradation [second term in (11)] is accounted for.

The prospects are bright for considerable reduction in the parasitic product ( $R_s C_b$ ) noise-sensitivity degradation at millimeter wavelengths.

1) Germanium, having a theoretical value 2.5 times lower than silicon for the bracket term of (12), recently has been applied with success to millimeter wavelengths.

2) The development of intermetallic semiconductors, such as Indium-Antimonide, with far higher mobilities promises much lower values for the bracket term than germanium.

3) Transistor<sup>25</sup> fabricating techniques permit new crystal rectifier geometry which also promises considerable reduction of the parasitic product ( $R_s C_b$ ).

Thus, the combination of high mobility semiconductors and new rectifier geometry should permit the 600°K flat part of the mixer noise curve ( $F_x - 2$ ) which is shown in Fig. 1 to be extended on up to 100,000 mc in the near future.

A marked reduction of crystal diode parasitics also should permit a reduction of the 1/f-type semiconductor noise in the time-average crystal-diode noise temperature  $\bar{i}$  discussed in Section II-C 2). The remaining thermal and shot-noise portion of  $\bar{i}$  is proportional linearly to absolute thermal temperature. All mixer performance previously discussed in this paper has been considered at the approximate room temperature of 290°K. Thus, from (10) it is indicated<sup>26</sup> that mixer noise ( $F_x - 2$ ) can be reduced linearly with absolute temperature if conversion loss  $L_0$  does not increase. Conversion loss is nearly independent of thermal temperature except for those temperatures with values too low to provide carriers in the semiconductor. This temperature is

<sup>23</sup> Bell Telephone Labs., "Millimeter Wave Research," final report to Office of Naval Research, Dept. of the Navy, under Contract NONR-687(00), ch. 5; October 1, 1955.

<sup>24</sup> G. C. Messenger and C. T. McCoy, "A low noise figure microwave crystal diode," 1955 IRE CONVENTION RECORD, pt. 8, pp. 68-73.

<sup>25</sup> Philco Res. Staff., "The surface-barrier transistor (five parts)," PROC. IRE, vol. 41, pp. 1702-1720; December, 1953.

<sup>26</sup> G. C. Messenger, "Cooling of crystal mixers and antennas," IRE TRANS., vol. MTT-5, pp. 62-63; January, 1957.

below 75°K for germanium suitable for microwave diodes. Cooling the crystal diode provides a further benefit to mixing because of the exponential coefficient  $\alpha$  in (8) and (9). This coefficient is inversely proportional to temperature; therefore, referring to Fig. 4, equally efficient conversion can take place with less local oscillator drive  $V$  which results in the further reduction of the  $1/f$ -type noise in  $\bar{i}$

It is not unreasonable to believe that in the relatively near future the parasitic product  $R_s C_i$  can be reduced by an order of magnitude from its best present value, and that present-day mixer noise ( $F_x - 2$ ) of 600°K can be reduced by a factor of 4 by cooling to liquid nitrogen temperature (75°K, about  $\frac{1}{4}$  of room temperature). Mixer noise, and thereby receiver noise, thus could be reduced to 150°K for all frequencies below 100,000 mc (see Fig. 1). This is not the lowest limit, for, provided semiconductors can be developed which will maintain conducting carriers at indefinitely lower temperatures, the mixer noise conceivably can be reduced without limit.

The vacuum-tube amplifier noise ( $F_r - 1$ ) curve of Fig. 1 and the discussion in Section II-B indicate that there will be difficulty in retaining the IF noise [second term in (7)] as a small part of the total receiver noise for cooled mixers; undoubtedly this will be accomplished by replacing the vacuum tube, that has a hot 1000°K cathode, with transistors that are developed for low

noise and are cooled by principles similar to those described for cooling the mixer diode.

### III. CONCLUSION

The low-noise capabilities of present-day microwave and millimeter crystal-superheterodyne receivers are determined primarily by the crystal mixer. The crystal-mixer noise, in essence, may be quantitatively related to a few fundamental physical parameters, namely: rectifying contact geometry, dielectric constant, carrier concentration, mobility, and temperature of the semiconductor.

For the future, improved contact geometry, better physical constants from new semiconductors, and lower temperatures promise limitless reduction in crystal-mixer and receiver noise. Therefore antenna noise will soon become the dominant limitation to over-all receiver sensitivity for all frequencies between 100 mc and 100,000 mc.

### IV. ACKNOWLEDGMENT

The author acknowledges that the subject matter on crystal physics of minimizing parameters and "cooled" mixers, as presented in this paper, originated with G. C. Messenger of the Philco Corp. research staff. The services of the Philco research report and drafting group in editing and illustrating this paper are appreciated.



# A High Resolution Radio Telescope for Use at 3.5 M\*

B. Y. MILLS†, A. G. LITTLE†, K. V. SHERIDAN†, AND O. B. SLEE†

**Summary**—A pencil-beam radio telescope of the cross type is described; it has a beamwidth of 49 minutes of arc and a sensitivity which approaches, under ideal conditions,  $2 \times 10^{-26}$  W m<sup>-2</sup> (cps)<sup>-1</sup>, that is, about 1/10,000 the flux density of the strongest radio source. To speed the collection of information the beam may be scanned, presenting information on five separate declinations quasi-simultaneously. Although it is intended primarily as a survey instrument, strong radio sources may be located with high accuracy; the probable errors in the measured positions of the stronger identified sources average less than a 1-foot arc. Methods of calibrating the flux density and temperature scales are described and some examples are given of the use of the radio telescope. The theory of operation and some of the design factors are discussed and it is concluded that, for a given size of antenna and the best snr on a typical radio source, the wavelength is rather well defined. This optimum generally lies in the range 2 m to 4 m, depending on details of the receiver and antenna design; other factors, however, play an important part in the choice of wavelength.

## I. INTRODUCTION

A TYPE of pencil-beam radio telescope which gives high resolution at meter wavelengths has been described by Mills and Little;<sup>1</sup> the directivity is obtained by multiplication of the fan-beam responses of two long crossed arrays. A large instrument of this form was constructed and has been in partial operation since May, and in full operation since August, 1954. A survey has been made of the distribution of 3.5-m radiation in the southern sky and a large number of individual astronomical bodies of interest have been investigated. The present paper describes the general theory and design of the radio telescope and gives some details of the construction, operation, and calibration; it is intended to supplement the observational papers already published and in preparation.

The need for such an instrument became clear as the result of investigations in 1950–1952 which showed that models of the distribution of radio emission, comprising “radio stars” and a slowly varying “background,” were inadequate.<sup>2,3</sup> In fact, it appeared that the distribution over the sky is very complex and includes emission features of all angular sizes. In these circumstances the use of conventional interferometer type instruments, which arbitrarily reject features above a certain size, is not desirable for general survey work; instead, pencil-beam

instruments of high resolution are indicated. The present instrument which was developed to meet this requirement has more than satisfied the original expectations and it is clear that it has marked advantages over the interferometric methods commonly employed at meter wavelengths. Not only can discrete sources be located accurately and unambiguously, but contour diagrams of extended objects can be obtained readily. The ability to detect faint radio sources is not normally limited by the resolution, as it is with a conventional meter wave interferometer, but by the statistical fluctuations of the received radiation and the receiver noise; the result is a much greater sensitivity for a given antenna gain. A disadvantage caused by an increase in side-lobe level in certain directions is found to be generally unimportant if the antenna is adjusted carefully.

## II. GENERAL DESCRIPTION

The instrument is located near Sydney at the Fleurs field station of the Radiophysics Laboratory (longitude = 150°46'.5 east, latitude = 33°51'.5 south). It comprises a cruciform arrangement of two arrays of dipoles each approximately 1500 feet long lying in the north-south and east-west directions, respectively. Each array consists of two rows of 250 half-wave dipole elements backed by a plane wire mesh reflector; the individual dipoles are aligned in an E-W direction. Photographs in Fig. 1 show the general arrangement. Each array has a fan-shaped response pattern of about 50° by 0°.6 between half-power points; a pencil-beam response is obtained by mixing the outputs of the arrays alternately in equal and opposite phases, approximately 430 times a second. Signals originating near the intersection of the two fan beams are received by both arrays and are modulated at the switching frequency of 430 cps; other signals have no modulation imposed. Consequently, by amplifying the modulated component alone, the response of the system is confined to the region of the intersection of the two fan beams and, in effect, a pencil-beam response is obtained. With the present arrangement this pencil beam is approximately circular in section and 49 minutes of arc between the half response points.

The pencil beam may be directed to different parts of the sky by altering either of the two fan beams by phase adjustment to the dipole elements of the arrays. Normally it is used as a transit instrument, that is, the movement of the pencil beam is confined to the meridian plane, for which it is necessary to phase the dipoles of the N-S array only. Two basic types of observation are made. In one, the pencil beam is directed to a fixed

\* Original manuscript received by the IRE, October 3, 1957.

† Radiophysics Laboratory, CSIRO, Sydney, Australia.

<sup>1</sup> B. Y. Mills and A. G. Little, “A high-resolution aerial system of a new type,” *Aust. J. Phys.*, vol. 6, pp. 272–278; September, 1953.

<sup>2</sup> B. Y. Mills, “The distribution of the discrete sources of cosmic radio radiation,” *Aust. J. Sci. Res.*, vol. A5, pp. 266–287; June, 1952.

<sup>3</sup> J. G. Bolton, G. J. Stanley, K. C. Westfold, and O. B. Snee, “Galactic radiation at radio frequencies. VII. Discrete sources with large angular widths,” *Aust. J. Phys.*, vol. 7, pp. 96–109; March, 1954.

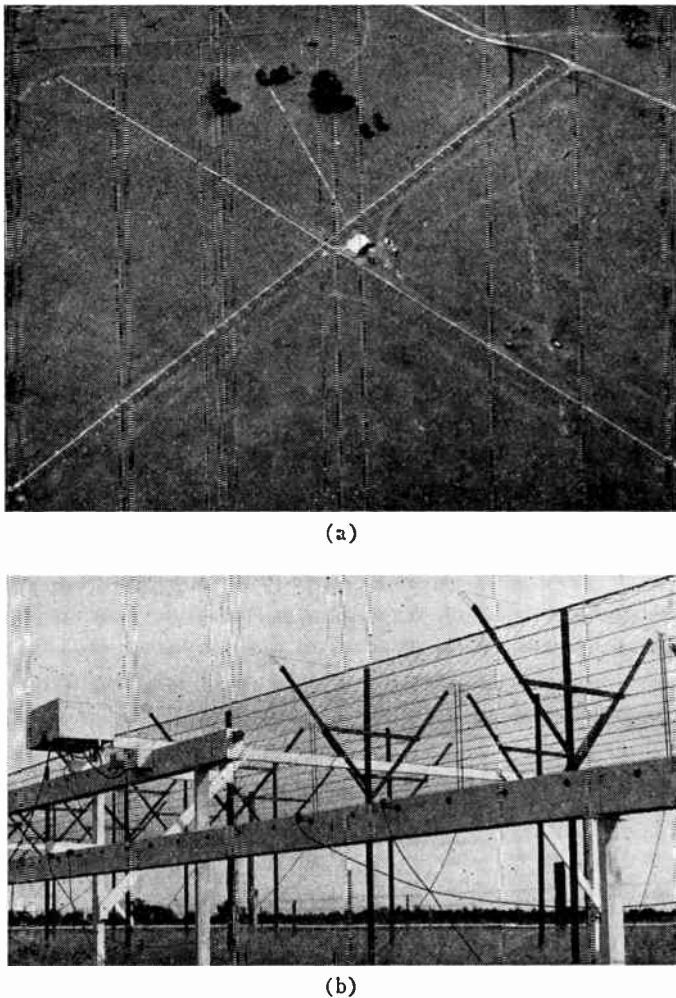
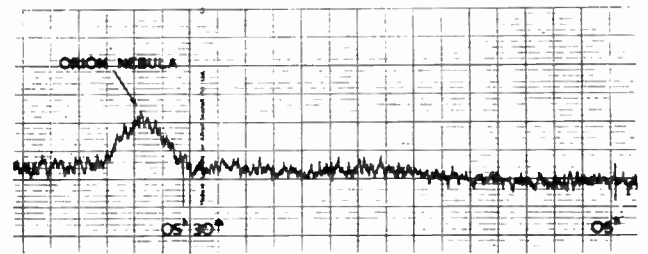
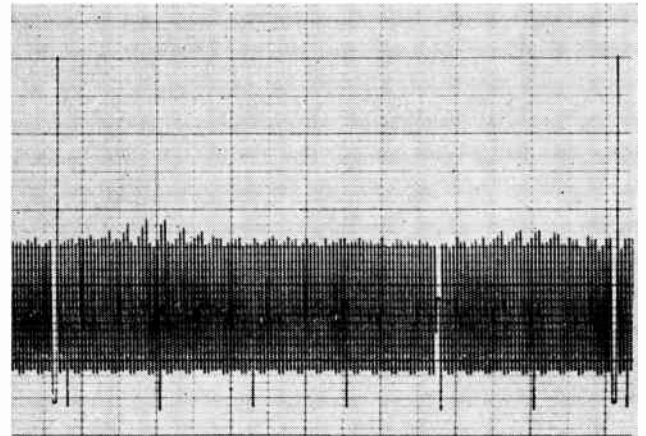


Fig. 1—Photographs of the radio telescope. (a) An aerial view of the instrument showing the general arrangement, (b) a close-up of one of the arrays showing the full-wave dipoles, the feed line, and coupling probes.

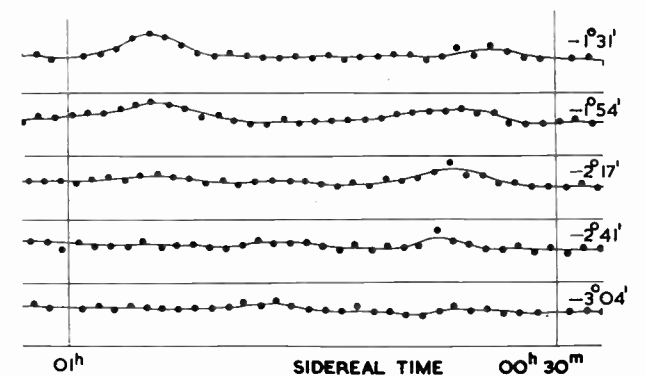
declination and the output recorded as the rotation of the earth sweeps the beam along a declination circle; this form of recording is illustrated in Fig. 2(a). Time marks are placed on the record at regular intervals, with a choice of 10, 20, or 30 minutes, and the time constant of the recording circuit can be varied from 1 to 12 seconds. The transit of a discrete source is shown. In the other method, shown in Fig. 2(b), the pencil beam is switched successively among five declinations slightly less than half a beamwidth apart at intervals which may be chosen to be 4, 8 or 12 seconds. During these intervals the signal is integrated on the recorder and returned to zero again at the end, forming a sawtooth pattern, the height of each "tooth" being proportional to the equivalent antenna temperature at the appropriate declination. It was shown before<sup>1</sup> that, to record the absolute brightness temperature in any direction, it is necessary to add the temperature derived from the pencil beam to a temperature derived from the arrays themselves. A modification in the present system, to be described later, requires the addition of the effective temperature of the N-S array only; this is added so as



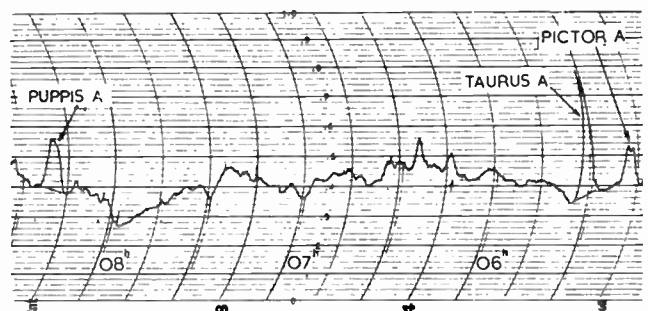
(a)



(b)



(c)



(d)

Fig. 2—Sample records obtained with the instrument. (a) A radio source of moderate intensity, the Orion Nebula, observed with fixed beam directed at a declination of  $-5^{\circ} 22'$ . (b) A section of "scanning" record centered on a declination of  $-2^{\circ} 17'$ . (c) Tracings of the individual declination sections in (b); two sources of moderate intensity are shown, the one on the right being complex. (d) A section of record obtained with the E-W array plus high-pass filter combination; radio sources are recorded over a range of declinations of about  $50^{\circ}$  or more. Some strong sources are noted.

to raise the base of the sawtooth by an amount proportional to the array temperature. Finally a bias is applied so that a sawtooth, which usually represents a temperature of about  $3000^\circ$ , is obtained in the absence of any signal; this is to eliminate difficulties with negative outputs, which often occur with this system. By plotting the tops of every fifth sawtooth separately as demonstrated in Fig. 2(c), five separate declination records may be obtained. The "scanning" method is used normally for obtaining isophotes and for general survey work; use is made of the fixed method when the greatest sensitivity and accuracy is required for the observation of a particular object.

Near the zenith and in regions of low sky brightness the sensitivity approaches  $2 \times 10^{-26} \text{ W m}^{-2} (\text{cps})^{-1}$  when using fixed recording. When scanning, only one fifth of the time is spent on each declination; statistical fluctuations therefore are increased by a factor of  $\sqrt{5}$  and the sensitivity correspondingly reduced. Two other factors can also result in reduced sensitivity. Firstly, in the neighborhood of the galactic plane, particularly near the galactic center, the background brightness increases markedly, increasing the noise fluctuation level. Secondly, at large zenith angles the gains of the arrays decrease because of the directivity of the individual dipole elements and the reflecting mesh, combined with foreshortening effects. Accordingly, the maximum zenith angle usually is restricted to  $\pm 45^\circ$  where the sensitivity has decreased by a factor of approximately two; however, greater angles have been used for special observations.

In addition to the above uses it is convenient to record the output of the E-W arm of the instrument separately. This arm has a fan-beam response normally confined to the meridian plane. The output is either recorded directly, or passed through an amplifier and high-pass filter combination which removes the variations in background level and leaves only the discrete sources and small scale irregularities. The record is useful for checking ionospheric effects and in the search for variable sources;<sup>4</sup> a sample is shown in Fig. 2(d).

### III. THEORY OF OPERATION

The basic theory of this type of radio telescope was outlined in a previous paper.<sup>1</sup> The present treatment is more general and includes the effects of errors in adjustments of the arrays and a more detailed account of the problems associated with the determination of absolute values for the sky brightness. Various idealized systems are treated to clarify the factors involved.

#### A. Arrays Without Cross Coupling

Consider first the case when the coupling between arrays is negligible. Let  $\bar{F}_1$ ,  $(\theta, \phi)$ , and  $\bar{F}_2(\theta, \phi)$  be the complex response patterns of the E-W and N-S arrays,

respectively. In the receiving case,  $\bar{F}_1$  and  $\bar{F}_2$  represent voltages produced at the mixing point in the receiver, when radiation is incident upon the antenna system from a direction fixed by angles  $\theta$  and  $\phi$ . The latter are measured from the E-W and N-S vertical planes passing through the antenna center. The voltage responses are normalized for maxima of unity and, of the factors determining their phases, only the contributions due to the orientation of the arrays with respect to the incident radiation, and the electrical path lengths to the mixing point, need be considered. In the transmitting case, which it is often useful to consider,  $\bar{F}_1$  and  $\bar{F}_2$  represent the normalized electromagnetic fields at a large distance from the antenna system.

If the power output from the system is due to a unit source with coordinates  $\theta, \phi$  is written as  $P_i$  when the arrays are connected in phase addition, and as  $P_0$  when the phase is changed by  $\psi$ , an angle which in practice is close to  $\pi$ , we have:

$$\begin{aligned} P_i &= K(\bar{F}_1 + \bar{F}_2)(\bar{F}_1 + \bar{F}_2)^* \\ P_0 &= K(\bar{F}_1 + \bar{F}_2 \exp i\psi)(\bar{F}_1 + \bar{F}_2 \exp i\psi)^* \end{aligned} \quad (1)$$

where  $K$  is a constant depending on the over-all gain of the system.

Assuming a square-law detector, the peak amplitude of the modulated signal output is therefore given by:

$$\begin{aligned} A_m = P_i - P_0 &= K\{(\bar{F}_1\bar{F}_2^* + \bar{F}_2\bar{F}_1^*)(1 - \cos\psi) \\ &\quad + i(\bar{F}_1\bar{F}_2^* - \bar{F}_2\bar{F}_1^*) \sin\psi\}. \end{aligned} \quad (2)$$

For convenience in evaluating this expression the phase of the signal from the E-W array, measured at the mixing point when the response is a maximum, will be taken as zero.

When the phase switching is exactly  $\pi(\psi = \pi)$ , and the arrays are symmetrical, and feeder lengths equal,  $\bar{F}_1$  and  $\bar{F}_2$  will be real at all angles and of positive or negative sign. Designating the responses in this case, as  $F_1$  and  $F_2$ , (2) reduces to

$$A_m = K \cdot 4F_1F_2. \quad (3)$$

If the final record deflection is proportional to  $A_m$ , the composite response pattern of the two arrays is then given by

$$R = F_1F_2. \quad (4)$$

These last two expressions were derived in an earlier paper;<sup>1</sup> they show that the effective polar diagram of the instrument is given by the product of the voltage diagrams of each array. Negative values for  $R$  occur when  $F_1$  and  $F_2$  differ in sign, as they may in the side-lobe responses.

In general, side lobes are likely to be particularly troublesome in directions in which either fan beam has its maximum response; *i.e.*, when  $F_1$  and  $F_2$  are large. Steps must therefore be taken to reduce such responses by tapering the current distribution along the arrays. We have adopted a truncated Gaussian distribution,

<sup>4</sup> O. B. Slee, "Apparent intensity variations of the radio source Hydra A," *Aust. J. Phys.*, vol. 8, pp. 498-507; December, 1955.

since side lobes may be reduced to any desired level, and the principal response is of circular or elliptical section and approximately Gaussian, leading to easy manipulation in data reduction processes. It is arranged that the current in the end dipoles is 1/10 that in the center; computation then indicates that side lobes are less than 1 per cent except for the first which is 2 per cent. Some other distributions are more efficient in the sense that a given beamwidth and side-lobe level may be obtained with a shorter array, but they are in general more critical in adjustment and, as we shall see later, adjustment errors are a major factor in causing spurious responses at large angles from the pencil beam. In Fig. 3 the computed beam shape is compared with the response to the "point" source Hydra A (IAU 09S1A).

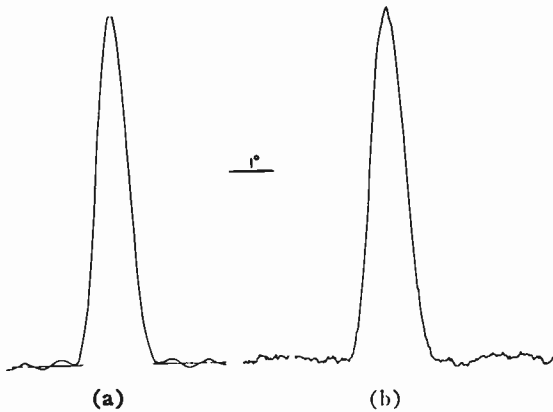


Fig. 3—A comparison between (a) the computed E-W response curve of the instrument and (b) the response to the transit of the radio source Hydra A (IAU 09S1A).

Before considering the effects of adjustment errors we will examine the effect of the neglected cross coupling between arrays on the response of a "perfect" system; *i.e.*, one in which the dipole currents all have their correct theoretical values and there are no extraneous effects.

### B. Coupling Effects in a "Perfect" System

When coupling is present, each antenna diagram is modified by the presence of the other array. The modified diagrams may be represented by  $\bar{F}_1(\theta, \phi) + \bar{E}_{21}(\theta, \phi)$  and  $\bar{F}_2(\theta, \phi) + \bar{E}_{12}(\theta, \phi)$  where  $\bar{E}_{12}$  and  $\bar{E}_{21}$  describe the effects of the coupling. In general the  $F$ 's and  $E$ 's are dissimilar functions of  $\theta$  and  $\phi$ , as coupling occurs only near the centers of each array.

The composite diagram is obtained from (2), thus:

$$R = \frac{1}{2} \{ (\bar{F}_1 + \bar{E}_{21})(\bar{F}_2 + \bar{E}_{12})^* + (\bar{F}_1 + \bar{E}_{21})^*(\bar{F}_2 + \bar{E}_{12}) \}. \quad (5)$$

If

$$\begin{aligned} \bar{E}_{12} &= x_{12} + iy_{12} \\ \bar{E}_{21} &= x_{21} + iy_{21} \end{aligned} \quad (6)$$

and  $\bar{F}_1$  and  $\bar{F}_2$  are real, as before, then

$$R = F_1F_2 + (F_1x_{12} + F_2x_{21}) + \frac{1}{2}(x_{12}x_{21} + y_{12}y_{21}). \quad (7)$$

Thus, two extra terms are added to the desired response, the first important in directions in which either or both arrays have a large response ( $F$  large) and the second, very small, but distributed over a large solid angle because coupling is confined to the array center. It has been found impossible to eliminate or compensate for these responses in any convenient way; accordingly, in actual operation, the coupling between arrays is reduced to a negligible value by removing dipoles near the center.

### C. Removing Central Dipoles in a "Perfect" System

In the experimental version of this instrument,<sup>1</sup> dipoles were removed from the centers of both arrays to eliminate interaction: this procedure, therefore, will be considered first. The voltage directional diagrams of the remaining dipoles may be obtained by subtracting the response of the array formed by the dipoles removed from that of the complete array. Since the arrays are assumed to be in perfect adjustment all responses are real. Thus, if  $\xi_1(\theta, \phi)$  and  $\xi_2(\theta, \phi)$  are the additional responses, normalized with respect to  $F_1$  and  $F_2$ , the resultant diagrams become  $F_1 - \xi_1$ , and  $F_2 - \xi_2$ . The composite diagram is given then by

$$\begin{aligned} R &= (F_1 - \xi_1)(F_2 - \xi_2) \\ &= F_1F_2 - (F_1\xi_2 + F_2\xi_1) + \xi_1\xi_2. \end{aligned} \quad (8)$$

The diagram again has unwanted responses of small amplitude represented by the last two terms. In contrast to the previous example, however, the response may be readily evaluated,  $\xi_1$  and  $\xi_2$  being known precisely. Now a thermodynamical argument shows that if such a system is placed in a constant temperature enclosure, the power output is independent of the phase difference between arrays and is the same whether they are connected in or out of phase; the net response is therefore zero, that is,

$$\int_{4\pi} R d\Omega = 0. \quad (9)$$

In order to indicate the correct temperature in these circumstances, the brightness temperatures indicated by each array were originally averaged and added to the temperature indicated by the composite system. This procedure gives an over-all response of the form

$$\begin{aligned} R &= F_1F_2 - (F_1\xi_2 + F_2\xi_1) + \xi_1\xi_2 \\ &\quad + k \{ (F_1 - \xi_1)^2 + (F_2 - \xi_2)^2 \} \end{aligned} \quad (10)$$

the factor  $k$  being chosen to yield the correct average temperature. It may be shown that the effect is to reduce the magnitude of the unwanted spurious responses, but it is clear from (10) that they are not eliminated.

An improvement is possible by increasing  $k$  until the second and fourth terms in (10) balance in a constant temperature enclosure, that is,

$$\int_{4\pi} (F_1\xi_2 + F_2\xi_1)d\Omega = k \int_{4\pi} \{(F_1 - \xi_1)^2 + (F_2 - \xi_2)^2\} d\Omega. \quad (11)$$

In practice, very few dipoles need to be removed and, consequently, each  $\xi$  represents a low amplitude response extending over a large angle in all directions, comparable with the wider response of each array. The integrands in (11), therefore, are similar functions of  $\theta$  and  $\phi$  and their contributions in (10) cancel approximately at all angles. The actual response then approximates a pencil beam,  $F_1F_2$ , to which is added a very wide-angle response of low intensity  $\xi_1\xi_2$ . The latter may be evaluated separately and corrections made where necessary. This appears to be a possible method of plotting absolute brightness temperatures, but we have found that a different procedure has advantages.

Consider a system in which dipoles are removed from the center of one array only, say the E-W array. The composite diagram then becomes

$$R = (F_1 - \xi_1)F_2 = F_1F_2 - F_2\xi_1. \quad (12)$$

The error is now reduced to a single small negative response elongated in the E-W direction. Since it is similar in form to the power response of the N-S array,  $F_2^2$ , a reasonably accurate compensation may be achieved by adding the latter to the composite diagram, thus:

$$R = F_1F_2 - F_2\xi_1 + kF_2^2. \quad (13)$$

Again if  $k$  is chosen so that

$$\int_{4\pi} F_2\xi_1 d\Omega = k \int_{4\pi} F_2^2 d\Omega \quad (14)$$

the correct temperature is indicated in a constant temperature enclosure and the similarity in form of the integrands insures that the remaining spurious responses are small. It is found necessary with the present instrument to remove six half-wave dipoles from the center of the E-W array to reduce cross coupling to a tolerable level. Under these conditions and when  $k$  is chosen according to (14), the spurious response to a point source, resulting from the inexact cancellation of  $F_2\xi_1$  and  $kF_2^2$ , nowhere exceeds  $\pm 0.4$  per cent of the principal pencil-beam response. As we show in Section V, this is of the same order as the spurious responses caused by adjustment errors in the E-W array. Large effects can be produced by "extended" sources because the cancellation errors are slowly varying functions of position, and the spurious response may be the result of integration over a large angle. In general it is easy to correct for such effects.

#### D. The Effect of Adjustment Errors

The principal effect of errors in the currents of individual dipoles is to cause a rise in the general side-lobe level; a secondary effect is to cause collimation errors in

the main beam. Errors in the E-W array will generate a random side-lobe pattern extending in the E-W direction and errors in the N-S array, a pattern extending in the N-S direction. We will evaluate approximately the effects in the former case; the latter may be derived similarly. Consider the array as a transmitter and let the error current in the  $n$ th dipole of the E-W array be  $a_n \exp i\chi_n$ . The directional diagram of the E-W array, including all such error currents, then becomes

$$F_1 + \frac{\sum a_n \exp i(\chi_n + n\pi \sin \phi)}{\sum I_n}$$

where  $I_n$  are the correct currents of the dipoles. The composite diagram is then found by substituting in (2), thus:

$$R = \frac{1}{2} \left[ F_1F_2(1 - \cos \psi) + \frac{F_2}{\sum I_n} \left\{ (1 - \cos \psi) \sum a_n \cos(\chi_n + n\pi \sin \phi) - \sin \psi \sum a_n \sin(\chi_n + n\pi \sin \phi) \right\} \right]. \quad (15)$$

When  $\psi = \pi$ , the extra term representing the error response becomes

$$E_1(\theta, \phi) = F_2 \frac{\sum a_n \cos(\chi_n + n\pi \sin \phi)}{\sum I_n}. \quad (16)$$

From expressions (15) or (16) the error response may be calculated in any direction, if the individual error currents are known. It is more practical to specify the magnitude of the random side-lobe level in statistical form, and the rms error response, in directions remote from the main beam, is given simply by

$$(\bar{E}^2)^{1/2} = F_2 \frac{(\sum a_n^2)^{1/2}}{\sum I_n} \quad (17)$$

since phases add randomly at large angles. It is usual to measure errors in the amplitude and phase of the *actual* current. Such measurements may readily be converted into a correct current plus an error current, but it is easier to apply them directly. Thus, if the error in amplitude is  $\Delta I_n$  and the error in phase  $\Delta\sigma_n$  we have, providing  $\Delta I \ll I$ :

$$a_n^2 = (\Delta I_n)^2 + \left( 2I_n \sin \frac{\Delta\sigma_n}{2} \right)^2$$

and

$$(\bar{E}^2)^{1/2} = F_2 \frac{\left( \sum (\Delta I_n)^2 + 4 \sum I_n^2 \sin^2 \frac{\Delta\sigma_n}{2} \right)^{1/2}}{\sum I_n}. \quad (18)$$

A determination of the collimation error of the pencil beam may be made in a similar way. In this case, only the phase errors  $\Delta\sigma$  need be considered, as amplitude errors enter as a second-order effect. We will derive the E-W collimation error as the result of phase errors in

the E-W array; the independent N-S collimation errors may be calculated similarly. In an E-W plane through the center of the main beam,  $F_2$  may be taken as unity and it will be assumed  $\psi = \pi$ .

Since  $\phi$  is small, the response is therefore, from (2) and (4),

$$R = \frac{1}{2} (\bar{F}_1 + \bar{F}_1^*) \\ = \frac{\sum I_n \cos(\Delta\sigma_n) + \pi n \phi_n}{\sum I_n} \quad (19)$$

Maximum response occurs when  $\partial R / \partial \phi = 0$ , i.e., when

$$\sum I_n n \sin(\Delta\sigma_n + \pi n \phi) = 0 \quad (20)$$

In any particular case the collimation error may be obtained from (20) by solving for  $\phi$ , but usually a statistical form of the result is sufficient. If  $\Delta\sigma$  is small, as is usual with the present antenna, and the collimation error is written as  $\Delta\phi$ , we have

$$\sum I_n n (\Delta\sigma_n + \pi n \Delta\phi) = 0$$

whence

$$\Delta\phi = \frac{\sum I_n n \Delta\sigma_n}{\pi \sum I_n n^2} \quad (21)$$

It follows that in a large number of independent determinations in which the probability of error is equal in all dipoles

$$(\overline{\Delta\phi^2})^{1/2} = \frac{1}{\pi} (\overline{\Delta\sigma^2})^{1/2} \cdot \frac{(\sum I_n^2 n^2)^{1/2}}{\sum I_n n^2} \quad (22)$$

With the present instrument an rms phase error of  $10^\circ$  leads to a probable collimation error of about 1/4 minute of arc.

#### IV. CHOICE OF EQUIPMENT PARAMETERS

The factors which must be considered in the design of a cross-type radio telescope are multifarious and some of the most important are not dictated by the astronomical requirements, for example, the funds available, the local interference problem, and the area of flat ground available. We limit ourselves here to a brief discussion of some of the purely scientific aspects, which form a background against which the practical decisions must be made.

The present equipment was conceived with the object of making two principal types of measurement, with the possibility of a third added later. These are 1) the plotting of radio brightness distributions with fairly high resolution, 2) the detection of a large number of discrete sources of radiation and the accurate measurement of their positions and flux densities, and 3) the possible measurement of angular sizes of distant radio galaxies by the use of a supplementary antenna forming an interferometer with a very long baseline.

The basic parameter of the instrument is its resolution. From information available in 1953, when the radio telescope was designed, it appeared that the beamwidth should be as small as possible and definitely less than  $1^\circ$ ; but practical considerations, such as cost, and the time taken to examine any region of interest, required that the beamwidth should be as large as is consistent with the astronomical requirements. A beamwidth of  $0^\circ.8$  was chosen as a reasonable compromise; it is not possible to discuss here the detailed considerations which led to the adoption of this figure. The operating frequency and dimensions were then chosen so as to produce a sensitivity commensurate with this resolution with the minimum cost. In order to see how this can be done, let us consider the effects of varying the operating frequency. The effects on the visibility of objects larger or smaller than the beamwidth are different and will be considered separately.

#### A. The Visibility of "Point" Sources

It will be assumed that the flux density of a typical "point" source is proportional to the wavelength over the range of interest, and that the brightness temperature of the cosmic background is of the form  $T = a\lambda^{2.5}$ , where  $a$  is a constant. The precise forms of these spectra are not known, but those assumed are consistent with the observational data and adequate for the present demonstration. Assuming that the antenna has collecting area  $A$  and ohmic efficiency  $\eta$ , that the receiver has noise factor  $N$  and over-all gain  $G$ , and that the ambient temperature is  $290^\circ\text{K}$ , the following relations hold:

Power output due to

- |                                           |                                |
|-------------------------------------------|--------------------------------|
| 1) a typical "point" source               | $\propto G\eta A\lambda$       |
| 2) cosmic background                      | $\propto G\eta a\lambda^{2.5}$ |
| 3) loss resistance at ambient temperature | $\propto G(1-\eta)290$         |
| 4) receiver noise                         | $\propto G(N-1)290$            |

Whence the signal-to-noise power ratio

$$\frac{\eta A \lambda}{\eta a \lambda^{2.5} + (1 - \eta)290 + (N - 1)290} \quad (23)$$

When the resolution, and therefore the observing time, is constant the visibility of a signal is also proportional to the square root of the bandwidth, which will be assumed inversely proportional to the wavelength. Therefore for constant visibility we have

$$A \propto \frac{a\lambda^{2.5} + (N/\eta - 1)290}{\lambda^{1/2}} \quad (24)$$

The factor  $a$  varies in different directions, being greatest near the galactic center in Sagittarius. We adopt a value of 40 which corresponds to the lower temperatures observed over the greater part of the sky. In the original design,  $\eta$  was chosen as 0.5 and, for the receiver, a 6AK5 cascode input stage was assumed, giving  $N \approx 2.5$  at 3-m wavelength. Thus the design was based on an

efficiency which seemed realizable and a receiver which, from long experience, was known to be satisfactory. With the latest techniques, much better values of noise factor can be reliably achieved and our experience indicates that higher efficiencies may also be used. In Fig. 4 are shown two curves representing the variation of  $A$  with wavelength both for the original design conditions and for a possible more efficient design ( $\eta=0.7$  and  $N=2.0$  at 1-m wavelength). In each case, it is assumed that  $N \propto \lambda^{-1/2}$  is over the range of interest. In the first case, minimum area is needed at wavelengths of about 3 m, in the second at wavelengths near 2 m.

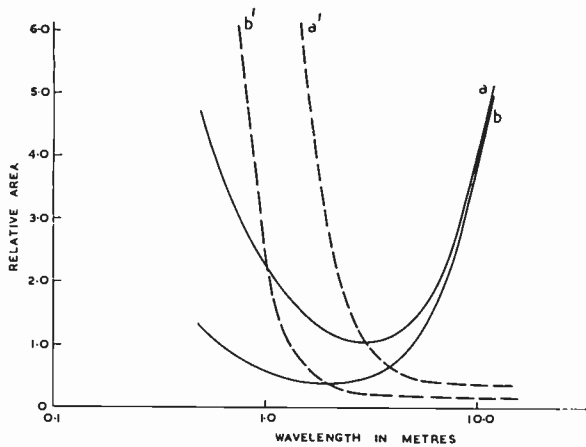


Fig. 4—The relative collecting area required for a constant snr on a typical source at different wavelengths. The solid curves refer to an unresolved source, the dotted curves to an extended source. (a) Curves based on the use of a 6AK6 cascode preamplifier and 50 per cent efficiency. (b) Curves based on the best available modern techniques.

### B. The Visibility of "Extended" Sources

For extended sources which are resolved by the pencil beam but not by the fan-beam system, different considerations apply. On the assumption that the basic spectrum is the same as before, the receiver power output due to such a source will now be proportional to brightness temperature rather than flux density, that is, to  $/G\eta A\lambda^3$ . Whence (24) is replaced by

$$A \propto \frac{a\lambda^{2.5} + (N/\eta - 1)290}{\lambda^{2.5}} \quad (25)$$

The dotted curves in Fig. 4 show the variation of  $A$  for a given visibility. With the receiver used, employing a 6AK5 input stage, a sharp increase in area is required below 3 m; with the hypothetical receiver a similar increase occurs below about  $1\frac{1}{2}$  m.

In general it is desirable to choose as short a wavelength as possible to reduce the effects of the ionosphere; the final choice of 3.5 m was based on a study of the local interference situation.

Having decided on beamwidth and operating frequency, the length of the array will be fixed. The remaining dimension is the width; this is ideally chosen to give sufficient area to observe all the detail permitted

by the resolution of the instrument. In practice, however, a certain relaxation of this requirement is not only possible but even desirable. There is no point, for instance, in the sensitivity being high enough to observe the spurious responses from a large number of discrete sources. Also, when the source density is large, the usefulness of the information is reduced by chance blending effects. An expression due to Mills and Slee<sup>5</sup> may be interpreted to show that this limit occurs when the source density approaches one per  $4\pi$  beamwidths, that is the number of sources which can be reliably observed over the whole sky by an antenna of beamwidth  $\Omega$  steradians is about  $\Omega^{-1}$ . The sensitivity to be aimed at could well be of the order required to detect this number of sources, the actual value being chosen according to the particular nature of the observations planned. Inserting some figures taken from the above paper, and assuming that flux density is proportional to wavelength, the minimum reliable flux density is given by

$$S_r = 6\lambda\Omega^{2/3} \times 10^{-24} \text{ W m}^{-2} (\text{cps})^{-1} \quad (26)$$

It may be shown that the minimum collecting area, including both arms, of a symmetrical cross required to detect reliably "point" sources of flux density  $S$  at low declinations and remote from the galactic center is given approximately by

$$A_{\min} \approx \frac{k\{40\lambda^{2.5} + (N/\eta - 1)290\}}{S\sqrt{\Phi\Delta F}} \quad (27)$$

where  $k$  is Boltzmann's constant,  $\Phi$  is the E-W beamwidth in degrees, and  $\Delta F$  is the bandwidth of the system.

It is characteristic of stationary cross-type antennas that the available sensitivity decreases as the zenith angle increases; it is therefore necessary to consider also the coverage desired. For the present instrument the maximum sensitivity given by (27) is about  $3 \times 10^{-26} \text{ W m}^{-2} (\text{cps})^{-1}$ , which is 0.4 times the value of  $S_r$  given by (26). This corresponds to an array width of two dipoles. Under ideal conditions the instrument actually has a sensitivity equal to or better than this figure.

Finally, it should be pointed out that gross departures from a design suggested by the above considerations are justified in special circumstances. For example, high resolution observations at wavelengths in the decameter range are of the utmost interest, but as shown by Fig. 4 enormous structures would be required to observe the "point" sources with the same sensitivity as may readily be achieved at shorter wavelengths. In a recently completed instrument designed by Shain at the Radiophysics Laboratory this sensitivity was sacrificed in the interests of size and cost.<sup>6</sup>

<sup>5</sup> B. Y. Mills and O. B. Slee, "A preliminary survey of radio sources in a limited region of the sky at a wavelength of 3.5 m," *Aust. J. Phys.*, vol. 10, pp. 162-194; March, 1957.

<sup>6</sup> C. A. Shain, "The Sydney 19.7-MC radio telescope," this issue, p. 85.

## V. THE ARRAYS

The performance and general usefulness of the instrument is dependent on the behavior of the antenna to a much greater degree than in a conventional radio telescope. Accordingly, it is desirable to give a rather detailed account of the critical features in the design, construction, and operation of the arrays.

### A. Description

Each array consists essentially of 500 half-wave dipole elements arranged in two parallel rows each 125 wavelengths long, and backed by a chicken-wire reflecting screen of width  $1.3\lambda$ , approximately  $\lambda/8$  beneath. The dipoles are lightly coupled to coaxial line feeders which run the length of the arrays and are terminated at each end by matched loads. Phasing of the dipoles to change the beam direction is achieved by changing the points at which the dipoles are coupled to the feed lines. Each dipole element is supported between the arms of Y-shaped wooden frames, as illustrated in Fig. 1(b).

The main feed lines are constructed in 150-foot lengths. The outer conductor is fabricated from 8-foot sections of 20# galvanized steel sheets, which are bent to form an open-bottomed box 6 inches deep and 4 inches wide. To the open bottom is soldered a strip of  $\frac{1}{2}$ -inch wire mesh which has the function of enclosing the line electrically, while allowing easy access for adjustment and for the removal of insect life. The inner conductor is of  $\frac{1}{4}$ -inch copper tubing; it is placed in the vertical plane through the center line of the outer conductor,  $1\frac{1}{2}$  inches from the closed top and  $4\frac{1}{2}$  inches from the wire-mesh bottom, giving a characteristic impedance of about  $200\Omega$ . The asymmetrical placing is required to reduce leakage. The inner conductor is supported at intervals by thin perspex beads and is connected to the outer at the ends through expanding joints which allow differential expansion. It is fed through a matching network by flexible coaxial cable of  $72\Omega$  impedance at a point  $\lambda/4$  from each short-circuited end. The dipoles are coupled to the line by capacity probes which may be inserted at intervals of  $11\frac{1}{2}$  inches (30 electrical degrees) through a series of holes along the length of the outer conductor, thus the dipole phases may be set with an error of less than  $15^\circ$ . The arrangement is illustrated in Fig. 5 which shows a bottom view of the feed line and coupling probe.

In the N-S array the dipoles are at right angles to the line of the array, thus the two rows of dipole elements form full-wave dipoles which are center fed, as illustrated in Fig. 6. A combined balun and matching transformer reduces the dipole impedance ( $\sim 5000\Omega$ ) to the  $72\Omega$  of the flexible feed cable. This cable, which has an electrical length of  $1.65\lambda$ , is terminated by the tuned transformer in the probe unit which raises the impedance at the probe to about  $1500\Omega$ . This somewhat complicated system is dictated by the desire to reduce the capacitive load on the feed line, which requires a

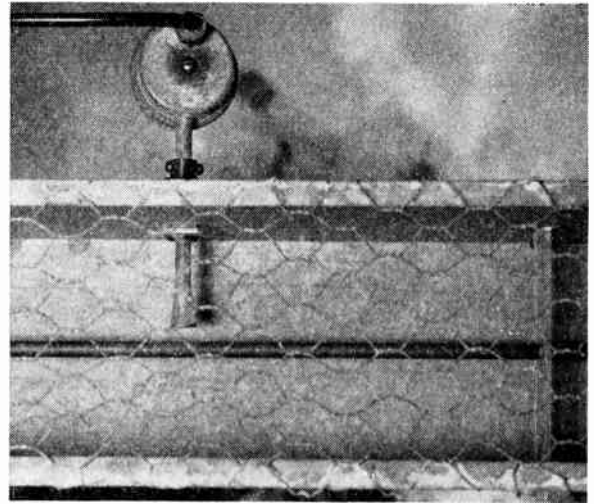


Fig. 5—A bottom view of the feed line and capacity probe combination.

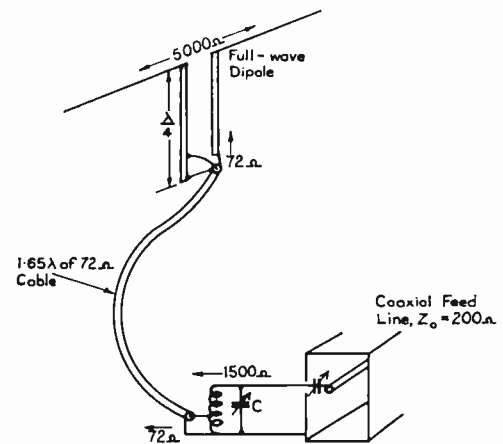


Fig. 6—The schematic feed arrangement for the full-wave dipoles in the N-S array.

high-impedance probe, and to reduce the effects of cross coupling between adjacent dipoles, which requires that the full-wave dipole should be fed by a low impedance source. The latter requirement is essential for easy setting up of the arrays. The amount of coupling, which is controlled by the distance between probe and inner conductor, is arranged so that the current distribution along the array is in the desired Gaussian form and about 50 per cent of the power is dissipated in the terminating resistances of the feed line. The rather low efficiency is desirable to reduce changes in current distribution which can occur as the result of changes in the radiation resistance of the dipoles when the beam is directed to different declinations, and also to reduce standing waves along the feed line which result from discontinuities caused by the dipole probes. The latter cause a standing wave generally less than 1.1 except within about  $1\frac{1}{2}^\circ$  of the zenith where the spacing approaches  $\lambda/2$ ; in these directions the discontinuities are tuned out by attaching capacitive plates to the inner conductor at appropriate places. The 150-foot line sec-

tions, 10 in all, are joined through manually-operated variable phase shifters and relay-operated stepped phase shifters. The former are used to correct phase errors which might occur along each line section, the latter for changing the declination in small discrete steps.

The E-W array is basically similar, but there are some notable differences. The most obvious is that the rows of dipoles are colinear so that the polarization is the same in both arrays. Also, half-wave folded dipoles are used, rather than full-wave dipoles, in order to permit a greater swing from the meridian plane, if required. Actually, this feature has not been used and the feed is arranged so that two adjacent dipoles are connected by a branched line to the same probe, as illustrated in Fig. 7. For ease of adjustment the feed is arranged as before so that the probe presents a high impedance to the feed line and each half-wave dipole is fed by, in this case, a high impedance source. In operation, the fan beam of the E-W array is directed about  $20^\circ$  north or south of the zenith, according to the setting of the N-S array, by introducing a phase shift of  $60^\circ$  between the rows of dipoles; this results in a more uniform over-all sensitivity. The change from north to south and vice versa is easily accomplished by interchanging the feed points of each row. In normal operation the beam is at right angles to the line of the array so that the feed points are at integral numbers of wavelengths; consequently, large standing waves might be expected in the main feed line. These are also tuned out by attaching capacitive plates to the inner conductor at appropriate points. Because this array is normally fixed, it is possible to use a tighter coupling and it is arranged that only 15 per cent of the power is dissipated in the terminating resistors.

### B. Adjustment of the Arrays

The successful operation of an antenna of this type requires facilities for the easy and accurate measurement of the currents in each dipole, both in phase and amplitude. The method adopted makes use of an electrostatically shielded pickup loop which may be affixed by jig in a standard position close to the current maximum in each dipole. A 5-watt crystal controlled oscillator is available at the operating frequency of 85.525 mc and the output is fed to the center of the array under test. To measure the current in a particular dipole the loop is placed in position and the voltage pickup compared in amplitude and phase with a standard voltage derived from a directional coupler inserted in the main feed line; the method is indicated in Fig. 8. Referring to the figure, the settings of the piston attenuator and tapping point in the coaxial line are adjusted to give a null in the receiver, the respective settings indicating the relative amplitude and phase of the dipole current. Intercomparison between dipoles is therefore easily made. Since the pickup loop and directional coupler are each placed at the end of 150 feet of flexible cable, it is

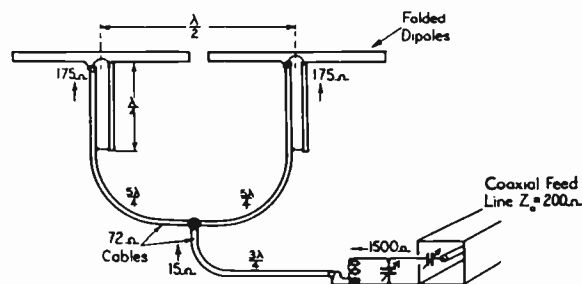


Fig. 7—The schematic feed arrangement for the folded half-wave dipoles in the E-W array.

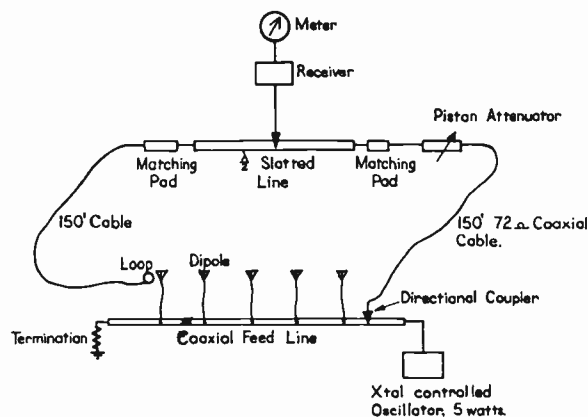


Fig. 8—The phase and amplitude comparator used in adjusting the dipole currents.

possible to measure the dipole currents over a distance of about 300 feet on either side of the array center, with the directional coupler fixed in position. Measurements may be extended over greater distances by a process of secondary calibration. In practice, it is found that measurements of phase and amplitude can, with care, be repeated to within  $1^\circ$  and 2 per cent, respectively. The principal variable factors are the 150-foot lengths of flexible cable; it is found that these should be old and well stretched for best results.

The initial adjustment of currents is similar in both arrays: as an example we will consider briefly the N-S array. Advantage is taken of the properties of the feed system of Fig. 6 to tune the transformer in the probe unit. This operation is performed with the pickup loop placed at the dipole under test, the probe removed from the feed line, and an adjacent dipole excited. The tuning capacitor is adjusted until the current induced in the dipole under test is a minimum, corresponding to a very low impedance across the feed point. This adjustment effectively controls the phase of the current; the coupling is then adjusted to give the required amplitude by inserting the probe at the appropriate feed point and adjusting its distance from the inner conductor by sliding it in the collar provided. By working from the centers to the ends of the arrays the current distribution is adjusted to the desired form and, finally, the proportion of power dissipated in the terminating resistors is measured. If necessary the currents are then readjusted

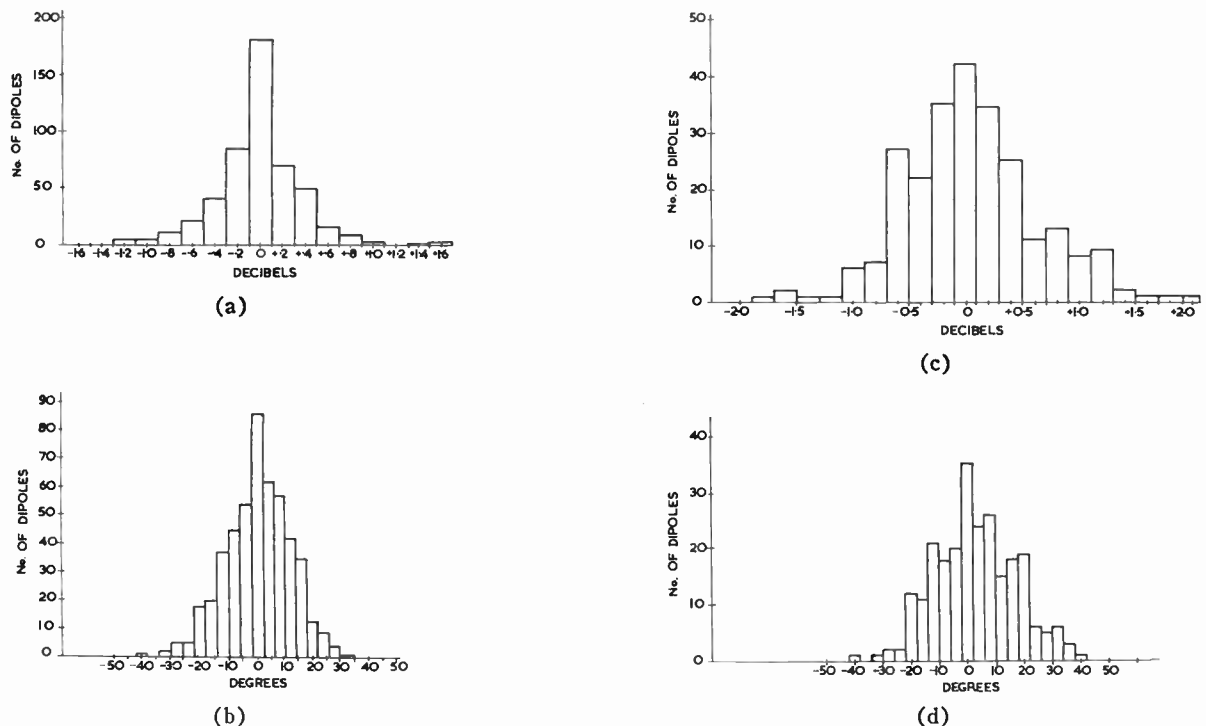


Fig. 9—Histograms of the errors in amplitude and phase of the dipole currents measured five months after setting up. (a) Amplitude errors, E-W array. (b) Phase errors, E-W array. (c) Amplitude errors, N-S array. (d) Phase errors, N-S array.

to make this power about 50 per cent of the total. By this method the individual currents may be set up with a relative accuracy of about 5 per cent in amplitude and  $10^\circ$  in phase; a greater phase accuracy is possible (about  $3^\circ$  or  $4^\circ$ ) by individual adjustment, but in general it is unnecessary.

In the course of time, errors arise, particularly in the N-S array which is frequently altered in declination. In Fig. 9 are shown histograms of the amplitude and phase errors in each array five months after setting up. This is about the normal period between readjustment. For the E-W array the rms errors in amplitude and phase are 0.35 db and  $7^\circ$  respectively, yielding an rms side-lobe level of about 0.6 per cent [calculated according to (18)] and a probable collimation error of less than  $\frac{1}{4}$ -foot arc (22). These values are undoubtedly upper limits, as the phase errors are not completely random but are, to a large extent, due to the integral nature of the phase adjustment and tend to be equal on each side. The corresponding values for the N-S array are 0.6 db and  $15^\circ$  yielding a side-lobe level of 1.7 per cent and a probable collimation error of about 1 foot.

In actual operation side lobes in a N-S direction appear to be of this order although, as to be expected, occasional ones are much larger. Very little evidence is available about the E-W array since in the areas of sky north of the zenith, which have been analyzed in detail, practically no such side lobes have been observed: south of the zenith it is found that they have little effect in the areas investigated although they are sometimes recognizable, the largest observed to date being 3 per cent.

### C. Beam Swinging

Changing the declination is accomplished by two methods; in one the probes are inserted at intervals so that a progressive phase shift exists along the array which produces a response pattern inclined to the vertical according to the relation  $\sin \theta = L/2\pi$ , where  $L$  is the phase change per wavelength. By using the *free space* wavelength in this calculation the beam direction is automatically compensated for tropospheric refraction<sup>7</sup> which is appreciable near the limits of coverage. This method is used for setting up a series of standard beam settings which, near the zenith, are an 80-foot arc apart. The zenith angle is defined by the relation

$$\sin \theta_n = 0.01163 + 0.02327(n - 1) \quad (28)$$

where  $n$  is an integer. The second method is generally used for obtaining intermediate beam positions at  $\frac{1}{4}$  this interval by means of the stepped phase shifters between sections of the feed line. An example of the beam positions available is given in Fig. 10.

In the former method adjustment is made manually according to a previously calculated schedule; it takes about one hour for one person to change the beam setting. In the latter, the stepped relays are actuated by a switch in the control hut or, in scanning operation, the relays are actuated automatically in such a manner that the direction is changed at 12-second intervals.

The arrangement of these phase shifters along the feed line and the corresponding phase shifts for the two

<sup>7</sup> B. Y. Mills, "The positions of six discrete sources of cosmic radio radiation," *Aust. J. Sci. Res.*, vol. A5, pp. 456-463; September, 1952.

BEAM SETTING	DECLINATION
	← -27 31
	• ← -27 11
	• ← -26 50.5
n = +6 → ●	← -26 30.5
	• ← -26 10
	• • ← -25 50
	• ← -25 29.5
n = +7 → ●	← -25 09.5
	• ← -24 49.5
	• • ← -24 29
	• ← -24 08.5
n = +8 → ●	← -23 48
	• ← -23 28
	• • ← -23 07.5
	• ← -22 47.5

Fig. 10—Examples of some of the standard beam positions available by manual setting (large dots) and automatic switching (small dots). The angles given refer to the declinations to which the beam is directed.

extra beam positions are given in Table I. The phase shifters at  $6\lambda$  from the center consist of three reactors which may be connected to the inner of the main feed line at spacings of  $\lambda/4$ . It was necessary to break up the central block of dipoles in this way to avoid too large a

introduce large side lobes. The spurious responses in the meridian plane have been calculated, using (16) for a beam change of  $-20$  minutes. They are shown in Fig. 12, p. 78, over a range of  $15^\circ$ ; for a change of  $+20$  minutes the signs are reversed. For a change of  $\pm 40$  minutes the responses are slightly smaller and spaced at double the distance; *i.e.*,  $4^\circ.6$ ; however, this case is not of importance because each such declination is observed twice and the results averaged, once with a beam setting 40 minutes to the north and  $-40$  minutes shift, and once with a beam setting 40 minutes south and  $+40$  minutes shift. The spurious responses are equal and opposite and therefore cancel. In general, the high side-lobe level in the  $\pm 20$  minutes of arc positions is not serious because such a side lobe is not repeated on adjacent declinations and therefore cannot be mistaken for a real source of emission; a method of correction is discussed in Section VII. In case of doubt an intermediate beam position may always be set up manually for checking.

D. Calibration

Measurement of flux density and brightness temperature requires a knowledge of the array gains at all zenith angles. A method has been developed for measuring the gains of large antennas in terms of the known gain of a reference antenna, which in this case is a half-wave dipole mounted  $0.21\lambda$  above an effectively infinite horizontal reflecting screen. Radio sources are observed using both arrays of the cross in normal operation and each array separately in an interferometer connection with the standard dipole. Thus, three different types of observation are made of each source, each giving a recorder deflection which is a function of the product of the gains of the two antennas used and the flux density of the source. By combining these three independent measurements it is possible to derive the flux density of the source and the gains of the two arrays in terms of the gain of the standard. A detailed description of the method is given by Little.<sup>8</sup>

For calibration, five strong "point" sources have been chosen (05S4A, 09S1A, 16N0A, 12N1A, and 05N2A), disposed over the range of useful zenith angles, and the effective areas of the arrays measured at the corresponding angles. These measured values, which have a probable error of about 10 per cent, are then fitted to a theoretical sensitivity curve derived below, and a value obtained for the maximum effective area of the arrays. This is used in conjunction with the theoretical sensitivity curve to give the effective area at any zenith angle.

Calculation of the sensitivity curve is comparatively simple with the form of feed employed, which has the property that the dipole currents in the N-S array do not vary significantly as the radiation resistance changes

<sup>8</sup> A. G. Little, "Gain measurements of large aeriels used in interferometers and cross-type radio telescopes," *Aust. J. Phys.*, submitted for publication.

TABLE I  
LOCATION OF THE PHASE SHIFTERS AND AMOUNT OF CHANGE

Distance of switch from array center	Phase shift for beam change near zenith of:	
	$\pm 20$ minutes of arc	$\pm 40$ minutes of arc
$\pm 6\lambda$	0	$\pm 28^\circ.5$
$\pm 12.5\lambda$	$\pm 51^\circ.5$	$\pm 51^\circ.5$
$\pm 25\lambda$	0	$\pm 51^\circ.5$
$\pm 37.5\lambda$	$\pm 51^\circ.5$	$\pm 51^\circ.5$
$\pm 50\lambda$	0	$\pm 51^\circ.5$

distortion of the antenna beam. All the other phase shifters are of the form illustrated in Fig. 11; they con-

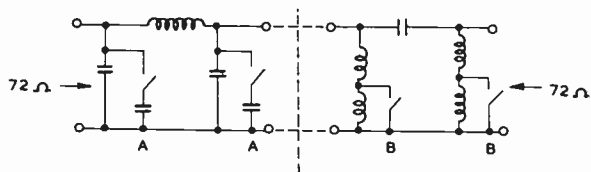


Fig. 11—A circuit of the switched phase shifters used in scanning the beam.

sist of advancing and retarding pi networks which, in the quiescent condition with all switches open, produce equal and opposite phase changes. By closing each pair of switches alternately the phases may be advanced or retarded by equal amounts without sensible change of characteristic impedance or over-all loss.

The principal effect of phase changing in steps is to

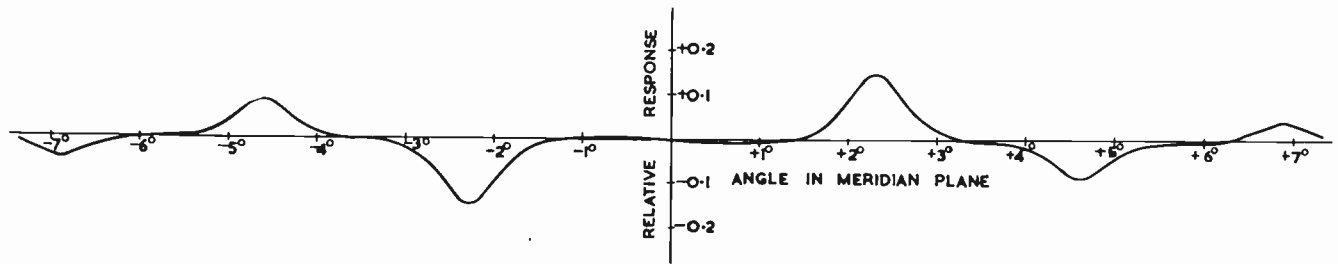


Fig. 12—The error response in the meridian plane near the zenith produced by switching the beam by  $-20$  minutes of arc from a manual position; when switched by a  $+20$  minutes of arc the signs of the responses are reversed.

with changing zenith angle. Between zero and  $40^\circ$  the current change has been measured as less than 5 per cent. Assuming constant current and considering the arrays as transmitters, we may compute the sensitivity at any declination by evaluating the product of the field intensities at a large distance.

For the N-S array, in the direction of maximum, the field will be proportional to that of a single dipole and reflector, thus:

$$F_{2(\phi=0)} \propto \sin(0.246\pi \cos \theta). \quad (29)$$

For the E-W array this response must be further modified due to the presence of two rows of dipoles separated by  $0.54\lambda$  and with relative phase difference of  $60^\circ$ . Thus:

$$F_{1(\phi=0)} \propto \sin(0.246\pi \cos \theta) \cos\left(0.54\pi \sin \theta \pm \frac{\pi}{6}\right). \quad (30)$$

The over-all response, after normalizing for the effect of the reflector, is therefore given by

$$R_{(\theta,0)} = \frac{\sin^2(0.246\pi \cos \theta)}{\sin^2 0.246\pi} \cos\left(0.54\pi \sin \theta \pm \frac{\pi}{6}\right). \quad (31)$$

In Table II are listed the total effective areas of the two arrays, including all losses, measured at the pre-amplifiers for the five zenith angles of the calibration sources. Also included are the total effective areas obtained by dividing the measured area by  $R_{(\theta,0)}$  of (31). The mean value of  $A/R_{(\theta,0)}$  is  $736 \pm 17$  square meters and

TABLE II  
THE TOTAL EFFECTIVE AREA OF THE ARRAYS MEASURED  
AT FIVE ZENITH ANGLES

Zenith angle $\theta$	Measured effective area $A$ square meters	$A/R_{(\theta,0)}$
$12^\circ$	816	860
$22^\circ$	616	709
$39^\circ$	382	683
$46^\circ.5$	278	695
$56^\circ$	176	735

this is adopted as the best estimate. In Fig. 13 is shown the derived curve based on this figure, compared with the measured areas. The fit is reasonable, within the uncertainty of the measurements, and it is concluded that adoption of the above curve is unlikely to produce errors greater than about 10 per cent. Possibilities of

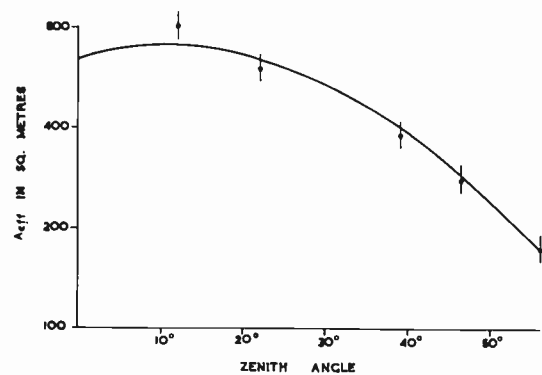


Fig. 13—The effective total area of the arrays (including ohmic losses) as a function of zenith angle. The solid curve is theoretically derived and fitted to the measured areas indicated by dots; the vertical "wings" indicate the probable errors of the measured points.

small systematic errors occur as the result of the neglected current changes and the effect of ground reflections at large zenith angles.

## VI. ASSOCIATED ELECTRONIC EQUIPMENT

### A. Description

The receiving and recording equipment follows conventional practice in many respects with a few novel additions dictated by the special requirements of the instrument. A block diagram of the essential functional elements of the system is shown in Fig. 14.

The output of each array at a wavelength of 3.5 m (85.5 mc) is connected via low-loss coaxial cables to a separate preamplifier using a 6AK5 cascode input stage. After amplification the signals are separately converted to the intermediate frequency of 25.5 mc using a common crystal-controlled local oscillator at a frequency of 111 mc. Phase switching is accomplished at a rate of 430 cps by inserting an electronic phase reversing switch between the local oscillator and one of the frequency changers. This arrangement has great stability as any small unbalance which may occur in the switch is largely removed by saturation in the mixing process. After some further amplification, the separate signals are combined at the input of the main intermediate frequency amplifier. This has a bandwidth of 250 kc between half-power points and defines the bandwidth and operating frequency of the system. The bandwidth

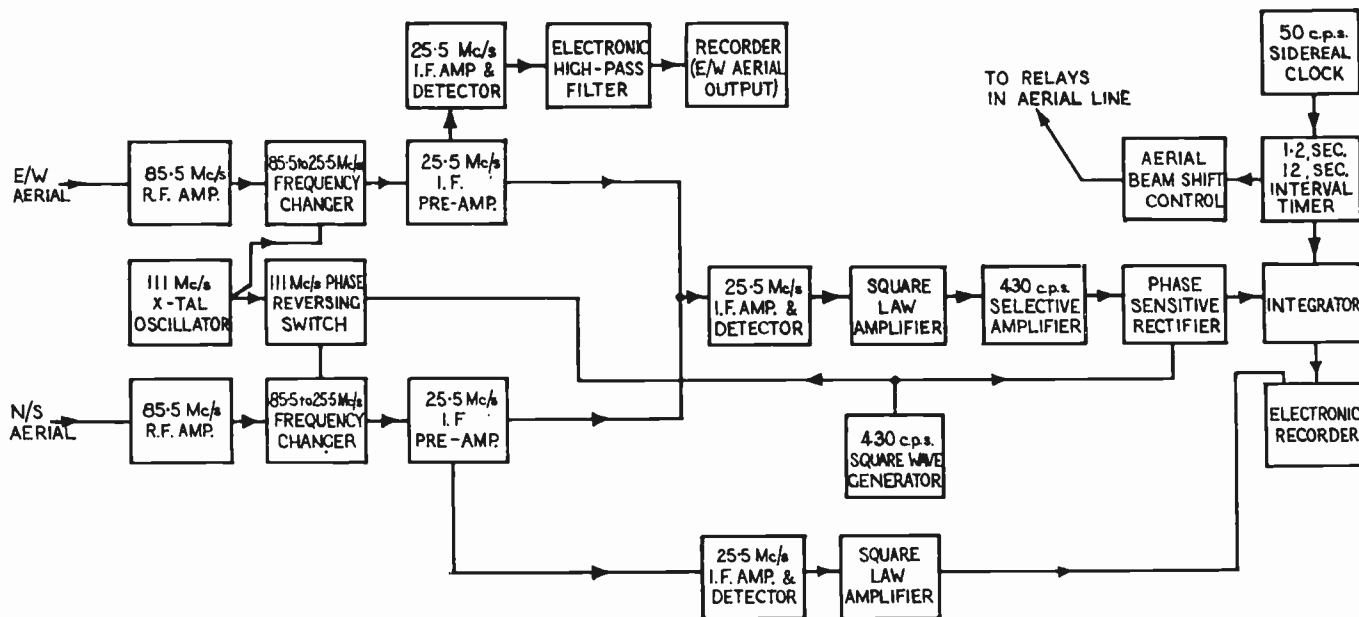


Fig. 14—A simplified block diagram illustrating the essential functional elements of the system.

is necessarily small because of the large path differences for radiation incident on different parts of the arrays, particularly at large zenith angles. The amplifier has a diode detector with output linear up to 5 volts with a noise signal.

The desired output is a modulated noise signal which is superimposed on a random signal comprising uncorrelated noise from each array, together with noise generated internally in the receiving system. In order that the modulated output should be independent of the random components it is essential that the final output of the receiver should be proportional to the power input. This condition has been achieved by squaring the rectified output voltage using a multigrid tube (6SA7) in a conventional multiplying circuit.

The 430-cps output from the squaring tube is passed through a tuned amplifier of bandwidth approximately 30 cps and converted to a dc noise signal by a phase-sensitive rectifier. The mean voltage is proportional to the power being received in the pencil beam. When the instrument is used with a fixed beam position, this voltage is smoothed with a resistance capacitance filter of time constant a few seconds (usually 12) and applied to the pen recorder. Typical recordings of the transit of radio sources have been shown in Fig. 2(a) and Fig. 3.

When the instrument is used for survey work, with the scanning beam, the arrangement is more complex. The basic recording circuit is shown in Fig. 15 in simplified form. During each 12-second interval, in which the beam is directed at a fixed declination, the switch *S* is closed for the first 1.2 seconds, which embraces the time required for the beam-switching relays to operate and the condenser to lose any accumulated charge, and then opened for 10.8 seconds. During the latter interval the output from the phase sensitive detector is integrated

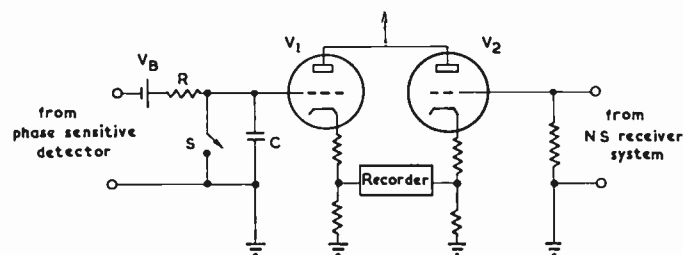


Fig. 15—A simplified circuit illustrating the recording method used when scanning the pencil beam.

by the resistance capacitance combination of time constant 100 seconds. At the end of the interval, before the switch is closed again, the voltage at the grid of *V*<sub>1</sub>, and therefore the recorder deflection, is the sum of three contributions; one is approximately proportional to the time integral of the voltage output from the phase sensitive detector, and therefore to the power received in the pencil-beam response pattern; the second is a fixed voltage due to the impression of a bias voltage *V*<sub>*B*</sub>, the third is a random noise voltage. The cycle of five separate declinations is repeated once a minute forming a sawtooth repetitive pattern on the recorder. As shown in Section III it is also necessary to include the effective temperature of the N-S array, which is derived from the lower receiver channel in Fig. 14. This is added to the grid of *V*<sub>2</sub> and displaces each sawtooth vertically by an amount corresponding to the brightness temperature at the appropriate declination.

A typical recording has been shown in Fig. 2(b). In this, the main sawtooth deflection is due to the bias voltage; radio sources can be seen on the right and left and the random fluctuations in the sawtooth peaks are the result of noise. Additional features on this recording are: 1) the connection of the preamplifiers to dummy

loads every half hour for a period of 12 seconds as a check on stability; the difference between this level and the bottom of the sawtooth pattern represents the added N-S temperature and 2) the negative-going deflections which mark a particular beam position.

The whole timing cycle is controlled by a quartz crystal clock running at sidereal rate, the switching intervals being determined by electronic counting circuits. For monitoring purposes, both the total power output from the main receiver and the phase-sensitive detector output are displayed directly on a double-pen recorder; this is very useful for interpretation of the main record in the presence of interference.

As described in Section II, the output of the E-W array is also recorded at high sensitivity. This is obtained from the upper receiving channel of Fig. 14, the output of which is filtered to remove the dc and the very low frequency components caused by the passage of the galaxy and slow drifts in the receiver: "point" sources are then recorded at a very high effective gain. The high-pass filter is of a type described by Bolton and Slee<sup>9</sup> which employs a long time constant agc circuit. A typical record obtained from this section is shown in Fig. 2(d); some well-known sources are indicated.

### B. Calibration and Adjustment

The flux density and temperature scales of the instrument are calibrated by means of a diode noise generator. This is a satisfactory standard at such a low frequency; the transit time effect is negligible and impedance transformation is small and easily corrected.

The flux density calibration is performed by injecting into each preamplifier attenuated signals of equal phase and amplitude derived from the noise generator. The resultant recorder deflection is then related to the input power, which in turn may be related to the flux density of a radio source by means of the array calibration. The flux density  $S$  of a source which produces the same recorder deflection as a current of  $I$  mA in the noise generator is given by the relation

$$S = 3.18 \times 10^{-22} \cdot \frac{Z_0 \alpha}{A_{\text{eff}}} I \quad (32)$$

where  $Z_0$  is the line impedance, which must be the same for the arrays, the noise generator, and the attenuators,  $\alpha$  is the attenuation, approximately 1/400 in the present arrangement, and  $A_{\text{eff}}$  is the effective area of the arrays as given by Fig. 13.

The main temperature scale presents more difficulty. In a conventional antenna the apparent brightness temperature of the sky is obtained simply by measuring the antenna temperature and dividing by an efficiency factor which is of the order of 60 per cent. Here, how-

ever, the relation between the sky brightness and the array temperature produced by the radiation in the pencil beam alone is not simple; the calibration must be made via the flux density standard. Consider a uniform area of brightness temperature  $T$  just filling the main pencil beam: this will produce the same deflection as a "point" source of flux density  $S'$  centered in the pencil beam, defined by the following equation, the integral being taken over the uniform bright area.

$$T = \frac{\lambda^2 S'}{2k \int_4 R d\Omega} \quad (33)$$

The flux density  $S'$  may be related to the recorder deflection by means of (32). The effective solid angle,  $\int R d\Omega$ , has been calculated from the theoretical response curve; it is  $(2.3 \times 10^{-4})/\cos \phi$  steradians, the cosine factor expressing the effect of foreshortening of the N-S array. Thus we may calibrate the "beam temperature"  $T_b$  in terms of noise generator current as follows:

$$T_b = 6.16 \times 10^5 \frac{Z_0 \alpha}{A_{\text{eff}}} I \cos \phi \quad (34)$$

The calibration of the N-S array is arranged so that, if it be contained in an enclosure at constant temperature  $T$ , the dc recorder deflection should be the same as the deflection of the sawtooth peaks due to a source of temperature  $T$  just filling the pencil beam. For calibration, the noise generator is connected directly, without attenuation, to the N-S preamplifier; the relation between the N-S array temperature and the noise generator current is given by the expression

$$T_{N-S} = \frac{5.75 Z_0 I}{\eta_{N-S}} \quad (35)$$

where  $\eta_{N-S}$  is the ohmic efficiency of the N-S array. The efficiency, which is a function of zenith angle, was obtained by direct measurement of the losses in the various circuits of the array; it was checked by comparison between the sky brightness measured with the array and with the comparison dipole, after making allowance for the different polar diagrams.

Errors may easily arise in matching  $T_{N-S}$  to  $T_b$ , but it is estimated that the total mismatch should not exceed 20 per cent, which is not expected to be of great consequence. The uncertainty is similar to that which arises in a parabolic antenna when converting "antenna temperature" to "beam temperature."

There are two adjustments which must be performed very carefully; these are the balance of the phase reversing switch and the law of the "square-law" amplifier (see Fig. 14). The phase-reversing switch is very stable and changes in mean level of the recorded output are often undetectable for weeks on end. However, any difference between the output of the switch in the two phase conditions results in a spurious signal which is

<sup>9</sup> J. G. Bolton and O. B. Slee, "Galactic radiation at radio frequencies. V. The sea interferometer," *Aust. J. Phys.*, vol. 6, pp. 420-433; December, 1953.

proportional to the mean noise power in the N-S receiver. Accordingly, the balance is checked frequently by connecting a diode noise generator to the N-S pre-amplifier and varying the diode current so that the total receiver power output varies over the normal range produced by the passage of the galaxy, about 4:1. If necessary, the balance of the switch is adjusted so that the mean output of the phase sensitive detector is zero over the whole range.

The second adjustment, that of the square-law amplifier, is essential to insure that the measured flux density should be independent of the receiver noise level. Any marked degree of dependence could well affect physical conclusions derived from a study of the statistics of radio sources in their relation to the galaxy. A check is made by injecting a fixed signal into each preamplifier from the calibrating noise generator in the normal way, plus a much larger amount of uncorrelated noise at the mixing point of the two preamplifier chains. This extra noise is arranged to vary the total receiver output over a range of 4:1. The recorder deflection is then checked for constancy. Any variation implies that the over-all response, including the diode detector, differs from the square law desired; adjustment is made by varying the bias of the multiplying tube. In practice it is not possible to obtain an exact adjustment as high-order terms are always present in the plate current of the multiplying tube; however, it is easy to arrange that the total variation should be less than about 3 per cent, which is quite adequate for our purpose.

## VII. USE OF THE INSTRUMENT

It has been shown how the various elements of the radio telescope function and how it may be calibrated; it remains to give some examples of the practical use of the instrument. The results of several observational programs have been fully described in the literature and they will be referred to when appropriate.<sup>10</sup> Here, discussion will be limited to general features particularly related to instrumental aspects of the observations. The two principal uses, the study of discrete sources of small angular size and the study of extended distributions, in particular the Milky Way, will be discussed separately; also some other forms of observation, for which it has been adapted, will be considered.

### A. Discrete Radio Sources

The method of detection and cataloging of discrete radio sources has been described in some detail by Mills and Slee.<sup>5</sup> In the preliminary catalog given, a total of 383

<sup>10</sup> It should be noted that in papers published prior to December, 1956, incorrect values of flux density and temperature are given, owing to errors in the preliminary calibration of the equipment. Flux densities should be approximately doubled: corrections to temperatures are less but no simple relationship holds. Corrected values for some important measurements are given in an article by B. Y. Mills, "Radio Frequency Radiation from External Galaxies" in "Handbuch der Physik," Springer-Verlag, Berlin, Germany, vol. 53, in press.

sources are listed in a limited area of about one steradian. Briefly, sources are recognized as "humps" on the record, which are visible on *at least* two adjacent beam positions with approximately the same right ascension; this criterion effectively disposes of the great majority of side-lobe responses. The observations are made with either a "fixed" or "scanning" beam depending on the particular requirement; examples are given in Fig. 2. Two points of interest are the accuracy with which the positions of the stronger sources may be measured, that is, the accuracy with which the direction of the pencil beam is known, and the reliability of the weaker sources, which may be influenced by spurious antenna responses.

The collimation errors were estimated in Section V from measurements of dipole phase errors, but observations of actual sources suggest that there may be small systematic errors which persist when the arrays are re-adjusted. There are six sources for which reasonably reliable identifications are available and which can be observed with sufficient signal to override any effects of finite resolution and noise. The differences between the measured positions and the optical centers of the identified objects are indicated in Table III. The meas-

TABLE III  
DIFFERENCES BETWEEN OPTICAL CENTERS AND MEASURED RADIO POSITIONS OF SOME IDENTIFIED SOURCES

Source IAU number	Declination nearest degree	Difference in position minutes of arc	
		Right ascension	Declination
05N2A	+22	-1.5	-1
12N1A	+13	-1.0	-2
16N0A	+5	-1.5	+2
09S1A	-12	-0.5	0
03S3A	-37	-1.5	+2
13S4A	-42	-0.5	+4

urements were made over a long period of time with readjustments in between. They suggest a collimation error of  $-1$  minute in right ascension and, possibly,  $+1\frac{1}{2}$  minutes in declination with a probable error in each observation of  $\pm 0.3$  minute in right ascension and about  $\pm 1\frac{1}{2}$  minutes in declination. The cause of the small systematic errors has not been established; in fact the declination error may not exist as it appears from a study of the brightness contours of 13S4A that the declination discordance in this case may be a real effect of the corona of emission surrounding the source.<sup>11</sup> If the declination measurement on this source is neglected the collimation error is negligible.

The number of sources which can be measured with the above accuracy is severely limited in practice by the effects of random noise. This increases the error at low flux densities and, while the effects may be removed by

<sup>11</sup> K. V. Sheridan, "An investigation of the strong radio sources in Centaurus, Fornax, and Puppis," in preparation.

multiple observations, the number required increases at a very steep rate. It may be shown that, in these circumstances, the total number of observations required is proportional to  $n^{7/3}$  where  $n$  is the number of sources to be measured. With the present equipment this sets a practical limit to  $n$  of the order of 5 per cent of the total number of observable sources; above this, the increase in information does not seem commensurate with the labor involved. With different instruments the limit may be different; in particular it is likely to be appreciably higher with an easily movable radio telescope, with which many observations may be made in rapid sequence.

The most important aspect, however, is the influence of the spurious responses of the instrument on the cataloging of weak radio sources. It is clear that such responses can only be troublesome when a strong source crosses one of the fan beams for, elsewhere, the side-lobe response is far less than that of a conventional antenna because of the careful tapering and adjustment of the arrays. In order to keep a check on the side-lobe structure, the beam settings and sidereal times at which all strong sources cross either of the fan beams, have been calculated. For the N-S beam this occurs at the right ascension of the source, for the E-W beam according to

$$\sin \theta_n = \cos \delta \sin L \cos H - \sin \delta \cos L \quad (36)$$

where  $\theta_n$  refers to the zenith angle of beam setting,  $n$ , in the meridian plane,  $L$  is the latitude, and  $\delta$  is the declination, and  $H$  the hour angle of the source.

The resulting pattern is shown in Fig. 16. The existence of a faint source is always questioned if it is located on any of the lines of interference. In general it would be rejected if located at the right ascension of a strong source because, as we have seen, the side-lobe level can be quite high in the meridian plane. Side-lobe responses due to all the sources diagrammed are usually visible on at least one of a set of five beam positions. In the E-W direction few side-lobe responses have been recognized and cataloged radio sources show no clustering along the lines of interference; such an effect, if present, might indicate the existence of unrecognized sidelobes. The sun, in fact, is the only source which is often detectable in these directions; it is several times stronger than the strongest southern celestial sources. Examination of Fig. 16 suggests greater difficulties might be experienced south of the zenith, but little cataloging has been done in this region so that it is not yet possible to give a positive opinion.

The cataloging of sources is continuing, with about 1200 sources listed at present in an area of 3.3 steradians. This is about 45 per cent of the area usefully accessible to the instrument.

### B. Contour Plotting

Although a number of contour maps of the distribution of radio emission across various emitting objects

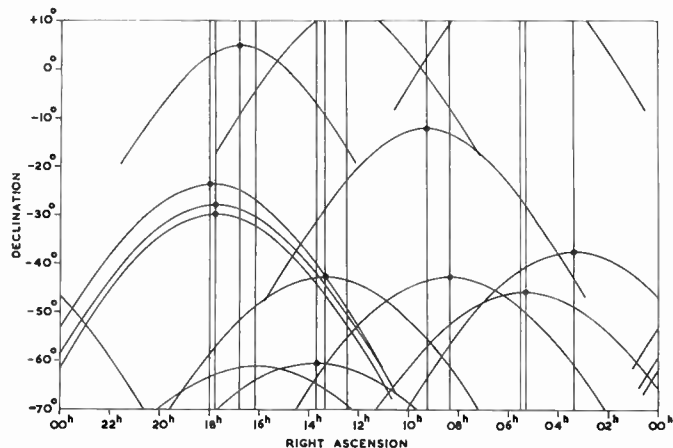


Fig. 16—The disposition of the "lines of interference;" the strong sources indicated by dots on the diagrams may produce spurious responses along these lines.

have been published,<sup>12-14</sup> no detailed account has been given of the preparation of the diagrams. While it is outside the scope of the present paper to give very detailed descriptions of this sort, it is possible to indicate the general methods employed.

Two types of objects are to be considered; in one, the variation in the N-S array temperature is small over the whole region and it is possible to plot difference temperatures only; in the other, absolute temperatures are required, either because a large area is involved or the total emission of a particular region must be measured. In either case the usual method is to write down the indicated temperatures over a grid measuring one or two minutes of time by one beam position ( $\approx 20$  minutes of arc). After any necessary corrections have been made, the resultant contours are drawn with smooth lines which, as far as can be judged, do not contain spurious high-frequency components not accepted by the arrays. When the contours are complex or closely crowded, temperatures may be read from the traced curves more frequently and interpolations in declination performed by methods described by Bracewell.<sup>15</sup> A process of filtering to remove any remaining spurious high frequency components, also described by Bracewell, is too complicated for hand reduction of data and has not been employed: in view of other uncertainties in the data, little is lost by this omission.

As an example of the form of diagram obtained, a version of the brightness temperature contours observed near the galactic center is shown in Fig. 17.<sup>13</sup> Two forms of correction have been applied to this diagram. In one,

<sup>12</sup> B. Y. Mills, "The observation and interpretation of radio emission from some bright galaxies," *Aust. J. Phys.*, vol. 8, pp. 368-389; September, 1955.

<sup>13</sup> B. Y. Mills, "The radio source near the galactic centre," *Observatory*, vol. 76, pp. 65-67; April, 1956.

<sup>14</sup> B. Y. Mills, A. G. Little, and K. V. Sheridan, "Emission nebulae as radio sources," *Aust. J. Phys.*, vol. 9, pp. 218-227; June, 1956.

<sup>15</sup> R. N. Bracewell, "Two dimensional aerial smoothing in radio astronomy," *Aust. J. Phys.*, vol. 9, pp. 297-314; September, 1956.

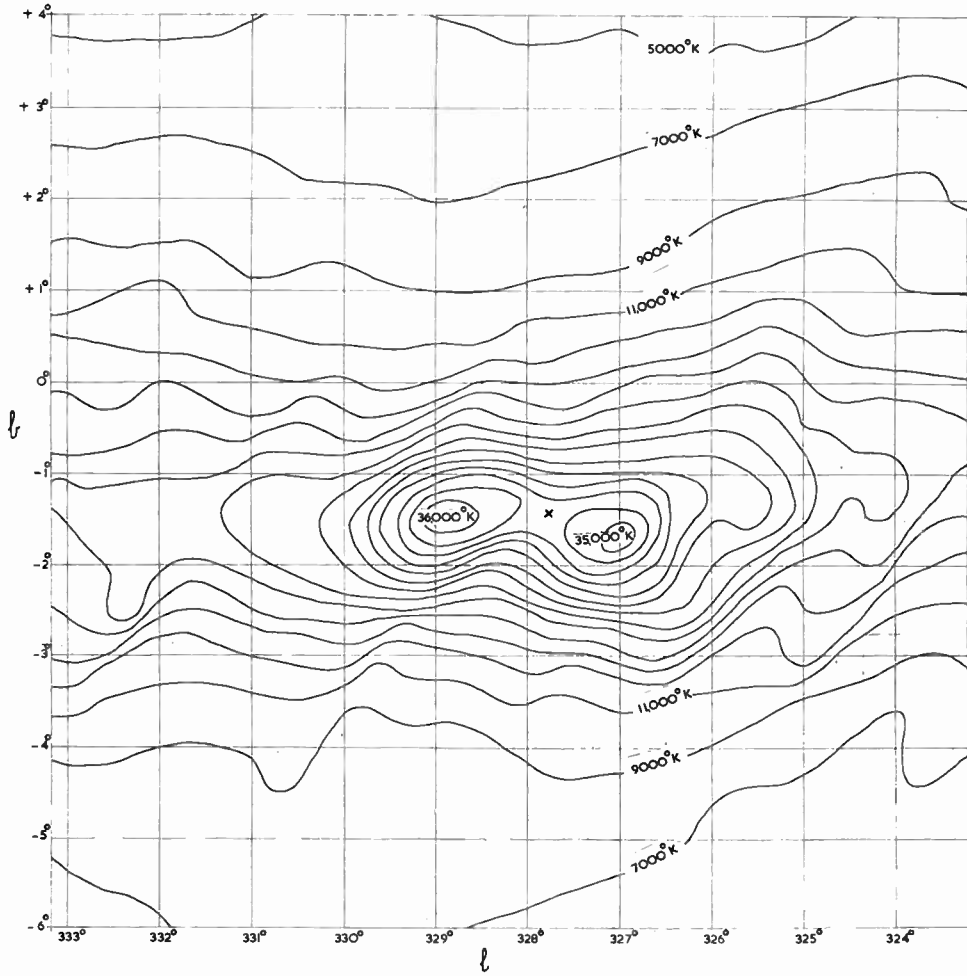


Fig. 17—An example of a brightness temperature contour diagram near the galactic center. The cross near the middle of the diagram indicates the position of a strong source observed at short wavelengths in the direction of the galactic center. At 3.5 m the source corresponds with an area of absorption, suggesting that it is a region of ionized hydrogen.

The relative calibration of adjacent beam settings is checked and adjusted, if required, by comparison of temperatures in the overlapping positions corresponding to beam changes of  $\pm 40$  minutes from the standard settings (Fig. 10). In two beam settings, out of the ten involved in the diagram, adjustments of this kind were necessary, one of +7 per cent and the other of -3 per cent. The second correction is desirable to remove the effects of spurious responses in the  $\pm 20$ -foot beam positions. These tend to produce "corrugated" contours since the errors are alternately positive and negative, but they may be corrected simply by application of a series derived from the error response of Fig. 12. For correction near the galactic plane two terms only appear sufficient to remove the major part of the effect, thus:

$$\begin{aligned} \Delta T_{n+1/4} &= 0.13(T_{n+2} - T_{n-1.5}) \\ &\quad - 0.06(T_{n+3.75} - T_{n-3.25}) \\ \Delta T_{n-1/4} &= 0.13(T_{n-2} - T_{n+1.5}) \\ &\quad - 0.06(T_{n-3.75} - T_{n+3.25}) \end{aligned} \quad (37)$$

here

$$\Delta T_{n+1/4} \text{ and } \Delta T_{n-1/4}$$

are the temperature corrections required at the beam positions on either side of the standard settings of (28); the other temperatures are similarly defined.

At present, work is proceeding on the preparation of contour maps covering a strip  $10^\circ$  wide extending the length of the southern Milky Way. Contour diagrams of a number of special regions of interest are also being prepared and will be published in due course.

### C. Miscellaneous Applications

Many special observations have been made with the instrument, some in which modifications to the usual mode of operation were required. Most of those which led to positive conclusions have been described in the literature; these include observations of astronomical objects of particular interest, such as emission nebulae,<sup>14</sup> nearby external galaxies,<sup>12</sup> and supernovae,<sup>16</sup> together with some observations of solar and lunar occultations

<sup>16</sup> B. Y. Mills, A. G. Little, and K. V. Sheridan, "Radio emission from novae and supernovae," *Aust. J. Phys.*, vol. 9, pp. 84-89; March, 1956.

of radio sources.<sup>17-19</sup> One of the latter was interesting in demonstrating the feasibility of making observations away from the meridian plane, by phasing the elements of the E-W array.<sup>19</sup> Also, as mentioned in Section II, the E-W array has been used continuously in a search for variable sources and a study of ionospheric effects.

Other uses of interest which, in general, have not been reported in the literature include the investigation of radio emission within the solar system and an investigation of the polarization of radiation from the galaxy and other radio sources. The sun itself is a powerful radio source and the distribution of emission has been studied by Little;<sup>20</sup> it is the only member of the solar system from which radiation has definitely been detected with this instrument. The other observations include particularly the planets Jupiter and Venus and the recent comet Arend-Roland: it is possible to say that in no case did continuous emission from these objects exceed about  $5 \times 10^{-26} \text{ W m}^{-2} \text{ cps}^{-1}$  at 3.5 m. Since the observations are of very limited duration, the possibility of sporadic emission is not eliminated. Other members of the solar system have also been investigated with negative results.

Polarization measurements were attempted using a single dipole plus reflector, forming an interferometer in conjunction with either the E-W or N-S arrays. The polarization of the single dipole was at right angles to that of the arrays. With this arrangement, no response

<sup>17</sup> O. B. Slee, "Occultation of a radio source by the solar corona," *Observatory*, vol. 76, pp. 228-231; December, 1956.

<sup>18</sup> H. Rishbeth, "An investigation of the radio source 06N2A in Gemini," *Aust. J. Phys.*, vol. 9, pp. 494-504; December, 1956.

<sup>19</sup> H. Rishbeth and A. G. Little, "A lunar occultation of the radio source associated with Kepler's supernova," *Observatory*, vol. 77, pp. 71-74; April, 1957.

<sup>20</sup> Radio Astronomy, IAU Symp. No. 4, The University Press, Cambridge, England, p. 288; 1957.

occurs if the polarization of the radiation is random or plane-polarized with the plane parallel to that of the arrays or the single dipole; with any other form of polarization an interference pattern might be expected.<sup>21</sup> No significant patterns were observed: for the radio sources 03S3A, 05N2A, 09S1A, and 12N1A, the deflections were less than 3 per cent of those obtained when the single dipole was aligned parallel to the array dipoles, and for 13S4A and the galactic center the deflection was less than 1 per cent. In all cases the limit was set by noise fluctuations.

With the completion of the survey of the southern sky, observations with the radio telescope have now practically ceased while work proceeds on the construction of the equipment for angular size measurement, mentioned in Section III. This involves a radio-link interferometer with base line approximately  $3000\lambda$ , of a type developed earlier by one of the authors.<sup>22</sup> It is anticipated that this should provide information very valuable for the identification of radio sources and also perhaps, for a cosmological investigation based on distant radio galaxies of very small angular size.

#### VIII. ACKNOWLEDGMENT

The authors express their gratitude to K. R. McAlister, who was responsible for the major part of the mechanical design of the arrays and who succeeded in reducing their cost below any reasonable expectation.

<sup>21</sup> B. Y. Mills and A. B. Thomas, "Observations of the source of radio-frequency radiation in the constellation of Cygnus," *Aust. J. Sci. Res.*, vol. A4, pp. 158-171; June, 1951.

<sup>22</sup> B. Y. Mills, "The radio brightness distributions over four discrete sources of cosmic noise," *Aust. J. Phys.*, vol. 6, pp. 452-470; December, 1953.



# The Sydney 19.7-MC Radio Telescope\*

C. A. SHAIN†

**Summary**—The construction and operation of the Sydney 19.7-mc "Mills Cross" radio telescope is described briefly, with special reference to the features peculiar to operation at this low frequency.

The results obtained so far are reviewed. They relate to the detection of ionized interstellar hydrogen, to the evaluation of the general background radiation from extremely distant external galaxies, to the study of discrete sources, and to the study of refraction in the ionosphere.

## INTRODUCTION

THE first observations in radio astronomy were made by Jansky<sup>1</sup> at a frequency of 18 mc. He discovered the broad band of radio emission which follows the Milky Way and which has since been studied intensively by radio astronomers, mainly at much higher frequencies. The lower frequencies, however, can yield unique information. The current interest is centered on observing, not so much Jansky's "primary waves themselves coming from a great many sources scattered throughout the heavens," but the effect on those "primary waves" of the absorption due to the great clouds of interstellar ionized hydrogen which tend to concentrate near the plane of the Milky Way. Because the absorption processes are similar, this is closely analogous to the study by radio engineers of the *D* region of the ionosphere through its absorption of radio waves reflected from the *E* and *F* regions.

As is common in radio astronomy, the greatest possible resolving power is required, because the clouds of ionized hydrogen occupy a band in the Milky Way only a few degrees wide. Some 18.3-mc observations by Shain and Higgins<sup>2</sup> gave indirect evidence for the existence of the interstellar absorption,<sup>3</sup> but direct experimental investigation required the construction of an antenna having a beamwidth of 1° or 2°; at 20 mc such an antenna must have linear dimensions of a few thousand feet.

The invention of the "Mills Cross"<sup>4</sup> made such an antenna practicable, and a system is now in operation near Sydney with a beamwidth of 1.4° at a frequency of 19.7 mc (a wavelength of 15.2 meters). The construction of a large antenna at these wavelengths is somewhat simpler than at shorter wavelengths, in spite of the great

increase in physical size for a given beamwidth, because of the much easier tolerances allowable, but there are certain problems—interference from radio stations, and the refraction and absorption effects in the ionosphere—which are much more serious on the lower frequencies. Previous experience at 18.3 mc showed that these difficulties could be overcome by suitable techniques.

The general principles of the "Mills Cross" have been given by Mills and Little<sup>4</sup> and by Burke.<sup>5</sup> Briefly, the "Cross" consists of two very long antenna arrays which are connected together in a receiver through a phase-switching system. That part of the receiver output which is modulated at the switching frequency is recorded. The over-all effect is to produce a pencil-beam response from the region of the sky common to the beams of the two arrays. The detailed theory, together with a description of the Sydney 85.5-mc Cross, is given in another paper.<sup>6</sup>

The 19.7-mc instrument is essentially similar to the 85.5 mc one described in the paper by Mills and his collaborators,<sup>6</sup> to which reference should be made. The present paper first describes the special features of the 19.7-mc equipment which have been developed to counter the difficulties peculiar to this low frequency, and then shows the types of results which are now forthcoming.

## SPECIAL FEATURES OF THE 19.7-MC EQUIPMENT

### Antenna

The particular requirements of this antenna are low sidelobes, a bandwidth not less than one quarter of a mc to accommodate slight variations in operating frequency, and simple means of changing the direction of the beam of the north-south array, and hence the declination setting, to make the most profitable use of the best recording times.

To keep the sidelobe level down, at the expense of broadening the main beam, both the north-south and east-west arrays of the Cross have a heavily-tapered current distribution. The effectiveness of this is shown by the fact that only a few of the strongest sources are troublesome in producing spurious responses at certain declination settings. The reduction of standing waves by the insertion of matching networks at intervals along the main feeders gives an acceptable bandwidth.

The N-S array is 3625 feet and the E-W array 3400 feet in length. Along each array runs a main feeder of

\* Original manuscript received by the IRE, October 3, 1957.

† Radiophysics Laboratory, CSIRO, Sydney, Australia.

<sup>1</sup> K. G. Jansky, "Directional studies of atmospherics at high frequencies," *PROC. IRE*, vol. 20, pp. 1920-1932; December, 1932; "Electrical disturbances apparently of extraterrestrial origin," *Proc. IRE*, vol. 21, pp. 1387-1398; October, 1933.

<sup>2</sup> C. A. Shain and C. S. Higgins, "Observations of the general background and discrete sources of 18.3 mc/s cosmic noise," *Aust. J. Phys.*, vol. 7, pp. 130-149; March, 1954.

<sup>3</sup> C. A. Shain, "A comparison of the intensities of cosmic noise observed at 18.3 mc/s and at 100 mc/s," *Aust. J. Phys.*, vol. 7, pp. 150-164; March, 1954.

<sup>4</sup> B. Y. Mills and A. G. Little, "A high-resolution aerial system of a new type," *Aust. J. Phys.*, vol. 6, pp. 272-278; September, 1953.

<sup>5</sup> B. F. Burke, "Mills cross radio telescopes," *Astron. J.*, vol. 6, pp. 167-168; May, 1956.

<sup>6</sup> B. Y. Mills, A. G. Little, K. V. Sheridan, and O. B. Slee, "A high resolution radio telescope for use at 3.5 m," this issue, p. 67.

polythene-insulated coaxial cable<sup>7</sup> to which the dipoles of the respective arrays are lightly coupled. In the case of the N-S array, in which the phases have to be adjusted, sections of the feeder are in the form of artificial lines constructed around the fixed contacts of switches spaced at intervals along the feeder. Each of the dipoles is coupled through a small capacitor to the moving contact of one of the switches, so that the phase of the dipole current with respect to the phase of the current at the input to the feeder is adjustable in steps of  $33^\circ$  with negligible change in amplitude. For convenience, the dipole connections are grouped in threes and one artificial line, with three independent moving contacts, suffices for each group. Provision is also made for scanning over five closely-spaced beam positions (with separations of  $33'$  arc at the zenith), by means of relay-operated phase-switching networks controlled from a central hut. The scanning-cycle period is one minute; a large change in declination, involving the manual alteration of all the dipole switches, takes about twenty minutes.

As an illustration of the type of construction, Fig. 1 shows a small section of the N-S array.

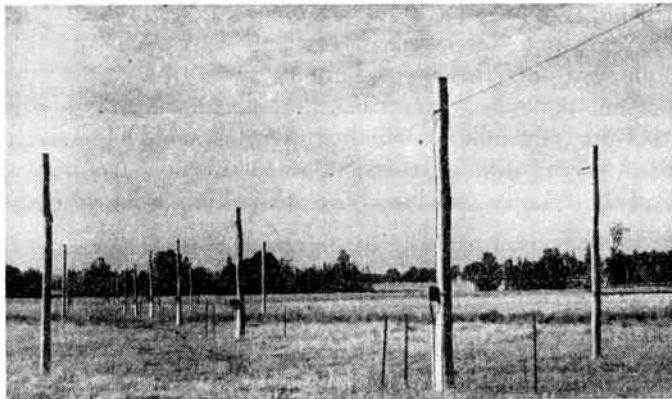


Fig. 1—The northern end of the N-S array. The dipoles are supported by wires, broken up by insulators, running along the sides of the array. Nine of the boxes containing the dipole phasing switches can be seen on the poles in the middle of the array. There are 51 of these boxes in the complete array.

### The Receiver and Its Operation

In planning the receiving equipment, two opposing considerations had to be kept in mind: the bandwidth should be as great as possible<sup>8</sup> in the interests of sensitivity, but the greater the bandwidth the more trouble is experienced from interfering radio stations.

The early work on 18.3 mc showed that although the radio spectrum near 20 mc was often crowded with interfering signals, there were generally some clear gaps several kilocycles wide in a range of 100 kc or so. These gaps would remain clear for several hours and only slight retuning was required; in fact, between midnight

<sup>7</sup> Type PT29M, similar to RG-11/U.

<sup>8</sup> An upper limit to the bandwidth is determined by the path differences between the ends of the array for radiation at different frequencies within the pass band, especially at large zenith distances. This restriction is not serious with the present equipment.

and dawn, owing to the poor ionospheric propagation conditions, there were often very few interfering signals. A similar state of affairs has been found on 19.7 mc, and accordingly the receiver was designed to take as much advantage as possible of the gaps between the stations. It is a double superheterodyne receiver, and a block diagram is shown in Fig. 2.

The first IF is 2 mc; the amplifier has a pass band 100 kc wide. This can be used directly on those occasions when the interference is very low, but generally the second IF amplifier is necessary. The 2 mc output from the first IF is mixed with a second oscillator on 1.75 mc, and the broad-band (200–300 kc) mixer output is passed to five separate narrow band channels. The first of these includes a mechanical filter,<sup>9</sup> centered on 250 kc with a bandwidth of 8.5 kc at 3 db down and 13 kc at 40 db down. The remaining channels each have two stages of amplification with variable tuning, so that each channel can be adjusted, independently of the others, to any frequency in the range 200 to 300 kc. The bandwidth of each tunable IF is 4.5 kc at 3 db down and 16 kc at 40 db down. The outputs of the five channels are combined immediately before the detector. The combined response is an IF pass band like a comb, the separation between the component pass bands being variable at will, and the maximum effective bandwidth, with all narrow-band IF's in operation, is 26 kc. A typical over-all response curve is shown in Fig. 3.

In operation, at first only the fixed-frequency channel is used. The first local oscillator frequency is varied between 21.6 and 21.8 mc to search for suitable gaps between stations. Having found the widest gap, the local oscillator is left fixed and as many as possible of the variable frequency IF channels brought into operation, with equal gains, in the same or nearby gaps. A beat oscillator is provided to cover the full range of the second IF pass band, and it has been found in practice that any interfering signal can be detected aurally in the loudspeaker when its strength is less than that required to affect the record. As often as possible an observer is in attendance for monitoring. To minimize ionospheric effects, the cosmic noise records are taken during the night, when possible after midnight, and under these conditions often all five narrow channels can be used, and occasionally the 100 kc bandwidth. At other times of the day it is often possible to use one narrow channel only.

Although the bandwidth may be limited to a few kilocycles, the sensitivity is sufficient to produce very useful records, and the results have justified the general design.

### OUTLINE OF THE CURRENT RESEARCH PROGRAM

The main observational program at present involves a survey of the 19.7-mc brightness distribution in a zone about  $15^\circ$  wide around the galactic equator. In this region the brightness temperatures at higher

<sup>9</sup> Collins Radio Company Type F 250A-85.

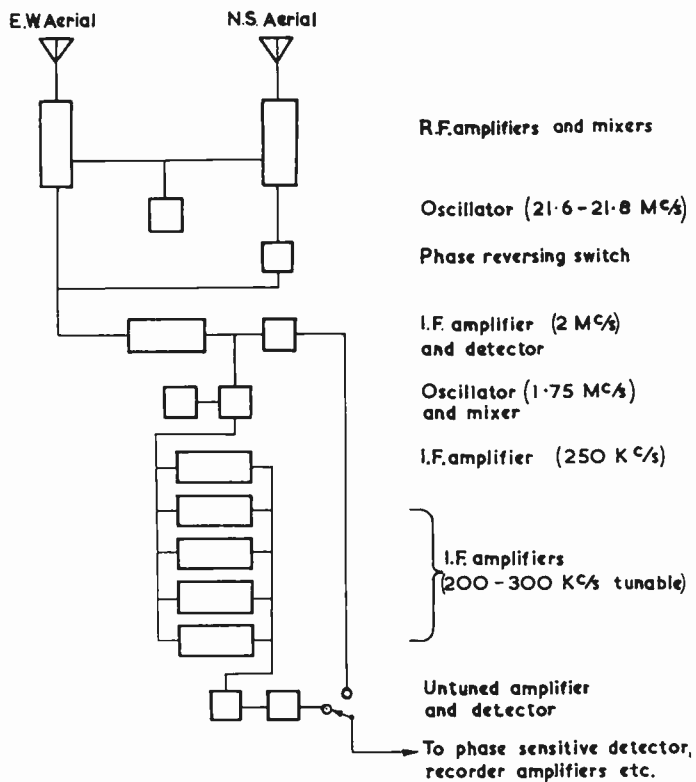


Fig. 2—Block diagram of the receiving equipment. Only the main units are shown. Among the units omitted are the square wave generator for the phase switch, the beat frequency oscillator, and a separate IF channel for recording the output from the N-S antenna separately.

frequencies (for example, 85.5 mc) show a sharp ridge, due to some form of nonthermal emission in the galaxy, rising to a maximum near the galactic center.<sup>10</sup> However, the regions of ionized hydrogen (the so-called HII regions) are also concentrated near the galactic plane, so that their absorption effects will be most pronounced in this region around the galactic equator. It has been found, in fact, that in the immediate vicinity of the equator the increased absorption near the galactic plane commonly outweighs the general nonthermal increase in brightness, and, instead of a ridge, a trough is seen.<sup>11</sup> A typical example is shown in Fig. 4. Detailed comparison of the 19.7 and 85.5-mc brightness distributions will throw much light on the distribution of ionized hydrogen in the galaxy. Indeed the recognition of absorbing clouds by this means appears to be the most sensitive method available to astronomers for detecting interstellar ionized hydrogen.

An interesting possibility that has come out of the preliminary work is that it may be possible to estimate distances to certain structural features of the galaxy. Even HII regions which are very dim optically may be completely opaque to 19.7-mc radiation, and therefore, any radio noise from their direction must have been

<sup>10</sup> B. Y. Mills, "The observation and interpretation of radio emission from some bright galaxies," *Aust. J. Phys.*, vol. 8, pp. 368-389; September, 1955.

<sup>11</sup> C. A. Shain, "The galactic absorption of 19.7 mcs radio waves," *Aust. J. Phys.*, vol. 10, pp. 195-203; March, 1957.

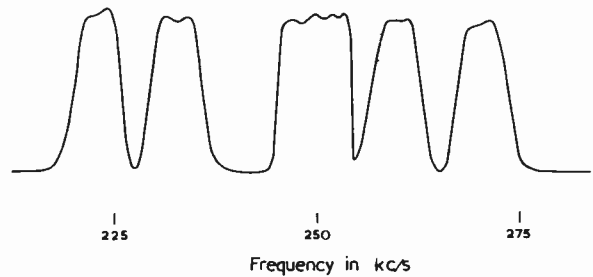


Fig. 3—Over-all response at the combined output of the 200-300 kc IF units. The broader, flat-top response centered on 250 kc corresponds to the fixed mechanical filter. The center frequencies of the other peaks may be varied independently.

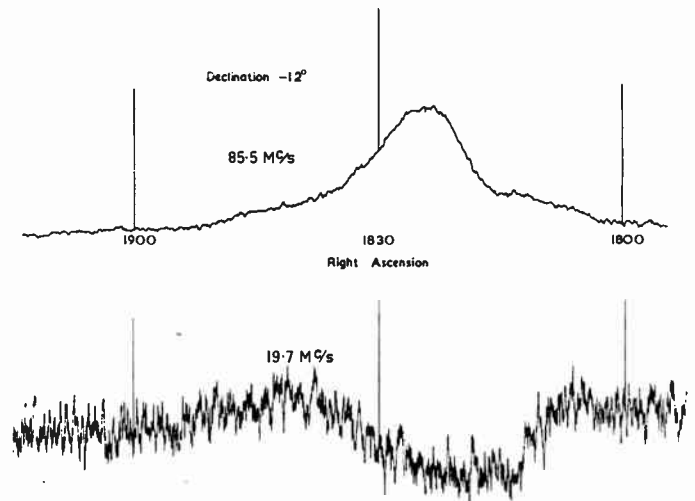


Fig. 4—Variation of brightness during a sweep across the Milky Way at declination  $-12^\circ$ . The upper record is at 85.5 mc and shows the sharp ridge characteristic of such records at this frequency. The lower record shows the trough observed at 19.7 mc due to interstellar absorption.

generated between the sun and the HII region. Correlation of 19.7-mc brightness temperatures with distances, derived optically, to known large and bright HII regions should give a value for the amount of radiation emitted per unit distance near the sun, for various directions in the galaxy. If this proves constant, 19.7-mc brightness could then be used to estimate distances to other absorbing HII regions, and it may be possible to trace out some part of the spiral structure of the galaxy.

When a radio telescope is directed to one of the galactic poles, the brightness temperatures observed are much higher than were expected. It is now known that this radiation comes from two sources—a roughly spherical "halo" surrounding the galaxy, and all the extragalactic sources in the universe<sup>12</sup>—but the estimation of their relative importance presents some difficulty. A new line of attack has come from 19.7-mc observations of the large Magellanic cloud and, in particular, of absorption by its giant HII region, 30 Doradus and its associated nebulosities. Since, in this case, the absorbing region is far outside our galaxy, the reduction in bright-

<sup>12</sup> J. E. Baldwin, "The distribution of the galactic radio emission," *Mon. Not. Roy. Astron. Soc.*, vol. 115, No. 6, pp. 690-699; 1955.

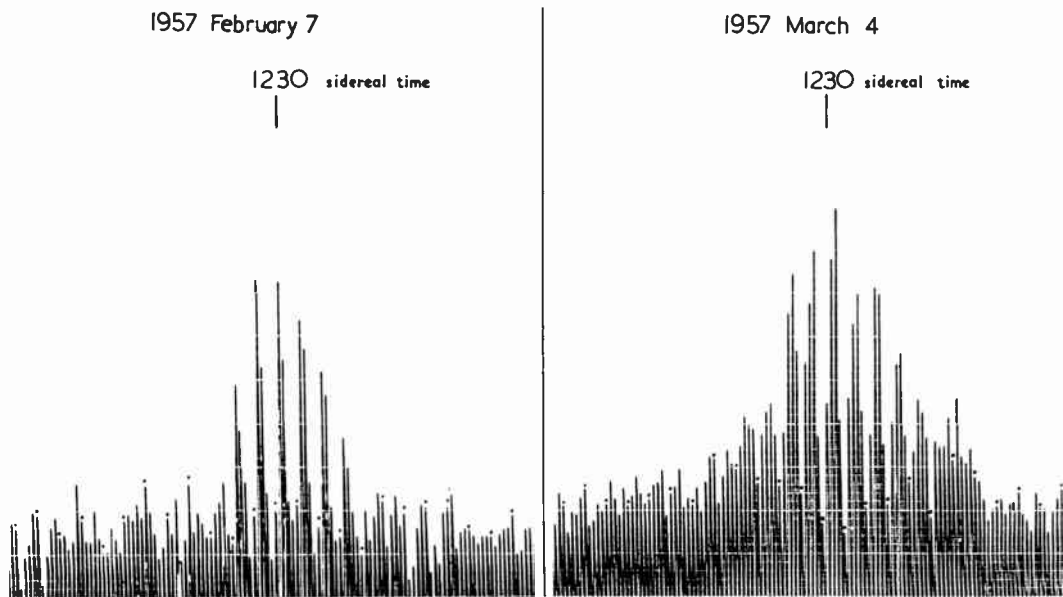


Fig. 5.—Records of the source Virgo-A on February 7 and March 4, 1957, using the scanning system. The length of one line is a measure of the energy received over a period of 12 seconds with the antenna directed to a particular declination; an adjacent line corresponds to a second declination, five declinations spaced at  $33'$  arc being scanned in succession and the sequence then repeated. The southernmost position is indicated by dots over appropriate lines and the antenna scans northwards, reading from right to left, from this position.

ness is due to the cutting off of radiation from the far side of the Magellanic cloud and extragalactic sources. It is possible to estimate the former component, and hence to determine the contribution to the general background of cosmic noise due to all the extragalactic sources. Preliminary results suggest that this is small.

Observations of discrete sources, especially those of small angular size, are troubled by ionospheric scintillations, which can be very severe at 19.7 mc. As mentioned above, the best time for observing is between midnight and dawn, just the period when scintillations are most severe. In general, the presence of scintillations makes the detection of a source more difficult, unless the number of records is increased to average them out. This is not practicable in a general survey of the sky, and it is not proposed to attempt to detect a great number of weak sources, but rather to observe a moderate number of the stronger sources known from the 85.5-mc survey, with a view to determining what different spectral classes of sources there are. Some of the brightest sources have comparatively large angular sizes and the directivity of this equipment is sufficient to study their brightness distributions in some detail. An interesting result coming out of this part of the program is the marked difference between the brightness distribution across the source Centaurus-A at 19.7 and 85.5 mc. The strong "point" source is much less prominent at 19.7 mc.

As a by-product of the earlier cosmic noise work on 18.3 mc, analysis of the records gave much information on the attenuation of radio waves passing right through the ionosphere. It is expected that the current records will also provide new material for ionospheric studies. This time, however, the directivity of the present aerial

will permit accurate measurements of ionospheric refraction. In any case, it will be necessary to make some study of refraction, if only to decide when it is seriously affecting the cosmic noise work. Refraction appears in two ways: firstly, the normal type of astronomical refraction which, since the equipment operates as a transit instrument, causes an apparent change in declination, and second, refraction in the east-west direction, causing an apparent change in right ascension, due to horizontal gradients of ionization in the  $F$  region.<sup>13</sup> The latter may be quite serious (perhaps  $1^\circ$ ) near sunrise. A further complication is that a source moves through the aerial beam in about 10 minutes, so that it is difficult to distinguish between short period changes in the ionosphere and its regular diurnal variation. A particular case is illustrated in Fig. 5, by two records of the source Virgo A. By comparing the relative amplitudes on the different positions of the declination scan, the apparent declination can be determined, and the time of maximum response gives the apparent right ascension. In this manner it is found that on February 7, Virgo A appeared to be about  $0.8^\circ$  to the north-east of its true position, and on March 4,  $0^\circ.4$  to the south.

From the experience already obtained with this 19.7-mc antenna, it is clear that, in spite of difficulties caused by interference and the influence of the ionosphere, it will yield much useful astrophysical information. Furthermore, the effects of the ionosphere on the cosmic noise observations may throw further light on the ionosphere itself.

<sup>13</sup> F. G. Smith, "Ionospheric refraction of 81.5 mcs radio wave from radio stars," *J. Atmos. Terr. Phys.*, vol. 2, no. 6, pp. 350-355 1952.

# An Antenna Array for Studies in Meteor and Radio Astronomy at 13 Meters\*

P. B. GALLAGHER†, MEMBER, IRE

**Summary**—The design of a high-frequency radar antenna making possible the detection of echoes from the ionized trails produced by very small meteors is described. Preliminary results indicate that the radar system, when fully completed, will be capable of detecting meteors down to the 15th visual magnitude, thus making possible radio studies of meteors five visual magnitudes smaller than the smallest which have heretofore been systematically investigated at back reflection. The results of these studies are expected to provide new information on the amount and distribution of interplanetary matter, the contribution of meteoric ionization to the lower ionosphere, and the radio propagation characteristics of vhf ionospheric scatter and meteor burst communication systems. The results of some preliminary measurements of meteors down to the 14th magnitude are presented. Other possible applications of the antenna are discussed.

## INTRODUCTION

AN ANTENNA array, designed for radar studies of very small meteors, has been constructed at Stanford University. The nominal radar power output is 100 kilowatts peak and 1000 watts average. The number of echoes actually detected with this system, with one half of the antenna in operation, indicates that it should be sensitive to meteors as small as the 15th visual magnitude. Thus this installation will permit studies of meteors five magnitudes smaller than the smallest which have been investigated systematically at back reflection in the past.

Studies of very small meteors have important application to the design of the antenna systems used in vhf ionospheric scatter communication systems. It is now clear that overlapping reflections from very small meteor trails represent an important component of the continuous ionospheric scatter signal.<sup>1</sup> In fact, the evidence suggests that at moderate latitudes, the meteoric component is by far the principal component during the evening hours when the scatter signal is at its daily low ebb. To improve circuit performance at this critical time of day, it is necessary to maximize the meteoric component of the signal; considerable improvement can be effected by employing antenna beams which intersect slightly to one side of the center of the great circle path. To predict the best intersection point for a given time of day, time of year, and geographical location, more needs to be known of the characteristics of very small meteors. In a similar manner, more information on

meteor characteristics is needed for the optimum design of the systems using the new technique of meteor burst communication.<sup>2</sup>

The radio studies of small meteors will also be applied to determine the number, velocities, orbits, and space distribution of meteoric particles 100 times lighter than those previously studied by radar means. Important questions to be studied are: 1) What is the size of the smallest particle that produces ionization in the upper atmosphere? 2) What is the total amount of ionization created by meteors of all sizes? 3) Are there enough of these small particles in interplanetary space to account for the zodiacal light, the F corona, and the gegenshein? 4) Are there any interstellar particles amongst the smaller meteors? 5) What is the number-mass distribution of the smaller meteors?

It is the purpose of this paper to discuss the design and testing of the antenna array used in the radar system, to outline some of the preliminary results of the studies on meteors, and to indicate some potential applications of the system in other radio astronomy research.

## EQUIPMENT

The operating frequency chosen, 23.1 megacycles, represents a compromise between sensitivity to small meteors on the one hand, and interference from ionospherically propagated ground backscatter on the other. To detect small meteors which burn out high in the atmosphere, a low radio frequency is needed. In the interests of obtaining high gain at minimum cost, the limitations of fixed-frequency operation were accepted.

A broadside antenna array configuration was selected for reasons of economy and flexibility. The most economical unit of this array was found to be a 4-element Yagi antenna, which offers high gain in a simple, easily mounted structure. The final layout called for 48 Yagi units in a colinear arrangement. The units are fed from a common transmission line and are spaced one wavelength apart along that line. A second colinear set of 48 units, placed parallel to the first, and spaced from it by several wavelengths, causes the basic fan beam to be broken up into lobes.

For small meteor studies, a beam pointing generally north was desired. As pictured in Fig. 1, the individual Yagi units are positioned at a 45° elevation angle and are mounted on wooden telegraph poles at an average height of 35 feet above ground. The two lines of Yagis extend 48 wavelengths (or 2000 feet) east and west, and

\* Original manuscript received by the IRE, October 3, 1954. The research reported in this paper has been sponsored by the Electronics Research Directorate of the AF Cambridge Res. Ctr., Air Res. and Dev. Command, under Contracts AF 19(604) 1031 and AF 19(604) 2193.

† Radio Propagation Laboratory, Stanford Univ., Stanford, Calif.

<sup>1</sup> K. L. Bowles, "Ionospheric forward scatter," *Annals of the IGY*, vol. 3, part IV, pp. 346-357; 1957.

<sup>2</sup> See PROC. IRE, vol. 45; December, 1957.

5) Errors resulting from variations in coupling coefficient at each coupler and variations in spacing of the couplers along the line were also evaluated. From measurements made at the output of each coupler, the rms errors were found to be  $\epsilon_6=0.07$  and  $\epsilon_7=0.07$  radian.

Bracewell has developed a theory of tolerances for large and complex antenna arrays.<sup>3</sup> He defines a directivity achievement factor

$$\zeta = \frac{\text{achieved directivity}}{\text{design directivity}} = \frac{1}{1 + \sum \epsilon_i^2}$$

where  $\epsilon_i$  is the complex fractional departure from the perturbed mean of the illumination along the array due to various causes  $i=1, 2$ , etc. The cumulative errors 1) through 5) result in  $\zeta=0.93$ , which is equivalent to a 0.29-db loss in forward gain. This is quite small compared to dissipative losses (1.25 db) and remaining uncertainties about ground and mutual impedance effects, even though individual amplitude and phase errors measured at the time of initial adjustment appeared almost prohibitively large. Therefore no further corrective adjustments were undertaken.

Field intensity measurements at 13 meters of radio star, solar, and other extra-terrestrial noise sources constitute a potential application of this array system. As such, the array could be used as part of a total power radiometer, sensitive only to the horizontally polarized component of the incoming wave. (The array can be adapted for cross polarization, if desired.) Fig. 3 shows a calibration of the azimuthal beam pattern of one line

echoes. The theoretical work of Kerr<sup>4</sup> at 30 mc has been scaled to fit the 13-meter wavelength. Using a 500-cps pre-detection bandwidth and 10-second post-detection integration time, the sun echo power for a quiet sun would exceed the noise threshold by about 5 db. (This presumes that ionospheric absorption, atmospheric, and station interference are on a par at both frequencies.) With an adjustment of parameters, but using the same antenna and transmitter power, it appears that planetary echoes (Venus and Mars) might also be detected.

One line of the array was completed in January, 1957. Since that time, studies in the field of meteor astronomy have included echo counts, determination of diurnal and day-to-day variations in echo rates, echo amplitude distributions, meteor velocities, and durations of echoes from ionization produced by meteors of the 14th visual magnitude and larger. These measurements have demonstrated the existence of short-period showers, and extreme fluctuations in day-to-day rates.

Fig. 4 is a record of typical radar meteor echo activity.

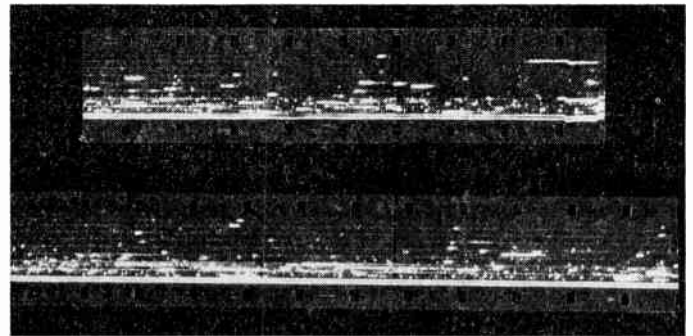


Fig. 4—Range-time display of meteor echo activity observed with the 13-meter array; 100-km range marks; one frame per 11 seconds; peak power 90 kw; January 24, 1957; 0400 PST.

Hourly echo rates as high as 6000 have been measured daily, during the two-hour pre-sunrise period. Outside this period the echo rate declines rapidly. The ratio of the daily maximum echo rate to the daily minimum echo rate for this radar has been found to be over 100:1, as compared to 20:1 for another lower-power, lower-directivity radar operating in the same frequency range on the Stanford campus.

Preliminary evidence also suggests that particles smaller than about the 13th visual magnitude may exist in space in greater numbers than would be indicated from an extrapolation of the mass distribution law that applies to meteors larger than 10th magnitude.

#### CONCLUSION

The feasibility of a very large broadside array for meteor detection at 13 meters has been demonstrated. The design offers notable flexibility, economy in con-

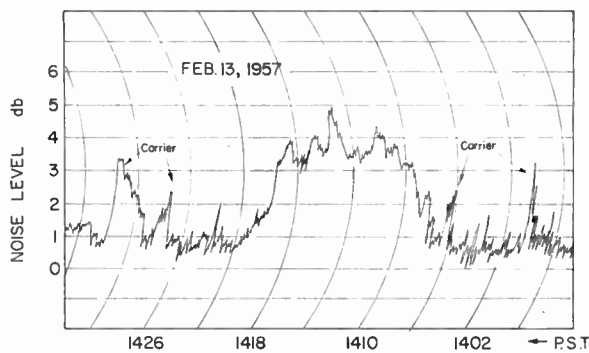


Fig. 3—Penmotor recording of the radio noise source Cassiopeia as it transits the 13-meter array beam, taken February 13, 1957. Each four-minute division represents one-half degree.

of the array using the relatively discrete source in Cassiopeia at the upper transit across the beam.

Calculations show that with a transmitter of the same peak power, but capable of transmitting very long pulses, the system may be capable of detecting solar

<sup>3</sup> R. N. Bracewell, "Radio Astronomy Techniques" in "Handbuch der Physik," vol. 54, Springer Verlag, Berlin, Germany, in press.

<sup>4</sup> F. J. Kerr, "On the possibility of obtaining radar echoes from the sun and the planets," Proc. IRE, vol. 40, pp. 660-666; June, 1952.

struction, and simplicity of adjustment but is limited to fixed-frequency operation. It can be modified for detection of echoes from the sun, as well as other studies in radio astronomy.

Performance degradation resulting from reasonable tolerances in layout and construction has been found to be negligible.

Preliminary results with a 100-kw pulsed transmitter have shown that the law relating size and number of meteoric particles is valid down to meteors of approxi-

mately the 13th visual magnitude. There is evidence that the law may break down for still smaller particles, but higher transmitter power will be required in order to answer this question.

#### ACKNOWLEDGMENT

The design of the antenna array and the feed system was conducted primarily by the antenna group of the Stanford Research Institute, under the direction of J. T. Bolljahn.

## Radio Telescope Antennas of Large Aperture\*

JOHN D. KRAUS†, FELLOW, IRE

**Summary**—Equations are derived for the number of sources which a radio telescope can detect and the number which it can resolve. Based on these relations curves for the number of sources which can be both detected and resolved, as a function of frequency and aperture, are presented. The need for large apertures in order that radio astronomy deal with significant numbers of sources is evident. It is also pointed out that there is a most economical frequency for radio astronomy in the vicinity of 300 mc.

A design for a radio telescope which provides a large aperture at low cost is described. It consists of a fixed standing parabolic reflector with a tiltable flat-sheet reflector. The advantages of the design are pointed out and the results with a scale model are described.

#### INTRODUCTION

PROGRESS in any science is dependent on improvements in observing techniques. Before Galileo, astronomy was restricted to the few thousand objects which could be observed with the unaided eye. With the invention of the optical telescope the number of observable objects increased sharply. Many previously known objects also could be studied in greater detail. As larger telescopes were built more objects came into view until with the largest present-day telescopes billions of objects can be observed. This development is actually the history of the increase of aperture from the  $\frac{1}{8}$ -inch pupil diameter of the human eye to the 200-inch diameter of the Mount Palomar telescope.

With the introduction of radio telescopes a new window has been opened on the universe. However, at present only one hundred or so radio sources are reliably known. This is hardly a statistically significant sample of the radio universe. Although the largest telescopes now or soon to be in operation may raise this number into the thousands, it is doubtful if the number will ap-

proach that of the stars that can be observed with the unaided eye (about 5000). Hence, until much larger radio telescopes are built radio astronomy will remain in the primitive status of even smaller numbers than the pre-Galilean era of optical astronomy.

The only way out is with telescopes of larger aperture. But it is not sufficient merely to plan bigger completely steerable parabolic dish telescopes. These cost millions of dollars for diameters of only 100 to 200 feet and the cost mounts exponentially as the size is increased. What is needed in order to break through the "aperture barrier" is an approach or design which can achieve apertures of several acres for thousands instead of millions of dollars, since then apertures of dozens of acres for a few millions of dollars become feasible.

In the next section basic relations between the number of sources which a telescope can observe and its aperture are developed and discussed in some detail. This is followed by a description of a telescope design which provides a large aperture per unit of cost.

#### APERTURE AND SOURCE NUMBER

In order to observe a celestial radio source a radio telescope must be able to do two things: 1) detect the source, and 2) resolve it.

Assuming a uniform source distribution, the number of sources which a radio telescope can detect is proportional to the cube of the telescope range. Thus,

$$N_d = K_0 R^3 \quad (1)$$

where

$N_d$  = number of sources which can be detected,

$K_0$  = constant,

$R$  = maximum range of telescope.

\* Original manuscript received by the IRE, October 3, 1957.

† Director, Radio Observatory, Ohio State University, Columbus, Ohio.

Now the range<sup>1</sup> of a radio telescope is given by

$$R = R_0 \sqrt{\frac{G_0}{G_{\min}}} \tag{2}$$

where

- $R$  = maximum range of telescope (meters),
- $R_0$  = range of reference source (meters),
- $G_0$  = power flux density of reference source (janskys) (1 jansky = 1 watt meter<sup>-2</sup> cps<sup>-1</sup>),
- $G_{\min}$  = minimum power flux density which can be detected with the telescope (janskys).

The *reference source* in (2) is one whose distance and flux density are both known. The range  $R$  is then the maximum distance at which this source or one like it can be detected.

A conservative single-valued estimate of the minimum flux density  $G_{\min}$  is given by

$$G_{\min} = \frac{2kTN}{aA_{em}\sqrt{n\Delta ft}} \tag{3}$$

where

- $G_{\min}$  = minimum detectable power flux density (janskys),
- $k$  = Boltzmann's constant (=  $1.38 \times 10^{-23}$  joules / °K),
- $T$  = receiver ambient temperature (°K),
- $N$  = receiver noise figure (dimensionless),
- $a$  = cable efficiency factor ( $0 \leq a \leq 1$ ) (dimensionless),
- $A_{em}$  = maximum effective aperture of telescope antenna (meters<sup>2</sup>),
- $n$  = number of observations or records (dimensionless),
- $\Delta f$  = receiver band width (cps),
- $t$  = receiver time constant (seconds).

Substituting (3) in (2) yields for the maximum range

$$R = R_0 \left[ \frac{aA_{em}G_0\sqrt{n\Delta ft}}{2kTN} \right]^{1/2} \tag{4}$$

where the symbols are as given following (2) and (3).

Assuming that the noise figure  $N$  is proportional to the square root of the frequency and that the bandwidth can be increased in proportion to the frequency, we have that the maximum range in meters is

$$R = K_1 R_0 \sqrt{A_{em} \lambda^x} \tag{5}$$

where

- $K_1$  = constant,
- $R_0$  = range of reference source (meters),
- $\lambda$  = wavelength (meters),
- $x$  = spectrum index of reference source ( $G_0 \propto \lambda^x$ ) (dimensionless).

It is assumed also in (5) that the number of observations  $n$  and the receiver time constant  $t$  and temperature  $T$  are fixed.

Substituting (5) into (1) yields the number of sources (like the reference source) that can be detected as

$$N_d = K_2 A_{em}^{3/2} \lambda^{1.5x} \tag{6}$$

where

- $N_d$  = number of detectable sources (dimensionless),
- $K_2$  = constant,
- $A_{em}$  = maximum effective aperture of antenna (meters<sup>2</sup>),
- $\lambda$  = wavelength (meters),
- $x$  = spectrum index of reference source (dimensionless).

The maximum effective aperture  $A_{em}$  of an antenna is related to the physical aperture by

$$A_{em} = \gamma A \text{ (meters}^2\text{)} \tag{7}$$

where

- $\gamma$  = efficiency factor ( $0 \leq \gamma \leq 1$ ) (dimensionless),
- $A$  = physical aperture (meters<sup>2</sup>).

For a circular aperture

$$A_{em} = \gamma \pi \frac{D^2}{4} \tag{8}$$

where

- $D$  = aperture diameter (meters).

Hence, (6), can also be written

$$N_d = K_3 D^3 \lambda^{1.5x} \tag{9}$$

where

- $K_3$  = constant.

For the common nonthermal type of radio source the spectrum index is between 0.5 and 1.0. If we take  $x = 2/3$  for this type of source (9) becomes

$$N_d = K_3 \lambda D^3. \tag{10}$$

Eq. (10) is at best an estimate, since it depends on assumptions concerning the frequency dependence of several quantities. Different frequency dependencies can result in an exponent for  $\lambda$  different from unity. However, (10) is suggestive of the trend with frequency and is useful for indicating the ultimate order of magnitude of  $N_d$ . Taking  $K_3$  equal to 1/10 yields an optimistic or ultimate quasi-empirical value for  $N_d$ .<sup>2</sup> In actual practice the number may be only 20 per cent to 50 per cent as great.

Turning next to the matter of resolution, the ultimate number of sources a radio telescope can resolve is by Ko's criterion,<sup>1</sup> equal to the sky area divided by the an-

<sup>1</sup> J. D. Kraus, "Resolution pattern effects, and range of radio telescopes," IRE TRANS., vol. AP-4, pp. 445-451; July, 1956.

<sup>2</sup> It is also assumed that  $t$  in (3) is of the order of a few seconds,  $n$  is unity, and  $\gamma$  and  $a$  are unity or nearly so.

tenna beam area. This is numerically equal to the directivity of the antenna.<sup>3</sup> Hence,

$$N_r = D_0 = \frac{4\pi A_{em}}{\lambda^2} = \frac{\pi^2 \gamma D^2}{\lambda^2} \quad (11)$$

where

$N_r$  = number of sources which can be resolved (dimensionless),

$D_0$  = directivity of antenna (dimensionless),

$A_{em}$  = maximum effective aperture of antenna (meters<sup>2</sup>),

$\gamma$  = antenna efficiency factor (dimensionless),

$D$  = antenna diameter (assuming circular aperture) (meters),

$\lambda$  = wavelength (meters).

For  $\gamma = 1$  (uniform aperture illumination), (11) can be written as

$$N_r \simeq 10 \left( \frac{D}{\lambda} \right)^2. \quad (12)$$

It is assumed in (11) and (12) that the entire sky is observable. Depending on the latitude of the telescope, a fraction of the sky will be observable as given by the factor

$$\frac{1 + \cos |L|}{2} \quad (13)$$

where  $L$  = latitude. Owing to the difficulty of observing close to the horizon, even less sky may, in practice, be observable. For these reasons, and also because the sources will not, in general, be uniformly distributed as assumed, (11) is an optimistic value for  $N_r$  and in actual practice the number may be only 20 per cent as great.<sup>4</sup> However, with this in mind (11) is useful for indicating the ultimate order of magnitude of  $N_r$ .

Eq. (11) gives the number of sources  $N_r$  which the radio telescope can resolve while (10) gives the number  $N_d$  which it can detect. If  $N_d$  is smaller than  $N_r$ , the telescope is *detection* (or sensitivity) *limited*; that is, it is capable of resolving more sources than it can detect. On the other hand, if  $N_r$  is smaller than  $N_d$ , the telescope is *resolution limited*; that is, it is capable of detecting more sources than it can resolve.

Taking  $K_3$  in (10) equal to 1/10 and  $\gamma = 1$  in (11), the values for  $N_d$  and  $N_r$  are presented in Fig. 1 as a function of frequency (and wavelength) for 4 apertures from 1/10 to 100 acres (1 acre = 43,560 square feet).<sup>5</sup> For a given aperture the maximum number of sources which can be both detected and resolved occurs where  $N_d = N_r$ . For

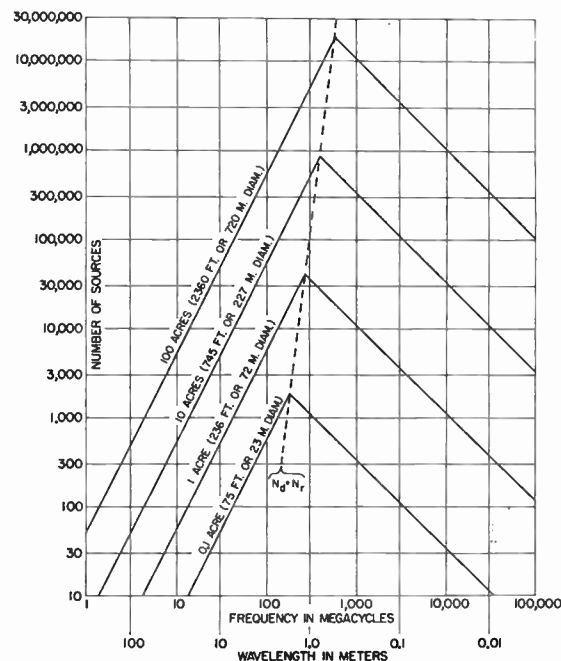


Fig. 1—Number of sources which a radio telescope can both detect and resolve as a function of frequency (and wavelength) and size of antenna aperture. The antenna aperture is given in acres (1 acre = 43,560 square feet). Although the aperture may be of any shape, the diameter in feet and meters is given for the case of a circular aperture. To the left of the dashed line ( $N_r = N_d$ ) the telescope is resolution limited and to the right it is detection limited.

example, a telescope antenna with a 75-foot aperture diameter (0.1-acre aperture) can detect and resolve a maximum of nearly 2000 sources at a frequency of about 200 mc. At higher frequencies the telescope is detection limited while at lower frequencies it is resolution limited.

For larger apertures the maximum occurs at somewhat higher frequencies as indicated by the dashed line for  $N_d = N_r$  in Fig. 1. For the apertures shown, the maximum occurs at frequencies between 200 and 600 mc. At frequencies above the maximum the number of sources decreases with frequency, this part of the graph being based on the common nonthermal type of radio sources. Of course, if thermal sources are taken into consideration the trend with frequency is more favorable.

Fig. 1 applies to apertures of any shape (rectangular, square, elliptical, circular, etc.) with the diameter given for the circular case.

As pointed out earlier, the values given in Fig. 1 are optimistic and in actual practice the numbers may be only 20 per cent to 50 per cent as great. This lends even more emphasis to the great importance of large aperture if large numbers of sources are to be observed. Thus, in order to observe a million radio sources (which is small compared to the number which can be observed optically) radio telescopes with apertures in the 10- to 100-acre range are needed.

Another way of stating the situation is to say that at present radio astronomy deals with only about 6 magni-

<sup>3</sup> J. D. Kraus, "Antennas," McGraw-Hill Book Co., Inc., New York, N.Y., pp. 24 and 54; 1950.

<sup>4</sup> J. L. Pawsey indicates that the number may be only 5 per cent to 10 per cent as great; that is 10 to 20 beam areas are required per source unequivocally resolved.

<sup>5</sup> A similar figure but with different values is given by E. G. Bowen and J. L. Pawsey, "A Proposal for a Giant Radio Telescope," Division of Radiophysics, CSIRO, Sydney, Australia, p. 28; 1955.

tudes; that is, a range of 24 db in flux density from the strongest to weakest observable sources (one magnitude = 4 db). On the other hand, optical astronomy encompasses over 20 magnitudes (a range of 80 db). To extend radio observations to weaker sources requires more antenna directivity and this in turn requires greater aperture.

As the frequency is raised the cost of a radio telescope of constant aperture increases since the antenna must be held to closer mechanical tolerance. Thus, the cost per source for a radio telescope of given aperture will be like the inverse of a curve in Fig. 1, but flatter at low frequencies and steeper above the breakover frequency ( $N_d = N_r$ ) as suggested by the curve in Fig. 2. If the largest number of (nonthermal) sources is the desired objective, Fig. 2 suggests that there is a most economical frequency at or close to the frequency for which  $N_d = N_r$ ; that is, in the vicinity of 300 mc.

To illustrate the effect of an increase in aperture, two signatures made with the Ohio State University helical-array radio telescope antenna<sup>1,8</sup> are shown in Fig. 3. These were taken of the same radio source (Virgo A) on different days, the only change being that the aperture area for the upper signature is 8 times that for the lower one. This was accomplished by using 96 helices (the full number) for the upper signature and one bay of 12 helices for the lower trace. Although the radio source is detectable as a broad gradual rise in the lower signature, it is not too obvious. However, in the upper trace it stands out sharply, the shape of the signature being an indication of the antenna pattern in right ascension. The horizontal coordinate of right ascension is indicated in hours below the lower signature. The spikes below the upper signature are time marks impressed automatically at 10-minute intervals. The gradual upward trend to the left in the records is due to a gradual rise in the background radiation in this direction.

#### STANDING PARABOLOID DESIGN

In order to obtain the largest possible apertures a radio telescope design is needed which provides a maximum of aperture per dollar of cost.

One answer to this aperture problem is afforded by the Mills cross antenna.<sup>7</sup> Although it provides a relatively high resolution, the effective aperture area is not commensurate. Furthermore, it is essentially a single-frequency device.

Another approach to the problem is one we have developed at the Ohio State University which possesses great potentialities in the large aperture field. It is of the reflector type, incorporating a fixed standing paraboloid and a tiltable flat reflector with the ground acting as part of the antenna structure both electrically and mechanically. It is a wide-band antenna that can

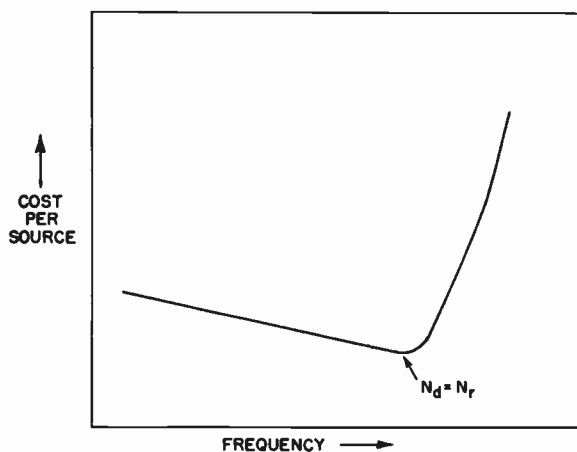


Fig. 2—Graph of radio telescope cost per observable radio source as a function of frequency. The minimum cost occurs at or close to the frequency for which the number of sources which can be detected ( $N_d$ ) is equal to the number which can be resolved ( $N_r$ ).

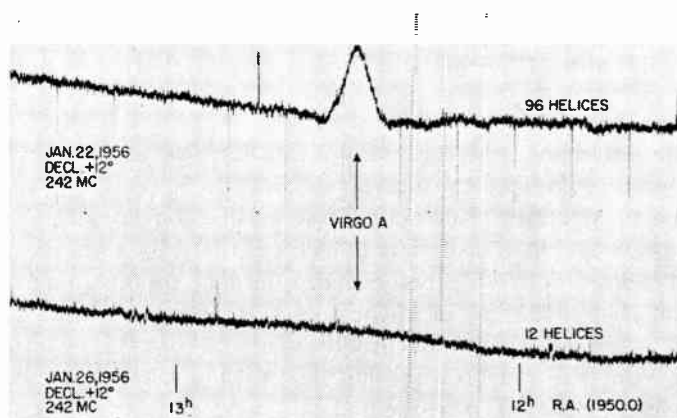


Fig. 3—Record of radio source Virgo A taken with 12 helices (lower trace) and with 96 helices (upper trace) showing improvement resulting from 8-fold increase in antenna aperture.

be operated over a frequency range of 50 to 1 or more and provides a very large aperture per unit cost. The design is especially well-suited for background mapping, source location, and spectrum observations. Although essentially a meridian-transit instrument, it can be arranged to track objects near the meridian for moderate intervals. And most important it provides a high resolution with a large aperture area for collecting the celestial radio waves.

The essential features of the design<sup>8-10</sup> are shown by the sketch in Fig. 4. Down-coming celestial radio waves are deflected by the tiltable flat-sheet reflector into the paraboloid and thence to a horn antenna at the prime focus. The reflecting surface of both paraboloid and flat sheet consists of coarse mesh wire screen or closely-spaced vertical wires. The only moveable structure is

<sup>8</sup> J. D. Kraus, "Radio telescopes," *Sci. Amer.*, vol. 192, pp. 36-43; March, 1955.

<sup>9</sup> J. D. Kraus and R. T. Nash, "A Design for a Large-Aperture, Low Cost Radio Telescope," Ohio State Univ., Columbus, Ohio, Radio Observatory Rep. No. 5; November 22, 1955.

<sup>10</sup> J. D. Kraus, "Radio telescope designs of large aperture and low cost," *Astron. J.*, vol. 61, p. 169; May, 1956.

<sup>6</sup> S. Matt and J. D. Kraus, "The effect of the source distribution on antenna patterns," *Proc. IRE*, vol. 43, pp. 821-825; July, 1955.

<sup>7</sup> B. Y. Mills and A. G. Little, "A high resolution aerial system of a new type," *Aust. J. Phys.*, vol. 6, p. 272; 1953.

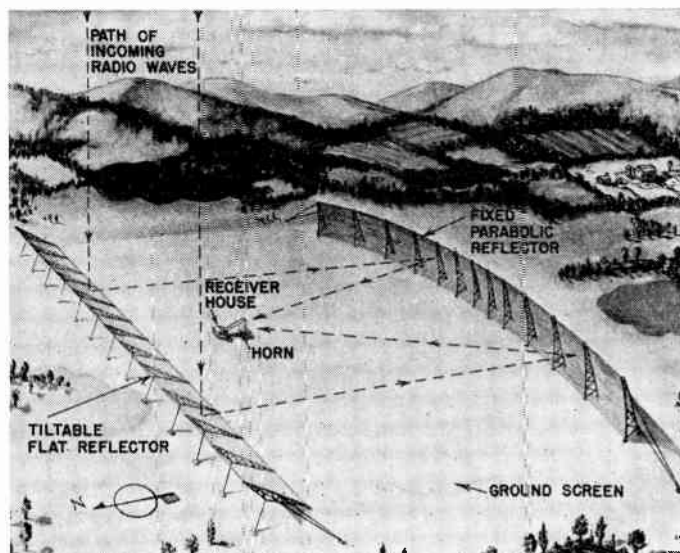


Fig. 4—Sketch showing arrangement of fixed standing paraboloid tiltable flat reflector radio telescope antenna with path indicated for incoming radio waves. An antenna of this design with parabolic reflector 360 feet long by 70 feet high is now under construction at the Ohio State-Ohio Wesleyan Radio Observatory near Delaware, Ohio.

the flat-sheet reflector. Since a flat surface can be very easily checked for any unevenness, it is not necessary that the tiltable reflector be a rigid structure. This results in a large saving in cost. The reflector is tilted by a number of independently operated hydraulic jack members and the desired degree of flatness of the reflector obtained by adjusting them individually while monitoring or observing the reflector for flatness with a small optical telescope set up near one end.

It is much more difficult to maintain tolerances on a curved surface such as a paraboloid, especially if it is moveable. This problem is avoided and the cost correspondingly reduced by making the paraboloid fixed. In this way the ground itself provides the basic mechanical support for the paraboloid and the amount of structure required to maintain the paraboloid tolerances is a minimum.

Furthermore, if the paraboloid were steerable it would be necessary for the focus or feed point to move with it as an integral part of the paraboloid structure and this would require a large and expensive supporting framework. This is avoided in the present design since, with the paraboloid fixed, the focus or feed point can be situated at ground level with the earth providing the necessary rigidity for proper alignment. In the present design, movement is required of only the simple flat reflector. At the latitude of Columbus, Ohio ( $+40^\circ$ ), nearly the entire sky observable from the latitude, that is, from  $-40^\circ$  to  $+90^\circ$  declination or a range of  $130^\circ$ , can be observed with a change in flat reflector tilt of only  $65^\circ$ . This results from the fact that for a given change in the flat reflector angle, the change in declination angle is twice as much.

By making the length of the reflectors considerably greater than the height there is an additional saving in

cost since the expense of a structure is approximately proportional to the cube of its height. Thus, a paraboloid 2000 feet long by 200 feet high (9.2-acres aperture) will cost no more than one 350 feet long by 350 feet high (2.7-acres aperture) but it will have over 3 times the aperture area. Furthermore, the lower over-all height makes the telescope less susceptible to interfering radio signals of terrestrial origin, since the strength of such signals increases rapidly with height above the ground.

In connection with the rectangular shape of the aperture it should be mentioned that the number of sources which an antenna can resolve or detect is a function of the size of the aperture area and not its shape. For example, an antenna with an aperture 100 feet long by 25 feet wide (2500-square foot aperture area) can resolve the same number of sources as an antenna of the same aperture area but 50 feet square. The pencil beam of a square or circular antenna aperture may be a convenience in some applications as compared to the fan beam of the rectangular aperture. However, in other cases the fan beam of the rectangular aperture may be more convenient, as in search and mapping observations with the earth's rotation sweeping the beam, since fewer changes in declination are required to map the sky to a given precision.

The ground is an integral part of both the mechanical and electrical structure of the telescope. It is covered with a conducting screen and acts as an image plane. The wave polarization used is vertical. Accordingly, the field intensity can be a maximum along the ground and the efficiency of utilization of the paraboloid may be correspondingly increased.

The flat reflector tilts on an east-west axis with observations being along the meridian. However, by displacing the primary antenna along an east-west line it is possible to track celestial objects for some distance either side of the meridian. The displacements may be achieved by moving the primary horn antenna on tracks or by installing several horns side-by-side forming the elements of a rudimentary radio camera.

To test the design a scale model 12 feet across was constructed.<sup>9,11</sup> When operating at 1.25-cm wavelength, the model simulates an antenna with paraboloid 700 feet long by 70 feet high operating at 70-cm wavelength. A photograph of the model, built by Robert T. Nash, is shown in Fig. 5. The standing paraboloid is at the right and the tiltable flat-sheet reflector is at the left with the horn feed at the prime focus just to the right of the base of the flat-sheet reflector. Since the entire model was made steerable by mounting it on a turntable it was necessary to provide a relatively more massive man-made supporting structure than would be the case in the full-size telescope which is fixed in azimuth

<sup>11</sup> R. T. Nash, "Design of a High Resolution Antenna for the Reception of Radio Waves of Extraterrestrial Origin," Ohio State University, Columbus, Ohio, Master thesis; June, 1955.

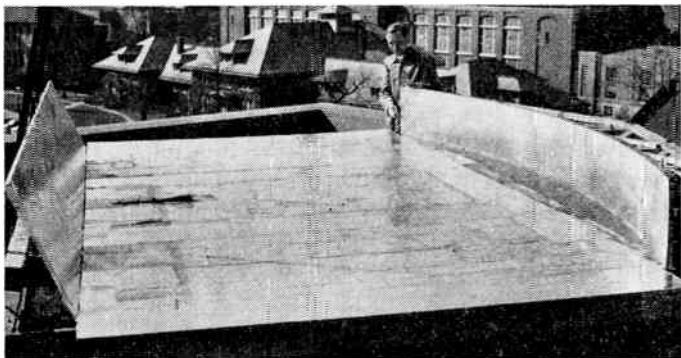


Fig. 5—Scale model operating at one-cm wavelength built to test performance of standing parabolic reflector type antenna.

and utilizes the ground as the principal supporting structure.

The far-field patterns, measured by Nash at 1.25 cm at a distance of 2 miles from the model, are shown in Fig. 6. The measured half-power beamwidth is  $0.26^\circ$  in right ascension and  $1.9^\circ$  in declination. These values agree closely with the calculated beamwidths. The measured gain of the antenna is about 75,000 or nearly 49 db. The model tests were so satisfactory that the unit has been used as an actual radio telescope for observations of the sun and moon at one-cm wavelength.

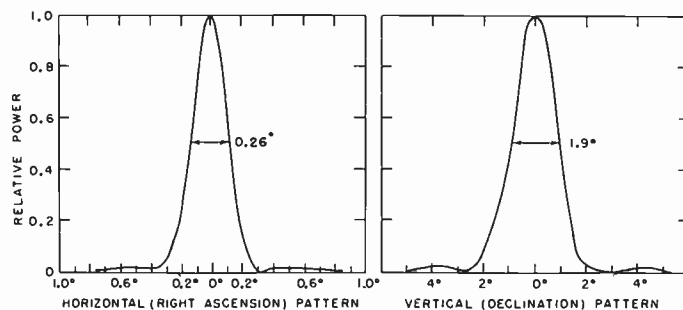


Fig. 6—Measured patterns of model standing parabolic reflector antenna. The half-power beamwidth is  $0.26^\circ$  (16 minutes of arc) in the horizontal plane and  $1.9^\circ$  in the vertical plane.

A grant of \$48,000 was received last year from the National Science Foundation for building the central half of a standing paraboloid antenna 700 feet long by 70 feet high. This antenna, which is now under construction, will have a standing paraboloid 360 feet long by 70 feet high with a tiltable flat reflector 360 feet long by 100 feet high. This antenna will have an effective aperture equal to that of a 190-foot diameter parabolic dish antenna. The 360- by 70-foot antenna will not only be useful for many types of radio astronomy observations but also will be valuable as a prototype for even larger units of the same design.

## Radio Interferometry of Discrete Sources\*

R. N. BRACEWELL, SENIOR MEMBER, IRE†

**Summary**—Salient features of the theory and practice of radio interferometry are presented with special attention to assumptions and to the specifically two-dimensional aspects of the subject. The measurable quantity on an interferometer record is defined as complex visibility by generalization from an analogous quantity in optical interferometry. Subject to conditions on antenna size and symmetry, the observed complex visibility is equal to the normalized two-dimensional Fourier transform of the source distribution, with respect to certain variables  $S_x$  and  $S_y$  which are defined. This transform is in turn identically equal to the complex degree of coherence  $\Gamma$  between the field phasors at the points occupied by the interferometer elements. The correlation between the instantaneous fields, and that between the instantaneous intensities are less general parameters which are, however, deducible from  $\Gamma$ . A theorem is proved according to which only certain discrete stations on a rec-

tangular lattice need be occupied for full determination of a discrete source distribution. Procedures in interferometry are discussed in the light of this result and an optimum procedure is deduced. Current practice is considered over-conservative, e.g, independent data in the case of the sun are obtainable only at station spacings of about 100 wavelengths on the ground, a fact which has not hitherto been taken into account.

### I. INTRODUCTION

IT IS well known that in the struggle to resolve detail in the radiofrequency emission from the sky, radio interferometers have played an important part. The observations of enhanced radiation from the sun (Hey<sup>1</sup>) and of a variable component of cosmic noise (Hey, Parsons, and Phillips<sup>2</sup>), posed two clear problems which called for angular resolution, and both were

\* Original manuscript received by the IRE, October 3, 1957. This research was supported by U. S. Air Force, Off. Sci. Res., Air Res. and Dev. Com., contract No. AF 18(603)-53. Reproduction in whole or part is permitted for any purpose of the United States Government.

† Radio Propagation Lab., Stanford Univ., Stanford, Calif. This work was carried out while the author was at Berkeley Astronomical Dept., on leave from Radiophysics Div., CSIRO, Australia.

<sup>1</sup> J. S. Hey, "Solar radiations in the 4-6 metre radio wavelength band," *Nature*, vol. 157, pp. 47-48; January, 1946.

<sup>2</sup> J. S. Hey, S. J. Parsons, and J. W. Phillips, "Fluctuations in cosmic radiation at radio frequencies," *Nature*, vol. 158, p. 234; August, 1946.

answered by interferometry. In the first case, a measurement of the angular width of the source of enhanced radiation was made in 1945 by McCready, Pawsey, and Payne-Scott,<sup>3</sup> and this, together with a position measurement, showed that the enhanced radiation came from a region having the general dimensions of a plage surrounding a sunspot group and that it lay over a group of spots visible on the sun at the time. In the second case Bolton and Stanley<sup>4</sup> demonstrated the existence of an intense discrete source in a certain position in the sky.

In each case, an important discovery depending on attainment of angular resolution was made with a very simple instrument. Even though interferometry has continued to contribute to radio astronomy, it is well to emphasize these achievements of the interferometer to counterbalance defects which have come to light in later comparisons with narrow beam instruments.

This paper is a contribution to the understanding of radio interferometry, and introduces a theorem which is of great importance for the practical conduct of observations with interferometers. The theorem is applicable to radiation fields in general, and has practical significance in optics, acoustics, and radio direction finding, but in this paper is discussed in terms of its application to radio astronomy.

Section II explains how an interferometer is used. We show that the unit experiment with an interferometer, whose elements are  $S$  wavelengths apart in an azimuth  $\theta$ , measures one complex number which we term the complex visibility  $Ve^{i\sigma}$  of an interference fringe system. In Section III the quantity  $Ve^{i\sigma}$  is shown to be equal, under certain conditions, to  $\bar{T}(S_x, S_y)/\bar{T}(0, 0)$ , which is a value of the normalized two-dimensional Fourier transform of the source distribution  $T(x, y)$  with respect to certain transform variables  $S_x$  and  $S_y$ , which, if the interferometer pointed vertically overhead, would be  $S \cos \theta$  and  $S \sin \theta$ . While  $V$  is readily measured,  $\sigma$  presents difficulties. The measurement of one value only of  $V$ , as in the work cited above, is equivalent to knowing one of the second moments of the distribution  $T(x, y)$ . Knowledge of  $V$  but not  $\sigma$  over a finite region of ground is equivalent to knowing the autocorrelation function of the *principal solution* for  $T(x, y)$ .

Section IV describes procedures for stationing the elements of interferometers and Section V interprets the procedure in terms of the complex degree of coherence  $\Gamma = \langle F_1 F_2^* \rangle$  between the phasors  $F_1$  and  $F_2$  representing the radiation field at the points occupied by the two elements of the interferometer.

Section VI proves a new theorem in interferometry according to which observations with an interferometer

need only be made at certain definite intervals, about 100 wavelengths for the sun, and about 1000 wavelengths for the smaller extragalactic sources.

Many special types of interferometer which are completely omitted from discussion in this paper may be found described in general works.<sup>5,6</sup> These include devices for lobe sweeping, lobe switching, frequency sweeping, polarimetry, wide-band operation, post-correlation detection, and aperture synthesis (Ryle<sup>7</sup>). The basic considerations of this paper enter however into all these special refinements of the simple interferometer.

## II. THE COMPLEX VISIBILITY OF AN INTERFEROMETER RECORD OF A DISCRETE SOURCE

By an interferometer we understand an antenna with two or more well separated parts, and in what follows we shall have in mind two identical antennas, pointing in the same direction and connected in parallel by equal feeders, to a pair of terminals. When a compact source of radiation moves through the beam of either antenna considered separately the record obtained shows a more or less periodic rise and fall as the signals received by the two antennas interfere. For a point source the two signals are equal in amplitude but change their relative phase as the path difference from the source to the two antennas varies. Therefore, if the two feeders have identical complex electrical lengths, the record obtained falls completely to zero at its minima. Fig. 1(a) shows a record of available power from a point source as it moves through the beam. The background level is partly receiver noise and partly cosmic noise.

When an extended source goes through the beam we have to deal with the simultaneous effects of many point sources. A small spread in the times when the constituent point sources go through the beam may suffice to destroy the quality of the interference nulls. At the same time the upper envelope [broken line in Fig. 1(a)] is smoothed out slightly, but if the source is small relative to the beamwidth of a single antenna, and this is the situation where interferometers have been applied, then the filling in of the nulls (and corresponding reduction of the maxima) is the principal effect. A record taken under such circumstances is illustrated in Fig. 1(b).

To specify a record such as that of Fig. 1(b) we shall need, in addition to the absolute level, a coefficient  $V$ , having the nature of modulation percentage, which we define by

$$V = \frac{p_{\max} - p_{\min}}{p_{\max} + p_{\min}},$$

<sup>3</sup> L. L. McCready, J. L. Pawsey, and R. Payne-Scott, "Solar radiation at radio frequencies and its relation to sunspots," *Proc. Roy. Soc. A*, vol. 190, pp. 357-375; August, 1947.

<sup>4</sup> J. G. Bolton and G. J. Stanley, "Observations on the variable source of cosmic radio-frequency radiation in the constellation of Cygnus," *Aust. J. Sci. Res. A*, vol. 1, pp. 58-69; March, 1948.

<sup>5</sup> J. L. Pawsey and R. N. Bracewell, "Radio Astronomy," Oxford University Press, New York, N. Y.; 1955.

<sup>6</sup> R. N. Bracewell, "Radio Astronomy Techniques" in "Handbuch der Phys.," vol. 54 (in press).

<sup>7</sup> M. Ryle, "The Mullard Radio Astronomy Observatory, Cambridge," *Nature*, vol. 180, pp. 110-112; July, 1957.

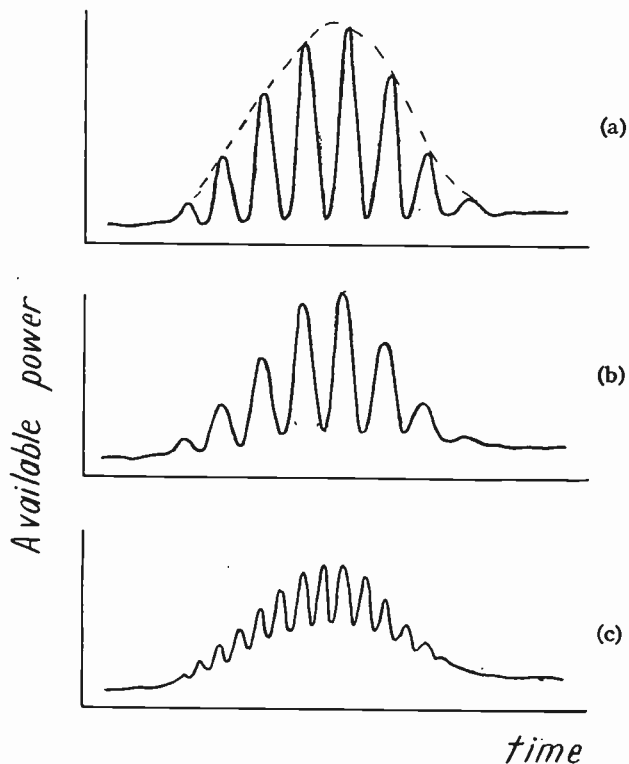


Fig. 1—Available power from an interferometer as (a) a point source, (b) an extended source of the same flux density, moves through the beam. In (c) we show the available power from the same extended source as observed with an interferometer consisting of the same antennas more widely spaced.

where  $p_{\max} - p_{\min}$  is the range of variation of available power, and  $p_{\max} + p_{\min}$  is twice the average available power. In Fig. 1(a)  $V$  has its maximum value of unity, in Fig. 1(b)  $V = 0.8$ , and in Fig. 1(c)  $V = 0.3$ . We shall refer to  $V$  as the visibility of the interference fringes, borrowing the optical terminology introduced by Michelson, and applying the word fringe to the temporal variation in the usual way. To complete the specification we need the phase  $\sigma$  of the interference pattern relative to the beam axis. Thus if the envelope maximum follows an interference maximum with a delay  $T_1$ , and if the time difference between successive maxima is  $T$ , then

$$\sigma = \frac{2\pi T_1}{T}$$

The complex quantity

$$U = V e^{i\sigma}$$

which includes both  $V$  and  $\sigma$ , will be referred to as the complex visibility of the interference pattern. A single record such as that of Fig. 1(b) may be regarded as yielding one measurement of complex visibility. Further records such as that of Fig. 1(c), made on the same extended source with the same component antennas more widely spaced, yield further measurements of complex visibility. Fig. 2 is a fringe visibility diagram, showing visibility against spacing, and includes the data from

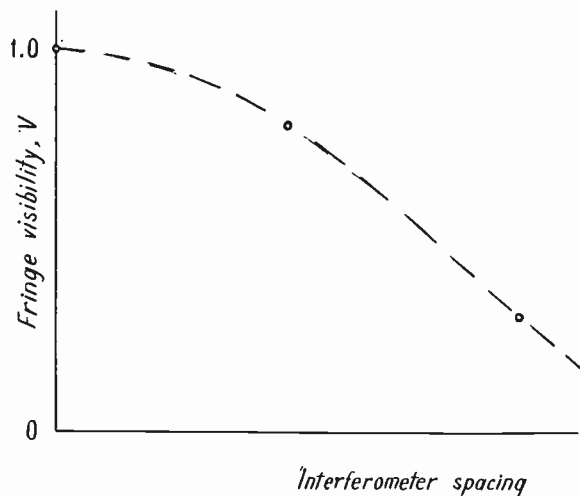


Fig. 2—Fringe visibility diagram for the source of Fig. 1(b) and 1(c).

Fig. 1(b) and 1(c). A little consideration will show that  $V = 1$  at zero spacing, and this point is also shown. The phase  $\sigma$  is not shown.

### III. THE FOURIER TRANSFORM RELATION BETWEEN THE COMPLEX VISIBILITY AND THE SOURCE DISTRIBUTION

It has been known since the earliest account of interferometry of radio sources by McCready, Pawsey, and Payne-Scott<sup>3</sup> that the amplitude and phase of a simple interference record are given by the Fourier transform of the source distribution. Consider an interferometer of spacing  $S$  wavelengths whose radiation pattern is thus

$$A(x, y)[1 + \cos \{2\pi(S_x x + S_y y)\}].$$

In this expression  $x$  and  $y$  are rectangular coordinates respectively along and across a circle of declination, and  $A(x, y)$  is the radiation pattern of one antenna alone, assumed sufficiently directional and used far enough away from the celestial pole that the rectangular coordinates are satisfactory.  $S_x$  and  $S_y$  are the spacings in wavelengths of the projections of the interferometer elements onto planes parallel to the  $x$  and  $y$  directions, respectively. For example, in a special case of particular interest, namely when the elements of a horizontal interferometer of spacing  $S$  wavelengths along a line making an angle  $\theta$  with the east-west direction are pointed at an elevation  $\alpha$  to the meridian, we have  $S_x = S \cos \theta$  and  $S_y = S \sin \theta \sin \alpha$ .

Let the source be described by a brightness temperature distribution

$$T(x - \Omega t, y),$$

where  $\Omega$  is the velocity of the sky in the  $x$  direction due to the earth's rotation, and the origin of coordinates is on the axis of the interferometer elements. Then the available power at the interferometer terminals will be, assuming equal and nondissipative feeders,

$$\begin{aligned}
& k\Delta f \iint T(x - \Omega t, y) A(x, y) [1 + \cos \{2\pi(S_x x + S_y y)\}] dx dy \\
&= k\Delta f \iint T(x, y) A(x + \Omega t, y) dx dy \\
&\quad + k\Delta f \cos(2\pi S_x \Omega t) \iint \cos \{2\pi(S_x x + S_y y)\} T(x, y) A(x + \Omega t, y) dx dy \\
&\quad - k\Delta f \sin(2\pi S_x \Omega t) \iint \sin \{2\pi(S_x x + S_y y)\} T(x, y) A(x + \Omega t, y) dx dy.
\end{aligned}$$

The first term is what would be the available power from a single antenna. The remainder terms take on a simple form under the condition that the distribution  $T$  is compact relative to  $A$  and is mainly concentrated around  $(x, y)$ . Then the available power becomes approximately

$$\begin{aligned}
& k\Delta f A(x_1 + \Omega t, y_1) \iint T(x, y) dx dy \\
&\quad + k\Delta f A(x_1 + \Omega t, y_1) \cos(2\pi S_x \Omega t) \iint \cos \{2\pi(S_x x + S_y y)\} T(x, y) dx dy \\
&\quad - k\Delta f A(x_1 + \Omega t, y_1) \sin(2\pi S_x \Omega t) \iint \sin \{2\pi(S_x x + S_y y)\} T(x, y) dx dy \\
&= k\Delta f A(x_1 + \Omega t, y_1) \iint T(x, y) dx dy \{1 + V \cos(2\pi S_x \Omega t - \sigma)\},
\end{aligned}$$

where

$$\begin{aligned}
V e^{i\sigma} &= \frac{\iint e^{-i2\pi(S_x x + S_y y)} T(x, y) dx dy}{\iint T(x, y) dx dy} \\
&= \frac{\bar{T}(S_x, S_y)}{\bar{T}(0, 0)}.
\end{aligned}$$

This final result lends definiteness to the Fourier transform relation, showing that the complex visibility of the interference pattern is the normalized two-dimensional Fourier transform of the source distribution, under the conditions implied and stated in the above derivation, and with respect to the variables  $S_x$  and  $S_y$ . As far as the author is aware this result has not been given quantitatively before, but it is probably fair to say that it contains nothing which is not well known among users of interferometers. The present derivation indicates the necessary generalization for sources not satisfying the condition of compactness relative to the antenna beam, and indicates, through the inequality of  $S_x$  and  $S_y$ , that motion of two interferometer elements on a circle in the ground plane is associated with an ellipse in the transform plane.

When  $\sigma$  has not been measured, only  $V$ , the information gathered is exactly that contained in  $\mathcal{V}\mathcal{V}^*$ . Now the two-dimensional Fourier transform of  $\mathcal{V}\mathcal{V}^*$  is the two-

dimensional autocorrelation function of  $T(x, y)$ ; therefore the information retained about  $T(x, y)$  is only that which is contained in its autocorrelation function. This is a useful concept and analogous to the partial knowledge of a waveform whose power spectrum only is given. If  $T(x, y)$  is an even function of  $x$  and  $y$ , as may

often be surmised from considerations of symmetry,  $\sigma$  must be zero or  $\pi$  everywhere, and  $T(x, y)$  may be fully reconstituted, provided that wherever  $V$  approaches zero precautions are taken to ascertain whether the phase has reversed. (One way of doing this is to couple a weak signal from a third antenna into the interferometer.) When  $T(x, y)$  is not even, then if one proceeds by ignoring phase and treating all phases as zero (or  $\pi$  as indicated), then one recovers a distribution  $T_0(x, y)$  in which all the two-dimensional Fourier sine components have been slipped in phase to become cosine components.

#### IV. PROCEDURES IN INTERFEROMETRY

The practice of moving one element  $B$  of an interferometer out along an east-west line from the other element  $A$ , which is kept stationary, is equivalent to exploring the transform on the  $S_x$  axis [Fig. 3(a)] out to a distance corresponding to the maximum spacing. Thus if stations  $B_1 \cdots B_4$  were occupied we would have values of the normalized transform at the 9 points shown on the  $S_x$  axis. The values on the negative  $S_x$  axis are deducible from those on the right since negative spacings (element  $B$  to the west of  $A$ ) are necessarily equivalent to positive spacings. The precise relation follows from the fact that brightness temperature is a real quantity; hence its transform, though complex in general, is subject to having its real part even and its

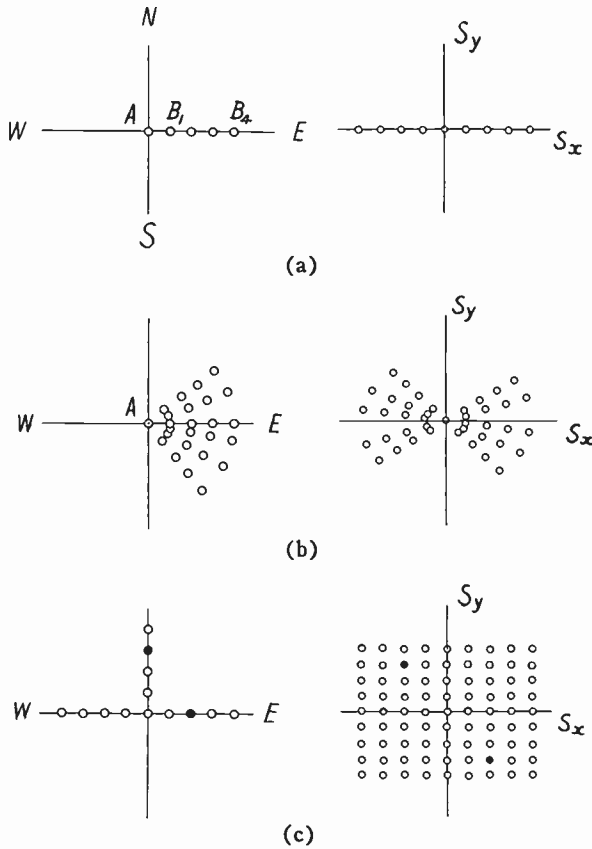


Fig. 3—Procedures for interferometry.

imaginary part odd. The values on the negative  $S_x$  axis are therefore complex conjugates of those on the positive half-axis.

Since the transform of an unknown brightness distribution only defines the distribution if it is known over the whole plane, it is clear that knowledge of the transform along only one finite line-segment is rudimentary. It, nevertheless, fixes certain parameters of the distribution. Suppose that  $\bar{T}(S_x, S_y)$  is known at three points on the  $S_x$  axis, viz.  $(-U, 0), (0, 0), (U, 0)$ . Of the three data, one pertains to the absolute level and the two remaining are equivalent to the first and second differences

$$\bar{T}(U, 0) - \bar{T}(-U, 0)$$

and

$$\bar{T}(U, 0) - 2\bar{T}(0, 0) + \bar{T}(-U, 0).$$

By a theorem proved in the Appendix, the first of these quantities is

$$- 2i \iint \sin 2\pi UxT(x, y)dx dy$$

and the second is

$$- 4 \iint \sin^2 \pi UxT(x, y)dx dy;$$

consequently these integrals are the parameters actually determined. In the common case where the source distribution is not very extended in the  $x$  direction, the first parameter is proportional to

$$\iint xT(x, y)dx dy$$

and therefore yields the abscissa of the centroid of the source distribution. The second parameter becomes proportional to

$$\iint x^2T(x, y)dx dy$$

and therefore contains the second moment of the source distribution about the  $y$  axis. This reasoning demonstrates the known result that an observation of a *small* source at one interferometer spacing gives 1) the flux density, 2) the transit time of the centroid, 3) the source width. If the source is not small (or the spacing is large) the modification is as given above. Since the source *shape* is not determined, only one of its radii of gyration about its centroid, different widths for the same source result from different assumptions. Different observers have used 1) width of equivalent rectangular strip  $w_x$ , 2) the diameter of the equivalent uniform disk  $D$ , 3) standard deviation of the equivalent two-dimensional Gaussian source  $\sigma_r$ . The familiar conversion factors are contained in the following relations between the various spread measures of a source of radius of gyration  $\sigma_x$  about the  $y$  axis through the centroid.

$$\sigma_x = \frac{w_x}{2\sqrt{3}} = \frac{D}{4} = \frac{\sigma_r}{\sqrt{2}}.$$

If two width measurements at right angles are possible,  $(\sigma_x^2 + \sigma_y^2)^{1/2}$  may be recommended. But if only one is available and if the source possesses circular symmetry, or if circular symmetry forms a suitable basis, then  $\sigma_r (= \sqrt{2}\sigma_x)$  is recommended.

The two-dimensional procedures may also be mentioned. In the first [Fig. 3(b)], the movable element  $B$  occupies a sequence of stations along many lines running out from the home base  $A$ . The transform is then known at the points indicated on the right. In the second [Fig. 3(c)], both elements are movable: one along an east-west line and one towards the north.

In practice it is difficult to measure  $\sigma$ , as compared with  $V$ . For it is necessary to equalize or measure the phase lengths of the two feeders, and to determine the line on which the phase centers of the two elements lie, at the time of the observation. Temperature and other effects make this difficult. However, if the interference pattern of Fig. 1(b) has an unknown phase origin, or is allowed to drift in phase, then provided the upper and lower envelopes remain determinate,  $V$  may still be measured, although  $\sigma$  is lost. To answer the question, what information about the source distribution has

been retained, we draw on the analogous situation where the power spectrum of a waveform is known, but not the phases of the spectral components. We know that the power spectrum determines the autocorrelation function of the waveform, and so if  $V(S_x, S_y)$  is all that is known about a source distribution, we have the two-dimensional autocorrelation function of the distribution.

It also happens universally that the transform is not known beyond a finite central area whose outline is set by the maximum spacings used. In this case our information refers to the principal solution (Bracewell and Roberts<sup>8</sup>) not to the source distribution itself.

V. CORRELATION AND COHERENCE

Interferometry is sometimes discussed in terms of the correlation which exists between the fields at different points in the receiving plane. According to this viewpoint the procedures for two-element interferometry are in essence procedures for exploring the autocorrelation function of the radiation field of the source. We now show the sense in which this is true.

Let  $E(t)$  be that part of the electric field at a receiving point to which attention will be paid by the receiving instrument. Then

$$E(t) = \Re F(t)e^{i\omega t},$$

where  $F(t)$  is the field phasor, a complex quantity whose modulus and phase change slowly with time at a rate set by the bandwidth of the equipment. All phases of  $F(t)$  are equally likely and the modulus has a Rayleigh distribution  $p(|F|)$  where

$$p(|F|) = \frac{2|F|}{\langle |F|^2 \rangle} \exp\left(-\frac{|F|^2}{\langle |F|^2 \rangle}\right),$$

and

$$\langle \dots \rangle \equiv \lim_{T \rightarrow \infty} \frac{1}{2T} \int_{-T}^T \dots dt.$$

If we form the product of the instantaneous fields  $E_1(t)$  and  $E_2(t)$  at two points and evaluate the time average, the result is contained in the average product of the field phasors  $F_1(t)$  and  $F_2^*(t)$ . Thus

$$\begin{aligned} \langle E_1 E_2 \rangle &= \langle \Re F_1 e^{i\omega t} \Re F_2 e^{i\omega t} \rangle \\ &= \left\langle \frac{F_1 e^{i\omega t} + F_1^* e^{-i\omega t}}{2} \frac{F_2 e^{i\omega t} + F_2^* e^{-i\omega t}}{2} \right\rangle \\ &= \frac{1}{4} \langle F_1^* F_2 + F_1 F_2^* \rangle \\ &= \frac{1}{2} \Re \langle F_1 F_2^* \rangle. \end{aligned}$$

We elect to deal in terms of

$$\langle F_1 F_2^* \rangle$$

which we define to be the complex degree of coherence following Zernike.<sup>9</sup>

Let an interferometer consist of two small antennas spaced  $S$  wavelengths apart in the  $x$  direction and connected together by feeders with over-all voltage transfer factors  $\alpha_1 e^{-i\delta_1}$  and  $\alpha_2 e^{-i\delta_2}$ . Let the function  $T(x - \Omega t, y)$  represent a slowly moving source, which is necessarily compact relative to the wide beams of the small antennas. Then the field phasor at one antenna is  $F_1 e^{-i\phi/2}$ , where

$$\phi = 2\pi S \sin \Omega t \approx 2\pi S \Omega t,$$

and the voltage phasor at the terminals of the interferometer will be

$$V_T = V_1 + V_2 = \alpha_1 e^{-i\delta_1} F_1 e^{-i\phi/2} + \alpha_2 e^{-i\delta_2} F_2 e^{i\phi/2}.$$

The instantaneous power will be proportional to  $V_T V_T^*$  where

$$\begin{aligned} V_T V_T^* &= \alpha_1^2 F_1 F_1^* + \alpha_2^2 F_2 F_2^* + \alpha_1 \alpha_2 (F_1 F_2^* e^{i(-\phi - \delta_1 + \delta_2)} \\ &\quad + F_1^* F_2 e^{-i(-\phi - \delta_1 + \delta_2)}). \end{aligned}$$

As time elapses the mean value  $\langle V_T V_T^* \rangle$  of the instantaneous power will measure the available power at the terminals, and under conditions where

$$\langle F_1 F_2^* \rangle = \langle F_2 F_2^* \rangle,$$

*i.e.* when behavior at one point is, on the average, the same as that another point nearby, we have

$$\begin{aligned} \langle V_T V_T^* \rangle &= \langle V_1 V_1^* \rangle + \langle V_2 V_2^* \rangle \\ &\quad + \frac{\sqrt{\langle V_1 V_1^* \rangle \langle V_2 V_2^* \rangle}}{\langle F_1 F_1^* \rangle} \{ \langle F_1 F_2^* e^{i(-\phi - \delta_1 + \delta_2)} \rangle \\ &\quad + \langle F_1^* F_2 e^{-i(-\phi - \delta_1 + \delta_2)} \rangle \} \\ &= \langle V_1 V_1^* \rangle + \langle V_2 V_2^* \rangle \\ &\quad + 2|\Gamma| \sqrt{\langle V_1 V_1^* \rangle \langle V_2 V_2^* \rangle} \cos(2\pi S \Omega t + \delta_1 \\ &\quad \quad \quad - \delta_2 - \phi + \Gamma), \\ &= \{ \langle V_1 V_1^* \rangle + \langle V_2 V_2^* \rangle \} \\ &\quad \cdot \left\{ 1 + \frac{2|\Gamma| \sqrt{\langle V_1 V_1^* \rangle \langle V_2 V_2^* \rangle}}{\langle V_1 V_1^* \rangle \langle V_2 V_2^* \rangle} \cos(2\pi S \Omega t \right. \\ &\quad \quad \quad \left. + \delta_1 - \delta_2 - \phi + \Gamma) \right\}, \end{aligned}$$

where

$$\Gamma = \frac{\langle F_1 F_2^* \rangle}{\langle F_1 F_1^* \rangle}.$$

Consequently as time elapses the available power rises and falls sinusoidally above and below a mean level  $\langle V_1 V_1^* \rangle + \langle V_2 V_2^* \rangle$  with a complex visibility

<sup>8</sup> R. N. Bracewell and J. A. Roberts, "Aerial smoothing in radio astronomy," *Aust. J. Phys.*, vol. 7, pp. 615-640; December, 1954.

<sup>9</sup> F. Zernike, "Concept of degree of coherence and its application to optical problems," *Physika*, vol. 5, pp. 785-795; August, 1938.

$$v = \frac{2\sqrt{\langle V_1 V_1^* \rangle \langle V_2 V_2^* \rangle}}{\langle V_1 V_1^* \rangle + \langle V_2 V_2^* \rangle} \Gamma e^{-i(\delta_1 - \delta_2)}$$

Thus when the interferometer is symmetrical the complex visibility of the interference record is equal to the complex degree of coherence between the field phasors at the points occupied by the interferometer, *i.e.*

$$v = \Gamma.$$

The above derivation, in which the opportunity has been taken to generalize to unequal feeders (or unequal antenna gains), shows that coherence should be regarded as a property of the field, and visibility as a measurable property of an interferogram. By adjustment of an interferometer for symmetry, or by a measurement of the relative proportions of the power contributed by each arm and the difference in arm lengths  $\delta_1 - \delta_2$ , coherence is deducible from the visibility observed with a small-antenna interferometer, for example,

$$|\Gamma| = \frac{\langle V_T V_T^* \rangle_{\max} - \langle V_T V_T^* \rangle_{\min}}{\langle V_T V_T^* \rangle_{\max} + \langle V_T V_T^* \rangle_{\min}} \cdot \frac{1}{2} \left\{ \sqrt{\frac{\langle V_1 V_1^* \rangle}{\langle V_2 V_2^* \rangle}} + \sqrt{\frac{\langle V_2 V_2^* \rangle}{\langle V_1 V_1^* \rangle}} \right\} = \frac{r^{1/2} + r^{-1/2}}{2} V,$$

where  $r$  is the ratio of available powers from the two antennas separately.

Had the nonzero extent of the antennas been retained in this as in the earlier sections, we would have found that the measurement of complex visibility led not to coherence but to a mean coherence weighted according to the autocorrelation function of the antenna aperture distribution. Since we showed earlier that complex visibility observed with a symmetrical interferometer was the normalized two-dimensional Fourier transform of the source distribution, provided it was compact relative to the spread of the antenna beam it is clear that  $\bar{T}(S_x, S_y)/\bar{T}(0, 0)$  and  $\Gamma$  are the fundamental properties of the source distribution alone. The following direct argument shows that they are equal.

Let the distant field in the direction  $(x, y)$  be represented by a phasor  $f(x, y)$ . Then  $\langle ff^* \rangle$  measures the brightness temperature in the direction  $(x, y)$ . The field distribution  $f(x, y)$  produces in the  $\xi\eta$  plane (a plane inclined to the ground in such a way that the  $\xi$  and  $\eta$  axes are respectively parallel to the  $x$  and  $y$  axes) a Fraunhofer diffraction field  $F(\xi/\lambda, \eta/\lambda)$  such that

$$F\left(\frac{\xi}{\lambda}, \frac{\eta}{\lambda}\right) \propto \iint f(x, y) e^{-i2\pi(\xi x/\lambda + \eta y/\lambda)} dx dy.$$

By the convolution theorem, the complex spatial autocorrelation function of  $F$  is then proportional to the Fourier transform of  $ff^*$ , *i.e.*,

$$\iint F^* \left( \frac{\xi}{\lambda} - \alpha, \frac{\eta}{\lambda} - \beta \right) F(\alpha, \beta) d\alpha d\beta \propto \iint f(x, y) f^*(x, y) e^{-i2\pi(\xi x/\lambda + \eta y/\lambda)} dx dy.$$

Now the expression on the left may be written

$$\langle F_1 F_2^* \rangle_{\text{spatial}},$$

where the averaging is done instantaneously over all pairs of points having the same spatial relationship, and under ergodic circumstances we may expect this to be equal to the time average

$$\langle F_1 F_2^* \rangle.$$

The expression on the right, under the same circumstances, represents  $\bar{T}$ , or the transform of  $\langle ff^* \rangle$  with respect to the variables  $\xi/\lambda, \eta/\lambda$  the spatial integration replacing the time averaging. Consequently  $\bar{T}$  is proportional to  $\langle F_1 F_2^* \rangle$ , and the normalized quantities, which are both equal to unity at the origin, are equal, *i.e.*

$$\Gamma = \frac{\bar{T}}{\bar{T}(0, 0)}.$$

Some further notes may be appended. First the normalized time correlation of the instantaneous fields is given by

$$\frac{\langle E_1 E_2 \rangle}{\langle E_1^2 \rangle} = \frac{\langle \Re F_1 e^{i\omega t} \Re F_2 e^{i\omega t} \rangle}{\langle (\Re F_1 e^{i\omega t})^2 \rangle} = \frac{\langle F_1 F_2^* + F_1^* F_2 \rangle}{2\langle F_1 F_1^* \rangle} = \frac{\langle 2 \Re F_1 F_2^* \rangle}{2\langle F_1 F_1^* \rangle} = \Re \Gamma.$$

Second, the instantaneous intensities  $E_1^2$  and  $E_2^2$  are correlated, partly by virtue of the correlation between  $E_1$  and  $E_2$  and partly by both having nonzero mean values; thus<sup>10</sup>

$$\frac{\langle E_1^2 E_2^2 \rangle}{\langle E_1^4 \rangle} = \frac{\langle E_1^2 \rangle \langle E_2^2 \rangle + 2\langle E_1 E_2 \rangle^2}{\langle E_1^4 \rangle} = \frac{\langle E_1^2 \rangle^2 + 2\langle E_1 E_2 \rangle^2}{3\langle E_1^2 \rangle^2} = \frac{1}{3} + \frac{2}{3} (\Re \Gamma)^2.$$

If the mean values are first subtracted, the additive constant must vanish and the normalization must bring the correlation to unity when  $\Gamma = 1$ ; hence

$$\frac{\langle (E_1^2 - \langle E_1^2 \rangle)(E_2^2 - \langle E_2^2 \rangle) \rangle}{\langle E_1^4 \rangle - \langle E_1^2 \rangle^2} = \frac{\langle E_1^2 E_2^2 \rangle - \langle E_1^2 \rangle^2}{2\langle E_1^2 \rangle^2} = (\Re \Gamma)^2.$$

Considering the correlation of the squared envelope  $F_1 F_1^*$  with  $F_2 F_2^*$  in the same way, we find by putting

$$F_1 e^{i\omega t} = E_1 + iE_2$$

$$F_2 e^{i\omega t} = E_2 + iE_1,$$

<sup>10</sup> A concise proof that  $\langle E_1^2 E_2^2 \rangle = \langle E_1^2 \rangle \langle E_2^2 \rangle + 2\langle E_1 E_2 \rangle^2$  is given by E. Wolf, "Intensity fluctuations in stationary optical fields," *Phil. Mag.*, ser. 8, vol. 2, pp. 351-354; March, 1957.

that

$$\begin{aligned} \langle F_1 F_1^* F_2 F_2^* \rangle &= \langle (E_1^2 + \hat{E}_1^2)(E_2^2 + \hat{E}_2^2) \rangle \\ &= 4\langle E_1^2 \rangle^2 + 2\langle E_1 E_2 \rangle^2 + \langle E_1 E_2 \rangle^2 + 2\langle E_1 E_2 \rangle^2 + 2\langle E_1 E_2 \rangle^2 \\ &= 4\langle E_1^2 \rangle^2 + 4\langle E_1^2 \rangle^2 (\Gamma \Gamma)^2 + 4\langle E_1^2 \rangle^2 (\mathcal{G} \Gamma)^2 \\ &= 4\langle E_1^2 \rangle^2 (1 + \Gamma \Gamma^*); \end{aligned}$$

whence by normalization the correlation between squared envelopes is

$$\frac{\langle F_1 F_1^* F_2 F_2^* \rangle}{\langle (F_1 F_1^*)^2 \rangle} = \frac{1}{2} + \frac{1}{2} \Gamma \Gamma^*$$

and the correlation between the fluctuating parts of the squared envelopes is therefore<sup>11</sup>

$$\frac{\langle (F_1 F_1^* - \langle F_1 F_1^* \rangle)(F_2 F_2^* - \langle F_2 F_2^* \rangle) \rangle}{\langle (F_1 F_1^* - \langle F_1 F_1^* \rangle)^2 \rangle} = \Gamma \Gamma^*.$$

## VI. A THEOREM IN INTERFEROMETRY OF DISCRETE SOURCES

In applying the procedures for interferometry described in Section IV the question arises, how many stations should be occupied, and in the two-dimensional case where an antenna is carried out in various azimuths, how many azimuths should be chosen? Since information will be lost if the choices are too coarse, observers have tended towards conservatism. The following theorem gives quantitative guidance, shows that the azimuth method is inferior, and reveals that observing stations may be much more widely spaced than has been customary.

Let  $T(x, y)$  represent the brightness temperature distribution over a source which is discrete in the sense that it does not extend beyond  $x = \pm x_c$ ,  $y = \pm y_c$ . Then the complex degree of coherence of the field which it produces on the ground is

$$\Gamma(S_x, S_y) = \frac{\bar{T}(S_x, S_y)}{\bar{T}(0, 0)}.$$

Suppose that  $\Gamma$  is observed only at the points of a rectangular lattice where

$$\begin{aligned} S_x &= \frac{m}{2x_c}, \\ S_y &= \frac{n}{2y_c}, \end{aligned}$$

$m$  and  $n$  being integers. Then the information about  $\Gamma$  is the same as that contained in

$${}^2III(2x_c S_x, 2y_c S_y) \bar{T}(S_x, S_y), \quad (2)$$

<sup>11</sup> This result is deducible from (16) and (19) of E. N. Bramley, "Diversity effects in spaced-aerial reception of ionospheric waves," *Proc. IEE*, pt. III, vol. 98, pp. 19-25; January, 1951, and is asserted explicitly by J. A. Ratcliffe, "Some aspects of diffraction theory and their application to the ionosphere," *Rep. Prog. Phys.*, vol. 19, pp. 188-267; 1956.

where the bed-of-nails function  ${}^2III$  is defined in terms of the two-dimensional delta function  ${}^2\delta$  by

$${}^2III(S_x, S_y) = \sum_{\mu=-\infty}^{\infty} \sum_{\nu=-\infty}^{\infty} {}^2\delta(S_x - \mu, S_y - \nu).$$

By the two-dimensional convolution theorem, the two-dimensional Fourier transform of (2) is proportional to

$${}^2III\left(\frac{x}{2x_c}, \frac{y}{2y_c}\right)^* T(x, y) \quad (3)$$

where the asterisk signifies the two-dimensional convolution integral, *i.e.*,

$$f(x, y) * g(x, y) = \int_{-\infty}^{\infty} \int_{-\infty}^{\infty} f(x - x^1, y - y^1) g(x^1, y^1) dx^1 dy^1.$$

We have made use of the property that  ${}^2III$  is its own two-dimensional Fourier transform-in-the-limit, for a proof of which see Bracewell.<sup>12</sup> But (3) represents an array of discrete sources, all identical with  $T(x, y)$  and spaced at intervals  $2x_c$  in the  $x$  direction and  $2y_c$  in the  $y$  direction. Since the sources of the array do not overlap (although at points they may touch),  $T(x, y)$  is clearly recoverable from (3), and hence also from (2), and thus in turn from the measurements of  $\Gamma$  made at the discrete intervals  $1/2x_c$  and  $1/2y_c$ . We therefore have the following theorem.

*A discrete source confined within  $x = \pm x_c$ ,  $y = \pm y_c$ , is completely specified by measuring the coherence of its field at discrete spacings such that  $S_x$  and  $S_y$  are integral multiples of  $(2x_c)^{-1}$  and  $(2y_c)^{-1}$ , respectively.*

Since a source which is confined within  $x = \pm x_c$ ,  $y = \pm y_c$  is also confined within  $x = \pm x_c^1$ ,  $y = \pm y_c^1$  where  $x_c^1 > x_c$  and  $y_c^1 > y_c$ , it follows that measurements at any finer interval also specify the source completely. However, there would be a degree of redundancy, for the measurements at finer intervals would be deducible from measurements at the greatest interval compatible with the theorem, and would not be fully independent. In a sense, therefore, we may think of the information about the source as being spread over the ground with a certain density, there being one independent datum per rectangular cell of dimensions as above. The smaller the source, the more thinly the information is spread; *e.g.*, if we consider a radio sun of diameter 0.01 radian observed at noon, then independent measurements of coherence require stations 100 wavelengths apart on the average in an east-west direction, and in the north-south direction the spacing must be increased by the secant of the sun's zenith distance.

The procedure illustrated in Fig. 3(c) is therefore appropriate, particularly if the north-south spacings are increased so as to bring the sampling points on the

<sup>12</sup> R. N. Bracewell, "Two-dimensional aerial smoothing in radio astronomy," *Aust. J. Phys.*, vol. 9, pp. 297-314; September, 1956.

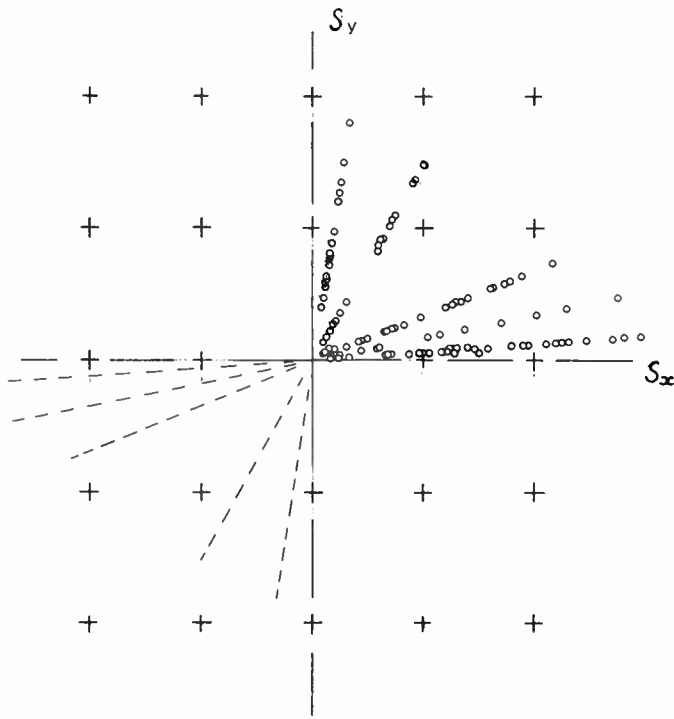


Fig. 4—Independent measurements may be made at the crosses. The circles show the amount of redundancy in an example drawn from current practice.

$(S_x, S_y)$  plane onto a lattice which is square, not rectangular as shown.

The procedure of Fig. 3(b) is shown to suffer from too closely packed sampling at low spacings, but apart from this is satisfactory provided the number of azimuths is such that the critical spacing is not exceeded on the periphery of the sampled area on the  $(S_x, S_y)$  plane.

An example of the impact of this theorem on current practice is afforded by Fig. 4 which shows the sampling points used by O'Brien and Tanberg-Hanssen<sup>13</sup> in an

<sup>13</sup> P. A. O'Brien and E. Tanberg-Hanssen, *Observatory*, vol. 75, pp. 11-13; February, 1955.

interferometric survey of the two-dimensional brightness distribution over the sun. Also shown are the cells containing one independent datum on the average. A certain amount of redundancy is desirable in order to guard against errors but it will be seen that the spacings chosen are extremely conservative. This comment applies to other published studies also and should not be taken as a criticism of the conclusions derived from the example cited, which was an important work in a still-continuing development of interferometric technique.

APPENDIX

Let

$$\bar{T}(S_x, S_y) = \int_{-\infty}^{\infty} \int_{-\infty}^{\infty} e^{-i2\pi(S_x x + S_y y)} T(x, y) dx dy.$$

Then

$$\begin{aligned} \bar{T}(U, 0) - \bar{T}(-U, 0) &= \int_{-\infty}^{\infty} \int_{-\infty}^{\infty} (e^{-i2\pi Ux} - e^{i2\pi Ux}) T(x, y) dx dy \\ &= -2i \int_{-\infty}^{\infty} \int_{-\infty}^{\infty} \sin 2\pi Ux T(x, y) dx dy, \end{aligned}$$

and

$$\begin{aligned} \bar{T}(U, 0) - 2\bar{T}(0, 0) + \bar{T}(-U, 0) &= 2 \int_{-\infty}^{\infty} \int_{-\infty}^{\infty} \cos 2\pi Ux T(x, y) dx dy \\ &\quad - 2 \int_{-\infty}^{\infty} \int_{-\infty}^{\infty} T(x, y) dx dy \\ &= 2 \int_{-\infty}^{\infty} \int_{-\infty}^{\infty} (\cos 2\pi Ux - 1) T(x, y) dx dy \\ &= -4 \int_{-\infty}^{\infty} \int_{-\infty}^{\infty} \sin^2 \pi Ux T(x, y) dx dy. \end{aligned}$$

These are the results used in Section IV.



# Restoration in the Presence of Errors\*

R. N. BRACEWELL, SENIOR MEMBER, IRE†

**Summary**—The observed antenna temperature due to a celestial source distribution differs from the true distribution in being smoother; various methods are known for operating on the observed distribution to gain better agreement with the true distribution. Current practice includes restoration by successive substitutions, by the chord construction, etc., but also shows a trend towards complete omission of any restoration, which is, no doubt, partly due to awareness that the true distribution is not fully determined by the observations. The isolation of a principal solution has, however, removed uncertainty as to the significance of nonuniqueness. The remaining question as to the degree of restoration which can be tolerated is solved here in terms of statistical properties of the errors. The solution shows that any proposed method of restoration must include mention of the character of the true distribution and of the errors; otherwise cases could be constructed where the proposed method led to deterioration. In the simplest case of independent random errors and a poorly resolved distribution, the rms level of the errors relative to the observed temperature is the relevant parameter (represented by  $(c/b)^{1/2}$  in Fig. 3); e.g., with a random error level as great as 15 per cent, agreement with the true distribution improves up to the third stage of restoration by successive substitutions (Table I) or on application of the chord construction.

## I. INTRODUCTION

SINCE the earliest surveys of the distribution of cosmic radio noise over the sky, the question of allowing for the smoothing effect of the antenna radiation pattern has obtruded itself during the reduction of the observations. Hey, Parsons, and Phillips<sup>1</sup> introduced an interesting scheme of approximate correction subject to test; the corrected distribution was subjected to a numerical operation resembling the effect of antenna smoothing and the result compared with observation. The correction itself was obtained by treating the observed distribution as an actual celestial distribution and noting the effect of operating on it numerically as above. It was found that the results were very good in that one or two stages of adjustment yielded a corrected distribution compatible with the observations, to their order of accuracy. This survey was made at 64 mc with a 14° beam.

This same scheme was followed by Bolton and Westfold<sup>2</sup> in their 100-mc survey with a 17° beam, again with satisfactory results. The method was set out sys-

tematically in mathematical form showing how a sequence of distributions could be derived by successive application of small corrections at each stage of comparison with observation. A mathematical argument which purported to show that the infinite sequence converted to the true distribution was later shown to be erroneous and has contributed perhaps to a reaction against the method itself. It is, therefore, worth emphasizing that the merits of the procedure rest on practical verification; one or two small corrections have usually brought the observations into compatibility with observation.

The survey by Allen and Gum<sup>3</sup> made with a 25° beam at 200 mc was corrected, at least in the vicinity of the galactic equator, by an adaptation of Eddington's formula, which is applicable to spectral lines broadened by a Gaussian instrumental profile. The same over-all test for compatibility with the observed data was applied.

Swarup and Parthasarathy<sup>4</sup> restored the solar profiles they obtained at 60 cm by means of the chord construction which is discussed in Section VI.

The correct theory of the method of successive substitutions, as the method will be termed, was given by Bracewell and Roberts<sup>5</sup> who showed that a solution, *i.e.*, a distribution compatible with observation, was not unique. This conclusion was important in reconciling discordant results (Brown and Hazard<sup>6</sup>) obtained by different observers, and alternative results obtained by the same observers (Christiansen and Warburton<sup>7</sup>). While some clashes were resolved, the self-checking feature of the method of successive substitutions was shown to engender false confidence, for an infinite number of distributions would possess the self-checking property. However, among these solutions is one, referred to as the principal solution, which is distinguished by absence of those spatial Fourier components which would be rejected totally by the antenna. Since the principal solution is a solution, it follows that those components which are not rejected totally by the antenna are present in the correct proportions.

\* C. W. Allen and C. S. Gum, "Survey of galactic radio noise at 200 Mc/s," *Aust. J. Sci. Res. A.*, vol. 3, pp. 224-233; June, 1950.

† Radio Propagation Lab., Stanford Univ., Stanford, Calif. This work was carried out while the author was at Berkeley Astronomical Dept., on leave from Radiophysics Div., CSIRO, Sydney, Australia.

<sup>1</sup> J. S. Hey, S. J. Parsons, and J. W. Phillips, "An investigation of galactic radiation in the radio spectrum," *Proc. Roy. Soc. A.*, vol. 192, pp. 425-445; February, 1948.

<sup>2</sup> J. S. Bolton and K. C. Westfold, "Galactic radiation at radio frequencies. I. 100 Mc/s survey," *Aust. J. Sci. Res. A.*, vol. 3, pp. 19-33; 1950.

<sup>3</sup> C. W. Allen and C. S. Gum, "Survey of galactic radio noise at 200 Mc/s," *Aust. J. Sci. Res. A.*, vol. 3, pp. 224-233; June, 1950.

<sup>4</sup> G. Swarup and R. Parthasarathy, "Solar brightness distribution at a wavelength of 60 centimetres. I. The quiet sun," *Aust. J. Phys.*, vol. 8, pp. 487-497; December, 1955.

<sup>5</sup> R. N. Bracewell and J. A. Roberts, "Aerial smoothing in radio astronomy," *Aust. J. Phys.*, vol. 7, pp. 615-640; December, 1954.

<sup>6</sup> R. H. Brown and C. Hazard, "A model of the radio-frequency radiation from the galaxy," *Phil. Mag.*, ser. 7, vol. 44, pp. 939-963; September, 1953.

<sup>7</sup> W. N. Christiansen and J. A. Warburton, "The distribution of radio brightness over the solar disk at a wavelength of 21 centimetres. II. The quiet sun—one dimensional observations," *Aust. J. Phys.*, vol. 6, pp. 262-271; June, 1953.

The principal solution is easily derivable from any other solution, and in the absence of any information about the true distribution, other than that contained in the observations, the incorporation of any components not present in the observations cannot be justified, thus, the principal solution is best fitted to represent the conclusion. Of course, if the antenna is too small for its purpose, the principal solution may still be a poor approximation to what is actually in the sky.

Once the status of the principal solution is understood, any step by step approach to a solution regains meaning. The filtering process necessary to remove the unwarranted components from any solution, once found, has been given by Bracewell<sup>8</sup> for the general two-dimensional case. However, it is very interesting to note that, under certain ideal conditions, the method of successive substitutions itself leads, in the limit, to the principal solution.

One of these conditions is freedom of the observed data from errors. From what has been said it is clear that correction for antenna smoothing is an important topic in practical radio astronomy, and it is proposed in this paper to pursue the effect of errors on the method of successive substitutions. It is hoped that the results to which this study leads will better fit the method for future application and provide a more informed basis for selecting the method for use. It is undoubtedly the lack of a thorough study of correction for antenna smoothing which has led in recent publications (Brown and Hazard,<sup>9</sup> Christiansen and Warburton,<sup>10</sup> Kraus and Ko,<sup>11</sup> Piddington and Trent<sup>12</sup>) to omission of a correction for antenna smoothing.

Yet although there are an infinite number of distributions which are compatible with the observations, the uncorrected observed distribution is not one of them.

Brown and Hazard<sup>9</sup> applied corrections for thermal emission from their feeder, thermal emission from the ground below and around their 218-foot paraboloid, and sky radiation received at the primary feed without being reflected from the paraboloid; but, they assumed that the brightness temperature of the sky was constant over the solid angle subtended by the main beam and its side-lobes. Piddington and Trent<sup>12</sup> simply multiplied all their observations by 100/65 on the basis of an estimate that, if the antenna were used to transmit, 0.65 of the radiated power would proceed in the direction of the beam axis and 0.35 would proceed towards cold sky differing negligibly from absolute zero in temperature. These cor-

rections are important but do not include the smoothing correction discussed here.

## II. OUTLINE OF THE PROBLEM

Let a true distribution of brightness temperature be  $T(x, y)$ , where we follow the notation and assumptions of previous papers in which rectangular coordinates  $(x, y)$  are suitable for considering surveys carried out by highly-directional antennas over zones of declination which are not too wide and not near the poles.

Let the antenna be so mounted that when it is pointed at  $(x, y)$  the position angle of the beam is always the same, irrespective of sidereal time, and let this position angle be the same for all points in the area surveyed. This condition rules out surveys conducted on alt-azimuth mountings, unless the antenna is used as a meridian instrument, and is wise for the present purpose of concentrating on the effect of errors. The phenomena associated with variable position angle have been discussed separately (Bracewell<sup>13</sup>).

Let the antenna pattern be the same when the antenna points in different directions within the area to be surveyed. This condition implies rigidity of the antenna (plus ground) and is an important simplifying assumption. If it cannot be made, and ground reflections may often vitiate it in some directions at least, there is no known way of allowing for significant changes in pattern. It is already virtually impossible to measure radiation patterns of highly-directional antennas for radio astronomy in more than one plane. This condition is regarded so seriously that Piddington and Trent<sup>12</sup> have insisted on the necessity of meridian observations for accurate surveys. Even so, declination has to be altered, and it would seem that in future solid paraboloids and feeds specially designed to reduce spillover will be necessary for improved accuracy.

Under the conditions stated, the effective antenna temperature  $T_a'$  observed at the terminals when the antenna is pointed at  $(x, y)$  is given by

$$T_a' = (1 - \eta)T_0 + \eta \int_{-\infty}^{\infty} \int_{-\infty}^{\infty} A(x', y') T(x + x', y + y') dx' dy',$$

where  $A$  is the radiation pattern of the antenna (plus ground),  $\eta$  is the ratio of the power radiated away to the power fed in at the terminals, and  $T_0$  is the temperature of the material in which the nonradiated fraction  $1 - \eta$  is dissipated. In these definitions we avail ourselves of the reciprocity theorem to speak as if the antenna were used to radiate. The infinite limits shown for the double integral are permissible under our assumption of a highly directional antenna and will be understood in the equations which follow.

<sup>8</sup> R. N. Bracewell, "Two-dimensional aerial smoothing in radio astronomy," *Aust. J. Phys.*, vol. 9, pp. 297-314; September, 1956.

<sup>9</sup> R. H. Brown and C. Hazard, "A radio survey of the Milky Way in Cygnus, Cassiopeia, and Perseus," *Mon. Not. Roy. Astron. Soc.*, vol. 113, pp. 109-122; 1953.

<sup>10</sup> W. N. Christiansen and J. A. Warburton, "The sun in two dimensions at 21 cm," *Observatory*, vol. 75, pp. 9-10; February, 1955.

<sup>11</sup> J. D. Kraus and H. C. Ko, "A detailed map of the radio sky," *Nature*, vol. 175, pp. 159-160; January 22, 1955.

<sup>12</sup> J. H. Piddington and G. H. Trent, "A survey of cosmic radio emission at 600 mcs," *Aust. J. Phys.*, vol. 9, pp. 481-493; December, 1956.

<sup>13</sup> R. N. Bracewell, "Strip integration in radio astronomy," *Aust. J. Phys.*, vol. 9, pp. 198-217; June, 1956.

Now let

$$T_a(x, y) = \iint A(x', y')T(x + x', y + y')dx'dy',$$

where  $T_a(x, y)$  has been referred to usually as the observed distribution, as it would be if the efficiency  $\eta$  of the antenna were unity, and if there were no errors. But owing to a variety of reasons, after allowing for  $\eta$  and  $T_0$ , the actual observation recorded is

$$T_a(x, y) + E(x, y)$$

where  $E(x, y)$  is the error temperature.

Among the sources of error are variations in  $T_0$  and  $\eta$ , changes in matching, motion of the antenna due to wind or heating, changes in receiver gain, statistical fluctuations in receiver output, timing errors, various undesirable properties of recorders, calibration errors of antenna setting circles and remote indicators, and collimation errors. This partial list of causes suggests that the usual normally-distributed error associated with many small effects will account for a good part of  $E(x, y)$ . There will, however, also be systematic contributions from many of the causes mentioned, and furthermore, one can expect correlation between the error and the actual signal level. As examples of this we have the statistical fluctuations which are strong when the signal is strong, and receiver gain changes which are associated with changed operating levels in the electron tubes. Effective correlation also is introduced by dependence of both signal level and system parameters on some third thing such as time of day or phase of operating cycle.

A good example of specification of over-all error is afforded by Christiansen's one-dimensional distribution over the quiet sun. Calling the observed distribution  $T_a(\Phi)$ , the errors were quoted as follows:

$T_a$	$\Phi$	Range
$\pm 0.020$	$\pm 0.2$	$\Phi < 10$
$\pm 0.030$		$10 < \Phi < 12$
		$\Phi > 12$

While this statement is incomplete, and in fact is not all that is known in this case, it is more than would be available usually, since the observations were repeated a great many times. It suffices to illustrate the dependence of the errors on the signal. The strong signal occurred in the range  $\Phi < 10$ , and zero signal where  $\Phi > 12$ . In the range  $10 < \Phi < 12$  the signal fell from full strength to zero. The error in  $T_a$  is, therefore, as great as the full signal (1.0) in that interval, which is locked to the behavior of the signal.

If there were no errors, the  $n$ th stage of restoration by successive substitutions would be given by

$$T_n(x, y) = \iint R_n(x - x', y - y')T_a(x', y')dx'dy',$$

where  $R_n$  is a restoring distribution, given explicitly by

Bracewell and Roberts,<sup>4</sup> and  $n$  could be taken as large as necessary. But when there are errors the question is how many stages of restoration can be tolerated. The physical situation is greatly clarified by considering the Fourier transforms of the quantities under discussion. Let

$$\bar{T}_a(u, v) = \iint T_a(x, y)e^{-i2\pi(ux+vy)}dxdy,$$

$$\bar{T}(u, v) = \iint T(x, y)e^{-i2\pi(ux+vy)}dxdy,$$

and

$$\bar{A}(u, v) = \iint A(-x, -y)e^{-i2\pi(ux+vy)}dxdy.$$

Then by the two-dimensional convolution theorem

$$\bar{T}_a(u, v) = \bar{A}(u, v)\bar{T}(u, v),$$

and

$$\bar{T}(u, v) = \frac{\bar{T}_a(u, v)}{\bar{A}(u, v)}, \quad \bar{A}(u, v) \neq 0.$$

The principal solution is defined by its Fourier transform  $\bar{S}(u, v)$ ,

$$S(u, v) = \begin{cases} \frac{\bar{T}_a(u, v)}{\bar{A}(u, v)}, & \bar{A}(u, v) \neq 0 \\ 0, & \bar{A}(u, v) = 0. \end{cases}$$

The correction factor  $\{\bar{A}(u, v)\}^{-1}$  becomes large for certain values of  $(u, v)$ , especially near the cutoff possessed by all finite antennas, but also elsewhere in the case of antennas having two or more distinct parts. Now if the Fourier transform of the error distribution had components near cutoff, or where the factor  $\{\bar{A}(u, v)\}^{-1}$  is large, it would be desirable to modify the correction.

Let a modified factor

$$\frac{a}{\bar{A}(u, v)}$$

be used. Then we may inquire what value  $a$  should assume in order to compensate for the presence of errors. Naturally the error itself will not be known and of course, if nothing at all were known about the error nothing could be done. In practice, however, one knows something about its order of magnitude from comparing successive records of the same part of the sky. Averages over ensembles of such records will be denoted below by sharp brackets.

We now seek to determine  $a$  in such a way that the restored distribution exhibits the best agreement, on the average, with the principal solution and *a fortiori* with the true distribution. And if restoration is being carried out by the method of successive substitutions, we consider at what stage the restoration is best terminated.

III. DERIVATION OF THE RESTORING DISTRIBUTION

Let

$$\begin{aligned} \bar{T}_a(u, v) + \bar{E}(u, v) \\ = \iint [T_a(x, y) + E(x, y)] e^{-i2\pi(ux+vy)} dx dy, \end{aligned}$$

and let the modified factor  $a/\bar{A}(u, v)$  be applied to  $\bar{T}_a(u, v) + \bar{E}(u, v)$ . The result so obtained in general will show a discrepancy from the Fourier transform of the principal solution  $\bar{S}(u, v)$  since  $\bar{E}(u, v)$  may assume various phases. As  $a$ , therefore, cannot be selected to reduce the complex discrepancy to zero, we impose the condition that the modulus of the discrepancy should be a minimum on the average and solve the resulting equation for  $a$ . Thus

$$\frac{\partial}{\partial a} \left\langle \left[ S(u, v) - \frac{a(\bar{T}_a(u, v) + \bar{E}(u, v))}{\bar{A}(u, v)} \right] \times \text{conjugate} \right\rangle = 0,$$

when, dropping the variables  $u, v$ ,

$$\begin{aligned} 0 &= \frac{\partial}{\partial a} \langle [\bar{T}_a - a(\bar{T}_a + \bar{E})] \times \text{conjugate} \rangle \\ &= \frac{\partial}{\partial a} \langle \bar{T}_a \bar{T}_a^* + a^2(\bar{T}_a + \bar{E})(\bar{T}_a^* + \bar{E}^*) \\ &\quad - a(\bar{T}_a + \bar{E})\bar{T}_a^* - a(\bar{T}_a^* + \bar{E}^*)\bar{T}_a \rangle \\ &= 2a[\bar{T}_a \bar{T}_a^* + \langle \bar{E} \bar{T}_a^* \rangle + \langle \bar{E}^* \bar{T}_a \rangle + \langle \bar{E} \bar{E}^* \rangle] \\ &\quad - 2\bar{T}_a \bar{T}_a^* - \langle \bar{E} \bar{T}_a^* \rangle - \langle \bar{E}^* \bar{T}_a \rangle. \end{aligned}$$

Therefore,

$$a = \frac{\bar{T}_a \bar{T}_a^* + \frac{1}{2} \langle \bar{E} \bar{T}_a^* \rangle + \frac{1}{2} \langle \bar{E}^* \bar{T}_a \rangle}{\bar{T}_a \bar{T}_a^* + \langle \bar{E} \bar{T}_a^* \rangle + \langle \bar{E}^* \bar{T}_a \rangle + \langle \bar{E} \bar{E}^* \rangle} \quad (1)$$

This result leads to the best restoring distribution  $R(x, y)$  through the Fourier transform relation,

$$R(x, y) = \iint \frac{a}{\bar{A}(u, v)} e^{i2\pi(ux+vy)} dudv \quad (2)$$

and contains all the special conclusions which follow.

It is, however, not general, since the right-hand side of (1) is seen on inspection to be real, a consequence of an earlier implicit assumption that  $a$  is real. This restriction may be removed readily and leads to a discussion of problems, not to be pursued here, in which the errors are correlated with  $T_a$  in a way which depends on the direction of scanning. Already such cases have arisen in practice when scanning at high speed relative to the beamwidth of the antenna and the bandwidth of the low-pass filter of a radiometer, and an analogous situation arises in scanning hydrogen line profiles.

The formula for  $a$  contains several different quantities which may be commented on in turn. First,  $\bar{T}_a(u, v)\bar{T}_a^*(u, v)$  is the squared modulus of the Fourier

transform of  $T_a(x, y)$ , and it is tempting to think of it as the power spectrum of  $T_a(x, y)$ , even though  $T_a(x, y)$  itself is already proportional to power. Provided this is kept in mind, it is illuminating to think of  $\langle \bar{E} \bar{E}^* \rangle$  as the average error power spectrum and of  $\frac{1}{2} \langle \bar{E} \bar{T}_a^* \rangle + \frac{1}{2} \langle \bar{E}^* \bar{T}_a \rangle$  as the mutual power spectrum. When the error and  $T_a$  are on the average incoherent, then the mutual terms vanish.

This section can be compared advantageously with the problem of so modifying a stationary complex time series  $T(t)$  afflicted with a disturbance  $g(t)$  that a best approximation to the message  $T(t)$  is obtained. The discussion of this problem by Wiener<sup>14</sup> contains implicitly a formula of the type derived here. Our problem differs in that the distributions sought are real, two-dimensional and nonstationary, and (for physical acceptability) nonnegative.

IV. SPECIAL CASES

1)  $EE^*$  is proportional to  $\bar{T}_a \bar{T}_a^*$  and  $\bar{E} \bar{T}_a^* + \bar{E}^* \bar{T}_a = 0$

In this case  $a$  is constant and the presence of the errors may be ignored for purposes of restoration except insofar as absolute temperature measurements are concerned.

2) The errors are small, i.e.,  $\langle \bar{E} \bar{E}^* \rangle \ll \bar{T}_a \bar{T}_a^*$

In this case the mutual terms may control the effect on  $a$  and we have

$$a \approx 1 - \frac{\langle \bar{E} \bar{T}_a^* \rangle + \langle \bar{E}^* \bar{T}_a \rangle - 2 \langle \bar{E} \bar{E}^* \rangle}{2 \bar{T}_a \bar{T}_a^*}$$

3) There is no correlation between the errors and  $T_a$

Then,

$$a = \frac{1}{1 + \frac{\langle \bar{E} \bar{E}^* \rangle}{\bar{T}_a \bar{T}_a^*}}$$

and if, further, the errors are small,

$$a \approx 1 - \frac{\langle \bar{E} \bar{E}^* \rangle}{\bar{T}_a \bar{T}_a^*}.$$

By further assuming specific forms of dependence on  $u$  and  $v$ , various restoring distributions can be obtained. One of the most interesting cases is that where  $\bar{T} \bar{T}^* = b$ ,  $\bar{A}(u, v) = (1 - |u|)(1 - |v|)$ , and  $\langle \bar{E} \bar{E}^* \rangle = c$ . This case arises when the antenna consists of a uniform square aperture, and the true distribution and the error distribution have uncorrelated flat spectra. Then

$$a = \frac{1}{1 + \frac{c}{\bar{T}_a \bar{T}_a^*}},$$

<sup>14</sup> N. Wiener, "Extrapolation, Interpolation and Smoothing of Stationary Time Series," New York, N. Y., sec. 3.1; 1949.

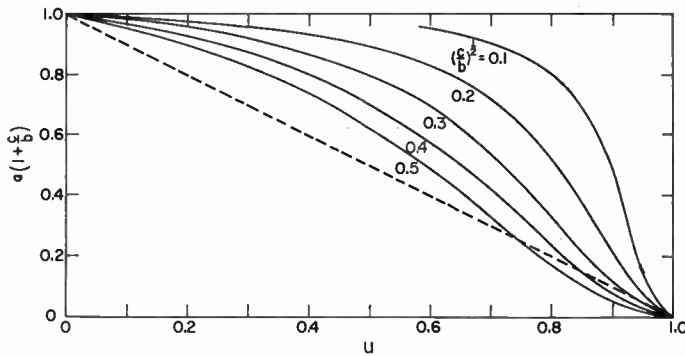


Fig. 1—The form of the modifying factor  $a$  in a certain simple problem.

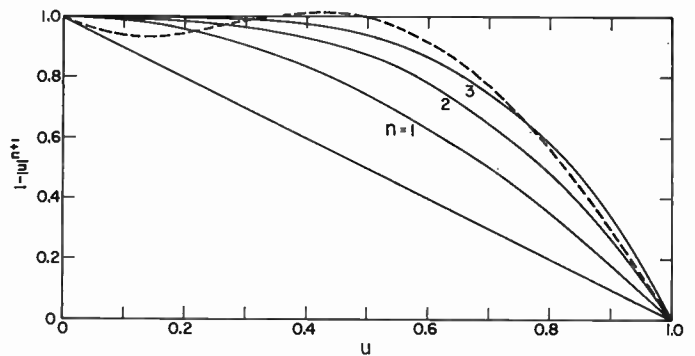


Fig. 2—Spectral factors corresponding to different stages of restoration by successive substitutions. The broken line refers to the chord construction.

and

$$\frac{a}{\bar{A}(u, v)} = \frac{\bar{A}}{\bar{A}^2 + \frac{c}{b}}$$

Fig. 1 illustrates the variation of  $a$  with  $u$  as  $v$  is held constant and equal to zero, for different values of  $(c/b)^{1/2}$ . Each curve has been normalized to have unit value at  $v=0$ . It will be seen that when  $(c/b)^{1/2} = 0.1$ , *i.e.* when  $(\overline{EE^*})^{1/2}$  is 10 per cent of  $(\bar{T}_a \bar{T}_a^*)^{1/2}$ , then the best restoration is quite close to the principal solution; and that when  $(c/b)^{1/2}$  is as great as 50 per cent, some improvement in agreement with the true distribution is still obtainable by a little restoration.

The normalization mentioned above is appropriate provided the shape and not the absolute level of the solution is important. But if it were a question of measuring the flux density of a source then the value of  $a$  at the origin would have to be taken into account and a correction factor  $(1+c/b)$  applied. The fact that improved agreement with the true distribution may entail depression of the absolute level has not been pointed out before.

### V. METHOD OF SUCCESSIVE SUBSTITUTIONS

In order to have some practical conclusions as simple as possible it is desirable to take a special case and show how to determine the number of stages which gives the best agreement with the true distribution. Thus, when  $\bar{A}(u, v) = (1 - |u|)(1 - |v|)$ , the Fourier transform of the  $n$ th restoration is (Bracewell and Roberts<sup>4</sup>)

$$1 + [1 - \bar{A}(u, v)] + [1 - \bar{A}(u, v)]^2 + \dots + [1 - \bar{A}(u, v)]^n \bar{T}_a(u, v),$$

and if only the cross section along  $v=0$  is considered this reduces to

$$\{1 + |u| + |u|^2 + \dots + |u|^n\} \bar{T}_a(u, 0);$$

and by substituting  $\bar{T}_a(u, 0) = (1 - |u|)\bar{S}(u, 0)$  we have

$$\{1 - |u|^n\} \bar{S}(u, 0).$$

The factor  $1 - |u|^n$  is shown in Fig. 2 for comparison with the corresponding curves of Fig. 1. It will be seen that the first stage of restoration approximates roughly to the restoration permitted when  $(c/b)^{1/2} = 0.3$  and that the second stage approximates to the curve  $(c/b)^{1/2} = 0.2$ .

To make these comparisons more definite and to illustrate a suitable approach we assume that  $n$  stages of restoration are to be made and then see how great the errors may be before  $n-1$  stages yield a better fit.

As a measure of discrepancy between the true distribution and the  $n$ th restoration let us take:

$$\begin{aligned} D &= \langle [(1 + |u| + |u|^2 + \dots + |u|^n)(1 - |u| + \bar{E}) - 1] \times \text{conjugate} \rangle \\ &= \langle (1 + |u| + |u|^2 + \dots + |u|^n)\bar{E} + |u|^n \rangle \times \text{conjugate} \rangle \\ &= \langle (1 + |u| + |u|^2 + \dots + |u|^n)^2 \overline{EE^*} + |u|^{2n} \rangle \\ &= \langle (1 + 2|u| + 3|u|^2 + \dots + 3|u|^{2n-2} + 2|u|^{2n-1} + |u|^{2n}) \overline{EE^*} + |u|^{2n} \rangle \\ &= \left( 1 + |u|^2 + |u|^3 + \dots + \frac{3|u|^{2n-1}}{2n-1} + \frac{2|u|^{2n}}{2n} + \frac{|u|^{2n+1}}{2n+1} \right) \overline{EE^*} + \frac{|u|^{2n+1}}{2n+1} \Big|_0^1 \\ &= \left( 1 + 1 + 1 + \dots + \frac{3}{2n-1} + \frac{2}{2n} + \frac{1}{2n+1} \right) \overline{EE^*} + \frac{1}{2n+1}. \end{aligned}$$

The first few of the expressions on the right are

$$\frac{7\overline{EE^*}}{3} + \frac{1}{5},$$

$$\frac{37\overline{EE^*}}{10} + \frac{1}{7},$$

$$\frac{533\overline{EE^*}}{105} + \frac{1}{9}.$$

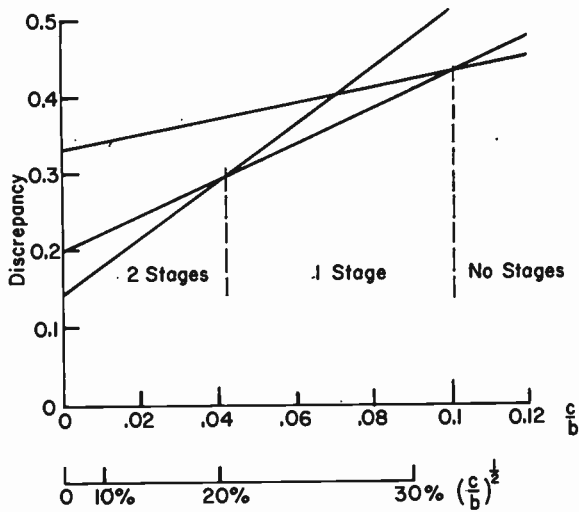


Fig. 3—How the discrepancy depends on the error level for different stages of restoration by successive substitutions.

Equating successive pairs of these expressions to find the intersections shown in Fig. 3 we have

$$\overline{EE}^* = 0.100, 0.042, 0.023, 0.015, \dots$$

These results add precision to the rough estimate made earlier by comparing Figs. 1 and 2 and may be summarized as in Table I.

TABLE I

Error level $(c/b)^{1/2}$ (per cent)	Best number of stages of restoration
32	0
20	1
15	2
12	3

### VI. THE CHORD CONSTRUCTION

In the preceding sections we have determined the best restoration under given circumstances of error, and the best stage of restoration by the method of successive substitutions. It is very important from the practical standpoint, however, that a proposed method of restoration should not involve too much effort, since the finely detailed two-dimensional maps now obtainable with instruments of high-resolving power will allow only the most elementary operations, if these are to be carried out by hand. An approach along these lines has been made (Bracewell<sup>16</sup>) which, in one dimension, leads

<sup>16</sup> R. N. Bracewell, "Correction for Gaussian aerial smoothing," *Aust. J. Phys.*, vol. 8, pp. 54-60; March, 1955.

to the chord construction (Bracewell<sup>16,17</sup>). This particularly simple operation on the data gives immediate restoration to the extent indicated by the broken line in Fig. 2.

The discrepancy can be evaluated as in Section V, but it is immediately clear that three stages of restoration by successive substitutions are roughly equivalent; hence if the level of error,  $(c/b)^{1/2}$ , does not exceed 15 per cent, correction by the chord construction will lead to improved agreement with the true distribution.

### VII. CONCLUSION

The problem of restoration in the presence of errors is solved in principle by convolution of the restoring distribution (2) (Section III) with the observations. Some special cases show that when the level of error is moderate, a considerable degree of restoration is warranted. In particular, two stages of correction by the method of successive substitutions are warranted when the error level  $(c/b)^{1/2}$  is as much as 20 per cent, and correction by the chord construction when the error is as much as 15 per cent. In recent published work where correction has been omitted there is no indication that the relative errors are this great. (The error in absolute level is usually greater but has no bearing on restoration.)

The special circumstances in some cases where restoration can be considered may render any of the three methods discussed here inapplicable. There is, however, an important inference from the full solution based on (1), *viz.* that any system of restoration should contain mention of 1) the character of the errors and 2) the character of the observed distribution. It is noteworthy that the method of successive substitutions satisfies these conditions inasmuch as the process is halted when "smoothing the trial distribution gives a result agreeing with  $T_a$  within the experimental error."

Only a very few one-dimensional special cases have been considered numerically here and those only for the purpose of establishing roughly the quantitative relation between error level and degree of restoration. Many important cases remain to be studied, especially the two-dimensional generalizations of the finite-difference method on which the chord construction is based.

Further topics not treated here are the physical acceptability of restored distributions, and the effect of uncertainties in the antenna pattern.

<sup>16</sup> R. N. Bracewell, "Simple graphical method of correcting for instrumental broadening," *J. Opt. Soc. Amer.*, vol. 45, pp. 873-876; October, 1955.

<sup>17</sup> R. N. Bracewell, "Chord construction for correcting aerial smoothing," *Aust. J. Phys.*, vol. 8, pp. 200-205; June, 1955.



# Discussion of 10.7-CM Solar Radio Flux Measurements and an Estimation of the Accuracy of Observations\*

W. J. MEDD†, MEMBER, IRE, AND A. E. COVINGTON†, MEMBER, IRE

**Summary**—The accuracy of the daily 10.7-cm solar flux measurements taken at the National Research Council, Ottawa, has been investigated. The various system parameters are examined and an auxiliary experiment, using a horn antenna, is described. These studies lead to a revision of the early values of the solar flux and require the use of conversion factors to some of the published data. It has been estimated that the relative error between observations separated by intervals of months may be  $\pm 10$  per cent during 1947 through 1949, and  $\pm 3$  per cent during subsequent years. The systematic error in 1952–1953 was estimated at  $\pm 7$  per cent.

## INTRODUCTION

OBSERVATIONS of solar radio emission on a wavelength of 10.7 cm have been made since 1947, at the laboratories of the National Research Council in Ottawa, using a four-foot-diameter parabolic reflector and an associated radiometer of the Dicke comparison type. In addition to a continuous monitor of any enhanced radiation or burst activity, measurements of the solar emission in flux units of watts per square meter per cps bandwidth are taken daily. Only the general method of calibration has been previously reported.<sup>1</sup> With the increasing significance of the radio data it becomes important to obtain an estimate of the absolute and relative accuracies of these measurements. This has involved a detailed examination of the system parameters and sources of error, and a review of certain results obtained from an additional radio telescope of different design operated in 1952–1953 concurrently with the standard equipment.

## THEORETICAL FORMULAS USED IN CALIBRATION

The magnitude of the open-circuit mean-square voltage and the absolute temperature of a resistor are related by Nyquist's formula,

$$\overline{v^2} = 4kTRdf, \quad (1)$$

where

- $\overline{v^2}$  = the mean-square noise voltage,
- $k$  = Boltzmann's constant,
- $T$  = the absolute temperature of the resistor,
- $R$  = the resistance in ohms, and
- $df$  = the bandwidth in cps.

The maximum power one is able to transfer from this resistance to the receiver occurs when the resistance is matched to the receiver input resistance. This power is called "available power" and is equal to  $kTdf$ . From a

consideration of thermal equilibrium, Burgess<sup>2</sup> has shown that the same formula applies to the radiation resistance,  $R_A$ , of an antenna enclosed in a black box at uniform temperature  $T_A$ . If the surroundings are not at uniform temperature, then  $T_A$  is taken as an average effective temperature given by

$$T_A = 1/(4\pi) \int G(\theta\phi)t(\theta\phi)d\omega, \quad (2)$$

where the direction gain  $G$  and the effective temperature  $t$  are functions of the angles  $\theta$  and  $\phi$ , and  $d\omega$  is an element of the solid angle.

An equivalent circuit of the form shown in Fig. 1 is



Fig. 1—Equivalent circuit of antenna and radiometer.

then assumed, where network 1 represents the ohmic resistance in the antenna, and network 2 the waveguide elements between the antenna and receiver. The effective temperature at  $B$ ,  $T_B$ , is obtained from an equation of power transfer; thus

$$T_B = (1 - \alpha)T_A + \alpha T_\alpha, \quad (3)$$

where  $\alpha$  is a fractional absorption coefficient and  $T_\alpha$  is ordinarily the ambient temperature  $T$ .  $(1 - \alpha)T_A$  is proportional to the signal power which reaches the receiver, while  $\alpha T_\alpha$  is proportional to the noise power emitted by the ohmic resistances of the antenna.

When the radiometer is connected to the antenna at  $B$ , the response in terms of recording meter deflections  $R$  has been found to follow the equation

$$R = a + cT_B. \quad (4)$$

$a$  includes the zero shift of the radiometer which arises principally from imperfect matching of the various components in the microwave system. When any adjustment of frequency or crystal current is made,  $a$  usually changes, but will otherwise remain constant for long periods of time.  $c$  is the sensitivity factor of the radiometer and is not as critical to matching conditions as  $a$ . The absorption coefficient  $\alpha'$  (see Fig. 1) is included in this constant.  $T_B$  and  $R$  take on different values depending upon the orientation of the antenna or the conditions

\* Original manuscript received by the IRE, October 14, 1957; revised manuscript received, October 28, 1957.

† National Research Council, Ottawa, Ont., Canada.

<sup>1</sup> A. E. Covington, "Some characteristics of 10.7 centimeter solar noise," *J. Roy. Astron. Soc. Can.*, vol. 45, p. 15; 1951.

<sup>2</sup> R. E. Burgess, "Noise in receiving aerial systems," *Proc. Phys. Soc., London*, vol. 53, p. 293; 1941.

TABLE I

Description of Situation	$T_A$ —Temperature of Radiation Resistance	$T_B$ —Effective Temperature at $B$	Recording Meter Deflection $R = a + cT_B$
1) Antenna pointing toward the sun	$T_{A1}$	$(1 - \alpha)T_{A1} + \alpha T$	$R_1$
2) Antenna pointing toward the sky remote from sun	$T_{A2}$	$(1 - \alpha)T_{A2} + \alpha T$	$R_2$
3) Antenna and ohmic losses in black box at ambient temperature $T$ Antenna replaced with resistance load at ambient temperature	$T_{A3} = T$ —	$(1 - \alpha)T + \alpha T = T$ $T$	$R_3$
4) Antenna and ohmic losses enclosed in black box at elevated temperature $T_4$ Antenna replaced with resistive load at other than ambient temperature	$T_{A4} = T_4$ —	$(1 - \alpha)T_4 + \alpha T_4 = T_4$ $T_4$	$R_4$

at the antenna terminals, and these are summarized in Table I.

Eqs. (1)–(4) will now be discussed further in more direct reference to the daily calibration procedure for determining the flux from the sun. The manner of dealing with (2) depends on the gain function,  $G(\theta\phi)$ , for the particular antenna used. The beamwidth of the antenna in use at Ottawa is about  $7^\circ$  to the half-power points. This is sufficiently wide that when pointing directly towards the sun, the gain may be taken as constant over the angular width of the sun, and equal to the maximum directive gain  $G_0$ . The gain becomes small at about  $10$  or  $15^\circ$  away from the maximum, and if the antenna is oriented some  $15^\circ$  or more from the sun, solar emission is not measurable with the present equipment since in the direction of the sun both the gain and the area of integration are small. However, at various angles away from the main beam there are side lobes where the gain, although small, may be of significance if the area of integration is large. These side lobes may exist at all angles from the main beam and collect an emission from the earth which will vary in magnitude as a function of the orientation of the antenna. The gain function is ordinarily not known in the side and back directions with sufficient accuracy to calculate the contributions of earth radiation by direct integration.

With the antenna pointing towards the sun, the effective temperature of the antenna radiation resistance is given by

$$T_{A1} = \frac{1}{4\pi} G_0 \Omega \bar{i}_{\text{sun}} + \frac{1}{4\pi} \int_{\text{sky}} G_{\text{sky}} d\omega + \frac{1}{4\pi} \int G_{\text{earth}} d\omega,$$

where  $\bar{i}_{\text{sun}}$  is the effective temperature of the sun usually averaged over the optical disk or corresponding solid angle,  $\Omega$ , and  $i_{\text{sky}}$  is the effective temperature of the sky. In accordance with the above discussion this equation will be written more simply as

$$T_{A1} = \frac{1}{4\pi} G_0 \Omega \bar{i}_{\text{sun}} + x(\alpha, \beta), \tag{5}$$

where  $x(\alpha, \beta)$  includes any contributions from the sky and earth, and is a function of the orientation of the an-

tenna as specified by the angles  $\alpha$  and  $\beta$ . The effective temperature at the antenna when pointed toward the zenith,  $T_{A2}$ , is taken as a second calibration level,

$$T_{A2} = \frac{1}{4\pi} G_0 \Omega i_{\text{sky}} + x(\alpha_0, \beta_0). \tag{6}$$

The temperature difference between these two levels is given by

$$T_{A1} - T_{A2} = \frac{1}{4\pi} G_0 \Omega (\bar{i}_{\text{sun}} - i_{\text{sky}}) + \Delta x(\alpha, \beta),$$

where the function  $\Delta x$  is the difference between the background temperatures in the directions of the sun and zenith. It is determined from a separate experiment. In terms of meter readings,

$$\begin{aligned} R_1 - R_2 &= c(1 - \alpha)(T_{A1} - T_{A2}) \\ &= c(1 - \alpha) \left[ \frac{1}{4\pi} G_0 \Omega \bar{i}_{\text{sun}} + \Delta x(\alpha, \beta) \right]. \end{aligned} \tag{7}$$

The approximation that  $\bar{i}_{\text{sun}} - i_{\text{sky}} = \bar{i}_{\text{sun}}$  has been made, as it is known that  $\bar{i}_{\text{sun}}$  is of the order of  $(10^4)^\circ$ , while  $i_{\text{sky}}$  is of the order of  $1^\circ$  or  $10^\circ$ . Attenuation through the earth's atmosphere has not been considered since, from other experimental work, it is known to be negligible.

The factor  $c(1 - \alpha)$  may be found from the difference between the readings  $R_3$ , for which the antenna is enclosed in a black box, and  $R_2$ , for which the antenna is in the sky or zenith position. Thus,

$$(R_3 - R_2)/(T - T_{A2}) = c(1 - \alpha).$$

When this is substituted in (7), the average effective temperature of the sun is given by

$$\frac{\bar{i}_{\text{sun}} G_0 \Omega}{4\pi} = \rho(T - T_{A2}) - \Delta x, \tag{8}$$

where

$$\rho = \frac{R_1 - R_2}{R_3 - R_2}.$$

It remains to establish the value of  $T_{A2}$ . This can be

found from (3), using readings  $R_2$ ,  $R_3$ , and  $R_4$  in Table I:

$$T_{A2z} = T - \frac{\rho_2}{1 - \alpha} (T_4 - T), \quad (9)$$

where

$$\rho_2 = \frac{R_3 - R_2}{R_4 - R_3}.$$

However, this direct method is not used in daily calibrations because of practical difficulties, and a constant value for  $T_{A2z}$  has been used, based upon isolated experiments which will be described later.

The flux,  $F$ , for two polarizations of radiation from the sun in units of watts per square meter for one cps bandwidth, is given by

$$F = \frac{2k\bar{I}_{\text{sun}}}{\lambda^2}.$$

In terms of observed quantities and system parameters,

$$F = \frac{8\pi k}{G_0\lambda^2} [\rho(T - T_{A2z}) - \Delta x(\alpha, \beta)]. \quad (10)$$

#### PRELIMINARY EXPERIMENTS

In 1946, the initial calibration of the radiometer associated with the four-foot reflector was based upon a black box which could be heated to various temperatures above ambient. At the same time investigations into the relative constancy of the sky temperature were being made, and it soon became evident that the sky would serve as a black box at very low temperatures.<sup>3</sup> These preliminary investigations, both with the heated black box and with heated waveguide terminations substituted for the antenna, indicated that the sky temperature was of the order of 50° K. At this time the antenna gain was also measured and found to be 700. Regular observations of the sun commenced in 1947, and the solar flux was calculated using a gain factor of 700 with an apparent sky temperature of 50° K.

In this method of calibration the sky temperature is important and its evaluation becomes a separate problem. Separate investigations were started with a horn antenna and a second radiometer whereby it was possible to replace the antenna with either a hot load or a load at ambient temperature. A continuously changing phase shifter was inserted between the radiometer and the antenna, or a substituted load, in an effort to minimize the zero-shift error due to residual mismatches. One series of observations, lasting just under a year, was obtained in 1948, during a period of considerable sunspot activity when variations in solar radio emission were large. No corresponding day-to-day changes were observed in the measured sky temperature nor was any difference found between day or nighttime readings, and sky temperature was therefore considered

to be essentially independent of any atmospheric effect dependent upon solar activity.

During the period 1947–1950, one radiometer was used with the four-foot radio telescope. Maintenance with a view to continuous observations was achieved by constructing certain spare components. Later, after 1950, two identical and complete radiometers were installed with a waveguide switch so that either set could be connected to the antenna. Calibrations were made periodically with both radiometers, and, in general, agreement was good. Differences up to 5 per cent occasionally appeared but were rectified by examination of the radiometers. The use of stand-by equipment has proven very helpful and produced more confidence in the results.

#### DETERMINATION OF SYSTEM PARAMETERS

##### *Zero Shift and Matching of Calibration Resistors*

When the radiation resistance of the antenna (or a substituted resistive element) is at the same temperature as the reference resistor in the waveguide chopper, the receiver output should ideally be zero. In general this is not so, and the fictitious output has been found to be related to the small residual mismatches which unfortunately occur when components are connected in a waveguide transmission line. The zero level depends upon the magnitude and phase of the impedance presented to the terminals of the receiver. In the derivation of (10) which gives the magnitude of solar radio flux, it is assumed that the zero shift,  $a$ , is constant and subtracts out. This certainly occurs when finding the difference between the sun and sky levels. However, there is a possibility of a change in the zero shift when any practical "black" box is placed around the dipole, and it was necessary to determine the magnitude of the mismatch error introduced. The standing-wave ratio was measured for two black boxes (18-inch cubes) which have been used in daily calibrations, and compared with that of the dipole looking into the reflector and, hence, into the sky. These measurements were made near the input terminals (point *C* in Fig. 1) looking toward the dipole through a 50-foot length of waveguide and several rotating couplers. The results are summarized in Table II.

TABLE II  
POWER STANDING-WAVE RATIOS

$\lambda$ (cm)	Box 1	Box 2	Sky Box Off	Phase of Mismatch
10.9	1.18	1.18	1.08	constant
10.8*	1.35	1.21	1.36	constant
10.7	1.34	1.40	1.40	constant
10.6*	1.08	1.15	1.06	constant
10.5	1.58	1.55	1.51	constant

\* Energy received in neighborhood of this wavelength.

The small differences shown in Table II would appear to have negligible effect on the zero shift, since the

<sup>3</sup> A. E. Covington, "Microwave sky noise," *J. Geophys. Res.*, vol. 55, p. 33; 1950.

values of solar flux as measured first with one box and then with the other show no difference. However, the zero error may become very critical with a poor mixer, and it is possible that an appreciable error has been present during some portions of the nine-year period of observations. A unidirectional transmission line was inserted between the crystal mixer and the rotating carbon disk in 1956, and resulted in an almost complete reduction in the mismatch error.<sup>4</sup>

### Linearity

It has been found that the relationship between effective antenna temperature,  $T_A$ , and radiometer response remains linear up to 5000° K, which is much higher than values ordinarily encountered. However, a small nonlinearity, independent of the range of  $T_A$ , may be introduced by the demodulator and recording meter combination, causing an error in calibration of less than one per cent.

### Receiver Noise and Stability

Associated with the accuracy of determining  $R$  or  $\rho$ , errors due to inherent receiver noise and drifts in gain during calibration can be made small by increasing the number of observations. Daily values are ordinarily based upon one or two good calibrations, but when repeated measurements are taken it is found that the majority of the values lie within 2 per cent of the average.

### Wavelength

The wavelength,  $\lambda$ , is measured and maintained constant to much higher accuracy than other parameters. Local oscillator wavelength, being an average value of the wavelengths at which energy is received, is used in (10).

### Temperature of Calibrating Black Box

The temperature of the black box is measured with Weston thermometers which are checked periodically. There is negligible error in these temperature determinations.

### Pointing Accuracy

The maximum of the receiving pattern of the antenna may be pointed towards the sun by varying the angular position of the antenna and finding maximum receiver output. This is not a critical adjustment. An auxiliary optical telescope has been calibrated as a finder and is used on clear days; on cloudy or rainy days the setting of the antenna is accomplished by radio means alone.

### Background Radiation

The term  $\Delta x$  in (8) is a small additive term and can be established to sufficient accuracy by experimental means in which readings of  $T_{A2}$  are taken for different

elevations and hour angles of the antenna. Unfortunately, in the earlier experimental work this term was erroneously considered negligible. The possibility of existence of this error was suggested in a private communication by Tanaka of Nagoya University,<sup>5</sup> who had found a small seasonal inconsistency between the Ottawa and Nagoya observations. The contribution of the term  $\Delta x$  has subsequently been re-investigated and necessitates a small correction to the values of solar flux reported. In spite of this, a relative inconsistency between the Ottawa and Nagoya observations still remains.

### Antenna Gain

The maximum directive antenna gain was redetermined in 1953 by a standard method which involves transmission between suitably separated antennas, and measurements of the reduction in power upon reception.<sup>6</sup> The following antennas were used in this experiment:

- 1) A horn about 10 feet in length with rectangular aperture 3 feet  $\times$  4 feet. This was also used for taking measurements of solar flux during 1952–1953.
- 2) A test horn identical with 1). Both are approximately optimum horns.
- 3) The four-foot parabolic reflector associated with the equipment used in daily measurements of solar flux. The focal length is 12 inches, and the focus is at the midpoint between a half-wave dipole and parasitic reflector.

Previously, antenna patterns in the two principal planes were taken, as a check that no objectionable side lobes were present. The weak side lobes far removed from the main lobe were not detected.

*Gain of Rectangular Horn:* The calculated gain using the formula of Schelkunoff<sup>7</sup> is shown graphically as a function of wavelength in Fig. 2. At 10.7 cm the value is 428. The theoretically calculated gain for a pyramidal horn has been confirmed in various reports and may be taken with more confidence than the following experimental determination, which was carried out under somewhat unsuitable conditions. However, it was desirable to see what correspondence with the theoretical value would be obtained, before proceeding with essentially the same setup to the gain measurements of the parabolic reflector.

The experimental work was carried out at the site of the Solar Radio Observatory. As towers of suitable height were not available, it was necessary to use a screen between the two antennas, to run through a portion of the diffraction pattern by raising and lowering

<sup>5</sup> H. Tanaka, "Some notes on the solar radio emission at centimeter regions around the period of sunspot minimum," *Proc. Res. Inst. Atmos.*, Nagoya University, vol. 3, p. 117; 1955.

<sup>6</sup> S. Silver, "Microwave Antenna Theory and Design," McGraw-Hill Book Co., Inc., New York, N. Y., p. 582; 1949.

<sup>7</sup> S. A. Schelkunoff, "Electromagnetic Waves," D. Van Nostrand Co., Inc., New York, N. Y., chap. 9; 1943.

<sup>4</sup> C. H. Mayer, "Improved noise power measurements through use of ferrites," *J. Geophys. Res.*, vol. 59, p. 188; 1954.

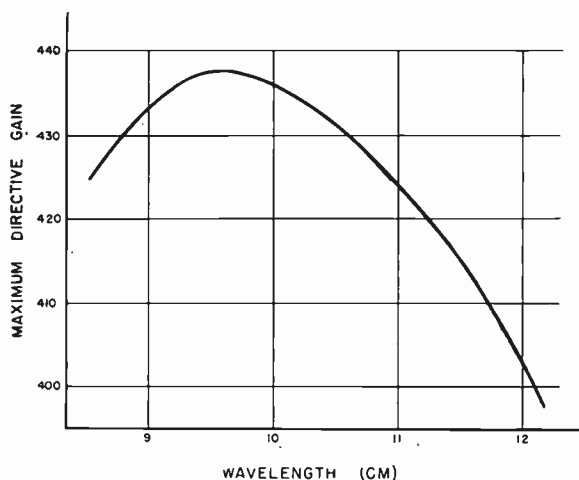


Fig. 2—Calculated maximum directive antenna gain of 3-foot  $\times$  4-foot aperture horn as a function of wavelength.

the test horn, and to take an average of the readings. The separation of the two 3-foot  $\times$  4-foot aperture horns was, on different occasions, 334, 280, and 276.5 feet. The distances were measured from the throat of each horn;<sup>8</sup> another method<sup>9</sup> which involves measuring from the horn face and applying correction factors yields approximately the same results—about 2 per cent lower—for this experiment. The experiment involves the use of a calibrated attenuator, and the manufacturer's statement of 0.2-decibel accuracy was accepted.

Values obtained for  $G_0$  were as follows: 427, 469, 459, 445, 426, 418, 421, 433, 409, 423, 441, 439, 441, and 422. The average of these 14 values is 434. Calculation of the ohmic losses in the horn and a small length of waveguide indicates that the measured effective gain should be increased by about 1 per cent to obtain a directive gain of 438 for the horn.

The probable error of this gain measurement was estimated as 6 per cent from a consideration of the various factors involved, predominantly the accuracy of the attenuator readings and the interpretation of the interference pattern. However, in subsequent calculations the theoretical antenna gain of 428 will be used, and it will then be necessary to place a probable error on this value. That the observed mean value in this experiment differs from the theoretical by only 2 per cent may be fortuitous, but a more refined experiment at 1.25 cm has been reported<sup>8</sup> in which a somewhat better check was obtained. It would thus seem certain that the probable error is small, and for the present purpose will be assumed as 2 per cent.

*Gain of Four-Foot Parabolic Reflector:* The gain,  $G_0$ , of the four-foot parabolic reflector was then determined

<sup>8</sup> W. C. Jakes, Jr., "Gain of electromagnetic horns," *PROC. IRE*, vol. 39, pp. 160-162; February, 1951.

<sup>9</sup> E. H. Braun, "Gain of electromagnetic horns," *PROC. IRE*, vol. 41, pp. 109-115; January, 1953.

by the same method using the 3-foot  $\times$  4-foot aperture test horn with the calculated gain of 428. Separations of 230 and 340 feet were used. On different occasions the following seven values of  $G_0$  were obtained: 673, 699, 716, 669, 691, and 743, with an average value of 704. (A weighted average was calculated as 698.) In making the calculations it was necessary to allow for attenuation through some waveguide pieces and rotating joints which are located near the dipole. This was determined experimentally to give a constant multiplying factor of 1.13, with a probable error estimated at about 5 per cent.

A further source of error is ohmic losses in the reflector and dipole proper, but this has been assumed small in comparison with other factors, and no correction has been attempted. The attenuator and the interpretation of the interference pattern may introduce an error of 6 per cent as indicated in the previous section, but in view of the close correspondence between the calculated and measured values of the horn, this may be reduced to about 4 per cent. The probable error in the gain of the parabolic reflector is then about 7 per cent, and the value of 704 for  $G_0$  has been therefore rounded off to 700. This is the same value as originally determined in the preliminary experiments.

#### Sky Temperature

Sky temperature has been used as one calibration level in view of its great convenience in making repeated calibrations, and because no uncertainties in "zero error" are present when the antenna is shifted from the sun to the sky. The disadvantage is that sky temperature must be determined separately. An accurate determination is not easy, since sky temperature is close to zero degrees, and must be evaluated in the presence of thermal emission from the ohmic losses in the antenna, and emission from the earth as received in the back lobes of the antenna pattern. Sky temperature proper may contain emission from the galaxy and from the earth's atmosphere. Galactic emission in the 10-cm range is very small and has not been detected with the present equipment, while attenuation of solar emission at sunset suggests the possibility of a small 10-cm emission from the earth's atmosphere.<sup>1</sup>

Of the various experiments which were performed in order to determine the sky temperature, the most reliable is a set of measurements taken in 1952 with a four-foot-square aperture horn. The method consisted of substituting two resistive loads as shown in Fig. 3, one at ambient temperature and the other heated to about 550° K. The interchange of resistances was made near the throat of the horn in order to minimize the ohmic losses.

The heated termination was made from carbon coated sand held in place by a piece of asbestos board placed diagonally across the waveguide. The sides of the waveguide were composed of heavy brass, with several small holes so that probing thermometers could

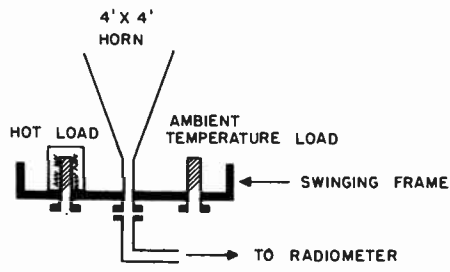


Fig. 3—Switching arrangement at antenna terminals for measurement of sky temperature.

be inserted. Several heating elements were clamped to the sides and controlled separately in order to obtain as uniform a temperature as possible around the sand. The temperature gradient within the load was about 3°. The temperature at the interior of the heated sand was read from a calibrated thermometer and its values used in calculation.

The shift in zero output was minimized by carefully matching to the radiometer the heated load, the ambient temperature load, and the antenna. Since the best possible matching can be obtained only over a small band of frequencies, the upper sideband of the radiometer was suppressed by a waveguide filter, although there was no definite evidence that this refinement was necessary.

For the final experimental setup the power standing-wave ratios to the flat load, heat load, and antenna were measured over the range of wavelengths required. These are shown in Fig. 4. In order to test for zero shift, additional mismatch was put into the waveguide and varied in phase. It was found that for any phase, mismatch differences considerably larger than any present in the system were required in order to produce discernible zero shift in the meter readings.

Eq. (9) gives the apparent sky temperature,  $T_{A2z}$ , in terms of the appropriate meter readings. A calculation of the factor  $1/(1 - \alpha)$  was made as approximately 1.009, which in this case included the attenuation in a short piece of waveguide at the throat of the horn. The following values of apparent sky temperature, in degrees Kelvin, were obtained:

1.5	0	0.5	-4	7.5	15	12.5	24
10.5	-2.5	2.5	1	9	-18.5	23	2.5

The average value is 5.5°; the probable error (aside from the theoretical limit of zero degrees) has been estimated as approximately 6°. This value of 5.5° is the apparent sky temperature for a particular 4-foot x 4-foot aperture horn, and includes the effect of back radiation, which has not been measured. It is assumed that the same value can be used in experiments employing the 3-foot x 4-foot aperture horn, since the back radiation, if not negligible, should not differ greatly for the two antennas. It is doubtful if this value should be used for the four-foot parabolic reflector which is a different type of antenna.

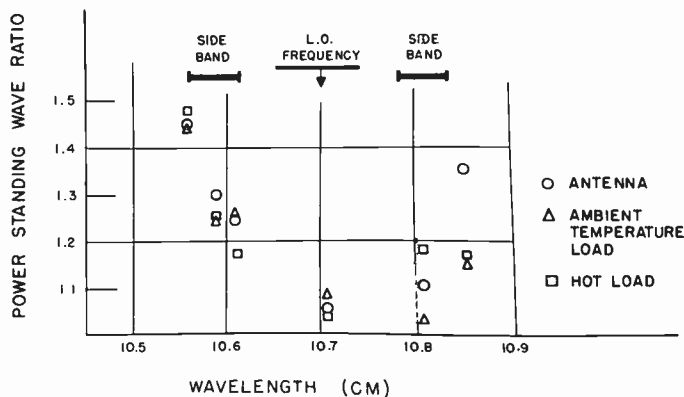


Fig. 4—Power standing-wave ratios of the 4-foot x 4-foot horn antenna, ambient temperature load, and hot load vs wavelength.

### MEASUREMENT OF SOLAR RADIO FLUX WITH HORN ANTENNA

During 1952 and 1953 some measurements of solar radio flux were taken with the 3-foot x 4-foot aperture horn. The associated radiometer was mounted directly behind the horn without any rotating couplers. The whole unit was steerable and could be pointed toward most parts of the sky. The radiometer was calibrated by using the "sky" position, and instead of a black box, a large black mirror which pointed toward the earth. Observations were taken with this instrument on 24 different days and the calculated values of flux,  $F_{horn}$ , may be compared with corresponding flux values obtained with the four-foot reflector,  $F_{reflector}$ . This is shown graphically in Fig. 5, where the values of  $F_{horn}$  have been calculated using an apparent sky temperature of 5.5° K (as measured on the 4-foot x 4-foot horn), and the theoretical value of 428 for the maximum directive gain; while the values of  $F_{reflector}$  have been calculated using the original values of  $G_0 = 700$  and  $T_{A2z} = 50°$  K. Since solar flux varies from day to day, the plots of simultaneous readings are shown as a scatter about the dashed line, which passes through the origin. The solid line represents the ideal case where measurements from the two different instruments give the same values of flux, and the following equation is satisfied:

$$\frac{\rho'}{G_0'} (T - T'_{A2z}) - \Delta x' = \frac{\rho}{G_0} (T - T_{A2z}) - \Delta x. \quad (11)$$

Here  $\rho = (R_1 - R_2)/(R_3 - R_4)$  as before; the symbols with the superscript refer to the 3-foot x 4-foot horn, and the others to the four-foot parabolic reflector.

There is an average discrepancy of about 20 per cent between the flux values as given by the two instruments. The total systematic error in  $F_{horn}$  is approximately 5 per cent, derived from the following estimates of individual parameter errors:  $G_0'$ , 2 per cent;  $T - T_{A2z}'$ , 4 per cent; and  $\rho'$ , 3 per cent. The total systematic error in  $R_{reflector}$  is considerably larger;  $G_0$  is accurate to only 7 per cent and the value of 50° K for  $T_{A2z}$  is not considered reliable in view of subsequent work. The values of

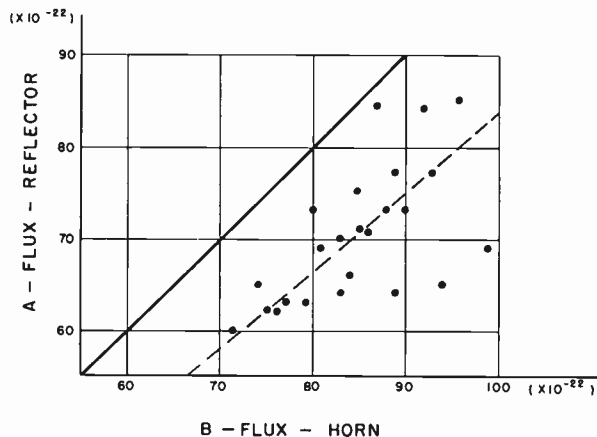


Fig. 5—Flux, as measured with the four-foot parabolic reflector, vs flux, as measured on corresponding days with the 3-foot  $\times$  4-foot aperture horn.

$F_{\text{reflector}}$  are therefore adjusted to conform with the measurements from the 3-foot  $\times$  4-foot aperture horn. From a consideration of the scatter of the observations it has been calculated that this adjustment can be made with an accuracy of 1 per cent, but because of an inconsistency found between readings taken in 1952 and in 1953, this has been revised upward to 4 per cent. Combining this with the accuracy of  $F_{\text{horn}}$ , it is estimated that the daily values of solar flux as measured with the four-foot parabolic reflector, and so adjusted, have a probable error of approximately 7 per cent.<sup>10</sup>

This adjustment of flux values implies an adjustment in one or both of the parameters  $G_0$  and  $T_{A_{2z}}$ . If  $G_0$  is taken as the measured value of 700, then from (11) the weighted mean value of  $T_{A_{2z}}$  is found to be about  $7^\circ$  K. It will be noted that this is an inaccurate method of determining  $T_{A_{2z}}$ , and that other pairs of values of  $G_0$  and  $T_{A_{2z}}$  may reasonably be assumed.

<sup>10</sup> One independent check on this result is available from the measurement of  $i_{\text{sun}}$  by J. S. Hey and V. A. Hughes at 10.5 cm on June 30, 1954; see "A method of calibrating centimetric radiometers using a standard noise source," this issue, p. 119. Their value of  $42,000^\circ$  is in close agreement with the value of  $43,000^\circ$  obtained at Ottawa on the same day.

## CONCLUSION

In 1952, in view of evidence essentially the same as presented in this paper, but with somewhat less data, the values of solar flux were revised.<sup>11</sup> The correction factor<sup>12</sup> to be applied to the original flux values is about 1.18 (1.17 in summer and 1.19 in winter, depending on ambient temperature).

As previously noted there has been an error in the neglect of the term  $\Delta x$  of (8) necessitating a further correction of a seasonal nature. In units of flux (unit =  $10^{-22}$  watts/m<sub>2</sub>/cps) daily values must be reduced by a quantity varying from approximately 5.5 in December to 0.5 in July, for all years previous to, and including, 1954. This is subsequent to the multiplicative correction of 1.18 for the years 1947 to 1952. A complete list of revised values may be obtained from the authors.

The magnitude of the systematic errors in these observations has been discussed and is estimated at  $\pm 7$  per cent. Relative error as between successive daily observations has been estimated from repeated observations taken on a single day during a quiet period. Differences of as much as 2 per cent from day to day are most probably indicative of a real change in solar emission. Seasonal variations or effects due to deterioration of the measuring equipment may cause a larger relative error between values separated by a longer period of time. To minimize instrumental errors, calibrations were taken with two different radiometers, infrequently in 1950 and 1951, and almost continually thereafter.

From a study of possible sources of error, such as zero-shift effects, and a review of the experimental data, it is estimated that a relative error between observations separated by months in time, may be 10 per cent during 1947, 1948, and 1949, and 3 per cent during subsequent years.

<sup>11</sup> A. E. Covington and W. J. Medd, "Variations of the daily level of the 10.7 centimetre solar emission," *J. Roy. Astron. Soc. Can.*, vol. 48, pp. 136-149; July-August, 1954.

<sup>12</sup> "Quarterly Bulletin on Solar Activity No. 104," IAU; October-December, 1953.



# A Method of Calibrating Centimetric Radiometers Using a Standard Noise Source\*

J. S. HEY† AND V. A. HUGHES‡

**Summary**—In order to compare radio-astronomical measurements of power flux observed on different occasions at different wavelengths, special attention must be paid to methods of calibration. A method is described which is suitable for a centimetric radiometer measuring antenna temperature over a range of 0 to 1000°K or more with an accuracy of about 1°K.

The power received by the radiometer is compared with that from a CV1881 argon discharge tube fed through a precision attenuator. An additional fixed amount of power is added to that of the radiometer to ensure that the effective temperature is above that of the room.

The intensity of solar radiation at  $\lambda = 10.5$  cm was measured by this method during the eclipse of June 30, 1954. The scale of the chart recording the radiometer output was effectively increased by adjusting the attenuator in steps each time maximum deflection was attained corresponding to about 20°K change of antenna temperature. Finally, to measure the brightness temperature of the un-eclipsed sun, the received power from the sun was compared with that from a known external noise source consisting of a horn radiator fed by a CV1881 argon discharge tube.

## INTRODUCTION

ACCURATE methods of calibration of radiometers used in radio astronomy are essential so that reliable comparisons can be made between observations on different occasions and at different wavelengths. The received power is usually expressed in terms of the antenna temperature which can be determined by comparing the received noise with that from a thermal noise generator. The radiometer may be required to measure antenna temperatures between 0°K and 10<sup>3</sup>°K, and to vary the temperature of a reference source, such as a resistor, over this range would be inconvenient for general use. This note indicates how a particular discharge tube, in conjunction with a precision attenuator, has been used as a standard variable noise source. The conversion of antenna temperature into brightness temperature of the radio astronomical source, such as the sun, involves a knowledge of the sensitivity pattern of the antenna. A more direct determination of brightness temperature can be achieved by using a standard source as an external radiator. The application of these techniques to a radiometer at  $\lambda = 10.5$  cm which was used for observation of the sun during the eclipse of June 30, 1954, is described.

## THE NOISE SOURCE

Mumford<sup>1</sup> first suggested that the gaseous discharge

\* Original manuscript received, October 14, 1957.

† Ministry of Supply, Royal Radar Est., Malvern, Worcs., Eng.

<sup>1</sup> W. W. Mumford, "A broad-band microwave noise source," *Bell Sys. Tech. J.*, vol. 28, pp. 608-618; October, 1949.

in an ordinary fluorescent lamp might be a suitable source of broad-band noise for measuring the noise factors of receivers. However, mercury-filled tubes are not very stable, and the noise power available depends on the ambient temperature of the tube. Argon discharge tubes were investigated by Johnson and DeRemer<sup>2</sup> and found to be more stable. Measurements at 10.5-cm wavelength by Hughes<sup>3</sup> on the argon tube, CV1881, matched into a waveguide, have shown that for a discharge current of 180 ma, the effective temperature is 11,140°K with a maximum error of 260°K (0.10 db), and that there is a high degree of stability and consistency between tubes. The effective temperature varies slightly with discharge current with the coefficient of  $-0.004$  db per ma. That the noise output of the tube is not critically dependent on frequency is indicated by comparison with measurements made by Sutcliffe<sup>4</sup> at a wavelength of 3 cm, where a similar effective temperature was obtained.

The effective temperature of the noise source may be varied by connecting in series a calibrated attenuator, which both attenuates the noise from the tube and contributes its own noise since it is at room temperature. If the coefficient of attenuation is  $\alpha$ , the effective temperature of the attenuator  $T_0$ , and that of the discharge tube  $T_D$ , then the effective temperature of the variable noise source is given by

$$T = \frac{T_D - T_0}{\alpha} + T_0.$$

Such a source, using an attenuator calibrated to an accuracy of 0.01 db, provided a variable standard temperature noise source for the radiometer now to be described.

## THE RADIOMETER USED FOR ECLIPSE MEASUREMENTS

Radiometers at centimeter wavelengths can measure, by means of wide rf bandwidths and long output time constants, changes of less than 1°K.

To reduce errors due to changes in gain or receiver noise factor, it is necessary not only to switch continually

<sup>2</sup> H. Johnson and K. R. DeRemer, "Gaseous discharge super-high-frequency noise sources," *Proc. IRE*, vol. 39, pp. 908-914; August, 1951.

<sup>3</sup> V. A. Hughes, "Absolute calibration of a standard temperature noise source for use with S-band radiometers," *Proc. IEE*, pt. B, vol. 103, pp. 669-672; September, 1956.

<sup>4</sup> H. Sutcliffe, "Noise measurements in the 3-cm waveband using a hot source," *Proc. IEE*, pt. B, vol. 103, pp. 673-677; September, 1956.

between the received noise from the antenna and a standard source,<sup>5</sup> but also to maintain the output of the standard source not greatly different from that to be measured. During a solar eclipse, a wide variation of antenna temperature occurs.

To fulfill the above requirements, the radiometer circuit, shown schematically in Fig. 1, was constructed. The received power was compared 30 times a second with that from a calibrated argon discharge tube source  $S$  by means of a waveguide switch. The antenna temperature to be measured is often below room temperature. In order to bring the two signals near the same level so as to improve the accuracy of measurement, a second discharge tube  $S'$  was arranged to add, by means of a directional coupler, a constant signal to that received by the antenna. The fine adjustment of the two signals to near equality could then be made by the precision attenuator connected to the reference source  $S$ .

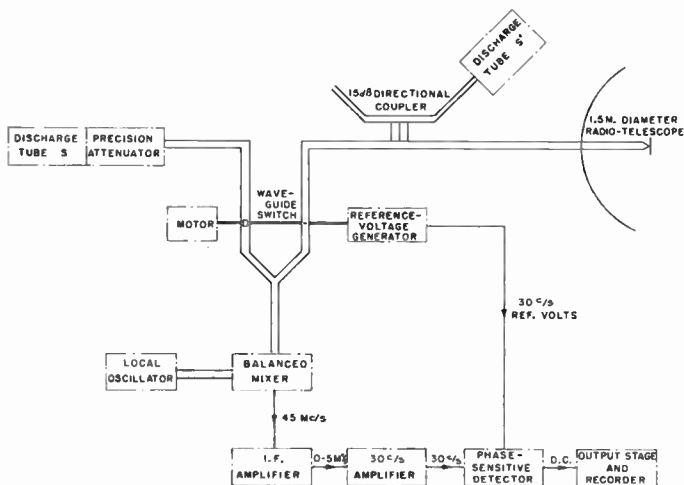


Fig. 1—Block schematic of radiometer.

The radiometer was used to measure the intensity of the radiation from the sun during the eclipse of June 30, 1954. The radiometer antenna which had a beamwidth of about  $4^\circ$  was automatically driven to follow the sun continuously. Prior to the eclipse, the power from the variable noise source was adjusted to equal that received by the antenna plus supplementary fixed noise source, so as to produce zero output from the radiometer. The gain was set so that a full-scale deflection on the recorder corresponded to approximately  $20^\circ\text{K}$  or 10 per cent of the total received power from the sun. As the eclipse progressed and the recorded output approached maximum deflection, the precision attenuator was readjusted to bring the reference signal back to near equality and the output at the recorder near zero again. This sequence was repeated as necessary throughout the eclipse, and a tracing of the recorded output is shown in

<sup>5</sup> R. H. Dicke, "The measurement of thermal radiation at microwave frequencies," *Rev. Sci. Instr.*, vol. 17, pp. 268-275; July, 1946.

Fig. 2. The successive readjustment 1) effectively allows the ordinate of the recording scale to be increased and so improves reading accuracy, 2) reduces the error due to gain fluctuations since the error is proportional to the difference in the two signals which is kept small, and 3) provides repeated calibrations of the recorder scale. By this method and with a time constant of about 10 seconds, the antenna temperature was measured throughout the eclipse to an accuracy better than  $1^\circ\text{K}$  corresponding to less than 0.5 per cent of the antenna temperature of the uneclipsed sun. The results, which were obtained at a site where the eclipse was partial, have been discussed elsewhere.<sup>6</sup>

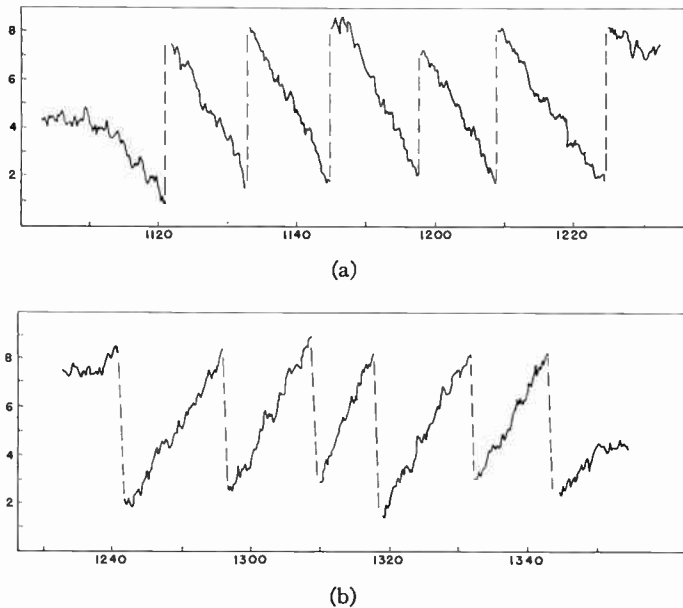


Fig. 2—Recorded output of radiometer during eclipse of June 30, 1954; (a) ordinates—relative power received, (b) abscissas—universal time.

#### BRIGHTNESS TEMPERATURE OF THE SUN

To interpret the power measured by the radiometer in terms of apparent brightness temperature of the solar disk<sup>7</sup> requires an accurate knowledge of the parameters of the antenna and of the losses in the waveguide transmission line between the antenna and waveguide switch. A more convenient method is to produce an external noise radiator of standard brightness temperature to make a direct comparison with the radiation from the sun. Such a comparison source is provided by a waveguide horn fed by an argon discharge tube. This noise radiator then has a brightness temperature equal to the effective temperature of the discharge tube and area equal to the effective area of the horn aperture. The effective area of the horn is directly proportional

<sup>6</sup> J. S. Hey and V. A. Hughes, "Centimetre wave observations of the solar eclipse of 1954 June 30," *Observatory*, vol. 76, pp. 226-228; December, 1956.

<sup>7</sup> The apparent disk temperature is defined as the brightness temperature of a uniformly bright disk equal in size to the observed optical disk.

to gain and it is possible to design a horn with a calculable gain.<sup>8</sup> Hence, if the radiometer antenna is directed towards the noise radiator and the increase in effective temperature noted, then from a knowledge of the distance between radiometer antenna and noise radiator an over-all calibration of the equipment is obtained. The radiator must obviously be sufficiently far away to be outside the Fresnel diffraction zone of the radiometer antenna, and hence limitations are placed on the size of antenna that may be calibrated. (Even with the largest antennas the radiator may be used in the near zone in order to provide a very simple method of comparing the operation of the equipment from day to day.)

The above method was used to obtain the apparent brightness temperature of the sun about the time of the eclipse of June 30, 1954. The radiometer antenna had a diameter of approximately 1.5 meters; and by spacing the noise radiator at a distance of 66 meters, the maximum path difference across the antenna was reduced to  $0.04\lambda$ . The apparent disk temperature of the sun will be given by

$$T_s = \frac{T_{AS}}{T_{AD}} \cdot T_D \frac{G_H \lambda^2}{4\pi R^2} \cdot \frac{1}{\Omega_S}$$

<sup>8</sup> W. T. Slayton, "Design and Calibration of Microwave Antenna Gain Standards," Naval Res. Labs., Washington, D. C., Rep. 4433; November, 1954.

where, under the conditions existing at the time of the calibration,

$T_{AS}$  = antenna temperature of the antenna directed towards the sun.

$T_{AD}$  = change in antenna temperature due to the noise radiator.

$T_D$  = effective temperature of discharge tube.

$G_H$  = gain of horn.

$R$  = distance between radiator and antenna.

$\Omega_S$  = solid angle subtended by optical disk of sun.

$\lambda$  = wavelength.

Substituting the experimental values,  $T_{AS} = 187.5^\circ\text{K}$ ,  $T_{AD} = 10.0^\circ\text{K}$ ,  $T_D = 11,140^\circ\text{K}$ ,  $G_H = 65.3$ ,  $R = 66$  meters,  $\Omega_S = 6.58 \cdot 10^{-5}$  steradians,  $\lambda = 10.5$  cm, the apparent brightness temperature of the solar disk at this wavelength is  $4.2 \cdot 10^4^\circ\text{K}$ . The main inaccuracy involved is in the gain of the horn which was calculated by Slayton's method. It appears unlikely that the error will exceed 5 per cent.

#### ACKNOWLEDGMENT

Acknowledgment is made to the Controller, H.M.B. Stationery Office, England, for permission to publish this paper.



# Measurements of Solar Radiation and Atmospheric Attenuation at 4.3-Millimeters Wavelength\*

ROBERT J. COATES†

**Summary**—Solar radiation and atmospheric attenuation were measured at 4.3-mm wavelength. The sun was scanned with a radio telescope consisting of a 10-foot precision paraboloid antenna (6.7-minute beamwidth) and a Dicke-type radiometer. Atmospheric attenuations were determined from the change in received solar radiation with changing elevation of the sun and from direct measurements of the thermal radiation from the atmosphere. The measured attenuations at the zenith for clear skies were between 1.6 and 2.2 db.

At 4.3-mm wavelength, the sun (when it is free of sunspots) appears to be a uniform disk nearly one per cent larger than its optical size. From a large number of measurements over a period of 6 months, the solar brightness temperature was found to be 7000 °K with an uncertainty of about 10 per cent. Sunspot regions are slightly brighter than the quiet areas; the largest observed enhancement is 2 per cent.

## INTRODUCTION

IN July, 1956, a program of absolute measurements of solar radiation and atmospheric attenuation was initiated at a wavelength of 4.3 mm at the U. S. Naval Research Laboratory. The observing wavelength is in the atmospheric window between the 5-mm oxygen line<sup>1</sup> and the 1.7-mm water-vapor line,<sup>2</sup> and consequently, there is considerable atmospheric attenuation from the wings of these lines. The sun and the moon are convenient signal sources for the measurements of such atmospheric attenuation.

Theoretical studies of the sun<sup>3,4</sup> have shown that solar radiation at millimeter wavelengths originates in the ionized solar atmosphere at a level a few thousand kilometers above the visible surface of the sun. This is thermal radiation from the ionized gas, and therefore, the results of the absolute measurements of this radiation can be used to calculate the characteristics (such as the electron temperature) of the emitting region.

## THE RADIO TELESCOPE

The radio telescope (Fig. 1) used for these observations has a half-power beamwidth of 6.7 minutes of arc. The antenna reflector is an aluminum paraboloid 10 feet in diameter with a focal length of 35.8 inches. This

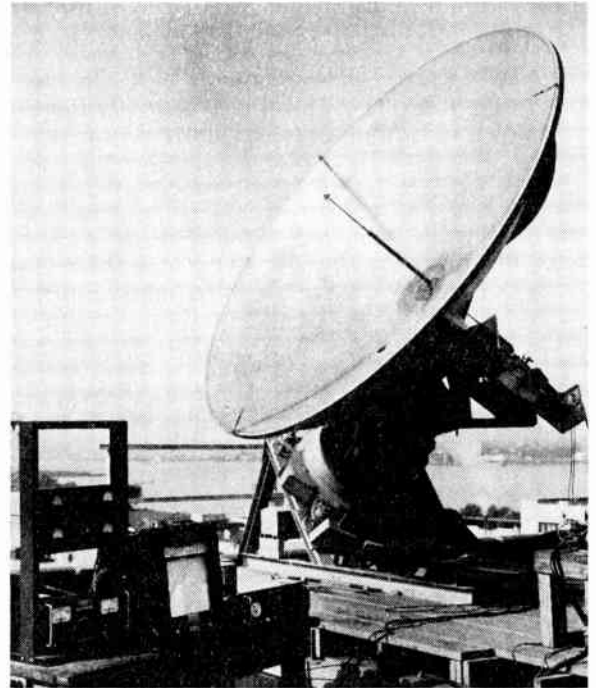


Fig. 1—10-foot radio telescope for 4.3-mm wavelength.

was cast in one piece and machined to sufficient tolerance for use at 4.3-mm wavelength.

A small horn is used to feed the reflector. A specially designed low-loss waveguide section connects the feed horn at the focus of the reflector to the receiver on the back of the antenna. This 4.5-foot section consists of a 16-inch tapered transition from 0.074×0.148 inch ID waveguide to 0.170×0.420 inch ID waveguide, then a long run of the large-size waveguide, followed by a second taper down to the small waveguide. The measured attenuation of this 4.5-foot waveguide section is 1.3 db as compared to 5-db attenuation measured for the same length of the small waveguide.

The polar mount for the antenna is an old radar pedestal, appropriately mounted. The hour-angle drive is controlled with a servosystem and the declination drive is operated manually.

The 4.3-mm receiver on the back of the antenna is a Dicke-type radiometer,<sup>5</sup> consisting of a superheterodyne receiver preceded by a calibrated attenuator and a motor-driven attenuator wheel (which modulates the incoming signal), and followed by an audio amplifier, a synchronous detector, and a recording meter. This

\* Original manuscript received by the IRE, October 3, 1957. This paper was chapter III in the author's Ph.D. dissertation for The Johns Hopkins University, Baltimore, Md.

† Radio Astronomy Branch, U. S. Naval Res. Lab., Wash., D. C.

<sup>1</sup> J. H. Van Vleck, "The absorption of microwaves by oxygen," *Phys. Rev.*, vol. 71, pp. 413-424; April 1, 1947.

<sup>2</sup> J. H. Van Vleck, "The absorption of microwaves by uncondensed water vapor," *Phys. Rev.*, vol. 71, pp. 425-433; April 1, 1947.

<sup>3</sup> J. P. Hagen, "Temperature gradient in the sun's atmosphere measured at radio frequencies," *Astrophys. J.*, vol. 113, pp. 547-566; May, 1951.

<sup>4</sup> S. F. Smerd, "Radio-frequency radiation from the quiet sun," *Aust. J. Sci. Res. A.*, vol. 3, pp. 34-59; March, 1950.

<sup>5</sup> R. H. Dicke, "The measurement of thermal radiation at microwave frequencies," *Rev. Sci. Instr.*, vol. 17, pp. 268-275; July, 1946.

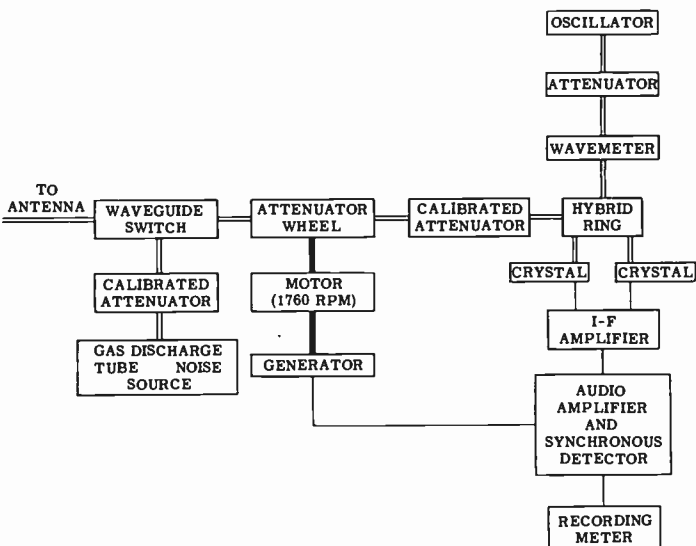


Fig. 2—Diagram of 4.3-mm radiometer.

arrangement is shown in the block diagram of the radiometer (Fig. 2) and in the photograph (Fig. 3).

When an observation is made with the radiometer, the signal from the antenna passes through the waveguide switch and is modulated by the attenuator wheel at a frequency of about 29.3 cps. The calibrated attenuator is set at zero attenuation and the modulated signal passes through to the balanced mixer consisting of the hybrid ring and the matched pair of crystals. The output from the mixer goes to the IF amplifier, which has a center frequency of 30 mc and a bandwidth of 5.5 mc. The audio output from the detector stage of the IF amplifier is amplified and detected in the synchronous detector. The synchronous-detector output is recorded on a Leeds and Northrop "Speedomax" recorder.

During calibration, the receiver is connected to the gas-discharge tube noise source<sup>6</sup> through the waveguide switch. This noise source was calibrated against a matched waveguide termination maintained at a uniform temperature of 620°C.

#### MEASUREMENTS

The observational program was designed to obtain scans across the sun for determining the brightness distribution, and to measure the atmospheric attenuation and the solar antenna temperatures for determining the solar brightness temperature. When observing, the antenna was pointed ahead of the sun and locked in position, and the radiometer output was recorded continuously as the earth's rotation carried the sun through the antenna beam. After the sun was past the antenna and the sky radiation had been recorded for a few minutes, 40 db of attenuation was inserted with the attenuator to give a zero-input reference reading. The receiver

<sup>6</sup> A. I. Reynard, "Precision Instruments for Calibrating Radiometers at 4.3 Millimeters Wavelength," Naval Res. Lab., Washington, D. C., Rep. 4927; May, 1957.

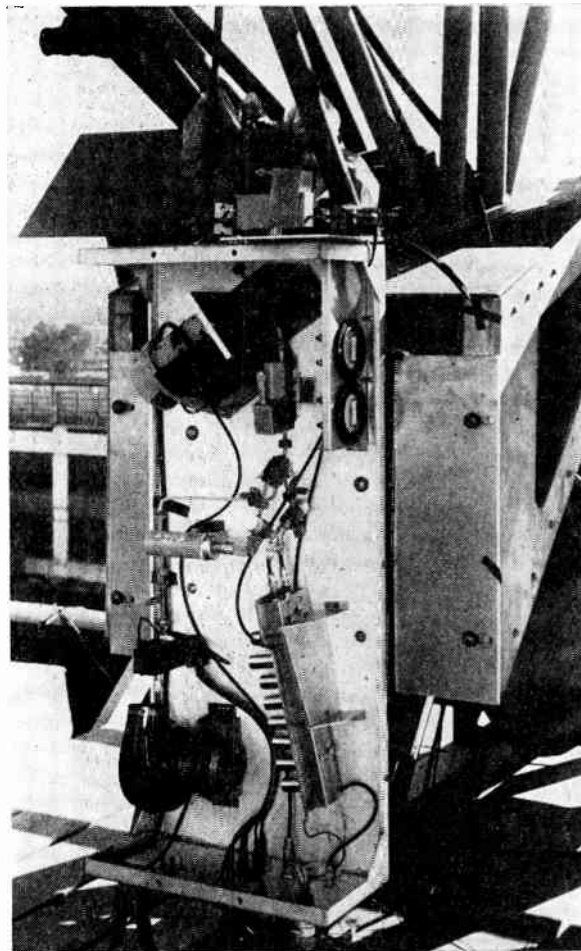


Fig. 3—4.3-mm radiometer.

was next switched to the gas-discharge noise source for measuring the receiver gain. After the gain measurement, the receiver was switched back to the antenna, the antenna was set ahead of the sun, and the sequence was repeated. In the middle of each sun scan, the sun was photographed through the optical sighting telescope with a 35-mm camera to record the path taken on each scan. The measurements were started when the sun was low in the sky and continued until the sun had passed the meridian. The series of measurements was broken once or twice for a complete radiometer calibration;<sup>7</sup> several times during a sequence of measurements the recording of the sky radiation was followed by several measurements of the radiation from an ambient black-body enclosure placed over the feed horn. This enclosure was a metal can lined on the inside with non-reflecting material. There was a small hole in the lid to

<sup>7</sup> The radiometer calibration procedure was as follows: the receiver was switched to the gas-discharge noise source, and the receiver attenuator was set to produce approximately a full-scale reading on the recorder. The output of the noise source was then attenuated in successive small steps by the calibrated attenuator between the noise source and the receiver, and the receiver output was recorded for each step covering the range between the zero level and full scale. A transcription of these readings gave a graph of input noise temperature vs recorder reading.

permit placement over the antenna feed horn. The wall lining was selected and mounted so that the impedance of the feed horn was the same with or without the can surrounding it. This is important because a different impedance would cause an error in the recording of the radiation from the can with respect to the recordings of the sky and the sun.

ANALYSIS

The power received from a thermal source usually is given in units of antenna temperature  $T$ , defined<sup>8</sup> as the temperature of a matched termination for which the available power at its terminals, in a frequency band between  $f$  and  $f+df$ , is equal to the received power  $P$  at the antenna terminals; *i.e.*,  $P=kTdf$ , where  $k$  is Boltzmann's constant. Antenna temperature is a convenient unit because the radiometer is calibrated by replacing the antenna with a matched noise source at a known effective temperature.

At a given wavelength, the brightness of a source is often specified in terms of a "brightness temperature," defined as the temperature of a black body at the source location for which the brightness of the thermal radiation would equal that actually observed.

When the antenna is pointed at the sun, the antenna temperature  $T_{\text{sun}}$  is given by

$$T_{\text{sun}} = \alpha_0 \int_{4\pi} \frac{A}{4\pi} [t_{\text{sun}}\alpha + t_e\alpha + (1 - \alpha)t_{\text{sky}}]d\Omega + (1 - \alpha_0)t_0 \tag{1}$$

where  $\alpha_0$  and  $t_0$  are the transmission and temperature, respectively, of the waveguide between the feed horn and the receiver;  $A$  is the gain pattern of the antenna;  $\alpha$  is the transmission of the atmosphere;  $t_{\text{sun}}$  is the brightness temperature of the sun;  $t_e$  is the brightness temperature of the ground;  $t_{\text{sky}}$  is the effective temperature of the atmosphere; and  $d\Omega$  is an element of solid angle.  $A$ ,  $t_{\text{sun}}$ ,  $\alpha$ ,  $t_e$ , and  $t_{\text{sky}}$  are functions of position. Radiation from radio stars and galactic background has been neglected, because at wavelengths as short as 4.3 mm this radiation is exceedingly small, as one can verify by extrapolating the radio source spectra<sup>9</sup> to short wavelengths. To date, radio stars have not been detected at millimeter wavelengths.

When the antenna is pointed at the sky, the antenna temperature  $T_{\text{sky}}$  is given by

$$T_{\text{sky}} = \alpha_0 \int_{4\pi} \frac{A}{4\pi} [t_e\alpha + (1 - \alpha)t_{\text{sky}}]d\Omega + (1 - \alpha_0)t_0. \tag{2}$$

In the series of sun scans just described, the antenna was fixed in position during each sun scan and a recording was made of both the sun and the sky at the same

position. The antenna temperature  $T_{\text{sun}}$ , with the sun in the center of the antenna beam, and the antenna temperature  $T_{\text{sky}}$ , with only sky in the beam, were deduced from the records for each sun scan with the aid of the calibration curve, gain measurements, and the ambient measurements. Thus, values of  $T_{\text{sun}}$  and  $T_{\text{sky}}$  were obtained at many antenna positions starting at a large zenith angle and ending at the minimum zenith angle at the meridian.

At each antenna position,  $\alpha$  can be considered as constant over the angle subtended by the sun; and therefore, subtracting (2) from (1),

$$T_{\text{sun}} - T_{\text{sky}} = \alpha_0\alpha \int_{\text{sun}} \frac{A}{4\pi} t_{\text{sun}}d\Omega = \alpha_0\alpha\Theta_{\text{sun}}$$

where  $\Theta_{\text{sun}}$  is the antenna temperature for the sun in the absence of atmospheric and waveguide losses.

For a uniform clear sky and zenith angles  $z$  less than  $80^\circ$ ,  $\alpha$  can be expressed in terms of the zenith transmission  $\alpha_0$  by  $\alpha = \alpha_0^{\sec z}$ . It follows that

$$\log (T_{\text{sun}} - T_{\text{sky}}) = \sec z \log \alpha_0 + \log (\alpha_0\Theta_{\text{sun}}).$$

Thus the attenuation at the zenith ( $-10 \log \alpha_0$ ) is obtained from the slope of a plot of  $\log (T_{\text{sun}} - T_{\text{sky}})$  vs  $\sec z$ , and the value of  $\Theta_{\text{sun}}$  is obtained from the extrapolated intercept at  $\sec z = 0$ . A typical plot is shown in Fig. 4.

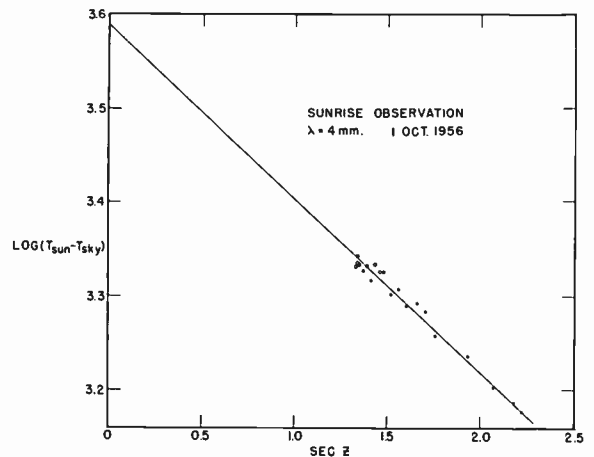


Fig. 4—Plot of  $\log (T_{\text{sun}} - T_{\text{sky}})$  vs  $\sec z$  for October 1, 1956.

Atmospheric attenuation also was calculated from the magnitude of the thermal emission from the atmosphere given in (2). With a narrow beam antenna that has very low side lobes, such as used in this investigation, the integral of the antenna pattern over the main beam and the first few side lobes is much larger than the integral over the remaining part of the  $4\pi$  solid angle. The thermal radiation from the sky is relatively high at  $\lambda$  4.3 mm because of the large attenuation. Therefore, for a first approximation, only the main beam and first few side lobes need be considered, and the atmospheric attenuation is essentially constant over

<sup>8</sup> J. L. Pawsey and R. N. Bracewell, "Radio Astronomy," Oxford Univ. Press, London, Eng., p. 21; 1955.

<sup>9</sup> N. G. Roman and F. T. Haddock, "A model for nonthermal radio-source spectra," *Astrophys. J.*, vol. 124, pp. 35-42; July, 1956.

this small angle. With this approximation, (2) may be written

$$T_{\text{sky}} = \alpha_0(1 - \alpha_0^{\text{sec } \theta})t_{\text{sky}} + (1 - \alpha_0)t_\theta. \quad (3)$$

In practice, it is very difficult to determine the absolute value of  $T_{\text{sky}}$  with high accuracy, because the radiometer output is affected by the impedance at the radiometer input. With a properly balanced mixer, a well-matched antenna, and a well-matched noise source, this effect is small but still not negligible. With the sun scans,  $T_{\text{sun}}$  and  $T_{\text{sky}}$  were measured in succession, and the impedance at the input of the radiometer was the same for both measurements. Therefore the errors resulting from the impedance effect were the same and canceled out in the reduction of the data when  $T_{\text{sky}}$  was subtracted from  $T_{\text{sun}}$ .

In order to cancel the impedance error in the measurement of the radiation from the atmosphere, the black-body enclosure at temperature  $t_c$  was placed over the antenna feed horn and the recorded antenna temperature  $T_c$  was subtracted from  $T_{\text{sky}}$ . Since  $T_c = \alpha_0 t_c + (1 - \alpha_0)t_\theta$ , subtracting  $T_c$  from (3) gives

$$T_c - T_{\text{sky}} = \alpha_0[t_c - (1 - \alpha_0^{\text{sec } \theta})t_{\text{sky}}].$$

This equation was used to compute  $\alpha_0$  from the measured values. Since the major part of the absorption occurs near the ground, the effective sky temperature  $t_{\text{sky}}$  was assumed to be approximately the air temperature near the ground.

The atmospheric attenuation at the zenith, deduced by both methods, and the values of the zero-loss antenna temperature for the sun are listed in Table I for several series of measurements made over a period of 6 months. Also included in Table I are results obtained from a measurement of a moonrise.<sup>10</sup> The measured vertical atmospheric attenuations for 4.3 mm were between 1.6 and 2.2 db for clear skies.

A few cloud observations, made by tracking the sun as clouds passed over, indicate additional attenuations of about 0.7 db for fair weather cumulus clouds. Further cloud measurements are in progress and the results will be reported at a later date.

The average of the solar measurements gives 5605°K for the observed solar antenna temperature, after correcting for atmospheric and waveguide attenuation. In order to convert this value to a solar brightness temperature, one must consider the directional character-

<sup>10</sup> This moonrise observation was at a lunar phase of two days before full moon. The procedure used for this observation was identical to that described for the sun; *i.e.*, repeated scans were made across the moon starting with the moon on the horizon and continuing until it passed the meridian. The scans were asymmetrical and showed that at 4.3-mm wavelength the sunlit part of the moon's surface is brighter than the dark part. The antenna temperature given in Table I was determined from the peak of each scan. Scans of the moon also have been made at a phase of 5 days before new moon, and the asymmetry of these scans verifies that the sunlit crescent is brighter than the dark portion. These observations are continuing and a more detailed analysis will be made after the completion of measurements for all phases of the moon.

TABLE I  
MEASURED ATMOSPHERIC ATTENUATIONS  
AND ANTENNA TEMPERATURES

Source	Date	Vertical Atmospheric Attenuation		Corrected Antenna Temperature $\Theta$
		A) Sunrise and Moonrise Measurements	B) Atmospheric Radiation Measurements	
Sun	September 10, 1956	1.8 ± 0.3 db	—	5330°K
	October 1, 1956	1.9 ± 0.1	2.0 ± 0.2 db	5620
	October 12, 1956	—	2.2 ± 0.3	5956
	November 15, 1956	1.6 ± 0.2	1.7 ± 0.3	5250
	December 4, 1956	1.6 ± 0.2	1.8 ± 0.3	5594
	February 12, 1957	—	1.9 ± 0.2	5880
Moon	November 15, 1956	1.7 ± 0.3	1.8 ± 0.3	202°K

Average  $\Theta_{\text{sun}} = 5605^\circ\text{K}$ .

istics of the antenna. If the antenna were completely surrounded by a source at a certain brightness temperature, then the antenna temperature would be equal to the brightness temperature. When the source does not completely surround the antenna, then the ratio between the antenna temperature and the brightness temperature is equal to the ratio of the integral of the antenna pattern over the source to the integral of the antenna pattern over  $4\pi$  solid angle. The 10-foot antenna at 4.3-mm wavelength has a beamwidth of  $\frac{1}{3}$  the diameter of the sun. Thus, the main beam and the first side lobe are entirely on the Sun, and the rest of the side lobes are off the sun.

By considering the antenna pattern, the antenna temperatures for the moon, and longer wavelength measurements with the Naval Research Laboratory 50-foot antenna, it was estimated that the observed antenna temperature is about 20 per cent lower than the solar brightness temperature. Therefore, dividing 5605° by 0.8 gives a value of  $7000^\circ \pm 700^\circ\text{K}$  for the 4.3-mm brightness temperature for the central region of the sun. The uncertainty is due mainly to the estimate of the 20 per cent factor.

#### THE SOLAR BRIGHTNESS DISTRIBUTION

Since July, 1956, numerous scans with the 4.3-mm telescope have been made across the solar disk under various sunspot conditions. Fig. 5 shows a scan across an active sunspot region on February 18, 1957, in which the increase in radiation from the active area is quite apparent. This is the largest sunspot enhancement observed at this wavelength. Scans across many other sunspots showed no detectable increase. Future research will investigate the characteristics of this enhanced radiation.

Only scans made across areas free from sunspots are usable for determining the brightness distribution for the quiet sun. The best scans for this purpose were made on February 12, 1957, and one of them is shown in Fig. 6(a). The path of that scan [illustrated in Fig.

6(b)] was across the center of the solar disk, and therefore it was well suited for determining the brightness distribution and the solar diameter at 4.3-mm wavelength.

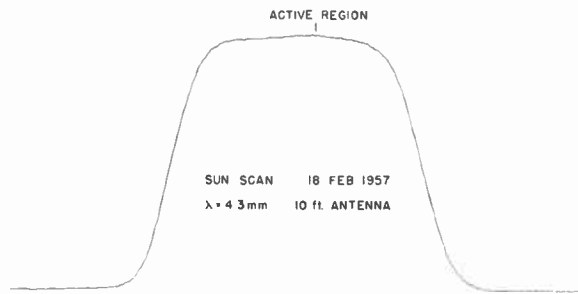


Fig. 5—A 4.3-mm scan across an active region on the sun on February 18, 1957.

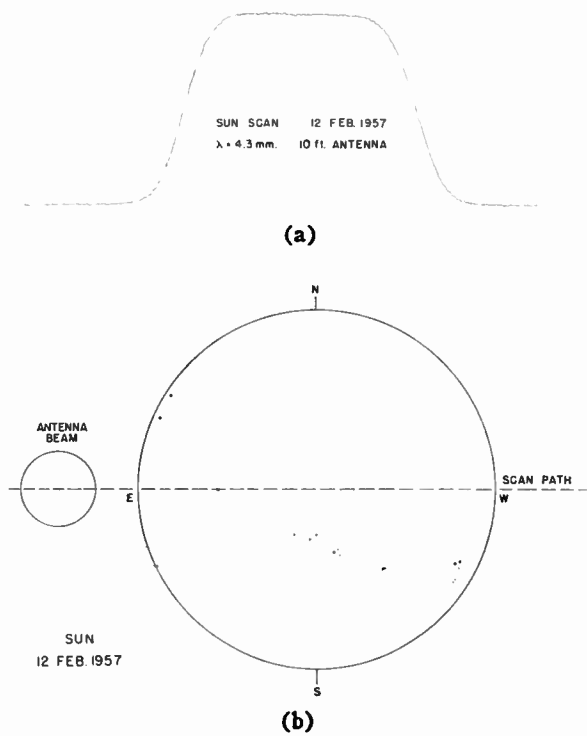


Fig. 6—(a) A 4.3-mm scan across a quiet region of the sun. (b) Map of scan path showing positions of sunspots.

Several theoretical sun scans were calculated for comparison with the observations. This involved integrating the antenna pattern over the sun [as set up in (1)] at successive positions of the sun relative to the antenna. Scans were calculated for a range of different solar diameters and brightness distributions. Fig. 7 shows a comparison between the observed solar scan, and one computed for a uniform sun equal in diameter to the optical disk. This comparison indicates that the 4.3-mm sun is larger than the optical sun. The best fit to the observations is obtained with a uniform disk one per cent larger than the optical disk. The scan for this model fits the observed scan within the experimental uncertainty over the entire curve. The agreement between this calculated curve and the observed curve, and the difference between it and the optical-disk curve, lead to the conclusions that the diameter of the 4.3-mm sun is  $1.01 \pm 0.005$  relative to the optical diameter, and the brightness temperature distribution is essentially uniform. The average brightness temperature of any 7-minute diameter area does not differ from the rest of the quiet sun by more than one per cent.

Since the above observations indicate that at 4.3-mm wavelength the sun is a uniform disk with a brightness temperature of  $7000^\circ\text{K}$  and a diameter about one per cent larger than the optical disk, the 4.3-mm radiation must originate in the lower chromosphere at heights less than 6000 km above the photosphere. From these data it may be concluded that the electron temperature of the emitting gas is of the order of  $7000^\circ\text{K}$  or less.

ACKNOWLEDGMENT

The author expresses his appreciation for the steady encouragement and valuable advice given by Dr. D. E. Kerr, Associate Professor of Physics of The Johns Hopkins University. Appreciation is also expressed to Dr. J. P. Hagen of the Naval Research Laboratory who originally suggested this area of research. Acknowledgment is made to A. E. Reynard for the development of the standard noise sources used to calibrate the 4.3 radiometer and to S. Edelson who helped operate the 4.3-mm radio telescope.

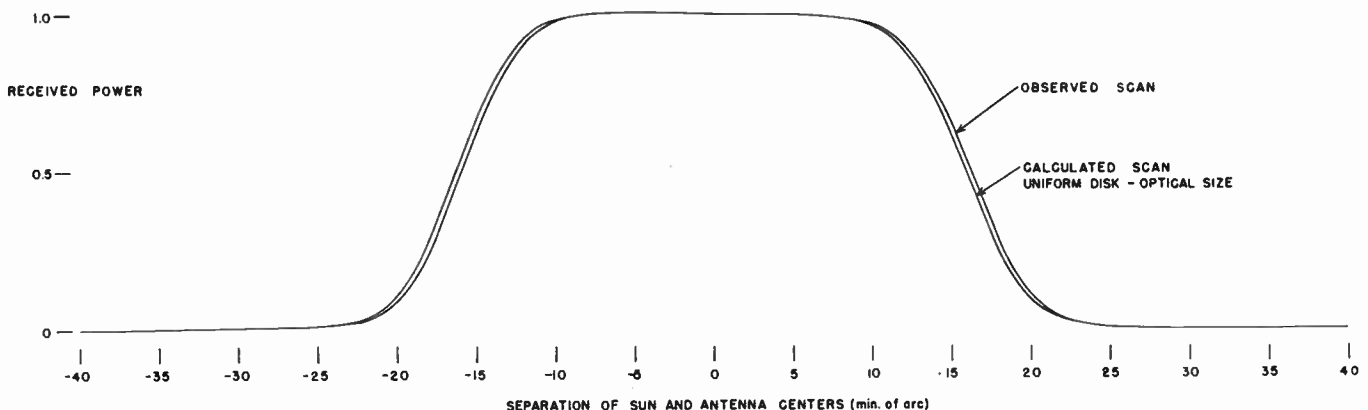


Fig. 7.—The observed 4.3-mm sun scan compared to a calculated scan for a uniform sun equal in diameter to the optical disk.

# Scanning the Sun with a Highly Directional Array\*

W. N. CHRISTIANSEN† AND D. S. MATHEWSON†

**Summary**—A survey is given of the very highly directive equipment and methods which have been devised to obtain details of the distribution of radio emission over the solar disk. A new instrument is described; it operates on a wavelength of 21 cm and gives, for the first time, radio pictures of the sun. This radio heliograph combines principles of the multielement interferometer and the Mills Cross. It consists of 64 parabolic antennas, 19 feet in diameter, arranged along two lines, each 1240 feet in length, in form of a cross.

Multiple pencil beams about 3' arc wide are produced by the system; by means of these, the sun is scanned television-wise. The radio heliograph is being used to produce daily pictures of the sun.

## I. INTRODUCTION

AMONG the millions of stars visible through telescopes, the sun alone is close enough to be seen in detail. Pictures of the sun taken in selected parts of the visible spectrum have told us of the existence in the solar atmosphere of vast disturbances, flares, prominences, and other unexpected features of the sun's atmosphere. The sun is a star of a common type and such solar observations have application to stars in general. The observations throw light also on the origin of some of the profound effects produced by the sun on the earth.

However, despite decades of optical studies the essential mechanisms at work in the solar atmosphere remain a mystery.

The discovery of radio waves from the sun about fifteen years ago provided a tool for investigating parts of the sun's atmosphere inaccessible to optical observations and gave promise of new information which might solve some of the problems of the sun. The discovery suggested immediately the possibility of producing radio "pictures" of the sun, but no antennas then in existence were capable of seeing detail in an object which subtends an angle of only one half of a degree. Nevertheless, means for obtaining directional information were developed and these have now reached the stage where we can obtain actual pictures using 21-cm radio waves.

This paper outlines the development of these directional methods and describes the new radio heliograph in operation at the Radiophysics Laboratory in Sydney.

## II. DEVELOPMENT OF DIRECTIONAL METHODS

An eclipse of the sun observed by Dicke and Beringer<sup>1</sup> provided the first directional discrimination in the study of solar radio waves. As the moon obscures the sun's disk it progressively cuts off the radiation from the different

parts of the sun and, if the actual emission is steady, the variation of received radiation with time gives information about the distribution of radio brightness over the solar disk; e.g. the covering of a small bright patch leads to a sudden decrease in received radiation. This method was used by Covington<sup>2</sup> to show the existence of a bright patch round a sunspot group. It was extended by Christiansen, Mills, and Yabsley<sup>3</sup> to locate bright areas by a sort of triangulation. They used simultaneous observations at places separated by hundreds of miles and located highly emitting spots at the intersections of arcs which represented the position of the edge of the moon at the times of sudden changes in received radiation. However, the method is severely limited; it can give information only at times of eclipses; it is open to serious ambiguities, and it fails if the solar emission itself varies during the eclipse.

The first application of a more conventional radio directional method was made by McCready, Pawsey, and Payne-Scott<sup>4</sup> when they observed on 200 mc the interference pattern as the sun rose over the sea. Interference occurs between the direct and sea-reflected waves and minima occur at known angles of elevation. From the position of minima they deduced the position of the radio source on the sun and, from the ratio of maximum to minimum, the angular size of the source. The position coincided with a very great sunspot on the sun at that time and the size was of the order, not of the sun, but of the sunspot. There would also have been an extended source corresponding to the body of the sun but at this time it was overshadowed by intense radiation from the sunspot region.

Observations such as these combined with systematic observations of the variation of intensity from the whole sun led to the recognition that the radiation from the sun could be divided into several categories. These are:

- 1) A group of components, prominent at meter wavelengths, which show rapid variations.
- 2) A component, prominent at decimeter wavelengths, which varies slowly over weeks or months. This originates in bright areas which have some connection with sunspots and is known as the "slowly varying component."

\* A. E. Covington, "Micro-wave solar noise observations during the partial eclipse of November 23, 1946," *Nature*, vol. 195, pp. 405-406; March, 1947.

† W. N. Christiansen, D. E. Yabsley, and B. Y. Mills, "Measurements of solar radiation at a wavelength of 50 centimetres during the eclipse of November 1948," *Aust. J. Sci. Res. A.*, vol. 2, pp. 506-523; December, 1949.

‡ L. L. McCready, J. L. Pawsey, and Ruby Payne-Scott, "Solar radiation at radio frequencies and its relation to sunspots," *Proc. Roy. Soc. A.*, vol. 190, pp. 357-375; August, 1947.

\* Original manuscript received by the IRE, October 3, 1957.

† Radiophysics Laboratory, CSIRO, Sydney, Australia.

<sup>1</sup> R. H. Dicke and R. Beringer, "Microwave radiation from the sun and moon," *Astrophys. J.*, vol. 103, pp. 375-376; May, 1946.

- 3) A component which is steady over months or years, at least, and is identified with the thermal radiation from the "quiet" sun.

The cliff interferometer may be considered as a two-element interferometer in which the two elements are the actual antenna and its image in the sea. An interferometer formed by two spaced antennas connected in parallel to a receiver is essentially similar and was first used in radio astronomy by Ryle and Vonberg.<sup>5</sup> The principle has been adapted to the observation of bursts of short duration by Little and Payne-Scott<sup>6</sup> who used a phase-swept version in which the antenna pattern was swept across the sun in a fraction of a second by a phase modulating the signal from one of the two antennas. They were able to show that the sources of certain solar bursts moved rapidly over the disk of the sun.

The two-element interferometer is still of value in solar studies, as it is the only method yet available to study the position, size, and motion of very short-lived disturbances. But apart from the restriction to one dimension, it has a basic deficiency. It relies, essentially, on direction finding by means of a zero in the directional pattern. Such direction finders cannot cope effectively with signals arriving simultaneously from a number of directions except in very special cases where something of the form of the distribution is known. It, therefore, is not adapted to the study of the complex distribution of radio brightness which is characteristic of the sun at decimeter wavelengths.

The simple two-element interferometer gives the position and a crude measure of the size of a source in a particular direction. It was pointed out by McCready, *et al.*<sup>4</sup> that observations at a single antenna separation, or height in the case of the cliff interferometer, gave the amplitude and phase of one component of the Fourier distribution of radio brightness measured one dimensionally (in strips) across the solar disk. A series of measurements at different separations would lead to a series of Fourier coefficients from which the complete strip distribution could be synthesized. This method was used by Stanier<sup>7</sup> to determine the one dimensional brightness distribution across the "quiet sun" at a wavelength of 60 cm. He did not measure the phase of his Fourier components but assumed them to be all the same, which implies a symmetrical source. His observations determined the distribution in an east-west direction; *i.e.*, the integrated emission in a series of north-south strips over the sun. Attempts some years later to repeat these measurements gave results which conflict with Stanier's. The disagreement may be due to a real

change in the distribution of brightness over the sun associated with change in the sunspot cycle or may be due to an error to which this type of measurement is particularly prone. Stanier attempted to eliminate the effect of the slowly varying component by working at times when he believed it to be absent. It is very difficult with such indirect observations to be sure of this and residuals of this component may have produced errors in the derived brightness distribution.

Stanier's measurement gave the distribution of brightness in one dimension only. In order to arrive at a result having simple physical significance he postulated that the sun is radially symmetric and so derived the consequent radial distribution. An important extension to two dimensions was made by O'Brien<sup>8</sup> who showed how, using a two-dimensional Fourier method, the two-dimensional brightness distribution could be derived from the interference patterns obtained at a series of antenna spacings in a series of directions covering the whole 180°.

This method is important in radio astronomy because two-element interferometers can operate at great spacings. It permits, in principle, the determination of very fine detail. Nevertheless, in practice it is exceedingly cumbersome involving, as it does, measurements with a great range of antenna spacings repeated in all directions; this is true even if a symmetrical source is assumed, so that only amplitudes and not phases of the different Fourier components need be measured. In general, phases also must be measured and this involves much more labor. This objection is particularly pertinent in the case of the sun because the whole series of observations must be completed before the emission pattern can vary. It has been applied to the "quiet sun" (a symmetrical source) at wavelengths of 60 cm and 140 cm.

While the multispaced, multidirectional interferometer technique was being developed in England, the construction of antennas, very large in one dimension, was in progress in Canada and Australia. Covington<sup>9</sup> built a slotted wave guide 450 wavelengths long which produced a knife-edge beam 8' arc wide at a wavelength of 10 cm. At the same time there was developed in Sydney<sup>10</sup> a multielement interferometer or "grating" (from the analogy with an optical diffraction grating) interferometer. The first multielement interferometer, which was built by one of the authors, consisted of thirty-two 6-foot diameter parabolic antennas equally spaced along an EW line 1000 wavelengths over all. It gave a series of knife-edged beams, each 3' arc to half power, through which the sun passed in succession. This "strip scan-

<sup>5</sup> M. Ryle and D. D. Vonberg, "Solar radiation on 175 mcs," *Nature*, vol. 158, pp. 339-340; September, 1946.

<sup>6</sup> A. G. Little and Ruby Payne-Scott, "The position and movement on the solar disk of sources of radiation at a frequency of 97 mcs," *Aust. J. Sci. Res. A.*, vol. 4, pp. 489-507; December, 1951.

<sup>7</sup> H. M. Stanier, "Distribution of radiation from the undisturbed sun at a wavelength of 60 cm.," *Nature*, vol. 165, pp. 354-355; March, 1950.

<sup>8</sup> P. A. O'Brien, "The distribution of radiation across the solar disk at metre wave-lengths," *Mon. Not. Roy. Astron. Soc.*, vol. 113, pp. 597-612; May, 1954.

<sup>9</sup> A. E. Covington and N. W. Broten, "Brightness of the solar disk at a wavelength of 10.3 cm.," *Astrophys. J.*, vol. 119, pp. 569-589; May, 1954.

<sup>10</sup> W. N. Christiansen and J. A. Warburton, "The distribution of radio brightness over the solar disk at a wavelength of 21 cm, I," *Aust. J. Phys.*, vol. 6, pp. 190-202; June, 1953.

ning" instrument showed clearly the existence of the bright disturbed areas responsible for the slowly varying component. These areas gave rise to peaks on the records which stood up above the "quiet sun" level. They moved across the solar disk with the rotation of the sun and tended to endure for a month or months.

A second 16-element interferometer was built at right angles to the first and with the two it became possible during the course of a year to obtain strip scans covering almost the whole range of directions from north-south to east-west. From the numerous scans available in each direction the contribution due to the "quiet sun" was recognized as the lower envelope of the scans and, using an extension of the two-dimensional Fourier method introduced by O'Brien, the distribution of 21-cm radio brightness over the "quiet sun" was derived.

The success of the strip-scanning technique was due largely to the circumstance that the antennas were constructed for use during the sunspot minimum phase of the solar cycle, so that the individual sources of radio emission on the sun were not numerous. With the change in the solar cycle it became apparent that the complicated situation on the sun, near the time of sunspot maximum, could be resolved only by the development of a much more highly directional antenna system on which the sun could be scanned by a pencil beam of size no more than 3' arc.

For a study of the slowly varying component the wavelength should be in the range from about 10 to 50 cm in which this component is very prominent.

We now turn to the description of the new instrument which scans the sun television-wise at a wavelength of 21 cm with a pencil beam of diameter 3' arc. A further instrument for use at 10 cm is being developed by R. N. Bracewell at Stanford University, California.

### III. THE PRINCIPLE OF THE CROSSED MULTIELEMENT INTERFEROMETER

The new instrument combines the principles of the multielement interferometer<sup>10</sup> and the Mills Cross.<sup>11</sup> It consists of two multielement interferometers placed at right angles to each other in cross formation. Each multielement interferometer produces a series of knife-edged antenna lobes and the two sets at right angles form a grid. The phase switching principle is then used to produce, from this, a number of pencil-beam lobes situated at the points of intersection in the grid.

The multielement interferometer consists of an array of identical antennas spaced at equal intervals, considerably greater than the antenna width, along a line. A photograph of the original instrument is shown in Fig. 1. If the array were continuous a single main antenna lobe would be produced, but the effect of the wide gaps in the array is to produce multiple main lobes. The directivity of such an array is calculated by use of the

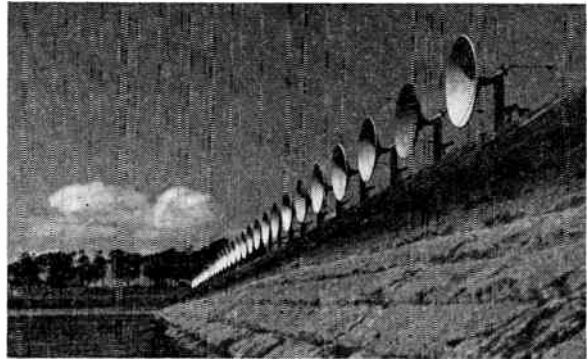


Fig. 1—The first 32-element interferometer at Potts Hill, near Sydney.

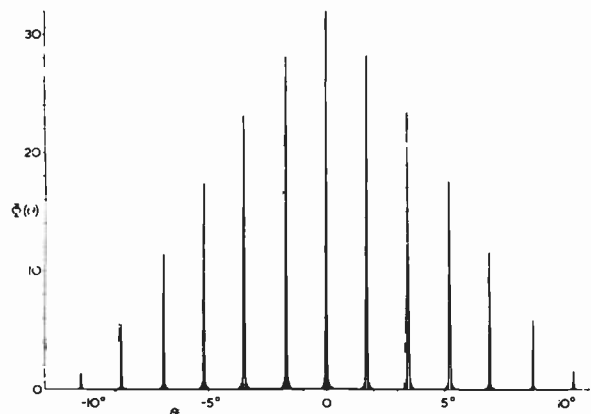


Fig. 2—Directivity of 32-element interferometer at Potts Hill  $\Phi(\theta)$  is power flux compared with that from one element of the array.  $\theta$  is the azimuth angle.

well-known expression for a one-dimensional array of radiating elements; a typical directivity diagram is shown in Fig. 2. Each of the main lobes has a width which is practically identical with that of a continuous array of the same over-all length. The spacing between adjacent lobes is dependent on the spacing between adjacent antennas of the array, the smaller the spacing of antennas the greater being the spacing between antenna lobes.

For solar observations this spacing is made large enough so that no two antenna lobes can fall on or close to the sun at the same time. Since at decimeter wavelengths the sun is the only bright body in the sky, the array then has effectively only a single lobe. The advantage of the multiple lobes, however, is that the sun may be repeatedly scanned by one lobe after another with no necessity to steer the array. Individual elements of the array, of course, must be steered since their individual directivity provides an envelope to the array directivity pattern and this envelope must be moved to follow the sun in its course through the sky.

In the crossed form of the multielement interferometer the antennas are arranged as in Fig. 3. The multielement interferometers individually produce a set of knife-edged antenna lobes as shown in Fig. 4. The outputs from these two systems are not added directly. The output of one is phase modulated, the phase being

<sup>11</sup> B. Y. Mills and A. G. Little, "A high resolution system of a new type," *Aust. J. Phys.*, vol. 6, pp. 272; September, 1953.

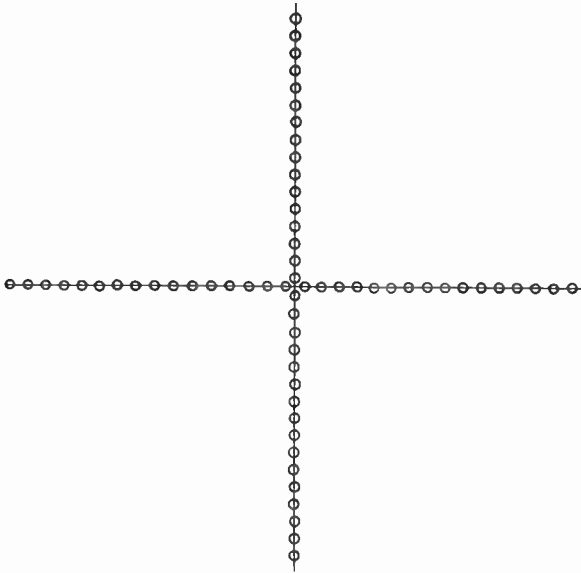


Fig. 3—Plan view of a crossed multielement interferometer.

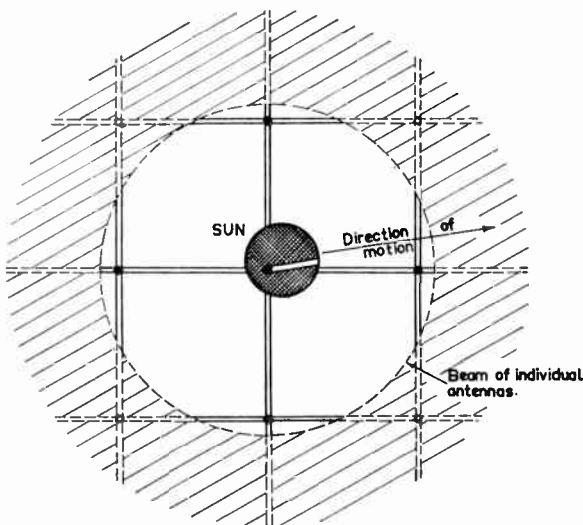


Fig. 4—Sketch showing the multiple lobes of the crossed multielement interferometer and the way in which the sun is scanned by one of these. The path of the scanning lobe across the solar disk is indicated.

changed by  $180^\circ$  in a periodic manner before it is added to the output from the other interferometer. This phase reversal affects the amplitude of any signal common to both systems but does not affect any that appear in one interferometer alone. Hence for the modulated component of the receiver output, the antenna has a directivity diagram which consists of a number of widely separated pencil beams or lobes, shown as small black circles at the intersection points in Fig. 4. The width of each lobe is a little greater than would be obtained if the cross were replaced by a rectangular antenna array having sides of the dimensions of the two arms of the cross.

In using this array for scanning the sun, the latter is allowed to drift in an EW direction through one of the antenna lobes in the manner described for a single multiple interferometer. After a short interval the sun en-

counters the next lobe. If this is to cover a new part of the sun, it is necessary that the second scan should take place with the antenna lobe slightly displaced in a NS direction with respect to the first, and the next displaced still further and so on. This happens naturally if observations are made in the morning or afternoon, since the sun moves in a circular path around the NS axis of the earth while the antenna lobes lie along circles about a horizontal NS line at the place of observation. Except at the equator these do not coincide, and at times other than at midday, the two sets of circles are inclined to one another. To make successive scans of the sun, one may then use the natural NS shift of the sun with respect to the antenna lobes. It is more convenient, however, to have some means for moving the lobes, and this can be done using phase shifters between adjacent antennas in the NS array. With these, successive scans may be separated by convenient amounts, so that the whole solar disk is adequately investigated. The results of all the scans are finally combined to produce a two-dimensional map of radio brightness over the solar disk.

#### IV. THE SYDNEY CROSSED MULTIELEMENT INTERFEROMETER

Each of the 64 individual elements of this array consists of a 19-foot parabolic reflector; each is fed by a half-wave dipole backed by a plane reflector. The antennas are mounted on individual equatorial mounts, as illustrated in Fig. 5 so that during the day only one movement is required to keep each antenna directed towards the sun.

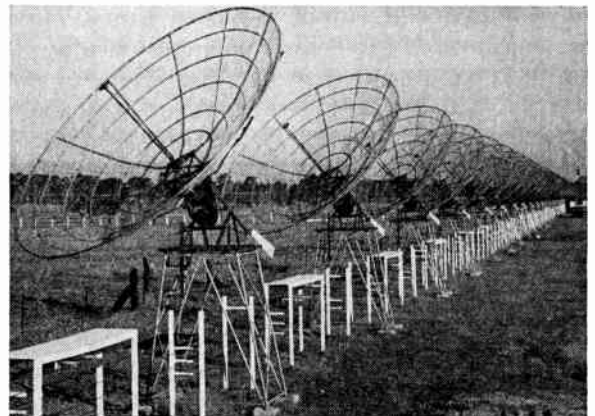


Fig. 5—Photograph of crossed multielement at Fleurs, near Sydney.

The antennas are arranged in two lines, one EW and the other NS, with a spacing of 40 feet between adjacent antennas. Each line, therefore, is 1240 feet long.

A branching system of closely spaced twin-wire feeder lines connects the antennas to the receiver. The length of transmission line between each antenna and the receiver is the same; thermal expansion of the feeder lines therefore affects all antennas equally.

To shift the antenna lobes in a NS direction it is necessary to vary the phase between adjacent antennas

through angles up to  $360^\circ$ . This is done by means of noncontacting slides (utilizing quarter-wave sections) which can move along the feeder lines, altering the positions of the junction points. These slides have a further function; they divide the power unequally at each branch (except the central one) to produce a "tapered" array. As is explained in the accompanying article on the Mills Cross,<sup>12</sup> tapering is necessary with a cross-type antenna if side lobes are to be kept small.

At the receiver, the output from the EW array is passed through a transmission-line network in which there are alternate paths differing in length by a half-wavelength. A rotating capacity switch causes the signal to change from one path to the other at a frequency equal to half that of the main power supply. By this means the signal from the EW array is  $180^\circ$  phase modulated. The output from this switched network is then combined with the output (unmodulated) from the NS array and fed to a superheterodyne receiver.

The receiver is of a conventional type with a tuned filter for image suppression followed by a crystal mixer, an IF amplifier, an audio amplifier tuned to the modulation frequency, a phase-sensitive detector, and finally at the receiver output, a chart recorder.

IF amplifiers of different bandwidth are employed. When the source under observation is near the zenith, a bandwidth of several mc is used. For sources far from the zenith, such as the sun in midwinter, the bandwidth has to be reduced to about 0.3 mc, which has the effect of increasing the amplitude of noise fluctuations. The narrowing of the bandwidth for directions away from the normal to the plane of the array is made necessary by the difference of the path length from the source to the different parts of the array. This difference in path length corresponds to a difference in phase which is not exactly the same at all frequencies in the pass band of the receiver. Hence for a given direction of the source, the bandwidth of the receiver must be kept sufficiently narrow so that phase differences over the pass band are not large enough to cause a significant deterioration in the performance of the array.

## V. PERFORMANCE

In a direction broadside to the array the beamwidth is  $3'$  arc. In other directions the dimensions of the beam increase, because of foreshortening of the array, in pro-

portion to the cosecants of the angles between the direction of the source and the line of each array. In midsummer in Sydney the sun is not far from the zenith at midday, and the antenna lobes used for scanning the sun will be approximately circular and  $3'$  arc wide. Observations at the time of writing have been made only in the months of winter and for these the calculated beamwidth at midday is  $3'$  arc in the EW direction and about  $5'$  arc in the NS direction. The beamwidth has, so far, been measured only roughly. For this, bright patches on the sun which are situated at the limb were used since they are foreshortened and hence appear smaller than those on the disk. The width of the beam appears to be approximately as calculated. A sample observation, shown in Fig. 6, is displayed with an optical sketch

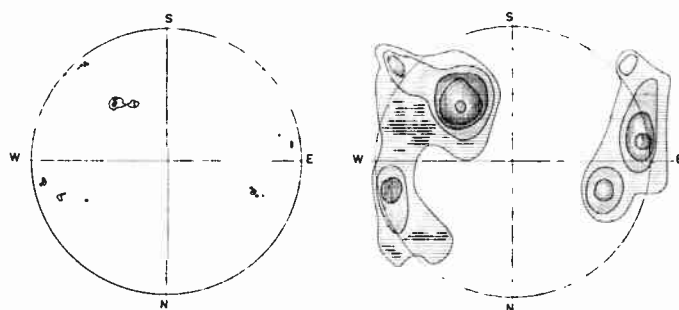


Fig. 6—A white-light sketch of the sun on June 27, 1957, showing sunspots and a radio picture of the sun showing the contours of radio brightness on the same day. The contours are at unit intervals from 2 to 6 on an arbitrary brightness scale and have not been taken down to the quiet-sun level of brightness.

of the sun for the same day. The close connection between the optical and radio features is apparent.

Pictures like this when obtained at daily intervals will allow a study to be made of the development and decay of individual radio sources on the sun and the general changes that these sources undergo during the solar cycle.

## VI. ACKNOWLEDGMENT

The authors wish to thank Dr. J. L. Pawsey for valuable discussions during the course of this work. The mechanical design was the work of K. R. McAlister. The workshops of the Division of Radiophysics were responsible for the construction and erection of the equipment. The skillful work done by members of the constructional team and by the installation team directed by C. Chenhall was an essential factor in the successful functioning of the equipment.

<sup>12</sup> B. Y. Mills, A. G. Little, K. V. Sheridan, and O. B. Slee, "A high resolution radio telescope for use at 3.5 m," this issue, p. 67.



# A Dynamic Spectrum Analyzer for Solar Studies\*

J. GOODMAN†, MEMBER, IRE, AND M. LEBENBAUM†, SENIOR MEMBER, IRE

**Summary**—A spectrum analyzer of the type originally built by Wild, *et al.*<sup>1,2</sup> is described. The analyzer covers the range of 90 mc to 580 mc at a rate of 3 sweeps per second in three overlapping bands. The output information is presented on three high-resolution oscilloscopes in a frequency-intensity display, and the time axis is provided by the continuous motion of the film used to photograph the displays. Modifications and improvements are suggested.

## INTRODUCTION

ANALYSIS of solar radiation in the radio frequency spectrum was carried out by many workers at discrete frequencies until Wild built a "dynamic spectrum analyzer" to cover the range of 40 mc to 240 mc. The results were of great interest and stimulated further independent studies aimed at obtaining data at higher frequencies with systems of increased sensitivity. This article describes several systems built for these studies, covering the range of about 90 mc to 580 mc. The equipments described were built for use by the Harvard Radio Observatory at Fort Davis, Texas, and subsequently for the Observatory of the University of Michigan, Ann Arbor, Mich.

## GENERAL DESCRIPTION

The dynamic spectrum analyzer consists of a series of swept receivers successively covering the frequency range of interest. They are fed from the special antenna, described elsewhere in this issue by Jasik, which tracks the sun. The outputs are fed to an indicator which consists of high-resolution cathode-ray tubes, mounted one above the other, on which the vertical deflection is proportional to frequency and the spot intensity is proportional to the strength of the received signal. A camera photographs the oscilloscopes on continuously horizontally-moving film, the resulting record being of the frequency-time-intensity type. Three receivers are used to cover the range from 90 mc to 580 mc; the three oscilloscope tubes are mounted as close as physically possible so that a single camera is used to record the data contained in the entire frequency range.

The receivers are of the superheterodyne type, utilizing two stages of rf amplification, a local oscillator, mixer, IF amplifier, second detector, and display cir-

cuitry. Each receiver covers about a 2:1 band, with the frequency ranges chosen to provide overlap at the band ends. A block diagram of a typical receiver and indicator is shown in Fig. 1. Tuning capacitors in the plate circuits of the two rf amplifiers and in the local oscillator tank circuit are ganged together and driven through a gear reduction system to give a sweep of 3 per second. By changing gears, a second sweep speed of 10 per second may be obtained. The receivers can also be used at spot frequencies by engaging a manual drive through a magnetic clutch. The rf drawer contains the rf amplifiers, mixer, local oscillator, discriminator for generating a sweep voltage, 30-mc IF preamplifier, and power supplies. The IF and video drawer contains the IF system (in the later model both linear and logarithmic amplification is provided, the latter giving a 60-db dynamic range), detectors, dc coupled amplifiers, sweep amplifiers and the sync pulse generators. The indicator contains the crt, magnetic deflection systems, and the blanking circuits. The equipment is rack mounted as shown in Fig. 2, a picture of the Harvard system. The three receivers, covering the ranges 90–180 mc, 170–330 mc, and 300–580 mc, each occupies one bay with their associated power supplies, and the three oscilloscopes comprising the display system are contained in the fourth. In the center receiver bay, a frequency-time marker generator is provided.

## DETAILED UNIT DESCRIPTION

### RF Units

A photograph of a typical rf drawer is shown in Fig. 3. The rf amplifiers, oscillator, mixer, and discriminator are contained in a single subassembly. The rf amplifiers are both WE 416B triodes operated in a grounded-grid configuration. The input of the first-stage is a broad-band, untuned circuit adjusted for a compromise between best noise figure and match; the latter being necessary because of the long transmission line between antenna feed and receiver input and the desire to maintain relatively constant gain across the band. The plate of the first stage feeds a parallel-tuned circuit with a special high-speed capacitor acting as the tuning element. The capacitor has a linear frequency vs rotation angle characteristic in both meshing and emerging positions; in this application, only 180° of the capacitor rotation is used in the rf amplifier stages, the display being blanked during the remaining half.<sup>3</sup> The output from the first stage is obtained from a tap on the

\* Original manuscript received by the IRE, October 18, 1957.

† Airborne Instruments Lab., Inc., Mineola, N. Y.

<sup>1</sup> "Observations of the spectrum of high intensity solar radiation at metre wavelengths," *Aust. J. Sci. Res.*

I. J. P. Wild and L. L. McCready, vol. 3, pp. 397–398; 1950.

II. J. P. Wild, vol. 3, pp. 399–408; 1950.

III. J. P. Wild, vol. 3, pp. 541–557; 1950.

IV. J. P. Wild, vol. 4, pp. 36–50; 1951.

<sup>2</sup> J. P. Wild, J. D. Murray, and W. C. Rowe, "Harmonics in the spectra of solar radio disturbances," *Aust. J. Phys.*, vol. 7, pp. 439–459; 1954.

<sup>3</sup> The receiver is operative during the other 180°, and the frequency-time characteristic is the mirror image of the first half of the rotation.

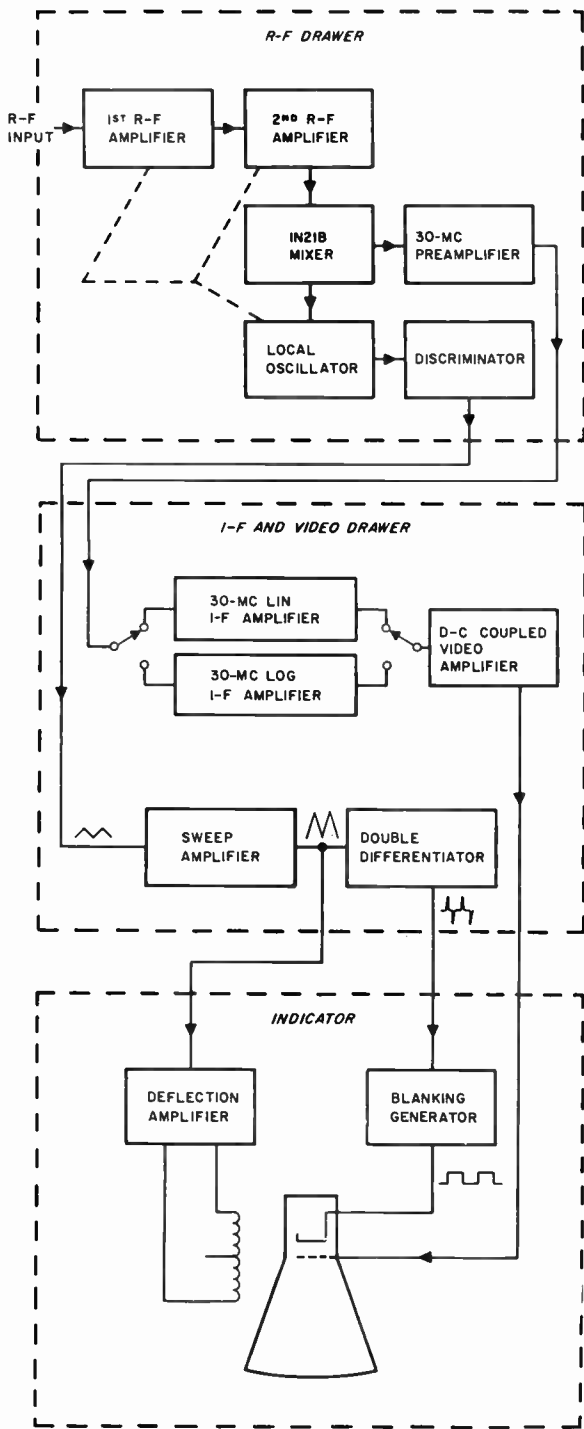


Fig. 1—Block diagram of a typical receiver and indicator.

inductance of the tank circuit, the loading being obtained from the input impedance of the second grounded-grid stage. The second-stage tank circuit is identical to the first, the output tap being connected to a 1N21B crystal mixer.

The local oscillator is a 5675 pencil triode operating in a Colpitts circuit. The tuning capacitor is identical to those used in the amplifiers. The oscillators are on the high side of the signal frequency in the lower two bands; in the highest band, the oscillator drives the

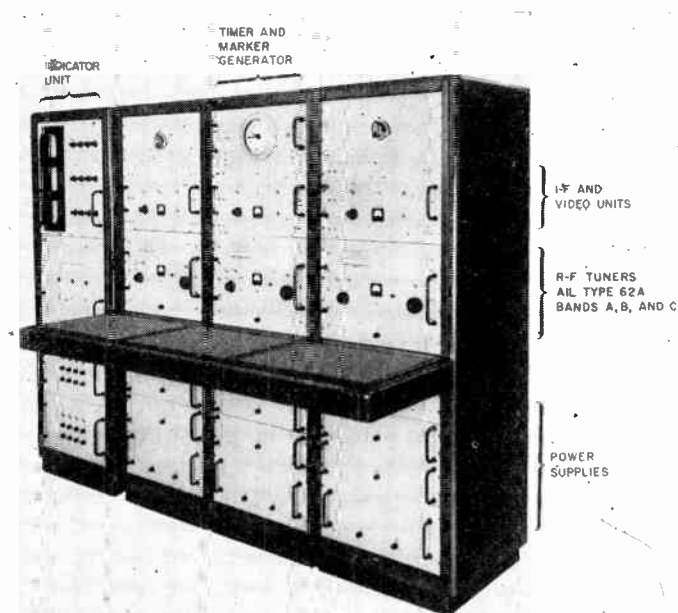


Fig. 2—Photograph of the dynamic spectrum analyzer.

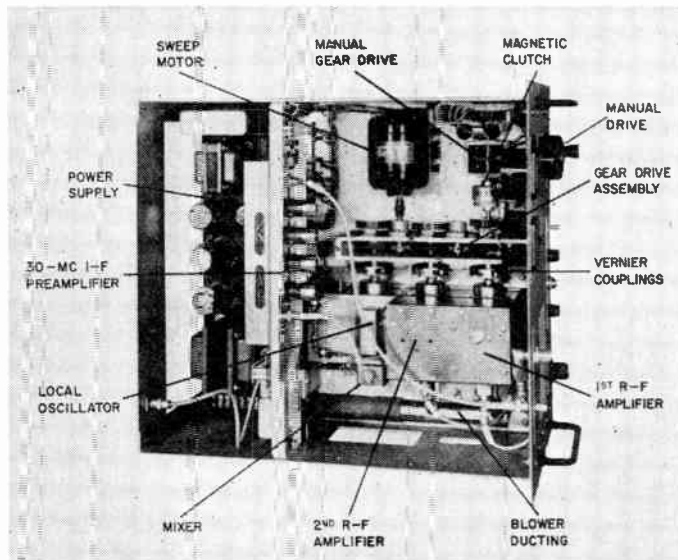


Fig. 3—A typical rf drawer.

mixer as a harmonic mixer and operates at half frequency (again with the second harmonic on the high side of the signal). A small amount of local oscillator power is fed to a discriminator circuit which gives a voltage output proportional to the frequency to which the local oscillator is tuned. The peak-to-peak output (from lowest to highest oscillator frequency) is about 1 volt. The voltage waveform out of the discriminator is triangular when the oscillator is swept, since both halves of the condenser are used in the oscillator. Half of the waveform is used as the sweep for the indicator, but both halves are used to produce the blanking sync pulses.

From the mixer, the signal is fed to a 30-mc low-noise preamplifier. The output from the preamplifier is fed

at a 50-ohm impedance level to the IF and video drawer.

It is necessary, when using the 416B triode to use special care in turning the plate and filament power on and off. An automatic system has been provided which applies the various potentials in the proper sequence to insure the best operating life for the tubes.<sup>4</sup> The sequence of operations is as follows:

- 1) AC power is applied to the filaments of the 416B and to the dc power supply. The relay contacts controlling application of dc to the amplifier tube are open. When dc appears at the output of the supply, a negative 10-volt bias is applied to the 416B.
- 2) After a suitable warmup period, a thermal time-delay relay closes, allowing plate voltage to be applied to the 416B. At the same time, the bias voltage is removed through a long time-constant network (about 5 seconds).
- 3) Current builds up in the 416B as the bias voltage is removed, reaching its final operating value of about 30 ma in a time determined by the time-constant network and of a value determined by a cathode degenerating resistor of about 1000 ohms.

It is not possible to turn off the supply without going through the complete cycle when turning it back on, so that momentary interruptions of ac cannot damage the tube.

#### *IF and Video Drawer*

The IF from the preamplifier is fed to either a linear or logarithmic IF amplifier, the latter being of the "successive detection" type<sup>5</sup> in which the plate decoupling filter acts as the video line. In either IF amplifier, the detected output is dc coupled through a video amplifier, which is, in effect, an impedance transformer. This amplifier delivers the signal at a low-impedance level through the output connecting cable to the indicator for direct application to the intensity grid of the oscilloscope. The linear IF amplifier has a large dynamic range, a 5763 being used in the last stage, and can develop a 30-volt signal at its output with good linearity. The logarithmic amplifier accurately compresses a 60-db range of input signals to about 20 db at its output.

The discriminator triangular waveform is amplified in dc coupled amplifiers and supplied to a deflection amplifier. This amplifier generates a triangular current waveform for driving the magnetic deflection yoke in the indicator unit, providing a vertical deflection proportional to frequency. The amplified triangular wave-

form is also double differentiated to develop sync blanking pulses at each end of the sweep. Unless the return sweep were blanked, the information for a small part of the trace at each end of a sweep on the oscilloscope would overlay the preceding and succeeding sweep; since the intelligence is contained in the intensity of the recorded signal, the overlay would destroy the information.

The power supply for the IF amplifiers is regulated to 1 part in 10<sup>4</sup>, the dc amplifiers are of the negative feedback type with a gain stability of 0.02 per cent, and the entire system, including power supplies, receives ac from an ac line regulator with a regulation of 1 part in 10<sup>4</sup>. The over-all receiver has a gain stability of better than 0.1 db for extended periods when operated under normal ambient conditions.

#### *Indicator*

The indicator tubes are Dumont Type K1207PAX, having a resolution of 1000 lines across the 5-inch face. Magnetic deflection is used. Since the signal information is presented in the form of intensity modulation, the intensifier grid is operated at ground to simplify the associated signal circuits. The blanking waveform is developed from the sync pulses, every return sweep being blanked, so that the trace appears on the film as in a television roster. The blanking waveform is applied to the cathode of the oscilloscope.

#### *Frequency Marker Generator and Timing Generator*

Two crystal oscillators, one at 10 mc and the other at 50 mc are used to generate a series of markers throughout the entire rf range covered by the receivers. The amplified oscillator signal is applied to crystal diode harmonic generators and the resulting signal loosely coupled to each rf head. The timing system is used to apply plate power to the proper crystal oscillator at a prescribed time. An ordinary 60-cycle timing clock with special contacts is used; one set closes for 3 seconds every other minute and applies power to the 50-mc oscillator; on alternate minutes, the second set closes, energizing the 10-mc oscillator. Once an hour, a third set closes for 10 seconds, holding one of the oscillators on for this additional time. This allows both time and frequency calibration marks to be recorded directly on the film without using the limited film width for photographing a clock face.

#### ELECTRICAL CHARACTERISTICS

Since these receivers are developmental in nature, they have been modified and improved over the last several years. Fig. 4(a) is a graph of noise figure of two Band C receivers showing the improvement obtained. The band A receiver noise figure averages 4.6 db over the 90-mc to 180-mc range; Band B averages 5.7 db over the 170-mc to 340-mc range; Band C averages 6.6 db. Fig. 4(b) is a plot of relative gain over the 300-mc to

<sup>4</sup> Actually it is most desirable to leave the tubes on continuously, and to provide 1 per cent filament regulation; power failures and inadvertent turn-off still make it desirable to incorporate the automatic turn-on procedure.

<sup>5</sup> For a review of the various types of logarithmic amplifiers, see T. H. Chambers and I. H. Page, "The high accuracy logarithmic receiver," Proc. IRE, vol. 42, pp. 1307-1314; August, 1954.

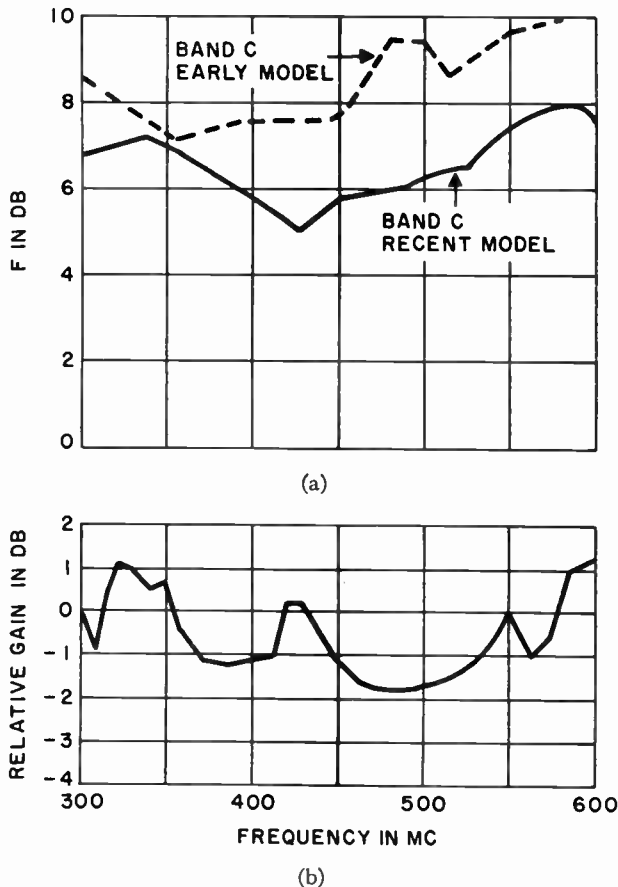


Fig. 4(a)—Noise figure of two Band C receivers. (b)—Relative gain of Band C receiver as a function of frequency.

580-mc range of Band C. It is important that the gain variation be small, for since the desired signal is noise, it cannot be distinguished from a gain fluctuation in the receiver. If the fluctuations are severe, some form of programmed gain control is required; a standard agc

is not adequate since the signal is identical in form to the receiver noise. Programmed control systems are undesirable since they add to the complexity of the over-all equipment.

#### IMPROVEMENTS

There is probably some room for improvement in both noise figure and gain "flatness," but the results attained with new models of the system approach closely the best results attainable at fixed-frequencies. Future improvements will be in the direction of simplicity and flexibility, and in improved data-handling systems. Particularly in the range above 500 mc, the use of broad-band low-noise twt amplifiers and voltage-tuned local oscillators allows great flexibility in sweep rates and in increasing the duty cycle to close to 100 per cent through the use of sawtooth rather than triangular frequency sweeps. With the rf system mounted at the feed, gain fluctuations can be reduced, and quantized outputs can be used to provide amplitude contours directly. The use of facsimile for data recording is then feasible, with the advantage of almost immediate availability of the signal information in a reduced form.

#### ACKNOWLEDGMENT

The contributions of S. Brass and W. Verba to the construction of the equipments is gratefully acknowledged. Throughout the design and construction phase, the guidance and counsel of Dr. Alan Maxwell, physicist-in-charge of the Harvard Radio Observatory at Fort Davis was invaluable, and since the installation of the equipment at Fort Davis in 1956, his unflagging efforts (and those of G. Swarup and S. Goldstein) have resulted in an equipment availability of 95 per cent of the possible observing time.

## A Wide-Band Antenna System for Solar Noise Studies\*

HENRY JASIK†, SENIOR MEMBER, IRE

**Summary**—A wide-band antenna system has been developed as part of a sweep frequency spectrum analyzer for solar noise studies in the 100 mc to 600-mc frequency range. The antenna system consists of an equatorially mounted 28-foot paraboloid illuminated by a unique feed combination which operates over the frequency range in three overlapping bands. Development of the antenna system has been carried out with the aid of scale models and two full size systems have been constructed. The resulting antenna has an effective

area which is reasonably constant over the entire range before reflection losses are considered. The feed configuration is described and performance characteristics are given.

#### INTRODUCTION

THIS paper treats the results obtained and the problems encountered in the development of an antenna system for a dynamic spectrum analyzer to be used for solar noise studies in the frequency range from 100 to 600 mc. Coverage of this total frequency

\* Original manuscript received by the IRE, October 3, 1957.  
† Jasik Labs., Westbury, N. Y.

range is by no means a trivial problem and it has been necessary to consider the systems aspects of the equipment in order to decide what compromises are acceptable in the antenna system. Some of these points have been treated previously in an unpublished report prepared by the author for Harvard College Observatory entitled "Instrumentation for the dynamic spectrum analyzer," dated May 31, 1955. However, for the sake of completeness, the considerations behind the design philosophy will be discussed briefly.

Basically, the performance desired of the antenna system is that it possess an effective collecting aperture of the order of 25 to 30 square meters over the frequency range from 100 to 600 mc. Since this antenna will primarily be observing the sun, which is the strongest radio source in the sky, side-lobe considerations are secondary. A point of considerable practical and economic importance is the requirement that the entire antenna system be capable of being mounted on a single pedestal with an equatorial drive. The last requirement which must be considered is that it be possible to use the same pedestal and antenna system in the frequency range of 2000 to 4000 mc at a later date.

The requirement of 2000 to 4000 mc operation, in addition to the 100 to 600 mc operation, makes the choice of a large parabolic reflector and multiple feed system virtually mandatory since a single antenna system operating over a 40 to 1 frequency range is somewhat beyond the present state of the antenna art. If operation over only the 100 to 600 mc range were required, an alternative possibility would have been the use of a group of four large pyramidal horns, each with a ridged waveguide feed. This type of structure is inherently capable of rather broad-band operation and would provide an essentially constant effective aperture over the 100 to 600-mc range with a good impedance match. However, the multiple horn structure would have been unusable at the 2000 to 4000-mc range so that an additional antenna system would have been required at a later date. In addition, the cost of a pyramidal horn system plus its mounting structure was estimated to be considerably greater than the cost of the parabolic reflector plus its feed.

For the above reasons, it was decided to use a 28-foot parabolic reflector of standard design and to develop a multiple feed system to properly illuminate the dish since this combination would provide the most economical arrangement for present and future use. Some reduction in electrical performance was to be expected because of the blocking of the aperture by the feed and the effect of the reflector on the feed impedance. However, this reduction in performance occurs primarily below 200 mc and is evidenced by a somewhat higher side-lobe level and an increase in standing-wave ratio on the transmission line to the feed. While the additional reflection losses in the cable will result in some loss of gain, this was not considered serious since the noise output

from the sun is extremely high below 200 mc. The more difficult aspect of this problem is the fact that the gain will have a periodic variation over the frequency range due to the reinforcement and cancellation of the reflection of the feed proper with the additional reflection caused by the parabolic reflector. However, it had been decided that the over-all system gain was to be stabilized by applying a suitable correcting voltage in the IF portion of the receivers, so that with some slight additional complication in the receiving equipment, it would be possible to compensate for the gain variations inherent in the reflector and multiple feed system as well as the gain variation of the receiver.

Subject to the limitations just discussed, the only remaining problem was that of a suitable feed since a standard reflector and pedestal design were available and high-performance scanning receivers were also available. The receivers available were capable of covering a continuous range of 2 to 1 in frequency which could be located anywhere in the 100 to 600-mc region. As it was considered feasible to design the individual components of the antenna feed so that they operated properly over approximately a 2 to 1 frequency range, it was decided to cover the 100 to 600-mc frequency range in three ranges, each range having a separate feed and receiver. By using cross polarization for the middle part of the frequency range, it is possible for all three feeds to operate simultaneously in the same location without cross-coupling between feeds. The frequency ranges which were finally arrived at are as follows.

Feed	Frequency Range	Polarization
A	100-180 mc	Vertical
B	160-320 mc	Horizontal
C	300-600 mc	Vertical

This arrangement provides continuous coverage with some overlap between ranges. Since the noise radiation from the sun normally is randomly polarized or circularly polarized, the cross polarization of Feed B is not expected to produce any serious problems in data interpretation. However, in the overlap regions, there will be data available in two orthogonal polarizations, so that a limited amount of information will be available on the polarization properties of solar noise.

In order to realize a combined feed for the three ranges, it was decided that an electromagnetic horn would be used for Feed C which covers the 300 to 600-mc range. This horn has a short flared section fed from a rectangular waveguide. Connection to the coaxial cable is made by means of a stepped ridge in the waveguide which transforms the waveguide impedance down to the 50-ohm level of the coaxial cable.

The frequency range of 100 to 180 mc is covered by Feed A which consists of a double dipole system and a plane reflector screen. These dipoles are located at the edge of the horn and are oriented to radiate energy of

the same polarization as that radiated by the horn. The side of the horn actually serves as the central part of each dipole radiator. Although these two feeds are identically polarized, there is no coupling between them since the axis of each dipole is located where the electric field in the horn is zero. Further, the dipoles cannot couple into the horn since the horn is below cutoff at the operating frequency of the dipoles.

The overlapping frequency range of 160 to 320 mc is covered by Feed B which consists of a dipole and reflector elements arranged in the form of a corner antenna. The dipole, which is center fed, is located in one plane of symmetry of the horn and is supported by two aluminum tubes which also form the balun. These two balun tubes in turn are supported by a square cross bar which fastens to two sides of the horn and is located in the  $H$  plane of the horn. The reflector elements are supported outside of the horn by dielectric members. Since Feed B is cross polarized to the other two feeds, it does not couple to them nor does it have any effect on their performance.

Finally, a fourth feed has been supplied to allow for operation in the 2000 to 4000-mc region. This feed is a horn which is a scaled down version of Feed C and is positioned between the two balun tubes of Feed B. Because of the large frequency separation between this feed and the other feeds, there is virtually no effect on the other feeds by the small horn. Although the 2000 to 4000-mc feed is slightly shadowed over a small angular region by the dipole of Feed B and the dielectric supporting members, the total amount of shadow angle is small and it is believed that the operation at 2000 to 4000 mc will be affected only slightly.

#### PATTERN STUDIES ON SCALE MODEL

##### *Primary Patterns*

Since it would have been quite time consuming and costly to have conducted the pattern studies in the development program on the full size 28-foot diameter paraboloid, all radiation pattern work was conducted on a scale model basis. For convenience, a scaling factor of 6.82 was chosen, since this corresponded to the ratio between the 12-foot focal length of the full size reflector and the 21.1-inch focal length reflector which was available in spun aluminum. Since it was necessary to maintain the same focal length to diameter ratio for the model studies, the scale model reflector had a diameter of  $49\frac{1}{2}$  inches.

For the  $f/d$  ratio of 0.428 used on both the model and full scale antenna, the angle intercepted by the dish as seen from the feed is  $\pm 60^\circ$ . In order to obtain the optimum gain factor from the feed and reflector combination, the primary pattern of the feed should be such that the illumination at the edge of the dish is approximately 10 db down from the illumination at the center of the dish. At this level, the best balance is obtained between the loss in gain due to energy spillover beyond the dish

and the increase in gain due to the shape of the illumination across the dish. Actually, the curve of gain factor vs level of illumination at the edge is quite broad and values between 7 db and 20 db will not cause any undue loss in gain.

Thus, the essential requirements for the feed system are that its pattern in both the  $E$  plane and the  $H$  plane be smooth and that at  $\pm 60^\circ$  from the normal, the intensity at the edge of the dish should have a value which is between 7 db and 20 db down from the intensity at the center. An additional requirement is that the phase centers of the various feeds be as close to one another as possible.

In developing the feed system, Feed C was designed first since the horn also acts as the central part of the dipole system for Feed A. Feed C actually operates in the 300 to 600-mc range, but all model pattern measurements were taken from 2040 to 4080 mc, corresponding to the 6.82-scaling factor. To prevent confusion, all further references here will be to the full scale operating frequencies, rather than to the model frequencies.

*Feed C:* In order to determine suitable dimensions for Feed C, primary patterns were measured for a number of horns. It was found that the most suitable radiator was a horn having an  $H$ -plane dimension the same as that of the waveguide section. The  $E$ -plane dimension was slightly less than the  $H$ -plane dimension and tapered down to the narrow waveguide dimension by means of a short flare section. The transition from rectangular waveguide to coaxial line was effected by the use of a three-section ridge waveguide transformer which changed the impedance level of the waveguide down to 50 ohms. Connection is made to the coaxial line at the back end of the low-impedance ridge. The back end of the waveguide is closed by a shorting plate which prevents rearward radiation. The position of the back plate with respect to the coaxial feed was chosen to provide a shunt reactance element which helps to compensate the input impedance.

The measured patterns for Feed C show that the illumination at the edge of the dish in the  $E$  plane varies from about 7 db down at the 300-mc end of the band to about 17 db down at the 600-mc end of the band. In the  $H$  plane, the illumination at the edge of the dish varies from about 6 db down at the low end of the band to about 12 db down at the high end of the band. Impedance measurements on the scale model showed that the input standing-wave ratio could be held below two to one.

*Feed A:* Feed A for the 100 to 180-mc range has the same polarization as Feed C. The main reason for this choice is that Feeds A and C are the most widely separated in frequency, so that the problem of reducing cross coupling between feeds would be considerably simplified. Another reason is the fact that the horn body must form the central portion of Feed A and if the frequency separation were too small, the central part of

Feed A would be too large in terms of wavelength to allow for effective control of the primary pattern.

The configuration of Feed A is a pair of dipoles at two front edges of the horn backed up by a reflecting grid in back of the horn. At each edge, a pair of dipole elements at the top and bottom of the horn effectively form a sort of sleeve antenna with the side of the horn acting as the central portion of the sleeve antenna. The two sets of dipoles at the edges of the horn behave as a two element array, in order to narrow the pattern in the  $H$  plane. The other control on the  $H$ -plane pattern of the feed is the size of the reflector grid and its spacing from the dipoles. The  $E$ -plane pattern of the feed is controlled by the over-all length of the dipoles and by the reflector grid.

In order to obtain the proper phase relationships in the dipole elements, it was necessary to feed the upper pair of elements from one side of a balun and the lower pair from the other side. For the scale model measurements, a conventional type of balun was used. The balun for the full size feed was of a somewhat more compact type consisting of a helical line type of structure.

Concurrently with the pattern studies, some preliminary impedance studies were conducted to make sure that the resulting feed structure could be properly matched. After taking a considerable number of measurements, a set of parameters was obtained which resulted in adequate primary pattern performance and impedance match.

The measured patterns in the  $H$  plane showed that the illumination at the edge of the dish varied from about 7 db down to about 10 db down over the 100 to 180-mc band. In the  $E$  plane, the illumination varied from about 10 db down to about 17 db down over the frequency range. At 180 mc, the  $E$ -plane pattern had a null just on the edge of the dish so that at higher frequencies the gain falls off somewhat due to the small area of the dish which is illuminated out of phase. This condition could have been corrected by shortening the dipole elements, but would have deteriorated the impedance performance at the low-frequency end of the band. However, since an overlap of 20 mc was considered sufficient at the 180-mc point, the dipole elements were left long enough to give suitable impedance performance at 100 mc. The pattern performance of the feed is actually adequate down to 90 mc, but the impedance characteristics leave something to be desired below 100 mc.

*Feed B:* Feed B for the 160 to 320-mc range is cross-polarized to Feeds A and C, so that the problem of cross coupling is not a factor in its design. However, the presence of the other feeds must be considered since Feed B must be so located that its center of radiation is reasonably close to that of the other two feeds. The structure finally chosen for Feed B is a balanced dipole placed slightly in front of the horn and located in the horn's  $H$  plane of symmetry. The dipole is supported by the two arms of its balun which in turn are supported by a

member running across the horn. Since the horn and the supporting member will not support transmission at the frequencies used by Feed B, there is a partial reflecting surface in back of the dipole, giving a broad unidirectional pattern for the dipole when it is mounted in front of the horn.

However, the pattern obtained is somewhat too broad to provide for efficient illumination of the dish. To improve this situation, three reflector rods were placed on either side of the horn in such a configuration as to form a corner reflector of approximately  $120^\circ$  included angle. The resulting patterns obtained from this arrangement provided quite satisfactory illumination over the frequency range. In the  $E$  plane, the illumination at the edge of the dish varied from about 8 db down to about 15 db down over the band, while in the  $H$  plane the illumination at the edge varied from about 6 db down to about 12 db down over the band.

Impedance measurements on the scale model showed a sizeable spread in the impedance characteristics. However, the curve did appear to be capable of proper compensation, as proved to be the case after the full scale antenna was constructed.

A view of the completely assembled scale model used for the pattern tests is shown in Fig. 1.

#### *Secondary Patterns*

To determine the performance of the scale model feed, the feed was mounted in a  $49\frac{1}{2}$ -inch diameter spun aluminum paraboloid. The positioning of the horn was such that the focal point of the reflector was located at a full scale distance of one inch inside of the aperture of the horn, Feed C. This location placed the center of phase of Feed C at the focal point and was close enough to the center of phase of the other feeds to produce a phase error of less than a quarter wavelength. Although some pattern measurements were made at positions slightly displaced from the above position, the original position proved to be the most satisfactory and all patterns taken for record purposes were measured at the position referred to above.

Prior to measuring a complete set of patterns, a brief investigation was made of the effect of the feed cable positioning. The mechanical and electrical complexity of the combined feed made it practically impossible to run the feed cables along the axis of the paraboloid to the back of the reflector. It therefore was necessary to run the feed cables along one of the three Fiberglas struts which supported the feed system. Since one of the feeds is cross polarized to the other two, this meant that the feed cables would have to be located in the  $E$  plane of at least one of the feeds. The secondary patterns for Feed B were then studied with the cable placed in both its  $E$  plane and its  $H$  plane. It was found that the effect of the cable positioning was negligible so that all further measurements were made with the cable located in the  $E$  plane of Feed B. This placed the cable in the  $H$  plane

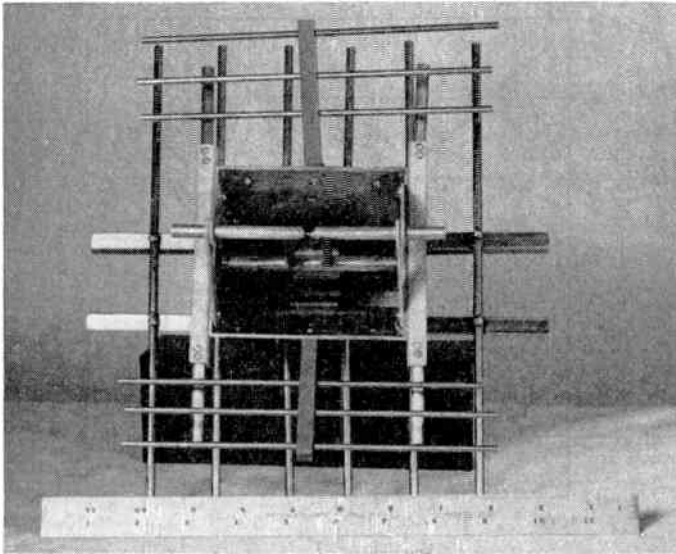


Fig. 1—Scale model of antenna feed used for primary pattern measurements.

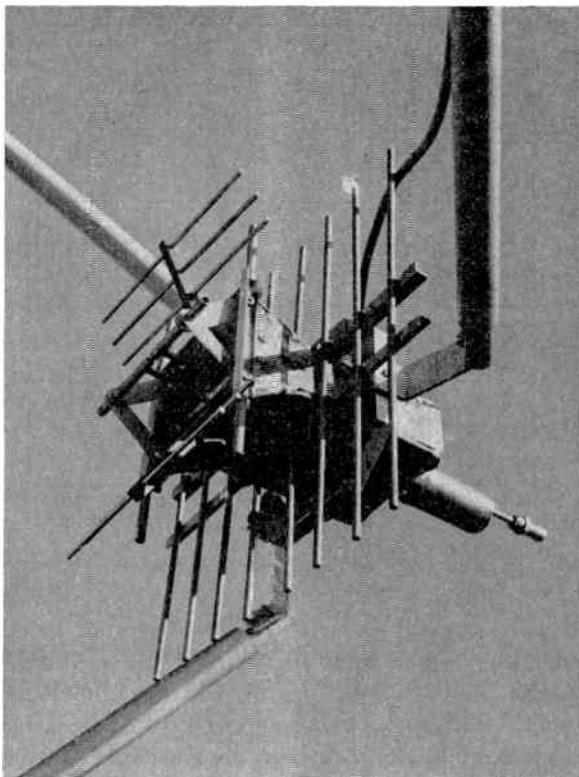


Fig. 2—Close-up view of scale model feed mounted in reflector.

of both Feeds A and C, where it has no effect since it is transverse to the electric field for these two feeds.

A close-up view of the feed structure is shown in Fig. 2. Fig. 3 shows a view of the feed structure mounted on the 49½-inch reflector, which in turn is mounted on a rotating pedestal used for pattern measurements in conjunction with an automatic recorder.

The principal characteristics of the secondary patterns are summarized in Figs. 4–6, p. 140 which show the 3-db beamwidth of the main beam as a function of

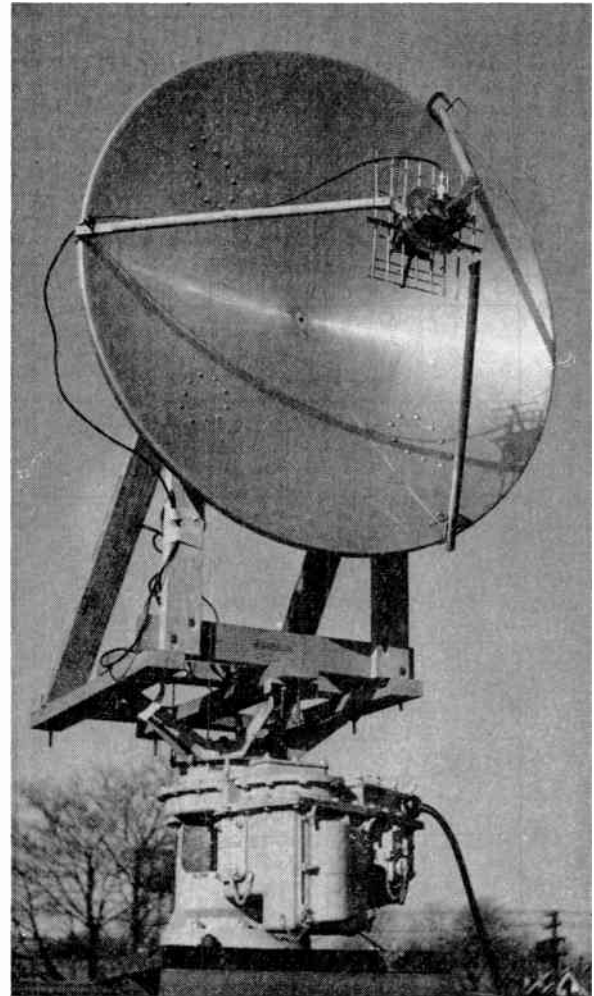


Fig. 3—Scale model of reflector and feed used for secondary pattern measurements.

frequency. Although all measurements were made at scaled frequencies, the results are presented in terms of the full scale frequencies. As would be expected, the beamwidth decreases for increasing frequency. One exception to this is the *E*-plane beamwidth for Feed A which rises slightly between 180 and 200 mc. This is due to the fact that the null of the primary pattern of Feed A falls slightly inside the reflector above 180 mc. For Feed C, it will be noted that the beamwidth increases slightly between 520 and 600 mc. It is believed that this particular rise is due to the measurement technique rather than the primary feed, since the measured primary patterns were quite satisfactory. At the time these measurements were made, insufficient oscillator power was available at the very highest frequencies to permit secondary patterns at a distance adequate to satisfy the far field criterion. This results in a slight broadening of the beam and it is felt that this would not have occurred had it been possible to make pattern measurements at sufficient range.

To obtain an estimate of the effective collecting aperture of the full size antenna, the gain at each frequency was first estimated by dividing 25,000 by the product of

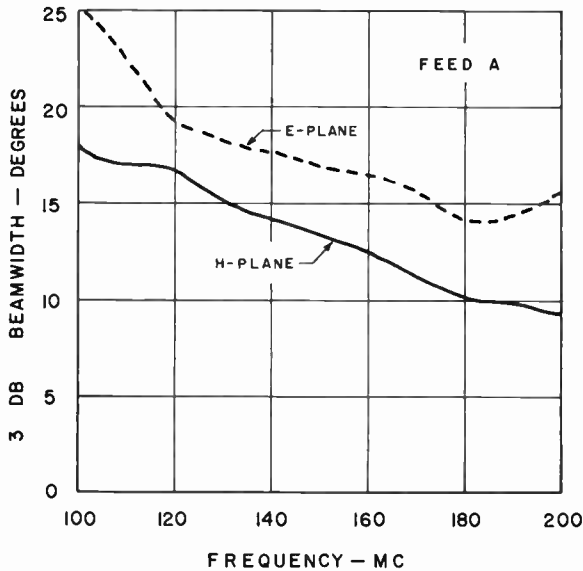


Fig. 4—Secondary pattern beamwidths for Feed A.

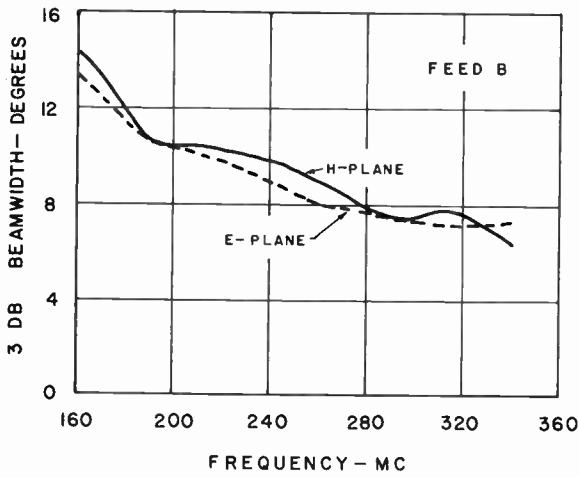


Fig. 5—Secondary pattern beamwidths for Feed B.

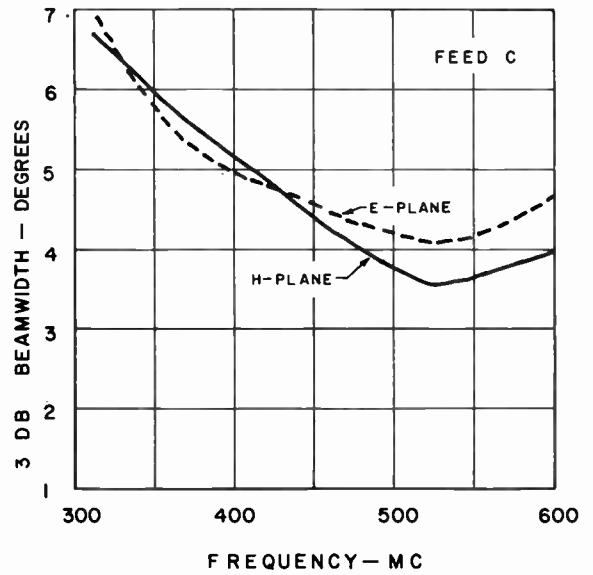


Fig. 6—Secondary pattern beamwidths for Feed C.

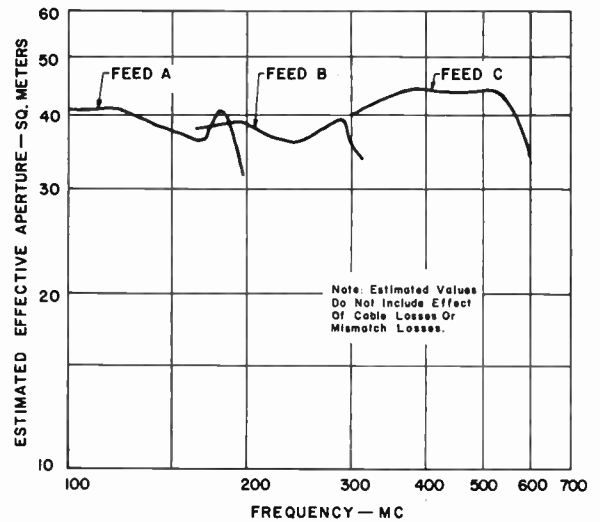


Fig. 7—Estimated effective aperture of antenna system.

the *E*-plane and *H*-plane 3-db beamwidths. This approximate calculation in the past has been found to give a reasonable agreement with actual gain measurements. Once the gain is known, the effective aperture can be determined by dividing the gain by  $4\pi$  and multiplying the result by the square of the wavelength. The results of this calculation appear in Fig. 7 and show estimated effective aperture for the final antenna. It should be noted that the actual collecting aperture finally realized will be somewhat lower due to cable losses and reflection losses caused by impedance mismatch.

FULL SCALE FEED

*Mechanical Considerations*

In designing the full scale version of the feed system, the linear dimensions of all radiating elements were increased by a factor of 6.82, corresponding to the frequency scaling factor. Thus, the primary patterns of the full scale feed would correspond identically to those of the model. A few minor changes were made for mechanical reasons. Some of the elements, which in the

model were circular in cross section, were changed to equal leg angles for the full scale feed. In so doing, the size of the angle was chosen to give the same electrical cross section as that of the circular rods used in the model. Use of angle members considerably simplified some of the design and assembly problems. Also, the dielectric supporting structure for the corner reflector elements was redesigned to provide a more rugged structure. The dielectric truss work, which consists of a number of Fiberglas channel sections and gusset plates, has a strength comparable to that of aluminum alloy. Because of the fact that the thickness of the Fiberglas is quite small in relation to the wavelength at 600 mc, its effect on the electrical performance is negligible.

In designing the antenna feed, structural members were chosen so that no element of the antennas would suffer permanent deformation at wind velocities below 120 mph. For lightness and corrosion resistance, 61ST aluminum alloy was used throughout the structure.

### Impedance Matching

Although it is readily possible to make radiation pattern studies on a scale model basis, the same is not true of impedance studies, because of the practical difficulties associated with the problem of scaling cable diameters and junction discontinuities. For this reason, it was not possible to design completely the impedance matching network on the scale model. Because the impedance compensating sections do not affect the radiation patterns, the final design of these sections was left for the full scale model.

Compensation of the full scale antenna was effected by a number of well-known techniques. In all cases, the impedance was measured when construction was completed, after which suitable compensating elements were added.

Feed C, the high-frequency horn, was matched by the use of stepped ridges in the waveguide section feeding the horn. Minor corrections were effected by a small impedance change in the short section of coaxial line connecting the ridges to the cable connector. The resulting input standing-wave ratio on the coaxial feed line was under 2 to 1 over the 300 to 600-mc range.

The S-band horn which was placed in the aperture of Feed C was a scaled version of the larger horn. Its impedance characteristics are such that its input standing-wave ratio is well under 2 to 1 over the 2000 to 4000-mc range.

Feed A for 100 to 180 mc consists of four dipole elements on the edges of the large horn plus its reflector screen. In order to obtain maximum band width, each element has its own compensating network since there is an appreciable length of cable between the dipole elements and the balun unit. The compensating network was a simple L section consisting of a shunt capacitive reactance and series inductive reactance at each dipole element. The balun unit itself was well matched and provided two pairs of balanced outputs to feed the dipole elements. The input standing-wave ratio of the antenna plus the balun was under 2.8 to 1 over the 100 to 180-mc range.

Feed B consists of a single balanced dipole plus its reflector elements. In order to compensate the dipole, it was necessary to use a transmission line section in series with the feed point to reduce the reactance spread. This transmission line section was located inside one of the dipole elements. The impedance curve was then shifted to the center of the impedance chart by two tandem transmission line transformer sections. The resulting impedance was such that the input standing-wave ratio of this antenna was under 2.8 to 1 over the 160 to 320-mc range.

Photographs of the complete feed system are shown in Figs. 8 and 9. The basic electrical configuration of the feed is not quite as evident as in Fig. 1, because of the Fiberglas truss work which was necessary to provide a sound mechanical structure.

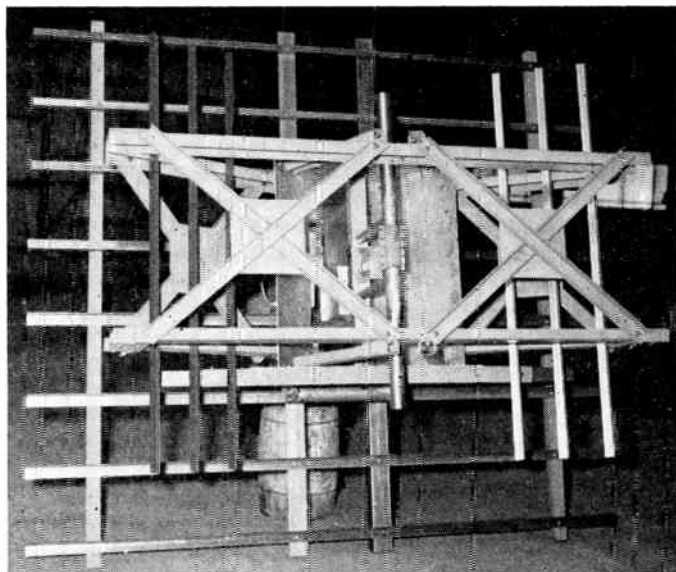


Fig. 8—Front view of full size feed.

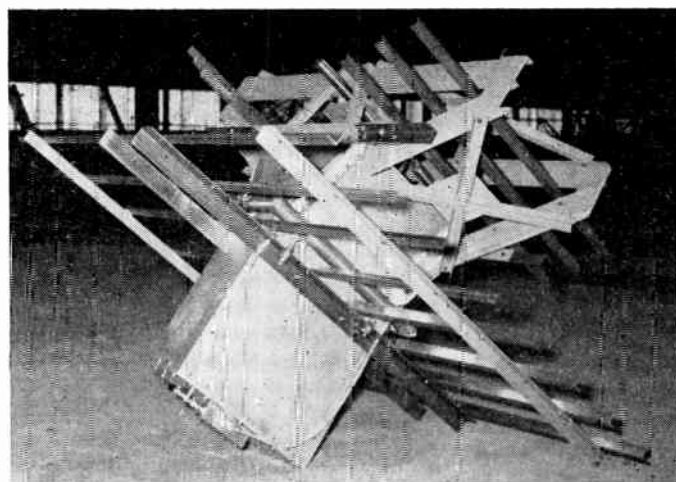


Fig. 9—Side view of full size feed.

Following installation of the feed in a 28-foot reflector, impedance measurements were taken to determine the amount of interaction between the feed and the reflector. As anticipated, the increase in the standing-wave ratio was relatively small above 200 mc. Below 200 mc, there was a somewhat larger increase in the standing-wave ratio at 155 mc and at 105 mc. Although this has the effect of reducing the effective area somewhat at these two frequencies because of the additional reflection loss, there is an ample amount of signal from the sun in this frequency range so that it is still possible to obtain excellent qualitative data on the noise spectrum of the sun. It is expected that more accurate quantitative measurements of the solar flux will be obtained after gain compensation has been applied to the scanning receivers.

Two versions of this antenna system have been built to date. The first has been installed at Harvard Observatory's field station at Fort Davis, Texas, and has been in operation for some time. Some rather interesting data



Fig. 10—Antenna system installed at Harvard Observatory Field Station, Fort Davis, Texas.



Fig. 11—Antenna system installed at University of Michigan, Ann Arbor, Mich.

has been obtained and it is expected that the results will be discussed in a paper to be published shortly by some members of the Harvard Observatory staff. A photograph of this antenna installation is shown in Fig. 10. The 28 foot reflector and its equatorial mount were supplied by the D. S. Kennedy Co., Cohasset, Mass. A second system has been in operation since August, 1957, at the Observatory of the University of Michigan, Ann Arbor, Mich. A photograph of this installation is shown in Fig. 11. The reflector and mount were also supplied

by the D. S. Kennedy Co. and are essentially identical to the first installation, except for the fact that the reflector surface is solid rather than being open mesh.

#### ACKNOWLEDGMENT

The development work described above was carried out under contract with the Harvard College Observatory whose work in the field of solar noise studies is being supported by the Geophysical Directorate of the Air Force Cambridge Research Center.

## The Radio Spectrum of Solar Activity\*

A. MAXWELL†, G. SWARUP†, AND A. R. THOMPSON†

**Summary**—Observations of the solar radio spectrum have been made at the Harvard Radio Astronomy Station, Fort Davis, Texas, daily from sunrise to sunset since September, 1956. The equipment comprises three separate receivers covering the total range 100–580

\* Original manuscript received by the IRE, November 12, 1957. This work forms part of a research program made possible by financial assistance from the Geophys. Res. Dir. of the USAF.

† Harvard Radio Astronomy Station, Fort Davis, Texas.

mc, and these are attached to a 28-foot-diameter paraboloid antenna. The outputs of the receivers are displayed on intensity modulated, high resolution cathode-ray tubes, and these are photographed by a continuous motion camera. Over-all, the system is approximately ten times more sensitive than any sweep frequency equipments used previously for solar observations. Examples of the records showing the four main types of radiation from active areas on the sun are given, and brief comments are made on the existing theories to account for them.

## INTRODUCTION

THE radio emission from the sun is composed of a background thermal emission from the solar atmosphere, and bursts of radiation, sometimes very intense, which originate in localized active areas on the disk. These bursts have complex characteristics, which make their classification very difficult from observations made with single frequency receivers. Observations over a large continuous band of frequencies, however, have made it possible to replace earlier empirical classifications of the radio bursts with a simple and natural classification based on their essential physical characteristics. The swept frequency technique, in which a narrow-band tunable receiver is repeatedly swept across a wide frequency range, was originally used by Wild and McCready<sup>1</sup> for solar observations in the range 70–130 mc, and subsequently by Wild, Murray, and Rowe<sup>2</sup> in the range 40–240 mc.

This paper is concerned with a new set of observations which have been taken at the Harvard Radio Astronomy Station, Fort Davis, Texas, since September, 1956. The new equipment covers the range 100–580 mc; it uses an antenna with five times the collecting area of that used by Wild and his colleagues, and its receiver noise figures are approximately 4 db lower. Because of its large frequency range and high sensitivity, the equipment is exceedingly vulnerable to interference, especially in the lowest 200 mc of its band, which is crowded with radio transmissions. It was therefore deemed necessary to set up the station in a remote part of the United States. A number of places were extensively surveyed for radio interference, and the site finally chosen was in the Davis Mountains of West Texas. The station (Fig. 1) is situated in a broad valley, and is surrounded by mountains 1500 feet higher; these give horizons of about 5° elevation at all azimuths. At frequencies above 35 mc, the station is virtually free from interference, apart from weak television signals on channels 2, 4, and 7, which have field strengths equivalent to 3, 1, and 4 microvolts at the terminals of a half-wave dipole; these are transmitted from the nearest large towns which are over 160 miles away.

Observations are taken daily from sunrise to sunset, and less than 5 per cent of the possible observing time has been lost. The station works in close cooperation with the Sacramento Peak Observatory, which forms its optical counterpart.

## EQUIPMENT

The frequency range of the equipment, 100–580 mc, is covered in three octave bands, 100–180, 170–330, and



Fig. 1—Laboratory and 28-foot paraboloid antenna, Harvard Radio Astronomy Station, near Fort Davis, Texas.

300–580 mc, by separate receivers. These sweep concurrently at a rate of 3 times per second, and are connected to separate broad-band primary arrays at the focus of a paraboloid antenna. The outputs are displayed on three intensity modulated cathode-ray tubes and recorded photographically.

*The Antenna*

The antenna has a diameter of 28 feet, a focal length of 12 feet, and is equatorially mounted. The primary arrays designed by Jasik<sup>3</sup> are described elsewhere in this issue. The low-frequency array is a double dipole and reflecting screen, the mid-frequency array a single dipole mounted in a corner reflector, and the high-frequency array an electromagnetic horn. They are mounted coaxially, and the mid-frequency array is cross polarized with the other two. The effective collecting area of the antenna varies between 38 and 45 square meters over the frequency range; this corresponds to an efficiency between 67 and 79 per cent, the geometric aperture being 57 square meters.

*The Receivers*

The receivers were built by Airborne Instruments Laboratory to meet the specifications of the Station. They are described in detail in another paper in this issue.<sup>4</sup> In each receiver the rf head consists of two grounded grid amplifier stages, an oscillator, and a crystal mixer. The local oscillator and the amplifier plate circuits are tuned by variable capacitors. These are geared to a synchronous motor and rotate at 3 rps. The full frequency sweep is achieved in 180° rotation, and the receiver output is rejected over the following half cycle where it is not possible to maintain alignment. The noise figures are 6, 7, and 8 db for the low, middle, and high-frequency bands, respectively, and are achieved by the use of Western Electric 416B triodes in the rf

<sup>1</sup> J. P. Wild and L. L. McCready, "Observations of the spectrum of high intensity solar radiation at metre wavelengths," *Aust. J. Sci. Res. A*, vol. 3, pp. 387–398; 1950.

<sup>2</sup> J. P. Wild, J. D. Murray, and W. C. Rowe, "Harmonics in the spectra of solar radio disturbances," *Aust. J. Phys.*, vol. 7, pp. 439–459; 1954.

<sup>3</sup> H. Jasik, "A wide-band antenna system for solar noise studies," this issue, p. 135.

<sup>4</sup> J. Goodman and M. T. Lebenbaum, "A dynamic spectrum analyzer for solar studies," this issue, p. 132.

stages. The IF bandwidths are 0.3, 0.5, and 1.0 mc, that is, about 1/300 of the range covered in each case.

### The Display Unit

The display unit comprises three high resolution cathode-ray tubes (DuMont K1207) which have a resolution of approximately 1000 lines across the 5-inch screen. A single vertical trace is produced on each tube by a deflection waveform which is derived from a discriminator fed by the local oscillator of the associated receiver; the spot displacement is therefore proportional to the instantaneous frequency of the receiver. The brightness is proportional to the receiver output. The three tubes are mounted one above the other, and are photographed by a continuous motion 35-mm camera in which the film moves horizontally at a speed of the order of 12 mm per minute. The pattern on the film is therefore an intensity modulated plot of frequency against time. The film used, Kodak Linagraph Panchromatic, was chosen to give the best compromise between speed and grain size. The whole system responds to intensity variations over a range of 30 db.

### OPERATION AND CALIBRATION OF THE EQUIPMENT

The equipment is switched on automatically at sunrise by a time clock. Minute marks are photographed on the films, and these are calibrated to an absolute accuracy of  $\pm 1$  second from the WWV transmissions. The films are developed to photometric standards.

After sunset each day the equipment is calibrated in frequency and intensity. For the frequency calibration, signal generators are used to provide six chosen frequencies within each octave band. Thus by interpolation one may deduce the frequency of the solar radio signals at any point on the film.

For the intensity calibration, the output of a noise diode source is fed into each of the receivers at 6 different levels covering a range of 18 db. The film density is thereby calibrated in terms of noise power applied to the receiver. It then remains to relate this input power to the intensity of the solar radiation incident on the antenna. This may be done as follows.

Let  $N$  = receiver input power corresponding to an antenna temperature  $T_A$ .  $N$  is a noise power, and is most conveniently expressed here in units of  $kT_0\Delta f$  (the power available from a matched resistor at ambient temperature) where  $k$  = Boltzmann's constant,  $T_0$  = ambient temperature,  $\Delta f$  = noise bandwidth of the receiver. The power applied to the receiver input may also be expressed in terms of  $T_A$  and the attenuation  $\alpha$  in the antenna cable.

Thus

$$NkT_0\Delta f = [\alpha T_A + (1 - \alpha)T_0]k\Delta f,$$

whence

$$T_A = \frac{1}{\alpha} (N + \alpha - 1)T_0. \quad (1)$$

The power delivered from the antenna terminals,  $kT_A\Delta f$ , is equal to that of the radiation absorbed by the antenna, that is,

$$kT_A\Delta f = \frac{1}{2} \Delta f \int \int_{4\pi} A B d\Omega.$$

Here  $A$  is the effective collecting area, and  $B$  the brightness in watts  $m^{-2}(cps)^{-1}$  steradian $^{-1}$  which is absorbed by the antenna. Both are functions of the direction of the solid angle  $d\Omega$ , and the factor 1/2 is introduced because the antenna absorbs radiation in one plane of polarization only. The integral may be evaluated in two separate parts, the first over the radio disk of the sun and the second over the remaining sky covered by the antenna beam. If  $B_1$  is the effective average value of the brightness over this remaining section of sky, then

$$kT_A = \frac{1}{2} A_0 \int \int_{\text{sun}} B d\Omega + \frac{1}{2} B_1 \int \int_{4\pi - \text{sun}} A d\Omega. \quad (2)$$

It has been assumed that the antenna beam is wide compared with the sun, so that for the first integral  $A$ , the effective collecting area may be taken as constant, and equal to  $A_0$ , the value corresponding to the center of the beam. On the same assumption the second integral is approximately that obtained by evaluating it over  $4\pi$  steradians. (This approximation is correct to  $\frac{1}{4}$  per cent at 100 mc, and to 3 per cent at 580 mc for the present equipment.)

Now,

$$\int \int_{\text{sun}} B d\Omega = I, \quad (3)$$

and

$$\int \int_{4\pi} A d\Omega = \lambda^2 \quad (4)$$

where  $I$  = intensity of solar radiation [watts  $m^{-2}(cps)^{-1}$ ], and  $\lambda$  = wavelength of the radiation. Also  $B_1$  is related to the equivalent value of temperature  $T_1$  by

$$B_1 = \frac{2kT_1}{\lambda^2}. \quad (5)$$

Combining (1) to (5),

$$I = \frac{2k}{A_0} \left[ \frac{1}{\alpha} (N + \alpha - 1)T_0 - T_1 \right].$$

Thus  $I$ , the intensity of the solar radiation, is determined in terms of  $N$ , which is directly related to the film density by the calibration. Of the other quantities involved,  $\alpha$  and  $A_0$  are known parameters of the equipment,  $T_0 = 300^\circ K$ , and  $T_1$  is the sky background temperature. (It is generally more convenient to express the sky radiation in terms of temperature than of brightness. The values of  $T_1$  depend on the sun's position in the sky; those values given in Table I indicate the order of magnitude.) From the value of  $I$  it remains only

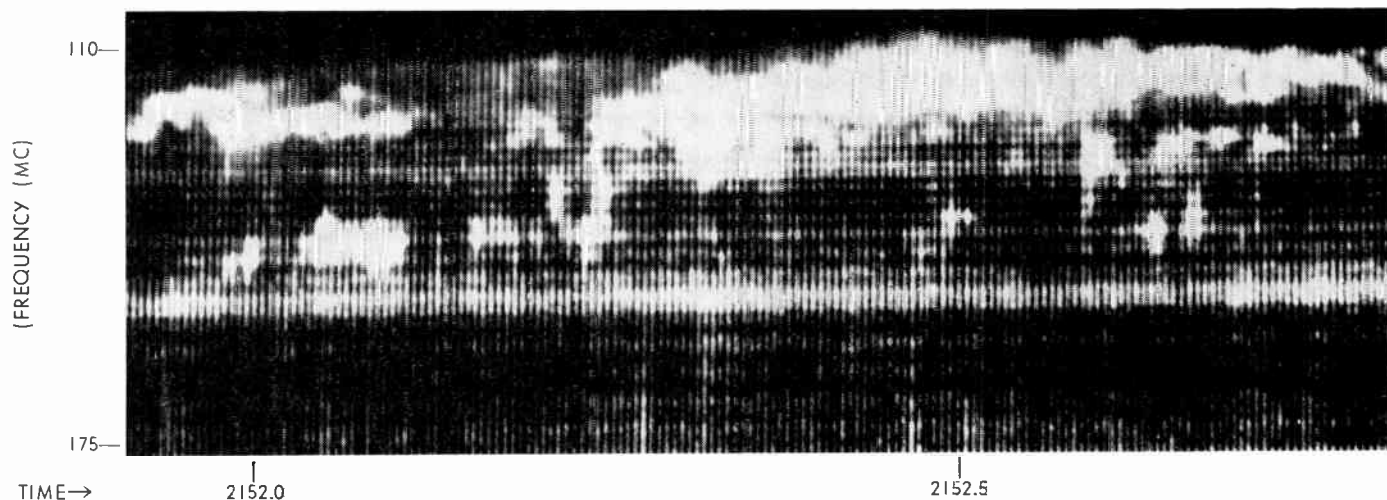


Fig. 2—Noise storm: January 19, 1957, 2152-53 U.T. The enlargement of this record is about four times greater than that of Figs. 3-8. The individual cathode-ray tube traces give the fine vertical structure.

to subtract the component due to the quiet sun to determine the intensity of the solar activity.

Approximate minimum detectable levels of solar activity at three frequencies are given for the present equipment in Table I.

TABLE I

Frequency	Background Sky Temperature ( $T_1$ )	Intensity of Quiet Sun	Minimum Detectable Solar Activity
100 mc	1000°K	$4 \times 10^{-22}$ watts $m^{-2}(cps)^{-1}$	$5 \times 10^{-22}$ watts $m^{-2}(cps)^{-1}$
300 mc	150°K	$4 \times 10^{-21}$ watts $m^{-2}(cps)^{-1}$	$5 \times 10^{-21}$ watts $m^{-2}(cps)^{-1}$
500 mc	50°K	$2 \times 10^{-21}$ watts $m^{-2}(cps)^{-1}$	$5 \times 10^{-21}$ watts $m^{-2}(cps)^{-1}$

#### OBSERVATIONS

The early spectral observations made by Wild and his co-workers established the fact that a great majority of the solar radio bursts belong to one of four distinct types. The classification is natural in the sense that the various types can be interpreted in terms of different physical processes on the sun. The present observations confirm that these identifications account for more than 95 per cent of the observed phenomena, but the greater sensitivity and different frequency range of the present equipment have given further information about the spectrum of the bursts. In this section the characteristics of the spectral classes are summarized briefly, and illustrated with examples from the records. A detailed description of the work will be given elsewhere, together with the correlation of the radio and optical solar data.

For the frequency band 100-580 mc, the assumption may be made that the solar radiation at a given frequency originates near a level in the solar atmosphere where the plasma frequency corresponds to that of the radiation. One may thus transform the frequency band

100-580 mc into a height range, which, at the present maximum of the solar cycle, lies roughly between 500-50-thousand km above the solar photosphere. It is therefore possible to interpret the frequency coordinates on the film records in terms of height. However, it must be emphasized that, although this interpretation gives the best physical picture so far suggested, and although it holds for the quiet (thermal) solar radiation, its validity is by no means established for the case of violent outbursts.

#### Noise Storms

A noise storm consists of a long series of short bursts continuing over hours or days. They are superimposed on a background of slowly varying enhanced radiation which has been described as a "continuum," although it is possible that the background may itself be composed of a large number of overlapping bursts. Noise storms are normally spread over a large frequency band but are rarely seen above 250 mc. On many occasions the bursts have bandwidths of a few megacycles and lifetimes extending from a fraction of a second to nearly one minute (Fig. 2). At other times bursts of bandwidth nearly 30 mc and lifetimes less than a second may predominate (Fig. 3).

Noise storms are caused by localized disturbances in the solar corona above active sunspot regions, but details of the radiation processes are not clearly understood.

#### Slow-Drift Bursts

A slow burst appears as a narrow band of intense radiation which drifts gradually, and sometimes irregularly, towards lower frequencies. Fig. 4 shows a typical example, where it will be seen that the average drift was  $-2.0$  mc. The spectra sometimes show the presence of a second harmonic (Fig. 5), but are often so complex as to preclude such identifications. Forty-six slow bursts have been recorded during the first 14 months' observations; their duration was 225 minutes which corresponds

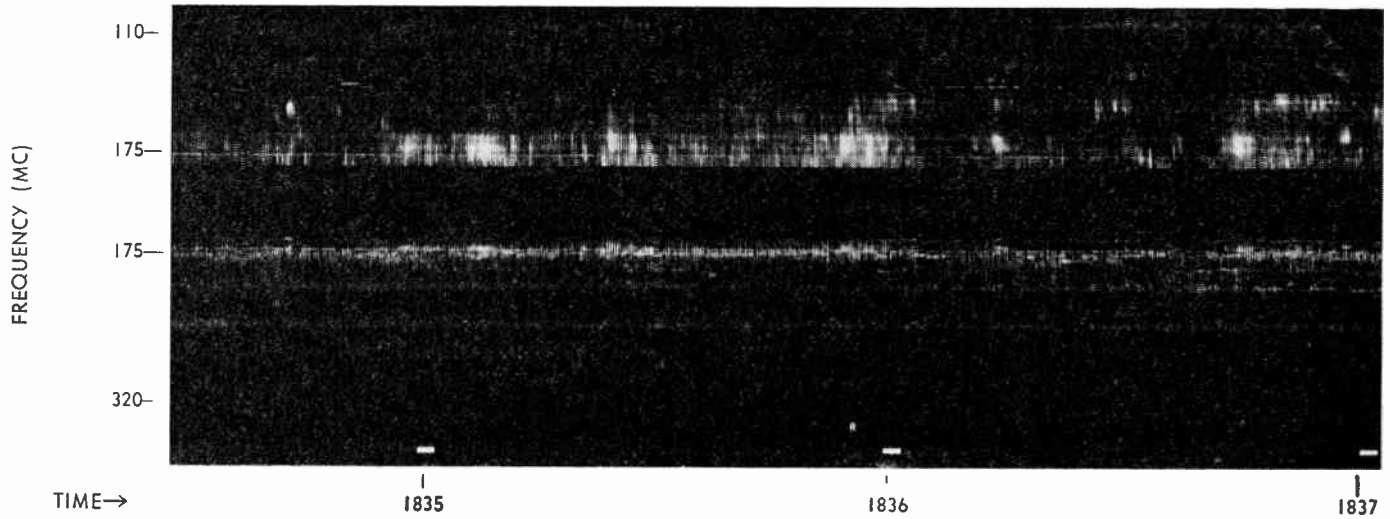


Fig. 3—Noise storm: October 12, 1957, 1835-37 U.T., showing wide-band, short duration bursts.

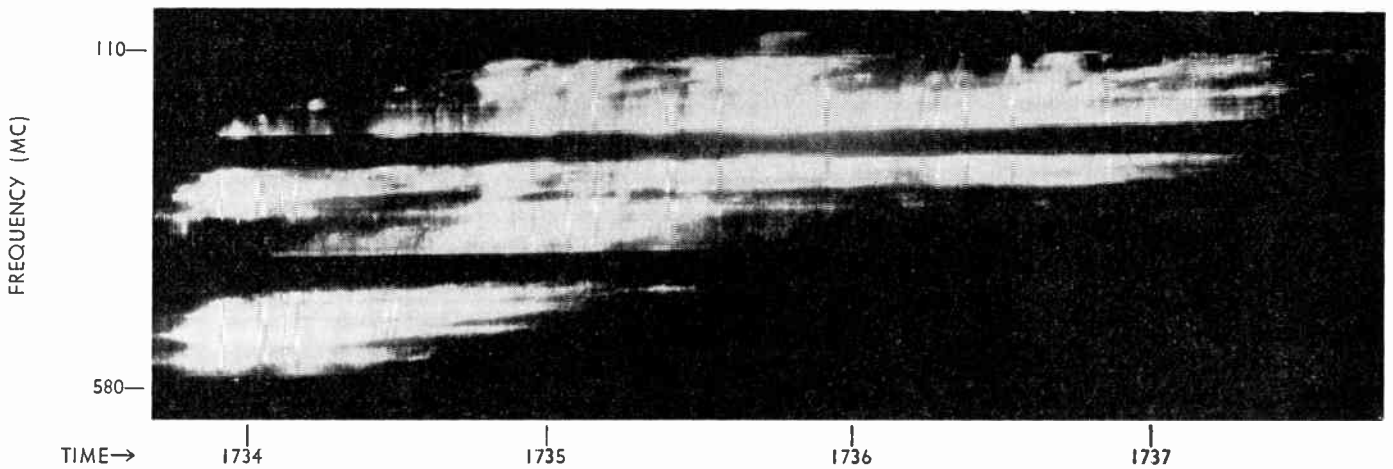


Fig. 4—High intensity slow-drift burst: January 7, 1957, commencing 1733.7 U.T. This burst, which is shown in its entirety, was completely isolated in time from any other activity. Unfortunately, there were no visual observations of the sun at that time.

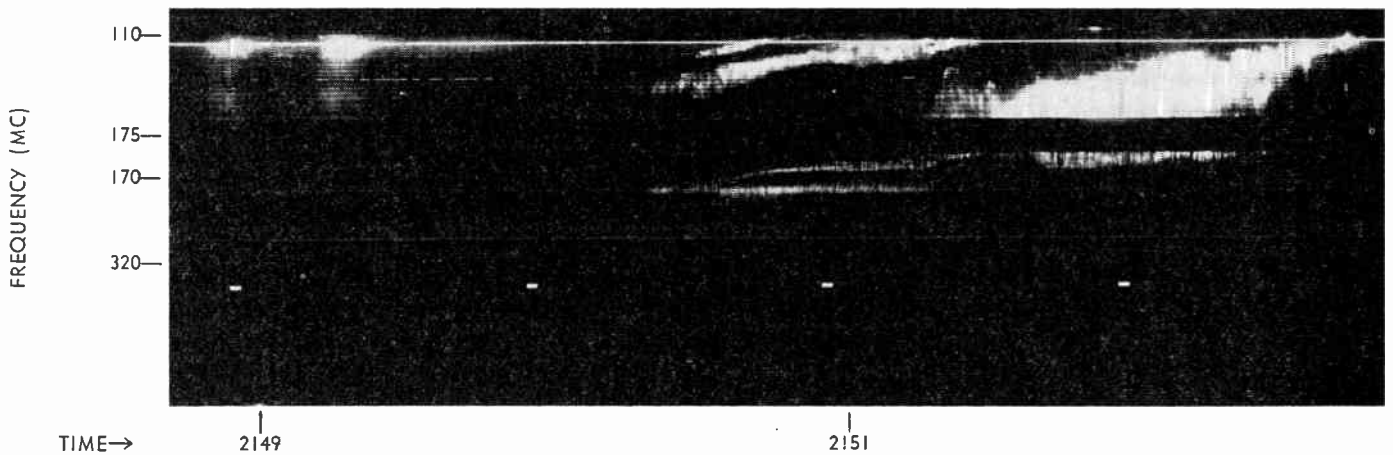


Fig. 5—Slow-drift burst with second harmonic: September 12, 1957, 2150 U.T. This was associated with a class-1 flare (beginning 2145, maximum 2148, end 2152 U.T.; 73° W, 12.5° S).

to a temporal probability of occurrence of 1 in 1300. The characteristic velocity of the solar disturbances which give rise to these slow bursts may be deduced from their rate of change of frequency. This velocity is of the order of 1500 km, and as it corresponds to that of

the so-called auroral corpuscular streams it has long been suggested that the slow bursts are caused by the passage of the streams through the solar atmosphere. Alternatively, the bursts may be caused by acoustic shock waves resulting from explosions in the lower at-

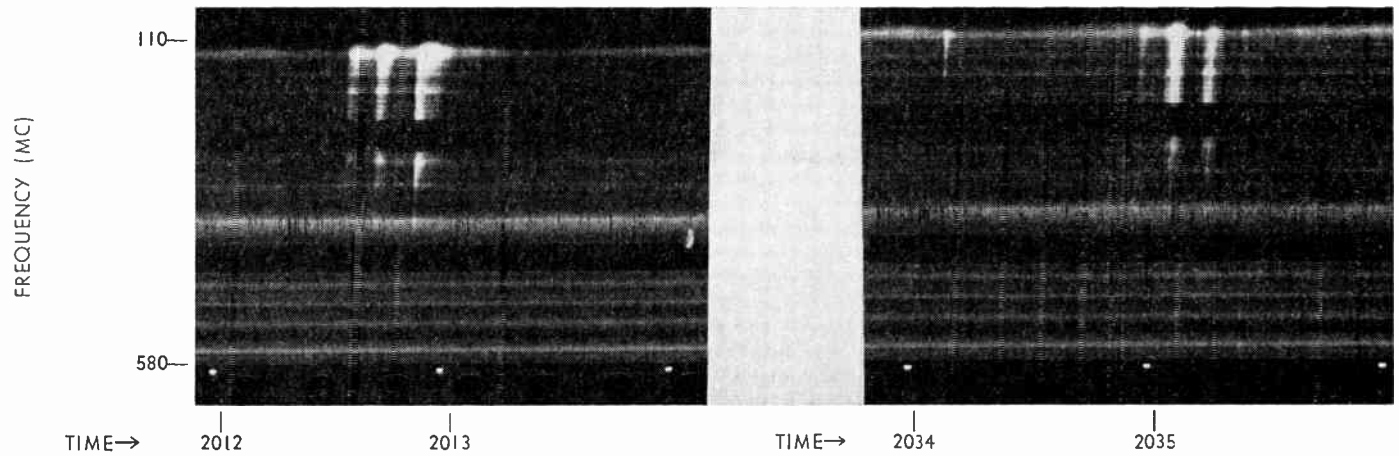


Fig. 6—Fast-drift bursts: November 25, 1956, 2013 and 2035 U.T. There were no optical observations at the time of the former. The latter was associated with a class-1 flare (beginning 2030, maximum 2035, end 2040 U.T.;  $36^{\circ}$  W,  $25^{\circ}$  S).

TABLE II  
ASSOCIATION OF FAST-DRIFT RADIO BURSTS WITH SOLAR FLARES  
(SEPTEMBER 1, 1956–JUNE 30, 1957)

Intensity in watts $m^{-2}(cps)^{-1} \times 10^{-22}$	Number of Bursts in Group	Number of Groups Recorded During Optical Observations	Percentage of Groups Associated with Flares
5–30 (Faint)	Not limited	610	47
30–100 (Moderate)	<10	246	45
30–100 (Moderate)	>10	82	56
>100 (Strong)	<10	82	56
>100 (Strong)	>10	64	72

mosphere. These waves, being propagated outward at some small multiple of the thermal velocity of the protons, would also be traveling at a velocity of the order of 1500 km.

#### Fast-Drift Bursts

Fast bursts, a very commonly occurring phenomenon, have durations of a few seconds and show exceedingly rapid drifts toward lower frequencies. They typically occur in groups of 3 to 10 with a total duration of less than 60 seconds, as illustrated in Fig. 6. During the period September 1, 1956–October 31, 1957, more than 9400 fast bursts were recorded. No definite correlation has previously been found between the bursts and solar optical phenomena. However, a comparison of the first ten months' observations at Fort Davis with the optical data shows the following: 1) during periods when optical observations were being made (approximately 50 per cent of the radio observing time) 50 per cent of the burst groups were associated with flares; 2) the positions of these flares were approximately uniformly distributed across the solar disk, and 3) the reverse correlation, that of 1215 flares with the radio bursts, was only 31 per cent. Details of this work will be published elsewhere; the association of the bursts with flares is summarized in Table II.

The observations have also revealed a new type of fast burst which appears on the records in the form of an inverted "U".<sup>5</sup> As in the example in Fig. 7, these bursts show a rapid decrease in frequency followed by an increase, and have a duration of a few seconds.

The source velocity which would be deduced from the slope of the fast bursts is of the order of 50,000 km. It has therefore been suggested that the bursts are caused by the outward passage of solar cosmic rays.<sup>6</sup> Alternatively it has been proposed that electron plasma shock waves may provide the mechanism.<sup>7</sup> On this latter hypothesis the "U" bursts would be caused by such waves being guided around a magnetic field of force.

#### Continuum

The continuum radiation is a steady enhancement of the background level over a wide band of the spectrum, and, as described earlier, is often associated with noise storms. At times, however, an extremely intense form of continuum radiation is observed covering a frequency

<sup>5</sup> Reported by G. Swarup at the American Astronomical Society Meeting, Cambridge, Mass.; May, 1957. Also, A. Maxwell and G. Swarup, "A new spectral characteristic in solar radio emission," submitted to *Nature*.

<sup>6</sup> J. P. Wild, J. A. Roberts, and J. D. Murray, "Radio evidence of the ejections of very fast particles from the sun," *Nature*, vol. 173, p. 532; March 20, 1954.

<sup>7</sup> M. Krook, unpublished.

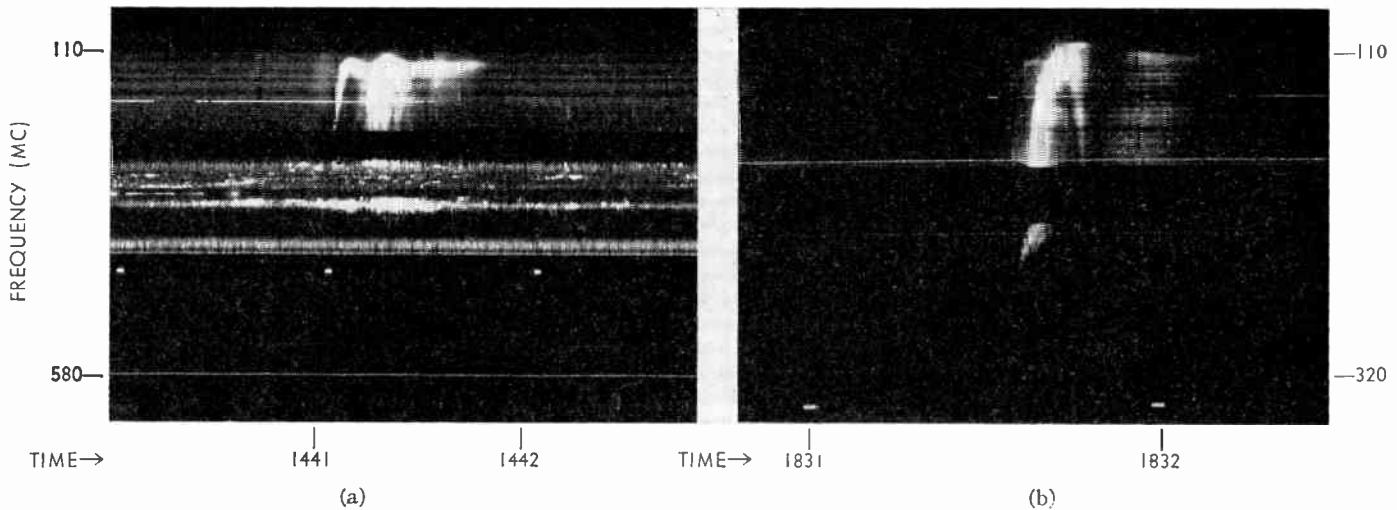


Fig. 7—Inverted “U” bursts: (a) February 26, 1957, 1441 U.T., associated with a class-1 flare (beginning before 1439, maximum 1440, end 1450 U.T.;  $75^{\circ}$  W,  $13^{\circ}$  N). Note the noise storm between 160 and 280 mc. (b) October 21, 1957, 1832 U.T. Note continuum, 200 mc wide, following burst. No optical observations were made at this time.

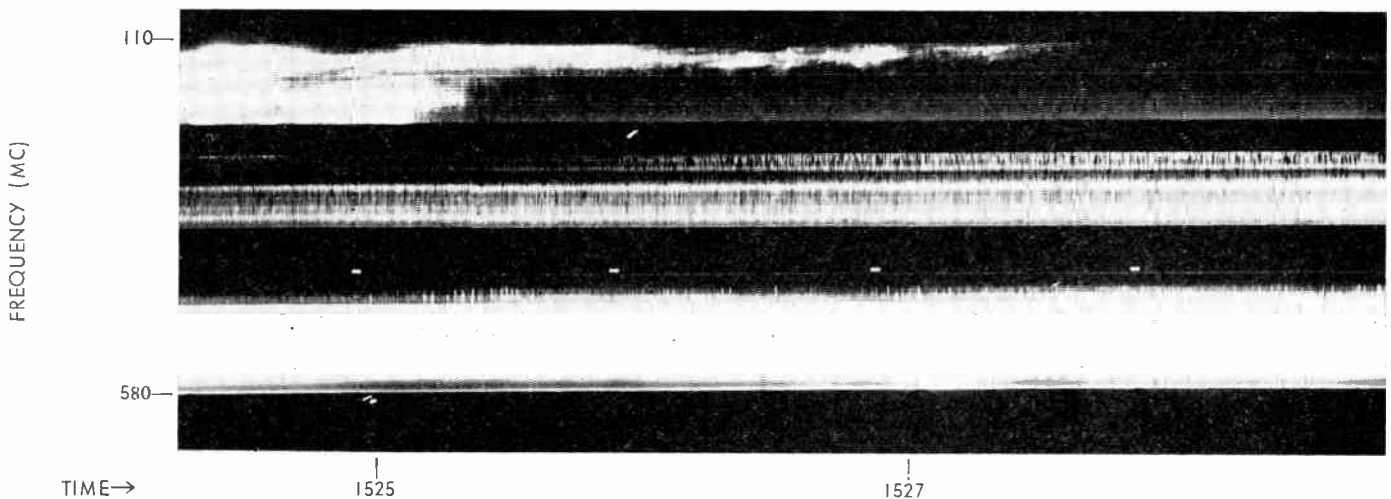


Fig. 8—Continuum: September 12, 1957. This is a small section from the record of a great solar radio outburst, which was associated with a class-2+ flare (beginning 1510, maximum 1517.5, end 1550 U.T.; intensity 35, which is the maximum;  $20^{\circ}$  W,  $12^{\circ}$  N). The continuum started at 1517 U.T., two minutes after the outburst commenced. Here it covers the range 180–580 mc and is gradually drifting downward in frequency. The end of a slow-drift burst can be seen on the low-frequency receiver, 100–180 mc.

band of more than 300 mc (Fig. 8). It occurs only after great outbursts, and lasts 10–60 minutes. This radiation probably corresponds to that described by Boisshot,<sup>8</sup> from single-frequency observations at 169 mc, as “Type IV” radiation.

Denisse<sup>9</sup> has suggested that it may be caused by the synchrotron mechanism.

<sup>8</sup> A. Boisshot, “Caractères d’un type d’émission hertzienne associé à certaines éruptions chromosphériques,” *Compt. Rend.*, vol. 244, pp. 1326–1329; 1957.

<sup>9</sup> J. F. Denisse, unpublished.

#### ACKNOWLEDGMENT

The authors are indebted to S. J. Goldstein for assistance with the initial observations and gratefully acknowledge the help and cooperation of Dr. H. Jasik, M. Lebenbaum, and J. Goodman in the construction of the equipment. They also wish to thank Prof. D. H. Menzel, of the Harvard College Observatory, and Dr. J. Evans and Dr. E. Dennison, of the Sacramento Peak Observatory, for invaluable help in establishing the Station.



# Studies at the McMath-Hulbert Observatory of Radio Frequency Radiation at the Time of Solar Flares\*

HELEN W. DODSON†

## THE COMPLEX FLARE PHENOMENON

### *H $\alpha$ and CaII Brightenings*

The principal optical aspect of the "flare event," and the one that is both necessary and sufficient at the present time for the identification of the phenomenon, is a relatively sudden increase in intensity of  $H\alpha$ , CaII, and other monochromatic radiations, in portions of the sun covering 50 to more than 1000 millionths of the solar hemisphere, for time intervals of the order of tens of minutes to several hours. The sudden brightenings generally take place in the bright plages that accompany or surround sun spots. The optical flare may be confined to the region of original brightening or may spread with time to quite distant areas.

### *Prominence Activity at the Time of the H $\alpha$ Brightening*

Visual and photographic studies also show that flare brightenings frequently are accompanied by certain types of prominence activity. With a small number of flares, a rapidly rising prominence is ejected from a region near the flare during the very early stages of the brightening.<sup>1</sup> These ejections, with velocities of the order of 1000 km are most easily observed as prominences when the associated flares are near the limb of the sun.

A much more usual type of flare-associated prominence is that indicated by the appearance on the disk of active dark flocculi in the postmaximum phase of flares. These primarily dark markings, exhibiting Doppler shifts of the order of a few hundreds of kilometers or less, probably are the disk counterparts of surge-type prominences seen at the limb. Visual and photographic records, made in the center of the  $H\alpha$  line, show that many of these active flocculi, during the first minutes of their lifetime, are *brighter* than the undisturbed  $H\alpha$  background.

In addition, certain flare-like events near the limb of the sun have shown that systems of very bright loops may develop and increase in size during the course of a flare. Finally, previously existing, relatively quiescent prominences, visible as "filaments" on the disk, may become active, show Doppler shifts, and be either partially or wholly dissipated during, or shortly after, flares in neighboring locations.

**Summary**—The complex flare phenomenon is described in terms of its photographic aspect on  $H\alpha$  spectroheliograms, associated prominence activity, terrestrial effects, and the general pattern of radio frequency emission. Flare-associated events at 2800 and 200 mc are reviewed, and the association between flares and the onset of 200-mc noise storms is discussed. Records of 2800 and 200-mc radiation at the time of 277 flares are compared. Flare-events at frequencies less than 200 mc are considered, and a study of 496 flares at 80 mc is summarized.

An effort is made to compare reports of dynamic spectra at radio frequencies with flare data and single frequency records.

The apparently close association between flares with "major early bursts" at frequencies  $< 200$  mc and geomagnetic disturbances is discussed.

## INTRODUCTION

THE long series of photographic records of solar activity at the McMath-Hulbert Observatory of the University of Michigan has made possible, throughout the past eight years, comparison of distinct solar events with concomitant solar emission at radio frequencies. Investigations into the relationships between optical features and radio frequency emissions have been, in large part, cooperative undertakings between staff members of the McMath-Hulbert Observatory, where the optical studies have been made, and staff members of the laboratories primarily devoted to radio frequency observations.

The work reported here stems from close cooperation with the School of Electrical Engineering of Cornell University whose excellent 200-mc solar records have been shared with us since 1950, and with the National Research Council of Canada at Ottawa, where for more than 10 years, A. E. Covington has recorded with great precision solar emission at 2800 mc. The daily 80-mc solar records of the Cavendish Laboratory, Cambridge, England, also have been made available to us and have been examined for the period January, 1949, to August, 1955.

Early in our investigations it became apparent that the complex solar event known as a *flare* was closely associated with many of the great enhancements at radio frequencies. Consequently, a large part of our work has been directed towards determining the general pattern of radio frequency emission at the time of solar flares. On the basis of both optical and radio frequency observations, a "flare" is a complex phenomenon and the interrelationships of its many aspects still are not clearly understood.

\* Original manuscript received by the IRE, November 6, 1957.

† McMath-Hulbert Observatory, University of Michigan, Ann Arbor, Mich.

<sup>1</sup> H. W. Dodson, E. R. Hedeman, and J. Chamberlain, "Ejection of hydrogen and ionized calcium atoms with high velocity at the time of solar flares," *Astrophys. J.*, vol. 117, pp. 66-72; January, 1953.

### Terrestrial Effects of Flares

Certain "terrestrial effects" provide evidence for additional aspects of the complex flare phenomenon. Ionospheric disturbances occur in close time association with a majority of flares and imply an increase in ultraviolet radiation or X rays at the time of the  $H\alpha$  brightening. Relationships between certain flares and subsequent geomagnetic storms indicate that at least some flares are accompanied by the actual ejection of material particles which, hours or days later, may impinge upon the earth's atmosphere and cause a geomagnetic storm and an aurora. Finally, there have been great increases in cosmic rays received on the earth within minutes or hours after the occurrence of a small number of great solar flares.

### General Pattern of Radio Frequency Radiation at the Time of Solar flares

Examination of daily 2800, 200, and 80-mc records for most of the 8-year interval, including 1949 and 1956, and records published in the literature for intermediate frequencies, has shown that the basic patterns of flare-associated radiation, within this frequency range, are fundamentally similar. At these frequencies, the fully developed flare event exhibits two parts, but either of the two parts may occur separately. With many flares there is no distinctive enhancement at radio frequencies. See Fig. 1.

The first or "early" part of the double pattern is a sudden burst that starts with the  $H\alpha$  flare and usually is over by the time  $H\alpha$  maximum has been attained. At 2800 and 200 mc, the second part is an enhancement that generally starts more gradually than the first part. At 200 and 80 mc the second part is definitely a "late" component, since it begins after  $H\alpha$  flare maximum has been attained and reaches its maximum late in the course of the flare. It may continue long after the  $H\alpha$  flare has faded.

#### FLARE EVENT AT 2800 MC<sup>2</sup>

At 2800 mc, the first or early part of the flare-associated event is a sudden single burst which may be either simple or complex in structure. (See Fig. 1.) In general, this burst starts with the onset of the flare and is over by the time maximum intensity has been attained by  $H\alpha$  radiation in the flare. For the flares that we have studied, the maximum of the 2800-mc burst precedes  $H\alpha$  maximum by an average of 3.4 minutes. Thus, the sudden burst type event at 2800 mc definitely is associated in time with the period of increasing  $H\alpha$  intensity in the flare.

The second or late part of the "flare event" at this frequency is a gradual diminution of excess flux. When

only the second part of the flare pattern occurs, the distinctive event is classified as a "gradual rise and fall." This type of event at 2800 mc appears to start with the  $H\alpha$  flare but has its maximum either at the time of  $H\alpha$  maximum, or later.

Our detailed study<sup>2</sup> in 1953 of 2800-mc solar radiation, as recorded at Ottawa, provided strong evidence that there is an outstanding event or disturbance in solar radiation at this frequency only when a flare or subflare is in progress. In recent years, the sensitivity of the Ottawa equipment has been increased, and less intense and more frequent events are reported. Spot checks continue to provide evidence for a very close

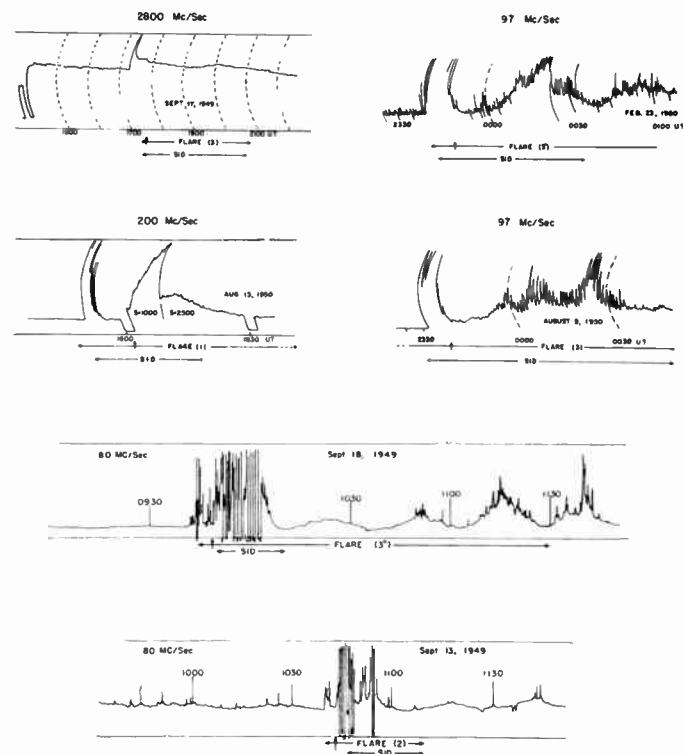


Fig. 1—Examples of 2800, 200, 97, and 80-mc radiation at the time of solar flares. Vertical arrows indicate times of flare maxima. The 80-mc records were made with an interferometer and show maxima and minima in the interference pattern as well as changes in solar emission.

association between 2800-mc events and optical phenomena. For example, on July 24, 1956, the report of 2800-mc outstanding events includes a "group of eight bursts," between 17<sup>h</sup>51<sup>m</sup>.2 and 24<sup>h</sup>30<sup>m</sup> U.T. Even though our calcium spectroheliograms for this date monitored only the large active center in the southeastern part of the solar disk, they showed small temporary brightenings in very close time association with four of the 2800-mc bursts. Ionospheric records, after the close of our photographic program at 2141 U.T., indicated the occurrence of flares with two more of the 2800-mc events. The data are summarized in Table I and an example of the brightenings is shown in Fig. 2(a).

<sup>2</sup> H. W. Dodson, E. R. Hedeman, and A. E. Covington, "Solar flares and associated 2800 mc/sec (10.7 cm) radiation," *Astrophys. J.*, vol. 119, pp. 541-563; May, 1954.

TABLE I

COMPARISON OF A GROUP OF 8 BURSTS AT 2800 MC JULY 24, 1956, (REPORTED BY COVINGTON, OTTAWA, CANADA) WITH CONCOMITANT PHOTOGRAPHIC AND IONOSPHERIC DATA

2800-MC Event			Small Brightenings in Southeastern Plage (Calcium Spectroheliograms)	Flares, as Indicated by Sudden Short- Wave Fades
Type	Time U.T.	Peak Flux $10^{-22}\text{wm}^{-2}(\text{cps})^{-1}$		
Single	1751.2-1752	9	No event in plage photographed	—
Single	1811 -1812	12	1810.5-1814	—
Single-simple	1908.3-1910.8	19	During a small flare, 1854-1920, but probably not associated	—
Single-simple	1934.5-1937.5	24	1934.5-1940	—
Single-simple	2025.8-2027	19	2025.5-2029	—
Single-simple	2048.3-2049.8	15	2048 -2051	—
Single-simple	2156.5-2207.5	*350		2158-2218
Precursor	2230	11	No spectroheliograms at these times	2237-2303
Single-simple	2233 -2245	200		
Post Increase	2245 ->2430	15		

\* Estimated.

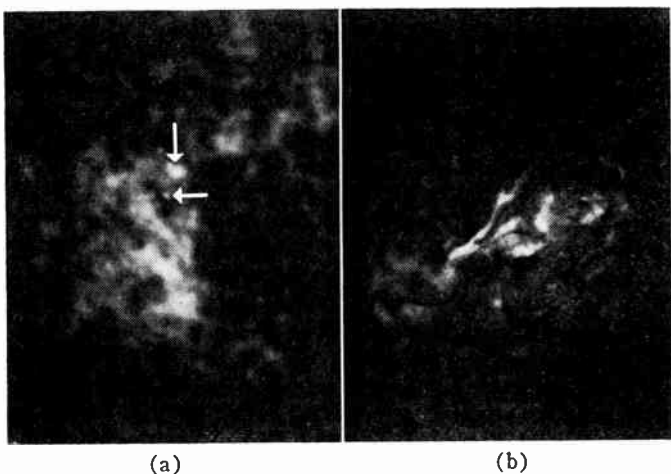


Fig. 2—Spectroheliograms showing solar phenomena at the time of certain distinctive events at radio frequencies. (a) Calcium spectroheliogram, 1956 July 24<sup>d</sup>19<sup>h</sup>34.<sup>m</sup>5 showing small round dot over umbra of spot and larger region near it that brightened simultaneously with small 2800-mc burst (see Table I). (b)  $H\alpha$  spectroheliogram 1951 June 16<sup>d</sup>17<sup>h</sup>27<sup>m</sup> showing large flare associated with great increase in 200-mc noise storm.

According to all of our studies there is very close time association between 2800-mc bursts and temporary brightenings visible on  $H\alpha$  and  $\text{Ca}^+$  spectroheliograms.

### FLARE EVENTS AT 200 MC<sup>3</sup>

#### Outburst-Type Phenomena

Starting times of the sudden burst-type features that constitute the early parts of flare events at this frequency cluster closely about the starting times of the flares. The "early burst" generally is over before, or close to the time of,  $H\alpha$  maximum. It is unfortunate that the great, early bursts are off scale, and therefore unmeasurable, on almost all of the calibrated records at low frequencies.

The second part of the flare-associated outburst at this frequency often appears to be a great increase in the

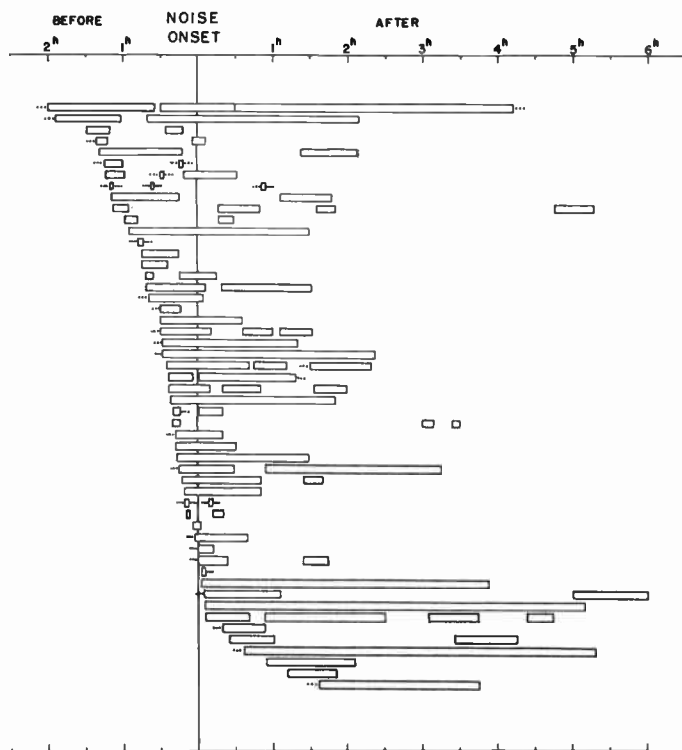


Fig. 3—Comparison of times of onset of 200-mc noise storms with occurrence and duration of  $H\alpha$  flares. The vertical line represents the time of start of the noise storm, and each horizontal entry represents a different storm. Small rectangles give the starting times and durations of  $H\alpha$  flares. Dots indicate that time of beginning or ending of a flare was not reported.

continuum or base level, without correspondingly great superposed bursts (see Fig. 1). The increase in flux generally starts as the  $H\alpha$  flare begins to fade and often lasts long after the  $H\alpha$  flare has ceased to be visible as a distinct solar feature. In some cases, the second part of the flare event at 200 mc is a noise storm of long duration with very great burst activity superposed on the increased base level. The relationship between these two types of enhanced 200-mc radiation during the post maximum phase of  $H\alpha$  flares must await more information on polarization, dynamic spectra, and better under-

<sup>3</sup> H. W. Dodson, E. R. Hedeman, and L. Owren, "Solar flares and associated 200 mc/sec radiation," *Astrophys. J.*, vol. 118, pp. 169-196; September, 1953.

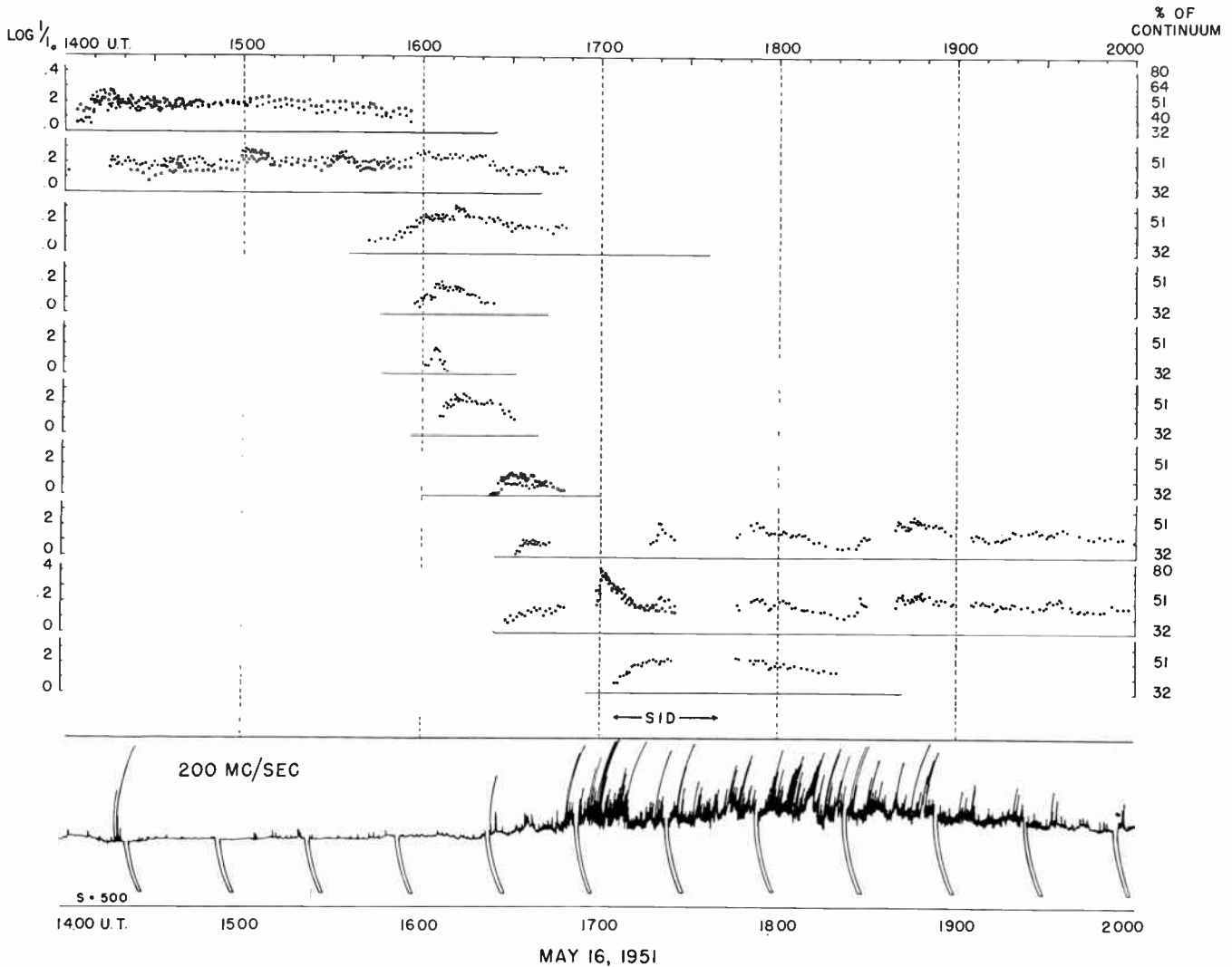


Fig. 4—200-mc record of May 16, 1951, showing onset of noise storm, and photometric light curves for concomitant flares in region very close to central meridian.

standing of the physical causation of the respective phenomena. The time relationships, with respect to flares, for the two types of enhancement are very similar.

#### Noise Storms

*Frequency of Association between Flares and Onsets of Noise Storms:* Association of very great bursts, or outbursts, with flares is well established, but the relationship between flares and noise storms at low radio frequencies is considerably less clear. Since this is the case, we have investigated the relationship between flares and all noise storms on the 200-mc Cornell records from April, 1950, when the daily 8-hour records were first made, to July, 1953. This study provides strong evidence for an association between flares and the well-defined onsets (or well-defined increases) of many noise storms. During this period, the Cornell records show 91 instances of the beginning of a protracted period of enhanced radiation of the type described as "noise storm." For 57 of the 91 cases, flares or subflares are known to have been in progress close to the starting times of the

200-mc enhancements. (See Fig. 3, p. 151, for a schematic representation of many of these cases.) In two additional cases, sudden ionospheric disturbances were reported, and for a third, brightenings (possibly of a flare-like nature) in a prominence accompanied the onset of the noise storm. For the times of 29 of the remaining 31 cases we have neither photographic nor visual observations and, therefore, cannot be certain of the solar circumstances. For the final 2 cases, intermittent visual observations were in progress at our observatory but flares were not reported. Thus, for 98 per cent of the recorded onsets of noise storms, there were either flares, SID's, or no observations.

The time relationships between the flares and the onsets of 200-mc "noise" in this investigation confirm the earlier study<sup>3</sup> in which "noise storms" were recognized as one of the "late" aspects of the flare-associated event at this frequency.

*Characteristics of Flares Associated with Onsets of Noise Storms:* H $\alpha$  flares identified and selected on the basis of their time association with the onsets of 200-mc

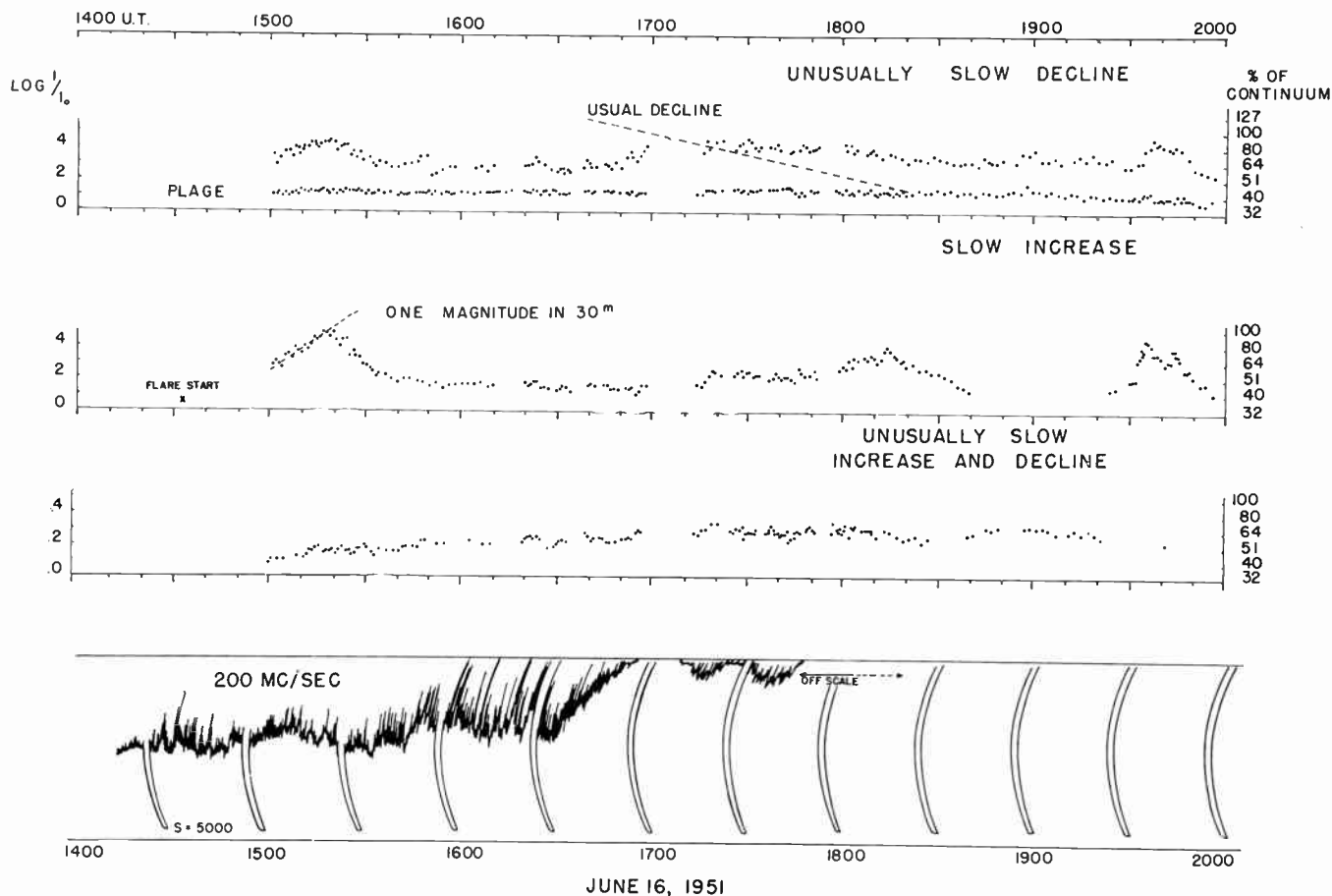


Fig. 5—200-mc record for June 16, 1951, showing a great increase in flux during a noise storm, and photometric light curves for concomitant flares in region 25 east of central meridian.

noise storms present a certain number of common characteristics. First of all, the group contains a high percentage of flares with such a complex structure and assorted brightenings that they do not lend themselves readily to representation by composite, representative light curves. More than half of the flare phenomena associated with the onset of noise storms were what might be termed "multiple flare events," in the sense that at the time of the noise storms several flares, in the same plage, followed each other in close succession. Our photographic records show that the flares were usually brightenings of different parts of the same plage rather than repeated brightenings of exactly the same region as so often happened. The 57 flare-associated noise storms involved a total of 98 separately reported flares. A number of these flares seemed to spread laterally with time, or to break out successively in a number of different regions within the plage. The photometric light curves shown in Fig. 4, for May 16, 1951, illustrate these complexities. The brightenings measured here were reported as 3 flares, each with multiple maxima, and each in a somewhat different part of the plage.

Many of the flares associated with the onsets of noise storms rose to maximum at a relatively gradual rate. The rate of increase of  $H\alpha$  intensity was often the slowest of the three general rates of rise found in our photo-

metric study of flares.<sup>4</sup> The rate of decline also was often very slow. The photometric light curves shown in Fig. 5, for the flares of June 16, 1951, illustrate these aspects. The flare at 1500 U.T. on this date was the only flare in our photometric program that reached a maximum intensity as great as that of the continuous spectrum at the slowest of the three rates of rise.

The  $H\alpha$  spectroheliogram of the flare of June 16, 1951, shown in Fig. 2(b), illustrates another characteristic of the flares associated with the onsets of noise storms. Frequently the "noise storm flares" must be described by the words patchy, stringy, outlines a dark filament, rather than by the more usual terms compact, clearly outlined, round.

In our photometric study<sup>4</sup> of flares, we have reported that the ionospheric effects of some of the "noise storm flares" were less than the large size and brightness of the flares led us to expect.

Finally, the flares associated with the onset of noise storms showed a higher than average concentration toward the central part of the solar disk. Seventy-eight per cent of the individual flares associated with noise storms occurred within  $40^\circ$  of the central meridian.

<sup>4</sup> H. W. Dodson, E. R. Hedeman, and R. R. McMath, "Photometry of solar flares," *Astrophys. J. Suppl. Ser.*, vol. 2, suppl. no. 20, pp. 241-270; February, 1956.

However, our study<sup>5</sup> of 2295 flares in the *Quarterly Bulletin* has shown that, in general, only 53 per cent of reported flares are observed in this portion of the solar disk.

*Center-To-Limb Effect in Noise Storms:* If it be assumed that the positions of flares associated with the onsets of noise storms provide information about the location of the source of enhanced 200-mc radiation, then a center-to-limb effect can be found in the relative intensities of continuum and superposed bursts.<sup>6</sup> When the flares were within 25° of the central meridian, the amplitude of the superposed noise storm bursts generally was less than the intensity of the continuum. For flares between 25° and 50° CMD, there were as many cases with burst amplitude greater than the continuum as the reverse. When the flares were more than 50° from the central meridian, the amplitude of the bursts was greater than the intensity of the continuum for more than 90 per cent of the cases. This variation from center-to-limb in relative intensity of storm-base-level and burst amplitude suggests that the two aspects of a noise storm may originate at different levels in the solar atmosphere. It also should be pointed out that the identification of the noise-emitting regions by associated flares indicates that 200-mc "storm" radiation is received from active regions at all meridian distances, even from regions on the solar limb.

The foregoing investigations have shown that the great, well-defined *onsets* of noise storms often take place when flares are in progress, or just over. Furthermore, near solar minimum in 1954, enhanced 200-mc radiation of the noise storm type occurred during the transit across the solar disk, of all regions in which flares were observed, but not during the transit of all bright calcium plages, nor of all regions with strong green coronal emission.<sup>7</sup> In spite of this evidence for a close association between flares and 200-mc noise storms, we have also found that there were, during the interval studied, certain very long periods of greatly enhanced 200-mc radiation for which the concomitant flare occurrence was relatively low. These cases must be studied further.

#### COMPARISON OF 2800-MC AND 200-MC RADIATION AT THE TIME OF 277 FLARES

##### *Morphology of the Events*

In order to permit direct comparison of flare-associated emission at 2800 and 200 mc, we have brought together data for the 277 flares between August, 1948 and

June, 1952 for which the two radio records were available to us for study.

For about 60 per cent of the flares, the general patterns of the radio frequency events at the two frequencies were basically similar, in the sense that flares that had "double" events at one frequency, had "double" events at the other, or only "early," or only "late" phenomena, respectively. Of the 163 flares for which there was no distinctive event at 2800 mc, 63 were also "null" at 200 mc and 52 more were associated with only very low energy or poorly defined events at the lower frequency. For the remaining 40 per cent of the flares, there were gross differences in the flare events at the two frequencies.

##### *Time Relationships*

For flares with "early," burst-like features at the two frequencies, the starting times of the bursts were very similar. The average difference was only 0.3 minute, and in the sense that the 2800-mc burst preceded the 200-mc burst. It should be remembered that, at best, we have been able to determine times only to the nearest tenth of a minute and that we are comparing records made at different institutions with different types of instruments.

The second or "late" parts of the flare events have a much greater difference in time of onset at the two frequencies than do the "early" parts. At 2800 mc, the second part apparently starts with the flare itself, or while the "early" burst is still in progress. At 200 mc the "second" part often is well separated from the first, and its onset usually does not occur until after flare maximum has been passed. In the second part of the flare event at radio frequencies, the longer wavelength radiation apparently lags behind the shorter.

##### *Basically Similar Flare Events at the Two Frequencies*

Direct comparison of flare-associated, distinctive events at the two frequencies is easiest when the events are the simplest. Often the single, and single-simple bursts at 2800 mc apparently mesh exactly with comparable events at 200 mc. There are even certain cases, though much rarer, when the "gradual rise and fall" at 2800 mc has a similar counterpart at 200 mc. See Fig. 6.

When the flare-associated bursts are more complex, even though the events may be similar in basic pattern at the two frequencies, they will often differ greatly in detail. To illustrate these complexities, we show in Fig. 7 the photometric  $H\alpha$  light curves, and the 2800 and 200-mc records for three flares of importance 2. It is hoped that in the future information from dynamic spectra will permit us to identify, on records such as these, the various spectral types of radio bursts, and the harmonics of lower frequencies. This information may make possible a clearer understanding of the significance of radio frequency emission at the time of flares.

<sup>5</sup> L. Goldberg, H. W. Dodson, and E. A. Müller, "The width of  $H\alpha$  in solar flares," *Astrophys. J.*, vol. 120, pp. 83-93; July, 1954.

<sup>6</sup> H. W. Dodson, "Relation between Optical Solar Features and Solar Radio Emission," IAU Symp. IV in "Radio Astronomy," ed. H. C. van de Hulst, Cambridge University Press, Cambridge, Eng., pp. 327-333; 1957.

<sup>7</sup> H. W. Dodson and E. R. Hedeman, "Resume of visually and photographically observed solar activity at time of 200 mc/sec noise storms near 1954 solar minimum," *Astrophys. J.*, vol. 125, pp. 827-830; May, 1957.

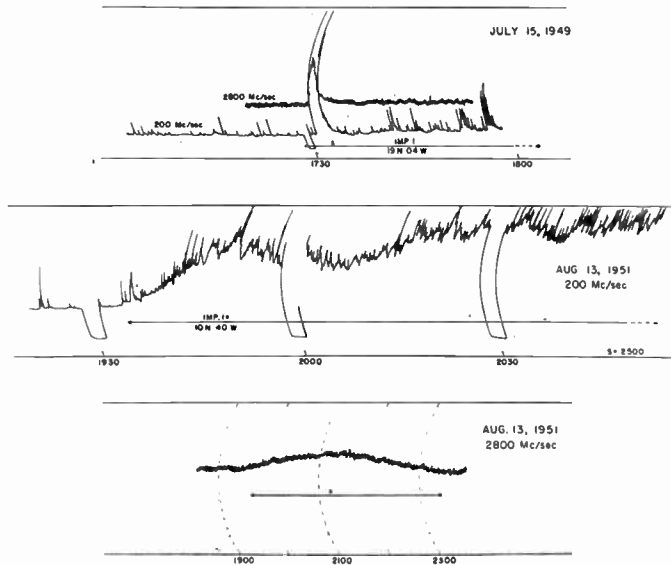


Fig. 6—Examples of "similar patterns" of flare-associated radiation at 2800 and 200 mc. Cross indicates time of flare maximum.

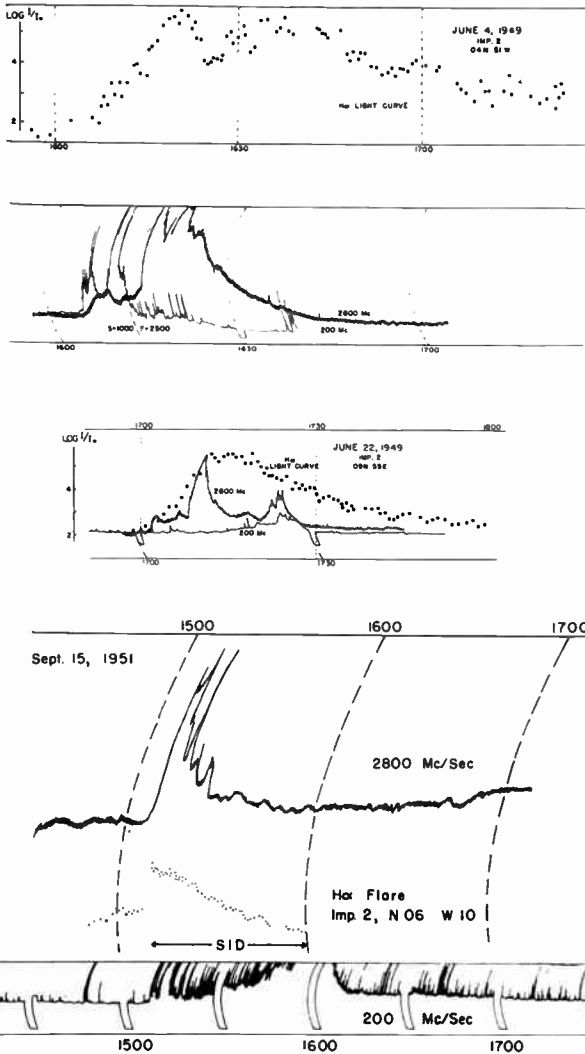


Fig. 7—Examples of complex flare events at 2800 and 200 mc and photometric light curves of concomitant  $H\alpha$  flares. Note change of sensitivity in 200-mc record for June 4, 1949.

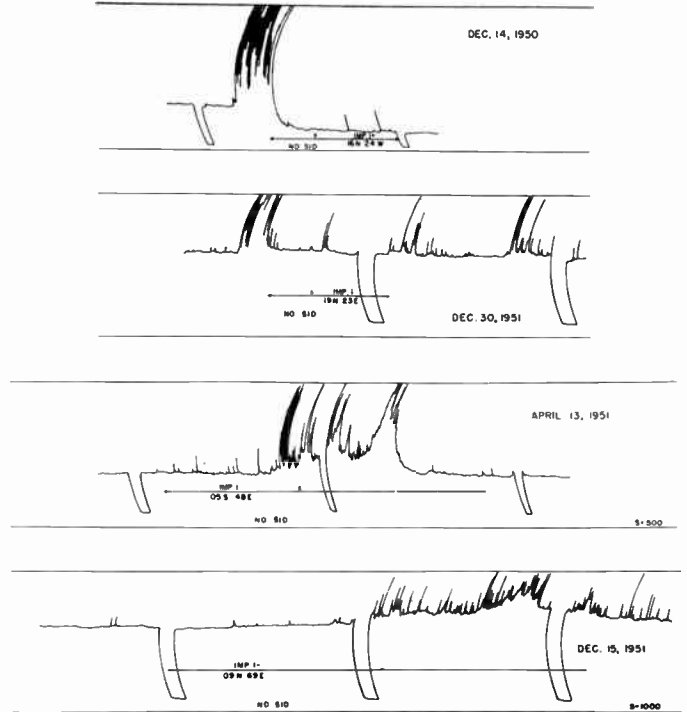


Fig. 8—Examples of 200-mc radiation at the time of flares for which there was no distinctive event at 2800 mc. The first two cases are premaximum events and the last two are primarily post-maximum. Crosses indicate time of flare maximum. Time scale is given by "dummy load" at 30-minute intervals.

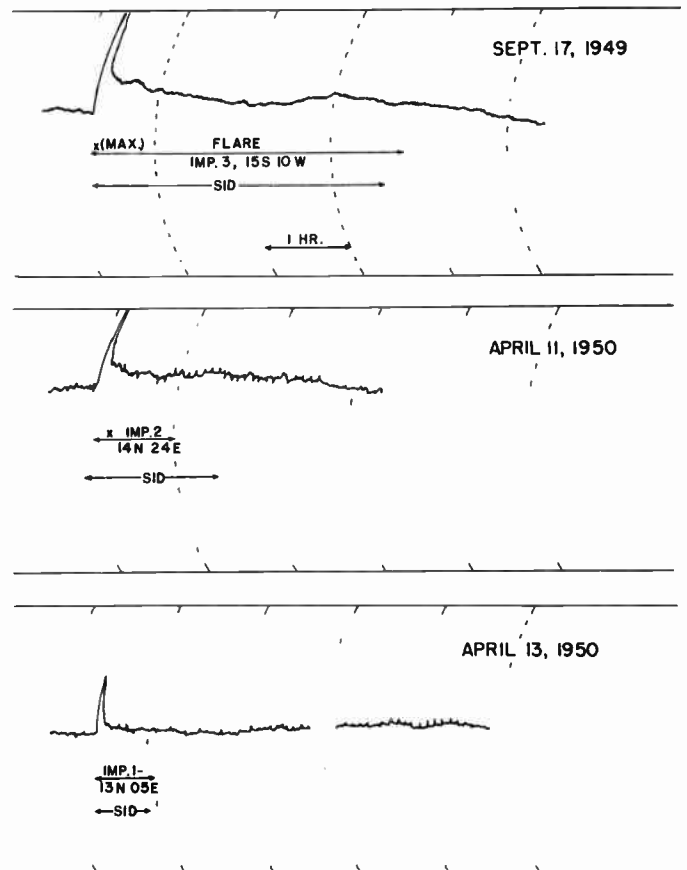


Fig. 9—Examples of 2800-mc radiation at the time of flares for which there was no distinctive event at 200 mc. Cross indicates time of flare maximum.

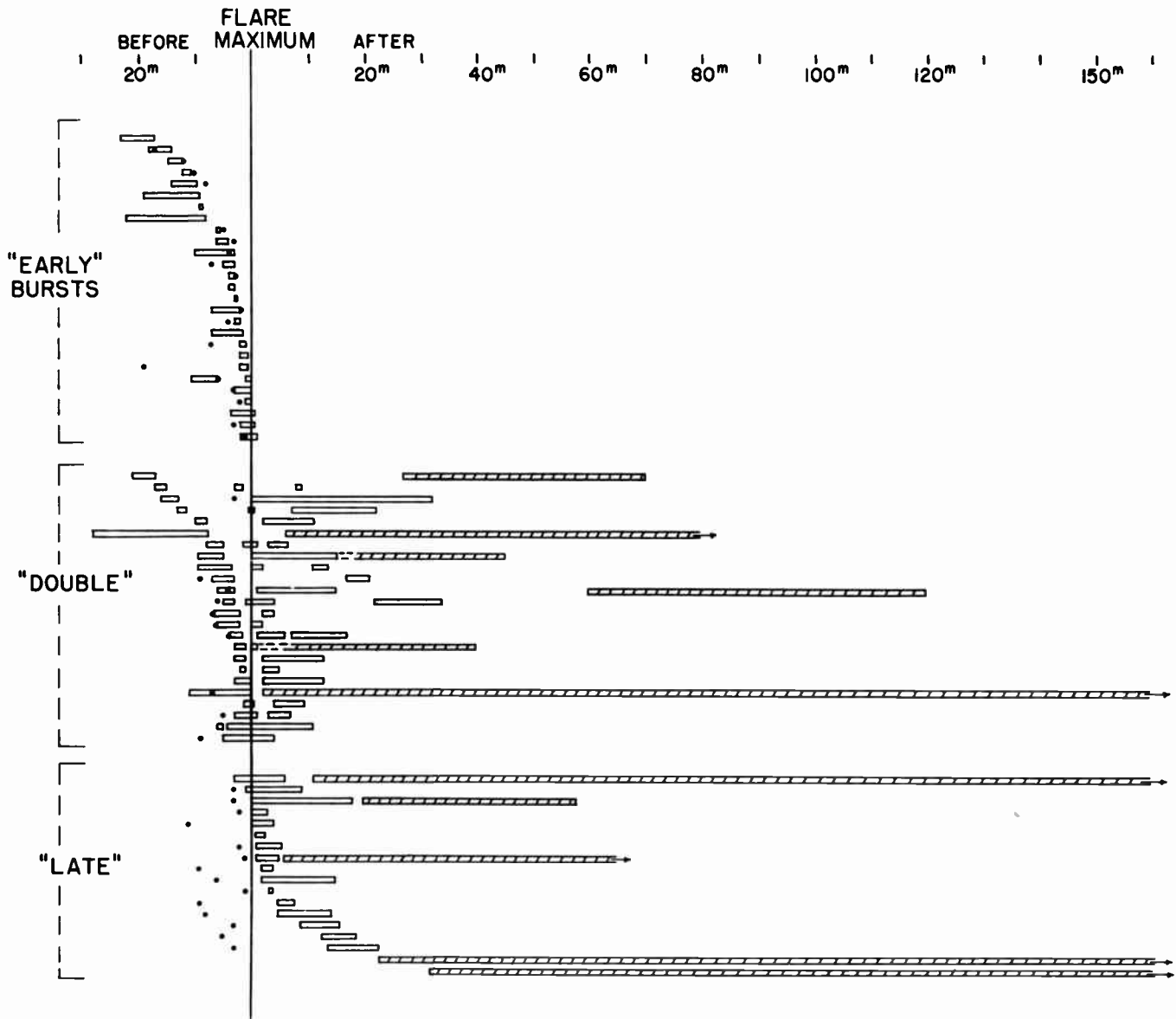


Fig. 10—Time relationships between 80-mc events and  $H\alpha$  flares. The vertical line represents the time of flare maximum. A dot gives the time of start of the flare, if known. Each horizontal entry represents, schematically, distinctive events on the 80-mc interferometer records of the Cavendish Laboratory at the time of a flare. The open rectangles indicate "noise storms." All flares in our study for which time of maximum was reported are included in the diagram.

#### Basically Different Events at the Two Frequencies

Differences between the two frequencies perhaps can be seen most clearly if our attention is drawn to flares for which there was a well developed event at one frequency and no evidence for distinctive, flare-associated emission at the other.

Of the 277 flares in the study, there were 100 flares for which we found no enhancement at 2800 mc, but for which there was evidence of an event at 200 mc. Of these 100 flares only two were of importance greater than one, and only 11 were accompanied by reported ionospheric disturbances. At 2800 mc, a high percentage of important flares have distinctive events and many of the less important flares do not. At 200 mc, the occurrence of flare-associated emission correlates much less

closely with the importance of the  $H\alpha$  flare. Fig. 8, p 155, shows four examples of 200-mc emission at the time of flares for which there was no concomitant enhancement at 2800 mc.

The converse group, null at 200 mc but with distinctive events at 2800 mc, is small and includes only 15 flares from our set of 277. However, a high percentage of this 200-mc "null" group were important flares, with reported ionospheric disturbances. Fig. 9, p. 155, shows three examples of 2800-mc emission at the time of flares for which there was no enhancement at 200 mc.

#### FREQUENCIES LOWER THAN 200 MC

##### Double Pattern

Our direct information on flare-associated radiation

at frequencies lower than 200 mc comes from examination of the 80-mc data, Cavendish Laboratory, for 1949–1955, from 18-mc bursts recorded July–October, 1957, on the IGY Indirect Flare Detector, McMath-Hulbert Observatory, and from inspection of occasional records published in the literature. At the lower end of the radio frequency spectrum, the “early” and “late” aspects of the flare-associated radiation apparently are still present. (See Fig. 1 and Fig. 10, pp. 150, 156.)

There is some indication that the “late,” postmaximum, part of the event at low frequencies is relatively greater, in comparison with the “early” part, than is the case at higher frequencies.

Furthermore, the 80-mc records show that during the postmaximum phase of some flares there may be, at this frequency, two types of enhanced emission. At, or immediately following,  $II\alpha$  maximum of certain flares there is a very great increase in flux, with duration of the order of tens of minutes. This great event, in turn, is followed by a protracted period of “storminess” with above average flux and many superposed bursts; see Fig. 1 and Fig. 10. This flare pattern, which perhaps should be called “triple” rather than double, is more obvious on the single-frequency traces at 80 mc than on comparable records at 200 mc. Fig. 10 shows schematically time relationships between 80-mc bursts and all  $H\alpha$  flares in our study for which the time of flare maximum was reported.

#### 80-MC Data

The 80-mc records at the Cavendish Laboratory were examined for the times of 791 flares. The equipment was not in use for the times of 260. The record was “confused” because of instrumental adjustments, calibration, or polarization measures at the time of 35 more. For the remaining 496 flares, there was evidence on the records for a distinctive event at the time of 261 flares, and no such event for 235. It should be pointed out that the 80-mc records were, in general, unmonitored interferometer records. Because they were unmonitored, a certain number of cases of terrestrial interference have undoubtedly been falsely identified as solar events. Because they are interferometer records, a certain number of flares have been designated incorrectly as “nulls” since their 80-mc emission may have occurred during the minimum in the interferometer pattern.

There were distinctive events on the 80-mc records at the times of flares in all importance categories and at all central meridian distances. Sometimes the events were very great and sometimes they were only small isolated bursts near the start of the flare. The percentage of flares with distinctive events *increased* with increasing flare importance, and *decreased* with increasing distance from the central meridian. See Table II and Table III.

It is questionable whether or not some of the lesser solar bursts here assigned to concomitant flares are, in truth, flare associated. However, until more is known

TABLE II  
PERCENTAGE OF FLARES IN DIFFERENT IMPORTANCE CATEGORIES WITH DISTINCTIVE EVENTS AT 80 MC

Flare Importance	Number of Flares		Percentage of Flares with 80-MC Event
	With 80-MC Event	“Null”	
1	145	176	45
1+	59	34	63
2	42	21	67
3	9	1	90
(?)	(6)	(3)	—
Total	261	235	53

TABLE III  
PERCENTAGE OF FLARES AT DIFFERENT DISTANCES FROM THE CENTRAL MERIDIAN WITH DISTINCTIVE EVENTS AT 80 MC

CMD	Number of Flares		Percentage of Flares with 80-MC Event
	With 80-MC Event	“Null”	
0°–10°	40	26	61
11°–20°	31	27	53
21°–30°	40	18	69
31°–40°	38	45	46
41°–50°	32	32	50
51°–60°	29	28	51
61°–70°	21	22	49
71°–80°	13	21	38
81°–90°	13	16	45
(?)	(4)		
Total	261	235	53

about spectra, polarization, or location of source, they have been included as flare events on the “circumstantial” evidence of time association.

#### COMPARISON OF DYNAMIC SPECTRA WITH SINGLE-FREQUENCY DATA FOR FLARES

The writer has not yet been able to study in detail a large number of flares with both single-frequency records and dynamic spectra. Nevertheless, certain relationships are beginning to emerge from the available data. According to the 1955–1956 *Quarterly Bulletin*, the Type III burst, with its rapid drift from high to low frequencies, is a very usual event when the sun is active. Single bursts of this type, or groups of them, apparently occur very close to the starting times of certain flares. This statement is based on: 1) evidence made available to us by Haddock for a small number of cases recorded by the recently completed University of Michigan Solar Radio Spectrograph at the time of flares observed at the McMath-Hulbert Observatory, and 2) comparison of *Quarterly Bulletin* radio-frequency and flare data for January, 1955, to June, 1956. In the latter comparison, direct flare reports were supplemented by data from 3750-mc bursts, on the assumption that 3750 mc resembles 2800 mc in its close flare association.

Type II bursts, with their much slower drift from high to low frequencies, apparently are relatively rare. Wild reported to the *Quarterly Bulletin* only 20 cases of

Type II bursts during the same 18 months in which he reported more than 1000 Type III events. Type II bursts seem to be closely associated with  $H\alpha$  flares. On the basis of evidence currently available to the writer, they tend to occur in the postmaximum, rather than in the premaximum stages of the flare.

Unfortunately, there are only very few flare or ionospheric observations available for comparison with the 20 cases of Type II bursts in the tables of the *Quarterly Bulletin*. However, by again assuming that a burst at 3750 mc provides indirect data on starting (and maximum) times for  $H\alpha$  flares, we have prepared the diagram in Fig. 11. This graph gives data for the 13 cases for which direct or indirect flare information could be located. It shows that in each case, the Type II burst, within the frequency range 240–40 mc, began from 1 to 21 minutes after the flare and/or 3750-mc burst. For the two cases for which the time of maximum of the  $H\alpha$  flare is known, the Type II burst definitely was a postmaximum event. These results are in agreement with our earlier study of Type II bursts.<sup>6,8</sup> Type III bursts also are shown in the diagram in Fig. 11 whenever they too occurred. Wild<sup>9,10</sup> already has pointed out that many of the radio-frequency bursts are flare associated and that Type II bursts frequently follow Type III bursts and, in turn, are sometimes followed by a long period of storminess (Type I). This apparently triple phenomenon is clearly shown in certain of the 80-mc records at the time of flares. See Fig. 1 and Fig. 10.

#### GEOMAGNETIC DISTURBANCES FOLLOWING FLARES WITH "MAJOR EARLY BURSTS" AT LOW RADIO FREQUENCIES

Radio frequency records at the time of solar flares not only provide new data that may lead to increased insight into the flare phenomenon, but they also give information that may help to identify the flares that are associated with geomagnetic storms. During our day by day examination of the Cornell 200-mc solar records, it was observed that flares with sudden bursts of great magnitude during the premaximum phase of the flare frequently were followed within one to four days by sudden-commencement geomagnetic storms. Conversely, certain important flares (importance 2+ or 3) without such "major early bursts" at 200 mc were not followed by geomagnetic disturbances.

In order to test these ideas, we have investigated the possible geomagnetic effects of all flares, using worldwide data, between January, 1949, and April, 1956, for which we had positive evidence of a "major early burst"

<sup>8</sup> H. W. Dodson, "The relation between observed solar features and solar radio emission," *Proc. NEC*, vol. 11, pp. 498-505; October, 1955.

<sup>9</sup> J. P. Wild, "Radio Observations of Solar Flares," *Trans. IAU*, ed. P. Th. Oosterhoff, Cambridge University Press, Cambridge, Eng., pp. 661-663; 1957.

<sup>10</sup> J. P. Wild, "Spectral Observations of Solar Activity at Metre Wave-Lengths," *IAU Symp. IV in "Radio Astronomy,"* ed. H. C. van de Hulst, Cambridge University Press, Cambridge, Eng., pp. 321-326; 1957.

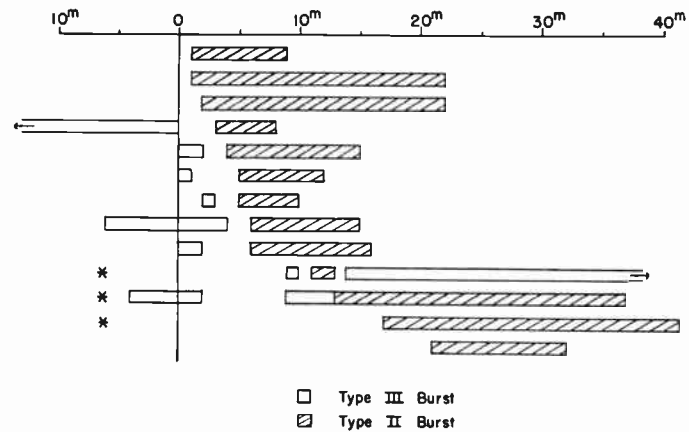


Fig. 11—Comparison of start of flares (or 3750-mc bursts) with Type II bursts reported in *Quarterly Bulletin*, January 1, 1955, to June 30, 1956. Type III bursts also are shown. The vertical line gives time of start of  $H\alpha$  flare and/or 3750-mc burst. Asterisks show cases for which  $H\alpha$  flare was observed. No data available for 7 of the 20 Type II bursts.

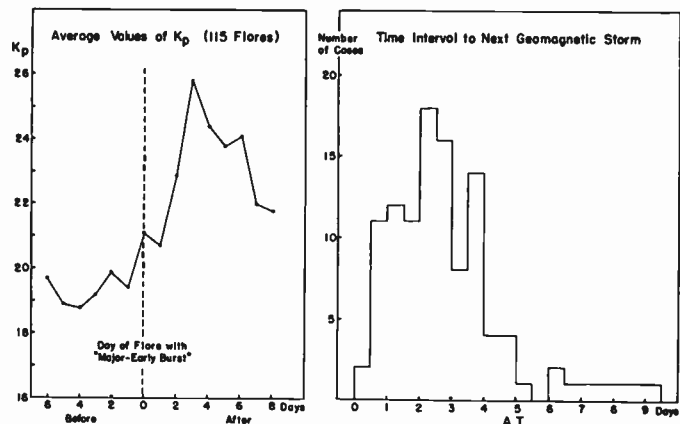


Fig. 12—Geomagnetic effects of flares with "major early bursts" at frequencies  $\leq 200$  mc.

at frequencies  $\leq 200$  mc. In this study, we tried to include only flares with premaximum bursts of duration  $\geq 2$  minutes and for which the intensity was very great. The study showed that flares with these great, premaximum events are relatively rare (115 cases) and that flares with such radio frequency emission indeed are followed by geomagnetic storms in a high percentage of cases. (See Fig. 12.) According to this study, the average time interval between the occurrence of flares with "major early bursts" and onsets of the next geomagnetic storms is about two and a half days, a time interval considerably longer than that usually given in studies of solar-terrestrial relationships. It should be pointed out that the study exclusively referred to the declining branch of the sun spot cycle and included small as well as great storms. These factors may be playing a part in the above time relationships, but the evidence for such a situation is not strong within the study itself.

The average time of two and one-half days between flare and start of storm, as found by the foregoing study, makes it very tempting to try to identify the ejection of

the storm-producing particles with the occurrence of the slowly drifting, flare-associated Type II bursts at radio frequencies. For Type II bursts, the inferred particle velocity is  $\sim 300\text{--}700$  km, corresponding to travel times from sun to earth of 2–5 days.<sup>9,10</sup> Future work may show that the above association is true. However, on the basis of present information, such an association is not yet justified. First, the 115 flares in the geomagnetic study<sup>11</sup> here considered were selected on the basis of a great *premaximum* burst, whereas Type II bursts, in the range 240 to 40 mc, as reported to date (through June, 1956, *Quarterly Bulletin*) are primarily postmaximum phenomena. It is true that many of the flares with major early bursts also had "late" components which indeed may have been Type II phenomena. Future studies should permit discrimination between the several parts of the flare event at radio frequencies and should provide clarification of these points. However, we do know that certain flares of importance 3, with only "late" components in their radio frequency emission, were not followed by geomagnetic storms within a small number of days.

Secondly, geomagnetic events following the 20 cases of Type II bursts reported through June, 1956, in the *Quarterly Bulletin* do not suggest an unusually close (or suitable) association between these phenomena and subsequent geomagnetic storms. The time interval between each reported Type II burst and the next geomagnetic storm is shown in Table IV. For certain bursts, a second time interval is also given, since particles moving with velocities of  $\sim 300\text{--}700$  km per second do not readily lend themselves to association with geomagnetic storms that begin within less than two days after the time of the burst.

#### CONCLUSION

Our studies have provided growing evidence that the flare mechanism is in some way intimately associated

<sup>11</sup> H. W. Dodson and E. R. Hedeman, "Geomagnetic disturbances associated with solar flares with major premaximum bursts at radio frequencies  $\lesssim 200$  mc/s," *J. Geophys. Res.*, in press, March, 1958.

TABLE IV  
TIME INTERVAL BETWEEN REPORTED TYPE II BURSTS AT RADIO FREQUENCIES AND START OF NEXT GEOMAGNETIC STORM.  
JANUARY 1, 1955–JUNE 30, 1956

Date and Time of Burst	Intensity	$\Delta t^*$
1955		
February 24 0104–0124	strong	3 <sup>d</sup> 21 <sup>h</sup>
June 9 0001–0033	weak	13 10
June 15 0400–0408	weak	7 6
June 21 2329–2354	strong	0 11 (10 <sup>d</sup> 16 <sup>h</sup> )
July 5 0215–0224	strong	6 22
July 7 0206–0213	moderate	4 22
September 10 0509–0520	weak	1 20
September 19 0152–0202	weak	7 23
November 15 0441–0505	weak	0 01 ( 2 22)
November 15 2205–2208	moderate	2 04
November 18 0242–0252	moderate	1 11 (13 06)
November 24 0442–0513	moderate	7 05
November 30 0544–0549	moderate	1 03 ( 5 16)
1956		
January 16 0031–0049	moderate	1 22 ( 3 07)
January 19 0026–0031	strong	2 17
February 14 0555–0620	strong	4 20
March 8 0321–0342	strong	1 18 (12 08)
April 25 2348–2419	weak	0 21 ( 2 17)
May 16 0007–0039	moderate	4 06
May 30 {2331–2333}	moderate	0 22 (14 20)
{ 2351 }	weak	

\* When the time to the first succeeding storm is  $\lesssim 2^d$  the time to the next storm is given in parentheses.

with much of the transient activity at radio frequencies. Either flares themselves or a stage of development of an active center such that flares can occur may be a necessary circumstance for the emission of greatly enhanced solar radiation at radio frequencies.

#### ACKNOWLEDGMENT

The author wishes to thank again those persons working in the field of solar radio astronomy at Cornell University, The National Research Council of Canada, and the Cavendish Laboratory whose generous cooperation throughout past years has made possible the studies here reported.

E. Ruth Hedeman has been a close and helpful colleague in the preparation of this review article, as well as in the original studies on which it is based.



# A Swept-Frequency Interferometer for the Study of High-Intensity Solar Radiation at Meter Wavelengths\*

J. P. WILD† AND K. V. SHERIDAN‡

**Summary**—The paper describes an interferometer which has been constructed for studying the various spectral types of solar activity at meter wavelengths. The instrument is a "swept-frequency" interferometer and is capable of measuring the one-dimensional position and angular size of a transient source on the sun's disk, and of determining the polarization and intensity of the received radiation. All these characteristics are determined as a function of frequency in the range 40–70 mc. Independent position measurements are made at one-second intervals, and source-size measurements at two-second intervals. Polarization measurements are made as an alternative at chosen times. The two antennas of the main interferometer are spaced 1 km apart on an east-west line. The two antennas of the polarization system are erected on a common axis maintained in the direction of the sun.

Some preliminary observations have given an indication of the spectrum of source size for activity of spectral Types I and III. In both cases the angular size is found to decrease from about 10 minutes of arc at 45 mc to about 6 minutes of arc at 65 mc.

## I. INTRODUCTION

THE sun's electromagnetic radiation in the meter-wavelength part of the radio spectrum is dominated by a spasmodic variable component which originates in active areas above certain sunspots. It consists of short-lived bursts of radiation lasting from a few seconds to several minutes, sometimes superimposed on a variable background continuum of longer duration. The majority of bursts conform to one of a relatively small number of spectral types of which three have been described in some detail.<sup>1-4</sup> Hypotheses have been advanced to interpret these spectra in terms of physical processes taking place in the solar corona. For example, in one of the commonest types of burst (spectral Type III) two frequency bands are emitted, one the second harmonic of the other, and these drift rapidly in the direction of decreasing frequency, sweeping through tens or hundreds of megacycles in a period of a few seconds. Reasons have been given for supposing that

the physical process responsible for such a burst is the excitation of plasma oscillations in the solar corona by a disturbance (e.g., a corpuscular cloud of ionized matter) traveling outwards through the corona exciting levels of continuously decreasing plasma frequency. The deduced velocity of an average disturbance is some 70,000 km and a possible connection with the cosmic rays of solar origin has been suggested.

Much the same interpretation has been given for the longer-lived bursts of spectral Type II, though here the deduced velocity is typically 500 km—of the order of the velocity of solar corpuscles responsible for auroras and magnetic storms on the earth. Also there are long-period storms of Type I bursts individually narrow in bandwidth, short in lifetime, and circular in polarization, which, together with other rarer spectral types, all remain without satisfactory explanation. In order to make further progress—to test the hypothesis on which the existing interpretations are based, and to explore the emissions of unknown origin—further information is required to supplement the spectral data.

In particular, we wish to know the position, angular size, and polarization of the radiating sources. Our present knowledge of the positions and motions of the sources on the sun's disk is very limited. In 1950, Payne-Scott and Little<sup>5</sup> made valuable directional observations of these sources with a swept-phase interferometer operating at a single frequency (97 mc). But to obtain a proper understanding of the origin of the bursts it seems essential to study the positions over a range of frequencies, since different frequencies are thought to originate from different levels in the corona. Also our knowledge of the angular size of the short-lived sources is almost nonexistent. Previous measurements of angular size,<sup>5-8</sup> which probably all refer to Type I storms, indicate that at frequencies between 97 and 200 mc the size is not more than a few minutes of arc. A quantita-

\* Original manuscript received by the IRE, October 18, 1957.

† Radiophysics Laboratory, CSIRO, Sydney, Australia.

<sup>1</sup> J. P. Wild and L. L. McCready, "Observations of the spectrum of high-intensity solar radiation at metre wavelengths. Part I—The apparatus and spectral types of solar burst observed," *Aust. J. Sci. Res.*, vol. A3, pp. 387–398; September, 1950.

<sup>2</sup> J. P. Wild, "Observations of the spectrum of high-intensity solar radiation at metre wavelengths. Part II—Outbursts (type II). Part III—Isolated bursts (type III). Part IV—Enhanced radiation (type I)," *Aust. J. Sci. Res.*, vol. A3, pp. 399–408; September, 1950, vol. A3, pp. 541–557; December, 1950, vol. A4, pp. 36–50; March, 1951.

<sup>3</sup> J. P. Wild, J. D. Murray, and W. C. Rowe, "Harmonics in the spectra of solar radio disturbances," *Aust. J. Phys.*, vol. 7, pp. 439–459; September, 1954.

<sup>4</sup> J. P. Wild, J. A. Roberts, and J. D. Murray, "Radio evidence of the ejection of very fast particles from the sun," *Nature*, vol. 173, pp. 532–534; March, 1954.

<sup>5</sup> R. Payne-Scott and A. G. Little, "The position and movement on the solar disc of sources of radiation at a frequency of 97 mc. Part II—Noise storms. Part III—Outbursts," *Aust. J. Sci. Res.*, vol. A4, pp. 508–525; December, 1951, vol. A5, pp. 32–49; March, 1952.

<sup>6</sup> L. L. McCready, J. L. Pawsey, and R. Payne-Scott, "Solar radiation at radio frequencies and its relation to sunspots," *Proc. Roy. Soc.*, vol. A190, pp. 357–375; August, 1947.

<sup>7</sup> M. Ryle and D. D. Vonberg, "An investigation of radio-frequency radiation from the sun," *Proc. Roy. Soc.*, vol. A193, pp. 98–120; April, 1948.

<sup>8</sup> Y. Avignon, E. J. Blum, A. Boischoit, R. Charvin, M. Ginat, and P. Simon, "Observation des orages radioélectriques polaires avec le grand interféromètre de Nancy," *Compt. Rend. Acad. Sci.*, vol. 244, pp. 1460–1463; March, 1957.

tive knowledge of source size is necessary both to gauge the scale and spread of the disturbed region and to calculate the intrinsic radio brightness of the sources. Polarization observations, notably those of Payne-Scott and Little<sup>6</sup> and Hatanaka,<sup>9</sup> have been more extensive, but apart from some recent observations of Komesaroff (in preparation), these have been restricted to single frequencies.

The instrument described in this paper is an interferometer constructed with the intention of making rapid measurements of the position and size (both in one dimension) and polarization of the transient sources over a substantial frequency range. These data are obtained side by side with records of dynamic spectra using the radio spectrograph at Dapto (40–240 mc). Hence it is hoped to obtain a fairly complete set of observable characteristics of the different spectral types of burst.

The instrument covers a frequency range of 40–70 mc, the lowest range of the spectrograph. There were several reasons for choosing the lowest range. The first is dictated by the nature of emitted spectra. Reference has already been made to the natural emission of harmonic frequencies, a phenomenon common to bursts of Types II and III. On current evidence it appears that the fundamental frequencies rarely exceed 100 mc, while harmonics are received over a much wider range. By choosing a frequency range below 100 mc, therefore, we should be in a position to observe the sources both in their fundamental and harmonic emissions. Second, it can be shown that an interferometer of given base line is capable of discriminating between the 40- and 70-mc plasma levels at the limb of the sun more efficiently than between the levels of a pair of higher frequencies (e.g., 70 and 120 mc) bearing a similar ratio<sup>10</sup>—this despite the sacrifice of angular resolution at the lower frequencies. Finally, the technical problems in the building of an accurate interferometer of given base line decrease with frequency. A disadvantage of low-frequency operation is the increase in errors of position due to refraction in the ionized atmospheres of the sun and earth.

To obtain a sequence of positions of sources which exist for no more than 5 or 10 seconds it is necessary to make measurements at intervals of about one second. Little and Payne-Scott<sup>11</sup> fulfilled this requirement at a single frequency by rapidly sweeping the phase of signals entering through one arm of their interferometer, thus causing the fringes in the antenna pattern to be

<sup>9</sup> T. Hatanaka, "Polarization of solar radio bursts," in "Radio Astronomy," H. C. van de Hulst, ed., Cambridge University Press, Cambridge, Eng., pp. 358–362; 1957.

— "The Faraday effect in the earth's ionosphere with special reference to polarization measurement of the solar radio emission," *Publ. Astron. Soc. Japan*, vol. 8, pp. 73–86; 1956.

<sup>10</sup> This merely expresses the fact that the distribution of electron density,  $N$ , in the solar corona is such that  $\sqrt{N}$  (proportional to plasma frequency) decreases outwards more slowly than exponentially.

<sup>11</sup> A. G. Little and K. Payne-Scott, "The position and movement on the solar disc of sources of radiation at a frequency of 97 mc. Part I—Equipment," *Aust. J. Sci. Res.*, vol. A4, pp. 489–507; December, 1951.

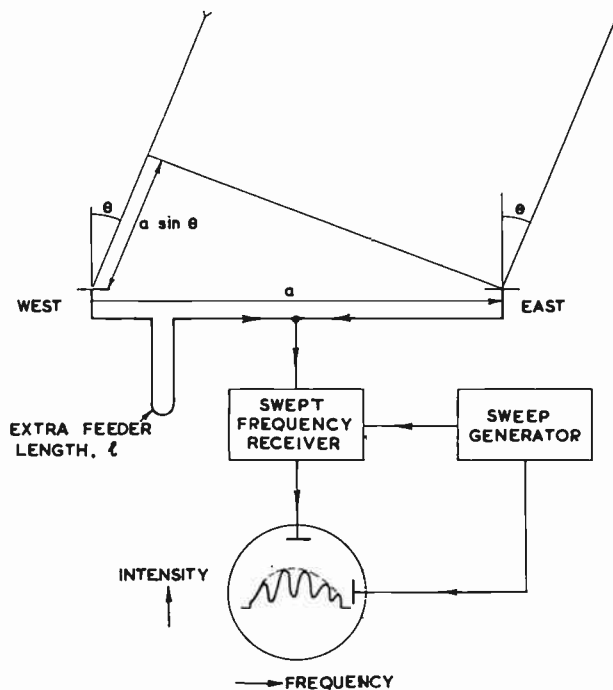


Fig. 1—The principle of the swept-frequency interferometer.

scanned rapidly across the sky. In the present case we need an interferometer in which both the antenna pattern and the frequency are swept. This has been achieved in a single operation; *i.e.*, sweeping the frequency in an asymmetrical two-antenna interferometer.

The principle of such a "swept-frequency" interferometer has previously been applied by Wild and Roberts<sup>12</sup> to the problem of radio-star scintillations.<sup>13</sup>

## II. THE SWEEP-FREQUENCY RECEIVER

### A. The Principle

The principle of the swept-frequency interferometer is illustrated in Fig. 1. Plane waves incident on an asymmetrical two-antenna interferometer at an angle  $\theta$  with the normal plane of the interferometer travel through the two antennas along paths which differ by  $a \sin \theta + l$ , where  $a$  is the spacing of the antennas and  $l$  the extra feeder length in one side. The interfering waves are received in a swept-frequency receiver and displayed on a cathode-ray tube which traces the pattern of intensity vs frequency. It is evident that this pattern will be just the spectrum of the source modulated with an interference pattern having maxima at wavelengths for which  $a \sin \theta + l = n\lambda$  and minima for which  $a \sin \theta + l = (n + \frac{1}{2})\lambda$ , where  $n$  is an integer. When all frequencies arrive from the same direction, such maxima occur at equal intervals,  $\Delta f$ , in the frequency scale, given by

<sup>12</sup> J. P. Wild and J. A. Roberts, "The spectrum of radio-star scintillations and the nature of irregularities in the ionosphere," *J. Atmos. Terr. Phys.*, vol. 8, pp. 55–75; February, 1956.

<sup>13</sup> The latter instrument was also used for some preliminary solar observations. See R. L. Loughhead, J. A. Roberts, and M. McCabe, "The association of solar radio bursts of spectral Type III with chromospheric flares," *Aust. J. Phys.*, in press.

$$\Delta f = \frac{c}{a \sin \theta + l} \quad ((\theta) < \pi) \quad (1)$$

where  $c$  is the free-space velocity of light. Thus measurement of the frequencies of maximum or minimum enables the position angle,  $\theta$ , to be measured at those frequencies. Provided the instantaneous position of the source is approximately independent of frequency, none of the ambiguities in position encountered with single-frequency interferometers arise since, for a given value of  $l$ ,  $\Delta f$  is a unique function of  $\theta$ . (The value of  $\Delta f$  can be adjusted to any desired value by varying the length  $l$ .) Also by measuring the maximum-to-minimum ratio of the intensity of the interference pattern we can obtain a useful measure of the angular size of the source if the latter is no wider than about one fringe spacing and no narrower than about one tenth of a fringe spacing.

While the simple interferometer shown in Fig. 1 is suitable for the rough measurement of position, difficulties arise when measurements of high precision are required (*e.g.*, a few hundredths of a fringe spacing). In the first place, the finite bandwidth of solar emissions can cause a considerable distortion of the sinusoidal pattern and so complicate the precise location of the true interference maxima and minima. Second, in the case of sources of relatively large angular width, the interference pattern is superimposed on a high-incoherent background with consequent loss in the visibility of the pattern. We have overcome these problems by measuring positions with an interferometer in which the signals entering the two antennas are multiplied together rather than added. This technique is familiar in radio-star interferometry where it is desirable to eliminate the galactic background.<sup>14</sup> Fig. 2(b) shows the kind of pattern obtained when a partially resolved source is viewed with a multiplying interferometer; this may be contrasted with the adding pattern shown in Fig. 2(a). With multiplication the receiver amplification may be increased as desired, and the phase of the pattern can be accurately measured using the points at which the pattern crosses the zero line.

However, the adding interferometer is still required for source-size measurements. Our instrument, therefore, has been made to combine both adding and multiplying facilities, and is automatically switched between the two conditions during alternate ( $\frac{1}{2}$ -second) sweep intervals. Where possible, the two systems make use of the same equipment. In describing them, however, it is convenient to regard them as two independent instruments.

So far we have restricted the discussion to problems of measuring position and source size. We shall continue to do so until Section IV-C, where it will be shown that polarization can be measured by replacing the spaced antenna system with a pair of crossed antennas.

<sup>14</sup> For example, see M. Ryle, "A new radio interferometer and its application to the observation of weak radio stars," *Proc. Roy. Soc.*, vol. A211, pp. 351-375; March, 1952.

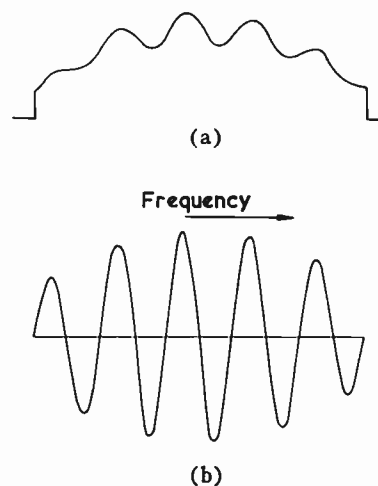


Fig. 2—Characteristic patterns of intensity (vertical) vs frequency obtained with (a) an adding interferometer and (b) a multiplying interferometer.

### B. The Adding Interferometer

A block diagram of the adding interferometer is shown in Fig. 3. For source-size measurements the signals are received in two identical broad-band, wide-beam antennas spaced 1 km apart on an east-west line. Connection to the receiver is made by long feeder lines, one of which includes a special section capable of being varied from 0 to 480 m in steps of 15 m. The signals are combined in a simple junction, detected by a 40-70 mc swept-frequency receiver<sup>3</sup> and displayed on a cathode-ray tube provided with a horizontal sweep synchronized to the receiver sweep. The receiver is swept at 2 revolutions per second, the operative period being  $\frac{1}{3}$  second. Thus traces of the form shown in Fig. 2(a) are generated twice per second, and these are photographically recorded. Facilities are provided for injecting standard power levels from a noise generator and frequency markers from a harmonic crystal generator.

The function of the variable line is to provide control of the frequency spacing between maxima in the interference pattern [ $\Delta f$  of (1)]. If this spacing is allowed to become too large, the interference pattern is liable to become confused with the envelope of the natural spectrum; also we would sacrifice the number of independent measurements across the frequency range. If the spacing becomes too small the interference pattern would become blurred by the finite bandwidth of the receiver (chosen to be fairly large, 0.5 mc, to minimize noise fluctuations) and the reading accuracy would decline. In practice the most suitable spacing is found to be  $\Delta f \sim 5$  mc, so that we need to arrange for the difference in the total path length from the source to the receiver through the two antennas to be approximately 60 m [see (1)]. Now as the earth rotates, the path length between the sun and the two antennas changes by up to  $\pm 1$  km in 12 hours. The present equipment has been designed to operate during the interval noon  $\pm 2$  hours, during which the path-length difference varies by about

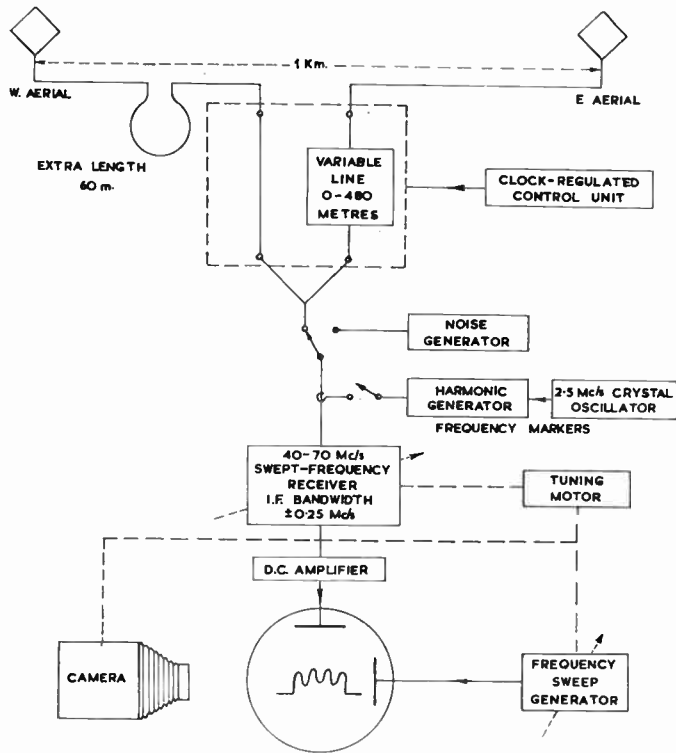


Fig. 3—The adding interferometer.

$\pm 480$  m. This path length is compensated by the variable line which is automatically inserted in the appropriate feeder line and adjusted to the correct length (see Section III-B).

For polarization measurements the two spaced antennas are replaced by two antennas having a common principal axis but orthogonal planes of polarization. An additional 60 m of feeder length is included in one arm. The reason for this will be discussed in Section IV-C.

C. The Multiplying Interferometer

A block diagram of the multiplying interferometer is shown in Fig. 4. The antenna and feeder arrangements are the same as those of the adding interferometer but the signals in the two arms are amplified and converted to the intermediate frequency (30 mc) before being combined. It is necessary to preserve the relative phase of the two signals up to the common mixing point and so the two converters are supplied by a common local oscillator. The frequency is swept by tuning, in synchronism, each radio-frequency amplifier and mixer, and the common local oscillator. The two 30-mc signals are then multiplied by phase switching and phase detection; the principle of this method is contained in (6) of Section IV and the technical arrangement is essentially similar to that used by Mills, Little, Sheridan, and Slee.<sup>16</sup> A high switching rate of 5 kc is used because it is required to make several switchings during the time

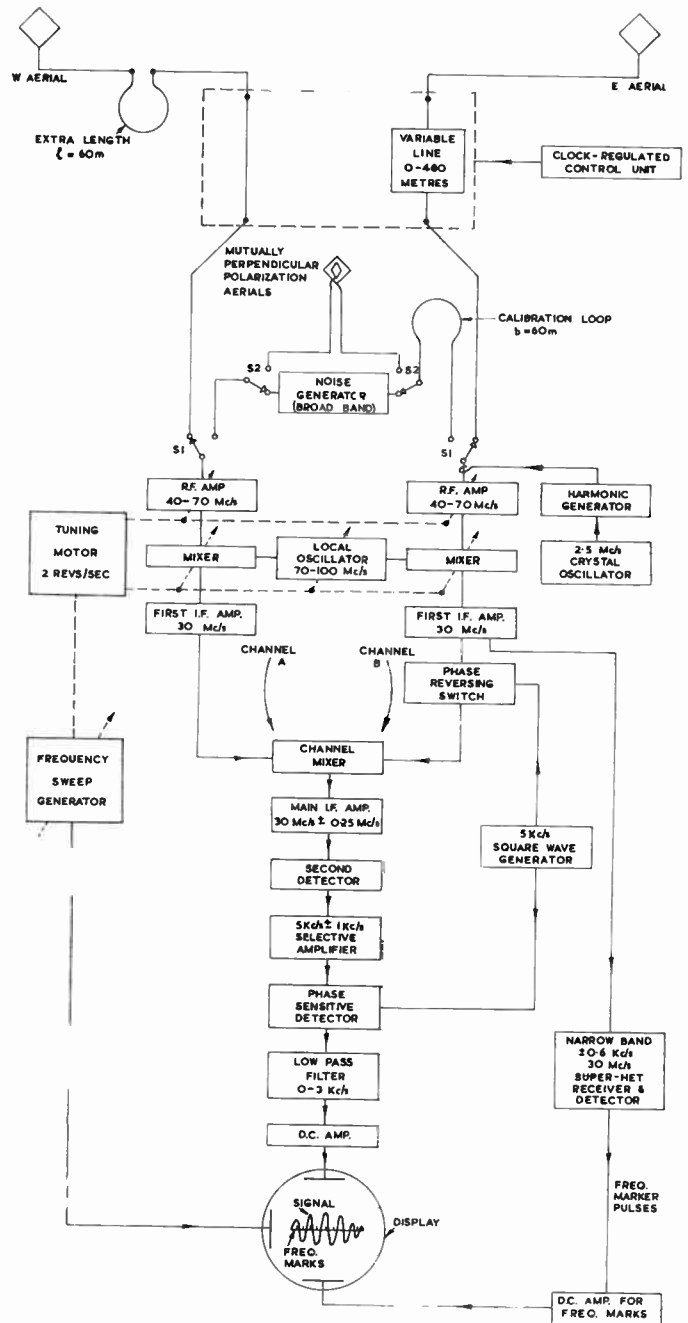


Fig. 4—The multiplying interferometer.

( $\sim 10^{-2}$  to  $10^{-3}$  seconds) taken for the frequency to be swept through one receiver bandwidth. The output of the phase-sensitive detector is passed through a low-pass filter to the Y plates of the cathode-ray tube.

The factors influencing the accuracy of position measurement will be discussed in Section IV, but two of the factors require instrumentation and should be mentioned now. The first is the provision of accurate sharp frequency markers. These are inserted automatically, at intervals of two seconds, by injecting harmonics of a 2.5-mc crystal oscillator into the input terminals of one of the rf amplifiers; at the same time the intermediate frequencies are diverted from the main IF amplifier (bandwidth 0.5 mc) into one of bandwidth one

<sup>16</sup> B. Y. Mills, A. G. Little, K. V. Sheridan, and O. B. Slee, "A high resolution radio telescope for use at 3.5 m," this issue, p. 67.

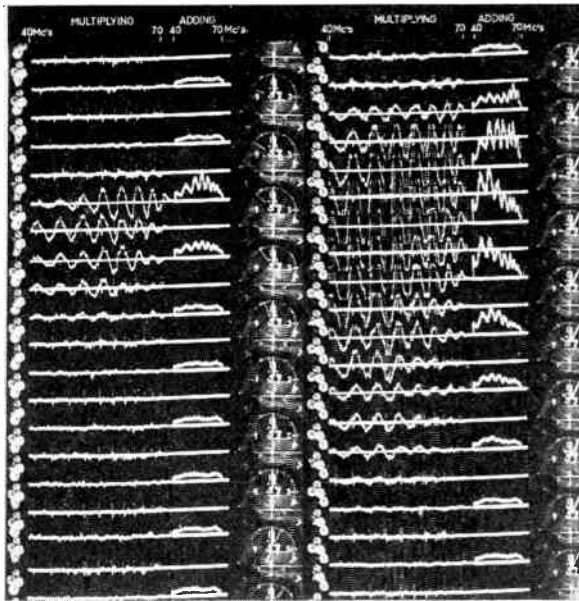


Fig. 5—Two typical records of Type III bursts obtained on July 3, 1957. As indicated by the clock, time advances vertically downwards. Patterns of the multiplying interferometer are displayed at one-second intervals, and those from the adding interferometer at two-second intervals.

kc, whence they are detected and displayed as a vertical deflection on the cathode-ray tube. The appearance of the marker pips is shown in Fig. 5.

The second calibration facility is the provision of a means of determining the relative shift in the phase of signals passing through the two receiver channels; the relative phase shift must be known as a function of frequency and determined at sufficiently short intervals of time. This is done by replacing the antennas and feeders with a pair of artificial phase-coherent sources of noise which generate an artificial swept-frequency interference pattern. Signals from a broad-band diode noise generator are split into two channels and attenuated in identical networks to prevent interaction between them. One is fed to receiver *A* through a cable of length *s*, the other to receiver *B* through a length *s* + *b*. Thus an interference pattern is set up on the display corresponding precisely to that from a celestial source for which the path difference through space and through the antenna feeders is *b*. In practice the length *b* is chosen to be 60 m giving fringes spaced at the desirable interval of 5 mc.

#### D. The Combined Display

A 12-inch cathode-ray tube is used to display all the required information, *viz.*, multiplying and adding interferometer patterns, and narrow-band frequency markers which are superimposed on the former. The tube is photographed with a 35-mm cine camera whose film is advanced by 1/10 inch between alternate scans (*i.e.*, at one-second intervals). The final record is illustrated in Fig. 5 and Fig. 6. The record also includes clock images at 2-second intervals and a bunch of illuminated numbers to indicate the setting of the variable line.

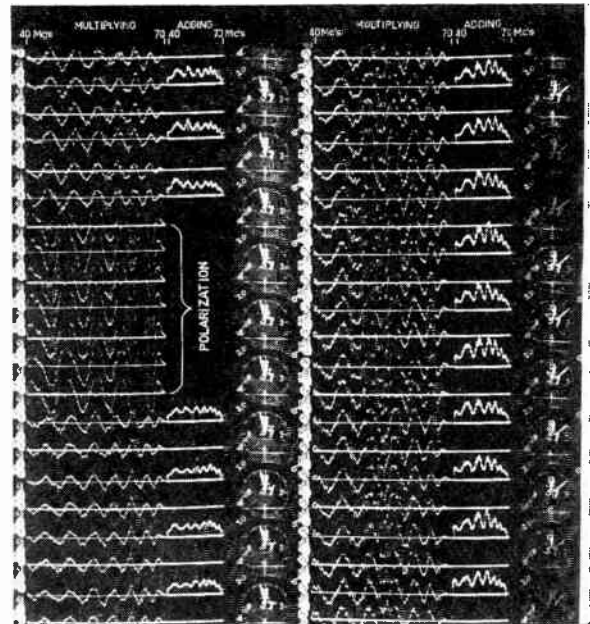


Fig. 6—Two sections of the record taken on June 20, 1957, during a Type I storm which was characterized by a high background continuum. (Note: During the "polarization" section, no adding pattern was recorded in this case.)

The combined display is produced automatically by using magnetically operated switches to control a cycle of operations which covers 4 scans (2 seconds). The scans in each sequence are shared as follows: 1) multiplying interferometer, 2) adding interferometer, 3) multiplying interferometer, and 4) frequency markers. During 2) the trace is deflected to the right and the horizontal sweep reduced in amplitude.

### III. THE ANTENNA FEEDER SYSTEM AND ITS CALIBRATION

#### A. Antennas and Feeders

The spaced antennas of the interferometer are single-wire rhombics each mounted on a wooden cross in the vertical north-south plane and pivoted at the center to allow for two different declination settings (summer and winter); no azimuth movement is necessary because the beamwidth of the antennas is wide enough to accommodate the sun's daily motion during the operating hours (noon  $\pm$  2 hours). The antennas are designed for uniformity of effective area in the frequency range 40–70 mc (see Wild and McCready<sup>1</sup>). Each side is of length 3.64 m, and the semiangle at the side corners is 27°, giving an effective area of about 9 m<sup>2</sup>. Each antenna has a characteristic impedance of about 700 ohms and is connected directly to 700-ohm open-wire transmission lines.<sup>16</sup> The length of each feeder is about 800 m, having a measured attenuation of about 4 db at 50 mc (see Section III-C). Near the receiving station the feeders are quasi-exponentially tapered to transform the char-

<sup>16</sup> These consist of a pair of copper wires of diameter 0.064 inch spaced 11 inches by thin perspex spacers at intervals of 30 feet and supported 10–15 feet above the ground on wooden poles.

acteristic impedance to 300 ohms to facilitate connection to the receivers.

Polarization measurements are made with a different pair of rhombic antennas which are mounted on a common axis and with their planes perpendicular. Each antenna has the same dimensions as the interferometer antennas, but the pair is equatorially mounted and driven to follow the sun. This allows polarization observations to be made throughout the day.

### B. The 0-480-Meter Variable Line

As explained in Section II-B, the function of the variable line is to maintain the frequency spacing between fringes in the interference pattern at a value of the order of 5 mc for different positions of the sun in the sky. While it would probably be feasible to develop a suitable compact nondispersive artificial line, we have preferred to minimize problems of matching, dispersion, and loss by the use of long lengths of the normal 700-ohm open-wire line.

The variable line consists of 5 loops of the open-wire line of length 15, 30, 60, 120, and 240 m, respectively. Each of these may be either switched into the antenna feeder line or by-passed with a direct connection. A plan view of two of the loop sections is shown in Fig. 7. The switches were designed to avoid appreciable reflections in the radio-frequency line and are operated by solenoids.<sup>17</sup>

Similar switches are used in a system to transfer the variable line from the eastern feeder to the western feeder at noon each day.

The six banks of solenoids operating the five loops and the "noon transfer" system are controlled by a clock-regulated unit which arranges for the total length of the eastern feeder to be decreased in 15-m steps before noon, and then the total length of the western feeder to be similarly increased after noon. By this means the quantity  $a \sin \theta + l$  in (1) is maintained in the vicinity of 60 m and hence the frequency interval  $\Delta f$  in the vicinity of 5 mc.

### C. Calibration of the Antenna Feeder System

One of the major technical problems encountered in making accurate position measurements with the interferometer is the determination of the electrical lengths of the antenna feeder system including the variable line. Since the switches in the variable line inevitably introduce some discontinuities, it is necessary to investigate carefully the consequent variations in electrical length with frequency. To measure apparent positions with an accuracy of  $\pm 1'$  arc ( $\pm 3 \times 10^{-4}$  radians), it is desirable to measure all relative electrical lengths to better than one part in  $3 \times 10^3$ , or  $\pm 30$  cm in our case.

<sup>17</sup> Each switch consists of a thin strip of phosphor bronze, one end of which is held in a plastic clamp; the other end contains small rhodium-plated contacts which bear against similar contacts in plastic mounts. The arm is linked through a long rigid plastic arm to its solenoid.

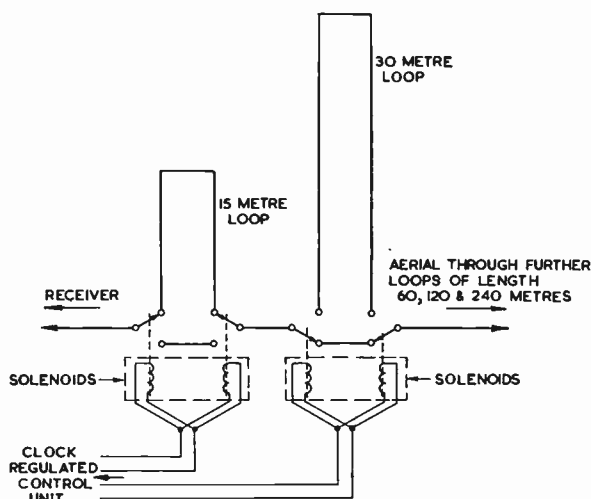


Fig. 7—Diagrammatic plan view of two sections of the variable line, in which only one of the two wires of each radio frequency line is seen. The complete line can be varied from 0 to 480 m in steps of 15 m.

Also, it will be shown that the measurement of source size requires that the relative attenuation of the pair of feeders be known as a function of frequency.

The lines were calibrated by recording, as a function of frequency, the impedance at the receiver terminals of each line with the antenna disconnected from the line. Let us assume initially that the line is uniform and has a characteristic impedance  $Z_0$ . The impedance,  $Z_R(f)$ , at the receiver terminals is then

$$Z_R(f) = Z_0 \coth \left\{ \alpha_L + \alpha_T + i \frac{2\pi f}{c} (l_L + l_T) \right\}, \quad (2)$$

where  $\alpha_L$  and  $l_L$  denote the attenuation and electrical length of the line being measured, and where the termination of the line (nominally an open circuit) is represented by a short line of length  $l_T$  and attenuation  $\alpha_T$ . In the general case, the attenuation and length parameters vary slowly with frequency.

In practice the attenuation per wavelength is extremely small, and so it follows from (2) that as the frequency is increased,  $Z_R(f)$  oscillates between extreme values

$$(Z_R)_{\max} = Z_0 \coth (\alpha_L + \alpha_T) \quad (3)$$

and

$$(Z_R)_{\min} = Z_0 \tanh (\alpha_L + \alpha_T), \quad (4)$$

and these occur at frequencies

$$f_n = \frac{nc}{l_L + l_T}$$

and

$$f_{n+1/2} = \frac{(n + \frac{1}{2})c}{l_L + l_T}, \quad (5)$$

respectively, where  $n$  assumes integral values.

The phase and amplitude of the pattern of  $Z_R(f)$

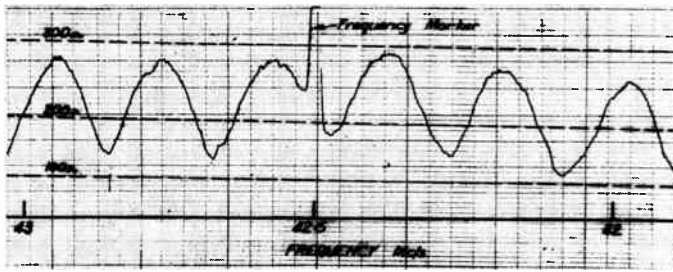


Fig. 8—A small section of an actual record of impedance at the receiver terminals (vertical vs frequency using the system described in the text for measuring electrical length and attenuation).

[see (2)] is measured by connecting the line across the terminals of the 40–70 mc swept-frequency receiver in parallel with a noise diode which acts as a *current* source of broad-band noise. The receiver includes a narrow-band (6-kc) IF amplifier, and the detected output is displayed on a pen recorder. As the receiver frequency is mechanically swept slowly across its range, an oscillatory pattern in phase with  $Z_R(f)$  is traced on the recorder.<sup>18</sup> A typical pattern is shown in Fig. 8. The phase is accurately read using frequency markers generated from harmonics of a crystal oscillator, and the electrical length  $l_L + l_T$  may be determined at many frequencies across the range using (5). Also the attenuation  $\alpha_L + \alpha_T$  is determined by measuring the ratio  $(Z_R)_{\max}/(Z_R)_{\min}$  with the aid of a series of calibration runs in which the network is replaced by several resistors of known value; it is calculated from (3) and (4), which give

$$\tanh(\alpha_L + \alpha_T) = \sqrt{\frac{(Z_R)_{\max}}{(Z_R)_{\min}}}$$

The measurements are then repeated for the line belonging to the other arm of the interferometer, which is terminated by an identical terminating impedance. Let the attenuation and length of the second line be  $\alpha_{L'}$  and  $l_{L'}$ , respectively. As before, we determine  $l_{L'} + l_T$  and  $\alpha_{L'} + \alpha_T$  as functions of frequency, and so obtain the required relative length  $l_L - l_{L'}$  and relative attenuation  $\alpha_L - \alpha_{L'}$ .

A sample set of length measurements ( $l_L + l_T$ ) is shown in Fig. 9. It is seen that the derived lengths at different frequencies are scattered about a mean value with a standard deviation of about 10 cm. This scatter includes the effects of the nonuniformity of the line (e.g., those due to switches in the variable line). Working within the required limits of  $\pm 30$  cm, we are clearly justified in regarding the line as a uniform, non-dispersive line whose length is given by the average at different frequencies.

A sample set of attenuation measurements is shown in Fig. 10. It is found that, within limits of about  $\pm \frac{1}{2}$  db (sufficient for source-size determinations), the measured attenuations can be adequately represented by a linear function of frequency.

<sup>18</sup> A small additional phase shift may occur in the receiving system. This effect tends to be cancelled when we come to measure differences in length between a pair of line networks.

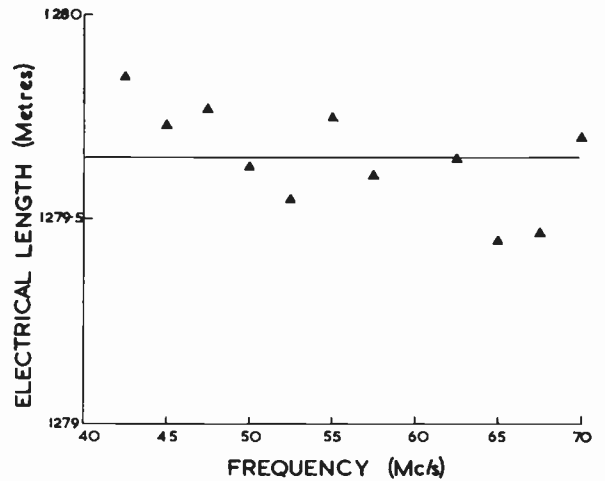


Fig. 9—A typical measurement of electrical length ( $l_L + l_T$ ) as a function of frequency. (This example refers to the west feeder with the variable line set to 450 m.)

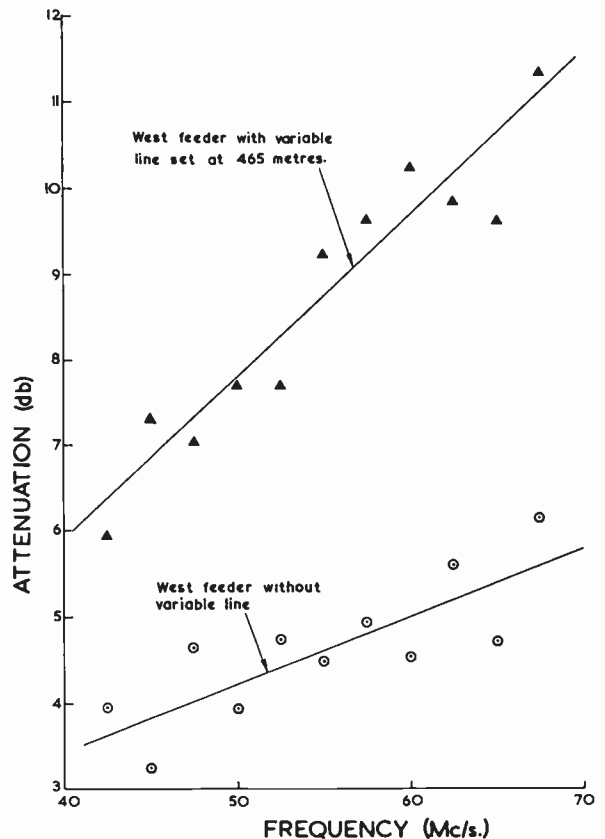


Fig. 10—Two sample measurements of attenuation ( $\alpha_T + \alpha_L$ ) as a function of frequency.

#### IV. THEORY OF MEASUREMENTS

##### A. The Measurement of Positions on the Sun's Disk

We now discuss the method of locating sources on the sun's disk with an E-W swept-frequency multiplying interferometer. The first step is to use the records to calculate the angle  $\theta$  between the incoming rays and the normal plane of the interferometer (see Fig. 1) taking into account phase shifts in the receiver. The second is to relate  $\theta$  with positions on the sun's disk.

1) *A Determination of the Angle  $\theta$* : The phase of the recorded interference pattern is determined by the difference in phase of the two signals reaching the mixing point in the channel mixer (see Fig. 4). At this point let us represent the voltage waveform of the signal passing through channel *A* as

$$E_A = |E_A| \sin 2\pi f_0 t,$$

where  $f_0$  is the intermediate frequency. Then that of the signal through channel *B* will be of the form

$$E_B = |E_B| \sin \left( 2\pi f_0 t + \phi_S + \phi_L + \phi_R + \frac{\pi}{2} \pm \frac{\pi}{2} \right)$$

where the  $\phi$ 's denote phase terms introduced by the difference in path length through the two channels in space ( $\phi_S$ ), in the antenna feeder lines ( $\phi_L$ ) and in the receiver circuits ( $\phi_R$ ). The term " $\pi/2 \pm \pi/2$ " is included to take account of the two positions of the phase switch. Denoting the two switched values of  $E_B$  by  $E_B^+$  and  $E_B^-$ , the output of the phase-sensitive detector is proportional to the time average

$$\begin{aligned} & \frac{(E_A + E_B^-)^2 - (E_A + E_B^+)^2}{2} \\ &= 4 |E_A| |E_B| \sin 2\pi f_0 t \sin (2\pi f_0 t + \phi_S + \phi_L + \phi_R) \\ &= 2 |E_A| |E_B| \cos (\phi_S + \phi_L + \phi_R). \end{aligned} \tag{6}$$

The phase terms  $\phi_s$  and  $\phi_L$  are given by

$$\begin{aligned} \phi_S &= 2\pi(a/\lambda) \sin \theta \\ \phi_L &= 2\pi(l/\lambda), \end{aligned}$$

where  $l$  is the length by which the western antenna feeder line exceeds the eastern, and  $a$  and  $\theta$  are defined in Fig. 1. Similarly, we write

$$\phi_R = 2\pi \{x(\lambda)/\lambda\},$$

where  $x(\lambda)$  is the difference in path length introduced by the two receivers. Substituting in (6) we obtain the swept-frequency interference pattern

$$2 |E_A| |E_B| \cos \frac{2\pi}{\lambda} \{a \sin \theta + l + x(\lambda)\}.$$

The wavelengths at which the interference pattern crosses the zero line occur at  $\lambda_n$ , given by

$$a \sin \theta + l + x(\lambda_n) = \frac{1}{2}(n + 1)\lambda_n, \tag{7}$$

where  $n$  takes integral values, and is even or odd according to the sign of the slope of the pattern as it crosses the zero line.

To determine the function  $x(\lambda)$  at a number of wavelengths, we replace the antenna system by the artificial source (noise generator) (see Fig. 4). This is connected to receivers by a pair of cables differing by a known length,  $b$ . We then obtain a second interference pattern whose zero points are given, by analogy with (7), by

$$b + x(\lambda_m) = \frac{1}{2}(m + 1)\lambda_m,$$

where  $m$  takes integral values.

The electrical length of  $l$  in (7) is measured by the method previously described and so  $\sin \theta$  is calculated. Providing that neighboring wavelengths  $\lambda_n, \lambda_{n+1}$  arrive from approximately the same direction, no ambiguity in choosing  $n$  will arise.

2) *Conversion of  $\theta$  to Solar Disk Coordinates*: The position of a source in the celestial sphere may be specified by the usual astronomical coordinates—hour angle,  $H$ , and declination,  $\delta$ . These are related to the measured quantity.

$$S = \sin \theta$$

by the well-known expression for an E-W interferometer<sup>19</sup>

$$S = \sin H \cos \delta. \tag{8}$$

Let the position of a source on the sun be referred to the center ( $S_0; H_0, \delta_0$ ) of the disk in the form ( $H_0 + \Delta H, \delta_0 + \Delta \delta$ ). Then, with sufficient accuracy, the small displacements  $\Delta H$  and  $\Delta \delta$  cause the value of  $S$  to become

$$S = S_0 + \Delta S,$$

where

$$\Delta S = \left( \frac{\partial S}{\partial H} \right)_0 \Delta H + \left( \frac{\partial S}{\partial \delta} \right)_0 \Delta \delta. \tag{9}$$

Thus for a given value of  $\Delta S$  there is a family of possible positions of the source which lie on a straight line whose equation, in the ( $\Delta H, \Delta \delta$ ) plane, is (9). Let us specify this line in terms of its (angular) distance,  $r$ , from the center of the sun and its inclination,  $\psi$ , with the  $H$  axis (see Fig. 11)—, *i.e.*, in the form

$$r = \cos \psi \Delta H - \sin \psi \Delta \delta. \tag{10}$$

Comparing (9) and (10) we obtain

$$\tan \psi = - \left( \frac{\partial S}{\partial \delta} \right)_0 / \left( \frac{\partial S}{\partial H} \right)_0 \tag{11}$$

and

$$r = \frac{\Delta S}{\sqrt{\left\{ \left( \frac{\partial S}{\partial \delta} \right)_0 \right\}^2 + \left\{ \left( \frac{\partial S}{\partial H} \right)_0 \right\}^2}} \tag{12}$$

Substituting for  $S$  in (11) and (12), using (8), we obtain the values of  $r$  and  $\psi$  in terms of the measured quantity  $S = \sin \theta$ , and the sun's position (available from the *Nautical Almanac*):

$$r = \frac{\sin \theta - \sin H_0 \cos \delta_0}{\sqrt{\frac{1}{2}(\cos 2H_0 \cos 2\delta_0 + 1)}} \tag{13}$$

$$\psi = \tan^{-1} (\tan H_0 \tan \delta_0). \tag{14}$$

<sup>19</sup> The treatment given here is for a horizontal E-W interferometer. The actual interferometer axis lies in a surveyed E-W vertical plane but is tilted a small angle  $\alpha$ , the W antenna being higher than the E. In this case (8) becomes  $S = \cos \alpha \sin H \cos \delta + \sin \alpha (\cos H \cos \phi \cos \delta + \sin \delta \sin \Phi)$ , where  $\Phi$  is the latitude of the observing station.

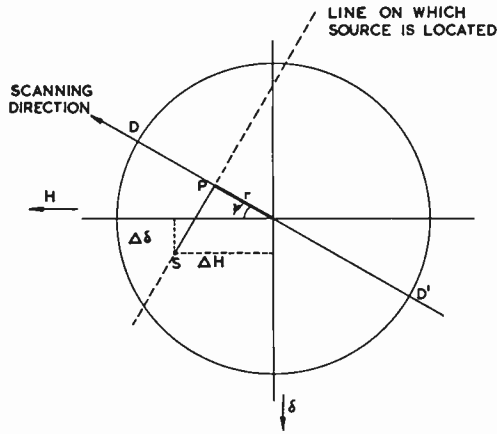


Fig. 11—Aspect of the sun as seen at noon from the southern hemisphere.

*B. The Measurement of Source Size*

The method of measuring the angular size of a source with an adding swept-frequency interferometer is closely analogous to the monochromatic method originally used in optical astronomy by Michelson and in radio astronomy by McCready, Pawsey, and Payne-Scott;<sup>7</sup> we simply measure the ratio of the maximum-to-minimum power in the interference pattern and hence calculate the half-power width of the source assuming a plausible shape of the source. The half-power width does not depend critically on the assumed shape if the latter is a smooth, single-humped curve. Here we shall assume the shape to be one period of a sine wave, such that the line-integrated brightness,  $B(\theta')$ , at an angle  $\theta'$  measured along the scanning direction is given by

$$\left. \begin{aligned} B(\theta') &= A \left( 1 + \cos \frac{\pi\theta'}{\Delta} \right) \dots \dots \dots | \theta' | \leq \Delta \\ B(\theta') &= 0 \dots \dots \dots | \theta' | > \Delta \end{aligned} \right\} \quad (15)$$

where  $\Delta$  is the half-power angular width of the source. The ratio  $P_{max}/P_{min}$  of the maximum-to-minimum power in the interference pattern at any desired frequency<sup>20</sup> is obtained from the records by drawing the upper and lower envelopes to the fringe pattern [Fig. 12(b)]. These are calibrated using special calibration records in which a series of six power levels, each separated by a 2:1 interval, is generated with a diode noise generator. The source-size calculation also depends on the relative attenuation,  $\alpha$ , of the feeder lines which is measured for different settings of the variable line by the technique previously described.

The dependence of source size upon  $P_{max}/P_{min}$  and  $\alpha$  is derived below. (Previous treatments describing the analogous monochromatic method have neglected the effects of attenuation which are important here.)

Let the attenuation, expressed as a power ratio, along the two feeder lines be  $k_A$  and  $k_B$ , respectively [Fig.

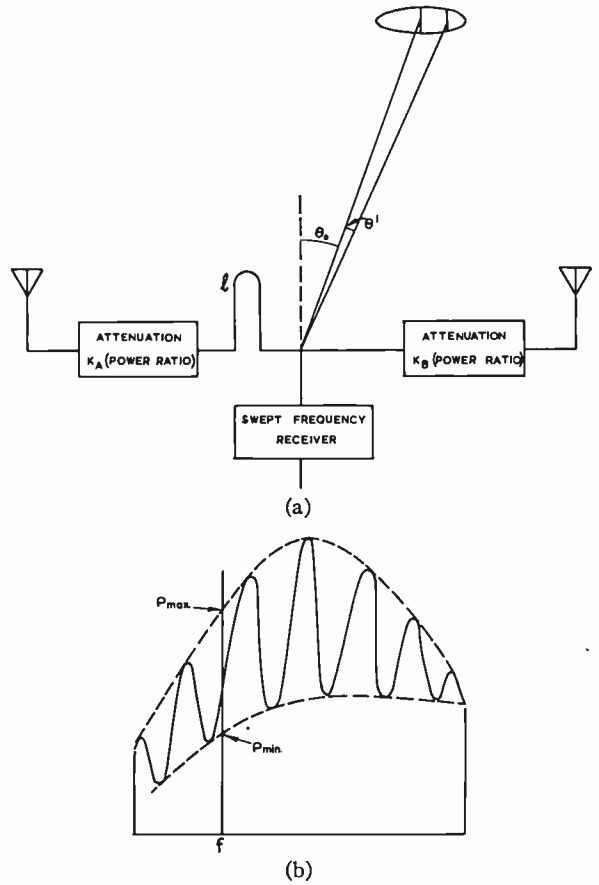


Fig. 12—Defining the symbols required for source-size measurements.

12(a)]. The power received from a point source of flux density  $S$  at position angle  $\theta_0$  is then proportional to the time average

$$\begin{aligned} & [(k_A S)^{1/2} \cos \{ 2\pi f t + \pi(f/c)(a \sin \theta_0 + l) \} \\ & + (k_B S)^{1/2} \cos \{ 2\pi f t - \pi(f/c)(a \sin \theta_0 + l) \}]^2 \\ & = \frac{1}{2}(k_A + k_B)S + (k_A k_B)^{1/2} S \cos \{ 2\pi(f/c)(a \sin \theta_0 + l) \} \end{aligned}$$

Similarly if the point source is replaced by a source of small but finite angular size having a line-integrated brightness  $B(\theta')$  at frequency  $f$ , the received power is proportional to

$$\begin{aligned} & \frac{1}{2}(k_A + k_B) \int_{-\infty}^{\infty} B(\theta') d\theta' \\ & + (k_A k_B)^{1/2} \int_{-\infty}^{\infty} B(\theta') \cos [2\pi(f/c) \{ a \sin (\theta_0 + \theta') + l \}] d\theta' \\ & \approx \frac{1}{2}(k_A + k_B) \int_{-\infty}^{\infty} B(\theta') d\theta' \\ & + (k_A k_B)^{1/2} \int_{-\infty}^{\infty} B(\theta') \cos \{ 2\pi(f/c)(\theta' \cos \theta_0 \\ & + a \sin \theta_0 + l) \} d\theta', \end{aligned}$$

where  $B(\theta')$  is taken as nonzero only for small values of  $\theta'$ . As  $f$  is varied, the above expression defines the swept-frequency interference pattern. It is simple to show that:

<sup>20</sup> In this section all quantities relating to the source [i.e.,  $B(\theta')$ ,  $A$ ,  $\Delta$ ,  $P_{max}$ ,  $P_{min}$ ,  $S$  and  $l$ ] are functions of frequency. So also are the instrumental quantities  $k_A$ ,  $k_B$  and  $\alpha$ .

1) The spacing between neighboring maxima is

$$\Delta f = \frac{a \sin \theta_0 + l}{c}$$

provided that  $B(\theta')$  does not change appreciably with frequency in the interval  $\Delta f$ , and

2) The maximum and minimum envelopes of the interference pattern due to a symmetrical source are proportional to

$$\frac{1}{2}(k_A + k_B) \int_{-\infty}^{\infty} B(\theta') d\theta'$$

$$\pm (k_A + k_B)^{1/2} \int_{-\infty}^{\infty} B(\theta') \cos \{2\pi a(f/c)\theta' \cos \theta_0\} d\theta'$$

Denoting these envelopes by  $P_{max}$  and  $P_{min}$ , we note that the visibility,  $\xi$ , of the fringes, defined by

$$\xi = \frac{P_{max} - P_{min}}{P_{max} + P_{min}}$$

is given, by

$$\xi = \frac{2(k_A k_B)^{1/2}}{k_A + k_B} \frac{\int_{-\infty}^{\infty} B(\theta') \cos \{2\pi\theta'(a/\lambda) \cos \theta_0\} d\theta'}{\int_{-\infty}^{\infty} B(\theta') d\theta'}$$

Thus  $\xi$  is just the ratio of the moduli of the Fourier components of the source distribution at angular "frequencies"  $(a/\lambda) \cos \theta_0$  and 0, with a factor of proportionality determined by the attenuation of the lines. If the relative attenuation is  $\alpha$  nepers ( $\alpha = \frac{1}{2} \log_e (k_A/k_B)$ ), this factor becomes

$$\frac{2e^\alpha}{e^{2\alpha} + 1} = \text{sech } \alpha$$

It remains to substitute the assumed source function (15), whence we obtain

$$\xi = \frac{P_{max}/P_{min} - 1}{P_{max}/P_{min} + 1} = \frac{\text{sech } \alpha \sin 2\pi v}{2\pi v(1 - 4v^2)}$$

where  $v = \Delta(a/\lambda) \cos \theta_0$ .

A plot of  $P_{max}/P_{min}$  vs  $v$  for different values of  $\alpha$  is given in Fig. 13. The conversion of  $v$  to the source size  $\Delta$  for the interferometer at Dapto is also given in this figure. It is seen that numerical values of source size can be assessed in the approximate range 1 to 20 minutes of arc. Outside this range upper and lower limits can be derived.

### C. The Measurement of Polarization

Polarization measurements are made by replacing the pair of spaced antennas of the interferometer by a pair of antennas mounted on a common axis, but with

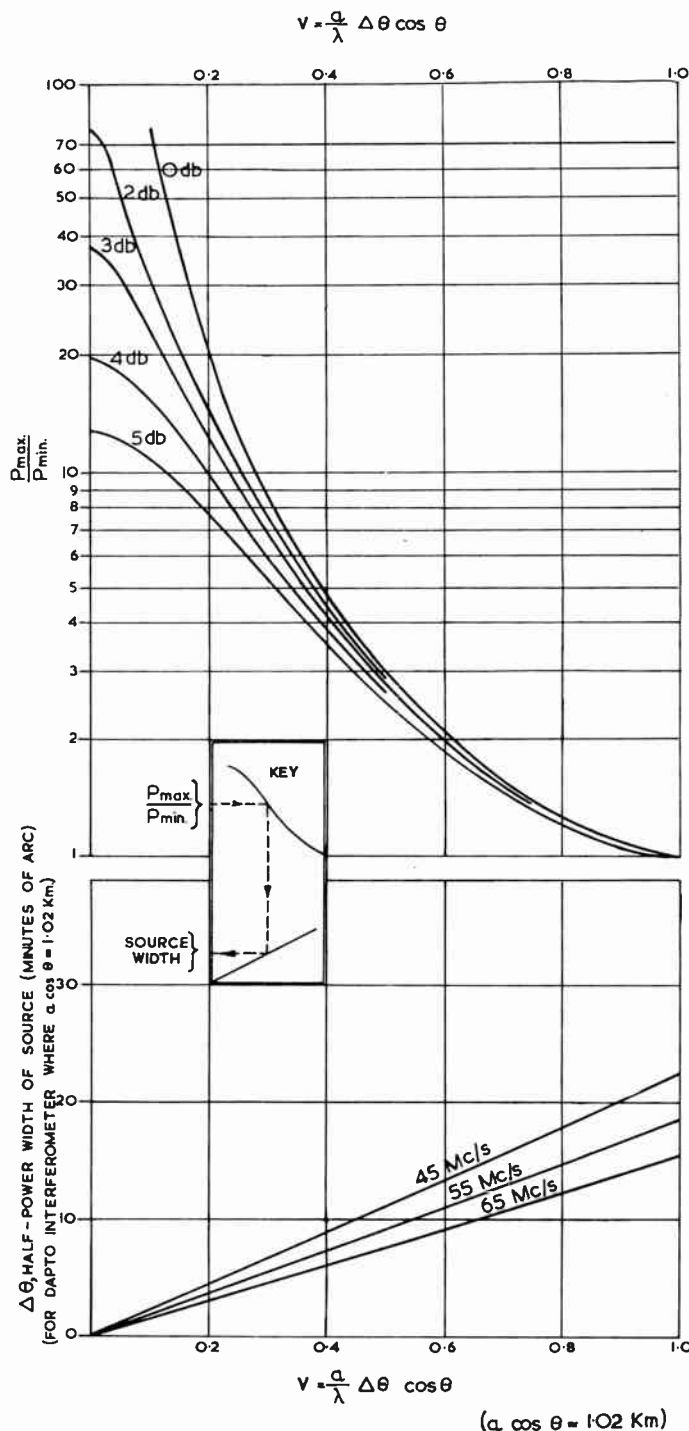


Fig. 13—The chart used for calculating sources size from the maximum-to-minimum power ratio ( $P_{max}/P_{min}$ ) in the interference pattern, and the relative attenuation of the feeders in decibels. The upper part of this figure is quite general, while the lower part contains parameters peculiar to the interferometer at Dapto.

mutually perpendicular planes of polarization. The antennas are connected to the adding and multiplying receiving systems through feeders differing by a known length  $b$  ( $= 60$  m) as shown in Fig. 4.

The signals generated in the two antennas by polarized radiation incident upon them will in general contain phase-coherent components. These components

will interfere with one another at the mixing point and, as the frequency is swept, will generate an interference pattern. With the multiplying system, this pattern is [cf. (6)]

$$\cos\left(\frac{2\pi fb}{c} + \phi_P + \phi_R\right),$$

where  $\phi_P$  is the difference in phase between the two received polarization components of the radiation, and  $\phi_R$  is the relative phase change introduced in the receivers. The latter term is determined in the calibration process and so the polarization phase,  $\phi_P$ , is determined (at 2.5-mc frequency intervals) from the frequencies of the null points in the interference pattern.

Past observations have shown that polarized radiation from the sun is mainly circular. In this case  $\phi = \pm\pi/2$ , the sign depending on the sense of rotation. Circular polarization can therefore be directly recognized and its sense determined from measurements of  $\phi_P$ ; also the degree of circular polarization is given by the depth of modulation of the pattern of the adding interferometer.

When the phase  $\phi_P$  indicates noncircular polarization the problem is more complicated. Linear polarization gives  $\phi_P = 0$  or  $\pi/2$ , but the depth of modulation depends both on the angle between the planes of polarization of the antenna and the radiation, and on the degree of polarization. Intermediate values of  $\phi_P$  correspond to elliptical polarization. In general, however, it is simple to show<sup>21</sup> that the complete polarization characteristics (*i.e.*, the percentage, eccentricity, orientation, and sense-of-rotation of elliptical polarization) can be determined from measurements of the following:

- 1) The phase,  $\phi_P$ , of the polarization (given accurately by the multiplying interferometer with crossed antenna system).
- 2) The maximum and minimum power in the polarization interference pattern (given by the adding interferometer with crossed antenna system).
- 3) The total power received in one polarization (given by the adding interferometer with the spaced antenna system).

Polarization observations are made at selected times by operating an antenna switch ( $S_2$ , shown in Fig. 4) which replaces the spaced-antenna system by the crossed-antenna system. A sample record in Fig. 6 shows strong circular polarization in storm radiation (spectral Type I).

## V. PRELIMINARY RESULTS

Trial observations with the interferometer were made daily between June 6 and July 6, 1957, and during this period numerous bursts and storms of solar radio emission were recorded. Analysis of these records is incom-

plete at the time of writing. The preliminary results given below are primarily measurements of the angular size of Type I and Type III sources recorded on two selected days.

### A. Observations of a Type I Storm—June 20, 1957, 11:30 to 12:30 E.A.S.T.<sup>22</sup>

Parts of the record are reproduced in Fig. 6, and the analysis is summarized in Fig. 14. The storm was characterized by an unusually intense background continuum in which the flux density attained a value of  $1.5 \times 10^{-19}$  W m<sup>-2</sup> (c/s)<sup>-1</sup>. The radiation was strongly polarized (right-handed circular).

At 12:08 the source was located on the line  $AA'$  in Fig. 14(a).<sup>23</sup> It was not possible to decide which of two large sunspot groups, one in the northern and one in the southern hemisphere, was associated with the source. However a further measurement made at 13:46 when the scanning angle had changed by  $11\frac{1}{2}^\circ$  favored the northern group.

Measurements of source size at 55 mc at intervals of about one minute are shown in Fig. 14(b). The frequency dependence of source size, averaged over the one-hour period, is shown in Fig. 14(c).

The mean size is seen to decrease from about 10' arc at 45 mc to 6' arc at 65 mc.

The maximum instantaneous brightness temperature in this period was estimated to be  $2.3 \times 10^{10}$  K.

### B. Observations of Type III Bursts—July 3, 1957, 10:15 to 12:30 E.A.S.T.

In this period 26 individual bursts, or small groups of bursts, were analyzed (Fig. 15). Records of two are reproduced in Fig. 5. Fig. 15(a) shows the location of a burst at 10:39 and indicates an origin above a large spot near a flare in progress.

Detailed source-size measurements indicated that at any one frequency the size remained approximately constant in the course of the rise and fall of an individual burst. Fig. 15(b) shows the distribution of source size at 55 mc, for the 26 bursts, and Fig. 15(c) the average size as a function of frequency. There appears to be no marked difference between the angular size of Type I and Type III emissions.

The maximum instantaneous brightness temperature in this period was estimated to be  $10^{10}$  K.

The above results show that both Type I and Type III sources cover a remarkably large part of the sun's disk frequently exceeding one tenth of the optical disk if circular symmetry is assumed. The result that the size increases with decreasing frequency suggests that the emitting region in the solar corona could be funnel-shaped, the diameter increasing with height. It should

<sup>22</sup> Eastern Australian Standard Time is 10 hours in advance of Universal Time.

<sup>23</sup> The sunspot pictures and flare observation in Figs. 14 and 15 were kindly made available by the Division of Physics, CSIRO, through the courtesy of Dr. R. G. Giovanelli.

<sup>21</sup> J. L. Pawsey and R. N. Bracewell, "Radio Astronomy," Clarendon Press, Oxford, Eng., pp. 59–62; 1955.

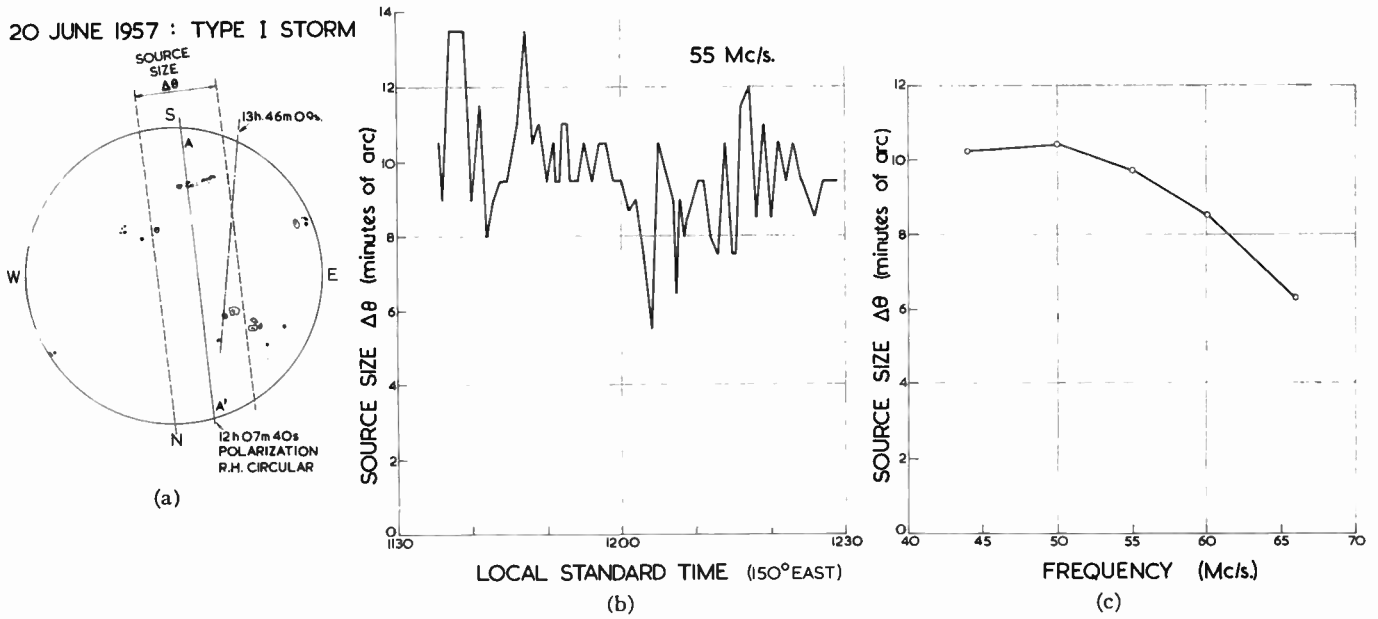


Fig. 14—Observations of a Type I storm. (a) A pair of instantaneous position measurements, averaged over frequency, (b) the variation with time of the apparent source size at 55 mc, (c) the average spectrum of source size over the period in (b).

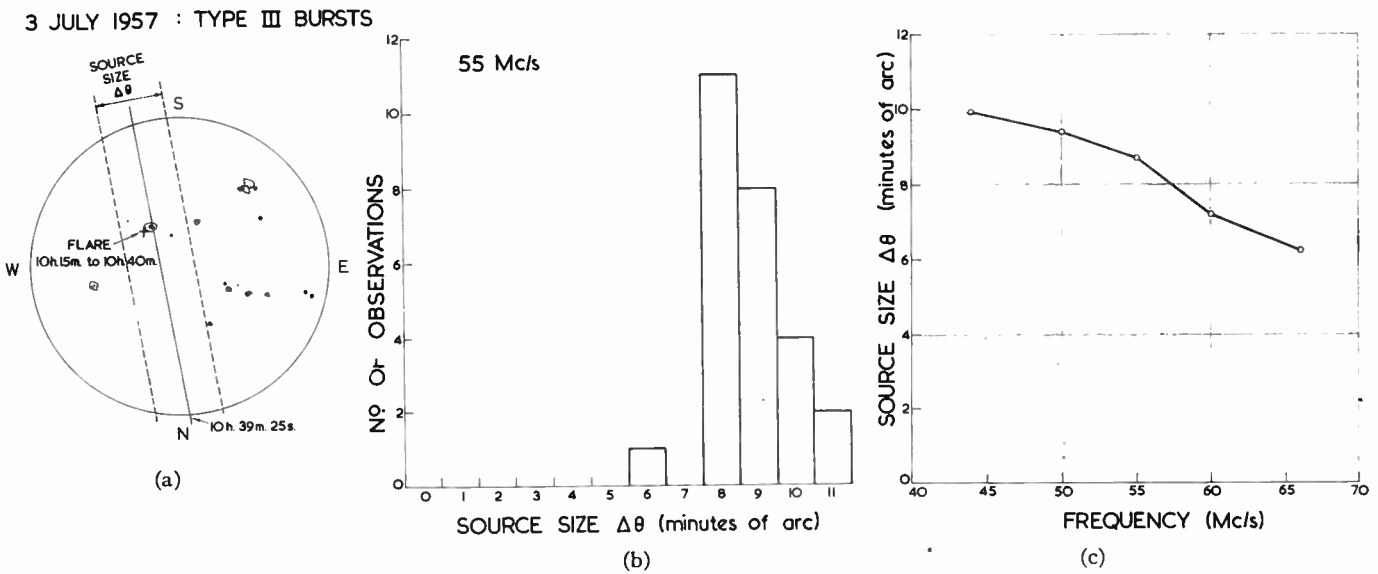


Fig. 15—Observations of Type III bursts. (a) An instantaneous position measurement, averaged over frequency, (b) histogram showing the distribution of source size in the 26 bursts (55 mc), (c) the average spectrum of source size during the bursts referred to in (b).

be pointed out, however, that the size we measure does not necessarily correspond to that of the actual emitting region since refraction and scattering in the solar atmosphere could disguise its true form. Further measurements of sources at different positions on the sun's disk should help to resolve this question.

VI. ACKNOWLEDGMENT

The authors wish to thank Dr. J. A. Roberts and M. M. Komesaroff who participated in the initial phases of this work. Much of the variable line assembly and its

control unit was constructed by Mr. Komesaroff. The authors also are indebted to G. H. Trent for valuable assistance in construction of equipment, taking of observations, and analysis of results, and to J. Joisce who assisted in the observing program. Considerable help was derived from H. Rabben, Fraunhofer Institute, Freiburg-in-Breisgau, during an extended visit to Dapto field station. Finally, thanks are due to Dr. J. L. Pawsey, Director, CSIRO Radiophysics Laboratory's radio astronomy group, for his interest in this work, and Dr. Roberts for helpful criticisms of the manuscript.

# Radio Astronomy Polarization Measurements\*

MARSHALL H. COHEN†, MEMBER, IRE

**Summary**—Various polarization measuring schemes are discussed in terms of the Stokes parameters. The methods are separated into three groups according to the number of components isolated by the antenna system. The dispersion resulting from the frequency dependence of the Faraday effect is considered, and the interpretation of polarization data in terms of these effects is discussed. Some results are that one polarization determination will allow limits to be placed on the axial ratio and polarization percentage at the source, and on the ray path integral of longitudinal magnetic field times electron density. A graphical presentation of Hatanaka's dispersion theory permits this to be done very quickly. With suitable assumptions, measurements at two frequencies or with two bandwidths will fix the three quantities.

Radio astronomy polarization observations are surveyed. The ionosphere, solar corona, and Crab Nebula are considered briefly in the light of possible Faraday effects. Mayer, McCullough, and Sloanaker's 3.15-cm observations on the Crab Nebula and the optical results are used to analyze lower frequency attempts to find polarized radiation from this object.

## I. INTRODUCTION

THIS introduction contains a brief survey of some polarization observations.

Section II reviews the Stokes parameters as a means of describing the state of polarization of radio noise. It is shown how the parameters are related to quantities which can be measured with antennas.

Section III is a survey of measurement techniques. A number of schemes are considered and categorized according to the number of components measured.

Section IV is a discussion of the Faraday effect. Several experiments for finding the parameters involved are considered.

Section V is a discussion of polarization observations of the sun and of the Crab Nebula in terms of possible Faraday rotation effects.

Circularly-polarized radiation from the sun was first observed in 1946, at an active time when a large sun spot was on the sun's disk.<sup>1</sup> The existence of the polarization was presumed to be associated with the magnetic field of the sun spot, and subsequent investigations showed that the sense of rotation generally corresponded to the ordinary mode of the magneto-ionic theory.<sup>2</sup> There were reports of elliptical and linear polarizations seen with an interference polarimeter,<sup>2,3</sup> but typically any polarized component in the solar radiation was

\* Original manuscript received by the IRE, October 14, 1957. Various aspects of this work have been supported by contracts with the Office of Naval Res. and the Rome Air Dev. Center, and by a grant from the Natl. Science Foundation.

† Cornell University, Ithaca, N. Y.

<sup>1</sup> J. L. Pawsey and R. N. Bracewell, "Radio Astronomy," Oxford University Press, London, Eng., p. 185; 1955.

<sup>2</sup> R. Payne-Scott and A. G. Little, "The position and movement on the solar disk of sources of radiation at a frequency of 97 mcs. II. Noise storms," *Aust. J. Sci. Res.*, vol. A 4, pp. 508-525; 1951.

<sup>3</sup> R. Payne-Scott and A. G. Little, "The position and movement on the solar disk of sources of radiation at a frequency of 97 mcs. III. Outbursts," *Aust. J. Sci. Res.*, vol. A 5, pp. 32-49; 1952.

taken to be circular. A number of observatories making routine observations of the sun made observations of both circular components, and computed a percentage of polarization on the basis that only circular polarization was present.<sup>4</sup> The circularly-polarized solar radiation is characteristic of noise storms, which are associated with sun spots. This has been observed over a very wide range of frequencies. At microwave frequencies the storms are missing, but the "slowly varying component" has been seen to be partly circularly polarized at 10 cm<sup>5</sup> and at 3 cm.<sup>6</sup>

In 1954 Hatanaka, Suzuki, and Tsuchiya<sup>7,8</sup> constructed a telescope-type (as opposed to an interference-type) polarimeter that made a complete determination of the four polarization parameters. They observed many partially-polarized, elliptical bursts from the sun at 200 mc. In 1956, however, Hatanaka<sup>9</sup> pointed out that at meter wavelengths the Faraday rotation in the earth's ionosphere would be great enough to destroy the precision with which orientation angle data could be extended back to the source. He also pointed out that there was a chance that the solar corona might produce a very large rotation and a consequent dispersion in orientation angles which would have the effect of depolarizing a wave. This raised the speculation that perhaps some of the unpolarized solar bursts were originally linearly polarized, but became unpolarized by the dispersion process.

The ionospheric Faraday effect has been directly observed by Evans,<sup>10</sup> who made a two-frequency radar experiment with the moon as the target. The Faraday rotation (one way) was 10 to 13 radians at 120 mc, near sunrise. The amount of rotation should be proportional to  $f^{-2}$  for frequencies well above the critical frequency.

Optical measurements of the photosphere<sup>11</sup> suggest the existence of a general solar dipole magnetic field with a strength of 1 Gauss at the poles. If this type of field exists, a radio ray resulting from thermal radiation

<sup>4</sup> *Quart. Bull. Solar Activity*, Internatl. Astron. Union, Zurich, Switzerland; January-March, 1949, and later issues.

<sup>5</sup> Pawsey and Bracewell, *op. cit.*, p. 171.

<sup>6</sup> N. L. Kaidanovsky, D. V. Korolkov, N. S. Soboleva, and C. E. Khaikin, "Observations of polarized radio waves from sun spots on a wavelength of 3 cm," *Solar Data*, no. 4, Acad. Sci. USSR; 1956.

<sup>7</sup> S. Suzuki and A. Tsuchiya, "A time-sharing polarimeter at 200 mc," this issue, p. 190.

<sup>8</sup> T. Hatanaka, S. Suzuki, and A. Tsuchiya, "Observations of polarization of solar radio bursts," *Proc. Japan Acad.*, vol. 31, pp. 81-87; 1955.

<sup>9</sup> T. Hatanaka, "The Faraday effect in the earth's ionosphere with special reference to polarization measurements of solar radio emission," *Publ. Astron. Soc. Japan*, vol. 8, pp. 73-86; 1956.

<sup>10</sup> J. V. Evans, "The measurement of the electron content of the ionosphere by the lunar radio echo method," *Proc. Phys. Soc.*, vol. B69, pp. 953-955; September, 1956.

<sup>11</sup> H. W. Babcock and H. D. Babcock, "The sun's magnetic field, 1952-1954," *Astrophys. J.*, vol. 121, pp. 349-366; March, 1955.

will be slightly circularly polarized because the two magneto-ionic modes will have different absorption coefficients. Smerd<sup>12</sup> has calculated the magnitude of this effect and has shown how the resultant polarization depends on the strength of the magnetic field and on the electron temperature. Rays from the northern and southern hemispheres of the sun will have opposite polarizations because the longitudinal components of magnetic field are opposite for the two cases, so the integrated flux from the whole sun will be unpolarized.

Attempts have been made to measure the differential polarization between the two halves of the sun, and thereby determine the strength of the general magnetic field in the corona. The results so far have been negative and have only given upper limits to the magnetic field. Christiansen, Yabsley, and Mills,<sup>13</sup> measuring at 50 cm during an eclipse, set an upper limit of 9 Gauss for the strength of the polar field. Conway,<sup>14</sup> measuring with a N-S interferometer at 60 cm, set a limit of 2.5 Gauss. A more recent interferometer measurement by Conway<sup>15</sup> gives a preliminary estimate of 1 Gauss for the limits. This required equipment which could detect a polarized component of 0.25 per cent.

The light from the radio source in Taurus (Crab Nebula) has been found to be strongly linearly polarized, and since this discovery there has been considerable interest in a possible polarization of the radio radiation.<sup>16</sup> Mayer, McCullough, and Sloanaker<sup>17</sup> have recently reported a polarization of about 7 per cent at 3 cm, observed with a rotating linear antenna in the NRL 50-foot dish. At lower frequencies the polarization would probably be less because of Faraday dispersion. At 22 cm Westerhout<sup>18</sup> set an upper limit of 1 per cent, and at 158 mc Hanbury-Brown, Palmer, and Thompson<sup>19</sup> set an upper limit of  $2\frac{1}{2}$  per cent, for the polarized flux, if linearly polarized.

The sources in Cassiopeia and Cygnus also have been examined for polarized radiation, with negative results.<sup>17-20</sup>

<sup>12</sup> S. F. Smerd, "The polarization of thermal 'solar noise' and a determination of the sun's general magnetic field," *Aust. J. Sci. Res.*, vol. A 3, pp. 265-273; June, 1950.

<sup>13</sup> W. N. Christiansen, D. E. Yabsley, and B. Y. Mills, "Measurements of solar radiation at a wavelength of 50 centimeters during the eclipse of November 1, 1948," *Aust. J. Sci. Res.*, vol. A 2, pp. 506-523; 1949.

<sup>14</sup> R. G. Conway, "The general magnetic field of the sun," *The Observatory*, vol. 76, pp. 106-108; June, 1956.

<sup>15</sup> Report to the XIIth General Assembly of URSI, Boulder, Colo.; August 26-September 5, 1957.

<sup>16</sup> J. H. Oort and T. H. Walraven, "Polarization and composition of the Crab Nebula," *Bull. Astron. Inst. Neth.*, vol. 12, pp. 285-308; May, 1956.

<sup>17</sup> C. H. Mayer, T. P. McCullough, and R. M. Sloanaker, "Evidence for polarized radio radiation from the Crab Nebula," *Astrophys. J.*, vol. 126, pp. 468-470; September, 1957.

<sup>18</sup> G. Westerhout, "Search of polarization of the Crab Nebula and Cassiopeia A at 22 cm wavelength," *Bull. Astron. Inst. Neth.*, vol. 12, pp. 309-311; May, 1956.

<sup>19</sup> R. Hanbury-Brown, H. P. Palmer, and A. R. Thompson, "Polarization measurements on three intense radio sources," *Monthly Notices Roy. Astron. Soc.*, vol. 115, pp. 487-492; 1955.

<sup>20</sup> M. Ryle and F. G. Smith, "A new intense source for radio-frequency radiation in the constellation of Cassiopeia," *Nature*, vol. 162, pp. 462-463; September, 1948.

## II. POLARIZATION PARAMETERS

The radio waves of concern are assumed to be partly-polarized noise signals. Such waves can be uniquely resolved into polarized and unpolarized (randomly-polarized) components.<sup>21</sup> The polarized part has a noise spectrum but has coherence between components at right angles. Its electric vector traces out an ellipse which is continually fluctuating in size but maintains a constant orientation, axial ratio, and sense of rotation, for intervals long compared with the period. The polarized part is specified by its intensity ( $I_e$ ), orientation ( $\chi$ ), and axial ratio ( $r$ ). The sense of rotation is contained in the sign of  $r$ :  $r > 0$  means left hand in the radio sense; and  $r < 0$  means right hand. See Fig. 1. The wave is propagating along the  $z$  axis, into the paper, and is right-hand polarized. The angle  $\chi$  is clockwise from the  $x$  axis, viewed in the direction of propagation.

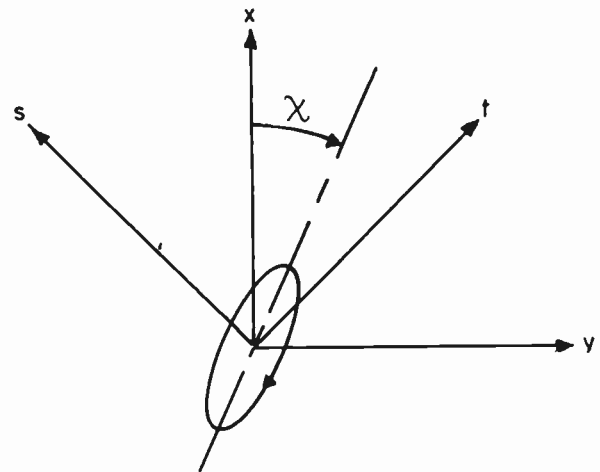


Fig. 1—Coordinate system.

The unpolarized part of the wave has a similar noise spectrum and has components at right angles which are independent. It is specified by a single parameter, intensity ( $I_u$ ). The total intensity ( $I$ ) is the sum of  $I_e$  and  $I_u$ . If we let  $m$  = polarization fraction =  $I_e/I$ , the four parameters that specify the wave are  $I$ ,  $m$ ,  $r$ , and  $\chi$ .

The Stokes parameters<sup>21</sup> are a set of four numbers that define the wave and have the advantage of being closely related to antenna measurements. They may be defined by

$$I = I \quad (1)$$

$$Q = I_e \cos 2\beta \cos 2\chi \quad (2)$$

$$U = I_e \cos 2\beta \sin 2\chi \quad (3)$$

$$V = I_e \sin 2\beta, \quad (4)$$

<sup>21</sup> S. Chandrasekhar, "Radiative Transfer," Oxford University Press, London, Eng., pp. 24-35; 1955.

where

$$\beta = \tan^{-1} r. \quad (5)$$

In these terms, the quantities  $m$ ,  $r$ , and  $\chi$  are given by

$$m = (Q^2 + U^2 + V^2)^{1/2}/I, \quad (6)$$

$$\sin 2\beta = V/I_s, \quad (7)$$

$$\tan 2\chi = U/Q. \quad (8)$$

The wave can be regarded as the sum of two independent elliptically-polarized components, with equal and opposite values of  $r$ , and perpendicular orientations.<sup>21</sup> These will be referred to as opposite polarizations. They include perpendicular linear components, and oppositely rotating circular components, as special cases. These are the only ones we shall use. If the wave is resolved into components along the  $x$  and  $y$  axes (Fig. 1), the intensities are (omitting impedance factors)

$$I_x = X^2 + \frac{1}{2}I_u, \quad (9)$$

$$I_y = Y^2 + \frac{1}{2}I_u, \quad (10)$$

$$I = I_x + I_y. \quad (11)$$

In these formulas  $X$  is the rms amplitude of the  $x$  component of the polarized part, and  $Y$  is the rms amplitude of the  $y$  component of the polarized part. These quantities are all defined for a certain frequency interval; say, the bandwidth of the receiver. The amplitudes  $X$  and  $Y$  have a fixed ratio so long as the polarization is constant. Moreover, there is a constant phase relationship between corresponding frequencies of the two components of the polarized part. Let  $\gamma_v$  be the angle by which the  $y$  components lead the  $x$  components. The value of  $\gamma_v$  is constant over the entire band under consideration.

Similar remarks can be made about components along the  $s$  and  $t$  axes at  $\pm 45^\circ$  to the  $x$ ,  $y$  axes, Fig. 1.

$$I_s = S^2 + \frac{1}{2}I_u, \quad (12)$$

$$I_t = T^2 + \frac{1}{2}I_u, \quad (13)$$

$$I = I_s + I_t. \quad (14)$$

The phase difference,  $\gamma_t$ , is similarly defined.

Corresponding definitions can be made in terms of circular components:

$$I_r = R^2 + \frac{1}{2}I_u, \quad (15)$$

$$I_l = L^2 + \frac{1}{2}I_u, \quad (16)$$

$$I = I_r + I_l. \quad (17)$$

$R$  and  $L$  are the mean amplitudes of the right and left circular components of the polarized part of the wave, and  $\gamma_r$  is the phase difference between them. For sinusoidal waves the circular components are defined in terms of the linear components:

$$\hat{R} = (\hat{X} + j\hat{Y})/\sqrt{2}, \quad (18)$$

$$L = (\hat{X} - j\hat{Y})/\sqrt{2}. \quad (19)$$

Except for a factor  $\sqrt{2}$ , this is the representation used by Rumsey.<sup>22</sup> The interpretation of these equations is considered in Appendix I.

In terms of the  $x$ ,  $y$  components the Stokes parameters are

$$I = I_x + I_y = X^2 + Y^2 + I_u, \quad (11)$$

$$Q = I_x - I_y = X^2 - Y^2, \quad (20)$$

$$U = 2XY \cos \gamma_v, \quad (21)$$

$$V = 2XY \sin \gamma_v. \quad (22)$$

This result is derived by Chandrasekhar.<sup>21</sup> In terms of the  $s$ ,  $t$  components,

$$I = I_s + I_t, \quad (14)$$

$$Q = 2ST \cos \gamma_t, \quad (23)$$

$$U = I_t - I_s, \quad (24)$$

$$V = 2ST \sin \gamma_t. \quad (25)$$

This is like the representation in  $x$ ,  $y$  components with  $Q$  and  $(-U)$  interchanged. This follows from (2) and (3); a rotation of  $45^\circ$  interchanges  $\cos 2\chi$  and  $(-\sin 2\chi)$ .

In terms of the circular components the parameters are

$$I = I_l + I_r, \quad (17)$$

$$Q = 2RL \cos \gamma_r, \quad (26)$$

$$U = 2RL \sin \gamma_r, \quad (27)$$

$$V = I_l - I_r. \quad (28)$$

This is derived in Appendix I.

The intensities  $I_x$ ,  $I_r$ , etc., are proportional to the powers that will be generated in linearly and circularly-polarized antennas. Eqs. (11), (14), (17), and (20) to (28) can therefore be regarded as defining the Stokes parameters in terms of signals induced on the appropriate antennas. The quantities involved are directly measurable. The intensities and phase shifts can be found by standard techniques, and the products  $XY$ , etc., are proportionat to the amplitudes of the cross-correlation functions of the signals in the oppositely-polarized antennas. To show this, let  $x(t)$  and  $u_x(t)$  be the voltages for the polarized and unpolarized parts, respectively, in the  $x$  antenna, and similarly for the  $y$  antenna. Then

<sup>22</sup> H. G. Booker, V. H. Rumsey, G. A. Deschamps, M. L. Kales, and J. I. Bohnert, "Techniques for handling elliptically polarized waves with special reference to antennas," Proc. IRE, vol. 39, pp. 533-552; May, 1951.

$$\rho(\tau) = \frac{[x(t) + u_x(t)][y(t + \tau) + u_y(t + \tau)]}{\{[x(t) + u_x(t)]^2[y(t) + u_y(t)]^2\}^{1/2}} \quad (29)$$

$$= \frac{x(t)v(t + \tau)}{(I_x I_y)^{1/2}}. \quad (30)$$

If the bandwidths are narrow,  $x$  and  $y$  are close to sine waves with phase difference  $\gamma_y$ , and so

$$\rho(\tau) = \frac{XY}{(I_x I_y)^{1/2}} \cos(\omega\tau + \gamma_y). \quad (31)$$

Sometimes polarization observations which are incomplete are made. This means that all four parameters are not determined, but if the wave has a known axial ratio the polarization percentage is fixed. Solar bursts have been observed in this fashion by a number of stations.<sup>4</sup> Right and left circular components are observed, and the quantity  $m_1$  is reported:

$$m_1 = (I_l - I_r)/(I_l + I_r) = V/I. \quad (32)$$

When the polarized part of the wave is circular (by far the most common case)  $Q = U = 0$  and  $m = m_1$  by (6). In the general case, from (2)-(6),

$$m_1 = m \sin 2\beta. \quad (33)$$

When the polarization is not known *a priori*, all one can say is that  $m_1 \leq m$ .

When the wave is circularly polarized, it is also possible to determine  $m$  by measuring the correlation product  $XY$  and the total intensity  $I$ . Let

$$m_2 = 2XY/I = (U^2 + V^2)^{1/2}/I. \quad (34)$$

When the polarized part of the wave is circular  $Q = 0$  and  $m = m_2$ , but in general,

$$m_2 = m(1 - \cos^2 2\beta \cos^2 2\chi)^{1/2}. \quad (35)$$

Again,  $m_2 \leq m$ .

Linear polarization has been sought in the radiation from radio stars, and determinations of a parameter  $m_3$  have been made. When the  $x$  and  $y$  intensities are measured the following quantity is computed,

$$\frac{I_x - I_y}{I_x + I_y} = \frac{Q}{I} = m_3 \cos 2\chi, \quad (36)$$

where

$$m_3 = m \cos 2\beta. \quad (37)$$

When the wave is linearly polarized  $m_3 = m$ , but otherwise  $m_3 < m$ . This particular case by itself is of limited use because  $\chi$  is indeterminate, and  $m_3$  cannot be found from (36). However, if  $I_s$  and  $I_t$  are also measured,

$$\frac{I_t - I_s}{I_t + I_s} = \frac{U}{I} = m_3 \sin 2\chi, \quad (38)$$

and  $m_3$  can be found from (36) and (38).

The quantities  $m_1$  (or  $m_2$ ) and  $m_3$  are sometimes spoken of as the circularly and linearly-polarized fractions. This is misleading because linear and circular polarizations are not "opposite," and a wave cannot uniquely be broken into a combination of linear and circular components.

### III. MEASUREMENT TECHNIQUES

The problem of determining the state of polarization of a completely polarized wave has been thoroughly discussed in the literature.<sup>22,23</sup> If two polarization components are measured the two intensities and the phase difference are required, but it is possible to avoid the phase measurement by measuring the intensities of three components. Thus, if right and left circular antennas are used, the measurement of intensities gives  $I$  and  $r$ ;  $\chi$  is found from the phase difference. If crossed linear antennas are used, all three measurements must be made to find either  $r$  or  $\chi$ , in general. If a linear antenna is used it may be convenient to rotate it, in which case the intensities can be measured at three orientations and used to deduce the three polarization parameters. This method, however, does not specify the sense of rotation. If a continuous record is made as the antenna is rotated, one gets the polarization "dumbbell" pattern, from which  $|r|$  and  $\chi$  are immediately found.

In the present case the wave is not completely polarized. A fourth parameter,  $m$ , is introduced, and therefore a fourth independent measurement must be made. If only two polarization components are measured, the extra quantity to be determined, in addition to two intensities and a phase difference, is the amplitude of the cross-correlation function. If three components are used, either phase or correlation may be measured in addition to the three intensities. If four independent components are used, the four intensities are sufficient, and neither phase nor correlation coefficient need be measured.

It is apparent that there is a great variety of ways for measuring polarization. In this section a number of schemes for making the complete polarization determination will be discussed. They are classified into three groups according to the number of polarization components measured. Reference will be made to methods which have been successfully used and reported in the literature; an attempt will be made to show the relations among them, and what they measure in terms of the Stokes parameters. Only the general principles of operation will be considered. For details of construction, circuits, calibration, etc., reference must be made to the original papers.

The nature of the source being studied introduces special requirements into the operation of a polarimeter for radio astronomy use. Solar bursts often are very short; there is not time to mechanically rotate an an-

<sup>23</sup> J. D. Kraus, "Antennas," McGraw-Hill Book Co., Inc., New York, N. Y., pp. 464-485; 1950.

tenna. This, though, is not serious since electronic switching or sweeping can accomplish the equivalent of antenna rotation if desired. A different complication comes about when radio stars are studied since they shine against a diffuse background and it is desirable to employ interference techniques, at least at the lower frequencies. This requires the use of antenna pairs rather than single antennas, but as far as the polarization is concerned the same quantities are measured.

A. Two Components

If two fixed antennas are used as a polarimeter, the measured quantities can be the two intensities, the phase difference, and the amplitude of the correlation function. The instrument at the Cornell Radio Observatory is of this type. This instrument is discussed in detail in a separate article.<sup>24</sup> The general operation is considered here. The simplified block diagram (Fig. 2) illustrates the operation. The antennas are oppositely polarized; suppose they are  $x$  and  $y$ -oriented dipoles.

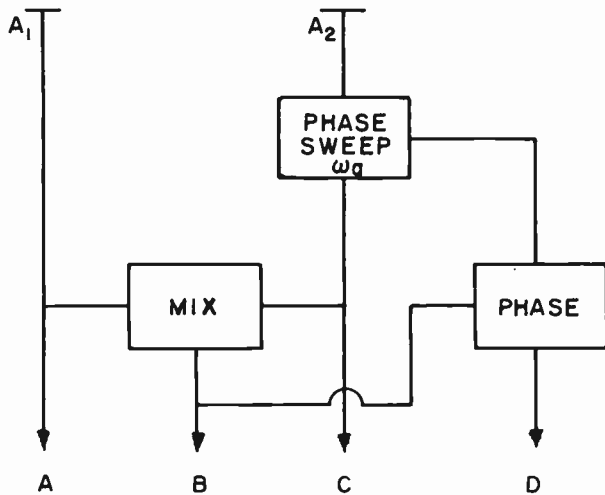


Fig. 2—Polarimeter which measures two components of polarization.

With square-law detectors the outputs at  $A$  and  $C$  are  $I_x$  and  $I_y$ , and the Stokes parameters  $I$  and  $Q$  are the sum and difference of them. The phase of the signal from  $A_2$  is continuously swept at an audio rate,  $\omega_a$ . If the downcoming wave is unpolarized, the signals in the two channels are independent, and the mixer does not have an output component at the audio sweep frequency. If the downcoming signal is partly polarized, the signals in the two channels are partly correlated, and the mixer does have an output component at the sweep frequency. Its amplitude can be shown to be proportional to the product of the polarized components,  $XY$ , as follows.<sup>25</sup> In a narrow band the  $x$  signal can be broken into two parts, polarized and unpolarized:

$$E_x = X \cos [\omega t + \phi(t)] + E_{ux} \cos [\omega t + \psi_x(t)]. \quad (39)$$

The angles  $\phi$  and  $\psi_x$  are independent random functions of time. At the mixer the  $y$  signal is

$$E_y = Y \cos [(\omega + \omega_a)t + \phi(t) + \gamma_y] + E_{uy} \cos [(\omega + \omega_a)t + \psi_y(t)]. \quad (40)$$

When these are multiplied the only term at the audio frequency is  $\frac{1}{2}XY \cos(\omega_a t + \gamma_y)$ . Some of the other terms may have spectra covering the audio band, but their amplitudes will be small, and proportional to the ratio of the audio to IF bandwidths. With a narrow-band filter and a linear detector, then, output  $B$  (Fig. 2) is approximately  $XY$ . The phase angle of the audio signal at  $B$  is  $\gamma_y$ ; it is measured by comparison with a reference voltage derived from the phase sweep and recorded at output  $D$ . The Stokes parameters  $U$  and  $V$  can now be found from (21) and (22), and  $m$ ,  $r$ , and  $\chi$  from (6), (7), and (8). In terms of the outputs  $A$ ,  $B$ ,  $C$ ,  $D$  (meaning, respectively,  $I_x$ ,  $XY$ ,  $I_y$ ,  $\gamma_y$ ) the desired parameters are

$$I = A + C, \quad (41)$$

$$m = [(A - C)^2 + 4B^2]^{1/2} / (A + C), \quad (42)$$

$$\sin 2\beta = (2B \sin D) / [(A - C)^2 + 4B^2]^{1/2}, \quad (43)$$

$$\tan^2 2\chi = (2B \cos D) / (A - C). \quad (44)$$

Note that  $m$  can be found from  $A$ ,  $B$ , and  $C$ ; but the phase measurement  $D$  must be made before  $r$  or  $\chi$  can be found.

Other methods for measuring phase and correlation could be used. This is true here as well as in the systems shown later. For example, the quantities  $(XY \cos \gamma_y)$  and  $(XY \sin \gamma_y)$  could be generated directly by adding phase sensitive detectors to Fig. 2. It would also be possible to obtain these quantities without the phase sweep. Fig. 2, however, represents a method which has been used several times in both interference and telescope instruments, and so it will be used for discussion.

If opposite circular antennas are used in Fig. 2, the four outputs  $A$ ,  $B$ ,  $C$ ,  $D$  are, respectively,  $I_r$ ,  $RL$ ,  $I_l$ , and  $\gamma_r$ . The Stokes parameters can then be found from (17) and (26) to (28), and the polarization parameters, from (6) to (8), are

$$I = A + C, \quad (45)$$

$$m = [(C - A)^2 + 4B^2]^{1/2} / (A + C), \quad (46)$$

$$\sin 2\beta = (C - A) / [(C - A)^2 + 4B^2]^{1/2}, \quad (47)$$

$$\chi = \frac{1}{2}D. \quad (48)$$

With circular antennas the measurements break into two independent sets:  $A$ ,  $B$ , and  $C$  determine  $I$ ,  $m$ , and  $r$ , and  $D$  determines  $\chi$ .

The Cornell instrument has provision for using either crossed linear or opposite circular antennas. The circular antennas have been used, however, because as shown above, the phase measurement is not needed unless the

<sup>24</sup> M. H. Cohen, "The Cornell radio polarimeter," this issue, p. 183.

<sup>25</sup> Pawsey and Bracewell, *op. cit.*, p. 60.

orientation data is desired. The Faraday effect in the earth's ionosphere changes  $\chi$  a great deal at meter wavelengths (see Section V), so that orientation data at these wavelengths is hard to interpret. At the present state of knowledge,  $\chi$  can be projected back through the ionosphere only very imprecisely.

An interference scheme which in essence would be identical to the above is shown schematically in Fig. 3. Connections (a) and (b) of Fig. 3 represent standard phase sweeping interferometers with "parallel" antennas. The phase sweeping in effect speeds up the standard pattern, and the audio component out of the mixer is the desired signal for the point source. From the point of view of determining polarizations, the phase sweeping is not important since the earth's rotation will do the same job, only more slowly.

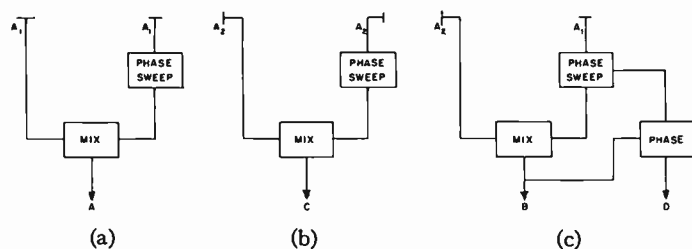


Fig. 3—Interference polarimeter.

The outputs  $A$ ,  $B$ ,  $C$ , and  $D$  record the same quantities as in Fig. 2. With regard to  $B$ , we may say that an unpolarized wave produces no interferometer pattern with crossed antennas, but a partly-polarized wave does. Its amplitude is proportional to the product of the  $x$  and  $y$  components of the polarized part. As pointed out earlier, the antennas can be any oppositely-polarized pair. The use of circularly-polarized antennas would again break the measurements into two independent sets, with  $D$  used only to find  $\chi$ .

The interference technique used by Little and Payne-Scott<sup>26</sup> is very close to the above scheme. It is simpler because only two antenna connections, Fig. 3(a) and 3(c) are used, but presumably it is less sensitive because the fourth output is the dc level at the mixer of Fig. 3(c). This is just the average value of the combined signals from the two antennas after one of them has been swept in phase. But since it is the average value it is not a result of the interferometer pattern, and so does not have the advantage of discrimination against a diffuse background. Little and Payne-Scott, however, were studying solar bursts, and this disadvantage probably is not important in this case.

Historically, an instrument like this was built first by Ryle and Vonberg.<sup>27</sup> It did not have a phase sweep,

<sup>26</sup> A. G. Little and R. Payne-Scott, "The position and movement on the solar disk of sources of radiation at a frequency of 97 mcs. I. Equipment," *Aust. J. Sci. Res.*, vol. A 4, pp. 489-507; December, 1951.

<sup>27</sup> M. Ryle and D. D. Vonberg, "An investigation of radio-frequency radiation from the sun," *Proc. Roy. Soc.*, vol. A 193, pp. 98-120; April, 1948.

but rather let the earth's rotation produce the pattern. It was mainly used to detect the presence of circular polarization in solar radiation. The version by Little and Payne-Scott did have a phase sweep and was also used to study solar bursts. An interference instrument similar to that used by Ryle and Vonberg was used by Ryle and Smith<sup>20</sup> in a search for polarized radiation from radio stars. The Cornell instrument<sup>24</sup> followed the work of Little and Payne-Scott. It was designed for solar studies also.

A microwave polarimeter recently built by Akabane<sup>28</sup> operates on two linear components but is somewhat different from the instruments discussed here. The modulation scheme is different from that shown in Fig. 2, and the quantities  $(XY \cos \gamma_v)$  and  $(XY \sin \gamma_v)$  are generated by synchronous detectors. The  $x$  and  $y$  intensities are not recorded, but rather the quantities  $(I + \frac{1}{2}Q)$  and  $Q$ , which are also generated by the modulation process and isolated with synchronous detectors.

### B. Three Components

A polarization determination with three antennas can be made as in Fig. 4. Five outputs are shown, but they are redundant. Either  $B$  or  $D$  can be not used. Antennas  $A_1$  and  $A_2$  are oppositely polarized, and  $A_3$  can be any different one. A convenient set is  $(xyt)$  oriented linear antennas (Fig. 1), but this cannot be one antenna which rotates since  $A_1$  and  $A_2$  must be used simultaneously to measure outputs  $B$  and  $D$ . If three linear antennas are used and the phase is not measured, the sense of rotation will not be determined.

An interference version of the scheme in Fig. 4 was used by Hanbury-Brown, Palmer, and Thompson<sup>19</sup> in an attempt to measure the polarization of the signals from the three strongest radio sources at 158 mc. Their system was as shown in Fig. 5. The outputs  $A$ ,  $B$ ,  $C$ ,  $E$  are the same as in Fig. 4, and the quantities they measure are shown on the diagram. The intensity along the  $s$  axis (Fig. 1) was also measured, although this is not shown in Fig. 5. This was redundant but presumably was useful as a check.

### C. Four Components

The intensities measured by four antennas are sufficient to specify the four polarization parameters. But the measurements must be independent; right and left circular and  $x$  and  $y$ -linear antennas will not do, whereas right and left circular and  $x$  and  $t$ -linear antennas will. In the former case the measurements are not independent by (11) and (17). Many combinations, of course, are possible.

Suzuki and Tsuchiya<sup>7</sup> have built a polarimeter of this type at the Tokyo Observatory. Their antennas are crossed dipoles, and by appropriate connections they get the two circular components, and four linear com-

<sup>28</sup> K. Akabane, "A polarimeter in the microwave region," this issue, p. 194.

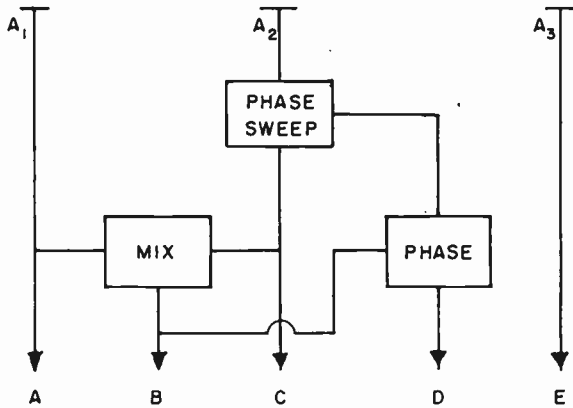


Fig. 4—Polarimeter which measures three components of polarization.

ponents:  $x, y, s, t$ . The information is redundant but presumably this is useful as a check. The intensity  $I$  can be found from (11), (14), and (17), and the other Stokes parameters can be found from (20), (24), and (28).

This instrument was designed for solar work. Since short-duration bursts are of interest, rapid switching techniques are used to sample the different antenna connections. Even so, the measurements are made at different times, and errors might be introduced if the burst is changing very rapidly.

This point could be overcome by using a series of networks to split the two dipole signals into isolated parts and then making all the combinations all the time, or by using four separate antennas. The former method has the disadvantage that the noise figure would effectively be raised since each network would reduce the signal by 3 db. The latter method has the obvious disadvantage of requiring twice as many antennas. Both methods have the further disadvantage that four separate receiver channels would be needed.

The two-component systems discussed in Section III-A above avoid this point because only two intensities are measured. Since they must be measured at the same time, two receiver channels are needed. They should have similar phase characteristics as well as similar gain and bandwidth characteristics. The absolute values of noise figure, gain, and phase shift do not have to be the same for the two channels, but they should be stable between calibration periods.

IV. FARADAY ROTATION AND DISPERSION

In a homogeneous magnetized ionized medium, a polarized electromagnetic wave is propagated in two independent modes which have different phase velocities. When the frequency is sufficiently high, the two modes are circularly polarized with opposite senses of rotation (except for the case where the magnetic field is almost exactly transverse). The axial ratio and sense of rotation of the resultant total wave do not change, but the plane of polarization does. The Faraday rotation of the plane of polarization,  $\phi$ , is given by

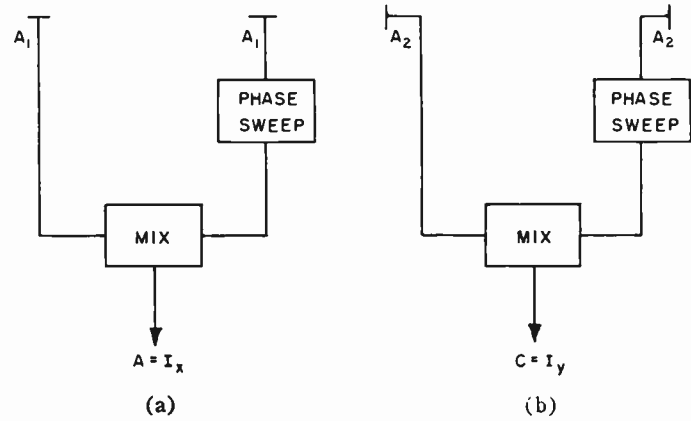


Fig. 5—Interference polarimeter.

$$\phi = (2.36 \times 10^{-3})f^{-2} \int_0^z nB_z dz, \tag{49}$$

where

- $\phi$  = radians,
- $f$  = megacycles,
- $n$  = number of electrons/cc,
- $B_z$  = longitudinal component of magnetic field (Gauss),
- $z$  = kilometers.

This result is used by Evans,<sup>10</sup> for example, in explaining the fading of moon echoes by a variable Faraday rotation in the ionosphere.

When the frequency is not high enough, there is a change in the shape of the ellipse in addition to the Faraday rotation. This general case has been discussed by Hatanaka.<sup>9</sup>

Since  $\phi$  is a function of frequency in (49), an elliptically-polarized noise signal containing a spectrum of frequencies is dispersed into a continuum of ellipses with a spread of orientations. This is depicted in Fig. 6. The angular dispersion rate is, from (49)

$$\frac{d\phi}{df} = -2 \frac{\phi}{f} \text{ radians/cycle.} \tag{50}$$

If  $\Delta f/f = (f_2 - f_1)/f \ll 1$ , then

$$\frac{\theta}{\phi} \approx 2 \frac{\Delta f}{f}, \tag{51}$$

where  $\theta$  is the dispersion angle corresponding to the frequency band limited by  $f_1$  and  $f_2$ .

The above formulas can be applied in the corona, but if the lower frequencies originate higher in the corona and have less medium to traverse, the frequency dependence may not be as great as suggested by (49) and (51). If a wide spectrum of frequencies originates at one place in the corona, high above the plasma level for the lowest frequency, then these equations will be correct. On the other hand, if each frequency originates at a sharp plasma level the frequency dependence will be slower than  $f^{-2}$  and the dispersion less than the value given in (51). This latter picture is probably artificial since the corona must be somewhat irregular, and any volume must generate a spectrum of frequencies, all of which come from the same level.

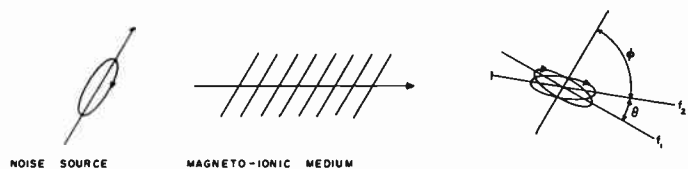


Fig. 6—Dispersion from Faraday effect.

Let us ignore this question of frequency dependence and consider what happens when a polarimeter operates on a dispersed elliptically-polarized wave. Let the dispersion be as in Fig. 6. Assume that  $f_1$  and  $f_2$  are the edges of the receiver pass band and that the spectrum is uniform between these limits. Then orientations spread over an angle  $\theta$  are received and interpreted as a partially-polarized signal. The resultant state of polarizations was first calculated by Hatanaka<sup>9</sup> for the case where the source is all polarized. His procedure was to integrate the Stokes parameters over the bandwidth. The results are

$$m = \left[ \frac{\sin^2 \theta}{\theta^2} + \sin^2 2\beta_0 \left( 1 - \frac{\sin^2 \theta}{\theta^2} \right) \right]^{1/2}, \quad (52)$$

$$\sin 2\beta = \left[ \frac{\sin^2 \theta}{\theta^2} \cot^2 2\beta_0 + 1 \right]^{-1/2}, \quad (53)$$

where  $\tan^{-1} \beta_0$  is the axial ratio of the wave at the source.

Astronomical sources cannot be expected to be fully polarized, in general. For example, when the source consists of synchrotron radiation from electrons in a magnetic field, it must be considered to have an appreciable depth, and the radio radiation from the bottom layer of electrons will suffer a Faraday rotation in its passage through the source itself. Even if the magnetic field is homogeneous, all the different levels will produce different planes of polarization at the top of the source, so it will be only partially polarized. This has nothing to do with the bandwidth; it is strictly a property of the source. Eq. (52) thus gives the percentage of polariza-

tion at a distant point only for that part of the flux which is subject to dispersion, *i.e.*, the part which is polarized at the source. The net percentage of polarization is found by multiplying (52) by  $m_0$ , the fraction of the flux which is originally polarized.

$$m = m_0 \left[ \frac{\sin^2 \theta}{\theta^2} + \sin^2 2\beta_0 \left( 1 - \frac{\sin^2 \theta}{\theta^2} \right) \right]^{1/2}. \quad (54)$$

The final axial ratio cannot be affected by the initial percentage of polarization, so (53) is unchanged in the general case. (54) can also be derived by direct recourse to the Stokes parameters in the way that (52) is derived.

These relations are shown graphically in Fig. 7. The abscissa and ordinate are  $r$  and  $m/m_0$ ; in the radio astronomy case  $r$  and  $\bar{m}$  are measured quantities. The curves are the families  $r_0 = \text{constant}$  and  $\theta = \text{constant}$ .

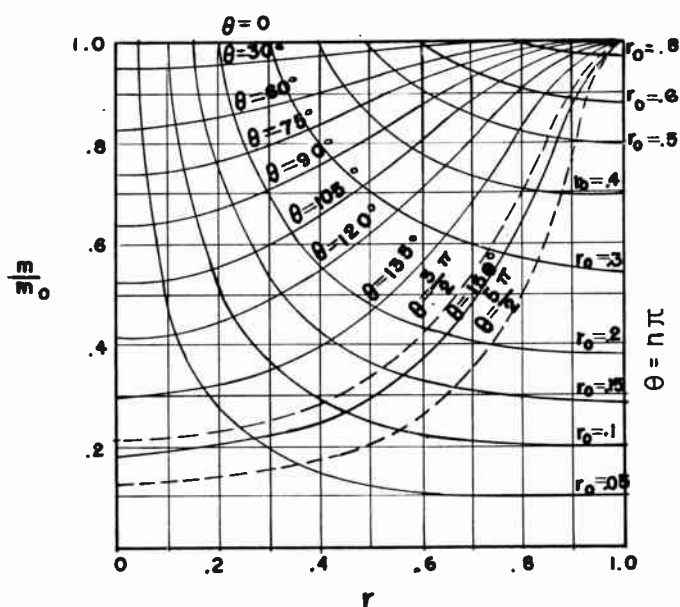


Fig. 7—Polarization parameters as functions of Faraday dispersion angle and initial polarization parameters.

The wave initially is represented by some point on the top line,  $\theta = 0$ . As the wave transverses the medium (or as the bandwidth is increased from zero) the point moves down the line  $r_0 = \text{constant}$ , until at  $\theta = \pi$  it reaches the right-hand boundary. At this point the polarized part, which is now circular, is smallest. As  $\theta$  further increases, the point comes back up the  $r_0 = \text{constant}$  line until it reaches the approximate limit  $\theta = 3\pi/2$ , the dashed line. Then it subsides until at  $\theta = 2\pi$  it is again at the right-hand side.

Fig. 7 also can be used to find the polarization of the source in simple cases like the above example, synchrotron radiation in a homogeneous magnetic field. At the outer boundary of the source the orientations are spread uniformly through the angle  $\phi_s$ , the rotation angle for the depth of the source. If  $m_0$  is taken as unity and  $\phi_s$  used for  $\theta$ , Fig. 7 will give the net polarization of the source. In the case of synchrotron radiation  $r_0 = 0$ .

At this point we outline the various assumptions and approximations which have been used. They pertain to the source, to the medium, and to the equipment. They must all be valid if the above formulas are to hold and if the succeeding material is to be valid.

- 1) Slowly-varying medium (homogeneous theory applies).
- 2) Circular magneto-ionic modes (high frequency and quasi-longitudinal propagation).
- 3) No selective absorption or other mechanism that would change the polarization.
- 4) Uniform spectrum.
- 5) Rectangular band-pass.
- 6) Narrow band.

The foregoing has shown that the Faraday dispersion may be significant whenever the product of rotation and relative receiver bandwidth is on the order of  $\frac{1}{2}$  or greater, for then  $\theta \geq 1$  by (51). The polarization parameters, in this case, are not an intrinsic property of the wave but rather depend upon the receiver frequency and bandwidth. Both these characteristics of the receiver should be given if proper interpretation is to be given to the measured values.

The quantities  $m_0$ ,  $r_0$ , and  $\chi_0$  are important because they specify the source. They are not the measured values  $m$ ,  $r$ , and  $\chi$  whenever the Faraday effect is important, but limits can be set on  $m_0$  and  $r_0$  from measurements of  $m$  and  $r$ . Limits can also be set on  $\theta$ . This quantity is important because it contains information on the medium between the source and the observer—the integrated product of magnetic field and electron density.

In any case where  $m$  and  $r$  are measured, one can find from Fig. 7 an upper limit to  $\theta$  and both upper and lower limits to  $r_0$ . The upper limit to  $\theta$  and lower limit to  $r_0$  are attained when  $m_0 = 1$ , whereas the upper limit to  $r_0$  is attained for  $\theta = 0$ . Furthermore, the initial value of polarization,  $m_0$ , is restricted because  $m_0 \geq m$ . As an example, when  $r = 0.4$  and  $m = 0.6$ ,  $m_0 \geq 0.6$ ,  $\theta \leq 112^\circ$ , and  $0.22 \leq r_0 \leq 0.4$ .

In the upper right corner of Fig. 7 where the  $\theta = \text{constant}$  lines converge, an accurate determination of the limit to  $\theta$  is critically dependent upon the measurement accuracy. For example, if a measured point is  $m = 0.98 \pm 2$  per cent,  $r = 0.75 \pm 5$  per cent, then the upper limit to  $\theta$  is somewhere between 0 and  $70^\circ$ . Much of the data reported by Hatanaka *et al.*<sup>8</sup> and by Cohen<sup>24</sup> on polarized bursts from the sun does fall in this region.

The determination of the limits from Fig. 7 uses only two of the four parameters that characterize the burst,  $m$  and  $r$ . The other two, the total intensity and orientation, are of no help for this. There is some difficulty in using orientation data directly. If the orientation of the original source is known (as it is in moon-echo experiments), then the total Faraday rotation can be found to within a half-integral number of revolutions. Astronom-

ical sources, however, generally do not have a known orientation. In fact, part of the problem in interpreting polarization data is to find the orientation of the source. However, the Faraday rotation in the earth's ionosphere alone is many radians at meter wavelengths, and this must be accurately known before orientation data can be extended outside the ionosphere.

The above discussion has been for a measurement at one center frequency with a specific bandwidth. If the parameters of the wave are measured at two frequencies, or with two bandwidths, far more information can be obtained. If orientation angles are measured at two frequencies, a dispersion can be directly calculated. This, though, must be interpreted cautiously. Solar bursts at different frequencies are thought to come from different levels in the corona; even if the two sources are parallel, the media between the source and observer are different for the two cases. An exception occurs when the two bursts are harmonically related and come from the same source. In this case, though, the rotation for the lower frequency is four times that for the higher frequency, and it would be difficult to fix the difference in orientations to within  $n\pi$ . The ionospheric rotation is variable, and this by itself would be enough to confuse the result unless high frequencies are used.

The above objections may not be valid if the two frequencies are so close that the bands are adjacent. The same information can then be obtained as from measurements made at one center frequency and two bandwidths, over the same total frequency range. The two experiments are different because they require different measurements. In the two-frequency experiment the dispersion information comes from the difference in orientation angles. Once  $\theta$  is found,  $\phi$  can be estimated from (51). If  $m$  and  $r$  are also measured,  $m_0$  and  $r_0$  can be found from Fig. 7. In the two-bandwidth experiment the orientations are the same and are not required for the analysis; what is needed are the values of  $m$  and  $r$ . Measurements of  $r$  at two bandwidths will fix  $r_0$  and  $\theta$  to within trigonometric ambiguities. If  $m$  also is measured at the two bandwidths, one can find the polarization percentage at the source.<sup>29</sup> This also gives a check which would be useful in resolving the ambiguities in  $r_0$  and  $\theta$ . The total rotation  $\phi$  can also be estimated as with the two-frequency experiment.

## V. DISCUSSION

### A. Ionosphere

The earth's ionosphere is a magneto-ionic medium. Measurements by Evans<sup>10</sup> have shown that the Faraday rotation in it is variable and greater than 10 radians in the daytime at 120 mc. At the lowest radio astronomy frequencies, around 20 mc, the rotation would be

<sup>29</sup> M. H. Cohen, "Interpretation of Radio Polarization Data in Terms of Faraday Rotation," Cornell Univ. School of Elec. Eng., Ithaca, N. Y., Res. Rep. EE 295; May, 1956.

greater than 360 radians. If the dispersion is to be insignificant ( $\theta \leq 1$ ) the relative bandwidth must be on the order of 0.0014 or less; so the bandwidth must be about 28 kc or smaller at 20 mc. This restriction is not serious since narrow bandwidths are customarily used at the low frequencies.

Even though the dispersion may be small, the rotation is not, at frequencies up to at least 500 mc. A correction for this effect has to be made whenever orientation angle data are extrapolated back through the ionosphere. The rotation is variable, and at the lower frequencies, where it is very large, the extrapolation will require a knowledge of the ionosphere at the time of observing the radio source.

### B. Corona

The solar corona is ionized and presumably contains some magnetic field. A Faraday rotation might therefore be expected for rays propagating through the corona. Hatanaka<sup>9</sup> has made estimates of the magnitude of the rotation. A model using the Allen-Baumbach formula for electron density and a general dipole magnetic field with a strength of 1 Gauss at the pole gives, at 200 mc,  $\phi$  from  $10^3$  to  $10^6$  radians for sources from 2 to 0.1 solar radii above the photosphere. The magnetic field is artificially smooth, but it may give the right order of magnitude for the rotation. Even if an irregular field is assumed, the rotation will be very large. A 30,000-km "blob" at  $h=0.2$  radius with a homogeneous longitudinal magnetic field of 0.2 Gauss and the above electron density gives a rotation of  $2 \times 10^4$  radians at 200 mc all by itself. If the magnetic field is stronger,  $\phi$  is proportionately greater, although if it is strong enough, several of the approximations listed above may be invalidated. The Faraday effect will still be present, but the results are not so simple, since the modes will not be circles. If the medium is highly turbulent, the homogeneous theory may not apply. In this case the two modes are coupled, and there will be no Faraday effect at all. However, estimates of the maximum gradients for uncoupled modes, based on Budden's theory,<sup>30</sup> give very large values: 0.04 Gauss/km for 300 mc at a height of one radius.<sup>29</sup> The gradients are probably smaller than this, so the magneto-ionic modes are uncoupled, and the Faraday effect can take place. Also, as noted in the previous section, the assumption of uncoupled modes is introduced often in explaining the circularly-polarized bursts by the independent propagation qualities of the two magneto-ionic modes.

Rotations of  $10^3$  to  $10^6$  radians might give large dispersions with the customary bandwidths for solar instruments. The resulting signals, then, would be some combination of circular plus random. These, in fact, are the most commonly observed polarizations for solar

bursts. However, these are also the polarizations that would commonly result from a source distributed in depth, as described above.

The polarimeter built by Suzuki and Tsuchiya<sup>7</sup> has a 100-kc bandwidth at 200 mc, and the instrument built by Cohen<sup>24</sup> has a 10-kc band at 200 mc. If the rotation of a 200-mc burst is  $10^6$  radians, the dispersions would be 100 and 10 radians respectively, according to (51), and the wave would be depolarized—to circular plus random—for both instruments. If the dispersions were 10 and one radians respectively, there would be substantial differences in the observations of partially elliptically-polarized waves with the two instruments. If the dispersions are much more or much less than 10 and one radians, the differences will be small.

The reported observations do show that the above values of dispersion are sometimes much too large. Payne-Scott and Little<sup>2,3</sup> saw several examples of linearly-polarized signals. Numerical values of  $m$  and  $r$  are not given, but presumably in Fig. 7 the points would have been near the left boundary, and not near the bottom. If their point gave  $\theta < 2$ , the corresponding limit to  $\phi$  would have been  $\phi < 10^3$  radians at 97 mc. Hatanaka *et al.*<sup>8</sup> have reported some observations which, when plotted on Fig. 7, give several points with  $\theta=0$  and a number with  $\theta \approx 90^\circ$ . The points with  $\theta=0$  are completely polarized, elliptical, and imply that  $\phi=0$ , but, as discussed above, small inaccuracies in  $m$  will make large changes in  $\theta$ . The points with  $\theta=90^\circ$  give  $\phi < 1.6 \times 10^3$  radians at 200 mc.

### C. Crab Nebula

Mayer, McCullough, and Sloanaker<sup>17</sup> have measured quantity  $m_3$  (37) for the Crab Nebula at a wavelength of 3.15 cm. The result is that the polarized component, if linear, is about 7 per cent of the total flux. Optical radiation from this object is strongly linearly polarized in patches, with a residual linear polarization of 9.2 per cent.<sup>16</sup>

It seems reasonable, therefore, to assume that the polarized component is linear at 3.15 cm, and that  $m = m_3 = 0.07$ . The reported orientation at 3.15 cm is about  $148^\circ$ , and at optical wavelengths it is  $159.6^\circ$ ; the difference is therefore about  $11^\circ$ .

Oort and Walraven<sup>16</sup> have estimated that at a wavelength of 21 cm the Faraday rotation in the interstellar space between the Crab Nebula and the earth would be 7 radians, and within the nebula itself the Faraday rotation would be 14 radians. At 3.15 cm the corresponding figures would be 0.16 and 0.31 radians respectively. If the  $11^\circ$  orientation difference measured by Mayer *et al.* is taken to result from interstellar rotation, it gives the value of  $\phi = 0.19$  radians; Oort and Walraven's value is close to that value. The orientation difference, of course, may be regarded as  $(0.19 \pm n\pi)$  radians, but even  $n=1$  gives a rotation much greater than the theoretically estimated one.

<sup>30</sup> K. G. Budden, "The theory of the limiting polarization of radio waves reflected from the ionosphere," *Proc. Roy. Soc.*, vol. A 215, pp. 215-233; November, 1952.

The amount of polarization measured at 3.15 cm is less than that at optical wavelengths by the factor  $(0.07/0.092) = 0.76$ . Let this be called the polarization factor.

If the depolarization is taken to result from the interstellar rotation, the required rotation can be deduced. The 3.15-cm equipment received two bands, each 5.5 mc wide, separated by 60 mc, and with a center frequency of 9530 mc. In Appendix II it is shown that two independent linearly-polarized waves with equal intensities and orientations  $\theta$  apart combine to give a polarization percentage  $m = \cos \theta$ . If  $m = 0.76$ ,  $\theta = 40^\circ$ ; by (51) the required rotation is 55 radians. This value is unreasonably large, and the depolarization probably does not result from the interstellar rotation.

If the polarization factor is taken to result from rotation within the nebula, the internal rotation is about  $72^\circ$ , from Fig. 7. That amount is four times Oort and Walraven's estimate of 0.31 radian. Oort and Walraven also pointed out that there would be extra radio depolarization because the less polarized outer parts of the nebula would contribute relatively larger amounts to the radio energy. This may be the source of most of the depolarization at 3.15 cm.

Several attempts at lower frequencies to measure the polarization in the Crab Nebula radiation were unsuccessful. At 22 cm Westerhout<sup>18</sup> determined that  $m_3 \leq 0.01$  for two bands, each 2 mc wide and separated by 68 mc. If we take the 3.15-cm interstellar rotation to be  $11^\circ$ , at 22 cm it will be 9.4 radians, and the dispersion in 68 mc will be  $52^\circ$ . The polarization factor is  $\cos 52^\circ = 0.61$ ; this would reduce the polarization from 9.2 per cent to 5.6 per cent. This effect would be eliminated by using only one band. The internal rotation within the nebula is much more important; if it is about 14 radians, at 22 mc, the polarization factor,  $m/m_0$  in (54), will be a maximum of about 0.07. This would reduce the polarization from 5.6 per cent to 0.4 per cent. The polarization might further be reduced because, as at 3 cm, the effective radiating region of the nebula may be greater than the optical region.

Hanbury-Brown, Palmer, and Thompson<sup>19</sup> made measurements of the Crab Nebula at 158 mc with a bandwidth of 400 kc. They set limits for both circular and linear polarization:  $m_2 \leq 0.04$  and  $m_3 \leq 0.025$ . This permits the computation of a limit for arbitrary polarization, for by (35) and (37)  $m \leq (m_2^2 + m_3^2)^{1/2}$ , so the measured value is  $m \leq 0.047$ .

The above estimates for rotation in the galaxy and in the interstellar medium give values smaller than these limits. If the interstellar rotation is  $11^\circ$  at 3.15 cm, it will be 700 radians at 158 mc; the dispersion in a 400-kc band is 3.5 radians. The polarization factor from Fig. 7 will be no more than 0.2, and the polarization would be reduced to about 2 per cent. If the reduction in polarization from interstellar rotation is to be insignificant ( $\theta \leq 1$ ), the bandwidth should be no more than 110 kc. The internal rotation in the nebula, however, would be

1100 radians at 158 mc, according to Oort and Walraven's estimate. This would reduce the polarization by a factor of  $10^3$ , and the source would be essentially unpolarized at 158 mc.

APPENDIX I

We consider the elliptically-polarized part of the wave to be generated by two oppositely rotating coherent circular components. See Fig. 8. The connection between the circular and linear components is essentially that used by Rumsey.<sup>22</sup> For each frequency component (18) and (19) hold, and by combining them, we have

$$\begin{aligned} \hat{R}e^{j\omega t} + (\hat{L}e^{j\omega t})^* &= \sqrt{2}\{X \cos \omega t + jY \cos(\omega t + \gamma_r)\} \\ &= E_x + jE_y. \end{aligned} \tag{55}$$

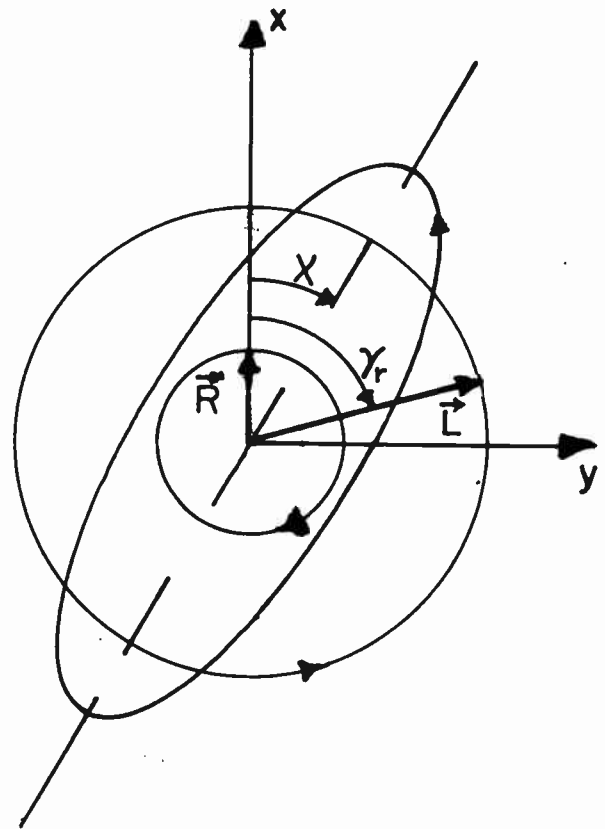


Fig. 8—Elliptical polarization.

The quantities  $(\hat{R}e^{j\omega t})$  and  $(\hat{L}e^{j\omega t})^*$  are interpreted as the right and left circular components with the real parts representing the  $x$  components and imaginary parts the  $y$  components of electric field. At the time instant shown in Fig. 8 the electric vector of the right-hand component,  $\vec{R}$ , is parallel to the  $x$  axis and so  $(\hat{R}e^{j\omega t})$  is real. At that instant  $(\hat{L}e^{j\omega t})^*$  is therefore  $(Le^{j\gamma_r})$ , where  $\gamma_r$  is the phase angle by which  $\hat{R}$  leads  $\hat{L}$ . The angular separation between the vectors is  $\gamma_r$ , and since they rotate in opposite directions,

$$\gamma_r = 2\chi. \tag{56}$$

The axial ratio, by definition, is the ratio of minor to major axes. From Fig. 8,

$$r = (L - R)/(L + R). \quad (57)$$

The quantities  $\cos 2\beta$  and  $\sin 2\beta$  are needed for the Stokes parameters:

$$\cos 2\beta = \frac{1 - r^2}{1 + r^2} = \frac{2RL}{I_e}, \quad (58)$$

$$\sin 2\beta = \frac{2r}{1 + r^2} = \frac{L^2 - R^2}{I_e}. \quad (59)$$

Upon substituting (56), (58), and (59) into (2), (3), and (4), we have

$$Q = 2RL \cos \gamma_r, \quad (26)$$

$$U = 2RL \sin \gamma_r, \quad (27)$$

$$V = L^2 - R^2 = I_l - I_r. \quad (28)$$

## APPENDIX II

Consider the superposition of two independent linearly-polarized waves traveling in the same direction, having equal intensities  $I_0$  with similar spectra, and orientations separated by the angle  $\chi$ . Let wave  $a$  be parallel to the  $xa$  axis and wave  $b$  be at angle  $\chi$  (Fig. 1). Then from (1) to (4),

$$I_a = I_0 \quad I_b = I_0, \quad (60)$$

$$Q_a = I_0 \quad Q_b = I_0 \cos 2\chi, \quad (61)$$

$$U_a = 0 \quad U_b = I_0 \sin 2\chi, \quad (62)$$

$$V_a = 0 \quad V_b = 0. \quad (63)$$

Since the waves are independent, the parameters for the total wave are the sums of the individual parameters; *i.e.*,  $I = (I_a + I_b)$ , etc., and

$$m = (Q^2 + U^2 + V^2)^{1/2}/I = \cos \chi. \quad (64)$$

# The Cornell Radio Polarimeter\*

MARSHALL H. COHEN†, MEMBER, IRE

**Summary**—The Cornell polarimeter operates on 201.5 mc with a bandwidth of about 10 kc. This bandwidth is an order of magnitude smaller than previously used. The instrument is basically similar to the interference polarimeter built by Little and Payne-Scott, although it does not operate on an interference basis. The two circular components and the phase and correlation are measured. Ratios of the measured quantities are used graphically to find the polarization percentage and axial ratio. The system is calibrated on a relative basis by transmitting noise from a distant vertical dipole. The errors introduced by inaccuracies in the antennas are discussed; it is shown that the measured inaccuracies might give errors on the order of  $\pm 0.05$  in axial ratio and polarization fraction.

The observed polarizations are similar to what has been reported by other observers, so qualitatively there is no gross "bandwidth effect." Mixed and variable polarizations have been seen. An example of a mixed polarization record is shown.

## INTRODUCTION

AT Cornell University, a polarimeter which has a center frequency of 201.5 mc and a bandwidth of 10 kc has been built. This instrument is being used to study solar bursts. The bandwidth is an order of magnitude smaller than that used in other in-

struments.<sup>1,2</sup> Thus one of the objectives is to look for evidence of coronal Faraday rotation, as manifested in a "bandwidth effect." Hatanaka<sup>3</sup> has shown how a large rotation would give a polarization dispersion proportional to the bandwidth; thus a narrow-band instrument possibly might see elliptical polarization where a wide-band one would see only circular plus random. This effect is also discussed by Cohen.<sup>4</sup>

The Cornell instrument is basically similar to the interference polarimeter built by Little and Payne-Scott,<sup>1</sup> although it does not operate on an interference basis. The two antennas are at one place. The other major differences are: 1) the antennas are not linear, but rather are circularly polarized; and 2) the intensities of the signals in the two antennas are recorded individually,

<sup>1</sup> A. G. Little and R. Payne-Scott, "The position and movement on the solar disk of sources of radiation at a frequency of 97 mcs, I. Equipment," *Aust. J. Sci. Res.*, vol. A 4, pp. 489-507; 1951.

<sup>2</sup> T. Hatanaka, S. Suzuki, and A. Tsuchiya, "Polarization of solar radio bursts at 200 mc/s. I. A time sharing radio polarimeter," *Publ. Astron. Soc. Japan*, vol. 7, pp. 114-120; 1955.

S. Suzuki and A. Tsuchiya, "A time-sharing polarimeter at 200 mc," this issue, p. 190.

<sup>3</sup> T. Hatanaka, "The Faraday effect in the earth's atmosphere with special reference to polarization measurements of solar radio emission," *Publ. Astron. Soc. Japan*, vol. 8, pp. 73-86; 1956.

<sup>4</sup> M. H. Cohen, "Radio astronomy polarization measurements," this issue, p. 172.

\* Original manuscript received by the IRE, October 14, 1957. Various aspects of this work have been supported by contracts with the Office of Naval Res. and the Rome Air Dev. Center, and by a grant from the Natl. Science Foundation.

† Cornell University, Ithaca, N. Y.

rather than using essentially the signal from one antenna orientation, and the crossed-antenna dc level.

These differences are pointed out by Cohen,<sup>4</sup> where several different classes of polarimeters are discussed. A more detailed discussion of the Cornell instrument follows.

OPERATION

Fig. 1 shows a block diagram of the instrument. There are two main receiver channels which are connected to right and left circular antennas. The two channels receive the same rf bands, but have them translated into IF bands shifted by 1000 cps. The IF signals are mixed (multiplied) and the 1000-cycle component is filtered out. The phase of the 1000-cycle output is measured also, with respect to a reference derived from the local oscillators. The signals are recorded on a six-channel high-speed recorder. Adjustable RC integration circuits and dc amplifiers follow the outputs shown.

The local oscillators differing in frequency by 1000 cps are used to determine the cross-correlation function of the signals in the two channels. If an unpolarized wave is incident on the antennas, the two signals are incoherent and there is no 1000-cycle component out of the mixer. If it is polarized partially, the signals are correlated partly and, as shown by Cohen,<sup>4</sup> the mixer output is proportional to the product of the polarized components in the two antennas. The discussion by Cohen<sup>4</sup> involves a continuous phase shifter in one channel, but the operation with separate local oscillators is identical.<sup>5</sup> The phase of the 1000-cycle component at B is the phase difference between the two circular components of the polarized part of the rf wave. This is just twice the orientation angle of the ellipse.<sup>4</sup>

The four outputs are calibrated to read the total right and left intensities,  $I_r$  and  $I_l$ , the product of the polarized components,  $RL$ , and the phase difference between them,  $\gamma_r$ . These are shown in Fig. 1. In terms of these measurements the Stokes parameters are<sup>4</sup>

$$I = I_l + I_r \tag{1}$$

$$Q = 2RL \cos \gamma_r \tag{2}$$

$$U = 2RL \sin \gamma_r \tag{3}$$

$$V = I_l - I_r. \tag{4}$$

In the data reduction we do not find all these parameters as such, but rather get directly the percentage of polarization,  $m$ ; axial ratio,  $r$ ; and orientation angle,  $\chi$ . These quantities are given by

$$m = I_o/I \tag{5}$$

$$\sin 2\beta = V/I_o \tag{6}$$

$$\tan 2\chi = U/Q, \tag{7}$$

<sup>5</sup> R. H. Brown, H. P. Palmer, and A. R. Thompson, "A rotating-lobe interferometer and its application to radio astronomy," *Phil. Mag.*, vol. 46, pp. 857-866; 1955.

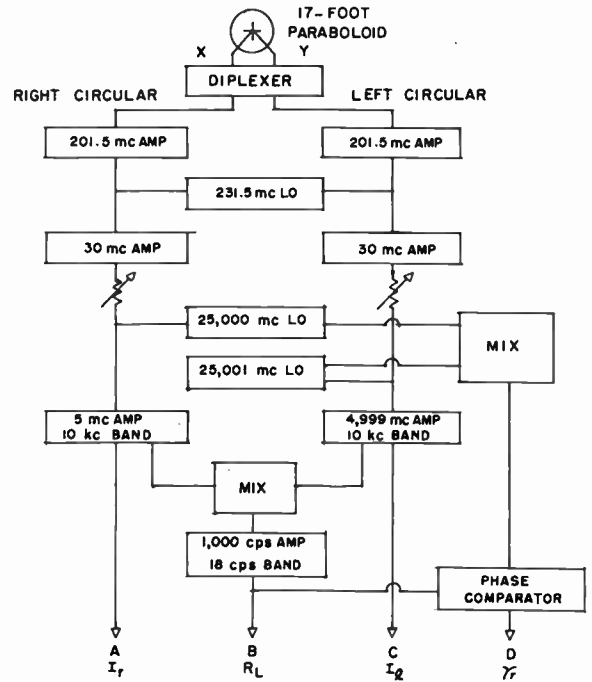


Fig. 1—Block diagram.

where

$$\tan \beta = r \tag{8}$$

and

$$I_o = (Q^2 + U^2 + V^2)^{1/2}.$$

When these equations are combined, we have

$$m = \{(1 - a)^2 + 4b^2\}^{1/2}/(1 + a), \tag{9}$$

$$\tan 2\beta = \frac{2r}{1 - r^2} = \pm \frac{a - 1}{4b}, \tag{10}$$

and

$$\chi = \frac{1}{2}\gamma_r, \tag{11}$$

where

$$\left. \begin{aligned} a &= I_r/I_l \\ b &= RL/I_l \end{aligned} \right\} \text{when } I_l > I_r, \tag{12}$$

$$\left. \begin{aligned} a &= I_l/I_r \\ b &= RL/I_r \end{aligned} \right\} \text{when } I_l < I_r. \tag{13}$$

Eqs. (9) and (10) are plotted in Fig. 2. The abscissa is the ratio of circular components, and the ordinate is the ratio of the correlator output to the larger component. The radial lines are lines of constant axial ratio, and the curved set are lines of constant percentage of polarization. The two quantities  $a$  and  $b$  are ratios of measured values, and  $r$  and  $m$  are read from the graph.

Note that the phase measurement is used only to find the orientation angle. The other parameters,  $I$ ,  $m$ , and  $r$ , are found independently from the other measurements,  $A$ ,  $B$ , and  $C$ , Fig. 1. The orientation angle is often not

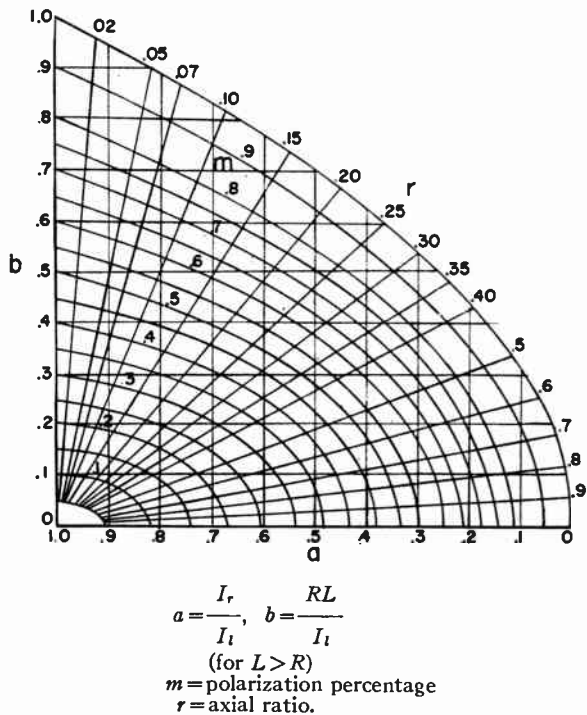


Fig. 2—Axial ratio and polarization percentage vs ratios of circular components.

important because, at meter wavelengths, it is confused by Faraday rotation in the ionosphere.<sup>4</sup> In such cases, then, only three measurements need be made to find the three parameters of interest. This is an advantage of circularly-polarized antennas, for with linear antennas both orientation angle and axial ratio depend on the phase measurement.

The design considerations were that the system should be able to resolve short solar bursts, small as well as large, and that the IF bandwidth should be small. These requirements are somewhat contradictory, since if the bandwidth is small the integration time must be long if small bursts are to be seen.

The receiver output fluctuates because both the signal and the receiver noise have a statistical nature. The relative fluctuations in power are on the order of  $(B\tau)^{-1/2}$ , and with  $B = 10$  kc and  $\tau = 0.1$  sec this gives  $\Delta P/P \sim 3$  per cent. The intensities in the two channels cannot be measured with greater precision, unless the burst is relatively long and smoothed averages can be taken. Longer time constants are also available for slower variations.

Unless the burst is large, its intensity will be smaller than the internal receiver noise plus the background noise. In this case, the measurement inaccuracy is greater than 3 per cent. In terms of antenna temperature, the fluctuations are  $\Delta T_A \sim \{(F-1)T_0 + T_A\} (B\tau)^{-1/2}$ . When looking at the quiet sun at 200 mc with a 17-foot dish  $T_A$  might be on the order of 500° K, with two thirds coming from the sun and one third from the background. If the noise figure is 6, these values give relative fluctuations, in terms of the quiet sun, of

$\Delta T_A/T_{QS} \sim 18$  per cent. Again, when the bursts have a long duration the accuracy is increased by taking an average value. In most cases, however, no attempt is made to analyze bursts which are not greater than the quiet sun.

Also, there are conflicting requirements on the audio amplifier bandwidth. It must be wide enough to allow short bursts to be seen, and it must be narrow to keep the excess noise developed in the mixer from being objectionable. This excess noise is proportional to the ratio of audio to IF bandwidths, thus the problem becomes more severe as narrower IF bands are used. An audio bandwidth of 18 cycles is being used presently.

The two second local oscillators are separately crystal controlled, with the two crystals in one oven. The frequency difference does not have to be fixed, but it must remain within the pass band of the audio amplifier. The oscillators need to be adjusted about once a week.

The phase comparator is patterned after a design by Kretzmer.<sup>6</sup> It reads continuously from 0 to 360°, and is approximately linear. The measured deviations from linearity are less than  $\pm 5^\circ$ . The entire scale is recorded on 40 mm of chart paper. If the accuracy of reading is  $\pm 1$  mm, the inaccuracies in phase are on the order of  $9^\circ$ . This corresponds to orientation inaccuracies of  $\pm 4.5^\circ$ . One of the inputs to the phase comparator is a 1000-cps sine wave; the other is a noise signal in an 18-cps band, centered on 1000 cps, with a superposed 1000-cps spike whenever an elliptically-polarized wave is incident. When the spike is absent, the phase comparator has a rapidly fluctuating output. An example of this can be seen in Fig. 4. When an elliptically-polarized wave of great enough amplitude is present, the phase comparator has a steady output.

#### ANTENNAS

The first part of the antennas consists of crossed dipoles at the focus of a 17-foot paraboloid on an equatorial mounting. The signals go through baluns and impedance matching arrangements to a circularly-polarized diplexer, and then the two circular components go to preamplifiers in a box on the dish. This is shown schematically in Fig. 3.

If the terminals  $R$  and  $L$  are isolated, the antenna polarizations will be "opposite," and if the net phase difference between  $ac$  and  $bd$  is  $90^\circ$  the two polarizations are circular.

The procedure used for setting the  $90^\circ$  phase shift is as follows. Impedances are adjusted until the dipoles are 50 ohms, as seen at terminals  $c$  and  $d$ . Then the antennas are disconnected at points  $a$  and  $b$  and the line stretcher is adjusted until  $Z_c Z_d = 2500$ . If the antenna systems are essentially the same, the impedances at  $c$  and  $d$ , for open circuits on  $a$  and  $b$  differ only by the extra length of line, and when it is  $90^\circ$  the above formula holds.

<sup>6</sup> E. R. Kretzmer, "Measuring phase at audio and ultrasonic frequencies," *Electronics*, vol. 23, pp. 114-118; 1949.

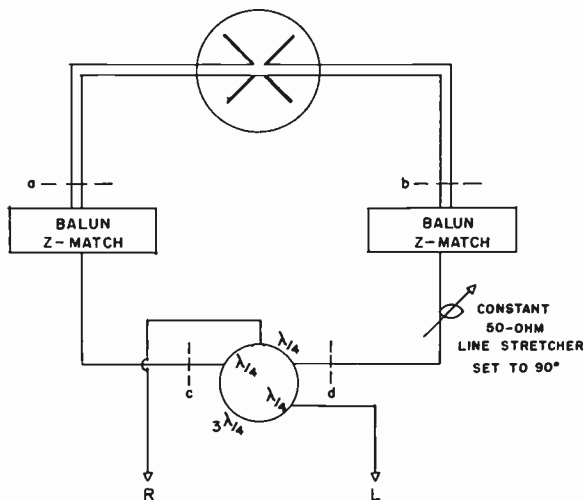


Fig. 3—Antennas.

The circularity of the antennas is tested by rotating the dish on its axis when it is illuminated by a linearly-polarized wave. The plane wave is generated by a vertical dipole on a 20-foot tower 125 feet away. When the dish is rotated, the variations in receiver output are about 0.3 db. This means that the axial ratio of the antennas is about 0.97 instead of 1.00. The determination of the axial ratio of an incoming signal will be in error by a maximum of 0.035, from this alone. (See the Appendix for details.) If maximum errors of 0.01 are desired, the antennas must be circular within 0.08 db, or else all the antenna parameters must be measured and the determination made in terms of their actual values.

A right-hand helix is also mounted on the tower supporting the vertical dipole. It is used on occasions when cables are changed, etc., as an absolute check on right hand vs left hand.

The crosstalk between the antennas, at terminals *R* and *L*, Fig. 3, is measured to be about -30 db. This inaccuracy, by itself, will make an unpolarized wave read 6 per cent polarized, linear. If the wave is entirely polarized, there will be no error in *m*, but there will be one in *r*. When the wave is circular, for example, the measured axial ratio will be about 0.94. (See the Appendix for details.) If the errors due to crosstalk are to be less than one per cent, the crosstalk must be smaller than -46 db. If the crosstalk is zero, the antennas are oppositely polarized, regardless of the circularity. Since the polarizations are opposite (9) or Fig. 2 will give correctly the percentage of polarization in this case.

In summary, the antenna inaccuracies, adding in a random fashion, might result in errors of ±0.05 in the determination of *r* and *m*. The final determination will be less accurate because of errors in other parts of the system, and the fluctuations previously discussed.

CALIBRATION

The system is calibrated by transmitting noise from the vertical dipole described above. The noise generator

for this purpose is simply a noisy, high-gain 201.5-mc amplifier. An attenuator with steps of 1 db allows its level to be changed by known amounts. The receiving antenna is pointed at the dipole and receives the noise signal plus the background from the sky. The equivalent temperature at the receiver input is then

$$T_{eq} = (F - 1)T_0 + T_b + qT_n, \tag{14}$$

where  $T_b$  is the background temperature,  $T_n$  is the temperature of the noise source when 40 db are inserted in the attenuator, and  $q$  is the factor by which the attenuation is decreased; *i.e.*, the factor by which the noise signal is increased above the -40 db reference level.

The indicators on the channels *ABC* of Fig. 1 are set to read zero when  $q=1$ . This level is not substantially bigger than that seen from the sky alone, since  $T_n \ll \{(F-1)T_0 + T_b\}$ . The attenuation is then decreased, and the three scales of channels *ABC* are calibrated in units of  $q$ . The values of  $q$ , when multiplied by  $T_n$ , give the excess antenna temperature from the source. The units are the same for the two circular channels because there is equal coupling between the dipole and the two circularly-polarized antennas. The same unit is used for the correlator channel because we wish it to be calibrated in units of  $(RL)$ , and since the wave is completely linearly polarized  $R=L$ , and  $RL=R^2=I_r=I_l$ .

When an arbitrarily-polarized wave is incident on the antennas, values of  $(qT_n)$  are needed to fix the three temperatures, of the right, left, and correlator components. The parameters  $m$  and  $r$ , however, are determined by the ratios of these temperatures, according to (9) and (10). These are, for the case  $I_l > I_r$ ,

$$a = \frac{I_r}{I_l} = \frac{q_r T_n}{q_l T_n} = \frac{q_r}{q_l}, \tag{15}$$

$$b = \frac{RL}{I_l} = \frac{q_{RL} T_n}{q_l T_n} = \frac{q_{RL}}{q_l}. \tag{16}$$

The scale readings on the right, left, and correlator channels are converted into values of  $q_r$ ,  $q_l$ , and  $q_{RL}$  by a calibration curve. The factor  $T_n$  drops out in (15) and (16), and so the absolute level of noise used is immaterial.

When solar bursts are being studied the  $q$  values used are the differences  $q_{burst} - q_{base\ level}$ . This subtraction also eliminates errors from variations in sky temperature between the calibration point and the sun.

The correlator output, when calibrated this way, is in error by the excess mixer noise which is in the audio pass band. This noise is proportional to the ratio of audio to IF bandwidths, and is, to the first order, dependent only on  $I_r$  and  $I_l$ , and not on the correlation between them. Thus it can be found by generating circular and random polarizations and noting the output at *B*. This is the amount to be subtracted, when a signal is incident, to find the product  $RL$ . The circular and

random signals are simulated by increasing the gains in the two receiver channels. If one side has its gain increased the internal noise will be amplified more, and the effect on the output is identical to what happens when a circularly-polarized wave is incident. Unpolarized waves are simulated by increasing the two gains the same amount, when  $q = 0$ .

The phase comparator is adjusted to read zero when the linear dipole is transmitting noise, and it is calibrated with a reversing switch connected in one input channel. The switch reverses the phase by  $180^\circ$  and calibrates the entire range, since the instrument is assumed to be linear. Since the antenna is on an equatorial mounting and the calibrating source is to the south, the measured orientations are with respect to the north-south line in the celestial sphere.

The calibration procedure gives only the relative polarization parameters, and not the absolute intensity. The intensity can be found in units of the quiet sun radiation if corrections are made for variations in the galactic background for different times of the year. If the absolute intensity were desired, the calibrating system would have to be compared against a standard noise generator. Further, the antenna gains would have to be known accurately.

#### OBSERVATIONS

Solar observations with the Cornell instrument have been made since December, 1956. The predominant polarizations for activity that have been seen are the same as those previously reported by others:<sup>7,8</sup> unpolarized, circular, and partially polarized, circular. Elliptical polarizations are relatively rare, and there has been somewhat of a tendency for the polarization percentage to become smaller as the axial ratio decreases (towards linear). Highly polarized, near linear, bursts are extremely rare. (This type is also confused because much interference resembles it.) The details of the observations will be published elsewhere.

The classes of polarizations that have been typically seen are what one would expect if there were a Faraday rotation in the sun's atmosphere that played a substantial role in the propagation.<sup>4</sup> Other observations with a much wider band system, however, have given similar results,<sup>8</sup> so that, on a qualitative basis, there has been no pronounced "bandwidth effect."

The different varieties of activity (storms, isolated bursts, etc.) commonly have characteristic polarizations.<sup>7</sup> Many exceptions also have been seen, however. The storm on March 4, 1957, was unpolarized, for example, although storms are almost always circular. Outbursts also have been seen in a wide range of partially

polarized, elliptical to pure circular, and to unpolarized states.

Some days data show "mixed" polarizations. Sometimes this takes the form of mixed right and left circular storms, and at other times there have been groups of bursts of mixed polarizations. These mixed polarizations are taken to result from there being several sources on the sun at one time. Solar activity has been at a very high level since our observations began, and on days when we saw mixed polarizations there generally were several active regions on the solar disk.

Occasionally we saw polarizations that are described as "variable." The polarization would drift rather than change in an essentially random fashion. The drifting occurred on slow (hours) and fast (seconds to minutes) time scales. These observations are probably similar to the variations in polarization at 97 mc during storms and outbursts reported by Payne-Scott and Little.<sup>9,10</sup> As an example of a slow variation, on February 26, 1957, a storm was partially polarized, left elliptical at the start of the observations (1340 U.T.), and it drifted roughly towards completely polarized, left circular during the first few hours. The fast variations were sometimes seen in outbursts, especially when they were accompanied by a so-called "second part." Several examples of this have been recorded. The drifting has been seen to proceed both ways, from unpolarized toward polarized, and vice versa.

An example of mixed polarizations is shown in Fig. 4. This is a sample from the record of June 20, 1957. The time marks on the bottom are one minute apart. The channels of information are labeled *A*, *B*, *C*, *D* according to the outputs on Fig. 1, and the gain on the correlator channel is much greater than the gains on the two circular channels. The bursts around 2353-54 appear to be mixed right and left circular. The outburst starting at 2355 is 20-30 per cent polarized, left circular, except for the second major dip, where the right circular channel has an extra burst. The signal in the correlator channel is essentially all excess noise, as discussed above. The phase comparator does not show any coherent phase.

The base levels above which the bursts occur are very high, since on these ranges for channels *A* and *C* the quiet sun is about one line. Since there are independent right and left circular bursts, it is simplest to assume that the base level increases are also independent, and there are two independent storms. The entire day's record suggests this. Occasionally right and left circular bursts occurred together. The total radiation was unpolarized or slightly polarized, but might have resulted from the chance coincidence of two of the independent storm

<sup>9</sup> R. Payne-Scott and A. G. Little, "The position and movement on the solar disk of sources of radiation at a frequency of 97 mcs. II. Noise storms," *Aust. J. Sci. Res.*, vol. A 4, pp. 508-525; 1951.

<sup>10</sup> R. Payne-Scott and A. G. Little, "The position and movement on the solar disk of sources of radiation at a frequency of 97 mcs. III. Outbursts," *Aust. J. Sci. Res.*, vol. A 5, pp. 32-49; 1952.

<sup>7</sup> J. L. Pawsey and R. N. Bracewell, "Radio Astronomy," Oxford University Press, London, Eng., ch. V; 1955.

<sup>8</sup> T. Hatanaka, S. Suzuki, and A. Tsuchiya, "Observations of polarization of solar radio bursts," *Proc. Japan Acad.*, vol. 31, pp. 81-87; 1955.

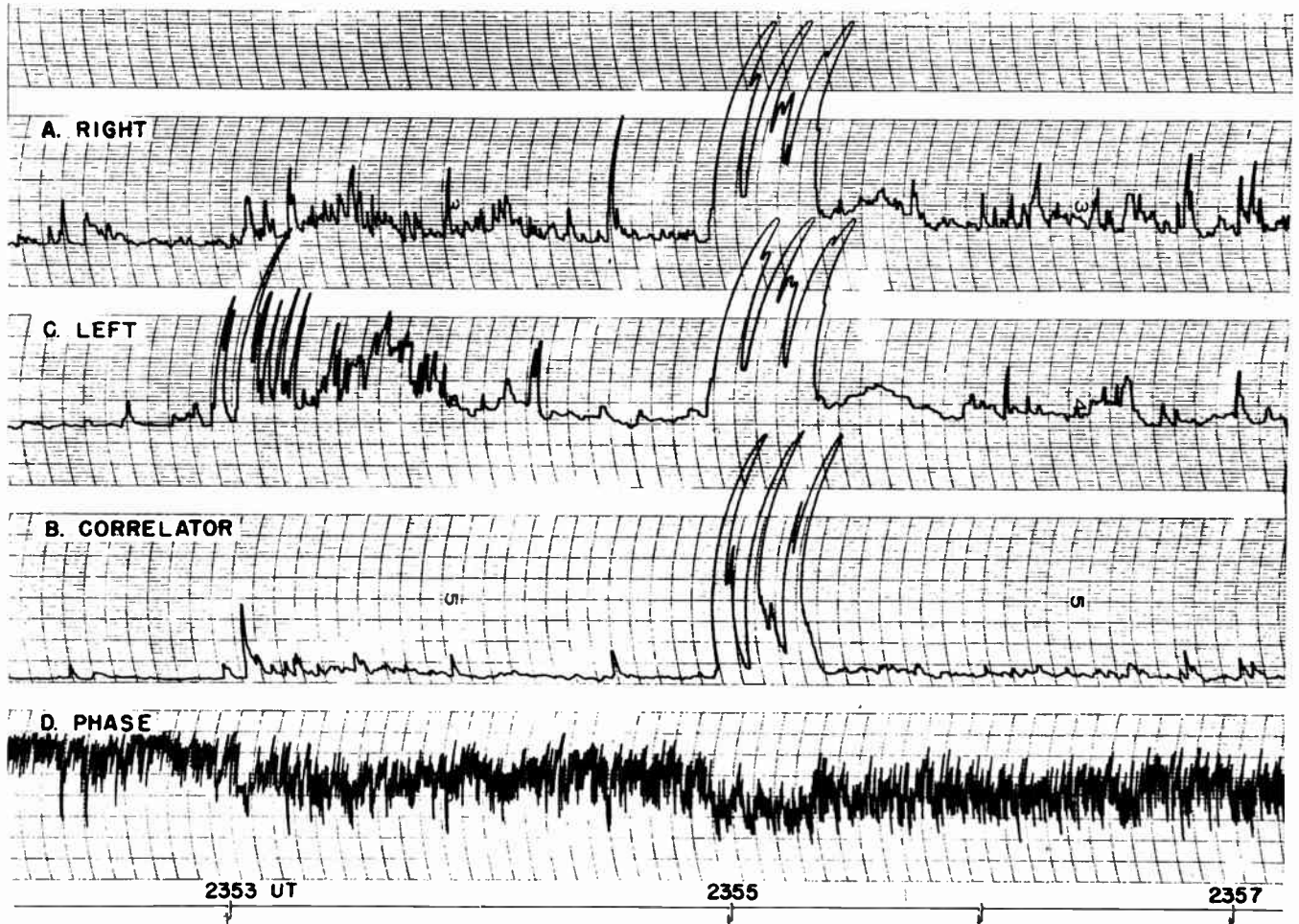


Fig. 4—Polarized solar radiation, June 20, 1957, 201.5 mc. Bandwidth 15 kc.

bursts. The outburst at 2355, and another longer one at 2405, could hardly have been such chance coincidences.

APPENDIX

ANTENNA ERRORS

Two antenna errors will be considered separately. The first is a noncircularity of the antennas, while maintaining complete isolation. This results when the antennas, assumed to be circular, are actually oppositely elliptically polarized. The ellipses are perpendicular and have  $r_1 = -r_2$ . The second error is a nonzero crosstalk.

*Noncircular, but Oppositely Polarized*

Let  $M$  and  $N$  represent opposite elliptical polarizations, with orientations at  $\pm 45^\circ$  to the  $x$  axis, and axial ratios  $r$ . There is no loss in generality in this discussion from choosing these specific orientations. A pure  $M$  wave would be generated by combining  $x$  and  $y$  components of equal amplitude and the proper phase separation,  $\phi$ . To find the value of  $\phi$  for an axial ratio  $r$ , use the Stokes parameter  $V$ . From Cohen<sup>4</sup>

$$V = 2|\hat{X}\hat{Y}|\sin\phi = I_o\sin 2\beta. \tag{17}$$

But

$$2|\hat{X}\hat{Y}| = I_o \tag{18}$$

and

$$\tan\beta = r, \tag{19}$$

so

$$r = \tan(\phi/2). \tag{20}$$

Let  $k$  be the departure of  $|r|$  from unity, and let  $\Delta\phi$  be the departure of  $|\phi|$  from  $\pi/2$ :

$$|r| = 1 - k, \tag{21}$$

$$|\phi| = \pi/2 - \Delta\phi. \tag{22}$$

Then for  $\Delta\phi \ll 1$ ,

$$k \approx \Delta\phi. \tag{23}$$

An elliptically-polarized wave can be specified by its  $(\hat{X}, \hat{Y})$  components, or by its  $(\hat{M}, \hat{N})$  components. The relations between the components are

$$\hat{M} = (\hat{X} + \hat{Y}e^{i\phi})/\sqrt{2} \tag{24}$$

$$\hat{N} = (\hat{X} - \hat{Y}e^{i\phi})/\sqrt{2}. \tag{25}$$

Suppose a polarimeter has  $M, N$  antennas and a partially-polarized wave is incident. It induces signals of intensity  $I_m$  and  $I_n$ :

$$I_m = |M|^2 + \frac{1}{2}I_u \tag{26}$$

$$I_n = |\hat{N}|^2 + \frac{1}{2}I_u. \tag{27}$$

Phasors are used for convenience, although the signals have the quality of noise.  $I_u$  is the intensity of the unpolarized part of the wave. The true Stokes parameters of the wave in terms of its  $(\hat{X}, \hat{Y})$  components are<sup>4</sup>

$$I = |\hat{X}|^2 + |\hat{Y}|^2 + I_u. \tag{28}$$

$$Q = |\hat{X}|^2 - |\hat{Y}|^2 \tag{29}$$

$$U = 2|\hat{X}\hat{Y}| \cos \gamma_v \tag{30}$$

$$V = 2|\hat{X}\hat{Y}| \sin \gamma_v, \tag{31}$$

where  $\gamma_v$  is the angle by which the  $y$  component of the wave leads the  $x$  component. The apparent Stokes parameters are calculated on the basis that the antennas are right and left circularly polarized. Apparent values of  $\hat{X}$  and  $\hat{Y}$  can be first calculated from (24) and (25). Let primes represent apparent quantities, on the basis that  $\phi = \pi/2$ .

$$\hat{X}' = (M + \hat{N})/\sqrt{2} = \hat{X} \tag{32}$$

$$\hat{Y}' = -j(\hat{M} - \hat{N})/\sqrt{2} = \hat{Y} \exp(-j\Delta\phi). \tag{33}$$

From (28) to (31), then:

$$I' = |\hat{X}'|^2 + |\hat{Y}'|^2 + I_u = I \tag{34}$$

$$Q' = |\hat{X}'|^2 - |\hat{Y}'|^2 = Q \tag{35}$$

$$U' = 2|\hat{X}'\hat{Y}'| \cos \gamma_{v'} = 2|\hat{X}\hat{Y}| \cos(\gamma_v - \Delta\phi) \tag{36}$$

$$U' = U \cos \Delta\phi + V \sin \Delta\phi \tag{36}$$

$$V' = V \cos \Delta\phi - U \sin \Delta\phi. \tag{37}$$

These give

$$I_e' = (Q'^2 + U'^2 + V'^2)^{1/2} = I_e \tag{38}$$

so

$$m' = m. \tag{39}$$

Note that this result,  $m' = m$ , does not depend on  $\Delta\phi$  having a small value. As long as the antennas are oppositely polarized  $I$  and  $I_e$  are correctly found.

The apparent axial ratio,  $r'$ , is found from  $r' = \tan^{-1}\beta'$ , where

$$\sin 2\beta' = V'/I_e' \tag{40}$$

by (17). Eq. (37) is now substituted for  $V'$  in (40) When the antennas are nearly circular  $\Delta\phi \approx k \ll 1$ ; if  $\Delta r = r - r'$ , this gives<sup>4</sup>

$$\Delta r \approx (1/2)k(1 + r^2) \sin 2\chi. \tag{41}$$

In this,  $r$  is the axial ratio of the wave and  $\Delta r$  is the error in its determination;  $k$ , assumed small, is the departure from unity of the axial ratio of the measuring antennas.

Eq. (41) does not hold when the wave is nearly circular; in this case.

$$\Delta r \approx k. \tag{42}$$

The measured value of  $k$  is 0.035. The error in axial ratio thus is less than 0.035. For polarizations near linear the error is less than 0.02, and for certain orientations the error is zero.

### CROSSTALK

If there is crosstalk between the antennas the polarizations are not opposite. They cannot, for example, be right and left circular. In the polarimeter the measured crosstalk is about  $-30$  db. Most of this comes from the magic ring, although a little results from asymmetry in the crossed dipoles.

In a few special cases the effect of crosstalk on the polarization determination can be found easily. For example, when the wave is completely polarized there is no error in the determination of  $m$ , since all the components are correlated anyway. In this case, however, there will be an error in axial ratio.

Let the crosstalk factor be  $k$ ; *i.e.*, when one volt is applied to terminal  $R$  of Fig. 3,  $k$  volts appear at terminal  $L$ . If the antennas are nearly circularly polarized, the apparent circular components will be, approximately,

$$\hat{R}' = \hat{R} + k\hat{L} \tag{43}$$

$$L' = L + k\hat{R}. \tag{44}$$

The extreme errors in magnitude occur for phases such that

$$|\hat{R}'| = |\hat{R}| + |kL| \tag{45}$$

$$|L'| = |L| - |k\hat{R}|. \tag{46}$$

The apparent axial ratio is

$$r' = \frac{|L'| - |\hat{R}'|}{|L'| + |\hat{R}'|}. \tag{47}$$

This gives an upper limit to the error in the determination of axial ratio. When  $|k| \ll 1$ ,

$$|\Delta r| \leq |k|(1 + r^2). \tag{48}$$

This result is obtained by expanding  $r'$ , (47), in powers of  $|k|$  and retaining only the first-order term.

The measured value of  $|k|$  is 0.03 ( $-30$  db). Thus, when the incident wave is nearly circular, the error in  $r$ ,  $|\Delta r|$ , is less than 0.06. When it is nearly linear, the error is less than 0.03.

If the wave is unpolarized, the signals at  $R$  and  $L$  will be slightly correlated because of the cross coupling. In this case the apparent intensities are approximately

$$I_r' = I_{ur} + |k|^2 I_{ul} \tag{49}$$

$$I_l' = I_{ul} + |k|^2 I_{ur}. \tag{50}$$

The total intensity is  $I = I_{ur} + I_{ul}$ . The apparent polarized intensity is

$$I_s' = \sqrt{Q'^2 + U'^2} = 2\overline{R'L'}, \quad (51)$$

since  $V' = 0$ .  $\overline{R'L'}$  is the average product of the correlated components and equals  $|k|I$ . Thus

$$m' = 2|k|. \quad (52)$$

A 6 per cent polarization will be read for an unpolarized wave, when the crosstalk is  $-30$  db.

#### ACKNOWLEDGMENT

The assistance of E. R. Schiffmacher and H. Goldberg in both system design and data analysis procedures is gratefully acknowledged. G. C. Chapel and others have been of great help in construction and data taking.

## A Time-Sharing Polarimeter at 200 MC\*

S. SUZUKI† AND A. TSUCHIYA†

**Summary**—A radio polarimeter at 200 mc of time-sharing type is described. This instrument observes a set of two circular and four linear components of polarization in 1/200 of a second, with 1/1200 of a second interval for each component, so that practically a simultaneous observation of rapidly varying phenomenon such as a solar burst is made possible. Some details on the electronic switching, the square-law detector, and the method of calibration and checking are discussed.

#### INTRODUCTION

IT IS KNOWN that four independent pieces of information are needed in order to describe the complete state of polarization of an electromagnetic wave [1, 2]. The best way to define the state of polarization is to use the Stokes parameters. Another way is to describe the total intensity, the degree of polarization, and the axial ratio and direction of the polarization ellipse of the radiation [3].

It is also important to use the same receiving system for each component as far as it is possible to avoid inevitable errors due to the difference or change in the gains and in the central frequencies of different receiving systems, especially for the observations of solar radio bursts which have rather narrow spectral bandwidths.

The polarimeter which was built in 1954 at the Tokyo Astronomical Observatory for use at 200 mc is the first attempt to determine the complete state of polarization by observing six components of polarization [1, 2]. It is operated on a time-sharing scheme to satisfy the latter requirement. A different principle is used for a 9000-mc polarimeter [4].

Let a pair of crossed dipoles be  $A$  and  $B$ . Let

$$\begin{aligned} e_a &= E_a \sin \omega t \\ e_b &= E_b \sin (\omega t - \delta) \end{aligned} \quad (1)$$

represent the instantaneous output voltages of the antennas  $A$  and  $B$ , respectively, where  $\omega$  is the circular frequency of the radiation under consideration. If we combine these two output voltages after putting a phase delay  $\phi$  to one of them, then the combined input voltage is

$$e_a + e_b(\phi) = E_a \sin \omega t + E_b \sin (\omega t - \delta - \phi), \quad (2)$$

and the power received by such a system is, by neglecting a factor for the reduction of voltage into power,

$$I(\phi) = I + U \cos \phi - V \sin \phi, \quad (3)$$

where  $I$ ,  $U$ , and  $V$  are three of Stokes parameters. If the directions of  $A$  and  $B$  are  $+45^\circ$  and  $-45^\circ$  from the vertical, respectively, we can obtain two linears, in vertical and horizontal directions, and two circulars, right handed and left handed, by putting phase delays of  $0$ ,  $\pi$ ,  $\pi/2$ , and  $-\pi/2$ , respectively. If we denote the power received with these connections by  $I(v)$ ,  $I(h)$ ,  $I(r)$ , and  $I(l)$ , we can write, by (3),

$$\begin{aligned} I(v) &= I(0) = I + U \\ I(h) &= I(\pi) = I - U \\ I(r) &= I(\pi/2) = I - V \\ I(l) &= I(-\pi/2) = I + V. \end{aligned} \quad (4)$$

The remaining parameter  $Q$  is given by

$$Q = I(a) - I(b). \quad (5)$$

Therefore, Stokes parameters are given by combining (4) and (5) and we have also the following equalities for check:

$$I = \frac{1}{2} \{ I(v) + I(h) \} = \frac{1}{2} \{ I(r) + I(l) \} = I(a) + I(b). \quad (6)$$

The polarization degree, the axial ratio, and direction of the polarization ellipse are calculated from these quantities by the standard method [3].

\* Original manuscript received by the IRE, October 14, 1957.

† Tokyo Astronomical Observatory, University of Tokyo, Japan.

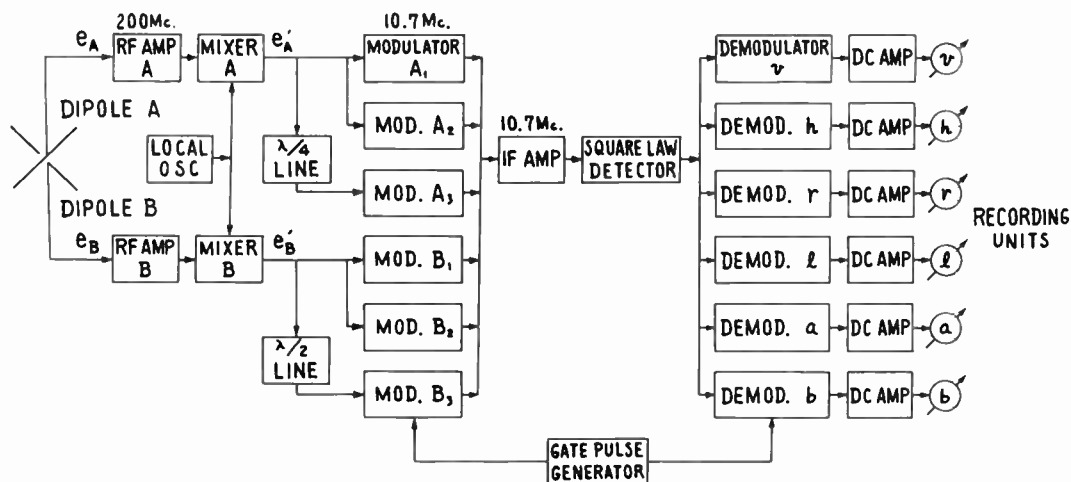


Fig. 1—Block diagram of the circuit.

GENERAL SCHEME

A functional block diagram of this system is given in Fig. 1. A pair of crossed dipoles *A* and *B* is put at the focus of a 10-meter paraboloid of equatorial mounting, the directions of the dipoles being  $\pm 45^\circ$  from the north-south direction in the celestial sphere. The antenna output voltages  $e_a$  and  $e_b$  at 200 mc are converted into 10.7 mc and then combined after putting suitable phase delays to get the necessary information. By the use of a common local oscillator the voltage and phase relationships are preserved in the process of frequency conversion.

After detection by a square-law detector, the six pieces of information are separated into six channels by time demodulators which are operated synchronously with the modulators, and are recorded by a six-pen recorder or other recorders. The bandwidth is 100 kc.

ANTENNA MATCHING

Low-loss coaxial cables, each about 40 meters in length, are used to feed the antenna outputs to the receiver. The matching is made at the receiver ends of these transmission lines since it seems difficult to make the matching devices stable against the outdoor weather conditions. The standing-wave ratios in the transmission lines are about 2.

ELECTRONIC SWITCHING

An electronic switching system is adopted instead of a combination of rotating capacity switches, since mechanical devices like the latter are not suitable for observing rapidly varying phenomena such as bursts.

The relation between the time modulators and demodulators is shown in Fig. 2. They are controlled by common gate pulses each having the duration of 1/1200 of a second. In the first 1/1200 of a second the modulators  $A_1$  and  $B_1$ , and the demodulator  $v$  are on. Then  $e_a'$  and  $e_b'$  (at the frequency of 10.7 mc) are combined in phase and give the  $v$  component of the polarization at

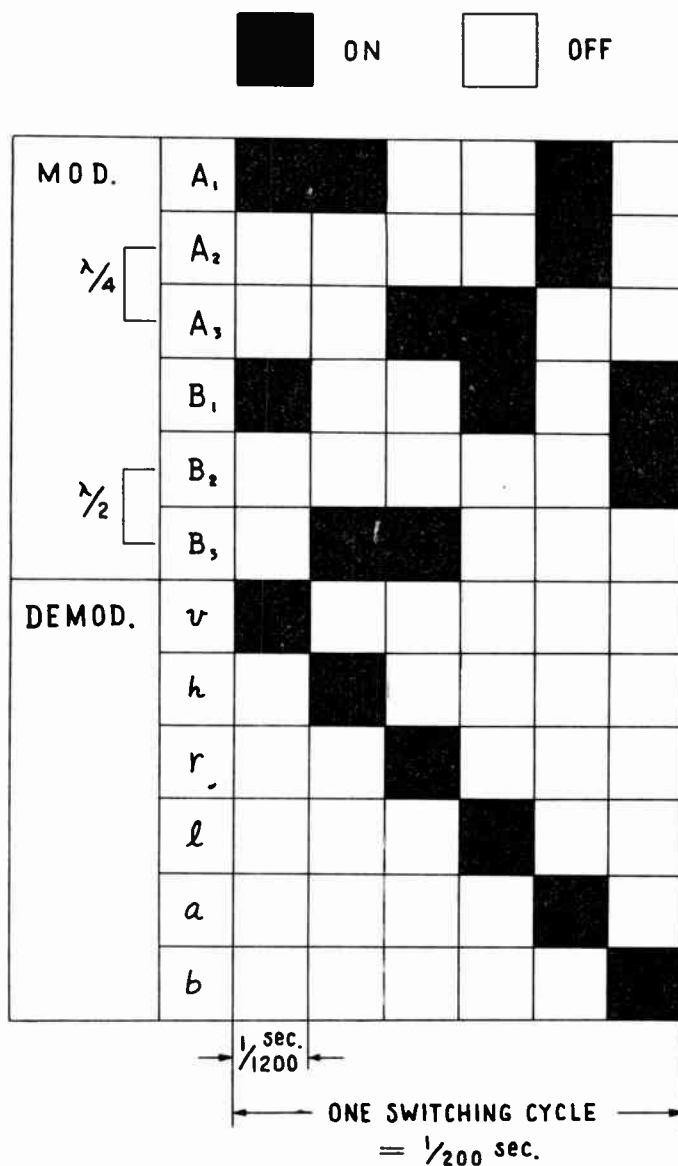


Fig. 2—Schematic diagram of the combination of modulators and demodulators.

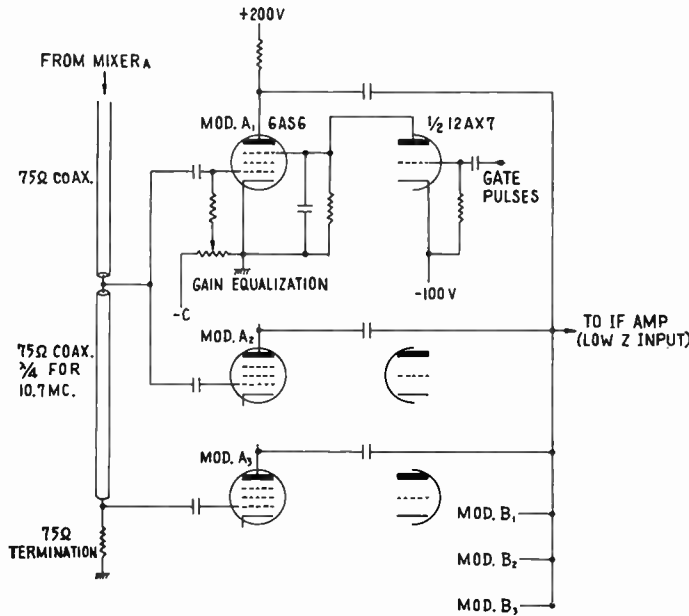


Fig. 3—Construction of the time modulators.

the output of the demodulator  $v$ . In the next  $1/1200$  of a second  $A_1$ ,  $B_3$ , and  $h$  are on, and the  $h$  component is measured, and so on. Thus, a set of six pieces of information is picked up in  $1/200$  of a second.

The gate pulses are generated by a scale-of-six counting tubes specially made for our purpose. It is a single-pulse type and has six outputs. By using somewhat longer control pulses there are gaps between adjacent gate pulses long enough to avoid the crosstalks between adjacent channels caused by the trails of the gate pulses.

The construction of the time modulators is shown in Fig. 3. The switching is made at the suppressor grids of the 6AS6 pentodes;  $1/2$  12AX7's are used as the switching tubes to clamp the suppressor potentials to zero during the "on" periods. The voltage gains of  $A_2$  and  $B_2$  are adjusted to be  $0.41 (= \sqrt{2-1})$  times as that of the other four so as to equalize the over-all gains of six channels. Thus, the outputs of the six components are all equal when the incident wave is randomly polarized. Coaxial lines terminated at their ends are used as the phase shifters to give the phase delays of  $\pi/2$  and  $\pi$ .

Four-diode constant output type demodulators are used as shown in Fig. 4. There is a cathode follower stage preceding the demodulators. Manual switching is also provided for checking purposes.

SQUARE-LAW DETECTOR

If a conventional linear detector is used, the deflection on the tape due to a solar burst is affected by the background noises which include receiver noise, galactic radiation, and the general radiation from the sun. So it is required to calculate the intensity of each component for each burst from the deflections of both the burst and the background.

To cut down the troubles of calculation for many numbers of bursts, square-law detection is desirable.

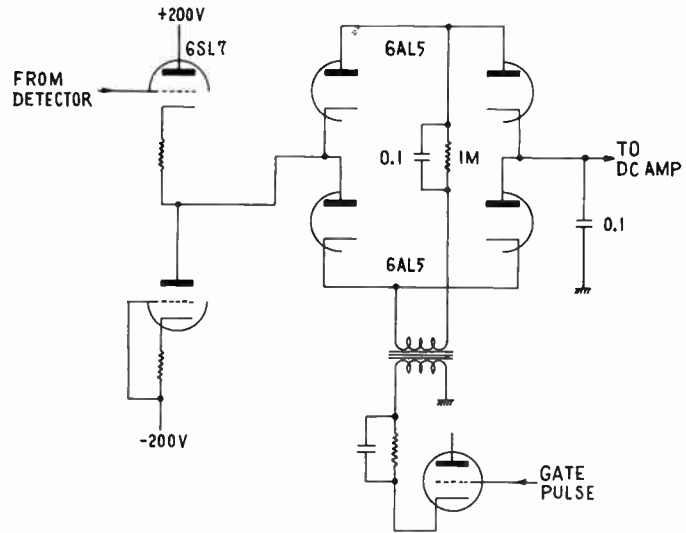


Fig. 4—Construction of the time demodulator.

Since the conventional square-law detectors are not suited for the observation of solar bursts, a new type of square-law detector which has fast response time and excellent stability has been developed in this Observatory.

In Fig. 5 the IF input signal is supplied to the two grids of the squaring tube 6SA7. (A similar performance can be obtained by 6L7.) The output circuit of the squaring tube is tuned to the second harmonics, *i.e.*, 21.4 mc in this case, of the input frequency.

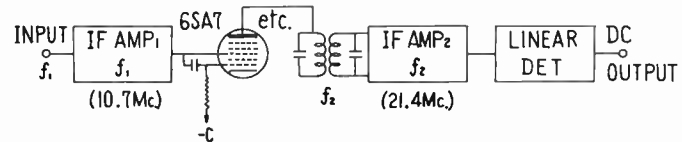


Fig. 5—Schematic diagram of the square-law detector.

Let the input signal be

$$e_i = E \sin \omega t. \tag{7}$$

The plate current of the squaring tube is

$$i_0 = kE^2 \sin^2 \omega t = \frac{1}{2} kE^2 (1 - \cos 2\omega t). \tag{8}$$

Thus the second harmonic output voltage is

$$e_0 = k'E^2 \cos 2\omega t. \tag{9}$$

After linear detection, a dc voltage proportional to the input power is obtained. It is necessary, of course, to make the bandwidth of the second harmonic amplifier wider by a factor or two of more than that of the main amplifier.

The square-law characteristics against the noise input are checked as shown in Fig. 6. A higher IF gain than that used in the normal operation is used to observe saturation. It is seen that the output voltage is linearly

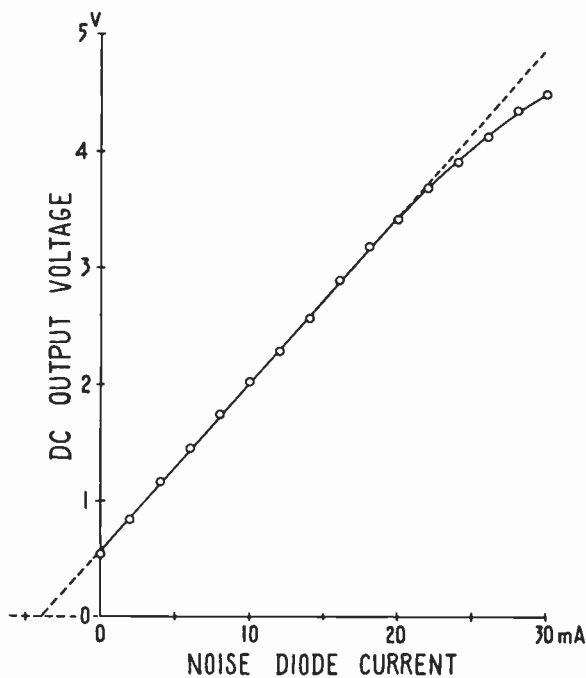


Fig. 6—Performance of the square-law detector.

proportional to the input power until the saturation takes place at about 3.5 volts.

By extrapolating the line to the left as shown in Fig. 6 we can get the magnitude of the receiver noise. In this case the receiver noise corresponds to about 4 ma. Since the impedance is 75 ohms, the noise factor of the receiver turns out to be 6.

As is seen from its construction this square-law detector has a shorter response time and a higher output voltage than the thermal type and better stability than the plate-detection type, so it seems to be suited for this kind of work.

#### STABILIZATION BY DC FEEDBACK

A dc feedback system, as developed by the Cornell Radio Astronomy Group, is applied to all rf and IF amplifier stages to stabilize the cathode currents. This stabilization was used originally for stabilizing the gain, but it is found to be also very effective for stabilizing the phase shifts in the rf amplifiers since it stabilizes the input impedances of the amplifier tubes.

#### CALIBRATION AND CHECKING

Built-in standard noise generators are provided at the input of the two rf amplifiers for the calibration and also for the checking and adjustment of the relative gain of each section.

A dipole which is short enough not to disturb the field of the main dipoles is mounted approximately in the  $v$  direction at the vertex of the paraboloid to send test signals for the phase adjustment. A cw test signal is used at present, since a high-power noise generator could not be obtained. If there is a phase error  $\Delta$  between two rf amplifiers, the outputs of  $r$  and  $l$  are

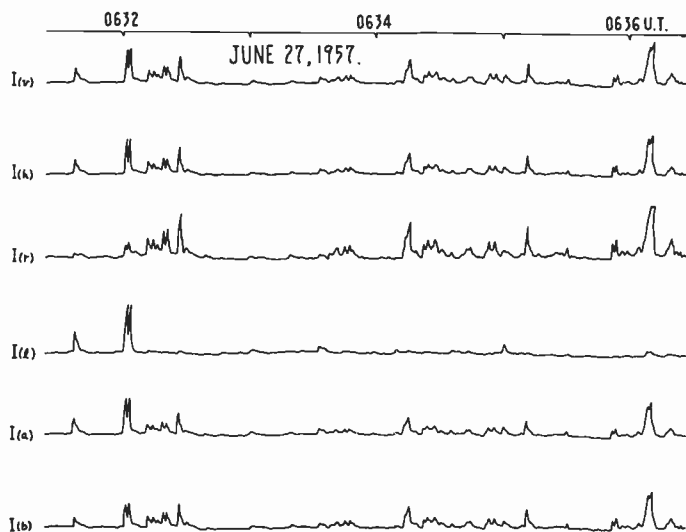


Fig. 7—An example of the observed tape. (The sun: June 27, 1957.)

$$I(r) = I(\pi/2 + \Delta) = I - U \sin \Delta,$$

$$I(l) = I(-\pi/2 + \Delta) = I + U \sin \Delta,$$

because  $V=0$ . Thus, we can align the two amplifiers by adjusting the phase until the  $r$  output becomes equal to  $l$  output.

As the relative phase shift has been found to be very small, the adjustment is being done by a slight detuning of the IF transformer. It can be shown by a simple analysis that this phase alignment is correct even if the gains of the two rf amplifiers are not equal. Therefore, we can finish by adjusting the phase shift first and then the relative gain between two rf amplifiers.

Although the gains of the rf amplifiers can be made equal by means of the noise generator, there remains the question of the equality of the gains of the two dipoles. It is checked by receiving the quiet sun radiation which is believed to be unpolarized.

There is a possibility that the state of polarization of an incident wave may be deformed before reaching the crossed dipoles, and if this deformation exists, it cannot be checked by the total power checking expressed by (6). The most doubtful point is the reflection caused by a ladder and stays attached in the dish. All one can say is that this deformation may not be so large, because the crosstalk between the antennas is  $-50$  db. A larger value of coupling could be observed if there were reflections to cause deformations of polarization.

The main source of errors in this equipment may be the crosstalk between the two rf amplifiers, mainly through the common local oscillator. This crosstalk is kept smaller than  $-50$  db by a careful buffering. Crosstalk may also be caused by the leakage at the modulators and the demodulators. Each of these leakages is smaller than  $-50$  db, so the errors in the receiver are considered to be very small.

An example of the tape is given in Fig. 7, on p. 193, of the solar observation.

ACKNOWLEDGMENT

The authors wish to express their hearty thanks to Prof. T. Hatanaka for his kind guidance and discussion and to N. Shibuya for his assistance in building the equipment. They are also grateful to the staff of the Radio Astronomy Section of the Observatory for valuable discussions.

BIBLIOGRAPHY

- [1] Hatanaka, T., Suzuki, S., and Tsuchiya, A., "Observations of Polarization of Solar Radio Bursts," *Proceedings of the Japan Academy*, Vol. 31, No. 2 (1955), pp. 81-85.
- [2] Hatanaka, T., Suzuki, S., and Tsuchiya, A., "Polarization of Solar Radio Bursts at 200 Mc/s. I. A Time Sharing Radio Polarimeter," *Publication of the Astronomical Society of Japan*, Vol. 7, No. 3 (1955), pp. 114-120.
- [3] Cohen, M. H., "Radio Astronomy Polarization Measurements," this issue, p. 172.
- [4] Akabane, K., "A Polarimeter in the Microwave Region," this issue, p. 194.
- [5] Suzuki, S., "A New Type of Square-Law Detector," *Publication of the Astronomical Society of Japan*, Vol. 7, No. 3 (1955), pp. 121-124.

# A Polarimeter in the Microwave Region\*

KENJI AKABANE†

**Summary**—A polarimeter at the frequency of 9000 mc for the observation of the solar-radio emission is described. The method of phase modulation at the rf circuit is applied to detect the polarized components in the incident waves. The amplitude modulation by ferrite switching also is used to get higher accuracy for the observation. The Stokes parameters ( $I$ ,  $Q$ ,  $U$ , and  $V$ ) in a partially-incident wave can be obtained directly. The minimum detectable intensities of these parameters are 3 for  $I+Q/2$  and  $V$ , and 6 for  $Q$  and  $U$  respectively in the units of  $10^{-22}$  mks. An example of the observation shows the complex polarization of a solar-radio burst at this frequency.

INTRODUCTION

THE polarization of the solar-radio emission has been observed already by some workers in meter wavelength region.<sup>1,2</sup> In the microwave region a few observations have been made, but there have been no detailed observations of the polarization of bursts in this region. However, such detailed observations seem quite important in relation to the magnetic field of the sunspot and also to the emission mechanism of the solar-radio noise. Thus, a new type of polarimeter in the microwave region has been constructed to observe the sun on a routine basis, including the period of the International Geophysical Year.

PRINCIPLE OF MEASUREMENTS

A rotating phase shifter in the waveguide modulates the incident wave for the detection of polarized components. The principle of this method is briefly as follows, considering a cw incident wave as a special case.

\* Original manuscript received by the IRE, October 14, 1957.  
 † Tokyo Astronomical Observatory, University of Tokyo, Japan.  
<sup>1</sup> T. Hatanaka, S. Suzuki, and A. Tsuchiya, "Observations of polarization of solar radio bursts," *Proc. Japan Acad.*, vol. 31, no. 2, pp. 81-85, 1955.  
<sup>2</sup> M. H. Cohen, "The Cornell radio polarimeter," this issue, p. 183.

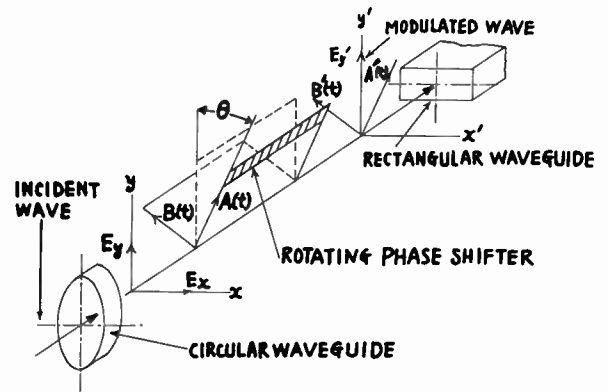


Fig. 1—Principle of phase modulation.

$E_x$  and  $E_y$  represent the incident wave at one point as shown in Fig. 1, and let

$$E_y = p \cos \omega t, \quad E_x = q \cos (\omega t + \phi). \quad (1)$$

The linear component parallel to the plane of the phase shifter is

$$\begin{aligned} A(t) &= p \cos \theta \cos \omega t + q \sin \theta \cos (\omega t + \phi) \\ &= [(p \cos \theta + q \sin \theta \cos \phi)^2 \\ &\quad + q^2 \sin^2 \theta \sin^2 \phi]^{1/2} \cos (\omega t + \Phi_1) \\ \tan \Phi_1 &= q \sin \theta \sin \phi / (p \cos \theta + q \sin \theta \cos \phi), \end{aligned} \quad (2)$$

where  $\theta = \omega_0 t$ , and  $\omega_0$  is the angular velocity of the rotating phase shifter. The other linear component perpendicular to the plane of the phase shifter is

$$\begin{aligned} B(t) &= p \sin \theta \cos \omega t - q \cos \theta \cos (\omega t + \phi) \\ &= [(p \sin \theta - q \cos \theta \cos \phi)^2 \\ &\quad + q^2 \cos^2 \theta \sin^2 \phi]^{1/2} \cos (\omega t + \Phi_2) \\ \tan \Phi_2 &= -q \cos \theta \sin \phi / (p \sin \theta - q \cos \theta \cos \phi). \end{aligned} \quad (3)$$

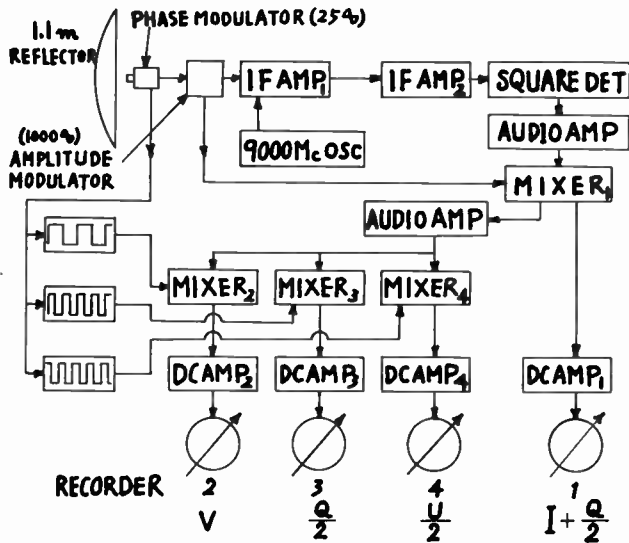


Fig. 2—Block diagram of the system.

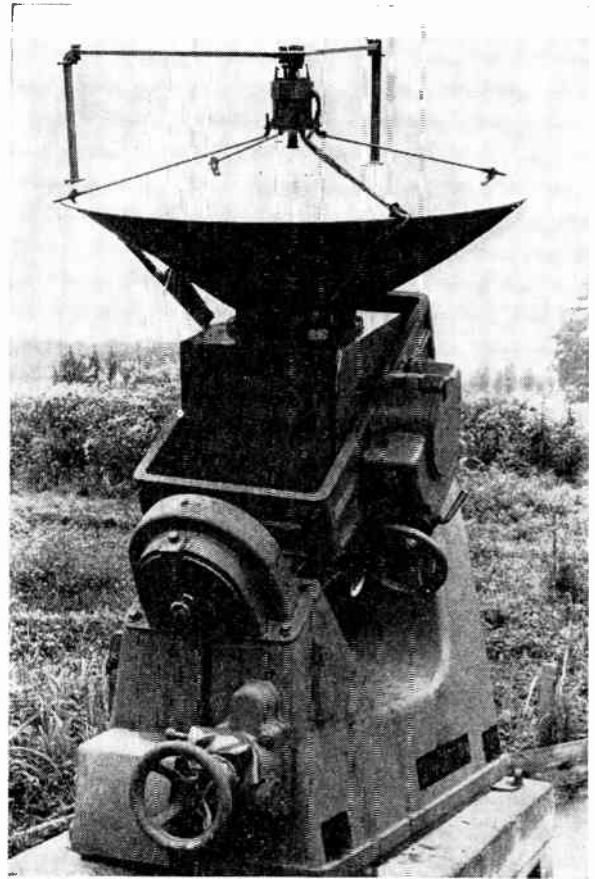


Fig. 3—Antenna.

The  $B(t)$  component has a normal phase shift during the transmission in the waveguide, but the  $A(t)$  component has an abnormal phase shift  $\pi/2$  larger than that of the  $B(t)$  component. Thus, the linear components are modulated into the following forms:

$$\left. \begin{aligned} A(t) \rightarrow A'(t) &= [(p \cos \theta + q \sin \theta \cos \phi)^2 \\ &+ q^2 \sin^2 \theta \sin^2 \phi]^{1/2} \cos \left( \omega t + \Phi_1 - \frac{\pi}{2} \right) \\ B(t) \rightarrow B'(t) &= [(p \sin \theta - q \cos \theta \cos \phi)^2 \\ &+ q^2 \cos^2 \theta \sin^2 \phi]^{1/2} \cos (\omega t + \Phi_2) \end{aligned} \right\} \quad (4)$$

One linear component ( $E_{y'}$  in Fig. 1) of the wave represented by  $A'(t)$  and  $B'(t)$  feeds the rectangular waveguide as shown in Fig. 1. The other linear component ( $E_{z'}$ ) is reflected to the outside of the system or absorbed by the matched load. From (4) we obtain for  $E_{y'}$ ,

$$\begin{aligned} E_{y'} &= A'(t) \cos \theta + B'(t) \sin \theta \\ &= \left[ \frac{3}{4} p^2 + \frac{1}{4} q^2 + pq \sin \phi \sin 2\theta + \frac{1}{4} (p^2 - q^2) \cos 4\theta \right. \\ &\quad \left. + \frac{1}{2} pq \cos \phi \sin 4\theta \right]^{1/2} \cos (\omega t + \Phi_3), \end{aligned} \quad (5)$$

and

$$\begin{aligned} |E_{y'}|^2 &= \left( \frac{3}{4} p^2 + \frac{1}{4} q^2 \right) + pq \sin \phi \sin 2\theta \\ &\quad + \frac{1}{4} (p^2 - q^2) \cos 4\theta + \frac{1}{2} pq \cos \phi \sin 4\theta. \end{aligned} \quad (6)$$

As the phase shifter rotates with the velocity of  $\omega_0$ , the modulated component is expressed by

$$\begin{aligned} |E_{y'}|^2 &= \left( \frac{3}{4} p^2 + \frac{1}{4} q^2 \right) + pq \sin \phi \sin 2\omega_0 t \\ &\quad + \frac{1}{4} (q^2 - p^2) \cos 4\omega_0 t + \frac{1}{2} pq \cos \phi \sin 4\omega_0 t. \end{aligned} \quad (7)$$

The time average of  $|E_{y'}|^2$  and the products of  $|E_{y'}|^2$  with reference signals such as  $\sin 2\omega_0 t$ ,  $\cos 4\omega_0 t$ , and  $\sin 4\omega_0 t$  provide the parameters of the polarized incident wave. That is,

$$\left. \begin{aligned} |E_{y'}|^2 &= \frac{3}{4} p^2 + \frac{1}{4} q^2 = \frac{1}{2} I + \frac{1}{4} Q, \\ |E_{y'}|^2 \sin 2\omega_0 t &= \frac{1}{2} pq \sin \phi = \frac{1}{4} V, \\ |E_{y'}|^2 \cos 4\omega_0 t &= \frac{1}{8} (p^2 - q^2) = \frac{1}{8} Q, \end{aligned} \right\} \quad (8)$$

and

$$|E_{y'}|^2 \sin 4\omega_0 t = \frac{1}{2} pq \cos \phi = \frac{1}{8} U,$$

where  $I$ ,  $Q$ ,  $U$ , and  $V$  correspond to the Stokes parameters. From these parameters, the elliptically-polarized component and the randomly-polarized component can be deduced for the incident wave.

When the incident wave has a certain bandwidth (IF bandwidth in general), the above mentioned analyses should be applied to each wave, incoherent with each other, existing in this bandwidth. Then  $I$ ,  $Q$ ,  $U$ , and  $V$  in (8) give the mean values over the bandwidth of the incident wave.

#### APPARATUS

The block diagram of the system is shown in Fig. 2. The antenna consists of a parabolic reflector 1.1 m in diameter and equatorially mounted as shown in Fig. 3. The feeder at the focus of the reflector is a cylindrical waveguide used in the  $H_{11}$  mode. The phase modulator shown in Fig. 4 rotates with a velocity of about 25 cps,

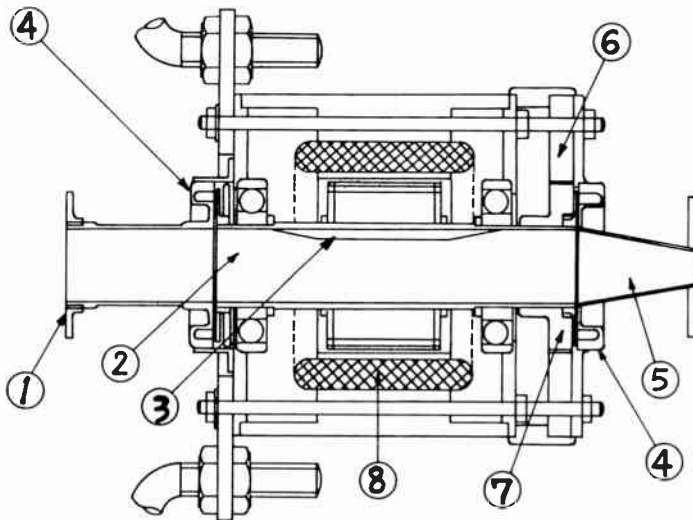


Fig. 4—Phase modulator—1) Feeder waveguide, 2) circular waveguide for modulation, 3) phase shifter, 4) choke coupling for transmission, 5) tapered waveguide, 6) magnet, 7) rotor for reference signal, and 8) coil for induction motor.

and is connected to the rectangular waveguide by a tapered waveguide. The amplitude modulator operates also with a ferrite-switching system at a frequency of 1000 cps which is independent of the frequency of the phase modulator. The IF amplifier has a central frequency of 60 mc and a bandwidth of 8 mc, and the image band is received as well as the signal band. The noise figure of the IF amplifier is about 12 db with the ferrite-switching system in operation, considering both the signal and the image bands. The output of the square-law detector<sup>3</sup> is amplified and mixed with the reference signal from the ferrite-switching system by the coherent detector. The time average of the output from the mixer 1 is linearly proportional to  $\overline{|E_{y'}|^2}$  in (8). The oscillating components of the output from mixer 1 are amplified again and mixed with the three other reference signals from the phase modulator. That is, the reference signals of  $\sin 2\omega_0 t$ ,  $\cos 4\omega_0 t$ , and  $\sin 4\omega_0 t$  are fed to mixers 2, 3, and 4 respectively, and the outputs of these mixers give  $\overline{|E_{y'}|^2} \sin 2\omega_0 t$ ,  $\overline{|E_{y'}|^2} \cos 4\omega_0 t$ , and  $\overline{|E_{y'}|^2} \sin 4\omega_0 t$  separately. The schematic diagram of these mixers is shown in Fig. 5. The time constants of the dc amplifiers are 0.3 second for  $I+Q/2$ , and 1 second for  $V$ ,  $Q$ , and  $U$ . Under these circumstances the minimum detectable intensities of the incident wave are 3 units for  $I+Q/2$  and  $V$ , and 6 units for  $Q$  and  $U$  (one unit is  $10^{-22}$  mks).

#### CALIBRATION AND ACCURACY

##### *The Temperature of the Sky (Around the Zenith)*

The output of the radiometer when the reflector is turned towards the empty sky is regarded as a standard of the daily measurement. Another standard is obtained

<sup>3</sup> S. Suzuki, "A new type of square-law detector," *Publ. Astron. Soc. Japan.*, vol. 7, no. 3, pp. 121-124; 1955.

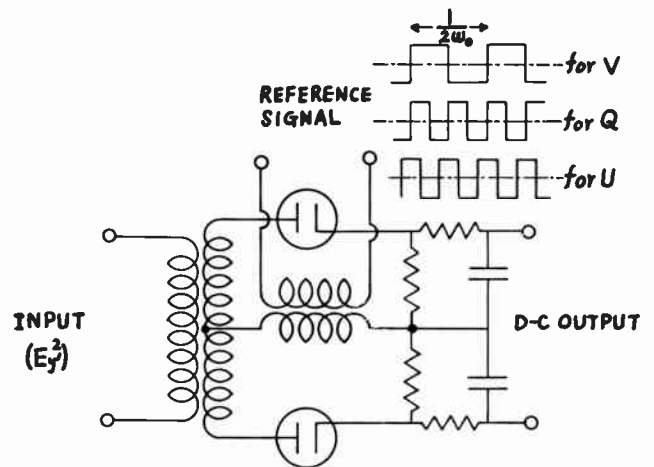


Fig. 5—Mixer for coherent detection.

by inserting a carefully matched load between the phase modulator and the amplitude modulator.

The emitted wave from the absorber in the ferrite system towards the reflector is partially reflected backwards to the receiver by the phase modulator, the feeder, and the parabolic reflector. When the reflector is pointed to the sky, the radiometer receives some radiation from the sky and some amount of the reflected wave. This reflected wave is to be considered an apparent incident wave to the receiver. Then the phase modulator is replaced by a carefully matched horn having the vswr of less than 1.05, and the horn is pointed directly to the clear sky. The output of the radiometer in this procedure is measured by the calibration of the hot load, and the temperature of the clear sky is roughly equal to  $0^\circ\text{K} \pm 10^\circ\text{K}$ . When the phase modulator and the parabolic reflector are in operation, the output of the radiometer rises to  $30^\circ\text{K} \pm 10^\circ\text{K}$  for the clear sky.

##### *Antenna Gain*

A standard horn has been used to calibrate the antenna gain. It has an aperture of  $205 \times 255$  mm and a calculated gain of 316 over an isotropic radiator. The output of the radiometer with this horn pointed to the sun is compared with the output obtained by the parabolic reflector pointed also to the sun. Thus, we obtain an antenna gain of  $4830 \pm 5$  per cent (an effective area of  $3820 \text{ cm}^2$ ) for the parabolic reflector, including the effect of the stays for the feeder and the mismatching of the feeder and the phase modulator. The half-width of the antenna beam is about  $\pm 1.2^\circ$ .

##### *The Calibration of the Sensitivity*

The sensitivity for  $I$  (the total intensity of the incident wave) is calibrated by the sky temperature and the radiation of an absorber inserted in the input waveguide at the ambient temperature. The sensitivity for  $V$  (the difference between right-handed and left-handed circular polarizations) is calibrated by a source of circular

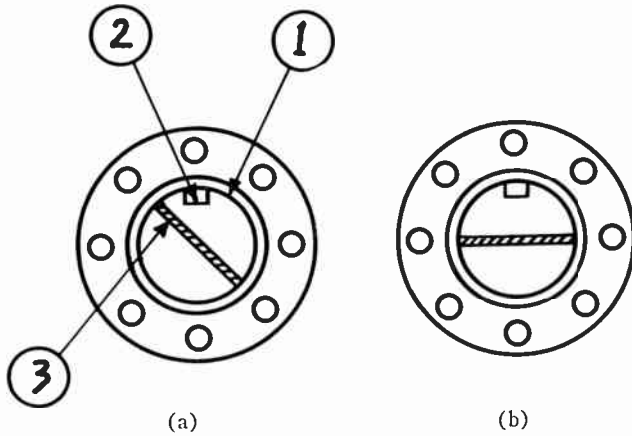


Fig. 6—Radiation source for the calibration of sensitivity—1) Circular waveguide, 2) phase shifter, and 3) lossy plate.

waves attached at the top of the waveguide. This source is a quarter-wave plate at ambient temperature, and is shown in Fig. 6(a). One linear component of the radiation emitted by the matched load in the ferrite system and other absorbers in the tapered waveguide, is absorbed by the lossy plate shown by 3 in Fig. 6(a), and the other linear component is radiated to the empty sky by the parabolic reflector. The source of radiation shown in Fig. 6(b) is used to find the sensitivities of  $Q$  and  $U$  (the difference of the linear components of the incident wave). Considering that the lossy plate in Fig. 6 is at the ambient temperature, we obtain calibrations on the recorder tapes for  $I$ ,  $Q$ ,  $U$ , and  $V$ .

### Accuracy

The character of the phase modulator is dependent on the rf frequencies in the bandwidth of the receiver, and the dc outputs for  $Q$ ,  $U$ , and  $V$  from the coherent detectors shown in Fig. 5 are not completely independent of each other because of leakages between the reference signals. That is,  $Q$ ,  $U$ , and  $V$  have a mutual coupling with each other, a leakage of about 15 per cent of  $V$  appears at the  $Q$  and  $U$  recorders, about 5 per cent of  $Q$  leaks to  $V$  and  $U$ , and about 5 per cent of  $U$  leaks to  $V$  and  $Q$ . This mutual coupling of  $Q$ ,  $U$ , and  $V$  is a serious source of errors.

Another source of errors for the observation of a polarized wave is the asymmetric structure of the parabolic reflector, including the stays supporting the feeder and the waveguides for the receiver. The radiation from the lossy plate in the ferrite system and from the other absorber inserted in the tapered waveguide shown in Fig. 4 is a randomly-polarized wave, and is radiated to the sky by the parabolic reflector. This radiation is partially reflected by the feeder, the stays, and the waveguides in front of the parabolic reflector, and turns back again to the receiver.

By measuring the polarization of this reflected wave, the asymmetry of the antenna system for the reflection has been roughly estimated. We concluded that the

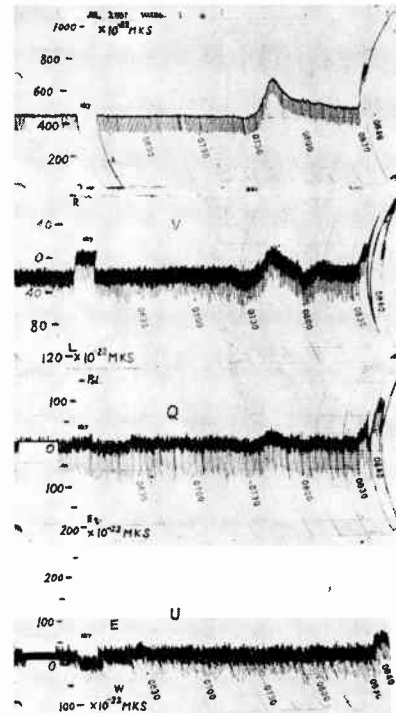


Fig. 7—An example of the observed tape (the sun: July 3, 1957).

asymmetry of the antenna system for the reflection (as well as for the incident wave) is less than 5 per cent for  $Q$  and  $U$ , and less than 3 per cent for  $V$ . This means that even though the incident wave has exactly random polarization,  $Q$  and  $U$  have apparent values of 5 per cent of the total intensity of the incident wave, and  $V$  has the apparent value of 3 per cent of the total intensity.

It might be noted that a parabolic reflector with a larger aperture than ours should be undesirable for the polarization measurement of the sun because the narrower beamwidth of the antenna would give rise to errors in the polarization measurement.

### OBSERVATION OF THE SOLAR RADIO EMISSION

Fig. 7 shows the outburst of solar-radio emission observed with this equipment on July 3, 1957. The steady flux of 450 units and the left-handed excessive polarization of 6 per cent of the total flux are shown by the upper two diagrams in this figure.

A slightly linear component of the steady flux is shown by the lower two diagrams ( $Q$  and  $U$ ). An outburst started at about 0730, and a more intense one started at 0831 U.T. It can be seen that these bursts have certainly some polarized component varying with time in a complex manner.

### ACKNOWLEDGMENT

The author wishes to express his sincere thanks to Dr. T. Hatanaka, S. Suzuki, and other staff members at the Observatory for their valuable discussion.

# Critical Frequency, Refractive Index, and Cone of Escape in the Solar Corona\*

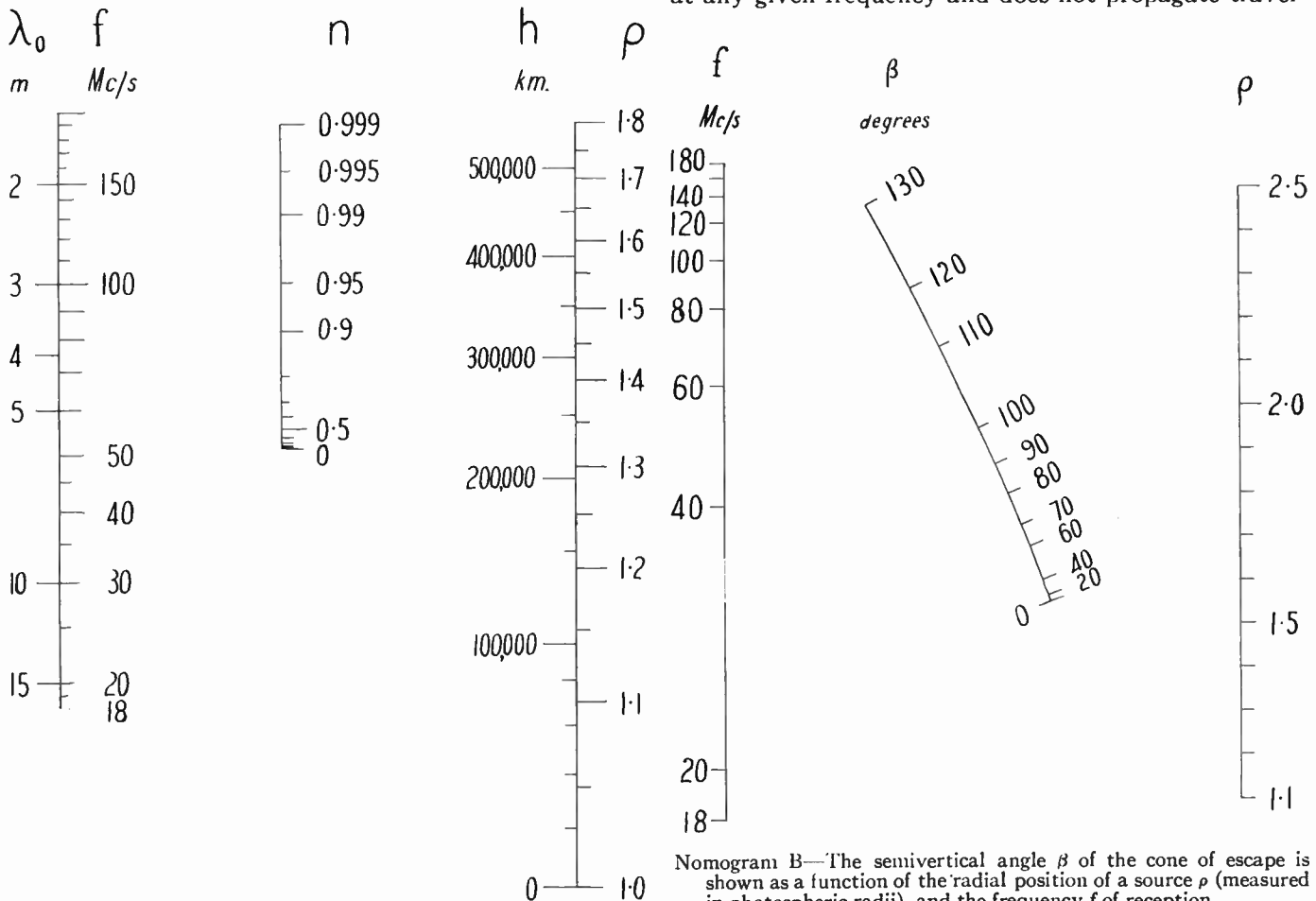
R. N. BRACEWELL†, SENIOR MEMBER, IRE, AND C. V. STABLEFORD‡

**Summary**—Nomograms give refractive index governing radio propagation in the solar corona and the semivertical angle of the cone of escape.

THE propagation and escape of radio waves in the solar corona, which is fully ionized, have much in common with propagation in the ionosphere, and since the corona has proved to be a source of radio-frequency power, radio people have become more and more interested in this problem. The accompanying

nomograms have been used to speed up the calculation of numerical results and are offered here for the use of others who are concerned with the same matter. They are based on an idealized model of the solar corona.

In making calculations about propagation in the corona one requires to know the refractive index of the medium, and, in some cases, the angle of the cone within which the rays from a point source may emerge,<sup>1</sup> given the height above the photosphere and the frequency. Further, below a certain level, the corona is overdense at any given frequency and does not propagate travel-



Nomogram A—The refractive index  $n$  of the solar corona is given as a function of position ( $h$  = height above photosphere, or  $\rho$  = number of photospheric radii from the sun's center) and frequency  $f$  or free-space wavelength  $\lambda_0$ . The critical frequency for any height and vice versa may be read off using the condition  $n = 0$ .

Nomogram B—The semivertical angle  $\beta$  of the cone of escape is shown as a function of the radial position of a source  $\rho$  (measured in photospheric radii), and the frequency  $f$  of reception.

ling waves in the steady state at all. Nomogram A allows one to determine the refractive index  $n$  of the corona, and hence the critical level or critical frequency, by using the condition  $n = 0$ . Nomogram B gives the semivertical angle  $\beta$  of the cone of escape.

\* Original manuscript received by the IRE, October 3, 1957.  
 † Radio Propagation Lab., Stanford Univ., Stanford, Calif. This work was carried out while the author was at Berkeley Astronomical Dept., on leave from Radiophysics Div., CSIRO, Sydney, Australia.  
 ‡ Astronomy Dept., University of California, Berkeley, Calif.

<sup>1</sup> J. L. Pawsey and R. N. Bracewell, "Radio Astronomy," Clarendon Press, Oxford, Eng., p. 81; 1955.

As basic data for nomogram A, we require the electron density  $N$  as a function of height in the corona. This information is available from photometry of the white light scattered from the coronal electrons at the time of total solar eclipse. It turns out that the electron density varies spatially and temporally, but by far the predominant variation is the dependence on the height  $h$ , above the photosphere. The adopted variation is represented by the formula<sup>2</sup>

$$N = 1.55 \times 10^{14} \rho^{-6} (1 + 1.93 \rho^{-10}) \text{ electrons/meter}^3,$$

where  $\rho$  is the distance from the sun's center in units of the photospheric radius. The refractive index  $n$  is related to the electron density of an ionized medium by

$$n^2 = 1 - \frac{Ne^2}{\epsilon_0 m (\omega^2 + \nu^2)},$$

where  $e$  and  $m$  are the charge and mass of the electron,

<sup>2</sup> C. W. Allen, "The spectrum of the corona at the eclipse of 1940, October 1," *Monthly Notices Roy. Astronom. Soc.*, vol. 107, p. 426; 1947.

$\omega$  is the angular frequency of the wave,  $\epsilon_0$  is the permittivity of free space, and  $\nu$  is the electron collision frequency. In the above formula  $\nu$  may be neglected since it is small relative to  $\omega$  throughout the corona.<sup>1</sup>

Nomogram B depends on a knowledge of the ray paths between the source and the observer, calculated in the way described by Jaeger and Westfold,<sup>3</sup> and in more detail by Bracewell and Preston.<sup>4</sup> The nomogram was established by an approximate method, and allows  $\beta$  to be read off to an accuracy of about 3 degrees.

It should be recalled that the effects of coronal irregularities and magnetic fields have been neglected and that therefore the results yielded by the nomograms are in any case approximate. It is suggested that their principal value lies in furnishing rapidly values of  $n$  and  $\beta$  consistent with an admittedly imperfect but widely adopted model.

<sup>3</sup> J. C. Jaeger and K. C. Westfold, "Equivalent path and absorption for electromagnetic radiation in the solar corona," *Aust. J. Sci. Res. A.*, vol. 3, pp. 376-386; 1950.

<sup>4</sup> R. N. Bracewell and G. W. Preston, "Radio reflection and refraction phenomena in the high solar corona," *Astrophys. J.*, vol. 123, pp. 14-29; January, 1956.

## Radio Sources and the Milky Way at 440 MC\*

N. G. ROMAN† AND B. S. YAPLEE†, MEMBER, IRE

*Summary*—The brighter radio sources and two regions of the Milky Way were surveyed at 440 mc with equipment mounted in the Naval Research Laboratory's 50-foot radio telescope. An attempt was made to keep the technique in this survey as similar as possible to that used at higher frequencies. Flux values are given for nine discrete sources and contour maps are presented for the section of the galactic plane near and north of the galactic center and for the area near the strong radio source, Cygnus A. The results obtained for five of the discrete sources and for two lines across the Milky Way are compared with the results of other observers at other frequencies, in an attempt to study the radio frequency spectra of astronomical objects.

### INTRODUCTION

BY 1955, the brighter radio sources had been observed at numerous frequencies between 10 mc and 10,000 mc. These observations indicated that, in most regions of the radio spectrum, the flux from radio stars is almost proportional to the inverse of the frequency. Further, theoreticians had shown that relativistic electrons moving in a magnetic field would produce a spectrum in which the flux is proportional to an inverse power of the frequency. However, observationally, the proportionality constant appeared to be

significantly different for the high and low frequencies—an effect unexpected theoretically. As the high-frequency measurements were made with parabolic reflectors and the low-frequency measurements with interferometers, it was possible that the differing techniques might produce this difference. For the theoretical interpretation of the results, it is important that its reality be established or disproved.

At the Naval Research Laboratory, a 440-mc receiver and a horn feed were constructed for the 50-foot radio telescope. A horn was chosen, in spite of its bulk at this frequency, because its dimensions could be scaled from the horn used at 1420 mc. Thus the illumination of the parabola was identical for NRL's 1420 and 440 mc-observations. With this equipment, antenna temperature measurements were made of the more intense radio sources and of the brighter portions of the Milky Way.

Results of several other surveys at intermediate frequency have been published recently, [1]–[3]. Other surveys are in progress.

### EQUIPMENT

A superheterodyne receiver, used as a dc radiometer, was mounted in a rectangular metal box located be-

\* Original manuscript received by the IRE, November 6, 1957.

† U. S. Naval Research Lab., Washington, D. C.

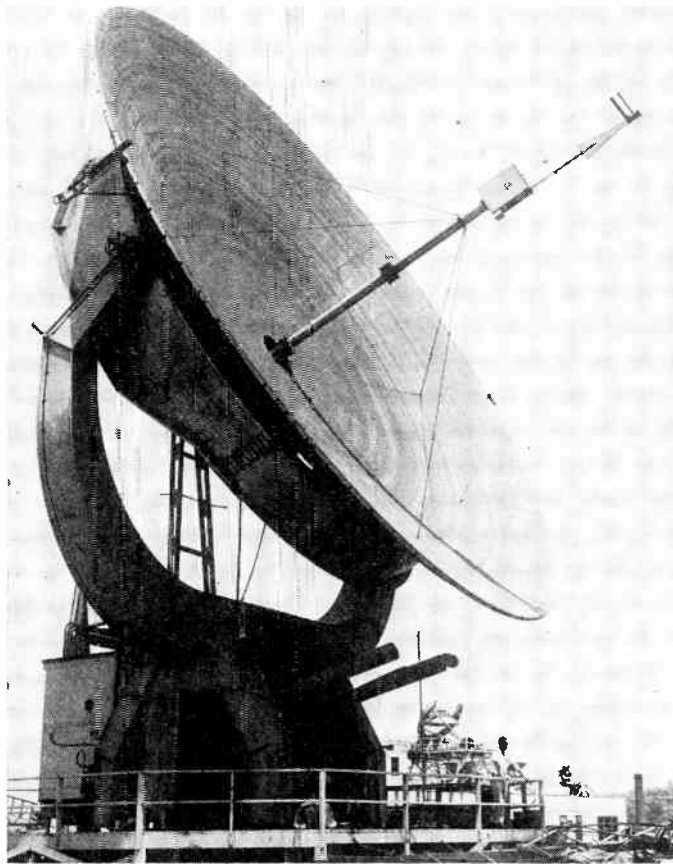


Fig. 1—The 440-mc feed horn and receiver mounted in the NRL 50-foot antenna.

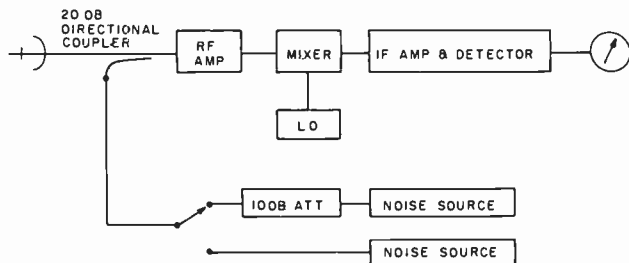


Fig. 2—The block diagram of the 440-mc receiver.

tween the center supporting post and the feed horn assembly (Figs. 1 and 2). The rf amplifier consisted of a GL 6299 planar triode in a cavity and of a quarter-wave transformer to match the tube to the antenna line. For convenience and simplicity, a GR Type 1209-B unit oscillator was used as the local oscillator. The IF amplifier was tuned to 30 mc with a bandwidth of approximately 1 mc. The difference between the output of the second detector and the bucking voltage from a battery, of the order of several millivolts, was dc coupled to a Leeds and Northrop Speedomax recorder through an RC network which provided various time constants for the radiometer output.

For calibration, noise was injected into the rf input through a 20-db directional coupler. Thus it appeared

as noise in excess of the background seen by the antenna. A copper foil helix wound on a teflon tube surrounding the fluorescent tube [4] coupled the noise from the fluorescent tube through type *N* connectors to a coaxial switch that allowed either a fluorescent tube or a fluorescent tube plus a 10-db attenuator to be connected to the directional coupler. The output of the directional coupler was calibrated against a heated resistor to determine the effective noise output in each position of the coaxial switch. The additional equivalent temperatures were 162°K and 14.9°K.

The system was quite sensitive to temperature changes, but a continual flow of outside air through the system prevented the baseline from drifting seriously during an observation under normal operating conditions.

The horn was a modified Cutler feed attached to the receiver box through nonstandard waveguide. The *E* dimension was reduced to feed the horn properly without a taper. A short length of RG 9/AU coaxial cable connected the waveguide, through a transition, to the receiver input.

The characteristics of the antenna pattern are illustrated in Fig. 3 by the mean of six drift curves at declination +40°36'. The ordinate is antenna temperature, a measure of the intensity of the source, and the abscissa is right ascension; at this declination, ten minutes of right ascension equals approximately 1.9°. The curve for the point source, Cygnus A, has been reflected about its peak right ascension and removed from the curve of the extended source, Cygnus X, to illustrate the appearance of the two sources if observed separately. The half-power level for Cygnus A and the theoretical half-power beamwidth also are indicated on this diagram.

#### OBSERVATIONS

The location of the NRL 50-foot antenna is such that interference is strong at frequencies below 1500 mc. To avoid the strongest of this interference, observations had to be made between 10:00 P.M. and 7:00 A.M. Therefore, two observing periods were needed to cover the sky visible from this latitude; one was during June and July, 1956 and the other in February, 1957. The equipment was unchanged between these periods and neither the calibration, performance, nor results showed any systematic differences between the two periods.

To minimize the effects of interference, the observations, with only a few exceptions, were made with the antenna stationary. Thus, those sources of interference which were constant in a given direction merely caused a base-line shift for the entire observation. The telescope was set at the declination of the source, approximately 5° ahead in hour angle; the earth's rotation carried the source through the antenna beam and the observation continued until a flat base-line was observed again, 4° or 5° beyond the source. As a further means of decreasing the effects of random interference, several drift curves were made of each source. This method also

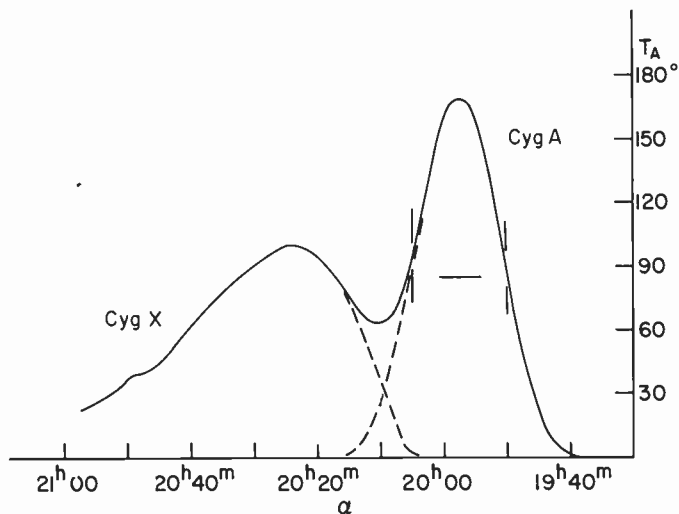


Fig. 3—The mean of six drift curves at declinations  $+40^{\circ}36'$ . The solid curve is the observed curve. The ordinate is the voltage output of the receiver which has been calibrated and converted to antenna temperature. The abscissa has been marked off in right ascension. At this declination, 10 minutes of right ascension equal  $1.9^{\circ}$  of arc. The right side of the curve has been reflected about the right ascension of Cygnus A,  $19^{\text{h}}57^{\text{m}}$  and is shown as a dashed line. This intensity has then been removed from the curve of Cygnus X, on the right, to give the other dashed curve. Thus, the degree of blending of the two sources is indicated. The horizontal and vertical lines of the Cygnus A curve are the observed half-power point and the predicted antenna beam half-width, respectively.

eliminated most of the effects of base-line drift caused by inadequate temperature control in the receiver box. A drift curve of Centaurus A is illustrated in Fig. 4.

Before and after each observation, two deflections were taken with each of the two fluorescent noise sources. As reduction of these calibration deflections indicated no significant nonlinearity and little or no change in the gain of the equipment during a night, all calibration measurements for each night were averaged.

From drift curves of Cassiopeia A and of the Sun, a standard drift curve was drawn. This standard drift curve was then photographed and reduced to various vertical and horizontal scales by means of a trace-scale converter built in the optics division of the laboratory [5]. Individual scans of the bright point sources were matched to the properly reduced standard pattern and their heights above the base-line measured. This method proved to be a rapid means of utilizing the entire upper half of each drift curve rather than merely the peak value. This was particularly important in the presence of interference which distorted portions of the curve. The few curves with obviously tilted base lines or other distortions were replotted to correct these faults. Many of the weaker sources were lost or nearly lost in the noise. For these, point by point averages were made and the mean curve only compared to the standard curves. For the drifts across portions of the Milky Way, the drift curves at each declination were averaged. The times at which each average curve crossed various values of antenna temperature were read and used to draw the contour maps.

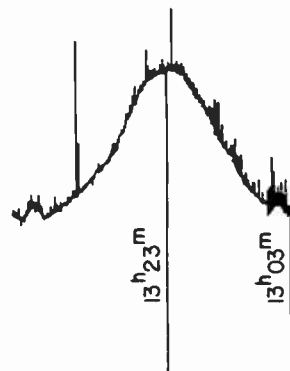


Fig. 4—A drift curve of the source, Centaurus A. The long vertical lines are time markers. The right ascensions to which the antenna was pointed at the times are indicated.

RESULTS

Table I lists the point sources observed in this investigation. The fluxes have been derived from the observed antenna temperatures and an assumed antenna efficiency of 0.65. The errors quoted are *internal* mean errors derived from the scatter among individual measurements of the drift curve heights. The large mean error for Cassiopeia A probably results from the inclusion of scans as well as drifts of this source. For the scans, the antenna was driven through the position of the source rather than held stationary. Only the intensity of each source above the neighboring background emission was determined.

TABLE I  
DISCRETE SOURCES

Source	$T_A$	$F_{440}$ [ $10^{-24}$ watt $\text{m}^{-2}(\text{cps})^{-1}$ ]	Remarks
Cas A	$245^{\circ} \pm 7^{\circ}$	57.2	
Cyg A	$166^{\circ}$	38.7	
Tau A	$56.5 \pm 2^{\circ}$	13.2	
Cen A	$52.2 \pm 2^{\circ}$	12.2	
Vir A	$22.3 \pm 2^{\circ}$	5.2	
IC 443	14.5	3.4	
Pup A	7.5	1.8	
Her A	6.4	1.5	
NGC 2244	21.9	$8.2 \pm 2$	Rosette Nebula (See Text)
NGC 1976	$\leq 11.4$		Orion Nebula
M 31	$\leq 3.4$	$\leq 2.4$	Andromeda Nebula
Hya A	$\leq 3.2$	$\leq 0.8$	

The results of the drift curves across two regions of the galactic plane are given in the form of contour maps. Fig. 5 shows the region near and north of the galactic center ( $\alpha=17^{\text{h}}43^{\text{m}}$ ;  $\delta=-29^{\circ}$ ) and Fig. 6 includes the region of Cygnus A ( $\alpha=19^{\text{h}}57^{\text{m}}$ ;  $\delta=+40^{\circ}36'$ ) and Cygnus X. No attempt has been made to reduce the data from the form of the measured antenna temperatures. The shapes of the outer contours tend to be somewhat uncertain as a small error in temperature in the wings of the drift curves usually corresponds to a large error in the position of the contour. The uncertainties in these plots are probably of the order of  $10^{\circ}$  of tempera-

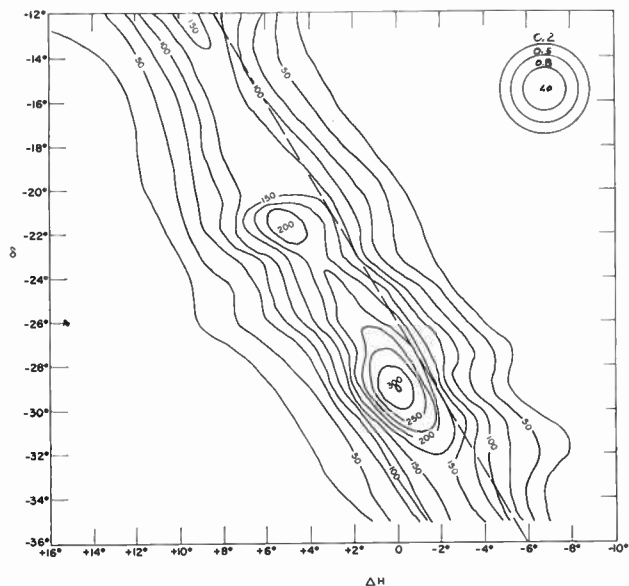


Fig. 5—A contour map of the galactic center region. The dashed line is the position of the galactic plane on the basis of the Lund pole. The numbers indicate the measured antenna temperatures. The ordinate and the abscissa are celestial coordinates corresponding to terrestrial latitude and longitude, respectively, except that  $\Delta H$  has been given in terms of true angular distance; *i.e.*, it has been corrected for the convergence of meridians of longitude. The concentric circles in the upper right corner show the observed antenna diagram to the same scale.

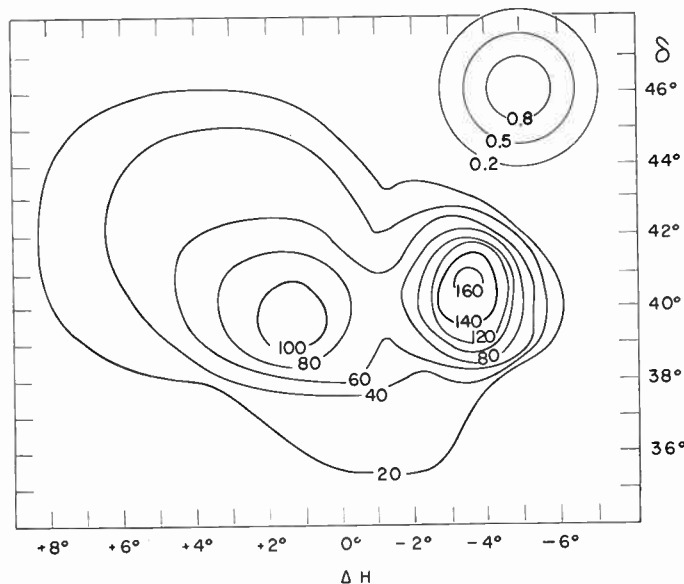


Fig. 6—A contour map of the Milky Way in Cygnus. Cygnus A is the smaller source on the right; the source on the left is Cygnus X. The concentric circles in the upper right corner show the observed antenna diagram to the same scale.

ture. As for the point sources, these temperatures are relative to the background at several degrees from the galactic plane. Comparisons with the surveys by McGee [1] and by Seeger [2] and their respective coworkers indicate that about  $80^\circ$  should be added to the observed temperatures. The concentric circles in the upper part of Fig. 6 indicate the observed antenna pattern for the equipment used.

The Rosette Nebula, NGC2244, probably is an extended source and its width must be taken into account in computing the flux. From the measured broadening of the beam, a half width of  $2.7^\circ$  is derived for this source. This leads to a flux of  $6.7$  to  $9.3 \times 10^{-24}$  watt  $m^{-2}(cps)^{-1}$  according to the intensity distribution assumed for the source. If the Rosette were very small, the flux corresponding to the observed antenna temperature would be  $5.1 \times 10^{-24}$  watt  $m^{-2}(cps)^{-1}$ . This may be taken as a lower limit to the flux observed in the present survey, but it disagrees with the fluxes previously observed:  $1.4 \times 10^{-24}$  watt  $m^{-2}(cps)^{-1}$  at 400 mc [2] and  $1.6 \times 10^{-24}$  watt  $m^{-2}(cps)^{-1}$  at 242 mc [6]. The cause of this discrepancy is unknown. There may be confusion with nearby sources or with the galactic background; also, the Rosette Nebula was near the Sun during the observing period. However, it seems unlikely that side lobes from the sun, with their changing position with respect to the nebula, could be responsible for the large measured flux. No correction has been made for the extension of Centaurus A.

Several unsuccessful attempts were made to observe the moon at 400 mc. From the estimated upper limits to the observed antenna temperatures and the probable background brightnesses, the moon appears to be fainter than  $150^\circ K$  at this frequency.

DISCUSSION

The fluxes quoted in Table I have been combined with others available for four of the brighter "radio stars" and have been plotted against frequency in Fig. 7 through Fig. 10. Although observations are now quite numerous between 20 and 1500 mc, the scatter of the results masks any fine detail in the spectra of these sources. Nevertheless, some conclusions can be drawn. At frequencies above 1200 mc, the slopes of the four spectra are essentially identical, but at lower frequencies they differ considerably. In each case the flux increases as the frequency decreases, but the increase is progressively steeper from Taurus A through IC 443 and Cassiopeia A to Cygnus A. The spectra are still consistent with the schematic picture of two regions in which the flux is inversely proportional to the frequency separated by a region of lesser slope [7]. Both the length and the position of this flatter region vary from source to source, making it unlikely that it is caused by instrumental effects.

The steep rise at the position of Sagittarius A (probably the galactic center) at 440 mc (see Fig. 5) can be explained only by the presence of a small, bright source superposed on the galactic background. The source appears to be a point source with a flux of  $2.3 \times 10^{-24}$  watt  $m^{-2}(cps)^{-1}$  with the  $3^\circ$  beamwidth, but the flux may be uncertain by as much as 50 per cent and the diameter may be as large as  $1^\circ$ . The spectrum of Sagittarius A is illustrated in Fig. 11. At very high frequencies, a small source, not more than  $10'$  in diameter is

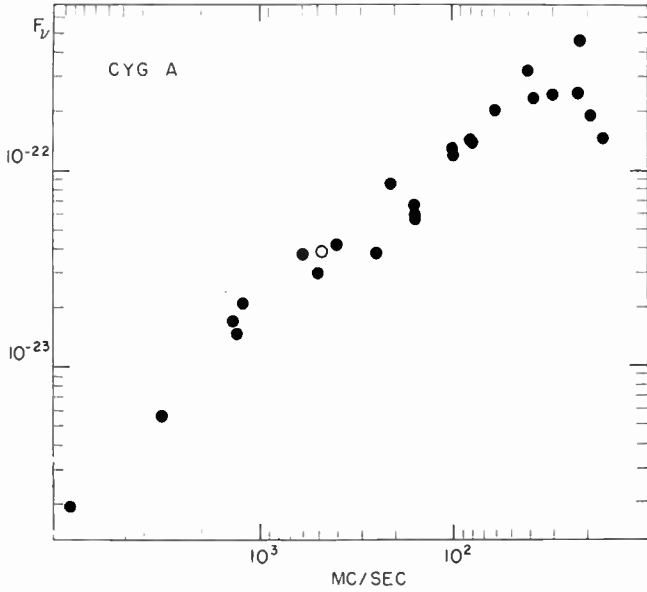


Fig. 7—The spectrum of Cygnus A. The points measured in the present survey are indicated by open circles in Fig. 7—Fig. 11, [2], [3], [8]–[21].

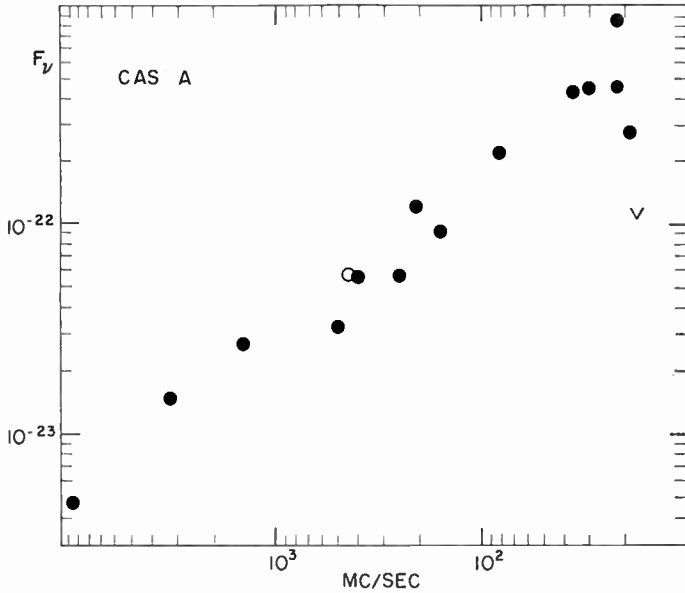


Fig. 8—The spectrum of Cassiopeia A, [2], [8], [10]–[15], [21].

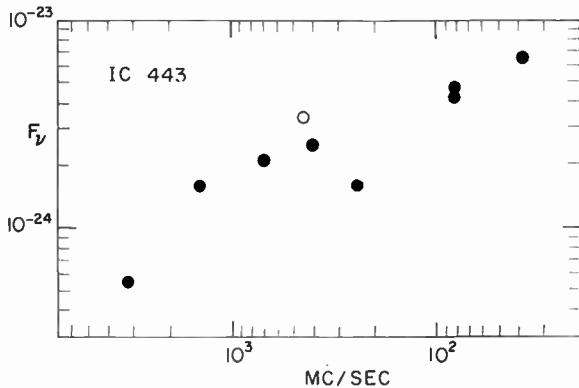


Fig. 9—The spectrum of IC 443, [2], [3], [6], [11], [12], [18], [22].

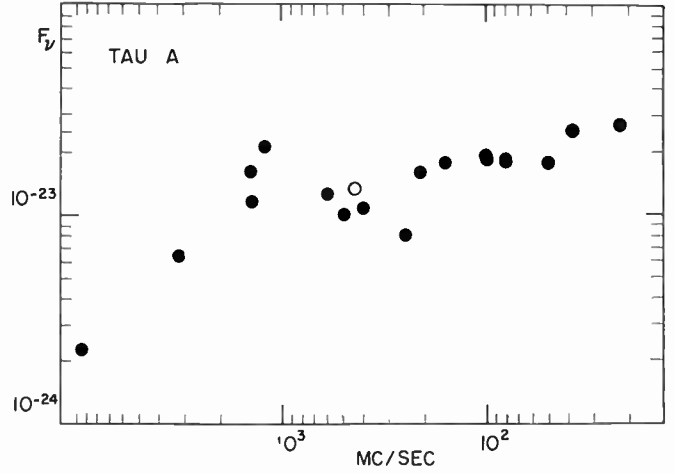


Fig. 10—The spectrum of Taurus A, [8], [10]–[12], [14], [16], [18]–[21], [24].

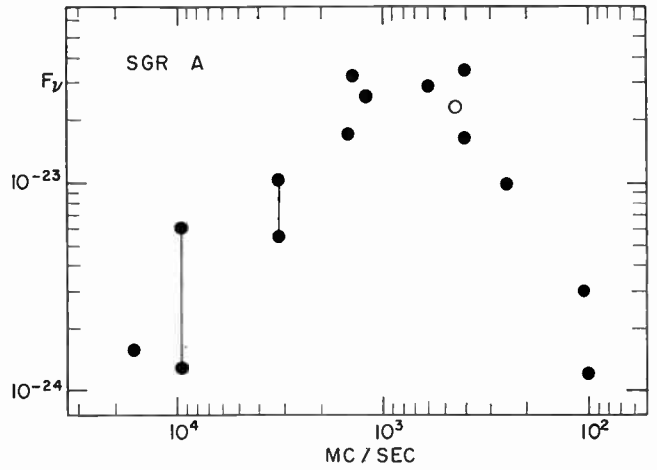


Fig. 11—The high frequency spectrum of Sagittarius A, [1]–[3], [9], [11], [12], [14], [16], [20], [25]–[27].

superposed on a much lower background, at least  $1^\circ$  across [4], [19], [20]. Therefore, at 3200 and 9530 mc, two points have been plotted. The lower refers only to the small source; the upper, to the entire flux received from a circular region centered on the small source and  $1^\circ$  in diameter. The latter is probably more appropriate for a comparison with the other flux measurements for this source. No background source has been observed at 16,000 mc [20]. The highest frequency points are definitely lower than those between 400 and 1500 mc. A spectrum of this shape can be explained by a nonthermal source behind a large, dense HII region (that is, a cloud of ionized gas, mainly consisting of hydrogen).

At low frequencies, the galactic background is definitely nonthermal. An attempt was made to investigate its character at high frequencies by comparing the contours in Figs. 5 and 6 with similar contours for frequencies between 400 and 3200 mc, but the uncertainty in the absolute level of the zero contours makes anything but highly tentative deductions impossible. The indications

are that the emission from the region of the Milky Way, 7° north of Sagittarius A, is predominately nonthermal at frequencies as high as 1500 mc. In the Cygnus X region, a strong nonthermal background appears to persist at 1500 mc, although emission from ionized gas also may be important. The latter probably predominates at 3000 mc.

#### ACKNOWLEDGMENT

The authors wish to express their appreciation to the members of the Radio Astronomy Branch who so generously assisted with the observing for this program. Particular thanks are due Robert Bruton who also assisted in the construction and testing of the radiometer and to C. J. Grebenkemper and C. H. Mayer, T. P. McCullough and R. M. Sloanaker who kindly placed their unpublished data at our disposal. We also wish to thank J. D. Purcell and J. Jackson of the optics division for making the antenna templates for us.

#### BIBLIOGRAPHY

- [1] McGee, R. X., Slee, O. B., and Stanley, G. J. "Galactic Survey at 400 mc/s Between Declinations  $-17^\circ$  and  $-49^\circ$ ," *Australian Journal of Physics*, Vol. 8 (September, 1955), pp. 347-367.
- [2] Seeger, C. L., Westerhout, G., and van de Hulst, H. C. "The Flux Densities of Some Radio Sources at 400 mc/sec.," *Bulletin of the Astronomical Society, Netherlands*, Vol. 13 (November, 1956), pp. 89-99.
- [3] Piddington, J. H., and Trent, G. H. "Cosmic Radio Sources Observed at 600 mc/s," *Australian Journal of Physics*, Vol. 9 (March, 1956), pp. 74-83.  
—, —, "A Survey of Cosmic Emission at 600 mc/s," *Australian Journal of Physics*, Vol. 9 (December, 1956), pp. 481-493.
- [4] Montague, H. A. *Coaxial UHF Noise Source*, United States Naval Research Laboratory Report 4560, August 3, 1955.
- [5] Purcell, J. D. *A Simple Analogue Computer with Application to the Reduction of the Photographic Density Traces of Spectra*, Report of NRL Progress, October, 1954.
- [6] Ko, H. C., and Kraus, J. D. *An Investigation of the Cosmic Radio Radiation in the Region of the Galactic Anti-Center*, Ohio State University Radio Observatory Report No. 4, June 22, 1955.
- [7] Roman, N. G., and Haddock, F. T. "A Model for Nonthermal Radio Source Spectra," *Astrophysical Journal*, Vol. 124 (July, 1956), pp. 35-42.
- [8] Adgie, R., and Smith, F. G. "The Radio Emission Spectra of Four Discrete Sources and of the Background Radiation," *Observatory*, Vol. 76 (October, 1956), pp. 181-187.
- [9] Bolton, J. G., Stanley, G. J., and Slee, O. B. "Galactic Radiation at Radio Frequencies VIII: Discrete Sources at 100 mc/s Between Declinations  $+50^\circ$  and  $-50^\circ$ ," *Australian Journal of Physics*, Vol. 7 (March, 1954), pp. 110-129.
- [10] Brown, R. H., and Hazard, C. "A Survey of 23 Localized Radio Sources in the Northern Hemisphere," *Monthly Notices of the Royal Astronomical Society*, Vol. 113 (April, 1953), pp. 123-133.
- [11] Haddock, F. T., Mayer, C. H., and Sloanaker, R. M. "Radio Emission from the Orion Nebula and Other Sources at  $\lambda 9.4$  cm," *Astrophysical Journal*, Vol. 119 (March, 1954), pp. 456-459.
- [12] Hagen, J. P., McClain, E. F., and Hepburn, N. "Detection of Discrete Radio Sources at 21 cm Wavelength," *PROCEEDINGS OF THE IRE*, Vol. 42 (December, 1954), p. 1181.
- [13] Hey, J. S., and Hughes, V. A. "Intensities of Discrete Radio Sources in Cygnus and Cassiopeia at 22.6 mc/s," *Nature*, Vol. 173 (May 1, 1954), pp. 819-820.
- [14] Kraus, J. D., Ko, H. C., and Matt, S. "Galactic and Localized Source Observations at 250 Megacycles per Second," *Astronomical Journal*, Vol. 59 (December, 1954), pp. 439-443.
- [15] Lambden, R. J., and Lovell, A. C. B. "The Low Frequency Spectrum of the Cygnus (19N4A) and Cassiopeia (23N5A) Radio Sources," *Philosophical Magazine*, Vol. 1 (August, 1956), pp. 725-737.
- [16] Mills, B. Y. "The Distribution of the Discrete Sources of Cosmic Radio Radiation," *Australian Journal of Scientific Research*, Vol. A5 (June, 1952), pp. 266-287.
- [17] Ryle, M., Smith, F. G., and Elsmore, B. "A Preliminary Survey of the Radio Stars in the Northern Hemisphere," *Monthly Notices of the Royal Astronomical Society*, Vol. 110 (December, 1950), pp. 508-523.
- [18] Shakeshaft, J. R., Ryle, M., Baldwin, J. E., Elsmore, B., and Thompson, J. H. *A Survey of Radio Sources Between Declinations  $-38^\circ$  and  $+83^\circ$* , Memoirs of the Royal Astronomical Society, Vol. 67 (1955), pp. 106-154.
- [19] Stanley, G. J., and Slee, O. B. "Galactic Radiation at Radio Frequencies II. The Discrete Sources," *Australian Journal of Scientific Research*, Vol. A3 (June, 1950), pp. 234-250.
- [20] Westerhout, G. "Continuous Radiation from the Direction of the Galactic Center at 22 cm," *Bulletin of the Astronomical Society, Netherlands*, Vol. 13 (November, 1956), pp. 105-109.
- [21] Haddock, F. T., and McCullough, T. P. (unpublished). Quoted in reference 7.
- [22] Baldwin, J. E., and Dewhirst, D. W. "Position and Identification of a Bright Extended Radio Source in Gemini," *Nature*, Vol. 173 (January 23, 1954), pp. 164-165.
- [23] Brown, R. H., and Hazard, C. "Radio-Frequency Radiation from Tycho Brahe's Supernova (AD 1572)," *Nature*, Vol. 170 (August 30, 1952), pp. 364-365.
- [24] Burke, B. F., Firor, J. W., Franklin, K. L., and Wells, H. W. *Radio Astronomy*, Carnegie Institution of Washington Yearbook No. 54 (1954-1955), pp. 43-49.
- [25] Piddington, J. H., and Minnett, H. C. "Observations of Galactic Radiation at Frequencies of 1210 and 300 mc/s," *Australian Journal of Scientific Research*, Vol. A4 (December, 1951), pp. 459-475.
- [26] Grebenkemper, C. J., and Sees, J. E. (private communication).
- [27] Mayer, C. H., McCullough, T. P., and Sloanaker, R. M. (private communication).



# Flux Measurements of Cassiopeia A and Cygnus A between 18.5 MC and 107 MC\*

H. W. WELLS†, FELLOW, IRE

**Summary**—Results of a series of measurements on the two most intense radio stars are given. Basic techniques for absolute and relative intensity measurements are described. Principal sources of error are discussed with special attention to the very controversial range below 30 mc. To minimize one common source of error, interferometer arrays using simple dipole antennas over reflecting screens were used for all absolute measurements of Cassiopeia A. For relative amplitude determinations, collinear arrays with higher resolution were employed. The absolute observations show flux densities which increase by a factor of two between 100 mc and 40–50 mc, and then continue a more gradual increase to 18.5 mc. The amplitude of Cygnus A relative to Cassiopeia A is between 0.5 and 0.6 over the entire range of frequencies.

## INTRODUCTION

ALTHOUGH cosmic radio waves were discovered in 1932 by Jansky,<sup>1</sup> an interval of sixteen years elapsed before Bolton and Stanley<sup>2</sup> detected the presence of *discrete* sources of these cosmic radio waves, sometimes called radio "stars." Their results were promptly confirmed and extended by Ryle and Smith.<sup>3</sup> Surveys followed in England, Australia, and the United States, leading to the identification of more than 100 discrete sources of radio waves from outer space. However, only a limited number have been positively associated with optical objects.

One of the basic questions concerning a radio star is its spectrum: How does the intensity or flux density vary with frequency? Precise answers are of fundamental importance to theories concerning the mechanism of generation of cosmic radio waves. Furthermore, the ability to intercompare spectra of different radio sources establishes facts concerning absorption in interstellar space which may, in some cases, aid in the establishment of a distance scale, and possibly different origins of the radiation.

Measurements of the intensity of the stronger radio sources have been made by several different investigators over a substantial range of frequencies but their results show a great amount of disagreement. The scatter in flux determined by each individual or group testifies to the inherent difficulty of making "absolute measurements." This lack of agreement among separate workers certainly has contributed to the surprising fact

that, as yet, we have no accepted spectrum for even the most intense radio star (Cassiopeia A). In a recent report to Commission V of URSI, Seeger<sup>4</sup> has reviewed the objectives, difficulties, and present status of absolute intensity measurements collected from all available sources of information. He pleads for more accurate measurements of several principal sources which subsequently may become reference standards for the much simpler relative intensity measurements.

This report will include only the simplest of statements regarding instrumentation. The reader who is interested in more specific information on instruments and other aspects of radio astronomy is referred to the book by Pawsey and Bracewell<sup>5</sup> which also includes a substantial bibliography for each chapter. The apparatus used for our measurements was a Ryle-type phase-switching interferometer.<sup>6</sup>

For absolute measurements the antennas were simple folded dipoles over extended ground screens. Antennas were constructed along east-west baselines and were separated by different spacings, usually between  $10\lambda$  and  $20\lambda$  depending on terrain factors. Each folded dipole was mounted between  $0.1\lambda$  and  $0.2\lambda$  above the ground screen so that it would match into a 50-ohm unbalanced transmission line through a 4:1 balun. Transmission lines were brought in directly to a network as shown in Fig. 1 without any preamplifiers in the lines.<sup>7</sup> It is seen that the signals from antenna No. 1 reach the receiver through: 1) a magic *T*-dividing network and 2) a capacity switch which introduces a  $\frac{1}{2}\lambda$  length of line at a rate of about 30 per second. Antenna No. 2 is connected to the receiver through another magic *T*. The purpose of the dividing networks is to permit the application of calibration signals from the noise source simultaneously with the recordings of radio stars. Experience has demonstrated that a network of this type is an essential factor in minimizing errors caused by receiver saturation or nonlinearity effects at frequencies below approximately 50 mc. The 3-db loss in each dividing network is no handicap because signal levels are quite ample.

The attenuator pads in each leg from the noise source

\* Original manuscript received by the IRE, November 5, 1957.

† Carnegie Inst. of Washington, Washington 15, D. C.

<sup>1</sup> K. G. Jansky, "Electrical disturbances apparently of extra terrestrial origin," *Proc. IRE*, vol. 21, pp. 1387–1398; October, 1933.

<sup>2</sup> J. G. Bolton and G. J. Stanley, "Observations on the variable source of cosmic radio frequency radiation in the constellation of Cygnus," *Aust. J. Sci. Res.*, vol. A 1, pp. 58–69; March, 1948.

<sup>3</sup> M. Ryle and F. G. Smith, "A new intense source of radio-frequency radiation in the constellation of Cassiopeia," *Nature*, vol. 162, pp. 462–463; September 18, 1948.

<sup>4</sup> C. L. Seeger, Report to URSI Commission V from Sub-Commission Vd; June, 1957.

<sup>5</sup> J. L. Pawsey and R. N. Bracewell, "Radio Astronomy," Clarendon Press, Oxford, Eng.; 1955.

<sup>6</sup> M. Ryle, "A new radio interferometer and its application to the observation of weak radio stars," *Proc. Roy. Soc. A*, vol. 211, pp. 351–375; March, 1952.

<sup>7</sup> H. W. Wells, "Flux measurements of discrete radio sources at frequencies below 30 mc," *J. Geophys. Res.*, vol. 61, pp. 541–545; September, 1956.

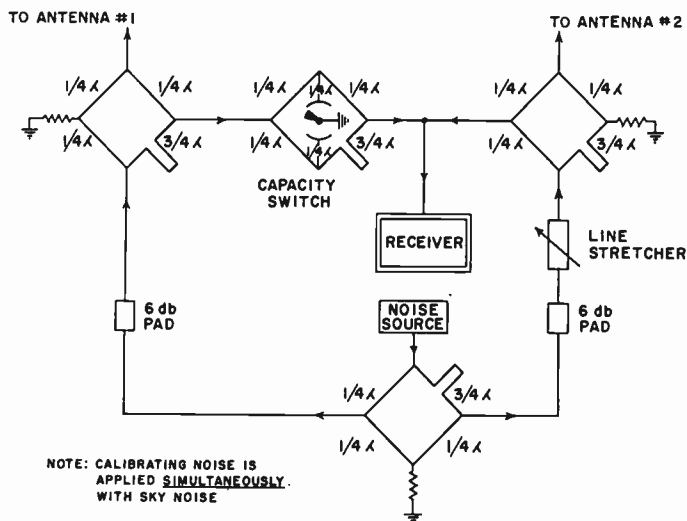


Fig. 1—Interferometer details. (Same as Fig. 1, *J. Geophys. Res.*, vol. 61; September, 1956.)

provide additional isolation and the line stretcher is used to compensate for any phasing unbalance in the separate paths of the calibrating signal. The receiver consists of three basic units: 1) a low-noise preamplifier; 2) the radio frequency amplifier; and 3) the detector, audio amplifier, phase detector, and bridge amplifier. Provision is made always to monitor the detector current since this is essential to measurements of noise figure and other basic adjustments.

Principal sources of error in the making of absolute intensity measurements are in the determination of the equivalent noise power or temperature of the radio source at the antenna and the computation of *effective* antenna aperture. These two factors are combined in the basic formula for the determination of flux:

$$S = kT/A$$

where

$S$  = flux density in units of watts per square meter per cycle per second

$T$  = equivalent temperature of the source at the antenna in degrees K

$A$  = effective aperture of the antenna in square meters.

In practice,  $T$  is determined from scalings of the amplitude of a record produced by a radio source. Scaled values are corrected to equivalent antenna temperature,  $T$ , by applying corrections for measured losses in transmission lines and distribution networks. The distribution system, shown in Fig. 1, was adopted after our discovery of substantial errors in early measurements at frequencies below 20 mc caused by receiver saturation or nonlinearity. (Initially the receiver was disconnected from the antennas and switched over to a noise source for calibration.) The noise source used for calibration was a simple device incorporating a Sylvania 5722 saturated noise diode. The output of this instrument was checked against a thermal source at each dif-

ferent operating frequency. The thermal source was a stable 50-ohm carbon resistor terminating a short section of special 50-ohm coaxial line. For intercomparison purposes the thermal source could be heated in a small electrical oven or immersed in boiling water.

The recordings of Cassiopeia A are confused with other sources when dipole antennas are used. The main contribution, from Cygnus A, can be effectively removed from the Cassiopeia A scalings since the position of the Cygnus source is well known. Most of the direct or absolute measurements were made on Cassiopeia A, while other sources were measured relative to Cassiopeia A using antenna arrays of higher resolution. Other errors in the determination of  $T$  may be caused by radio star scintillation and by absorption in the ionosphere. At frequencies below 50 mc, scintillations are very common. Recordings must continue over a long enough time interval to establish accurate scalings for periods free of scintillation. The effects of ionospheric absorption are eliminated nominally by recording in the hours between midnight and sunrise when the observing frequency is three or four times greater than the ionospheric critical frequency at vertical incidence. It has been demonstrated by Mitra and Shain<sup>8</sup> that ionospheric absorption is negligible under these conditions.

Although the theoretical characteristics of many antennas and arrays have been computed, the properties *actually* achieved are extremely difficult to determine. The problem becomes worse at the meter wavelengths since physical dimensions get large. Usually it is necessary to employ antenna arrays for resolution between radio sources and perhaps for greater signal power. The one antenna which has been the subject of the most exhaustive theoretical and practical examination is the dipole. The fact is often overlooked that a dipole backed by an infinite conducting screen has a gain of 6 db over a dipole in free space. This is equivalent to a collecting area of  $\frac{1}{2}\lambda^2$  as shown by Kraus,<sup>9</sup> and normally is adequate for the detection of principal radio sources up to 200 mc or higher. Even with dipoles, the measured pattern sometimes disagrees with the theoretical pattern.

Tests were conducted to assess the efficiency of the ground screens. Comparisons were made between a dipole over a large metal plate and an identical dipole over the ground screen actually used for recording. A differential radiometer was used and a balance was obtained by adjusting a variable attenuator in the leg from the dipole over the large metal plate. Efficiencies between 90 and 95 per cent were measured. However, it is fully recognized that the dimensions of all reflecting screens used for these measurements are finite and perhaps too small. Plans are being made to repeat some measurements under conditions which more closely ap-

<sup>8</sup> A. P. Mitra and C. A. Shain, "The measurement of ionospheric absorption using observations of 18.3 mc/s cosmic radio noise," *J. Atmos. Terr. Phys.*, vol. 4, pp. 204-218; 1953.

<sup>9</sup> John D. Kraus, "Antennas," McGraw-Hill Book Co., Inc., New York, N. Y.; 1950.

proach that of an infinite reflecting screen. Any subsequent revision of  $A$  would probably be to smaller values resulting in a proportionate upgrading of  $S$ .

For relative amplitude measurements rather simple 4 or 5-element collinear arrays were found to be adequate since the principal requirement was one of resolution between Cygnus A and Cassiopeia A. Once a radio source has been resolved, the other requirement reduces to an accurate means of intercomparing the intensity of the source being measured with that of the reference standard. Although the above remarks are oversimplified, the fact remains that relative amplitude measurements are much simpler than absolute measurements and, as a result, are often considered to be more reliable.

#### ABSOLUTE MEASUREMENTS OF CASSIOPEIA A

The results of our absolute measurements on Cassiopeia A are shown in Table I and are plotted in Fig. 2.

TABLE I  
MEASUREMENTS ON CASSIOPEIA A

Frequency (mc)	18.5	27	50	87	108
Flux density ( $S$ ) in units of $10^{-24} \text{ w m}^{-2}(\text{cps})^{-1}$	500	430	380	200	200

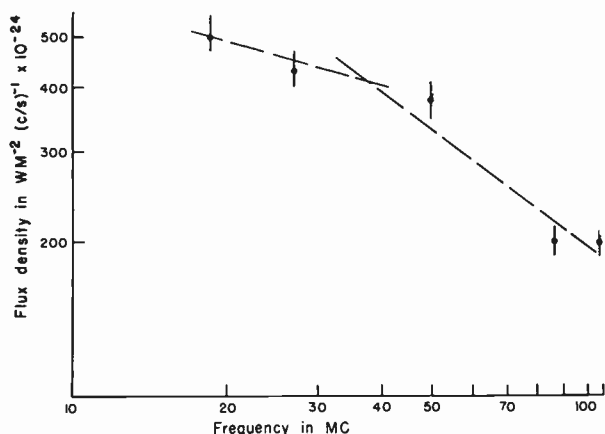


Fig. 2—Cassiopeia A, Derwood, Md., CIW, DTM (1957).

Since authors always have a tendency to draw lines between points, the dashed lines of Fig. 2 show one way of interpreting the observations. The slope of spectrum from 100 mc to about 40 mc is in surprisingly good agreement with a composite spectrum of Cassiopeia A prepared by Seeger<sup>4</sup> from all available data, showing a slope of  $-0.82$ . But in the vicinity of 40-50 mc there appears to be a break or change in slope. This has been anticipated on theoretical grounds and it is perhaps surprising that the flux of Cassiopeia A is found to be slowly *increasing* even at frequencies as low as 18.5 mc. The same lower frequency region, below 40 mc, is also the area of greatest disagreement among the limited number of investigators who have reported "absolute" measurements.

At present, measurements are being undertaken at 207 mc in order to extend the series over three octaves of frequency.

A recheck is being made at 50 mc and a new series of measurements are planned for about 38 mc, interference permitting. All of these are significant to a classification of the spectrum of Cassiopeia A. As soon as the present sunspot cycle abates sufficiently to permit operations below 20 mc without excessive ionospheric interference, it is planned to resume investigations and to extend the series to the lowest possible frequencies.

Questions are frequently raised concerning the accuracy of these measurements. Most of the possible sources of error have been discussed earlier in this report except perhaps errors due to the use of dipoles in a phase-switching interferometer such as ours. We are satisfied that there is no progressive error introduced by our use of dipoles on Cassiopeia A since the spacing in wavelengths between antennas of the interferometer was changed at each different frequency. Hence, the lobe structure was different at each frequency and the lobe including Cassiopeia A was compared with switched lobes in different sections of the dipole polar diagram. Admittedly, there remains a slight possibility that conditions of geometry peculiar to any single measurement could influence the results. We like to think that the results around 100 mc are accurate to  $\pm 10$  per cent, but the scatter of the ratio measurements suggests that this is optimistic. Between 40 mc and 100 mc there is good agreement with Adgie and Smith.<sup>10</sup> At 18.5 mc we estimate accuracy at  $\pm 25$  per cent but we are inclined to weigh the results more heavily toward *higher* values recognizing the possibility of some ionospheric absorption.

#### RELATIVE AMPLITUDE MEASUREMENTS

The relative amplitude measurements have been conducted primarily to determine the strength of Cygnus A relative to Cassiopeia A. The radio source in Cygnus A is the second strongest but is also one of the most distant which has been identified. Baade and Minkowski<sup>11</sup> interpreted their optical evidence as indicating that the Cygnus-A source consists of two galaxies in head-on collision. The distance to this nebula is estimated at nearly 200 million light years. On the other hand, the Cassiopeia-A source is known as a new type of galactic nebulosity, a mere one thousand light years. Accordingly, any significant difference in the spectra of these two sources could suggest a difference in the generating mechanism, or interstellar absorption due to distance or clouds of material between source and the earth.

Our measurements of the ratio Cygnus A/Cassiopeia

<sup>10</sup> R. Adgie and F. G. Smith, "The radio emission spectra of four discrete sources and of the background radiation," *Observatory*, vol. 76, pp. 181-187; October, 1956.

<sup>11</sup> W. Baade and R. Minkowski, "Identification of radio sources in Cassiopeia, Cygnus A and Puppis A," *Astrophys. J.*, vol. 119, pp. 206-214; January, 1954.

A have been conducted with collinear arrays with sufficient resolution to separate these two principal sources. At the lower frequencies this ratio is 0.5 to 0.6. However, measurements just completed at 87 mc indicate a substantial strengthening of Cygnus A, boosting the ratio to 0.72. At 108 mc no measurements with arrays have been conducted as yet. These ratios undoubtedly include a small contribution from Cygnus X along with Cygnus A since our antennas do not resolve these sources. However, the net augmentation of apparent flux is believed to be insignificant, especially at the lower frequencies. In view of the existing controversy regarding relative amplitudes, especially at the lower frequencies, the record in Fig. 3 showing a ratio of approximately 0.5 is particularly significant.

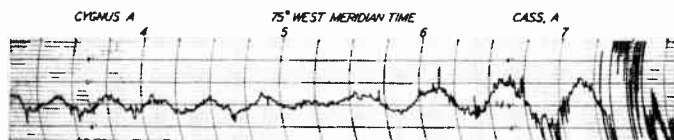


Fig. 3—Interferometer record of Cygnus A and Cassiopeia A at 18.5 mc, May 27, 1956, Derwood, Md., CIW, DTM. (The ratio of Cassiopeia A to Cygnus A is approximately 2 to 1.)

## CONCLUSION

It is believed that a healthy and balanced development in the new science of radio astronomy dictates increased efforts toward the sound establishment of spectra for a few principal radio sources. Agreement, even on one, would be a major step forward leading perhaps to a new yardstick for distance determination or to other fascinating discoveries of conditions within our universe.

## ACKNOWLEDGMENT

Helpful contributions resulting from discussions with associates are gratefully acknowledged. The capacity switch used in the interferometer is a modification of the Cambridge design provided by F. G. Smith. The calibration technique is patterned after a development by B. F. Burke for use with the Mills Cross. Receiver components for 200 mc and other helpful suggestions have come from J. W. Firor. Also, much of the success of the experiments is due to the continued efforts of R. W. Reuschlein in helping maintain the continuity of observations.

# The Distribution of Cosmic Radio Background Radiation\*

H. C. KO†, MEMBER, IRE

**Summary**—The results of a survey of cosmic radio background radiation at 250 mc using the Ohio State University 96-helix radio telescope are described. The antenna has beam widths of about 1.2° in right ascension and 8° in declination between half-power points. Radio maps, covering about 75 per cent of the sky, are presented in celestial and galactic coordinates. The greater resolving power of the antenna has revealed a number of fine features of the background radiation as well as numerous radio stars.

Radio maps made at other frequencies by various groups are summarized. To present an over-all picture of the sky at different frequencies, eight maps are shown for frequencies from 64 mc to 910 mc. All maps are modified to have the same scale, coordinates and units to facilitate intercomparison.

An intercomparison of these radio maps shows some consistent features of the galactic background radiation. These features may be represented by three symmetrical distributions and several unsymmetrical or irregular distributions. The symmetrical distributions are as follows:

1) a narrow belt about 3° wide lying in the galactic plane and concentrated towards the galactic center, 2) a very broad band of radiation concentrated within about 15° to 30° of galactic latitude and having its maximum near the galactic center, and 3) an approxi-

mately isotropic distribution. The first component indicates a mixture of thermal and nonthermal origin, while the other two are non-thermal.

## INTRODUCTION

ONE of the important observations in radio astronomy is the determination of the distribution of continuous background radiation over the celestial sphere. The radio brightness of background radiation received on the earth varies from different directions over the sky and may be conveniently specified by its equivalent brightness temperature. The brightness temperature of the sky at a given frequency is defined as the temperature of a black body—subtending the same solid angle as the region of the sky under consideration—that would produce the same brightness as observed at that frequency. Radio maps of the sky are made from the measurements of the sky brightness temperature distribution. Each map at a particular frequency shows how the sky would appear if our eyes were sensitive to radio waves instead of light and were as poor in resolving power as the radio telescope antenna.

\* Original manuscript received by the IRE, October 3, 1957.

† Radio Observatory, Dept. of Elec. Eng., Ohio State University; Columbus, Ohio.

TABLE I  
SURVEYS OF COSMIC RADIO BACKGROUND RADIATION

Observers	Frequency (mc)	Antenna Beamwidth (deg)	Range of Observation	
			R.A.	Dec.
1. Reber and Ellis <sup>1</sup>	0.5-2.0			
2. Friis and Feldman <sup>2</sup>	9.5, 18.6	16° × 4°, 11° × 3°		
3. Higgins and Shain <sup>3</sup>	9.15	31° × 26°		
4. Jansky <sup>4</sup>	20.5	30° × 37°		
5. Shain and Higgins <sup>5</sup>	18.3	17° × 17°	0 <sup>h</sup> -24 <sup>h</sup>	-52° to -12°
6. Shain <sup>6</sup>	19.7	1.4° × 1.4°	17 <sup>h</sup> -18 <sup>h</sup>	-22° to -33°
7. Fränz <sup>7</sup>	30	30° × 30°		
8. Herbstreit and Johler <sup>8</sup>	25-110			
9. Cottony and Johler <sup>9</sup>	25-110			
10. Moxon <sup>10</sup>	40, 90, 200	35° × 70°		
11. Sander <sup>11</sup>	60	20° × 30°		
12. Hey, Parsons, and Phillips <sup>12</sup>	64	13° × 14°	0 <sup>h</sup> -24 <sup>h</sup>	-30° to +50°
13. Baldwin <sup>13</sup>	81	2° × 15°	0 <sup>h</sup> -24 <sup>h</sup>	-28° to +82°
14. Mills <sup>14</sup>	85.7	0.8° × 0.8°	17 <sup>h</sup> -18 <sup>h</sup>	-34° to -24°
15. Bolton and Westfold <sup>15</sup>	100	17° × 17°	0 <sup>h</sup> -24 <sup>h</sup>	-90° to +40°
16. Hanbury Brown and Hazard <sup>16</sup>	158.5	2° × 2°	19 <sup>h</sup> -05 <sup>h</sup>	+38° to +68°
17. Reber <sup>7</sup>	160	12° × 12°	0 <sup>h</sup> -24 <sup>h</sup>	-40° to +90°
18. Allen and Gum <sup>18</sup>	200	25° × 25°	0 <sup>h</sup> -24 <sup>h</sup>	-90° to +40°
19. Dröge and Priester <sup>19</sup>	200	16.8° × 16.3°	0 <sup>h</sup> -24 <sup>h</sup>	-20° to +90°
20. Ko and Kraus <sup>20</sup>	250	1.2° × 8°	0 <sup>h</sup> -24 <sup>h</sup>	-40° to +60°
21. Atanasijevic <sup>21</sup>	255	10° × 10°	17 <sup>h</sup> -04 <sup>h</sup>	-30° to +90°
22. McGee, Slee, and Stanley <sup>22</sup>	400	2° × 2°	15 <sup>h</sup> -20 <sup>h</sup>	-49° to -19°
23. Seeger, Westerhout, and van de Hulst <sup>23</sup>	400	2° × 2°	16 <sup>h</sup> -19 <sup>h</sup>	-15° to -35°
24. Reber <sup>24</sup>	480	4° × 4°	0 <sup>h</sup> -24 <sup>h</sup>	-40° to +90°
25. Piddington and Trent <sup>25</sup>	600	3.3° × 3.3°	0 <sup>h</sup> -24 <sup>h</sup>	-90° to +51°
26. Denisse, Leroux, and Steinberg <sup>26</sup>	910	3.5° × 3.5°	16 <sup>h</sup> -22 <sup>h</sup>	-35° to +50°
27. Westerhout <sup>27</sup>	1360	1.9° × 2.8°	17 <sup>h</sup> -18 <sup>h</sup>	-20° to -35°

The existence of cosmic radio waves was first discovered by Jansky<sup>4</sup> in 1932 at a frequency of 20.5 mc. Subsequent measurements of this radiation were made by Reber<sup>17,24</sup> who published the first maps of the cosmic radio radiation at frequencies of 160 mc and 480 mc. He confirmed that the radiation is concentrated along the galactic equator and towards the galactic center, and

also found several subsidiary maxima in regions of the constellations of Cygnus, Cassiopeia, and Taurus. During the past decade, a number of other radio surveys have been made at various frequencies. These surveys are summarized in Table I.

<sup>1</sup> G. Reber and G. R. Ellis, "Cosmic radio-frequency radiation near one megacycle," *J. Geophys. Res.*, vol. 61, pp. 1-10; March, 1956.

<sup>2</sup> H. T. Friis and C. B. Feldman, "A multiple unit steerable antenna for short-wave reception," *Proc. IRE*, vol. 25, pp. 841-917; July, 1937.

<sup>3</sup> C. S. Higgins and C. A. Shain, "Observations of cosmic noise at 9.15 mc/s," *Aust. J. Phys.*, vol. 7, pp. 460-470; September, 1954.

<sup>4</sup> K. G. Jansky, "Directional studies of atmospheric high frequencies," *Proc. IRE*, vol. 20, pp. 1920-1923; December, 1932. See also, "Electrical disturbances apparently of extraterrestrial origin," *Proc. IRE*, vol. 21, pp. 1387-1389, October, 1933.

<sup>5</sup> C. A. Shain and C. S. Higgins, "Observations of the general background and discrete sources of 18.3 mc/s cosmic noise," *Aust. J. Phys.*, vol. 7, pp. 130-149; March, 1954.

<sup>6</sup> C. A. Shain, "Galactic absorption of 19.7 mc/s radiation," *Aust. J. Phys.*, vol. 10, pp. 195-203; March, 1957.

<sup>7</sup> Kurt Fränz, "Rauschtemperatur des antennenstrahlungswiderstandes," *Hochfreq. und Elektroak.*, vol. 59, pp. 143-144; May, 1942.

<sup>8</sup> J. W. Herbstreit and J. R. Johler, "Frequency variation of the intensity of cosmic radio noise," *Nature (London)*, vol. 161, pp. 515-516; April 3, 1948.

<sup>9</sup> H. V. Cottony and J. R. Johler, "Cosmic radio noise intensities in the vhf band," *Proc. IRE*, vol. 40, pp. 1053-1060; September, 1952.

<sup>10</sup> L. A. Moxon, "Variation of cosmic radiation with frequency," *Nature (London)*, vol. 158, pp. 758-759; November 23, 1946.

<sup>11</sup> K. F. Sander, "Measurement of galactic noise at 60 mc/s," *J. IEE*, pt. III A, vol. 93, pp. 1487-1489; 1946.

<sup>12</sup> J. S. Hey, S. J. Parsons, and J. W. Phillips, "An investigation of galactic radiation in the radio spectrum," *Proc. Roy. Soc. A*, vol. 192, pp. 425-445; 1948.

<sup>13</sup> J. E. Baldwin, "A survey of the integrated radio emission at a wavelength of 3.7 m," *Monthly Notices Roy. Astron. Soc.*, vol. 115, pp. 684-689; 1955.

<sup>14</sup> B. Y. Mills, "The radio source near the galactic center," *Observatory*, vol. 76, pp. 65-67; April, 1956.

<sup>15</sup> J. G. Bolton and K. C. Westfold, "Galactic radiation at radio frequencies, I. 100 mc/s survey," *Aust. J. Sci. Res. A*, vol. 3, pp. 19-33; 1950.

<sup>16</sup> R. Hanbury Brown and C. Hazard, "A radio survey of the milky way in Cygnus, Cassiopeia and Perseus," *Monthly Notices of the Roy. Astron. Soc.*, vol. 113, no. 2, pp. 109-122; 1953.

<sup>17</sup> G. Reber, "Cosmic static," *Astrophys. J.*, vol. 100, pp. 279-287; November, 1944.

<sup>18</sup> C. W. Allen and C. S. Gum, "Survey of galactic radio-noise at 200 mc/s," *Aust. J. Sci. Res. A*, vol. 3, pp. 244-233; 1950.

<sup>19</sup> F. Dröge and W. Priester, "Durchmusterung der allgemeinen radiofrequenz-strahlung bei 200 mhz," *Z. Astrophys.*, vol. 40, no. 4, pp. 236-248; 1956.

<sup>20</sup> H. C. Ko and J. D. Kraus, "A radio map of the sky at 1.2 meters," *Sky and Telescope*, vol. 16, pp. 160-161; February, 1957.

<sup>21</sup> I. Atanasijevic, "Mesures du rayonnement de la voie lactee sur 255 mc/s," *Compt. Rend. (Paris)*, vol. 235, pp. 130-132; July 16, 1952.

<sup>22</sup> R. X. McGee, O. B. Slee, and G. J. Stanley, "Galactic survey at 400 mc/s between declinations -17° and -49°," *Aust. J. Phys.*, vol. 8, pp. 347-367; September, 1955.

<sup>23</sup> C. L. Seeger, G. Westerhout, and H. C. van de Hulst, "The flux densities of some radio sources at 400 mc/s," *Bull. Astron. Inst. Neth.*, vol. 13, pp. 89-99; November 26, 1956.

<sup>24</sup> G. Reber, "Cosmic static," *Proc. IRE*, vol. 36, pp. 1215-1218; October, 1948.

<sup>25</sup> J. H. Piddington and G. H. Trent, "A survey of cosmic radio emission at 600 mcs," *Aust. J. Phys.*, vol. 9, pp. 481-493; December, 1956.

<sup>26</sup> J. F. Denisse, E. Leroux, and J. L. Steinberg, "Observations du rayonnement galactique sur la longueur d'onde de 33 cm," *Compt. Rend. (Paris)*, vol. 240, pp. 278-280; January 17, 1955.

<sup>27</sup> G. Westerhout, "Continuous radiation from the direction of the galactic center at 22 cm," *Bull. Astron. Inst. Neth.*, vol. 13, pp. 105-109; November 26, 1956.

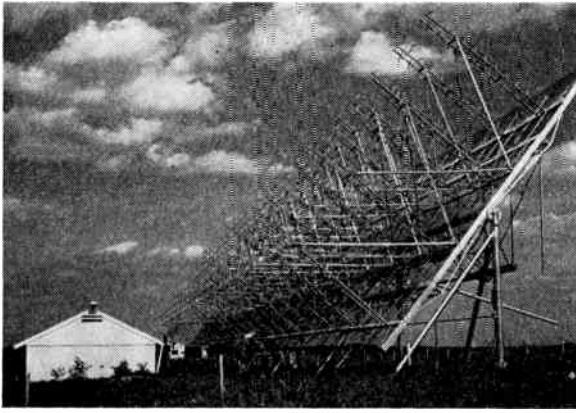


Fig. 1—Photograph of the Ohio State University 96-helix radio telescope. The antenna has a beam approximately 1.2 degrees wide in right ascension and 8 degrees in declination at a frequency of 250 mc. The telescope receiver is housed in the building adjacent to the antenna.

To construct a radio map, it is necessary to measure the brightness temperature variation over the sky. The smallest measurable temperature difference is determined by the receiver sensitivity, while the measurable detail is a function of the antenna resolving power. Because any practical antenna has a beam width that is not infinitely sharp, the true brightness distribution is blurred and the observed distribution is smoother than the true one. The lower the resolving power of the antenna, the greater is the smoothing effect. It has been shown by Bracewell and Roberts<sup>28</sup> that detailed structure less than the half-power beam width is lost because of antenna smoothing and cannot be restored by subsequent graphical or other processes.

Most of the older surveys were made with antennas of large beam widths, the order of 15 to 30 degrees between half-power points. Thus, any detailed structure smaller in angular size than these beam widths did not appear. Recently, several surveys made with antennas of narrow beam widths, the order of 1 to 3 degrees between half-power points, have been published. However, these surveys were either restricted to selected small regions of the sky or made at higher frequencies. It is obvious that radio surveys of large areas of the sky made with antennas of high resolution are of considerable interest and importance. Such surveys would reveal detailed structure of the background radiation and contribute to studies of the galactic structure and origin of the galactic radio radiation.

The results of observations at 1.2-meters wavelength (250 mc) using the high resolution beam of the Ohio State University 96-helix radio telescope will be described first. Some preliminary results of these observations have been presented by Kraus and Ko.<sup>20,29</sup> The present survey covers about 75 per cent of the entire celestial sphere. Radio isophotes of the background ra-

<sup>28</sup> R. N. Bracewell and J. A. Roberts, "Aerial smoothing in radio astronomy," *Aust. J. Phys.*, vol. 7, pp. 615-640; December, 1954.  
<sup>29</sup> J. D. Kraus and H. C. Ko, "A detailed radio map of the sky," *Nature (London)*, vol. 175, pp. 159-161; January 22, 1955.

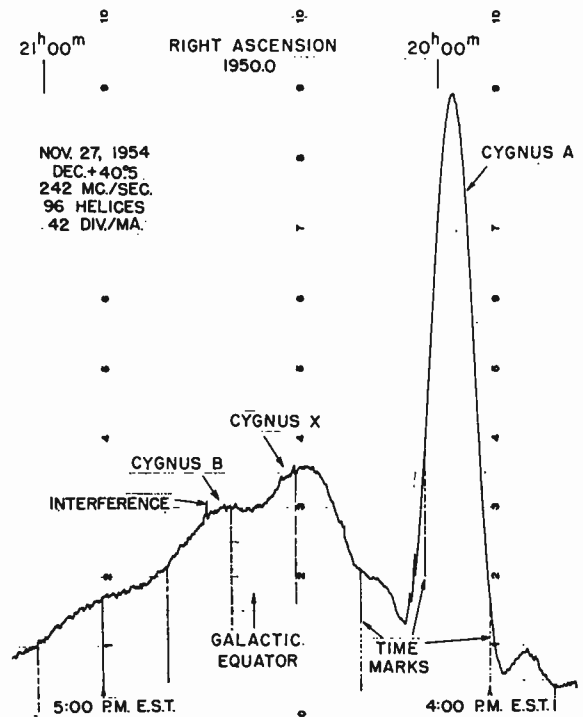


Fig. 2—Sample profile taken with the Ohio State University 96-helix radio telescope in the Cygnus region. The deflections due to the transit of radio stars Cygnus A, Cygnus X, and Cygnus B are shown superposed on the gradual rise due to the general background radiation.

diation are shown by radio maps plotted in celestial and galactic coordinates. The greater resolving power of the antenna has revealed a number of fine features of the background radiation as well as numerous radio stars.

Radio maps made by others at various frequencies are then summarized and comparisons of the 250-mc survey with these maps show a number of interesting features.

#### OBSERVATIONS

The Ohio State University 96-helix radio telescope consists of a rectangular array of 96 right-handed helices arranged in 4 rows of 24 as shown in Fig. 1. The antennas are mounted on a ground plane which is 160 feet long by 22 feet wide. The entire array pivots on a horizontal east-west axis and operates as a meridian transit-type instrument. The antenna pattern is fan-shaped, with a half-power beam width of 1.2 degrees in right ascension and 8 degrees in declination at a frequency of 250 mc. The directivity is about 2270. The main lobe occupies about 70 per cent of the total beam area, while the rest is distributed among the minor lobes. The receiving system is of the total power type.

The observations were made by setting the antenna at a fixed declination, a narrow zone of declination being swept out by the antenna beam as the earth rotates. The power intercepted is recorded as a function of right ascension. The measurements were repeated at four degree steps in declination until a sufficient number of good records were obtained at each step. The sky survey

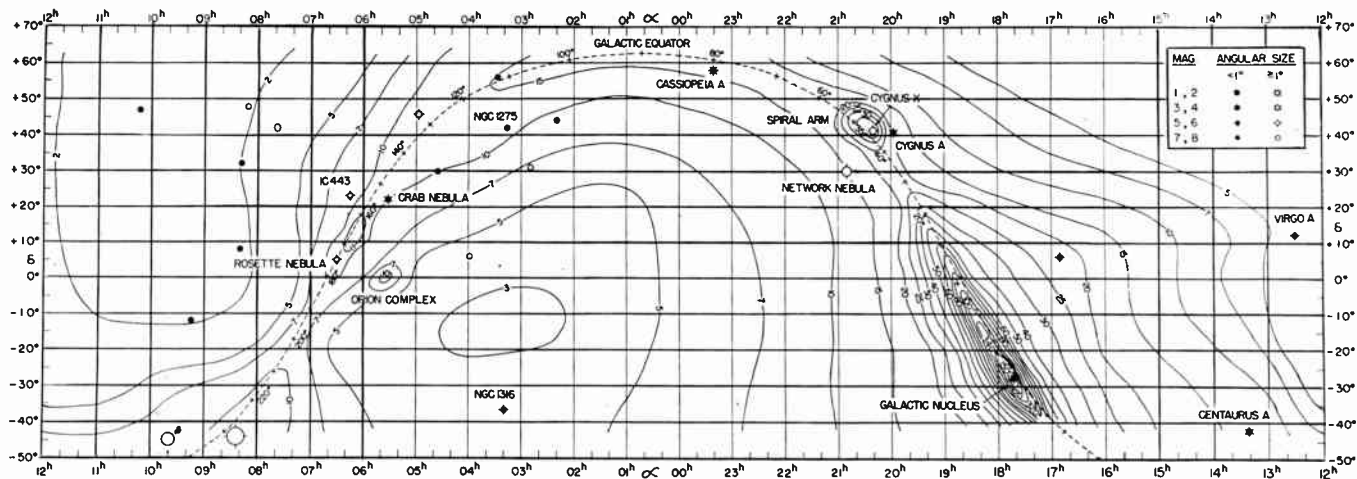


Fig. 3.—Radio map of the sky in celestial coordinates made with The Ohio State University 96-helix radio telescope at 250 mc. The contours show the radio brightness of the sky background radiation while the small circles indicate the location of radio stars.

extends from about Dec.  $-40^\circ$  to  $+60^\circ$ , covering about 75 per cent of the whole celestial sphere.

In general, radio profile at each declination consist of abrupt humps due to the presence of radio stars and more gradual elevations of the background where the galactic equator is crossed. Fig. 2 is a sample profile obtained at a declination of  $+40.5^\circ$  between right ascension  $19^{\text{h}}40^{\text{m}}$  and  $21^{\text{h}}10^{\text{m}}$ , showing radio stars Cygnus A, Cygnus X, and Cygnus B as well as a general background rise. The narrow antenna beam has successfully separated the detailed feature of this complex region. Scores of such profiles taken at different declinations were then combined to produce the radio map. In constructing the map, the humps on the profiles due to radio stars were removed, so that the contours show only the continuous background radiation.

The resulting map is shown in Fig. 3, which consists of contours of equal brightness plotted directly in celestial coordinates (Epoch 1950). The numbers on the contours in the map give the radio brightness temperature increase in units of  $6^\circ\text{K}$  above the base sky temperature corresponding to the coldest part of the sky. The accurate measurement of this base temperature is very difficult because of its low value. Our measurements indicate that it is about  $80^\circ\text{K} \pm 30^\circ\text{K}$ .

During the survey, a number of radio stars were also detected. The presence of a radio star is noted as an abrupt hump on the recorded profile as shown in Fig. 2. If the radio star is a point source, the signature on the record is a direct measure of the antenna pattern. For a radio star of large angular extent (radio nebula), a broadening of the antenna pattern is observed. The detection of radio stars becomes very difficult if the stars are superposed on a steep continuous background rise. This masking effect is pronounced near the galactic equator, especially in the regions near the galactic center. The positions of intense radio stars detected are shown in the map by solid dots for the localized radio stars (angular extent less than  $1^\circ$ ) and open circles for

the extended radio stars (angular extent  $1^\circ$  or more). The magnitude scale has been arbitrarily chosen so that the first magnitude corresponds to a flux density of  $10^{-22}$  watts/m<sup>2</sup>/cps. (1 magnitude = 4 db.)

#### DISTRIBUTION OF CONTINUOUS BACKGROUND RADIATION AT 250 MC

Fig. 4 is a map of the continuous background radiation at 250 mc plotted in galactic coordinates.<sup>30</sup> The contours give the absolute brightness temperature in degrees Kelvin.

The general features of the contour lines are similar to those shown in earlier surveys by others. The radio isophotes show a concentration along the galactic equator. As a function of galactic longitude, the brightness temperature increases toward the galactic center and shows a general decrease toward the galactic anti-center. The position of the highest brightness temperature lies very close to that of the galactic center. There are also a number of details which were not disclosed in the earlier surveys. Thus, the minimum or col along the galactic equator does not occur at a galactic longitude  $148^\circ$ , which is the direction of the anticenter, but at about galactic longitude  $193^\circ$ . The degree of concentration of isophotes toward the equator and also toward the galactic center is much greater than that previously obtained by low-resolution antennas at neighboring frequencies.

The distribution of the radiation may be conveniently divided into three distinct subsystems:

- 1) a narrow, bright belt of radiation about  $3^\circ$  wide lying in the galactic plane and concentrated towards the galactic center,
- 2) a very broad band of radiation concentrated within about  $15^\circ$  to  $30^\circ$  of galactic latitude, and
- 3) an approximately spherical component distributed in the whole celestial sphere.

<sup>30</sup> Based on the galactic pole, R. A.  $12^{\text{h}}40^{\text{m}}$ , Dec.  $+28^\circ$  (1900).

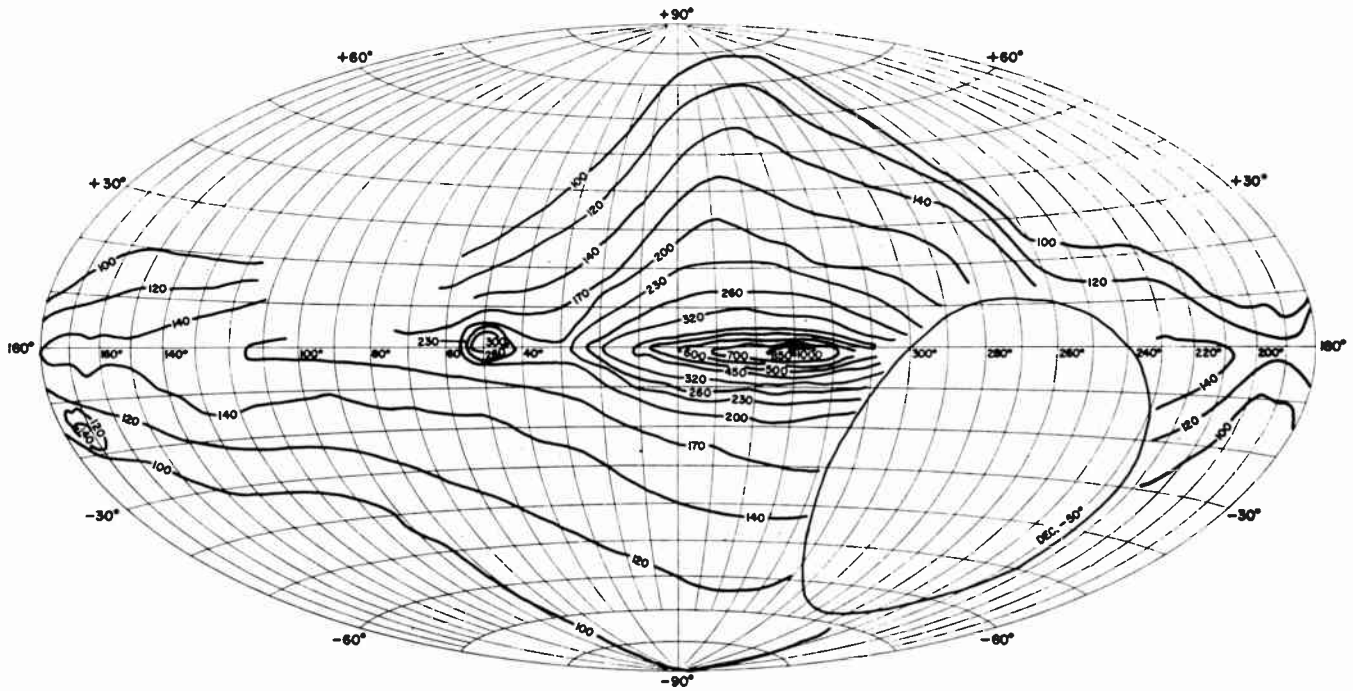


Fig. 4.—250 mc radio isophotes of the general background radiation in galactic coordinates. The numbers on the contours give the absolute brightness temperature in degrees Kelvin.

The latitude of the ridges of maximum brightness temperature in the isophotes shows a significant bias to the south of the galactic equator at both galactic center and anticenter regions. The amount of bias varies with galactic longitude and reaches several degrees at certain places. This indicates that the radio galactic plane is biased to the south of the optical galactic plane and, in addition, the radio galactic pole is tilted from the Lund pole.

Similar effects also have been noted by Piddington and Trent<sup>25</sup> at 600 mc and by Seeger and Williamson<sup>31</sup> at 205 mc. It also can be seen from Fig. 4 that the width between half-brightness points also changes with galactic longitude.

In addition to the above general features, there have been found a number of irregular structures. These structures have a well-defined boundary of large angular extent, the order of 5 degrees to 15 degrees. Four of them are in the regions of Cygnus, Orion, Vela, and Puppis and are probably a complex of less extended sources. It is significant that these complexes are located near Gould's belt and in the areas rich in diffuse nebulosities, H II regions, and dark nebulas. It is very probable that these complexes belong to some local structural feature in the neighborhood of the sun. Another noteworthy feature of the map is a long finger or peninsula of radiation extending from the galactic equator toward the north galactic pole along galactic longitude 350 degrees. There is also a narrow belt of emission along R. A. 13<sup>h</sup> covering at least from Dec.

−15° to +15°. This belt has been attributed by Kraus and Ko<sup>32</sup> to radiation from the local supergalaxy.

#### RADIO MAPS OF THE SKY AT OTHER FREQUENCIES

Table I lists radio maps of the sky made to date by various workers at different frequencies. These surveys are arranged in order of increasing frequency and other pertinent data are also listed. The list summarizes our present knowledge of the radio sky.

Published radio astronomy observations of continuous background radiation cover frequencies ranging from less than 1 mc up to 1360 mc. Although there are a considerable number of radio maps made at frequencies between 60 mc and 900 mc, there are very few radio maps at lower or higher frequencies.

The presently available radio maps are scattered in a wide variety of publications and are presented in various coordinates (galactic and celestial), different projections (Mercator, Aitoff, etc.), and a variety of units (antenna temperature, sky temperature, brightness, etc.). Thus, intercomparison of these maps is inconvenient and difficult. To show the over-all picture of the radio sky at various frequencies, eight maps have been selected for presentation here. These eight maps cover the frequency range 64 mc to 910 mc and each map covers a reasonably complete area of the whole celestial sphere. To facilitate convenient intercomparison between the maps, they have been modified from their originals so that all are in celestial coordinates (Epoch 1950) and of a uniform size, while the contours give the absolute sky brightness

<sup>31</sup> C. L. Seeger and R. E. Williamson, "The pole of the galaxy as determined from measurements at 205 mc/sec," *Astrophys. J.*, vol. 113, pp. 21-49; January, 1951.

<sup>32</sup> J. D. Kraus and H. C. Ko, "Radio radiation from the supergalaxy," *Nature (London)*, vol. 172, pp. 538-539; September 19, 1953.

temperature in degrees Kelvin. These eight maps are presented in Fig. 5–Fig. 12, on the following page. The size and shape of the antenna beam used on each survey is also shown superposed on each map.

In comparing the maps one must take the instrumental effects involved into account. For example, the brightness temperature measured by an antenna in a particular direction of the sky is not determined by the true brightness temperature in that direction alone, but by a weighted average of the brightness temperature in all the directions over the entire antenna beam. If the antenna beam is sharp enough compared with the variation of the brightness temperature distribution, then the observed brightness temperature is a good approximation to the true brightness temperature of that part of the sky under consideration. On the other hand, the observed temperature may differ from the true one considerably if the antenna beam width is much larger than the variation of the brightness temperature distribution. The same is true for the structure of radio isophotes in the maps. The observed structure is a good approximation of the true one if the antenna beam is sharp compared with the variation of the distribution. In general, the observed structure is smoother than the true one due to poor antenna resolving power. These antenna smoothing effects are most pronounced at the galactic equator and especially near the galactic center where the variation of the distribution is rapid. The degree of these effects depends upon the beam width of the antenna used.

Another factor to be considered in comparing the maps is the limited receiver sensitivity at the higher frequencies. At frequencies above 200 mc, the brightness temperature of the coldest parts of the sky is so low that its accurate measurement becomes very difficult. Thus, in many surveys at the higher frequencies, the relative temperature was measured above the base temperature corresponding to the coldest parts of the sky, but the absolute value of this base temperature was not accurately determined.

The accuracy of the absolute temperature in the maps varies from  $\pm 25$  per cent to  $\pm 50$  per cent. The relative accuracy of each map, or the temperature of one portion of the sky relative to another on a single map, is generally much better, being perhaps in the range of 5 to 20 per cent.

Besides its astronomical value, the radio maps of the sky are useful to radio engineers. The noise level and range of radio and radar equipment may be greatly affected by the amount of galactic noise picked up. The amount is a function of the antenna pattern and the region of the sky in the beam at the moment. By means of radio maps, such as presented here, a radio engineer may be able to make substantial improvements in the range and reliability of radio and radar equipment.

## DISCUSSION

All of the sky surveys have a general similarity, but

they differ in local structure. The general structure of the isophotes may be conveniently represented by symmetrical distributions with respect to the galactic equator and unsymmetrical or irregular distributions. In the following discussion distinctions between the distributions are made only for descriptive convenience and do not imply that each distribution has a different mechanism of radiation. Thus, there are three symmetrical distributions as follows.

1) A narrow, bright belt of radiation about  $3^\circ$  wide lies in the galactic plane and concentrated towards the galactic center. This bright belt dominates the radio maps entirely at frequencies above 400 mc. At lower frequencies, the belt is shown only in the radio maps made with high resolution antennas, such as those at 85.7 mc<sup>33</sup> and 250 mc. It is obvious that radio maps made at low resolution fail to resolve this narrow belt. The existence of this belt was first noted in the interferometer measurements of the galactic plane regions by Scheuer and Ryle.<sup>33</sup> In Shain's map<sup>6</sup> of the galactic center region at 19.7 mc, the radio isophotes show a trough near the galactic plane with a considerable rise in brightness on either side of the trough. The existence of this trough is due to absorption effects of the H II regions near the galactic plane. Thus, the radiation from this belt has both thermal and nonthermal components. However, the relative proportions of these components can not be accurately determined.

2) A very broad band of radiation is concentrated within about  $15^\circ$  to  $30^\circ$  of galactic latitude and has its maximum brightness at the region of the galactic center. The brightness increases rapidly as the frequency decreases and this band dominates the radio maps at frequencies less than about 250 mc. Above 400 mc, this band is very weak. The radiation from this system has a nonthermal spectrum.

3) There is a roughly isotropic component of radiation distributed over the whole celestial sphere. The brightness of this component decreases rapidly as the frequency increases and its spectrum is of nonthermal type. Above 200 mc, the brightness is so low that its accurate measurement becomes difficult.

In addition to these symmetrical distributions, there are a number of unsymmetrical or irregular distributions, as follows:

1) A long finger or peninsula of radiation extending along galactic longitude  $350^\circ$  from the galactic plane towards the north galactic pole is observed in the radio maps at frequencies between 64 mc and 910 mc. This feature is even evident in low-resolution surveys. At 600 mc<sup>25</sup> and 910 mc,<sup>26</sup> this finger becomes shorter and appears as a localized source at galactic coordinates of about  $l=360^\circ$  and  $b=+16^\circ$ .

2) A weak band of emission appears at about  $l=270^\circ$

<sup>33</sup> P. A. G. Scheuer and M. Ryle, "An investigation of the H II regions by a radio method," *Monthly Notices Royal Astron. Soc.*, vol. 113, pp. 3–17; 1953.

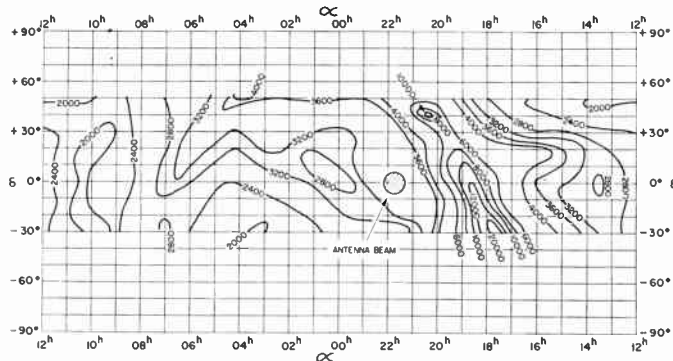


Fig. 5—Map of the radio sky background at 64 mc (after Hey, Parsons, and Phillips<sup>13</sup>). The contours give the absolute brightness temperature of the radio sky in degrees Kelvin.

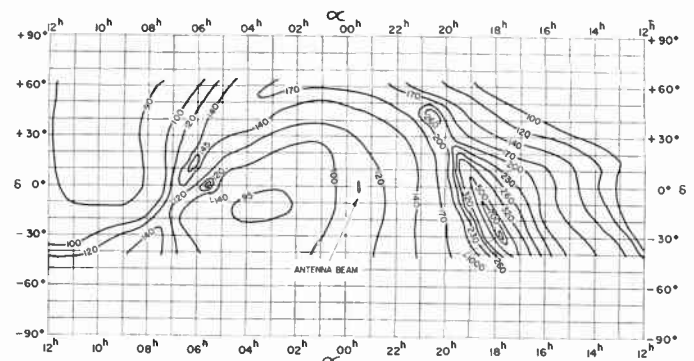


Fig. 9—Map of the radio sky background at 250 mc (after Ko and Kraus<sup>20</sup>). The contours give the absolute brightness temperature of the radio sky in degrees Kelvin.

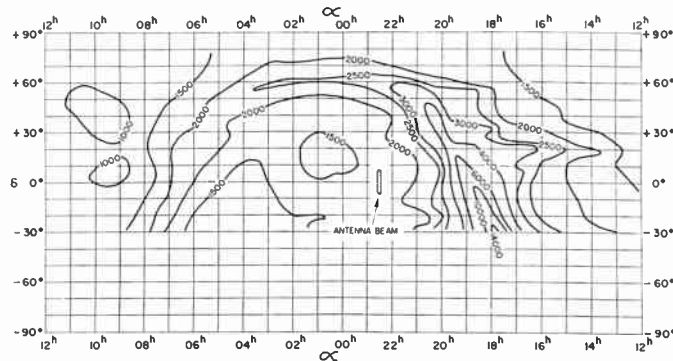


Fig. 6—Map of the radio sky background at 81 mc (after Baldwin<sup>14</sup>). The contours give the absolute brightness temperature of the radio sky in degrees Kelvin.

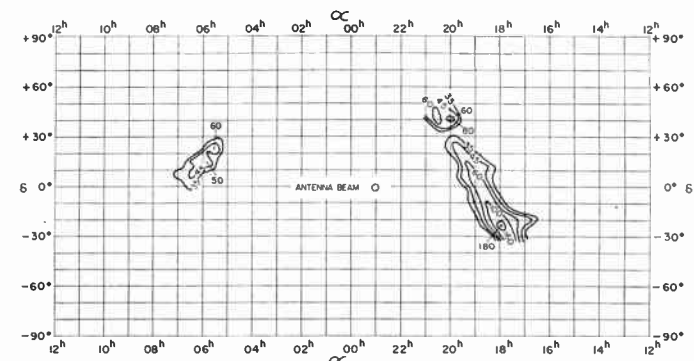


Fig. 10—Map of the radio sky background at 480 mc (after Reber<sup>24</sup>). The contours give the absolute brightness temperature of the radio sky in degrees Kelvin.

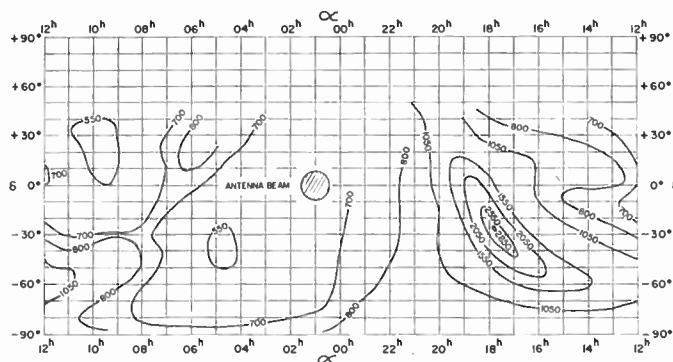


Fig. 7—Map of the radio sky background at 100 mc (after Bolton and Westfold<sup>14</sup>). The contours give the absolute brightness temperature of the radio sky in degrees Kelvin.

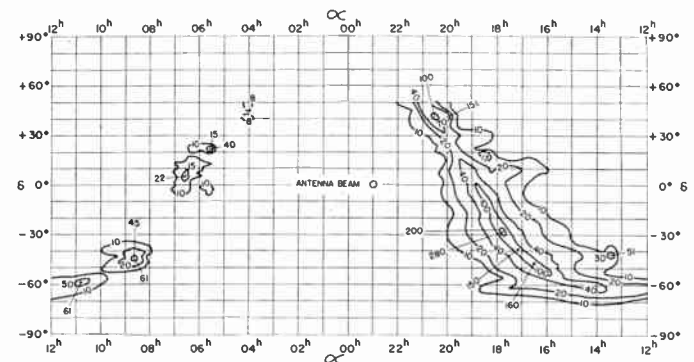
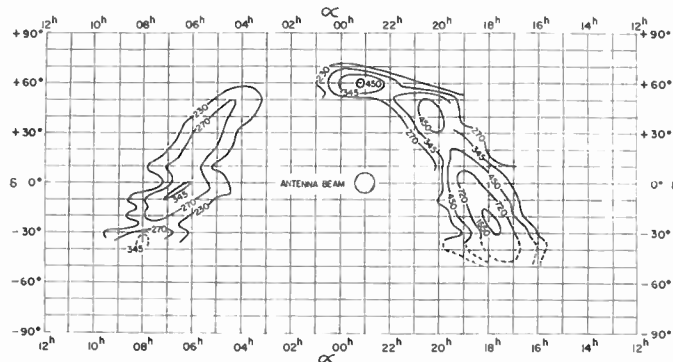


Fig. 11—Map of the radio sky background at 600 mc (after Piddington and Trent<sup>25</sup>). The contours give the absolute brightness temperature of the radio sky in degrees Kelvin.



and  $b = +50^\circ$ . This band has been attributed to radiation from the local supergalaxy. The band is observed at frequencies of 81 mc,<sup>13</sup> 158 mc,<sup>34</sup> and 250 mc.<sup>32</sup>

3) There are large radio complexes in the regions of Cygnus, Orion, Vela, and Puppis. These complexes have an angular extent of 5 to 15 degrees, and appear more prominent in the radio maps at higher frequencies. There is some evidence that these complexes have a thermal spectrum.

4) There are discrepancies between some of the radio maps for a number of localized regions in Taurus, Cassiopeia, Cygnus, Virgo, and Centaurus. There are intense radio stars in these regions and the discrepancies between the maps can mostly be reconciled when allow-

\* R. Hanbury Brown and C. Hazard, "An extended radio frequency source of extra-galactic origin," *Nature (London)*, vol. 172, pp. 997-998; November 28, 1953.

ance is made for the effects of antenna smoothing and the spectra of the radio stars.

It can be shown that these distributions are incompatible with the existing radio models of the galaxy, derived only from low-resolution surveys. A detailed study of this problem will be presented later.

#### ACKNOWLEDGMENT

The author is indebted to Professor John D. Kraus for his continued help and advice and to Donn Van Stoutenburg for maintaining the radio telescope equipment. This work was aided in part by grants from the development fund and the fund for basic research of the Ohio State University, grants from the National Science Foundation, and by support from the U. S. Air Force Cambridge Research Center (Electronics Research Directorate) received through a contract with the Ohio State University Research Foundation.

# A Galactic Model for Production of Cosmic Rays and Radio Noise\*

L. MARSHALL†

## PART I

RECENTLY, radio surveys of several galaxies at 3.5 meters made by Mills<sup>1</sup> have led him to conclude that "intermediate type" galaxies ( $S_b$  and  $S_c$ ), which are those with observable arms, are more efficient emitters of nonthermal radio frequency radiation than other kinds of galaxies. It is the purpose of the present paper to suggest an explanation for Mills' observation, the significance of which has been emphasized by Minkowski.<sup>2</sup> One may assume that all galaxies with spiral arms have magnetic fields along the galactic arms as does our galaxy. It is proposed here that the magnetic field of the spiral arms together with a magnetic halo which is a natural extension of the field of the arms make the parts of a Fermi accelerator for charged particles. Accordingly, galaxies having these two components should accelerate charged particles to energies such that the high energy tail approximates a cosmic ray spectrum and the more numerous lower energy particles account for the radio noise of the galaxy.

\* Original manuscript received by the IRE, November 11, 1957.

† Inst. of Advanced Study, Princeton University, Princeton, N. J.

<sup>1</sup> B. Y. Mills, "The observation and interpretation of radio emission from some bright galaxies," *Aust. J. Phys.*, vol. 8, pp. 368-389; 1955.

<sup>2</sup> R. Minkowski, "Radio sources outside our galaxy," *Sky and Telescope*, pp. 61-62; December, 1957.

## PART II

The presently known features of the magnetic fields of our galaxy include, on the one hand, a magnetic field which runs parallel to the spiral arms of the galaxy and, on the other hand, a magnetic halo more or less spherical which surrounds the entire galaxy. In order to satisfy the condition,  $\text{Div } B = 0$ , these individual parts may be represented respectively as the inner and outer components of a single magnetic entity, the lines of force threading in through one arm and out through the other arm of the galaxy, returning through the halo to the starting point. The simplest representation having these properties is that of a magnetic dipole, and has been proposed previously by Heidmann.<sup>3</sup>

On this assumption, the average magnetic fields of the halo and the galactic arm are approximately related according to  $H_{\text{halo}} \sim H_{\text{arm}} \times 3(r/R)^3 \ln(R/r)$  where  $r$  is the radius of the optically visible galactic spiral and  $R$  is the radius of the halo. The ratio  $r/R$  may be taken as  $1/2$  in which case  $H_{\text{halo}} = (1/4)H_{\text{arm}}$ , about the same ratio as that assumed by Burbidge<sup>4</sup> to account for the observed radio emission of the halo.

<sup>3</sup> J. Heidmann, "Sur un schéma de théorie de l'origine des rayons cosmique," *Compt. Rend.*, vol. 240, pp. 511-513; January, 1955.

<sup>4</sup> G. R. Burbidge, "Halo of radio emission and origin of cosmic rays," *Phys. Rev.*, vol. 101, pp. 906-907; January, 1956.

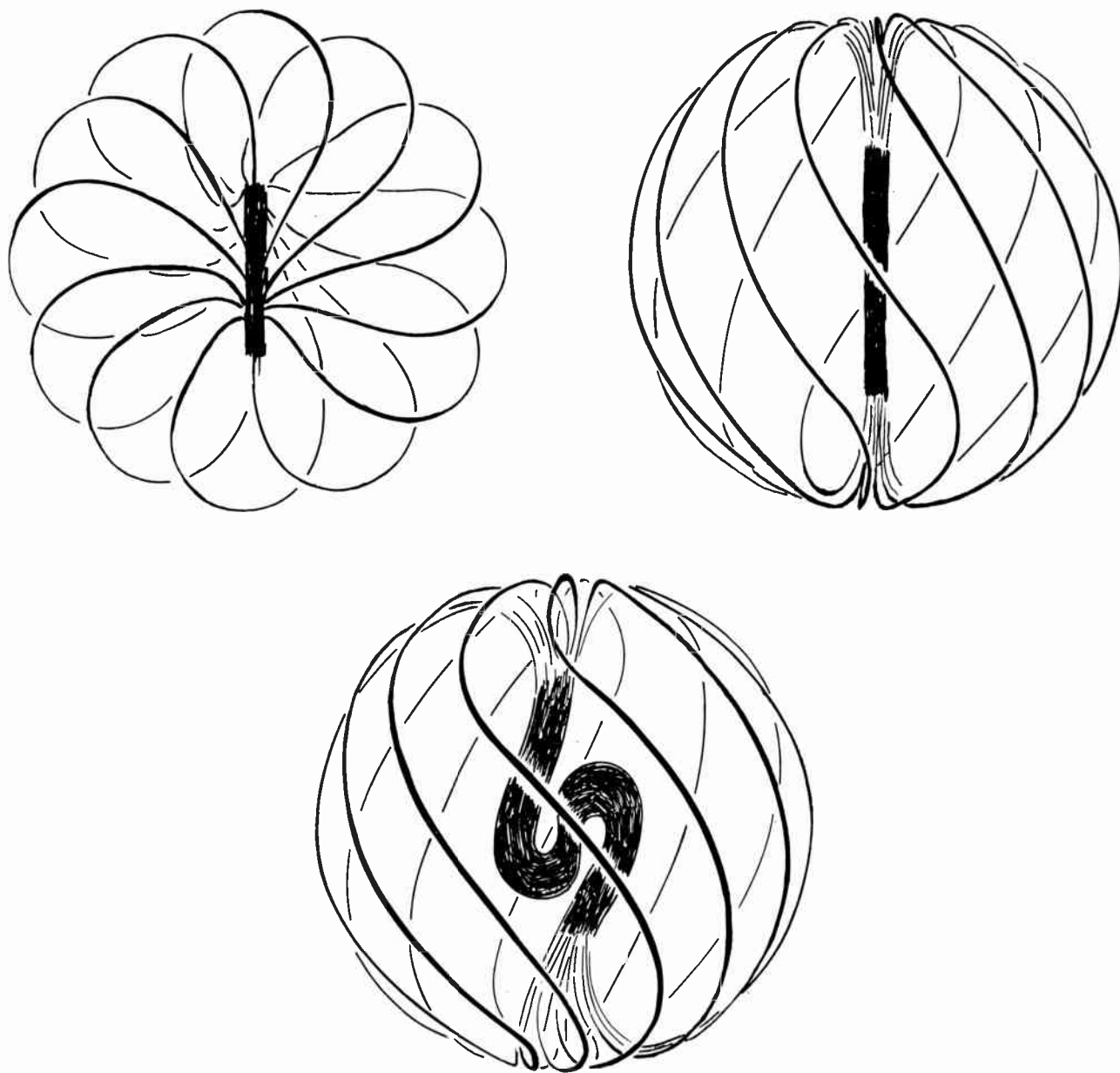


Fig. 1—Three views of a hypothetical galaxy made in the form of a twisted magnetic dipole.

Three drawings of such a magnetic field are shown in Fig. 1, and in Fig. 2, for comparison, three photographs of galaxies show what may be visible parts of halos, NGC 2685, NGC 3718, and M 81. It is assumed that differential rotation of the spiral arms has twisted the lines of force of the original dipole into a spiral, and the resulting deformations extend also into the halo. Consider a galaxy having a differential rotation such that the arms trail, *i.e.*, such that the velocity of rotation first increases as a function of radius and then decreases. The effect of galactic rotation on any initial magnetic lines of force is to stretch them azimuthally, *i.e.*, build an azimuthal component of  $H$ . Consequently after a few rotations the direction of  $H$  lies along the arm of the galaxy. This feature is in agreement with the interpretation of experimental observations on our galaxy.

Each arm of the galaxy is now a magnetic mirror, the lines of force diverging from the galactic center toward the halo, with a pitch of about  $5^\circ$  for many galaxies. In addition, because the differential rotation of the Milky Way galaxy is in such a direction that its arms are winding up,<sup>5,6</sup> the divergent lines of force of the magnetic mirrors are folding together with time. Consequently, a charged particle trapped in the arm sees the mirror moving toward it with a velocity which is the differential of

<sup>5</sup> H. C. van de Hulst, C. A. Muller, and J. H. Oort, "The spiral structure of the outer parts of the galactic system derived from the hydrogen emission at 21 cm wavelength," *Bull. Astron. Inst. Neth.*, vol. 12, pp. 117-149; May, 1954.

<sup>6</sup> K. K. Kee, C. A. Muller, and G. Westerhout, "The rotation of the inner parts of the galactic system," *Bull. Astron. Inst. Neth.*, vol. 12, pp. 211-222; December, 1954.

the velocity of galactic rotation with respect to radius, namely  $\sim 1 \times 10^6$  cm.

For at least one other galaxy, namely NGC 253, there is evidence<sup>7</sup> that the galaxy is winding up, that is, that the arms are trailing. It is perhaps not unjustified to assume that all galaxies with well-defined arms are winding up and have magnetic fields directed along the arms, and therefore they have moving magnetic mirrors as an intrinsic feature of their structure.

A recent report<sup>8</sup> of a violet shift of the 21-cm radio signal from the galactic halo may be interpreted as indicating motion of lines of force of the halo toward the plane of the galaxy. According to the present model, this effect tentatively may be caused by winding up of the lines of force in the arms. An amplification of this statement is given in the Appendix. In this case, an upper limit can be set for kinetic energy density of matter in the halo in order that the drag caused by inertia of matter be insufficient to stretch the lines of force. This limit is  $\frac{1}{2}\rho v^2 \sim (2 \times 10^{-6} \text{ Gauss})^2 / 8\pi = 0.16 \times 10^{-12} \text{ ergs/cm}^3$ , namely less than 1/10 of that in the disk.

In addition, a lower limit may be set for the flux of electrons, in order that hydrogen atoms shall be coupled to and therefore forced to move with the velocity of the lines of force, the coupling resulting from collision with electrons circling around the lines of force. This limit is given by the requirement that the probability for 2000 collisions in  $\sim 10^9$  years be  $> 1$ , where the factor,  $2000 = m_e / M_p$ , is the number of collisions for an electron to exchange energy with a proton. Assuming an electron-atom cross section of  $10^{-14} \text{ cm}^2$ , the required flux is  $N_e v > 2000 / (3 \times 10^{16} \text{ seconds}) \sigma = 6 \text{ electrons/cm}^2$ .

Looked at in somewhat finer detail, this tentative interpretation requires that at intermediate galactic latitudes some parts of the halo shall show a red shift and others a violet shift. Fig. 3(b) shows a schematic map of the plane of the galaxy with representative lines of force winding into the galactic arm. The 21-cm signal from hydrogen tied to the magnetic field should be red shifted or blue shifted depending whether the line of force at the particular position in question is being moved relatively away from the sun or toward the sun by the winding up process. Namely, hydrogen at positions 1 and 4 should show a blue shift, as the winding pulls them closer to the sun. On the other hand, hydrogen at positions 2 and 3 should show a red shift because these lines are winding up into the arm at a radius from the galactic center greater than that of the sun. Consequently, hydrogen at positions 2 and 3 has a smaller rotational velocity than does the sun and therefore gradually moves away from it. These features are in agreement with observations of 21-cm radiation at galactic latitudes of  $\pm 15^\circ$  to  $\pm 40^\circ$  which were reported in the work

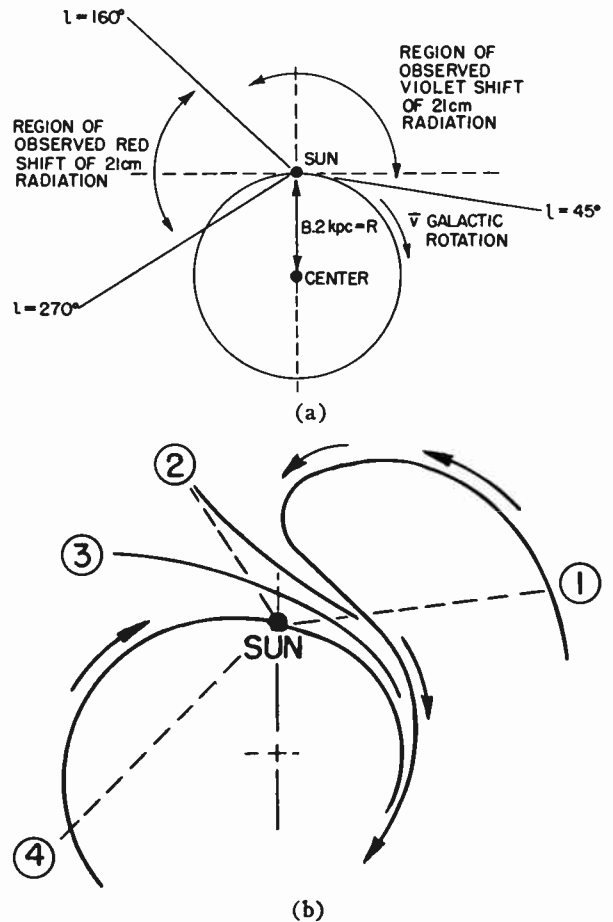


Fig. 3—Plan view of galaxy showing regions of red and violet shifted 21-cm signal as a function of galactic longitude.

of Matthews<sup>9</sup> and Westerhout.<sup>10</sup> At galactic longitude  $45^\circ$  to  $160^\circ$  Matthews observed a violet shift [see Fig. 3(a)] of up to  $\sim 30$  km. This effect can be understood in Fig. 3(b) as resulting from movements of lines of force like No. 1 toward the position of the sun. Furthermore he observed from galactic longitude  $170^\circ$  to  $270^\circ$  a red shift of up to  $\sim 60$  km which in Fig. 3(b) can be represented as resulting from movements of hydrogen tied to lines of force No. 2 and No. 3, rotating more slowly than the sun and therefore gradually moving away from it.

The violet shift to be expected from lines of force like No. 1 and No. 4 at those positions where they are approximately perpendicular to a radius vector to the sun is given by  $V_{\text{blue}} = v / 2\pi$  where  $v$  is the velocity of winding up of the line of force. Taking  $v$  as  $\sim 200$  km from which it follows that  $V_{\text{blue}} = 30$  km. The red shift for lines of force No. 2 and No. 3 is given by  $V_{\text{red}} = v \sin \theta$  where  $\theta$  is the angle between the radius vectors from the center of galaxy to the sun and from the sun to hydrogen at positions 2 or 3; e.g. for  $0 \sim 70^\circ$ ,  $V_{\text{red}} = 60$  km.

<sup>9</sup> T. A. Matthews, "Distribution of Neutral Hydrogen between Galactic Longitudes  $60^\circ$  and  $135^\circ$ ," Harvard Univ., Cambridge, Mass, Doctoral dissertation; 1956.

—, private communication; 1957.

<sup>10</sup> G. Westerhout, "Progress report on 21 cm research," in "Radio Astronomy," H. C. van de Hulst, ed., Cambridge University Press, Cambridge, Eng., pp. 22-28; 1957.

<sup>7</sup> D. S. Evans, "The sense of rotation of NGC 253," *M.N.*, vol. 116, pp. 659-661; May, 1956.

<sup>8</sup> H. L. Helfer and H. E. Tatel, "Preliminary 21-cm meridian plane surveys," *Astrophys. J.*, vol. 121, pp. 585-603; 1955.

If further experimental evidence sustains this very tentative viewpoint, it may enable one to map the direction of lines of force of the halo and their connection to the field of the galactic arms.

### PART III

In the galactic arm, the moving magnetic mirror makes one half of a Fermi accelerator for cosmic rays, the other half of which is formed by fluctuations in magnetic lines of force, *i.e.*, the Alfvén waves, produced by disturbances in the halo, and traveling into the magnetic mirror along the connecting lines of force. The main source of energy for production of the necessary disturbances in the halo is probably that very hydrogen which the 21-cm radiation observations show to be mainly moving in toward the plane of the galaxy, according to the present hypothesis having recoiled from collision with electrons circling around the lines of force of the halo. Presumably, the hydrogen gas exists in clouds of all sizes less than the dimensions of the halo, producing on this account Alfvén waves of corresponding wave lengths and amplitudes in the recoiling magnetic field lines of the halo. Because the present model provides that the energy for production of cosmic rays in the galaxy comes directly from kinetic energy of hydrogen clouds, the cosmic ray energy density in the entire galaxy can be estimated from the requirement that it shall not exceed the kinetic energy density of hydrogen in the halo, the upper limit for which we shall take from Part II, namely  $<0.16 \times 10^{-12}$  ergs/cm<sup>3</sup>, *i.e.*, at least 10 times smaller than the energy density of cosmic rays in the galactic arms.

The Fermi cosmic ray accelerator implicit in this model and composed of the two kinds of magnetic mirrors moving against each other has two attractive features. One point is that the rate of gaining energy is first order in the quantity  $a = (V_{\text{mirror}}/v_{\text{particle}})$  because all collisions are head on. The Alfvén waves are of all sizes (presumably even up to  $\sim 1/10$  radius of halo  $\sim 2$  kpc); consequently, although an energetic particle moving out of the arm may penetrate several waves as it spirals along a line of force, eventually it meets a wave of sufficient amplitude to reverse it and reflect it back into the arm.

A second point is that the average distance between the two opposing mirrors is small, essentially because every Alfvén wave travels into the arm as far as it may until it is damped out by ion atom collision. The result is that the heavy ions of cosmic rays can be accelerated in a distance short compared with  $L$ , their mean free path for nuclear collision, thus removing the well-known difficulty of acceleration of heavy nuclei. It follows from this model that cosmic ray particles are accelerated for the most part in the galactic arms and remain there during their life. Accordingly the radio signal from synchrotron radiation should be strongest in the arms and center of the galaxy. To a large extent only the most energetic particles are able to penetrate the bar-

rage of Alfvén waves to reach the outer halo, a feature which fits with the suggestion of Burbidge<sup>11</sup> that the radio noise of the halo is produced mainly by electrons made in the halo in nuclear collisions of cosmic rays of 1–100 bev with interstellar hydrogen. All his arguments and conclusions may be taken directly into the framework of this model, excepting his postulate that the energy density of cosmic radiation of the halo shall be equal to that in the galactic disk. Instead, in this framework, that for the halo must be reduced at least by a factor 10.

According to the well-known Fermi cosmic accelerator hypothesis, the rate at which a particle gains energy  $E$  is given by

$$dE/dt = Ea/T_1$$

where  $a = V/v$ ,  $V$  is the mirror velocity or in this case the velocity of incoming Alfvén waves,  $v$  is the particle velocity;  $T_1 = d/v$  is the time for collision with a mirror,  $d$  being the distance between the mirrors. The rate for catastrophic processes which remove a particle from acceleration is given by

$$dN/dt = -N/T_2$$

where  $N$  is the density of particles and  $T_2 = L/v$  is the life time for removal from acceleration,  $L$  being the distance for removal. Then

$$N/N_0 = 1/E \left( \frac{T_1}{aT_2} \right).$$

Plausible numbers such as  $V = H/\sqrt{4\pi\rho} = 1 \times 10^7$  cm for  $H = 10^{-6}$  Gauss and  $\rho = 10^{-27}$  grams/cm<sup>3</sup> in the halo, and  $d = 5 \times 10^{18}$  cm for average distance between mirrors, are consistent with increase of energy by  $10^{10}$  in  $10^6$  years. To agree with the experimentally observed cosmic ray spectrum one requires that  $T_1/aT_2 = 1.5$  from which it follows that for high energy particles with  $v \sim c$  the catastrophic mean free path is  $L = cT_1/1.5a = c/1.5V = (3 \times 10^{10})(5 \times 10^{18})/1.5 \times 10 \sim 10^{22}$  cm. This length is small compared with the mean free paths for nuclear collision for protons,  $5 \times 10^{25}$  cm, and for Fe nuclei,  $4 \times 10^{24}$  cm.<sup>12</sup> Consequently the heavy nucleonic component may have the same energy spectrum as does the protonic component, provided that the catastrophic lifetime  $T_2$  is the same for both.

One may ask what is the nature of the process that removes particles from the accelerator in a distance of  $10^{22}$  cm. On the one hand it may be leakage along the lines of force leading to the halo. On the other hand it may be collision with a hypothetical region of high density at the very center of the galaxy. The mass required such that essentially all cosmic rays entering the region make  $n$  catastrophic collisions is  $\sim 100$  grams/cm<sup>2</sup>, and if spread over a length  $\sim 300$  parsecs gives a density of  $6 \times 10^4$  hydrogen/cm<sup>3</sup> and a total mass of  $100 \times (10^{21})^2$

<sup>11</sup> G. R. Burbidge, "Galactic radio emission and the energy released in nuclear collisions of primary cosmic-ray protons," *Phys. Rev.*, vol. 103, pp. 264–265; July, 1956.

<sup>12</sup> P. Morrison, S. Olbert and B. Rossi, "The origin of cosmic rays," *Phys. Rev.*, vol. 94, pp. 440–453; April, 1954.

$= 10^{44}$  grams. This is about equal to one half the total mass of the galaxy and would require to be atomic or molecular gas or dust, *i.e.*, of small dimension, a somewhat awkward stipulation. Such catastrophic collisions, however, would produce a large number of electrons, in agreement with the strong radio signal observed from the galactic center.

Calculations of Piddington<sup>13</sup> and Cowling<sup>14</sup> show viscous damping of Alfvén waves in the halo to be negligible; *i.e.*, for  $H = 7 \times 10^{-6}$  Gauss,  $\rho = 10^{-3}$  atom/cm<sup>3</sup>, at 100°K, for amplitudes  $\sim 5$  pc the damping time is  $\sim 10^{18}$  years. The damping caused by charged particle acceleration is almost certainly greater, but an estimate of its magnitude depends on an estimate of leakage from the arms.

#### APPENDIX

A proof that winding up of the magnetic lines of force of the arms must cause the lines of force in the halo to be reeled in, *i.e.*, shortened, is not known to the author. But a plausibility argument can be made from the fact that a galactic arm with magnetic field directed along the arm is stable against elongation. Using arguments similar to those of Chandrasekhar and Fermi,<sup>15</sup> this is readily shown for a section of cylinder containing a magnetic field parallel to its axis, and containing incompressible matter uniformly distributed. The section of cylinder is stable against elongation in this case because such a deformation increases both its magnetic energy and its gravitational energy.

The flux in the section of cylinder, of original radius  $R$  and magnetic field  $H_0$ , is  $\pi R^2 H_0$ . We require the flux to stay constant as the cylinder is elongated, a condition which gives a relation between initial and subsequent magnetic field, that is,  $H_0 \pi R^2 = H \pi (R - \epsilon)^2$ , where  $\epsilon$  is the decrease in radius accompanying an elongation  $l$  for a section of cylinder of original length  $L$ .

We require the volume to remain constant, namely  $\pi (R - \epsilon)^2 (L + l) = \pi R^2 L$ , which means  $l/L = 2(\epsilon/R)$ . The initial magnetic energy is given by

$$M_0 = 2 \int_0^R \int_0^L (H_0^2/8\pi) \pi r dr dz = (H_0^2/8\pi) \pi R^2 L$$

and after elongation the magnetic energy is

$$\begin{aligned} M &= 2 \int_0^{R-\epsilon} \int_0^{L+l} (H^2/8\pi) \pi r dr dz \\ &= (H_0^2/8\pi) \pi R^2 (L+l) = M_0 (1+l/L). \end{aligned}$$

<sup>13</sup> J. H. Piddington, "Solar atmospheric heating by hydromagnetic waves," *M.N.*, vol. 116, pp. 314-323; January, 1956.

<sup>14</sup> T. G. Cowling, "The dissipation of magnetic energy in an ionized gas," *M.N.*, vol. 116, pp. 114-124; November, 1956.

<sup>15</sup> S. Chandrasekhar and E. Fermi, "Problems of gravitational energy in the presence of a magnetic field," *Astrophys. J.*, vol. 118, pp. 116-141; 1953.

The increase in magnetic energy corresponding to fractional elongation  $l/L$  is  $M = (l/L) M_0 = 2(\epsilon/R) M_0$ .

It may be seen immediately that elongation of the cylinder causes the gravitational energy term to increase also. That is, the process of elongation of the cylinder, if it is elongated to infinity, is the process of removing the particles in the cylinder infinitely far from each other along the  $z$  axis, against their gravitational forces.

Thus, work must be done on the system to produce such an elongation, work both against the gravitational forces and against the magnetic forces. On the contrary however, if the cylinder contracts its length, potential energy of both magnetic and gravitational fields is converted to kinetic energy. In the arm where kinetic energy dominates, the differential rotation of the galaxy forces the arms to elongate and forces kinetic energy of rotation to be converted to magnetic energy of a field directed along the arms. In the halo, if the magnetic field energy dominates as has been assumed here, then the system moves in such a way that lines of force shorten and magnetic energy is converted to kinetic energy.

#### PART IV

The galactic model discussed here 1) provides an explanation for the experimental observation that galaxies with well-defined arms are radio emitters, 2) offers a tentative explanation for the sign and magnitude of the observed red and violet shifts of the 21-cm radio signal from the halo, 3) requires that the nonthermal radio signal from the arms is stronger toward the center of the galaxy, and 4) provides that the magnetic field direction of the arm should be parallel to the galactic arm after the galaxy has made a couple of turns. It postulates the same ratio of fields for halo and disk as those found by Burbidge to explain the observed radio noise. It provides for the acceleration of cosmic rays as a direct result of the structure of the magnetic fields in the spiral arms, and removes the previously existing difficulty with acceleration of the heavy nucleonic component. It provides that kinetic energy of matter moving other than in the galactic plane shall be converted to cosmic rays. On the other hand, this model seems to offer no intrinsic explanation for the nature of the process required to remove particles from the Fermi cosmic ray accelerator.

#### ACKNOWLEDGMENT

The author is grateful for the hospitality of the Department of Astronomy of California Institute of Technology during the course of this work, and for many informative conversations, in particular for those with L. Davis and J. Greenstein.



# Absorption Techniques as a Tool for 21-CM Research\*

A. E. LILLEY† AND E. F. McCLAIN‡, SENIOR MEMBER, IRE

**Summary**—Hyperfine transitions between the  $F=0$  and  $F=1$  levels of interstellar hydrogen gas have been observed to produce absorption lines in the spectra of radio stars. Elementary relations are developed which describe the action of an  $L$  band radiometer connected to an antenna, if the antenna is viewing an assembly of gas which is illuminated by a radio star. The consequences of the absorption line studies are reviewed. They include: high resolution studies of the interstellar gas, the structure and physical state of interstellar HI regions, minimum distances to radio stars, and experiments of interest in cosmology.

## INTRODUCTION

EARLY efforts in radio astronomy were concerned primarily with radiation from the Sun, the Milky Way, and certain of the stronger discrete radio sources. In all cases the radiation studied was, in effect, broad-band noise or continuum radiation. In some instances the radiation has a flat spectrum, in others, the intensity per unit bandwidth is an inverse function of the frequency. Such radiation, while yielding valuable information regarding the physics of the generating body, nevertheless possesses limitations as far as dynamical studies of these objects in their environment are concerned. A spectral line was required which would permit investigations in radio astronomy, based on the Doppler effect, similar to those which had been employed by optical astronomers. The paper by van de Hulst in 1945, which predicted the existence of line radiation from the neutral hydrogen atom, was the first step which led to the present major investigative programs employing the 1420-mc hydrogen line.<sup>1</sup> While the existence of the line was predicted in 1945, it remained for Ewen and Purcell to make the first astronomical measurement of this radiation from a cosmic source.<sup>2</sup> As an indication of the significance which astronomers attached to the existence of this line, scientists in Holland and Australia confirmed the work of Ewen and Purcell within weeks, so that the issue of *Nature* which carried the discovery by Ewen and Purcell also contained the confirmations by the Dutch and Australians. Since the initial discovery in 1951, hydrogen line investigations have accounted for a major part of the effort in radio astronomy.

In their original paper, Ewen and Purcell pointed out that while the hydrogen responsible for 1420 mc radiation has a characteristic or state temperature, the radiation background against which the hydrogen might appear also would have a finite temperature and therefore, the hydrogen might be detected either as an emission line against a cold background or an absorption line seen against a relatively hot background. As it turned out, except for selected regions or positions in the sky, the background radiation is normally cooler than the hydrogen state temperature and the initial detection and much of the subsequent investigation utilized the emission from ground state hydrogen. Notable among the studies based primarily on emission have been the work of Heesch, Lilley,<sup>4</sup> and Menon<sup>5</sup> at Harvard, who were concerned with specific regions of the Milky Way the work of the Dutch investigators who, until recently, have been concerned primarily with mapping the northern Milky Way, and the Australians who, in addition to mapping the southern Milky Way, have made extensive investigations of emission from the Magellanic Clouds.

Early in 1954, Hagen and McClain, at the Naval Research Laboratory, became interested in continuum emission from radio sources at a wavelength of 21 cm just outside the hydrogen emission band.<sup>6</sup> A hydrogen radiometer was employed for the continuum studies and since the radio sources constitute the necessary hot background, the first measurements of hydrogen in absorption were obtained. The initial measurements employed the source in the direction of the galactic center and the radio source Taurus A as sources of background radiation. Almost simultaneously, Williams and Davies made similar studies in the direction of the radio sources Cassiopeia A and Cygnus A.<sup>7</sup> Subsequently, Hagen, Lilley, and McClain, made a detailed study of absorption in the direction of Cassiopeia A which revealed unexpected fine structure in the ab-

\* D. S. Heesch, "Some features of interstellar hydrogen in the section of the galactic center," *Astrophys. J.*, vol. 121, pp. 569-584; May, 1955.

<sup>4</sup> A. E. Lilley, "Association of gas and dust from 21-cm hydrogen radio observations," *Astrophys. J.*, vol. 121, pp. 559-568; May, 1955.

<sup>5</sup> T. K. Menon, "A 21-cm investigation of the Orion region," Doctoral dissertation, Harvard University, Cambridge, Mass.; April, 1956.

<sup>6</sup> J. P. Hagen and E. F. McClain, "Galactic absorption of radio waves," *Astrophys. J.*, vol. 120, pp. 368-369; September, 1954; paper read at joint meeting of URSI, IRE, and AGU (abstr), Washington, D. C.; May, 1954.

<sup>7</sup> D. R. W. Williams and R. D. Davies, "A method for the measurement of the distance of radio stars," *Nature*, vol. 173, pp. 1182-1183; June, 1954.

\* Original manuscript received by the IRE, October 3, 1957.

† Yale University Observatory, New Haven, Conn. Formerly with Radio Astronomy Branch, U. S. Naval Research Lab., Washington, D. C.

‡ Radio Astronomy Branch, U. S. Naval Research Lab., Washington, D. C.

<sup>1</sup> H. C. van de Hulst, *Nederl. Tij. Natuurkunde*, 's-Gravenhage-martinus Nyhoff, vol. 11, p. 201; 1945.

<sup>2</sup> H. I. Ewen and E. M. Purcell, "Observation of a line in the galactic radio spectrum," *Nature*, vol. 168, p. 356; September, 1951.

sorption profile.<sup>8</sup> As will be explained later, these initial investigations, utilizing absorption rather than emission, have resulted in the beginnings of an independent distance scale to the radio sources. In addition, they have opened new studies of astrophysical and cosmological interest.

A block diagram of one type of hydrogen receiver is shown in Fig. 1. Two pass bands are so arranged that one having a width of approximately 2 mc is used as a reference against which to compare a second narrow band which is tuned across the hydrogen line. If such a receiver is connected to a directive antenna and pointed at an isolated hydrogen cloud the hydrogen recorder will display only an emission profile. The height or intensity of the profile is determined by the state temperature of the gas, the number of atoms in the line of sight and the line broadening mechanism. The width is determined primarily by the Doppler effect due to thermal motions and any turbulence which may be present in the cloud. If the cloud possesses gross motions toward or away from the antenna, the center frequency of the profile will of course be shifted to a higher or lower frequency respectively. In this case, with no background radiation field, the comparison band does not see a signal and no indication will be present on the continuum recorder.

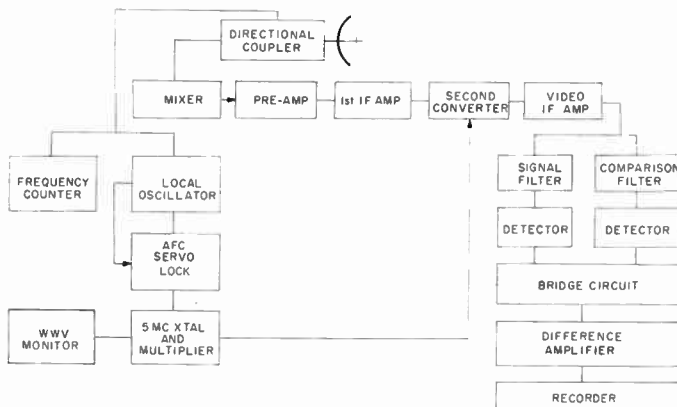


Fig. 1—Block diagram of NRL hydrogen radiometer. The receiver is an L band radiometer employing a crystal mixer and double conversion. Signal and comparison bands provide a comparison of the spectral intensity received by the antenna in two regions of the spectrum. A stable local oscillator is tuned in frequency, translating the signal and comparison bands through the spectrum. The difference in energy received in the two bands is presented at the recorder.

If the same radiometer system is pointed at a discrete radio source or "radio star," the signal and comparison bands will see equal temperatures and the continuum recorder will display the antenna temperature of the radio star, while the hydrogen recorder will indicate zero temperature difference between signal and comparison bands. If one now places a hydrogen cloud behind the radio source, and provided the angular extent of the

radio star is small compared to the antenna beam width, the signal band would receive additional radiation and would plot the true hydrogen profile as the receiver was tuned. The continuum recorder would continue to indicate the antenna temperature of the radio source. The term antenna temperature requires some clarification.

#### ANTENNA TEMPERATURE

In the absorption problem we are confronted with a gaseous medium which is a monochromatic emitter and absorber. Imbedded in this medium are the radio stars which are emitting a continuum of radiation. We will examine some simple relations which govern the action of the interstellar gas on the spectrum of the radio stars.

It is convenient in treating many problems in radio astronomy to make use of "temperatures" by use of the Rayleigh-Jeans formula relating temperature and intensity. The radiation transfer problem can then be treated in terms of temperatures. Both the optical and some radio investigations indicate that radio stars are not uniformly bright in appearance but rather, exhibit a filamentary appearance. The surface brightness of such a radio star may be represented by a temperature distribution  $T(\theta, \phi)$ , the effective temperature presented by the source in an element of solid angle whose position is specified by  $\theta$  and  $\phi$ . Effective temperature is used without specifying whether the radiation mechanism of the source is thermal or nonthermal. By effective temperature is meant the temperature required by a black thermal emitter (having the same geometrical configuration and location as the actual source) in order to produce the same flux observed at the antenna.

With the definition given above for the source, we may write the antenna temperature presented by the source as

$$T_A = \frac{1}{4\pi} \int T(\theta, \phi) G(\theta, \phi) d\omega \quad (1)$$

where  $G(\theta, \phi)$  is the gain function of the antenna over an isotropic radiator.

However, because of the generally small size of radio telescopes, the beam widths in use are quite large compared to the angular sizes subtended by the radio stars. This condition enables us to make use of an average brightness temperature,  $T_B$  and an average solid angle,  $\Omega_S$ , for each source. Then for a particular antenna, the main beam may also be assigned an effective solid angle  $\Omega_B$  and the antenna temperature may be written simply as

$$T_A = T_B \frac{\Omega_S}{\Omega_B} \quad (2)$$

#### THE ABSORPTION EFFECT

If an antenna views a cloud of gas which is spectrally emitting and absorbing microwave radiation (see Fig. 2) then the observed line intensity may be written as

<sup>8</sup> J. P. Hagen, A. E. Lilley, and E. F. McClain, "Absorption of 21 cm radiation by interstellar hydrogen," *Astrophys. J.*, vol. 122, pp. 361-375; November, 1955.

$$T_H(\nu) = T_G(1 - e^{-\tau(\nu)}). \quad (3)$$

$$\Delta T'(\nu) = (T_G - T_B)(1 - e^{-\tau(\nu)}). \quad (6)$$

In (3),  $T_G$  is the temperature which is effective in establishing the population of the two states responsible for the spectral line, and  $\tau(\nu)$  is the opacity of the cloud. The opacity of the cloud may be regarded in one sense as an attenuation factor, *viz.*: if  $I_0$  were the intensity of some extraneous radiation passing through the cloud, then the emergent radiation intensity would be given by  $I_0 e^{-\tau(\nu)}$ .

It is evident from (6) that the relative sizes of  $T_G$  and  $T_B$  determine whether there will result an emission line, no line, or an absorption line.

Profiles produced by hydrogen gas in the interstellar medium are spectrally confined to widths generally less than one megacycle and thus their radiation excites only the signal band of the radiometer.

Most of the radio stars are small in angular extent, however, and (6) must be modified to take this into account. We may still regard the gaseous medium as filling the beam, but we shall assign a solid angle  $\Omega_S$  to the radio star.

Using the diagram shown in Fig. 4, we may again write down the contributions to the signal and comparison bands

$$T_S = T_G(1 - e^{-\tau(\nu)}) + T_B \frac{\Omega_S}{\Omega_B} e^{-\tau_B(\nu)}, \quad (7)$$

$$T_C = T_B \frac{\Omega_S}{\Omega_B}. \quad (8)$$

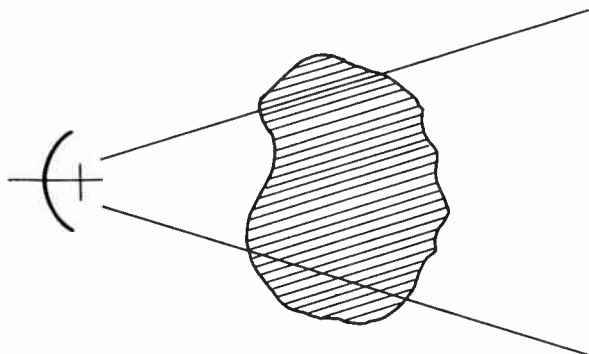


Fig. 2—Antenna viewing an interstellar cloud of hydrogen gas. This is a schematic representation of an antenna viewing a spectrally emitting gas cloud which completely fills the antenna beam.

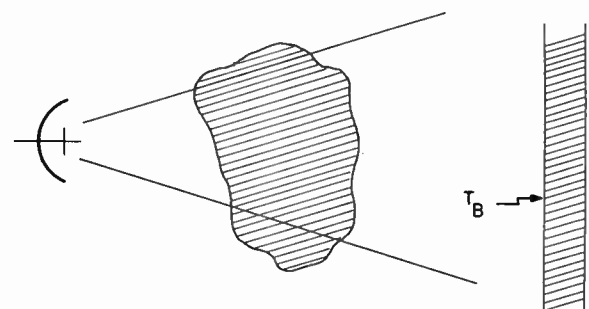


Fig. 3—Antenna viewing an interstellar cloud illuminated by a continuum source. The spectrally-emitting cloud fills the antenna beam and the cloud is illuminated from behind by a continuum source of uniform brightness temperature  $T_B$ .

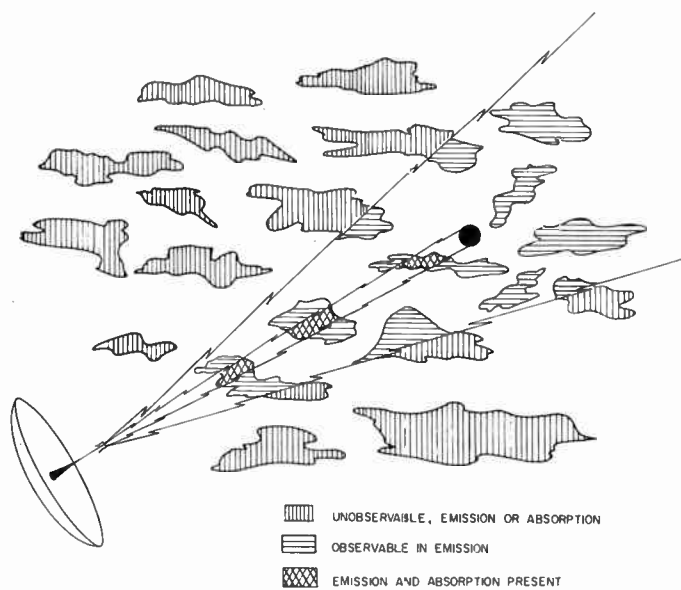


Fig. 4—Antenna viewing an assembly of interstellar gas clouds and a radio star included within the beam. Two beams are evident: the cone subtended by the radio star, and the cone defined by the beam of the antenna. Emission and absorption effects are indicated in the figure.

The gaseous profile can be altered in shape and amplitude from the form given by (3) if the antenna also views a continuum radiation field. Suppose that behind the cloud there exists a uniform radiating source of surface brightness temperature  $T_B$  and that both the cloud and the continuum source completely fill the antenna beam as shown in Fig. 3. We write down the thermal contribution to both the signal and the comparison bands, respectively  $T_S$  and  $T_C$ ,

We distinguish between  $\tau(\nu)$ , the effective opacity spread over  $\Omega_B$ , and  $\tau_S(\nu)$ , that part of  $\tau(\nu)$  which is confined to  $\Omega_S$ . We also replace  $T_G(1 - e^{-\tau(\nu)})$  with  $\overline{\Delta T}(\nu)$  and, because this represents simply the contribution of the gas alone, we call it the expected profile. The expected profile is the profile which would be observed in the absence of the radio star, and may be determined by obtaining profiles from adjacent comparison regions or by drift curves through the source at various fixed frequencies.

$$T_S = T_G(1 - e^{-\tau(\nu)}) + T_B e^{-\tau(\nu)} \quad (4)$$

The difference between (7) and (8) again yields the observed profile,

$$T_C = T_B \quad (5)$$

$$\Delta T'(\nu) = \overline{\Delta T}(\nu) - T_A(1 - e^{-\tau_S(\nu)}). \quad (9)$$

and the difference between (4) and (5) is the quantity displayed by the radiometer, given by

All the quantities in (9) are available through the observational data with the exception of  $\tau_S(\nu)$ . The solution

for this quantity in terms of the observables is

$$\tau_s(\nu) = -\ln \left[ 1 - \frac{\overline{\Delta T'(\nu)} - \Delta T'(\nu)}{T_A} \right]. \quad (10)$$

The absorption data thus permit the determination of the opacity  $\tau_s(\nu)$ , and it is this quantity which contains considerable information of astronomical interest. One of the striking consequences is the angular resolution involved. Because  $\tau_s(\nu)$  is produced by gas confined to the solid angle subtended by the radio star, the resolution is equivalent to truly enormous antennas. Absorption investigations on some of the brighter radio sources present angular resolutions equivalent to antennas having diameters from one-tenth to approximately a full mile. The greatest resolution available to 21-cm research is likely to remain in absorption rather than emission studies.

#### DISTANCE DETERMINATIONS TO RADIO STARS

We shall take the absorption effects observed on the Cassiopeia A radio star to illustrate the problems of distance determination. At wavelengths near 21-cm, Cassiopeia A has the greatest apparent intensity of all the radio stars. This source of radio radiation was identified optically by Baade and Minkowski of Mount Wilson and Palomar Observatories, and a new type of filamentary nebulosity is now known by virtue of their studies.<sup>9</sup>

In addition to their optical studies of the physical processes operating in this new type nebulosity, they have obtained spectra yielding radial velocities and photographs which demonstrate changes of position of the emission filaments, or transverse motions. Statistically combining the position change and radial velocity data, Baade and Minkowski have concluded that the distance to the radio source nebulosity is about 1500 light years.

Now let us examine the Cassiopeia A radio absorption data for distance information. All 21-cm absorption data show the spectrum, and hence the radial velocity distribution, of the absorbing gas. It is the velocity distribution, and in addition, the knowledge that the absorbing gas must lie between the observer and the radio source, which allows one to estimate a *minimum* distance to the radio source by radio observations.

The radio data consist of the intensity distribution of the hydrogen radiation as a function of frequency. The ability to determine distances by means of hydrogen line profiles requires a knowledge of the large-scale dynamics of the interstellar medium, which allows one to interpret radial velocities and hence frequencies as measures of distances. In order to interpret quantitatively the relation between radial velocity and distance-from-the-earth, the gross behavior of the material in the plane

of our own galaxy must be known. The phenomenon of galactic rotation describes the fundamental feature of the large-scale motions of material in the galactic plane.

The interpretations of the hydrogen-line profiles, obtained in the plane of our Milky Way by Dutch and Australian workers, show that the interstellar hydrogen gas is concentrated into spiral arms. These concentrations are revealed by separate maxima in the hydrogen spectrum at particular celestial positions.

The general shape of emission profiles which are observed in directions adjacent to the Cassiopeia A radio star is characterized by two distinct emission maxima as shown in Fig. 5(a). By employing a model of galactic rotation the variation of radial velocity of the interstellar clouds with distance from the sun along a particular line of sight may be predicted. Conversely, if the profile produced by the radio receiver shows maxima at particular radial velocities, the maxima are interpreted as arising from condensations of gas lying in spiral arms located at different distances along the line of sight. On this interpretative basis, the two maxima which characterize the profiles originating in directions near the Cassiopeia A radio source have been assigned distances from the sun. The Dutch group places the most distant of the Cassiopeia region spiral arms at a distance of about 9000 light years. Now the 21 cm profile obtained for the exact direction of the Cassiopeia A source, Fig. 5(b), shows the effects of absorption in both maxima.<sup>8</sup>

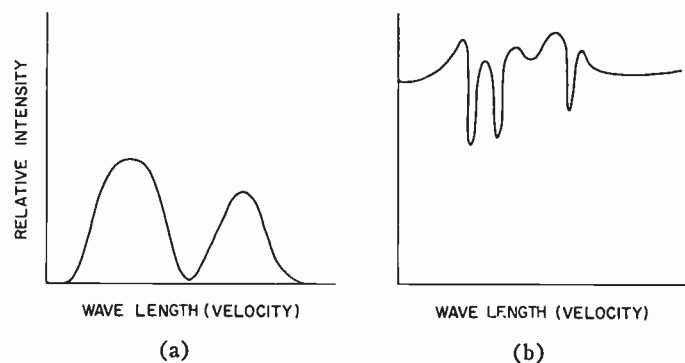


Fig. 5—Behavior of 21-cm profiles in the direction of Cassiopeia A. Profiles obtained in the general direction of Cassiopeia A show a shape characteristic of the curve marked A. (a) Only emission is present. (b) In the exact direction of Cassiopeia A, the profile shows considerable distortion in shape and exhibits absorption features. The higher level of (b) is due to the antenna temperature of the Cassiopeia A source.

Moreover, the absorption profile displays the strongest absorption effects in the frequency interval occupied by the gas which exists in the second and most distant of the two major spiral arms. Immediately there is the reasonable interpretation that the radio source must lie at a distance which is at least as great as the second spiral arm. If there were no other information existing which enabled the distance to the source to be evaluated, the minimum distance to the source of 9000 light years resulting from the radio data would not be disturbing. But the minimum radio distance is a factor of

<sup>9</sup> W. Baade and R. Minkowski, "Identification of the radio sources in Cassiopeia, Cygnus A, and Puppis A," *Astrophys. J.*, vol. 119, pp. 206-214; January, 1954.

six greater than the optically evaluated distance. A recent absorption investigation of the Cassiopeia source by Muller,<sup>10</sup> using the Dutch 83-foot instrument, has verified the principal absorption features and left the radio distance interpretation unchanged.

The distance problem remains unresolved and, until it is clarified, the exact distance to the Cassiopeia A source remains in doubt. The ability of the radio or optical data to provide valid distance information also remains doubtful. Admittedly, the optical determination is based on a statistical study of limited scope imposed by the source itself, but to stretch the optical data to accommodate the minimum radio distance is a stretch whose magnitude is unacceptable to the optical investigators. A factor of two error in the optical distance would still leave the optical distance only one third of the way out to the minimum radio distance. Clearly, one of the distance determinations has an unknown effect which is misleading either the optical or the radio investigations. The vulnerable point of the radio data is clear. All one really knows about the radio absorption effect is that the gas responsible for the absorption lies between the observer and the Cassiopeia A source. If the source is really as close as the optical studies place it, then the radial velocity distribution of the absorbing gas must be given an interpretation which is not straightforward. Two possibilities present themselves. First, we may be dealing with two nearby interstellar clouds which happen to have anomalous radial velocities which are just equal to the value expected from galactic rotation in the second spiral arm. Or second, the absorbing gas may be located very close to the radio source and dynamically associated with it. The random cloud argument is possible, but it also is "special." Gas associated with the source is a possibility but an adequate physical discussion would be complicated. The proximity of the intense radio source would bathe the adjacent hydrogen gas clouds in microwave radiation density of a magnitude much greater than gas clouds normally experience in typical interstellar regions. The presence of the high-radiation density would affect the absorbing properties of the gas, adjusting the state temperature and essentially reducing the attenuating property of the gas. But the opacity is fixed and may be determined with reasonable accuracy from the radio data. Therefore, the amount of gas present on this hypothesis is, for a fixed opacity, greater than the amount needed to produce the same opacity in more normal regions of interstellar space.

Either random nearby clouds or gas physically very near the source with radial motions away from the source could produce an absorption profile which would mislead the radio minimum distance determined by means of a galactic rotation analysis. Whether the radio data have effects such as these involved, or whether

there are unknown systematic dynamical properties of the optical filaments are problems that have stimulated studies presently in process which hopefully will satisfactorily resolve the distance problem.

#### SAGITTARIUS A

One of the most intriguing problems today is the matter of the galactic center region. In this direction the classical model of the galaxy would display no radial velocity and one might expect a narrow intense emission line. Actually, the region exhibits a complex hydrogen emission profile as first pointed out by Heesch.<sup>3</sup> In addition, the region contains an intense discrete source of continuum radiation at longer wavelengths which has been suggested as the galactic center by McGee and Bolton.<sup>11</sup> Investigations of the continuum at cm wavelengths by Haddock and McCullough, and Haddock, Mayer, and Sloanaker suggest the possibility of two sources, one behind the other.<sup>12,13</sup> More recently Mills has obtained additional evidence at 3.5 meters, that the continuum radiation may arise from two regions at different distances and that the nearer source may be an HII or ionized hydrogen region.<sup>14</sup>

The first hydrogen absorption measurement made by Hagen and McClain used the galactic center as a source of background radiation.<sup>6</sup> This measurement employed a receiver bandwidth of 55 kc which was too wide to reveal a great amount of detail subsequently found by McClain using a bandwidth of 5 kc.<sup>15</sup> Fig. 6 shows the expected and observed profiles obtained in the latter experiment using the NRL 50-foot antenna. The extent of the absorption features in velocity was compared with the angular extent of the gas at various velocities and a distance scale assigned to the hydrogen profile. This treatment of the data indicated the probable existence of a continuum source at a distance between 2 and 6 kiloparsecs (kpc) with a most probable position at 3.4 kpc but did not exclude the possibility of an additional weak source at a greater distance. Measurements by Williams and Davies, utilizing a somewhat different absorption technique, also suggest the existence of an HII region at approximately 3 kpc.<sup>16</sup>

Dutch investigators utilizing the absorption technique in combination with their new 83-foot antenna have recently published a partial profile of the galactic

<sup>11</sup> R. X. McGee and J. G. Bolton, "Probable observation of the galactic nucleus at 400 mc," *Nature*, vol. 173, pp. 985-987; May, 1954.

<sup>12</sup> F. T. Haddock and T. P. McCullough, "Extension of radio source spectra to a wavelength of 3 cm," *Astrophys. J.*, vol. 60, pp. 161-162; June, 1955.

<sup>13</sup> F. T. Haddock, C. H. Mayer, and R. M. Sloanaker, "Radio emission from the Orion nebula and other sources at 9.4 cm," *Astrophys. J.*, vol. 119, pp. 456-459; March, 1954.

<sup>14</sup> B. Y. Mills, "The radio source near the galactic center," *Observatory*, vol. 76, pp. 65-67; April, 1956.

<sup>15</sup> E. F. McClain, "An approximate distance determination for radio source Sagittarius A," *Astrophys. J.*, vol. 122, pp. 376-384; November, 1955.

<sup>16</sup> R. D. Davies and D. R. W. Williams, "An alternative identification of the radio source in the direction of the galactic center," *Nature*, vol. 175, pp. 1079-1081; June, 1955.

<sup>10</sup> C. A. Muller, "21 cm absorption effects in the spectra of two strong radio sources," *Astrophys. J.*, vol. 125, pp. 830-834; May, 1957.

center region exhibiting an absorption feature in the blue wing at  $-50$  km. This investigation by Woerden, Rougoor, and Oort suggests the presence of a small spiral arm near the center and requires the existence of a source of continuum radiation at the center or beyond.<sup>17</sup>

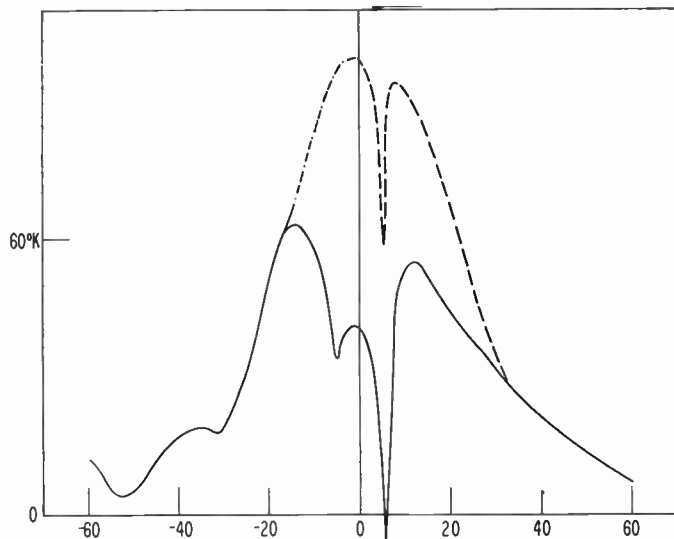


Fig. 6—Expected and observed profiles for Sagittarius A. In this diagram the ordinate is in  $^{\circ}\text{K}$  and the abscissa is in kilometers per second. The upper curve is the emission profile expected in the absence of the source while the lower curve is the observed curve.

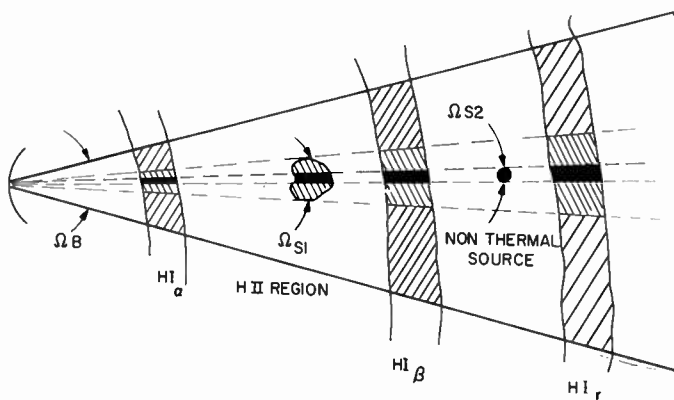


Fig. 7—Possible configuration of gas clouds and continuum emitters in the direction of Sagittarius A. The configuration is discussed in the text.

Based on present evidence one is forced to consider at least two sources of continuum radiation and three interleaved hydrogen regions in discussing the region of the galactic center. A possible configuration is shown in Fig. 7. An alternative concentric configuration has been suggested by Mills.<sup>14</sup> In such a complex situation where the continuum sources may be either thermal or nonthermal and of different sizes, one should expect

<sup>17</sup> H. van Woerden, W. Rougoor, and J. Oort, "Expansion d'une structure spirale dans le noyau du système galactique, et position de la radiosource Sagittarius A," *Compt. Rend. Acad. Sci.*, vol. 244, pp. 1691–1695; March 25, 1957.

profiles in which certain portions are a function of antenna size and other portions may remain relatively unchanged with larger antennas. A complete quantitative solution of the case presented in Fig. 7 requires the determination of at least 27 parameters. The inherent advantage of a larger antenna results from a reduction in the number of angular diameters that one must consider. It is probable that this region will remain an interesting and fruitful area of study for some time.

#### EXTRAGALACTIC STUDIES

Finally, in our survey of the observational possibilities of the absorption effect, we shall consider its application to extragalactic objects. In the early studies which were confined to observing the line in emission, the first step of the hydrogen line out of our galaxy was made by the Australian team of Kerr, Hindman, and Robinson.<sup>18</sup> They succeeded in detecting 21 cm emission from the Magellanic Clouds and the investigators in Australia have profitably pursued the initial detection by studying the dynamics and distribution of hydrogen gas in our closest extragalactic system.

The period following the detection of the Magellanic Clouds saw several hydrogen line groups attempting to detect other of our nearby galactic neighbors. A favorite object was Messier 31, the great spiral nebula in the Constellation Andromeda. But the early attempts failed, primarily because of the poor resolution of antennas available in 1954–1955, and attempts were shelved until recently when larger antennas were available.<sup>19</sup> It became clear that in the detection of the hydrogen line remote galactic objects were going to be difficult. But the possibility of finding the radio line in a remote system was intriguing. Ever since the discovery of the line, an interesting experiment was evident; a comparison of optical and radio red shifts on a common extragalactic.

From the work of Hubble, Humason, and others, we have the red-shift law through which arises the concept of the expansion of the universe. The Doppler effect interpretation of red-shifts of extragalactic objects shows that galaxies in space are receiving from each other with velocities which are proportional to their distances apart.

There have been alternative suggestions advanced to explain the red-shift-distance relation exhibited by extragalactic nebulas which allows a red-shift-distance relation in a static universe. Even though the Doppler interpretation is the straightforward one, astronomers, physicists, and cosmologists have sought additional tests of the Doppler interpretation. Such tests are important because of their intrinsic interest and because the fundamental expansion property of the

<sup>18</sup> F. J. Kerr, J. F. Hindman, and B. J. Robinson, "Observations of the 21 cm line from the Magellanic Clouds," *Aust. J. Phys.*, vol. 7, No. 2, pp. 297–314; 1954.

<sup>19</sup> Heesch and Dieter, "Extragalactic 21 cm line studies," this issue, p. 234.

universe rests observationally on the Doppler interpretation of the red-shift law.

Several tests have been proposed for examining the Doppler hypothesis. An obvious possibility which presented itself with the discovery of the hydrogen line, was the measurement of the hydrogen line red-shift on a distant extragalactic object having a large and an optically determined red-shift. The optical and radio red-shifts could then be compared over a wavelength base in the electromagnetic spectrum that covers a wavelength ratio of about 500,000 to 1. If the red-shifts are produced by the Doppler effect, then for a common test object, the observed shift should be the same for the optical and radio determinations.

The early emission studies, as outlined above, were not able to move very far into extragalactic space. But the discovery by Baade and Minkowski that the second most intense radio star was a collision of two galaxies at a distance of approximately  $10^8$  light years, and with the simultaneous development of 21-cm absorption line studies, an experiment suggested itself that stimulated interest in a red-shift experiment.

Considering the two galaxies in collision which comprise the Cygnus A radio star, there is a chance that peripheral hydrogen associated with the two systems might exist in neutral, unionized form. (See Fig. 8.) This associated gas could absorb spectrally part of the continuum radiation originating in the deeper regions of the collision producing an absorption line in the continuum which originated at the source. Baade and Minkowski, using the 200-inch Hale telescope, measured the optical red-shift of the Cygnus A colliding system and found that the red-shift corresponded to a recessional velocity of approximately 16,830 kilometers per second.<sup>9</sup> Since the peripheral gases in the Cygnus A system are dynamically part of the system, the radio absorption line should show a Doppler shift corresponding to the recessional velocity of 16,830 km. For the 1420-mc rest frequency of the 21-cm line, a radial velocity of 16,830 km would decrease the observed frequency by about 81 mc.

With these considerations in mind, the authors began a study in late 1955 of various ways to search observationally for the suspected absorption line. Two problems were evident: the suspected line was likely to be both weak and broad. Both the anticipated weakness and the breadth of the line meant that the usual scanning techniques using signal and comparison bands would probably be unsatisfactory and a completely different approach would be required.

The breadth of the absorption line is fixed and not subject to control but the observed line intensity would depend on the antenna size viewing the Cygnus A source. A very large antenna would assist the study significantly. The Cygnus A radio source has a declination such that it passes near the zenith for the geographical latitude of Washington, D. C. and so a special

possibility presented itself. A large stationary antenna could be constructed which would have the Cygnus A source transit the antenna main beam once a day near the zenith. A special receiver could also be constructed which would record the transit of Cygnus A on a number of channels distributed in frequency outside and within the range where the absorption line was expected.

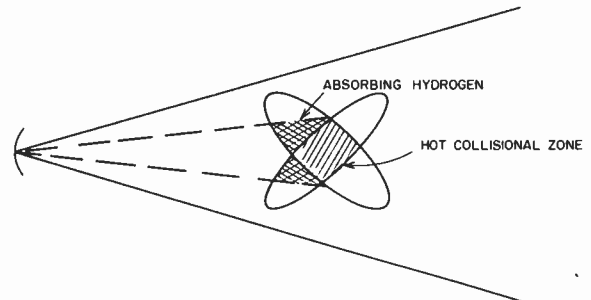


Fig. 8—Schematic representation of colliding galaxies in the Cygnus A system. The collision produces a source of continuum radiation and nearby associated hydrogen can spectrally absorb part of the continuum radiation.

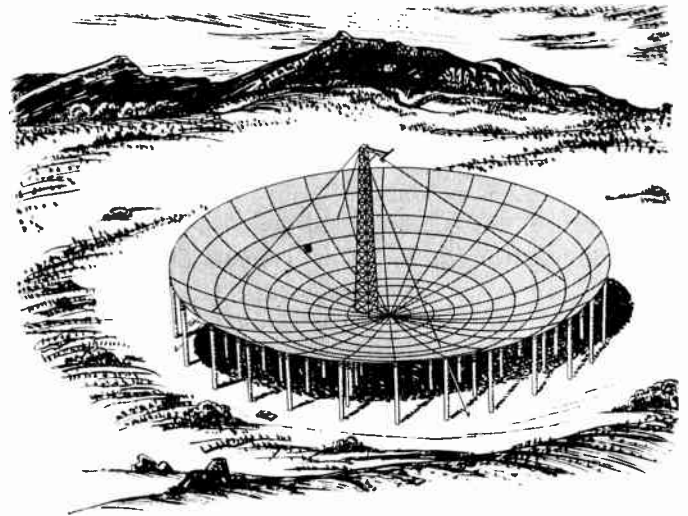


Fig. 9—Proposed 500-foot antenna for Cygnus A absorption measurements. This antenna is discussed in the text.

A 500-foot parabolic antenna made of chicken wire panels and mounted on telephone poles seemed to be a reasonable approach for a special experiment and the antenna was designed (see Fig. 9).<sup>20</sup>

During the interval when the 500-foot chicken wire antenna was being designed, it seemed reasonable to make a serious effort with the 50-foot antenna and its associated comparison radiometer. Scanning techniques were eliminated because of the anticipated line width and the receiver was converted to a straight radiometer, displaying only the energy received in the comparison band.

<sup>20</sup> W. R. Ferris, "Design of a 500-Foot-Diameter Faceted Paraboloidal Antenna," U. S. Naval Research Lab. Rep., No. 4881; pp. 1-7; January 25, 1957.

There are many effects that can distort the output of a receiver connected to an antenna and a broad weak line is particularly susceptible to these effects. Ground reflections and variation of the radiometer zero with frequency are two troublesome examples. Trouble can arise in two forms: the equipment can present a "line" which is purely instrumental in origin, or the equipment tuning effects can obscure the actual line originating in the gaseous assembly.

In order to avoid such instrumental difficulties as these, a second source, Cassiopeia A, was used as a standard and a comparison was made of the relative intensities of Cassiopeia A and Cygnus A at various frequencies. The problem of detecting a weak line could be assisted by the usual method of accumulating enough data so that a statistical increase in sensitivity would result.

The search was carried out with the 50-foot antenna and a weak absorption feature was found in the position anticipated from the Doppler interpretation.<sup>21</sup> The position of the radio absorption feature agrees very well with the optical value. Slight differences would be expected because of the physically different locations and velocity distributions of the gases involved in the radio and optical studies. Since the absorption line red-shift measurement on the Cygnus A system, the constancy of  $\Delta\lambda/\lambda$  for radio and optical measurements has been confirmed with a larger antenna. Heesch, using the new 60-foot Agassiz Station Radio Telescope of Harvard Observatory, has succeeded in detecting a faint 21 cm emission line from the rich Coma cluster of galaxies. The red-shift of the Coma cluster is approximately only one third of the red-shift of the Cygnus A system, but the radio red-shift agrees satisfactorily with the optical red-shift of the cluster.<sup>22</sup>

Although the Cygnus A radio red-shift represents a crude first attempt, the resulting demonstration of the constancy of  $\Delta\lambda/\lambda$  for optical and radio wavelengths improves our knowledge of the constancy by about  $10^5$ .

In addition, the radio results suggest that one is likely to find  $\Delta\lambda/\lambda$  constant for a particular extragalactic object wherever a red-shift measurement is made in the electromagnetic spectrum.

The constancy of the radio and optical red-shifts is a natural consequence of the Doppler interpretation. It is not a categorical demonstration of the expansion of the universe but it is very suggestive.

The successful detection of an absorption line in the Cygnus A collision raises an interesting question concerning the number of similar measurements which might be performed with larger antennas. There are two additional radio sources, NGC 5128 in Centaurus and NGC 4486 in Virgo which, although not studied as

yet, might be detected in absorption using the NRL 50-foot antenna. While both sources are probably rich in hydrogen, they exhibit antenna temperatures approximately 25 per cent of the Cygnus value, and the possibility of a successful measurement is reduced correspondingly. If we assume that colliding galaxies are distributed uniformly throughout space, the number detected should go as the third power of the antenna diameter. We might, therefore, expect an antenna in the 500- to 600-foot range to have between 1000 and 3000 such sources available for study.<sup>23</sup>

#### ADDITIONAL ABSORPTION LINE EXPERIMENT

In our survey of the potentialities of the absorption technique, two points concerning the content and physical state of the interstellar medium require mentioning. First, concerning the content of the interstellar medium, the absorption technique with larger antennas presents an opportunity for the detection of other spectral lines. As antennas increase in size, the antenna temperature of a small source increases at a rate proportional to the square of the aperture. Thus the thermal amplitude of a given absorption line increases with increasing antenna size thereby increasing the signal size with respect to the minimum detectable temperature difference of the radiometer. This results in an effective increase in sensitivity for line detection by virtue of significantly improving the chances of detecting lines which have very small opacities.<sup>24</sup> Small opacities will result because of the small cosmic abundances of atoms and radicals which have expected lines.

A second point concerns the direct detection of interstellar magnetic fields. Bolton and Wild have proposed using the Zeeman-splitting of the radio absorption lines to measure interstellar magnetic fields of the order  $10^{-5}$  to  $10^{-6}$  Gauss.<sup>25</sup> The splitting of the two  $\sigma$  components of the hydrogen line (the upper level splits into three components) is approximately 2.8 mc per Gauss. For a Gaussian line the minimum detectable magnetic field is given approximately by

$$H_{\min} \cong 4 \times 10^{-7} \frac{\Delta\nu \Delta T_{\min}}{T_l} \quad (11)$$

where  $T_l$  is the maximum absorption line depth expressed as a temperature,  $\Delta T_{\min}$  is the minimum temperature change detectable by the radiometer, and  $\Delta\nu$  is the half-width of the absorption line.

For an antenna of the 140-foot size to be built at the National Radio Observatory, (11) leads to  $H_{\min}$  in the range between  $10^{-5}$  and  $10^{-6}$  Gauss, provided the observations are made on the Cassiopeia A radio star.

<sup>23</sup> E. F. McClain, "A note on the potentialities of large radio telescopes," *Astrophys. J.*, vol. 123, pp. 367-368; March, 1956.

<sup>24</sup> A. E. Lilley, "A note on the galactic microwave spectrum," *Astrophys. J.*, vol. 122, pp. 197-198; July, 1955.

<sup>25</sup> J. G. Bolton and J. P. Wild, "On the possibility of measuring interstellar magnetic fields by 21-cm Zeeman splitting," *Astrophys. J.*, vol. 125, pp. 296-297; January, 1957.

<sup>21</sup> A. E. Lilley and E. F. McClain, "The hydrogen line redshift of radio source Cygnus-A," *Astrophys. J.*, vol. 123, pp. 172-175; January, 1956.

<sup>22</sup> D. S. Heesch, "21-cm line emission from the Coma cluster," *Astrophys. J.*, vol. 124, pp. 660-662; November, 1956.

A variety of evidences suggest that magnetic fields of the order  $10^{-5}$  and  $10^{-6}$  Gauss may exist in the interstellar medium.

A second interesting possibility exists in the measurement of the density of the intergalactic medium. As yet no measurement has revealed the existence of material in average regions of intergalactic space although it is generally supposed that very low density hydrogen might be present. If ground state hydrogen were present it would be effective in absorbing continuum radiation from distant radio sources of the Cygnus A type.

The intergalactic gas may be ionized; the time for recombination is expressed in billions of years. However, the physical state of the intergalactic medium is at present unknown and it is of considerable interest to ask what density of ground state hydrogen could be detected in the intergalactic medium. Intergalactic gas lying between the observer and a source of the Cygnus A type would absorb continuum radiation from the source. The density detectable under this circumstance is given approximately by

$$\rho \sim \text{constant} \frac{T_S H \Delta T_{\min}}{T_A} \quad (12)$$

where  $T_A$  is the antenna temperature of the source used as a background,  $H$  is Hubble's constant,  $\Delta T_{\min}$  is the

minimum detectable temperature of the radiometer employed and  $T_S$  is the state temperature of the intergalactic gas.<sup>26</sup> A 140-foot radio telescope viewing the Cygnus A source could detect a density of the order  $10^{-30} T_S \text{ gm cm}^{-3}$ . It is apparent that two major unknowns will control the fate of this experiment, the state temperature and fractional ionization of the intergalactic medium. It remains nevertheless an experiment which radio astronomers are obligated to attempt.

A new approach to the absorption line problem is being carried ahead by Bolton at the California Institute of Technology. He plans to apply interferometer techniques to the absorption line studies of galactic and extragalactic radio sources. It is clear that objects of the Cygnus A type can be detected and usable measurements made at distances significantly greater than distances at which similar optical measurements can be made provided means can be found for selection of suitable sources. Therefore it may be possible to extend the radio red-shift measurements to velocities which are significant fractions of the velocity of light. The future of absorption line studies with larger antennas and improved receivers should be very interesting and rewarding.

<sup>26</sup> A. E. Lilley, "Radio Astronomical Measurements of Interest to Cosmology," Conference on Role of Gravitation in Physics, Wright Air Dev. Ctr. Tech. Rep., 57-216; March, 1957.



# Hydrogen Line Study of Stellar Associations and Clusters\*

T. K. MENON†

**Summary**—This paper describes the results of recent investigations at Harvard College Observatory on the interstellar structure around a number of stellar associations and clusters. The results were obtained from analyses of the 21-cm profiles of neutral hydrogen in these systems using the 24-foot and 60-foot radio telescopes at the Agassiz Station of Harvard College Observatory. Investigations of the associations Orion I and Orion II showed expansion of neutral hydrogen around these associations. Preliminary results of studies of other associations Lacerta, Cygnus II, Cygnus VI, NGC 2244, and NGC 2264 are described. Observations of hydrogen content of some galactic clusters were found to show a strong age effect. The significance of the above results for studies of stellar evolution is discussed.

## INTRODUCTION

THE discovery by Ewen and Purcell<sup>1</sup> of the 21-cm radiation from neutral hydrogen has proved to be of very great importance for studies of the structure of our galaxy and the interstellar medium. After the initial surveys to obtain the broad outlines of the distribution of hydrogen in our galaxy, astronomers have started detailed investigations of specific astrophysical problems. Those relating to stellar evolution have been stressed especially at the Agassiz Station of the Harvard College Observatory. This paper reviews the results obtained so far and surveys the potentialities of this field of research.

One of the most fruitful recent hypotheses with regard to stellar evolution is that due to Ambartsumian<sup>2</sup> who introduced the concept of a new type of stellar system called an association. An association is defined as a concentration of stars of similar spectral type. Two types of stellar associations have been studied in some detail. Those consisting of *O*- and *B*-type supergiant stars are known as *O* associations; and those consisting primarily of variable stars of the *T* Tauri type, and other variables of similar spectra, are known as *T* associations. Ambartsumian has shown that these associations cannot be stable systems and must disintegrate in a few million years. They are hence systems of positive total energy. Ambartsumian suggested that the stars in these systems should be expanding with a velocity of a few kilometers per second. A brilliant confirmation of

this prediction was made by Blaauw's<sup>3</sup> analysis of the proper motions of the  $\zeta$  Persei group of *O*- and *B*-type stars which showed a mean expansional velocity of 12 km and an age of 1.3 million years. Since then similar expansions have been found for the associations Lacerta by Blaauw and Morgan,<sup>4</sup> Cepheus II by Markarian,<sup>5</sup> and Scorpius by Kolopov.<sup>6</sup>

Since there is every reason to believe that these expansions are connected with the mode of origin of the associations, one should expect to find corresponding motions in the neutral hydrogen surrounding these associations. In selecting those for a study we have to bear in mind two requirements. First, the associations chosen should preferably be situated away from the galactic plane to avoid confusion due to extraneous hydrogen. Second, they should be situated near regions of small galactic rotation effect in radial velocities so that systematic motions other than galactic rotation can be studied.

One of the first associations studied at Harvard was that in Orion.<sup>7,8</sup> This is the nearest *O* association known at present and is also one of the largest observed. As long ago as 1894, Barnard observed a ring of emission nebulosity with a diameter of about 17° surrounding most of the early type stars. Since the distance of the association is about 450 parsecs the diameter is found to be about 136 parsecs. The region observed with the 24-foot radio telescope at the Agassiz Station of Harvard College Observatory extended from  $l=160^\circ$  to  $184^\circ$  and from  $b=-10^\circ$  to  $-25^\circ$ . Barnard's loop is centrally situated within this region. From some of the 21-cm profiles shown in Fig. 1 it is immediately seen that the profiles for the region between  $l=172^\circ$  to  $175^\circ$ ,  $b=-22^\circ$  to  $-16^\circ$  are asymmetrical, with a secondary maximum on the negative velocity side. Since the galactic rotation effect in radial velocity is positive for this region, the asymmetry can be naturally interpreted as due to an expansion of the neutral hydrogen in the line of sight. From the 21-cm profiles one can obtain the number of

<sup>3</sup> A. Blaauw, "The age and evolution of the Persei group of *O*- and *B*-type stars," *Bull. Astron. Inst. Neth.*, vol. 11, p. 405; June, 1952.

<sup>4</sup> A. Blaauw and W. W. Morgan, "Expanding motions in the Lacerta aggregate," *Astrophys. J.*, vol. 117, p. 256; March, 1953.

<sup>5</sup> B. A. Markarian, "Expansion of the open star cluster IC 2602," *Cont. Burakan. Obs.*, No. 11, p. 19; 1953.

<sup>6</sup> P. N. Kolopov, "Stellar association around the open cluster NGC 6231 in Scorpius," *Russ. A. J.*, vol. 28, p. 472; November, 1951.

<sup>7</sup> T. K. Menon, "A 21-CM investigation of the Orion Region," IAU Symposium on Radio Astronomy, Cambridge University Press, Cambridge, England; 1957, in press.

<sup>8</sup> T. K. Menon, "Interstellar structure of Orion region I," *Astrophys. J.*, in press.

\* Original manuscript received by the IRE, October 18, 1957. The various investigations reported here have been supported by the National Science Foundation.

† Harvard College Observatory, Cambridge, Mass.

<sup>1</sup> H. I. Ewen and E. M. Purcell, "Observations of a line in the galactic radio spectrum. I. Radiation from galactic hydrogen at 1420 mc/sec," *Nature*, vol. 168, p. 356; September, 1951.

<sup>2</sup> V. A. Ambartsumian, "Stellar associations," *Russ. A. J.*, vol. 26, p. 3; January, 1949.

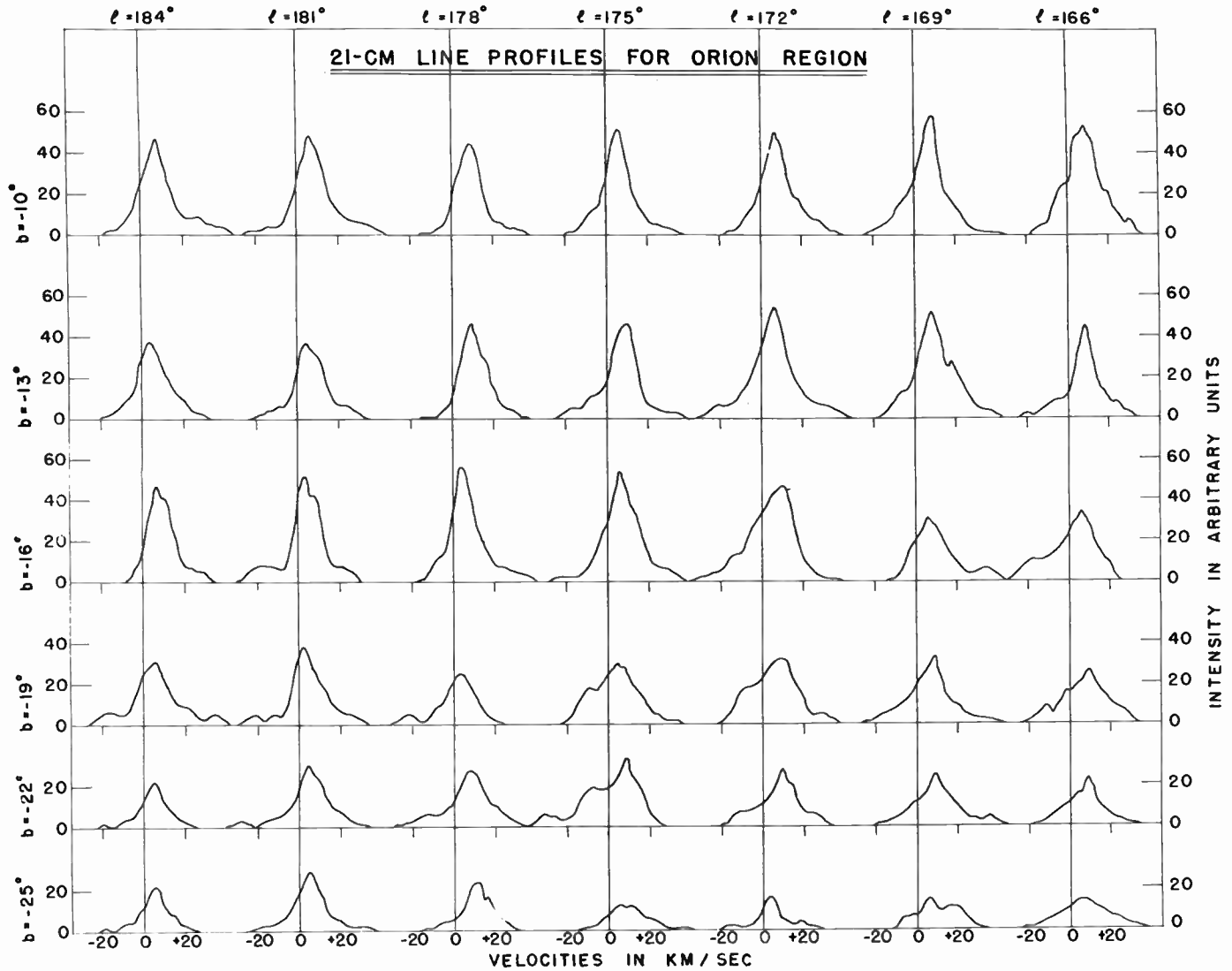


Fig. 1.

hydrogen atoms in a column one square centimeter in cross section in the line of sight and convert this into density by assuming a path length. Combining this information with the shape of the profiles one can derive a model of the expansion of neutral hydrogen. Such a model is shown in Fig. 2. The center of expansion is found to be at  $l=173.5^\circ$ ,  $b=-18^\circ$ . This is in satisfactory agreement with the center of expansion of three stars moving away from the Orion region found by Blaauw and Morgan.<sup>9,10</sup> The age of expansion,  $2.6 \times 10^6$  years, derived from the 21-cm observations is in agreement with that of the two stars found by Blaauw and Morgan but does not agree with the third one. This might have some evolutionary significance. The early observations with the 24-foot telescope at Harvard

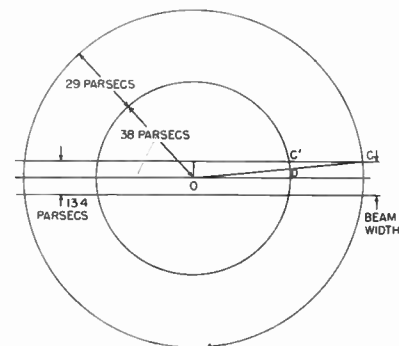


Fig. 2—Model of expansion of the Orion region.

<sup>9</sup> A. Blaauw and W. W. Morgan, "The space motions of AE Aurigae and Columbae with respect to the Orion nebula," *Astrophys. J.*, vol. 119, p. 625; May, 1954.

<sup>10</sup> A. Blaauw, "On the luminosities, motions, and space distribution of the nearer northern O-B5 stars," *Astrophys. J.*, vol. 123, p. 408; May, 1956.

indicate that the mass distribution in the expanding region is not symmetrical. This can be tentatively interpreted as due to the inclination of the Orion spiral arm to the line of sight. The total mass of neutral hydrogen in the expanding shell is about 50,000 solar masses.

A number of theories have been proposed in recent years for the origin of stellar associations. The first one,

due to Öpik,<sup>11</sup> suggests that the explosion of a supernova would cause a compression and expansion of the surrounding interstellar medium. According to Öpik, new stars could be formed in such compressed regions and hence would have the expansion velocity of the interstellar gas clouds from which they were formed. In the second theory, proposed by Oort,<sup>12</sup> the role of the supernova is taken over by an early type star. Öpik's theory fails to explain the Orion observations, since the stars near the 21-cm center of the expansion fail to show any expansion whereas the gas far away from the center is still expanding. A similar criticism applies to Oort's theory, in addition to the fact that it cannot provide for the expansion of the high velocity stars of Blaauw and Morgan. In any case, the region is a very complex one and has to be studied in much more detail both theoretically and observationally before we can arrive at a satisfactory interpretation of all observations.

A study of the association Orion II, which contains the *O* star  $\lambda$  Orionis, has been made by Wade<sup>13</sup> at Harvard. Around the star  $\lambda$  Orionis is a large H II region of diameter  $8^\circ$  which is bordered by a dark ring. Wade has found from his observations with the 60-foot radio telescope that across a line of constant latitude passing through the center of the H II region the number of atoms in the line of sight reaches a maximum at the outer edge of the H II region and decreases to a minimum at the center of the H II region. At the same time he finds that the halfwidth of the 31-cm profiles is minimum at the edge of the H II region and reaches a maximum at the center. Figs. 3 and 4 show his results. From these observations he has derived a model of radial density distribution and expansion of the H I shell. The total mass of neutral hydrogen in the shell is found to be 40,000 solar masses and the expansion velocity is about 8 km.

In recent years theories of an expanding H II region around an early type star have been proposed by Oort and Spitzer<sup>14</sup> and by Savedoff and Greene.<sup>15</sup> With the known parameters of the  $\lambda$  Orionis system, Wade finds that the velocity expected from the Oort and Spitzer model is only 0.54 km. This value is very much lower than that observed. Since 96 per cent of the  $\lambda$  Orionis cloud is still neutral the theory of Oort and Spitzer probably does not apply to this case. According to the theory of Savedoff and Greene, the shock front can be ahead of the ionization front by about 2 per cent

<sup>11</sup> E. Öpik, "Stellar associations and supernovae," *Irish Astr. J.*, vol. 2, p. 219; December, 1953.

<sup>12</sup> J. H. Oort, "Outline of a theory on the origin and acceleration of interstellar clouds and O-associations," *Bull. Astron. Inst. Neth.*, vol. 12, p. 177; September, 1954.

<sup>13</sup> C. M. Wade, "A 21-CM Study of an Expanding H II Region," Harvard University Doctoral dissertation; 1957.

<sup>14</sup> J. H. Oort and L. Spitzer, "Acceleration of interstellar gas clouds by O-type stars," *Astrophys. J.*, vol. 121, p. 6; January, 1955.

<sup>15</sup> M. P. Savedoff and J. Greene, "Expanding H II region," *Astrophys. J.*, vol. 122, p. 477; November, 1955.

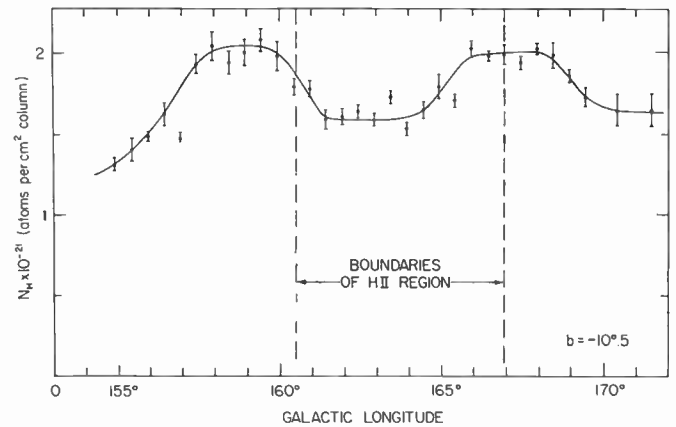


Fig. 3—Number of neutral hydrogen atoms in the line of sight per square centimeter column as a function of galactic longitude at  $b = -10^\circ.5$ .

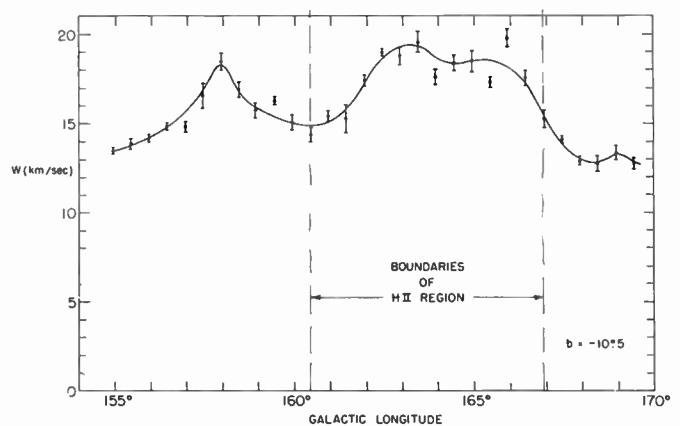


Fig. 4—Width of the 21-cm line between points of half-maximum intensity as a function of galactic longitude at  $b = -10^\circ.5$ .

of its radius at most. Observationally, however, the region in which the neutral gas is moving outwards has more than twice the radius of the ionized region. Hence, Wade thinks that the density and velocity distributions that we observe must reflect the past history of the region as well as what is now occurring. Obviously, considerable theoretical and observational work needs to be accomplished before we can get a clear picture of the phenomena.

Among other associations being studied at Harvard are NGC 2244, NGC 2264, II Cygni, VI Cygni, and Lacerta. Preliminary observations<sup>16</sup> of NGC 2244 indicate that this association is situated exactly at a branching point of the Orion spiral arm. A similar preliminary study<sup>16</sup> of NGC 2264 showed a decrease in 21-cm intensity in the vicinity of the cluster, which indicates either a decrease in kinetic temperature or real paucity of hydrogen in its surroundings. A detailed study of these associations by R. J. Davis is in progress in order to elucidate the spiral structure in their vicinity.

A study of the region around the associations II Cygni and VI Cygni has been completed by Mrs. May

<sup>16</sup> T. K. Menon, "A 21-cm study of NGC 2244 and NGC 2264," *Astrophys. J.*, vol. 61, p. 9; February, 1956.

Kassim. This region is quite complicated because of excessive obscuration. She finds that there are definite maxima in neutral hydrogen distributions in the vicinity of these associations. A detailed optical and 21-cm analysis is in progress; it should provide interesting information about the expansion of these associations.

In all the associations mentioned above no noticeable expansion of the stars has been established. Since we do not know the mode of formation of an expanding association we cannot as yet predict the relative motion of the gas and the stars in the cases where expansion of the stars has been found. Of the four associations for which definite expansion of the stars has been established, II Persei and I Lacerta have been studied at Harvard. Matthews<sup>17</sup> from his observations with the 24-foot radio telescope found remarkable increases in neutral hydrogen density in the vicinity of these associations. He also noted that there are small discrepancies between the velocities of the clusters and the velocity of hydrogen associated with them. However, the existence of increased density in the cluster regions seems to be well established. The detailed study of I Lacerta is being made by W. E. Howard with the 60-foot telescope and his results corroborate Matthews' work. Howard finds an apparent relative motion of the gas and the stars, which could reasonably be explained as resulting from momentum balance. He has constructed a three-dimensional model which suggests that these motions are intimately connected with the origin and evolution of the association as a whole.

Optical studies of many of these associations are in progress in many observatories throughout the world and in the next few years 21-cm studies will have added considerable new information. Since the associations are believed to be the youngest of stellar clusters, the importance of this information in solving the problem of star formation is obvious.

Another aspect of stellar evolution which has been studied in considerable detail in recent years is the problem of the color-luminosity arrays of globular and galactic clusters. We shall restrict this discussion to the galactic clusters. From the study of the color-luminosity arrays, it has been possible to determine the relative ages of a number of clusters. For example, the cluster  $h$  and  $\chi$  Persei is found to be young, whereas the cluster M67 is found to be one of the oldest. The most massive stars of type  $O$  are known to have initial contracting stages of evolution lasting only a few hundred thousand years, whereas stars with mass of the order of one solar mass take many millions of years to reach the main sequence. Hence, one would expect to find in the youngest clusters and associations large numbers of overluminous stars above the main sequence at the lower branch of the main sequence. These stars would be in the process of

contraction before arriving at the main sequence. This fact was strikingly confirmed by the discovery by Parenago<sup>18</sup> and Walker<sup>19</sup> of a large number of such stars in the Orion association and NGC 2264. The question then arises whether there are any stars in galactic clusters still in the proto-star stage.

Before answering we shall look at the problem from a different point of view. From the observational work of Van Rhijn,<sup>20</sup> Luyten,<sup>21</sup> McCusky<sup>22</sup> and others, we have fairly accurate values of the luminosity function  $\phi(M_v, sp)$ , the density of stars in the solar neighborhood of absolute visual magnitude between  $(M_v - \frac{1}{2})$  and  $(M_v + \frac{1}{2})$  in a certain range of spectral class. Since stars of all ages exist in the galactic system, this general luminosity function is the sum of the distribution functions at the times of star formation, modified by the effects of stellar evolution. Salpeter<sup>23</sup> has shown how one can obtain the time dependent function  $\psi(M_v)$  from  $\phi(M_v)$ , under the assumptions that 1) the rate of formation of stars in the solar neighborhood has been uniform since the beginning of the galaxy, and 2) that all stars leave the main sequence after a certain characteristic time when about 7 per cent of the hydrogen has been changed to helium. That Salpeter's arguments are essentially correct is shown by the recent work of Sandage<sup>24</sup> who extended Salpeter's work to the observed parts of the luminosity function of a number of galactic clusters and one globular cluster. From this work it is possible to compute the amount of mass still in the proto-star stage in each cluster. F. D. Drake at Harvard has done this for five galactic clusters,  $h$  and  $\chi$  Persei, Pleiades, Coma Berenices, Praesepe, and M67, which are listed in order of increasing age. From the Salpeter formation function and the known ages of the clusters, Drake finds the mass of low-mass dwarf stars in proto-star stage for these clusters to be 3400, 63, 13, 13, and 0 solar masses, respectively. In an effort to find out whether the gas in these proto-stars is in the form of neutral hydrogen, Drake has determined, using the 60-foot Agassiz radio telescope, the amount of excess of 21-cm radiation from these clusters. When he converted the observed excess radiation into mass of neutral hydrogen he found the respective masses to be 5000, 77, 25, 24, and less than 40 solar masses showing a strong age effect. Other arguments indicate that these masses are more

<sup>18</sup> P. P. Parenago, "The stars in the Orion nebula," *Russ. A. J.*, vol. 30, p. 249; 1953.

<sup>19</sup> M. F. Walker, "Studies of extremely young clusters NGC 2264," *Astrophys. J.*, Suppl., vol. 2, p. 365; October, 1956.

<sup>20</sup> P. J. Van Rhijn, "The absorption of light in interstellar galactic space and the galactic density distribution," *Groningen Pub.*, No. 47; 1936.

<sup>21</sup> W. Luyten, "The luminosity function," *Ann. N. Y. Acad. Sci.*, vol. 42, p. 201; October, 1941.

<sup>22</sup> S. McCusky, "Variations in the stellar luminosity function VIII. A summary of results," *Astrophys. J.*, vol. 123, p. 458; May, 1956.

<sup>23</sup> E. E. Salpeter, "The luminosity function and stellar evolution," *Astrophys. J.*, vol. 121, p. 161; January, 1955.

<sup>24</sup> A. Sandage, "Observational approach to evolution I. Luminosity function," *Astrophys. J.*, vol. 125, p. 422; March, 1957.

<sup>17</sup> T. A. Matthews, "The Distribution of Neutral Hydrogen Between Galactic Longitudes 60° and 135°," Harvard University Doctoral dissertation; 1956.

probably in the form of condensations and not uniformly distributed. Since Drake's preliminary observational results do, in fact, agree remarkably well in the hydrogen mass with the mass of proto-stars predicted by the Salpeter function, we can tentatively conclude that the observed cluster hydrogen is actually in the form of proto-stars within the clusters. Further observations are in progress to improve the accuracy of the mass determinations, to study a few more clusters, and to clarify the observed positional structure in the neutral hydrogen distribution in some of the bigger clusters.

The problems described above are in general connected with the large-scale systematic motions and content of neutral hydrogen in associations and clusters. There are a number of questions that should be studied in detail in order to provide some picture of the energy-

dissipative mechanisms inside these stellar systems. The first of these concerns the small-scale random motions inside a system and their systematic variations with position, both inside a system and in different parts of the galaxy. This will provide a clue to the interpretation of the observations that some clusters contain only massive stars, while others contain a mixture of massive and dwarf stars. The second question is that of the relative importance of gas and dust in controlling motions near early type stars. The third is concerned with the possible effects of a galactic magnetic field on general interstellar motions and possible ways of detecting it by a study of a 21-cm profile. Research along these lines is in progress at Harvard and is expected to add to our general knowledge of physical processes in the interstellar medium and of stellar evolution.

## Extragalactic 21-CM Line Studies\*

D. S. HEESCHEN† AND N. H. DIETER‡

**Summary**—The study of neutral hydrogen in extragalactic systems by means of its 21-centimeter line emission is a relatively new field of radio astronomy research. To date, radiation has been observed from seven galaxies and three clusters of galaxies. In this paper some of the results of these observations are described. Although the observational material presently available is quite limited, it does indicate the great potential power of extragalactic 21-centimeter line studies.

### INTRODUCTION

THE 21-centimeter line emission of neutral atomic hydrogen has proven a valuable tool for studying the distribution and properties of interstellar hydrogen in our galactic system. With the advent of larger antennas and more sensitive receivers, research at 21 centimeters has naturally been extended into the "Realm of the Nebulae"—to other galaxies and clusters of galaxies. Extragalactic nebulae should provide radio observers, as they do optical observers, with more direct information about the over-all structure of stellar systems than is obtainable from observations of our own galaxy from within. Both radio and optical observers are handicapped, however, by the great distances of these objects. In only a few cases are the angular diameters of the galaxies larger than the beamwidths of existing antennas, and the 21-centimeter radiation, reduced in proportion to the square of the distance, lies near the limit of detectability with present receivers.

Nevertheless, the amount of astronomical information to be gained is so great as to justify the considerable effort required. For example, 21-centimeter line observations of an extragalactic system can, in principle, yield directly the red shift (a Doppler-frequency shift of spectral lines toward long wavelengths) of the system, and the distribution, internal motions, and total mass of neutral hydrogen within the system. Indirectly, comparison of optical and radio data should yield further information concerning the nature and evolution of galaxies and clusters of galaxies.

### 21-CENTIMETERS LINE EMISSION FROM GALAXIES

Up to the present time only a few galaxies have been observed, but these indicate some of the results which can be expected from more extensive surveys. For example, Lilley and McClain,<sup>1</sup> using the Naval Research Laboratory 50-foot antenna, measured the red shift of the Cygnus-A radio source by observing the 21-centimeter line absorption in the spectrum of the source. This is the only existing extragalactic observation of the 21-centimeter line in absorption. It is of great significance in that it demonstrates the constancy of the red shift over the wide wavelength range from optical to radio. It also suggests the possibility of determining the red shifts of very distant objects by this technique.

\* Original manuscript received by the IRE, November 6, 1957.

† Natl. Radio Astronomical Observatory, Green Bank, W. Va.

‡ Harvard College Observatory, Cambridge, Mass.

<sup>1</sup> A. E. Lilley and E. F. McClain, "The hydrogen-line red shift of radio source Cygnus A," *Astrophys. J.*, vol. 123, pp. 172-175; January, 1956.

Twenty-one-centimeter line absorption studies are described in detail in another paper in this issue.<sup>2</sup>

All other observations so far made have been of the emission of neutral hydrogen radiation by more or less normal galaxies. Galaxies may be classified according to their appearance, using a system introduced by Hubble.<sup>3</sup> Elliptical galaxies (type E) show little or no internal structure and very little interstellar gas and dust. The SO systems form a transitional group to the highly flattened spiral galaxies, which are subdivided as follows: Sa systems have a prominent nucleus and tightly wound spiral arms; Sb's, such as the Andromeda nebula, show a smaller nucleus and more conspicuous spiral structure; Sc's, like M33 in Triangulum, have a pinwheel appearance of small nucleus and intricate, branching spiral arms. There remain the irregular systems like the Magellanic Clouds which do not fit any of these categories. The classification has greater significance than that of appearance alone in that the more advanced the spiral nature of the system, the more population I-type material it contains; that is, associations of young hot stars and interstellar dust and gas. From the point of view of 21-centimeter observations these normal galaxies fall into two groups—those that are near enough and large enough to permit detailed survey, and those that can be observed only as a whole. In the first group there are now only four galaxies, and we see little prospect of greatly increasing the number at the present time. They are the large and small Magellanic Clouds in the southern sky, and the two great spiral nebulas, M31 in Andromeda and M33 in Triangulum, in the northern. These four (along with our own galaxy) are likely to provide the basic data for much of the research on more distant systems. Although a good deal is already known about all four systems, information about the neutral interstellar hydrogen within them has until recently been completely lacking.

The Magellanic Clouds were the first extragalactic objects from which 21-centimeter line emission was observed. They have been extensively observed by Kerr and his associates,<sup>4,5</sup> using an antenna having a beamwidth of 1.5°. Since the clouds are the closest extragalactic systems, and each covers 7° or 8° in the sky, the Australian<sup>6</sup> observers were able to make a detailed study of them. From their observations they found directly the mass and velocity distribution of the neutral hydrogen within each galaxy and, from their observed rotational velocities, the total mass in each

system. These values are given in Table I, where the results of all available 21-centimeter line observations of galaxies are summarized.

M31, the Great Nebula in Andromeda which covers about 6° by 1.5° in the sky, has been investigated by van de Hulst and Raimond,<sup>6</sup> with their 25-meter, 31-minute beamwidth paraboloid. Their observations consist effectively of velocity profiles of the HI at various points along the major axis of the galaxy. They derive the rotation curve and HI distribution in M31, as well as estimates of the total mass and HI mass present. Their results are given in Table I. There is some evidence, from observations of M31 with Harvard's 60-foot radio telescope, that considerable hydrogen may be present at large distances from the major axis. If so, this would increase the present estimate of HI mass in M31.

TABLE I  
MASS OF NEUTRAL HYDROGEN AND TOTAL MASS OF GALAXIES

1	2	3	4	5	6	7
	Type	Dist. kpc	$M_H/M_\odot$	$M_T/M_\odot$	$M_H/M_T$	References
Galaxy	Sb		$1.4 \times 10^9$	$0.7 \times 10^{11}$	0.02	6
M31	Sb	440	$1.9 \times 10^9$	$1.5 \times 10^{11}$	0.01	6
M81	Sb	2600	$1.0 \times 10^{10}$	$8.2 \times 10^{10}$	0.12	9
M33	Sc	425	$1.2 \times 10^9 \ddagger$	$1 \times 10^{10}$	0.12	7
M51	Sc	1200	$4.6 \times 10^9$	?	?	9
LMC*	Ir	46	$0.6 \times 10^9$	$3.0 \times 10^9$	0.2	4
SMC†	Ir	46	$0.4 \times 10^9$	$1.3 \times 10^9$	0.3	4
M32	E2	440	$> 8 \times 10^8$ $< 4 \times 10^7$	$2.5 \times 10^{10}$	$> 0.0003$ $< 0.0015$	9

\* Large Magellanic Cloud.

† Small Magellanic Cloud.

‡ Not corrected for antenna efficiency.

A survey of M33 is in progress at Harvard, with a 49-minute beamwidth antenna, and has produced some interesting preliminary results.<sup>7</sup> Optically, M33 has an extent of about 60 minutes by 30 minutes,<sup>8</sup> so that with such low-angular resolution one might not expect to find much detail in the hydrogen distribution and velocity. However, the neutral hydrogen radiation comes from a much larger area in the sky than present photographs indicate for the visual radiation. Measurable signals have been found at 80 minutes from the center in the direction of the major axis, more than twice the optical radius, and 60 minutes from the center in the minor axis direction. The velocity structure is complex and not yet investigated in detail, but estimates of the total mass and the mass of neutral hydrogen have been made on the basis of observations to date. The results are shown in Table I.

<sup>2</sup> A. E. Lilly and E. F. McClain, "Absorption techniques as a tool for 21-CM research," this issue, p. 221.

<sup>3</sup> E. Hubble, "The Realm of the Nebulae," Yale Univ. Press., New Haven, Conn.; 1936.

<sup>4</sup> F. J. Kerr, J. V. Hindman, and B. J. Robinson, "Observations of the 21-cm line from the Magellanic Clouds," *Aust. J. Phys.*, vol. 7, pp. 297-314; June, 1954.

<sup>5</sup> F. J. Kerr and G. de Vaucouleurs, "Rotations and other motions of the Magellanic Clouds from radio observations," *Aust. J. Phys.*, vol. 8, no. 4, pp. 508-522; 1955, and "The masses of the Magellanic Clouds from radio observations," *Aust. J. Phys.*, vol. 9, no. 1, pp. 90-111; 1956.

<sup>6</sup> H. C. van de Hulst and E. Raimond, "Rotatie en waterstof-dichtheid van de Andromeda Nevel afgeleid uit waarnemingen van de 21 cm lijn," *Afd. Naturkunde*, vol. 65, pp. 157-160; 1956.

<sup>7</sup> N. H. Dieter, "Observations of neutral hydrogen in M33," *Publ. Astron. Soc. Pacific*, vol. 69, pp. 356-357; August, 1957.

<sup>8</sup> N. U. Mayall and L. H. Aller, "The rotation of the spiral nebula Messier 33," *Astrophys. J.*, vol. 95, pp. 5-23; January, 1942.

Three galaxies—M32, M51, and M81—have been observed at Harvard by Heesch, <sup>9</sup> using the 60-foot antenna. M32 is a small elliptical companion to M31, while M51 and M81 are large Sc and Sb spirals, respectively. The optical size of M51 is smaller than the 49-minute beamwidth used in the observations, but the angular extent of 21-centimeter line emission was found to be 2°. In the case of M81 too, a large angular extent of neutral hydrogen was found. The radial velocity of M81, relative to the sun, is only about -50 km, so there is the possibility, even though M81 is at +42° galactic latitude, of confusing the emission from M81 with that from local galactic hydrogen. Because of this possibility, a detailed study of the distribution of HI in M81 is rather difficult. However, the HI emission shows such symmetry with respect to both the position and orientation of M81 as to make relatively certain the conclusion that there is an extensive distribution of neutral hydrogen in M81. The masses of neutral hydrogen in these two galaxies, derived from the 21-centimeter observations, are given in Table I. The observations of the elliptical galaxy, M32, are as yet incomplete, and only upper and lower limits to the mass of HI can be determined. The diameter of M32 is less than the antenna beamwidth and, therefore, only an upper limit of 49 minutes can be set by observations. It is probable that the neutral hydrogen all lies within the optical diameter of the galaxy, which is about 8 minutes.

These, then, are the observations to date of external galaxies, and the one thing which stands out in all of the spirals is the large extent of HI. Each of them seems to be imbedded in a cloud of hydrogen that extends far beyond the optical limits of the galaxy, and which accounts for a good part of the 21-centimeter radiation received. Thus, there may be two types of distribution of hydrogen in a spiral galaxy; the relatively dense concentrations associated with the spiral arms, and a less dense but much more extensive cloud in which the spiral structure is imbedded. Pickelner and Shklovsky<sup>10</sup> on theoretical grounds, have postulated the existence of a halo of neutral hydrogen around our own galaxy, and it may be that this is what we are observing in the above galaxies. If the hydrogen in M51 is assumed to be distributed in a spherical halo, the density of HI in the halo is about 0.006 atom per cubic centimeter, in good agreement with the predictions of Pickelner and Shklovsky.

From galaxies in this nearby group we should be able to obtain new information on the structure and content of galaxies in general which can be applied to the more distant ones. We should, for example, be able to make a new determination of the total mass of a galaxy which

is independent of the optical determination. The mass of a single galaxy can best be determined by its rotation curve; that is, the dependence of rotational velocity on distance from the center. Beyond the point in the galaxy where the velocity begins to decrease with increasing radius the relation is assumed to be Keplerian; that is, all the mass is assumed to be concentrated at the center and the outer mass elements considered to be moving independently. The observed relation between velocity and position then gives the total mass. Optically, the velocities are determined from the Doppler displacement of spectral lines in small isolated emission nebulosities. The 21-centimeter determination of the velocities, however, depends on all the gas in the line of sight within the rather large beamwidth. This has the advantage of averaging out any peculiar motions of small portions of the galaxy; but the disadvantage of possible confusion because of the enormous volume included. However, any improvement or check on the values of masses of these nearby galaxies is of very great importance because they are the basis for the mass-luminosity relation by which most of the masses of distant galaxies are estimated. With this or other determination of the total mass and the direct determination of the mass of HI we shall be able to find in each case the percentage of the mass of the galaxy that exists as interstellar neutral hydrogen. It may be hoped also that in the future a discussion of the variation of the mass-luminosity ratio in different parts of a galaxy may be supplemented by a comparison of the luminosity and HI mass in the region considered. Right now, however, one of the most striking problems is the direct determination of how the neutral hydrogen associated with a galaxy is distributed in space and how it varies in velocity. Even from our limited view now it seems obvious that 21-centimeter observations of galaxies hold rich and varied promise. The size of galaxies in neutral hydrogen radiation may permit us to include several other systems in group one—the group which we can study in some detail. If other systems exceed their optical diameter by as much as those so far observed, we may be able to observe structure in some of them even with existing antennas. With the larger antennas now planned, or under construction, even spiral structure, at least in M31, may be detectable.

The number of galaxies in the second group—in which only the mass and velocity dispersion of hydrogen can be determined—should increase very rapidly. Table II gives estimates of maximum antenna temperatures that might be expected for a number of galaxies when observed with a 60-foot or 140-foot antenna. The estimates are obtained from<sup>9</sup>

$$\Delta T_m = 4.2 \times 10^{10} M_H \Delta V^{-1} \theta_0^{-2} s^{-2}, \quad (1)$$

where

$M_H$  = mass of HI (grams),

$\Delta T_m$  = maximum antenna temperature (°K),

<sup>9</sup> D. S. Heesch, "Neutral hydrogen in M32, M51, and M81," *Astrophys. J.*, vol. 126, in press; 1957.

<sup>10</sup> S. B. Pickelner and I. S. Shklovsky, "On the Nature of the Galactic Halo." Paper presented at the symposium, Gas Dynamics of Cosmic Clouds, Harvard Observatory New Haven, Conn.; June, 1957.

TABLE II  
MAXIMUM EXPECTED ANTENNA TEMPERATURES FOR SEVERAL GALAXIES

Galaxy	Type	$M_T/M_\odot$	$M_H/M_\odot$	$s$ kpc	$\frac{1}{2}\Delta V$	$\Delta T_m$	
					km	60 feet	140 feet
M82	Ir	$8 \times 10^9$	$2 \times 10^9$	1300	50	5	30
M101	Sc	$2 \times 10^9$	$3 \times 10^8$	1100	10	6	30
M66	Sb	$1 \times 10^{11}$	$5 \times 10^9$	2200	100	2	10
M104	Sa	$5 \times 10^{10}$	$1 \times 10^9$	1500	100	1	6
NGC 3115	E6	$1.6 \times 10^{10}$	$8 \times 10^7$	1700	100	0.1	0.4

$\Delta V$  = total line width to  $\frac{1}{2}$  intensity (cm per second),  
 $\theta_0$  = observed angular diameter to  $\frac{1}{2}$  intensity (radians),

$s$  = distance to the source (cm),

$\nu, \Delta\nu$  = frequency and Doppler shift.

In Table II, the mass of HI present has been estimated from the type of galaxy, the total mass, and the data in column 6 of Table I. The total masses are from Holmberg.<sup>11</sup> The values of  $\Delta V$  are assumed values, based on the results of observations that have been made of other galaxies. In all cases  $\theta_0$  has been taken as the antenna beamwidth.

Perhaps the most obvious quantity to be derived from such observations is the radial velocity of the galaxy, and this can be done quite simply and accurately if the system can be observed at all. For example, M51 was found to have a velocity relative to the sun of  $+421 \text{ km} \pm 5 \text{ km}$ , while the optical velocity is given as  $+438 \text{ km per second} \pm 35 \text{ km}$ .<sup>12</sup> For more distant systems the improvement in accuracy will no doubt be still greater.

One of the most interesting parameters to be derived from 21-centimeter observations of galaxies is the variation of the amount of neutral hydrogen with galaxy type. From a practical point of view, this variation may make possible better estimates of the mass of systems beyond the reach of dynamical methods; that is, methods based on motions within, or interactions between, galaxies. If, in our local group of galaxies, we can find the percentage of hydrogen in the different types of galaxies (irregular, Sb, Sc, and E2 observed so far) we can perhaps extrapolate this to other systems and for a particular type of galaxy estimate the total mass from the mass of neutral hydrogen. Since, at the present time, estimates are based only on a mass-luminosity relation, this additional criterion may be useful despite the small sample on which it is based. This dependence of the amount of interstellar neutral hydrogen on galaxy type is also of interest from the point of view of the age and evolution of the stellar systems. It can, perhaps, provide data for investigating the balance between condensation

of stars out of the original hydrogen and its return to the interstellar medium. For this reason a search for other ellipticals to supplement the information on M32 should certainly be carried out although the signals can be expected to be very small indeed. Perhaps those showing some sign of the presence of dust would be the most likely objects to begin with. There are as yet no direct observations of Sa or S0 systems which would be needed to fill in the sequence.

#### 21-CENTIMETER LINE EMISSION FROM CLUSTERS OF GALAXIES

Twenty-one-centimeter line emission has been observed from three clusters of galaxies to date.<sup>13,14</sup> The data derived from these observations are given in Table III, together with optical data for the clusters. The optical velocities are from Humason, Mayall, and Sandage.<sup>12</sup> The probable error in radial velocity from a 21-centimeter line measurement is about  $\pm 200 \text{ km}$ . The results shown in Table III suggest that 21-centimeter line observations may provide precise determinations of the recessional velocities of distant clusters.

TABLE III  
OBSERVED CLUSTERS OF GALAXIES

Cluster	Distance, mpc	$\Delta T_m$	Diameter	Radial vel km	
				HI	Optical
Coma	25	2.0	$5^\circ$	+7000	+6680
Hercules	58	1.5	$4^\circ.5$	+10,040	+10,277
Corona Borealis	120	1.0	$1^\circ$	+21,024	+21,530

The antenna temperature in the hydrogen line,  $\Delta T_A$ , due to a source brightness temperature  $T_B$ , is given approximately by

$$\Delta T_A = T_B \frac{\Omega_s}{\Omega_A}$$

where  $\Omega_s$  and  $\Omega_A$  are solid angles, subtended respectively by the source and antenna beam, to half-intensity

<sup>11</sup> E. Holmberg, "On the masses and luminosities of extragalactic nebulae," *Lund Meddelunde, Ser. I*, no. 180, pp. 1-13; 1952.

<sup>12</sup> M. L. Humason, N. U. Mayall, and A. R. Sandage, "Redshifts and magnitudes of extragalactic nebulae," *Astron. J.*, vol. 61, pp. 97-162; April, 1956.

<sup>13</sup> D. S. Heeschen, "21-CM line emission from the Coma cluster," *Astrophys. J.*, vol. 124, pp. 660-661; November, 1956.

<sup>14</sup> D. S. Heeschen, "Neutral hydrogen emission from the Hercules and Corona Borealis clusters of galaxies," *Publ. Astron. Soc. Pacific*, vol. 69, pp. 350-351; August, 1957.

points. This expression is a good approximation only for  $\Omega_s \ll \Omega_A$ . For  $\Omega_s \gg \Omega_A$ ,  $\Delta T_A \approx T_B$ . Putting in appropriate expressions for  $\Omega_s$  and  $\Omega_A$  we get

$$\Delta T_A \approx T_B \left( \frac{d}{D} \right)^2 \frac{1}{\Omega_0} \left( 1 - \frac{HD}{c} \right)^2,$$

where  $d$  is the linear diameter of the source,  $D$  its distance,  $\Omega_0$  the solid angle subtended by the antenna at the undisplaced frequency of the line, and  $H$  is the Hubble red shift parameter. Table IV gives the antenna temperature expected from clusters similar to the Coma cluster at various distances, when observed with a 140-foot or 1000-foot paraboloid. In using the above equation,  $\Delta T_A$ ,  $T_B$ , and  $d$  were obtained from the Coma cluster results shown in Table III, and  $H$  was assumed to be 180 km per megaparsec.<sup>15</sup> The table shows that with a 140-foot telescope we should be able to determine from hydrogen line observations the red shifts of clusters of galaxies out to at least 800 megaparsec. Such measurements should be useful additions to optical measurements for studying the relation between red shift and distance of distant clusters.

TABLE IV  
ANTENNA TEMPERATURES EXPECTED FROM "COMA-LIKE"  
SOURCE AT VARIOUS DISTANCES

D mpc	$\Delta\nu/\nu$	$\nu$ mc	$\Delta T_m$	
			140 feet	1000 feet
200	0.12	1250	2.0	
400	0.24	1080	1.0	
600	0.36	910	0.3	
800*	0.42	830	0.15	
1000	0.5	710	0.07	2.0
1200	0.6	575		1.6
1400	0.7	425		0.6
1600	0.86	204		0.1

\* For this and succeeding distances, the relativistic Doppler effect has been used.

By conventional optical spectroscopic techniques, red shifts of distant galaxies have been measured to values of  $\Delta\nu/\nu$  of about 0.2. Recently Baum has developed a photoelectric technique with which he has measured red shifts and magnitudes of galaxies in clusters to  $\Delta\nu/\nu = 0.4$ .<sup>16</sup> It is clear from Table IV that hydrogen line red shift measurements can also be made to this distance and may therefore provide an accurate and important check on optically determined red shifts.

Red shift determinations of distant clusters of galaxies by measurements of the HI line emission are very time-consuming at the present, involving as they do the measurement of antenna temperatures of less than 1° K. Corresponding optical determinations are still more time consuming, however. Optically, there seems to be

little hope of either decreasing the time required or of extending the observations to still more distant clusters. In the case of the HI line observations, however, considerable improvement may be expected. Receiver techniques will undoubtedly improve greatly in the next few years. Researches now in progress on the solid state maser, low temperature crystal mixers, and transistorized IF amplifiers; and techniques for improving receiver stability all look promising in this respect.

With a 1000-foot diameter antenna it appears not impossible that red shifts of clusters of galaxies may be measured to  $\Delta\nu/\nu = 0.8$ . As far as the writers know, there are, at present, no definite plans anywhere for construction of an antenna with 1000-foot, or greater, aperture. However, very large antennas are being discussed and will undoubtedly be built in the future. If observations with the large antennas now available or soon to be available bear out the predictions made here with regard to red shift measurements, a very considerable expenditure for still larger antennas would be justified on this basis alone. As receiver techniques improve, a point will be reached where antenna noise rather than receiver noise is the limiting factor in the measurement of weak signals. Improvement of signal to noise ratio at this stage can be accomplished only by increasing antenna gain and efficiency.

The 21-centimeter line observations needed to measure the red shift of a cluster of galaxies also serve to determine the random motion and total mass of neutral hydrogen within the cluster. In addition, it should be possible to determine the distribution of hydrogen within some of the nearer clusters. Table V gives data for some of the better known nearby clusters of galaxies.

TABLE V  
PREDICTED ANTENNA TEMPERATURES FOR CLUSTERS OF GALAXIES

Cluster	Distance, mpc	Radial velocity, km	No. of galaxies	Predicted $\Delta T_m$	
				60 feet	140 feet
Peg I	21	3800	100	10° K	10° K
Pisces	26	4700	30	2	2
Cancer	27	4900	150	9	9
Perseus	30	5433	500	6	6
U Ma I	86	15,519	300	3	4
Haufen A	88	15,781	420	3	3
Leo	108	19,489	300	2	3
Gemini	130	23,365	200	0.9	2
Bootes	218	39,367	150	0.2	1
U Ma II	224	40,360	200	0.2	1

The predicted antenna temperatures shown in the last two columns are based on the assumptions that the ratio of hydrogen to number of galaxies in the cluster is the same for these clusters as it is for the Coma cluster, and that the mean random motion is the same. All of these clusters have easily detectable hydrogen line emission if the above assumptions are correct. The question of the validity of the assumptions is an important topic for investigation. Is the density of hydrogen in a

<sup>15</sup> One megaparsec equals  $3.262 \times 10^6$  light years or  $3.086 \times 10^{24}$  cm.

<sup>16</sup> W. A. Baum, "Photoelectric determinations of redshifts beyond 0.2c," *Astron. J.*, vol. 62, p. 6; January, 1957.

cluster constant from one cluster to another, and if not, on what does it depend? Is the hydrogen mass dependent on the number of galaxies in the cluster? Is it dependent on the types of galaxies in the cluster, or on the mass-luminosity ratio of the cluster? Is it dependent on the age of the cluster? We hope some progress toward answering these questions can be made through 21-centimeter line observations and related optical studies.

The antenna temperature produced by 21-centimeter line emission from a cluster of galaxies is given by (1) used previously for individual galaxies,

$$\Delta T_A = 4.2 \times 10^{19} M_H \Delta V^{-1} \theta_0^{-2} s^{-2}. \quad (2)$$

All of the quantities in this equation except  $M_H$  and  $s$  can be directly determined from observations. Thus if the distance to a cluster is known from optical measurements the mass of hydrogen may be obtained from the 21-centimeter observations. The mass of hydrogen in clusters is of value in assessing the mean density of matter in the universe, a quantity of great importance to cosmological theories. If, from 21-centimeter line and optical studies of clusters with known distances, we can find a relationship between the mass of hydrogen within a cluster and some other measurable property of the cluster, it may be possible to use this relation to obtain the distance of more distant clusters. At the present time all distances of faint clusters are determined from the magnitudes of the brightest galaxies in the cluster. Such determinations can be quite accurate, but uncertainties arise because assumptions and corrections to the observational data are required. Another, completely independent, method for the determination of distances of faint clusters is highly desirable. It is hoped that 21-centimeter line observations will provide the answer.

The hydrogen line observations that so far have been made of clusters of galaxies do not suffice to determine the important question of whether the neutral hydrogen observed is concentrated principally in the galaxies, or

in the intergalactic region, of a cluster. Most clusters appear to consist mainly of type E and S0 galaxies—population II objects with presumably little HI. It has been suggested<sup>17</sup> that the reason so few spiral galaxies are to be found in clusters is that collisions between galaxies sweep out the gas and dust before spiral structure has time to develop. The Coma cluster observations suggest that the hydrogen is between the galaxies, rather than in them; the large mass of hydrogen found,  $10^{14} M_\odot$  appears to be too great to be due to the 1000 galaxies of the cluster, particularly since most of the galaxies are types E and S0. The evidence is far from conclusive, however, and more observations with antennas of high resolution are needed. Higher resolutions studies may enable us to compare the distribution of hydrogen in a cluster with that of the galaxies in the cluster and thereby shed some light on this problem. If it should be established that the neutral hydrogen in clusters of galaxies is intergalactic, the question still remains as to whether it is there as the result of collisions, or whether some or all of the intergalactic hydrogen is the residue of a primordial gas cloud from which the cluster formed. It is possible, for example, that much of the hydrogen swept out of galaxies by collisions would remain ionized and therefore not contribute to the 21-centimeter line emission.

It is clear that 21-centimeter line observations potentially provide a very powerful means for studying the properties of galaxies and clusters of galaxies. Those few observations, described here, that are available at present have raised many more questions than they have answered, and all of the work to date is in need of verification and expansion. Extragalactic 21-centimeter line studies should be a fruitful and exciting field for many years and, together with optical studies, may be expected to add greatly to our knowledge of extragalactic systems and the nature of the universe.

<sup>17</sup> W. Baade and L. Spitzer, "Stellar populations and collisions of galaxies," *Astrophys. J.*, vol. 113, pp. 413–418; March, 1957.



# Excitation of the Hydrogen 21-CM Line\*

GEORGE B. FIELD†

**Summary**—The importance of spin temperature for 21-cm line studies is reviewed, and four mechanisms which affect it are studied. Two of the mechanisms, collisions with free electrons and interactions with light, are studied here in detail for the first time. The results are summarized in Table II of Section VI, in the form of certain *efficiencies* which can be used with (15) to calculate the spin temperature. In Section VI the results are applied to a variety of astronomical situations, and it is shown that in the usual situation collisions with H atoms are very effective in establishing the spin temperature equal to the kinetic temperature. Under conditions of low-density and/or high-radiation intensity, however, important deviations from the usual are noted. The significance of such deviations for absorption studies of radio sources and the galactic halo is discussed. In Section VII the deuterium line at 91.6 cm is considered in like fashion. It is shown that for deuterium also, the spin temperature probably is close to the kinetic temperature.

## I. INTRODUCTION

GR<sup>E</sup>AT advances have been made in the understanding of the interstellar medium by studying the distribution of 21-cm emission. (See, for example, van de Hulst, Muller, and Oort,<sup>1</sup> and Muller and Westerhout.<sup>2</sup>) Absorption by interstellar clouds of radiation emitted by radio sources has also been observed, particularly by Williams and Davies,<sup>3</sup> Hagen, Lilley, and McClain,<sup>4</sup> and Muller.<sup>5</sup> The phenomenon of absorption, when connected with radio sources, has permitted studies of hydrogen distribution with the high-effective angular resolution resulting from the small diameters of the sources observed. The same phenomenon, when connected with emission features, has complicated interpretation of emission profiles as saturation is approached.

Several authors, including Hagen, Lilley, and McClain,<sup>4</sup> have discussed the theory of 21-cm absorption. For our purpose, the equation for a simple case is sufficient. Let a cloud (large compared to a beamwidth) of "spin temperature"  $T_S$  be placed in front of a radio source of antenna temperature  $T_B$  in the continuum. If

the detector operates as a comparison system, the observed antenna temperature is

$$\Delta T_A = (T_S - T_B)(1 - e^{-\tau_\nu}), \quad (1)$$

where  $\tau_\nu$  is the frequency-dependent opacity of the cloud.  $\Delta T_A$  is thus the sum of the diminished source radiation,  $T_B e^{-\tau_\nu}$ , and the self-absorbed cloud radiation,  $T_S(1 - e^{-\tau_\nu})$ , less the undiminished source radiation,  $T_B$ , detected outside the line and hence subtracted from the total.

If the equation is applied to a radio source and to a point close enough to the source to assure that the beam is in the same cloud as when on the source, we see that both  $(T_S - T_B)(1 - e^{-\tau_\nu})$  and  $T_S(1 - e^{-\tau_\nu})$  may in principle be determined. Direct radiometry outside the line determines  $T_B$ , and hence we may obtain  $T_S$  and  $\tau_\nu$  separately. If the equation is applied to a point with little continuum emission, the extra data afforded by absorption of a source of known brightness are missing, and it is impossible to obtain  $T_S$  and  $\tau_\nu$  separately; only the combination  $T_S(1 - e^{-\tau_\nu})$  is known. It has been the practice to assume (e.g., Muller, *et al.*)<sup>1</sup> that  $T_S$  is everywhere equal to its value determined toward the galactic center, *viz.*, 125°K, and to interpret all emission profiles on that basis.

If absorption observations are made and  $T_S$  determined, the relation of  $T_S$  to properties of the cloud is of interest. If emission observations are made, the reliability of assumptions concerning the value of  $T_S$  is important. In either case, it is worthwhile to relate  $T_S$  to physical properties of the cloud which may be predicted theoretically or observed in other ways. Previous considerations of this problem gave a simple answer;  $T_S = T_K$ , the gas kinetic temperature of the cloud.<sup>6-8</sup> In the present paper, this conclusion is substantiated for a wide variety of conditions, while in certain situations divergences are found.

## II. SPIN TEMPERATURE

The 21-cm line is a transition between the two hyperfine states of the  $1^2S_{1/2}$  ground level of hydrogen. These states differ only in the value of the total spin angular momentum  $F$ , which is the sum of electron and proton spins:

$$F = S + I. \quad (2)$$

<sup>6</sup> H. I. Ewen and E. M. Purcell, "Radiation from galactic hydrogen at 1420 mc," *Nature*, vol. 168, p. 356; September, 1951.

<sup>7</sup> S. A. Wouthuysen, "On the excitation mechanism of the 21-cm interstellar hydrogen emission line," *Astrophys. J.*, vol. 57, pp. 31-32; April, 1952.

<sup>8</sup> E. M. Purcell and G. B. Field, "Influence of collisions upon population of hyperfine states in hydrogen," *Astrophys. J.*, vol. 124, pp. 542-549; November, 1956.

\* Original manuscript received by the IRE, November 6, 1957.

† Harvard College Observatory, Cambridge, Mass.; presently at Princeton Univ. Observatory, Princeton, N. J.

<sup>1</sup> H. C. van de Hulst, C. A. Muller, and J. H. Oort, "The spiral structure of the outer part of the galactic system derived from hydrogen emission at 21-cm wavelength," *Bull. Astron. Inst. Neth.*, vol. 12, pp. 117-149; May, 1954.

<sup>2</sup> C. A. Muller, G. Westerhout, *et al.*, "A catalogue of 21-cm line profiles," *Bull. Astron. Inst. Neth.*, vol. 13, pp. 151-195; March, 1957, and the four papers following in the same number.

<sup>3</sup> D. R. W. Williams and R. D. Davies, "A method for the measurement of the distance of radio stars," *Nature*, vol. 173, pp. 1182-1183; June, 1954; also, *Phil. Mag.*, Ser. 8, vol. 1, p. 622; July, 1956.

<sup>4</sup> J. P. Hagen, A. E. Lilley, and E. F. McClain, "Absorption of 21-cm radiation by interstellar hydrogen," *Astrophys. J.*, vol. 122, pp. 361-375; November, 1955.

<sup>5</sup> C. A. Muller, "21-cm absorption effects in the spectra of two strong radio sources," *Astrophys. J.*, vol. 125, pp. 830-834; May, 1957.

Since  $S$  and  $I$  are each  $\frac{1}{2}$  (in units  $\hbar$ ),  $F$  takes the value 0 or 1, splitting the ground level into a hyperfine doublet. In a magnetic field, the  $F=1$  state is further split into three components and is therefore called a triplet; the  $F=0$  state is a singlet. The triplet state lies above the singlet an amount  $h\nu_{10}$  with  $\nu_{10}=1420.405$  mc, so the  $1\rightarrow 0$  transition results in the emission of a quantum of 21-cm radiation. The energy difference between the singlet and triplet is due to the different orientations of electron and proton magnetic moments (parallel in the singlet, antiparallel in the triplet) which results in a magnetic interaction analogous to that between two bar magnets. The  $1\rightarrow 0$  transition then is equivalent to a "spin flip," the electron spin going from parallelism with the proton spin to antiparallelism.

The probability for a spontaneous  $1\rightarrow 0$  transition is given by the Einstein  $A$  quoted by Wild:<sup>9</sup>

$$A_{10} = \frac{64\pi^4\beta^2}{3h\lambda^3} = 2.85 \cdot 10^{-15} \text{ sec}^{-1}, \quad (3)$$

where  $\beta$  is the Bohr magneton. Such an extremely small value for  $A$  corresponds to a lifetime of the triplet state of  $1.1 \times 10^7$  years against spontaneous radiation and is responsible for the importance of collisions as against radiation in establishing the population of the triplet. Twenty-one-cm radiation incident on the atom can cause  $0\rightarrow 1$  transitions (absorptions) and  $1\rightarrow 0$  transitions (induced emissions). These processes have probabilities given by

$$I_\nu B_{01} = \frac{g_1}{g_0} B_{10} I_\nu = 3A_{10} \frac{\lambda^2 I_\nu}{2h\nu_{10}}, \quad (4)$$

and

$$I_\nu B_{10} = A_{10} \frac{\lambda^2 I_\nu}{2h\nu_{10}},$$

respectively. In these equations  $I_\nu$  is the specific intensity of 21-cm radiation and  $g = 2F+1$  the statistical weight of the state.

A beam of 21-cm radiation, therefore, causes absorption and induced emission on passing through a hydrogen cloud. Absorptions subtract photons from the beam while induced emissions add them; consequently the induced emissions act like negative absorptions. Suppose that we know the absorption coefficient, per cm, calculated on the assumption that all atoms are in the singlet state. If we call this quantity  $K_{01}$ , the effective absorption coefficient is

$$K = K_{01}(1 - g_{01}n_1/g_1n_0), \quad (5)$$

when corrected for stimulated emission, as can be seen from the relative probabilities expressed in (4). If the cloud were in thermodynamic equilibrium at some temperature  $T$ , we could say that

<sup>9</sup> J. P. Wild, "The radio-frequency line spectrum of atomic hydrogen and its applications in astronomy," *Astrophys. J.*, vol. 115, pp. 206-221; March, 1952.

$$g_0n_1/g_1n_0 = \exp(-h\nu_{10}/kT), \quad (6)$$

according to Boltzmann's law. Even if it is *not* in thermodynamic equilibrium, it is convenient to *define* a "spin temperature,"  $T_S$ , by such a relation, so that

$$g_0n_1/g_1n_0 \equiv \exp(-h\nu_{10}/kT_S). \quad (7)$$

At this point a radical difference emerges between ordinary and radio astronomy. Interstellar temperatures which are directly observable are in the range 100°K to 10,000°K, with few exceptions. But  $h\nu/k$  for most optical lines is 20,000°K or more. Hence in the optical case the exponential is small, most atoms are in the ground state, and a determination of  $K$  then refers to  $K_{01}$  and hence to practically all of the atoms. For the 21-cm line,

$$h\nu_{10}/k \equiv T_* = 0.0681^\circ\text{K}, \quad (8)$$

and the exponential is close to unity. Therefore,  $K$  is determined by the small difference in populations of the singlet and triplet, this difference depending on the usually unknown spin temperature,  $T_S$ . It follows that determinations of opacity lead directly to densities in the optical realm, but not in the radio. On the other hand, because an assignable fraction of atoms is in the upper state in 21-cm work, emission is easily interpreted in terms of numbers of atoms.

It may be mentioned that since  $T_S$  is usually much greater than  $T_*$ ,

$$K = 32,000 n_{0f}(\nu)/T_S \quad (9)$$

follows from (7), when we use  $K_{01} = 3n_0A_{10}\lambda^2f(\nu)/8\pi$ , where  $f(\nu)$  is the line shape function. Eq. (9) reduces to one of Wild's<sup>9</sup> if we put the number of singlet atoms,  $n_0$ , equal to  $g_0/(g_1+g_0) = \frac{1}{4}$  of the total. When  $Kl$  is substituted for  $\tau_\nu$  in (1) and assumed small; and if  $T_B=0$  so that only emission is effective, we see that  $T_S$  cancels; the observed emission is independent of  $T_S$  as long as there is no saturation. Thus it is that  $T_S$  is of no consequence as long as we study optically thin clouds in emission. When we study absorption, however, it forms a vital link in the interpretation.

### III. STATISTICAL EQUILIBRIUM

The spin temperature,  $T_S$ , is merely a convenient shorthand for the relative population of the singlet and triplet. What then determines these populations physically? If the cloud were isolated from space by a wall, we could apply statistical mechanics to calculate the distribution of the available energy over the various energy levels. There would then be a unique temperature for all kinds of energy modes, including energy of translation, radiation, and discrete atomic levels including the hyperfine levels. Thus the spin temperature would be equal to this unique temperature, whatever it might be.

But the cloud is not isolated from space; it continu-

ally receives radiation from the stars and emits it again into space. Our basic principle is to balance input and output. Given the rates of the various processes, it is then possible to compute the steady state populations. The final temperature which characterizes any mode of energy depends on the way that mode is coupled to other modes. There are temperatures appropriate to the translational energies of particles, to total radiation density, to the grains, to atomic levels, to the color of the light from stars. These can vary over wide limits depending on the degree to which the mode is coupled to the hot stars on the one hand and to free space on the other. In our case there are three temperatures of special interest to us; the brightness temperature of 21-cm radiation, averaged over all directions,  $T_R$ ; the kinetic temperature of the atoms and electrons,  $T_K$ ; and the color temperature of certain kinds of light,  $T_L$ . The brightness temperature of radio radiation at 21 cm is defined in the usual way:

$$T_R = \frac{\lambda^2}{2k} \bar{I}_\nu \tag{10}$$

with  $\bar{I}_\nu$  the brightness at 21 cm averaged over the whole sky and over all Doppler shifts occurring in the group of H atoms.  $T_L$  will be defined later.

Evidently, there are fundamentally two kinds of excitation mechanisms, collisional and radiative. Each of these can excite the transition directly by exchange of a quantum of energy equal to  $h\nu_{10}$ . But conceivably, higher levels of the hydrogen atom can be excited from one hyperfine state with de-excitation occurring to the alternate hyperfine state. Since the  $n=2$  level is the lowest level above the ground state, a transition  $n=1$  to  $n=2$ , corresponding to the Lyman- $\alpha$  line in the spectrum of hydrogen (1216Å, and 10.2 ev.), is required to accomplish this. Certainly the scattering of Lyman- $\alpha$  should be taken into account, and possibly higher Lyman lines. But we need not consider high energy collisions because the fraction of particles with energies enough to excite  $L\alpha$  collisionally is proportional to  $10^{-(61,000/T_K)}$ , while the fraction which can ionize the atom is proportional to  $10^{-(68,000/T_K)}$ . Hence if the value of  $T_K$  is such as to make the first value significant, the second factor will be only slightly less, and ionization will occur. Thus, we find that regions hot enough for high-energy collisions will be ionized and thus unobservable. We are left with the low energy collisions and both low- and high-energy radiative transitions as important mechanisms. We write  $P^{C,R,L}$  for the rate of transitions (per second) caused by collisions, radio frequency, and light, respectively. Using (4), (8), and (10), we find

$$\left. \begin{aligned} P_{01}^R &= 3 \frac{T_R}{T_*} A_{10}, \\ P_{10}^R &= \left(1 + \frac{T_R}{T_*}\right) A_{10}, \end{aligned} \right\} \frac{P_{01}^R}{P_{10}^R} \simeq 3 \left(1 - \frac{T_*}{T_R}\right), \tag{11}$$

for the transitions caused by 21-cm radiation of average brightness,  $I_\nu = 2kT_R/\lambda^2$ .

Collisional transitions have probabilities which will be calculated in Section IV, but the ratio of  $P_{01}^C$  to  $P_{10}^C$  is easily derived. For any type of colliding particle, the rate is proportional to the number of such particles, times some function of the kinetic temperature. Hence, the ratio of the upward to downward rates is a function of the kinetic temperature alone and is, therefore, the same as in a closed system at the same temperature. The latter will be just that for thermodynamic equilibrium, and (6) holds in addition to the condition of steady state so we find that

$$n_0 P_{01}^C = n_1 P_{10}^C = \frac{g_1}{g_0} n_0 P_{10}^C \exp(-T_*/T_K),$$

so

$$\frac{P_{01}^C}{P_{10}^C} = \frac{g_1}{g_0} \exp(-T_*/T_K) \simeq 3 \left(1 - \frac{T_*}{T_K}\right). \tag{12}$$

(We shall always assume all  $T$ 's  $\gg T_*$ .) Since the argument holds for each kind of collision, it holds for any combination of collisions.

We note that (12) for the ratio holds also for 21-cm radiation, with  $T_K$  replaced by  $T_R$ . Inasmuch as it follows from a thermodynamic argument involving the energy source, we may assume that the argument holds also for the case of excitation by Lyman radiation. In this case, the value of the "temperature of the light" follows from a detailed argument which will be considered in Section V. For the present let us define  $T_L$ , the light temperature, by

$$\frac{P_{01}^L}{P_{10}^L} = 3 \left(1 - \frac{T_*}{T_L}\right). \tag{13}$$

The hypothesis of equilibrium states that the populations of singlet and triplet do not change with time. Therefore, the number leaving the triplet equals the number entering the triplet, per second. This leads to

$$\begin{aligned} \frac{n_1}{n_0} &= \frac{g_1}{g_0} \exp(-T_*/T_S) \simeq 3 \left(1 - \frac{T_*}{T_S}\right) \\ &= 3 \frac{\frac{T_R}{T_*} A_{10} + \left(1 - \frac{T_*}{T_K}\right) P_{10}^C + \left(1 - \frac{T_*}{T_L}\right) P_{10}^L}{A_{10} \left(1 + \frac{T_R}{T_*}\right) + P_{10}^C + P_{10}^L} \end{aligned} \tag{14}$$

when (6), (11), (12), and (13) are applied. Upon rearranging, we find

$$T_S = \frac{T_R + y_C T_K + y_L T_L}{1 + y_C + y_L},$$

$$y_C = \frac{T_*}{T_K} \frac{P_{10}^C}{A_{10}}, \quad y_L = \frac{T_*}{T_L} \frac{P_{10}^L}{A_{10}} \tag{15}$$

are normalized probabilities or "efficiencies." Eq. (15) shows that  $T_S$  is a weighted mean of the three temperatures  $T_R$ ,  $T_K$ , and  $T_L$ ; when any one of the efficiencies is very large,  $T_S$  takes on the corresponding temperature value. Our next step is to discuss the efficiencies and to show how they are related to certain properties of the interstellar medium.

#### IV. COLLISIONS

We have calculated in the previous section the *ratio* of the de-excitation to the excitation probability, which holds for any type of collision. Let us now consider what the rate of de-excitation is. Since  $y_c$  is proportional to  $P_{10}^c$ , we must calculate the probability for a given triplet atom that a de-excitation takes place via a collision of that atom with another particle. Evidently, since the large mass of the proton makes it sluggish compared to the electron, the forces induced in the atom by a collision are much more likely to cause the electron spin to flip than the proton spin to do so. An electron spin flip can be caused magnetically by the action of magnetic forces on the magnetic moment of the electron, or electrostatically by forcing out the original electron and replacing it with one of opposite spin.

The latter process of substitution of an "up" for a "down" electron, called spin-exchange, can occur whenever the colliding particle contains electrons and, in particular, if the colliding particle is a hydrogen atom or a free electron. The total density of H atoms and electrons is always greater than that of any other species since the number of H atoms plus electrons is greater than the number of hydrogen nuclei (protons) by the number of free electrons originating in the ionization of other elements, while the proton density usually exceeds the helium density by a factor 10 and other atoms by a factor 1000. It is clear that H atoms and free electrons will always play a dominant role then; the latter assumes relative importance whenever the ionization of hydrogen is more than a few per cent. It may be added that the spin-exchange process for collisions with H atoms and free electrons is much more probable than the magnetic spin flip alluded to above, because the magnetic interaction induced by the atomic or free electron, as the case may be, is less than the electrostatic interaction by roughly  $v^2/c^2$ . This quantity is  $5 \times 10^{-6}$  for atomic electrons and only  $4 \times 10^{-6}$  for free electrons at  $10^4$ K.

It seems very probable, therefore, that by far the most frequent collisions will be with other H atoms and free electrons. The H atom case is treated in detail by Purcell and Field.<sup>8</sup> They showed that the atomic encounter can be treated semiclassically, and that the strong dependence of the interatomic forces on the separation makes the collision cross section relatively independent of energy; it was found to vary as  $T_K^{-0.27}$  over the range  $1^\circ$  to  $10^4$ K. The collision effectiveness,  $y_H$ , was computed and presented in Table I of their

paper. Since it is proportional to  $n_H$ , the density of hydrogen atoms,  $y_H/n_H$  was actually given. The resulting values of  $y_H/n_H$  are listed in Table II of the present paper.

The treatment of the free electron spin exchange is of necessity quantum mechanical, the angular momenta of the important collisions being less than  $\hbar$  because of the small electron mass. Although this particular problem is not solved in the literature, the problem of scattering of a polarized beam of electrons by a ground state hydrogen atom has been treated by many authors, in various energy ranges and using various approximations. An excellent discussion of this work is given by Seaton.<sup>10</sup>

Our problem can be related to the scattering problem as follows. (See Appendix for a rigorous demonstration.) The scattering problem results in "scattering amplitudes,"  $T(\theta)$  and  $S(\theta)$ , which are functions of the polar angle of the scattered beam with the incident beam, and which refer to the cases in which the incident and atomic electrons are in the triplet state [ $T(\theta)$ ], or singlet state [ $S(\theta)$ ]. The *differential scattering cross section* in direction  $\theta$  is well known to be  $\frac{3}{4}|T|^2 + \frac{1}{4}|S|^2$  for an unpolarized beam. The analogous *differential cross section for electron exchange* is  $\frac{1}{4}|T-S|^2$ . Since, however, only half of the exchanges are with electrons having opposite spin, the *electron spin exchange cross section* is half of this quantity. Furthermore, half of the electron spin exchanges with a hyperfine triplet result only in a transition to another component of the triplet, so the *de-excitation cross section* is only half of the spin exchange cross section. Thus, the differential de-excitation cross section for which we seek is

$$\frac{d\sigma}{d\omega} = \frac{1}{16} |T - S|^2, \quad (16)$$

where  $d\omega$  is an element of solid angle in direction  $\theta$ . Now all of the calculations we shall use are based on *S*-wave scattering, in which  $T$  and  $S$  are independent of  $\theta$ . (That this is a good approximation up to  $10,000^\circ$ K follows from the study of *P* waves by Chandrasekhar and Breen.<sup>11</sup>) Consequently we have the total de-excitation cross section for triplet atoms by free electrons:

$$\sigma = \frac{\pi}{4} |T - S|^2. \quad (17)$$

Naturally, the scattering amplitudes and  $\sigma$  depend on the energy of the incident electron. Here we may divide the energy range into two domains: one, right around zero energy, the other extending up to perhaps one volt. The higher energies were treated by two variational

<sup>10</sup> M. J. Seaton, "The application of variational methods to atomic scattering problems. V. The zero energy limit of the cross-section for elastic scattering of electrons by hydrogen atoms," *Proc. Roy. Soc. A*, vol. 241, pp. 522-530; September, 1957.

<sup>11</sup> S. Chandrasekhar and F. H. Breen, "The motion of an electron in the Hartree field of a hydrogen atom," *Astrophys. J.*, vol. 103, pp. 41-70; January, 1946.

principles by Massey and Moiseiwitsch.<sup>12</sup> The results using the two variational principles were in good agreement for the triplet amplitude, and we can use them directly. For the singlet amplitude the results disagreed by 10 per cent, but the authors preferred the Hulthen (H) method with a free parameter (b). Thus we may use the H-b results for the singlet. Seaton<sup>10</sup> feels that the H-b results are accurate to about 20 per cent up to energies at which *P* waves become important (presumably 10,000°K). On the other hand, the low-energy data for the singlet are considered dubious by Seaton, who introduces a different trial function and finds agreement between his results using the two variational methods for zero energy of the incident electron. However, he found a 6 per cent discrepancy in the zero energy singlet amplitude which he had calculated, and the H-b singlet amplitude of Massey and Moiseiwitsch extrapolated to zero energy. I find, however, that the two agree within a per cent or so.

Borowitz and Greenberg<sup>13</sup> also calculated scattering amplitudes near zero energy (up to 0.04 ev). Their results are presented in Table I in terms of the scattering amplitudes for singlet and triplet at zero energy in units  $a_0 = 5.3 \times 10^{-9}$  cm. These amplitudes are called "scattering lengths." A second parameter which gives the dependence on energy near zero energy, called the "effective range," is also tabulated. For comparison, we also give the same quantities as calculated by Seaton<sup>10</sup> and deduced from Massey and Moiseiwitsch.<sup>12</sup>

We note that the zero energy triplet amplitudes agree well, but while Seaton agrees with Massey and Moiseiwitsch for the singlet, they both disagree with Borowitz and Greenberg. Furthermore, the form of the variation near zero energy is quite different as determined by the effective range in the two papers for both the singlet and triplet. Inasmuch as Borowitz and Greenberg do not attain high energies anyway and the Massey and Moiseiwitsch data agree with Seaton's at zero energy, it seems advisable to adopt Massey and Moiseiwitsch's results over the entire energy range.

Their data are given in terms of phase shifts,  $\delta$ , which are related to the amplitudes by

$$T \text{ or } S = k^{-1} \sin \delta_{l,s} e^{i\delta_{l,s}}, \tag{18}$$

where  $k$  is the momentum of the incident electron divided by  $\hbar$ . When these definitions are inserted in (17) for the cross section, we find

$$\sigma = \frac{\pi}{4k^2} \sin^2 (\delta_t - \delta_s). \tag{19}$$

<sup>12</sup> H. S. W. Massey and B. L. Moiseiwitsch, "The application of variational methods to atomic scattering problems. I. The elastic scattering of electrons by hydrogen atoms," *Proc. Roy. Soc. A.*, vol. 205, pp. 483-496; March, 1951.

<sup>13</sup> S. Borowitz and H. Greenberg, "Variational calculation of the scattering of electrons by hydrogen atoms at near zero energy," *Bull. Amer. Phys. Soc.*, pt. II, vol. 2, p. 172; April, 1957.

TABLE I  
SCATTERING PARAMETERS FOR ZERO ENERGY ELECTRONS

Author	Scattering Length		Effective Range	
	Singlet	Triplet	Singlet	Triplet
MM	7.00	2.34	2.46	1.40
S	7.01	2.33	—	—
BG	7.75	2.35	3.80	0.81

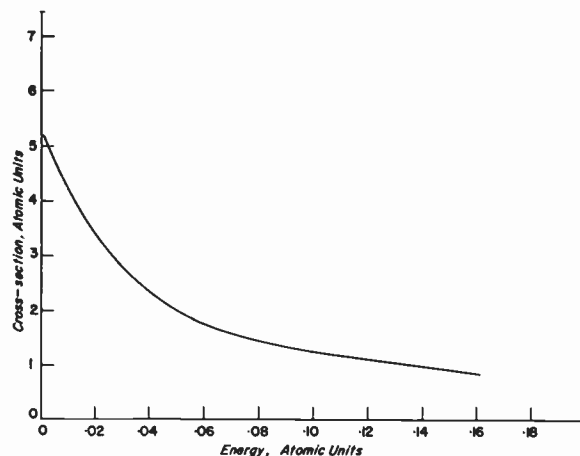


Fig. 1—Cross section for de-excitation of the hyperfine triplet by electrons. Energies are in Rydbergs (13.6 ev) and cross sections in units  $\pi a_0^2 = 8.8 \times 10^{-17}$  cm<sup>2</sup>.

The resulting cross section in units  $\pi a_0^2$  using Massey and Moiseiwitsch phase shifts is plotted vs the electron energy in units of 13.6 ev in Fig. 1.

The cross section may be averaged over a Maxwellian distribution of electron speeds, using the formula due to Jeans:<sup>14</sup>

$$P_{10}^e = n_e \sqrt{\frac{8kT_K}{\pi\mu}} \bar{\sigma}(T_K), \tag{20}$$

$$\bar{\sigma}(T_K) = \int_0^\infty u e^{-u} \sigma(u) du,$$

$$u = m_e E / \mu k T_K.$$

*E* is the incident electron energy, and  $\mu$  the reduced mass of the electron-atom system. Since  $\mu$  is about equal to  $m_e$ ,  $u$  is very close to  $E/kT_K$ , and we have for the value of  $y_e$ , defined by (15),

$$y_e = \frac{2h\nu_{10}}{kA_{10}} \sqrt{\frac{2k}{\pi m_e}} n_e \bar{\sigma}(T_K) T_K^{-1/2}. \tag{21}$$

The ratio between this equation and the analogous one of Purcell and Field<sup>8</sup> is seen to be

$$\frac{8}{\sqrt{2}} \left( \frac{m_H}{m_e} \right)^{1/2}.$$

<sup>14</sup> J. Jeans, "Dynamical Theory of Gases," Cambridge University Press, Cambridge, Eng., p. 36; 1925.

The factor 8 arises from our use here of  $\bar{\sigma}$  as the de-excitation cross section and there as the strong collision cross section, and the  $\sqrt{2}$  arises from the fact that here the relative velocity is just the electron velocity, not  $\sqrt{2}$  times the atom velocity. The results of averaging the cross section over electron speeds are shown in Fig. 2, and the values of  $y_e/n_e$  are given in Table II.

V. LIGHT

In Section III we pointed out that light could cause hyperfine transitions in the ground level via the intermediate step of transitions to higher optical levels in the atom. The lowest of these levels is  $n=2$ , for which the excitation energy is 10.2 volts, or 1216 Å, the  $L\alpha$  line. In a complete theory,  $n=3, 4, \dots$  should be considered, as well as the continuum of levels for the ionized state. The principles, however, can be made clear by discussing only  $L\alpha$  light. Furthermore, there is every reason to suspect that  $L\alpha$  will be particularly important in the interstellar medium, because radiation at this wavelength has a very short mean free path in hydrogen gas and yet endures many scatterings since the possibility of splitting into two photons via permitted transitions to an intermediate level is closed to it.<sup>15</sup> In consequence, every  $L\alpha$  photon is enormously more effective than an  $L\beta$ , for example, in scattering from ground level hydrogen atoms and hence in causing hyperfine transitions since the  $L\beta$  quickly splits into  $H\alpha$  and  $L\alpha$ .

We consider a triplet atom moving at speed  $v$  through an isotropic radiation field which has intensity  $I_\nu(\nu)$  in the neighborhood of  $L\alpha$ . We see that if the atom is initially in the ground level hyperfine triplet it may absorb a photon and thus reach the  $n=2$  level, returning however to the hyperfine singlet by emission of a more energetic photon. The probability of doing so depends on  $I_\nu(\nu)$ , where here  $\nu$  is the precise frequency corresponding to the upward transition in question, Doppler shifted by the speed  $v$ .

Similarly, a singlet atom can absorb a slightly higher frequency to reach the same upper state, so that the rates of leaving the singlet and triplet depend on the relative intensities at the two frequencies in question, while the rate of return is independent of the latter. Consequently, if there are more red photons than blue, the singlet becomes more heavily populated than the triplet.

More precisely, refer to the energy level diagram of Fig. 3, p. 246.  $2S$  level is omitted, as it is connected with  $1S$  only by a forbidden transition.  $2P$  is split into  $J=3/2$  and  $1/2$  by spin-orbit interaction; each of these levels is again doubled by hyperfine interaction with  $F=J\pm 1/2$ . The  $L\alpha$  line consists of the totality of transitions labelled in the figure. However, the transitions

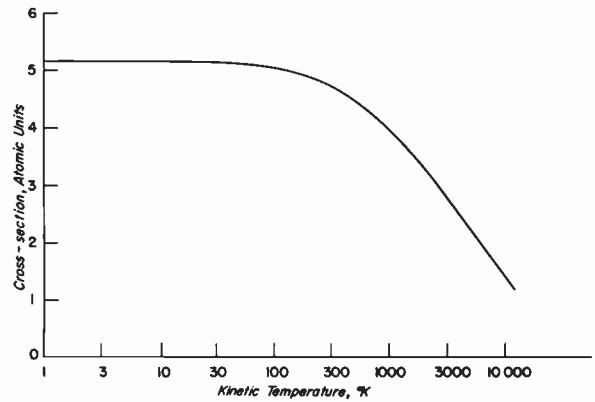


Fig. 2—Cross section for de-excitation, averaged over electron speeds at temperature  $T_K$ .

TABLE II  
EFFICIENCIES FOR COLLISIONS AND  $L\alpha$ , AND CRITICAL IONIZATION

(1) $T_K(^{\circ}K)$	(2) $y_H/n_H$	(3) $y_e/n_e$	(4) $y_\alpha/n_\alpha$	(5) $(n_e/n_H)_c$ per cent
1	1200	6700	$5.9 \times 10^{11}$	18
3	490	3900	$1.1 \times 10^{11}$	13
10	190	2100	$1.9 \times 10^{10}$	9
30	85	1200	$3.6 \times 10^9$	7
100	35	650	$5.9 \times 10^8$	5
300	16	350	$1.1 \times 10^8$	5
1000	6.7	130	$1.9 \times 10^7$	5
3000	3.3	66	$3.6 \times 10^6$	5
10000	1.3	18	$5.9 \times 10^5$	7

$2P_{3/2} \rightarrow 0S_{1/2}$  and  $0P_{1/2} \rightarrow 0S_{1/2}$  are forbidden since they involve  $\Delta F=2$  and  $0 \rightarrow 0$ , respectively. The relative strengths for the downward transitions are noted on the diagram. They were found from the usual rules for  $LS$  coupling of the hyperfine doublets given by Condon and Shortley<sup>16</sup> together with the observation that the relative strengths of the  $P_{3/2}$  and  $P_{1/2}$  lines are 2:1 in accordance with the  $LS$  coupling to form  $J$ . In the following we shall discuss only the transitions to and from the  $1P$  states since the transitions to and from  $2P$  and  $0P$  via the "complementary transitions" of Fig. 3 cannot mix the ground state populations as they are paired with forbidden transitions.

Let us call  $\nu_0$  and  $\nu_1$  the frequencies, Doppler shifted by a speed  $v$  (which we hold constant for the present) from the ground level singlet and triplet up to the  $1P_{1/2}$ , and  $\nu_0'$  and  $\nu_1'$  similarly up to  $1P_{3/2}$ . If  $I(\nu)$  is the intensity at those frequencies and  $B$  the corresponding Einstein probability, the rate at which a singlet atom is excited to  $1P_{1/2}$  is  $B_0 I(\nu_0)$ . It has a chance  $A_1/(A_0 + A_1)$  of returning to the triplet (if we ignore stimulated emission in the  $L\alpha$  line as is legitimate in interstellar space) thus effectively exciting the triplet state. Since the same can happen with  $1P_{3/2}$  the rate of excitation is, for  $\nu$  atoms

<sup>16</sup> E. U. Condon and G. H. Shortley, "The Theory of Atomic Spectra," Cambridge University Press, Cambridge, Eng. p. 243; 1953.

<sup>15</sup> Although two photon processes destroy even  $L\alpha$  after many scatterings, via transitions through a virtual level.

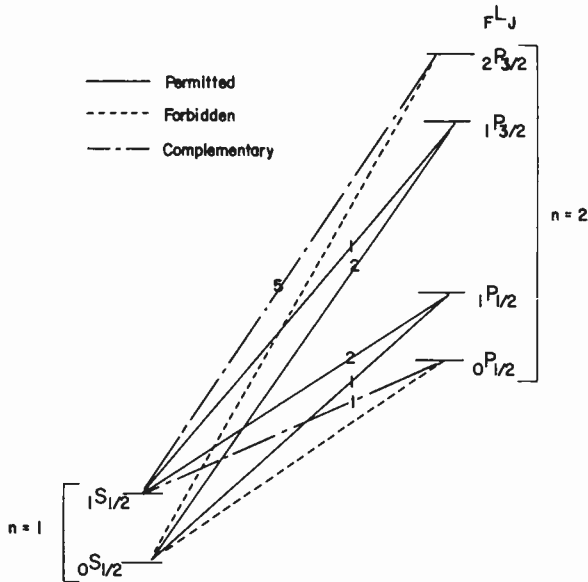


Fig. 3—The 1S and 2P levels of hydrogen, showing the particular transitions in the  $L\alpha$  line which excite the triplet (dark lines). The numbers in the center are relative strengths.

$$P_{10}^L = B_0 I(\nu_0) \frac{A_1}{A_0 + A_1} + B_0' I(\nu_0') \frac{A_1'}{A_0' + A_1'}; \quad (22)$$

similarly,

$$P_{10}^L = B_1 I(\nu_1) \frac{A_0}{A_0 + A_1} + B_1' I(\nu_1') \frac{A_0'}{A_0' + A_1'} \cdot \quad (22')$$

With the relations between  $B$ 's and  $A$ 's, and the relative strengths of Fig. 3, one can show that

$$P_{01}^L = \frac{B_0 A_1}{A_1 + A_0} [\bar{I}(\nu_0) + I(\nu_0')], \quad (23)$$

$$P_{10}^L = \frac{g_0}{g_1} \frac{B_0 A_1}{A_1 + A_0} [\bar{I}(\nu_1) + \bar{I}(\nu_1')].$$

Each expression of (23) is correct for any speed  $v$ . The bar signifies averaging over all  $v$ 's,  $I(\nu)$  being a function of  $\nu$  through the dependence of  $\nu$  on  $v$  in each case.

From (23), it is clear that the probabilities depend on the intensity profile of the radiation near  $L\alpha$ , and hence on the solution of a difficult scattering problem, the exact premises of which depend on physical conditions. For example, the radiation near a star would have a profile which depended on the atmosphere of the star, while radiation which has been scattered many times in the interstellar medium may have a profile dependent on the Doppler effects in the medium. It is the latter case which is of greatest interest:  $L\alpha$  is generated by recombination in an HII region and, scattering an enormous number of times, penetrates an HI region where it causes observable effects on 21-cm excitation. In fact, Wouthuysen<sup>7</sup> originally called attention to this possibility, and while it was dropped for a time in view of the

high efficiencies of collisions, it now seems that the  $L\alpha$  mechanism can be of import when the gas is dilute enough. In a forthcoming paper<sup>17</sup> the question of a  $L\alpha$  profile within a cloud will be treated. The work so far shows that if a portion of photons is scattered  $t$  times on the average by hydrogen atoms in a cloud having Doppler width  $\nu_D$ , the line will progressively broaden to  $\pm \nu_D (2 \ln t)^{1/2}$ , while flattening in the center between those limits. That is, the line profile approaches an ever widening "mesa" function. However, the flat portion slopes slightly down toward the blue as a consequence of photon energy losses through recoil, this slope being constant to a first approximation and equal in slope to the Planck curve corresponding to the atom kinetic temperature,  $T_K$ . Thus the radiation via recoil comes to quasi-equilibrium with the matter in a narrow range around the center of  $L\alpha$ , as predicted on general grounds by Wouthuysen.<sup>7</sup>

From the detailed scattered profile discussed above, it follows that we may put

$$\bar{I}(\nu_1) + I(\nu_1') = 2 \frac{h\nu_\alpha}{4\pi} \frac{n_\alpha c}{2\nu_D},$$

$$\bar{I}(\nu_1) - \bar{I}(\nu_0) = \bar{I}(\nu_1') - I(\nu_0') = \frac{h\nu_\alpha}{4\pi} \frac{n_\alpha c}{2\nu_D} \frac{h\nu_{10}}{kT_K}, \quad (24)$$

where there are  $n_\alpha$   $L\alpha$  photons per  $\text{cm}^3$  within  $\pm \nu_D$  of the line center. The error in this procedure comes from those scattering processes outside the straight line part of the line profile, *i.e.*, at distances greater than  $\nu_D (2 \ln t)^{1/2}$  from the center. But the fraction of scatterings at such frequencies is only  $\exp(-\nu^2/2\nu_D^2) = t^{-1}$ , which we may take to be a very small number. Using (13), (23), and (24), we see that

$$\frac{T_*}{T_L} \equiv \frac{h\nu_{10}}{kT_L} = \frac{h\nu_{10}}{kT_K}; \quad T_L = T_K. \quad (25)$$

This result, first pointed out by Wouthuysen,<sup>7</sup> follows, for the special case of radiation trapped in a cloud, from the detailed calculations summarized here. Using it, we have also

$$y_\alpha = \frac{h(\lambda c)^2}{36\pi k} \sqrt{\frac{m_H}{k}} \frac{A_\alpha}{A_{10}} \frac{\nu_{10}}{\nu_\alpha} \frac{n_\alpha}{T_K^{3/2}}, \quad (26)$$

when the various constants are inserted in (23). Note from (15), that we may not, however, draw Wouthuysen's conclusion that  $T_s$  depends only on  $T_K$  (which describes the "color" of the  $L\alpha$  radiation) but not on  $P_{10}^L$ , the frequency of  $L\alpha$  collisions. Clearly, this conclusion is valid only if  $L\alpha$  collisions dominate, *i.e.*, if  $y_\alpha \rightarrow \infty$ . In any case it is of interest that  $L\alpha$  does serve to couple  $T_s$  even more strongly to  $T_K$ . The values of  $y_\alpha/n_\alpha$  are given in Table II.

<sup>17</sup> G. B. Field, "The time dependent scattering of a resonance line by a dilute gas," to be published.

TABLE III  
FIVE EXAMPLES OF SPIN TEMPERATURE

Cloud	$T_K$	$T_R$	Atoms		Electrons		Photons		Contributions to $T_S$				$T_S$
			$n_H$	$y_H$	$n_e$	$y_e$	$n_\alpha$	$y_\alpha$	Radio	Atoms	Elec- trons	Pho- tons	
1) Remote	$10^2$	10	1	35	$10^{-3}$	0.65	$<10^{-13}$	$<10^{-4}$	0.27	95.30	1.78	0	97.35
2) Near HII (Orion)	$10^2$	20	1	35	$10^{-3}$	0.65	$4 \times 10^{-3}$	$2.4 \times 10^8$	$<10^{-5}$	$10^{-3}$	$<10^{-4}$	100	100.0
3) Source:													
Cygnus A	$10^2$	$2 \times 10^5$	1	35	$10^{-3}$	0.65	0	0	5450	95.3	1.8	0	5547
Virgo A	$10^2$	$2 \times 10^3$	1	35	$10^{-3}$	0.65	0	0	54.5	95.3	1.8	0	151.6
4) Galactic													
Halo	$10^4$	10	$10^{-2}$	$1.3 \times 10^{-2}$	$10^{-2}$	0.18	$4 \times 10^{-6}$	$2.4 \times 10^4$	$<10^{-3}$	$<10^{-2}$	0.12	$10^4$	$10^4$
5) Intergalactic	$10^3$	1	$10^{-5}$	$6.7 \times 10^{-5}$	$10^{-5}$	0.0013	—	1.6	0.38	0.03	0.49	615	616

VI. APPLICATIONS

In Table II we have collected the efficiencies for collisions with H atoms, electrons, and  $L\alpha$  quanta. We see that  $y_e/y_H$  is about 6 to 20 on a per particle basis. This implies that a small ionization will make electrons more important than atoms. The critical ratio at which this occurs,  $(n_e/n_H)_c$ , is listed in column 5. It indicates that in an HI region, electrons are unimportant since  $(n_e/n_H)_c \simeq 10^{-3}$ . In the galactic halo and in the intergalactic medium electrons may be important because coexistence of roughly equal numbers of atoms and electrons is possible at low densities.

$y_\alpha/n_\alpha$  exceeds the other efficiencies by large factors, mostly because  $c/v$  is large while the cross sections are not so different. We may thus be led to expect that Wouthuysen was correct in his original estimate of the importance of  $L\alpha$ . Obviously what matters is  $n_\alpha$ , and we shall see that the range of  $n_\alpha$  is such as to make  $L\alpha$  important under some conditions, while not in others.

We consider five examples of the application of (15) and Table II:

- 1) A remote cloud,
- 2) A cloud near a source of  $L\alpha$  (HII region),
- 3) A cloud near or in a radio source,
- 4) A cloud in the galactic halo,
- 5) An intergalactic cloud.

In Table III are estimates of  $T_K$ ,  $T_R$ ,  $n_H$ ,  $n_e$ , and  $n_\alpha$  for all five cases. Although we shall to some extent justify these estimates, in many cases they are mere guesses. Table III serves only to illustrate various possibilities for, using the parameters therein, we may compute the contributions to the spin temperature implied by (15) and summing the results, compare  $T_S$  with  $T_R$  and  $T_K$ . It should be remembered that while we have used  $T_L = T_K$  here in accordance with (25), one could use a more general light temperature defined by

$$\frac{T_*}{T_L} = - \frac{d \log \bar{I}_\nu}{d(\nu/\nu_{10})}, \tag{27}$$

in which case,

$$y_\alpha = 5.9 \times 10^{11} n_\alpha / T_L T_K^{1/2}. \tag{28}$$

Cases 1) and 2) are meant to differ only in the amount of  $L\alpha$ . In a remote cloud,  $T_R$  may be estimated by averaging 21-cm profiles in the vicinity of the plane<sup>1</sup> over a band width of 15 km/sec and allowing a few degrees for radiation near the poles and continuous emission. Case 2) may have a somewhat larger  $T_R$  owing to the radio emission of the HII region.

Case 3) is meant to demonstrate the effect of large  $T_R$ —the other parameters can be taken as equal to those of a remote interstellar cloud, although it is of course not certain what the real parameters are, of a cloud imbedded in high-velocity material. Both Cygnus A and Virgo A are treated, the former being the brightest, and the latter, the faintest among the five bright sources at 21 cm.  $T_R$  was estimated from the measures of Hagen, McClain, and Hepburn<sup>18</sup> together with angular dimensions at lower frequencies from Pawsey's<sup>19</sup> list.

Case 4) is based on Pickelner and Shklovsky's<sup>20</sup> model of the galactic halo, in which the hydrogen is about half-ionized. Case 5) adopts speculative parameters for the intergalactic medium.  $T_K$  is no more than a guess, while  $T_R = 1^\circ\text{K}$  is a reasonable extrapolation of results at lower frequencies near the galactic pole. The densities approximate the smoothed out densities of galactic matter, and the ionization may be 50 per cent.

We have not yet mentioned  $L\alpha$ . Of course what is needed is a detailed theory of the transfer of  $L\alpha$  from stars into the interstellar medium. Lacking this, we may calculate  $n_\alpha$  roughly by various means. First of all, HI regions such as 1) and 2) must receive their  $L\alpha$  from stars. Near a hot star, there will be an HII region where  $L\alpha$  is generated copiously by recombination after photoionization of the neutral hydrogen by stellar ultraviolet.

<sup>18</sup> J. P. Hagen, E. F. McClain, and N. Hepburn, "Detection of discrete radio sources at 21-cm wavelength," Proc. IRE, vol. 42, p. 1811; December, 1954.

<sup>19</sup> J. L. Pawsey, "A catalogue of reliably known discrete sources of cosmic radio waves," *Astrophys. J.*, vol. 121, pp. 1-5; January, 1955.

<sup>20</sup> S. B. Pickelner and I. S. Shklovsky, "An investigation of the properties and energy dissipation of the galactic halo," *Astrophys. J. USSR*, vol. 34, pp. 145-158; March-April, 1957. (In Russian, English abstract.)

This process has been studied by Zanstra,<sup>21</sup> who shows that

$$n_{\alpha}(\text{center}) = \frac{R}{c} \frac{dn_{\alpha}}{dt} = \frac{R}{c} \alpha n_e^2, \quad (29a)$$

$$n_{\alpha}(\text{edge}) = S_m^{-1} n_{\alpha}(\text{center}), \quad (29b)$$

where  $S_m$  is the optical depth of  $L\alpha$  at the line center corresponding to the radius,  $R$ , of the nebula.  $\alpha n_e^2$  is the number of recombinations per  $\text{cm}^3$  per sec in the nebula.  $S_m$  for a classical HII region may be taken as  $10^4$ , while for the Orion nebula,<sup>22</sup>  $n_e = 10^3 \text{ cm}^{-3}$ ,  $\alpha = 4 \times 10^{-13}$ , and  $R = 1 \text{ psc}$ . Consequently, for the Orion nebula

$$n_{\alpha}(\text{edge}) = 4 \times 10^{-3} \text{ cm}^{-3}. \quad (30)$$

On the other hand, these photons are scattered very frequently on their way into the HI region, and thus traverse large distances in order to make radial progress. It can easily be shown that the effective mean free path in the radial direction is reduced, because of absorption in the interstellar dust, to

$$l_e = (l_a l_s)^{1/2} = 0.04 \text{ psc}, \quad (31)$$

for a mean free path against scattering,  $l_s = 5 \times 10^{-6} \text{ psc}$ , and a mean free path against absorption,  $l_a = 300 \text{ psc}$ . It follows that the density of  $L\alpha$  given by (30) holds only a minute distance from the edge of the Orion nebula and at larger distances will be reduced by  $e^{-25d}$ , where  $d$  is the distance to the HII region in parsecs. Since the typical remote cloud will be a parsec or more from an HII region,

$$n_{\alpha}(\text{remote cloud}) < 10^{-13} \text{ cm}^{-3}, \quad (32)$$

and hence is entirely negligible. For the same reasons we put  $n_{\alpha} = 0$  in case 3).

In the halo, however,  $L\alpha$  is being generated locally by recombination in the partially ionized gas; furthermore, the absorption by dust is probably very low. In this case, (29a) will be appropriate, giving  $n_{\alpha} = 4 \times 10^{-5} \text{ cm}^{-3}$  for  $n_e = 10^{-2}$ ,  $\alpha = 4 \times 10^{-13}$ , and  $R = 10 \text{ kpc}$ . The case of the intergalactic medium again needs special treatment because of the peculiar transfer effects in an expanding medium. Here we find that the situation is dominated by the escape of red  $L\alpha$  photons from the local region; this will be shown elsewhere<sup>17</sup> to give  $P_{10}^L = 6.5 \times 10^{-11}$  and hence  $y_{\alpha} = 1.6$  for the adopted model.

Although we must emphasize that Table III is based on speculative values of the parameters in many cases, we may draw some conclusions of a general sort. First of all, the contribution of the radio transitions to  $T_S$  is small in every case but near a radio source. There,  $T_S$  is

<sup>21</sup> H. Zanstra, "On scattering with redistribution and radiation pressure in a stationary nebula," *Bull. Astron. Inst. Neth.*, vol. 11, pp. 1-10; March, 1947.

<sup>22</sup> D. E. Osterbrock, "Electron densities in the Orion nebula," *Astrophys. J.*, vol. 122, pp. 235-239; September, 1955.

increased 50 per cent in the weak source, while it is multiplied by 50 in the stronger one over what it would be in the absence of radio frequency emission. We conclude that absorption in the vicinity of strong sources can not be safely interpreted<sup>23</sup> in terms of mass of HI at the present time, in view of (9) and Table III, as even the  $T_S$  of Table III is still dependent on the unknown parameters of the absorbing cloud.

A comparison of cases 1) and 2) shows that while  $L\alpha$  can be very important in the immediate vicinity of an HII region, it is of no consequence at remote points. Even when it is important, it drives  $T_S$  toward  $T_K$  just as collisions would. On the other hand, 3), the  $T_S$  in the galactic halo is apparently completely determined by its own  $L\alpha$ . Should  $L\alpha$  not act as we have supposed,  $T_S$  in the halo would drop from  $10^4$  to something nearer  $10^3 \text{ }^\circ\text{K}$ . In any case, it seems quite hopeless to observe absorption in the halo until very large antennas are available, as the opacity can be expected to be between  $10^{-3}$  and  $10^{-4}$ . It is interesting to note that in the halo electrons become important, contributing 10 times the temperature that the atoms do, albeit a small fraction of the  $L\alpha$  contribution.

The intergalactic cloud depends almost entirely on  $L\alpha$ ; were it not present in the estimated quantity,  $T_S$  would fall to  $1^\circ\text{K}$ . Hence, the presence of  $L\alpha$  will make the intergalactic medium rather transparent if the temperature is high.

## VII. APPLICATION TO THE DEUTERIUM LINE

Recently there have been attempts<sup>24-26</sup> to observe absorption at 327 mc which could be attributed to interstellar deuterium. Inasmuch as the absorption coefficient for such a line depends inversely on the spin temperature,  $T_S'$ , of the deuterium (D) atoms, it is of interest to see whether  $T_S' = T_K$  as it does for the hydrogen (H) in remote interstellar clouds. Radio-frequency, collisional, and optical excitations will be considered, using the same notation as previously, but with primes on the parameters for D.

The D hyperfine structure results from an  $I$  value of 1 for the deuteron, giving rise to a hyperfine doublet  $F = 3/2$  (upper) and  $\frac{1}{2}$  (lower). The separation is 327 mc or 91.6-cm wavelength. The partial sum line strength  $S(aB)$  for any one of the four levels,  $a$ , of the quartet is found to be  $(4/3)\beta^2$  rather than simply  $\beta^2$  as in H. Conse-

<sup>23</sup> A. E. Lilley and E. F. McClain, "The hydrogen-line red shift of radio source Cygnus A," *Astrophys. J.*, vol. 123, pp. 172-175; January, 1956.

<sup>24</sup> G. G. Getmanzev, K. S. Stankevitch, and V. S. Troitzky, "Detection of the spectral line of deuterium from the center of the galaxy on the wavelength of 91.6 cm." IAU Symposium No. 4, Cambridge University Press, Cambridge, Eng., pp. 90-91; 1957. Also *Dok. Akad. Nauk. USSR*, vol. 103, pp. 783-786; August, 1957.

<sup>25</sup> G. J. Stanley and R. Price, "An investigation of monochromatic radio emission of deuterium from the galaxy," *Nature*, vol. 177, pp. 1221-1222; June, 1956.

<sup>26</sup> R. L. Adgie and J. S. Hey, "Intensity of the radio line of galactic deuterium," *Nature*, vol. 179, pp. 370-371; February, 1957.

quently, the spontaneous transition probability,  $A'$ , which is proportional to  $S(aB)$  and to  $\lambda'^{-3}$ , is

$$A' = \frac{4}{3} \left( \frac{\lambda}{\lambda'} \right)^3 A = 0.0163A = 4.65 \times 10^{-17} \text{ sec}^{-1}. \quad (33)$$

As a result, radio-frequency transitions are weak relative to those in H, and this is reflected in increased values of the efficiencies for collisions and light. Radio-frequency transitions in our formulas are specified by the quantity  $T_R'$ , which is the average brightness temperature over the sky at 91.6-cm wavelength. An estimate based on Allen and Gum's<sup>27</sup> observations at 200 mc, corrected by a  $\lambda^{-2.5}$  law, yields  $T_R' = 40^\circ\text{K}$  for interstellar clouds near the sun.

Collisions will occur at very nearly the same rate as for H, differing only by reduced-mass factors near unity. Remembering the definition of  $y_c$  (15), we have, neglecting such effects,

$$y_c' = \frac{T_*'}{T_*} \frac{A}{A'} y_c = 14.1 y_c. \quad (34)$$

We may put  $T_K$  equal to that taken previously for a remote cloud,  $100^\circ\text{K}$ . Then  $y_c = 35$  if  $n_H = 1$  and  $y_c' = 494$  and  $y_c' T_K = 49,400^\circ\text{K}$ . We have ignored electron collisions, as is usual for HI regions.

Finally optical transitions take place at the rate<sup>28</sup>

$$P_{10}'L = A_\alpha \frac{\lambda^4}{18\pi h\nu} \frac{dE}{d\lambda}, \quad (35)$$

where  $dE/d\lambda$  is the spectral energy density at  $L'\alpha$ . In the case of H, we wrote (27) in a form suited to a profile drastically affected by scattering in the interstellar gas. Here the situation is quite different owing to the isotope shift of  $L'\alpha$  0.33 Å shortwards of  $L\alpha$ , together with the small ratio  $n(\text{D})/n(\text{H}) \simeq 1/7000$ . The blue shift is about 7 Doppler widths for  $L\alpha$  with an rms velocity of 8.5 km, so that the interstellar scattering due to H at the wavelength of  $L'\alpha$  is due to the  $L\alpha$  damping wings and has a coefficient of about one parsec<sup>-1</sup>, if  $n_H = 1 \text{ cm}^{-3}$ . On the other hand, D itself exhibits a scattering coefficient of about 27 psc<sup>-1</sup>, and hence a mean free path,  $l_s$ , of 0.037 psc in the line center. The effective mean free path against absorption in the dust (defined in the previous section) with  $l_a = 300 \text{ psc}$  is then

$$l_e = (l_a l_s)^{1/2} = 3\frac{1}{3} \text{ psc}, \quad (36)$$

and a considerable amount of  $L'\alpha$  will find its way to remote clouds. The precise amount which does so depends on a detailed calculation of the scattering, as outlined above. Since, however,  $3\frac{1}{3}$  parsec is not small compared to distances between the stars, we may consider  $dE/d\lambda$  in (35) as given by dilution only. The best esti-

mate is probably that of Lambrecht and Zimmerman,<sup>29</sup> who found

$$\left( \frac{dE}{d\lambda} \right)_{1215\text{Å}} = 1.2 \times 10^{-16} \text{ erg cm}^{-3}(\text{Å})^{-1}, \quad (37)$$

which, when put in (35) yields

$$P_{10}'L = 1.310 \times 10^{-10} \text{ sec}^{-1},$$

$$y_{\alpha'} = \frac{T_*'}{T_L'} \frac{P_{10}'L}{A'} = \frac{45,000}{T_L'}. \quad (38)$$

This time it may not be wise to put  $T_L' = T_K$ , which is true only when the  $L\alpha$  profile is shaped by many scatterings. The scattering coefficients already calculated indicate that the situation is marginal, so that  $T_L'$  may approach  $T_K$  or, on the other hand, it may more nearly reflect the spectral gradient to the blue of  $L\alpha$  in the starlight itself. Even in this case we cannot specify  $T_L'$ , for if the spectral gradient approximated that of a black body of temperature  $T_c$ ,  $T_L'$  would be near  $T_c$ , or perhaps  $50,000^\circ\text{K}$ .<sup>29</sup> On the other hand,  $T_L'$  may reflect primarily the structure of the stellar  $L\alpha$  line. It seems reasonable to suppose, however, that  $T_L'$  will be between  $T_K$  and  $T_c$ . We conclude that if  $T_L' = T_K$ ,

$$y_{\alpha'} = 450; \quad y_{\alpha'} T_L' = 45,000^\circ\text{K}, \quad (39)$$

while if  $T_L' = T_c = 50,000^\circ\text{K}$ ,

$$y_{\alpha'} = 0.90; \quad y_{\alpha'} T_L' = 45,000^\circ\text{K}. \quad (40)$$

Putting the results together we find that  $T_R'$  is negligible, as expected, and

$$T_s' = \begin{cases} 100^\circ\text{K} & \text{if } T_L' = T_K, \\ 191^\circ\text{K} & \text{if } T_L' = T_c, \end{cases} \quad (41)$$

which indicates that an extreme assumption concerning the effectiveness of light at most only doubles the spin temperature. Therefore, it seems justified to put  $T_s' = T_K$  in discussions of the deuterium line, although a different result for the interstellar radiation field near  $L\alpha$  would upset this conclusion.

## APPENDIX

### ELECTRON DE-EXCITATION CROSS SECTION

Let  $a$  be an up proton spin function and  $\alpha$  and  $\beta$  up and down electron spin functions. One component of the hyperfine triplet is  $u(r_2)a\alpha(2)$ , where (2) refers to the atomic electron and  $u$  is the hydrogen ground state. An unpolarized beam of electrons of unit flux is  $2^{-1/2}[e^{i\gamma}\alpha(1) + \beta(1)]e^{ikz_1}$ , aside from a constant velocity factor, where (1) refers to the incident electron and  $k$  its wave number.  $\gamma$  is a random phase. Since the part of the beam containing  $\alpha(1)$  cannot possibly cause a spin flip, the initial wave function of the system hyperfine triplet

<sup>27</sup> C. W. Allen and C. S. Gum, "Survey of galactic radio-noise at 200 mcg," *Aust. J. Sci. Res., A*, vol. 3, pp. 224-233; June, 1950.

<sup>28</sup> This rate is taken to be that for H; there may be factors of order unity resulting from the exact calculation.

<sup>29</sup> H. Lambrecht and H. Zimmermann, "New calculation of the interstellar radiation field, II," *Wiss. Z. Fr. Schiller Univ. (Jena)*, vol. 5, pp. 217-220; 1955.

plus incident unpolarized beam is  $2^{-1/2}u(r_2)e^{ikz_1}\alpha(2)\beta(1)$ , which is written decomposed into an electron triplet and singlet as

$$2^{-3/2}u(r_2)ae^{ikz_1} \times [\{\alpha(2)\beta(1) + \alpha(1)\beta(2)\} + \{\alpha(2)\beta(1) - \alpha(1)\beta(2)\}].$$

Now as long as we ignore magnetic interactions, the spin functions do not change in the scattering. Nevertheless, the singlet and triplet scatter with different amplitudes because the requirement of over-all antisymmetry when  $r_1$  and  $r_2$  are comparable leads to different electrostatic interactions for the two cases. Hence the scattered wave is, in general,

$$2^{-3/2}u(r_2)a \frac{e^{ikr_1}}{r_1} [\{\alpha(2)\beta(1) + \alpha(1)\beta(2)\}T(\theta_1) + \{\alpha(2)\beta(1) - \alpha(1)\beta(2)\}S(\theta_1)],$$

where  $T(\theta_1)$  and  $S(\theta_1)$  are the triplet and singlet scattering amplitudes. The final spin state we are interested in

is the hyperfine singlet  $2^{-1/2} \times [a\beta(2) - b\alpha(2)]$ , and the product of this with the scattered wave, or

$$2^{-2}u(r_2) \frac{e^{ikr_1}}{r_1} \alpha(1) \times [T(\theta_1) - S(\theta_1)],$$

is the amplitude corresponding to de-excitation. The differential cross section for the process of de-excitation is thus  $r_1^2$  times the absolute square of this amplitude, summed over  $r_2$ , or

$$\frac{d\sigma}{d\omega} = 2^{-4} |T - S|^2,$$

agreeing with (16).

#### ACKNOWLEDGMENT

The author is particularly grateful to Prof. E. M. Purcell, who originated much of the work developed here. Fruitful discussions were also had with Dr. T. Wu, Dr. K. Gottfried, Prof. L. Spitzer, and Dr. M. J. Seaton. Dr. Leo Sartori kindly read the manuscript.

## Spectral Lines in Radio Astronomy\*

A. H. BARRETT†

**Summary**—A review of the elements of microwave spectroscopy as it concerns, or is likely to concern, radio astronomy is presented. This review attempts to show how atomic and molecular resonance lines arise in the radio frequency spectrum and to discuss the important parameters of spectral lines. Finally, it is shown how the intensity of radio emission received from the galaxy is modified by the presence of an interstellar atomic gas having a resonance transition at the frequency of observation.

### I. INTRODUCTION

THE frequency spectrum of radio frequency radiation received from a typical region of the galaxy is without discontinuities or irregularities for the most part. However, in a relatively narrow frequency interval centered about 1420.4 mc ( $\lambda = 21$  cm) the intensity is approximately double that of adjacent portions of the spectrum. It was predicted in 1944 by van de Hulst, a Dutch astronomer, that the galactic radiation at 1420.4 mc might be different from the neighboring frequencies. This was shown to be the case by Ewen and Purcell in 1951<sup>1</sup> and was verified immediately thereafter, by workers in the Netherlands<sup>2</sup> and in Aus-

tralia.<sup>3</sup> Subsequently, this frequency band has become the most studied part of the spectrum and will most likely continue to be. Undoubtedly there are similar such increases, or decreases, in the level of galactic radiation at other frequencies many times less intense which so far have escaped detection. It is the purpose of this paper to review briefly the origin of the radiation at 1420.4 mc and at other frequencies which might exhibit similar behavior. Although this is not a new subject, it is intended here to present more background material than has usually been given in the more detailed papers on this subject.<sup>4-9</sup> Accordingly, this paper

\* J. L. Pawsey of Radio Phys. Lab., CSIRO, Sydney, Australia, has reported in a telegram the success of W. N. Christiansen and J. V. Hindman in detecting the 1420-mc hydrogen line, *Nature*, vol. 168, p. 358; September, 1951.

† I. S. Shklovsky, "On the monochromatic radio radiation of the galaxy and the possibility of observing it," *Astron. Zhur. USSR*, vol. 26, pp. 10-14; January, 1949.

E. M. Purcell, "Line spectra in radio astronomy," *Proc. Amer. Acad. Arts and Sci.*, vol. 82, pp. 347-349; December, 1953.

I. S. Shklovsky, "The possibility of observing monochromatic radio emissions from interstellar molecules," *Dok. Akad. Nauk USSR*, vol. 92, pp. 25-28; July, 1953.

C. H. Townes, "Microwave spectra of astrophysical interest," *J. Geophys. Res.*, vol. 59, p. 191; March, 1954.

C. H. Townes, "Microwave and Radiofrequency Resonance Lines of Interest to Radio Astronomy," IAU Symposium No. 4, in "Radio Astronomy," ed. H. C. van de Hulst, Cambridge Univ. Press, Cambridge, Eng. 1957.

J. P. Wild, "The radio-frequency line spectrum of atomic hydrogen and its applications in astronomy," *Astrophys. J.*, vol. 115, pp. 206-221; March, 1952.

\* Original manuscript received by the IRE, November 6, 1957.

† University of Michigan Observatory, Ann Arbor, Mich.

<sup>1</sup> H. I. Ewen and E. M. Purcell, "Radiation from galactic hydrogen at 1420 mc/sec," *Nature*, vol. 168, pp. 356-357; September 1, 1951.

<sup>2</sup> C. A. Muller and J. H. Ort, "The interstellar hydrogen line at 1420 mc/sec and an estimate of galactic rotation," *Nature*, vol. 168, pp. 357-358; September, 1951.

is divided into two parts; the first is a review of the basic essentials of microwave spectroscopy, and the second is a discussion of the formation of absorption and emission lines as applicable to radio astronomy. It is hoped that this paper will provide an idea of some of the physical interactions in atoms and molecules which produce radio frequency lines and how the radiation from the galaxy is modified by the presence of the emitting and absorbing gas.

## II. ELEMENTS OF MICROWAVE SPECTROSCOPY

The change in intensity of galactic radiation as a function of frequency near 1420 mc is due to the inherent properties of the hydrogen atom. The frequency at which similar abrupt changes in the level of galactic radiation may occur will be determined by the properties of other atoms or molecules. Thus, a discussion of the fundamental characteristics of atomic and molecular systems and their interaction with electromagnetic radiation will be given. No attempt at completeness is intended; only those aspects of radio frequency spectroscopy having a bearing on understanding and interpreting the results of radio astronomy are included. Several excellent books which treat the material in detail are available on the general subject of radio frequency spectroscopy.<sup>10-12</sup> In this section a summary will be given of the theory of energy levels, dipole matrix elements and selection rules, transition frequencies, and widths of spectral lines.

### A. Energy Levels

In atomic and molecular systems the electrons and nuclei can take up only those motions and orientations that yield a discrete set of internal energies, *i.e.*, energy levels or states. Since a continuous range of internal energies is not possible in a bound system, the energy is said to be "quantized." Similarly, the various angular momenta associated with the electrons, nucleus, or both are quantized. Angular momentum can be represented by a vector,  $\mathbf{J}$ , whose magnitude is restricted to the values  $\sqrt{J(J+1)}h/2\pi$  where  $J$  is a pure number, the angular momentum quantum number, and  $h$  is Planck's constant and equals  $6.625 \times 10^{-27}$  erg-sec. The projection of the vector  $\mathbf{J}$  on the axis of quantization is limited to the values  $m_J h/2\pi$ , where  $m_J$  is the magnetic quantum number and must satisfy  $-J \leq m_J \leq J$ . The angular momenta necessary to specify the energy states of an atom are: 1) the total electronic orbital angular momentum  $\mathbf{L}$ , 2) the total electronic spin momentum  $\mathbf{S}$ , 3) the total electronic angular momentum  $\mathbf{J} = \mathbf{L} + \mathbf{S}$ , 4) the nuclear spin momentum  $\mathbf{I}$ , and 5) the total atomic

angular momentum  $\mathbf{F} = \mathbf{I} + \mathbf{J}$ . The additions of these momentum vectors are illustrated in Fig. 1. The resultant of the addition of two angular momentum vectors may assume one of several possible values. Thus for a given value of  $L$  and  $S$ , the possible values of  $J$  are  $L+S$ ,  $L+S-1$ ,  $L+S-2$ ,  $\dots$ ,  $|L-S|$ . Similar remarks apply to  $\mathbf{F}$ .

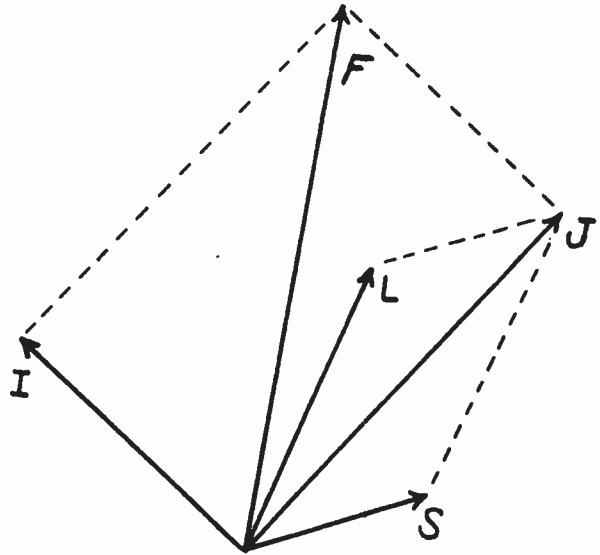


Fig. 1—Addition of atomic angular momentum vectors.

Energy levels in atoms arise from electric and magnetic interactions of the atomic electrons amongst themselves and with the nucleus. The most important of these interactions from the standpoint of radio astronomy is that between the magnetic field of an electron and the magnetic moment of the nucleus, the so-called "hyperfine energy." The electron, because of its inherent properties and because of its motion about the nucleus, produces a magnetic field at the nucleus. This creates different energies of the system for various orientations of the nuclear magnetic moment with respect to this field. This interaction always occurs in atomic systems when neither the nuclear angular momentum  $\mathbf{I}$  nor the total electronic angular momentum  $\mathbf{J}$  are zero. The semiclassical picture of the interaction is sufficiently quantitative to give the correct form for the resulting change in energy.<sup>13</sup> If the internal energy of the atom without inclusion of hyperfine effects is  $E_0$ , the total internal energy becomes

$$E = E_0 + E_M = E_0 - \boldsymbol{\mu}_I \cdot \mathbf{H}_J \quad (1)$$

where the magnetic interaction energy  $E_m$  is the negative of the vector dot product of the nuclear magnetic moment  $\boldsymbol{\mu}_I$  and the magnetic field due to the electron  $\mathbf{H}_J$ . The nuclear magnetic moment is related to the nuclear spin momentum by

<sup>10</sup> W. Gordy, W. V. Smith, and R. F. Trambarulo, "Microwave Spectroscopy," John Wiley & Sons, Inc., New York, N. Y.; 1953.

<sup>11</sup> C. H. Townes and A. L. Schawlow, "Microwave Spectroscopy," McGraw-Hill Book Co., Inc., New York, N. Y.; 1955.

<sup>12</sup> D. J. E. Ingram, "Spectroscopy at Radio and Microwave Frequencies," Butterworths Scientific Publications, London, Eng.; 1955.

<sup>13</sup> N. F. Ramsey, "Nuclear Moments," John Wiley & Sons, Inc., New York, N. Y.; 1953.

$$\mathbf{u}_I = g_I \mu_N \mathbf{I} \quad (2)$$

where  $g_I$  is the "nuclear  $g$  factor" which is characteristic of a particular nucleus and may be positive or negative, and  $\mu_N$  is the nuclear magneton ( $5.0504 \times 10^{-24}$  erg Gauss $^{-1}$ ). The magnetic field of the electron can be resolved into components parallel and perpendicular to  $\mathbf{J}$ , the total angular momentum of the electron. Thus

$$\mathbf{H}_J = \frac{\mathbf{H}_J \cdot \mathbf{J}}{J \cdot J} \mathbf{J} + (\mathbf{H}_J \cdot \mathbf{K}_0) \mathbf{K}_0 \quad (3)$$

where  $\mathbf{K}_0$  is a unit vector normal to  $\mathbf{J}$ . Upon combining (1) through (3) the dot product of  $\mathbf{I}$  and  $\mathbf{K}_0$  results. This term has a time average value of zero and can be dropped from further consideration. The magnetic energy is now

$$E_M = -g_I \mu_N \frac{\mathbf{H}_J \cdot \mathbf{J}}{J \cdot J} \mathbf{I} \cdot \mathbf{J}. \quad (4)$$

The magnetic field  $\mathbf{H}_J$  is composed of two parts, the field due to the electron's magnetic moment and the field due to the motion of the electron about the nucleus. The first of these is just the field of a magnetic dipole and can be written as

$$\mathbf{H}_s = -\frac{1}{r^3} \left[ \mathbf{u}_e - \frac{3(\mathbf{u}_e \cdot \mathbf{r})}{r^2} \mathbf{r} \right] \quad (5)$$

and the second follows from classical electromagnetic theory and can be written as

$$\mathbf{H}_L = \frac{e}{cr^3} \mathbf{V} \times \mathbf{r} = \frac{-e}{mcr^3} \mathbf{r} \times m\mathbf{V} \quad (6)$$

where  $\mathbf{r}$  is a radius vector from the nucleus to the electron,  $\mathbf{V}$  is the velocity of the electron,  $e$  and  $m$  are its charge and mass, respectively, and  $c$  is the velocity of light. The electron magnetic moment  $\mathbf{u}_e$  is related to the electron spin momentum  $\mathbf{S}$  by a relation analogous to (2).

$$\mathbf{u}_e = -2\mu_B \mathbf{S} \quad (7)$$

where  $\mu_B = eh/4\pi mc = 0.92732 \times 10^{-20}$  erg Gauss $^{-1}$  and is called the Bohr magneton. Eq. (6) can be written in terms of the orbital angular momentum  $\mathbf{L}$  since

$$\mathbf{L} \frac{h}{2\pi} = \mathbf{r} \times m\mathbf{V}. \quad (8)$$

Combining (5)–(8) and remembering that  $\mathbf{H}_J$  is the sum of  $\mathbf{H}_L$  and  $\mathbf{H}_S$  we have

$$\mathbf{H}_J \cdot \mathbf{J} = -\frac{2\mu_0}{r^3} [\mathbf{L} - \mathbf{S} + 3(\mathbf{S} \cdot \mathbf{r}_0) \mathbf{r}_0] \cdot (\mathbf{L} + \mathbf{S}) \quad (9)$$

where use has been made of the relations  $\mathbf{J} = \mathbf{L} + \mathbf{S}$  and  $\mathbf{r}_0 = \mathbf{r}/r$ . Eq. (9) must be averaged over the electron's motion and, when this is done, the  $\mathbf{L} \cdot \mathbf{r}_0$  term will average to zero and the  $\mathbf{S} \cdot \mathbf{r}_0$  term will average to  $\pm \frac{1}{2}$ . The

factors  $\mathbf{L} \cdot \mathbf{L}$  and  $\mathbf{S} \cdot \mathbf{S}$  must be replaced by their quantum mechanical equivalents  $L(L+1)$  and  $S(S+1)$ , respectively, where  $S = \frac{1}{2}$  for a single electron atom such as hydrogen. Thus

$$\mathbf{H}_J \cdot \mathbf{J} = -2\mu_0 \left[ \frac{1}{r^3} \right] [L(L+1)]. \quad (10)$$

The average of  $r^{-3}$  can be calculated from quantum mechanics. The result for hydrogen-like atoms is

$$\frac{1}{r^3} = \frac{Z^3}{a_0^3 n^3 L(L+1/2)(L+1)} \quad (11)$$

where  $Z$  is the atomic number,  $a_0 = h^2/(4\pi^2 m e^2) = 0.52917 \times 10^{-8}$  cm, and  $n$  is a quantum number determining the gross characteristics of the energy of the atom, *i.e.*,  $n$  largely governs the value of  $E_0$  in (1).

Since  $\mathbf{F} = \mathbf{I} + \mathbf{J}$  the  $\mathbf{I} \cdot \mathbf{J}$  factor of (4) can be evaluated from the vector relation

$$\mathbf{F} \cdot \mathbf{F} = \mathbf{I} \cdot \mathbf{I} + \mathbf{J} \cdot \mathbf{J} + 2\mathbf{I} \cdot \mathbf{J}. \quad (12)$$

Thus we can write

$$\mathbf{I} \cdot \mathbf{J} = \frac{1}{2} [F(F+1) - I(I+1) - J(J+1)] \quad (13)$$

where the quantum mechanical equivalents of the squares of the angular momentum vectors have been used, as above. It is now possible to combine (4), (10), (11), and (13) to get the result

$$E_M = g_I \left( \frac{m}{M} \right) \frac{\alpha^2 h c R Z^3}{n^3} \left[ \frac{F(F+1) - I(I+1) - J(J+1)}{J(J+1)(2L+1)} \right] \quad (14)$$

where the "fine structure constant"  $\alpha = 2\pi e^2/hc = 7.2973 \times 10^{-3}$ , the Rydberg constant  $R = 2\pi^2 m e^4 / ch^3 = 1.09737 \times 10^5$  cm $^{-1}$ , and  $(\mu_N/\mu_0) = m/M$  where  $M$  is the nuclear mass. This equation represents the energy of interaction between the magnetic field of the electron and the nuclear magnetic moment. When the nuclear spin momentum is zero, corresponding to  $\mathbf{u}_I = 0$ ,  $F = J$  and (14) goes to zero. However, for a given  $I$  and  $J$  not zero, various values of  $F$  are possible corresponding to different orientations of  $\mathbf{J}$  relative to  $\mathbf{I}$  and (14) yields the different values of the energy for the different orientations.

Eq. (14) has been developed on a semiclassical basis but it may be shown to be valid by a rigorous quantum mechanical calculation if one ignores higher order effects.<sup>14</sup> It is a curious fact that (14) is valid for all states of hydrogenic atoms even though it would seem from (10) that states having  $L = 0$ , the so-called  $S$  states,

<sup>14</sup> H. A. Bethe and E. E. Salpeter, "Quantum Mechanics of One- and Two-Electron Systems," in "Handbuch der Physik," Springer-Verlag, Berlin, Ger., vol. 35, pp. 193-200; 1957.

would show zero hyperfine structure. The average of  $r^{-3}$  for  $L=0$  is not infinite as (11) predicts, but remains finite when suitably computed for  $S$  states,<sup>14</sup> thus this is not the way out of the dilemma. The calculations have assumed the nucleus to be a point particle, a particle of zero radius. If one removes this restriction for the  $L=0$  states the hyperfine effect can be calculated. It is then seen that an energy splitting arises because there is a probability of finding the electron inside the assumed boundaries of the nucleus. Were it not for this finite probability, the hyperfine splitting of the energy levels with  $L=0$  would be zero.

Another type of magnetic interaction occurs in atoms and causes a splitting of the energy levels larger than the hyperfine interaction. This effect, which gives rise to the "fine structure" of atomic spectra, is the interaction between the electron's spin momentum  $S$  and its orbital angular momentum  $L$ . The fine structure splitting can be calculated semiclassically in a manner quite analogous to the above hyperfine calculation. The electron revolves about the nucleus in the electric field of the nucleus, thus experiencing a magnetic field given by

$$\mathbf{H} = \frac{\mathbf{E} \times \mathbf{V}}{c} \quad (15)$$

where the field of the nucleus  $\mathbf{E}$  is given by

$$\mathbf{E} = \frac{Ze}{r^3} \mathbf{r}. \quad (16)$$

The fine structure energy  $E_{fs}$  is that of the interaction of the electron's magnetic moment with the field of (15); thus

$$E_{fs} = -\boldsymbol{\mu}_e \cdot \mathbf{H} \quad (17)$$

Combining (15) and (16), averaging  $\mathbf{H}$  over the electron's orbit, and using (7) and (11) gives

$$E_{fs} = \frac{2\alpha^2 hc R Z^4}{n^3 L(L+1/2)(L+1)} \mathbf{L} \cdot \mathbf{S}. \quad (18)$$

The  $\mathbf{L} \cdot \mathbf{S}$  factor can be evaluated as in (13) and inserted in this expression. However, the rigorous derivation of the fine structure energy is exactly half the value obtained above. The discrepancy is due to the omission of a relativistic effect in the above derivation; when this is included its effect is opposite to the magnetic interaction and of one half the magnitude.<sup>15</sup> Thus the final result is

$$E_{fs} = \frac{\alpha^2 hc R Z^4}{n^3 L(L+1/2)(L+1)} \left[ \frac{J(J+1) - L(L+1) - S(S+1)}{2} \right]. \quad (19)$$

<sup>15</sup> See, for example, H. E. White, "Introduction to Atomic Spectra," McGraw-Hill Book Co., Inc., New York, N. Y., p. 126; 1934.

Thus states of different  $J$ , arising from a given  $L$  and  $S$  and representing different orientations of  $\mathbf{L}$  with respect to  $\mathbf{S}$ , will have different energies. Note that the fine structure energy is of order  $\alpha^2 hc R$  while the hyperfine energy is of order  $(m/M)\alpha^2 hc R$ . Since  $m/M \sim 1/2000$ , the fine structure energy is about 2000 times larger than the hyperfine energy.

There exists another type of fine structure splitting of atomic energy levels. This type, known as the "Lamb shift," has been extensively studied, both experimentally and theoretically, since its discovery by Lamb and Rutherford in 1947.<sup>16</sup> Unfortunately, the Lamb shift is not adaptable to a semiclassical calculation, as above, but requires quantum electrodynamics for its theoretical explanation. Prior to 1947, atomic theories predicted that certain levels of the hydrogen atom would coincide and no strong experimental evidence existed to refute this prediction. However, when radio frequency methods were applied to the study of the energy levels of hydrogen it was found that these levels were not exactly coincident, but were separated by energies corresponding to radio frequencies. These energy differences had previously escaped detection because the energy separations were just below the limit of careful optical spectroscopy. The Lamb shift has been studied in ionized helium, also.<sup>17</sup>

Molecular systems, like atomic systems, possess energy levels that are sufficiently closely spaced that radio frequency transitions can occur between them. As in atoms, there are several properties of molecules that produce these levels. Perhaps the most familiar origin of radio frequency transitions in molecules is that of molecular rotation. This is also adaptable to a classical evaluation, at least to a first approximation. Consider a diatomic molecule, two atoms bound together to form a molecule and separated by a distance  $r_e$ , the internuclear distance. This system is capable of rotation about its center of mass with an angular velocity  $\omega$  and a moment of inertia  $I = \mu r_e^2$  where  $\mu$  is the reduced mass of the molecule. The rotational energy is given by the familiar relation

$$E = \frac{1}{2} I \omega^2 = \frac{1}{2} \mu r_e^2 \omega^2 \quad (20)$$

and the molecule's angular momentum is quantized so that

$$I\omega = J \frac{h}{2\pi} \quad (21)$$

where  $J$  is the quantum mechanical angular momentum vector. Combining (20) and (21) and remembering that the square of  $J$  must be replaced by  $J(J+1)$  gives

<sup>16</sup> For a review of this subject see W. E. Lamb, Jr., "Anomalous fine structure of hydrogen and ionized helium," *Reps. Prog. Phys.*, vol. 14, pp. 19-63; 1951. See also Bethe and Salpeter, *op. cit.*, p. 189.

<sup>17</sup> R. Novick, E. Lipworth, and P. F. Yergin, "Fine structure of singly ionized helium," *Phys. Rev.*, vol. 100, pp. 1153-1173; November 15, 1955.

$$E = hBJ(J + 1) \quad (22)$$

where  $B = h/8\pi^2\mu r_s^2$  is the "rotational constant" of the molecule. Corrections must be applied to this formula when the molecule is vibrating as well as rotating, but these are usually quite small compared to the pure rotational term.

In addition to the rotational transitions, molecules exhibit radio frequency spectra because of fine and hyperfine structure of their energy levels. Of the molecules having hyperfine transitions in the range of frequencies of interest to radio astronomy, none have been studied in the laboratory. Consequently, their structure and energy parameters have not been determined with precision. Since it is not possible to determine the frequencies of the transitions of such molecules, they are not of immediate interest in radio astronomy. One exception exists, however; it is possible to calculate the energy levels of the ionized hydrogen molecule ( $H_2^+$ ) with reasonable precision and its hyperfine structure will yield radio frequency lines.<sup>8,18</sup> The calculation has not yet been performed.

There are several possible forms of molecular fine structure which are of importance in microwave spectroscopy. The form of fine structure of most interest to radio astronomy is the so-called "A doubling" which can occur in many of the molecules of astrophysical importance. A detailed discussion of the origin of A doubling is quite complex and only a crude description of it will be given here. In the vast majority of molecules, the electrons in their lowest energy states will pair off so that the spin axis of one is opposite in direction to that of the other in the pair. Thus the total spin angular momentum will be zero. Clearly, molecules with an odd number of electrons cannot have all their spins paired off and these represent exceptions to the rule. The orbital angular momentum of the molecular electrons is not constant but the projection of this momentum on the molecular axis is constant; furthermore, this projection is quantized and denoted by the quantum number  $\Lambda$ . Many molecules have  $\Lambda = 0$ , but those molecules for which  $\Lambda \neq 0$  will show A doubling in their spectra. The rotational energy of a molecule having a total angular momentum  $J$  and electronic orbital angular momentum  $L$  can be written

$$E = Bh[(J_x - L_x)^2 + (J_y - L_y)^2] \quad (23)$$

where it has been assumed for simplicity that the total spin momentum is zero, that the molecular axis is the  $z$  axis, and that the moment of inertia about the  $z$  axis is zero. Since

$$J_z = L_z = \Lambda \quad \text{and} \quad J_x^2 + J_y^2 + J_z^2 = J(J+1), \quad (24)$$

(23) becomes

<sup>18</sup> B. F. Burke, "Comments at Washington conference on radio astronomy," *J. Geophys. Res.*, vol. 59, p. 191; March, 1954.

$$E = Bh[J(J + 1) - \Lambda^2] - 2Bh(L_x J_x + L_y J_y) \quad (25)$$

where a term  $B(L_x^2 + L_y^2)$  has been omitted because it is a constant, independent of  $J$ . The first term of (25) represents the usual rotational energy modified by  $B\Lambda^2$ , and is independent of the orientation of  $L$ . For example, if the magnitude of  $\Lambda$  is one, the rotational energy is the same for  $\Lambda = +1$  or  $-1$ , corresponding to the two possible positions of  $\Lambda$  on the molecular axis. The second term, however, gives rise to a coupling between  $L$  and  $J$  which splits each rotational energy level into two levels. The second term is usually much smaller than the first term and can be treated by perturbation methods. Note that for  $L=0$ , (25) reduces to the expression for the energy of a simple rigid rotor, (22). The evaluation of the second term is complex because  $L$  is not a constant, however, quite complete theories of A doubling are available and reference should be made to these papers for actual cases.<sup>19,20</sup>

### B. Dipole Matrix Elements and Selection Rules

Atoms and molecules can interact with electromagnetic radiation by making a transition from one energy level to another; that is, a change from one value of internal energy, corresponding to a particular motion and orientation of the electrons and nucleus, to another value of the energy, corresponding to different motions and/or orientations. If the final energy of the atom is greater than the initial energy, the difference in energy must have been supplied by the incident radiation field, thus the process is one of absorption of radiation. Conversely, when energy is added to the radiation field the process is one of emission and the atom will have made a transition from an initial level to a final level of lower energy. The frequency  $\nu$  of radiation emitted (or absorbed) is given by the well-known Bohr condition

$$\nu = \frac{E_f - E_i}{h} \quad (26)$$

where  $E_f$  and  $E_i$  are the energies of the final and initial states of the atom, respectively.

It is a fortunate circumstance that transitions between *any* two atomic states are not possible. Were it not for this fact, the interpretation of atomic spectra would be exceedingly complicated since it would be difficult to assign initial and final energies to the large number of frequencies which would result. Very definite rules, called "selection rules," can be given which enable one to predict which pairs of levels can give rise to a transition and, hence, be capable of emitting or absorbing radiation.

If one inquires into the theory of the interaction of an

<sup>19</sup> G. C. Dousmanis, T. M. Sanders, Jr., and C. H. Townes, "Microwave spectra of the free radicals OH and OD," *Phys. Rev.*, vol. 100, pp. 1735-1754; December, 1955.

<sup>20</sup> J. J. Gallagher and C. M. Johnson, "Uncoupling effects in the microwave spectrum of nitric oxide," *Phys. Rev.*, vol. 103, pp. 1727-1737; September, 1956.

atom or molecule with electromagnetic radiation a quantity arises which is a measure of the effectiveness of the radiation on the atom. This quantity is the dipole matrix element and may be thought of as the quantum mechanical analog of the classical dipole moment often encountered in the theory of radio transmission. The dipole matrix element depends on the initial and final states of the transition and, like its classical counterpart, can be classified as either electric or magnetic. When a transition takes place, the intensity of emitted radiation is proportional to the square of the matrix element and this provides the key to the selection rules. When the matrix elements are calculated quantum mechanically, many cases turn out to be zero and it becomes possible to predict quite generally which combinations of initial and final state quantum numbers will give results different from zero. It is these transitions that will have intensities different from zero. As an example, consider a diatomic molecule rotating with angular momentum  $J$  and energy  $E = \hbar B J(J+1)$  as given by (22). The selection rule for this case is that the initial and final values of  $J$  must differ by unity. Thus, if the molecule absorbs a quantum of energy, its energy must increase in such a way that its angular momentum quantum number is only one unit larger than originally. Again, from (22), its energy must now be  $E = \hbar B (J+1)(J+2)$ , where  $J+1$  has been substituted for  $J$ . From (26) we see that the frequency of the quanta must have been  $2B(J+1)$ . Similarly, if the molecule in state  $J$  emits radiation its energy will be less after emission corresponding to state  $J-1$ . The frequency of the emitted quanta will be  $2BJ$ . Thus for a diatomic molecule the selection rule is  $\Delta J = \pm 1$  and the frequencies for emission and absorption for a molecule originally in state  $J$  are:

$$\begin{aligned} \nu &= 2B(J+1) \quad (\text{absorption, } J \rightarrow J+1, \Delta J = +1) \\ \nu &= 2BJ \quad (\text{emission, } J \rightarrow J-1, \Delta J = -1). \end{aligned} \quad (27)$$

Selection rules exist for transitions between the other levels discussed above. For hyperfine transitions the rule is  $\Delta F = 0, \pm 1$ ; for fine structure transitions it is  $\Delta J = 0, \pm 1$ .

Matrix elements which are not zero have values which may be grouped into two ranges. This subdivision corresponds to a more fundamental division of matrix elements into "electric dipole" and "magnetic dipole" matrix elements depending on whether it is the electric or magnetic field of the radiation which is effective in producing a transition within the atom. The difference between the two cases is made clear by an example. Consider the hyperfine energy levels given by (14) which arise from different relative orientations of the electron and nuclear magnetic moments. Clearly, if the incident radiation is to cause a transition it must cause the electronic or nuclear magnetic moment to change its orientation with respect to the other moment, thereby altering the internal energy of the atom. A change of

magnetic moment can only result from the *magnetic* field of the incident wave, thus the transition will have a magnetic dipole matrix element. The same is true of the magnetic fine structure energy levels discussed above. On the other hand, the "Lamb shift" fine structure levels, the rotational levels, and the  $\Lambda$ -doublet levels are connected by electric dipole matrix elements. In the case of a diatomic molecule composed of two different atoms, the center of mass of the molecule is the center of rotation, but the center of charge will not, in general, coincide with the center of mass. Thus to change the rotational energy of the molecule and cause a transition, the rotation of the center of charge must be altered and this is accomplished by the action of the *electric* field of the incident radiation which gives rise to electric dipole matrix elements. Note, that for homonuclear molecules, molecules composed of two identical atoms, the centers of mass and charge coincide and the above argument would predict that external radiation would be ineffective in producing rotational transitions. This is borne out by experimental results. The familiar microwave spectrum of molecular oxygen ( $O_2$ ) is not in conflict with this general result. The  $O_2$  spectrum results from transitions between molecular fine structure levels, similar to  $\Lambda$  doubling, of a given rotational level. Thus transitions are not between rotational levels. Furthermore, a magnetic dipole matrix element is associated with the  $O_2$  microwave spectrum.

Calculation of matrix elements can only be made by quantum mechanics, but a reliable order-of-magnitude estimate can be made from classical reasoning. The displacement of the charge center from the mass center in a molecule will be of the order of  $0.2 \times 10^{-8}$  cm, and the net charge displaced by this amount can be taken as one electron,  $5 \times 10^{-10}$  esu, thus the electric dipole moment, the product of the charge and the displacement, is of the order of  $10^{-18}$  esu. The magnetic dipole moment may be estimated by considering an electron revolving about a proton at a radius  $a_0$  as in the ground state of the hydrogen atom. The electron constitutes a "current" of  $ev/2\pi a_0$ , where  $v$  is the electron velocity, and the area of the orbit is  $\pi a_0^2$ . The classical magnetic moment of a circular current is  $IA/c$ , which for the revolving electron gives  $IA/c = eva_0/2c$ . The angular momentum  $mva_0$  is of the order of  $\hbar/2\pi$ , thus  $IA/c = e\hbar/4\pi mc$  which equals  $10^{-20}$  erg/Gauss. Thus the electric dipole moment is of the order of 100 times the magnetic dipole moment. More complete calculations bear out this result. Since the intensity of emitted radiation varies as the square of the dipole matrix element, electric dipole transitions are some  $10^4$  times as intense as magnetic dipole transitions. This is an important point and we shall return to it later.

### C. Transition Frequencies

Eq. (26) allows the prediction of the transition frequencies if the energies of the states and selection rules

are known. For instance, atomic hyperfine energies of hydrogen are given by (14) and the selection rule for hyperfine transitions is  $\Delta F = \pm 1, 0$ . Thus the frequency of the transition from a state  $F+1$  to a state  $F$  is given by

$$\nu = 2g_I \left( \frac{m}{M} \right) \frac{\alpha^2 c R Z^3}{n^3} \frac{F+1}{J(J+1)(2L+1)} \quad (28)$$

and it is possible to predict the transition frequencies for all the hydrogen hyperfine levels from this expression.

For the  $1^2S_{1/2}$  state of atomic hydrogen, for which  $n=1$ ,  $L=0$ ,  $S=\frac{1}{2}$ , and  $J=\frac{1}{2}$ , the possible values of  $F$  are 1 and 0. The frequency of this transition has been determined very precisely in the laboratory,<sup>21,22</sup> the frequency being 1420.40576 mc. Table I gives the frequencies of several hydrogen, helium, and other atomic hyperfine transitions. Note that for He<sup>3</sup> the state of highest energy has the lower  $F$  value. This is a consequence of a negative nuclear  $g$  factor [cf. (2)].

Radio frequency transitions can occur between fine structure levels also. Eq. (19) illustrates the general trend for hydrogen but does not include the effects of the Lamb shift. Fortunately, the fine structure of hydrogen has been studied extensively and the transition frequencies are accurately known. Table II gives the frequencies of the Lamb shift lines for the  $n=2$  and  $n=3$  levels of hydrogen and the  $n=2$  level of ionized helium. Also given in Table II are the fine structure lines for neutral helium. These frequencies are not predictable from (19) because various interactions present in atoms with more than one electron were omitted in the derivation of (19).

Rotational transition frequencies have been measured in the laboratory for many molecules, but not many of these are of immediate interest to radio astronomy. Diatomic molecules, especially hydrides, appear to be the important molecules of interstellar space, but even the lowest rotational frequencies of these molecules are quite high by present standards. Table III gives the frequencies of a few diatomic molecules that may be important in interstellar regions. Some of the heavier, more complicated, molecules might be detected in planetary atmospheres, but this does not appear imminent.

Of the various molecular fine structure transitions, only  $\Lambda$  doubling has been considered here. This type of transition has been measured for OH<sup>19</sup> and NO<sup>20</sup>. In the case of OH, the  $\Lambda$ -doublet frequencies were measured in states other than the lowest rotational state, thus one must rely on theory to predict the lowest  $\Lambda$ -doublet frequency, which is the one of interest to radio astronomy. The calculation yields the frequencies 1665.0 mc and

<sup>21</sup> J. P. Wittke and R. H. Dicke, "Redetermination of the hyperfine splitting in the ground state of atomic hydrogen," *Phys. Rev.*, vol. 96, pp. 530-531; October, 1954.

<sup>22</sup> P. Kusch, "Redetermination of the hyperfine splittings of hydrogen and deuterium in the ground state," *Phys. Rev.*, vol. 100, pp. 1188-1190; November, 1955.

TABLE I  
ATOMIC HYPERFINE TRANSITIONS

Atom	State	Frequency
H <sup>1</sup>	$1^2S_{1/2} \quad F=1 \rightarrow 0$	1420.4 mc
H <sup>1</sup>	$2^2S_{1/2} \quad F=1 \rightarrow 0$	177.6
H <sup>2</sup>	$1^2S_{1/2} \quad F=3/2 \rightarrow 1/2$	327.4
H <sup>2</sup>	$2^2S_{1/2} \quad F=3/2 \rightarrow 1/2$	40.9
He <sup>3</sup> I	$1^2S_{1/2} \quad F=0 \rightarrow 1$	8665.6
He <sup>3</sup> II	$2^2S_{1/2} \quad F=0 \rightarrow 1$	1083.4
He <sup>3</sup>	$2^3S_1 \quad F=1/2 \rightarrow 3/2$	6739.7
H <sup>3</sup>	$1^2S_{1/2} \quad F=1 \rightarrow 0$	1516.7
N <sup>14</sup>	$4^3S_{3/2} \quad F=5/2 \rightarrow 3/2$	26.1
N <sup>14</sup>	$4^3S_{3/2} \quad F=3/2 \rightarrow 1/2$	15.7
Na <sup>23</sup>	$2^2S_{1/2} \quad F=2 \rightarrow 1$	1771.6

TABLE II  
ATOMIC FINE STRUCTURE TRANSITIONS

Atom	State	Frequency
H	$2^2S_{1/2} \rightarrow 2^2P_{1/2}$	1058 mc*
H	$2^2P_{3/2} \rightarrow 2^2S_{1/2}$	9910*
H	$3^2S_{1/2} \rightarrow 3^2P_{1/2}$	315*
H	$3^2P_{3/2} \rightarrow 3^2S_{1/2}$	3250*
He	$2^3P_0 \rightarrow 2^3P_1$	29640
He	$2^3P_1 \rightarrow 2^3P_2$	2291.7
He	$3^3P_0 \rightarrow 3^3P_1$	8113.6
He	$3^3P_1 \rightarrow 3^3P_2$	658.6
HeII	$2^2S_{1/2} \rightarrow 2^2P_{1/2}$	14043
HeII	$2^2P_{3/2} \rightarrow 2^2S_{1/2}$	161453

\* Uncorrected for hyperfine structure.

TABLE III  
MOLECULAR ROTATIONAL TRANSITIONS

Molecule	State	Frequency
CaH	$J=1/2 \rightarrow 1/2$	250,000 mc*
	$J=1/2 \rightarrow 3/2$	
CO	$J=0 \rightarrow 1$	115,271.2
NO	$J=1/2 \rightarrow 3/2$	150,372.8†
CS	$J=0 \rightarrow 1$	48,991.0

\* Approximate frequency.

† Uncorrected for fine and hyperfine structure.

1667.0 mc for the two strongest hyperfine components of the  $J=3/2$   $\Lambda$  doublet of the  $2\pi_{3/2}$  state of O<sup>16</sup>H<sup>1</sup>. The frequencies of these lines are currently being measured in the laboratory so that values will be available that are not dependent on molecular theory of  $\Lambda$  doublets.<sup>23</sup>

More complete listings of radio frequency spectral lines of interest to radio astronomy have been published and reference should be made to these papers for other cases.<sup>4-9</sup> Perhaps it should be pointed out that Shklovski has calculated the  $\Lambda$ -doublet frequency of the  $J=3/2$ ,  $2\pi_{3/2}$  state of CH as 7025 mc<sup>6</sup> but this appears to be in error. On the basis of improved molecular constants,<sup>24</sup> and improved theory,<sup>19</sup> the frequency is calculated to be 620 mc. However, this calculation is based on constants determined from optical spectra, thus the constants are not accurate by microwave standards and

<sup>23</sup> C. H. Townes, private communication.

<sup>24</sup> R. Coutrez, J. Hunaerts, and A. Koeckelenbergh, "Radio emission from Comet 1956 h on 600 mc," this issue, p. 274.

the 620 mc might be in error by as much as 50 mc or so. Nevertheless, this transition might be important in explaining the radio radiation from comets, as suggested by Coutrez, Hunaerts, and Koeckelenbergh as a result of their recent observations of Comet Arend-Roland.<sup>24</sup>

#### D. Line Widths

Eq. (26) and the energies of Section II-B predict that emission or absorption in atomic or molecular systems will occur at a single frequency, *i.e.*, the processes are monochromatic. This property has led to the practice of referring to such transitions as "spectral lines," however, as might be expected, the processes are not strictly monochromatic. All lines have a finite width which is usually a very small fraction of the resonant frequency so that the term "line" is really quite appropriate.

There are two sources of line width that are important for most cases in radio astronomy. The first of these is due to the fact that the atom emitting or absorbing radiation is not stationary but is constantly in motion. This leads to the familiar Doppler or thermal broadening and turbulent broadening. If the atom is moving along the line of sight with a velocity  $v$ , the frequency of its transition will appear shifted by an amount given by the well-known Doppler formula

$$\nu - \nu_0 = \frac{\nu_0}{c} v \quad (29)$$

where  $\nu$  is the observed frequency and  $\nu_0$  is the resonant frequency of the stationary atom. If the atoms are moving with a Maxwellian velocity distribution, the probability of finding velocities between  $v$  and  $v+dV$  is

$$f(v) = \sqrt{\frac{M}{2\pi kT}} e^{-Mv^2/2kT} \quad (30)$$

where  $M$  is the mass of the atom,  $k$  is the Boltzmann constant, and  $T$  is the kinetic temperature of the atoms. The intensity distribution of the emitted radiation will be given by<sup>15</sup>

$$I(\nu) = I_0 e^{-M/2kT(\nu-\nu_0)^2/\nu_0^2} \quad (31)$$

where  $I_0$  is the peak intensity. The line width, full width at half maximum, is readily found for this type of intensity distribution to be

$$\Delta\nu = 2 \frac{\nu_0}{c} \sqrt{\frac{2kT}{M} \ln 2} \quad (32)$$

These equations demonstrate how an atom's velocity can result in a broadening of its emitted radiation. In actual circumstances which arise in radio astronomy, these formulas may have to be modified to take account of 1) a distribution of velocities other than Maxwellian, 2) galactic rotation, and 3) turbulence.

A second mechanism by which spectral lines may be broadened results from the possibility that one or both

of the energy levels of the transition may have a short lifetime. Thus, an atom in such a level or state will not remain in that state if it can make a transition to a state of lower energy with the emission of a photon. This process, which can take place in the absence of an external radiation field, is called "spontaneous emission." If an atom is assumed to be in a particular state at time  $t=0$ , the probability of finding the atom in that level at time  $t$  is  $e^{-A t}$ . The atomic constant  $A$ , known as the "Einstein  $A$  coefficient," is the reciprocal of the mean lifetime of the state and can have a wide range of values. For spontaneous emission of visible radiation,  $A$  is of the order of  $10^8 \text{ sec}^{-1}$ , but for radio radiation it is of the order of  $10^{-15} \text{ sec}^{-1}$ .

It can be seen classically that this spontaneous emission from a level gives rise to radiation that is not strictly monochromatic.<sup>25</sup> By a Fourier analysis of the radiation from an oscillator whose amplitude is decaying with time according to  $e^{-(1/2)At}$  (its energy is decreasing at the rate  $e^{-At}$ ), one obtains a frequency spectrum of the form

$$I(\nu) = I_0 \frac{1}{(\nu - \nu_0)^2 + (A/4\pi)^2} \quad (33)$$

Clearly this is a frequency distribution having a line width  $\Delta\nu = A/2\pi$ . This result is substantiated by the quantum mechanical theory of radiation where it is shown that  $A$  is a property of the energy level and any radiation involving that level will be broadened by this amount. The theory also yields the value of  $A$ :<sup>25</sup>

$$A = \frac{64\pi^4 \nu^3 |\mu|^2}{3hc^3} \quad (34)$$

where  $|\mu|^2$  is the square of the dipole moment (cf. Section II-B). The tremendous range of values for  $A$  is accounted for by the variation of  $A$  as the third power of the frequency of the emitted radiation.

Line broadening can also be caused by the interaction of the radiating atom with other atoms. This source of line width, called "pressure broadening," is not important in radio astronomy because interstellar clouds and interstellar space in general are so rarefied that collisions between atoms are insignificant. However, pressure broadening may be the dominant source of line width in planetary or solar atmospheres.

### III. FORMATION OF EMISSION AND ABSORPTION LINES

With this brief review of microwave spectroscopy, we will now inquire as to how the presence of a microwave resonance transition in the atoms of interstellar space will alter the intensity of radio energy received. This requires a knowledge of the atom's ability to emit and absorb radiation at its resonant frequency when illuminated by external radiation.

<sup>25</sup> W. Heitler, "The Quantum Theory of Radiation," Oxford University Press, London, Eng., 3rd ed.; 1954.

Consider an atomic gas having  $n_1$  and  $n_0$  atoms per  $\text{cm}^3$  in the upper and lower energy levels, respectively, and let  $\nu_0$  be the resonant frequency defined by these levels. Radiation incident on this gas in a range of frequencies close to  $\nu_0$  will be absorbed by atoms initially in the lower state. The incident radiation will supply energy  $h\nu_0$  necessary to cause an atom to make a transition from the lower to the upper energy level and a photon of energy  $h\nu_0$  will be removed from the radiation field. Similarly, the radiation can induce or stimulate transitions in the reverse direction, from the upper to the lower energy level, and this "stimulated emission" will add a photon of energy  $h\nu_0$  to the radiation field. The net absorption by the gas is the difference between the number of absorptions and the number of emissions. If an atom in the lower state is capable of absorbing energy of frequency  $\nu$ , the probability of absorption per atom per second is  $B_{01}\rho(\nu)$ , where  $\rho(\nu)d\nu$  is the energy density of the incident radiation in the frequency range between  $\nu$  and  $\nu+d\nu$ , and  $B_{01}$  is an atomic constant known as the "Einstein  $B$  coefficient." The number of atoms per  $\text{cm}^3$  capable of absorbing energy at frequency  $\nu$  can be written as  $n_0f(\nu)$  where  $f(\nu)$  is the fraction of atoms able to absorb at frequency  $\nu$ . The fraction  $f(\nu)$  will depend on the atomic velocities in the case of a Doppler broadened line, or on the width of the energy levels in the case of a line broadened by stimulated emission. In any case,  $f(\nu)$  is the function specifying the line shape and must be subject to the condition

$$\int_0^{\infty} f(\nu)d\nu = 1 \quad (35)$$

as can be seen from the definition of  $f(\nu)$ . Thus the number of absorptions per  $\text{cm}^3$  per second at frequency  $\nu$  is

$$n_0f(\nu)B_{01}\rho(\nu). \quad (36)$$

Similarly, the number of induced emissions per  $\text{cm}^3$  per second is

$$n_1f(\nu)B_{10}\rho(\nu) \quad (37)$$

where  $B_{10}$ , the coefficient of stimulated emission, is related to  $B_{01}$  by the relation

$$g_0B_{01} = g_1B_{10} \quad (38)$$

The statistical weights,  $g_0$  and  $g_1$ , are pure numbers of order unity and represent the number of sublevels which compose the energy levels 0 and 1, respectively.

The net number of absorptions can be written as

$$n_0f(\nu)B_{01}\rho(\nu) \left[ 1 - \frac{g_0n_1}{g_1n_0} \right] \quad (39)$$

where use has been made of (38). It should be pointed out that (39) neglects the effects of spontaneous emission, but it can be shown that spontaneous emission is very small compared to stimulated emission in the radio frequency domain. This is not true for optical fre-

quencies; in fact, spontaneous emission is much more frequent than stimulated emission for optical frequencies.

The relative number of atoms in levels 1 and 0 can be related by a Boltzmann distribution law

$$\frac{n_1}{n_0} = \frac{g_1}{g_0} e^{-h\nu_0/kT_s} \cong \frac{g_1}{g_0} \left( 1 - \frac{h\nu_0}{kT_s} \right) \quad (40)$$

where the second form of the expression follows since  $h\nu_0/kT_s$  is small compared to unity in the radio frequency domain. Eq. (40) does not imply that the atoms are in thermal equilibrium, but may be taken as the definition of  $T_s$ , the "state temperature."

The change in energy density  $d\rho(\nu)d\nu$  per unit path length  $dl$  through the gas is  $h\nu/c$  times the net absorptions per  $\text{cm}^3$  per second and thus, from (39) and (40), gives

$$\frac{d\rho(\nu)d\nu}{dl} = \frac{n_0f(\nu)B_{01}\rho(\nu)h^2\nu^2}{ckT_s}. \quad (41)$$

The absorption coefficient  $\gamma(\nu)$ , the fractional change in energy density per unit length, becomes

$$\gamma(\nu) = \frac{n_0f(\nu)B_{01}h^2\nu^2}{ckT_s}. \quad (42)$$

From the theory of the interaction of radiation with matter, the value of  $B_{01}$  to be inserted in (42) is<sup>25</sup>

$$B_{01} = \frac{8\pi^3 |\mu|^2}{3h^2}. \quad (43)$$

In astronomical work, the quantity usually used to specify absorption is not the absorption coefficient per unit length  $\gamma(\nu)$  but the opacity  $\tau(\nu)$ , the integrated absorption over the entire path length. Thus

$$\tau(\nu) = \int \gamma(\nu)dl. \quad (44)$$

Combining (42)–(44) and letting  $N_0$  be the number of atoms in level 0 in a column along the line of sight of one  $\text{cm}^2$  cross section ( $N_0 = \int n_0 dl$ ), we finally obtain

$$\tau(\nu) = \frac{8\pi^3 N_0 \nu^2 |\mu|^2}{3ckT_s} f(\nu). \quad (45)$$

For a line broadened only by spontaneous emission, the line shape function  $f(\nu)$  is

$$f(\nu) = \frac{1}{\pi} \frac{\Delta\nu}{(\nu - \nu_0)^2 + (\Delta\nu)^2} \quad (46)$$

which resembles (33) and satisfies (35).

Having obtained an expression for the opacity of the gas, it is now possible to describe how the presence of the gas will affect the intensity of radiation received by a radiometer. When frequency scanning radiometer is tuned in the range of the resonant frequency, the intensity received will be

$$I(\nu) = I_s[1 - e^{-\tau(\nu)}] + I_A e^{-\tau(\nu)} \quad (47)$$

where the first term represents the radiation from the gas itself, and the second term represents the attenuation by the gas of continuum radiation.  $I_s$  is the intensity that would be received from the gas if it were opaque,  $\tau(\nu) = \infty$ , and  $I_A$  is the intensity that would be received if the gas were absent or transparent,  $\tau(\nu) = 0$ . If the radiometer is tuned off resonance,  $\tau(\nu) = 0$  and the intensity received is  $I_A$ . Thus, the change in intensity of received energy as the radiometer is tuned through the resonant frequency is (47) minus  $I_A$ , or

$$\Delta I(\nu) = (I_s - I_A)[1 - e^{-\tau(\nu)}]. \quad (48)$$

In radio astronomy, it is customary to employ the Rayleigh-Jeans approximation whereby the intensity of radiation is related to a temperature by the familiar relation

$$I(\nu)d\nu = \frac{2kT\nu^2}{c^2} d\nu. \quad (49)$$

Thus the temperature difference detected by a radiometer with an absorbing gas in the antenna beam is

$$\Delta T(\nu) = (T_s - T_A)[1 - e^{-\tau(\nu)}] \quad (50)$$

where  $T_A$  is the "antenna temperature" of the continuum radiation, and  $T_s$  is defined by (40). If  $\tau(\nu)$  is small compared with unity, (50) can be combined with (45) to give

$$\Delta T(\nu) = \left(1 - \frac{T_A}{T_s}\right) \frac{8\pi^3 N_0 \nu^2 |\mu|^2}{3ck} f(\nu). \quad (51)$$

Eq. (51) illustrates several important points. Note that if  $T_s > T_A$ , the resonance line will appear in emission, whereas if  $T_A > T_s$ , the line will appear as an absorption line. For an emission line, if  $T_s \gg T_A$  the radiometer output will be independent of  $T_s$ .

Several assumptions are inherent in the above development. It has been assumed that the gas is uniform and, also, that the source of continuum radiation lies entirely behind the source of resonance radiation. Removal of these assumptions invalidates (47). Finally, it must not be assumed that  $T_s$  is the kinetic temperature  $T$  of the atoms [cf. (30)]. In laboratory spectroscopy,  $T_s$  is invariably equal to  $T$  (with the exception of recent work on masers), but in interstellar space a careful analysis must be made of the various processes which are competing to establish the relative populations of the energy levels. Such an analysis has been made for the hydrogen 1420-mc line and it is found that  $T_s = T$  for all expected galactic densities.<sup>26,27</sup> However, for lines

<sup>26</sup> E. M. Purcell and G. B. Field, "Influence of collisions upon population of hyperfine states in hydrogen," *Astrophys. J.*, vol. 124, pp. 542-549; November, 1955.

<sup>27</sup> G. B. Field, "Excitation of the hydrogen 21-cm line," this issue, p. 240.

having electric dipole matrix elements,  $T_s$  may depart appreciably from  $T$ , especially for high frequency lines.<sup>28</sup>

Equations of the form of (45), (50), and (51) are basic for the interpretation of spectral lines in terms of the number of atoms present. It should be noted that the opacity depends on the square of the dipole matrix element and, thus, the opacity of an electric dipole transition is some  $10^4$  times as large as that of a magnetic dipole transition, other factors remaining equal. This is an important point for it allows  $N_0$  to be smaller by  $10^4$  in the case of electric dipole transitions and still preserve the detectable opacity.

#### IV. CONCLUSION

At the writing of this paper, only the 1420-mc line of atomic hydrogen has been detected in the spectrum of radiation from our galaxy. The study of this line, however, has produced rich dividends, and still more can be expected. Perhaps it should be pointed out that the hydrogen radio line enables one to study interstellar hydrogen in the ground, or lowest, state which would otherwise be unobservable by optical methods except under limited circumstances. Because of this, it has been possible to map the hydrogen distribution in large regions of the galaxy where the gas is entirely in its ground state.

Russian observers have reported the detection of the hyperfine transition in deuterium at 327.4 mc,<sup>29</sup> but this has not been confirmed by other radio astronomers after extensive searches.<sup>30,31</sup> The most recent of these efforts<sup>31</sup> is able to set an upper limit on the abundance ratio of deuterium to hydrogen of 1/2000 which can be compared with the terrestrial abundance ratio of 1/6670.

A similar search for the OH lines at 1665 mc and 1667 mc failed to produce any positive result.<sup>32</sup>

As advances are made in techniques, the minimum detectable temperature difference in radiometer output will undoubtedly be lowered, thus fewer atoms will be required to produce a detectable spectral line. Also, as larger antennas are constructed, it should be possible to study planetary atmospheres, for instance, and the detection of spectral lines in these atmospheres should be feasible. In the meantime, the study of the hydrogen line will have to suffice, but that will not be without its rewards.

<sup>28</sup> A. H. Barrett and A. E. Lilley, "On the detection of microwave spectral lines in radio astronomy," *Astron. J.*, vol. 62, p. 4; January, 1957.

<sup>29</sup> G. G. Getmanzev, K. S. Stankevitch, and V. S. Troitsky, "Detection of monochromatic radio emission of deuterium from the center of the galaxy on a wavelength of 91.6 cm," *Dok. Akad. Nauk USSR*, vol. 103, pp. 783-786; February, 1955.

<sup>30</sup> G. J. Stanley and R. Price, "An investigation of monochromatic radio emission of deuterium from the galaxy," *Nature*, vol. 177, pp. 1221-1222; June 30, 1956.

<sup>31</sup> R. L. Adgie and J. S. Hey, "Intensity of the radio line of galactic deuterium," *Nature*, vol. 179, p. 370; February, 1957.

<sup>32</sup> A. H. Barrett and A. E. Lilley, "A search for the 18 cm line of OH in the interstellar medium," *Astron. J.*, vol. 62, p. 5; January, 1957.

# Measurements of Planetary Radiation at Centimeter Wavelengths\*

C. H. MAYER†, MEMBER, IRE, T. P. McCULLOUGH†, AND R. M. SLOANAKER†

**Summary**—Radiation from the planets, Venus, Mars, and Jupiter, has been measured at a wavelength of 3.15 cm using the Naval Research Laboratory 50-foot reflector and a narrow-band radiometer. The apparent blackbody temperatures for Mars and Jupiter derived from the radio measurements agree reasonably well with the results of infrared radiometric measurements. For the case of Venus, the apparent blackbody temperature derived from the 3.15-cm measurements is about a factor of two higher than the value derived from the infrared measurements. A measurement of the radiation from Venus at 9.4-cm wavelength was made using the same antenna. The apparent blackbody temperature derived from this measurement agreed well with the value derived from the 3.15-cm measurement, but the accuracy of the 9.4-cm result was low because of the small flux density of radiation and the small number of observations.

## INTRODUCTION

THE PLANETS are expected to emit radio radiation by ordinary thermal processes; for example, the earth is known to radiate as a gray body at a temperature near 300°K. At wavelengths as long as radio wavelengths and for temperatures in the hundreds of degrees absolute, thermal radiation is governed by the Rayleigh-Jeans approximation. For this case, the flux density of radiation varies as the inverse-square of the wavelength. The best opportunity for the detection of thermal radio radiation from other planets is presented therefore at the very short radio wavelengths. Even here, the largest antennas available and special receiving and measurement techniques are necessary to measure the extremely weak thermal emissions of other planets.

Observations of thermal radio radiation from the planets are of interest to supplement the infrared observations. This is especially true for the planets with extensive atmospheres, for in general, the much longer wavelength radio radiation would be expected to penetrate the atmospheres more readily than would the infrared radiation. Observations of planetary radiation have additional interest to the radio astronomer because the positions in the sky of other radio sources of small angular diameter are not accurately known.

Unexpected strong bursts of long-wavelength radio radiation from Jupiter were discovered by Burke and Franklin<sup>1</sup> in 1955. These observations were subse-

quently confirmed by several observers.<sup>2</sup> A similar type of radiation from Venus has been detected by Kraus.<sup>3</sup> The generating mechanism of this radiation is not known, but the spectrum of the impulsive radiation from Jupiter apparently falls off rapidly with decreasing wavelength.<sup>4</sup> This type of planetary radiation has not been reported at wavelengths shorter than about 11 meters. There is no evidence at the present time to indicate that the long-wavelength impulsive radiation has any connection with the radiation at centimeter wavelengths which is presumably of thermal origin.

In May, 1956, a radiometer at a wavelength of 3.15 cm was installed in the Naval Research Laboratory 50-foot paraboloid to observe the close approach of Venus. The wavelength near 3 cm was considered a good compromise between the desire to use as short a wavelength as possible, and the limitations in the aiming and focusing ability of the 50-foot antenna. It was estimated that the flux density of radiation from Venus at this wavelength and at closest approach would be roughly  $6 \times 10^{-26}$  watts  $m^{-2}$  (cps)<sup>-1</sup> which would correspond to a change in antenna temperature of roughly 2°C. Subsequently, a measurement of the radiation from Venus was attempted at 9.4-cm wavelength. The flux density of radiation at this wavelength was expected to be an order of magnitude below that at 3.15 cm.

In September, 1956, the 3.15-cm radiometer was used with the 50-foot antenna to observe the close approach of Mars. The flux density of radiation from Mars at closest approach was expected to be about  $7 \times 10^{-26}$  watts  $m^{-2}$  (cps)<sup>-1</sup> corresponding to a change in antenna temperature of about  $\frac{1}{4}$ °C.

A few observations of Jupiter at 3.15-cm wavelength were made in May and June, 1956; but, results were quite inaccurate because of antenna pointing errors. An improved series of measurements of radiation from Jupiter was made in March, 1957. The estimated flux density and antenna temperature for thermal radiation from Jupiter were expected to be about twice those for Mars.

\* C. A. Shain, "18.3 mc/s radiation from Jupiter," *Aust. J. Phys.*, vol. 9, pp. 61-73; March, 1956. J. D. Kraus, "Some observations of the impulsive radio signals from Jupiter," *Astron. J.*, vol. 61, pp. 182-183; May, 1956.

† J. D. Kraus, "Impulsive radio signals from the planet Venus," *Nature*, vol. 178, p. 33; July, 1956.

—, "Radio observations of the planet Venus at a wave-length of 11 meters," *Nature*, vol. 178, pp. 103-104; July, 1956.

—, "Class II radio signals from Venus at a wave-length of 11 meters," *Nature*, vol. 178, pp. 159-160; July, 1956.

—, "Recent observations of radio signals from Venus at 11 meters wave-length," *Astron. J.*, vol. 62, p. 21; January, 1957.

† F. G. Smith, "A search for radiation from Jupiter at 38 mc/s and at 81.5 mc/s," *Observatory*, vol. 75, pp. 252-254; December, 1955.

\* Original manuscript received by the IRE, October 3, 1957. Detailed descriptions of the observations are given in NRL Rep. Nos. 4998 and 5021 and in two papers which have been submitted by the authors to the *Astrophys. J.* for publication: "Observations of Venus at 3.15 CM Wavelength" and "Observations of Mars and Jupiter at a Wavelength of 3.15 CM."

† Radio Astronomy Branch, U. S. Naval Research Lab., Washington, D. C.

1 B. F. Burke and K. L. Franklin, "Observations of a variable radio source associated with the planet Jupiter," *J. Geophys. Res.*, vol. 60, pp. 213-217; June, 1955. K. L. Franklin and B. F. Burke, "Radio observations of Jupiter," *Astron. J.*, vol. 61, p. 177; May, 1956.

## APPARATUS

## 3.15-CM Radiometer

The radiometer used at 3.15-cm wavelength for the observations of Venus, Mars, and Jupiter was a modification of the Dicke radiometer.<sup>5</sup> A ferrite circulator was used to switch the receiver alternately between the 50-foot antenna and a small horn antenna pointed at the sky.<sup>6</sup> This arrangement gave the advantage of increased radiometer stability since the antenna temperatures of the 50-foot antenna and the small comparison horn differed by only a few degrees when the 50-foot antenna was pointed at the sky or at weak sources of radiation like the planets. The inherent impedance isolation of the ferrite circulator greatly improved the accuracy of calibrating the radiometer and also further improved the radiometer stability by suppressing variable impedance errors. The radiometer circuit is diagrammed in Fig. 1.

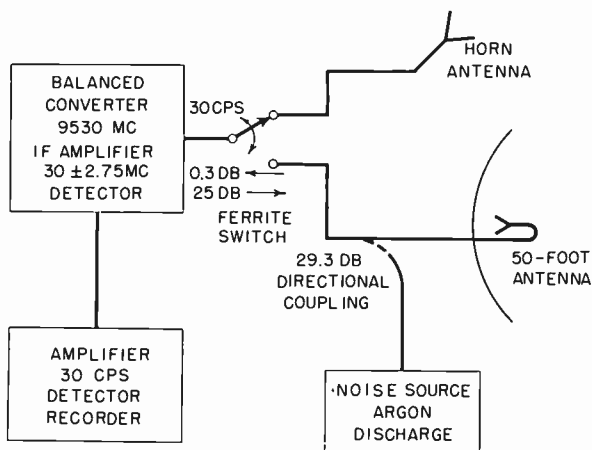


Fig. 1—Block diagram of 3.15-cm radiometer.

The ferrite circulator was switched at a 30-cps rate. The insertion loss of the switch in the preferred direction was 0.3 db and the switching ratio was greater than 25 db over the bandwidth of the receiver. The ferrite switch was followed by a balanced crystal converter which was transformer coupled to a 30-mc IF amplifier with a 2.2-db noise factor and a bandwidth of 5.5 mc. Two types of mixer crystals were used at different times, the 1N263 and the 1N23E. There was no input preselection except that associated with the crystal mixers, so that both the signal and image bands were converted to the intermediate frequency. The receiver noise factor measured at the feed horn terminal using an argon discharge noise source in waveguide was about 4.7 in power ratio. From this it can be inferred that the same receiver with reactive input preselection which would pass only the signal band would have a noise factor of about 8.4 in

power ratio on the average. Since the radiometer was used to measure broad-band, noise-type radiation, the former figure is the more significant. The 30-cps modulation from the second detector was amplified and the dc component was extracted in a half-wave coherent detector using two thermionic diodes. The reference voltage for the coherent detector and the drive for the ferrite switch were derived from the same audio-frequency signal generator with an adjustable phase-changer in the reference voltage line. The output of the coherent detector was filtered by a two-stage RC network and applied to a Leeds and Northrup potentiometer-type recorder with a full scale response time of 1 second. The over-all output time constant of the radiometer was 5 seconds.

The 3.15-cm radiometer basically was calibrated with thermal noise sources, but an argon discharge noise source was used as a secondary calibration standard. As indicated in Fig. 1, a small noise power from the argon tube could be fed to the receiver input through a directional coupler in the antenna line. The secondary standard was used so that the radiometer could be calibrated accurately at frequent intervals during the observations. A second advantage was that the calibration signal was applied at the same input power level as was the measured signal. In order to do this directly, thermal noise sources at very low temperatures would be necessary. The change in antenna temperature when the argon tube was turned on was calibrated by direct comparison with thermal noise sources. The thermal noise sources were constructed using matched resistive terminations of the lossy-wall waveguide type. The terminations with their associated waveguide transmission lines were immersed in agitated water baths. The temperatures of the water baths were measured with precision thermometers. To make the calibration, the comparison horn was replaced by a matched termination at ambient temperature, and two such thermal noise sources were substituted for the feed horn in turn. One of the thermal noise sources was maintained at ambient temperature while the other was maintained at a temperature slightly above ambient by means of an immersion heater in the water bath. The change in the radiometer output deflection when the argon tube was turned on was compared with the change when the two thermal noise sources with a known temperature difference were interchanged. To make accurate comparisons the temperature of the heated noise source was adjusted and allowed to reach equilibrium so that the changes in the radiometer output deflections for the two cases were nearly equal. By this procedure the change in antenna temperature corresponding to the argon discharge noise source was found to be 13.8°C with a standard deviation for individual readings of about 0.3°C. A number of these calibrations were made at several times during the interval covered by the observations so that the mean error in this figure is much less than the standard deviation for individual measurements. The error introduced

<sup>5</sup> R. H. Dicke, "The measurement of thermal radiation at microwave frequencies," *Rev. Sci. Instr.*, vol. 17, pp. 268-275; July, 1946.

<sup>6</sup> C. H. Mayer, "Improved microwave noise measurements using ferrites," *IRE TRANS.*, vol. MTT-4, pp. 24-28; January, 1956.

—, "Improved noise power measurements through the use of ferrites," *J. Geophys. Res.*, vol. 59, pp. 188-199; March, 1954.

by the change of impedance when the noise sources were substituted for the antenna feed horn was tested and found to be negligible.

The radio-frequency and intermediate-frequency circuits of the radiometer were mounted adjacent to the focus of the paraboloid so that rigid transmission lines could be used for the high frequencies. This part of the radiometer was located in the pyramidal box shown in Fig. 2. The mounting of the feed horn and the comparison horn also are shown. The 30-cps modulation was cabled to the control cabin of the antenna where the low-frequency circuits and the power and recording units were located. The power line was regulated to 0.1 per cent with a Sorensen ac regulator. All of the vacuum tube filaments in critical circuits were heated by dc from a Sorensen Nobatron regulated to 0.2 per cent. All vacuum tube plates were supplied from electronically regulated power supplies.

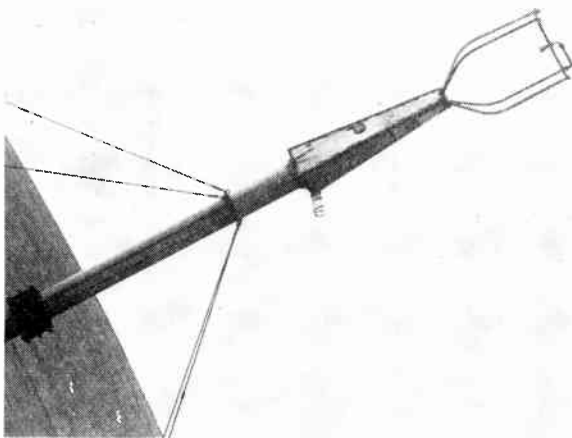


Fig. 2—3.15-cm radiometer mounted in the 50-foot reflector.

### 3.15-CM Antenna

A plane-polarized pyramidal horn used for the feed antenna was located at the focus of the 50-foot paraboloid. The horn was designed so that the illumination at the edge of the reflector was about 15 db below that at the vertex.

The radiation patterns of the 50-foot antenna at 3.15-cm wavelength were measured using a transmitting antenna mounted in the top of the Washington Monument at a distance of about 5 miles. The results of the pattern measurements are shown in Fig. 3 where the horizontal-plane pattern and the vertical-plane pattern are plotted on both linear and logarithmic scales. These patterns were measured both for horizontal and vertical polarizations, but the results were nearly identical and the differences could be easily accounted for by measurement inaccuracies. The horizontal-plane patterns showed a somewhat broadened beamwidth and merged sidelobes. A check on the horizontal-plane pattern with the reflector pointed to an elevation angle of about 70° was made using the Crab Nebula as a source. This check

indicated that the half-power width of the horizontal-plane pattern for this antenna attitude was nearly the same as the 8.5 minutes of arc measured for the vertical-plane pattern at the horizon and that the broad skirts caused by merged sidelobes had disappeared. No comparable check of the vertical-plane pattern at high elevation could be made.

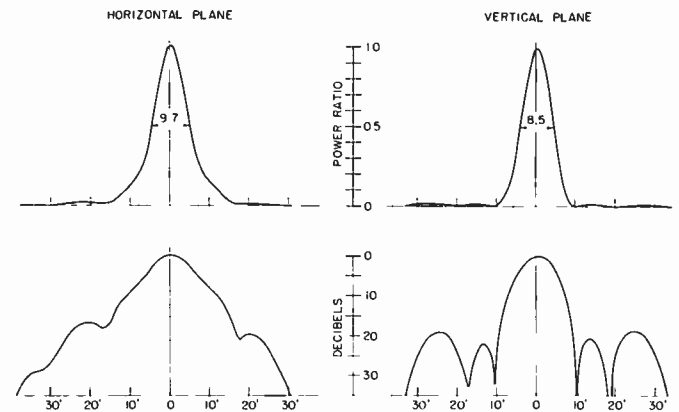


Fig. 3—Radiation patterns of the 50-foot reflector measured at 3.15-cm wavelength.

The gain of the antenna at 3.15-cm wavelength was measured using a transmitting antenna at a distance of about 13 miles with a line of sight path. The measurement was made by comparing the signal received by the 50-foot antenna with the signal received by a standard horn with a gain of 22.15 db. Calibrated waveguide attenuators were inserted in the transmission line from the 50-foot antenna and a superheterodyne receiver was used to match the outputs. This measurement gave a gain of 60.7 db for the 50-foot antenna when pointed at the horizon. The greatest uncertainty in the gain measurement was considered to be the incomplete knowledge of the field across the paraboloid compared to the field sampled by the standard horn. The standard horn was moved horizontally across the aperture of the paraboloid at about the height of the lower rim and vertically from about this height to about the height of the axis of the paraboloid when it was pointed at the horizon. These scans indicated a maximum variation in the field of about 1 db. From these scans the field at the normal position of the standard horn was corrected by about  $\frac{1}{2}$  db to approximate what was estimated to be a representative field over the aperture. Since the characteristics of the antenna apparently change with elevation angle, a check was made by taking drift scans through the intense radio sources Cassiopeia-A and the Crab Nebula over a range of elevation angles. Although these observations did not give a highly accurate calibration for the gain variation with antenna attitude, they indicated that the gain at the average elevation angle of the observations was about  $\frac{1}{2}$  db higher than the value measured at the horizon. This correction was applied to the measured gain for the data reduction. The final estimate for the gain of the 50-foot paraboloid at

the average elevation angle of the observations was 61.2 db with an estimated mean error of about  $\frac{1}{2}$  db.

#### 9.4-CM Radiometer

The 9.4-cm radiometer used a rotating lossy-card chopper similar to that described by Dicke<sup>5</sup> to effect the 30-cps input modulation. A ferrite isolator was inserted in the antenna line for impedance isolation. The chopper was followed by a balanced converter using 1N21C crystals. The remainder of the radiometer was the same as the 3.15-cm radiometer. The receiver noise factor measured with an argon discharge noise source was about 5 in power ratio including the loss of the ferrite isolator and considering both signal and image bands as useful. An argon discharge noise source was used in the same manner as already described for the 3.15-cm radiometer except that in this case the experimental error of the planetary measurement was so high that the same effort was not expended to achieve accurate calibration of the argon tube signal. Instead the coupling ratio of the directional coupler was accurately measured and the change in antenna temperature was calculated from the coupling ratio, the effective noise temperature of the argon tube, and the loss of the antenna line. The resulting change in antenna temperature when the argon tube was turned on was 12.7°C referred to the antenna feed terminal, with an estimated mean error of about 1°C. In this case the rf and IF circuits were mounted behind the vertex of the paraboloid and were connected to the feed antenna with a waveguide transmission line.

#### 9.4-CM Antenna

The waveguide reverted-horn feed antenna which was used for the previous observations of radio sources at 9.4-cm wavelength was used here.<sup>7</sup> The antenna patterns were not remeasured. The antenna gain has not been measured at this wavelength. The gain was originally assumed to be 51.5 db;<sup>7</sup> however, in the light of the measured gain at 3.15 cm this figure was raised to 51.9 db for the present analysis.

### OBSERVATIONS

#### Venus

Radiation from Venus at 3.15 cm was first detected on May 2, 1956; however, the observations were taken in a slight rain so these data are not included in the analysis. Regular observations were made on 34 days spread over the period May 5, 1956, to June 23, 1956, a period just prior to and including inferior conjunction. The observations were made by setting the antenna ahead of Venus in hour angle and letting the rotation of the earth sweep the beam of the antenna through the

position of Venus or through a position above or below Venus. In all, about 1400 such drift curves were made. From these, about 600 were selected for which the peak of the antenna beam missed the position of Venus by less than 1 minute of arc. These peak drift curves were averaged for each day and the average antenna temperatures are plotted in Fig. 4. The data from June 20 to June 23 are less reliable because during this period Venus and the Sun were in nearly the same direction and solar radio radiation was picked up in the sidelobes of the antenna. As Venus approached the earth during the period, the solid angle subtended by the visible disk increased as indicated by the solid curve in Fig. 4. It can be seen that the measured antenna temperature changed very nearly according to the solid angle of the visible disk. Since the maximum angular diameter of Venus was small compared with the half-power width of the antenna beam, no correction is needed for source size and this result indicates that the radiating temperature of Venus was nearly constant over this period. No differences in the amplitudes of single drift curves during a day were noted which could not have been caused by radiometer output variations or antenna pointing errors.

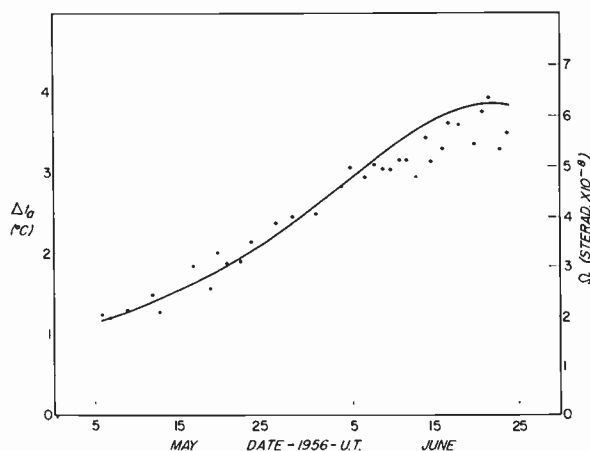


Fig. 4—Daily averages of the measured antenna temperatures for Venus plotted along with the change in the solid angle subtended by the optical disk of Venus.

The temperature of a blackbody radiator which would subtend the same solid angle as Venus and which would correspond to the measured flux density of radiation was  $620 \pm 110^\circ\text{K}$  (mean error) near the beginning of the period, and  $560 \pm 73^\circ\text{K}$  (mean error) near the end of the period. A sample of the radiometer output trace during a drift scan through Venus on June 17, 1956, is reproduced in Fig. 5(b).

An attempt was made to put rough limits on the spectrum of the radio radiation from Venus by making two observations at 9.4-cm wavelength. Observations were made on June 24, 1956; however, the interference of the Sun in the sidelobes of the antenna was more serious than at 3.15-cm wavelength and no usable data were obtained. On June 25, the interference from the Sun was still present but was sufficiently lessened to allow four

<sup>7</sup> F. T. Haddock, C. H. Mayer, and R. M. Sloanaker, "Radio emission from the Orion nebula and other sources at  $\lambda$  9.4 cm," *Astrophys. J.*, vol. 119, pp. 456-459; March, 1954.

—, "Radio observations of ionized hydrogen nebulae and other discrete sources at a wave-length of 9.4 cm," *Nature*, vol. 174, p. 176; July, 1954.

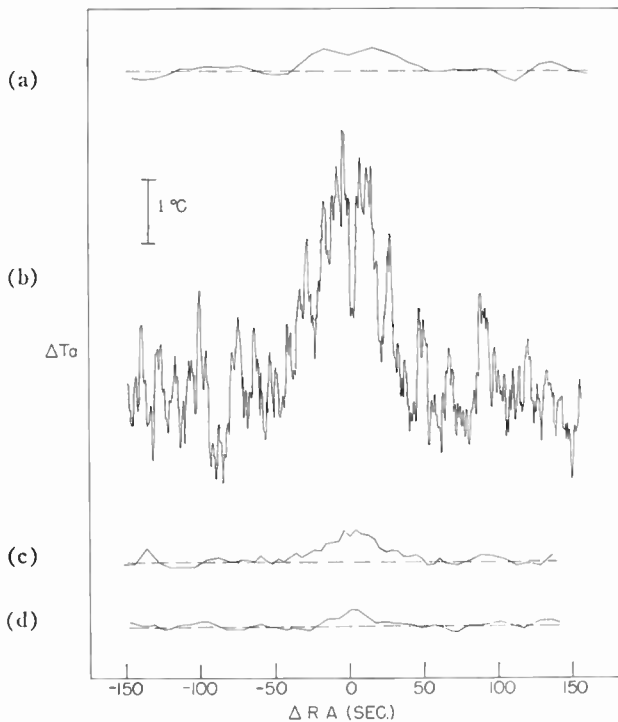


Fig. 5—Summary of the measurements of planetary radiation. (a) Average of eleven drift scans through Venus made at a wavelength of 9.4 cm. (b) A reproduction of the output trace of the 3.15-cm radiometer as Venus drifted through the beam on June 17, 1956. (c) Average of forty-five drift scans through Jupiter made at 3.15-cm wavelength. (d) Average of seventy-one drift scans through Mars made at 3.15-cm wavelength.

usable drift scans to be made. These four drift scans were averaged and the result indicated a change in antenna temperature of about  $0.3^{\circ}\text{C}$ . This corresponds to a flux density of about  $8 \times 10^{-26}$  watts  $\text{m}^{-2}$  (cps) $^{-1}$  and an apparent blackbody temperature for Venus of about  $430 \pm 215^{\circ}\text{K}$  (mean error). Because of the added uncertainty due to sun interference in the sidelobes of the antenna, the 9.4-cm radiometer was again installed in the 50-foot antenna on July 27, 1956. At this time seven good drift scans through Venus were obtained which when averaged gave a change in antenna temperature at the position of Venus of about  $0.25^{\circ}\text{C}$ . This corresponds to a flux density of about  $6 \times 10^{-26}$  watts  $\text{m}^{-2}$  (cps) $^{-1}$  and an apparent blackbody temperature for Venus of about  $740 \pm 370^{\circ}\text{K}$  (mean error). The average of the two 9.4-cm measurements of the blackbody temperature of Venus was  $580^{\circ}\text{K}$  which compares favorably with the result at 3.15-cm wavelength. Although the accuracy of the 9.4-cm results is very poor, these measurements suggest that no great percentage of the radio radiation from Venus at centimeter wavelengths has a spectrum very different from that of thermal radiation. An average of the eleven drift scans through Venus at 9.4-cm wavelength is plotted in Fig. 5(a).

### Jupiter

During May, 1956, a limited number of drift scans through or near the position of Jupiter were made. An average line was drawn through the radiometer output

traces for twenty-nine scans, the values of the average lines were read off at specified intervals, and the twenty-nine scans were averaged together numerically. The drawing of the average line was checked by reading the actual recorder trace at discrete points. The average of the twenty-nine scans indicated a change in antenna temperature of  $0.21^{\circ}\text{C}$ . However, the antenna pointing calibration using the Crab Nebula radio source indicated that the peak of the antenna beam missed the position of Jupiter by several minutes of arc for many of the drift scans included in the average. A large correction had to be applied to the measured antenna temperature to take this into account. After this correction and a small correction for atmospheric absorption, the best estimate for the change in antenna temperature with Jupiter at the peak of the main beam was about  $0.35^{\circ}\text{C}$ . This corresponds to a blackbody temperature for Jupiter of about  $140^{\circ}\text{K}$  using the solid angle calculated from the mean diameter of the visible disk. The uncertainty on this value was so high, perhaps 40 per cent mean error, that it was not considered to be of much quantitative value.

A second series of observations of Jupiter with improved accuracy was made on seven days between March 23 and April 1, 1957. The radio sources associated with the Crab Nebula and the Orion Nebula were used as pointing objects. In this series of observations drift scans were made not only at the expected declination of Jupiter, but also at declination settings 4 minutes of arc above and below the expected declination. A change in antenna pointing of 4 minutes of arc from the peak of the beam corresponds roughly to half-power response. These extra measurements indicated that the declination settings for the central scans were accurate to about  $\frac{1}{2}$  minute of arc so that no appreciable correction was necessary for systematic pointing errors. The result of averaging forty-five drift scans at the central declination setting is shown in Fig. 5(c). The measured change in antenna temperature was  $0.48^{\circ}\text{C}$  and after corrections of 2 per cent for atmospheric absorption and 4 per cent for random antenna pointing errors the corrected antenna temperature was  $0.51^{\circ}\text{C}$ . This corresponds to an incident flux density of  $1.4 \times 10^{-25}$  watts  $\text{m}^{-2}$  (cps) $^{-1}$  and a temperature for a blackbody radiator which would subtend the same angle as the mean diameter of the disk of Jupiter of about  $145^{\circ}\text{K}$ . The estimated mean error is 18 per cent.

### Mars

The observations of Mars were made on seven days between September 9 and September 21, 1956. The pointing of the antenna beam was checked each day against the radio source associated with the Omega Nebula. The average of seventy-one drift scans through the position of Mars is shown in Fig. 5(d). The measured change in antenna temperature was  $0.2^{\circ}\text{C}$ . The antenna pointing was uncertain because the true position of the Omega Nebula radio source is not accurately known.

TABLE I

Planet	Infrared Blackbody Temperature °K	Date of Observation	Wavelength of Observation cm	Antenna Temperature* °K	Flux Density watts m <sup>-2</sup> (cps) <sup>-1</sup>	Radio Blackbody Temperature† °K
Venus	240 <sup>8</sup>	June 25 and July 27, 1956 May 5-18, 1956 June 15-23, 1956	9.4 3.15 3.15	0.28 1.42 3.54	7 × 10 <sup>-26</sup> 3.8 × 10 <sup>-26</sup> 9.6 × 10 <sup>-26</sup>	580 ± 230 (ME) 620-110 560-73
Jupiter	130 <sup>9</sup>	May 13 and May 31, 1956 March 23 to April 1, 1957	3.15 3.15	0.35 0.51	9.5 × 10 <sup>-26</sup> 1.4 × 10 <sup>-26</sup>	140 ± 56 145 ± 26
Mars	260 <sup>10</sup>	September 9-21, 1956	3.15	0.24	6.5 × 10 <sup>-26</sup>	218 ± 76

\* Corrected for atmospheric absorption and antenna pointing errors.

† Based on the solid angle calculated from the average diameter of the visible disk.

For this reason a sizeable correction and comparable uncertainty were applied to the measured value. An additional correction of 2.3 per cent was applied for atmospheric absorption. The resulting best estimate for the change in antenna temperature due to Mars at the peak of the antenna beam and in the absence of atmospheric absorption was 0.24°C. This corresponds to a flux density from a point source of  $6.5 \times 10^{-26}$  watts m<sup>-2</sup> (cps)<sup>-1</sup> and a temperature for a blackbody radiator which would subtend the same solid angle as Mars of 218°K. The estimated mean error is about 35 per cent.

#### DISCUSSION

The radiometer output response due to Venus was sufficiently large that individual drift scans could be inspected and no definite evidence for short-time variability in the received radiation was observed. Because of the altitude-azimuth mounting of the antenna, the plane of polarization accepted by the antenna rotated by more than 90° with respect to the meridian through Venus from rising to setting. No systematic change in the measured radiation with this rotation was noted which indicates that no substantial part of the radiation was plane polarized. In this case, the usual assumption that the antenna will accept only  $\frac{1}{2}$  of the incident flux was partially justified experimentally. The same assumption was made for Mars and Jupiter.

The antenna temperature for a given antenna is specified<sup>11</sup> by

$$T_a = \frac{D}{4\pi} \int \int_{4\pi} T_b \left( \frac{A}{A_0} \right) d\Omega \quad (1)$$

where  $D$  is the directivity of the antenna at the peak of the main lobe,  $A/A_0$  is the normalized antenna pat-

tern, and  $T_b$  is the brightness temperature. In the case of the small comparison horn, the beamwidth was about 37° between half-power points, and the directivity was so small that no known source of radiation in the sky except the sun would produce a detectable response. The antenna temperature of the comparison horn during the observations can be considered constant during a drift scan. The change in the measured antenna temperature during a drift scan is then a measure of the change in the integral for the 50-foot antenna. Since the brightness temperature of the sky background is very small compared to the brightness temperatures of the planets for short wavelengths, and since the radiation collected from the earth may be considered constant during a drift curve, the change in antenna temperature during a drift curve is a measure of the flux density of radiation from the planet.

The total flux density of radiation  $S$  from a point source is related to the maximum change in antenna temperature  $\Delta T_a$  during a drift scan by

$$S = \frac{2k\Delta T_a}{A_0} \quad (2)$$

where  $k$  is Boltzmann's constant, and  $A_0$  is the effective area of the antenna for reception at the peak of the beam.

The total flux density of radiation at a wavelength  $\lambda$  from a blackbody radiator at a temperature  $T$ , subtending a solid angle  $\Omega$ , is given to sufficient accuracy by the Rayleigh-Jeans approximation.

$$S = \frac{2kT\Omega}{\lambda^2} \quad (3)$$

The flux densities of radiation and the corresponding blackbody temperatures for the planets can be calculated from the observed change in antenna temperature using these expressions. The angular diameters of the planets were small compared with the half-power diameter of the antenna beam so that no appreciable error is introduced by the finite size of the source. The errors caused by reflected solar radiation from the planets is estimated to be negligible.

<sup>8</sup> E. Pettit and S. B. Nicholson, "Temperatures on the bright and dark sides of Venus," *Pub. Astron. Soc. Pacific*, vol. 67, pp. 293-303; October, 1955. W. M. Sinton: Cited from D. H. Menzel and F. L. Whipple. "The case for H<sub>2</sub>O clouds on Venus," *Pub. Astron. Soc. Pacific*, vol. 67, pp. 161-168; June, 1955.

<sup>9</sup> D. H. Menzel, W. W. Coblenz, and C. O. Lampland, "Planetary temperatures derived from water-cell transmissions," *Astrophys. J.*, vol. 63, pp. 177-187; April, 1926.

<sup>10</sup> G. de Vaucouleurs, "Physics of the Planet Mars," Eng. ed., Faber and Faber Ltd., London, Eng., p. 171; 1954.

<sup>11</sup> J. L. Pawsey and R. N. Bracewell, "Radio Astronomy," Clarendon Press, Oxford, Eng., p. 24; 1955.

The present measurements are summarized in Table I, p. 265, along with the blackbody temperatures measured by infrared radiometric methods. The region of emission of the radio radiation is probably not the same as for the infrared radiation for the cases of Venus and Jupiter, and consequently the blackbody temperatures would not necessarily agree. The transparencies of the atmospheres are difficult to predict because of possible molecular absorptions, and no attempt to do this will be made in the present discussion. Appreciable absorption in a heavily-ionized atmosphere does not seem very likely at these wavelengths, but this possibility cannot be rejected completely without further study. The great apparent discrepancy between the blackbody temperatures for Venus measured at radio and infrared wavelengths is as yet unexplained. For the case of Mars there does not seem to be much possibility for large atmospheric absorption of radio waves, but they may be emitted from a different level in the crust.

The measurements suggest that the blackbody temperature of Venus decreased slightly over the measurement period. Such a decrease could be connected with the rotation of the planet or with the phase of solar illumination. Over this period the sunlit crescent of Venus decreased from about 36 per cent of the visible disk to nearly zero. The present radio observations are considered inadequate to define a correlation.

The accuracy of these first measurements of planetary radiation at centimeter wavelengths is not high; however, these experiments demonstrate that such measurements are practical with existing apparatus and present techniques.

#### ACKNOWLEDGMENT

The authors express their thanks to J. W. Boland for his assistance in making the observations and reducing the data. They also wish to thank F. Hennessey for many valuable discussions about antenna measurement problems.

## Planetary and Solar Radio Emission at 11 Meters Wavelength\*

JOHN D. KRAUS†, FELLOW, IRE

*Summary*—Observations are described of radio emissions from the Sun, Jupiter, and Venus during 1956 and early 1957 at a wavelength of 11 meters. Records are presented of solar 11-meter radiation at the time of a large (importance 3) flare on August 31, 1956, and during other periods of solar activity. The effect of scintillation on records of radio stars also is illustrated.

A number of records of impulsive radiation from Jupiter at both slow and fast recorder speeds is shown. The radiation is of a bursty or intermittent nature which can be classified into two main types: one which may persist for several seconds and produces a rumbling sound in the loudspeaker and another which is of very short duration (10 milliseconds or less) and produces a cracking or clicking sound. Many of the short pulses consist of distinct pairs or triplets which fall into two main groups, one having pulse separations of about one-quarter second and the other, pulse separations of about one tenth this value. An echo mechanism to explain the multiple pulses is postulated and observed trends in pulse separation compared to those expected with such a mechanism. The stronger Jupiter pulses indicate a peak radiated radio power at the source of the order of 10 kilowatts per cps bandwidth.

Observations of 11-meter radio emission from Venus are described and one record is presented for which the probability is only about one in a hundred thousand that it is due to a random process instead of Venesian radiation.

\* Original manuscript received by the IRE, October 14, 1957.

† Radio Observatory, Ohio State University, Columbus 10, Ohio.

#### INTRODUCTION

THE discovery of radio emission from Jupiter by Burke and Franklin<sup>1</sup> has opened a new phase of "long-wave" radio astronomy. The impulsive Jupiter signals have been observed only at wavelengths of the order of 10 to 15 meters, which is in the long wavelength range of the radio astronomy spectrum.

Observations of Jupiter signals began at Ohio State University early in 1956, following the construction of an interferometer antenna consisting of two colinear arrays each made up of six horizontal half-wavelength elements one-quarter wavelength above ground. Each array was backed up by a reflector element, which formed, with the ground, a rudimentary corner reflector.<sup>2,3</sup>

The colinear arrays were separated by about 400 feet on an east-west axis or about 11 wavelengths at the 11-

<sup>1</sup> B. F. Burke and K. L. Franklin, "Observations of a variable radio source associated with the planet Jupiter," *J. Geophys. Res.*, vol. 60, pp. 312-317; June, 1955.

<sup>2</sup> J. D. Kraus, "The corner reflector antenna," *PROC. IRE*, vol. 28, pp. 513-519; November, 1940.

<sup>3</sup> J. D. Kraus, "Antennas," McGraw-Hill Book Co., Inc., New York, N. Y., pp. 328-338; 1950.

meter wavelength employed. The beam envelope was fan-shaped with the beam maximum adjusted to various azimuthal angles by orienting the colinear arrays in different but always parallel directions. The receiver consisted of a radio frequency preamplifier, a standard communications receiver with 50-kc bandwidth, a one-stage dc amplifier with variable time constant (one-fourth to two seconds), and an Esterline-Angus recorder. With this equipment set up on the author's farm near Columbus, Ohio, observations of Jupiter signals were made from January to March of 1956, and also of solar and Venusian emissions later in the year.

In November, 1956, the receiving equipment was moved to the site of the Ohio State-Ohio Wesleyan Radio Observatory near Delaware, Ohio, where it was connected to an interferometer array consisting of two colinear arrays each of two horizontal half-wavelength elements about one-quarter wavelength above ground. Each array was oriented east-west and the arrays were separated by about five wavelengths (180 feet). The beam envelope was fan-shaped and fixed with the maximum on the meridian. This system was in operation for several months and with it one very significant record of Venus radiation was obtained on November 30, 1956.

Late in February, 1957, a new lobe-sweeping antenna was put into operation on 27 mc at the Observatory site. The antenna consists of three right-handed helical beam antennas<sup>4</sup> 24 feet long by 11 feet in diameter mounted side-by-side on an east-west line, as shown in Fig. 1, with the helix axes pointing at the intersection of

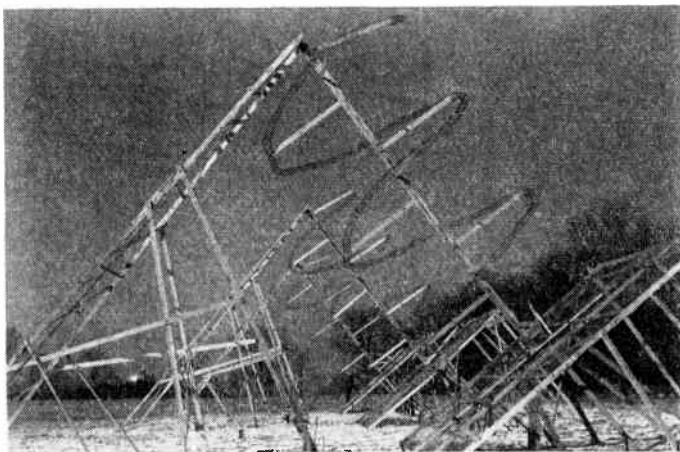


Fig. 1—Three-helix lobe-sweeping antenna at the Ohio State-Ohio Wesleyan Radio Observatory. The center helix is fixed while the outer two rotate in opposite directions.

the meridian and the celestial equator. The helices have 2.5 turns each and are spaced 50 feet apart. The center helix is fixed while the outside helices rotate on their axes in opposite directions at a constant synchronous speed of about 30 revolutions per hour. Depending on the rotation direction, the rotation of the helix advances or retards the phase of the received wave by an electrical

angle equal to the angle through which the helix is turned. As a result of the continuous rotation, a fan beam, about 12° wide in right ascension by about 60° in declination, is swept over a sector of the zodiac several hours in right ascension both sides of the meridian once every two minutes. With this arrangement a celestial source appears to move across the sky by a small increment for each sweep. The system is well adapted for observing variable radio sources, particularly those which may emit sporadically for only a few minutes at a time.

In the following discussion, the above three radio telescope systems will be referred to as the 11-wavelength interferometer, 5-wavelength interferometer, and the rotating helix (or lobe-sweeping) array.

#### SOLAR OBSERVATIONS

Using the 11-wavelength interferometer, a large number of observations were made of 11-meter solar radiation. One of the most interesting occurred on August 31, 1956, at the time of a large (importance 3) solar flare. Associated with the flare was an intense radio outburst, producing the record shown in Fig. 2(a). The outburst began on 11 meters at 7:37.5 A.M. (EST) and one-half minute later the recorder was off scale. Within a few minutes the disturbance subsided but secondary peaks occurred at 7:42.5 and 7:45 A.M.

The outburst shows prominently even though the sun was far outside the main beam of the antenna. The beam envelope is about 1.5 hours wide at half-power with maximum on the meridian. On August 31, the sun was on the meridian about 12:32 P.M. The interferometer pattern can be distinguished near noon on August 31 [Fig. 2(a)], but was much clearer on the preceding day, as shown in Fig. 2(b). The interferometer pattern is sketched in Fig. 2(c). The envelope is shown by the dashed curve.<sup>5</sup> Note that the pattern in Fig. 2(c) is in rectangular coordinates while the patterns of Fig. 2(a) and 2(b) are in the curved coordinates of the recorder.

Since the antenna response is well down five hours from the meridian, the intensity of the outburst on August 31 was actually of the order of 50 times the noon intensity that day instead of twice as large as indicated on the record. Between 8:30 and 11:00 A.M. on August 31 it would appear that solar activity was at a relatively high level (considerably above the noon level) but well below the peak outburst level.

According to data of the Bureau of Standards and the High Altitude Observatory,<sup>6</sup> the radio outburst was observed to begin on 167 and 460 mc at 7:37.1 A.M. (EST), while the flare of importance 3 was observed optically to reach a maximum at 7:58 A.M.

The fact that the outburst was observed on 167 mc 0.4 minute before it appeared at 27 mc may be of signifi-

<sup>5</sup> The pattern is in relative power and all records in this paper are in relative power or nearly so.

<sup>6</sup> "Preliminary Reports of Solar Activity," High Altitude Observatory and Natl. Bur. Stand., Boulder, Colo.; 1956.

<sup>4</sup> *Ibid.*, pp. 173-216.

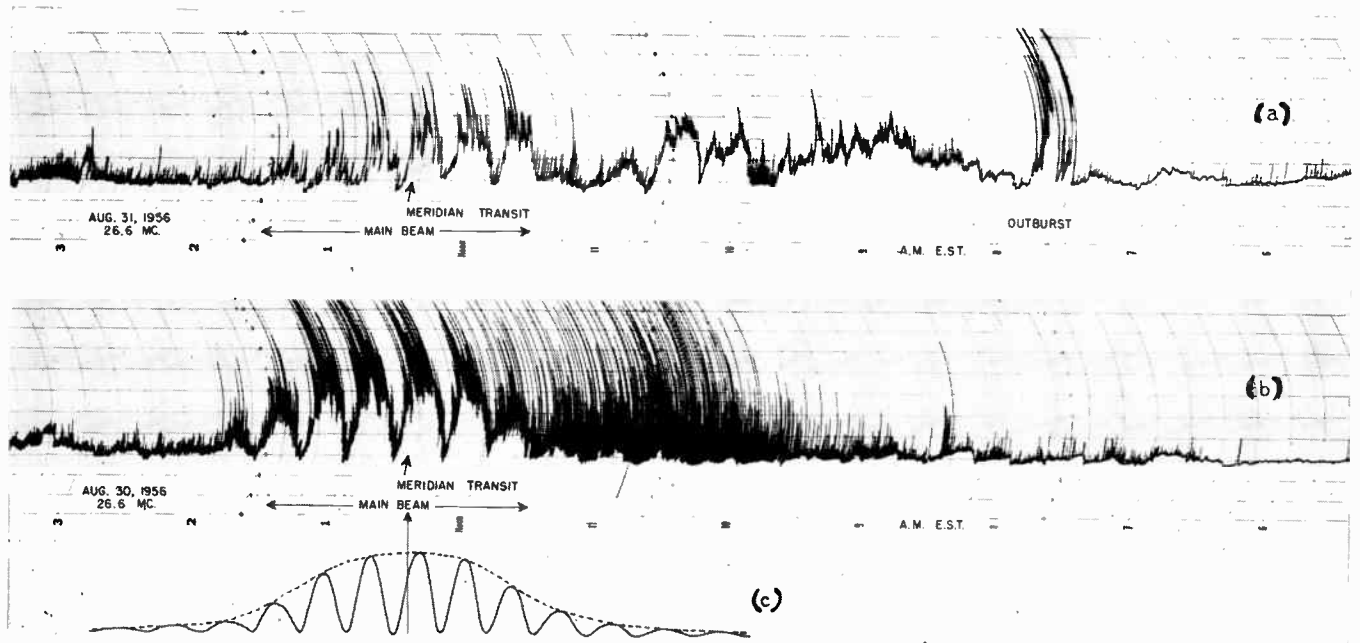


Fig. 2—(a) Record of 11-meter solar radiation on August 31, 1956, at and following a large solar flare. The large deflection labeled "outburst" occurred close to the time of the flare. (b) Record of solar noise on August 30, 1956. (c) Interferometer antenna lobe pattern with envelope (dashed).

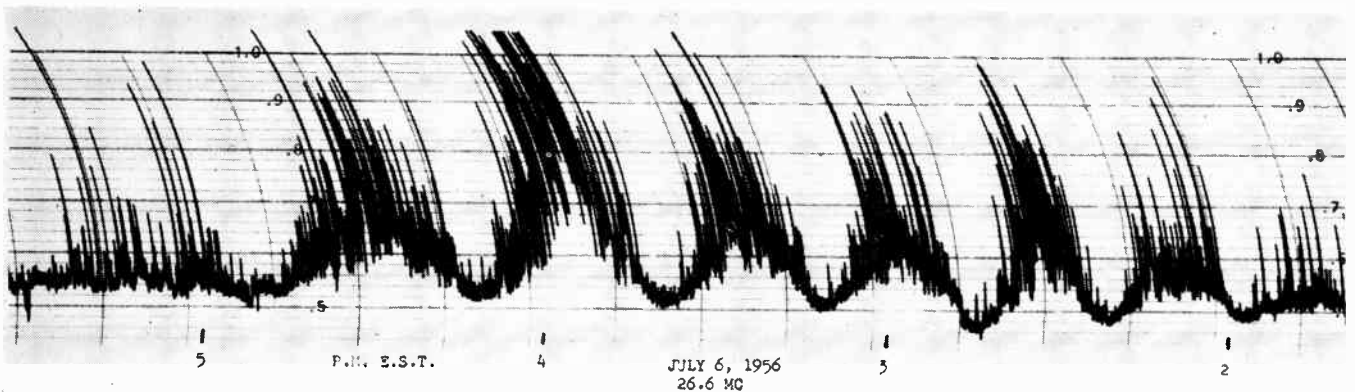


Fig. 3—Record of 11-meter solar noise on July 6, 1956.

cance as an indication of the rate of movement of the disturbance outward through the solar corona.

It is interesting to note that the deflections at meridian transit on August 30 are larger than on August 31 after the outburst. Also, the fluctuations due to individual small bursts are more intense, rapid, and numerous on August 30 than on August 31.

Solar observations are useful not only as records of solar activity but also as a means of checking or calibrating the antenna pattern. Radio stars such as Cygnus A are also valuable for calibrating the antenna pattern. Another record of solar activity obtained on July 6, 1956, is shown in Fig. 3. In this case the antenna beam was oriented so the sun crossed through the envelope maximum about 4:00 P.M. (EST). On most days the solar activity was too low to give a record, because the equipment sensitivity was too small to detect the quiet or undisturbed sun at 11 meters wavelength.

#### SCINTILLATION OBSERVATIONS

A solar related phenomenon readily observed on 11 meters is the scintillation or fluctuation in intensity of radio stars. This effect is of ionospheric origin<sup>7</sup> and while ordinarily not large, may be very pronounced on some occasions. Two records of strong scintillation of Cygnus A obtained with the 11-wavelength interferometer on May 24 and June 1, 1956, are shown in Fig. 4. The recorder time constant was about one-fourth second. The upper record (May 24) shows large and rapid fluctuations, some peaks being several times the normal peak amplitude of the source. The fact that the strong scintillation effects of May 24 and June 1 occurred seven and 15 days, respectively, after a large solar flare

<sup>7</sup> C. G. Little, "A diffraction theory of the scintillation of stars on optical and radio wavelengths," *Monthly Notices Roy. Astron. Soc.*, vol. 111, p. 289; 1951.

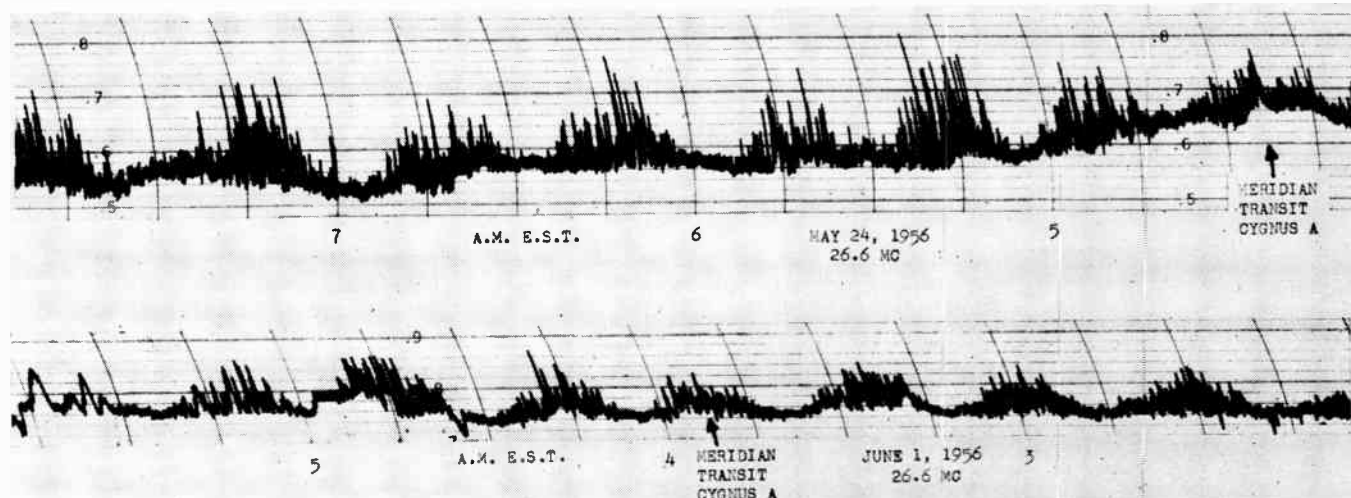


Fig. 4—Interferometer lobe patterns of Cygnus A showing large scintillation effect.

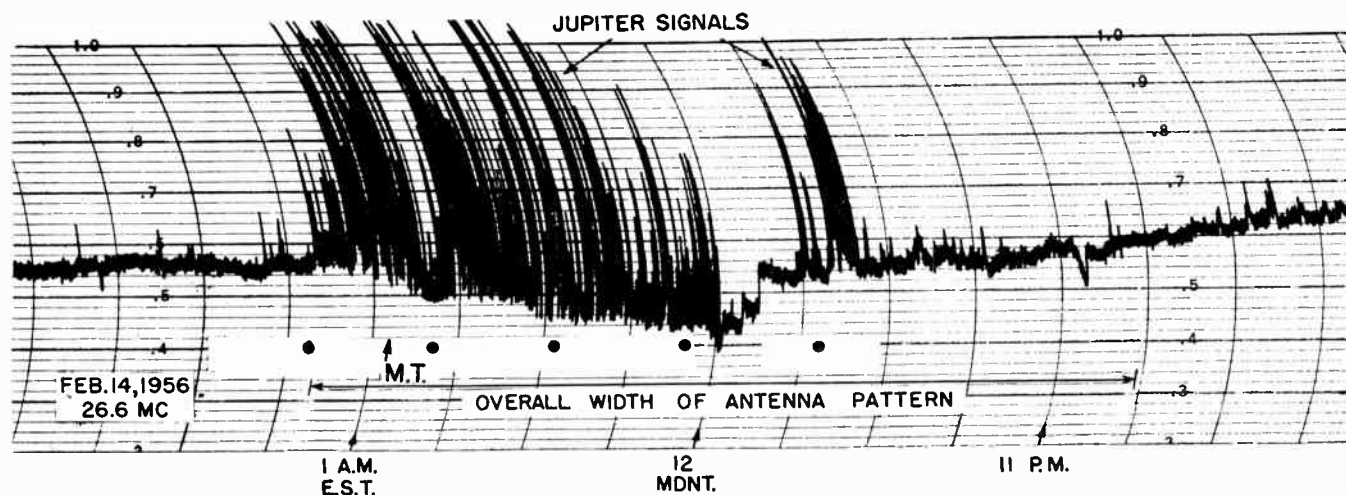


Fig. 5—11-meter Jupiter noise recorded February 14, 1956, at a tape speed of three inches per hour.

(importance 3) may be of significance.<sup>8</sup> The scintillation undoubtedly indicates that the ionosphere was in a disturbed or turbulent condition on these dates and that this condition was produced by slow particles emitted from the sun bombarding the ionosphere.

In Fig. 4 the time of meridian transit is indicated by the arrows. On May 24 the beam was directed 18° north of west so that the response to Cygnus A is greatest after meridian transit, while on June 1 the beam was reversed (directed 18° south of east) so that the response is strong before meridian transit.

JUPITER OBSERVATIONS

The discovery of Jupiter radiation by Burke and Franklin<sup>1</sup> (on 22 mc) was confirmed by Shain<sup>9</sup> on some 18.3 mc records taken in 1950–1951 which showed a se-

ries of bursts previously assumed to be terrestrial interference. Shain demonstrated that the phenomenon seems to be related to one or more localized regions on the planet, a principal region of activity in 1950–1951 appearing to have been associated with one of the white spots of the South Temperate Belt. However, observations during the winter of 1955–1956 by Franklin and Burke<sup>10</sup> show some evidence of a correlation between the large Red Spot and the occurrence of the radio emissions.

During January and February, 1956, extensive observations of the Jupiter signals were made at about 27 mc at Ohio State University with the 11-wavelength interferometer.<sup>11,12</sup> Fig. 5 shows a record obtained on the night of February 13–14 during one of the most ac-

<sup>8</sup> J. D. Kraus, "Relation of 11-meter solar system phenomena to solar disturbances," *Nature*, vol. 179, pp. 371–372; February 16, 1957.

<sup>9</sup> C. A. Shain, "18.3 mcs radiation from Jupiter," *Aust. J. Phys.*, vol. 9, pp. 61–73; March, 1956.

<sup>10</sup> K. L. Franklin and B. F. Burke, "Radio observations of Jupiter," (abstract), *Astron. J.*, vol. 61, p. 177; May, 1956.

<sup>11</sup> J. D. Kraus, "Radio noise from Jupiter," *Sky and Telescope*, vol. 15, p. 358; June, 1956.

<sup>12</sup> J. D. Kraus, "Some observations of the impulsive radio signals from Jupiter," (abstract), *Astron. J.*, vol. 61, p. 182; May, 1956.

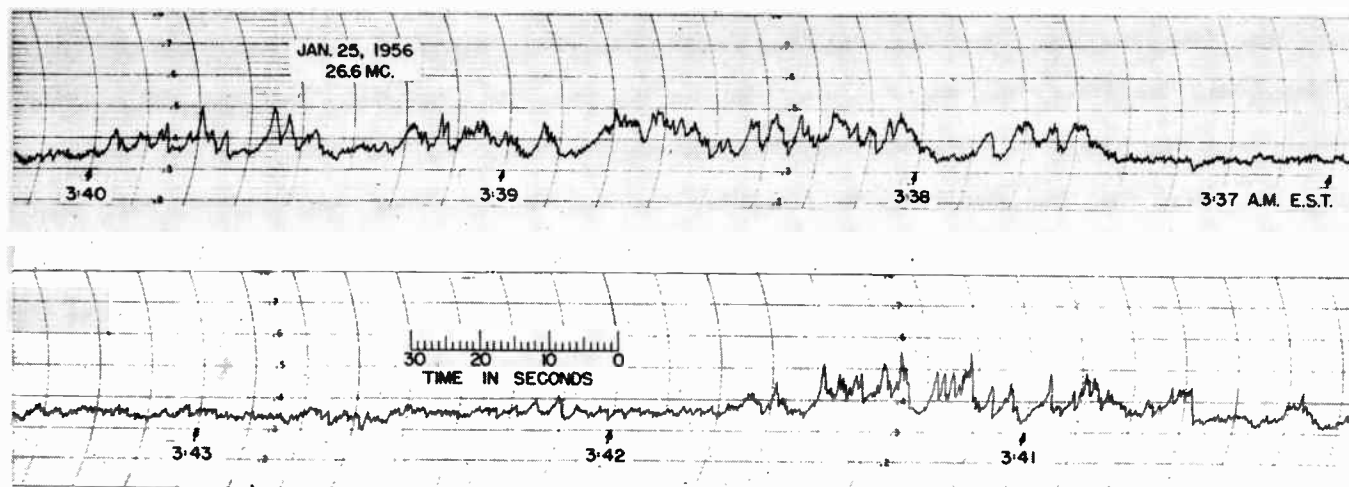


Fig. 6—11-meter Jupiter noise on January 25, 1956, recorded at a tape speed of six inches per minute. The noise corresponds to the peaks beginning about 3:37.5 A.M. and extending to about 3:41.5 A.M.

tive periods in the months of January and February. Between 11:30 and 11:45 P.M. (EST) there was strong activity followed by about 15 minutes of inactivity, after which an intense active period began that lasted almost without interruption for about one hour and 10 minutes. Some of the breaks in the activity on the record apparently occurred when Jupiter drifted through the nulls of the interferometer pattern. The calculated null positions are shown in Fig. 5 by the small solid circles. However, it is to be noted that the null at 12:28 is very indistinct, possibly because the Jupiter emission was exceptionally strong at the time. The recorder time constant was about one-fourth second and it is to be noted that even with so short a time constant the background noise level was noticeably raised for intervals of nearly 25 minutes while Jupiter was between the nulls of the antenna pattern.

Owing to the highly variable intensity of the Jupiter signals, the interferometer patterns were generally quite indistinct. The pattern in Fig. 5 was the best one obtained. The unique characteristics of the Jupiter signals, however, made it possible to correlate the observed noise with Jupiter with some certainty without the need in every case of distinct interferometer patterns for identification.

The Jupiter signals are characterized by their impulsive or pulse-like nature, in many respects appearing similar to static from a terrestrial thunderstorm. In the early days of radio, the terrestrial static or "atmospherics" were commonly classified into "clicks" and "grinders." The Jupiter signals are reminiscent of these types, since some are of very short duration and have a clicking or popping sound when listened to with a loudspeaker, while others are of a more sustained character and exhibit a rumbling or grinding sound. The clicks may be of only a few milliseconds duration and may be single or multiple. The multiple clicks are usually double with an occasional triplet. The spacing between these multiple clicks is of the order of one-fourth second

or less. Individual rumbles or grinders, however, may last for several seconds, and these may come in sufficiently rapid succession to raise and sustain the background noise at an enhanced level for several minutes. A recorder with a long integration time responds well to these rumble groups while a very short recorder time constant is necessary to respond to the short pulses or clicks.

Another characteristic of the Jupiter signals is their very intermittent nature; a period of activity was observed only once in many days of listening. When a source on Jupiter is active it can sometimes be observed for 60° of planet rotation before and after the central meridian passage. However, there may be many days of negligible detectable activity even at those times when the presumed active region is on or near the central meridian. When activity does occur, it may persist with some interruptions for several hours, the activity tending to occur in a succession of noisy periods. On the other hand, the active period may persist for only 10 or 15 minutes. Sometimes isolated clicks may occur without other evidence of activity.

In Fig. 5 the recorder tape speed was three inches per hour. Fig. 6 shows a record with a tape speed of 360 inches per hour (six inches per minute) and it is possible to see more fine structure. This activity occurred on the morning of January 25, 1956. Starting at about 3:37.5 A.M. (EST) there are a series of peaks corresponding to rumbles that occurred roughly at five-second intervals in groups of four or five. The groups are spaced about one-half minute apart. The record of Fig. 6 was obtained as a re-recording of the rectified audio signal recorded on a magnetic sound tape operated at  $1\frac{7}{8}$  inches per second.

Fig. 7 is another re-recording of a magnetic sound tape taken on January 20, 1956. At 5:44 A.M. (EST) a strong rumble occurred, preceded about five seconds by a double crack or pair of sharp clicks with a separation of about one-fourth second. The actual peak intensity

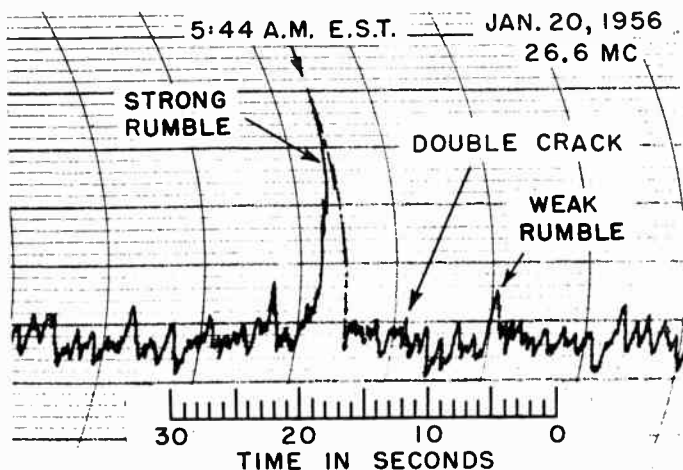


Fig. 7—11-meter Jupiter noise of January 20, 1956, recorded at six inches per minute showing small peak due to very short double crack or click followed about five seconds later by a strong rumble.

of these clicks was probably greater than that of the strong rumble, but their duration was only of a few milliseconds, so the actual deflection was small with the recorder time constant about one-half second. The phenomenon in Fig. 7 occurred about three minutes after the start of a 10-minute series of bursts.

The multiple clicks appear to fall into at least two main groups, one group having pulse separations of about one-fourth second and the other group, pulse separations of one tenth this value. The individual pulses are of the order of 10 milliseconds or less.

Fig. 8 shows cathode-ray oscillograms of three double and two triple pulses or cracks re-recorded from a magnetic sound tape made during an active period on the morning of February 2, 1956. Time increases to the left as on the other records. The time interval between pulses is shown in seconds. It is to be noted that in all cases the second pulse is weaker than the first and, where a third is present, it is weaker than the second. This is suggestive of an echo phenomenon in which the second and third pulses are echos of the first. The triple pulse with approximately 0.3-second spacing is particularly significant in this connection since each succeeding pulse not only becomes smaller in amplitude, but more spread out in time.

Another approach to the problem is illustrated by Fig. 9 in which about 50 strong multiple pulses, which occurred during a three-hour period of Jupiter activity on February 2, 1956, are analyzed on a time diagram. The pulse separation time is plotted as ordinate and elapsed time as abscissa. The open circles are double pulses or cracks while the solid circles are triple pulses. Where two solid circles are connected by a vertical line, it signifies that the time between the first and second pulses was different than that between the second and third.

The pulse separation times fall mostly into three groups: a short interval of about 25 milliseconds, an intermediate interval of about one-fourth second, and

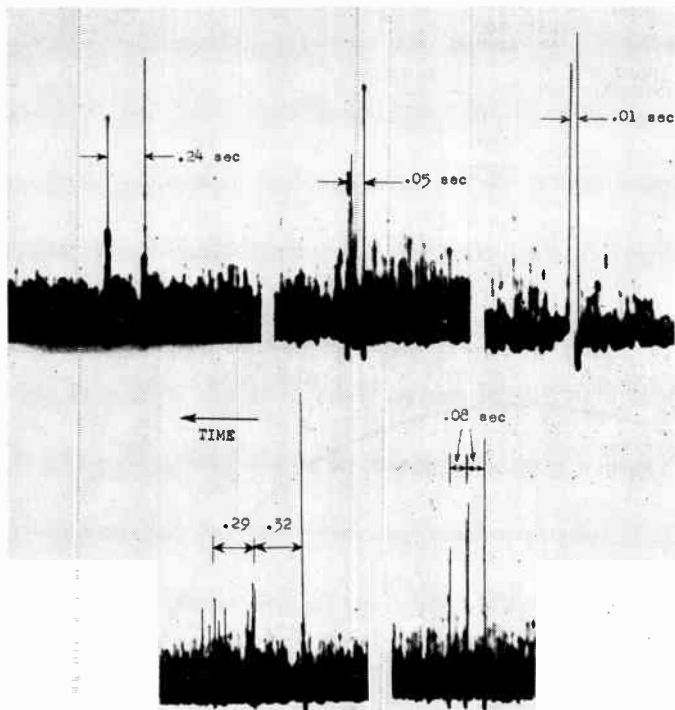


Fig. 8—Cathode-ray oscillograms of 11-meter Jupiter multiple pulses or cracks showing three pulse pairs and two triplets. The pulse separation is given in seconds. Photograph partly retouched for clarity.

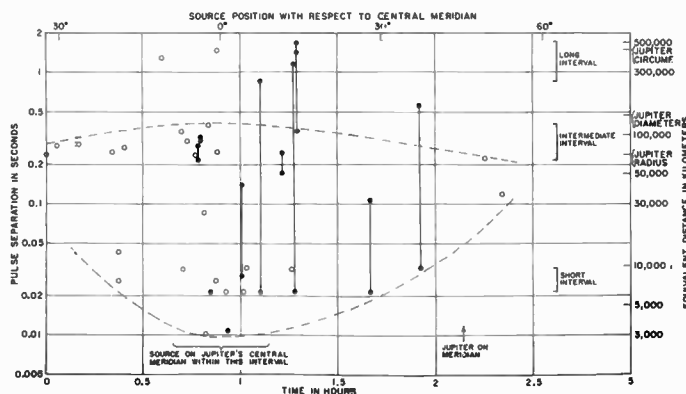


Fig. 9—Chart in which pulse separation (ordinate) is presented as a function of time of observation (abscissa) for about 50 strong multiple Jupiter pulses or cracks observed during a three-hour period on February 2, 1956. The position of the presumed source on Jupiter with respect to the central meridian is shown along the top and the distance equivalent to the pulse separation is given at the right (velocity of light assumed).

a long interval of the order of one second. It is uncertain whether the pulses belonging to this long interval group are single pulses which happened to occur close together or genuine doublets or triplets. Note, however, that this long interval corresponds approximately to the time required for a signal to travel once around the planet.

Excluding this long interval group, an apparent trend is evident in the other two as indicated by the dashed lines. Thus, the longest intermediate intervals occurred at the same time as the shortest short intervals. Furthermore, as determined by independent data based on

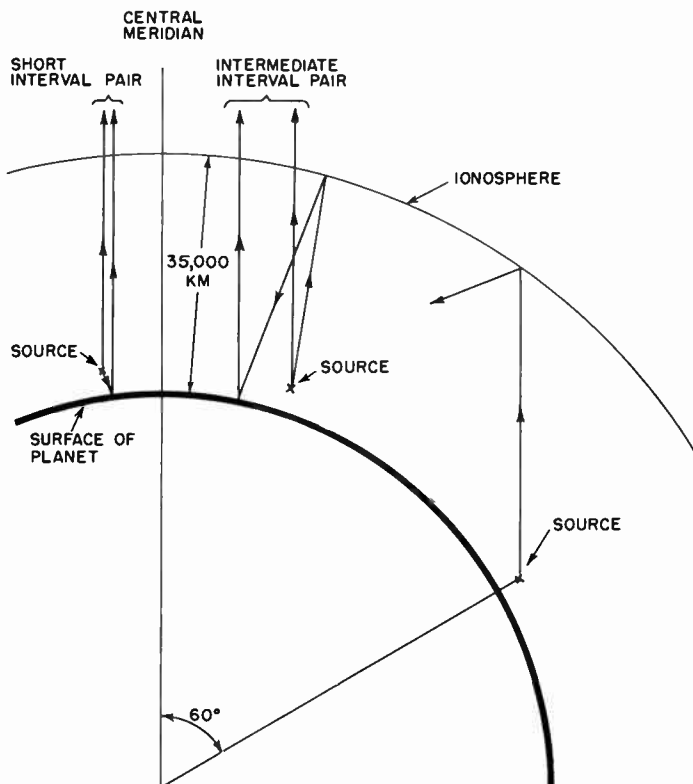


Fig. 10—Diagram illustrating possible wave paths for explaining multiple Jupiter pulses separated by short and intermediate intervals by means of an echo mechanism.

previous activity periods and a knowledge of the rotation period, the radio source was presumed to be on the central meridian of Jupiter at this same time. On this basis the source position, with respect to the central meridian, is shown along the top of Fig. 9.

Postulating an echo phenomenon, the variation of the time separation of the pulses of the intermediate interval group can be explained with the aid of Fig. 10. Assuming that at a height of about 35,000 km the planet has an ionosphere which is partially transparent at the frequency of observation, the direct and reflected ray paths of a pulse pair might be as suggested. As the source rotates farther from the central meridian the reflected ray path becomes slightly shorter, which corresponds to the observed decrease in the longest intervals in the intermediate group. With still further rotation the rays become totally internally reflected by the ionosphere, which would account for the observed disappearance of activity considerably before the source reaches the limb of the planet. Although the echo phenomenon provides a plausible explanation for the multiple pulses, the observations are not adequate to draw definite conclusions and the multiple pulses may be caused by some other phenomenon.

The intermittent and sporadic nature of the Jupiter signals is well illustrated by their behavior on February 26, 1957. On this date, as Jupiter crossed the meridian at 2:09 A.M. (EST), a tremendous burst of activity began which lasted about 18 minutes. About 29 minutes

after meridian transit or at 2:38 A.M., another almost as intense burst took place for about 18 minutes. Finally, about 61 minutes after meridian transit or at 3:10 A.M., a third period of activity began which lasted for 17 minutes and which, although intense, was weaker than the second period. About one hour before meridian transit there had also been a precursor interval of activity lasting about 15 minutes (from 1:09 to 1:24 A.M.) but this period was considerably weaker than the three periods of activity following meridian transit. Aside from occasional weak activity and a few isolated strong brief bursts there was no other activity for three hours before and after meridian transit.

Strong Jupiter activity was recorded also on February 27 and 28 and March 1 and 2, 1957, but little or no Jupiter activity was recorded during the following 15-week period; no observations were made after June 14, 1957.

It is of interest that the intense Jupiter activity of February 26, 1957, occurred about four and a half days after a very large solar flare on February 21 rated of importance  $3+$ .<sup>6</sup> Also, the intense Jupiter activity of February 14, 1956, shown in Fig. 5, occurred about three and a third days after the great eruptive solar prominence (rated as an importance 3 flare) which shot off the solar disk at the record velocity of 1100 km<sup>13</sup> on February 10. The February 14, 1956, Jupiter activity was the strongest observed from the planet during January and February. Although these sequences may be entirely coincidental, they do suggest the possibility that the mechanism producing the Jupiter radiation may be initiated or triggered by particles emitted from the sun.

During the January-February, 1956, observations the times of occurrence of Jupiter activity indicated that it originated in a localized region on the planet. However, the February 26 to March 2, 1957, observations suggested that the activity was widespread or originated in two or more localized regions.

Peaks of Jupiter activity are commonly observed which are at least 10 times the intensity of Cygnus A. Taking the intensity of Cygnus A as  $38 \times 10^{-24}$  janskys (watts meter<sup>-2</sup> cps<sup>-1</sup>) at 250 mc and assuming a spectrum proportional to wavelength for Cygnus A, the peak radiated power at the source on Jupiter is about 10 kw per cps of bandwidth. In this calculation the distance to Jupiter is 4.4 astronomical units, it is assumed that the source has a hemispherical radiation pattern, and that the power flux density attenuation is proportional to the inverse square of the distance.

A power of 10 kw per cps is several orders of magnitude greater than the estimated peak radio power from a terrestrial lightning stroke. However, this does not rule out the possibility that a lightning-like mechanism on Jupiter is responsible, since the dense Jovian at-

<sup>13</sup> D. H. Menzel, E. P. Smith, H. DeMastus, H. Ramsey, G. Schnable, and R. Lawrence, "The record prominence of 10 February 1956," (abstract), *Astron. J.*, vol. 61, p. 186; May, 1956.

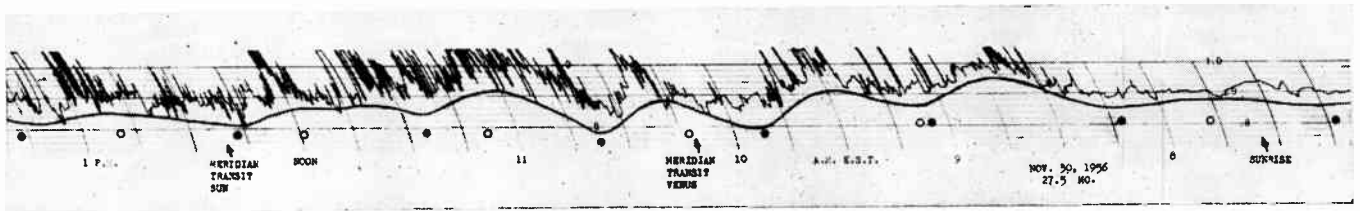


Fig. 11—Interferometer pattern of radiation from Venus observed on November 30, 1956.

mosphere may permit higher voltages to build up and more energy to be stored before the dielectric medium ruptures.

The Jupiter observations of Burke and Franklin<sup>1</sup> were made at 22 mc. Shain's observations<sup>9</sup> were made at 18.3 mc, while observations at the National Bureau of Standards have been made at 18 and 20 mc.<sup>14</sup> Other observations at the Department of Terrestrial Magnetism have been made at 27 mc, which when compared to the 22-mc observations indicate the Jupiter radiation is not part of a continuum<sup>10</sup> as there is no correlation between the occurrence of individual bursts. The observations at Ohio State have been made at about 27 mc (26.6 mc in 1956 and 27.6 mc in 1957). While making observations of the Jupiter signals on the morning of March 2, 1957, Mukherjee, Ohio State University research assistant, tuned the receiver repeatedly to higher frequencies between 2:52 and 3:10 A.M. (EST) finding peaks of intensity at the following: 27.6, 29.8, 35.6, 40.0, 40.9, and 43.0 mc. There was little or no signal observed at intermediate frequencies and none above 43 mc. These observations should be regarded with caution since antenna and transmission line response and resonances may be at least partially responsible for this peaking effect. However, they do suggest that the Jupiter emission may have a complex spectrum. To the best of our knowledge, 43 mc is the highest frequency at which the impulsive (nonthermal) Jupiter signals have been reported.

Smith<sup>15</sup> has reported the absence of Jupiter radiation at 38 mc in 1952 and 1953 and at 81.5 mc in 1955. The fact that no radiation was noted on 38 mc may or may not be significant with respect to the spectrum since the observations totaled only 16 days and Jupiter may have been quiescent at the times of observation.

The Jupiter signals are not only of astronomical interest, but should also interest the communications engineer looking ahead to the era of space travel and interplanetary communications, since their quasi-coherent and bursty or pulse-like nature may make it possible to draw significant conclusions about the reliability and information capacity of interplanetary radio circuits. This problem is complex since it involves com-

munications between two rotating, moving spheroids with a communication path through two ionospheres (one on each planet) and an interplanetary medium.

#### VENUS AND OTHER OBSERVATIONS

Using the 11-wavelength spacing interferometer a number of patterns were obtained indicating radiation from Venus. A record<sup>16</sup> obtained May 30, 1956, has minima corresponding to the interferometer pattern nulls for an hour before and after the meridian transit of Venus, with the background level raised between the minima. Another more significant record was obtained by Dr. M. Krishnamurthi using the 5-wavelength spacing interferometer at the Ohio State-Ohio Wesleyan Radio Observatory site on November 30, 1956. This record, shown in Fig. 11, has an interferometer pattern for several hours before and after the meridian transit of Venus and was the only record suggesting Venusian radiation obtained over a two-month period of observations. The irregular line at top is the actual recording (time constant about three seconds). The line under the actual record is sketched in accordance with the smoothed background variation. The solid circles indicate the calculated null positions for a source at the coordinates of Venus while the open circles indicate the calculated null positions for a source at the coordinates of the sun. All of the eight observed minima agree closely with those calculated for Venus whereas only one is close to a calculated null position for the sun. Known radio sources other than the sun were either completely out of the antenna beam during the observation period or too weak or both to be a factor. Furthermore, if the pattern were produced by a random phenomenon the probability that such a chance process could yield the observed agreement with the calculated null positions for Venus is only about one in a hundred thousand. Accordingly, the probability is high that the radiation recorded in Fig. 11 was of Venusian origin with the emission being of a relatively sustained type.

Using the lobe-sweeping array, apparent sources were observed to cross the meridian on March 9, 10, 21, and 24, 1957 at the meridian transit time of Venus within the experimental error of the system (about three minutes).

On March 14, 1957, a peculiar record was obtained in which a source appeared for only about 45 minutes,

<sup>14</sup> R. M. Gallett, "The results of the observations of Jupiter's radio emissions on 18 and 20 mc in 1956 and 1957," (abstract), *IRE TRANS.*, vol. AP-5, pp. 327-328; July, 1957.

<sup>15</sup> F. G. Smith, "A search for radiation from Jupiter at 38 mcs and at 81.5 mcs," *Observatory*, vol. 75, pp. 252-254; December, 1955.

<sup>16</sup> J. D. Kraus, "Radio observations of the planet Venus at a wavelength of 11 meters," *Nature*, vol. 178, pp. 103-104; July 14, 1956.



Fig. 12—Three-helix lobe-sweeping array patterns obtained during transit of source on March 14, 1957. Horizontal chart width corresponds to lobe displacement of  $20^\circ$  either side of meridian (vertical line). East of the meridian is to the right and west to the left.

being observed to cross the meridian about 47 minutes before the meridian transit of the sun (about 21 minutes before the meridian transit of Venus). Selected tracings of the swept-lobe records of this source are shown in Fig. 12. The motion of the source (from right to left with time) is obvious with the source being on the meridian (vertical line) about 11:55 A.M. Since no known radio source of large enough intensity crossed the meridian sufficiently close to this time, the apparent "source" is due either to some spurious effect or else is a real source of transient or temporary nature.

#### ACKNOWLEDGMENT

This research was supported in part by grants from the National Science Foundation and the fund for basic research of the Ohio State University. The three-helix lobe-sweeping array was constructed by R. H. McFarland as part of his master's thesis problem. Dr. Krishnamurthi, who obtained the record of Fig. 11 and assisted in some of the swept-lobe array observations, was an American Wheat Loan Exchange Post Doctoral Fellow at Ohio State University in November–December, 1956, and during 1957.

## Radio Emission from Comet 1956 h on 600 MC\*

R. COUTREZ†, J. HUNAERTS†, AND A. KOECKELENBERGH†

**Summary**—Radiation from Comet 1956 h has been observed on 600 mc at perihelion. An attempt to identify this emission, which presented a rather stable character, has been made. It appears that this radiation may arise from transitions between fine structure components resulting from  $\Lambda$ -type doubling of the level  $J=3/2$  of the  $^2\Pi_{1/2}$  state of CH molecule. The observed flux density leads to a number of molecules of the order of  $10^{20}$ – $10^{21}$ , which is compatible with admitted numbers in cometary atmospheres.

#### INTRODUCTION

IT has long been known that a comet consists of a rather small nucleus of compact material, surrounded by a highly tenuous atmosphere which may extend to considerable distances when the object reaches the vicinity of the sun. The "head" of the comet, in the neighborhood of the nucleus, is formed by molecules or free radicals (OH, NH, CH, CN,  $C_2$ ,  $C_3$ ,  $CH^+$ ,  $OH^+$ ,  $NH_2$ ) together with possible other components emitted from compact materials, by desorption processes under the influence of solar heating, and possible other mecha-

nisms. The "tail," directed opposite to the sun under the effect of selective radiation pressure, contains ionized material and forms a plasma, often extending at considerable distances from the nucleus. The mechanism by which a second tail or "egret" directed towards the sun is formed, principally for the new comets near perihelion, is not clearly understood at the present time, though this feature seems to be not infrequent for telescopic comets. On the other hand, comets show activity in the tail; it seems that this activity occurs in connection with solar activity under the effect of electromagnetic and corpuscular solar radiation.

The mechanisms by which a comet may give rise to electromagnetic radiation on long wavelength, pertaining to the radio astronomical interval, have been discussed by Poloskov<sup>1</sup> from a theoretical point of view.

<sup>1</sup> S. M. Poloskov, "Monochromatic radio emission of cometary molecules," *Proc. Liege Symp. 1956*, published under the title "Les Molécules dans les Astres," Institut d'Astrophysique, Cointe-Sclesin, Belgium, pp. 118–123; 1957.

———, "Cometary radio emission," *Astron. J. USSR*, vol. 30, pp. 68–75; January–February, 1953. (In Russian.)

\* Original manuscript received by the IRE, November 6, 1957.

† Royal Observatory of Belgium, Uccle, Belgium.

TABLE I

COMET 1956 H MEASURED FLUX DENSITIES ON 600 MC

April	Time (U.T.) of observ.	Eq. Coordinates		$r$ (A.U.)  $\Delta$ (A.U.)		Flux density [ $\text{wm}^{-2}$ (cps) $^{-1}$ ]
		$\alpha$	$\delta$	(after Candy) <sup>4</sup>		
9	11.31	0 <sup>h</sup> 51 <sup>m</sup>	- 5°10'	0.320	0.834	56 × 10 <sup>-24</sup> 70
	11.40	0.47	- 7.04			
12	12.14	0.53	- 3.30	0.343	0.717	56* 42
	14.16	0.45	- 3.45			
24	18.15	—	—	0.555	0.594	35†
26	21.43	2.33	+50.50	0.598	0.625	28‡ 28
	21.45	2.47	+50.00			

\* Peak at  $84 \times 10^{-24} \text{wm}^{-2} (\text{cps})^{-1}$ .

† No certain identification.

‡ The flux may be double.

Owing to the faint electronic densities in the tail and the low electronic temperatures as deduced from optical observations, there seems to be no possibility of detecting a thermal radiation with a continuous spectrum even for the largest comets at perihelion. However, non-thermal radiation (from plasma effects) may be observed. Another possibility is *monochromatic* radiation of molecular origin, resulting from transitions between fine structure components due to the so-called  $\Lambda$ -type doubling of rotational levels in the fundamental electronic state. Only *heteropolar* radicals having  $\Pi$  levels are to be considered here because they only have  $\Lambda$ -type doubling, and particularly OH and CH owing to their relative abundance in the cometary heads. This observational possibility might occur exclusively for the largest comets in the vicinity of perihelion. However, there is at present no satisfactory theoretical model for the molecule so the predicted wavelengths for these transitions are still uncertain.

#### OBSERVATION OF A RADIOFLUX FROM COMET 1956 H ON 600 MC

The Comet 1956 h seems to belong to a class of comets with very long periods and has apparently carried out one of its first, if not the first, passages at perihelion in April, 1957. The large angular dimensions of the cometary head, as predicted from previous optical observations, and the probable abundance of free radicals at perihelion, engaged the radio astronomy group of the Royal Observatory, Uccle, Belgium, in an attempt to detect such an electromagnetic radiation on 600 mc. The observations were made at the station of Humain-Rochefort with a Wurzburg paraboloid of 30-foot aperture, mounted azimuthally, and equipped with a highly stable receiver, on April 9 and 12 when the comet passed in the vicinity of perihelion, and on April 24 and 26 at the vicinity of minimum geocentric distance. The method used consisted simply of sweeping the antenna beam back and forth, from west to east and conversely, on the probable region of the comet as determined from the Hasegawa ephemeris,<sup>2</sup> and of recording at the same time the output on a Speedomax chart. This sweeping was made at fixed zenithal distances. Passing over the comet, it seemed that a radioflux was detected above the level of the ordinary fluctuations of the receiver's output.<sup>3</sup> Moreover, this flux seemed rather *stable*, and with a slow motion in azimuth in the direction of diurnal motion or conversely, a rather clear difference was observed in the duration of the elongation as seen on the record. Extracts of these records are reproduced in Figs. 1-7, pp. 276-277, with the corresponding regions of the sky and the shape of the antenna lobe. The observational results are described in Table I.

<sup>2</sup> J. Hasegawa, IAU Circular No. 1580; January 10, 1957.<sup>3</sup> R. Coutrez and P. Bourgeois, IAU Circular No. 1954; April 11, 1957.

In Table I,  $r$  and  $\Delta$ , the heliocentric and geocentric distances of the Comet 1956 h, have been deduced from the ephemeris computed by Candy. No certain identification has been obtained for April 24 owing to an error of setting (observation made at too low a declination). Taking into account the fluctuations of the receiver's output, the flux densities are given with a probable relative error of 50 per cent. Many records were obtained on the probable region, and it appeared clearly that the position of the radio source computed from the horizontal coordinates of the antenna beam corresponded well to the position of the Comet 1956 h as computed from the ephemeris. Moreover, the flux seemed to originate in the lower part (head or egret), the tail producing less or no radiation on this frequency.

It is perhaps interesting to mention that the distribution of observed centers of emission, on April 9, 1957, led to the impression that the comet was preceded by an emissive region directed towards the sun. The presence of such an "egret" was actually confirmed by subsequent visual observations.

#### CHARACTERISTICS OF THE RECEIVER AND CALIBRATION OF OUTPUT

As measured in the laboratory at Uccle, the noise factor of the receiver is of the order of 6, with a total gain of 120 db and a bandwidth (at 3 db) of 7 mc. The image frequency is 540 mc with a reduction of gain of 3 (approximately). Great care has been taken in order to improve the stability of the receiver (use of dc degeneration in the intermediate-frequency amplifiers, highly stable power supplies giving a precision of 1/20,000 on continuous voltages and 1/4000 on heating currents, precision local oscillator on 570 mc in a thermostated cabin). With an amplification corresponding to 100 divisions on the recorder's chart for 3 ma of anodic current of an adapted noise diode (Bendix TT 1 in coaxial mount), the record on a dummy load was found to be a

<sup>4</sup> M. P. Candy, IAU Circular No. 1585; February 20, 1957.

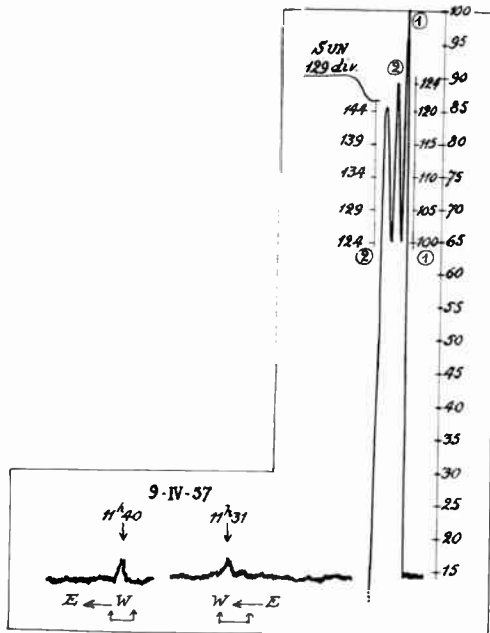


Fig. 1—Sketch of records on the Sun and Comet 1956 h, on 600 mc. Note the zero shift for the sun.

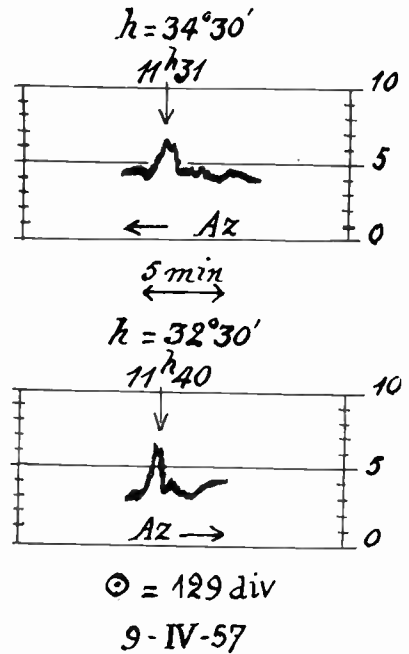


Fig. 2—Deviation obtained on the comet's region on April 9, 1957. In the upper figure the antenna beam has the same direction as the diurnal motion; in the lower figure, the opposite.

perfectly straight line in the laboratory conditions with the time constant of 1 second. However, in the observational conditions on the antenna, the record with the same amplification was still presenting irregular drifts of 1 division, with a rather short period; this fact seems to be due to thermal variations of the rf head. The scale of the record is linear in power to a few per cent.

The antenna gain has been deduced from the lobe shape, taking into account the law of illumination of the paraboloid by the slotted dipole in focus. The comparison noise diode is placed right at the input of the receiver, at the extremity of the antenna line. Taking into account antenna gain and losses in the transmission line, the formulas giving the corrected antenna temperature and the corrected flux density are, respectively, in our case,

$$T_{corr} = 365 I_{ma} \text{ (diode) } (^\circ K)$$

and

$$S = 6.0 \times 10^{-22} I_{ma} \text{ (diode) } [w m^{-2} \text{ (cps)}^{-1}]$$

This corresponds very well to our common base of  $30 \times 10^{-22} w m^{-2} \text{ (cps)}^{-1}$  for 5-ma diode, as deduced from the comparison of our regular measurements of solar flux with other data.<sup>5</sup> On the other hand, the internal position of the feed in the Wurzburg parabola gives a low antenna gain but has the advantage of lowering the first secondary lobe level, which is 33 db below the principal lobe. This excludes any possibility of a contribution due to a passage of the sun's disk in the secondary lobe, even in case of outburst. Moreover, an examination of the relevant records has been made and it was found that the sun, at the dates given in Table I, has had no special activity on 600 mc.

Quart. Bull. Solar Activity, IAU,

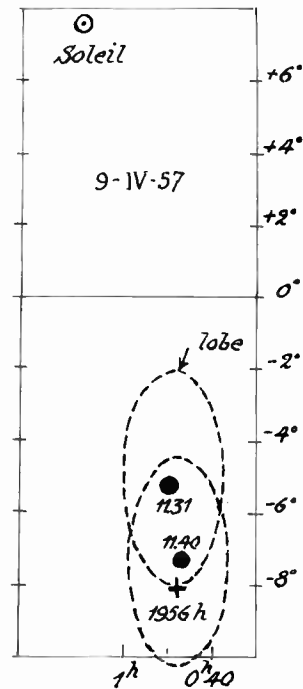


Fig. 3—Relative positions of the sun and the comet on April 9, 1957. The contours of antenna lobes are given. The cross indicates the position of the comet, after Candy's ephemeris. The black circles are the lobe centers for observations recorded in Fig. 2.

The calibration of the records has been made by comparison with the deviation given by the sun in the antenna beam. For example, on April 9, the sun gave a deviation of 129 divisions on the Speedomax chart; this deviation calibrated with the noise diode was found to correspond to  $36 \times 10^{-22} w m^{-2} \text{ (cps)}^{-1}$ ; then, if the scale is linear in power to this extent, a deviation of 2 divisions on the comet corresponds to an antenna tem-

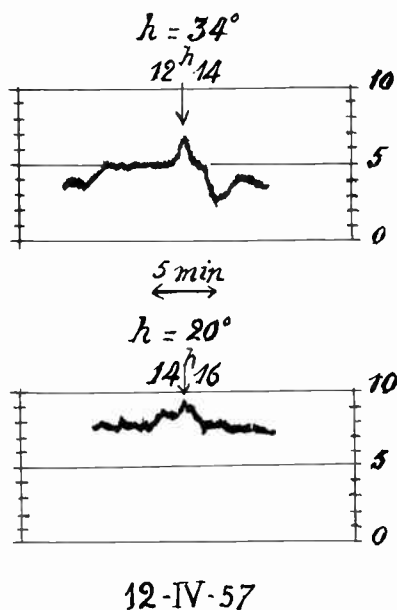


Fig. 4—Deviation obtained on the comet's region on April 12, 1957. In the upper figure the antenna beam has the same direction as the diurnal motion; in the lower figure, the opposite.

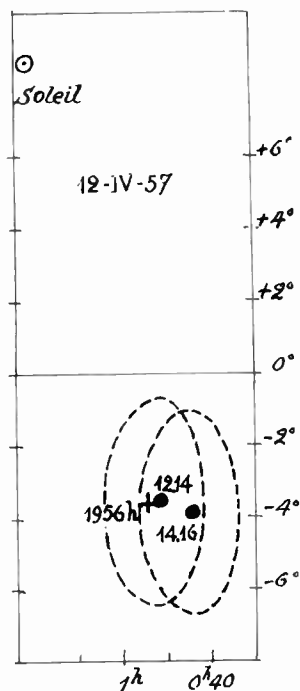


Fig. 5—Relative positions of the sun and the comet on April 12, 1957. The contours of antenna lobes are given. The cross indicates the position of the comet, after Candy's ephemeris. The black circles are the lobe centers for observations recorded in Fig. 4.

perature of 34°K or to a flux density of  $36 \times 10^{-24} \text{wm}^{-2} (\text{cps})^{-1}$ . The same method has been applied to the whole set of data entered in Table I.

NUMBER OF EMITTED PHOTONS AND LIFETIME OF EMITTING SYSTEMS

The radioflux of Comet 1956 h on 600 mc was found rather stable. This contrasts with the observations made by the German observers of the University of Bonn on

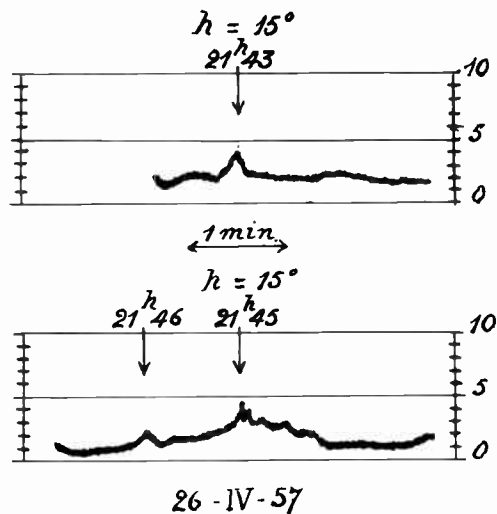


Fig. 6—Deviation obtained on the comet's region on April 26, 1957. In the upper figure the antenna beam has the same direction as the diurnal motion; in the lower figure, the opposite.

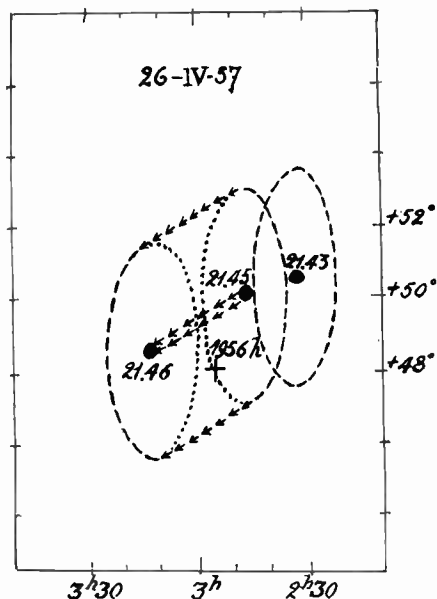


Fig. 7—Lobe contours and positions of the radio sources on April 26, 1957. The cross indicates the position of the comet, after Candy's ephemeris.

1420 mc<sup>8</sup> and by Kraus<sup>7</sup> which detected also radioflux originating from this comet. On the other hand, observations made on April 9 may be taken as an example in order to determine the number of emitted photons per unit time, independently of any assumption concerning the origin of this radioflux.

We have examined the possibility of continuous emission, due to free-free transitions under the effect of ordinary solar radiation; however, taking into account the physical conditions in the comet, this hypothesis seemed to us improbable. We did not examine the possibility of

<sup>8</sup> H. G. Müller, W. Priester, and G. Fischer. Universitäts Sternwarte, Bonn, Germany. Prepublication. These results have been obtained with the 25-m paraboloid at Stockert.

<sup>7</sup> J. D. Kraus, IAU Circular No. 1596; April 29, 1957.

nonthermal radiation (plasma effects), but our impression is that the radiation on 600 mc might present a monochromatic character and be concentrated in a line, of width  $\Delta\nu$ . For the calculations, we adopted the values

$$\Delta\nu = 10^4 \text{ cps corresponding to a Doppler broadening at } 5000^\circ\text{K, and}$$

$$\Delta\nu = 10^3 \text{ cps corresponding to a Doppler broadening at } 50^\circ\text{K or to a natural width, respectively.}$$

At geocentric distance  $\Delta = 0.834 \text{ A.U.} = 133 \times 10^{11} \text{ cm}$ , the comet sees 1 square cm at the antenna corresponding to a solid angle  $\Omega = 5.6 \times 10^{-27} \text{ sterad}$ . For the whole sphere, the power per (cps) radiated by the whole comet is then

$$P\nu = 4\pi S\nu/\Omega = 10^8 \text{ erg sec}^{-1} (\text{cps})^{-1}.$$

If the radiation is concentrated in a line of width  $\Delta\nu$ , and with the preceding values, the total (integrated) power radiated per unit time is, respectively,

$$P = 10^{12} \text{ erg sec}^{-1} (\Delta\nu = 10^4)$$

and

$$P = 10^{11} \text{ erg sec}^{-1} (\Delta\nu = 10^3).$$

Since a photon at 600 mc represents an energy  $E = h\nu = 4 \times 10^{-18} \text{ erg}$ , the total number of photons emitted by the whole comet on this frequency is, respectively,

$$N = 25 \times 10^{28} \text{ sec}^{-1} (\Delta\nu = 10^4) \text{ and}$$

$$N = 25 \times 10^{27} \text{ sec}^{-1} (\Delta\nu = 10^3).$$

This total number of photons represents the total number of emission processes per second, for the whole comet, on 600 mc. In correspondence with a plausible number of emitting systems, we therefore obtain the results expressed in Table II.

TABLE II  
NUMBER AND LIFETIME OF EMITTING SYSTEMS

Number of systems	Number of processes per second and per system		Lifetime of a system	
	(1) ( $\Delta\nu = 10^4$ )	(2) ( $\Delta\nu = 10^3$ )	(1)	(2)
$10^{32}$	$25 \times 10^{-4}$	$25 \times 10^{-5}$	400 seconds	4000 seconds
$10^{31}$	$25 \times 10^{-3}$	$25 \times 10^{-4}$	40	400
$10^{30}$	$25 \times 10^{-2}$	$25 \times 10^{-3}$	4	40

DISCUSSION ON THE INTERPRETATION OF RADIOFLUX BY MONOCHROMATIC EMISSIONS

Let us now examine on the basis of the preceding calculated number of emitting systems, the possibility of interpreting the observed radioflux emitted by the comet by molecular radiation resulting from transitions between fine structure components, due to the  $\Lambda$ -type doubling of rotational levels in the fundamental electronic state. Only the heteropolar radicals OH and CH are to be considered.

For molecule OH, according to Poloskov, the transition between sublevels  $J = 3/2$  of  ${}^2\Pi_{3/2}$  state gives rise

to a radiation at  $\lambda = 18.25 \text{ cm}$  which excludes the possibility of interpreting the emitted flux.

The CH molecule seems to present a better possibility of identification. In order to improve the wavelength of the transition between sublevels, we have made a new determination of the  $\Lambda$ -type doubling of  ${}^2\Pi$  state for the intermediate case between Hund's cases (a) and (b) by Van Vleck's formula<sup>8</sup>

$$\delta\nu(J) = [(\frac{1}{2}p + q)(\pm 1 + 2X^{-1} - YX^{-1}) + 2qX^{-1}(J - \frac{1}{2})(J + \frac{3}{2})](J + \frac{1}{2})$$

where

$$X = [4(J + \frac{1}{2})^2 + Y(Y - 4)]^{-1/2}$$

and

$$Y = A/B.$$

$A$  and  $B$  are the coupling and rotational constants.

This theoretical relation, which is not a rigorous one, notwithstanding is a satisfying one and represents very well the observational data.<sup>9</sup> These are given by the work of Gerö.<sup>10</sup> We considered the lines from (0-0) bands of the  $A^2\Delta - X^2\Pi$  and  $B^2\Sigma - X^2\Pi$  transitions. The values of the parameters  $p$  and  $q$  deduced from this computation are

$$p = 0.0376; \quad q = 0.0387.$$

These values may be compared with those given by Mulliken and Christy,<sup>11</sup>

$$p = 0.032; \quad q = 0.037.$$

In Table III, opposite, we give the results of our determination, for the  $\Lambda$ -type doubling of the  ${}^2\Pi_{3/2}$  state.

We see that the  $\delta\nu$  resulting from the  $\Lambda$ -type doubling deduced by us is in better agreement with the experimental values than those calculated by adopting Mulliken and Christy's parameters  $p$  and  $q$ . Thus the wavelength  $\lambda = 50.0 \text{ cm}$  obtained by us for the transition between sublevels  $J = 3/2$  of state  ${}^2\Pi_{3/2}$  for the CH molecule appears as being more compatible with the optical spectrum's data than the value  $\lambda = 45.45 \text{ cm}$  as given by Poloskov, whose results are identical to those calculated with the parameters adopted by Mulliken and Christy.

The interpretation of CH emission spectrum in the cometary conditions for the visible light has been made previously by Hunaerts<sup>12</sup> and gives the possibility of computing the time interval between absorption processes giving rise to this spectrum, for the conditions in

<sup>8</sup> J. H. Van Vleck, "On  $\Lambda$ -type doubling and electron spin in the spectrum of diatomic molecules," *Phys. Rev.*, vol. 33, pp. 467-506; 1929.

<sup>9</sup> Poloskov, *loc. cit.*

<sup>10</sup> L. Gerö, "Vervollständigung der analyse der CH-banden," *Z. Phys.*, vol. 118, pp. 27-36; May, 1941.

<sup>11</sup> R. Mulliken and R. Christy, " $\Lambda$ -type doubling and electron configurations in diatomic molecules," *Phys. Rev.*, vol. 38, pp. 87-119; July 1, 1931.

<sup>12</sup> J. Hunaerts, "Interprétation du spectre d'émission de CH dans les comètes," *Ann. Obs. Roy. de Belgique*, 3me sér., T.6, fasc. 4; 1954.

TABLE III  
MOLECULE CH  $\Lambda$ -TYPE DOUBLING FOR STATE  ${}^2\Pi_{3/2}$

$J$	Observed	Calculated	
	(1)	(2)	(3)
	cm <sup>-1</sup>	cm <sup>-1</sup>	cm <sup>-1</sup>
1.5	—	0.020	0.023
2	0.085	0.083	0.080
2.5	—	0.157	0.156
3	0.275	0.254	0.250
3.5	0.370	0.370	0.362
4	0.545	0.506	0.486
4.5	0.667	0.661	0.642
5	0.860	0.835	0.810
5.5	1.070	1.029	0.996
6	1.255	1.242	1.201
6.5	1.467	1.474	1.424
7	1.795	1.726	1.666
7.5	1.973	1.997	1.926

(1) The observed values are deduced from the measurements of Gerö. In the case of a  ${}^2\Delta - {}^2\Pi$  transition we have

$$\delta\nu_{dc}(J) = R_{cd}(J) - R_{dc}(J) = Q_d(J) - Q_c(J) = P_{cd}(J) - P_{dc}(J)$$

whereas, in the case of  ${}^2\Sigma - {}^2\Pi$  transition,

$$\delta\nu_{dc}(J) + \delta\nu_{dc}(J+1) = [R(J) - Q(J)] - [Q(J+1) - P(J+1)]$$

and we may write

$$\delta\nu_{dc}(J) + \delta\nu_{dc}(J+1) \sim 2\delta\nu_{dc}(J + \frac{1}{2}).$$

In this case, we get in this way not the real doublet separation for actual values of  $J$ , but instead the separation  $\delta\nu(J+1/2)$  for fictitious  $J$  values (the entire values of Table III).

(2) Values calculated with the parameters  $p$  and  $q$  as determined in this work.

(3) Values calculated with the parameters  $p$  and  $q$  as determined by Mulliken and Christy.

which the comet has been observed. This interval is given by

$$\tau_{\text{abs}} = 1/\Sigma B\rho\nu'$$

where the sum is extended to the whole set of absorptions from the same level. Here,  $B$  is the absorption probability and

$$\rho\nu' = \beta I \cdot \rho\nu$$

the solar radiation density, account being taken of the dilution factor  $\beta = 5.41 \times 10^{-6} r^{-2}$ , of the absorption percentage  $I$  by the Fraunhofer lines, and of the radiation density  $\rho\nu = 4\pi\lambda^2 F_\lambda/c^2$  for a mean disk intensity  $F_\lambda$ . Then, at 1 A.U. from the sun and for a wavelength interval of 100 Å between  $\lambda$  4250 and  $\lambda$  4350 Å,

$$\rho\nu' = 33 \times 10^{-21} \text{ erg cm}^{-3}.$$

On the other hand,  $\Sigma B$  has the same value  $3.25 \times 10^{17}$  for each rotational level and, then,

$$\Sigma B\rho\nu' = 21.5 \times 10^{-3} \text{ (at } r = 1 \text{ A.U.)}$$

owing to the fact that each line has a double effect resulting from the  $\Lambda$ -type doubling of  ${}^2\Pi$  states.

On April 9, ( $r = 0.320$ ),

$$\Sigma B\rho\nu' = 2 \times 10^{-1} \text{ sec}^{-1}.$$

It results that the time interval between two absorptions giving rise to the visible spectrum is of the order of 5 seconds.

An emission process giving rise to radiation on 600 mc from transitions between two sublevels resulting from

$\Lambda$ -type doubling is only admissible, when this time interval between two absorptions is much less than the lifetime of the molecule on the upper sublevel. Referring to Table II, it appears that the number of molecules which might explain the observed radioflux is of the order of  $10^{30}$  to  $10^{31}$ . This value agrees well with that given by Wurm<sup>13</sup> for the atmosphere of comets.

### CONCLUSION

A radioflux on 600 mc, which seemed rather stable, has been observed from the Comet 1956 h at the vicinity of perihelion. This stability does not mean that the flux may not present considerable variations from day to day.

The antenna characteristics (proportion of secondary lobes) and the absence of relevant solar activity at the observation days imply that the observed deviations on the comet region are probably real and are not due to solar direct radiation on 600 mc.

The position of the radio source, as observed, corresponds well to that given by the ephemeris of the Comet 1956 h.

An examination of the possibility of continuous emission by free-free transitions caused by ordinary solar radiation has been made; this assumption has been excluded owing to the faint electronic density and the low temperature. Our impression is that the radiation might present a monochromatic character on 600 mc.

The number of emitted photons by the whole comet in the whole sphere has been determined on the assumption that the linewidth is comprised between  $10^4$  and  $10^8$  cps, corresponding to admissible temperatures. The lifetime of an individual emitting system can be computed as a function of the number of systems. With reasonable number of molecules in cometary conditions, this lifetime lies between 4 and 4000 seconds for the observed flux density on 600 mc, and is inversely proportional to the line-width.

There seems to be a possibility of interpreting the observed radiation on 600 mc on the basis of transitions between sublevels  $J=1.5$  of state  ${}^2\Pi_{3/2}$  resulting from  $\Lambda$ -type doubling for the molecule CH. A new determination of the wavelength of this transition has been made, and led to the conclusion that an improved value of this wavelength is 50.0 cm, rather than 45.45 cm as given previously.

An emission process giving rise to radiation on 600 mc from transitions between two sublevels  $J=1.5$  of state  ${}^2\Pi_{3/2}$  of CH is only admissible, when the time interval between two absorption processes giving rise to the optical spectrum is much less than the lifetime of the molecule on the upper sublevel, otherwise the optical spectrum could not be emitted. Referring to previous results, it is seen that the number of molecules which might explain the observed radioflux is of the order  $10^{30}$ , to  $10^{31}$ , which agrees well with the admitted numbers in the cometary atmospheres.

<sup>13</sup> K. Wurm, "Die natur der kometen," *Vierteljahrsschr. Astron. Ges.*, vol. 78, pp. 18-87; January, 1943.

# Lunar Thermal Radiation at 35 KMC\*

JOHN E. GIBSON†, ASSOCIATE MEMBER, IRE

**Summary**—Measurements of the thermal radiation of the moon were made at a frequency near 35 kmc to investigate further the variation of the radio-wavelength brightness temperature with lunar phase first observed by Piddington and Minnett at 24 kmc. The subject measurements, when referred to the equivalent blackbody temperature for the center of the lunar disc, show a complex rather than sinusoidal variation with phase, varying between 225° and 145°K. The directivity of the antenna (about 0.2° of arc between half-power points) was sufficient to indicate the lunar equatorial (east-west) brightness distribution; this was found to vary in the expected manner and was in agreement with the form of the central brightness variation during a lunation. Observations of two total lunar eclipses showed that no measurable change in lunar radiation occurs during the few hours of an eclipse. Comparison of these results with calculations by Jaeger suggests the lunar surface is composed of a layer of fine dust of very low thermal conductivity, the average depth of which is estimated as one inch or more.

## INTRODUCTION

Thermal radiation due to the surface heat of the moon is measurable by thermocouple techniques in the infrared frequency range and by directive radio receiving systems at radio frequencies. The variation in apparent temperature of the moon during the lunar cycle was first investigated at radio frequencies by Piddington and Minnett<sup>1</sup> at 24 kmc. They found an approximately sinusoidal variation with lunar phase, and deduced the apparent temperature range to extend from about 200°K to about 300°K. A phase lag (relative-to-optical phase) in the occurrence of these extremes was observed, which was interpreted as indicative of a stratified lunar surface in the form of a thin surface cover of fine dust overlaying a subsoil of greater thermal conductivity.

Following much the same method, the observations were repeated at the Naval Research Laboratory during 1953, at a higher frequency near 35 kmc. The antenna beamwidth of 0.2° available for these observations greatly reduced the extrapolation required in determining lunar temperatures from observed readings. Moreover, this beam directivity was sufficient to permit the coarse measurement of the changing brightness variation along the lunar equatorial region. More recently, lunar temperature measurements at other radio frequency bands have been reported.<sup>2,3</sup>

\* Original manuscript received October 3, 1957. Adapted from U. S. Naval Research Lab. Rep. 4984.

† Radio Astronomy Branch, U. S. Naval Research Lab., Washington, D. C.

<sup>1</sup> J. H. Piddington and H. C. Minnett, "Microwave thermal radiation from the moon," *Aust. J. Sci. Res.*, vol. A 2, p. 63; March, 1949.

<sup>2</sup> K. Akabane, "Lunar radiation at 3000 mc/s," *Proc. Japan Acad.*, vol. 31, p. 161; March, 1955.

<sup>3</sup> M. R. Zelinskaya and V. C. Troitski, "Absolute methods for the measurement of the radio temperatures of the sun and moon at centimeter wavelengths, and results obtained at  $\lambda=3.2$  cm," *USSR Acad. Sci., Trans. Fifth Conf. on Questions of Cosmogony, (Moscow)*, p. 99; March 9-12, 1955. (In Russian.)

The present paper summarizes the experimental facilities, methods and results of the NRL observations at  $K_a$ -band,<sup>4</sup> and indicates their relation to present concepts of the physical characteristics and structure of the moon's surface.

## EQUIPMENT

The radio system used to obtain these measurements was identical in electrical characteristics to the present  $K_a$ -band system shown in Fig. 1. The antenna mount of this present equipment provides greater mechanical stability than the modified radar pedestal used in the former system.

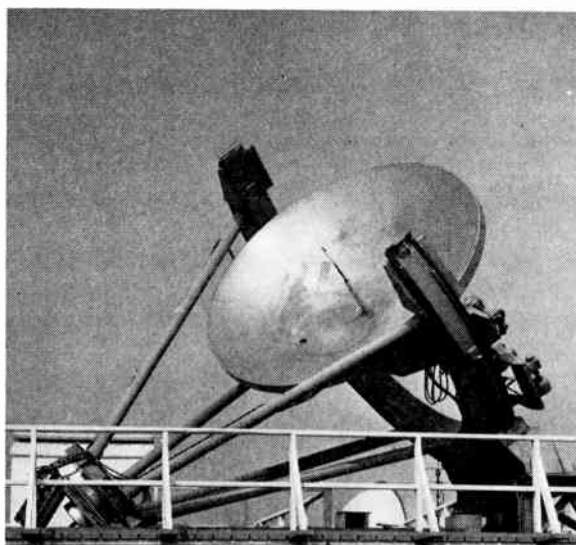


Fig. 1—Receiving system for cosmic radiation at 35 kmc.

The antenna reflector is ten feet in diameter and three feet in focal length, and was machined from an aluminum casting. The antenna feed is a small horn of 0.280-inch square aperture, from which the received radiation is transmitted through 0.140 by 0.280-inch silver-lined waveguide to the receiver mounted behind the antenna.

The receiver is the rapid-comparison type introduced by Dicke,<sup>5</sup> and follows quite closely the design of Dicke for 1.25 cm wavelength. The principal differences are the use of the hybrid ring instead of the Magic-T balanced mixer circuit, the omission of agc, and the use of a twin diode rather than a pair of pentodes as the coherent detector.

To provide absolute calibration signal levels, a waveguide switch at the receiver input permits the antenna

<sup>4</sup>  $K_a$ -band extends from 33 to 36 kmc.

<sup>5</sup> R. H. Dicke, "The measurement of thermal radiation at microwave frequencies," *Rev. Sci. Instr.*, vol. 17, p. 268; July, 1946.

to be replaced by either a dissipative dummy antenna termination at ambient temperature, or by a heated termination whose temperature is usually about 250°C, but which may be increased to near 600°C if desired. Received noise radiation whose power corresponds to low noise temperatures can be measured by scaling from the marker levels for the calibrating terminations. For high noise temperatures and for determining the receiver input-output response characteristic, an argon gas-discharge noise tube is used in conjunction with a calibrated variable attenuator.

Details of the mechanical and electrical design of the antenna and receiver, together with an analytical discussion of the receiver characteristics, have been given in a separate publication,<sup>6</sup> and it is necessary here to mention only two system parameters, the antenna directivity and the receiver sensitivity. The antenna radiation pattern is a pencil beam about 0.2° in width between half power points. The illumination of the reflector by the feed is tapered to about 15 db down at the edge; thus the side lobes of the radiation pattern are low. The plane of electric polarization is north-south.

For a receiver of this type which is open to both the signal and the image channels, and in which the IF pass band has the approximate frequency response of a single-tuned resonant circuit, the rms value of the flicker in the output indicator is given by

$$\Delta t = \frac{\pi}{4\sqrt{2}} \left[ FT_0 + \frac{3}{2}(t - T_0) + \dots \right] \frac{1}{\sqrt{\tau B}},$$

where

$F$  = noise factor referred to signal channel reception only, in accord with the IRE definition,

$T_0 = 290^\circ\text{K}$ ,

$t$  = noise temperature of received radiation,

$\tau$  = time constant (in seconds) of the output integrator (not to be confused with the atmospheric opacity  $\tau$  mentioned later), and

$B$  = equivalent noise bandwidth of the IF channel, in cycles per second.

For selected Sylvania type 1N53 mixer crystals, the noise factor ranges from 15 to 20 (12 to 13 db). With  $B \approx 4 \times 10^6$  and  $\tau = 1$ , the calculated value for  $\Delta t$  is 1.2° when  $t \approx T_0$ . The observed flicker is in good agreement, and is about three degrees in the peak-to-peak excursion.

### THE OBSERVATIONAL METHOD

The variation in lunar temperature during a synodic month (29.53 days) can be traced adequately from measurements spaced about a day apart. However, adverse weather conditions generally preclude the possibility of obtaining an unbroken series of daily measurements at  $K_a$ -band, where the attenuation due to clouds

<sup>6</sup> J. E. Gibson, "Comparison-Type Receivers for White Noise Radiation at 0.86 CM Wavelength," U. S. Naval Research Lab. Rep. 4864; December, 1956.

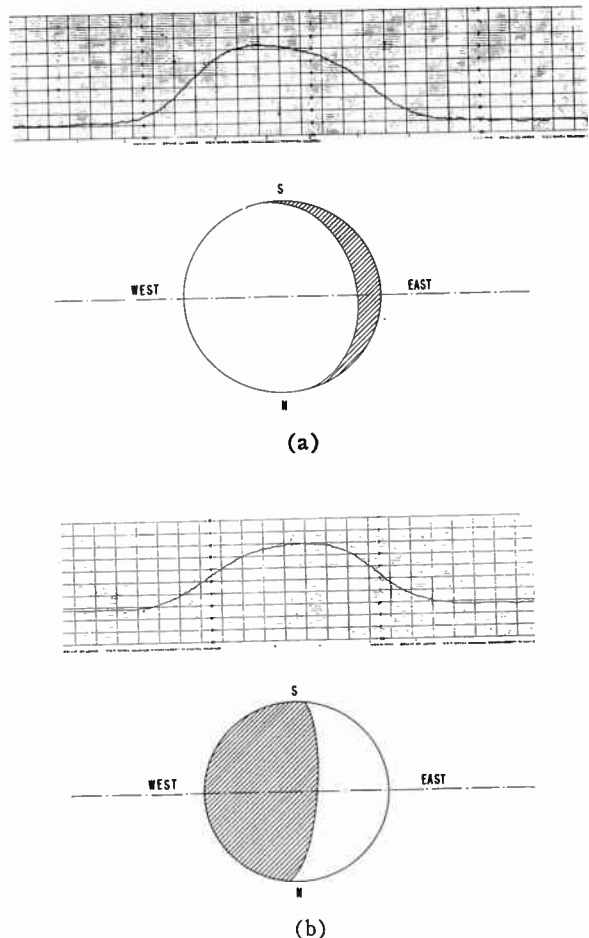


Fig. 2—Recordings of lunar thermal radiation received during the moon's transit of the stationary antenna beam. The moon is shown to scale for the two cases, and is so oriented that the west-east brightness variation across the moon is indicated by the corresponding recorded deflection. The receiver output time constant was one second, and the recorder chart speed was three inches (four divisions) per minute. (a) Lunar phase 139°; apparent diameter 33.07'. (b) Lunar phase 283°; apparent diameter 29.75'.

and precipitation is variable and difficult to determine. Therefore, the observations during the early part of 1953, were discontinuous, and since the equipment and observational technique were modified somewhat in this period, the early observations were regarded as preliminary. Finally, a long period of favorable weather in autumn provided the opportunity to obtain a complete set of data under unified conditions.

In order to measure both lunar temperature and equatorial brightness distribution, a scanning method was followed. The antenna was pointed just west of the moon's position and held stationary during the transit of the antenna beam caused by the diurnal movement of the moon (Fig. 2). A representative series of these scans was obtained for each daily observational period. Following groups of two or three scans, calibration marker levels were recorded for a receiver input termination at about 250°C and for an ambient temperature termination (about 15°C). The atmospheric attenuation for each day's observations was determined from

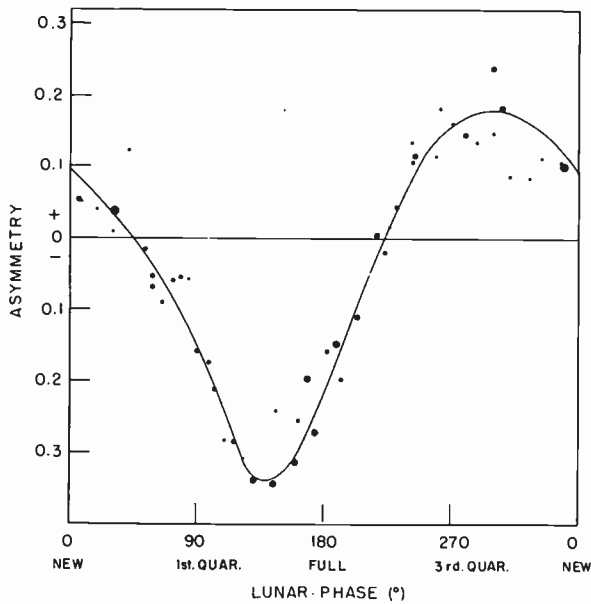


Fig. 3—Asymmetry of the lunar scan curve as a function of phase.

measurements of the apparent sky temperature at elevation angles of  $60.2^\circ$ ,  $16.3^\circ$ , and  $8.8^\circ$ , taken just prior to or following the recording of the lunar scans.

#### REDUCTION OF DATA

##### Equatorial Brightness Distribution

The scan recordings of Fig. 2 were chosen to show the asymmetry resulting from the radio brightness variation along the lunar equatorial region. Since comparable scans along the polar axis have not yet been obtained, direct analysis of these recordings in terms of relative brightness across the lunar disk has not been attempted. However, a secondary index of the brightness variation is the asymmetry itself, which may be defined in the form of a comparison of the slopes of the two sides of the recording. Points were marked off at 10 per cent and 90 per cent down from the crest, and the asymmetry was defined as

$$\text{Asymmetry} = \frac{\text{Rise Time} - \text{Fall Time}}{\text{The Shorter of the Two Times}}$$

The asymmetry data are plotted in Fig. 3. Here the variation in apparent lunar diameter is indicated by the sizes of the dots (not to scale). The curve is the estimated asymmetry for the moon at its largest diameter.

The asymmetry is seen to alternate about the axis according to phase in the manner suggested by Fig. 2. The two times at which the brightness variation across the moon is greatest are at about midway between first quarter and full moon, and shortly after third quarter, the latter being somewhat less pronounced. The intermediate nodes do not represent occurrences of a uniform brightness distribution, but instead they are the occasions when the sequence of the changing solar illumination brings the radio temperature of the central region

of the lunar disk near an extreme, and the temperature variations from the center toward the east and west limbs are comparable in their integrated effect on the form of the scan recording. Thus at the node near  $225^\circ$  in phase the temperature decreases toward the limbs. The most striking feature of the asymmetry variation is its phase lag compared to the phase of solar illumination. The low resolution for this antenna beam width makes it necessary to interpret the detailed meaning of the asymmetry variation jointly with the measured temperature variation.

##### Lunar Apparent Temperature

The transfer equation for the radiation received when pointed toward the moon may be written in terms of temperature in  $^\circ\text{K}$  as

$$t_m = \alpha T_0 + (1 - \alpha)(T_e + \epsilon^{-\tau \sec z} T_m),$$

where

$t_m$  = effective temperature of noise signal at receiver input,

$\alpha$  = fractional absorption of antenna transmission line,

$T_0$  = ambient temperature,

$T_e$  = apparent temperature of the atmosphere,

$\tau$  = opacity of the atmosphere,

$z$  = zenith distance ( $90^\circ$ —altitude), and

$T_m$  = apparent lunar temperature for a particular antenna directivity.

The coefficient of  $T_m$  is the fractional transmission through the atmosphere.

If  $t_{sk}$  denotes the effective temperature of the noise signal appearing at the receiver input when the moon has passed out of the antenna beam (when  $T_m = 0$ ), the value of  $T_m$  is given by

$$T_m = \frac{t_m - t_{sk}}{(1 - \alpha)\epsilon^{-\tau \sec z}}$$

The temperature difference ( $t_m - t_{sk}$ ) is readily calculable by means of a scale factor determined from calibration marker levels. For the equipment used here, the value of  $\alpha$  was 0.3, corresponding to 1.5 db attenuation. The values of the zenith angle  $z$  were determined for the times of these observations by reference to the American Nautical Almanac and equatorial to alt-azimuth coordinate conversion tables.

A major task in connection with these lunar observations was the development of a satisfactory technique for determining atmospheric attenuation. This has been treated in a separate publication,<sup>7</sup> in which the determinations of the variable opacity<sup>8</sup>  $\tau$  for these lunar measurements are given. The method used is a refinement of

<sup>7</sup> J. E. Gibson, "Atmospheric Attenuation at  $k$ -Band Radio Wavelengths," U. S. Naval Research Lab. Rep. 4966; August, 1957.

<sup>8</sup> The term opacity used by the author is frequently called optical depth.

that of Dicke *et al.*<sup>9</sup> In brief, an expression for the apparent temperature of the atmosphere was derived by formal integration of the product of the theoretical incremental fractional absorption, the temperature, and the fractional transmission along a ray from an extraterrestrial source to ground level. From this formula, families of curves relating the apparent temperature  $T_e$  to  $\sec z$  were computed, with the ground level relative humidity and  $\tau$  as parameters. The curves were computed for wavelengths of 0.86 cm and 1.8 cm, and those for 0.86 cm are reproduced in Fig. 4. The curves obtained experimentally were compared with the theoretical curves to obtain values for  $\tau$ , which ranged from 0.043 to 0.090.

The variation of  $T_m$  with lunar phase is shown in Fig. 5. The values plotted correspond to the maximum deflections recorded in scanning the moon, rather than the values for the antenna beam centered on the moon; however, the distinction is very minor.

Since the quantity  $T_m$  considered here is the effective lunar brightness temperature, which is a function of the antenna directivity and the brightness variation over the lunar disc, it is of interest to determine the brightness temperature more specifically, such as at the center of the apparent disc (normal incidence). The observed value  $T_m$  is the integral of the apparent temperature times the antenna gain over the sphere surrounding the antenna, or

$$T_m = \frac{1}{4\pi} \int_0^{4\pi} T(\theta, \phi) G(\theta, \phi) d\omega,$$

where the temperature  $T$  and the gain  $G$  are functions of the coordinates  $\theta$  and  $\phi$ , and  $d\omega$  is an elemental solid angle. The temperature at the center of the lunar disk may be computed using numerical integration, which may be formulated as

$$T_m = \sum T_m' B(\theta, \phi) W,$$

where  $T_m'$  is the central disk brightness temperature,  $B(\theta, \phi)$  is the factor by which the brightness temperature for a particular elemental solid angle differs from  $T_m'$ , and  $W$  is the fractional weight of the element. Since the brightness distribution determining  $B(\theta, \phi)$  has not been defined in detail experimentally, it is assumed here that the brightness variation with lunar longitude corresponds to the variation as seen at normal incidence during a lunation, and the brightness is assumed to vary as the fourth root of the cosine of the lunar latitude. The theoretical weights of concentric rings centered on a pencil-beam axis have been computed by Swanson, McCoy, and Hepperle.<sup>10</sup> Since the brightness distribution

<sup>9</sup> R. H. Dicke, R. Beringer, R. L. Kyhl, and A. B. Vane, "Atmospheric absorption measurements with a microwave radiometer," *Phys. Rev.*, vol. 70, p. 340; September, 1946.

<sup>10</sup> L. W. Swanson, D. O. McCoy, and C. M. Hepperle, "Theoretical Analysis of the Reception of Thermal Radiation at Radio Frequencies by the Use of Highly Directional Antennas," Collins Radio Co. Rep. CER-149; November, 1948.

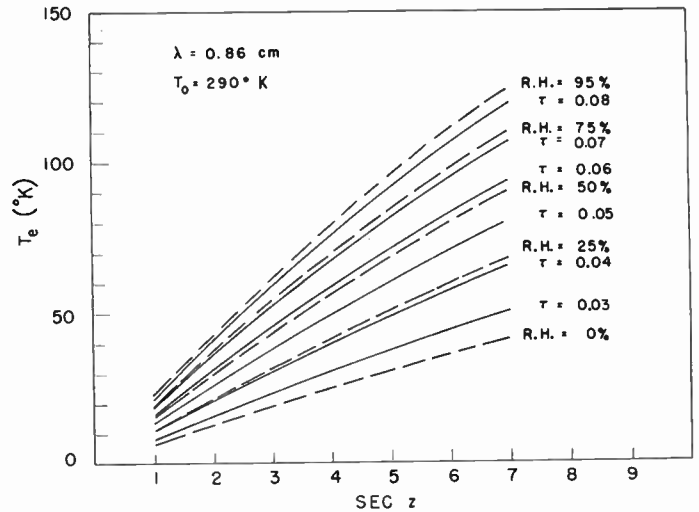


Fig. 4—Apparent sky temperature as a function of the secant of the zenith angle ( $90^\circ$ —altitude). The dependence of the opacity  $\tau$  upon atmospheric relative humidity at ground level is shown by plotting both as parameters.

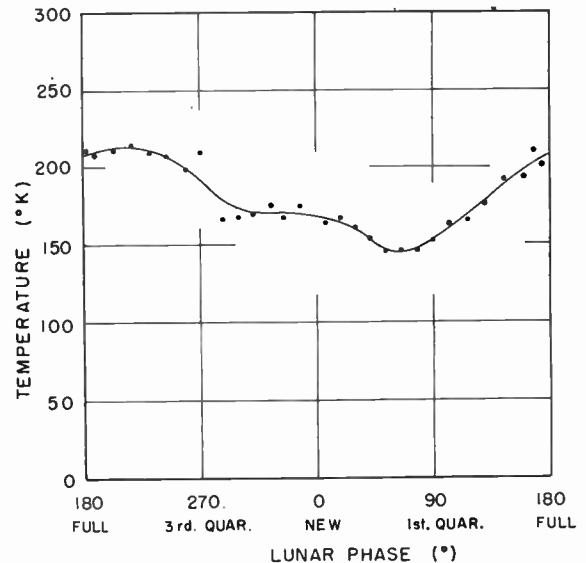


Fig. 5—The maximum antenna temperature for the moon, corrected for atmospheric attenuation, with a pencil-beam antenna radiation pattern  $0.2^\circ$  in width between half-power points.

is not circularly symmetrical in the case of the moon, the rings may be considered in suitable segments.

Theoretical and experimental considerations too lengthy to include here indicate that the summation of the weights out to the periphery of the moon totals more than 0.9 for this antenna in actual practice. On the basis of theoretical calculations for an idealized radiation pattern, the weights would total 0.97. In the present work, the latter value is assumed, and the possibility of the correct value being smaller is treated as an uncertainty which permits the deduced value for  $T_m'$  to be uncertain within a range up to about 10 per cent greater than the nominal value.

The variation of  $T_m'$  with phase is indicated by the

dashed line of Fig. 6, and the solid curve is a calculated plot which will be discussed later. The temperature is seen to vary from a maximum occurring several days after full moon to a minimum at first quarter. Although the times of these extremes do not coincide with the times for maximum and minimum visual brilliance of the moon at full moon and new moon, the radio-wavelength variation is really not at all surprising, since the times of the radio extremes are analogous to midafternoon and sunrise on earth, when similar extremes in the daily temperature variation are reached. The analogy is not overdrawn greatly, since the moon keeps one face toward the earth, and the temperature  $T_m'$  applies to a fixed selenographic area. However, the lunar day is as long as 29 earthly days, and this slowness of rotation partly accounts for the relatively large temperature variation observed at radio wavelengths.

### LUNAR ECLIPSE OBSERVATIONS

The radio-wavelength temperature variation for a more rapid change in solar illumination was investigated during two total lunar eclipses, those of January 29, 1953, and January 18, 1954, both of which were observed with a clear sky. The former eclipse began before moonrise, with the visible portion beginning just before the start of totality. The second eclipse was visible in all phases. During the visible portion of each eclipse a series of equatorial scans were recorded, together with calibration markers. Analysis of the data showed that no important radio temperature change occurred, and the asymmetry during the eclipses corresponded to the asymmetry for full moon.

### INTERPRETATION

Prior to the several series of microwave observations of recent years, infrared measurements have been available and attempts have been made to deduce from them information about lunar surface properties. Of these various studies, recent work by Jaeger<sup>11,12</sup> is of particular interest. He has given the results of numerical calculations of a) the fall in surface temperature during a lunar eclipse as seen at infrared wavelengths, b) the variation in surface temperature at the lunar equator during a lunation, again as seen at infrared wavelengths, and c) the variation in microwave temperature at the equator during a lunation. Two models of the lunar "land" are considered, the first of which is a homogeneous solid composed of either igneous rock, or a granular or cellular substance such as pumice or lava gravel, or a fine dust in vacuo. The second model is that of a stratified soil<sup>13</sup> having a thin topsoil of dust of negligible heat capacity

<sup>11</sup> J. C. Jaeger, "The surface temperature of the moon," *Aust. J. Physics*, vol. 6, p. 10; January, 1953.

<sup>12</sup> J. C. Jaeger, "Conduction of heat in a solid with periodic boundary conditions, with an application to the surface temperature of the moon," *Proc. Camb. Phil. Soc.*, vol. 49, p. 355; April, 1953.

<sup>13</sup> The term soil is used for aptness, but does not imply organic matter.

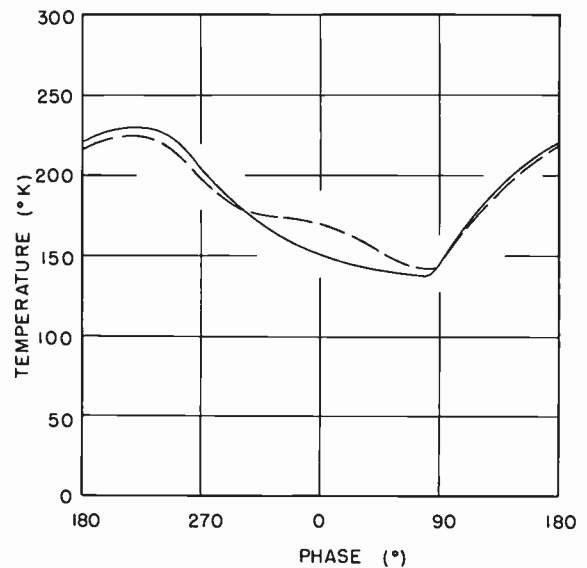


Fig. 6—Comparison of the brightness temperature for the center of the lunar disk (dashed) with a calculated curve (solid) for a lunar surface of deep dust.

covering a subsoil of denser material having better thermal conductivity.

Jaeger assumed that heat is lost by radiation according to the fourth power law. For the calculation of the fall in surface temperature during an eclipse, he took the initial surface temperature to be 370°K and the emissivity to be 1. In the calculation of the temperature variation during a lunation, he assumed the insolation of the moon's surface at normal incidence to correspond to 0.0258 calorie  $\text{cm}^{-2} \text{sec}^{-1}$ , and again assumed the emissivity to be 1.

In the surface (infrared) temperature calculations the thermal conductivity  $K$ , the density  $\rho$  and the specific heat  $c$  are combined in the parameter  $(K\rho c)^{-1/2}$  which describes the soil. Using cgs units, calorie, and °K, this soil parameter ranges from about 20 for rock to about 1000 for dust in vacuo. For the dust surface Jaeger followed Wesselink<sup>14</sup> and assumed

$$K = 2.8 \times 10^{-6} \text{ cal cm}^{-2} \text{ sec}^{-1} (\text{°K cm}^{-1})^{-1}$$

$$\rho = 1.8 \text{ gm cm}^{-3}$$

$$c = 0.2 \text{ cal gm}^{-1}.$$

The stratified surface introduces an additional parameter

$$D = P^{1/2}(K\rho c)^{-1/2}\tau^{-1},$$

where  $\tau$  is the thermal resistance of the top layer,  $P$  is the period of a lunation ( $P=29.53$  days), and the values of  $K$ ,  $\rho$ , and  $c$  are those for the subsoil. Comparison of the calculated curves for the infrared surface temperature with measurements during eclipses and through a luna-

<sup>14</sup> A. F. Wesselink, "Heat conductivity and nature of the lunar surface material," *Bull. Astron. Inst. Neth.*, vol. 10, p. 351; April, 1948.

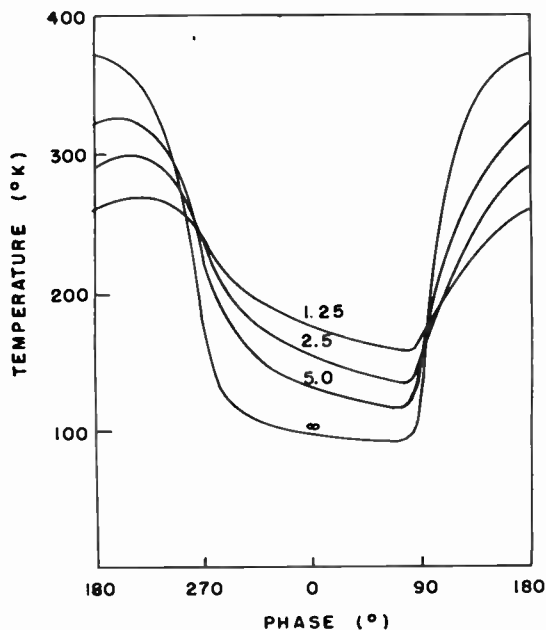


Fig. 7—Calculated microwave temperatures for a homogeneous lunar surface for which  $(K\rho c)^{-1/2} = 1000$ . The numbers on the curves are the values of  $C = \alpha_m(KP/\rho c)^{1/2}$ . (Jaeger, *Aust. J. Phys.*)

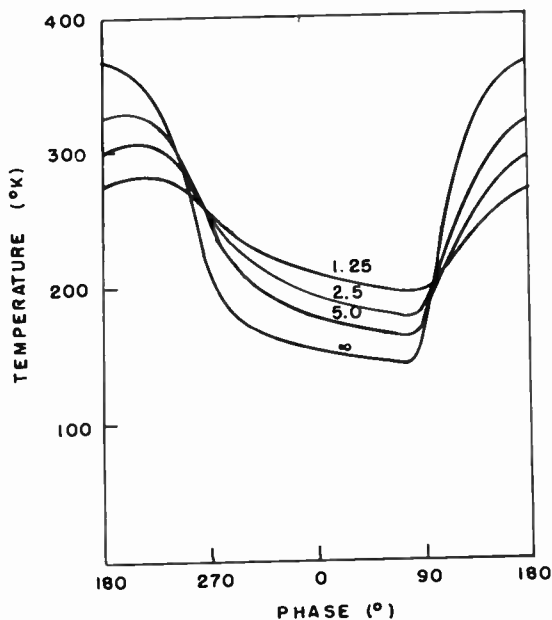


Fig. 8—Calculated microwave temperatures for a homogeneous lunar surface for which  $(K\rho c)^{-1/2} = 125$ . The numbers on the curves are the values of  $C = \alpha_m(KP/\rho c)^{1/2}$ . (Jaeger, *Aust. J. Phys.*)

tion showed that the best agreement is obtained for either a homogeneous dust surface or for a dust layer somewhat less than one centimeter in thickness covering a better-conducting substratum.

Since the attenuation of microwave radiation through a poor electrical conductor such as soil is much less than the attenuation at infrared or optical wavelengths, the microwave radiation originates throughout a comparatively large range of depths in the soil, and the measured microwave temperature bears no simple relation to the actual temperature, either at the surface boundary or at a greater depth. For a homogeneous surface material the microwave temperature at normal incidence is given by

$$T_m' = (1 - R)\alpha_m \int_0^\infty T(x)\epsilon^{-\alpha_m x} dx,$$

where

- $R$  = reflectivity of the surface boundary,
- $\alpha_m$  = an attenuation constant, and is a function of the wavelength and the electrical conductivity of the material,
- $x$  = depth below the surface boundary,
- $T(x)$  = temperature as a function of depth.

This relation simply expresses the microwave temperature as the summation of the thermal emission  $\alpha_m T(x) dx$  from various depths, each being transmitted partially to the surface by the factor  $\exp(-\alpha_m x)$ . The reflectivity is related to the dielectric constant  $\kappa$  by

$$R = \left( \frac{\sqrt{\kappa} - 1}{\sqrt{\kappa} + 1} \right)^2$$

and  $1 - R$  is the emissivity.

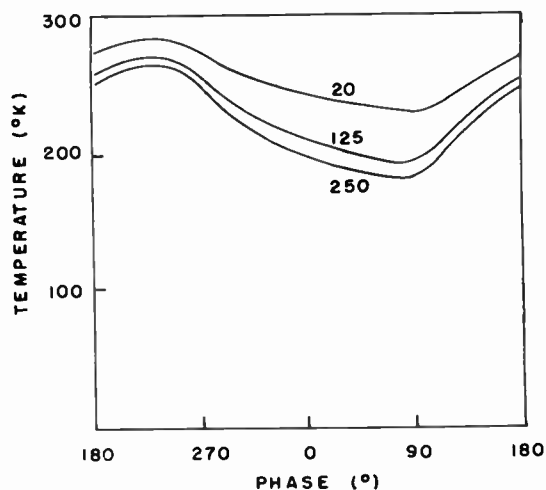


Fig. 9—Calculated microwave temperatures for a solid with a surface skin, for which  $D = C = \sqrt{2\pi}$ . The numbers on the curves are the values of  $(K\rho c)^{-1/2}$  for the substratum. (Jaeger, *Aust. J. Phys.*)

In the calculation of microwave temperature two parameters,  $(K\rho c)^{-1/2}$  and  $C = \alpha_m(KP/\rho c)^{1/2}$  are involved for the homogeneous solid model of lunar surface. The stratified surface model requires a third parameter, the  $D$  used in the infrared calculations. Jaeger's curves for the homogeneous model composed of dust are reproduced in Fig. 7, and the homogeneous pumice or lava gravel soil is represented by Fig. 8. Fig. 9 gives one set of results for the stratified model.

The closest parallel to the NRL data is the curve for  $C = 1.25$  in Fig. 7. Since Jaeger assumed the emissivity to be unity, it is necessary to reduce this curve somewhat in order to approximate the actual microwave brightness temperature  $T_m'$ . If the soil dielectric constant

is assumed to be about 5, the emissivity is about 0.85. Reducing Jaeger's curve for  $C=1.25$  by this factor, the solid curve in Fig. 6 is obtained.

The agreement between the calculated and measured curves is seen to be fairly close, with the most obvious discrepancy being the high observed temperature near new moon. This characteristic was noted in the preliminary measurements not given here, and seems to be a real effect. However, a satisfactory explanation is not known.

The choice of the homogeneous surface of dust as the representation which most nearly conforms to the microwave results is dependent upon two assumptions involved in the curves of Fig. 6, first, that the summation of the antenna beam weighting factors used in determining  $T_m'$  total nearly unity for the lunar disc, and secondly, that the lunar soil dielectric constant is about 5. The uncertainty of the former assumption permits the measured curve for  $T_m'$  to be raised by some factor not greater than 10 per cent, which would bring the measured results into agreement with a gravel-like soil. However, this possibility is countered by the uncertainty in the dielectric constant; a value of 3 may be considered possible, in which case the calculated curve is increased by about 10 per cent.

The infrared results point to a surface of dust; this might be compatible with the possibility a gravel soil is indicated by the microwave results, if the soil is stratified. However, the amplitude of the calculated microwave temperature variation is reduced in the case of the stratified soil; thus it appears the soil structure which

corresponds best to both infrared and microwave results is the homogeneous dust model.

The depth thus required for the dust surface need not be great, although it must be significantly greater than the thickness of the layer of negligible heat capacity assumed in the stratified model calculations. For the values of  $K$ ,  $\rho$ , and  $c$  for dust, a value for  $C$  of 1.25 corresponds to  $\alpha_m = 0.28$  per cm. If the dust layer were 10 cm deep, about six per cent of the radiation arising at this depth would appear at the surface. Thus deviations in the soil characteristics at depths of a few inches would not be evident from the observed microwave temperature variation. It seems reasonable to say that the dust layer is probably one inch or more in depth, as an average over the lunar surface.

The absence of significant change in microwave temperature during an eclipse indicates the temperature change is restricted to a very shallow depth of the soil, when the insolation is removed for a period of a few hours. This is consistent with a very low thermal conductivity for the surface layer.

#### ACKNOWLEDGMENT

The work was proposed by Dr. John P. Hagen, to whom the author is indebted for his early support and interest. Also due particular acknowledgment is R. J. McEwan who worked with the author during the observations.

The reproduction of illustrations from Dr. Jaeger's paper was made possible by the kind permission of the publishers of the *Australian Journal of Physics*.

## Lunar Radio Echoes\*

JAMES H. TREXLER†, ASSOCIATE MEMBER, IRE

**Summary**—High-power radars at the Naval Research Laboratory have been used to study the reflecting properties of the earth's moon. Experimental work over the last six years at frequencies in the 30-mc to 3000-mc band has revealed a lunar surface phenomenon which produces a "highlight." Measurements made at 198 mc have shown that more than 50 per cent of the echo energy is reflected in the first 50 microseconds after the leading edge of a short incident pulse contacts the moon. This fortunate situation permits many interesting astronomical observations and suggests the use of wide-band communication signals in a circuit using the moon as a passive relay. Many types of modulation have been successfully passed over the lunar circuit, including amplitude modulation by voice.

#### INTRODUCTION

THE HISTORY of attempts to study the moon by radio methods is a long one. One of the first published papers describing the problem was by Gernsback in 1927.<sup>1</sup> As early as 1924 and continuing through the 1930's, Young and his associates at the Naval Research Laboratory searched for moon echoes in their "back splash" and "round the world" research at frequencies up to 60,000 kc. In 1935, they probed for the moon with a high-power meter-wave radar and with

\* Original manuscript received by the IRE, November 11, 1957.

† Naval Research Laboratory, Washington 25, D. C.

<sup>1</sup> H. Gernsback, "Can we radio the planets," *Radio News*, vol. 8, pp. 946-948; February, 1927.

each new search-radar development an effort was made at the Laboratory to obtain moon echoes. By the end of World War II, equipment advances had progressed to the point where positive and repeated success theoretically was possible. At least ten groups of investigators from six countries have carried on such work with varying degrees of success. The United States Signal Corps announced successful radar contact in March, 1946, followed by Mofenson's paper in April.<sup>2</sup> Bay, in Hungary, closely followed the US work and he also reported his findings in April, 1946.<sup>3</sup> The Russians claimed almost simultaneous results through newspaper releases in Europe. Reports of experimental work and theoretical studies followed by Webb,<sup>4</sup> Kaufman,<sup>5</sup> Grieg, Metzger, and Wear,<sup>6</sup> Kerr, Shain, and Higgins,<sup>7</sup> DeWitt and Stodola,<sup>8</sup> Kerr and Shain,<sup>9</sup> Sulzer, Montgomery, and Gerks,<sup>10</sup> Kerr,<sup>11</sup> Bateman and Smith,<sup>12</sup> Shklovski,<sup>13</sup> Kaiser,<sup>14</sup> Murray and Hargreaves,<sup>15</sup> Brown, Evans, Hargreaves, and Murray,<sup>16</sup> Winter,<sup>17</sup> Lovell<sup>18</sup> and Kerr.<sup>19</sup> In general, however, the results of the experiments before 1950, had been limited by marginal conditions, such as low-transmitted powers with the attendant necessary narrow receiver bandwidths, and small antennas. It was apparent that additional work in this field could be very productive if equipment parameters were improved. With this in mind preparations were started in 1950, at the Naval Research Laboratory,

to assemble large radars designed specifically for moon work. The first of these equipments was placed in operation in the summer of 1951, followed by five additional systems all of which have provided data of considerable interest to astronomy, the radio propagation field, and radio communications. The first instrumentation was at a frequency of 198 mc and was used successfully in the moon circuit in October, 1951. This work was followed by 220-mc work in 1954; 300-mc work in 1955; and 30-mc, 2000-mc, and 3000-mc work in 1957. This paper is concerned specifically with the early 198- and 220-mc experiments. A companion paper by Yaplee *et al.*, describes the more recent 3000-mc work.<sup>20</sup> Description of the other work will be published at a later date.

#### EXPERIMENTAL

The most important element of the NRL meter-wave installations is a parabolic reflector which has an aperture of a little over one acre. This antenna is an off-center section of a parabola of revolution having an elliptical opening 220 by 263 feet along the minor and



Fig. 1—Air view of moon radar antenna.

major axes. Fig. 1 is an air view of the parabola which was cut in the earth by road-building machinery. The surface was paved by conventional asphalt black top methods with a galvanized iron grid having openings three inches by three inches being attached to provide a reflecting surface good for wavelengths of one meter or more. The surface, at all points, lies within three inches of a true parabola providing a measured antenna power gain of 10,000 at 198 mc. At the same frequency the half-power beamwidth is approximately  $1.4^\circ$  in both the *E* and *H* planes. The beam of the antenna can be steered in celestial coordinates of right ascension and declina-

<sup>20</sup> B. S. Yaplee, R. H. Bruton, K. J. Craig, and N. G. Roman, "Radar echoes from the moon at a wavelength of 10 cm," this issue, p. 293.

<sup>2</sup> J. Mofenson, "Radar echoes from the moon," *Electronics*, vol. 19, pp. 92-98; April, 1946.

<sup>3</sup> Z. Bay, "Reflection of microwaves from the moon," *Hung. Acta Phys.*, vol. 1, pp. 1-22; April, 1946.

<sup>4</sup> H. D. Webb, "Project Diana—army radar contacts the moon," *Sky and Telescope*, vol. 5, pp. 3-6; April, 1946.

<sup>5</sup> H. Kaufman, "A DX record; to the moon and back," *QST*, vol. 30, pp. 65-68; May, 1946.

<sup>6</sup> D. D. Grieg, S. Metzger, and R. Waer, "Considerations of moon-relay communication," *PROC. IRE*, vol. 36, pp. 652-663; May, 1948.

<sup>7</sup> F. J. Kerr, C. A. Shain, and C. S. Higgins, "Moon echoes and penetration of the ionosphere," *Nature (London)*, vol. 163, pp. 310-313; February 26, 1949.

<sup>8</sup> J. H. DeWitt, Jr. and E. K. Stodola, "Detection of radio signals reflected from the moon," *PROC. IRE*, vol. 37, pp. 229-242; March, 1949.

<sup>9</sup> F. J. Kerr and C. A. Shain, "Moon echoes and transmission through the ionosphere," *PROC. IRE*, vol. 39, pp. 230-242; March, 1951.

<sup>10</sup> P. G. Sulzer, G. F. Montgomery, and I. H. Gerks, "An uhf moon relay," *PROC. IRE*, vol. 40, p. 361; March, 1952.

<sup>11</sup> F. J. Kerr, "On the possibility of obtaining radar echoes from the sun and planets," *PROC. IRE*, vol. 40, pp. 660-666; June, 1952.

<sup>12</sup> R. Bateman and W. Smith, "Lunar DX on 144 mc/s," *QST*, vol. 37, pp. 11, 12, 116; March, 1953.

<sup>13</sup> I. S. Shklovski, "Radioastronomiya," (Radio Astronomy), Gosudarstvennoe izdatel'stvo Tekhniko-Teoreticheskoi Literatury, Moscow, Russia, p. 216; 1953.

<sup>14</sup> T. R. Kaiser, "Radio echoes from the aurora and the moon," *Occ. Notes, Roy. Astr.*, sec. 3, no. 16, p. 50; 1954.

<sup>15</sup> W. A. S. Murray and J. K. Hargreaves, "Lunar radar echoes and the Faraday effect in the ionosphere," *Nature (London)*, vol. 173, pp. 944-945; May 15, 1954.

<sup>16</sup> I. C. Browne, J. V. Evans, J. K. Hargreaves, and W. A. S. Murray, "Radio echoes from the moon," *Proc. Phys. Soc.*, vol. 69, pt. 9, pp. 901-920; September, 1956.

<sup>17</sup> D. F. Winter, "Radar Reflections from the Moon," Electronic Research Directorate, AF Cambridge Res. Ctr., Air Res. and Dev. Command, AFCRC-TR-56-106.

<sup>18</sup> A. C. B. Lovell, "British Work Carried out in Radio Astronomy Since 1954," presented at URSI 12th General Assembly, Boulder, Colo.; 1957.

<sup>19</sup> F. J. Kerr and C. A. Shain, "Reflexion of radio waves from the moon," *Nature (London)*, vol. 179, p. 433; February 23, 1957.

tion by a set of cables that move the boom supporting the focal point feed structure. The boom is gimbal mounted at the parabola's vertex which lies 10 feet outside the aperture. By providing a geometry that effects an equatorial mount, the feed can be moved in a simple way by varying one cable length to follow the moon in its path. At 198 mc, the antenna has a useful pattern for about one hour for celestial targets and is very near full gain for approximately 20 minutes or a time equal to three and one-half beamwidths. This small scanning angle is caused by the unsymmetrical shape of the reflector's surface segment used and the small focal length to aperture ratio. If the antenna were completed around its axis the focal length to aperture ratio or  $f$  number would be about 0.22 which places the focal point well inside the *latus rectum* of the parabola. This compromise in design which resulted in limited steering time was made to simplify the feeds and to shorten the focal point supporting the boom.

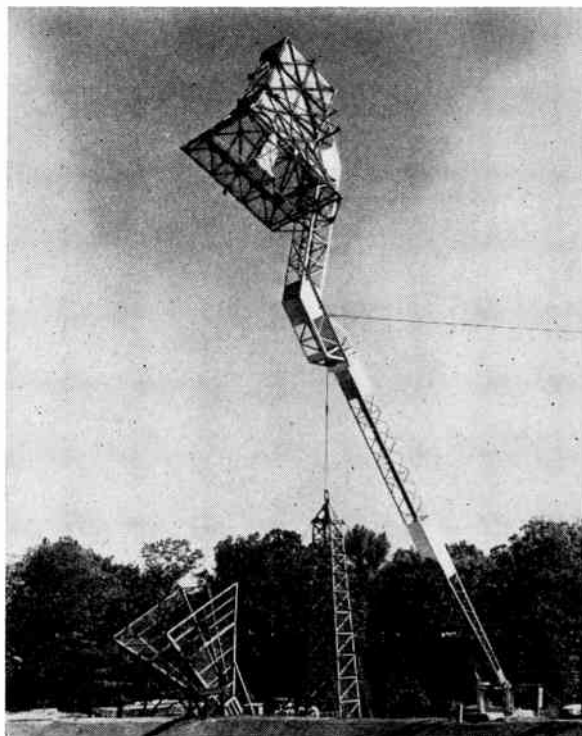


Fig. 2—Horn-type antenna feed on moon radar antenna.

Fig. 2 shows one of the many feed structures used at the focal point which is 90 feet above the dish. Considerable effort was expended in tailoring the primary radiation pattern and phase front of the feeds in an attempt to maximize the over-all antenna gain. It is very important for work in the vhf band to suppress pickup from terrestrial sources such as atmospheric and interference from fm and tv broadcast. As aids in this effort side and back gain of the feeds were reduced through careful shaping of the horns and the use of choke sections surrounding the structures which provide isolation from currents induced in the outer surface of the

feeds. This particular feed is for work at frequencies from as low as 45 mc to nearly 400 mc. The larger horn is more than 17 feet across. It is made of magnesium and weighs approximately 700 pounds. The over-all antenna system was measured for gain and beamwidth by using the sun as a source and a horn-type antenna as a gain standard. One of the gain standards used for 198-mc measurements can be seen in the lower left-hand corner of Fig. 2. All horn standards were modeled in pairs at 3000 mc to check their gains precisely.

The pulse transmitter for the 198-mc project consisted of a 1 megw, 12  $\mu$ sec Navy radar which was later modified to produce 1.2 megw with 10  $\mu$ sec pulses. A 100-watt communication transmitter tunable from 220 mc to 390 mc was used for cw checks. Power outputs of all transmitters were measured carefully by the use of calorimeter techniques, and the voltage standing-wave ratios on the antenna transmission lines were continually measured and maintained below 1.1:1. All transmission lines were coaxial 3-inch copper, air filled. The specially built receivers utilized the Western Electric 416A and later the 416B in grounded grid triode tube circuits that obtained noise figures between 2 db and 3 db. Receiver bandwidths were adjustable in steps from as narrow as 100 cps to as wide as 250 kc. Because of the long range to the target, the pulse rate stability requirements were exacting. Secondary frequency standards were used to provide the pulse rate. These secondary standards were equipped with counter circuits to determine range and comparator circuits to allow standardization with the basic time from the Naval Observatory.

Fig. 3 shows a single strobe A-Scope radar trace of the moon's echo taken near 1310 universal time on October 22, 1951. This trace is about average in shape, with some echoes being shorter and some longer. The total sweep length is 1000  $\mu$ sec. The transmitted pulse length was 12  $\mu$ sec, transmitter power 750 kw peak, and the receiver bandwidth was 250 kc to assure minimum distortion of the echo. Careful examination of many of these traces using a planimeter technique has indicated that more than half the echo power is returned in the first 50  $\mu$ sec. Fig. 4 is an example of a short echo and Fig. 5 is an example of a long echo. Figs. 3-5 are of echoes spaced about 30 seconds apart. Fig. 6 is a plot of the per cent of echo energy received as a function of time after the beginning of the echo. The contribution of noise to the signal has been removed by determining the noise level before the echo started and assuming this level to be constant during the 350  $\mu$ sec following the beginning of the echo. This plot is an average of many echoes randomly-sampled over a 5 minute period. Fig. 7 shows a consecutive group of echoes at a repetition rate of 10 per second. The high correlation of echo shape from pulse to pulse can be seen. The sweep length is 1000  $\mu$ sec in Fig. 7. A slight range drift can be seen which carried the echo steadily across the frame at the rate calculated for range change over the earth-moon path at the time of the exposure. This was the first posi-

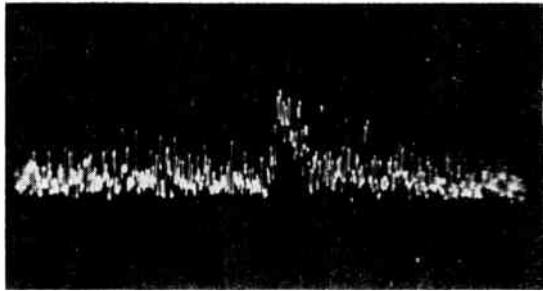


Fig. 3—Typical 198-mc lunar echo.

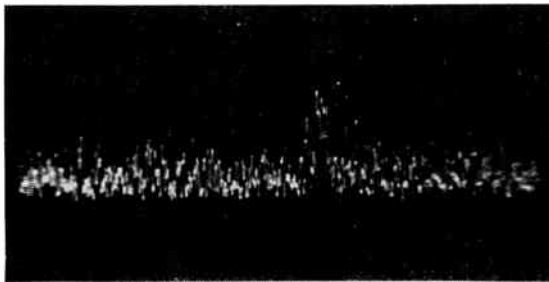


Fig. 4—A short 198-mc lunar echo.

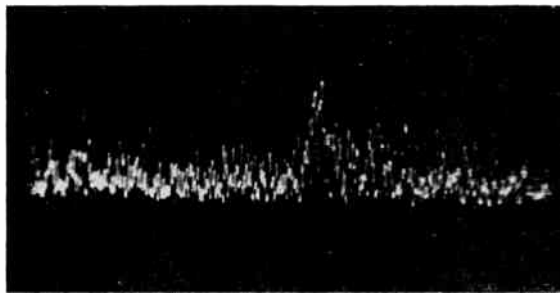


Fig. 5—A long 198-mc lunar echo.

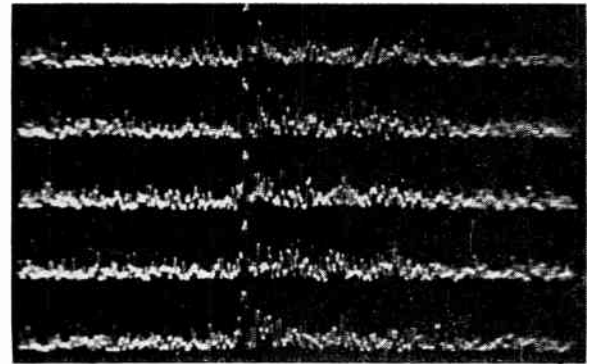


Fig. 7—Lunar echoes spaced 0.1 second apart.

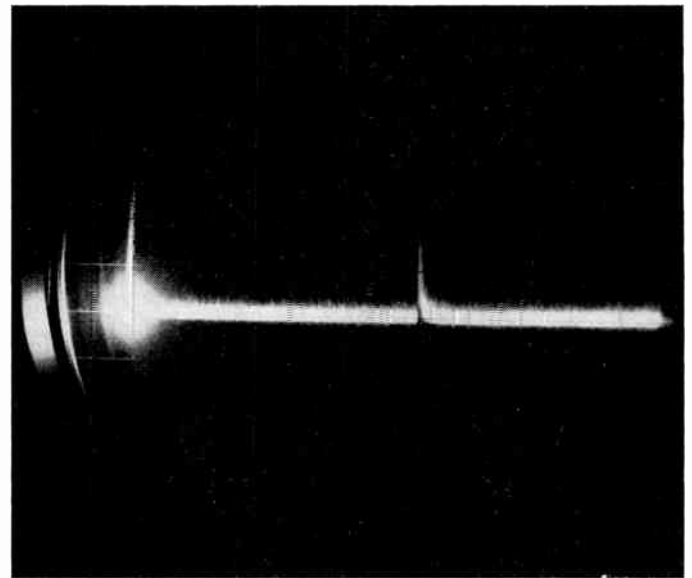


Fig. 8—Fifty superimposed lunar echoes.

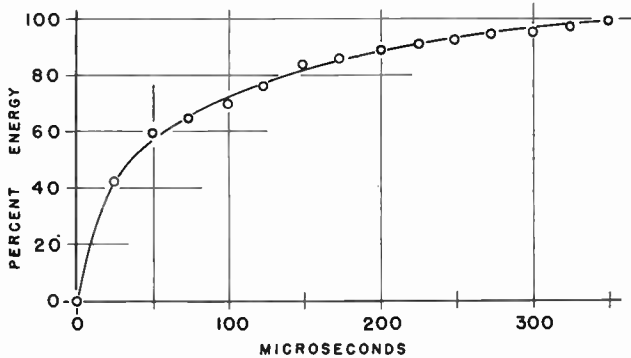


Fig. 6—Relative energy as a function of time.

tive check of target identification aside from range measurements. Visual observation of the echo gives the impression that several fixed or slowly moving echo areas exist following the first high-amplitude return. At signal-to-noise ratios of 12 db, the maximum delay of such echoes behind the leading edge was about 500  $\mu$ sec or 600  $\mu$ sec. With signal-to-noise ratios of 20 to 24 db, the delay was as great as 1000  $\mu$ sec.

Fig. 8 is a time exposure of an A-Scope radar trace

showing the superposition of 50 moon echoes from a train of 10- $\mu$ sec pulses. The transmitter peak power was 1.2 megw; the pulse rate was 15 per second which placed some 39 pulses "in flight" at all times. The bandwidth of the receiver was adjusted to provide maximum signal-to-noise ratios without disturbing the envelope of the signal. For this case the bandwidth is near 100 kc and the signal-to-rms-noise ratio is near 20 db. Note that none of the 50 returns falls to the baseline.

Theoretical considerations by early workers based on a rough reflector had predicted that the echo from so short a pulse would have a fast rise but a slow fall. Since the limb of the moon is some 1080 miles farther away than the closest point, the echo should persist for about 11.6 milliseconds which is the time required for the extra 2160-mile round trip to the limb. Actually, the theory indicates that after ten milliseconds the echo would drop out of sight into the noise if the peak level were only 20 db above the noise. Fig. 9 shows the theoretical signal as calculated from the US Army's Red Bank work.<sup>8</sup> Above and below the theoretical signal are two examples of the experimental signal at the same

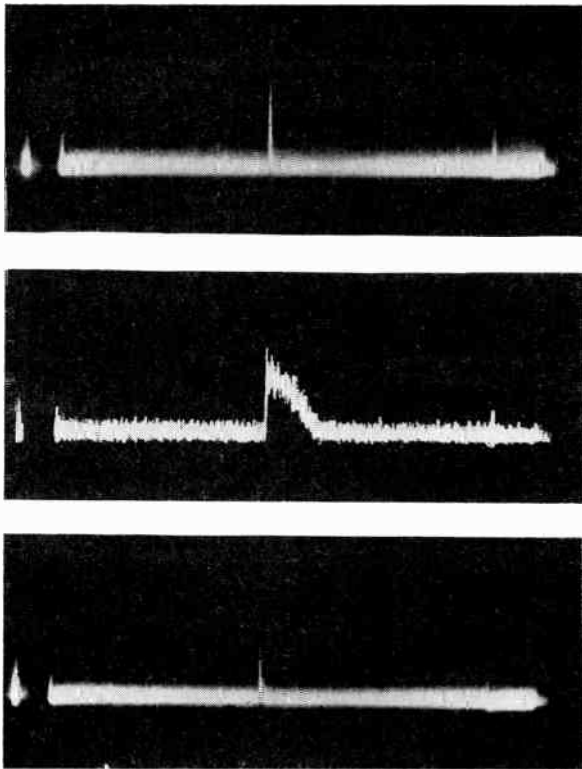


Fig. 9—Comparison of theoretical and two experimental lunar echoes.

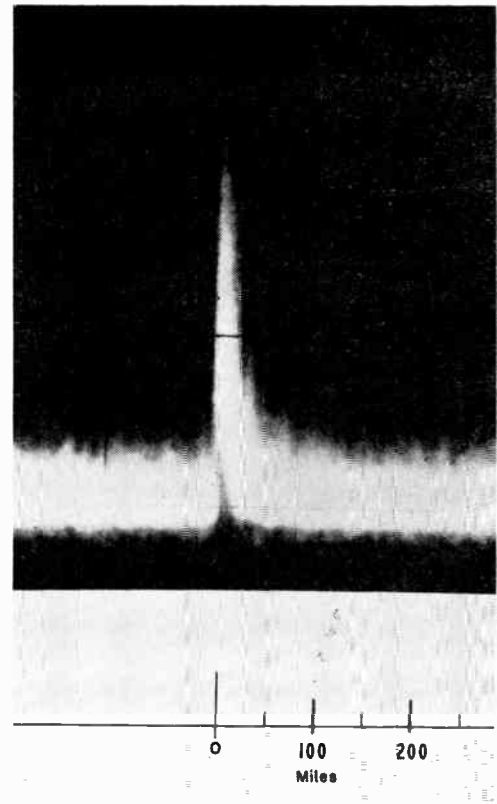


Fig. 10—Lunar echo length in miles.

signal-to-noise ratio. Experimentally there seems to be little echo left at the end of one millisecond and most of the return is in the first 100  $\mu$ sec. While the old theoretical model indicated a circuit bandwidth of 50 cps, the experimental results indicate that possibly a 10,000-cps band exists.

Fig. 10 is an enlargement of the echo trace with a radar range scale in miles below it. As can be seen, the most distant echoes are only 100 miles beyond the leading edge. Fig. 11 shows an A-Scope photograph with the leading edge of the moon drawn to scale below. The echoes that come from 100 miles farther back than the leading edge must lie in a circle 900 miles in diameter or a circle having a diameter somewhat less than half that of the moon. That part of the echo that contains the first 50 per cent of the reflected power comes from the first five miles of "depth" or a circle only 210 miles in diameter which is almost exactly one-tenth the diameter of the moon. Thus, half the power in the echo is confined to a small "highlight" approximately three minutes of arc in diameter.

All of the previous discussion assumed that the echo is formed at the nearest point on the moon and not by some peculiar formation elsewhere on the surface. Elaborate attempts were made to resolve this problem of the reflection point location by measuring the radar range very accurately. This was done with the crystal-controlled counters described earlier. The method did not prove practical at the time, since the complex problems of earth-moon mechanics were strained to achieve the necessary absolute accuracy in computed range. The

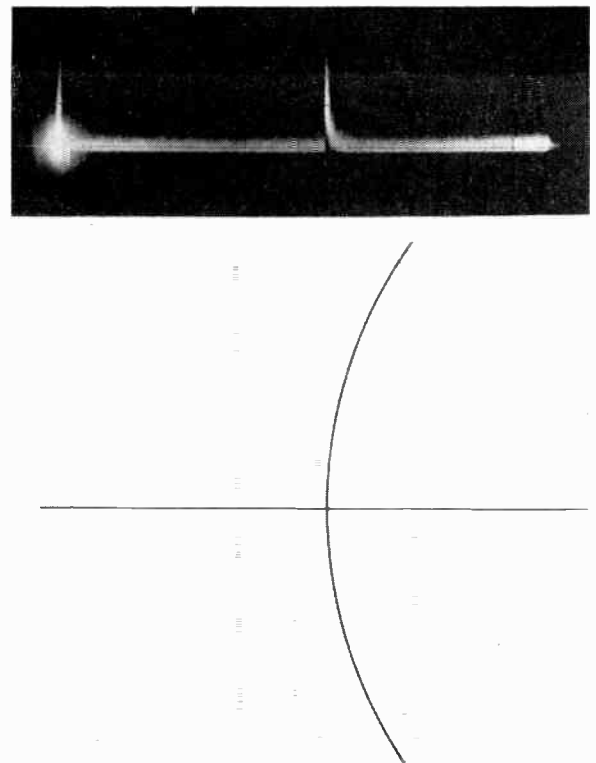


Fig. 11—Lunar echo compared in scale to curvature of the moon.

measurements of range made on October 22, 1951 indicated a radio transit time of 2.64793 seconds at 1310 universal time. Recent calculations of the transit time of the 1951 test made on the Navy's EXOS IBM 650

computer indicate values varying from 2.64791 to 2.64795 seconds or a difference of 20  $\mu$ sec which is a range error of about 2 miles. After the first five days of work in 1951, the transit time tests were discontinued with only rough checks being made through 1953. The trend seemed to indicate positive errors in range with some errors running into the milliseconds. Possibly this investigation could lead into many interesting fields, such as a means of studying the density of matter in the earth-moon space and refined measurements of the earth-moon geometry. The paper by Yaplee, *et al.*,<sup>20</sup> describes the work now underway at the Naval Research Laboratory in these fields.

In all of the short-pulse echo work the leading edge of the echo was sharply defined with no evidence of a precursor. This led to the assumption that the sharp rise point was, in fact, the nearest point to the earth on the moon's surface. This conclusion would suggest that no special or peculiar surface phenomenon is responsible, since it is extremely unlikely that such a surface area would correspond exactly to the moon center as seen from the earth. One exception to this assumption is the possible existence of a tidal bulge on the moon facing the earth. Such a bulge, if it exists, might tend to sharpen the echo, but the maximum height calculated for such a bulge is too small to appreciably modify the reflecting properties of the surface. The theory of a remelt surface proposed by some selenologists may help to account for the echoes observed. Such remelts are described as starting beneath the surface in the moon's geological past then breaking through and flooding the valleys and crater floors leaving only the highest mountains and crater rims projecting above the ocean-like lava seas which later cooled providing large areas that have only slightly roughened with time. These large smooth areas may provide the predominant echo completely overshadowing the random scattering from the mountains and crater walls. Fig. 12 is a photograph of the central area of the moon. The short echo results are not incompatible with measurements taken from the air above the surface of the earth. For example, Grant and Yaplee<sup>21</sup> have shown that dry desert-like terrain also produced a bright or "highlight" spot directly below the observing position. In the companion paper by Yaplee, *et al.*,<sup>20</sup> it is shown that this bright spot exists on the moon at 3000 mc which is a frequency approximately 15 times higher than the one used for the results shown here. The consistency of results over such a wide range of frequencies is interesting.

The fact that the echo seems to be different in shape from that predicted would suggest that the echo amplitude might also be different than predicted. The circuit loss was carefully measured and found to be 271 db between an isotropic radiator and collector when 10- $\mu$ sec



Fig. 12—Central area of the moon.

pulses were used at a frequency of 198 mc. This value is 17 db more loss than the average value of 254 db obtained by other investigators working near the same frequency with very long pulses. This additional loss for short pulse signals has been called modulation loss and results from the interference within the modulation cycle caused by echo components returned from reflection areas separated by distances large compared with the wavelength of the modulation frequency. The DeWitt-Stodola rough moon theory<sup>8</sup> predicted a 27-db loss for a 10- $\mu$ sec pulse compared to the longer pulses which completely engulf the moon. This is 10 db more than the 17 db indicated by measurements. To check the measuring techniques used, a 100-watt cw transmitter was placed in the system as a substitute for the larger pulse transmitter. A circuit loss of 252.5 db, only 1.5 db from the average of other workers, was found. The loss resulting from modulation by 10- $\mu$ sec pulses while using the same terminal equipment as was used for cw, except for the transmitter, was 18.5 db which is still 8.5 db less loss than predicted theoretically. The relatively good check between the cw work of others and the work reported here places some confidence in the pulse measurements. A review of all available data on the earth-moon-earth circuit loss indicated that the loss from an isotropic radiator on the earth to the moon and back to an isotropic collector on the earth increases at 6 db per octave from 20 mc to 3000 mc passing through 258 db at 300 mc. An uncertainty of 4 db covers most data. The signal levels given here are taken from the maximum echo levels. This level is quite constant if polarization

<sup>21</sup> C. R. Grant and B. S. Yaplee, "Back-scattering from water and land at centimeter and millimeter wavelengths," *PROC. IRE*, vol. 45, pp. 976-982; July, 1957.

and selective fading effects are eliminated. The polarization problem is primarily one of Faraday rotation as described by Murray and Hargreaves,<sup>15</sup> while selective fading manifests itself as signal level changes only for very narrow-band transmissions where it can be overcome by frequency diversity. At frequencies above 198 mc, no unaccounted-for long period fading has been observed. At frequencies below 30 mc where the ionosphere is very important, many unexplained fades are observed. Experience at the Naval Research Laboratory between 30 mc and 198 mc is as yet too limited to report on here. It is believed that many reports of long periods of low-signal level were due to polarization rotation or excessive ionospheric disturbance at near horizon transmission angles. A detailed analysis of the available data on transmission loss will be published soon.

To study further the cw signal characteristics, a local oscillator was provided to beat against the returning signal. The predicted Doppler shift caused by the relative motions of the earth and the moon was observed and the note was steady and clean. In Fig. 13 there is an audio frequency spectrograph of one such echo. The transmitter was started five seconds to the left of the section shown. At time 0 the transmitter was cut off and during the remaining 2.6 seconds the echo was received. Notice the Doppler shift in frequency, the high signal-to-noise ratio, and the steadiness of the signal. The upper trace is made with a narrow-band scanning filter providing frequency resolution. The lower trace is made with a broad-band filter to give time resolution.

Amplitude modulated signals were passed over the circuit first with fixed tones and later with frequency-

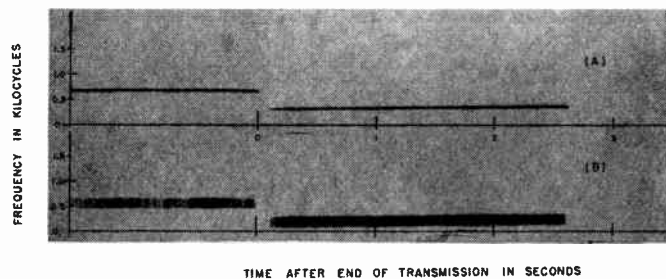


Fig. 13—Audio spectrograph of lunar echo.

sweeping signal generators as modulators. Attempts were successfully made in 1954, to send cw and modulated cw code over the circuit using the same basic 100-watt transmitter. Finally, voice transmissions were tried using amplitude modulation and a receiver bandwidth of 3 kc. The mean snr for these voice tests was near 14 db. Within the limitations of analysis possible with low-snr amplitude modulated signals no detectable loss of intelligence was noted. The voice was perfectly recognizable and there was no evidence of reverberation.

#### ACKNOWLEDGMENT

The outstanding work of many Naval Research Laboratory personnel made this experiment possible. The author particularly wishes to acknowledge the fine instrumentation work of R. A. Carpenter and the transmitter work of A. Q. Tool. A. B. Youmans carried out the range calculation check with the assistance of the Navy's EXOS computer staff and J. Ihnat did the energy-time studies. Throughout the program L. C. Young and H. O. Lorenzen have provided encouragement, advice, and support.



# Radar Echoes from the Moon at a Wavelength of 10 CM\*

B. S. YAPLEE†, MEMBER, IRE, R. H. BRUTON†, K. J. CRAIG†, AND N. G. ROMAN

**Summary**—Radar contact has been made with the moon with short pulses at 2860 mc, beginning a program of short-pulse lunar radar. The principal objective of the program is to obtain more accurate moon-to-earth distances than presently are known. Other information may result from the program, such as the earth's diameter, the interplanetary electron density, and the lunar surface characteristics. To date, the program has yielded the following results: earth-moon distances have been measured over several days with consistencies of less than one-half mile; several rough reflectivity measurements have been made which indicate that the radar cross section of the moon is 975 square miles at 2860 mc with pulses of 2- $\mu$ sec duration, and the fine structure of echoes may be correlated with lunar topography.

## INTRODUCTION

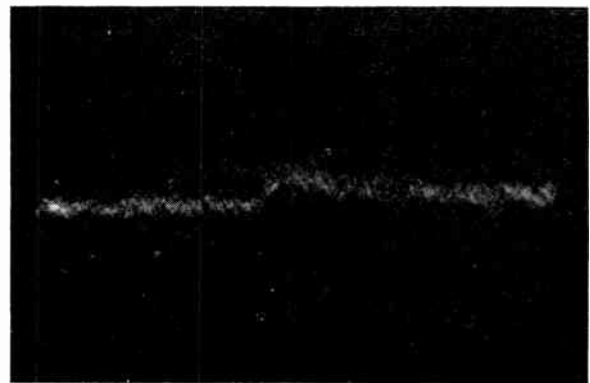
ATTEMPTS to obtain radar echoes from the moon have had a long history. The U. S. Army Signal Corps<sup>1,2</sup> first reported successful radar contact with the moon in 1946. In the same year, Bay<sup>3</sup> of Hungary, working in comparative isolation, also was successful. He used a novel electrolytic signal-output integrator to obtain increased sensitivity. In 1951, Kerr and Shain<sup>4</sup> at 20 mc showed the importance of fading due to libration of the moon and to ionospheric effects. Fading caused by Faraday rotation of polarization of the pulse was discovered by the group at the University of Manchester<sup>5</sup> in 1954. At the 1957 URSI meeting Trexler<sup>6</sup> reported experiments made in 1951 at the Naval Research Laboratory which indicated that the moon was not as rough a reflecting surface as had been thought, but was sufficiently smooth to produce almost specular reflections. Lovell,<sup>7</sup> at the same meeting, reported that the main scattering of the radio waves takes place from a small area on the visible hemisphere of the moon with a radius of about one third the moon's radius.

In 1956, the Radio Astronomy Branch of NRL started a program to determine: 1) the feasibility of ob-

serving echoes from the moon with a radar operating at a frequency of 2860 mc using 2- $\mu$ sec pulses, and 2) how accurately the radar distance to the moon could be measured. Using a high transmitter frequency, the difficulties of fading encountered at lower frequencies would be lessened. Preliminary results indicate that the radar distance may be measured to within 1000 to 2000 feet.



(a)



(b)

Fig. 1—(a) First echo from the moon at S band (arrow), and (b) expanded sweep of echo. (Fifty- $\mu$ sec postdetection integration used.)

\* Original manuscript received by the IRE, November 8, 1957.

† Radio Astronomy Branch, U. S. Naval Research Lab., Washington, D. C.

<sup>1</sup> J. Mofensen, "Radar echoes from the moon," *Electronics*, vol. 19, pp. 92-98; April, 1946.

<sup>2</sup> J. H. Dewitt, Jr. and E. K. Stodola, "Detection of radio signals reflected from the moon," *PROC. IRE*, vol. 37, pp. 229-242; March, 1949.

<sup>3</sup> Z. Bay, "Reflection of microwaves from the moon," *Hung. Acta Phys.*, vol. 1, pp. 1-22; April, 1946.

<sup>4</sup> F. J. Kerr and C. A. Shain, "Moon echoes and transmissions through the ionosphere," *PROC. IRE*, vol. 39, pp. 230-242; March, 1949.

<sup>5</sup> W. A. S. Murray and J. K. Hargreaves, "Lunar radar echoes and the Faraday effect in the ionosphere," *Nature, London*, vol. 173, pp. 944-945; May 15, 1954.

<sup>6</sup> J. H. Trexler, "Lunar radio echoes," this issue, p. 286.

<sup>7</sup> A. B. C. Lovell, "British Work Carried Out in Radio Astronomy Since 1954," presented at URSI XIIth General Assembly, Boulder, Colo.; 1957.

## RESULTS

### The Signal (Circuit Loop Loss)

The first objective was met when radar contact was made on the morning of February 24, 1957. Fig. 1 shows the radar echo with 50- $\mu$ sec postdetection integration as photographed on that morning. One must remember, as he views these pictures, that the echo he sees was transmitted some 600 pulses before the transmitter pulse shown. The magnitude of this echo as compared to the signal generator pulse is  $-108.3$  db; the minimum detectable signal is  $-114.3$  db. The average peak power of the magnetron as measured on a power bridge is 2.3

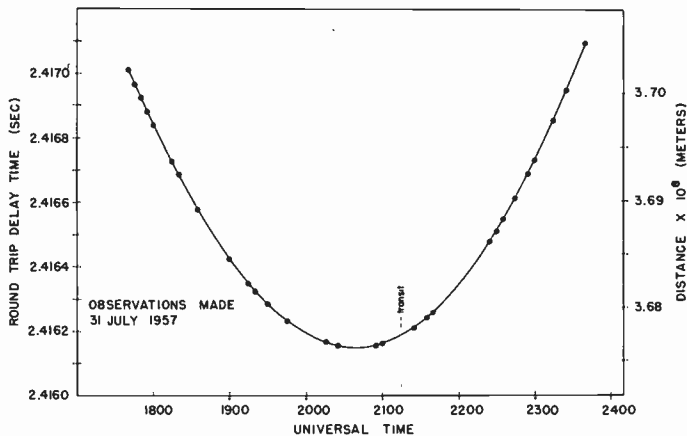


Fig. 2—Distance to the moon as measured by radar for a single six-hour observation period.

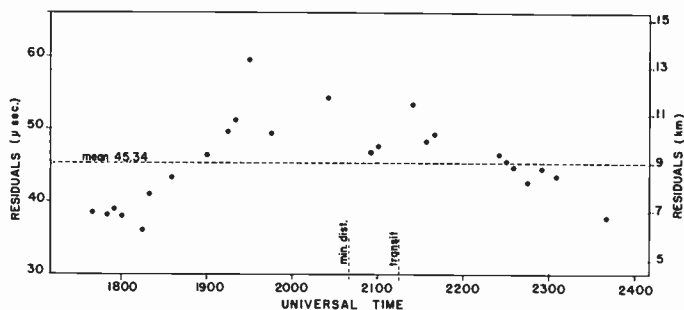


Fig. 3—Distance residuals, the differences between the observed and calculated distance.

megawatts. Thus the calculated loss from the transmitter to the moon and back to the receiver, using the 50-foot parabolic antenna, is 200 db, with an uncertainty of 4 or 5 db. For this particular loop loss, the radar cross section<sup>8</sup> of the moon is 975 square miles for a 2-μsec transmitter pulse.

The peak signal returned is about 5 db higher than that predicted by Dewitt and Stodola.<sup>2</sup> This increase in received signal agrees with the specular reflection characteristics of the moon as reported by Trexler<sup>6</sup> and Lovell.<sup>7</sup> As early as 1929,<sup>9</sup> if not earlier, predictions were made that the moon is covered with a layer of dust or small particles. It is interesting to note, as reported by Grant and Yaplee,<sup>10</sup> that dry sandy soil also exhibits specular reflection characteristics for microwave frequencies at normal incidence.

Results of Ranging

The second phase of this experiment has just commenced and preliminary results are very encouraging. The result of one day's observations are reported here to indicate the potentialities, but specific conclusions should not be drawn until observations over several lunar cycles have been obtained.

Shown in Fig. 2 is the measured distance as a function of time. The minimum distance is displaced from the time of transit (meridian passage) as a result of the elliptical orbit of the moon. The observed distances are compared with the computed distances, and the residuals are shown in Fig. 3. There are two apparent features in the residuals: 1) They are all positive, indicating a possible systematic error, and 2) they seem to deviate systematically from a straight line. For the sake of discussion a mean is shown; the rms deviation of a

single observation from this mean is 5.6 μsec, which indicates an accuracy of the order of a half mile. These residuals were determined from 0.1-second samples of the echo. Observations of the return show that the leading edge of the echo actually disappears into the noise for several seconds at a time. This fluctuation of the leading edge accounts for a large percentage of the scatter of the residuals shown in Fig. 3. However, if one analyzes one-minute samples of the returned signal, the actual leading edge of the echo may be determined and the distance measured more accurately.

Fig. 4 shows the geometry from which the distance to the moon was calculated. The following outline indicates the constants and parameters used.

- $c = 299,792.8$  km velocity of light,<sup>11</sup>
- $a = 6,378,270$  m equatorial radius of earth,<sup>12</sup>
- $b = 1,740,000$  m equatorial radius of moon,<sup>13</sup>
- $r = 6,369,910$  m radius of the earth at NRL,<sup>14</sup>
- $\pi =$  horizontal parallax of the moon,<sup>15</sup>
- $\phi = 38^{\circ}49'18.9''$  N geocentric latitude of NRL's 50-foot antenna,
- $\lambda = 77^{\circ}01'36.7''$  W longitude of NRL's 50-foot antenna,
- $\gamma =$  hour angle of the moon, and
- $\Delta =$  distance from observer to the surface of moon.

The reductions and calculations of the instantaneous distances of the moon are being done on an IBM 650.

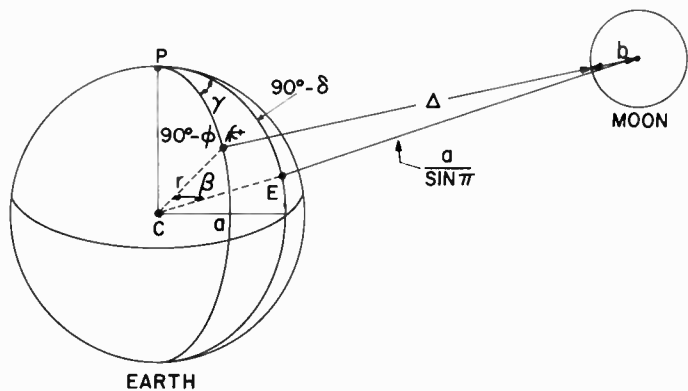
It is interesting to note that the distance from the center of the earth to the center of the moon is determined by

$$\frac{a}{\sin \pi}$$

where  $a$  = equatorial radius of the earth and  $\pi$  = horizontal parallax of the moon. Sin  $\pi$  is of the order of 0.02

<sup>8</sup> D. E. Kerr, "Propagation of Short Radio Waves," M.I.T. Rad. Lab. Ser., McGraw-Hill Book Co., Inc., New York, N. Y., vol. 13; 1951.  
<sup>9</sup> E. Epstein, "Settling of gases and constitution of the atmosphere," abstract, *Phys. Rev.*, vol. 33, p. 269; February, 1929.  
<sup>10</sup> C. R. Grant and B. S. Yaples, "Back scattering from water and land at centimeter and millimeter wavelengths," *PROC. IRE*, vol. 45, pp. 976-982; July, 1957.

<sup>11</sup> J. F. Mulligan and D. F. MacDonald, "Some recent determination of the velocity of light," *Amer. J. Phys.*, vol. 25, pp. 180-192; March, 1957.  
<sup>12</sup> Obtained from the U. S. Army Map Service.  
<sup>13</sup> Value obtained from C. W. Allen, "Astrophysical Quantities," Univ. of London, The Athlone Press, England; 1955.  
<sup>14</sup> Calculated from a formula in "The American Ephemeris and Nautical Almanac," Government Printing Office.  
<sup>15</sup> Taken from "Improved Lunar Ephemeris, 1952-1954," Government Printing Office, Washington, D. C.



$$(\Delta + b)^2 = r^2 + \frac{a^2}{(\sin \pi)^2} - \frac{2ra}{\sin \pi} \cos \beta$$

$$\cos \beta = \sin \phi \sin \delta + \cos \phi \cos \delta \cos \gamma$$

$$\Delta = -b + \sqrt{r^2 + \frac{a^2}{(\sin \pi)^2} - \frac{2ra}{\sin \pi} \cos \beta}$$

$$\frac{2\Delta}{C} = N \times (\text{pulse repetition period}) + \text{delay}$$

Fig. 4—Diagram of the earth-moon distance problem.

or less and any error in the value of *a* is multiplied by a factor of 50 or more. Since there is a large systematic error in our one day's result, the value of *a* was changed from 6,378,270 meters<sup>14</sup> given by the Army Map Service to 6,378,388 meters<sup>15</sup> given by the American Ephemeris in subsequent computations and the resultant systematic error then reduced to near zero.

Fig. 5 shows a nine-second sample of the recorded data. The pictures were taken at one-second intervals with about 26 traces per picture. The sweep length used is 260 μsec. No electrical integration was used so that fine structure in the echo is preserved. Sporadic structure has been seen as far as 400 μsec from the leading edge of the echo. No attempt has been made to correlate the fine pulse structure with the topography of the moon or with other phenomena.

The average peak amplitude of the return signal is about 7 db above noise. This average has on occasion gone up to 12 or 13 db for several hours at a stretch, and at other times has dropped to 4 or 5 db for even longer periods. However, in over 100 hours of observation there has never been a complete loss of the signal that could not be attributed to malfunctioning of the equipment. No serious effort has been made to correlate this apparent fading with atmospheric conditions or sunspot activity. However, during periods of extremely heavy rains the signal appears enhanced by several db and in the last instance of heavy rain the signal received was about 16 db above the noise.

The return echo is composed of a large number of individual spikes; however, when viewed on fast camera film, the number of spikes seems to average about four or five for each transmitter pulse. Each spike has a width of from 2 to 4 μsec, and the spacing between spikes varies from 2 to 20 μsec during visual observation of the echo. An individual spike within the first 10 μsec

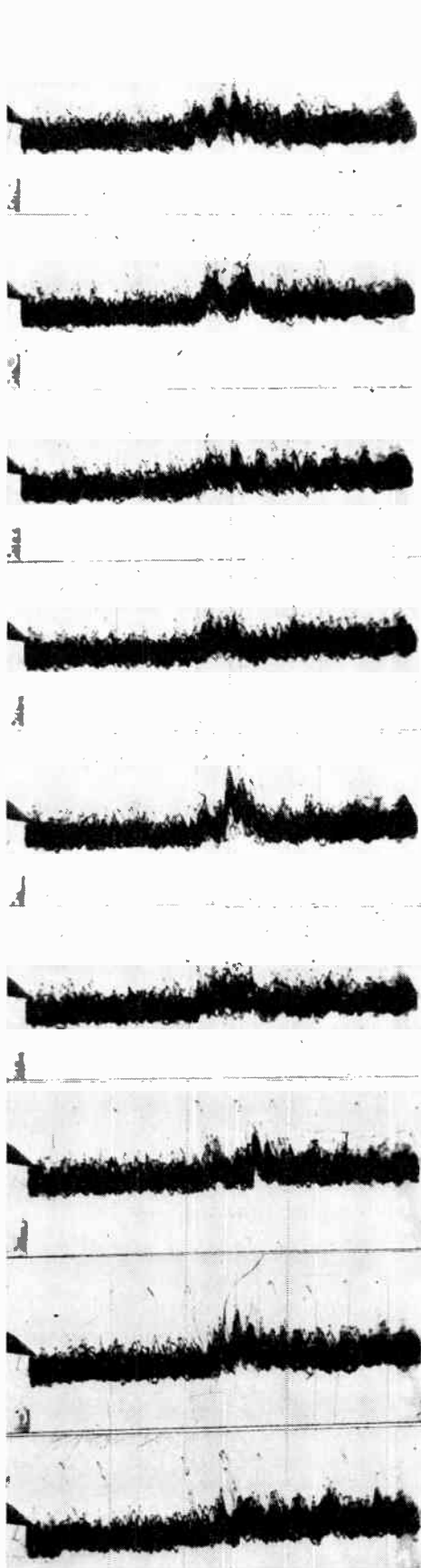


Fig. 5—Nine-second sample of recorded data which illustrates fluctuations and fine structure. (Sweep length 260 μsec.)

of the returned signal may persist for as much as one second and may disappear into the noise for several seconds. The fluctuation rate appears to increase linearly with range and is about doubled for signals 10 to 20  $\mu\text{sec}$  from the leading edge and perhaps tripled for signals at 30 to 40  $\mu\text{sec}$ , etc. This effect perhaps is caused by changes due to libration, in the multiple interference among several strong scattering areas on the moon.

#### DETERMINATION OF THE NUMBER OF IN-FLIGHT PULSES

It is necessary to determine the number of in-flight pulses,  $N$ , that is, the number of pulses which have left the transmitter since the one whose echo is being observed in order to calculate the radar distance. Conventional astronomical methods can determine the distance to the moon within a few miles and certainly well within the 400-mile uncertainty to which an ambiguity in  $N$  would lead. Hence,  $N$  can be determined from the computed distance to the moon, and arrangements have been made to do this as part of the data reduction procedure. However, if the ion density between the earth and moon were sufficiently large, the velocity of propagation of the pulses might be sufficiently less than their velocity of propagation in a vacuum to affect the computation of  $N$ .

Two methods have been used to determine  $N$  observationally. In one, the transmitter is turned off while a fast camera is used to photograph individual sweeps on the scope. The number of sweeps between the last transmitter pulse and the last received echo is  $N$ . The low signal-to-noise ratio makes this method marginal, but the observed values agreed with the calculated ones.

In the other method, the pulse repetition period is decreased by 10  $\mu\text{sec}$ . If one changes the period ( $p$ ) from 4000  $\mu\text{sec}$  to ( $p'$ ) of say 3990  $\mu\text{sec}$ , the  $N$ th pulse will move with respect to the echo at a rate of 2500  $\mu\text{sec}$  per second, for approximately 2.4 seconds. The echo which one sees on an oscilloscope will appear to move to the right through one or two ( $n$ ) transmitter pulses. When the echo stops, one may record a new value of delay ( $d'$ ); the total ranging time will now be

$$T = (N + n)p' + d'.$$

Now if one determines by interpolation on the film recording what the value of  $d$  would have been at the instant he recorded  $d'$ , he may evaluate the integer  $N$  from

$$Np + d = (N + n)p' + d'.$$

#### EQUIPMENT

The radar is located in NRL's 50-foot radio telescope. (See Fig. 6.) To avoid the use of rotary joints, the transmitter is mounted on beam girders behind the paraboloid as in Fig. 7. Since the magnetron, type QK 428, must operate within 15° of a horizontal position, the



Fig. 6—Antenna used in obtaining radar echoes from the moon at S band.

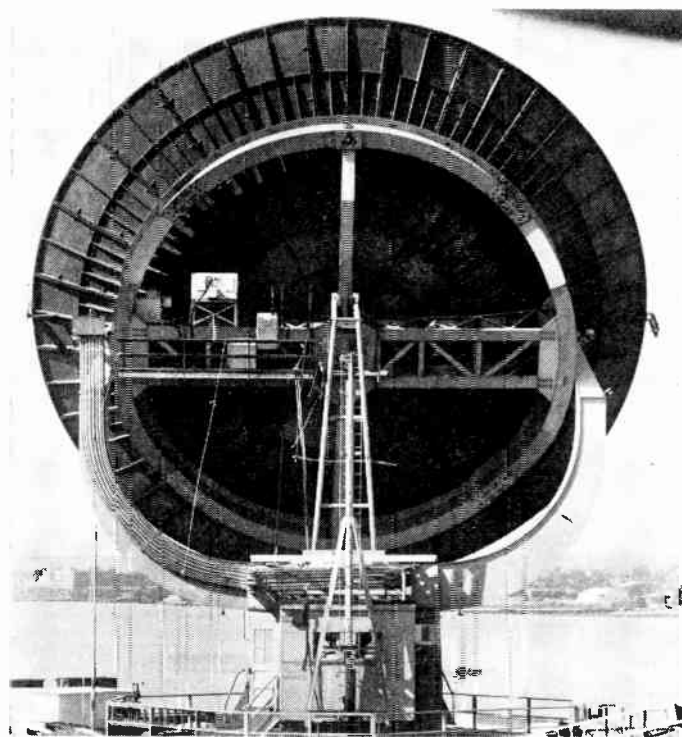


Fig. 7—View of equipment mounted on back of the 50-foot antenna.

transmitter was tilted 30° on its mount, thus permitting observations between 15° and 45° elevation. Rotary joints probably will be used in the future for more extensive observations. The telescope is driven to compensate for the rotation of the earth but manual corrections

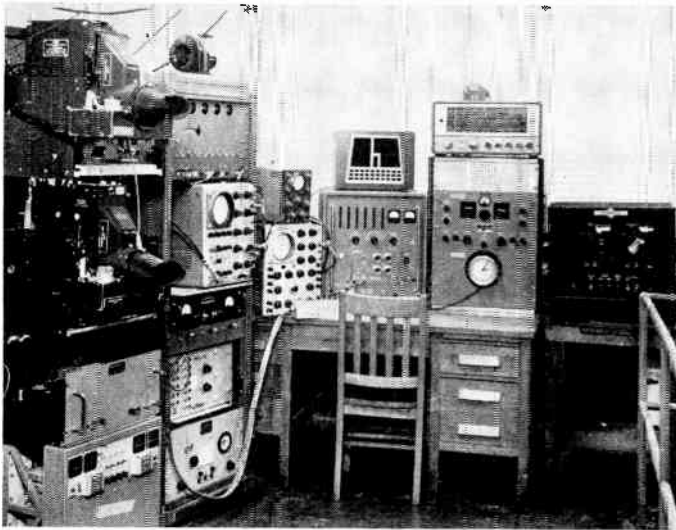


Fig. 8—Timing, monitoring, and camera recording equipment.

to its pointing are necessary to allow for the motion of the moon with respect to the stars.

A highly stable pulsing system was developed for this radar. The video display on the *A* scopes is triggered by a synchronizing pulse *N* periods later than the one whose echo is displayed. With a pulse repetition rate of 250 pps and the distance between the earth and the moon of about a quarter million miles, *N* is of the order of 500 to 700. Therefore, it is necessary for the pulsing system to have low jitter and high-frequency stability. All timing and pulse circuits are derived from a highly stable 100-kc frequency standard; count-down circuits provide the pulse repetition rate and one-second markers. The basic frequency source, which is stable to better than one part in  $10^8$  per day, is converted into pulses and one pulse is gated out at a regular interval for the synchronizing pulse. The one-second pulses, which key all counters and cameras, are phased to coincide with the WWV second marks. The moon echoes displayed on

the *A* scopes are photographed on 35-mm film 30  $\mu$ sec after the WWV-second with an exposure of 110 msec (26 pulses). Fig. 8 shows the equipment used.

The conventional superheterodyne receiver used with this radar system includes a balanced mixer input, a preamplifier, and an IF amplifier with a 350-kc bandwidth. At the outset of this experiment, an 8-db noise figure was achieved using 1N21E crystals, but leakage of the high peak power caused the crystals to deteriorate rapidly and it was impossible to maintain a good noise figure. This problem was solved by placing a low-noise traveling-wave amplifier (RCA 6861) between the tube and the balanced mixer. The power limiting feature of the traveling-wave tube prevented crystal burnout and maintained a consistent noise figure.

#### CONCLUSION

The preliminary results of short-pulse microwave radar of the moon are presented. Indications are that ranging the moon is entirely possible with a high degree of accuracy. A distance accuracy of better than a half-mile seems possible. A determination of the earth's equatorial diameter and NRL's distance from the axis of the earth can be made. The shape of the earth could be determined by similar observations at many points on the surface of the earth.

#### ACKNOWLEDGMENT

The authors express their appreciation to R. H. Larsen and J. J. McCullough, of EXOS Data Processing Branch, Navy Department Administrative Office, for their help in programming and processing the data. They also thank D. G. Chase for his extensive contributions to the preliminary phases of this program; the Wave Propagation Branch of the Naval Research Laboratory for the loan of its oscilloscope and photographic recording equipment, and Dr. J. L. Pawsey and Prof. F. T. Haddock for their valuable comments.



# The Use of Radio Stars to Study Irregular Refraction of Radio Waves in the Ionosphere\*

H. G. BOOKER†, FELLOW, IRE

**Summary**—The observations and the theory of radio star scintillation are reviewed, and the following conclusions are reached.

1) The frequency variation of amplitude and phase scintillations agrees with theory.

2) All observers agree that there is a marked increase of amplitude scintillation with increase in zenith angle. The Cambridge data agrees with theory, but the Manchester data does not. No available zenith angle data is adequate to determine the height of scintillation.

3) The available observations of phase scintillation are inadequate for almost all purposes.

4) At present, the Hewish method of locating height by comparing amplitude and phase scintillation is seriously hampered by lack of satisfactory observations. On existing data the method gives heights that are spread over a range of about five to one; all of these heights are above the *E* region and refer to nighttime scintillation.

5) All observers agree that there is a maximum of amplitude scintillation in the middle of the night.

6) In addition, Australian observers report a maximum of amplitude scintillation at midday. This is only weakly observed, if at all, in the northern hemisphere, where, however, observational conditions are different.

7) Australian observers report maxima of amplitude scintillation at the solstices and minima at the equinox, but observers in the northern hemisphere report little seasonal variation.

8) The rate of scintillation increases under magnetically disturbed conditions, due to increased drift velocity.

9) There is a good general correlation between the occurrence of radio star scintillation and spread *F* reflections. This correlation suggests a value of the order of 250–300 km for the height of radio star scintillation at night.

10) There is some correlation between the occurrence of radio star scintillation and sporadic *E* reflections, especially in Australia.

11) The physical cause of the fluctuations in electron density associated with radar star scintillation is uncertain, but there is little doubt that some of the other phenomena involving irregularities of electron density in the ionosphere are due to turbulence.

12) The scale of irregularities of electron density at the level responsible for amplitude scintillations is of the order of a kilometer. The scale is probably somewhat greater parallel to the earth's magnetic field than transverse to the field.

13) The most striking puzzle in connection with radio star scintillation is the cause of the nighttime maximum.

## I. INTRODUCTION

SHORTLY after discovery was made of the existence of a discrete source of cosmic noise in the constellation of Cygnus, it was found that the strength of the source, as received at ground level in the vhf band, was variable. At first it was thought that this indicated a variation in the power radiated by the source. It was discovered, however, by Smith [16] and by Little and Lovell [17] that there was no correlation between the fluctuations received at two points on the ground sepa-

rated by a distance of the order of 100 km, although fairly good correlation was obtained when the receivers were separated by a distance of the order of a kilometer. This led to the identification of the cause of the fluctuations as irregular refraction in the ionosphere. Thus, study of the scintillation of radio stars is an important method for studying irregularities of electron density in the ionosphere, although it is not yet clear at what height in the ionosphere the irregularities principally responsible for radio star scintillations exist. This paper is a review of the experimental evidence concerning radio star scintillation and of the theory that so far has been developed to explain it.

## II. METHODS OF OBSERVATION

The fluctuation in the radiation from the discrete sources of cosmic noise, such as those in the constellations of Cygnus or of Cassiopeia, can be seen with equipment that in principle is simple, although in practice certain technical difficulties have to be overcome. A moderately directional antenna looking at the appropriate part of the sky is connected to a radio receiver having a bandwidth usually of the order of a megacycle. The video-frequency output from the receiver is connected to a pen recorder having a time constant usually of the order of one second. The effect of the finite bandwidth of the receiver and of the time constant of the recorder is to smooth out much of the noise fluctuation, so that a comparatively smooth trace is obtained. By pointing the antenna in different parts of the sky, different strengths of cosmic noise are recorded. If the antenna is directed at Cygnus or at Cassiopeia, then fluctuations in the curve frequently are observed at the rate of a few per minute. These are the fluctuations caused by irregular refraction in the ionosphere.

Roughly speaking, the irregular patches of electron density in the ionosphere cast shadows on the surface of the earth, and by measuring the size of these radio shadows, we may estimate the size of the irregularities in the ionosphere. This may be done by observing the scintillation at two spaced receivers. If the receivers are side by side, the fluctuations observed are identical. As the receivers are moved apart, the fluctuations that they record become progressively less correlated until, for sufficiently large spacings, there is no correlation at all. The distance between the receivers, when the correlation in the fluctuations has dropped to some specified value such as one-half, is a measure of the size of the irregularities of field strength over the surface of the earth; these in turn are related to the size of the irregu-

\* Original manuscript received by the IRE, October 14, 1957. Prepared under U. S. Signal Corps Contract No. DA-36-039-SC-72812.

† Cornell University, Ithaca, N. Y.

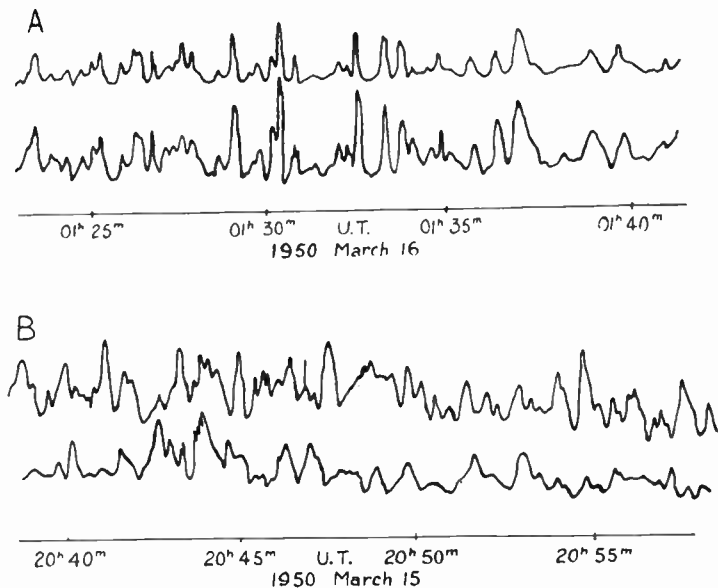


Fig. 1—Cassiopeia fluctuation records taken simultaneously by two receivers 11 km apart on a north-south base line. Records A: Correlation 0.9 (effective base line 4.1 km). Records B: No correlation (effective base line 7.7 km).

larities of electron density in the ionosphere. Fig. 1 shows examples of records taken by Little and Maxwell [4] at a pair of spaced receivers at the Jodrell Bank Experimental Station of the University of Manchester. Records A show good correlation between the fluctuations at the two receivers, while Records B show poor correlation.

Another way of observing the scintillation of radiation from discrete sources of cosmic noise is to measure the fluctuation in the phase difference of signals arising at two spaced receivers. The fluctuations in this phase difference may be interpreted as a flicker in the direction of arrival. The best way of doing this is to use the phase-switching interferometer invented by Ryle [1]. The phase-switching interferometer eliminates the effect of a uniform background of cosmic radiation in the sky from the presentation, and also has a number of other advantages. If the two antennas have a spacing large compared to the radio wavelength and are connected in phase, they have a polar diagram such as that indicated by curve *a* in Fig. 2. If, on the other hand, the antennas are connected in antiphase, then they have a polar diagram of the type indicated by curve *b* in Fig. 2. By suitable electronics, it is possible to record the difference between the power received by the interferometer when the antennas are connected in phase and that received when they are connected in antiphase. As the radio star moves through the polar diagram of the interferometer, we obtain records as shown in Fig. 3. Where the trace crosses the reference line in Fig. 3, reception by the interferometer in the two switch positions is identical, and the radio star is at one of the angles in Fig. 2 where curve *a* crosses curve *b*. Flicker in the angle of arrival of the radiation thus will cause an irregular variation in

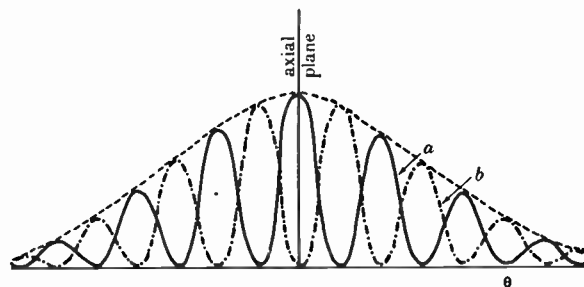


Fig. 2—Reception pattern of two spaced antennas: (a) connected in phase and (b) connected in antiphase.

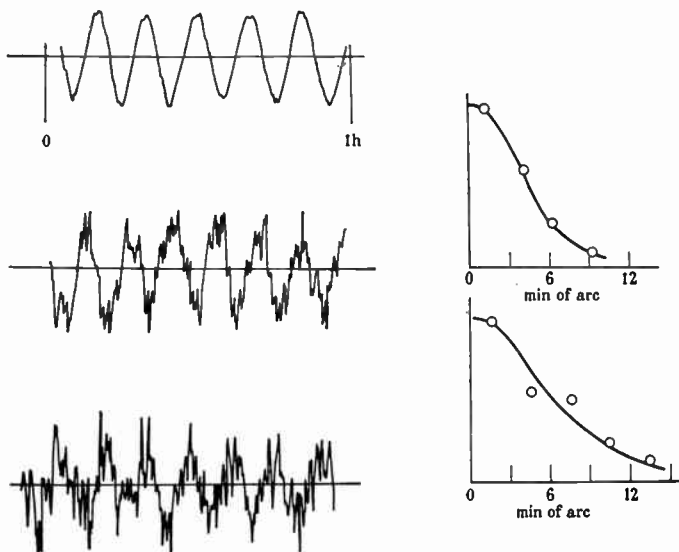


Fig. 3—Typical records of source 23.01 made with a high resolution interferometer on 8 m. The angular deviation deduced from the records is shown on the right.

the spacing between the zero points in Fig. 3. By measuring the irregularity in the crossing points, we may deduce the probability distribution of the flicker in the direction of arrival as shown on the right-hand side of Fig. 3.

A phase-switching interferometer, besides measuring the angular flicker in the direction of arrival, also measures the fluctuation in the amplitude of the radiation received from the source. This is illustrated in Fig. 4, where the results of the analysis of two records for probability of amplitude distribution are shown.

Wild and Roberts [12] have developed the above methods so that observations can be made almost simultaneously over the frequency range from 40 to 70 mc per second. This has been done by sweeping across the band in one-eighth of a second with a receiver having an acceptance bandwidth of half a mc per second. Rhombic antennas were used to achieve the necessary bandwidth. Presentation was on a cathode ray oscilloscope, with frequency varying in the vertical direction from 40 to 70 mc per second and time in minutes varying horizontally as shown in Fig. 5. Fig. 5 shows, by means of sketches, the various types of record obtained.

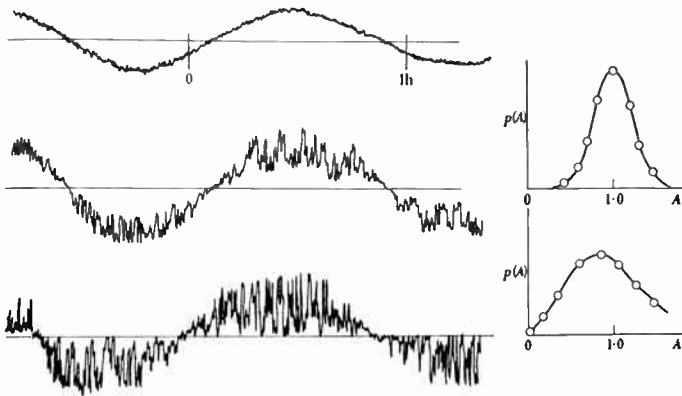


Fig. 4—Observations of the intensity fluctuations of source 23.01 made with a phase-switching receiver on 6.7 m. The probability distribution of amplitude  $p(A)$  deduced from the records is shown on the right.

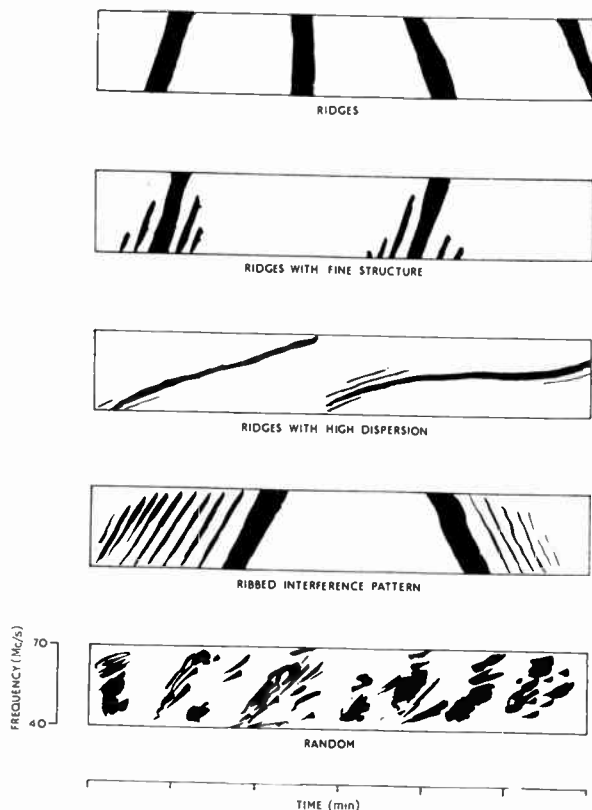


Fig. 5—Sketches showing idealized examples of the principal types of dynamic spectra observed.

### III. OBSERVATIONAL RESULTS

The intensity of radio star scintillation is likely to vary with 1) the radio frequency at which the observations are made, 2) the time of day, 3) the season of the year (and possibly the year in the sunspot cycle), and 4) the zenith angle of the source under observation. It also is necessary to make a study of the rate of scintillation and of the way in which it varies with the same parameters. Moreover, study also is required of the size, shape, and drift of irregularities of field strength over the surface of the earth, so that deductions can be made

about the size, shape, and drift of irregularities of electron density in the ionosphere. To aid in the determination of the height in the ionosphere at which the scintillation occurs, separate studies are required of the phase and amplitude scintillations at the ground.

Our knowledge of radio star scintillation depends mainly upon observations made at Cambridge, England, at Manchester, England, and at Sydney, Australia, although work has also been done in a number of other countries. In comparing the observations of these workers it should be noticed that the conditions of observation are substantially different at Cambridge, Manchester, and Sydney. At Cambridge, the antennas were well adapted for high angular resolution. The antennas were not, however, well adapted, or at any rate were not used, for measurements at low angles of elevation. Thus, Cambridge observations refer to the ionosphere generally overhead in a latitude of  $52^\circ$  north. At Manchester, measurements have been made of amplitude scintillation but not of phase scintillation. On the other hand, steerable antennas were used with which the sources could be followed to low angles of elevation. At low angles of elevation the sources were in a generally northerly direction. Thus, many of the Manchester observations refer to the ionosphere well to the north of Manchester. At Sydney, latitude  $34^\circ$  south, practically all observations were made at low angles of elevation in a generally northerly direction. Thus, most Australian observations refer to the ionosphere nearer to the equator than Sydney. It, therefore, must be borne in mind that all Sydney observations are at low angles of elevation. Even in comparing the Australian observations with the Manchester observations at low angles of elevation, it must be remembered that the Australians were looking more or less towards the equator, whereas the Manchester observers were looking more or less away from the equator.

In comparing the observations of different groups of workers it should be noticed that quantities with similar or identical names are sometimes interpreted differently by different authors. Thus the Cambridge workers describe the strength of amplitude scintillations by means of a "fluctuation index" derived by dividing the root-mean-square fluctuation in amplitude by the mean amplitude received from a source. Records are made on a linear power scale, and numerical conversion is made from power to amplitude. The Manchester workers used an index of fluctuation described as the "amplitude of fluctuations expressed as a percentage of the mean intensity from the source." This index of fluctuation is obtained from observations recorded on a linear power scale, and no numerical conversion is made from power to amplitude. Moreover, fluctuations on the Manchester records were assessed from the "peaks" of the scintillations, whereas on the Cambridge records they were assessed on a root-mean-square basis. Altogether the Manchester index of fluctuation, even if expressed as a fraction instead of a percentage, is probably about five

times larger than the Cambridge fluctuation index for weak scintillation conditions. Whether this same ratio applies for strong scintillation conditions, however is unclear. In Australia, Bolton, Slee, and Stanley [7] have also defined a "scintillation index." Whether their scintillation index agrees with the Cambridge index or the Manchester index, or represents yet a third index is unclear. In this paper, "fluctuation index" is used in the Cambridge sense, since this seems better adapted to comparison with theory.

Another confusion exists in the literature in connection with the use of the word "scale" to describe the size of irregularities of electron density in the ionosphere responsible for star scintillation. From an irregular function of position in space, it is possible to form an autocorrelation function. This function is unity for zero separation and zero for large separations. The correlation is reduced to a specified value, such as 0.5, for a separation that we denote by  $L$ . Now the irregular function of position may be Fourier analyzed, and from the spectrum we may pick out the component of greatest importance. This component has a repetition distance of  $2\pi L$ . The scales quoted by Cambridge workers appear to be estimates of  $2\pi L$ , whereas those quoted by Manchester workers are estimates of  $L$ . For the Australian workers, there is some uncertainty of interpretation, but it appears that their estimates of scale are measures of  $2\pi L$ . In this paper, it is the quantity  $L$  that is called the scale of the irregularities.

#### IV. THE FREQUENCY VARIATION OF AMPLITUDE SCINTILLATIONS

All workers agree that the fluctuation index usually is small at the high-frequency end of the vhf band, and that it increases as the frequency decreases through the vhf band. At the low-frequency end of the vhf band, the fluctuation index often approaches unity. According to Hewish [3], the fluctuation indexes at 40 mc per second are about four times stronger than at 80 mc per second, and similar results are reported by Bolton, Slee, and Stanley [7].

#### V. DIURNAL AND SEASONAL VARIATIONS OF AMPLITUDE SCINTILLATIONS

The time of day at which a given source is at a given angle of elevation varies progressively from day to day and moves through the 24 hours during the course of a year. If the fluctuation index is measured for a particular source at a particular angle of elevation each day for a year, we obtain a variation of fluctuation index that could be due to a seasonal phenomenon or to a diurnal phenomenon. By using a number of sources, each of which reaches a given angle of elevation at a different time of day, it is possible to separate the diurnal and seasonal variations. Using four sources Ryle and Hewish found that the temporal variation in fluctuation index almost entirely could be explained as a diurnal

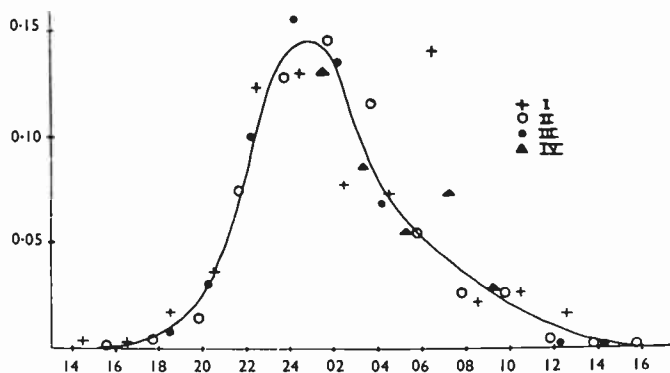


Fig. 6—Variation of the "fluctuation index" for the four sources plotted as a function of the time of observation. Ordinates: Fluctuation index. Abscissae: Local time.

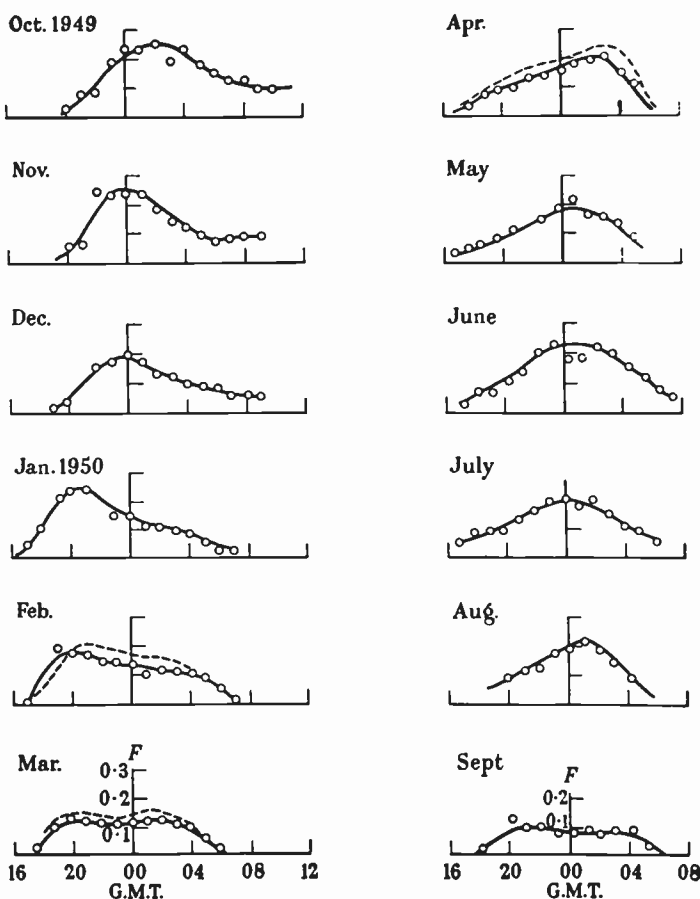


Fig. 7—The diurnal variation of the fluctuation index ( $F_{rms}$ ) deduced from observations of source 23.01 on 6.7 m. The dotted curves were obtained during the following year on 8 m.

phenomenon as shown in Fig. 6. Thus, at relatively high angles of elevation at Cambridge, amplitude scintillation reaches a maximum shortly after midnight and is almost absent during the daytime. What little seasonal variation is involved is shown in Fig. 7.

At Manchester, Little and Maxwell [4] also found that fluctuations were largest at night. They found, however, that at low angles of elevation, fluctuations always were observed independent of the hour of day.

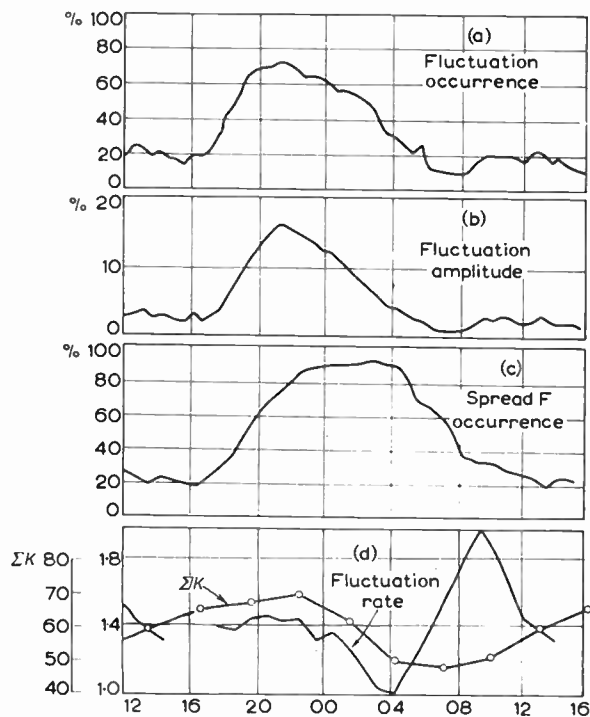


Fig. 8—Yearly average diurnal variations of radio star scintillations (August, 1954 to July, 1955): (a) fluctuation occurrence, (b) fluctuation amplitude, (c) occurrence of spread *F* at Inverness, and (d) fluctuation rate compared with summation of magnetic *K* indexes (*K*).

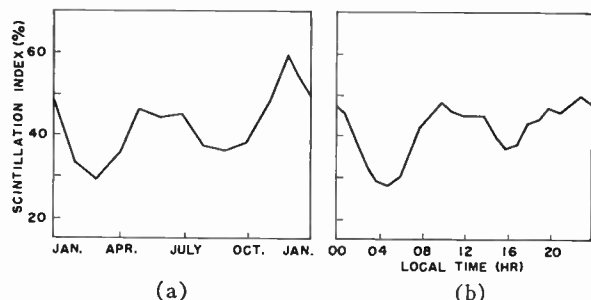


Fig. 9—(a) Mean monthly scintillation index plotted against the month of observation. (b) As in (a), but plotted against the local time of observation.

A summary of data recently published by Dagg [34] is shown in Fig. 8.

In Australia, Bolton, Slee, and Stanley [7], observing only at low angles of elevation in a generally equatorward direction, also found that fluctuations were observed both by day and by night. However, their observations showed a seasonal variation in fluctuation index comparable in importance with the diurnal variation, as shown in Fig. 9. There are minima at the equinoxes and maxima at the solstices. Moreover, although the diurnal variation shows a maximum around midnight, there is also a maximum at midday of comparable importance.

Using only one source, an analysis has been made by Harrower [14] of the diurnal and seasonal variations in the occurrence of amplitude scintillations at Ottawa.

The source used was Cygnus, which was visible at all times. An over-simplified description of the method of analysis is as follows: By averaging a year's data, the dependence upon zenith angle of the occurrence of amplitude scintillations first was obtained. By means of this curve, all data were converted to zenith observations. This corrected data then gave the diurnal and seasonal variations illustrated in Fig. 10. It will be observed that the nighttime maximum in the rate of occurrence appears throughout the year. There is, however, a daytime maximum in winter and a trace of a daytime in summer.

## VI. VARIATION OF AMPLITUDE SCINTILLATIONS WITH ZENITH ANGLE

By averaging a year's data it is possible to smooth out the diurnal and seasonal variations and thus ascertain the way in which the fluctuations vary with the zenith angle of the source. Because the path length through an ionospheric layer is proportional to the secant of the zenith angle of the source measured at an appropriate level in the ionosphere, one might expect the fluctuation index to increase with an increase in the zenith angle. Observations at both Cambridge and Manchester agree with this prediction. The Cambridge observations are shown in Fig. 11, p. 304 and the Manchester observations in Fig. 12. It is clear that amplitude fluctuations increase more rapidly with zenith angle than with the secant of the zenith angle.

## VII. SCINTILLATION RATE

All observers agree that the scintillation rate usually is of the order of a few fluctuations per minute and does not vary with the ratio frequency at which observations are made.

Both the Manchester and Cambridge observers find that the fluctuation rate is several times faster during periods of high-geomagnetic activity than during quiet periods. The relation between the fluctuation rate and the geomagnetic *K* index found by Dagg [33] is shown in Fig. 13. Little and Maxwell [4] also have found that, on the average, the scintillation rate at Manchester is several times greater at low angles of elevation than at high. It should be noted, however, that low angles of elevation at Manchester imply scintillation in the ionosphere in the general vicinity of the zone of maximum auroral activity. At Manchester, it was feasible on a number of occasions to observe the scintillation of sources in the northern sky under conditions when there was auroral activity in the northern sky. Under these circumstances high scintillation rates were observed, but there was no special increase in the fluctuation index [10]. On some occasions partial absorption of the radiation from the source, apparently due to attenuation in auroral ionization, was observed. Observations have also been made at Manchester [33] of marked increases in the rate of scintillation associated with marked

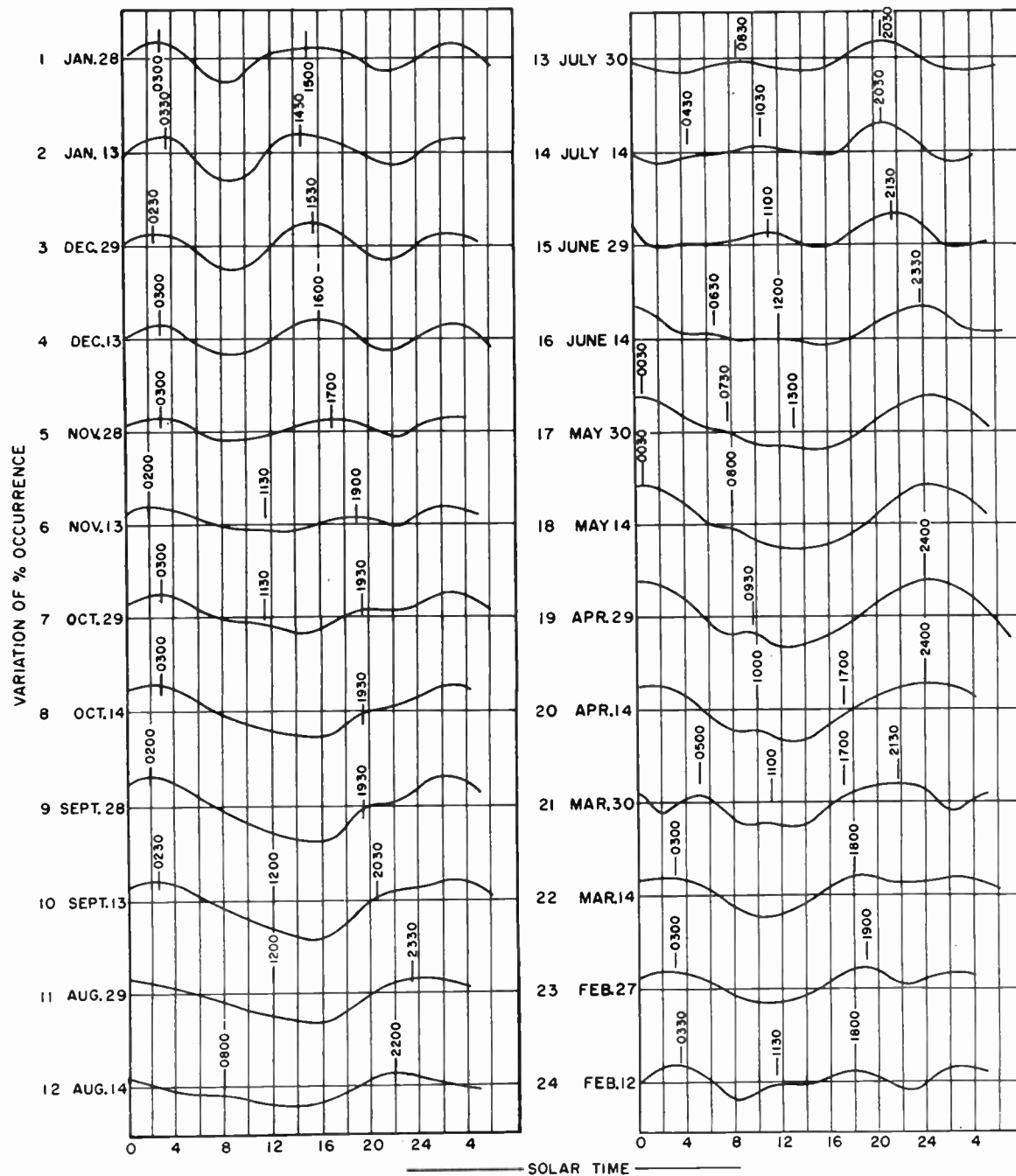


Fig. 10—Each of the 24 graphs shows variation of the percentage occurrence of scintillations plotted against local mean solar time for a given 15-day interval centered about the date written beside the graph. The numbers from 1 to 24 are used to identify 24 positions of the earth on its orbit around the sun in the course of one year. The hours marked along the curves indicate the times during the day at which the occurrence of scintillations passed through a maximum.

changes in the components of the earth's magnetic field. Fig. 14 illustrates these observations. However, Fig. 14 is unusual in one respect. On this occasion there also was a marked change in the fluctuation index. More frequently there is no marked change in the fluctuation index, but only a change in the fluctuation rate.

#### VIII. PHASE SCINTILLATIONS

All of the observations reported above are observations of the fluctuation in the amplitude of the radiation

received from sources. Equipment has been in use at Cambridge and in Australia with which measurements could be made of the fluctuations in the phase difference between the radiation received with two spaced antennas forming an interferometer. By dividing this fluctuation in phase difference by  $2\pi$  times the antenna separation in wavelengths, we derive the angular fluctuation in the direction of arrival of the radiation. Hewish [3] reports that, at a frequency of 40 mc per second, angular flicker is of the order of two to three

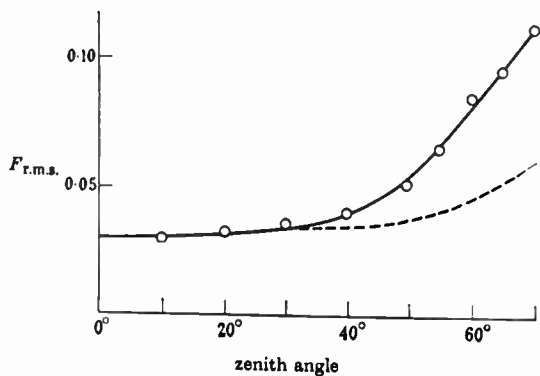


Fig. 11—The dependence of the fluctuation index ( $F_{r.m.s.}$ ) upon the zenith angle of the source. The secant of the angle of incidence on the ionosphere at a height of 400 km is shown by the dotted curve.

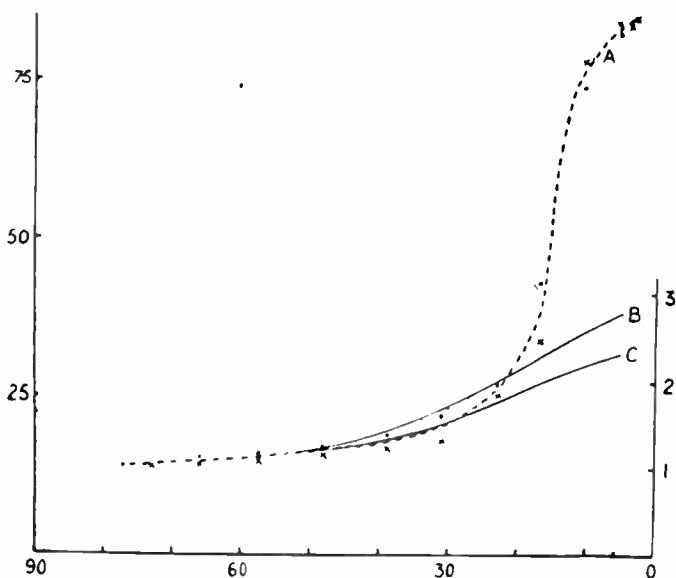


Fig. 12—Curve A: Amplitude of Cygnus fluctuations with elevation  $\times$  source setting,  $\cdot$  source rising (averages over 12 months). Curves B and C: Ratio of effective thickness of disturbing region in line of sight to zenith thickness—(Curve B for a disturbing region of assumed minimum height 300 km and maximum height 500 km; Curve C for assumed minimum height 250 km and maximum height 1000 km).

minutes of arc on a typical occasion (see Fig. 3), but may be as much as half a degree under "highly disturbed conditions." The rate of angle flicker is of the same order of magnitude as the rate of fluctuation in amplitude. Estimates of angular flicker on wavelengths of 8, 3.7, and 1.4 meters have indicated that the angular flicker is approximately proportional to the square of the wavelength.

It is stated by Hewish [3] that fluctuations in intensity are always accompanied by fluctuations in the phase difference between the antennas of an interferometer. However, it is not stated whether the converse is true. No analysis seems to have been made of the diurnal, seasonal, or zenith angle variations in phase fluctuations, and there does not seem to be any good reason for supposing that they are the same as for amplitude fluctua-

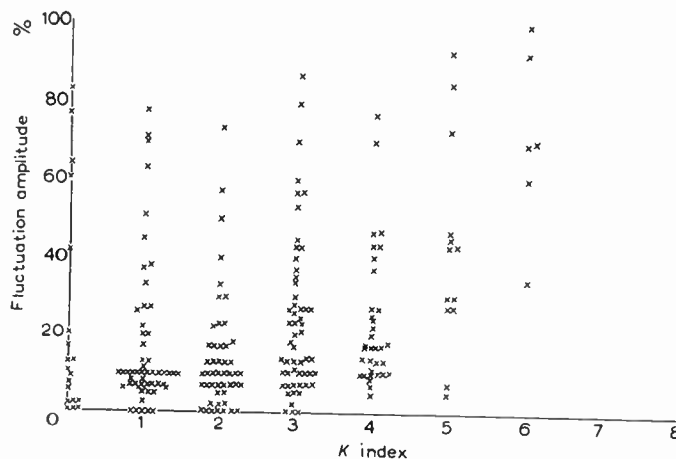


Fig. 13—Comparison of radio star scintillation amplitude with the magnetic  $K$  index.

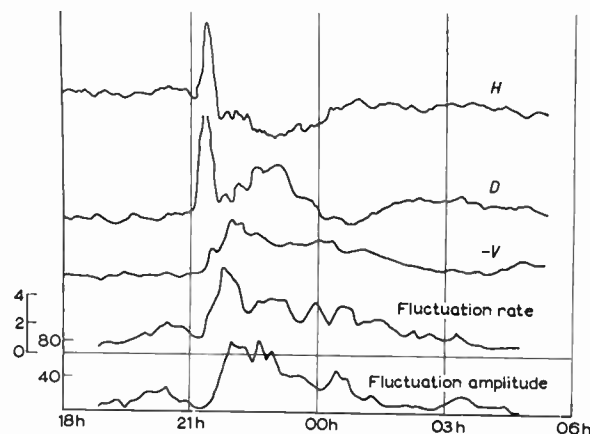


Fig. 14—Lerwick magnetogram April 1-2, 1955. Cassiopeia fluctuations. The fluctuation rate is the number of maxima per minute. The fluctuation amplitude is expressed as a percentage of mean source intensity.

tations. Wild and Roberts [12] in Australia, using their frequency-sweeping equipment, have reported frequency dispersion phenomena that seem to require much larger phase irregularities by day than by night: the dispersion over the ground of a particular irregularity in the band from 40 to 70 mc per second was about five times greater by day than by night.

### IX. DRIFT OF IRREGULARITIES

It is frequently observed that if the fluctuations in amplitude of a source are measured at two receivers separated in an east-west direction by a distance of the order of a kilometer, then the fluctuations are similar, except for a time shift. From this it has been concluded that the irregularities of intensity on the ground, and consequently, the irregularities of electron density in the ionosphere, are drifting horizontally. By using three receivers at the vertices of a triangle and by measuring the time shifts between the arrival of corresponding maxima at the three sites, it is possible to deduce the magnitude and direction of the velocity of drift [40].

Observations at Manchester and in Australia have shown little evidence of a north-south component of drift. All observers agree, however, that there is an important drift in the east-west direction. Overhead in England Maxwell and Dagg report drift from west to east before midnight and from east to west after midnight, with no observations during the daytime. Speeds are of the order of a hundred meters per second under quiet geomagnetic conditions, but rise to a thousand meters per second under disturbed geomagnetic conditions. In Australia, Wild and Roberts [12] looking roughly equatorward obtained a west to east drift of the order of about a hundred meters per second at night with no systematic drift in the daytime.

If scintillation is caused by the drift of a more or less stationary pattern of irregularities across the receiver, then there should be a linear relation between the scintillation rate and the drift speed. The extent to which this is true is illustrated in Fig. 15 using observations of Hewish [3].

### X. SIZE OF IRREGULARITIES

From the size of irregularities in field over the ground, it is possible to make deductions about the size and shape of irregularities of electron density in the ionosphere. Estimates of this type may be made by the following three methods.

- 1) Using an interferometer, the fluctuations in phase difference may be converted into angle flicker and from the cone angle thereby obtained, one may deduce a size of irregularity of electron density in the ionosphere.
- 2) One can measure the size of irregularities of amplitude over the ground, and hence of electron density in the ionosphere, ascertaining how far apart two receivers must be placed before the correlation in the irregularities is reduced to a specified value, such as 0.5.
- 3) Under conditions when there is known to be steady drift of a more or less stationary pattern across the receiver with a known velocity, the duration of an irregularity in time may be converted to the size of an irregularity over the ground.

Using method 2), Little and Maxwell arrived at a figure of four kilometers for the scale in the north-south direction. Using method 3), Ryle and Hewish [2] arrived at a figure of 5 km for  $2\pi$  times the scale in the east-west direction. At first the agreement between these two figures was thought to be good. Subsequently, however, it was realized that, because of confusion about the definition of scale, there was in reality a discrepancy between the two observations. The discrepancy subsequently was cleared up by Spencer [11], who showed that the shape of the irregularities over the ground varied with the direction of the source in such a way as to suggest irregularities of electron density in the ionosphere that are constricted perpendicular to the direction of the earth's magnetic field. Spencer quotes a figure of one to five for the ratio of the scale perpen-

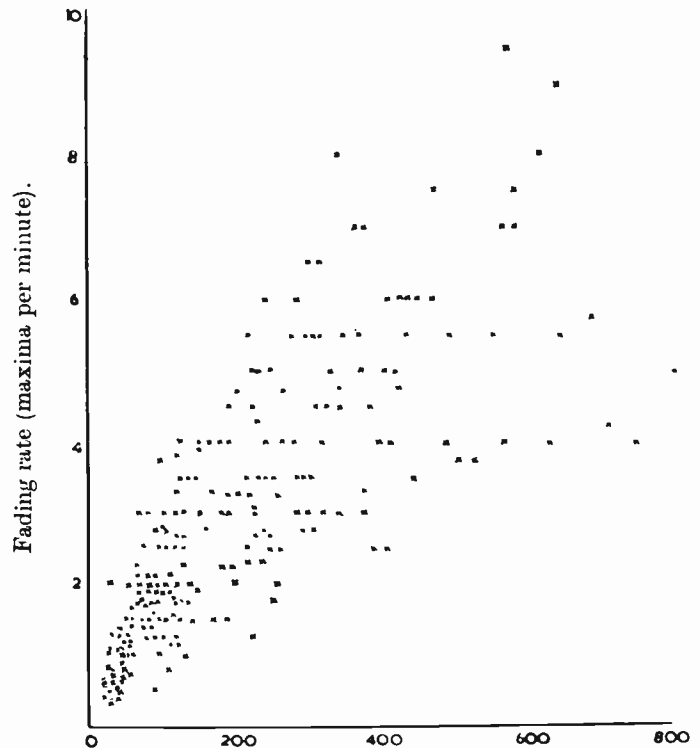


Fig 15—Drift speed in meters per second. *F*-region drift speed vs fading rate.

dicular to the earth's magnetic field to that along the earth's magnetic field, though he also mentions occasions when the two scales appear to be much more unequal. Cambridge and Manchester observations are thus in agreement with the view that the intensity scintillations observed at the ground are caused by irregularities in the ionosphere that have a scale parallel to the earth's magnetic field of the order of a few kilometers and a scale perpendicular to the earth's magnetic field somewhat less than a kilometer. These figures are derived from nighttime observations.

Observations of scale have also been made in Australia. The conditions of observation, however, were not so favorable, partly because of the low angle of observation, and partly because of a smaller angle between the direction of the star and the direction of the earth's magnetic field. The Australian observations made at night do not appear to contradict those made in England. During the daytime, however, the shape of irregularities in field over the ground was somewhat elongated, but the direction of elongation was random. Observations of the shape of irregularities of the field over the ground in the USSR also have indicated a random direction of elongation [36].

### XI. CORRELATION BETWEEN RADIO STAR SCINTILLATION AND *F*-REGION PHENOMENA

In England, a striking correlation has been obtained between fluctuations in the intensity of sources and the ionospheric phenomenon known as spread *F*. Spread *F* involves a situation in which the usually well defined

traces on an ionogram become diffuse, as indicated in Fig. 16 [41]. In some cases the  $F$ -region echo is even more diffuse than is shown in Fig. 16, and no sharp edges to the echo can be recognized. Spread  $F$  occurs primarily at night with a maximum of occurrence in the middle of the night. It is more frequent in winter than in summer [25, 26]. Although the phenomenon of spread  $F$  has been observed for at least twenty years, there still is no explanation of its occurrence. In particular, it is not known why it is primarily a nighttime phenomenon.

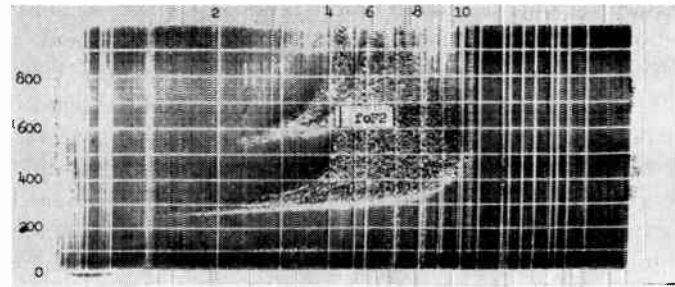
The diurnal variation of spread  $F$  clearly is very similar to that obtained for radio star scintillation by workers in England. Both at Cambridge and at Manchester, a high correlation has been found between the occurrence of scintillations in the intensity of the sources and the occurrence of spread  $F$  at ionospheric observatories in the British Isles (see Fig. 8). The correlation was, in fact, about as high as could be expected in view of the fact that the scintillation observations and the spread  $F$  observations referred to places in the ionosphere hundreds of kilometers apart. To obtain perfect correlation, observation of scintillations should be made for a source close to the zenith and compared with ionograms made at the same location, but this experiment does not seem to have been performed.

Briggs [37] has pointed out that, if the phenomena of spread  $F$  and of radio star scintillation occur at a common level, then the degree of correlation between the two phenomena when not observed in the zenith depends upon the height assumed. Therefore, he has adjusted the height to obtain maximum correlation and in this way has arrived at a height of from 250 to 300 km.

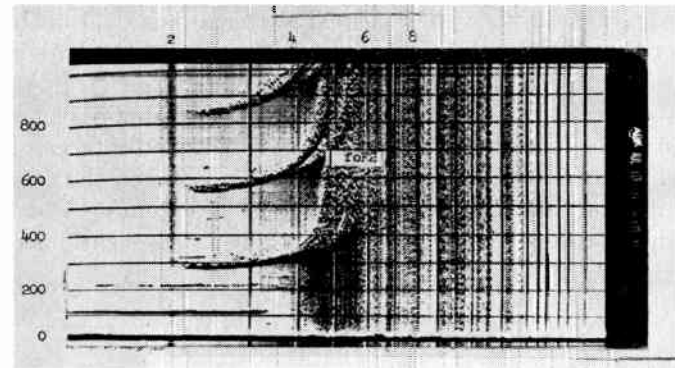
The close correlation between the amplitude scintillations and spread  $F$  that has been obtained in England is not observed in Australia. Such a correlation would be impossible in view of the fact that the diurnal variation of scintillations observed by the Australian workers shows a maximum at midday as well as at midnight, while spread  $F$  does not occur during the daytime. However, a partial correlation has been obtained by Mills and Thomas [6] between the fluctuation index and a measure of  $F$ -region "activity" that incorporate, among other things, the occurrence of spread  $F$ .

## XII. CORRELATION OF SCINTILLATIONS WITH $E$ -REGION PHENOMENA

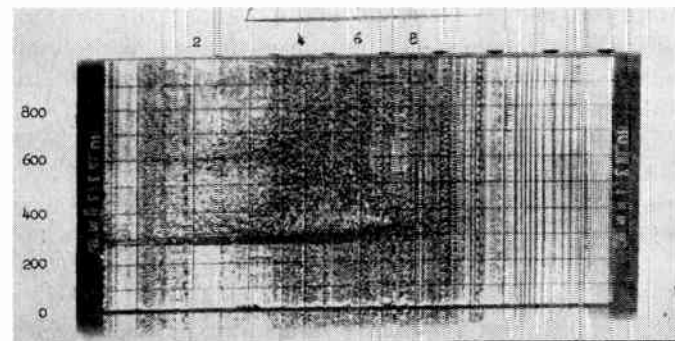
The existence of a maximum of scintillation at midday in the Australian observations led Bolton, Slee and Stanley to consider the possible role of the  $E$  region in causing scintillations. They obtain a partial correlation between the occurrence of scintillations and the occurrence of the phenomenon of sporadic  $E$ , in spite of the fact that the two sets of data refer to places in the ionosphere many hundreds of kilometers apart. A similar correlation has been obtained by Dueño [35], and recently by Dagg [34].



(a)



(b)



(c)

Fig. 16—Spread  $F$  Echoes—high, medium, and low latitudes. (a) Spread echo of the type commonly observed at high latitudes. Godhavn 1640 December 22, 1951. (b) Middle latitude spread echo. Adak 2015 July 10, 1955. (c) Equatorial-type spread echo. Huancayo 0400 June 3, 1952.

It has to be remembered that the Australian observations, unlike those made by other workers, have been made at low angles of elevation looking in a roughly equatorward direction. It seems reasonably clear that, under these circumstances, two scintillation phenomena are observed. One of these leads to a maximum of fluctuation index at night and presumably is the same as the phenomenon reported in England. The other phenomenon leads to a maximum of fluctuation index at midday, and nothing corresponding to it has yet been reported from England.

## XIII. DISPERSION EFFECTS IN RADIO STAR SCINTILLATION

It will be observed from Fig. 1 that fluctuations in the intensity of sources lead to a trace in which the up-

ward peaks are sharper than the downward peaks. Special attention has been drawn to a phenomenon of this type by the frequency-sweeping observations of Wild and Roberts [12]. They found that the times of occurrence of the peaks varied systematically with frequency over the band from 40 to 70 mc per second, leading to records of the type shown in Fig. 5. They found that the average spacing between fluctuations was typically 2 to 5 times the duration. Moreover, individual fluctuations were sometimes accompanied by "side lobes," as shown in Fig. 5. Thus, they were led to picture radio star scintillation as a "systematic" phenomenon rather than as a random phenomenon. Analysis of the statistical distribution of the amplitudes of fluctuations leads, however, to a Rayleigh distribution

#### XIV. THEORY

We shall assume that, apart from irregularities, the electron density  $N$  in the ionosphere is a function of height  $h$  only. From the electron density at a particular height, we derive the plasma wavelength  $\lambda_N$  in accordance with the equation

$$\lambda_N^2 = \frac{1}{r_e N}, \quad (1)$$

where  $r_e$  is the classical radius of the electron given by

$$r_e = 2.8 \times 10^{-15} \text{ meters.} \quad (2)$$

Neglecting the effect of the earth's magnetic field, the refractive index  $n$  at a particular point is derived from

$$n^2 = 1 - \frac{\lambda^2}{\lambda_N^2}, \quad (3)$$

where  $\lambda$  is the wavelength at which observations are made. We shall assume that  $\lambda$  is small compared to  $\lambda_N$ , so that no distinction need be drawn between the wavelength in the ionosphere and the wavelength in free space.

We assume that, in the ionosphere, there are irregularities of electron density that result in a mean square departure of electron density from mean denoted by  $(\overline{\Delta N})^2$ . For simplicity, we neglect possible restriction of irregularities of electron density perpendicular to the earth's magnetic field, and assume that the irregularities are isotropic. At this stage, it is not necessary to make any detailed assumptions about the cause of the irregularities. However, since turbulence is a possible, and even likely, cause of the irregularities, it is necessary to mention that, in this case, there would be a wide range of sizes of irregularities. Since, however, in radio star scintillation we are concerned with forward scattering, it would only be the irregularities of largest scale that would be of importance. Therefore, whatever the cause of the irregularities, it is satisfactory to assume that the ones with which we are concerned are all of

much the same size and may be characterized by a scale  $L$ . This scale is as defined in Section III and, in the case of turbulence, would correspond to the scale of the large eddies. The variation  $\Delta N$  in electron density produces a corresponding variation  $\Delta n$  in refractive index, calculated from (3). We derive

$$\left(\frac{\Delta n}{n}\right)^2 = \frac{\lambda^4}{\lambda_N^4} \left(\frac{\Delta N}{N}\right)^2 \quad (4)$$

$$= r_e^2 \lambda^4 (\overline{\Delta N})^2, \quad (5)$$

showing that the variations in refractive index decrease proportionally to the square of wavelength.

Let us consider a plane wave of wavelength  $\lambda$  passing through the ionosphere, and let us calculate the mean-square deviation in phase introduced into it for a distance  $D$  of travel. For a single irregularity, the mean-square difference of phase introduced is

$$\left(\frac{2\pi L}{\lambda}\right)^2 \left(\frac{\Delta n}{n}\right)^2. \quad (6)$$

In a distance  $D$  the number of irregularities passed through is of the order of  $D/L$ . For a reason that will be explained later, we actually shall take the number of irregularities passed through in distance  $D$  as

$$\frac{D}{2L}. \quad (7)$$

Assuming that the phase fluctuations introduced by successive irregularities add up on a random walk basis, we derive from (6) and (7) the following expression for the mean-square phase fluctuation introduced in a distance  $D$  of travel:

$$(\overline{\Delta\phi})^2 = \frac{D}{2L} \left(\frac{2\pi L}{\lambda}\right)^2 \left(\frac{\Delta n}{n}\right)^2. \quad (8)$$

Substituting from (5) into (8), we obtain for the mean-square-phase fluctuation introduced per unit distance of travel

$$\frac{1}{D} (\overline{\Delta\phi})^2 = 2\pi^2 r_e^2 \lambda^2 L (\overline{\Delta N})^2. \quad (9)$$

If  $dz$  denotes an element of length of the path large compared to the size of an irregularity, then the total mean-square deviation of phase introduced by the entire ionosphere is given by

$$(\overline{\Delta\phi})^2 = 2\pi^2 r_e^2 \lambda^2 \int L (\overline{\Delta N})^2 dz, \quad (10)$$

where the integral is taken along the whole length of path. If  $dh$  is the element of height corresponding to the path length  $dz$  and  $\chi$  is the zenith angle of the path at this level, then  $dz$  in (10) may be replaced by  $\sec \chi dh$ .

If we assume that over the important interval of height involved in the integration there is no significant variation of  $\chi$ , then (10) may be rewritten,

$$\overline{(\Delta\phi)^2} = 2\pi^2 r_e^2 \lambda^2 \sec \chi \int L(\overline{\Delta N})^2 dh. \quad (11)$$

If we further assume that the integrand in (11) is important only over an interval of height  $\tau$  and that in this interval of height the integrand may be given a mean value, then (11) becomes

$$\overline{(\Delta\phi)^2} = 2\pi^2 r_e^2 \lambda^2 \sec \chi L(\overline{\Delta N})^2. \quad (12)$$

The thickness  $\tau$  in (12) would probably be of the order of magnitude of the scale height of the atmosphere at the level in question. From (11) and (12) we notice that the mean-square phase fluctuation should be proportional to the square of wavelength and to the secant of the zenith angle at the level where phase scintillations are introduced.

It should be noted that these equations give the fluctuation in the phase of the wave compared to the phase that it would have had in the absence of fluctuations. This is not what is measured in practice. Indeed, with a noise source this could not be measured. What is measured is the fluctuation in the difference of phase between two points separated by a distance  $d$ . Let us assume that the separation between the receivers is perpendicular to the direction of the source and that there is a correlation coefficient  $\rho$  between the phase fluctuations at the two points. Then the mean square fluctuation in phase difference is given by

$$\overline{\{\Delta(\phi_1 - \phi_2)\}^2} = 2(1 - \rho)\overline{(\Delta\phi)^2}. \quad (13)$$

The correlation coefficient may be taken as

$$\rho = \exp\left(-\frac{d^2}{L^2}\right), \quad (14)$$

since it is assumed that any structure of scale less than  $L$  that may exist in the irregularities of electron density in the ionosphere does not appear in the irregularities of field at the ground. If we substitute from (14) into (13) and assume that the separation  $d$  between the receivers is small compared to the scale  $L$ , we derive

$$\overline{\{\Delta(\phi_1 - \phi_2)\}^2} = 2\left(\frac{d}{L}\right)^2 \overline{(\Delta\phi)^2}. \quad (15)$$

Substituting from (12) into (15), we derive

$$\overline{\{\Delta(\phi_1 - \phi_2)\}^2} = 4\pi^2 r_e^2 d^2 \lambda^2 \sec \chi \frac{1}{L} \overline{(\Delta N)^2} \tau. \quad (16)$$

This may be expressed more accurately as an integral with respect to height throughout the ionosphere by means of

$$\overline{\{\Delta(\phi_1 - \phi_2)\}^2} = 4\pi^2 r_e^2 d^2 \lambda^2 \sec \chi \int \frac{1}{L} \overline{(\Delta N)^2} dh. \quad (17)$$

From the fluctuations in the phase difference between two antennas, we may derive an expression for the fluctuation in the direction of arrival of a phase front. The mean square variation in the direction of arrival is

$$\overline{\theta^2} = \left(\frac{\lambda}{2\pi d}\right)^2 \overline{\{\Delta(\phi_1 - \phi_2)\}^2}, \quad (18)$$

and if we substitute from (15) into (18), we derive

$$\overline{\theta^2} = 2\left(\frac{\lambda}{2\pi L}\right)^2 \overline{(\Delta\phi)^2}. \quad (19)$$

As is to be expected, this is independent of the separation between the antennas. Substituting from (12) into (19), we derive

$$\overline{\theta^2} = r_e^2 \lambda^4 \sec \chi \frac{1}{L} \overline{(\Delta N)^2} \tau. \quad (20)$$

The more accurate expression involving an integral with regard to height throughout the ionosphere is

$$\overline{\theta^2} = r_e^2 \lambda^4 \sec \chi \int \frac{1}{L} \overline{(\Delta N)^2} dh. \quad (21)$$

We notice that the root-mean-square angular deviation is proportional to the square of the wavelength and the square root of the zenith angle measured at the level where phase scintillations are imposed.

Let us now turn our consideration to fluctuations in amplitude. Let us suppose that a plane wave of amplitude  $A$  passes through the ionosphere and is scattered by the irregularities of electron density existing therein. To simplify the calculation, let us suppose that the wave emerging from the ionosphere is not weakened substantially by scattering, and that multiple scattering may be neglected. We would then expect to receive below the ionosphere the remnant of the unscattered wave, together with waves scattered from the various irregularities. Under simple circumstances the phase addition of these various contributions would be given by a vector diagram, such as that shown in Fig. 17. The large vector represents the remnant of the unscattered wave, and the small vectors represent the scattered waves from the various irregularities. Under these circumstances we can see that, if  $\Delta A$  is a measure of the amplitude deviations in the resultant signal and  $A$  is the mean amplitude, then the associated deviations in phase should be of the order of magnitude of  $\Delta A$  divided by  $A$ . We write this relation in the form

$$\overline{\left(\frac{\Delta A}{A}\right)^2} = \overline{(\Delta\phi)^2}. \quad (22)$$

Fig. 17 is drawn on the assumption that the expressions in (22) are small compared to unity. If  $(\Delta\phi)^2$  is large compared to unity, then the random vectors in Fig. 17 are large compared with the vector representing the remnant of the incident wave. Under these circumstances the original incident wave has been removed by scattering and all field received arises from multiple scattering. The mean-square fractional deviation of amplitude  $(\Delta A/A)^2$  is then of the order of unity and the probability distribution of amplitude is Rayleigh. A limitation on the validity of (22) is, therefore, that the mean-square phase fluctuation should be less than unity.

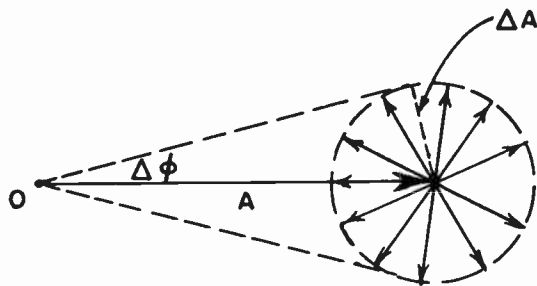


Fig. 17—Vector diagram showing addition of scattered waves to wave from source.

Another limitation on the validity of (22) arises in the following way. The waves scattered from an individual irregularity whose size is large in comparison with the wavelength consist of a roughly parallel beam in the direction of the incident wave out to a distance  $z_F$  from the irregularity, such that from this distance the irregularity subtends one Fresnel zone. The expression for the Fresnel zone distance  $z_F$  in terms of the scale  $L$  of the irregularities is

$$z_F = \frac{(2\pi L)^2}{\lambda} \tag{23}$$

At greater distances from the irregularity than  $z_F$ , scattering is in the form of a conical beam whose semi-vertical angle is of the order of

$$\frac{\lambda}{2\pi L} \tag{24}$$

and whose axial direction coincides with the direction of incidence. Therefore, the concept of radial scattering from irregularities only applies at distances from the irregularities large compared to  $z_F$ . Eq. (22) therefore applies when each scatterer is at a distance from the receiver in excess of its Fresnel zone distance  $z_F$ , and when the total root-mean-square fluctuation of phase is less than one radian. Under these circumstances an independent calculation of the mean-square fractional deviation of amplitude can be made; it should yield the expression already derived for the mean-square fluctuation of phase.

Consider an ionospheric scattering slab of thickness  $\tau$ , as shown in Fig. 18. Let  $R$  denote the receiver and  $X$  the direction of the source. Let the direction from  $R$  to  $X$  intercept the ionospheric slab at a distance  $r$  from the receiver. Assume that  $r$  is large compared to the Fresnel zone distance  $z_F$  given by (23). Also, assume that each irregularity in the ionospheric slab scatters energy in accordance with a formula such as that of Booker and Gordon [21]. For present purposes, this formula may be simplified by assuming that scattering takes place only near the forward direction within a small angle from the direction of incidence given by (24). We may assume further that, within this small angle, the intensity of the scattered wave is constant and equal to that in the forward direction. The relevant formula for the power scattered within the cone angle (24), measured per unit incident power density, per unit volume, and per unit solid angle, is

$$\sigma_F = \frac{1}{\lambda} \left( \frac{2\pi L}{\lambda} \right)^3 \left( \frac{\Delta n}{n} \right)^2 \tag{25}$$

Substituting from (5), (25) becomes

$$\sigma_F = r_e^2 (2\pi L)^3 (\overline{\Delta N})^2 \tag{26}$$

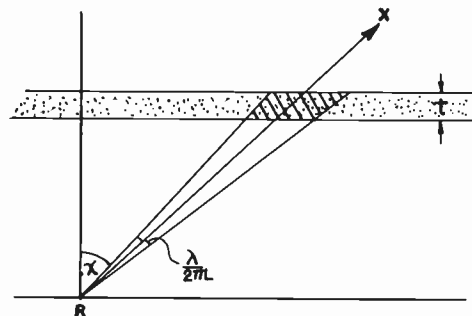


Fig. 18—Illustrating calculation of amplitude fluctuations.

Since we are assuming that scattering only takes place within the small angle (24) of the forward direction, the region of the ionospheric layer from which scattering reaches the receiver is the shaded area in Fig. 18. This is the part of the layer intercepted by a cone of semi-vertical angle (24), with vertex at  $R$  and axis in the direction of  $RX$ . The scattering volume is, therefore,

$$V = \pi r^2 \left( \frac{\lambda}{2\pi L} \right)^2 \sec \chi \tag{27}$$

If  $S$  is the aperture area of the antenna at  $R$ , the solid angle subtended by this antenna at a scattering irregularity is  $S/r^2$ . Therefore, for an incident power density of  $p$ , the scattered power received is

$$p\sigma_F V \frac{S}{r^2} \tag{28}$$

where  $\sigma_F$  and  $V$  are given by (26) and (27). In the absence of the irregularities, the power received by the antenna would be

$$pS. \quad (29)$$

By dividing (28) by (29), we derive the ratio of the scattered power received to the power received directly from the source, assuming that this is not seriously weakened by scattering. This ratio is the mean-square fractional deviation of amplitude at the receiver. Hence,

$$\overline{\left(\frac{\Delta A}{A}\right)^2} = \frac{\sigma_F V}{r^2}. \quad (30)$$

By substituting from (26) and (27) into (30), we derive

$$\overline{\left(\frac{\Delta A}{A}\right)^2} = 2\pi^2 r_e^2 \lambda^2 \sec^3 \chi \overline{L(\Delta N)^2}. \quad (31)$$

For a continuous distribution of scattering layers throughout the ionosphere, we may rewrite (31) as

$$\overline{\left(\frac{\Delta A}{A}\right)^2} = 2\pi^2 r_e^2 \lambda^2 \sec^3 \chi \int L \overline{(\Delta N)^2} dh. \quad (32)$$

We observe that (11) and (32) fit in with (22) in the way that they should. It should be noted, however, that the arguments leading to (11) and (32) only have a factor of two accuracy, whereas (22) has a higher accuracy. It was for this reason that a factor of two was introduced into (7).

It must be noted that (22) only applies when the distance of the scattering irregularities from the receiver exceeds the Fresnel zone distance given by (23). Hewish [19] has shown that when the distance  $z$  of the scatterers from the receiver is small compared to the Fresnel zone distance  $z_F$ , then

$$\overline{\left(\frac{\Delta A}{A}\right)^2} = \frac{z^2}{z_F^2} \overline{(\Delta \phi)^2}. \quad (33)$$

We therefore take the mean-square fractional deviation of amplitude to be given by (22) when  $z$  is greater than  $z_F$ , and by (33) when  $z$  is less than  $z_F$ . It should be noted, however, that while the mean-square fluctuation in phase can exceed unity, the mean-square fractional fluctuation of amplitude cannot.

Let us suppose that all of the irregularities in the ionosphere with which we are concerned are at distances from the receiver small in comparison with the Fresnel zone distance  $z_F$ . Substituting from (23) into (33), we obtain

$$\overline{\left(\frac{\Delta A}{A}\right)^2} = \frac{\lambda^2 z^2}{(2\pi L)^4} \overline{(\Delta \phi)^2}. \quad (34)$$

If we assume, for simplicity, that observations at low angles of elevation are not involved, then, for a layer at a height  $h$ ,

$$z = h \sec \chi. \quad (35)$$

Substituting from (12) and (35) into (34), we obtain

$$\overline{\left(\frac{\Delta A}{A}\right)^2} = \frac{1}{8\pi^2} r_e^2 \lambda^4 \sec^3 \chi \frac{h^2}{L^3} \overline{(\Delta N)^2} \tau. \quad (36)$$

Expressed as an integral throughout the ionosphere (36) is replaced by

$$\overline{\left(\frac{\Delta A}{A}\right)^2} = \frac{1}{8\pi^2} r_e^2 \lambda^4 \sec^3 \chi \int \frac{h^2}{L^3} \overline{(\Delta N)^2} dh. \quad (37)$$

This equation shows that if the irregularities with which we are concerned are larger than the Fresnel zone, then the mean-square fractional deviation of amplitude is proportional to the 4th-power wavelength and to the cube of the secant of the zenith angle.

It should be noticed that the integrals involved in (32) and (37) are different. The relative importance of different levels in the ionosphere is different according to whether the irregularities are large or small compared to their Fresnel zone: for large irregularities, those that are sufficiently close to the receiver are relatively unimportant for amplitude fluctuations. It also should be noted that the integral involved in (17) is different from either of those involved in (32) or (37). This means that the relative importance of different levels in the ionosphere is different for amplitude fluctuations and for fluctuations in the phase difference between the arms of an interferometer. It is possible, therefore, that the level in the ionosphere principally responsible for producing amplitude scintillations could be substantially different from that principally responsible for producing angular scintillations.

In spite of what has just been said, let us assume that the level responsible for amplitude fluctuations is the same as that responsible for phase fluctuations. This implies neglect of the different weighting of different ionospheric heights implied by the integrals in (11) and (37). Let us at the same time assume that the sizes of irregularities are large compared with the Fresnel zone. In these circumstances, as pointed out by Hewish, (34) can be solved for the distance  $z$  from the receiver to the layer in which it is assumed that all scintillation occurs. If we assume, for simplicity, that low angles of elevation are not involved, we may substitute from (35) into (34) and write the result as

$$h = \frac{(2\pi L)^2}{\lambda} \cos \chi \left\{ \frac{\overline{(\Delta A/A)^2}}{\overline{(\Delta \phi)^2}} \right\}^{1/2}. \quad (38)$$

Thus, simultaneous measurements of the amplitude and phase fluctuations, combined with a knowledge of the scale of the irregularities, should determine the height at which scintillation occurs, provided that the various assumptions used in deriving (38) are satisfied. Since it is the fluctuation in the phase difference be-

tween the arms of an interferometer that would be measured in practice, it is better to substitute from (15) into (38) and obtain

$$h = 4\sqrt{2}\pi^2 \frac{Ld}{\lambda} \cos \chi \left[ \frac{(\overline{\Delta A/A})^2}{\{\overline{\Delta(\phi_1 - \phi_2)}\}^2} \right]^{1/2}. \quad (39)$$

In all of the above calculations the scale  $L$  has been the scale of irregularities at the relevant level in the ionosphere. The scales actually measured, however, are scales of irregularities of field strength at the surface of the earth, and the question of the relation of the two scales arises. This matter has been studied by Booker, Ratcliffe, and Shinn [15] and by Hewish [19]. If  $(\overline{\Delta\phi})^2$  is less than unity, the situation is comparatively straightforward. Irregularities of scale  $L$  in the ionosphere produce scattering over a cone angle  $\lambda/(2\pi L)$ . An angular spectrum spread over this angle combines at the surface of the earth to give an irregular distribution of field strength for which the scale is  $L$ , the same as in the ionosphere. Passing from the irregularities in the ionosphere to the angular spectrum of scattering involves a Fourier transformation, and passing from the angular spectrum of scattering to the distribution of field strength over the ground involves a further Fourier transformation. As a result of this double Fourier transformation, the scale of irregularities over the ground is the same as that for the electron density in the ionosphere. On the other hand, if  $(\overline{\Delta\phi})^2$  is greater than unity, multiple scattering is involved. The path then may be divided into sections for each of which  $(\overline{\Delta\phi})^2$  is equal to unity. The number of sections is then the number of scatterings involved. Thus, when  $(\overline{\Delta\phi})^2$  is large compared to unity, there are  $(\overline{\Delta\phi})^2$  scatterings in passing through the ionosphere. On a random walk basis, therefore, the mean-square scattering angle is

$$\left( \frac{\lambda}{2\pi L} \right)^2 (\overline{\Delta\phi})^2. \quad (40)$$

It follows that when the mean-square fluctuation of phase exceeds unity, the correlation distance at ground level for the amplitude fluctuations is given by  $L/\{(\overline{\Delta\phi})^2\}^{1/2}$ . Thus, if  $L$  is the scale of irregularities of electron density in the ionosphere, then the scale measured by a spaced receiver experiment at ground level is

$$L \quad \text{if } (\overline{\Delta\phi})^2 < 1, \quad (41)$$

$$L/\{(\overline{\Delta\phi})^2\}^{1/2} \quad \text{if } (\overline{\Delta\phi})^2 > 1. \quad (42)$$

Thus, the scale of irregularities in the ionosphere may be obtained directly from the correlation distance measured at ground level, provided that it is known that the mean-square deviation of phase is less than unity. If the mean-square deviation of phase is greater than unity, then the measured correlation distance at ground level is less than the scale of irregularities in the ionosphere.

### XV. COMPARISON BETWEEN THEORY AND EXPERIMENT

Very satisfactory agreement exists between theory and experiment in the matter of wavelength dependence. In accordance with (21) the mean-square fluctuation in the angle of arrival should be proportional to the 4th-power of wavelength. This means that angle flicker should be proportional to the square of wavelength, and this is what is reported by Hewish [3].

So far as the variation of fluctuation index with wavelength is concerned, we notice that the mean-square fractional deviation of amplitude is proportional to the square of wavelength according to (32), and to the 4th-power of wavelength according to (37). To decide which equation is appropriate, we have to decide whether the size of the irregularities is small or large compared to the size of the Fresnel zone. The figure quoted by Hewish for  $2\pi L$  in (23) is five km, and the resulting value for the Fresnel zone distance  $z_F$  is 4000 km. There is little doubt, therefore, that the irregularities with which we are concerned are at distances from the receiver small compared to the Fresnel zone distance  $z_F$ . Consequently, the appropriate formula for the mean-square fractional deviation of amplitude is given by (37) rather than by (32).

Now Hewish has shown experimentally that the root-mean-square fractional deviation of amplitude is proportional to the square of wavelength. Therefore, we should expect the mean-square fractional deviation of amplitude to be proportional to the 4th power of wavelength, and this is in agreement with the appropriate theoretical formula, namely (37).

There also is agreement between theory and experiment concerning the wavelength dependence of the rate of scintillation. Whether the rate of scintillation is associated with the drift of a fixed pattern of irregularities or with the irregular motion of irregularities, a fading rate independent of wavelength would be expected, and this is what all observers have reported. Thus, all aspects of the wavelength dependence of radio star scintillation show agreement between theory and experiment.

Let us now turn to the dependence of scintillation upon zenith angle. Eq. (17) shows that the mean-square fluctuation in phase difference between two antennas forming an interferometer should be proportional to the secant of the zenith angle. Eq. (37) points out that the mean-square fractional deviation of amplitude should be proportional to the cube of the zenith angle. Let us compare this theoretical result with the observations made at Cambridge (Fig. 11) and Manchester (Fig. 12). These two sets of observations are replotted in Fig. 19, together with an appropriate theoretical curve based on (37). In replottting the Manchester observations it has been assumed that the discrepancy between the zenith observations at Manchester and Cambridge are due to the differences in the way the records were handled. It is observed from Fig. 19 that the agreement

between the Cambridge observations and the theory is good, but that the agreement with the Manchester observations is poor, in spite of the attempt to apply an appropriate correction. This is unfortunate since the Manchester observers are the only ones to have made zenith angle observations from essentially  $0^\circ$  to  $90^\circ$ . Had these observations shown behavior similar to the Cambridge observations it would have been possible to derive a value for the height of amplitude scintillation by studying the effect of the earth's curvature for values of the zenith angle near  $90^\circ$ . This cannot be done from the Cambridge observations themselves because measurements were not made at zenith angles greater than  $70^\circ$ . It cannot be done from the Australian observations because measurements were not made at zenith angles less than  $75^\circ$ .

zenith angle data is in fact at high angles of elevation and consists of a disagreement in the range of zenith angles from  $0^\circ$  to  $70^\circ$  between the Manchester observations and theory, as well as between the Manchester observations and the Cambridge observations.

Because of the absence of suitable observational data in the literature, it almost is impossible to test the zenith angle dependence given by (17) for the fluctuations, in the phase difference between the antennas of an interferometer.

Hewish [3] quotes eight observations made at a zenith angle of  $6^\circ$  and five made at a zenith angle of  $70^\circ$ . These observations would fit in with (17), but the spread in the observational data is large. Confidence in this agreement is reduced by the fact that measurements of amplitude fluctuations at the two zenith angles were made at the same time, and these show much poorer agreement with (37) than that shown by the average of all of the data at these two zenith angles (see Fig. 11).

We have seen that the dependence upon the zenith angle of amplitude and phase fluctuations, in principle, is capable of giving an estimate of the height at which scintillation occurs, but that observations published so far are inadequate to achieve this.

Let us now turn to the use of (39) for determining the height of scintillation. In connection with this use of (39), Hewish [3] made thirteen simultaneous observations of phase and amplitude fluctuation. The conditions necessary for the application of (39) appear to be reasonably well satisfied, with the possible exception of the assumption that phase and amplitude scintillations occur at the same height. Here again we are plagued by the paucity of observations, particularly in phase fluctuations, and by the wide scattering of the few observations that are available. Each of Hewish's points leads to a determination of the height of scintillation. The points corresponding to observations at a zenith angle of  $6^\circ$  give a four to one variation in the height determined. The observations made at a zenith angle of  $70^\circ$  are much more consistent, but yield a height only one-third of that given by the observations at a zenith angle of  $6^\circ$ . The discrepancy between the height determined from the  $6^\circ$  data and that determined by the  $70^\circ$  data arises from the fact that the ratio of the fluctuation index at a zenith angle of  $6^\circ$  to that at a zenith angle of  $70^\circ$  is substantially different for the sample of data in use and for the much more extensive data on fluctuation index summarized in Fig. 11. Thus, because of the shortcomings of the experimental data available for use in connection with (39), there is a five to one spread in the height deduced for the level at which scintillation occurs.

In these circumstances, it is doubtful whether any average height should be deduced from the data. Hewish mentioned a figure of 400 km, and since then this has been repeated uncritically by many authors. It is doubtful, however, whether the data does more than establish that the nighttime scintillation phenomena occur in the ionosphere above the *E* region.

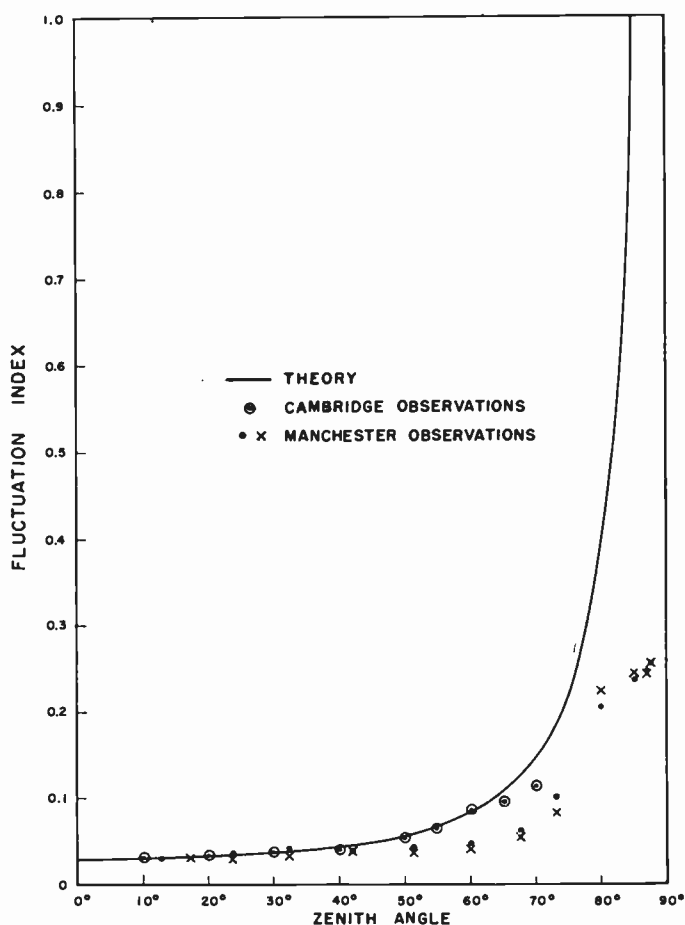


Fig. 19—Comparison between a theoretical curve for the zenith angle dependence of fluctuation index and observations made at Cambridge and at Manchester.

Note that Fig. 19 upsets the Manchester contention, based on Fig. 12, that the fluctuation index at low angles of elevation was affected to a major extent by auroral phenomena. The theoretical curve drawn in Fig. 12 must be replaced by the theoretical curve drawn in Fig. 19. It is then seen that, instead of the low-angle fluctuation index at Manchester being high compared to the zenith value, it is low. The anomaly in the Manchester

## XVI. DISCUSSION

The outstanding puzzle concerning radio star scintillations is concerned with the diurnal variation of the phenomenon. While there may be some disagreement between various observers operating under different conditions about the existence of a midday maximum of scintillation, all observers agree that there is a nighttime maximum of scintillation. No satisfactory explanation of this nighttime maximum has yet been proposed. It was the occurrence of this nighttime maximum that led Ryle and Hewish [2] to propose that scintillations were associated with ionization created by particles falling into the sun. This idea has been criticized by Maxwell [38] but developed by Harrower [14]. Harrower concluded that the particles would have to be either hydrogen atoms or protons. It is easy to see how such particles might create an ionized layer at night. However, it is less easy to see how such particles would create irregularities of ionization unless they could cause heating and hence turbulence [39]. What is required is a mechanism for causing irregularities in the ionization, of which there are plenty in any case in the ionosphere.

In considering the cause of irregularities in the ionosphere responsible for star scintillation, it is appropriate to remember that this is only one of many phenomena that indicate irregularities of electron density in the ionosphere. Other phenomena are:

- 1) fading of radio waves reflected from the ionosphere,
- 2) the diffusion of long duration visible meteor trails, and,
- 3) various phenomena of back scattering from the ionosphere.

It is possible that the irregularities of electron density associated with radio star scintillation have no relation to the irregularities that are required to explain other ionospheric phenomena; however, it seems more reasonable, with the present state of our knowledge, to assume a common origin for all irregularities of electron density in the ionosphere. The only likely common cause would seem to be atmospheric turbulence.

Atmospheric turbulence as a cause of irregularities of electron density in the ionosphere has been studied by Maxwell [38], Booker [22], Booker and Cohen [23], and Booker [24]. The subject, however, is controversial. Booker [22, 24] has pointed out that the degree of constriction of irregularities of electron density perpendicular to the earth's magnetic field observed by Spencer [11] suggests that the level at which intensity scintillations occur may not differ much from the level where the collisional frequency for ions is equal to the gyro-magnetic frequency for ions. This level is about 140 km, and therefore suggests that attention should be given to the region between the *E* and *F* regions as a possible location for the level where amplitude scintillations are imposed.

While a theory of radio star scintillation based upon atmospheric turbulence is capable of explaining many

features of the observations, at the present time it does not explain the nocturnal maximum of scintillation. The intensity of irregularities should be proportional to the gradient of electron density corrected for adiabatic variations with height. On the undersides of ionospheric layers this gradient maximizes in the daytime, leading to a simple explanation of any scintillation phenomenon that maximizes around midday. Above the level of maximum electron density in the *F* region, one would not expect much diurnal variation in the gradient of electron density. The only level in the ionosphere, therefore, where the gradient of electron density could vary in such a way as to produce a maximum at night is between the *E* and *F* regions. This again directs attention to the interval of height between the *E* and *F* regions as a possible location for the origin of scintillations in intensity. It seems, however, that the effect is not quantitatively large enough to explain the observed nocturnal maximum of amplitude scintillations.

Another effect to be considered is that of electromagnetic damping of turbulence. Associated with the irregular motions there would be irregular currents that would remove energy from the turbulent motion by collision processes. Electromagnetic damping of turbulence is proportional to ionization density and therefore maximizes in the daytime. Qualitatively, therefore, electromagnetic damping of turbulence could be used to explain a nighttime maximum in radio star scintillation, but quantitatively the effect has not been shown to be adequate.

Therefore, the position seems to be that atmospheric turbulence is the most likely source of the irregularities of electron density in the ionosphere that cause scintillation of radio stars, spread *F*, and many other ionospheric phenomena. However, no satisfactory explanation has been forthcoming for the nighttime maximum of radio star scintillation and spread *F*.

## BIBLIOGRAPHY

- [1] Ryle, M., "A New Radio Interferometer and Its Application to the Observation of Weak Radio Stars," *Proceedings of the Royal Society*, Vol. 211 (February-March, 1952), pp. 351-375.
- [2] Ryle, M. and Hewish, A., "The Effects of the Terrestrial Ionosphere on the Radio Waves from Discrete Sources in the Galaxy," *Monthly Notices of the Royal Astronomical Society*, Vol. 110 (1950), pp. 384-394.
- [3] Hewish, A., "The Diffraction of Galactic Radio Waves as a Method of Investigating the Irregular Structure of the Ionosphere," *Proceedings of the Royal Society*, Vol. 214 (August-October, 1952), pp. 494-514.
- [4] Little, C. G. and Maxwell, A., "Fluctuation in the Intensity of Radio Waves from Galactic Sources," *Philosophical Magazine*, Vol. 42 (1951), pp. 267-278.
- [5] Stanley, G. J. and Slee, O. B., "Galactic Radiation at Radio Frequencies, II. The Discrete Sources," *Austrian Journal of Physics*, Vol. A3 (1950), pp. 234-250.
- [6] Mills, B. Y. and Thomas, A. B., "Observations of the Source of Radio Frequencies Radiation in the Constellation of Cygnus," *Austrian Journal of Physics*, Vol. A 4 (1951), pp. 158-171.
- [7] Bolton, J. G., Slee, O. B., and Stanley, G. J., "Galactic Radiation at Radio Frequencies. VI. Low Altitude Scintillation of the Discrete Sources," *Austrian Journal of Physics*, Vol. A 6 (1953), pp. 434-451.
- [8] Smith, F. G., "Ionospheric Refraction at 81.5 Mc/s Radio Waves from Radio Stars," *Journal of Atmospheric and Terrestrial Physics*, Vol. 2 (1952), pp. 350-355.

- [9] Little, C. G. and Maxwell, A., "Scintillation of Radio Stars During Aurorae and Magnetic Storms," *Journal of Atmospheric and Terrestrial Physics*, Vol. 2 (1952), pp. 356-360.
- [10] Maxwell, A. and Dagg, M., "A Radio Astronomical Investigation of Drift Movements in the Upper Atmosphere," *Philosophical Magazine*, Vol. 45 (January-June, 1954), pp. 551-569.
- [11] Spencer, M., "The Shape of Irregularities in the Upper Atmosphere," *Proceedings of the Physics Society*, Vol. 68B (1955), pp. 493-503.
- [12] Wild, J. P., and Roberts, J. A., "The Spectrum of Radio Star Scintillations and the Nature of Irregularities of the Ionosphere," *Journal of Atmospheric and Terrestrial Physics*, Vol. 8 (1956), pp. 55-75.
- [13] Hartz, T. R., "Radio Star Scintillations in the Ionosphere," *Canadian Journal of Physics*, Vol. 33 (1955), pp. 476-482.
- [14] Harrower, G. A., "A Consideration of Radio Star Scintillations as Caused by Particles Entering the Ionosphere," *Canadian Journal of Physics*, Vol. 35 (1957), pp. 512-522, 792.
- [15] Booker, H. G., Ratcliffe, J. A., and Shinn, D. H., *Transactions of the Royal Society*, Vol. 242 (1950), p. 579.
- [16] Smith, F. G., "Origin of the Fluctuations in the Intensity of Radio Waves from Galactic Sources," *Nature*, Vol. 165 (1950), pp. 422-423.
- [17] Little, C. G., and Lovell, A. C. B., *Nature*, Vol. 165 (1950), pp. 423-424.
- [18] Little, C. G., "Diffraction Theory of the Scintillations of Stars on Optical and Radio Wavelengths," *Monthly Notices of the Royal Astronomical Society*, Vol. 111 (1951), pp. 289-302.
- [19] Hewish, A., "The Diffraction of Radio Waves in Passing Through a Phase-Changing Ionosphere," *Proceedings of the Royal Society*, Vol. 209 (1951), pp. 81-96.
- [20] Ratcliffe, J. A., "Some Aspects of Diffraction Theory and Their Application to the Ionosphere," *Reports on the Progress of Physics*, Vol. 19 (1956), pp. 188-267.
- [21] Booker, H. G., and Gordon, W. E., "A Theory of Radio Scattering in the Troposphere," *PROCEEDINGS OF THE IRE*, Vol. 38 (June, 1950), pp. 401-412.
- [22] Booker, H. G., "Turbulence in the Ionosphere with Applications to Meteor-Trails, Radio-Star Scintillation, Auroral Radar Echoes, and Other Phenomena," *Journal of Geophysical Research*, Vol. 61 (December, 1956), pp. 673-705.
- [23] Booker, H. G., and Cohen, R., "A Theory of Long-Duration Meteor Echoes Based on Atmospheric Turbulence with Experimental Confirmation," *Journal of Geophysical Research*, Vol. 61 (December, 1956), pp. 707-733.
- [24] Booker, H. G., "Theory of Radio Star Scintillation with Application to Spread F," paper presented at spring URSI meeting, Washington, D. C., May, 1957.
- [25] Reber, G., "Spread F over Washington," *Journal of Geophysical Research*, Vol. 59 (1954), pp. 445-448.
- [26] Reber, G., "Worldwide Spread F," *Journal of Geophysical Research*, Vol. 61 (1956), pp. 157-164.
- [27] Chandrasekar, S., "A Statistical Basis for the Theory of Stellar Scintillations," *Monthly Notices of the Royal Astronomical Society*, Vol. 112 (1952), pp. 475-483.
- [28] Seeger, C. L., "Some Observations of the Variable 205 Mc/Sec Radiation of Cygnus A," *Journal of Geophysical Research*, Vol. 56 (1951), pp. 239-258.
- [29] Seeger, C. L., *Bulletin of the Astronomical Institutes of the Netherlands*, Vol. 13 (1956), p. 89.
- [30] Fejer, J. A., "The Diffraction of Waves in Passing Through an Irregular Refracting Medium," *Proceedings of the Royal Society*, Vol. 220 (October-December, 1953), pp. 455-471.
- [31] Keller, G., *Fluctuations of Starlight and Skylight*, Columbus: Ohio University, Perkins Laboratory, Technical Report No. 1.
- [32] Megaw, E. C., *Proceedings of the IEE*, Part C, Monograph No. 236 R.
- [33] Dagg, M., *Journal of Atmospheric and Terrestrial Physics*, Vol. 10 (1957), p. 194.
- [34] Dagg, M., *Journal of Atmospheric and Terrestrial Physics*, Vol. 10 (1957), p. 204.
- [35] Dueño, B., paper presented at spring URSI meeting, Washington, D. C., May, 1956.
- [36] Vitkevitch, V. V., work reported at XIIth General Assembly of URSI, Boulder, Colorado, August, 1957.
- [37] Briggs, work reported by A. Hewish at XIIth General Assembly of URSI, Boulder, Colorado, August, 1957.
- [38] Maxwell, A., "Turbulence in the Upper Ionosphere," *Philosophical Magazine*, Vol. 45 (July-December, 1954), pp. 1247-1254.
- [39] Gold, T., Discussion at XIIth General Assembly of URSI, Boulder, Colorado, August, 1957.
- [40] Phillips, G. J., and Spencer, M., "The Effects of Anisometric Amplitude Patterns in the Measurement of Ionospheric Drifts," *Proceedings of the Physical Society (London)*, Vol. 68B (1955), pp. 481-492.
- [41] Wright, J. W., and Knecht, R. W., *Atlas of Ionograms Compiled for the URSI/AGI Special Committee on World Wide Ionospheric Soundings*, Boulder: National Bureau of Standards, 1957.



# An Investigation of the Perturbations Imposed Upon Radio Waves Penetrating the Ionosphere\*

ROBERT S. LAWRENCE†

**Summary**—A new method has been devised to measure continuously the phase deviations introduced by the ionosphere into the signals from discrete sources. Sample recordings of measurements at frequencies of 53, 108, and 470 mc are given. An experiment combining this phase measuring technique and standard ionospheric soundings at the point of penetration of the line of sight is in progress and is expected to shed light upon the height of origin of ionospheric scintillations.

## INTRODUCTION

THE National Bureau of Standards has undertaken a program to study the perturbations imposed upon radio waves penetrating the ionosphere. The program consists primarily of observations of extra-terrestrial discrete radio sources, loosely called "radio stars." These sources undergo apparent fluctuations in intensity, called "amplitude scintillations," and fluctuations in position, called "phase scintillations."<sup>1-9</sup> The observations will emphasize phase scintillations, and are designed to improve our knowledge of variations with radio frequency of the magnitude and rate of these ionospheric effects.

An important aspect of the program is the effort to determine the region or regions in the ionosphere responsible for the observed phenomena. The times of occurrence of various scintillation effects are to be compared with several types of vertical-incidence soundings. The sounding station is situated so as to observe the same ionosphere which causes the scintillations. The soundings to be made include sweep-frequency

ionograms,<sup>10</sup> phase-path observations at fixed frequency,<sup>11</sup> and measurement of ionospheric "winds."<sup>12,13</sup>

## SCINTILLATIONS

### *The Problem of Measuring Phase Scintillations*

When observed through the ionosphere, a radio star seems to fluctuate in both intensity and position in a manner analogous to the twinkling and dancing of visible stars. These fluctuations, known as "amplitude scintillations" and "phase scintillations," respectively, are produced by diffraction effects in the ionosphere.<sup>14-20</sup>

In principle, amplitude scintillations may be measured with a receiver and a wide-beamed antenna, tracking the mean position of the star. Output fluctuations of amplitude larger than those permitted by the product of bandwidth and time constant of the system will be caused by amplitude scintillations uncontaminated by effects of the phase scintillations. In practice, some sort of interferometer is generally used to determine that the fluctuations are in the source rather than caused by interference or variations in system gain.

The complementary process of measuring uncontaminated phase scintillations is more difficult. A standard method involves the use of the Ryle interferometer<sup>21</sup> in which the difference in the signal from two complemen-

\* Original manuscript received by the IRE, November 6, 1957. This work has been supported by the USAF under Contract DO-56-WDD-4-1.

† National Bureau of Standards, Boulder, Colo.

<sup>1</sup> J. S. Hey, S. J. Parsons, and J. W. Phillips, "Fluctuations in cosmic radiation at radio frequencies," *Nature*, vol. 158, p. 234; August 17, 1946.

<sup>2</sup> J. G. Bolton and G. J. Stanley, "Variable source of radio frequency radiation in the constellation of Cygnus," *Nature*, vol. 161, pp. 312-313; February 28, 1948.

<sup>3</sup> C. G. Little and A. C. B. Lovell, "Origin of the fluctuations of the intensity of radio waves from galactic sources," *Nature*, vol. 165, pp. 423-424; March 18, 1950.

<sup>4</sup> F. G. Smith, "Origin of the fluctuations in the intensity of radio waves from galactic sources," *Nature*, vol. 165, pp. 422-423; March 18, 1950.

<sup>5</sup> R. H. Brown and C. Hazard, "Radio survey of the Cygnus region," *Monthly Notices Roy. Astron. Soc.*, vol. 111, pp. 576-584; 1951.

<sup>6</sup> K. Burrows and C. G. Little, "Simultaneous observations of radio star scintillations on two widely spaced frequencies," *Jodrell Bank Ann.*, vol. 1, p. 29 ff; December, 1952.

<sup>7</sup> A. Maxwell, "The scintillation of the radio stars," *Occ. Notes Roy. Astron. Soc.*, vol. 3, pp. 65-70; April, 1954.

<sup>8</sup> M. Spencer, "The shape of irregularities in the upper ionosphere," *Proc. Phys. Soc. B, London*, vol. 68, pp. 493-503; August, 1955.

<sup>9</sup> C. G. Little, W. M. Rayton, and R. B. Roof, "Review of ionospheric effects at vhf and uhf," *PROC. IRE*, vol. 44, pp. 992-1018; August, 1956.

<sup>10</sup> J. M. Carrol, "Automatic ionosphere recorder," *Electronics*, vol. 25, pp. 128-131; May, 1952.

<sup>11</sup> J. W. Findlay, "The phase and group paths of radio waves returned from region E of the ionosphere," *J. Atmos. Terr. Phys.*, vol. 1, pp. 353-366; 1951.

<sup>12</sup> S. N. Mitra, "A radio method of measuring winds in the ionosphere," *Proc. IEE*, pt. III, vol. 96, pp. 441-446; September, 1949.

<sup>13</sup> B. H. Briggs and M. Spencer, "Horizontal movements in the ionosphere," *Reps. Prog. Phys.*, vol. 17, pp. 245-280; 1954.

<sup>14</sup> H. G. Booker, J. A. Ratcliffe, and D. H. Shinn, "Diffraction from an irregular screen with applications to ionospheric problems," *Phil. Trans. Roy. Soc. A*, vol. 242, pp. 579-607; 1950.

<sup>15</sup> C. G. Little, "A diffraction theory of the scintillation of stars on optical and radio wavelengths," *Monthly Notices Roy. Astron. Soc.*, vol. 111, pp. 289-302; 1951.

<sup>16</sup> A. Hewish, "The diffraction of radio waves in passing through a phase-changing ionosphere," *Proc. Roy. Soc. A, London*, vol. 209, pp. 81-96; October, 1951.

<sup>17</sup> J. A. Fejer, "The diffraction of waves in passing through an irregular refracting medium," *Proc. Roy. Soc. A, London*, vol. 220, pp. 455-471; December, 1953.

<sup>18</sup> E. N. Bramley, "The diffraction of waves by an irregular refracting medium," *Proc. Roy. Soc. A, London*, vol. 225, pp. 515-518; September, 1954.

<sup>19</sup> J. P. Wild and J. A. Roberts, "The theory of ionospheric focussing with applications to the study of radio star scintillations," unpublished; 1955.

<sup>20</sup> J. A. Ratcliffe, "Some aspects of diffraction theory and their application to the ionosphere," *Reps. Prog. Phys.*, vol. 19, pp. 188-267; 1956.

<sup>21</sup> M. Ryle, "A new radio interferometer and its application to the observation of weak radio stars," *Proc. Roy. Soc. A, London*, vol. 211, pp. 351-375; March, 1952.

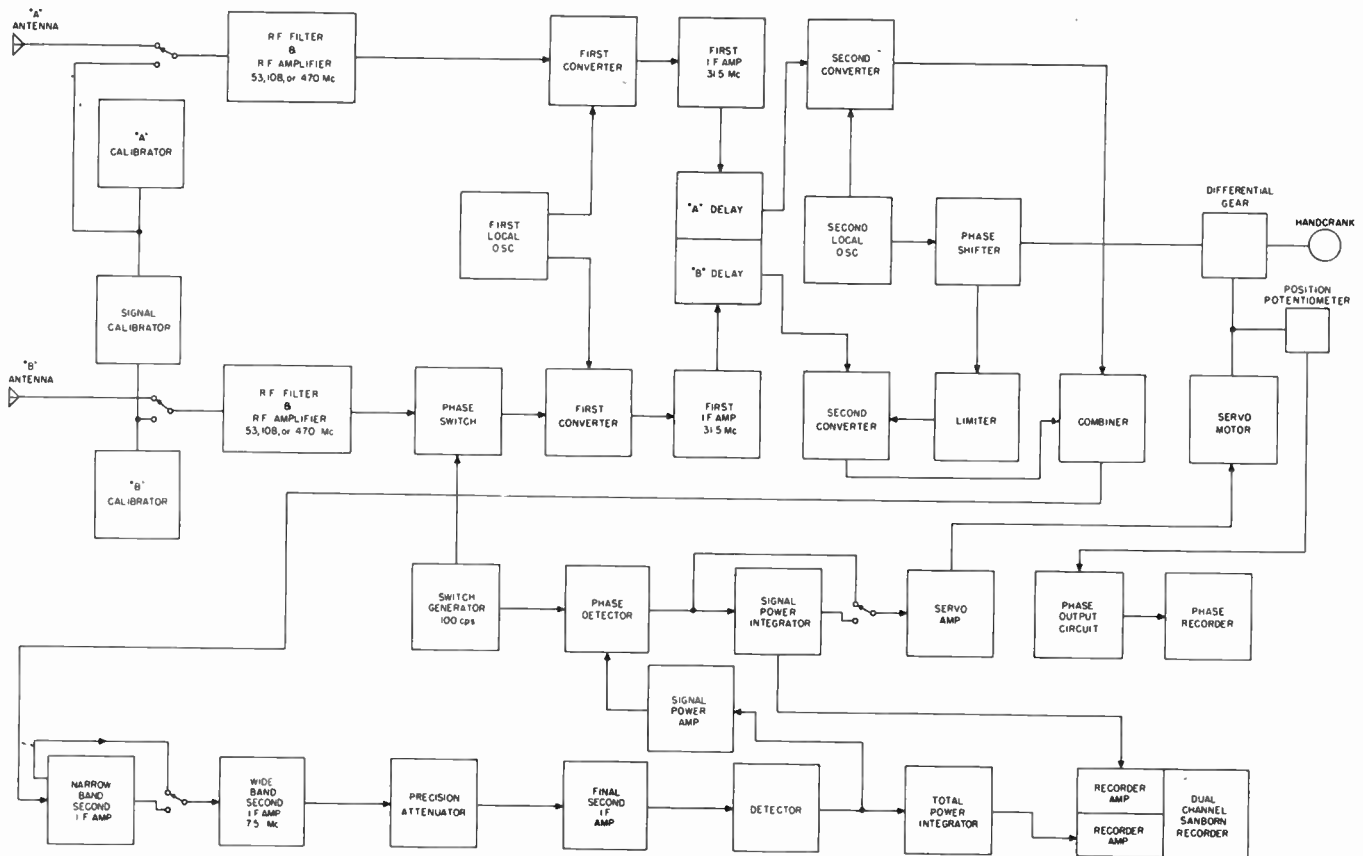


Fig. 1—Block diagram of phase scintillation receiver.

tary interferometer patterns is recorded. When a source moves steadily across the pattern of such an interferometer the recorded output passes through zero at regularly spaced intervals. The actual times of zero crossing may be compared with the times as computed from the diurnal motion of the source. Differences in these times provide a measure of the apparent deviations in the angular position of the source from its diurnal path. Such determinations can be made only at the times of zero crossings; thus, this method can give at most three or four measurements per minute. It cannot provide anything approaching a continuous record from which the higher-frequency components of the phase scintillations may be studied.

#### Principle of the Scintillation Receivers

Fig. 1 shows the block diagram of an instrument designed to provide a continuous measurement of apparent position. The instrument is a Ryle interferometer to which a rotary phase shifter has been added so that the whole interferometer pattern may be moved at will. A servomotor drives the phase shifter so as to keep the output of the interferometer always at a null; *i.e.* to keep the source always at a zero crossing. Under this condition the position of the shaft of the phase shifter continuously mimics the apparent position of the source.

The instrument consists of nearly identical signal channels for the interferometer's two antennas. Each signal is filtered to remove high-level interference outside

the desired frequency band, and amplified. Channel *B* then passes through a phase switch which, at the rate of 100 cycles per second, alternately inserts and removes an extra half-wavelength of transmission line.

The radio frequency is then converted to 31.5 mc and further amplified. The first local oscillator and the rf filters and amplifiers can be tuned easily over a range of  $\pm 2$  mc from their nominal frequencies. Each channel then passes through a delay line which may be manually selected to provide 0.0, 0.5, or 1.0 microsecond of delay. When the interferometer is used for sources near its plane of symmetry no delay is needed. However, if it is desired to observe a source in, say, the one-hundredth lobe with a bandwidth which is one hundredth of the center frequency, serious loss of visibility will occur because the lobe pattern is frequency dependent. When the source is directly on the lobe as measured at the center frequency, it will be half way between lobes as measured at a frequency near the edge of the pass band. This cancellation of the lobe pattern is removed by insertion of a delay which will, in effect, move the zeroth lobe away from the plane of symmetry and into the vicinity of the source.

After the delay has been introduced the signal is converted to 7.5 mc. For channel *A* the second converter is operated directly by the local oscillator, but for channel *B* a variable phase shift is introduced. The shifter is a rotary device which translates shaft rotation directly into electrical phase. Its shaft is operated

through a differential gear so that it may be controlled either by a hand crank or by the servomotor. Sufficient friction is introduced so that the motor and the crank will turn only the phase shifter and not each other. The servomotor also operates a linear potentiometer which is used to drive a recorder.

The converted signals then are combined and passed through amplifiers which determine the system bandwidth. Provision is made for manual selection of either of two bandwidths. Then an adjustable precision attenuator and further amplification precede detection of the signal. The detected signal is used in two ways. It is passed through an adjustable low-pass filter and recorded as "total power" received by the system; also through a band-pass filter centered on the 100-cps switching frequency and presented to the phase detector.

The phase detector rectifies the varying 100-cps signal synchronously with respect to the phase switch. In effect, its output is proportional to the difference in input power in the two positions of the phase switch. This output is passed through an adjustable low-pass filter and recorded as the "signal power" received by the system. The signal power, either before or after integration by the low-pass filter, is amplified and used to operate the servomotor.

Three noise diodes are provided as an alternate input to the receivers. Two of these, called the *A* and *B* calibrators, are connected independently to the two receivers. Since the noise they produce is uncorrelated, they will have no effect upon the signal power recorder except to increase the random fluctuations always present when noise is being measured. Thus, they affect the system in the same way as does the general background of galactic noise, and may be used to simulate that background. The third noise diode is the signal calibrator, connected simultaneously to both receivers with a direct effect upon the observed signal power. Thus it can be used to simulate a discrete source.

#### *Design Parameters of the Scintillation Receivers*

Inspection of a list of discrete sources<sup>22</sup> quickly shows that four of the ones available to northern observers are considerably more intense than all others. Of these four, the two brightest are Cygnus A and Cassiopeia A. The angular diameter of Cygnus A is sufficiently smaller than the others to suggest that it is the best choice of all sources for our purpose. More detailed considerations, involving the intensity of galactic background in the neighborhood of each source, the path through the sky for north temperate latitudes, and the spectra of the sources, do nothing to change this situation.

If one computes for a given antenna aperture the ratio of signal power to background power as a function of frequency, the optimum frequency for the study of scintillations appears to lie in the range 100 to 200 mc.

<sup>22</sup> J. L. Pawsey, "A catalogue of reliably known discrete sources of cosmic radio waves," *Astrophys. J.*, vol. 121, pp. 1-5; January, 1955.

Then, choosing an antenna size and assuming an inverse-square law of frequency dependence for scintillations, one can estimate the maximum frequency range over which useful scintillation observations can be made. From such considerations three frequencies were chosen for observations of phase scintillations. The exact frequencies, and the reasons for their choice are:

1)  $53 \pm 2$  mc. The low end of this range lies in an amateur radio band and as such is relatively free from nearby, high-powered transmitters. The upper end lies in television channel 2 and will be usable and quite vacant during the early morning hours.

2)  $108 \pm 2$  mc. This range is centered on the frequency which is planned for the earth satellite. Observations of the satellite with this equipment would be of more than passing interest. Local interference in this frequency range seems to be at least as scarce as at any nearby portion of the spectrum.

3)  $470 \pm 2$  mc. The upper end of this range lies in television channel 14, a channel in which no stations are known to be operating, with the possible exception of Worcester, Mass. Experience with the lower end of this range shows that while it is used sporadically for communication in the Rocky Mountain area, it is usually possible to find a frequency which will remain vacant for several months.

The bandwidth of the 53 and 108-mc receivers is 50 kc or 500 kc at the option of the operator. For the 470-mc receiver the operator has the option of 200-kc or 2-mc bandwidths. Considerable attention has been paid to the problem of suppression of interfering signals. For example, the response of the 53-mc receiver is down by 100 decibels at all frequencies more than 1.1 mc from the center frequency. Signals of 20 millivolts at frequencies more than 1.5 mc from the center frequency have no effect upon the recorder deflection.

The integrating networks for the total power and signal recorders permit manual selection of time constants of 0.2, 2, 5, 10, or 20 seconds.

#### *Geometry of the Scintillation Experiment*

The scintillation observations will be made at the NBS field site on Table Mesa (latitude  $40^{\circ} 7'.7$  N, longitude  $105^{\circ} 14'.3$  W), about 12 miles north of Boulder, Colo. The associated ionospheric observations will be made from a site (latitude  $42^{\circ} 5'$  N, longitude  $102^{\circ} 20'$  W) near Ellsworth, Neb.; beneath the point where the line of sight from Table Mesa to Cygnus A penetrates the *E* region when Cygnus A is rising at an elevation angle of  $15^{\circ}$  from Table Mesa.

The interferometer, consisting of two 40-foot paraboloidal reflecting antennas, is arranged on a east-west base line 475 meters in length. The 108 mc lobe pattern to be expected for an east-west interferometer at Table Mesa is shown in Fig. 2. An east-west base line has been chosen rather than a northwest-southeast one despite the fact that the latter arrangement would permit con-

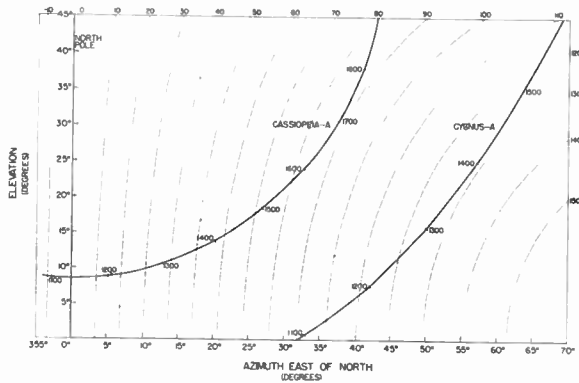


Fig. 2—108-mc lobe pattern from Table Mesa. Small numbers along starpath are local sidereal time. Every tenth lobe, numbered from the plane of symmetry, is shown as a dotted line.

tinuous observation of the rising Cygnus A in low-order lobes and would eliminate the need for the delay lines in the receivers. The east-west arrangement, like a north-south one, is symmetrical for rising and setting and thus, in effect, doubles the possible observing time for a given star. The east-west arrangement has the further advantages of allowing observations of Cassiopeia A near lower culmination and of providing a more versatile instrument for use with other sources.

The 475-meter spacing of the antennas was determined by the following considerations: Increased base length means closer lobe spacing and therefore greater angular resolution. It is essential, however, that the lobe spacing be larger than the source; otherwise the source will not appear on the signal recorder. In addition, the lobes must be separated far enough to prevent phase scintillations from jumping lobes. If this should happen, the ambiguity inherent in an interferometer would prevent quantitative conclusions from being reached. At 470 mc the 475-meter spacing gives a minimum lobe separation of 4.6 minutes of arc, just slightly greater than the diameter of Cassiopeia A. At 53 mc the minimum lobe spacing is 43 minutes, probably large enough to prevent lobe jumping. The antennas and receivers have been designed to permit estimation of the position of Cygnus A to within about one tenth of a lobe. The precision of measurement of phase scintillations is therefore better than 1 minute at 470 mc and 108 mc, and better than 6 minutes at 53 mc.

### Antennas

The two 40-foot paraboloidal reflecting antennas are modifications of the standard 28-foot paraboloids manufactured by the D. S. Kennedy Company. The extensions to 40 feet were designed and constructed at NBS. Each extension consists of 252 radial whips of  $\frac{3}{8}$ -inch aluminum tubing fastened together by 15 circular tension members of  $\frac{1}{8}$ -inch aluminum wire. Around the edge is a 2-inch  $\times$   $\frac{1}{8}$ -inch band of aluminum. The entire structure forms a grid with holes less than six inches square and weighs less than 200 pounds. This simple extension has proved to be both stable and accurate enough for use at 470 mc. One of the antennas is shown in Fig. 3.



Fig. 3—One of the two 40-foot paraboloidal reflectors.

The feed, designed and constructed by Jasik Laboratories, serves for all three frequencies simultaneously. Multicouplers permit the use of a single coaxial transmission line for the three frequencies.

### Recording and Analysis of Scintillation Data

Three output voltages are recorded from each of the three receiving systems. The total power record provides information on system gain, interference, and stability. The signal power record can be used in two ways. When the servoloop is disconnected and the phase shifter is either stationary or driven at a uniform rate, the signal power record shows the amplitude of the source, giving information about amplitude scintillations. When the servo is operating the signal power record remains close to zero. Deviations provide an indication of servo failure or of phase scintillations which are too rapid for the servo to follow.

The principal information to be obtained from the system is a record of servomotor shaft position, *i.e.*, of phase deviation. Such records, called "phase recordings," are obtained from the three recording systems and presented on three channels of a single sheet of paper. In the absence of phase scintillations the phase recording is a regular series of slanting lines, following the diurnal motion of the source. Phase scintillations are evidenced by deviations from linearity of these traces. A refinement which may be introduced is to drive the hand crank on the phase shifter at such a slowly variable rate as to compensate for the diurnal motion. This would straighten the traces on the phase records so that only phase scintillations would be apparent. Sample records appear in Fig. 4.

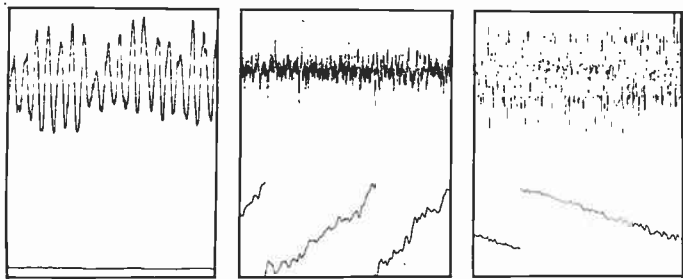


Fig. 4—Sample 108-mc recordings of the radio source Cassiopeia A. The left record shows the signal power (above) and the total power when the servomotor is driven at a constant speed so as to sweep the lobes across the sky. Amplitude scintillations are evident. The middle record shows the signal power (above) and phase recording 10 minutes later when the servo is tracking. Phase scintillations of moderate size show clearly. The right-hand record is similar to the middle one but was taken during strong atmospheric interference and at a time when phase scintillations were almost completely absent. Each record is 6 minutes long.

The paper charts just described contain essentially all the information to be gleaned from the scintillation observations. Their analysis involves various simple but repetitive scaling and statistical operations. Most of this labor is avoided by supplementing the paper records with automatically prepared punched paper tape which can be handed directly to an electronic computer. The signal power, the phase-shifter shaft position, or both are represented on the paper tape by a six-bit binary number. A seventh bit is used for identification and control information. The output from a single channel may be sampled as frequently as twice per second, or multiple channels may be sampled sequentially.

#### ASSOCIATED IONOSPHERIC OBSERVATIONS

##### Introduction

Existing information concerning the levels at which scintillations originate seems to be inconclusive. In England, Ryle and Hewish<sup>23</sup> observed a correlation between the time of occurrence of scintillations and spread *F*. Also in England, Little and Maxwell<sup>24</sup> reported such a correlation for scintillations observed at high angles of elevation. They found scintillations to be present continuously at low angles. About the same time Mills and Thomas<sup>25</sup> in Australia found no correlation between low-angle scintillations and sporadic *E* or spread *F*. However, an index of *F*-region activity prepared by Munro correlated significantly. Unfortunately, the observing times used by Munro did not usually cover the period of scintillation observations. Later, Hewish<sup>26</sup>

found that scintillations sometimes occurred during times when 2.4-mc echoes from the *F* region exhibited no fading. From this he concluded that the level of occurrence of scintillations must be greater than the level of reflection of 2.4-mc signals, *i.e.*, greater than 350 to 450 km. Comparison of the theory of diffraction through a thin phase-changing screen with the observed relationship between amplitude and phase scintillations suggested to Hewish that the irregularities are situated at a height of about 400 km.

About this same time, Little and Maxwell,<sup>27</sup> observing in England, found a fourfold increase in scintillation rate during auroras. They attributed this to an increased velocity of ionospheric wind. In their paper<sup>28</sup> they state categorically that this velocity pertains to the *F* region because the scintillations are caused by "sporadic *F* conditions." Meanwhile Bolton, Slee, and Stanley,<sup>29</sup> in Australia, were finding correlation only during the winter between low-elevation scintillations at 100 mc and spread *F*. They report a general, not detailed, correlation with sporadic *E* observed a few hundred kilometers from the point of penetration of the *E* region.

With regard to the correlation with spread *F*, Wells<sup>30</sup> pointed out that while the diurnal characteristics of scintillations and spread *F* are in good agreement, the lack of seasonal variations in scintillations casts doubt upon the reality of the relationship. In this country, Dueño<sup>31</sup> found some correlation with sporadic *E*, but none with spread *F*. However, his observations of the ionosphere were made at a point 300 km from the optimum for *E* effects and 1500 km from the optimum for *F* effects. By contrast, Hartz<sup>32</sup> reports that, on a yearly basis, he found a small positive correlation between 50-mc scintillations in Canada, abnormally high critical frequencies of the *F* region, and spread *F*; and a small negative correlation with sporadic *E*. None of his correlations was good on an hourly or daily basis. He concluded the *F* region is responsible for scintillations.

Recently Booker<sup>33</sup> has shown that turbulence cannot exist in the upper *F* region, and therefore that scin-

<sup>27</sup> C. G. Little and A. Maxwell, "Scintillation of radio stars during aurorae and magnetic storms," *J. Atmos. Terr. Phys.*, vol. 2, pp. 356-360; 1952.

<sup>28</sup> A. Maxwell and C. G. Little, "A radio-astronomical investigation of winds in the upper atmosphere," *Nature*, vol. 169, pp. 746-747; May 3, 1952.

<sup>29</sup> J. G. Bolton, O. B. Slee, and G. J. Stanley, "Galactic radiation at radio frequencies VI; low-altitude scintillations of the discrete sources," *Aust. J. Phys.*, vol. 6, pp. 434-451; December, 1953.

<sup>30</sup> H. W. Wells, "*F*-scatter at Huancayo, Peru and its relation to radio star scintillations," *J. Geophys. Res.*, vol. 59, pp. 273-277; June, 1954.

<sup>31</sup> B. Dueño, "Study and interpretation of low angle fluctuations from the radio star Cassiopeia as observed at Ithaca, N. Y.," Cornell Univ. School of Elec. Eng., Ithaca, N. Y., Tech. Rep. No. 27; September 25, 1955.

<sup>32</sup> T. R. Hartz, "Radio star scintillations and the ionosphere," *Can. J. Phys.*, vol. 33, pp. 476-482; August, 1955.

<sup>33</sup> H. G. Booker, "Turbulence in the ionosphere with applications to meteor trails, radio star scintillations, auroral radio echoes, and other phenomena," *J. Geophys. Res.*, vol. 61, pp. 673-705; December, 1956.

<sup>23</sup> M. Ryle and A. Hewish, "The effects of the ionosphere on radio waves from discrete sources in the galaxy," *Monthly Notices Roy. Astron. Soc.*, vol. 110, pp. 381-394; 1950.

<sup>24</sup> C. G. Little and A. Maxwell, "Fluctuations in the intensity of radio waves from galactic sources," *Phil. Mag.*, ser. 7, vol. 42, pp. 267-278; March, 1951.

<sup>25</sup> B. Y. Mills and A. B. Thomas, "Observations of the source of radio-frequency radiation in the constellation of Cygnus," *Aust. J. Sci. Res.*, ser. A, vol. 4, pp. 158-171; June, 1951.

<sup>26</sup> A. Hewish, "The diffraction of galactic radio waves as a method of investigating the irregular structure of the ionosphere," *Proc. Roy. Soc. A, London*, vol. 214, pp. 494-514; October, 1952.

tillations produced by turbulence must arise below 300 km. Wild and Roberts<sup>34</sup> found in Australia a strong correlation between low-angle nighttime scintillations and spread *F*, and weaker evidence of association of daytime scintillations with sporadic *E*. Some confirmation of the conclusion that nighttime scintillations are *F*-region and daytime scintillations are *E*-region phenomena comes from the velocity of the pattern on the ground. If the apparent drift is attributed entirely to the rotation of the earth, the derived heights of the scintillations are 500 km at night and 100 km by day.

Preparations are underway for a series of associated ionospheric experiments which will be operated in conjunction with the NBS scintillation program. The primary purpose of these experiments is to procure definitive evidence of the level of origin of the scintillations. These experiments will be vertical-incidence echo measurements, so the optimum location for comparison with the scintillation observations at Boulder is beneath the point of penetration of the disturbing ionospheric level by the line of sight to the radio star. For any particular level the diurnal motion of the star causes the optimum point to follow a regular and symmetrical path.

Ellsworth, Neb., lies on the *E*-region curve for Cygnus A at the point where the star is rising with an elevation angle of 15° from Boulder. This site has been chosen for the field station rather than a site on the *F*-region curve because *E*-region phenomena are known to vary more rapidly with geographical location than do *F*-region effects. Anyway, the *F*-region curve approaches within 80 km of Ellsworth when the elevation angle is 40°.

#### *Ionosphere Recorder*

The principal instrument at Ellsworth will be an NBS Model C-2 sweep-frequency ionosphere recorder.<sup>10</sup> This is a combination pulse transmitter and receiver which can be tuned rapidly from 1.5 to 25 mc and will display on film a plot of virtual height vs frequency. These records, called ionograms, will show the gross characteristics of the ionosphere such as critical frequencies, stratification of the *E* or *F* regions, sporadic *E*, spread *F*, etc. The intention is to secure such records frequently, perhaps every five or ten minutes, during the time when the radio star is rising at Boulder.

#### *Phase-Path Recorder*

An instrument to measure minute changes in the phase path of a pulse reflected from the ionosphere is a useful device which may be attached to the ionosphere recorder for fixed-frequency operation. This device was first used by Findlay<sup>11</sup> to study variations in the virtual height of the *E* region. It consists of a local oscillator which is detuned from the transmitted frequency by

a few kilocycles. The returning echo is mixed with this oscillator and the resulting beat frequency modulates the echo so that its trace appears banded. If the round-trip phase path to the ionosphere remains constant or varies slowly with time, the bands appear horizontal or slightly inclined, but systematic and regular. If, on the other hand, the phase path varies from minute to minute by more than, say, a radian the bands become distorted, irregular, or even discontinuous, suggestive of a turbulent or at least irregular reflecting region. It is reported to be common to observe irregular *E*-region echoes at the same time when *F* echoes are smooth and well behaved. This suggests strongly that, as we should expect from the larger retardation, the phase path is primarily influenced by the reflecting region. We believe that comparison of phase-path records with times of occurrence of scintillations may be very informative.

#### *Wind Recorder*

Also at Ellsworth, measurements will be made of winds or drifts by the spaced-receiver technique.<sup>12</sup> These observations will utilize pulses of some appropriate frequency in the range 2 mc to 6 mc received on three antennas placed at the corners of a 122-meter equilateral triangle. In general, the observed fading will correlate with a time lag for any pair of antennas. From the time lag, the component of the drift velocity in the direction of the line joining the antennas may be deduced. In addition, Briggs, Phillips, and Shinn<sup>35</sup> have shown that a comparison of the cross correlograms and the autocorrelogram of the fading can yield information concerning the turbulent or random velocity which alters the fading pattern on the ground. Incidentally, power spectrum of the fading can be found as a by-product of these data. Considerable progress has been made in interpretation of fading records of this type,<sup>36-38</sup> and comparison with scintillations may well prove illuminating.

#### ACKNOWLEDGMENT

Major contributions to the present state of the project have been made on a contract basis by H. I. Ewen, P. Strum, and H. Penfield of the Ewen-Knight Corporation; R. J. Grenzeback and C. W. Creaser of the D. S. Kennedy Company; and H. Jasik of the Jasik Laboratories. It is a pleasure to acknowledge the substantial assistance from R. Carle and E. Schiffmacher of NBS, and the benefits of many discussions with D. Farmer of the Ramo-Wooldridge Corporation, and with J. Warwick of the High Altitude Observatory.

<sup>35</sup> B. H. Briggs, G. J. Phillips, and D. H. Shinn, "The analysis of observations on spaced receivers of the fading of radio signals," *Proc. Phys. Soc. B, London*, vol. 63, pp. 106-121; February, 1950.

<sup>36</sup> G. J. Phillips and M. Spencer, "The effects of anisometric amplitude patterns in the measurement of ionospheric drifts," *Proc. Phys. Soc. B, London*, vol. 68, pp. 481-492; August, 1955.

<sup>37</sup> D. G. Yerg, "Notes on correlation methods for evaluating ionospheric winds," *J. Geophys. Res.*, vol. 60, pp. 173-185; June, 1955.

<sup>38</sup> N. F. Barber, "A correlation treatment of fading signals," *J. Atmos. Terr. Phys.*, vol. 8, pp. 318-330; 1956.

<sup>34</sup> J. P. Wild and J. A. Roberts, "Regions of the ionosphere responsible for radio star scintillations," *Nature*, vol. 178, pp. 377-378; August 18, 1956.

# A Phase Tracking Interferometer\*

HAYS PENFIELD†, MEMBER, IRE

**Summary**—A series of radio telescope receivers has been developed to operate in a switched interferometer system of the type described by Ryle.<sup>1</sup> The new features of the equipment include automatic tracking and recording of the phase difference of a coherent signal at the two receiver input terminals. Chart recorded outputs of total power, signal power, and signal phase are provided. The receiver utilizes dual low-noise rf amplifiers with a high degree of frequency selectivity. Fixed delay lines are available in both receiver channels to allow operation on the higher order lobes of the interference pattern. Front panel controls include a precision gain control, a receiver bandwidth selector, manual and automatic phase tracking controls, and signal power and total power integration time constant switches. Background and signal noise sources are provided for direct calibration of the receiver. Three of these receivers are currently in operation on frequencies of 53 mc, 108 mc, and 470 mc in a two-antenna drift interferometer at the National Bureau of Standards Laboratory in Boulder, Colo.

## INTRODUCTION

SINCE its initial use about a decade ago,<sup>2</sup> the radio interferometer has been used extensively in the field of radio astronomy to study both the location and size of extraterrestrial radio sources. The early interferometer systems operated on a total power principle in which the outputs of the two antennas were combined vectorially and fed to a receiver with the variation in total power output serving to indicate the presence of a coherent signal. The block diagram of the total power interferometer is shown in Fig. 1(a).

The problems of receiver gain instability in combination with the low signal to background noise ratio led to the development of the phase switching interferometer.<sup>1</sup> The block diagram of the phase switching interferometer is shown in Fig. 1(b). The distinguishing feature of this type of interferometer is the half-wave phase switch, which periodically inserts an additional half-wave section of transmission line in one channel of the receiver. This half-wave switching produces a lobe shift or inversion in the interferometer pattern such that the positions of the maxima in the unshifted pattern correspond to those of the minima in the shifted pattern. Thus, in the presence of a coherent input signal, the combined receiver output will contain an amplitude modulation component at the switching frequency. The output of the receiver is synchronously detected, thus cancelling out the background level and responding only to signals which are coherent at the two receiver inputs.

The phase tracking interferometer embodies the phase switching operation and goes one step further to

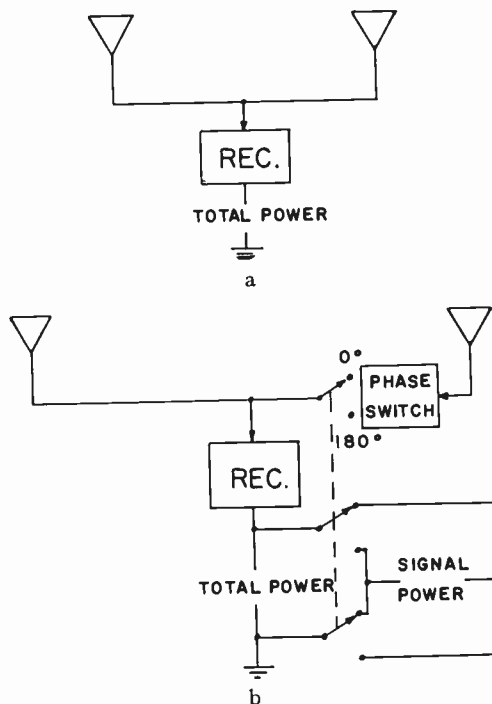


Fig. 1—Interferometer block diagrams. (a) Total power interferometer, (b) phase switching interferometer.

provide a controllable phase shifter in one of the receiver channels. The block diagram of the phase tracking interferometer is shown in Fig. 2. The phase shifter is connected in a feedback loop which acts to maintain a null condition at the synchronous detector output. This null condition corresponds to a  $90^\circ$  phase relation of the coherent signal at the point of combination. Thus, as the relative phase of a coherent signal in the two receiver channels changes, the phase shifter is driven in the proper direction to maintain the null output at the synchronous detector.

The two receiver channels utilize identical double conversion superheterodyne receivers with the combining of the two channels being made at the second IF. The local oscillator signals used in both receiver channels are derived from common local oscillators.

The phase shifter is located in the second local oscillator feed line to the second converter of one of the receiver channels.

Delay lines are provided in the two receiver channels to compensate for the large path length difference to the antennas when the signal source lies in the higher order lobes of the interferometer pattern. Normally these higher order lobes would be smeared out by the integration over the predetection bandwidth of the receiver.

The predetection bandwidth of the receiver is con-

\* Original manuscript received by the IRE, October 18, 1957.

† Ewen-Knight Corp., Needham, Mass.

<sup>1</sup> M. Ryle, "A new radio interferometer and its application to the observation of weak radio stars," *Proc. Roy. Soc. A*, vol. 211, pp. 351-375; March, 1952.

<sup>2</sup> M. Ryle and D. D. Vonberg, "An investigation of radio-frequency radiation from the sun," *Proc. Roy. Soc. A*, vol. 193, pp. 198-203; September, 1948.

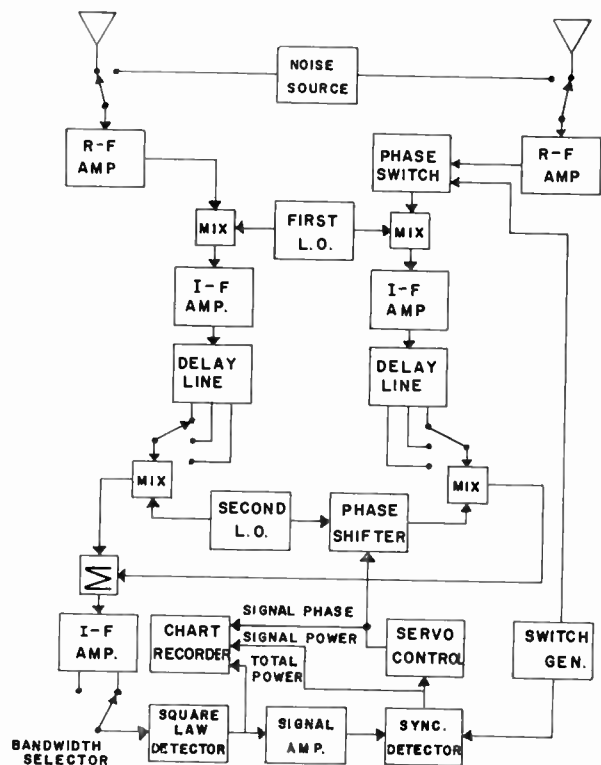


Fig. 2—Phase tracking interferometer block diagram.

trolled by the IF filter in the combined receiver channel, and a square law detector is utilized to give a dc output voltage which is proportional to the output power of the IF filter.

The phase switch modulation is amplified in the signal amplifier and fed to the synchronous detector which gives a dc output voltage proportional to the coherent signal power, and which has a polarity related to the phase of the phase switch modulation.

Fig. 3 shows the front view of the phase tracking interferometer receiver. The equipment is housed in two enclosed consoles with the block diagram engraved on the front panels. Front panel meters and controls are located at their appropriate position in the block diagram to facilitate equipment operation.

#### PERFORMANCE

The performance of the phase tracking interferometer may be described on the basis of the following parameters:

$T_s$  = the temperature contribution at the receiver input due to a discrete point source; this is the coherent signal.

$T_b$  = the temperature contribution at the receiver input due to galactic background radiation.

$T_r$  = the excess temperature of the receiver.

$\alpha$  = the ratio of power gains in the two receiver channels.

$\Delta f$  = the predetection noise bandwidth of the receiver.

$\tau$  = the receiver postdetection integration time constant.

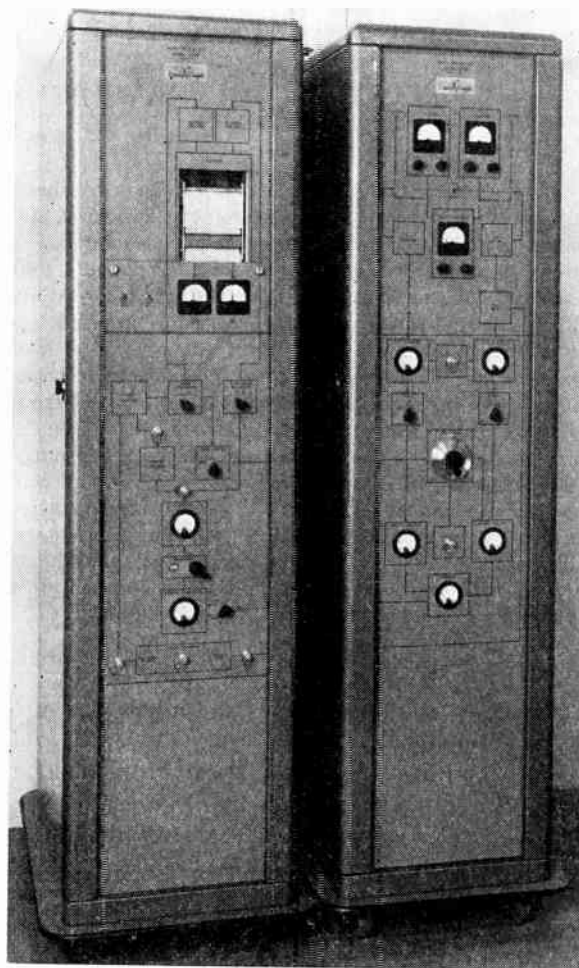


Fig. 3—Photograph of phase tracking interferometer receiver showing front panel engraving, meters, controls, and test points.

$\phi$  = the relative phase angle of the coherent signal,  $T_s$ , at the two receiver inputs.

$\theta$  = the phase angle introduced in one receiver channel by the phase shifter.

$f_c$  = the fundamental frequency of the phase reversal modulation produced in one channel by the phase switch.

The input signals to the receiver are assumed to have a flat power density spectrum over the frequency band-pass of the receiver and to have a Gaussian amplitude distribution. The receiver power levels are expressed in terms of effective temperature which is the usual notation in radio astronomy.

When the signals in the two channels are combined, the noncoherent voltages due to galactic background radiation and excess receiver noise add in direct proportion to the square root of the sum of the squared voltages and the coherent voltages due to a discrete source add directly with account being taken of the relative phase angle. The square law detector gives a dc output voltage proportional to the input power. Thus the voltage at the output of the square law detector will be directly proportional to the effective receiver input temperature and will consist of a dc level,

or total power term, plus a modulation component related to the coherent signal. The dc level is proportional to the sum of the effective receiver input temperatures due to the discrete source, the galactic background, and the excess receiver noise. The modulation component is a square wave function in which the magnitude is proportional to the product of the effective input temperature of the coherent signal and to the cosine of the sum of the relative phase angle of the coherent signal at the two receiver inputs and the phase angle introduced in one receiver channel by the phase shifter. Eq. (1) expresses the square law detector output voltage,  $E_0(t)$ , in terms of the parameters mentioned above and the receiver power gain constant,  $K_1$ .

$$E_0(t) = K_1 \left\{ (1 + \alpha)(T_s + T_b + T_r) + 2\sqrt{\alpha}T_s \cos [\phi(t) + \theta(t)] \left[ \sum_{n=\text{odd}}^{\infty} \frac{4}{n\pi} \sin 2\pi n f_c t \right] \right\}. \quad (1)$$

The synchronous detector performs a cross-correlation operation which results in an output voltage with an average (dc) level directly proportional to the magnitude of the coherent signal modulation component, and with a polarity determined by the phase of the modulation component relative to the phase of the reference signal in the synchronous detector. The output of the synchronous detector will fluctuate about this average level with a Gaussian distribution. The rms value of this fluctuation<sup>3</sup> is given by (2).

$$\text{rms fluctuation} = (1 + \alpha)K_1K_2 \frac{\pi 3/2}{8} \frac{1}{\sqrt{\Delta f \tau}} (T_b + T_r). \quad (2)$$

We may now investigate the phase tracking interferometer performance from a consideration of the signal-to-noise voltage ratio at the synchronous detector output. This signal-to-noise voltage ratio is defined as the average level due to a coherent signal divided by the rms fluctuation. Eq. (3) gives the expression for the synchronous detector output signal-to-noise voltage ratio.

$$\text{snr} = \frac{2\sqrt{\alpha}}{1 + \alpha} \frac{8}{\pi 3/2} \sqrt{\Delta f \tau} \frac{T_s}{T_b + T_r} \cos [\phi(t) + \theta(t)]. \quad (3)$$

The effects of the various terms of (3) on the interferometer performance are illustrated in Fig. 4 and Fig. 5. Fig. 4 shows the reduction in sensitivity which occurs when the ratio of power gain in the two receiver channels,  $\alpha$ , is changed by a factor of eight in both directions from unity. The decrease in sensitivity as  $\alpha$  departs from unity is a rather slow function and for differences in channel power gain of 3 db or less, the loss in snr is less than 6 per cent.

Fig. 5 illustrates the effect of predetection bandwidth and postdetection integration time on the rms fluctua-

<sup>3</sup> J. L. Pawsey and R. N. Bracewell, "Radio Astronomy," Oxford University Press, London, Eng., p. 43; 1955.

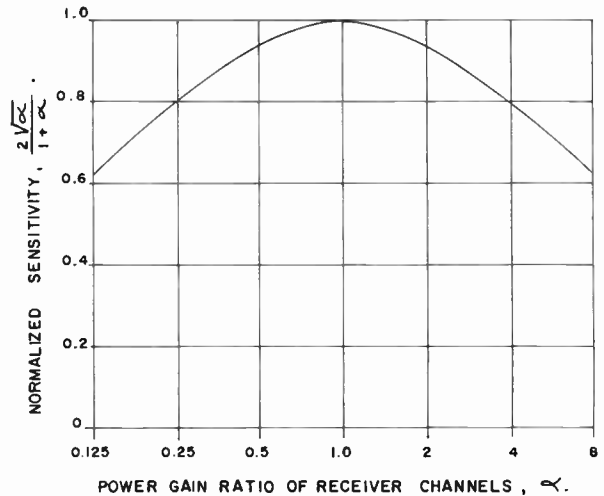


Fig. 4—Curve of reduction in receiver sensitivity as a function of power gain ratio in the two receiver channels.

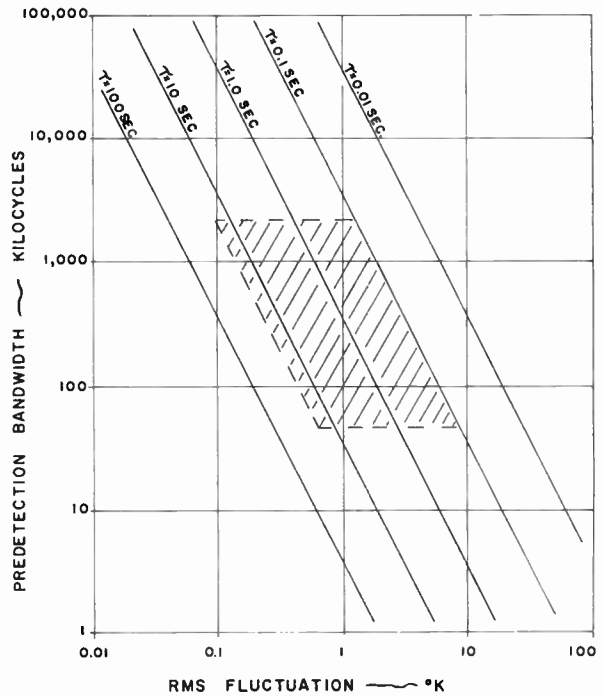


Fig. 5—Plot of rms fluctuation at the synchronous detector output as a function of predetection bandwidth for postdetection integration time constants of 0.01, 0.1, 1, 10, and 100 seconds. The rms fluctuation is given in degrees Kelvin for a background radiation plus excess receiver noise level of 1000° Kelvin.

tion in the synchronous detector output. The rms fluctuation is given in degrees Kelvin for a background radiation plus excess receiver noise level of 1000° Kelvin. The shaded area represents the range of predetection bandwidth and postdetection integration time used in the phase tracking interferometers.

In phase tracking operation the phase angle introduced by the phase shifter will be such that at the point of combination of the two receiver channels, the relative phase of the coherent signals will differ from 90° by a small error angle. The magnitude of this error angle will be a function of the servo loop gain, the postdetection

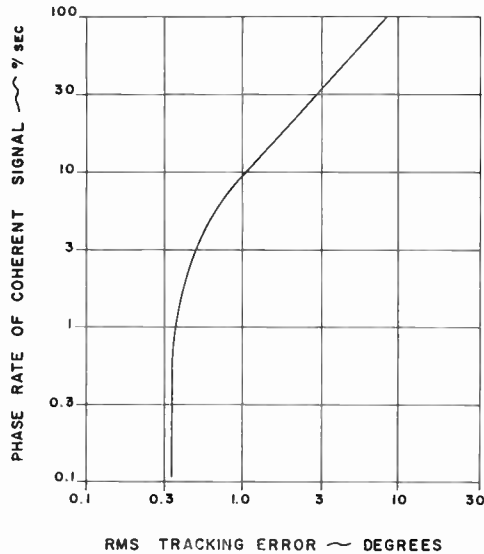


Fig. 6—Curve of rms tracking error angle as a function of rate of change of coherent signal phase at the two receiver inputs. Predetection bandwidth of 500 kc, a postdetection integration time constant of 0.2 second, a unity ratio of power gain in the two receiver channels and a ratio of input signal temperature to background plus excess receiver noise temperature of 0.05.

integration time constant, the rate of change of the relative phase of the coherent signal at the two receiver inputs, and the signal-to-noise voltage ratio at the output of the synchronous detector. The expression for the rms phase tracking error angle is given in (4) in terms of the previously defined system parameters and the servo loop gain constant,  $K_s$ .

$$\theta_{\text{Error}} = \frac{1 + \alpha \pi^{3/2}}{2\sqrt{\alpha}} \frac{1}{8} \frac{1}{\sqrt{\Delta f \tau}} \frac{T_b + T_r}{T_s} \frac{\left(\frac{d\phi}{dt} \tau + 1\right)}{K_s} \quad (4)$$

It should be noted that this expression has been simplified by considering only the single  $RC$  integration time constant and neglecting the other time constants associated with the servomotor and servoamplifier. This simplification is valid because these other time constants are very small relative to the  $RC$  integration time constant. Fig. 6 shows the rms tracking error angle as a function of rate of change of phase of a coherent signal at the two receiver inputs for a predetection bandwidth of 500 kc, a postdetection integration time constant of 0.2 second and a ratio of input signal temperature to background plus excess receiver noise temperature of 0.05.

Fig. 7 illustrates some typical recordings of signal power and signal phase made with one of the phase tracking interferometers. The signal phase recording is made in a linear fashion across the chart with a rapid flyback occurring at the end of each  $360^\circ$  of phase change. It should be noted that during phase tracking operation the signal power output will be maintained at or near its zero level. The signal phase recording plots the apparent change in phase of the coherent signal at the two antennas as a function of time. Any departure

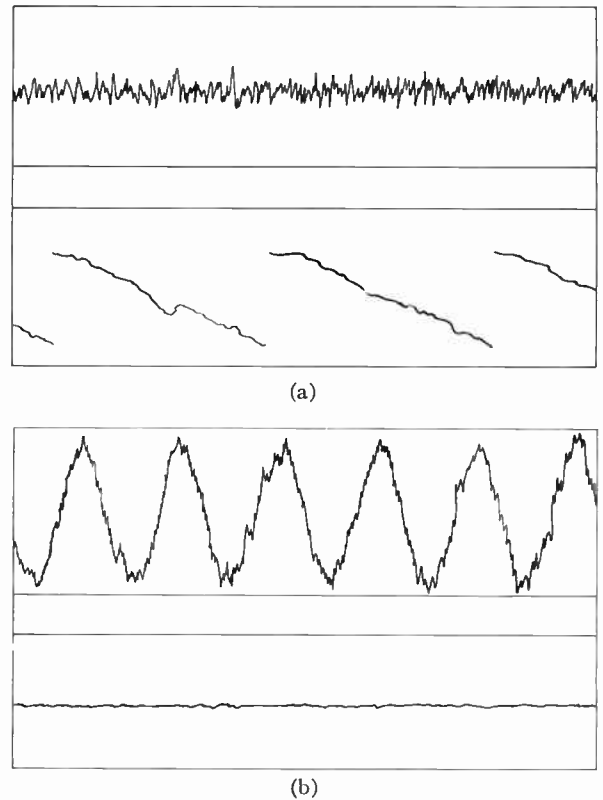


Fig. 7—Typical output recordings of the phase tracking interferometer. (a) Tracing of signal power and signal phase record made on Cassiopeia A at 108 mc with a predetection bandwidth of 500 kc and a postdetection integration time constant of 1 second. (Note the phase scintillation in the left-hand signal phase trace.) (b) Tracing of signal power and total power record made using the internal noise calibration sources. Operating frequency is 108 mc, predetection bandwidth of 50 kc, a postdetection integration time constant of 1 second, and a signal temperature to background plus excess receiver noise ratio of 0.045.

from the expected diurnal rate, therefore, represents a scintillation effect due to distortion of the coherent wave front in the earth's atmosphere. For this reason the phase tracking interferometer will be of particular value in studying the scintillation effects on radio waves passing through the earth's atmosphere. It is also expected that the interferometer receiver on 108 mc will give useful tracking data on the earth satellite.

The characteristics of the 53-mc, 108-mc, and 470-mc phase tracking interferometers are listed in Table I.

### PHASE SHIFTER DISCUSSION

The phase shifter used in the phase tracking interferometer is a rotary capacitor in which the stator plate is made up of four independent, symmetrically spaced segments. These four segments are driven successively by cables differing in electrical length by one-quarter wavelength at the second local oscillator frequency. Thus, as the rotor plate revolves, it couples successively to the segments giving a smooth transition through the complete  $360^\circ$  of electrical phase rotation. The rotor and stator plate angles and spacing are chosen to give a linear electrical phase shift as a function of the mechanical angular rotation of the rotor. The rotor shaft is

TABLE I  
CHARACTERISTICS OF THE 53-MC, 108-MC, AND 470-MC  
PHASE TRACKING INTERFEROMETER RECEIVERS

Operating Frequency	53 MC	108 MC	470 MC
$F$ (Noise Figure)	4 db	3 db	5 db
$T_r$	450°K	300°K	650°K
$T_b$ (Typical)	7500°K	1500°K	45°K
$\Delta f$	50 kc 500 kc	50 kc 500 kc	0.2 mc 2.0 mc
$\tau$	0.1 second ↓ 20 seconds	0.1 second ↓ 20 seconds	0.1 second ↓ 20 seconds

mechanically linked to a two-phase servomotor through a differential gear system. A hand crank is also connected to the phase shifter through the differential gear system to allow for manual control of the phase angle. A shaft-position potentiometer converts the mechanical shaft position at the servomotor input to the differential gear into dc voltage which is used to drive the signal phase recorder.

## CONCLUSION

The development of the phase tracking interferometer has come as a natural step in the development of the interferometer as a tool of the radio astronomer. The addition of the phase tracking feature allows for a more detailed study of the phase behavior of signals from outer space. In particular, the scintillation effect on these signals caused by the earth's atmosphere may be studied and correlated with other observations on atmospheric conditions.

A major contribution to the success of the equipment development has been the design and development of a simple and reliable phase shifter to operate at high radio frequencies.

## ACKNOWLEDGMENT

Credit for the original concept of these phase tracking interferometers must be given to Dr. R. S. Lawrence of the National Bureau of Standards, Boulder, Colo. The author is also indebted to Dr. H. I. Ewen and Peter D. Strum for their guidance and council during the design and construction of the equipment.

# Radio Astronomy Measurements at VHF and Microwaves\*

J. AARONS†, ASSOCIATE MEMBER, IRE, W. R. BARRON†, AND J. P. CASTELLI†

**Summary**—Radio astronomy measurements of atmospheric absorption, refraction, and scintillation, taken during the summer of 1956, and the spring of 1957, were made at 3.2 cm and 8.7 mm with the Sun as the source, and at 218 mc with solar energy and radiation from Cassiopeia A. Large tropospheric scintillations at angles below 3° made elevation accuracy difficult in the 8.7-mm and 3.2-cm bands. Refraction at 218 mc was greater than at the microwave wavelengths. Scintillations at 218 mc were present during periods of auroral activity. The information obtained has been useful in assessing radar angle-of-elevation accuracy and demonstrates the use of the sun and other celestial bodies as radiation sources for antenna pattern measurements.

## INTRODUCTION

IN THE radiofrequency spectrum, celestial bodies can be used as transmitters or reflectors. The one-way (transmitter) use concerns direct radiation from the object; the reflector (radar) use concerns earth-based or celestial radiation that is reflected from cele-

stial bodies. For our experiments we used the Sun and radio star Cassiopeia A as rf transmitters to obtain refraction, scintillation, and absorption data at 3.2 cm and 8.7 mm and refraction and scintillation data at 218 mc. This involved studying the effect of the earth's atmosphere. The sun and Cassiopeia A were used as sources of energy in the meter wavelength portion of the spectrum. In the microwave region, only the sun was used because the size of the equipments available (small parabolas) was insufficient to provide the very large collecting area required to obtain adequate signals at centimeter and millimeter wavelengths.

## FIELD SITES

The two sites used, one at Ipswich, Mass., and one at Scituate, Mass., are approximately 38 air miles apart. Both sites overlook the ocean. The Ipswich measurements, taken at sunrise, were made during the summer of 1956. For the microwave experiment, a series of altitudes was arbitrarily chosen, the azimuths calculated from the spherical trigonometry formula, and drift

\* Original manuscript received by the IRE, November 12, 1957.

† AF Cambridge Res. Center, Air Res. and Dev. Command, Bedford, Mass.

measurements taken. The parameters for the Ipswich equipments used are listed in Table I.

The two microwave antennas were placed on a single mount (see Fig. 1). Measurements were taken simultaneously at both bands. Individual fluctuations of the signals, as well as other data, could be compared.

The meter wavelength equipment at Scituate consisted of a 218-mc radio astronomy receiver and the Billboard antenna. This antenna, originally designed for an experimental radar, is in effect a sea interferometer. Energy reflected from the surface of the sea divides its radiation pattern into lobes. The lobes are maximum when

$$\frac{4\pi h \sin \theta}{\lambda} = \pi, 3\pi, 5\pi, \dots (2n - 1)\pi, \quad (1)$$

where  $h$  is the height above sea level and  $\theta$  is the elevation angle.

TABLE I  
IPSWICH MICROWAVE PARAMETERS

	X Band	$K_a$ Band
Parabolic antenna size	4'	18"
Measured half-power beam angle	2°	1° 40'
Attenuation of feed waveguides	4 db	0.8 db
Bandwidth	10 mc	10 mc
Time constants	2 seconds	6 seconds
Minimum detectable temperature difference	2°	2°
Wavelength	3.2 cm	8.7 mm
Frequency	9375 mc	32,320 mc

The Scituate antenna is 30 feet high by 75 feet wide with a nominal beam angle of 8° by 4°. Its mean height above sea level is 77 feet. The theoretical pattern of the Billboard antenna in the vertical plane is illustrated in Fig. 2. For low-angle measurements the two halves of the antenna are fed in phase. For measurements at higher angles, the transmission line to the upper bays of the antenna is lengthened by  $\lambda/2$  (antiphase position, denoted by  $A$  in Fig. 2).

A typical solar drift pattern is shown in Fig. 3. To record the solar coronal radiation, the receiver is initially set at its most sensitive position. As the sun rises and



Fig. 1—Microwave antenna assembly (4-foot parabola—3 cm; 18-inch parabola—8 mm) at Ipswich, Mass.

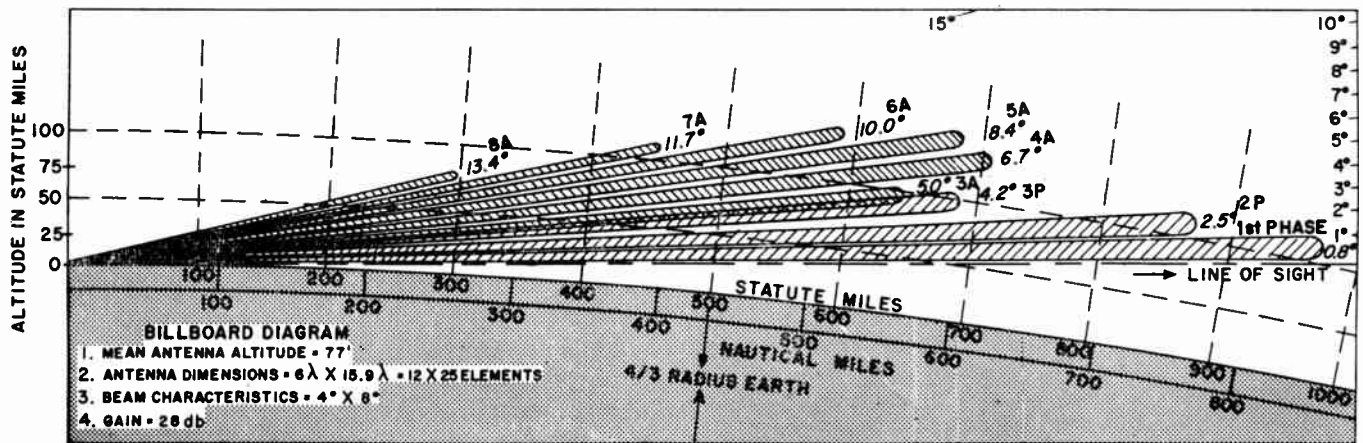


Fig. 2—Sea interferometer lobe pattern produced by reflections from the sea.

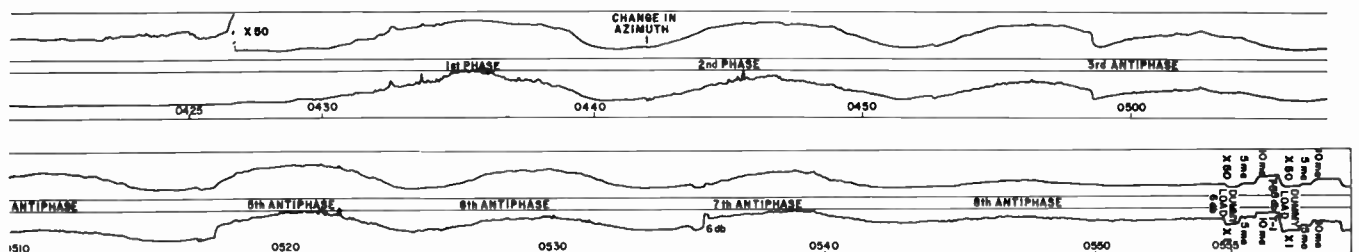


Fig. 3—Solar drift curves at 218 mc.

the intensity of radiation increases, the gain is turned down; as the sun drifts through each lobe in the pattern, the azimuth is changed.

Since the main attempt in the 218-mc experiment was to measure refraction and solar phenomena, the anti-phase position was used after the number 3 phase position. This position gave additional lobes at higher altitudes, with amplitudes considerably greater than the phase position could give in the same range of altitudes.

The Dicke radiometer used in all three units compares the power from a 50-ohm resistor with the power absorbed by the antenna and, by a phase-detecting system, amplifies only the difference. The upper half of Fig. 3 shows the radiometer power at 218 mc; the lower half shows the total receiver power (receiver energy plus antenna power).

### SOLAR DRIFT MEASUREMENTS

The basic technique for this experiment involved making a series of solar drift measurements. Antenna was set at a fixed elevation, azimuth and the sun allowed to drift through the pattern. A radio receiver tuned to WWV provided time markers for the record. After the sun passed through the antenna beam, antenna was set at the next elevation and azimuth position in the series.

The refraction at each position was measured by noting the time of transit at each elevation and comparing it with the astronomically calculated position of the center of the sun's disk. Fig. 4 is an example of the drift curves of the two microwave bands at two angles of elevation,  $1^{\circ}40'$  and  $7^{\circ}35'$  (the scale is changed with increasing altitude).

The scintillations, also seen with the antenna fixed in position for each of the drift curves, were measured for duration and depth of fade as the sun moved through the "blob" structure within the troposphere.

To measure absorption correctly, a tracking antenna must be corrected for refractive errors at low angles. Failure to correct for these errors will yield lower values for the apparent solar temperatures than the correct "middle of the beam" pattern.

For refractive measurements the altitude of the center of the antenna beam must be measured exactly although the azimuth may be only approximate. If the refraction is solely in the vertical plane the drift technique combined with accurate time measurements will correctly yield the refractive errors.

### THE MICROWAVE EXPERIMENTS

#### *Absorption and Sky Temperatures*

*Absorption:* In the microwave region studied, molecular oxygen and water vapor account for the absorption and scattering of energy. At 8.7 mm, attenuation is due about equally to water vapor and oxygen. At 3.2 cm the major part of the attenuation is produced by the oxygen.

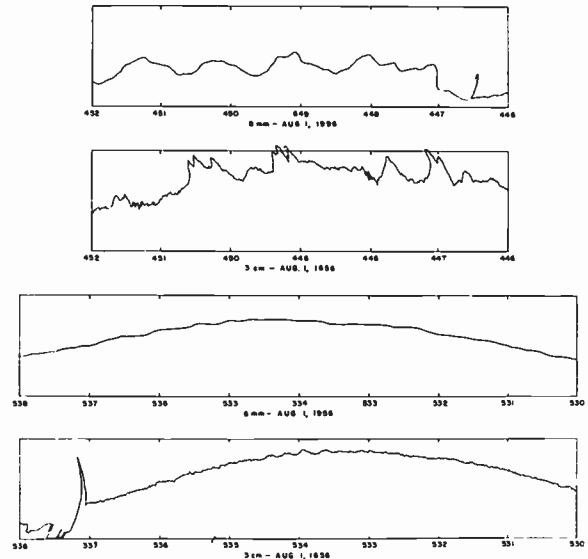


Fig. 4—Drift curve of sun (8 mm and 3 cm) at  $1^{\circ}40'$  and  $7^{\circ}35'$ .

Ground measurements by others made on both bands have yielded a mean absorption of 0.0097 db/km at 3.2 cm and 0.07 db/km at 8.7 mm.<sup>1</sup>

The advantages of the radio astronomy technique are several. The technique is comparative, the solar temperatures being compared at different altitudes where the recorded temperatures are directly related to the path length over which the energy travels through the atmosphere. Only one receiver has to be used; other techniques of measuring atmospheric attenuation require a ground plane and more than one receiver.

Another advantage in measuring by radio astronomy is that the absorption data (see Fig. 6 and Fig. 7) can be extrapolated to a height above the atmosphere to obtain an indication of the total attenuation.

Absorption was measured by recording the apparent temperature and sky background as the path length through the atmosphere decreased. Fig. 5 gives the path length as a function of altitude of a source, based on a curved earth model and 11.1 km as the assumed height of the atmosphere.

The temperatures of the sun and sky background at 14 different elevation angles were recorded for 40 days between July 30, and September 30, 1956. From the average temperature computed for each elevation angle, we subtracted the mean sky temperatures at the same elevation angles and azimuth overlooking the ocean. The data obtained is plotted in Fig. 6 for the 3.2-cm wavelength and in Fig. 7 for the 8.7-mm wavelength. At 3.2 cm the average solar temperature (extrapolated to beyond the earth's atmosphere) was  $16,000^{\circ}\text{K}$ , with an assumed solar diameter<sup>2</sup> of  $34'$ ; and at 8.7 mm it was  $5280^{\circ}\text{K}$ , with an assumed solar diameter of  $32'$ .

<sup>1</sup> J. H. Van Vleck, "Propagation of Short Radio Waves," Mass. Inst. Tech. Rad. Lab. Ser., vol. 13, McGraw-Hill Book Co., Inc., New York, N. Y., p. 641; 1951.

<sup>2</sup> S. F. Smerd, "Radio-frequency radiation from the quiet sun," *Aust. J. Sci. Res. A*, vol. 3, pp. 34-59; March, 1950.

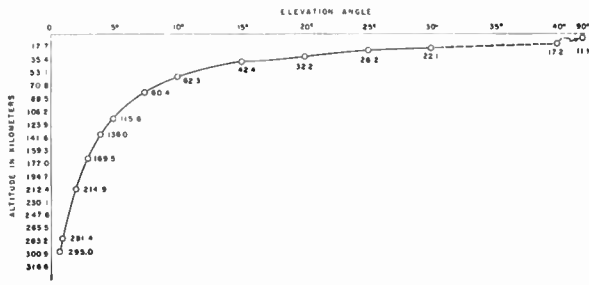


Fig. 5—Path length through atmosphere as a function of elevation. Angle assuming 11.1 km of atmospheric spherical earth model.

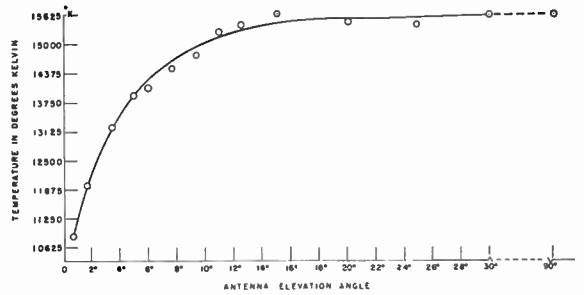


Fig. 6—Average temperature of sun (40 days), Ipswich, Mass., July 30–September 30, 1956.  $f=9375$  mc—ant BW=2° at  $P/2$ . Diameter of sun 0°34'.

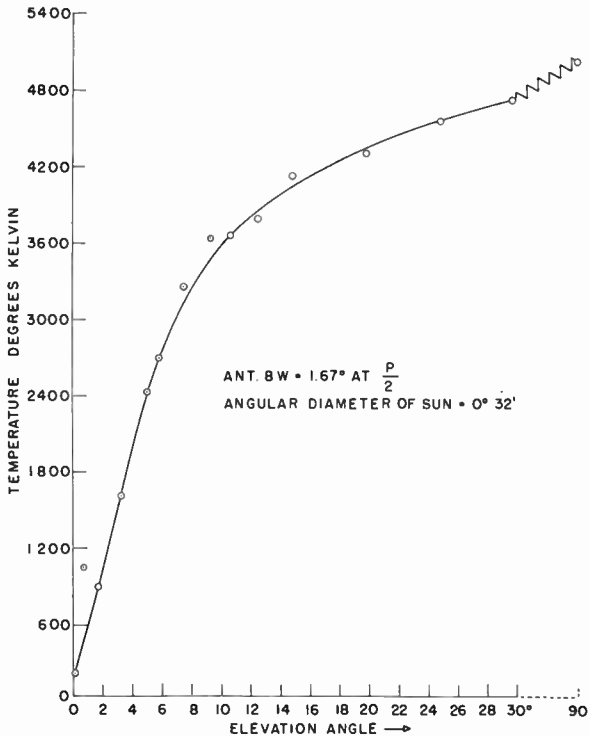


Fig. 7—Average temperature of sun, July 30–September 30, 1956. AFCRC, Ipswich, Mass.  $f=32,900$  mc.

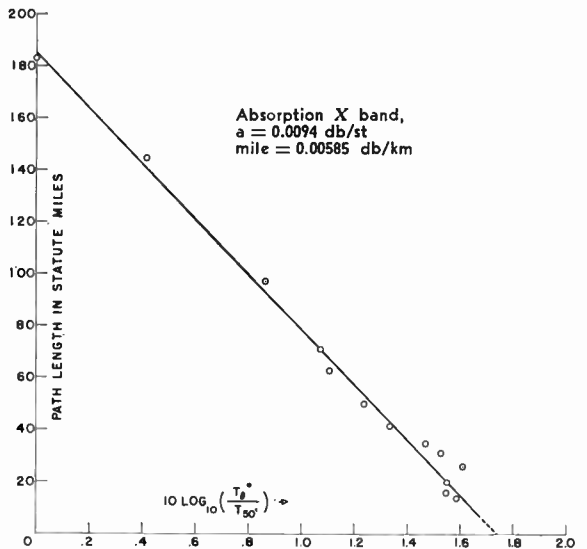


Fig. 8—Absorption 3.2 cm.

A plot of the ratio of

$$10 \log_{10} \frac{T \text{ at the antenna elevation angle}}{T \text{ at } 50' \text{ elevation}}$$

vs the path length in statute miles is shown in Fig. 8 for 3.2 cm and in Fig. 9 for 8.7 mm. The straight line drawn through the high elevation readings in the 8.7-mm curve denotes that these are more reliable than the readings at the lower altitudes, which were obscured by absorption and fluctuations.

The mean absorption is 0.033 db/km for the 8.7-mm region, in substantial agreement with ground measurements of the attenuation (previous measurements<sup>3</sup> by radio astronomy techniques have shown 0.044 db/km); X-band data yields a value of 0.00585 db/km.

<sup>3</sup> G. R. Marnier, "Radiometric Measurement of 8.7-mm Atmospheric Attenuation," Collins Radio Co., Cedar Rapids, Iowa, Tech. Rep. CER-479.

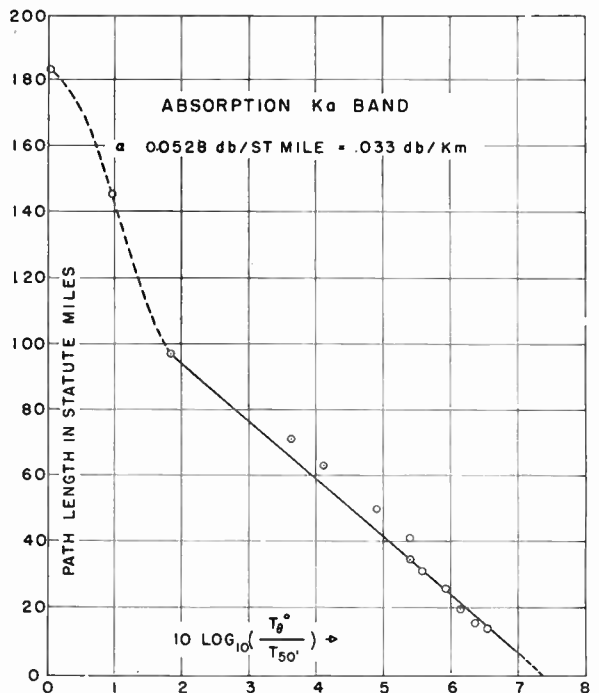


Fig. 9—8-mm absorption.

*Sky Temperatures:* It may be worth noting the sky temperatures that formed the background signals. It is hard to evaluate the temperatures obtained because ground radiation and reflectivity as well as atmospheric conditions contribute to the energy absorbed by the antenna. The measurements are necessarily limited to a particular antenna pattern and a particular site.

At 3.2 cm at zero elevation the temperature on a clear day was 89°K; on a day when there were heavy cloud formations, it was 90°. At zenith, however, the temperature was 54° for the cloudless day and 66° for the other.

At 8.7 mm the variations were considerably greater. The clear-day temperatures varied from 199° at zero elevation to 38° at zenith. For the day with heavy clouds the range ran from 229° at zero to 120° at zenith.

The low temperature readings obtained for the sun at 8.7 mm are highly uncertain because average sky backgrounds were inserted for corrective purposes. The great variations in sky temperatures could easily have affected the readings. In the 3.2-cm case, however, the larger solar signals and smaller variations make the solar temperatures obtained more valid.

### Refraction

In the microwave region, the deviation of rays in the lower atmosphere is influenced by the pressure of dry air, by water vapor pressure, and by the temperature. The microwave refraction is somewhat greater than optical refraction, owing to the high refractivity of water vapor at radio wavelengths.<sup>4</sup>

The optical refraction at sunrise is shown in a series of exposures (Fig. 10) made at the Ipswich site as an analog to the radiofrequency experiments. The curvature in the photograph indicates the deviation from the straight path of the sun (for this date), which is seen before it is on the horizon since its astronomical position is below the photographed path.

Simultaneous observations of the time of peak were made in order to measure the range of refraction at 3.2 cm and 8.7 mm. The time of the sun's transit at each elevation of the antenna was compared with the known astronomical position of the sun at that time to give the difference in altitude, or amount of refraction.

Fig. 11 is a plot of the refractive error as a function of the apparent altitude of the source. The range for 17 days is shown for each of the specific elevation angles. The optical refraction is also plotted (dotted curve).

Below an elevation angle of 3° the time of the sun's transit could only be roughly estimated from the fluctuating readings. In some cases, an integrated curve was artificially superimposed on the scintillations and a transit time taken. It is therefore emphasized that for



Fig. 10—Optical refraction at sunrise, Ipswich, Mass.

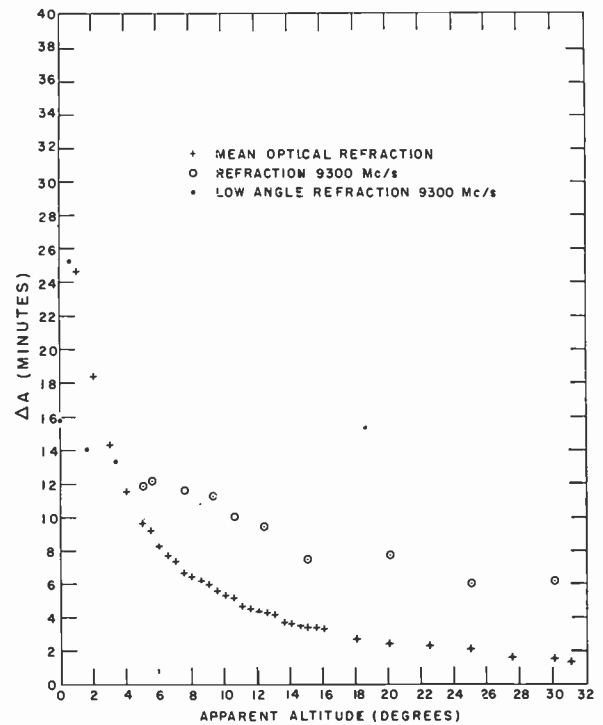


Fig. 11—Refractive error as a function of apparent altitude of source: 9375 mc and optical.

elevation angles below 3° the transit times in the drift curves were chosen merely as indications of the probable error. The values are rather nebulous.

At elevation angles above 3° the pattern fits the theoretical refraction curve in its downward trend; above 15° the curve flattens off, indicating a possible constant height error of several minutes of elevation. The error in reading was such that the timing accuracy was plus or minus 2 minutes of elevation. We are not following the usual procedure in refraction calculations, which is to

<sup>4</sup> J. L. Pawsey and R. N. Bracewell, "Radio Astronomy," Clarendon Press, Oxford, Eng.; 1955.

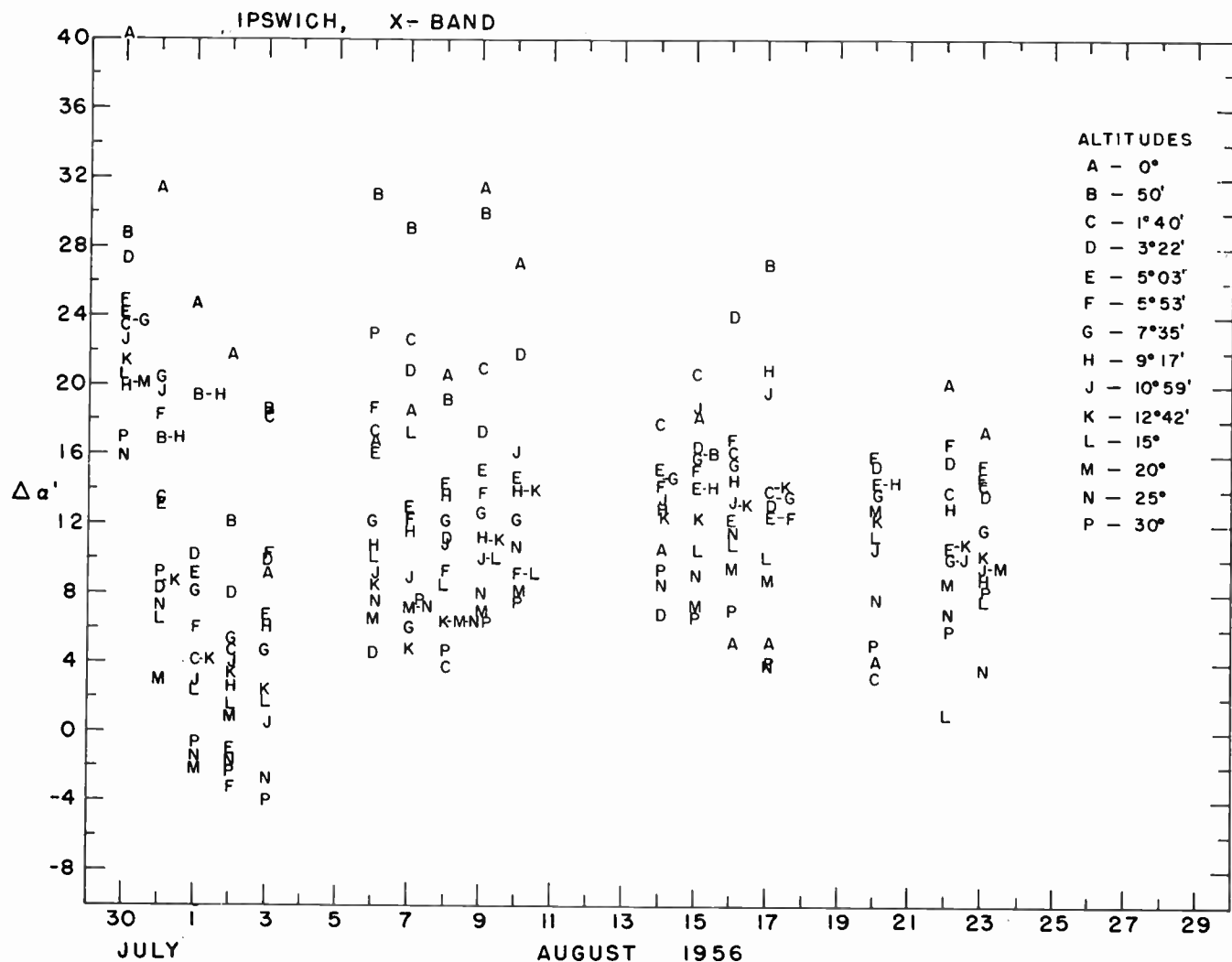


Fig. 12—Daily range of refractive errors 9375 mc.

use the upper angle values obtained from the data as the point of zero refraction and then reduce all values by this amount, but are presenting the raw data to allow evaluation of the excursions from the average value. The possibility of a small refractive error even at high altitudes is not excluded.

The range and mean of the readings does not give a dynamic picture of how the refraction changes within short periods of time. Refraction at a specific elevation can be slightly greater than at a lower angle. Fig. 12 illustrates two points. One is the irregularity during a single day. The other is the play in range on various days, the refraction tightly centered around one value on some days and ranging from maximum to minimum elevation on others. The "negative" refraction readings may result because the center of the sun's radio-frequency energy is not always the same as its optical center.

During periods when clouds, haze, and fog were present in the path, the measurements gave general indications of greater refraction at 8.7 mm than at 3.2 cm.

*Scintillations*

Fluctuations in the microwave region are most likely tropospheric in origin. The several theories on the origin of the fluctuations are concerned with the size of the irregularities in the lower atmosphere and the manner in which they are naturally arranged.

By Rayleigh's theory, the refractive index of a medium is a function of time, wind speed, and atmospheric conditions. As rays pass through different refractive media they bend through varying angles and thereby produce an irregular pattern in the signal detected on the ground.

Little's<sup>6</sup> theory is that diffraction is caused by an irregular screen in the layers; in the lower atmosphere considered in this paper, the screen is composed of tropospheric blobs.

Since tropospheric refraction is independent of frequency, Rayleigh's theory would lead us to expect that

<sup>6</sup> C. G. Little, "A diffraction theory of the scintillation of stars at optical and radio wavelengths," *Monthly Notices Roy. Astron. Soc.*, vol. 111, pp. 289-302; 1951.

scintillations from the same source would be the same on two frequencies. On the other hand, since a diffraction screen forms different patterns as the wavelength is varied, Little's theory would indicate dissimilar irregularities on two frequencies. A good proof of the theories therefore, would appear to be found in the extent of correlation between the scintillations at 3.2 cm and 8.7 mm. The evidence is that there are times when each is borne out. The data is now being sifted to determine the conditions prevailing in both cases.

#### THE SCINTILLATION DATA

The scintillation in both bands shows deep fades for long periods at elevation angles below  $3^\circ$ , and much smaller fluctuations for shorter periods at higher angles.

Fig. 13 illustrates sets of curves taken at the same altitude ( $1^\circ 40'$ ) but on two successive days (August 23, and 24, 1956). On both days the amplitudes of the fluctuation component of the 3.2-cm data were approximately equal, amounting to 5 per cent of the maximum signal level. On August 23, the 8.7-mm fade-to-signal ratios were extremely large but on August 24, the absorption practically wiped out the fades. August 24 could be described as a period of high, but relatively uniform water vapor absorption. The weather during the sunrise period was cloudy with light rain. Fog was present from midnight until 0845 EST. August 23, a clear day, appears to have been a period when a diffraction pattern was set up by the blob structure of the atmosphere but there was little correlation between the fades on 3.2 cm and 8.7 mm.

Periods do occur when the fluctuations are similar at the two wavelengths. Fig. 4 (top) illustrates a case at an elevation of  $1^\circ 40'$ . The general rise and fall of the fluctuations within the drift curves are similar when we consider the difference in the time constants used (2 seconds at 3.2 cm and 6 seconds at 8.7 mm). This is in contrast to the data in Fig. 13 (top), where little correlation between individual fades is seen. The explanation is that the Rayleigh theory of fluctuations holds in the former (Fig. 4) because the similarity in individual fluctuations is not frequency-dependent.

#### SCINTILLATION AMPLITUDE AND PERIOD

Scintillations are likely to occur at any elevation. Fluctuations on both bands are maximum up to  $3^\circ$ , decreasing to very small amplitudes after  $5^\circ$ .

The depth of fade at any wavelength is a function of the altitude and atmospheric conditions, varying from a fraction of 1 per cent of the antenna signal to as much as 20 per cent. The average fluctuation at the most disturbed elevation is between 5 and 10 per cent, regardless of the signal frequency band.

The correlation between scintillations and weather is most difficult to establish. It does appear, however, that on days when the dewpoint is highest the fluctuations are greater at  $X$  band than at  $K_a$  band—perhaps twice as much. This may be related to the finding that  $K_a$  sig-

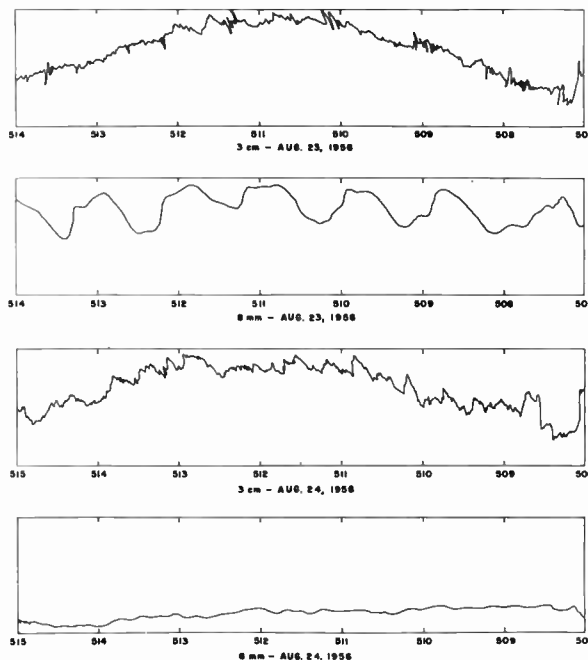


Fig. 13—Solar drift curves August 23, 24, 1956 at an elevation of  $1^\circ 40'$ .

nals are most attenuated on this kind of day. On the other hand, fair weather seems to bring out fewer scintillations at  $X$  band and more at  $K_a$ . On hazy to partly cloudy days the fluctuation depths at the two signal frequencies vary the least. On some clear days the fade percentage at the  $K_a$  band is three times that at  $X$ .

The duration of the scintillation cycle varies from 0.5 second to 60 to 70 seconds. The average period at  $X$  band is generally 15 to 22 seconds, or about one-half the average 35- to 55-seconds fluctuation at  $K_a$ . There are occasional exceptions, however, when the scintillations at  $X$  band are of longer duration than those at  $K_a$ . At  $X$  band some drift curves show faster jiggles during a slow scintillation. The scintillation period decreases with elevation, only fast scintillations being seen at the higher angles.

#### OPTICAL EVIDENCE

Optical studies of scintillations have provided guideposts in the rf field. In the visible range of the spectrum the amplitude of fluctuation is proportional to the cosine of the angle of elevation from  $10^\circ$  to  $90^\circ$ . The small amplitude fades seen at zenith in one study<sup>6</sup> were about 2 per cent of the mean light level and the largest about 10 per cent. At angles lower than  $10^\circ$ , low-frequency scintillation (approximately 5 cps) predominates. At the high elevations, fluctuation is continuous and relatively fast; there are no deep slow fades. The results obtained in this experiment are fundamentally in agreement with optical evidence on these points.

Optical evidence further indicates that with large

<sup>6</sup> M. A. Ellison and H. Seddon, "Some experiments on the scintillation of stars and planets," *Monthly Notices Roy. Astron. Soc.*, vol. 112, pp. 73-87; 1952.

apertures the pulse is flatter than with narrow apertures. Large antennas should therefore not experience the very deep fades that were frequently seen in our studies at low elevations.

### 218-MC EXPERIMENT

#### Refraction

Solar refraction was measured by comparing the nulls in the interference pattern of the sea interferometer with the actual position of the sun at the time the nulls appeared. These nulls occur at multiples of  $2\pi$  in (1). Peak times were not measured because at meter wavelengths they are difficult to discern during solar disturbances.

Two factors that affect the null points considerably are the height of the sea and the radiofrequency center of the sun. The changes in the height of the sea at the site at Scituate, Mass., have been tabulated by the US Coast and Geodetic Service, and the mean height of the antenna above the sea has been corrected for the changes in tides. The center of the sun's disk is more difficult to find.

The technique commonly used for finding both the height of the sea and the sun's center is to take the highest angle as the zero refraction point and correct all values accordingly. Applications of this technique are limited, especially when the maximum elevation obtainable is  $13.4^\circ$ . The sea interferometer was used in our studies because it produces a rather sharp image of the sun as it rises. To determine the appearance of the outer layers of the sun's corona the sensitivity of the equipment was initially raised to its maximum value. After the sun rose above the horizon the gain was turned down. The refractive errors at zero elevation were obtained for 21 days. On the basis of a solar radius of  $15'$ , the mean refractive error for the period was about  $1^\circ 05'$ , varying from a maximum of  $1^\circ 35'$  to a minimum of  $45'$ .

#### Antenna Pattern and Solar Temperatures

The antenna pattern in the vertical plane was measured by plotting daily solar drift curves such as illustrated in Fig. 3. To obtain the upper half-power point, the peak values were calculated as a function of angle. The deflections were reduced to equivalent temperatures by means of calibrating noise diodes in the system. Since the power absorbed by the antenna and delivered to the receiver is equal to  $kTB(F-1)$ , where

- $k$  = Boltzmann's constant,
- $T$  = Antenna temperature in  $^\circ\text{K}$ ,
- $F$  = Noise figure,
- $B$  = Bandwidth,

the half-power points and the half-temperature points are equal.

For the vertical plane the theoretical curve and the calculated curves were nearly equivalent, being  $8^\circ$  in the former and  $7^\circ 25'$  in the latter. The azimuth value, taken from other measurements, was  $4^\circ$ .

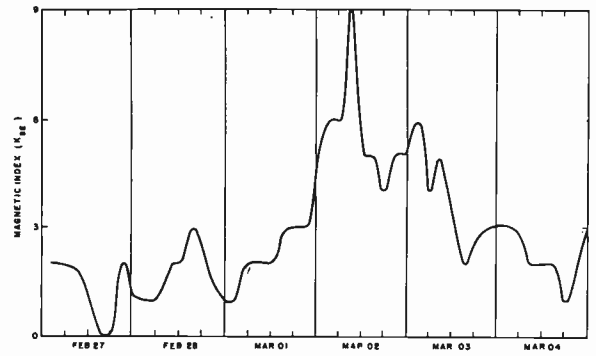


Fig. 14— $K_{BE}$  index for the period February 27–March 4, 1957.

The equivalent solar temperature, neglecting attenuation, was obtained from the product of the temperature reading and the ratio of solid angle of the antenna to solid angle of the source (assuming the sun to be its optical size). The solar temperatures averaged  $1,000,000^\circ\text{K}$ . A disturbed "base level" maximum of  $4,000,000^\circ$  during a solar disturbance was reached.

#### Scintillations

Fluctuations in solar energy are too large in amplitude at meter wavelengths to permit scintillation measurements with the sun as the source of energy. The scintillation study was made by observing the Cassiopeia A radio star at its lower culmination. When this source went through the beam the increase in signal amplitude amounted to a  $100^\circ$  increase in temperature. Fluctuations were concurrent during certain ionospherically disturbed periods.

The antenna pointed north at an altitude of  $11^\circ$ . It had a beamwidth of approximately  $12^\circ$ . Detailed analysis was made of the data collected during the period February 28 to March 3, 1957. Disturbances recorded during this time were associated with solar and terrestrial disturbances. A class 3 flare was observed at  $00^{\text{h}}05^{\text{m}}$  UT on February 28 and the sudden onset of a geomagnetic storm at Belvoir was noted at 0800 EST on March 1. The magnetic index taken at Belvoir is shown in Fig. 14. The recordings of the passage of Cassiopeia A through the beam are shown in Fig. 15.

While detailed correlation cannot be attempted, the association of the scintillations with the aurora (reported on the night of March 2) and the magnetic disturbances is well-defined. For this particular period, data analysis by Dr. Gerald Hawkins and his group at the Harvard College Observatory, shows that the signal periodicity ranged from its time constant (10 seconds for the records given) to 3 minutes, with most of the variations occurring at periods between 10 and 60 seconds. The signal was 3 db below the mean level for 7 per cent of the time and 1.8 db above the mean for 3 per cent of the time.

This period was unusual in that a large auroral disturbance took place. Observations are continuing for

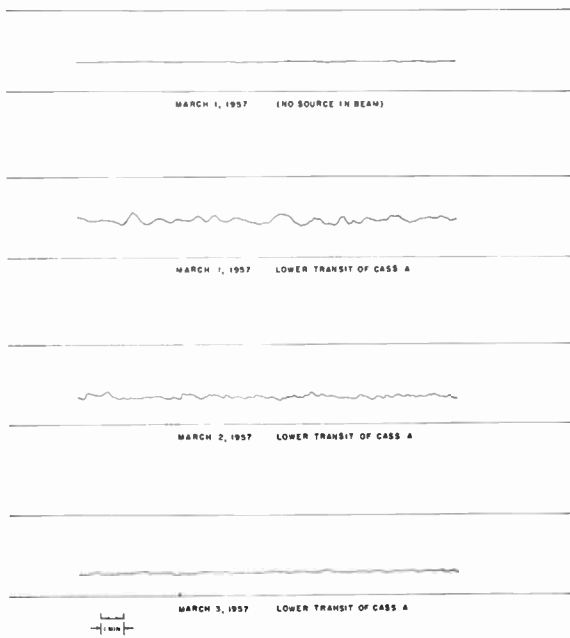


Fig. 15—Scintillations of Cassiopeia A during auroral period February 28–March 3, 1957.

the purpose of establishing the scintillation level when the lower transit of Cassiopeia A occurs during daytime periods.

#### CONCLUSION

##### *Atmospheric Attenuation*

*Microwave:* Molecular oxygen and water vapor account for the greater part of atmospheric absorption. The experiment described gave the following attenuation values:

X band (3.2 cm) 0.00585 db km  
 $K_a$  band (8.7 mm) 0.033 db km

The average measured solar temperatures at these frequencies were  $16,000^\circ\text{K}$  at 3.2 cm and  $5280^\circ\text{K}$  at 8.7 mm.

*218 MC:* VHF attenuation studies were not made. The average solar temperature for the period of the study was  $1,000,000^\circ\text{K}$ , with a maximum of  $4,000,000^\circ\text{K}$  noted during a period of disturbed solar activity.

##### *Refraction*

The refraction at the frequencies studied was generally greater than the optical refraction, primarily because of the water vapor in the atmosphere.

Refraction measurements made concurrently at the microwave frequencies of 3.2 cm and 8.7 mm showed that the refraction was not the same for the two frequencies at the same time. From day to day the amount of refraction would vary, one day greater at 3.2 cm and another day greater at 8.7 mm.

The 218-mc refractive error at sunrise averaged about  $1^\circ 05'$ , varying from  $1^\circ 35'$  to  $45'$ . The effect of change in antenna height because of tidal action of the sea was detectable though small.

##### *Scintillation*

The microwave scintillations considered were of tropospheric origin and their characteristics varied with changing altitude. At the lower altitudes the scintillations were of relatively large amplitude and long period. At the higher observed altitudes, from  $15^\circ$  to  $30^\circ$ , they were of small amplitude and short period. The 3.2-cm fluctuations were fairly consistent from day to day but those at 8.7 mm showed greater susceptibility to changes in the weather. A general explanation of the scintillation effects was possible, sometimes by refraction theory and sometimes by diffraction theory.

The 218-mc fluctuations in solar energy were too large to study atmospheric scintillation at this frequency. With Cassiopeia A as a source it was found that unusual solar and auroral activity enhanced scintillations.

#### ACKNOWLEDGMENT

This study was carried out under the general supervision of Dr. P. Newman. C. Ferioli, A. Orange, and R. Straka assisted with the sunrise observations. The work on Cassiopeia A scintillations was initiated in collaboration with Dr. G. Hawkins of the Harvard College Observatory and continued by AF Cambridge Research Center personnel. The Harvard College Observatory graciously allowed the use of its 24-foot equatorial parabola for the Cassiopeia A measurements. The Ewen-Knight Corporation built the 218-mc receiver. Dr. J. Casey instrumented portions of the microwave equipment.



# Some Measurements of High-Latitude Ionospheric Absorption Using Extraterrestrial Radio Waves\*

C. G. LITTLE† AND H. LEINBACH‡

**Summary**—This paper describes the manner in which 30-mc extraterrestrial radio waves have been used to study the radio absorption characteristics of the arctic ionosphere. It opens with a brief discussion of the theory of ionospheric absorption, followed by a description of the basic principles involved in the technique. Two different types of equipment which have been used in these absorption measurements are then discussed and typical records presented. The observations have shown that the regions of anomalous high-latitude absorption typically have lateral dimensions in excess of 100 km, and that marked differences can occur during disturbed periods between stations 800 km apart. Almost all the absorption of the extraterrestrial radio waves occurs below the *E* region. The absorption correlates well with the local geomagnetic *K* index, and apparently is associated with the bombardment of the upper atmosphere by the corpuscular streams which produce the aurora. The increase of absorption during daylight hours is thought to be due to a decrease in effective height of the absorbing layer, resulting from a photo detachment of electrons at heights of the order of 60–80 km, rather than to an increase in the strength of the corpuscular bombardment.

## SUMMARY OF THEORY OF IONOSPHERIC ABSORPTION

THE Appleton-Hartree magneto-ionic theory<sup>1</sup> shows that a radio frequency wave will be attenuated while traversing an ionized medium in which the free electrons undergo collisions with other particles. This absorption process is analogous to a frictional loss since the free electrons are caused to oscillate at the frequency of the incident radio wave and will give up some of their oscillatory energy, derived from the radio field, when they collide with other particles.

Quantitatively, the absorption of energy is given by

$$A = -20 \log_{10} \frac{E}{E_0} \text{ db},$$

where *A* = the absorption in decibels, *E*<sub>0</sub> = the field strength of the incident plane wave, and *E* = the field strength after traversing a distance *s* through the ionized medium. *E* and *E*<sub>0</sub> are related by

$$E = E_0 e^{-ks},$$

\* Original manuscript received by the IRE, November 6, 1957. This work was supported by a National Science Foundation grant, from April, 1954 to June, 1956, and from July, 1956 to March, 1957, by Signal Corps Contract No. DA-36-039-SC-71137.

† Geophys. Inst., University of Alaska, College, Alaska.

<sup>1</sup> E. V. Appleton, "Wireless studies of the ionosphere," *J. IEE*, vol. 71, p. 642; 1932.

H. G. Booker, "The application of the magneto-ionic theory to the ionosphere," *Proc. Roy. Soc. A*, vol. 150, pp. 267–286; June, 1935.

F. T. Farmer and J. A. Ratcliffe, "The absorption of wireless waves in the ionosphere," *Proc. Roy. Soc. A*, vol. 151, pp. 370–383; September, 1935.

where

$$k = \frac{2\pi e^2}{mc} \cdot \frac{1}{\mu} \cdot \frac{N\nu}{\nu^2 + (w \pm w_L)^2} \quad (1)$$

In this equation, *e* and *m* are the electronic charge and mass, *μ* is the refractive index of the ionized medium in which the electronic density is *N* and the electron collision frequency is *ν*, *w* is the angular frequency of the incident radio wave, and *w*<sub>L</sub> is the angular-gyromagnetic frequency corresponding to the longitudinal component of the magnetic field. The positive sign denotes the ordinary wave, the negative sign the extraordinary wave.

In studies of ionospheric absorption using extraterrestrial radio waves, the observing frequency is usually several times the critical frequency, and under such circumstances the refractive index in the absorbing region may be taken as unity. Also, the electron collision frequency in the absorbing region is usually very small compared with the radio frequency, and therefore, usually can be neglected when compared with (*w* ± *w*<sub>L</sub>). Under these conditions, the preceding equation reduces to

$$k = \frac{2\pi e^2}{mc} \cdot \frac{N\nu}{(w \pm w_L)^2} \quad (2)$$

Since both *N* and *ν* will vary with height, the total absorption along the line of sight will be given by

$$A = -20 \log_{10} \frac{E}{E_0} \text{ db} = 8.69 \int_s k ds, \text{ db}$$

or

$$A = \frac{8.69}{(w \pm w_L)^2} \cdot \frac{2\pi e^2}{mc} \int_s N\nu ds, \text{ db} \quad (3)$$

where *s* is the path length along which the product *Nν* is significant.

A determination of *A* (the attenuation in decibels) at a single frequency can therefore be used to determine the value of  $\int_s N\nu ds$ , since the other quantities in the above equation are all known. The measurement does not, however, give any indication of the variation of *Nν* with height.

## THE MEASUREMENT OF IONOSPHERIC ABSORPTION USING EXTRATERRESTRIAL RADIO WAVES

### Basic Principles

The principle behind the use of extraterrestrial radio

waves for the study of ionospheric absorption is essentially very simple. The radio noise power incident at a point outside the earth's atmosphere from a given direction in space is believed to be constant with respect to time. (See below for certain exceptions to this statement.) The radio noise power received on a fixed receiving system at the earth's surface should be, therefore, a function only of sidereal time, since each day the antenna beam will explore the same strip of sky as the earth rotates. The transparency of the earth's atmosphere at a particular instant of time, therefore, is given by the ratio of the signal strength actually received to that received at the same sidereal time under conditions of negligible ionospheric absorption. The actual details of the technique are discussed below.

When dealing with the reception of random noise signals from diffuse sources, it is often convenient to make use of the concept of equivalent antenna temperature. It can be shown that a power  $P_n = T_k k B$  could be extracted from a matched antenna installed in an enclosure at temperature  $T^\circ K$ , where  $k$  is Boltzmann's constant and  $B$  is the observing bandwidth. Using this fact, it is possible to relate any noise power  $P_n$ , received over a given bandwidth  $B$ , to its equivalent radio noise temperature  $T_e$  given by

$$P_n = T_e k B.$$

Consider, therefore, the case of a receiving system whose antenna beam is directed at a region of the sky whose effective radio temperature in the absence of any ionospheric absorption is  $T_1$ . Under these circumstances the antenna signal power would be given by  $P_1 = T_1 k B$ . If now, some absorbing medium (such as the ionosphere) with a uniform power transmission coefficient  $\alpha_2$  and temperature  $T_2$  is inserted over the full width of the antenna beam, the received signal power from the sky would be reduced to  $\alpha_2 T_1 k B$ . However, the absorbing medium would, itself, radiate radio noise in proportion to its temperature and effectiveness as an absorber. The antenna would therefore receive an additional signal,  $P_2 = (1 - \alpha_2) T_2 k B$ , from the ionosphere.

In the case where the antenna signal is transferred to the receiver via a matched transmission line whose power transmission coefficient is  $\alpha_3$ , the transmission line will itself act as both an attenuator and a generator of radio noise. The noise power reaching the receiver will be given by

$$P = k B [\alpha_3 \alpha_2 T_1 + \alpha_3 (1 - \alpha_2) T_2 + (1 - \alpha_3) T_3]$$

where  $T_3$  is the temperature of the transmission line. It is assumed that the antenna and the receiver are both matched to the transmission line and that the power transfer from the antenna to the receiver is complete apart from the effect of absorption of energy within the transmission line.

This received noise power will add to the noise power generated within the receiver itself, which is given by the expression

$$P_4 = (F - 1) T_A k B,$$

where  $T_A$  is room temperature, normally taken as  $293^\circ K$ , and  $F$  is the noise figure of the receiver.

If the above system is now used to observe extra-terrestrial radio noise, the power output of the receiver may be written as

$$P_0 = G(P_1 + P_2 + P_3 + P_4 + I), \quad (4)$$

where

$P_0$  = output noise power from the receiver,

$P_1$  = noise power from sky =  $\alpha_2 \alpha_3 T_1 k B$ ,

$P_2$  = noise power from ionosphere =  $\alpha_3 (1 - \alpha_2) T_2 k B$ ,

$P_3$  = noise power from antenna transmission line =  $(1 - \alpha_3) T_3 k B$ ,

$P_4$  = noise power from receiver =  $(F - 1) T_A k B$ ,

$I$  = power from interfering signals,

$G$  = receiver power gain.

#### *The Simple Ionospheric-Absorption Measuring Equipment*

The simplest equipment capable of ionospheric-absorption measurements by the "cosmic-noise" method consists of a receiver connected to an antenna by means of a transmission line, and a monitoring system (usually a pen recorder) to measure the receiver output noise power.

The absorption measurements made with a simple receiving system such as that described above are based on the comparison of the observed values of  $P_0$  with those obtained at the same sidereal time under conditions of negligible absorption. After correction, wherever possible, for variations in the other parameters in (4), any residual discrepancy is attributed to variations in  $P_1$  which is equal to  $(\alpha_2 \alpha_3 T_1 k B)$ . Since  $k$  is a constant and under normal operating conditions  $\alpha_3$ ,  $T T_1$ , and  $B$  are also constant, it is possible to attribute the residual discrepancy to  $\alpha_2$ , the transparency of the ionosphere at the frequency concerned.

It is clear that the simple equipment described above is very susceptible to uncertainties due to variations in receiver gain  $G$ , and also to a lesser degree, to changes in  $P_2$ ,  $P_3$ ,  $P_4$ , and  $I$ . These factors are discussed in the succeeding paragraphs.

*Variations of Receiver Gain:* Since the measurements of ionospheric absorption are based entirely upon the comparison of  $P_0$  on different days, their accuracy will be critically affected by the stability of the receiver gain,  $G$ . For this reason, it is important to try to stabilize the gain in receivers of the type indicated above. At the Geophysical Institute, this has been done by using electronically stabilized ac and dc power supplies to the receiver and by temperature stabilization of the equipment environments.

Even when all the above steps have been taken, it is important to check the stability of the receiver. This was done by periodically disconnecting the antenna from the receiver and feeding a standard, fixed quantity of noise power from a noise diode source into the receiver. It has been found desirable that these calibrations be done at several levels of noise diode power, since this enables the complete input-output calibration of the receiver to be checked, rather than just one point on the curve. As an example, one of the equipments at the Geophysical Institute makes use of a one-revolution per hour electric motor and a series of microswitches to calibrate the receiver automatically at three different levels of noise diode input power. As an additional check, the noise diode current is itself recorded continuously. A typical record from this equipment is shown in Fig. 1(a), in which the calibrating levels are readily seen.

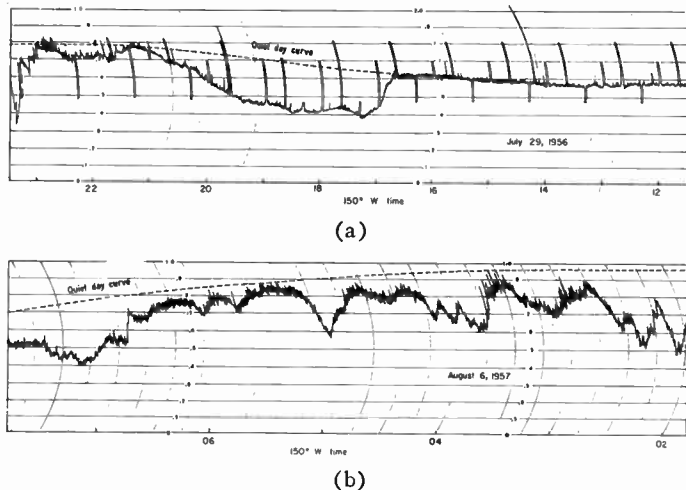


Fig. 1—Ionospheric absorption of 30-mc cosmic noise, (a) recorded by a total power system and (b) recorded by a servo-controlled self-balancing system. In both cases the signal level expected under ionospherically quiet conditions is shown by the dashed line.

*Variations of Extraterrestrial Radio Noise Power:* In the above discussion, it has been assumed that the strength of the extraterrestrial signal reaching the earth's upper atmosphere from a particular direction in space is constant and, therefore, that any variation in the signal received at ground level can be attributed to ionospheric effects.

The sun, however, provides an important exception to this statement. At wavelengths of the order of 10 meters the signal power from the sun, when undisturbed, is less than one per cent of the signal power from the diffuse background of radio noise observed on a wide beam antenna and, therefore, can normally be neglected. When active sunspot groups are present, and also occasionally at other times, the sun's radio output at these frequencies may increase enormously and render this absorption measuring technique useless during the daytime

for the duration of the activity. This must be regarded as a serious fault of the technique since it is often at these times that one desires information on the ionospheric absorption. The effect can often be limited to the major phases of the activity by utilizing a polar diagram that discriminates against the sun, e.g., an antenna beamed toward the Pole Star.

Four other minor sources of variation in  $P_1$  may be mentioned. Three of these are due to true variations in the signal power from discrete sources, namely, the planets Jupiter and Venus and a source recently discovered by the Australian workers. In these cases, the ratio of source signal power to diffuse background signal power is so low as to render their effects negligible on a wide-beam antenna. The fourth source of variations in  $P_1$  is the scintillation of the discrete sources due to diffraction effects in the ionosphere. These scintillations take the form of variations (of period about 30 seconds) in the intensity of the localized sources, but average out for the diffuse background radiation. When one of the more intense sources, such as Cygnus A or Cassiopeia A, is in the antenna beam, these scintillations may result in fluctuations of the order of two or three per cent of the input power on a wide-beam antenna. However, their effect is rarely serious since the power received from a source, averaged over several fluctuations, is unaffected by the presence of scintillations.

The above discussion relates to the variations in the extraterrestrial signal power reaching the antenna. The proportion actually received by the receiver is determined by the power transfer efficiency factor  $\alpha_3$  of the transmission line and by the accuracy of the impedance matching at each end of the line. In order to minimize the effect of the receiver noise, it is important that the efficiency of power transfer should be as high as possible. For accurate absorption measurements, it is also important that this efficiency should remain constant with time. It was found desirable to bury the main length of rf cable from the antenna to the receiver in the ground and to shield the remainder from direct sunlight. This precaution served to minimize the temperature variations in the cable and any resultant variations in attenuation or impedance matching.

*Radio Noise from the Ionosphere:* The intensity of the radio noise originating in the ionosphere will normally be very small compared with that of extraterrestrial origin for frequencies significantly above the vertical incidence ionospheric penetration frequency. For example, at 30 mc the equivalent antenna temperatures are about  $20,000^\circ\text{K}$  while electron temperatures in the absorbing region are not likely to be in excess of a few hundreds of degrees Kelvin. Moreover, to determine the magnitude of the ionospheric contribution to the antenna noise power, it is necessary to multiply the ionospheric temperature by the ionospheric absorption coefficient  $(1 - \alpha_2)$  which is usually less than 10 per cent at 30 mc. Under extreme conditions and at low frequencies, where the absorption of the extraterrestrial

signal is much greater, uncertainty in the value of  $T_2$  could limit the accuracy of the measurement of the absorption.

*Radio Noise from the Transmission Line:* It is possible to correct for the radio noise from the transmission line since the temperature of the cable and the attenuation within it can be determined with fair accuracy. In general, however, and particularly in the case of the low-loss cables actually used, no correction is required.

*Radio Noise Generated within the Receiver:* By careful design, it is possible to reduce the equivalent input noise power from a matched radio frequency amplifier to, say, three times that generated in the matched input resistor, assuming this to be at room temperature. In this case, the noise power generated within the receiver itself is  $2TkB$  since  $TkB$  is the noise power supplied by the input resistor at temperature  $T$ . The equivalent noise temperature of the receiver input due to receiver noise alone would therefore be about  $600^\circ\text{K}$ , *i.e.*, considerably less than the equivalent antenna temperature.

For accurate work, it is clearly important to know what proportion of the output noise power is generated within the receiver since this determines the base level from which all other signals must be measured. Its value can be obtained by means of a noise diode calibration of the receiver input-output characteristic and of the noise factor. Periodic checks of the receiver noise figure are necessary since it is likely to change as the input tubes age.

*Interference:* The signal powers used in these absorption measurements are weak, and the equipments are very susceptible to interfering signals, whether man-made or of natural origin. It is therefore important to use a site where man-made interference due to power lines, electrical machinery, automobiles, etc., is at a minimum and to try to use frequencies that are not affected by transmitted signals. The latter problem is particularly severe since there is no assurance that an interference-free channel will remain clear indefinitely. For this reason, it was found necessary to use a sweep frequency receiver and filtering circuits to record the *minimum* signal intensity received during the frequency sweep. The width of the frequency sweep was made about 20 times the IF bandwidth, to insure high probability of at least one clear channel per sweep.

In addition to the above experimental uncertainties, there remains a fundamental practical limitation to the accuracy with which the noise power can be measured. As has been shown by Machin, Ryle, and Vonberg,<sup>2</sup> there is a statistical fluctuation in the output level, whose rms value is given by

$$\Delta P_0 \simeq \frac{P_0}{(Br)^{1/2}}$$

<sup>2</sup> K. E. Machin, M. Ryle, and D. D. Vonberg, "The design of an equipment for measuring small radio-frequency noise powers," *Proc. IEE*, vol. 99, pts. III-IV, pp. 127-134; May, 1952.

where  $B$  is the input bandwidth as far as the second detector and  $\tau$  is the output time constant. Typical values of  $B$  and  $\tau$  for absorption measuring equipments are  $10^4$  cps and one second, respectively. Hence,  $\Delta P_0$  is of the order of one per cent of the output power (0.05 db). Greater accuracy can be obtained only by using wider input bandwidths and longer output time constants, or by integrating over several output fluctuations. In practice, the input bandwidth can be increased only at the risk of increasing the amount of interference from man-made transmitters. The time constant is usually kept fairly short in order to be able to follow rapid changes in signal and to have a fast recovery time after a burst of interference.

### The Continually Self-Calibrating System

The above discussion has been limited to the simplest form of absorption measuring equipment in which the gain of the receiver is implicitly assumed to remain constant for the period (usually many minutes) between automatic gain calibrations. However, a very elegant radiometer developed by Ryle and his colleagues<sup>2</sup> for use in radio astronomical work may be used with advantage in the study of ionospheric absorption.

The basic principles of the equipment are as follows: the receiver input connection is switched at a rapid rate (many cycles/second) between the antenna and a noise diode; if any inequality exists between the noise power fed into the receiver from these two sources, a square wave component at the switch frequency will appear at the output of the receiver. This signal is amplified in an amplifier tuned to the switch frequency and fed into a phase-sensitive detector; this stage produces a dc signal whose amplitude is proportional to the inequality of the two noise signals, and whose polarity is dependent upon which of the two signals is the greater. This dc signal is then used to adjust the filament temperature, and hence the noise power, of the noise diode in such a way as to make the two input signals equal in strength. As the antenna signal varies in strength, the power from the noise diode is therefore automatically adjusted to bring it into equality. To measure the antenna noise power it is therefore necessary only to record the current through the noise diode since this current is accurately proportional to the noise power generated by the temperature-limited noise diode.

In such an equipment the receiver is used as a null detector, and the accuracy of the reading is therefore not affected by relatively large variations of receiver gain. Since the equipment operates under balanced conditions, (4) is replaced by

$$P_{nd} = P_1 + P_2 + P_3 + \Delta P_4 + I, \quad (5)$$

where  $P_{nd}$  is the noise power from the noise diode (proportional to the current flowing through it),  $P_1$ ,  $P_2$ ,  $P_3$ , and  $I$  have the same meaning as in (4), and  $\Delta P_4$  is the difference between the equivalent noise input power of

the receiver when connected to impedances equal to the antenna impedance and noise diode impedance, respectively. The accuracy of the readings is no longer dependent upon variations in receiver gain; also,  $\Delta P_4$ , the change in receiver noise power as the receiver switches from antenna to noise diode, is normally very much smaller than  $P_4$ , and the equipment is therefore relatively insensitive to changes in receiver noise figure. A third important advantage is that the recording system is now linear with input power. To compare two signal powers, it is necessary only to divide the corresponding currents through the servo controlled noise diode. This is far easier than the procedure for the simple equipment, for which it is necessary first to correct the observed receiver output readings for possible gain variations and then to use a receiver input-output calibration to determine the actual received powers.

This servo system, which can result in increased accuracy and in simplification of the data scaling, requires careful design if these advantages are to be fully realized. The problem of receiver stability is now replaced by that of accurate, stable switching between the two noise sources. In practice, this was done by diode switches at the end of quarter-wavelength transmission lines. Considerable attention was paid to impedance matching, since the  $\Delta P_4$  of (5) would be zero only if the noise diode and the antenna present equal impedances to the receiver input when connected via the switch. Care was also taken to insure that the noise diode was operated with a sufficiently high plate voltage since it is only under temperature-limited conditions that the noise power would be accurately proportional to the current flowing through the diode. The equipment also required that the precautions already outlined in the discussion of the simple equipment be taken to ensure that the antenna and the transmission line were functioning satisfactorily.

Using a self-balancing radiometer of this type with a carefully designed antenna and transmission line system, it has been found that relative signal powers can be measured with a long-term accuracy of better than 0.2 db, with a short-term accuracy probably limited by temperature effects in the receiving system. A record from such an equipment is reproduced in Fig. 1(b).

#### *Advantages of the Cosmic-Noise Method of Measuring Ionospheric Absorption*

Until quite recently, the normal method of investigating ionospheric absorption was to measure the strength of manmade signals reflected by the ionosphere. Such a method, in essence, measures the total attenuation undergone by the radio signals and includes contributions due to partial reflections, polarization phenomena, ionospheric scattering, and deviative absorption.

The use of extraterrestrial radio waves to investigate the transparency of the ionosphere has several important advantages, especially at high latitudes. These ad-

vantages include the relative simplicity of the equipment since no transmitter is required, and the fact that the whole ionosphere is traversed instead of only that region below the point of reflection. Also, since frequencies well above the vertical incidence penetration frequency are used, the absorption to be measured is very much reduced, and data can be obtained during polar blackouts. (Such conditions, often experienced at high latitudes, occur when the absorption is so large at frequencies below the critical frequency that any reflected signals are undetectable.) The use of frequencies well above the gyromagnetic and critical frequencies has the further advantage that uncertainties arising from polarization effects and deviative absorption are much reduced. Also, owing to the omnidirectional nature of the transmissions, the absorption can more readily be measured as a function of azimuth and elevation.

#### THE GEOGRAPHICAL EXTENT OF THE ABSORBING "CLOUDS"

Three different short-term experiments have been conducted to determine the geographic extent and position of the regions of anomalous high-latitude absorption. These experiments are now discussed.

##### *Rotating Antenna Experiment*

In the first experiment, a horizontally directed 3-element Yagi antenna was rotated about a vertical axis at one revolution per 4 minutes. The antenna was horizontally polarized and was mounted one wavelength above the ground. On the assumption of perfect reflection by the ground, the main lobe of the antenna would be at an elevation of about  $14^\circ$ , with 3-db points at about  $7^\circ$  and  $22^\circ$  elevation. As the antenna rotated, the absorption layer (assuming a height of 85 km) would be crossed at a range of about 280 km from College, Alaska. Since the equipment integrates the extraterrestrial signal over the whole antenna beam, the rotating-antenna equipment actually explored the absorption conditions in a broad ring defined by radii of approximately 200 km and 500 km centered on College.

Owing to the nonuniform distribution of extraterrestrial signal power across the sky, the receiver output was not constant as the antenna rotated, the actual form of the variation being a function of sidereal time. Quiet day curves for four azimuths, geographical NW, NE, SE, and SW, were prepared as a function of sidereal time and the data were scaled against these four curves. An example of the manner in which the absorption varied as a function of time for these four azimuths during a single absorption event is shown in Fig. 2 in which the ordinates are antenna signal power. The maximum absorptions recorded during this event in these four directions are also shown and compared with the maximum zenithal absorption recorded simultaneously on another equipment.

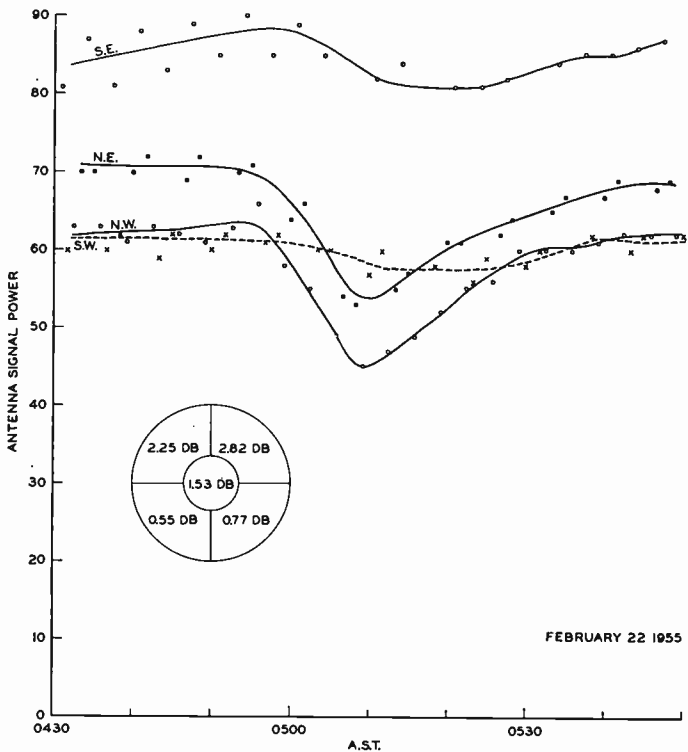


Fig. 2—Absorption of cosmic noise recorded as a function of direction. The circular insert shows the maximum absorption observed during the event for each quadrant and for the zenith.

Twenty-two major absorption events observed during the March, 1955 equinox have been analyzed in this way, and the ratio of the absorption in decibels to that observed in the NE direction determined. The median values of the ratios are shown in Fig. 3, from which it will be seen that the absorption was typically strongest in the northern quadrants. It is of interest that the NE direction typically showed the greatest absorption and the SW direction the least. It is tempting to suggest, since magnetic north is 30° east of true north at College, that this effect is due to the absorption varying with magnetic rather than geographic latitude (see Fig. 4). Although on some occasions the absorption in decibels was constant (to within 20 per cent) in the four main directions, on many occasions this was not true and ratios of at least 5:1 were observed, indicating a five-fold variation of the integrated product of electron density and collision frequency  $\int Nvdz$  along the different lines of sight.

A similar series of observations during the September, 1955 equinox gave similar results in that the absorption was usually greatest in the northern quadrants, though this effect was considerably less marked than during the spring equinox. The evidence suggests that the zone of maximum absorption had moved further south, possibly associated with the increase in sunspot number during that period.

The results of this experiment therefore suggest that the anomalous high-latitude absorption primarily occurs north of College and that marked azimuthal vari-

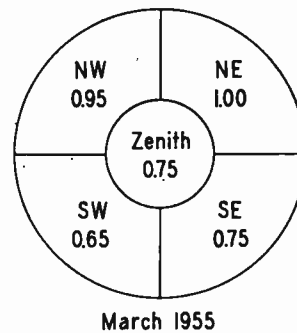


Fig. 3—Median values of the ratio of absorption to that in the NE direction for the zenith, and NW, SE, and SW directions, based on twenty-two events in March, 1955.

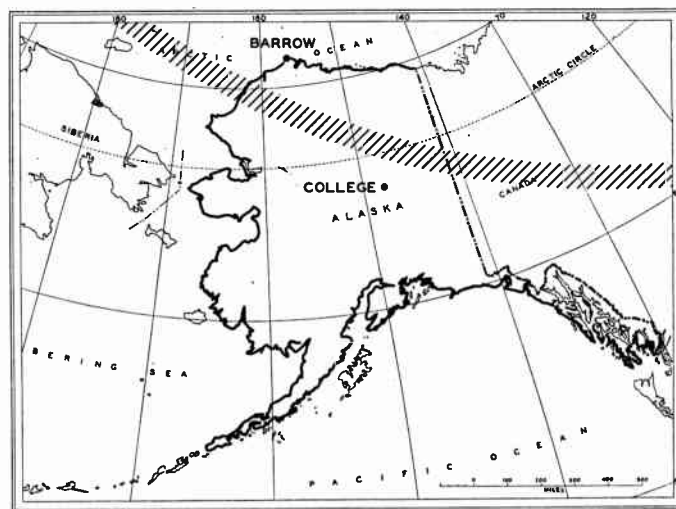


Fig. 4—Map showing the position of Barrow and College, Alaska, relative to the zone of maximum occurrence of visual aurora.

ations in absorption are frequently observed as observations are taken around a ring of some 300–400-km radius centered on College.

### Two-Antenna Experiment

Since the absorption measuring equipment accepts extraterrestrial radio waves over a wide cone of angles, the actual absorption measured is a mean value, averaged over the polar diagram. More exactly, if the distribution of extraterrestrial radio waves in power across the sky is given by  $P(\theta, \phi)$  and  $F(\theta, \phi)$  is the power polar diagram of the receiving antenna, then the fractional absorption recorded is given by

$$\frac{\int_0^{\pi/2} \int_0^{2\pi} P(\theta, \phi) \cdot F(\theta, \phi) \cdot A(\theta, \phi) \cdot d\theta \cdot d\phi}{\int_0^{\pi/2} \int_0^{2\pi} P(\theta, \phi) \cdot F(\theta, \phi) \cdot d\theta \cdot d\phi}$$

where  $A(\theta, \phi)$  describes the variation of the transparency of the ionosphere across the sky. At temperate latitudes,  $A(\theta, \phi)$  would be expected to be approximately uniform across the polar diagram, apart from the effect of changing obliquity. At high latitudes, however,

and particularly during auroral activity, marked irregularities in ionospheric absorption might be expected since individual visual auroral forms frequently are confined to a few kilometers or less in width.

During the summer of 1956, a two-antenna experiment was conducted at College with the object of determining if irregularities in the absorbing region, having lateral extent of the order 5–50 km, existed in the ionosphere. A broad- and a narrow-beam antenna, both directed at the zenith, were switched alternately into the input of the receiver, the complete switching cycle lasting three minutes. The pen recorder was operated at a chart speed of three inches per hour to permit separation of the noise recorded on each antenna.

The narrow-beam antenna consisted of a vertically directed broadside array of eight full-wave dipoles (at an operating frequency of 30.5 mc) spaced  $\frac{1}{2}$  wavelength apart. The entire array was suspended  $\frac{1}{8}$  wavelength above a chicken-wire ground screen. Physical dimensions of the ground screen were approximately 50 feet  $\times$  150 feet. The broad beam antenna consisted of a 3-element Yagi with the  $E$  vector in the geographic east-west plane.

The polar diagrams of each antenna were measured by making special flights with an airborne transmitter. The main lobe of the narrow-beam antenna was about  $15^\circ$  wide between the half-power points in the  $H$  plane and about  $60^\circ$  wide to the half-power points in the  $E$  plane. The  $H$  plane was aligned along the magnetic meridian. The Yagi antenna had a beamwidth of approximately  $60^\circ$  in the east-west  $E$  plane and somewhat over  $100^\circ$  in the north-south  $H$  plane. The areas of ionosphere investigated in the  $D$  region by the two beams were therefore of the order 20 km  $\times$  90 km for the narrow beam and 200 km  $\times$  90 km for the broad beam.

The traces were scaled relative to quiet day curves which were determined separately for each antenna using data for a few quiet days in August, 1956. On days during which precipitation occurred, unusual "absorption" events were found which affected only the records from the narrow-beam antenna. These events were shown to be due to the presence of moisture on the open wire transmission lines of this antenna. For this reason, data from days during which precipitation occurred were discarded from this study.

Six selected days were scaled by noting the value of absorption occurring on the hour for each of the 24 hours of the day (hereafter such values are called hourly values). The data were later reduced to 72 hourly values, owing to a persistent residual "absorption" which affected only the narrow-beam antenna throughout two of the days. The remaining 72 hourly values taken from data in the period 20–31 August are shown on the scatter diagram, Fig. 5. In general, the values do not depart far from the line of equal absorption on both antennas.

The peak absorption was also scaled for major singular events occurring during the interval 00–05 hours  $150^\circ$ W time. In this usage a "singular" event is defined

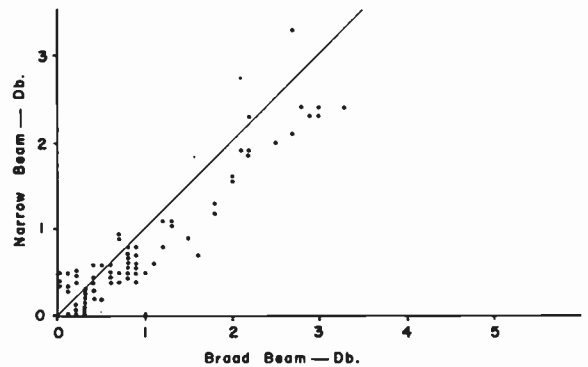


Fig. 5—Hourly values of absorption observed simultaneously on broad- and narrow-beam antennas at College. The straight line is that of equal absorption on the two antennas.

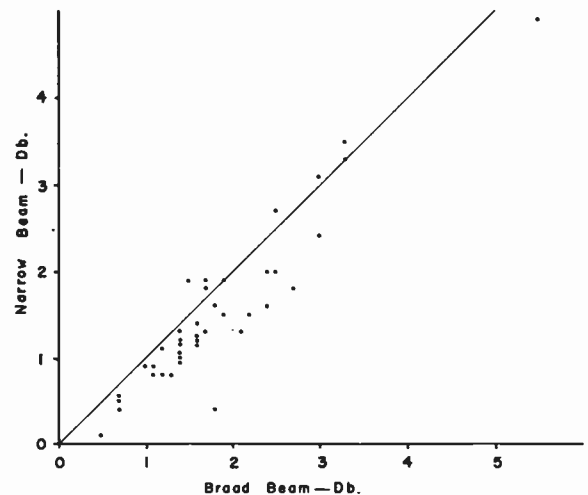


Fig. 6—Peak absorption during singular events observed simultaneously on broad- and narrow-beam antennas at College. The straight line is that of equal absorption on the two antennas.

as any occasion during which the absorption increased markedly from the predisturbance value and then decreased again to approximately the original level within 15 minutes or less. Such events are connected with the presence of visual aurora during the early morning hours. Thirty-nine singular events occurring during the period September 1–7, 1956, were scaled, and the results are shown in the scatter diagram of Fig. 6.

The two-antenna experiment indicates that the absorption is approximately equal on the two antennas. This fact is seen both from the equal-interval sampling, obtained by taking hourly values of the absorption, and even more strikingly from the analysis of the 39 singular events shown in Fig. 6. There is a trend for the broad beam antenna to show slightly more absorption than does the narrow-beam antenna. Such an effect can readily be explained as due to the increased effective thickness of the absorbing layer at oblique incidence.

The equality of the absorption on the two antennas shows that the ionospheric absorbing regions must normally have filled the broad-beam antenna and, therefore, must have had dimensions greater than 200 km in lati-

tude and 90 km in longitude. The absence of cases in which the absorption was markedly stronger on the narrow beam than on the broad beam indicates that isolated regions of absorption having dimensions of the order 5–50 km did not occur overhead during the period of observation.

Even though the absorption on the narrow beam during singular events is equal to or slightly less than that on the broad beam, the changes of absorption from predisturbance levels were on several occasions larger on the narrow beam antenna than on the broad beam antenna. Four examples of the change from predisturbance level to the peak absorption in singular events are shown in Table I.

TABLE I

Broad beam absorption (db)			Narrow beam absorption (db)			
Predisturbance value	Peak value	Change in absorption	Predisturbance value	Peak value	Change in absorption	
1)	1.1	1.8	0.7	0.3	1.6	1.3
2)	0.8	3.3	2.5	0.2	3.5	3.3
3)	1.0	3.3	2.3	0.1	3.3	3.2
4)	1.5	2.2	0.7	0.5	1.5	1.0

The most plausible explanation for these particular cases is that, originally, the absorption was not distributed uniformly across the sky, but was strongest over some region outside the narrow beam. This is indicated by the fact that the predisturbance values were originally greater on the broad-beam antenna than on the narrow beam antenna. Later, the absorption expanded into the zenithal region, thereby causing a relatively large increase in the absorption registered on the narrow beam. Such motions of regions of absorption have been observed while using a rotating antenna and are consistent with the greatly variable position and intensity of auroral luminosity.

#### Barrow-College Experiment

It has been realized for some time that one of the most important problems of high-latitude radio wave absorption is to determine its geographical distribution.

This problem has already received some attention, notably through the investigations of Cox and Davies<sup>3</sup> and Agy.<sup>4</sup> The results of Cox and Davies were, in part, based on the study of blackout time recorded by ionosondes at vertical incidence that were distributed in latitude across the auroral zone roughly along the 90° W meridian. Agy studied the outage time for various oblique incidence transmission paths across the auroral zone along the same meridian. Agy indicates, in part, that the absorption is low north of the auroral zone, that

the zone of absorption is centered near the center of the zone of maximum visual aurora, and that the zone may be less than 6° wide. Cox and Davies indicate that short duration blackouts seem to be localized in space.

At College the two-antenna and the rotating antenna experiments, described above, had indicated that the absorption was often nonuniform across the sky with a tendency for the absorption to be greater to the north of the station. These observations indicated a need for performing an experiment by use of the cosmic radio noise technique in which absorption would be simultaneously observed from two widely separated stations. Such an experiment was therefore conducted during the spring equinox of 1957. Barrow, Alaska, was selected for the second site because it is north of the auroral zone, while College, Alaska, is on the south side. Fig. 4 shows the location of Barrow and College relative to the auroral zone.

Each station was provided with a vertically directed 3-element Yagi antenna; these antennas were mounted in essentially identical fashions. The antennas were fed with 52-ohm coaxial line matched to the driven element through a balun and "T" match section. Earlier measurements of the polar diagram of a vertical 3-element Yagi had indicated a pattern of approximately 60° width between the half-power points in the *E* plane and somewhat over 100° in the *H* plane. Assuming a layer height of 85 km, these half-power beam dimensions correspond to viewing an elliptical section of the sky of some 100 km × 200 km, centered above the observing site. Because of the 800-km separation of the sites, there is no overlap between the ionospheric areas monitored by the two stations.

A quiet day curve was constructed for each station on the basis of an ionospheric undisturbed period which occurred during mid-March. Absorption was then measured by taking the ratio between the cosmic noise received and that which would have been received on a quiet day at the same sidereal time. The absorption at each station was scaled on the hour for each of the 24 hours of the day; the peak absorption occurring during each hourly interval was also noted. The accuracy of the data is believed to be within ±0.2 db, and is limited primarily by uncertainties in the quiet day curves.

Fig. 7 shows a scatter diagram of the hourly values of absorption at College and at Barrow. The diagram includes the 391 points constituting the available data for March, 1957. The linear correlation coefficient between absorption values at the two stations is 0.60. The "least squares" line of this set of data has a slope 0.38. In other words, the absorption at College was on the average some 2.6 times stronger than at Barrow.

Two specific periods were considered to determine if this degree of correlation is uniform throughout the day; the resulting scatter diagrams are shown in Fig. 8 and Fig. 9. The period 10–16 hours (Fig. 8) 150° W time was selected as representing the time during which daytime absorption was most likely to occur, whereas

<sup>3</sup> J. W. Cox and K. Davies, "Statistical studies of polar radio blackouts," *Can. J. Phys.*, vol. 32, pp. 743–756; December, 1954.

<sup>4</sup> V. Agy, "The location of the auroral absorption zone," *J. Geophys. Res.*, vol. 59, pp. 267–272; June, 1954.

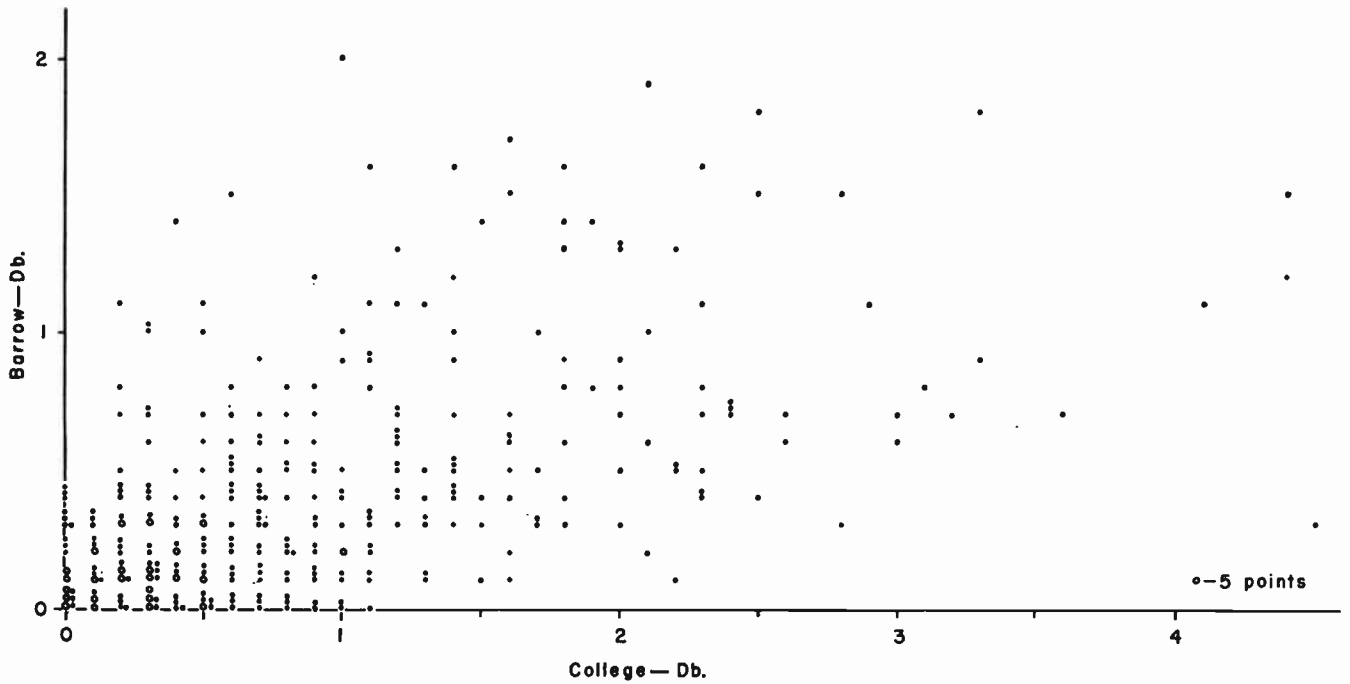


Fig. 7—Scatter diagram of hourly values of zenithal absorption of 30-mc cosmic noise at Barrow and College, Alaska, during March, 1957.

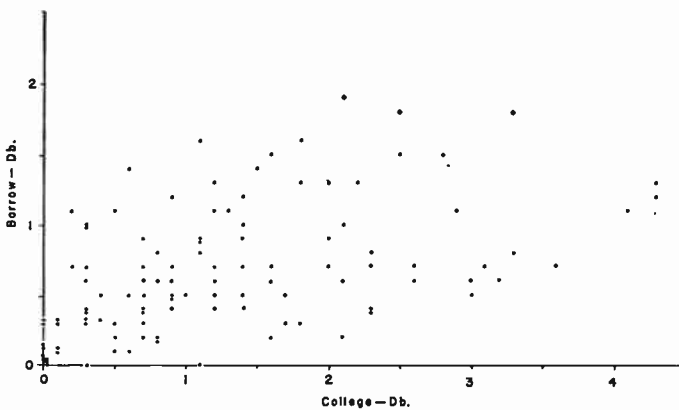


Fig. 8—Scatter diagram of hourly absorption values for the period 10<sup>h</sup>–16<sup>h</sup> 150° W, March, 1957.

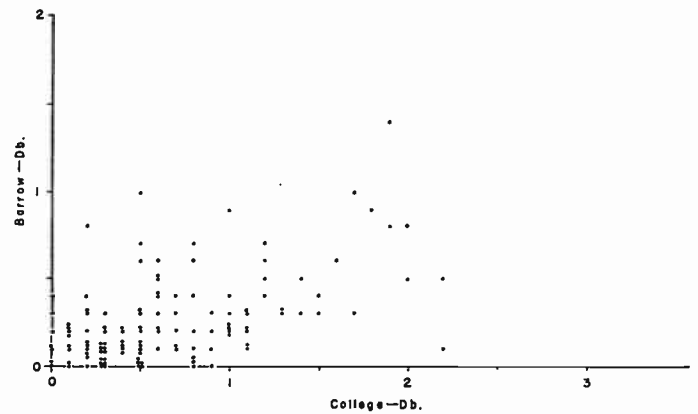


Fig. 9—Scatter diagram of hourly absorption values for the period 00<sup>h</sup>–06<sup>h</sup> 150° W, March, 1957.

the period of 00–06 hours 150° W time (Fig. 9) was selected as representing the time of night during which aurorally associated absorption was most probable. The correlation coefficient for the former period is 0.57 and for the latter period 0.43. It is noted that larger hourly values of absorption came during the daytime. This result is discussed in more detail below.

The diurnal variations of absorption at the two stations are illustrated in Fig. 10 and Fig. 11 (opposite). Fig. 10 shows the average hourly value of absorption for each hour of the day during March. In general, the two curves are similar; both show a relatively slow and smooth build-up of absorption after midnight, an early afternoon peak, and a very rapid fall-off of absorption in the early evening hours. At both stations, the most quiet part of the day is during the period 18–23 hours. It is

interesting to note that even on a very disturbed day the absorption generally recovers to the order of 0.5 db or less at 30 mc during this period. Under closer scrutiny there are some differences between the two curves which require explanation. For example, there is a strong peak at around 16 hours at College, and likewise a smaller peak centered at about 0.8 hours. The 16-hour peak is barely present at Barrow, while there is little or no evidence of the 08-hour peak on the Barrow data.

The differences between the two stations are further emphasized when the peak absorption during each hourly interval is considered rather than the values on the hour. Fig. 11 shows the average of the peak absorption during each hourly interval for both stations for the same period as covered in Fig. 10. The 08-hour peak is now emphasized at College but again is barely, if at all,

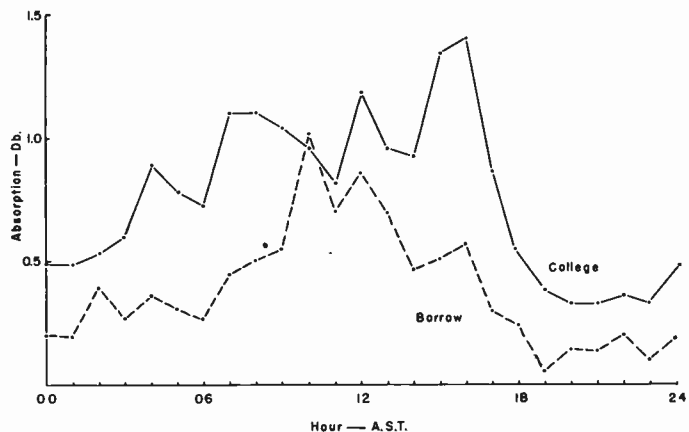


Fig. 10—Average diurnal variation of the hourly absorption values for March, 1957, Barrow and College, Alaska.

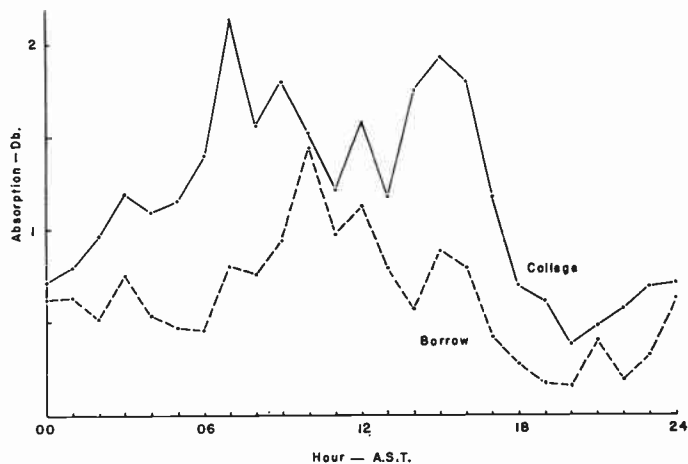


Fig. 11—Average diurnal variation of the peak absorption during each hourly interval for March, 1957, Barrow and College, Alaska.

present at Barrow. Again, the 16-hour peak is very strong at College, though still only weakly present at Barrow.

Because of the relatively large amount of data available for correlation between the absorption at College and Barrow, the correlation coefficient of 0.6 has high probability of statistical significance. From this high correlation coefficient it can be concluded that during periods of "storminess," the affected area is often at least as large as 800 km. On the other hand, smaller scale irregularities of absorption do exist as indicated by the rotating antenna and the two-antenna experiments; it is these irregularities which limit the degree of correlation between the two stations. Although the difference is not large between the correlation coefficients for the periods 00-06 hours ( $\rho=0.43$ ) and 10-16 hours ( $\rho=0.57$ ), it is probably significant.

Nighttime absorption at high latitudes is directly related to the presence of auroral activity and, more specifically, to the type of aurora present. Some of the strongest auroral-associated absorption corresponds to the period of breakup; that is, the transition from non-active homogeneous and rayed auroral forms to the

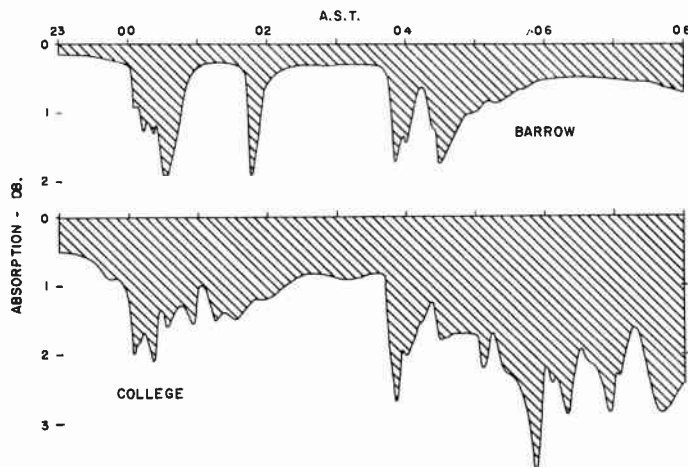


Fig. 12—30-mc zenithal absorption, College and Barrow, Alaska, on the night of March 5-6, 1957.

violently active rayed forms. It is, of course, well known that such breakups may be very restricted in geographical extent at any given time. Thus, one could expect, and indeed does find, numerous strong nighttime events present at one of the stations and not at the other (Fig. 12). The greater correlation between the two stations during the day, if significant, indicates that the corpuscular bombardment is more widely spread during the day than at night.

Another difference between the two periods of the day is evident from examination of the slope of the "least squares" lines of fit. This slope is 0.20 for the period 00-06 hours and 0.41 for the period 10-16 hours. Here again the conclusion is that the absorption is more nearly equal at the two stations during the day than at night, although the daytime ratio between College and Barrow absorption in decibels is still greater than 2:1.

The physical significance of the large ratio between the absorption measured at the two stations can be seen by considering the fundamental absorption equation. Assuming reasonable collisional frequencies and critical frequencies in the absorbing layer, the absorption in decibels is proportional to the integral  $\int_s N\nu ds$  where  $N$  is the electron density and the collision frequency is  $\nu$ . The total absorption is dependent on the path  $s$  over which the product  $N\nu$  is still appreciable. Thus, the absorption can be increased by increasing the number of electrons at a given height, by decreasing the height at which the electrons are formed, or by a combination of the two effects (the collision frequency  $\nu$  is dependent on the atmospheric density and hence height of the layer).

During particle bombardment, fluctuations in electron density are believed to be the primary factor involved in changes of absorption. From this assumption it appears that during March, 1957, College was closer to the auroral zone (or the zone of maximum bombardment) than Barrow. If the effect is entirely one of

differences in electron density, the average *D*-region electron density during disturbances must have been greater by a factor of two at College than at Barrow. The inference is that the auroral zone is quite sharply limited on its north side, because visual observations indicated that the auroral zone was north of College during this period.

The other possibility is that the height of the absorbing layer differs sufficiently between the two stations to account for the greater absorption at College. A fairly sharp focusing of the primary particles of higher energy, leading to a greater depth of penetration, might cause such a difference. These differences could also occur if ionization due to secondary effects, such as X rays, is likewise concentrated in a fairly narrow zone. X rays can ionize the atmosphere at lower heights than would be expected from the normal energy spectrum of the primary particles (Chapman and Little<sup>5</sup>). However, in view of the lack of detailed information on the height of the absorbing region, variations of the electron density are here assumed to account for the differences of the average absorption between the two stations.

The differences between the diurnal curves of the two stations (Figs. 10 and 11) seem to be real. The most plausible explanation of the presence of the 08-hour peak at College is the occurrence of pulsating aurora at College at this time of the day. Earlier studies by Heppner, Byrne, and Belon<sup>6</sup> have shown that the greatest percentage of blackout time observed by the College ionosonde corresponded to periods of pulsating aurora. During the period studied by those authors, there was more than 70 per cent blackout time during pulsating aurora, with all other auroral forms averaging 30 per cent or less. A small number of visual and photometric observations of aurora made at College during the winter of 1956–57, have also shown that pulsating aurora was present in the early morning hours (05–08) coincident with marked absorption at 30 mc.

The absence of the early morning absorption peak at Barrow can be explained by the hypothesis that pulsating aurora is not present at that station. Heppner,<sup>7</sup> studying extensive visual observations obtained at College in the period 1950–1952, found that the frequency of occurrence of pulsating aurora was quite low north of geomagnetic latitude 66° and that the zone of maximum occurrence of the pulsating aurora was at about 64°, well south of the zone of maximum occurrence of other types of aurora. Visual observations at Barrow by Franzke of the Geophysical Institute staff indicate that pulsating aurora rarely occurred there during the winter

of 1956–1957. It should be added that no such marked difference between the two stations is evident for other auroral forms.

At present there is no similar definite evidence by which one can explain the peak of absorption at 16 hours which was very noticeable at College and less so at Barrow. Tentatively, it is suggested that a secondary daytime maximum of particle bombardment occurred in the afternoon, the effect of which was enhanced by solar control of the absorbing region. However, further observations will be required in order to confirm this suggestion.

#### THE HEIGHT OF THE ABSORBING REGION

A basic weakness of the extraterrestrial radio wave technique of measuring ionospheric absorption is that it does not permit direct measurement of the height of the absorbing region above the earth's surface. However, by comparing the absorption data with the data from the C-3 ionospheric sounder (operated by the Geophysical Institute under contract with the National Bureau of Standards), it has been possible to show that the large majority of the absorption of the extraterrestrial radio waves during disturbed periods occurs below the *E* region.

The C-3 ionospheric sounder consists of a pulsed radar system which sweeps in frequency from 1–25 mc in 15 seconds. The pulses are transmitted vertically and are received after reflection from the ionosphere at frequencies up to the vertical incidence penetration frequency. Among the parameters scaled each hour is the minimum frequency  $f_{\min}$  at which echoes are actually observed. For a given equipment operating under constant conditions, this minimum frequency is primarily determined by the nondeviative absorption which, as stated above, is proportional to

$$\frac{1}{\nu^2 + (w \pm w_L)^2} \quad (6)$$

Using this expression, it is possible to calculate the ratio between the nondeviative absorption at 30.5 mc and at some other frequency  $f$ . Fig. 13 shows the manner in which this ratio varies with frequency for ordinary waves at College, assuming that  $\nu = 10^6$  (corresponding to a height of approximately 85 km). It is also possible, by measuring or estimating the pertinent parameters of the C-3 system, to predict the number of decibels of absorption required at a given frequency to give a barely detectable echo from the *E* or *F* region on the C-3 equipment. Fig. 14 is the result of such calculations, in which the C-3 equipment was supposed to be operating with the following characteristics throughout the range 1–8 mc:

Transmitter peak pulse power	= 10 kw,
Antenna area (transmitting)	= 1500 m <sup>2</sup> ,
Minimum detectable received signal	= $2.5 \times 10^{-14}$ watts,
Antenna area (receiving)	= 1500 m <sup>2</sup> .

<sup>5</sup> S. Chapman and C. G. Little, "The nondeviative absorption of high-frequency radio waves in auroral latitudes," *J. Atmos. Terr. Phys.*, vol. 10, pp. 20–31; January, 1957.

<sup>6</sup> J. P. Heppner, E. C. Byrne, and A. E. Belon, "The association of absorption and Es ionization with aurora at high latitudes," *J. Geophys. Res.*, vol. 57, pp. 121–134; March, 1952.

<sup>7</sup> J. P. Heppner, "A Study of Relationships between the Aurora Borealis and the Geomagnetic Disturbances Caused by Electric Currents in the Ionosphere," Calif. Inst. of Tech., Pasadena, Calif. Ph.D. dissertation; 1954.

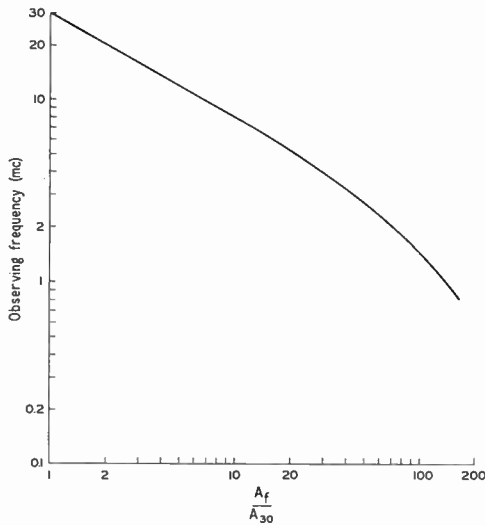


Fig. 13—Ratio,  $A_f/A_{30}$  of the absorption at any frequency  $f$  (less than 30 mc) to the absorption at 30 mc, as a function of frequency  $f$ . The curve is calculated for the ordinary wave assuming a constant collision frequency  $\nu$  of  $10^6$  per second, and gyromagnetic frequency  $\omega_L$  of  $10^7$  radians per second.

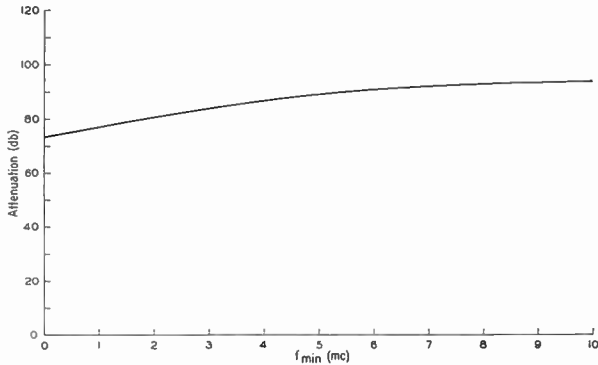


Fig. 14—Sensitivity curve of the C-3 ionosonde in terms of attenuation in db required to produce an observed minimum frequency of the  $E$  layer,  $f_{\min}E$ .

A total of 10 db was allowed for polarization and transmission line losses and for losses in the matching loads terminating the crossed delta transmitting and receiving antennas.

Using the ratios given in Fig. 13 for the relative magnitude of the absorption at 30.5 mc and at a frequency  $f$ , it is possible to compute from Fig. 14 the absorption required at 30.5 mc to produce a given value of  $f_{\min}$  on the C-3 equipment. Curves expressing this function are reproduced in Fig. 15, in which simultaneously measured values of  $f_{\min}E$  and zenithal absorption of the 30.5-mc extraterrestrial radio waves are also plotted. Similar data for the  $F$  region are given in Fig. 16. In each case, due allowance is made for the fact that the 30.5-mc extraterrestrial signal traverses the whole ionosphere once, while the C-3 transmission has to travel twice through any absorbing region below the reflecting layer before being recorded on the ground. The two curves shown in Fig. 15 were computed assuming that either all or one half of the 30.5-mc absorption occurred

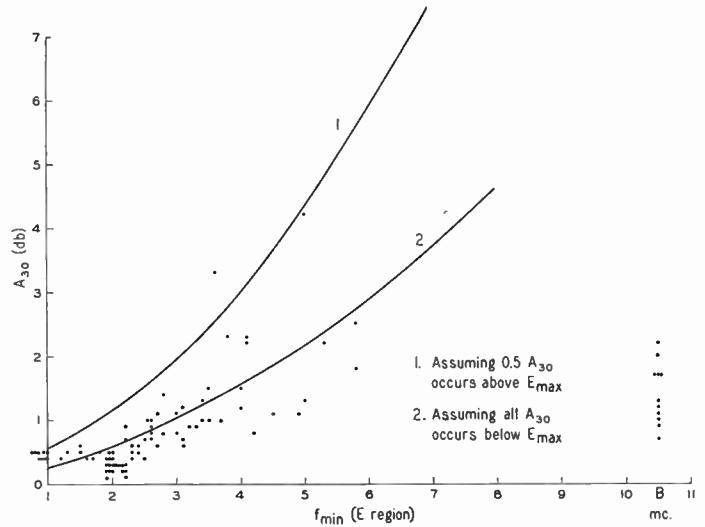


Fig. 15—Absorption at 30 mc using the cosmic noise technique plotted against  $f_{\min}E$  for the C-3 ionosonde, College, Alaska. Curve 1 is a theoretical curve assuming that one half of the absorption of 30-mc cosmic noise occurs above the point of reflection,  $E_{\max}$ . Curve 2 assumes that all of the 30-mc cosmic noise absorption occurs below  $E_{\max}$ . The dots are experimental points, with those at the mark  $B$  indicating values of 30-mc absorption occurring simultaneously with no signal return (blackout) on the C-3.

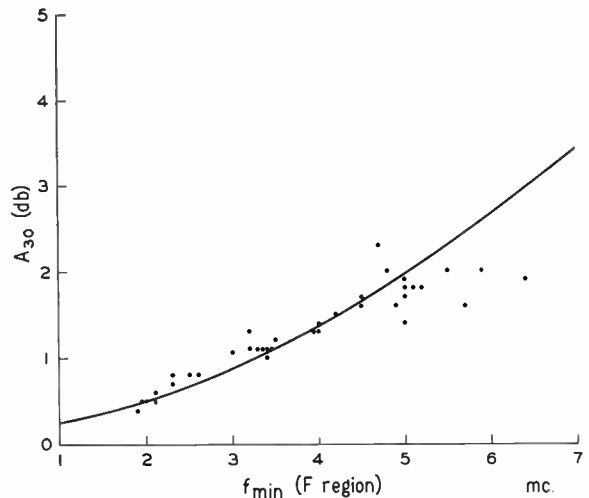


Fig. 16—Absorption at 30 mc using the cosmic noise technique, vs  $f_{\min}F$  ( $F$  layer). The solid curve is the theoretically predicted curve, assuming all absorption occurs below the point of reflection from the  $F$  layer. The dots are experimental points.

below the reflecting layer. It will be seen that the C-3 data indicate that virtually all the absorption occurs below the  $E$  region and is therefore traversed twice by  $E$ - or  $F$ -region echoes. Since the  $E$  region at College is at a height of about 100 km, this means that the absorption must be occurring below that height. The shape of the experimental curves, relating the  $f_{\min}$  and  $A_{30}$ , further suggests that the absorption must be occurring at heights above 60 km since below that height the  $\nu^2$  term in the denominator of (6) would be the dominant one, and the 30-mc absorption would have been approximately constant with frequency for the lower  $f_{\min}$  values.

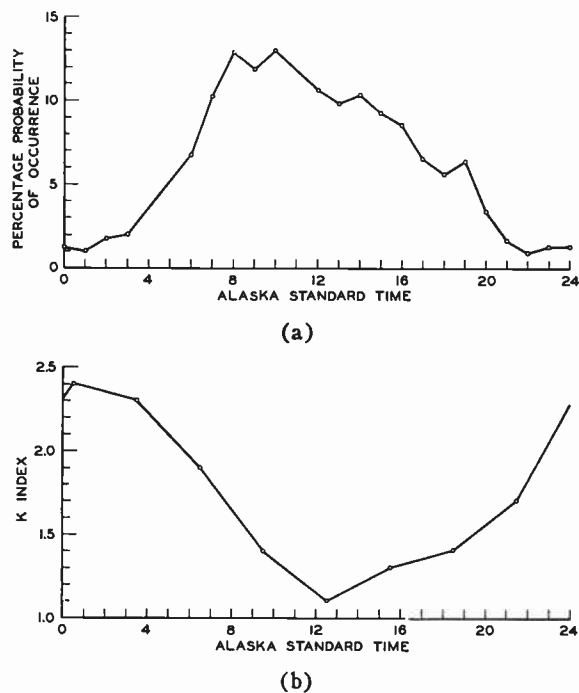


Fig. 17—(a) Average diurnal variation of polar blackouts (no signal return from the C-3), College, Alaska for 1954, and (b) average diurnal variation of the mean magnetic  $K$  index, at College for 1954.

#### CORRELATION BETWEEN MAGNETIC ACTIVITY AND IONOSPHERIC ABSORPTION

It has been known for many years that a good correlation exists in polar regions between magnetic activity, auroral activity, and ionospheric storms. It was therefore natural that a study be made of the correlation between magnetic activity and ionospheric absorption at College. Several different correlation studies have been made and are presented below.

The vertical incidence ionosonde data from College taken during 1954, was used to study the mean daily and seasonal variations of the incidence of absorption at College. The hourly scalings of the ionograms for the year were used to determine the percentage probability of occurrence of polar blackouts as a function of time of day and month. These hourly and monthly percentages are compared in Fig. 17 and Fig. 18 with the corresponding College  $K$ -index data. Two points are immediately obvious: first, the seasonal variation curves of  $K$  index and percentage blackout are very similar and both show pronounced equinoctial maxima; second, the mean diurnal variations of  $K$  index and blackout probability, averaged over the year, are very different in that the blackouts are most prevalent during the daytime, while the mean  $K$  index is at a maximum shortly after midnight. A further investigation, based on 50 days of continuous data using the cosmic noise technique, was therefore made to try and resolve the apparent discrepancy between the good positive seasonal correlation and the inverse diurnal correlation of absorption and magnetic activity.

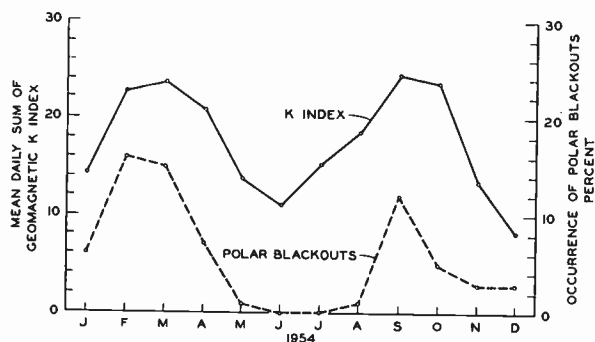


Fig. 18—Seasonal variation of geomagnetic  $K$  index and the incidence of polar blackouts at College, Alaska during 1954.

The magnetic three-hour  $K$  index was again selected as being a readily available and standard index of magnetic activity at College. The choice of a corresponding absorption index was dictated, in part, by the form of the available absorption data. These data have been tabulated by giving the maximum amount of absorption occurring in each half-hour interval during the day. Three different absorption indexes were established on the basis of these data, namely: 1) the average of the six half-hourly values of absorption obtained during each three-hour  $K$ -index period, 2) the peak absorption registered in the six half-hour intervals of each three-hour period, and 3) the greatest change in absorption between the half-hour peak values in the three-hour period. A trial correlation was run between each of these indexes and the  $K$  index for a specific  $K$ -index period. The peak absorption index showed the best correlation for the period tested and this index was therefore adopted for the remainder of the study.

Magnetic data for the Finnish station, Sodankylä, which is at a similar latitude but about 12 hours away in solar time, were also available, and the absorption at College was correlated with the Sodankylä  $K$  index as well as the College  $K$  index. Fifty-days data, from February 15 through April 5, 1955, were used for this study. Fig. 19 and Fig. 20 show the mean daily variation of the indexes for the fifty-day period for  $K$ (College) and Abs(College) and for  $K$ (Sodankylä) and Abs(College), respectively. The linear correlation coefficients between  $K$ (College) and Abs(College) and  $K$ (Sodankylä) and Abs(College) are also plotted in the respective figures. The following points are to be noted concerning these mean index curves.

1) The mean daily  $K$ (College) curve shows a pronounced maximum during the  $K$  periods 09–12 and 12–15 U.T. (23–02 and 02–05 hours local time at College).

2)  $K$ (Sodankylä) shows a diurnal peak in the interval 18–21 and 21–24 hours U.T. (corresponding to 19–22 and 22–01 hours local time at Sodankylä).

3) Except for a pronounced minimum during the period 06–09 U.T. (20–23 hours local time at College), the absorption index shows a much flatter diurnal curve than does either  $K$ (College) or  $K$ (Sodankylä).

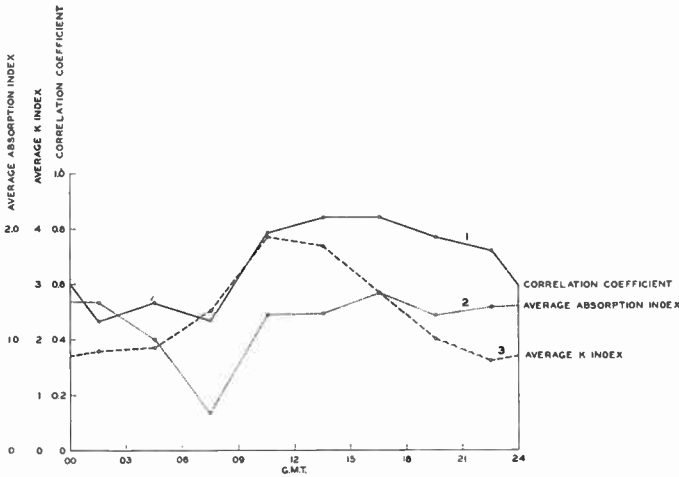


Fig. 19—Diurnal variation of the absorption and K index at College. Curve 1 shows the diurnal variation of correlation between K(College) and absorption(College). Curves 2 and 3 show the mean diurnal variations of K(College) and absorption(College).

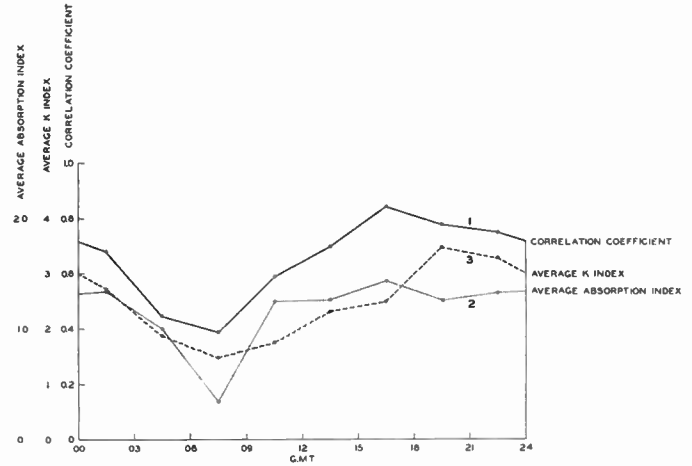


Fig. 20—Diurnal variation of the absorption at College and K index at Sodankylä. Curve 1 shows the diurnal variation of correlation between K(Sodankylä) and absorption(College). Curves 2 and 3 show the mean diurnal variations of K(Sodankylä) and absorption(College).

4) The sharp minimum of absorption activity during the evening hours is substantiated by absorption data obtained later at both College and Barrow, Alaska. (See College-Barrow experiment above.)

Linear correlation coefficients were calculated for Abs(College) vs K(College), Abs(College) vs K(Sodankylä), and K(College) vs K(Sodankylä) for each of the eight three-hour K-index periods, using the data from 50 successive days, February 15 through April 5, 1955, (Table II). The correlation between the two K indexes is statistically significant for all eight K-index periods. The high degree of correlation, averaging 0.75 for the eight groups, each of 50 observations, attests to the fact that magnetic storm activity tends to be widespread around the auroral zone.

TABLE II

CORRELATION COEFFICIENTS BETWEEN MAGNETIC ACTIVITY AND IONOSPHERIC ABSORPTION, BASED ON THE 50-DAY PERIOD OF FEBRUARY 15 THROUGH APRIL 5, 1955

K Index		Correlation Coefficient		
Time Period		K(College) vs K(Sodankylä)	Abs(College) vs K(College)	Abs(College) vs K(Sodankylä)
UT	150° W			
00-03	14-17	0.72	0.47	0.68
03-06	17-20	0.81	0.55	0.45
06-09	20-23	0.59	0.47	0.39
09-12	23-02	0.68	0.79	0.59
12-15	02-05	0.78	0.85	0.70
15-18	05-08	0.91	0.85	0.84
18-21	08-11	0.81	0.78	0.78
21-24	11-14	0.73	0.73	0.75
Mean		0.75	0.69	0.65

The correlation of absorption with both K(College) and K(Sodankylä) is likewise significant for all K-index periods. The period of best correlation of K index and absorption is during the night hours at College ( $\rho = 0.85$ ). The lowest correlation comes during the early evening

hours at College, when absorption activity tends to be at its minimum. It is important to note that the average correlation between K(Sodankylä) and Abs(College) is approximately equal to that between K(College) and Abs(College). The nighttime magnetic disturbances at Sodankylä are associated with the corpuscular bombardment of the upper atmosphere in the general region of Sodankylä; the fact that they correlate well with daytime absorption events at College and with relatively weak daytime magnetic effects at College suggests that a weak bombardment of the daytime side of the auroral zone occurs simultaneously with the major bombardment of the nighttime side of the zone.

The results of this more detailed correlation study show that the absorption activity is closely related to the simultaneous magnetic activity at all hours of the day. The different mean diurnal variations of the two phenomena must be due to some additional factor which causes the ratio of magnetic-to-absorption activity to vary between night and day. The corpuscular bombardment of the upper atmosphere is apparently at a maximum during the midnight hours, as evidenced by the visual and radar investigations of aurora, as well as by the magnetic data. Some mechanism is, therefore, required to enhance the daytime absorption (or alternatively, to suppress the nighttime absorption), relative to the corresponding magnetic activity. One plausible mechanism is the photodetachment during daylight hours of electrons attached to oxygen molecules located at heights of the order of 60-80 km. As discussed by Chapman and Little,<sup>5</sup> electrons could be produced at such heights by the absorption of X rays generated as bremsstrahlung in the aurora. These electrons would have considerable effect upon the ionospheric absorption since they occur at a region where the collision frequency  $\nu$  is high. They would, however, have little effect upon the electrical currents flowing in the ionosphere since they occur in a region where the electrical

conductivity is low. During the night electrons created at such heights would speedily be lost by attachment, resulting in relatively little absorption during the dark hours. Some evidence in favor of the solar daylight control of ionospheric absorption is presented in Fig. 21 which shows the variation of ionospheric absorption with time for the four days around the major solar outburst of February 23, 1956. The sunrise and sunset effect was particularly marked on February 24, and could still be detected on the two succeeding days. A detailed examination of the College ionosonde data during 1954 and 1955, also shows evidence of a solar daylight control of high latitude absorption associated with corpuscular bombardment, in that the narrow midday winter peaks of absorption broaden month by month as the daylight hours increase.

#### RELATIONS BETWEEN VISUAL AURORA AND ABSORPTION

Heppner, Byrne, and Belon have made an exhaustive study of the correlation of polar blackouts and visual aurora. As pointed out above, they found that pulsating aurora was accompanied by a blackout of a vertical ionosonde for more than 70 per cent of the cases studied. All other auroral forms were accompanied by 30 per cent or less blackout time.

The small amount of correlation work to date between visual aurora and absorption of cosmic noise received on a broad beam antenna confirms the conclusions of the above cited authors. The observed relations between aurora and absorption at College can be summarized as follows:

- 1) The prebreakup auroral forms, such as glows, homogeneous arcs, and quiet rayed arcs and bands, are accompanied by little or no absorption at 30.5 mc. If absorption is present, it is usually relatively constant with time.

- 2) The breakup phase of the aurora, characterized by violently active, moving rayed bands and draperies, may or may not be accompanied by moderate to strong absorption events. The absorption, when marked, sets in at the time of the breakup.

- 3) Pulsating and flaming aurora which sometimes follow breakup are usually accompanied by strong and variable amounts of absorption. Auroral associated absorption of 30.5-mc cosmic noise often reaches values in excess of 4 db during these periods.

A striking, but not unusual, example of the relation of aurora and absorption occurred on the night of August 31–September 1, 1956. On this night a spectacular auroral breakup occurred, marked by the formation of very active rayed bands with red lower borders. However, the accompanying absorption was less than 1 db, even though the bright aurora covered most of the sky. Some fifteen minutes later the breakup subsided, leaving fainter and more diffuse ray bundles and draperies. Shortly thereafter, the zenithal region of the

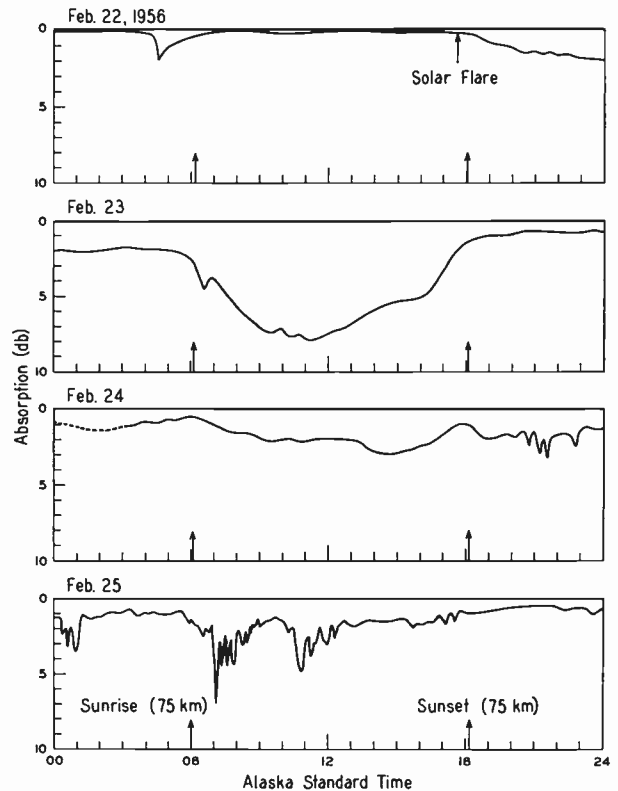


Fig. 21—Zenithal absorption of 30-mc cosmic noise recorded with a wide-beam antenna, College, Alaska, prior to and following the great solar flare of February 23, 1956 at 03:40 UT. Solar control of the absorption is particularly marked during the daylight hours of February 23, 150°. First indications of aurorally associated absorption are on the night of February 24–25.

sky was suddenly covered by violently flaming aurora. Simultaneously with the beginning of the flaming aurora, the absorption increased, reaching a value of approximately 5 db within two minutes. As the flaming aurora gradually subsided over the next half hour, the absorption also decreased in intensity.

Our observations confirm that pulsating and flaming aurora, unlike other auroral forms, are closely associated with major absorption events. The limitation of the northern extent of pulsating aurora and the presence (during March, 1957) of the early morning peak in absorption at College and its absence at Barrow are points which were discussed above (College-Barrow experiment). These differences in the absorption characteristics of the different auroral forms add weight to the suggestion that the physical mechanisms causing pulsating and flaming aurora differ significantly from those giving rise to other forms of auroral luminosity. In particular, the presence of strong absorption during pulsating and flaming aurora suggests an increase in the number and/or energy of X ray photons produced in the ionosphere by bremsstrahlung from electrons.

#### ACKNOWLEDGMENT

The authors wish to acknowledge the assistance they received from Dr. S. Chapman, Dr. W. M. Rayton, and Dr. G. W. Swenson, Jr., during the course of this work.

# Cosmical Electrodynamics\*

J. H. PIDDINGTON†

**Summary**—The spectacular results of radio astronomy have increased interest in the broader field of *electromagnetic phenomena in cosmical physics*. This subject is introduced here by a discussion of the various possible types of disturbance which may propagate in a magneto-ionic medium. The results are then applied in some regions of interest, particularly those from which nonthermal radio emission takes place.

In the solar atmosphere many otherwise mysterious phenomena are explained as electromagnetic effects: the heating of the corona to  $10^6$ °K, flares, the violent motion of the gases and emission of radio waves, as well as X rays and the corpuscles which cause magnetic storms. Interstellar space, the interior of a mysterious nebula and radio source (the Crab nebula), and interplanetary space provide more examples of electromagnetic phenomena.

One of the most fundamental problems concerns the origin of cosmic rays, now believed to result from electromagnetic processes. Evidence is provided of an even more fundamental process: the creation of magnetic field on such an enormous scale that nuclear energy sources are indicated.

## I. INTRODUCTION

RADIO astronomy largely has been responsible for the increasing interest in the broader field of *electromagnetic phenomena in cosmical physics*, an interest evidenced at an international conference under that title held in Stockholm, Sweden, in 1956, and attended by some 90 delegates from 14 countries.

Some of the phenomena concerned are directly associated with the emission of radio waves; for example, the occasional violent disturbances in the solar atmosphere which result in radio bursts, as well as flares and subsequent geomagnetic effects. Other of these phenomena have no apparent connection with radio emission; for example disturbances occurring in the interior of magnetic stars. However, even these may have an indirect association with radio emission and may warrant study by the radio astronomer.

The major portion of cosmical electrodynamics now is referred to as hydromagnetics or magnetohydrodynamics—the study of the movement of an electrically conducting fluid in the presence of a magnetic field. Perhaps the earliest work in this field was concerned with the origin of the cosmic magnetic fields themselves. According to these “dynamo” theories certain movements of the conducting fluid result in an increase (or at least maintenance) of the magnetic fields of the earth, the sun, and magnetic stars. These theories have been reviewed recently in some detail.<sup>1,2</sup> An important discovery in hydromagnetics was made by Alfvén, who

first described hydromagnetic shear waves and showed that they could transport magnetic energy.<sup>3</sup> More recently, hydromagnetic theory has largely been concerned with various mechanical effects of cosmical magnetic fields. These include magnetic control of sunspot and coronal structure, instability caused by magnetic fields, and oscillations of magnetic stars. They have been reviewed recently by Cowling.<sup>4,5</sup>

Of greater interest to the radio astronomer are theories of electromagnetic heating, including solar coronal heating, flares, and the acceleration of cosmic rays. Some have been reviewed by Cowling<sup>4,5</sup> and other more recent ones are discussed below. Also of interest in radio astronomy is the observational work of Babcock<sup>6</sup> on the magnetic fields of the sun and certain stars. Other observational work on the field of the galaxy and of the Crab nebula is mentioned below in Sections IV and V.

Hydromagnetic theory usually is simplified by neglecting electron inertia effects and displacement current. This means that plasma oscillations (or electric space-charge oscillations) are not considered. In some circumstances, notably in connection with the generation of solar radio bursts, these may be important. A review of these effects, with numerous references, has been given.<sup>7</sup> Finally, in certain problems, the motion of individual ions must be studied. This is the case for the acceleration of cosmic rays and their subsequent motion in a magnetic field, when they emit radio waves as suggested by Alfvén and Herlofson.<sup>8</sup> This latter mechanism probably is responsible for most cosmic radio emission and perhaps some (but not a large proportion<sup>9</sup>) of solar radio emission.

An approach to cosmical electrodynamics may be made by a study of sinusoidal waves in a magneto-ionic medium (fully or partially ionized gas permeated by a magnetic field). From such simple waves more complex disturbances may be synthesized and the electromag-

<sup>3</sup> H. Alfvén, “Cosmical Electrodynamics,” Oxford University Press, New York, N. Y., pp. 76–97; 1950. References are given to Walén’s work on sunspot fields and Lundquist’s experimental demonstration of hydromagnetic waves.

<sup>4</sup> T. G. Cowling, “The Sun,” G. P. Kuiper, Ed., University of Chicago Press, Chicago, Ill., vol. 1, pp. 532–591; 1953.

<sup>5</sup> T. G. Cowling, “Magnetohydrodynamics,” Interscience Publishers, New York, N. Y., 1957.

<sup>6</sup> A review will be given in the proceedings of the Conference on Electromagnetic Phenomena in Cosmical Physics, Stockholm, Sweden; 1956, in press.

<sup>7</sup> P. L. Bhatnager, M. Krook, and D. H. Menzel, “Preliminary Report of the URSI Committee on Dynamics of Ionized Media;” 1952.

<sup>8</sup> H. Alfvén and N. Herlofson, “Cosmic radiation and radio stars,” *Phys. Rev.*, vol. 78, p. 616; June, 1950.

<sup>9</sup> J. H. Piddington, “Thermal theories of the high-intensity components of solar radio-frequency radiation,” *Proc. Phys. Soc.*, vol. 66, pp. 97–104; January, 1953.

\* Original manuscript received by the IRE, November 18, 1957.

† CSIRO, Radiophysics Lab., Sydney, Australia.

<sup>1</sup> T. G. Cowling, “Vistas in Astronomy,” A. Beer, Ed., Pergamon Press, London, Eng., and New York, N. Y., vol. 1, pp. 313–322; 1955.

<sup>2</sup> W. M. Elsasser, “Hydromagnetism,” *Amer. J. Phys.*, vol. 23, pp. 590–609, December, 1955, and vol. 24, pp. 85–110; February, 1956.

netic field, gas movements, energy transport, and heating studied. Such disturbances appear to be the basis of most, if not all, nonthermal cosmic radio emission, as well as cosmic rays and other phenomena. In Section II some recent advances in magneto-ionic wave theory are described briefly.

In the later sections, these theoretical results are applied for the conditions observed in the different regions of interest. The solar atmosphere is, perhaps, of greatest interest, since it provides us not only with radio emissions of various types, but also high-energy quanta which create the ionosphere and particles which cause magnetic storms and aurorae. All these phenomena appear to have their origins in hydromagnetic effects. Other regions discussed are interplanetary space and interstellar space, both now known to be magneto-ionic regions in which interesting electromagnetic effects occur. Finally, the interior of a 900-year old supernova, the Crab nebula, is discussed. This powerful radio source contains a magnetic field of enormous total energy (roughly  $10^{41}$  joules, or the total energy radiated by the sun in  $10^7$  years) and may provide clues as to the origin of the galactic magnetic field and cosmic rays and hence, of most of the galactic radio emission.

## II. WEAK WAVES IN A MAGNETO-IONIC MEDIUM

Most phenomena (apart from atomic processes) in a magneto-ionic medium may be discussed in terms of the various possible waves present. A full nonlinear theory of strong waves is very complex, so that attention mainly has been confined to weak waves which provide an insight into many important effects. The radio engineer is well acquainted with two of these waves, the ordinary (*O*) and extraordinary (*E*) radio waves; however, because it makes certain simplifying assumptions (heavy ion motion and electron gas pressure are neglected), the well-known magneto-ionic theory fails to disclose various other waves. These are the two hydromagnetic waves discovered by Alfvén and applied by him and others to astrophysics.<sup>8</sup> There should be a sound wave, modified perhaps by the magnetic field; there also should be a space-charge or plasma wave.

A more complete "magneto-ionic" theory<sup>10</sup> discloses four and only four possible waves.<sup>11</sup> There are two shear type hydromagnetic waves, sometimes called Alfvén waves or magnetohydrodynamic waves. These have

<sup>10</sup> J. H. Piddington, "The four possible waves in a magneto-ionic medium," *Phil. Mag.*, vol. 46, pp. 1037-1050; October, 1955. This paper is concerned with the identification of different types of waves and not with their damping rates. Subsequently, the effects of collisions between various types of gas particles may be considered and the damping rate for each type of wave determined.

<sup>11</sup> When account is taken of viscosity a corresponding "viscosity wave" is introduced near a shearing boundary. See, for example, H. Lamb, "Hydrodynamics," 6th ed., Dover Press, New York, N. Y., p. 620; 1945. However, this wave is critically damped and does not seem to merit inclusion with the traveling waves. When account is taken of variation of thermal conductivity with pressure, "conductivity waves" may occur (A. Banos, Jr., "Normal modes characterizing magnetoelastic plane waves," *Phys. Rev.*, vol. 104, pp. 300-305; October, 1955), but these appear to have limited physical significance and are not discussed here.

been called the *O* and *E* hydromagnetic waves, because they correspond to the *O* and *E* radio waves; the latter being the simpler limiting cases at frequencies so high that heavy ion motion is negligible. The other two waves comprise a "magnetic sound" (*S*) wave and a plasma (*P*) wave.

The properties of the *O* and *E* waves have been investigated in some detail.<sup>12</sup> Like the corresponding radio waves, they are elliptically polarized, tending to circular and plane when propagated along and perpendicular to the steady-magnetic field. The gas always moves in a direction perpendicular to the magnetic field, suggesting the description "shear" waves. When the wave frequency is far below the gyromagnetic frequency of the heavy ions, the velocities of these waves are independent of the frequency, being  $V \cos \theta$  and  $V$ , respectively, where  $V = H_0(4\pi\rho)^{-1/2}$ ,  $\theta$  is the angle between the steady-magnetic field  $H_0$  and the wave normal, and  $\rho$  is the mass density of the gas.

The *S* hydromagnetic wave<sup>12</sup> is essentially a longitudinal or compression wave. At frequencies well below the ion gyrofrequency, it has the velocity of sound and, when propagated along the magnetic field, it is almost a pure sound wave (the magnetic field plays no part, but there is a weak electric space-charge effect). Finally the *P* wave is the more general case of the well-known electric space-charge or "plasma" wave whose properties have been modified by the presence of the magnetic field.<sup>10</sup>

In the following sections, the great importance of the shear hydromagnetic waves in cosmical electromagnetics is made evident. They constitute a back-and-forth change of energy from kinetic to electromagnetic. They transport this energy from one place to another (by their Poynting vector), dissipating some of it as heat and occasionally in other forms, such as excitation and ionization of some gas particles and as the energy of cosmic rays. Of particular interest is their rate of attenuation which, in an isotropically conducting medium, depends only on the electrical conductivity  $\sigma$  (emu) and the wavelength  $\lambda$ : the wave decays by a factor  $\exp 1$  in a time approximately  $\sigma\lambda^2$ . Unfortunately, in a magneto-ionic medium the situation is much more complicated; the electrical conductivity is a tensor with components  $\sigma_0$  along the magnetic field,  $\sigma_1$  perpendicular to the field and in the plane of the electric vector and  $\sigma_2$  perpendicular to both (Hall conductivity).

But the difficulties were not as formidable as they appeared; the effective conductivity recently has been determined<sup>13,14</sup> as  $\sigma_3 \equiv \sigma_1 + (\sigma_2^2/\sigma_1)$ , a result which allows

<sup>12</sup> See, for example, J. H. Piddington, "Hydromagnetic waves in ionized gas," *Monthly Notices Roy. Astron. Soc.*, vol. 115, pp. 671-683; 1955.

<sup>13</sup> J. H. Piddington, "Electromagnetic field equations for a moving medium with Hall conductivity," *Monthly Notices Roy. Astron. Soc.*, vol. 114, no. 6, pp. 638-650; 1954.

<sup>14</sup> T. G. Cowling, "The dissipation of magnetic energy in an ionized gas," *Monthly Notices Roy. Astron. Soc.*, vol. 116, no. 1, pp. 114-124; 1956.

rates of decay of hydromagnetic waves to be determined easily. It also allows the time of decay of a magnetic field in a conductor of dimensions  $L$  to be found, or the time of decay of a kink of dimensions  $L$  in a more extensive magnetic field. These are both given by  $\sigma_3 L^2$ .

This useful result has been used to determine rates of absorption in the solar atmosphere and interstellar space (Sections III and IV below) and consequent heating of the gas.

### III. THE SOLAR ATMOSPHERE

The solar atmosphere provides a laboratory with a wide variety of electromagnetic experiments, involving violent movement of gas and magnetic field and the emission of various types of radio noise, of ultraviolet light, X rays, and at times cosmic rays. None of these phenomena are fully understood; indeed, there is not yet agreement on the most basic problem of how the corona, situated between the relatively cold sun and colder space, is maintained at a temperature of about  $10^6$ °K and in places  $10^7$ °K (near sunspots).

It is fairly certain that the atmosphere is heated from below, the energy being provided by subsurface movement of material. Some of these movements cause the observed "granules"; these may be supersonic jets emerging from the surface of the sun. The upward transport of this energy must be by one of the four waves discussed above and each has been considered. There are strong arguments against the  $S$  and  $P$  waves and, until recently, this also seemed to be the case for the shear waves (which had been proposed earlier by Alfvén<sup>8</sup>). In calculating the electrical conductivity of the solar atmosphere it was thought that neutral atoms could be neglected. The reason was that, because of their very small collision cross section (compared to ions), they had negligible influence on the electron collision frequency. When the effects of neutral atoms are neglected, the electrical conductivity  $\sigma_3$  is so high that negligible wave damping occurs and thus negligible heating of the gas.

In a more recent investigation,<sup>15</sup> however, the role of neutral atoms was found to be vital. In fact, under typical chromospheric conditions the presence of 10 per cent neutral atoms could decrease the conductivity by a factor of about  $10^8$  and increase the absorption accordingly. The  $O$  and  $E$  waves are then able to explain the observed heating.

This remarkable effect of neutral atoms prompts an enquiry into its physical nature. This may be explained crudely by likening the magnetic lines of force to elastic strings on which the heavy ions and electrons are strung like beads. A hydromagnetic wave is an elastic wave which travels along these strings,<sup>16</sup> causing them to

vibrate and the ions to oscillate back and forth. Both positive and negative ions share this motion, their only relative motion being a slight drift constituting the electric current which is part of the wave. Thus a collision between ions is a very minor affair. The picture is greatly changed when neutral atoms are present—these are not forced into oscillation by the moving magnetic field and so may attain large velocities relative to the ions. A collision between an atom and a heavy ion may then involve a large transfer of energy from the wave to the gas.

In the case of weak waves the result is heating of the whole gas—in this way the high temperature of the solar atmosphere may be explained.<sup>15</sup>

Above sunspots, the observed violent movement of material, with velocities up to several hundred km sec<sup>-1</sup>, indicates the presence of more powerful hydromagnetic waves. Observations of thermal radio emission indicate gas temperatures above  $10^7$ °K. This intense heating may again find an explanation in terms of  $O$  and  $E$  waves, but these are now so powerful that they may give rise to other, more spectacular, effects.

When the relative velocity of the ion plasma and neutral atom gas is high enough, about 50–100 km sec<sup>-1</sup>, collisions between heavy ions and neutral atoms will excite and ionize the latter. The gas may reach a state of excitation and ionization far above that consistent with its "temperature" as measured by the purely random velocities of its particles. This situation results in the strong emission of light, ultraviolet and X rays. We have, in effect, a *glow discharge*, the electric field being an induction field due to the motion of the magnetic lines of force past the neutral atoms. The known properties of flares seem to be explicable in terms of such a mechanism.<sup>17</sup>

A flare usually is accompanied by the emission of intense radio noise and it would be reassuring to find an explanation of this emission in the same disturbance. The actual mechanism is not understood, but there is good reason to believe that emission takes place from outward traveling surfaces of discontinuity in the electron density. These have been thought to be the surfaces of electron clouds moving bodily. They could equally well be wave phenomena.

Measured velocities of two outward moving surfaces originating with the same flare have been approximately  $10^3$  and  $10^5$  km sec<sup>-1</sup>. The velocity of a weak  $S$  wave in a region of temperature  $10^7$ °K is a few hundred km sec<sup>-1</sup>, but it is likely that on moving into regions of lower density these waves would develop into shock waves and travel faster. Such waves may well account for the slow moving disturbance and, a day or so later, may cause the geomagnetic effects usually observed after a flare—a magnetic storm, ionospheric disturbance, and aurorae.

<sup>15</sup> J. H. Piddington, "Solar atmospheric heating by hydromagnetic waves," *Monthly Notices Roy. Astron. Soc.*, vol. 116, no. 3, pp. 314–323; 1956.

<sup>16</sup> In fact, the  $O$  and  $E$  waves may travel freely in any direction, because there also is an elastic repulsive force between adjacent lines of force.

<sup>17</sup> J. H. Piddington, "Solar atmospheric heating and flares," *Observatory*, vol. 76, pp. 21–23; February, 1956.

The explanation of the fast moving disturbance is more speculative. Both the shear waves ( $O$  and  $E$ ) and the plasma wave ( $P$ ) have been proposed, but in each case there are some difficulties.

In the case of a few very intense flares, yet one more type of emission has been observed—cosmic rays. Once again the origin may be explained in terms of the  $O$  and  $E$  waves associated with the flare. The requirement is merely a set of random hydromagnetic waves of sufficient strength and sufficiently short wavelength. The way in which these waves may accelerate ions to cosmic ray energies is described in Section IV.

The above discussion suggests that the physical theory of the solar atmosphere is largely a matter of electromagnetics. The same is likely to be true for the many stars which have been shown to have magnetic fields.

#### IV. INTERSTELLAR SPACE

Until a few years ago, it seemed most unlikely that any significant electromagnetic effects could occur in the cold, dead space between the stars. The visible galaxy, outlined mainly by these stars, is a disc shaped object of radius about 50,000 light years. Near the plane of the disc (the Milky Way) lie irregular clouds of gas and dust from which new stars continually are being created. The gas in these clouds (density about  $10\text{--}100$  atoms  $\text{cm}^{-3}$ ) is partially or fully ionized. Even the space between the clouds contains some gas (about  $0.1$  atom  $\text{cm}^{-3}$ ) which is at least partially ionized. Thus, the whole of interstellar space is an ion plasma and an efficient electrical conductor.

With the discovery, from optical observations, of an interstellar magnetic field, the whole galaxy was recognized as a magneto-ionic medium. It is possible then, that electromagnetic effects, in particular hydromagnetic disturbances, are significant in the space between stars. The criterion is that magnetic energy density  $H^2/8\pi$  is comparable with the kinetic energy density of random motion of the gas clouds. The magnetic field strength  $H$  is about  $5 \times 10^{-6}$  Gauss, the average ion density and random velocity about  $1 \text{ cm}^{-3}$  and  $10 \text{ km sec}^{-1}$  in the spiral arms, so that the ratio of magnetic to kinetic energy is about unity. Hydromagnetic waves, therefore, are likely to be highly significant.

Further interest was added when it recently was discovered that the galaxy visible in radio emission extends far beyond that visible in optical emission.<sup>18</sup> It is in the form of a sphere of about the same radius as the visible disk. The gas density in the additional part is very low and its significant features are a magnetic field and cosmic rays. The latter may be regarded as a very tenuous gas at an enormous temperature ( $10^{12}$ °K or more); its expansion into outer space is prevented by the magnetic field. The radio emission from this medium

is by the "synchrotron" process, electrons, and perhaps also positrons spiralling in the magnetic field and emitting radio waves because of this acceleration.

New problems, mainly electromagnetic in nature, are posed by these discoveries. Other long outstanding problems, such as the origin of cosmic rays, may find simple solutions in terms of electromagnetic effects.

The first problem, of course, is the origin of the magnetic field itself. On the earth we think of fields growing when an emf is applied to a conductor and causes a current to flow. On a cosmic scale the enormous self-inductance of the circuits concerned seems to exclude this simple mechanism.<sup>19</sup> It is more probable that the conducting material (ionized gas), in which an initial weak magnetic field is embedded, moves in such a way as to stretch the magnetic lines of force and so increases magnetic energy at the expense of kinetic energy.<sup>1</sup> The gas motion concerned at first was thought to be its turbulence; this would create a tangled magnetic field. However, the galactic field appears to be rather ordered in form as though resulting from ordered motion. The differential rotation of the galaxy might be effective, if the original weak field had a radial component. The lines of force would then be like elastic strings connecting two concentric, differentially rotating wheels. They would be continually stretched and rolled up between the wheels. This "magnetic spinning wheel" mechanism may also operate in the Crab nebula, as mentioned in Section V.

The galactic magnetic field is of particular significance in connection with cosmic rays. It acts as a container for these energetic ions which spiral around the magnetic lines of force and remain so trapped for millions of years. It also may be responsible for creating the cosmic rays by a mechanism first suggested by Fermi.<sup>20</sup> In its crudest form the theory considers the galactic magnetic field to consist of individual bundles of magnetic lines of force, each associated with a gas cloud. These clouds have random velocities of about  $10 \text{ km sec}^{-1}$  and may be regarded as enormous molecules of a gas mixture. Their masses are also enormous, equal to that of the sun or greater. Other molecules in this gas mixture are the heavy ions which are to become cosmic rays. These ions collide elastically with isolated clouds of magnetic field and on an average they gain energy. It is well known that in a gas mixture there is a tendency to equipartition of energy between the component particles. Similarly, in the galactic mixture the ions are accelerated until after a million years or so some of them attain cosmic ray energies.

In its simplest form this theory has proved quantitatively unsatisfactory. In a modified version the individual blobs of magnetic field are replaced by hydromagnetic waves and acceleration is by a statistical beta-

<sup>18</sup> For a summary of evidence, see L. Spitzer, Jr., "On a possible interstellar galactic corona," *Astrophys. J.*, vol. 124, pp. 20-34; July, 1956.

<sup>19</sup> The time constants involved exceed the age of the galaxy.

<sup>20</sup> E. Fermi, "On the origin of cosmic radiation," *Phys. Rev.*, vol. 75, pp. 1169-1174; April, 1949.

tron process,<sup>21</sup> due to fluctuations in intensity of the field, as well as the simple "collision" mechanism due to changes in its distribution. Whether or not the observed cosmic ray intensity can be accounted for in these terms depends on the intensity of the hydromagnetic waves which may be maintained from available energy sources. The intensity, in turn, depends on the rate of absorption of the waves.

In a recent investigation<sup>22</sup> it was found that, just as in the solar atmosphere, neutral atoms are a critical factor in controlling the damping of  $O$  and  $E$  galactic waves. In regions where the gas is fully ionized, damping due to ordinary viscosity and to the finite electrical conductivity is small and the Fermi acceleration process is likely to be efficient. However, when neutral atoms are present, the picture changes completely. Even when only the helium present (perhaps 10 per cent of the whole gas) is neutral, the absorption rate<sup>23</sup> is increased by a factor of more than  $10^5$ . The actual state of ionization is not known, but it is likely that neutral atoms are widely enough spread to cause considerable damping. If so, then Fermi's theory of acceleration, at least in its application to the galaxy as a whole, may fail. A possible alternative is mentioned in the following section.

Another galactic electromagnetic problem is posed by the disruptive effect of the magnetic field. We are accustomed to think of a magnetic field, for example that of a steel magnet, as dynamically stable. The stability is due to the cohesive forces in the steel, and apart from these the whole field and the magnet would fly to pieces. When the field is due to currents in an ionized gas cloud, the latter tends to be disrupted and this presumably is so for the galactic magnetic field. Assuming a balance to be maintained by gravitational attraction, the strength of the magnetic field may be estimated. The value so found<sup>24</sup> agrees with that estimated by other methods.

A somewhat similar problem is met in the gravitational contraction of galactic gas to form stars. This is strongly opposed by the magnetic field which itself is compressed and strengthened. An important factor may be that, as mentioned above, the neutral atoms can move past the magnetic lines of force and so contract to form the star.<sup>25</sup> The magnetic field and ion plasma are left in the original expanded state.

These few examples may serve to show that the physical theory of the space between the stars is largely a matter of electrodynamics.

<sup>21</sup> L. Davis, Jr., "Modified Fermi mechanism for the acceleration of cosmic rays," *Phys. Rev.*, vol. 101, pp. 351-358; January, 1956.

<sup>22</sup> J. H. Piddington, "Galactic turbulence and the origins of cosmic rays and the galactic magnetic field," *Aust. J. Phys.*, in press.

<sup>23</sup> Calculated for the "intercloud" region which comprises most of the volume concerned and in which the average gas density is about  $0.1 \text{ atom cm}^{-3}$ . The calculation refers to waves about one light year or less in length, thought to be effective as accelerators.

<sup>24</sup> S. Chandrasekhar and E. Fermi, "Problems of gravitational stability in the presence of a magnetic field," *Astrophys. J.*, vol. 118, pp. 116-141; July, 1953.

<sup>25</sup> L. Mestel and L. Spitzer, Jr., "Star formation in magnetic dust clouds," *Monthly Notices Roy. Astron. Soc.*, vol. 116, no. 5, pp. 503-514; 1956.

## V. THE CRAB NEBULA

The Crab nebula visually is a rather insignificant object (NGC 1952), because of its distance (about 3000 light years). However, it is the result of a vast supernova explosion, which occurred 900 years ago, and is an expanding shell of gas, already about 5 light years in diameter. It also is a powerful radio emitter (IAU 05N2A) of unusual spectrum and the whole interior of the shell glows with a peculiar light. It is found that all the observational data may be interpreted as electromagnetic effects and that these are of particular interest.

The curious optical and radio emission spectra defied explanation until it was suggested by Shklovsky<sup>26</sup> that in both cases emission was due to electrons spiralling in a magnetic field. Thus, the optical and radio spectra are part of a common spectrum due to a single mechanism, the synchrotron effect which also explains the main galactic radio emission. The truth of this theory was established when the optical emission was found partially plane polarized as predicted by the theory.

The next step was to reconstruct the physical situation in the nebula necessary to account for the emission. A magnetic field of strength about  $10^{-3}$  Gauss and extent about 3 light years is required, together with a cosmic ray gas with pressure about  $10^5$  times or more than that of average interstellar space.<sup>27</sup> The general shape of this field and its relation to the glowing core of the nebula may be seen in Fig. 1. Each of the short lines

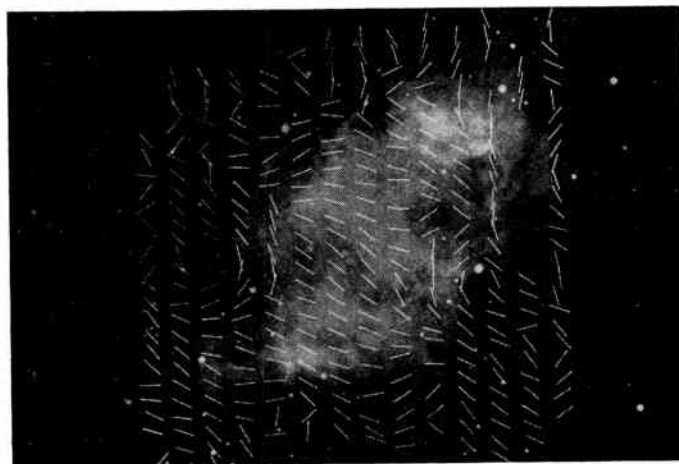


Fig. 1—The magnetic field of the Crab nebula (the radio source IAU 05N2A). The photograph of the nebula was taken by Baade<sup>28</sup> in continuous emission and shows the central region without the irregular outer shell. The directions of the magnetic field, shown by the white lines, are inferred from polarization data published by Oort.<sup>29</sup>

<sup>26</sup> I. S. Shklovsky, "The nature of the luminescence of the crab-shaped nebula," *Dok. Akad. Nauk, U.S.S.R.*, vol. 90, no. 6, pp. 983-986; 1953.

<sup>27</sup> J. H. Oort and T. Walraven, "Polarization and composition of the Crab nebula," *Bull. Astron. Inst. Neth.*, vol. 12, pp. 285-308; May, 1956.

<sup>28</sup> W. Baade, "The polarization of the Crab nebula on plates taken with the 200-inch telescope," *Bull. Astron. Inst. Neth.*, vol. 12, p. 312; May, 1956.

<sup>29</sup> J. H. Oort, "The Crab nebula," *Sci. Amer.*, vol. 196, pp. 52-60; March, 1957.

shows the average direction of the field in a small area. The outstanding feature, apart from the vast extent of this field, is its remarkable uniformity. As seen below, this poses an astrophysical problem of fundamental and outstanding importance.

The outward pressure of the magnetic field and cosmic ray gas (trapped in the field almost like gas in a balloon) render the nebula a virtually exploding bomb. It also is found that the cosmic rays radiating by the synchrotron process will dissipate their energy in a period of about 200 years or less. Since the explosion took place some 900 years ago, a source of energy and an accelerating mechanism must have been available until recently and presumably are still available. The necessary power supply has the incredible value of about  $10^{28}$  kw, more than  $10^4$  times the total power (of all forms) radiated by the sun.

A more recent investigation<sup>30</sup> of electromagnetic effects in the Crab nebula includes the question of the origin of the magnetic field. One possibility is that it was contained in the star before the explosion. However, it is found that the necessary pressure and energy of the magnetic field, when reduced to the proportions of a star, are impossibly high. Other possible origins, such as creation by turbulent motion of the shell also are excluded.

The conclusion is that most of the field was created after the explosion and perhaps is still being created at an average rate corresponding to an energy flow of more than  $10^4$  times the total output of solar energy.<sup>31</sup> Such a flow would seem to require nuclear reactions which must be continuing in or near the central star. There must be some mechanism for converting nuclear energy more or less directly to magnetic energy. An important clue is that the resulting magnetic field has a remarkably ordered form as can be seen from Fig. 1.

This conclusion may point to the origin of magnetic fields other than that in the Crab nebula, perhaps to the main galactic field; if so, it may be regarded as the starting point of a major part of radio astronomy.

In speculating on possible mechanisms, the magnetic spinning wheel suggests itself. The central star, having an initial poloidal field of perhaps a few thousand Gauss, spins and so creates a toroidal field between the star and the heavy nonspinning shell. Such motion would soon be arrested under the influence of electromagnetic forces if these were not opposed. However, if nuclear reactions are taking place in the central star some products in the form of ions may be ejected and must travel out along the magnetic lines of force. The sequence of events is then as follows. The ions leave the central con-

figuration which is spun by their rocket propulsion effect. The ions reach a kink in the magnetic field, where they lose velocity and energy which is used to stretch the field and increase magnetic energy. The strong field "spun" in this way is blown out to fill the nebula, becoming weaker in the process.

An even more fundamental mechanism for creating magnetic field suggests itself as worth investigating; it depends on the recent reports of nonconservation of parity.<sup>32</sup> It would be expected that radioactive atoms lined up in a magnetic field would, on exploding, emit as many particles of a particular type in one direction as in the opposite direction. This principle of parity appears to fail on occasions and one might anticipate as a possible result a net electric current and perhaps a stronger magnetic field.

Whatever the origin of the magnetic field of the Crab nebula, its large strength and extent suggests that at least a good part of the galactic magnetic field could originate within supernova shells, of which perhaps  $10^7$  have been formed in the history of the galaxy. After sufficiently expanding, these fields would merge to form a general field.

It has been suggested<sup>33</sup> that most (galactic) cosmic rays are created at the time of nova and supernova explosions. One difficulty, however, is that the (previously presumed) steadily expanding and diminishing magnetic field of the nebula would decelerate the cosmic rays by a sort of inverse Fermi process. The results of the Crab nebula investigation suggest that this theory may now require modification—if the magnetic field is created after the explosion and fed out from the central region, then it may create cosmic rays in a continuous Fermi process *after* the explosion. The interpretation of the radio observations<sup>27</sup> suggests that cosmic rays are still being created and the later investigation<sup>30</sup> provides a mechanism and also overcomes the previous difficulty of deceleration.

Another "radio star" which emits synchrotron radiation and in which a strong magnetic field and cosmic ray electrons must coexist<sup>34</sup> is the Virgo source (IAU 12N1A). Whereas the magnetic field strength appears to be much the same as in the Crab nebula, its volume is perhaps  $10^9$  times greater. This source, lying in an external galaxy, provides an unbelievable concentration of magnetic and cosmic ray energy and further stresses the importance of understanding the origin of this energy—perhaps the most fundamental theoretical problem yet met in radio astronomy.

While the detailed processes involved are not understood, the broad picture seems to be a hydromagnetic

<sup>30</sup> J. H. Piddington, "The Crab nebula and the origin of interstellar magnetic fields," *Aust. J. Phys.*, in press.

<sup>31</sup> This is of the same order as that required to replenish the cosmic rays mentioned above. The problem previously posed, footnote 27 (the origin of the cosmic rays), is replaced by another (the origin of the field). Once the field is accounted for the cosmic rays can be readily explained in terms of the Fermi process and the growing field.

<sup>32</sup> A brief review is given by B. Bleaney, "Non-conservation of parity," *Nature (London)*, vol. 179, pp. 1101-1102; June, 1957.

<sup>33</sup> V. L. Ginzburg, S. B. Pikelner, and I. S. Shklovsky, "Acceleration of particles in the envelopes of novae and supernovae," *Akad. Nauk. U.S.S.R., Astron. J.*, vol. 32, no. 6, pp. 503-513; 1955.

<sup>34</sup> G. R. Burbidge, "On synchrotron radiation from Messier 87," *Astrophys. J.*, vol. 124, pp. 416-429; September, 1956.

process of energy transfer: large numbers of ions transmute their kinetic energy to magnetic energy to form a large-scale "ordered" field. In so doing (and perhaps subsequently) the direction of energy flow is reversed for a few favored ions (presumably those already possessing an unusually large amount of kinetic energy) which are supplied with energy and become cosmic rays.

## VI. INTERPLANETARY SPACE

It is surprising that, compared with the other regions discussed above, so little is known about the interplanetary medium. Until recently, it was thought that, apart from occasional streams of solar gas which caused magnetic storms, the interplanetary medium was substantially a vacuum. It now seems that even as far away from the sun as the earth's orbit, the gas particle density is about  $500 \text{ cm}^{-3}$ , increasing towards the sun. The gas is mainly ionized hydrogen and its temperature may be  $10^5$ – $10^6$ °K.<sup>35</sup> From the point of view of a solar physicist we are situated *in* the solar corona. From the point of view of an ionospheric physicist the extreme outer ionosphere is at a temperature of  $10^5$ °K or more and its plasma or resonant frequency is about  $200 \text{ kc sec}^{-1}$ .

While the above results seem reasonably well established, there are other important factors about which we know little or nothing. Most important is the magnetic field or interplanetary space. Its average interstellar value is perhaps  $5 \times 10^{-6}$  Gauss, corresponding to a pressure of about  $10^{-12}$  dyne  $\text{cm}^{-2}$ . The pressure of the

interplanetary gas near the earth, assuming a temperature of  $10^6$ °K is about  $10^{-8}$  dyne  $\text{cm}^{-2}$ . If, as seems likely, this gas has an average outward drift from the sun, it will push back the magnetic field leaving the earth in a magnetic vacuum. Such a result could have important effects on cosmic ray intensities and their variations.

On the other hand, it has been suggested that when puffs of gas are emitted from the sun's atmosphere, these may contain their own magnetic fields. Such fields conceivably could be of substantial intensity (compared with the interstellar field), the limitation being imposed by equality of gas and magnetic pressures. The gas pressure is perhaps  $10^{-8}$  dyne  $\text{cm}^{-2}$ , corresponding to a magnetic field of about  $5 \times 10^{-4}$  Gauss near the earth. Stronger fields would be able to expand more or less freely and, having no effective retarding force, would soon dissipate. The strongest field possible, assuming a gas temperature of  $10^6$ °K, is about  $10^{-3}$  Gauss. These magnetic clouds also would have marked effects on cosmic ray intensities at the earth and they have been invoked to explain certain observed variations.

For many years, the Chapman-Ferraro theory of magnetic storms has served a useful purpose in indicating some of the main effects leading to a storm. In view of the new ideas about the interplanetary medium it now seems probable that the theory will need considerable revision. Instead of a jet of solar gas sweeping past the earth, the phenomenon may be more like a wave in the medium: a shock hydrodynamic wave if the magnetic field is weak enough to neglect ( $\ll 10^{-3}$  Gauss), otherwise a shock hydromagnetic wave. In any case, the problem becomes one of hydromagnetics when the wave encounters the earth's magnetic field.

<sup>35</sup> S. Chapman, "Notes on the solar corona and the terrestrial ionosphere," *Smithsonian Contrib. Astrophys.*, vol. 2, no. 1, pp. 1–12; February, 1957.



# Correspondence

## The Effects on Radio Astronomical Observations Due to Longitudinal Propagation in the Presence of Field-Aligned Ionization\*

Clouds of ionization of electron density higher than that of their surroundings have been demonstrated by means of back-scatter experiments to exist frequently at ionospheric heights.<sup>1</sup> From the echo statistics observed in these radar experiments, electron densities in the clouds are estimated to lie in the range between  $10^{11}$  and  $10^{14}$  electrons/meter<sup>3</sup>. These electron concentrations also have been shown to possess unique orientations which appear to be in alignment with the earth's magnetic field at the region of back-scatter.

### TOTAL REFLECTION FROM ELECTRON CLOUDS

It can be shown that discontinuities in density of the order of magnitude mentioned above are sufficient to cause total reflection of uhf signals if the energy is incident on the field-aligned surfaces at modest grazing angles. The relationship given by:

$$\sin g_m = \frac{8.97}{f} \sqrt{N} \quad (1)$$

where  $g_m$  is the maximum grazing angle for total reflection,  $f$  is the observing frequency, and  $N$  is the volume. Electron density provides the criterion for total reflection at an ionized boundary.<sup>2</sup> Note that  $g$  is here defined as the angle between the radio ray and the discontinuity. Table I illustrates the magnitude of these critical grazing angles for several frequencies.

A great deal of experimental research by radio astronomers is devoted to vhf and uhf tracking of celestial bodies. The celestial paths of the moon and radio point sources, with respect to certain observers on the earth, is such as to permit grazing and/or near-grazing angles (of the same order of magnitude as presented in Table I) between radiation from source to observer and the magnetic fields in the ionosphere. From the preceding, it may be deduced that when these tracking observations are coincident with the presence of electron density discontinuities aligned with the field, certain

TABLE I

$\frac{N \text{ electrons/m}^3}{f_{\text{mc}}}$	Frequency—meps			
	100	200	400	800
$10^{11}$	1.60°	0.80°	0.40°	0.20°
$10^{12}$	5.15°	2.57°	1.29°	0.64°
$10^{13}$	16.47°	8.16°	4.07°	2.03°
$10^{14}$	63.77°	26.65°	12.96°	6.44°

regions beyond the ionosphere will, because of energy redirection resulting from the reflection process, either be obscured or non-uniformly illuminated.

### THE REFLECTION GEOMETRY

It will be assumed throughout this note that the discontinuities can be represented by an ensemble of long (with respect to a wavelength), cylindrical, field-aligned columns of electron concentration.

Consideration of the geometry of the earth's magnetic field<sup>3</sup> will show that an observer in the northern hemisphere is required to look in azimuthal directions toward the magnetic South Pole and at elevation angles corresponding approximately to the magnetic inclination at the observing location, in order to view these columns at grazing or near-grazing incidence.

It may be shown that the relationship existing among these angles can be approximated by

$$g^2 = e_1^2 + I_1^2 - 2e_1 I_1 \cos(\theta + D) \quad (2)$$

where

- $g$  = the grazing angle,
- $e_1$  = complement of the elevation angle,
- $I_1$  = complement of the magnetic inclination,
- $D$  = magnetic declination,
- $\theta$  = azimuth angle.

For the purposes of illustration, Figs. 1 and 2 have been constructed for two active radio astronomy observatory locations, namely Ottawa, Canada, and Fairbanks, Alaska. The figures are contours of constant grazing angle,  $g$ , on a polar coordinate plot. The modulus is scaled to the complement of the elevation angle,  $e_1$ , and the argument to the azimuth angle,  $\theta$ . To a first approximation the region of the celestial sphere, affected by total reflection from the columns, lies within the contour defined by a value of  $g$  corresponding in (1) to the assumed value of electron density.

Fig. 1 also contains two representative examples of moon transits<sup>4</sup> on the arbitrarily chosen dates of March 8 and 13, 1957. Fig. 2 contains the orbits of the point source radio stars in Cassiopeia and Cygnus.

### EFFECT ON EXTRATERRESTRIAL RADIATION PATTERNS

The major effects on the extraterrestrial radiation patterns are such as to produce amplitude scintillations and fades at the

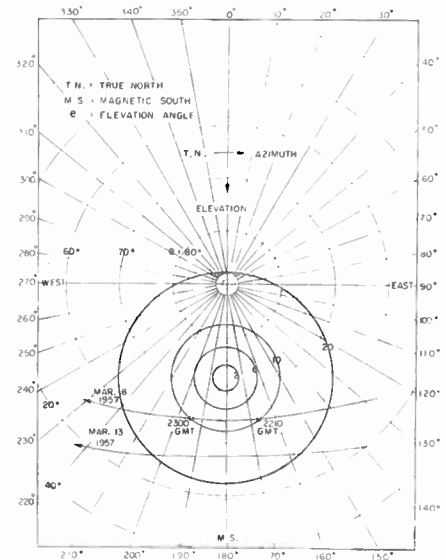


Fig. 1—Ottawa, Ont., Canada.

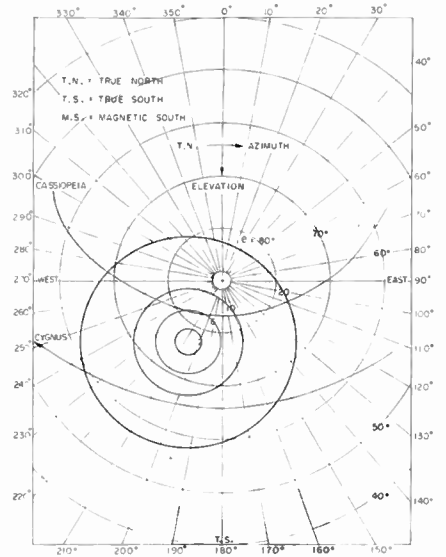


Fig. 2—Fairbanks, Alaska.

ground-based antenna. The manner in which these anomalies arise can best be illustrated by reference to a ray-tracing diagram, e.g., Fig. 3. The rays pictured in this diagram lie in the plane containing the antenna and the magnetic axis of the earth. It can be seen that the result of uniformly illuminating a large area on either side of the magnetic zenith is to produce a region in this plane enclosed by the parallel line pairs,  $A$  and  $B$ , and  $C$  and  $D$ . It is to be noted that rays  $A$  and  $B$  pass through widely separated portions of the ionosphere. Hence, perturbations on these paths due to ionospheric disturbances will be uncorrelated, giving rise to frequent scintillations. Also, the broad region of the ionosphere which produces parallel rays acts like a very large antenna

\* Received by the IRE, October 24, 1957.  
<sup>1</sup> R. L. Leadabrand, "Radio Echoes from Auroral Ionization Detected at Relatively Low Geomagnetic Latitudes," Stanford Univ., Stanford, Calif., Tech. Rep. No. 98; December 9, 1955.  
<sup>2</sup> A. M. Peterson, O. G. Villard, R. L. Leadabrand and P. B. Gallagher, "Regularly Observable Aspect-Sensitive Radio Reflections from Ionization Aligned with the Earth's Magnetic Field within the Ionospheric Layers at Middle Latitudes," Stanford Univ., Stanford, Calif., Tech. Rep. No. 93; September 30, 1955.  
<sup>3</sup> S. Chapman, "The geometry of radio echoes from aurorae," *J. Atmos. Terr. Phys.*, vol. 3, pp. 1-29; March, 1952.  
<sup>4</sup> H. G. Booker, "A theory of scattering by monisotropic irregularities with application to radar reflections from aurora," *J. Atmos. Terr. Phys.*, vol. 8, pp. 204-221; August, 1956.  
<sup>5</sup> M. Spencer, "The shape of irregularities in the upper ionosphere," *Proc. Phys. Soc. B*, vol. 68, p. 493; August, 1955.  
<sup>6</sup> "Ionospheric Radio Propagation," Natl. Bureau of Standards, Washington, D. C. Circular 462; June 25, 1948.

<sup>3</sup> Chapman and Bartels, "Geomagnetism," Oxford Univ. Press, London, vols. 1 and 2; 1940.  
<sup>4</sup> "The Air Almanac," Naut. Almanac Off., U.S. Naval Observatory, published quarterly.

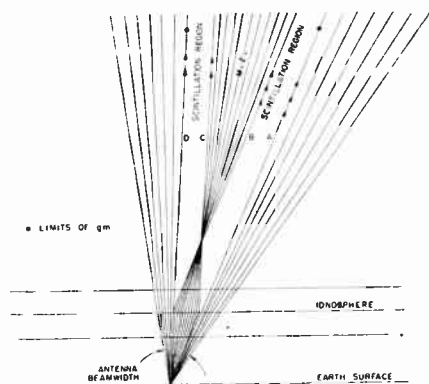


Fig. 3—Ray tracing for the wide-beam case.

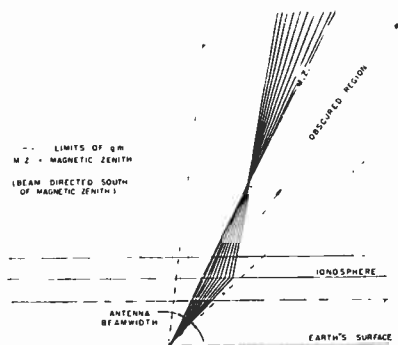


Fig. 4—Ray tracing for the narrow-beam case.

aperture with an extremely narrow beam-interference pattern. The amplitude of signal returns resulting from such patterns are very sensitive to angular shifts between antenna and source. Thus the relative motions of the earth and stars, for example, may be expected to produce scintillating signals.

When the antenna system employed possesses sufficient directivity to illuminate principally a region on one side of the magnetic zenith, the parallel ray structure is not produced. Instead a relatively large "hole" is formed in which a celestial body would be obscured. This latter condition is illustrated in Fig. 4.

An interesting by-product of the analysis shows that at times of obscuration, the narrow-beam antenna could be redirected to other elevations (on the opposite side of the magnetic zenith), thereby taking advantage of column reflections to fill in the obscured region.

#### POSSIBLE EXPERIMENTAL VERIFICATION

The observatories of the Defence Research Board and Geophysical Institute at Ottawa and Fairbanks, respectively, were chosen as examples for this paper since it appears that certain of their recent radio astronomical observations may be associated with the reflection effects described herein, although it is not anticipated that this approximate model and analysis will precisely fit the available data. The results, however, do appear potentially to be very powerful and it is expected that these and other active researchers will, very shortly, publish results which can be used to test further the predictions made on the basis of the analysis described. Should there be a strong correlation

between theory and experiment, a new and sensitive tool will become available for estimating electron densities in the ionosphere and the magnitude of disturbances of the magnetic field at ionospheric heights.

S. RUSH  
AND L. COLIN  
Rome Air Dev. Center  
Griffiss Air Force Base  
Rome, N.Y.

### Launching IGY Satellites\*

Having investigated possibilities in Australia and New Zealand,<sup>1</sup> the writer reports an observation concerning measurements, particularly of the earth's magnetic field, expected from rocket-launched satellites moving in geo-eccentric orbits reaching out eventually to several earth radii in the first instances. In harnessing the natural centrifugal acceleration of the earth at the surface launching point, the rocketed ascent of satellites therefrom, and that of the respective initial orbit, are described nominally on the plane of the great circle taken as produced out through the geographical bearing of the selected launching way.

The attainable ordinal number and value of the prescribed angle of inclination,  $i$ , of the plane of the satellite orbit to that of the plane of the geographical equator, determine the scientific desirability of any selected existing, conjectured, or feasible launching point and way. The Cape Canaveral point (28°28'N lat., 80°23'W long.) offers a value of  $i$  about  $35^\circ \pm 2^\circ$ . Any Australian point at the environs of Woomera would offer no greater value of  $i$  and any remotely envisioned ascent therefrom of satellite space rockets (of advanced design by the writer and/or with the Martin Company) would be retarded by natural centrifugal and other geodynamic influences. The conjectured point at the northerly environs of Murmansk, Russia, with a geographical bearing about  $34^\circ$  east of true north, offers a value of  $i$  about  $78^\circ \pm 1^\circ$ , but natural and complex density distribution, generated by the rotation of the nonuniformly shaped earth, at high northern latitudes are certain to produce incommodious ascent paths.

A small area of ground, less than 1 mile square, above high-tide sea level at the environs of Port Pegasus, Stewart Island, New Zealand (approximate lat. 47°11'S, long. 167°40'E), is an accessible and universally feasible launching way and point. Numerous values of  $i$  to  $90^\circ$  are offered for orbits of satellites (especially those carrying proton precessional magnetometers, radiation balance sensing arms, infrared cloud cover optical scanners, and other important instrumentation) required to pass through ionospheric layers of the auroral zones and over the geomagnetic poles and, where so prescribed or resulting from insufficiently

well-aligned orbit entry, out beyond the farthest presumed limit of the ectosphere. Natural placing of islands to the northeast, east and southeast, and south about the meridian, surrounding the land mass of Antarctica, indicate that ascent path perturbations ought to be relatively negligible. These topographical features could be used for the purpose of setting up radio and optical tracking, acquisition, and tele-metered data-recording stations. A commanding position on Mt. Allen (Stewart Island) is available for setting up the necessary telecontrol launching blockhouse. Facilities for ground installations could be set up close by. Given early sponsorship or an appointment to proceed, it is within the experience and available knowledge of the writer that scientific and technical arrangement to implement the Port Pegasus site—between the United States and New Zealand in the first instance at any rate—could be finalized before April, 1958. Attention is invited<sup>2</sup> from all nations participating in the IGY or subscribing to the United Nations.

WILLIAM H. FINLAY  
Canberra  
A.C.T.  
Australia

\* F. L. Whipple and J. A. Hynek, "A research program based on the optical tracking of artificial earth satellites," Proc. IRE, vol. 44, pp. 760-764; June, 1956.

### Mobile Single-Sideband Equipment\*

The viewpoints<sup>1</sup> on this problem of Richardson and myself reflect different approaches; in my case an elimination of continuous carrier with resultant greater power output for a given final amplifier, and hence somewhat improved range.

Considerable experience with essential service mobile systems makes simplicity of control obviously very desirable, and if system stability can be improved to  $\pm 200$  cycles, provision of a speech clarifier is hardly necessary, except that in conditions of fairly heavy noise or interference, adjustment to give speech a higher-pitched tone generally does increase intelligibility. In its present state of development, the Motorola equipment would be in a difficult situation with the possibility of other transmissions on adjacent frequencies in the same channel, as in such chaotic conditions the receiver might lock on an undesired signal. Conversely, without radiated carriers, if system stability were sufficiently improved, an SSB transmission even only 2 kc from the reference frequency to which the receiver is tuned becomes unintelligible and merely a noisy background against which a signal of equal strength is tolerably readable.

R. E. MORROW  
Worth Communications Services  
Birmingham, England

\* Received by the IRE, October 8, 1957.  
<sup>1</sup> W. H. Finlay, "Satellite observatories in nearby space," *Aust. J. Sci.*, vol. 19, p. 26; January, 1957.

\* Received by the IRE, October 7, 1957.  
<sup>1</sup> R. E. Morrow and R. A. Richardson, Proc IRE, vol. 45, pp. 1736-1737; December, 1957.

## Space-Charge Waves Along Magnetically-Focused Electron Beams\*

In a recent publication,<sup>1</sup> Labus has repeated his earlier criticism<sup>2</sup> of the analytical procedure usually employed in those problems of small-signal, slow-wave propagation along electron beams, in which small transverse ac displacements can take place. In its stead, he proposes a method which appears to be novel in concept, and certainly leads to results which differ materially from those found earlier by conventional techniques.<sup>3,4</sup> Although the questions at issue are procedural, and indeed go back to Hahn's first paper on the subject,<sup>5</sup> it is simpler to confine the discussion to the framework of one of the problems considered by Labus, that of axial-symmetric waves along a smooth cylindrical beam in Brillouin flow.<sup>3</sup>

Labus' procedure differs from that of Rigrod and Lewis<sup>3</sup> in two respects:

- 1) He takes account of the ac radial charge displacements by introducing increments of ac space-charge density throughout the volume of the beam, rather than on its surface.
- 2) He retains, in the electron dynamics equations, contributions due to the ac magnetic field  $B$  and the azimuthal component  $E_\phi$  of the ac electric field.

The second of these items is chiefly of theoretical interest and will be discussed later. The large discrepancies between the results of Labus' computations and those of Rigrod and Lewis<sup>3</sup> and of Brewer<sup>4</sup> are due entirely to the first item in dispute, which accordingly will be examined in some detail.

In the work of Rigrod and Lewis,<sup>3</sup> the radial charge displacements were treated by assigning an unknown ac space-charge density  $\rho$  to the interior of the beam, and replacing the boundary disturbance by an equivalent surface charge density. The perturbed boundary (associated with any one traveling wave) will have a profile given by the radial displacement of the outermost electrons:

$$(\tilde{\Delta r})_b \exp j(\omega t - \gamma z), \quad (1)$$

where  $r=b$  is the undisturbed boundary,  $\omega$  is the radian frequency, and  $\gamma$  the slow-wave propagation constant.

Suppose, in Fig. 1, that the solid curved line represents this boundary profile at any instant. Then the total charge in the beam equals that contained within the unperturbed boundary, plus that represented by the shaded areas:

$$Q_t = \int_0^{b+(\tilde{\Delta r})_b} (\rho_0 + \rho) 2\pi r dr \\ \cong \int_0^b (\rho_0 + \rho) 2\pi r dr + 2\pi b \rho_0 (\tilde{\Delta r})_b. \quad (2)$$

\* Received by the IRE, July 15, 1957.

<sup>1</sup> J. Labus, "Space charge waves along magnetically focused electron beams," Proc. IRE, vol. 45, p. 854-861; June, 1957.

<sup>2</sup> J. Labus and K. Poeschl, "Raumladungswellen in ionenfreien elektronenstrahlen," Arch. elek. Übertragung, vol. 9, pp. 39-46; January, 1955.

<sup>3</sup> W. W. Rigrod and J. A. Lewis, "Wave propagation along a magnetically focused cylindrical electron beam," Bell Sys. Tech. J., vol. 33, pp. 399-416; March, 1954.

<sup>4</sup> G. R. Brewer, "Some effects of magnetic field strength on space-charge-wave propagation," Proc. IRE, vol. 44, pp. 896-903; July, 1956.

<sup>5</sup> W. C. Hahn, "Small signal theory of velocity modulated electron beams," GE Rev., vol. 42, pp. 258-270; June, 1939.

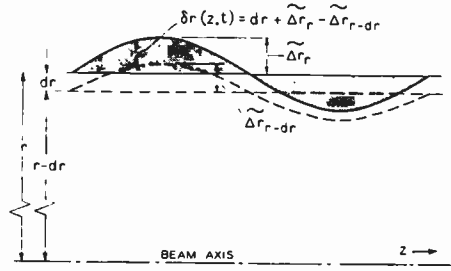


Fig. 1

The second term can be regarded as a surface charge, in which  $\rho$  is dropped when ac quantities are linearized. To this same approximation, the surface ripple has no measurable thickness and can only be equivalent to a sheet of charge or current.

This method of summation does not neglect the effect of the radial displacements within the beam, and does not assume that the surface charge is made up solely of the outermost electrons, as Labus suggests. The ac surface charge is produced by the unbalanced radial motions of all of the particles shown in the shaded areas of Fig. 1, which constitute a time-varying excess or deficiency of charge relative to that contained within the undisturbed boundary,  $r=b$ . The radial displacements within this boundary ( $r < b$ ) are related through the radial velocities at each point,  $v_r$ , and the charge-continuity equation, to the volume space-charge density  $\rho$ ; and, in addition, determine the radial current density within the beam.

In a small-signal approximation, the ac surface charge together with the dc velocity constitute an ac surface current density, with components

$$G_s = \rho_0 v_0 (\tilde{\Delta r})_b \quad (3)$$

$$G_\phi = \rho_0 v_\phi (\tilde{\Delta r})_b. \quad (4)$$

The wave admittance at the beam boundary, which must be equated to that of the circuit, can be written (using mks units) in the form

$$Y_e = \frac{H_\phi + \Delta H_\phi}{E_s} = \frac{H_\phi + G_s}{E_s}. \quad (5)$$

In this formulation, therefore, the surface current density (3) is equal to an increment  $\Delta H_\phi$  over the value of  $H_\phi$  computed as though the surface were undisturbed.

Labus prefers to compute  $\Delta H_\phi$  by adding up the equivalent ac charges due to radial displacements everywhere in the beam, in the form of increments to the volume space-charge density,  $\Delta\rho$ . He divides the beam into hollow-beam elements of infinitesimal thickness  $\delta r$ , bounded by surfaces whose profiles are the instantaneous radial displacements at the inner and outer radii of these elements, respectively. In Fig. 1, the solid curve  $(\tilde{\Delta r})_r$  is now understood to show the perturbed locus of particles originally at some radius  $r$  inside of the beam  $r < b$ . The dashed sinusoid is the locus  $(\tilde{\Delta r})_{r-dr}$  of particles whose undisturbed location would be  $(r-dr)$ .

Labus then evaluates the total charge in the curved hollow-beam elements, per unit length of beam, as follows:

$$dQ_t = 2\pi(r + \tilde{\Delta r})\delta r(\rho_0 + \rho) \\ = 2\pi r \delta r(\rho_0 + \rho + \Delta\rho). \quad (6)$$

This charge is equated to that of a similar hollow-beam element in a smooth cylindrical beam, to which the fictitious space-charge density increment  $\Delta\rho$  has been added to replace the charge produced by the radial motion:

$$(\tilde{\Delta r})\delta r(\rho_0 + \rho) \cong (\Delta r)\delta r \cdot \rho_0 = (r \cdot \tilde{\Delta\rho})\delta r \quad (7)$$

$$\Delta\rho = \rho_0 \frac{(\tilde{\Delta r})}{r}. \quad (8)$$

The mistake made in (6)-(8) is that Labus has assumed the two displacement amplitudes  $(\tilde{\Delta r})_r$  and  $(\tilde{\Delta r})_{r-dr}$  to be equal, separated by a constant distance  $\delta r$ , which is equal to the infinitesimal separation between the undisturbed surfaces at  $r$  and  $r-dr$ . This displacement, however, is some function of radius and becomes zero at the beam axis.

For the sake of clarity, the charge  $dQ_t$  of (6) will be recalculated properly in two different ways:

1) Following Labus,  $dQ_t$  equals the volume space-charge density times the volume between the surfaces  $(\tilde{\Delta r})_r$  and  $(\tilde{\Delta r})_{r-dr}$ :

$$dQ_t = (\rho_0 + \rho)\pi[(r + \tilde{\Delta r})^2 - (r - dr + \tilde{\Delta r}_{r-dr})^2] \\ = 2\pi(\rho_0 + \rho) \\ \cdot [r(\tilde{\Delta r}_r - \tilde{\Delta r}_{r-dr}) + \tilde{\Delta r}_{r-dr} dr + r dr]. \quad (9)$$

As  $\tilde{\Delta r}$  is a function of  $r$ ,

$$\tilde{\Delta r}_r - \tilde{\Delta r}_{r-dr} = \frac{\partial}{\partial r}(\tilde{\Delta r}) dr \quad (11)$$

$$dQ_t = 2\pi(\rho_0 + \rho) dr \left[ r \frac{\partial}{\partial r}(\tilde{\Delta r}) + \tilde{\Delta r} + r \right] \\ = 2\pi r dr(\rho_0 + \rho) \left[ 1 + \frac{1}{r} \frac{\partial}{\partial r}(r\tilde{\Delta r}) \right]. \quad (12)$$

Here second-order terms in  $(\tilde{\Delta r})$  as well as in the infinitesimal  $dr$  have been neglected. To a linear approximation, further,  $(\tilde{\Delta r})$  can be evaluated at  $r$  in (11) and (12). The increment in space-charge density  $\Delta\rho$  is then found as in (6):

$$\Delta\rho = (\rho_0 + \rho) \frac{1}{r} \frac{\partial}{\partial r}(r\tilde{\Delta r}) \\ \cong \rho_0 \frac{1}{r} \frac{\partial}{\partial r}(r\tilde{\Delta r}). \quad (13)$$

2) Another approach is to compute directly that portion of  $dQ_t$  which is due to the radial motion only. This charge increment is the charge due to the displacement at  $r$ , less the charge due to the displacement of  $r-dr$ . Each displacement is measured as above, relative to the original disturbed surface,  $r$  and  $r-dr$ , respectively. The net charge increment is therefore

$$(dQ)_{\text{radial motion}} = 2\pi r(\tilde{\Delta r})_r(\rho_0 + \rho) \\ - 2\pi(r-dr)(\tilde{\Delta r})_{r-dr}(\rho_0 + \rho). \quad (14)$$

Here the charge due to each displacement is the volume space-charge density times the volume swept out by the displacement amplitude; *i.e.*, effectively a surface charge, as in (2). As before, the ac charge density  $\rho$  drops out in a linear approximation, and with (11), the expression simplifies as:

$$(dQ)_{\text{radial motion}} \\ = 2\pi\rho_0 \left[ r \frac{\partial}{\partial r}(\tilde{\Delta r}) + (\tilde{\Delta r}) \right] dr \quad (15)$$

$$= 2\pi\rho_0 \frac{\partial}{\partial r}(r\tilde{\Delta r}) dr. \quad (16)$$

The total charge in each of these elementary volumes equals this charge plus that between the undisplaced surfaces at  $r$  and  $r - dr$ :

$$dQ_i = 2\pi r \left[ \rho_0 + \rho + \rho_0 \frac{1}{r} \frac{\partial}{\partial r} (r\tilde{\Delta r}) \right] dr. \quad (17)$$

The charge increment  $\Delta\rho$  so found is the same as in (13). Corresponding to it there is an increment  $\Delta i_z$  in axial current density  $i_z$ , and therefore in  $H_\phi$  at each radius in the beam:

$$\frac{1}{r} \frac{\partial}{\partial r} [r(\Delta H_\phi)_r] = \Delta i_z = v_0 \Delta\rho. \quad (18)$$

The total increment in  $H_\phi$  at the surface of the beam is found by integration:

$$\int_0^b \frac{\partial}{\partial r} [r(\Delta H_\phi)_r] dr = \rho_0 v_0 \int_0^b \frac{\partial}{\partial r} (r\tilde{\Delta r}) dr \quad (19)$$

$$b \cdot (\Delta H_\phi)_b = \rho_0 v_0 b (\tilde{\Delta r})_b$$

$$(\Delta H_\phi)_b = \rho_0 v_0 (\tilde{\Delta r})_b. \quad (20)$$

This is the same as  $G_s$  in (3) and (5); *i.e.*, both methods arrive at the same solution.

Concerning the second point in dispute, it can be demonstrated readily that the force terms due to the ac magnetic field are negligible for electron beams with velocities less than that corresponding to about 10,000 volts; whereas for beam velocities above this region, where such forces do become significant, it is incorrect to use the equations of nonrelativistic dynamics. Since the beams considered here are of the lower-voltage variety, the former stricture applies.

Since the axial dc velocity  $v_0$  is usually much greater than the tangential,  $v_{\phi 0}$ , it is sufficient to examine the terms in the force equations containing  $v_0$ . The ratio of interest in the radial force equation can be evaluated with the aid of the radial component of the field equation connecting  $H$  and  $J$ :

$$\text{curl } H = J + j\omega\epsilon E \quad (21)$$

$$H_\phi = \frac{\omega\epsilon}{\gamma} \left[ E_r + \frac{J_r}{j\omega\epsilon} \right]. \quad (22)$$

In true plasma waves, such as in an unbounded confined-flow beam, the displacement current is equal and opposite to the convection current. In beams of finite cross section and in finite magnetic fields, the convection current can be relatively larger, but is limited by the small-signal condition and practical limitations on beam permeance to a factor of about 5, or of the order of  $c/v_0$  at most:

$$J_i = - (j\omega\epsilon E_i) F_i \quad (i = r, \phi, z) \quad (23)$$

$$F_i \leq c/v_0. \quad (24)$$

The ratio of the forces due to the ac magnetic and electric fields, respectively, in the radial force equation, is given by

$$\left| \frac{v_0 B_\phi}{E_r} \right| \cong \frac{v_0 \mu \epsilon}{\gamma} |1 - F|$$

$$= \frac{v_0}{c} \cdot \frac{k}{\gamma} |1 - F|. \quad (25)$$

In these expressions,  $\epsilon$  and  $\mu$  are the dielectric constant and permeability of free space, respectively,  $k$  the free-space wave number, and  $c$  the velocity of light. This ratio is therefore negligibly small, for "slow" waves:

$$\frac{k}{\gamma} \approx \frac{v_0}{c} \ll 1. \quad (26)$$

When the fields have axial symmetry, the equation for curl  $E$  leads to the relation

$$E_\phi = - \frac{\omega}{\gamma} B_r. \quad (27)$$

The fields in the tangential force equation appear as the sum

$$E_\phi + v_0 B_r = v_0 B_r \left[ 1 - \frac{\omega}{\gamma v_0} \right] \approx 0. \quad (28)$$

The net contribution of  $E_\phi$  and  $v_0 B_r$  to the dynamics equations is therefore negligible, one being nearly equal and opposite in sign to the other, and each negligible in magnitude compared with  $E_r$  and  $E_z$ . The latter are directly excited by the initial modulation and are predominantly irrotational, whereas  $E_\phi$  is solenoidal, being induced indirectly by the currents of the moving charges.

This can be verified in greater detail as follows. The principal source of  $E_\phi$  is the surface current  $G_\phi$  given by (4), which in turn is dependent on  $E_r$ . The magnitude of such TE-TM coupling can be evaluated using the fact that  $G_\phi$  measures the maximum amplitude of  $H_z$ , approximately. This, taken together with the two field equations, (21) and (27), and the slow-wave condition (26), shows directly that  $E_\phi$  is negligible relative to  $E_r$ . When, in addition, the TE and TM fields are not coupled by the external circuit, as is the case in a drift region, the TE fields can be entirely disregarded. (Such circuit coupling does take place at a helical boundary; but only sufficient to affect the propagation constants, not the electron trajectories.)

With  $E_\phi$  equal to zero, the expressions given by Labus for the ac quantities inside of the beam—velocity, current-density, and fields—all reduce to the corresponding expressions previously published by Rigrod and Lewis,<sup>3</sup> in the case of Brillouin flow, and to those in Brewer's work,<sup>4</sup> in the case of the smooth beam with flux threading the cathode.

There are two conclusions: *First*, the results presented by Labus<sup>1,2</sup> are incorrect, whereas those of Rigrod and Lewis<sup>3</sup> and Brewer<sup>4</sup> are correct. *Second*, Labus' method of representing radial electron displacements by means of ac space-charge density increments throughout the beam volume can, when properly employed, lead to the same results as those obtained by using an equivalent surface charge density.

W. W. RIGROD  
Bell Telephone Labs.  
Murray Hill, N. J.

*Author's Comment*<sup>6</sup>

In problems dealing with the propagation of a perturbation within a bounded medium, the boundary conditions usually are given at the source of the perturbation. The present problem is more complicated because the shape of the medium is changed by the perturbation in an unknown way. In exact theory, that change should be included in the result. That theory however, would become laborious, unless the small signal meth-

od is justified and the separation of one or two of the variables is legitimate. In our problem, the separation is based on the assumption of the law of propagation along a preferred variable. The corresponding Ansatz that will be introduced into the differential equation requires that the boundary conditions are satisfied along a constant value of the remaining variables.

In the papers by Rigrod and Lewis<sup>3</sup> and Labus and Pöschl,<sup>2</sup> the conventional Ansatz  $\exp j(\omega t - \gamma z)$ , corresponding to a plane wave, was used, in order to separate the variables  $t$  and  $z$  of the partial differential equation. The boundary conditions (the continuity of field components) then are fulfilled along a constant value of  $r$  ( $r = b$ ) representing the surface of the undisturbed beam. In order to legitimize that procedure, additional field components (or currents) are introduced. Rigrod and Lewis' assume that "the rippled beam is equivalent to a uniform cylindrical beam with an ac surface charge density  $\rho_0 \tilde{r}$ , or a surface current density." Labus and Pöschl<sup>2</sup> consider the radial displacements of the flow within hollow cylinders of the radius  $r$  ( $0 < r < b$ ) and of the radial extension  $\delta r$ . According to Rigrod's note, the solutions obtained by those methods lead to the same result if the dependence of  $\delta r$  on  $r$  is properly taken into account.

In the work of Labus and Pöschl,<sup>2</sup> the field component  $E_\phi$ , and thus the coupling between TM and TE waves, had been taken into account, because it was believed that they may not be negligible, except for moderate values of magnetic fields, current densities, and beam radius. From the differential equations of the problem

$$L_0(E_z) = \frac{\omega L \gamma}{\omega(\omega_s^2/\omega_p^2 - 1)} L_0(rE_\phi)$$

$$L_1(E_\phi) = - \frac{\omega \omega_L}{\gamma c^2} r L_0(E_z)$$

$$\left( \text{herein } L_0 = \frac{\partial^2}{\partial r^2} + \frac{1}{r} \frac{\partial}{\partial r} - \gamma^2, \right.$$

$$\left. L_1 = \frac{\partial^2}{\partial r^2} + \frac{1}{r} \frac{\partial}{\partial r} - \left( \frac{1}{r^2} + \gamma^2 \right), \right.$$

$\omega_L = eB_0/2m$ ,  $\omega_s = \omega - \gamma u_0$ ) it becomes evident that the coupling between TM and TE waves depends on the magnitude of the magnetic field  $B_0$  and other parameters. In (11) of Labus' and Pöschl's work,<sup>2</sup> following from the boundary conditions, the coupling referred to is represented by the parameter  $\delta = \omega_L b/2c$ , containing the beam radius, besides  $B_0$ . The conditions for which its influence on the result had been disregarded in that paper, however, may not be true in general.

With regard to what had been said in (1), any solution of the considered problem that is based on the Ansatz  $\exp j(\omega t - \gamma z)$  will, in all cases, give rise to criticism. Therefore, the results of Labus and Pöschl<sup>2</sup> should not be called incorrect, unless the correct solution of the problem is known. In the conclusion of Labus' work,<sup>1</sup> the author pointed to further experiments, which perhaps might

settle these questions. However, he is aware of the difficulties encountered in obtaining reliable results. They depend on the accuracy of measuring the diameter of the unperturbed beam. In addition, a constant ripple along the beam, due to initial conditions can hardly be avoided. Therefore, an improved though more elaborate attack on that problem seems to be justified.

J. LABUS  
Siemens & Halske Aktiengesellschaft  
München, Germany

### A Plea for Maximum Utility in Government Contract Reports Covering Research and Development\*

Greater results from research and development programs, at no cost, can come from an increase in efficiency of the scientists and engineers working on them. This article discusses the effect on this efficiency of various ways of preparing government contract reports, particularly the regular quarterly report intended to cover all the work done in the interval. It is suggested that completeness of detail in such reports is not a sufficient measure of their utility to the government agency concerned, or to other scientists and engineers.

A fundamental premise in reporting on research and development to a government agency is that everything of value should be included. However, our scale of value extends not from zero to the positive but includes negative value as well. Thus, an incorrect or misleading result does not have zero value; it has a *harmful* effect on other workers and actually subtracts from their output. Such misleading results must not be confused with correctly determined negative results; e.g., a result that correctly indicates that a desired effect is not possible under given circumstances. These correct but negative results have *positive* values, since they have a beneficial effect on other workers.

In a research report, it is extremely important to maximize the utility to others by observing the following rules:

- 1) Eliminate negative values altogether.
- 2) Devote very little space and avoid detail in presenting results with a value that hovers around zero on the scale.
- 3) Describe in detail, and with full emphasis, a result that has a clearly discernible positive value.
- 4) When there are many results, proportion the detail and the emphasis to the value, so that the most valuable result is described in the most comprehensive terms.

When a paper is prepared for publication in one of our better journals, it is reviewed

by one or more independent readers who use exactly these criteria. Unfortunately, contract reports are not independently reviewed. We have all seen such reports with hundreds of pages of text, curves, photographs, and diagrams, all of which can easily be dismissed as much ado about nothing. Equally unfortunate is the report that describes an obviously valuable result in so little detail that it cannot be repeated elsewhere without duplicating much of the original work. But worst of all is the report with results that cannot be relied upon and are later found to be in error.<sup>1</sup>

The major difficulty in following the rules mentioned lies in the evaluation of research results. When the author of a report does not see the true value of his work, positive or negative, he will certainly be unable to avoid wasting the time of others. There seems to be little that can be done about this except a careful review by a supervisor or a colleague with better judgment.

*However, and this is the main thesis of this article, in most instances the research investigator himself is the most competent judge of value, and he does correctly evaluate; it does not follow that the most useful report is prepared.* There are many pressures on a writer of a contract report to deviate from the path of maximum utility. He may have worked for three months and have accumulated only data of extremely doubtful or even negative value. Since others may not share his insight, he is often praised when he submits an excellently written and complete report; yet, if he were asked to submit the same data to a technical journal, he would hesitate immediately to subject it to the scrutiny of critical review. He may have been encouraged to present *all* his work, good and bad, by a policy which assumes that proper evaluation will be done by each competent reader; at best, this is an extremely wasteful process. There may also be temptation to deviate from the best policy when a very important result is achieved. In such an instance, there may be a temporary advantage over hypothetical competitors by withholding key information from the report or by underemphasis of the important result and overemphasis of relatively unimportant data. To repeat, then, though a research investigator correctly evaluates the importance of his work, his evaluation may not always be used to the maximum benefit of others.

The effect of reports that depart widely from the rules leading to maximum utility is to mislead the government agency concerning the progress which is being made and to reduce markedly the efficiency of research and development workers who endeavor to use the contract reports to further their own work. Certain astute scientists are known to ignore the average contract report, preferring to wait for journal publication in which the author has more nearly approached a proper balance between emphasis and value.

<sup>1</sup> J. R. Pierce, in a report on "Basic Research in Electronics" prepared for the Technical Advisory Panel on Electronics, states, "... the greatest retarding influence on an art is inadequate or incompetent work. ... It wastes the time of other competent workers in following it, and it misleads the less competent as to what is desirable or possible."

In summary, the persons responsible for research direction in governmental organizations, in industry, and in academic institutions should try to instill in the research investigator a clear comprehension of the over-all benefit to be obtained by preparation of contract reports so as to be of greater use to others. These benefits are of exactly the same nature as those that come from a universal publication policy in science; each scientific worker is aided far more by the ability to use work *of* others than he loses by preparing his own work for use *by* others. The taxpayer, whose objective is to obtain a maximum return from each dollar spent on government-sponsored science, has an equal interest in improving the utility to society of government contract reports.

E. W. HEROLD  
Member, Advisory Group on  
Electron Tubes  
and RCA Laboratories  
Princeton, N. J.

### Properties of Ion Filled Waveguides\*

In the course of an investigation of so-called "ion plasma oscillations" in drifting electron beams, an analysis of some of the electromagnetic properties of an ion filled waveguide was made. The idealized system analyzed was the following: a metallic waveguide of rectangular cross section filled with a uniform charge density  $\rho_0$  of ions. The ions were assumed to have fixed average positions (no thermal or drift velocities), their charge to mass ratio was  $q/M$ , and the usual plasma frequency definition  $\omega_p^2 = q\rho_0/\epsilon_0 M$  was used. A dc, axial magnetic field  $B_0$  was assumed, giving a cyclotron frequency  $\omega_c = qB_0/M$ . The response of the system to a harmonic excitation  $e^{i\omega t}$  was studied under the assumption that solutions could be found of the form  $e^{-i\beta_z z}$  or  $\cos \beta_z z$ . The effect of dc space-charge fields was ignored.

A dispersion equation was found by expanding Maxwell's curl equations, including the ion vector current density  $J_i = \rho_0 v_i$ , where  $v_i$  is the vector ac ion velocity that is found by integrating the Lorentz force equation. The resulting "electromagnetic" dispersion equation is

$$\left[ -\beta^2 + k^2 \left( 1 - \frac{\omega_p^2}{\omega^2} \right) \right]^2 \left[ 1 - \frac{\omega_p^2}{\omega^2} \right] - \frac{\omega_c^2}{\omega^2} \left[ -\beta^2 + k^2 \left( 1 - \frac{\omega_p^2}{\omega^2} \right) + \frac{\omega_p^2}{\omega^2} \beta_z^2 \right] \left[ -\beta^2 + k^2 \right] = 0 \quad (1)$$

where  $\beta^2 = \beta_x^2 + \beta_y^2 + \beta_z^2$ ,  $\beta_x = l\pi/x_0$ ,  $\beta_y = m\pi/y_0$ , and  $x_0$  and  $y_0$  are the transverse waveguide dimensions. A much simpler equation can be derived by assuming that  $\beta_z \gg k = \omega/c$  (slow waves). In this case  $H \approx 0$ , and  $\vec{E} \approx -\text{grad } V$ . Then we can

\* Received by the IRE, October 16, 1957. This article originally appeared in the *AGET News Bulletin*, October 1, 1957.

\* Received by the IRE, October 7, 1957.

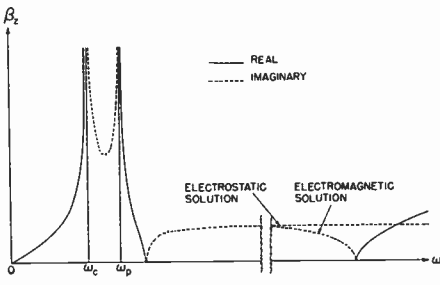


Fig. 1— $\beta_z$  vs  $\omega$  for  $\omega_c' < \omega_p$ .

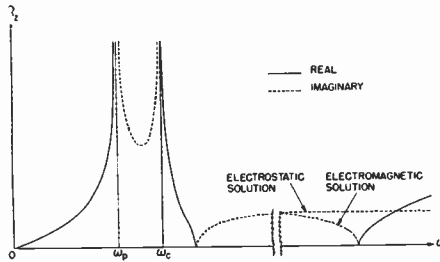


Fig. 2— $\beta_z$  vs  $\omega$  for  $\omega_p < \omega_c$ .

start with Poisson's equation to get the "electrostatic" relation

$$\beta_z^2 = \frac{\omega^2(\omega_p^2 + \omega_c^2 - \omega^2)}{(\omega_p^2 - \omega^2)(\omega_c^2 - \omega^2)} (\beta_x^2 + \beta_y^2). \quad (2)$$

Eq. (1) yields two different solutions for  $\beta_z^2$ . One solution behaves very much like the empty waveguide solution. The other solution of (1) behaves very much like (2) at low frequencies, and like the empty waveguide at high frequencies. Eq. (2) and the second solution of (1) are plotted in Figs. 1 and 2 for the cases  $\omega_c < \omega_p$ , and  $\omega_c > \omega_p$ . For reasonable values of the parameters  $\omega$ ,  $\omega_p$ ,  $\beta_x$ ,  $\beta_y$ , and assuming atomic or molecular ions rather than electrons, the frequencies to the left of the break in the abscissa are of the order of a few mc. Frequencies to the right of the break are of the order of a few kmc.

To us, the unexpected features of these curves are the two pass bands below the usual waveguide pass band. One extends from  $0 < \omega < \omega_c$  or  $0 < \omega < \omega_p$  (depending on whether  $\omega_c < \omega_p$  or  $\omega_c > \omega_p$ ). The other extends from  $\omega_p < \omega < \sqrt{\omega_p^2 + \omega_c^2}$  or  $\omega_c < \omega < \sqrt{\omega_p^2 + \omega_c^2}$ ; this region is characterized by  $\partial\beta/\partial\omega < 0$ , which implies a group velocity opposite to the phase velocity.

L. D. SMULLIN  
AND P. CHORNEY  
Mass. Inst. Tech.  
Cambridge, Mass.

### On the Forward Characteristic of Semiconductor Diodes\*

In books and elsewhere, the expression for the current-voltage characteristic of a semiconductor diode is still sometimes

\* Received by the IRE, September 3, 1957.

quoted without qualification as

$$I = I_0(e^{qV/kT} - 1), \quad (1)$$

$I_0$  being a constant,  $q$  the electronic charge,  $k$  Boltzmann's constant, and  $T$  the temperature. Actually, the characteristic almost never follows that form over any range beyond two or three tenths of a volt in the forward polarity ( $I$  and  $V$  positive) and a volt or so in the reverse polarity. The large signal region, which is often of the most practical interest, is not described well at all. The situation is almost as if a thermionic diode were described in terms of its region of very small currents, where the behavior is exponential; and the region of great practical interest, where the characteristic follows a three-halves power law, entirely disregarded. It would seem, as far as the forward part of the characteristic is concerned, that the common practice of plotting the characteristic on semilogarithmic coordinates helps to perpetuate this situation, since such a plot gives the low-current part of the characteristic a prominence out of all proportion to its importance in many practical applications.

The deviation of the reverse characteristic of a diode from the ideal form of (1) can arise from many reasons, some of them fundamental, some of them more or less accidental (e.g., surface conduction). It would be impossible to deal with these matters in a letter. Fortunately, some of them are often of small practical importance. What is desired here is to give some thought to the matter of the forward characteristic.

Hall<sup>1</sup> showed that, for certain types of diode, the  $qV/kT$  in (1) should be replaced by  $qV/2kT$ , and this form has had considerable use,<sup>2,3</sup> but even this seldom fits the facts very well above about one-half volt. Herlet<sup>4</sup> has given a theory which leads to a square-law relationship for large currents.

Recently, Fletcher<sup>5,6</sup> has given a rather rigorous treatment of the forward characteristic and matters related thereto, but the resulting expressions are not very convenient for practical application.

Actually, as can be seen by inspection, the forward characteristic of these diodes almost invariably starts out as an exponential, but approaches a straight line.<sup>7</sup> Armstrong, *et al.* proposed to take this into account, and to represent the characteristic by<sup>8</sup>

$$V = I \frac{R_R I + V_0}{I + I_N}. \quad (2)$$

<sup>1</sup> R. N. Hall, "Power rectifiers and transistors," *PROC. IRE*, vol. 40, pp. 1512-1518; November, 1952.

<sup>2</sup> E. Spence, "Durchlass- und Sperrigenschaften eines *p-i*-Metall Gleichrichters," *Z. Naturf.*, vol. 11a, pp. 440-456; June, 1956.

<sup>3</sup> H. S. Veloric and M. B. Prince, "High-voltage conductivity-modulated silicon rectifier," *Bell. Sys. Tech. J.*, vol. 36, pp. 975-1004; July, 1957.

<sup>4</sup> A. Herlet, "Das Verhalten von *p-n*-Gleichrichtern beim Hohen Durchlassbelastungen," *Z. Naturf.*, vol. 11a, pp. 498-510; June, 1956.

<sup>5</sup> N. H. Fletcher, "General semiconductor junction relations," *J. Electronics*, vol. 2, pp. 609-610; May, 1957.

<sup>6</sup> N. H. Fletcher, "The high-current limit for semiconductor junction devices," *PROC. IRE*, vol. 45, pp. 862-872; June, 1957.

<sup>7</sup> R. G. Shulman and M. E. McMahon, "Recovery currents in germanium *p-n* junction diodes," *J. Appl. Phys.*, vol. 24, pp. 1267-1272; October, 1953.

<sup>8</sup> H. L. Armstrong, E. D. Metz, and I. Weiman, "Design theory and experiments for abrupt hemispherical *p-n* junction diodes," *IRE TRANS.*, vol. ED-3, pp. 86-92; April, 1956.

$R_R$ , the "residual resistance" of the diode; the limit approached by the spreading resistance for large currents, is the resistance represented by the straight line to which the characteristic is asymptotic, while  $V_0$  is the intercept of that straight line on the  $V$  axis.  $I_N$  is just a constant of the diode. Given a characteristic,  $R_R$  and  $V_0$  can be found by drawing the asymptote, while  $I_N$  can be found by trial, or by the fact that when  $V = V_0$ ,  $I = (V_0 I_N / R_R)^{1/2}$ . Eq. (2) is really an asymptotic approximation to a theoretical characteristic, and involves some drastic approximations, but it is found to fit the facts quite well. Accordingly, it could, if desired, be considered just as an empirical interpolation formula. Since it fits the facts best for large currents it will give a rather large relative error at low currents, but the absolute error is quite small over the characteristic; and in calculating the action of rectifiers, etc., it is the absolute error, averaged over the working range, which is of interest.

Eq. (2) works best when voltage is to be found as a function of the current. Of course, it can be solved for the current, but the resulting expression, involving surds, may not be so convenient for further calculations.

Eq. (2) even attempts to represent the reverse part of the characteristic, in that  $I$  approaches  $-I_N$  as  $V$  approaches minus infinity. However,  $I_N$  will usually be two or three orders of magnitude greater than the reverse saturation current (if the reverse current *does* saturate). The representation can be improved in this respect; it can be shown that the complete expression developed by Armstrong *et al.*<sup>8</sup> is fitted a little better by the form

$$V = I \frac{R_R I^2 + V_0 I + V_0 I_N}{(I + I_N)(I + I_S)}. \quad (3)$$

$I_S$  being the reverse saturation current, it is readily seen that as  $I$  approaches  $-I_S$ ,  $V$  approaches minus infinity. On the other hand, for moderate or large forward currents, (2) and (3) are indistinguishable. Thus, (3) gives a better representation of the total characteristic, but at the cost of greater complexity; in particular, to solve for  $I$  it is now necessary to solve a cubic equation. For many applications dealing with the forward characteristic, (2) will prove both adequate and convenient.

In summary, it is proposed that (2) will represent the forward characteristic of a semiconductor diode quite well up to very high operating levels, and it will do so in a form convenient for use in many calculations.

H. L. ARMSTRONG  
Pacific Semiconductors, Inc.  
Culver City, Calif.

### Poles and Zeros Squared\*

The recent popularity of poles and  $z$  is mainly due to their use in the study of frequency response  $H(j\omega)$ . With

\* Received by the IRE, September 6, 1957.

$$\begin{aligned} p_i &= r_i e^{\pm j(\pi - \theta_i)} \\ \bar{p}_i &= r_i e^{\pm j(\pi - \theta_i)} \end{aligned} \quad (1)$$

the singularities of  $H(p)$ , the problem of determining the frequency dependence of the response is simplified if  $H(j\omega)$  is factored into vectors from  $j\omega$  to the fixed points  $p_i$ . We maintain that a further simplification is possible if instead of the  $p_i$ 's one considers their squares

$$\begin{aligned} w_i &= p_i^2 = r_i^2 e^{\pm j2\theta_i} \\ \bar{w}_i &= \bar{p}_i^2 = r_i^2 e^{\pm j2\theta_i} \end{aligned} \quad (2)$$

One can then determine the amplitude characteristic,

$$A(\omega) = |H(j\omega)|, \quad (3)$$

from the lengths of a smaller number of vectors.

Indeed with

$$h(p^2) = H(p)H(-p) = h(w) \quad (4)$$

where

$$w = p^2 \quad (5)$$

we have

$$A^2(\omega) = h(-\omega^2). \quad (6)$$

In obtaining  $A(\omega)$  from (3), one will have to determine the lengths of the  $n$  vectors from  $j\omega$  to the points  $p_i$ ; the fact that the  $p_i$ 's might be complex conjugate is not utilized since the point  $j\omega$  is not on the real axis. In obtaining  $A(\omega)$  from (6), one will again have to determine the length of  $n$  vectors, because  $h(w)$  has the same number of singularities as  $H(p)$ ; however, since  $-\omega^2$  is real, its distances to the points  $w_i$  and  $\bar{w}_i$  are equal, hence we need consider fewer vectors (half as many if all roots are complex). The above is demonstrated in Fig. 1 and its usefulness is shown in the following examples.

ONE PAIR OF COMPLEX POLES  $p_i = r e^{\pm j(\pi - \theta)}$

In the  $p$  plane we have

$$A(\omega) = \frac{1}{\textcircled{1} \textcircled{2}}$$

where  $\textcircled{1}$  and  $\textcircled{2}$  are the lengths of the vectors from  $j\omega$  to  $p_1$  and  $\bar{p}_1$ , respectively. To determine the condition for overshoot and the value  $\omega_m$  of the frequency for maximum response, we have from the  $w$  plane

$$A^2(\omega) = \frac{1}{\textcircled{A}^2}$$

where  $A(\omega)$  is maximum when  $\textcircled{A}$  is minimum. From Fig. 2 we trivially obtain

$$\omega_m^2 = r^2 |\cos 2\theta|$$

condition for overshoot (over-in the double-tuned circuit terms is given by

$$\theta > \frac{\pi}{4}$$

and  $\bar{p}_1'$  we have critical or  $\theta < \pi/4$  ( $p_1''$  and  $\bar{p}_1''$ ) the overcoupled case the condition is given by

$$\frac{r^2}{\sin 2\theta} = \frac{1}{|\cos 2\theta|}$$

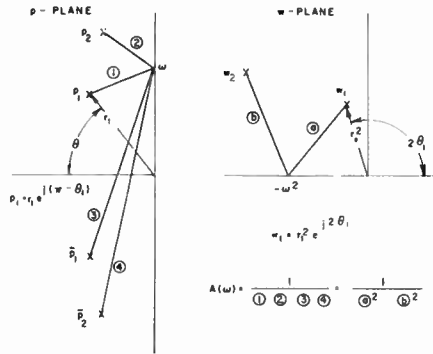


Fig. 1

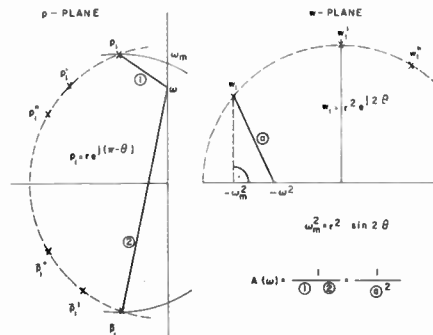


Fig. 2

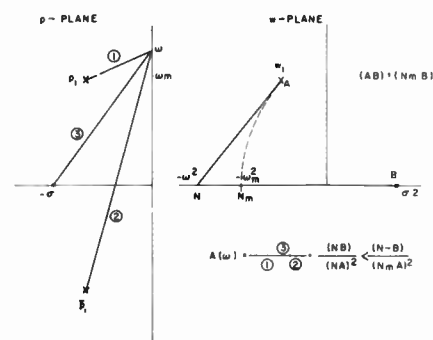


Fig. 3

ONE ZERO  $p = -\sigma$  AND ONE PAIR OF

COMPLEX POLES  $p_i = r e^{\pm j(\pi - \theta)}$

From the  $p$  plane it is not easy to see for what value of  $\omega$  the response (Fig. 3)

$$A(\omega) = \frac{\textcircled{3}}{\textcircled{1} \textcircled{2}}$$

is maximum. In the  $w$  plane

$$A^2(\omega) = \frac{(NA)}{(NB)^2}$$

where  $(NA)$  is the distance from  $-\omega^2$  to the pole  $w_1 = r^2 e^{j2\theta}$  and  $(NB) = \omega^2 + \sigma^2$ . It is easily seen that  $A(\omega)$  is maximum for  $\omega = \omega_m$  such that

$$(N_m A) = (AB)$$

hence  $\omega_m$  is given by

$$(\omega_m^2 + \sigma^2)^2 = r^4 + \sigma^4 - 2r^2\sigma^2 \cos 2\theta$$

and the condition for overshoot by

$$r^2 > 2\sigma^2 \cos 2\theta.$$

TWO PAIRS OF COMPLEX POLES

The analysis of the double-tuned circuit is simple when the  $Q$ 's are high and the resulting band narrow. One assumes then that the vectors to the points  $p_1$  and  $p_2$  are constant and considers only the variation of the two vectors to the points  $\bar{p}_1$  and  $\bar{p}_2$ . In the  $w$  plane this assumption is not necessary and the analysis of the wide-band case can be given as easily. Thus to obtain equal peaks in the response, we must have

$$r_1^2 \sin 2\theta_1 = r_2^2 \sin 2\theta_2$$

because then the poles  $w_1 = r_1^2 e^{j2\theta_1}$  and  $w_2 = r_2^2 e^{j2\theta_2}$  are equidistant from the real axis.

A. PAPAULIS  
Polytechnic Institute of Brooklyn  
Brooklyn, N. Y.

Effect of Correlation on Combiner Diversity\*

For reliable communications under conditions of rapid fading the advantages of combiner diversity, wherein the signals are combined by adding the squares of the individual signal-to-noise ratios, have been recently pointed out in the literature.<sup>1-3</sup> The analysis<sup>4</sup> of the probability distribution of the resultant signal has been made under the assumption that the individual signals are uncorrelated. It is the purpose of this letter to indicate how the effect of correlation may be taken into account and to give the resulting distribution function in the case of dual diversity. This permits a more reliable calculation of the spacing required for good diversity action. It should be pointed out that this has been done for the case of switch diversity by Staras<sup>5</sup> and the results obtained were similar to those obtained here.

The method of approach used in solving this problem is to convert the correlated variables, by means of a coordinate transformation, into uncorrelated variables having modified mean-square values.

Under rapid fading conditions the signal strength has a Rayleigh distribution having the probability-density function

$$p(z) = \frac{2z}{\sigma^2} \exp\left(-\frac{z^2}{\sigma^2}\right).$$

\* Received by the IRE, September 9, 1957. This work was supported by the Department of Defense.

<sup>1</sup> L. R. Kahn, "Ratio squarer," Proc. IRE, vol. 42, p. 1704; November, 1954.

<sup>2</sup> D. G. Brennan, "On the maximum signal-to-noise realizable from several noisy signals," Proc. IRE, vol. 43, p. 1530; October, 1955.

<sup>3</sup> C. L. Mack, "Diversity reception in uhf long range communications," Proc. IRE, vol. 43, pp. 1281-1289; October, 1955.

<sup>4</sup> H. Staras, "The statistics of combiner diversity," Proc. IRE, vol. 44, p. 1057; August, 1956.

<sup>5</sup> H. Staras, "Diversity reception with correlated signals," J. Appl. Phys., vol. 27, pp. 93-94; January, 1956.

eros  
i the

The variable  $z = \sqrt{x^2 + y^2}$  may be resolved into two variables  $x$  and  $y$ , each of which is normally distributed,

$$b(x) = \frac{1}{\sqrt{\pi\sigma^2}} \exp\left(-\frac{x^2}{\sigma^2}\right)$$

and similarly for  $y$ . Considering two correlated variables  $z_1$  and  $z_2$  having the components  $(x_1, y_1)$  and  $(x_2, y_2)$ , respectively, we assume a simple linear correlation

$$x_2 = \rho x_1 + u, \quad y_2 = \rho y_1 + v$$

where  $u$  and  $v$  are the uncorrelated portions of  $x_2$  and  $y_2$ . It has been shown<sup>6</sup> that the correlation coefficient  $c_1$  for  $z_1$  and  $z_2$  is given by

$$c = \frac{\pi}{4(4 - \pi)} \left( \rho^2 + \frac{\rho^4}{16} + \frac{\rho^6}{64} + \dots \right) \approx \rho^2.$$

We now consider the variables defined by the linear transformations:

$$\sqrt{2}\xi_1 = x_1 + x_2 = x_1(1 + \rho) + u,$$

$$\sqrt{2}\xi_2 = x_1 - x_2 = x_1(1 - \rho) - u,$$

$$\sqrt{2}\eta_1 = y_1 + y_2 = y_1(1 + \rho) + v,$$

$$\sqrt{2}\eta_2 = y_1 - y_2 = y_1(1 - \rho) - v.$$

These variables are normally distributed since they are linear combinations of normally distributed variables.<sup>7</sup> They are also uncorrelated as may be seen from the following:

$$2\xi_1\xi_2 = \overline{x_1^2} - \overline{x_2^2} = \sigma^2 - \sigma^2 = 0,$$

$$2\eta_1\eta_2 = \overline{y_1^2} - \overline{y_2^2} = \sigma^2 - \sigma^2 = 0,$$

$$2\xi_1\eta_1 = \overline{x_1y_1 + x_1y_2 + x_2y_1 + x_2y_2} = 0,$$

$$2\xi_2\eta_2 = \overline{x_1y_1 - x_1y_2 - x_2y_1 + x_2y_2} = 0,$$

$$2\xi_1\eta_2 = \overline{x_1y_1 - x_1y_2 + x_2y_1 - x_2y_2} = 0,$$

$$2\xi_2\eta_1 = \overline{x_1y_1 + x_1y_2 - x_2y_1 - x_2y_2} = 0,$$

since the only correlation between the  $x$ 's and  $y$ 's is that between  $x_1, x_2$  and  $y_1, y_2$ . In the case of normally distributed variables this is sufficient to prove that they are independent.<sup>8</sup>

Now combine these variables to form new variables,

$$\omega_1^2 = \xi_1^2 + \eta_1^2 \text{ and } \omega_2^2 = \xi_2^2 + \eta_2^2$$

which are Rayleigh distributed and uncorrelated. We have, furthermore,

$$\begin{aligned} \omega^2 &= \omega_1^2 + \omega_2^2 = \xi_1^2 + \eta_1^2 + \xi_2^2 + \eta_2^2 \\ &= x_1^2 + x_2^2 + y_1^2 + y_2^2 = z_1^2 + z_2^2 \end{aligned}$$

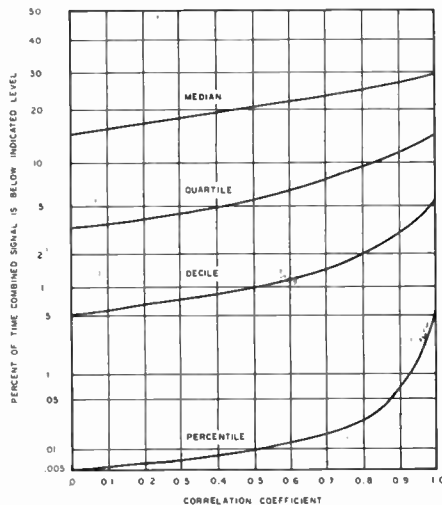


Fig. 1—Combiner diversity with correlated signals.

so that we have expressed the desired resultant,  $\omega$ , in terms of uncorrelated variables. It only remains to find the second moments of  $\omega_1$  and  $\omega_2$ .

We first note that

$$2\xi_1\xi_2 = \overline{x_1^2}(1 - \rho^2) - \overline{u^2} = 0$$

so that

$$\overline{u^2} = (1 - \rho^2)\sigma^2$$

and similarly

$$\overline{v^2} = (1 - \rho^2)\sigma^2.$$

Also

$$\overline{ux_1} = \overline{vy_1} = 0$$

since these variables are uncorrelated by definition. From these relations we have

$$\begin{aligned} \overline{\xi_1^2} &= \frac{1}{2} \overline{(x_1^2(1 + \rho)^2 + 2ux_1(1 + \rho) + u^2)} \\ &= \frac{1}{2} [\sigma^2(1 + \rho)^2 + \sigma^2(1 + \rho^2)] \\ &= \sigma^2(1 + \rho) \end{aligned}$$

$$\begin{aligned} \overline{\xi_2^2} &= \frac{1}{2} \overline{(x_1^2(1 - \rho)^2 - 2ux_1(1 - \rho) + u^2)} \\ &= \frac{1}{2} [\sigma^2(1 - \rho)^2 + \sigma^2(1 + \rho^2)] \\ &= \sigma^2(1 - \rho) \end{aligned}$$

$$\overline{\eta_1^2} = \sigma^2(1 + \rho)$$

$$\overline{\eta_2^2} = \sigma^2(1 - \rho)$$

and so we obtain for the probability-density functions of  $\omega_1^2$  and  $\omega_2^2$ ,

$$p(\omega_1^2) = \frac{1}{\sigma^2(1 + \rho)} \exp\left(-\frac{\omega_1^2}{\sigma^2(1 + \rho)}\right)$$

$$p(\omega_2^2) = \frac{1}{\sigma^2(1 - \rho)} \exp\left(-\frac{\omega_2^2}{\sigma^2(1 - \rho)}\right).$$

The probability-density function of the resultant is

$$b(\omega^2) = p(\omega_1^2)p(\omega_2^2) = \frac{1}{\sigma^4(1 - \rho^2)} \cdot \exp\left(-\frac{\omega_1^2}{\sigma^2(1 + \rho)}\right) \exp\left(-\frac{\omega_2^2}{\sigma^2(1 - \rho)}\right).$$

From this we may readily find the probability distribution for any value  $R$  of  $\omega^2$ , which is

$$\begin{aligned} P(R) &= \int_0^R \int_0^{R-\omega_1^2} p(\omega^2) d(\omega_1^2) d(\omega_2^2) \\ &= \int_0^R \exp\left(-\frac{\omega_2^2}{\sigma^2(1 - \rho)}\right) \left[ \int_0^{R-\omega_2^2} \frac{1}{\sigma^4(1 - \rho^2)} \cdot \exp\left(-\frac{\omega_1^2}{\sigma^2(1 + \rho)}\right) d(\omega_1^2) \right] d(\omega_2^2). \end{aligned}$$

Evaluating these integrals we have the final result, letting  $c = \rho^2$ ,

$$P(R) = 1 - \frac{1 + \sqrt{c}}{2\sqrt{c}} \exp\left(-\frac{R}{\sigma^2(1 + \sqrt{c})}\right) + \frac{1 - \sqrt{c}}{2\sqrt{c}} \exp\left(-\frac{R}{\sigma^2(1 - \sqrt{c})}\right)$$

which is the joint probability distribution for dual combination diversity when the two signals have a correlation coefficient,  $c$ .

In the limit  $c=1$ , we find

$$P(R)_{c=1} = 1 - e^{-R/2\sigma^2}$$

which is the distribution for a single variable having double the second moment of the individual variables. For  $c=0$ , we find

$$P(R)_{c=0} = 1 - e^{-R/\sigma^2(1 + R/\sigma^2)}$$

which is the distribution for dual combiner diversity with uncorrelated signals.

The joint distribution obtained above provides the results shown in Fig. 1. The curves represent the percentage of time which the combined signal falls below the level indicated. The particular level refers to that which each Rayleigh variable will fade below the indicated percentage of time. For example, the percentile curve refers to Rayleigh variables which fade below a given threshold 1 per cent of the time, whereas the combined signal only fades below this level 0.5 per cent of the time in the case of complete correlation and 0.005 per cent of the time for independent signals. It is apparent from these results that most of the advantage of combiner diversity is obtained even if the correlation coefficient is as high as 0.5. This conclusion is the same as that drawn from Staras' analysis of switch diversity.<sup>5</sup>

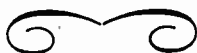
The writer wishes to acknowledge the valuable advice of W. D. White.

KARLE S. PACKARD  
Airborne Instruments Laboratory, Inc.  
Mineola, N. Y.

<sup>6</sup> H. G. Booker, J. A. Ratcliffe and D. H. Shinn, "Diffraction from an irregular screen with applications to ionospheric problems," *Phil. Trans. Royal Soc. (London)*, vol. 242, pp. 579-607; September, 1950.

<sup>7</sup> H. Cramer, "Mathematical Methods of Statistics," Princeton Univ. Press, Princeton, N. J., p. 213; 1946.

<sup>8</sup> *Ibid.*, p. 289



# Contributors

Jules Aarons (S'44-A'51) was born in New York, N. Y., in October, 1921. He received the B.S. degree from the College of the City of New York in 1942,



J. AARONS

the M.A. degree from Boston University in 1949, and the Ph.D. degree from the University of Paris, in 1954. He served as a radar and radio officer with the U. S. Army Air Force from 1943 to 1946. From 1946 to the present, he has been employed as a physicist with the Air Force Cambridge Research Center, where, since 1955, he is Chief of the Ionospheric Section of the Propagation Laboratory of the Electronics Research Directorate. He has engaged in studies of low-frequency fluctuations of the earth's magnetic field, solar-terrestrial relationships and their effects on radio communications, and at present is engaged in radio astronomy studies of atmospheric absorption, refraction, and scintillation.



Ned L. Ashton was born in Clinton, Iowa, on January 30, 1903. He received the Bachelor of Engineering degree and the Master's degree in both hydraulics and structural engineering, both from the State University of Iowa, in 1925 and 1926, respectively.



N. L. ASHTON

A professor of civil engineering at the State University of Iowa, he is now on academic leave while acting as a special consultant on the design of the 140-foot radio telescope for the Associated Universities, Inc., New York, N. Y. For the past two and one half years, he has been a consultant on special feasibility studies of large antennas for the Office of Naval Research and on the design of an aluminum highway bridge for the Research Board of the Iowa State Highway Commission. Currently, he also is acting as a consultant on special bridge design problems for the cities of Burlington and Iowa City, Iowa, and for the Cedar Rapids and Iowa City Railway Co. He is also an advisor on several large steerable antennas for the Air Force for Collins Radio Co., Cedar Rapids, Iowa.

Among the societies to which he belongs are the American Society of Civil Engineers, American Welding Society, Society of American Military Engineers, American Society for Metals, Sigma Xi, Tau Beta Pi, and Chi Epsilon.

He is a registered Professional Engineer in both Missouri and Iowa.

Kenji Akabane was born in Matsumoto, Japan, on November 20, 1926. He attended the University of Tokyo. In 1951, he received the B.A. degree in applied physics from that university. Since that time, Mr. Akabane has been employed at the Tokyo Astronomical Observatory, where he has been engaged in radio astronomy research with special emphasis in the microwave region.



K. AKABANE

He is a member of the Astronomical Society of Japan.



Alan H. Barrett was born in June, 1927, in Springfield, Mass. After service in the Navy, 1944-1946, he entered Purdue University, Lafayette, Ind., and received the B.S. degree in electrical engineering. He received the M.A. and Ph.D. degrees in physics from Columbia University, in 1953 and 1956, respectively. His thesis research was in microwave spectroscopy.



A. H. BARRETT

Dr. Barrett held a National Research Council, Naval Research Laboratory Postdoctoral Associateship from January, 1956, to January, 1957, during which time he was engaged in radio astronomy research at the Naval Research Laboratory, Washington, D. C. He is currently engaged in similar work at the University of Michigan.

He is a member of the American Physical Society, American Astronomical Society, Eta Kappa Nu, and Sigma Xi.



William Barron was born in Bridgeport, Conn., in September, 1928. He received the B.A. degree from Bowdoin College, Brunswick, Me., in 1950.



W. BARRON

He taught physics and mathematics at the secondary school level for five years before starting to work in the Ionospheric Section of the Propagation Laboratory, Air Force Cambridge Research Center, Hanscom Field, Bedford, Mass., in 1955. At present, he is engaged in studies in radio astronomy and atmospheric physics.

Emile-Jacques Blum was born in Floing, Ardennes, on July 27, 1923. After service in the French Army from 1943 to 1945, he received the Licence ès Sciences from Paris University in 1947.



E. J. BLUM

He was at the Laboratoire de Physique de l'École Normale Supérieure from 1948 to 1952. Mr. Blum was employed in research for the French Navy and joined the Radioastronomy Group. He obtained the Doctorat ès Sciences at Paris University in 1952. Since 1954, he has been at the Meudon Observatory, Paris, with the Radioastronomy Group. He was appointed "Astronome Adjoint" in 1956. He now is engaged in studies of radioastronomical receivers and technical developments, chiefly on meter wavelengths and in measurements made at the Nançay field station.



Henry G. Booker (SM'45-F'53) was born at Barking, Essex, Eng., in 1910. He was educated at Cambridge University where he received the B.A. degree in 1933, and the Ph.D. degree in 1936, specializing in radio wave-propagation. He was awarded the Smith's prize in 1935, and became a Research Fellow of Christ's College in the same year. From July, 1937, to July, 1938, he was visiting scientist at the Department of Terrestrial Magnetism of the Carnegie Institution of Washington, D. C. During World War II, he was in charge of theoretical research at the Telecommunications Research Establishment in England. After the war, he returned to Cambridge University as a lecturer, and in 1948, became a professor of electrical engineering at Cornell University. He was awarded the Duddell Premium in 1946, the Institution Premium in 1947, and the Kelvin Premium in 1948, by the Institute of Electrical Engineers, London.



H. G. BOOKER

Dr. Booker is an Associate Member of the IEE, and a Fellow of the Royal Meteorological Society. He is the author of numerous papers on radio wave propagation in the ionosphere and in the troposphere.



R. N. Bracewell (SM'56) was born in Sydney, Australia, in 1921. He graduated from the University of Sydney in 1941 with

the B.Sc. degree in mathematics and physics, later receiving the degrees of B.E. (1943) and M.E. (1948) in communications with first class honors. During the war, he worked on electromagnetic theory and microwave radar development in the Radiophysics Division of the CSIRO. From 1946 to 1949, he made experimental studies of solar ionospheric phenomena using very long waves, in the Cavendish Laboratory, Cambridge, and there he received the Ph.D. degree. A developing interest in the astronomical aspects of radio science led to his spending 1954-1955 as a visiting professor at the Berkeley Astronomical Department, University of California, on leave from CSIRO with a Fulbright grant. He has been associate professor of electrical engineering in the Radio Propagation Laboratory at Stanford University since 1955, where he is engaged in solar research.



R. N. BRACEWELL

He is a Fellow of the Institute of Physics, Associate Member of the Institution of Electrical Engineers, Fellow of the Royal Astronomical Society, life member of the Astronomical Society of the Pacific, and a member of Sigma Xi.



Robert H. Bruton was born in Annapolis, Md., on February 23, 1934. He was a student at the U. S. Naval Academy from 1953 to 1955. He now is attending Lehigh University, Bethlehem, Pa., where he received the B.A. degree in June, 1957. He will have completed his work for the B.S. degree in June, 1958. He worked at the Radio Astronomy Branch of the U. S. Naval Research Laboratory, Washington, D. C., for two summers as a student trainee; during 1956, on a 400-mc survey of cosmic radio sources and during 1957, on a short-pulse lunar radar project.



R. H. BRUTON

John Castelli was born in Lexington, Mass., in November, 1916. He was educated in the Lexington schools and received the A.B. and M.A. degrees from Boston College, Boston, Mass., in 1938 and 1939, respectively.



J. CASTELLI

During World War II, Mr. Castelli served in the U. S. Army Air Force as a radar officer. In 1946, Mr. Castelli entered the Civil Service at the Air Force Cambridge Research Center, where he has mainly worked on the rocket projects and various phases of radar systems.

W. N. Christiansen was born in Melbourne, Australia, on August 9, 1913. He received the B.S. and M.S. degrees in physics at the University of Melbourne in 1934 and 1935, and the degree of D.Sc. in 1953.



W. N. CHRISTIANSEN

After postgraduate work at Melbourne University, he joined the Commonwealth X-ray and Radium Laboratory. From 1937 until 1947, he was employed in the Research Laboratories of Amalgamated Wireless (A/asia) Ltd., where he was principally engaged in communications work, including the development of multiple-rhombic antenna arrays for use in long distance radio circuits. From 1948 to the present time, he has been working as a radio astronomer in the Division of Radiophysics of the CSIRO. His main work has been connected with high-resolution radio studies of the sun.

Dr. Christiansen is a Fellow of the Institute of Physics (Aust.), an Associate Member of the IEE (London), and a Fellow of the Royal Astronomical Society.



Robert J. Coates (A'47-M'55-SM'56) was born on May 8, 1922 in Lansing, Mich. He received the B.S. degree in electrical engineering from Michigan State University in 1943, the M.S. degree in electrical engineering from the University of Maryland in 1948, and the Ph.D. degree in applied physics from The Johns Hopkins University in 1957.



R. J. COATES

Dr. Coates joined the Naval Research Laboratory in 1943, where he worked on microwave radar development. Since then, he has done research in microwave propagation, pulsed communications, millimeter wavelength components, and millimeter wavelength systems. At present he is engaged in research in solar radio astronomy and in atmospheric physics.

Dr. Coates is a member of Tau Beta Pi, Phi Kappa Phi, Sigma Xi, RESA, URSI, the American Physical Society, and the American Astronomical Society. He is a registered Professional Engineer in Washington, D. C.



Marshall H. Cohen (S'47-A'50-M'56) was born in Manchester, N. H., on July 5, 1926. He received the B.E.E. degree from

Ohio State University in 1948, and the M.S. and Ph.D. degrees in physics from Ohio State University in 1949 and 1952. He was a re-



M. H. COHEN

search associate at the Antenna Lab. of Ohio State University Research Foundation from 1951 to 1954, where he worked primarily on miniature antennas and radar scattering. In 1954, he became an assistant professor in the School of Electrical Engineering at Cornell University.

He is a member of the American Physical Society and American Astronomical Society.



Raymond A. J. Coutrez was born in Ath, Belgium, on July 29, 1916. After his studies in mathematical physics and astronomy at the University of Brussels, Belgium, and Ecole Normale Supérieure, Paris, he received the Doctor's degree in science in 1941 and a special Doctor's degree in 1948.



R. A. COUTREZ

His principal works concerned statistical mechanics, stellar astronomy, solar physics, and radio astronomy, from theoretical and experimental points of view. In 1941, he joined the staff of the Royal Observatory, Belgium, where he is head of the solar and radio astronomy department and heads the radio astronomy station Humain-Rochefort.

He is a fellow of the Royal Astronomical Society of Great Britain, the Belgian Societies of Astronomy, Statistics, etc., and a past Advanced Fellow of the Belgian American Educational Foundation. He is also a member of Commissions 10, 11, and 40 of the IAU and Secretary of Commission V, URSI.



A. E. Covington (M'49) was born in Regina, Saskatchewan, Canada, on September 21, 1913. He received the B.A. degree in physics and mathematics in 1938, and the M.A. degree in 1940 from the University of British Columbia, Vancouver, B.C. He took postgraduate studies at the University of California at Berkeley, from 1940 to 1942. Since then, he has been with the National Research Council of Canada at Ottawa.



A. E. COVINGTON

He is a member of the American Astronomical Society and the Royal Astronomical Society of Canada.

Kalen J. Craig was born in Larned, Kan., on March 29, 1921. He is studying electrical engineering at George Washington University, Washington, D. C.



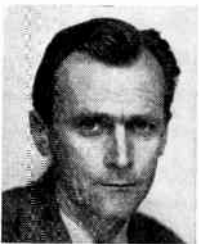
K. J. CRAIG

From 1942 to 1946, he served with the U. S. Marine Corps, and graduated from the Radio Materiel School of the U. S. Naval Research Laboratory; he also acquired experience with naval radar equipment and radio-controlled aircraft. He joined the Wave Propagation Branch of the Naval Research Laboratory in 1952 and engaged in the study of electromagnetic propagation in the troposphere.

Since he became affiliated with the Radio Astronomy Branch early in 1957, Mr. Craig has worked on the moon radar project.



Jean-François Denisse was born in Saint-Quentin, France, on May 16, 1915. He entered the Ecole Normale Supérieure in 1936



J. F. DENISSE

where he received the Licence ès Sciences and the Agrégation de Physique from Paris University, Paris, France. After service in the French Army in France and in Africa, he was at the Laboratoire de Physique de l'Ecole Normale Supérieure from 1945, working on problems related to radio astronomy and ionosphere research. He spent 1948 to 1949 at the National Bureau of Standards as a guest worker and he obtained the Doctorat ès Sciences in 1949. After two years as assistant professor in physics, he joined the Meudon Observatory, Paris, in 1953, where he is leading the Radio-astronomy Group. He was appointed full Astronomer of the Paris Observatory in 1956.



Nannielou H. Dieter was graduated Phi Beta Kappa, in 1948, from Goucher College, Baltimore, Md. During her junior and senior summers, she was Lydia S. Hinchman Fellow at the Maria Mitchell Observatory in Nantucket, Mass.



N. H. DIETER

From 1948 until early in 1951, she worked in the Gravity and Astronomy Section of the U. S. Coast and Geodetic Survey. From 1951 until 1955, she worked in the Radio Astronomy Branch of the U. S. Naval Research Laboratory. In 1955, she went to the Harvard University Graduate School.

Helen W. Dodson (Mrs. E. L. Prince) was born in Baltimore, Md., in 1905. She received the A.B. degree from Goucher College in 1927, the M.A. and Ph.D. degrees from the University of Michigan, and the Sc.D. (Hon) degree from Goucher College. She was on the faculty of Wellesley College from 1932 through 1945; a staff member at the Radiation Laboratory, M.I.T., from 1943 through 1945; and a member of the faculty of Goucher College from 1945 through 1950. From 1947 to the present time, she has been on the faculty of the University of Michigan, where she is professor of astronomy at the McMath-Hulbert Observatory. She has been engaged in research on solar flares, prominences, solar radio-frequency emission, and solar-terrestrial relationships.



H. W. DODSON

Dr. Dodson is a member of the American Astronomical Society, American Geophysical Union, Phi Beta Kappa, and Sigma Xi.



Frank D. Drake (M'57) was born on May 28, 1930, in Chicago, Ill. He received the B.E.P. degree in 1952 from Cornell University, Ithaca, N. Y., and the M.A. degree in astronomy from Harvard University, Cambridge, Mass., in 1956. From 1952 to 1955, he was an electronics officer in the United States Navy.



F. D. DRAKE

Since 1955, he has been associated with the Agassiz Station Radio Astronomy Project of Harvard University, working principally in 21-cm astronomical research and in infrared techniques and optical astronomy. Also, he presently is director of the astronomical research group of the Ewen Knight Corp., Needham Heights, Mass.

Mr. Drake is a member of the American Astronomical Society, Tau Beta Pi, and Sigma Xi.



Richard M. Emberson was born in Columbia, Mo., on April 2, 1914. He received the A.B., A.M., and Ph.D. degree in physics from the University of Missouri in 1931, 1932, and 1936, respectively. He did three years post-graduate work as a Bemis Fellow at the Harvard College Observatory. For one year he was an instructor in biophysics at the University of Pittsburgh Medical School. He also has been a staff member of the Radiation Laboratory,



R. M. EMBERSON

Massachusetts Institute of Technology, from 1941-1946; a radio engineer at the Naval Research Laboratory during 1946; and secretariat at the Research and Development Board, from 1946 through 1951. He has been assistant secretary and assistant to the President of Associated Universities, Inc., from 1951 to the present.

He is a member of the AAAS, and the Astronomical Society, and a Fellow of the Association of Physics Teachers and the Physical Society.



H. I. Ewen (SM'54) was born on March 15, 1922, in Chicopee, Mass. He received the B.A. degree in mathematics and astronomy



H. I. EWEN

from Amherst College, Amherst, Mass., in 1943; the M.A. degree in physics from Harvard University, Cambridge, Mass., in 1948; and the Ph.D. degree in physics from Harvard in 1951. He was an instructor at Amherst College in 1943. From 1943 to 1946, he was a Lieutenant in the United States Navy, serving as an airborne radar observer in the European Theatre. In 1952, he became research director of the Scientific Specialties Corp. He was acting director of the microwave communications division of the National Co., Malden, Mass., from 1954 through 1955. He was a member of the National Radio Astronomy Facility Study Group in 1955, and a member of the Advisory Panel for the National Radio Astronomy Laboratory in 1956.

Dr. Ewen was one of the founders of the Agassiz Station Radio Astronomy Project of Harvard University in 1952, and since that time has been codirector of that project. He presently is a member of the astronomy committee of the Office of Naval Research. In 1951, he founded the Ewen Knight Corp. of Needham Heights, Mass., and is the president of that corporation at present.

Dr. Ewen is a Fellow of the AAS, a Fellow of the American Association for the Advancement of Science, and a member of the American Astronomical Society, Phi Beta Kappa, and Sigma Xi.



George B. Field was born in 1929 in Rhode Island. He received the B.S. degree in physics from the Massachusetts Institute of



G. B. FIELD

Technology in 1951, whereupon he commenced working on military problems at the Naval Ordnance Laboratory. He then attended Princeton University, where he was awarded the Ph.D. degree in astronomy, in 1955.

For the next two years, Dr. Field held a Junior Fellowship in the Harvard Society of Fellows. While a Junior Fellow, Dr. Field was a guest at the

Harvard College Observatory, where he worked with the George R. Agassiz radio telescope. At present, he is an assistant professor of astronomy at the Princeton University Observatory.



John Wilson Findlay was born in Kineton, Warwickshire, Eng., on October 22, 1915. He graduated with first class honors in physics from Cambridge University, England, in 1937 and received the Ph.D. degree from that University in 1950.



J. W. FINDLAY

Mr. Findlay was a research student at the Cavendish Laboratory, Cambridge, Eng., from 1937 to 1939. At the start of the second World War in 1939, he

worked for the Air Ministry on radar for the R.A.F. in France. From 1940 to 1942, he was at the R.A.F. headquarters of the Middle East Command engaged in planning, siting, and evaluating ground radar stations throughout the Command.

From 1942 to 1945, he was scientific advisor to the Command Radar Officer at Air Headquarters, New Delhi, India, and he assisted the R.A.F. in the development of ground radar defenses in India, Burma, and Ceylon.

Dr. Findlay was a fellow of Queen's College, Cambridge, and a university demonstrator in physics at the Cavendish Lab., from 1945 to 1953. His research was in ionospheric physics and he spent six months during 1952 as a guest investigator at the Department of Terrestrial Magnetism, Carnegie Institution of Washington, Washington, D. C.

From 1954 to 1956, he was a senior principal scientific officer in the Ministry of Supply in London, working on basic electronics research and on the development of ground radar for the R.A.F. and Army. From 1956 to the present time, he has been employed by Associated Universities, Inc., at the National Radio Astronomy Observatory, Green Bank, West Va.

He is a member of the O.B.E., an Associate Member of the IEE (G. Brit.), and a Fellow of the London Physical Society.



Philip B. Gallagher (S'51-M'57) was born in Tacoma, Wash. on August 22, 1927. He received the B.E.E. degree in 1949 from the University of Santa Clara. After attending Illinois Institute of Technology, Chicago, for one year, he went to Stanford University, Stanford, Calif., where he received the M.S. degree in 1951. From 1951 to 1955, he was a research assistant with the Radio Prop-



P. B. GALLAGHER

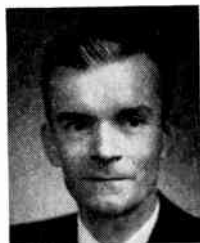
agation Laboratory at Stanford University. In 1956 he received the Ph.D. degree in electrical engineering specializing in radio propagation.

He is now continuing at the Stanford Radio Propagation Laboratory as a research associate, working on problems in ionospheric radio propagation.

Dr. Gallagher is a member of Sigma Xi, Tau Beta Pi, and Eta Kappa Nu.



John E. Gibson was born in Gibson, N. C. on December 25, 1914. In 1939, he received the B.S. degree in physics from the University of North Carolina, Chapel Hill, N. C.



J. E. GIBSON

He joined the Naval Research Laboratory in 1940, where, during the war years, he was engaged initially in very-high frequency communication transmitter development and later in research and invention concerning centimeter-wavelength rf circuits for car-tridge triodes and diodes.

Since 1951, Mr. Gibson has been connected with the radio astronomy program of the Naval Research Laboratory, where in addition to developing receiving systems and conducting observational studies of solar and lunar radiation, he participated in solar eclipse expeditions to the Sudan in 1952 and to Sweden in 1954.

Mr. Gibson is a member of U.S.A. Commission 5 of the International Scientific Radio Union.



Jesse Goodman (S'43-A'48-M'55) was born in New York, N. Y., on February 25, 1921. He received both the Bachelor's degree and the Master's degree in electrical engineering from New York University, New York, N. Y., in 1946 and 1949, respectively.



J. GOODMAN

From 1946 to 1948, Mr. Goodman was a development engineer with Hazeltine Electronics Corporation, Little Neck, N. Y. where he was mainly concerned with the design of radar receivers.

In August, 1948, he joined the receiver group at Airborne Instruments Laboratory, Mineola, N. Y. and participated in the development of countermeasures radar diversity and propagation equipments and receivers for radio astronomy applications. Mr. Goodman is now project engineer at Airborne Instruments Laboratory in the Applied Electronics Department, where he is in charge of the design of large-scale special purpose receiving systems.

Fred T. Haddock (A'42-M'55) was born in Independence, Mo., on May 31, 1919. He received the S.B. degree in physics from the Massachusetts Institute of Technology in 1941. He was awarded the M.S. degree in physics by Maryland University in 1950. In 1941, he joined the Naval Research Laboratory, where he did research in the field of microwave components and antennas. After 1946, he was engaged in radio astronomy research at NRL. Since February, 1956, he has been an associate professor in the Departments of Electrical Engineering and Astronomy at the University of Michigan, where he is in charge of the radio astronomy project.



F. T. HADDOCK

He is US Chairman of the URSI Commission on radio astronomy. He is a member of the American Physical Society, American Astronomical Society, International Astronomical Union, a Fellow of the Royal Astronomical Society, and Sigma Xi.

❖

D. S. Heeschon was born in Davenport, Iowa, in 1926. He received the B.S. degree in engineering physics from the University of Illinois, Urbana, Ill., in 1949, and the Ph.D. degree in astronomy from Harvard University, Cambridge, Mass., in 1954. He then taught for one year at Wesleyan University, Middletown, Conn. In 1955, he returned to Harvard as a lecturer and research associate. He is now with the National Radio Astronomy Observatory.



D. S. HEESCHON

Dr. Heeschon is a member of the American Astronomical Society, URSI, and Sigma Xi.

❖

J. S. Hey was born in Nelson, Eng., in 1909. He majored in physics and was graduated from the University of Manchester in 1930. This was followed by research work in X-ray crystallography for which he received the M.Sc. degree in 1931. He joined the Ministry of Supply in 1940, as a member of an operational research group dealing with radar problems. After World War II, he carried out research in radio astronomy and was awarded the degree of D.Sc. at the University of Manchester in 1950. He is now on the staff of the Royal Radar Establishment, Malvern, Eng.



J. S. HEY

❖

Mr. Hey is a Fellow of the Royal Astronomical Society and a Fellow of the Physical Society of Great Britain.



V. A. Hughes was born in Manchester, Eng., in 1925. He received the B.Sc. degree from the University of Manchester in 1944.



V. A. HUGHES

Following a period at the Telecommunications Research Establishment, he returned to the University of Manchester for three years of research in radio astronomy at the Jodrell Bank Experimental Station and he received the M.Sc. degree in 1950. Mr. Hughes is now a member of the staff of the Royal Radar Establishment, Malvern, Eng.

Mr. Hughes is a Fellow of the Royal Astronomical Society and a Fellow of the Physical Society of Great Britain.



Joseph J. Hunaerts was born in Brussels, Belgium, on July 6, 1912. He specialized in astrophysics at the University of Brussels, Belgium, where he received the degree of Doctor of Science.



J. J. HUNAERTS

In 1936, he joined the staff of the Royal Observatory of Belgium. He contributed many papers on the molecular spectra of the sun and the comets. He is now engaged in ionospheric research and particularly in the interpretation of the behavior of the ionosphere during solar eclipses.

Dr. Hunaerts is a member of Commissions 15 (cometary physics) and 36 (spectrophotometry) of the IAU.



C. M. Jansky, Jr. (A'18-M'25-F'28) was born on November 28, 1895 in Barry County, Mich. He received the B.S. degree in physics in 1917 and the M.S. in 1919, both from the University of Wisconsin. Mr. Jansky taught and supervised undergraduate and post-graduate work in radio communication and electronics at the University of Minnesota, from 1920 to 1929, where he was an associate professor in radio engineering.



C. M. JANSKY, JR.

In 1920, he established the first radio broadcasting station west of the Mississippi, in Minneapolis, Minn.

Mr. Jansky served as a member of the four radio conferences called by the U. S. Government to deal with radio regulation and proposals for new legislation, resulting in the passage of the Radio Act of 1927. During World War II, he was Special Consultant to the Secretary of War, attached to the headquarters of the Army Air Force. He was concerned with operational research, dealing with the use of radar and radio communication in air defense. During the war, he was also a member of the communications division of the National Defense Research Committee of the Office of Scientific Research and Development.

Mr. Jansky was a member of the U. S. delegation to International Conferences on Marine Radio Aids to Navigation, London, 1946, and New York and New London, Conn., 1947. He was chairman of Panel 5 on Frequency Modulation Broadcasting of the Radio Technical Planning Board from 1944 to 1945. He was the industry advisor to the U. S. delegation, International Telecommunications Conference in 1947 and chairman of the panel on Marine Navigation of the Committee on Navigation, Research and Development Board, the Department of Defense, from 1942 to 1952.

He was a member of the U. S. delegation to the Maritime VHF Telephone Conference, The Hague, Netherlands, January, 1957. He was a member of the U. S. Observer Delegation to the Baltic and North Sea Telecommunications Meeting on Rescue Cooperation, Goteborg, Sweden, September, 1955. In July, 1957, he was honored guest at the Radio Astronomy Conference, Essen, Germany. Mr. Jansky is a member of the U. S. Dep't. of Commerce, Bureau of Foreign Commerce, delegation to the U. S. Trade Mission to Scandinavia, and the International Trade Fair, Stockholm, Sweden, September, 1957. Mr. Jansky is a registered Professional Engineer in the District of Columbia.

Mr. Jansky was president of the IRE in 1934; he was on the Board of Directors from 1929-1942. He served on the Executive committee and various Committees of the Radio Tech. Commission for Marine Services since 1947. He is a member of the IEE, and the American Radio Relay League since 1920. He is a member of Sigma Xi, the Cosmos Club of Washington, D. C., the U. S. Observer Delegation to the Baltic and North Sea Telecommunications Meeting on Rescue Cooperation, Goteborg, Sweden, September, 1955.



Henry Jasik (A'40-SM'47) was born in New York, N. Y. on March 12, 1919. He received the B.S.E.E. degree from the Newark College of Engineering, in 1938, and the D.E.E. degree from the Polytechnic Institute of Brooklyn, in 1953.



H. JASIK

Dr. Jasik worked with the Navy Department from 1938 to 1939, and with the Civil Aeronautics Administration from 1939 to 1944. From 1944

to 1946, he served as an officer in the U. S. Navy, stationed at the Naval Research Laboratory, where he worked on the development of airborne radar and communications antennas. From 1946 to 1949, he was associated with Andrew Alford, Consulting Engineers as senior project engineer and as vice-president of the Alford Manufacturing Company. From 1949 to 1952, he was employed by the Airborne Instruments Laboratory. Here he was associated with the Special Devices Section and with the Antenna Section, where he was assistant supervising engineer.

Since September 1952, Dr. Jasik has been engaged as an independent consulting engineer. In 1955, he organized Jasik Laboratories. He has been active in the antenna field and allied fields for the past 15 years and is currently working on antenna problems in the radio astronomy field. During the past several years, he has developed the feed systems for a number of large radio telescopes in this country.

Dr. Jasik is a member of Sigma Xi and Eta Kappa Nu and is a registered Professional Engineer in the State of New York.



André Koeckelenbergh was born in Haselt, Belgium, in 1929. He received the M.A. degree in physical science in 1951 from Brussels University, Belgium.



A. KOECKELENBERGH

In 1952, he joined the staff of the Royal Observatory of Belgium at the department of solar physics and radio astronomy. With Dr. Coutrez and Mr. Pourbaix, he made the determination of localized radiosources on meter wave in the solar corona from the radio observations of the solar eclipse on February 25, 1952 in Lwiro and N'Gili (Belgian Congo) and Dakar. Since 1954, he has been engaged as assistant astronomer in charge of solar visual and radio observations.



Hsien Ching Ko (S'53-M'56) was born in Formosa, China on April 28, 1928. He received the B.S. degree in electrical engineering from the National Taiwan University in 1951 and worked as a junior engineer at the Radio Wave Research Laboratories in China.



H. C. KO

In 1952, he entered Ohio State University, from which he received the M.S. and Ph.D. degrees in electrical engineering in 1953 and 1955, respectively. From 1952 to 1955, he was engaged in research in radio astronomy as research assistant at the Ohio State University Radio Observatory.

In 1955, Dr. Ko joined the staff of Ohio State University, where he is now an assistant

professor of electrical engineering and assistant director of the Radio Observatory.

Dr. Ko is a member of Sigma Xi, Pi Mu Epsilon, Eta Kappa Nu, and the American Astronomical Society.



John D. Kraus (A'32-M'43-SM'43-F'54) was born in Ann Arbor, Mich., on June 28, 1910. He attended the University of Michigan, receiving the B.S. degree in 1930, the M.S. degree in 1931, and the Ph.D. degree in physics in 1933. From 1934 to 1935, he did research on industrial noise reduction problems and from 1936 to 1937, was engaged in nuclear research with the newly completed University of Michigan cyclotron.



J. D. KRAUS

From 1938 to 1940, Dr. Kraus was an antenna consultant. In 1940, he joined the Naval Ordnance Laboratory, Washington, D. C., working on the degaussing of ships, and in 1943 he became a member of the Radio Research Laboratory at Harvard University. In 1946, he joined the faculty of the Ohio State University, where he is now professor of electrical engineering, professor of physics and astronomy, and Director of the Radio Observatory. Professor Kraus is the author of books on antennas and electromagnetic theory and of numerous articles on antennas and radio astronomy topics. He is responsible for the development of the helical beam antenna, the corner reflector antenna, and other antenna types.

He is a member of the American Astronomical Society and the American Physical Society.



Robert S. Lawrence was born on October 28, 1925 in Worcester, Mass. After serving for three years in the U. S. Army, he attended Worcester Polytechnic Institute and received the B.S. degree in physics in 1949. After receiving the M.S. degree from Yale University in 1950, he joined the radio division of the National Bureau of Standards. He soon became associated with the radio astronomy work of the



R. S. LAWRENCE

laboratory and is now project leader of that work. His present activities include study of the ionosphere by means of radio noise from the sun, discrete radio sources, and artificial satellite transmissions. He visited Harvard College Observatory, 1954-1955, where he was engaged in 21-cm radio astronomy research.

Mr. Lawrence is a member of Sigma Xi, RESA, the American Astronomical Society, and U. S. Commission 5 of URSI.

Matthew T. Lebenbaum (A'42-M'46-SM'46) was born in Portland, Ore., on November 29, 1917. He received the B.A. degree from Stanford University, in 1938, and the M.S. degree from the Massachusetts Institute of Technology, in 1945. After two years as a research and teaching assistant, at M.I.T., he joined the American Gas and Electric Service Corporation as a system planning engineer. From 1942



M. T. LEBENBAUM

to 1945, he was a research associate at the Radio Research Laboratory of Harvard University and participated in countermeasures receiver development at Harvard and in England with TRE and ABL-15. In 1945, he joined Airborne Instruments Laboratory and is now head of the Applied Electronics Department, where his work has been largely concerned with special receiver design for countermeasures, radar, and propagation and radio astronomy applications.



Harold Leinbach was born in Fort Collins, Colo. on January 7, 1929. He received the B.S. degree from South Dakota State college in 1949, and the M.S. degree in astronomy from California Institute of Technology, Pasadena, Calif., in 1950.



H. LEINBACH

Prior to his Army service, Mr. Leinbach spent three years in auroral studies at the Geophysical Institute, College, Alaska. Since his return in 1956, he has been active in the study of high-latitude radio wave absorption. He has participated in the development of the "riometer," a device designed for the routine measurement of ionospheric absorption during IGY.



A. E. Lilley was born in Mobile, Ala., May 29, 1928. He graduated from the University Military School in 1946. He received Bachelor's and Master's degrees in physics, in 1950 and 1951, respectively, from the University of Alabama. During 1951 to 1954, he attended Harvard University, where he received the Ph.D. degree in astronomy. From 1954 to 1957, he was a member of the Radio Astronomy Branch at



A. E. LILLEY

the Naval Research Laboratory engaged in various radio astronomical problems. At present, he is assistant professor of astronomy at Yale University.

A. G. Little was born on February 2, 1925, in Sydney, New South Wales, Australia. As a part-time student, he received a diploma in applied physics in 1950 from the Sydney Technical College, while employed by the Commonwealth Scientific and Industrial Research Organization. Later he attended the N.S.W. University of Technology and received the B.Sc. degree in applied physics in 1954.



A. G. LITTLE

At present he is engaged in research on radio astronomy at the Radiophysics Division of CSIRO.



C. Gordon Little (M'56) was born in Liu Yang', Hunan Province, China, on November 4, 1924. Before graduating from the University of Manchester, England in 1948 with the B.Sc. in Honours Physics, he worked in industrial research laboratories for three years on the design of high-voltage rectifiers and electrometer tubes.



C. G. LITTLE

After carrying out graduate studies at the Jodrell Bank Radio Astronomy Research Center of the University of Manchester, Dr. Little was awarded the Ph.D. degree in 1952. In January, 1954 he took up an appointment as visiting professor of geophysics and senior research scientist at the Geophysical Institute of the University of Alaska. Since July, 1954, Dr. Little has been deputy director of the Geophysical Institute and is in charge of the research programs in ionospheric physics and arctic radio wave propagation.

Dr. Little is a Fellow of the Royal Astronomical Society, London, and an Associate Member of the Arctic Institute of North America.



Mrs. Leona Marshall was born in 1918. She received the B.S. and Ph.D. degrees both from the University of Chicago, in 1932 and 1943, respectively. From 1942 through 1944, Dr. Marshall was a research associate, Manhattan District, and, from 1944-1946, she was a consultant at the E. I. du Pont de Nemours & Co., Hanford, Wash. She returned to the University of Chicago, where she was a post doctoral fellow from 1946 through 1948, a research



L. MARSHALL

associate, from 1948–1954, and assistant professor at the Fermi Institute, from 1954 to the present time.

❖

D. S. Mathewson was born in Brisbane, Australia, on June 21, 1929. He received the B.S. and M.S. degrees in physics from the University of Queensland in 1952 and 1954, respectively. From 1950 to 1955, he was employed in the Radiation Physics Department of the University of Queensland investigating problems in medical physics, particularly the application of photographic film in  $\gamma$  and  $\beta$ -ray dosimetry. He



D. S. MATHEWSON

joined the Division of Radiophysics of the CSIRO in 1955 and has been primarily engaged in the building of the crossed multiple interferometer at St. Marys, Sydney.

❖

Alan Maxwell was born in Auckland, New Zealand, on October 21, 1926. He received the degrees of B.Sc. and M.Sc (Hons)



A. MAXWELL

in physics from the University of New Zealand, and the Ph.D. degree in physics from the University of Manchester, Eng. From 1950–1955, he did research work in radio astronomy at the Jodrell Bank Experimental Station of the University of Manchester, and, from 1952–

1955, also lectured in the Department of Physics. In 1955, he joined Harvard University to lead a new research program in solar radio astronomy.

Dr. Maxwell is a Fellow of the Royal Astronomical Society, the Physical Society of London, a member of the American Astronomical Society, and a Fulbright Scholar.

❖

Cornell H. Mayer (M'47) was born on December 10, 1921, in Ossian, Iowa. He received the B.S. degree in electrical engineering from the State University of Iowa in 1943, and the M.S. degree in electrical engineering from the University of Maryland in 1951.



C. H. MAYER

In 1943, he joined the staff of the Naval Research Laboratory, Washington, D. C., to work on the development of micro-

wave radar. Since 1948, he has been associated with the Radio Astronomy program at the Naval Research Laboratory.

Mr. Mayer is a member of the Scientific Research Society of America, and the American Astronomical Society.

❖

Edward F. McClain (M'49–SM'53) was born in Carrollton, Mo. on August 22, 1921. He attended Missouri School of Mines from 1939 to 1942 and received the B.E.E. degree from George Washington University in 1950.



E. F. McCLAIN

Mr. McClain has been employed by the Naval Research Laboratory since February 1942. He was in charge of a group doing research and development on microwave radar until 1947. At that time he was placed in charge of a program which culminated in the development of the first doppler airborne navigation system. An outgrowth of this work is the Navy's recently announced AN/APN-67 automatic navigator. Mr. McClain was placed in charge of a 21-cm research group at NRL in 1953 and shortly thereafter made the first 21-cm absorption measurements. Under this program, absorption measurements on a number of radio stars, as well as the hydrogen line red-shift experiments were conducted. In September, 1956, Mr. McClain was placed in charge of the Radio Astronomy Branch in which capacity he has continued until the present.

Mr. McClain is a member of the American Astronomical Society, URSI, Sigma Tau, and RESA.

❖

Claudius T. McCoy, for a photograph and biography please see page 1295 of the September, 1957 issue of PROCEEDINGS.

❖

Timothy P. McCullough was born in Vardaman, Miss. on December 9, 1910. He received the B.A. degree in physics from the University of Mississippi in 1936, and the M.S. degree in physics from North Carolina State College in 1937.



T. McCULLOUGH

From 1937 to 1942, he was an instructor in physics at Mississippi State College. In September, 1942, he joined the Physics Department, University of Mississippi, and in August, 1943, went on military leave as a commissioned officer in the Naval Reserve, where he served as instructor in physics at the U. S. Naval Academy until

July, 1946. Mr. McCullough joined the Naval Research Laboratory, Washington, D. C., in July, 1946 and has been engaged in radio astronomy research, except for a three year period during the Korean War. During this time, he was on active military duty as technical adviser at the Navy Training Publication Center, Washington, D. C.

❖

Wilford J. Medd (M'54) was born on August 17, 1914, in Nobleford, Alberta, Canada. He studied at the University of Alberta, Edmonton, Alberta, from which he received the B.S. degree in engineering physics in 1946.



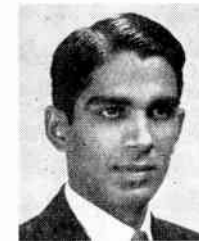
W. J. Medd

Mr. Medd then joined the staff of the National Research Council of Canada at Ottawa, where he has been engaged in research in the field of radio astronomy.

He is a member of the Royal Astronomical Society of Canada.

❖

T. K. Menon was born on December 19, 1926 in Tattamangalam, South India. He obtained the degree of B.Sc. (Hons.) in physics from Annamalai University, Madras State, in 1947. He studied electrical communication engineering at the Indian Institute of Science, Bangalore, South India and received the E.C. degree in 1950.



T. K. MENON

Mr. Menon was a research assistant in the department of Electrical Communication at the Indian Institute of Science from 1950–1952. He worked on problems of instrumentations for inospheric studies. Mr. Menon joined Harvard in 1952. He received the S.M. degree in applied physics in 1953 and the Ph.D. in astronomy in 1956, both from Harvard University.

Since July, 1956, Dr. Menon has been a lecturer in astronomy, and the Agassiz Radio Astronomer at Harvard College Observatory. Since February, 1957, Mr. Menon has been in charge of the Agassiz Station Radio Astronomy Project.

He is a member of the American Astronomical Society.

❖

B. Y. Mills was born on August 8, 1920, in Sydney, Australia. He received the degree of B.Sc. in 1940, the B.E. in 1942, and the M.E. in 1950, all from the University of Sydney, Australia. He joined the staff

of the Division of Radiophysics, Commonwealth Scientific and Industrial Research Organization, in 1942 and in the ensuing



B. Y. MILLS

four years was engaged in the design and development of radar equipment. From 1946 to 1948, he worked in the Valve Laboratory of the Division, developing a high voltage X-ray tube employing a magnetron-fed resonant cavity. In 1948 he joined

the radio astronomy group engaging in the investigation of various aspects of this new science.

Mr. Mills is a Fellow of the Royal Astronomical Society.



Hays Penfield (S'51-A'53-M'57) was born on October 26, 1926, in Philadelphia, Pa. He received the B.A. degree in physics from Williams College, Williamstown, Mass., in 1952, and the B.S.E.E. and the M.S.E.E. degrees from Massachusetts Institute of Technology, Cambridge, Mass., in 1952.



H. PENFIELD

From 1944 to 1946, he was a petty officer with the U. S. Navy.

He joined the General Electric Co. in 1950 as a cooperative student and worked on the development and design of aircraft fuel mass gages and fuel mass flow meters, and the design and construction of automatic electronic test equipment for production-line testing.

Later, as staff member with M.I.T.'s Lincoln Laboratory, he was concerned with research and development work on radar systems using correlation techniques and information theory. He developed and designed low-noise receiver front ends, IF amplifiers, limiters, video amplifiers, pulse circuits, electromechanical delay lines, signal generators, target simulators and other associated equipment.

In his present work as a project engineer with the Ewen Knight Corporation, he has developed special uhf radiometric and interferometric equipment.

Mr. Penfield is a member of Phi Beta Kappa, Sigma Xi, and Eta Kappa Nu.



J. H. Piddington was born on November 6, 1910 in Wagga, New South Wales, Australia. He received the B.Sc. degree from the University of Sydney in 1931 and the B.E. degree in 1933. He carried out research in electronics, mainly radar, at Sydney and Cambridge, Eng., where he received the Ph.D. degree in 1938. Fulltime work on radar at Sydney University and then at the Radiophysics Laboratory of CSIRO, Syd-

ney, Australia, continued until 1945, during which time he designed the LW/AW air warning set used by US and Australian



J. H. PIDDINGTON

forces. From 1945 to 1947, he was engaged in the development of civil aviation radio navigational aids, including the Australian version of distance measuring equipment (dme). In 1947, he turned to radio astronomy and headed an experimental microwave team until 1953; during this period he became increasingly interested in the theoretical aspects of this work. Now, in addition to this theoretical work, he is concerned with general cosmical electromagnetics.



Grote Reber was born in Chicago, Ill., on December 22, 1911. He graduated from the present Illinois Institute of Technology in



G. REBER

1933. He worked in an engineering capacity for several radio manufacturers in Chicago from 1933-1947. He was at the National Bureau of Standards, from 1947 to 1951, as a radio physicist. From 1951 to the present, he has been associated with the Research Corporation, conducting various experiments relating to radio astronomy in Hawaii and Tasmania.



Nancy G. Roman was born in Nashville, Tenn., on May 16, 1925. She attended Swarthmore College, Swarthmore, Pa., receiving the B.A. degree in 1946. She then attended the University of Chicago, Chicago, Ill., and received the Ph.D. degree in 1949. From 1946 to 1949, she worked at the University of Chicago in the department of astronomy and astrophysics, as a research assistant. In 1949,



N. G. ROMAN

she became a research associate. She was appointed an instructor in 1951 and became an assistant professor in 1954. In 1955, she was employed by the United States Naval Research Laboratory as an astronomer in the radio astronomy branch. She is, at present, section head of the Microwave Spectroscopy Section. Dr. Roman's field of research has been in observational astronomy with emphasis on galactic structure and stellar motions. This has included: spectral classification, photoelectric photometry, and radial velocity measurements,

particularly as applied to star clusters, high velocity stars, and stellar population problems. Research in radio astronomy has been concerned with the spectra of radio "stars."

She is a member of the American Astronomical Society, Royal Astronomical Society, IAU, US Commission V of URSI, and the Scientific Research Society of America.



C. A. Shain was born in Sandringham, Victoria, Australia, on February 6, 1922. He received the B.S. degree from the University of Melbourne in 1943



C. A. SHAIN

while serving with the Australian Army. Since 1943, he has been with the Division of Radiophysics of the Commonwealth Scientific and Industrial Research Organization, Sydney, Australia. Following several years of radar development during the war, since 1946 he has been working in the field of radio astronomy. This work has included studies of moon echoes, the absorption of extraterrestrial radiation in the ionosphere, and radiation from Jupiter; however, Mr. Shain's main interest is the study of cosmic noise at frequencies below 20 mc.

Mr. Shain is a Fellow of the Royal Astronomical Society.



Kevin V. Sheridan was born in Brisbane, Australia, on August 4, 1918. He joined the Radio Physics Division of the CSIRO in



K. V. SHERIDAN

Laboratory.



O. B. Slee was born in Adelaide, South Australia, on August 10, 1924. Upon completing his high school education, he joined



O. B. SLEE

the radar section of the R.A.A.F. in which he served for four years during World War II. After the war, he joined the staff of the Division of Radiophysics, Commonwealth Scientific and Industrial Research Organization in Sydney, and since then has been

working on some of the many radio astronomy projects conducted by the Laboratory. He was awarded diplomas in radio engineering and applied physics by the New South Wales University of Technology in 1952 and 1955, respectively, and is currently working towards a physics degree from the same institution.

❖

Russell M. Sloanaker, Jr. was born on October 29, 1921 in Philadelphia, Pa. He received the B.S. degree in physics from the Pennsylvania State University in September, 1943. He joined the staff of the Naval Research Laboratory, Washington, D. C., in November, 1943, where he worked until 1948 on the development and testing of radar equipment. During this time, he was on active duty in the U. S. Navy, assigned to the Laboratory, for one year.



R. M. SLOANAKER

From June, 1948 until the present, he has worked at the Naval Research Laboratory in the field of radio astronomy.

❖

Charles V. Stableford was born in Kingman, Ariz., on May 5, 1931. He received the B.S. degree in chemistry and mathematics at Arizona State College, Flagstaff, Ariz. From 1951 to 1953, he was employed at the Lowell Observatory, Flagstaff, Ariz., as a research assistant.



C. V. STABLEFORD

In the autumn of 1953, Mr. Stableford entered the University of California, Berkeley, Calif., where he is doing graduate work in astronomy.

❖

Jean-Louis Steinberg was born in Paris, France, on June 7, 1922. He received the Licence ès Sciences from Paris University, Paris, France, in 1943. Captured by the German Forces in 1944, he spent a year in a concentration camp in Poland. He entered the Laboratoire de Physique de l'Ecole Normale Supérieure in 1945 and started with others a radio astronomy program. He obtained the Doctorat ès Sciences Physiques in 1950. Since



J. L. STEINBERG

1956, he has been at the Meudon Observatory, Paris, with the Radioastronomy Group. He was appointed Astronome Adjoint in 1957. Mr. Steinberg is now engaged in the development of microwave equipments for radio astronomy and investigation of solar radiation at 3-cm wavelength and its propagation through the terrestrial atmosphere.

❖

Peter D. Strum (A'45-SM'55) was born in Brunswick County, Va., on April 25, 1922. He received the B.E.E. degree with honors from North Carolina State College, Raleigh, N. C., in 1945, and the M.S. degree in electrical engineering from Stanford University, Stanford, Calif., in 1947.



P. D. STRUM

Mr. Strum was an instructor at North Carolina State College in 1944 and 1945, following the completion of his undergraduate studies.

In 1947, he joined the engineering staff of Airborne Instruments Lab., Mineola, N. Y., where he participated in receiver research and the development of receivers, beacons, automatic direction finders, and test equipment. In 1952, he was appointed assistant supervising engineer of the Applied Electronics Section.

In May, 1955, Mr. Strum joined the staff of National Company, Malden, Mass., as chief engineer of the receiver department, concerned with the development of communication receivers.

Since October, 1955, Mr. Strum has been with the Ewen Knight Corporation, Needham Heights, Mass., where he is concerned with the development of radio astronomy receivers.

Mr. Strum is a member of Sigma Xi, Tau Beta Pi, and Eta Kappa Nu.

❖

Shigemasa Suzuki was born in Tokyo, Japan on March 14, 1920. He received the undergraduate degree of Bachelor of Science in electrical engineering from Waseda University in 1942.



S. SUZUKI

After working for radio manufacturing companies, Mr. Suzuki joined the staff of Tokyo Astronomical Observatory in 1949, where he has been concerned with the development of observational equipments in the field of radio astronomy.

Mr. Suzuki is a member of the Astronomical Society of Japan.

Govinda Swarup was born in 1929 in Thakurdwara, U. P., India. He studied at Allahabad University, Allahabad, India, where he obtained the M.Sc. degree in physics and electronics, in 1950. From 1951 to 1953, he worked as Secretary to the Radio Research Committee, CSIR, India. Since 1953, he has been studying the characteristics of radio emission from the sun. From 1953 to 1955, he worked at the Radio Physics Laboratory, CSIRO, Sydney, Australia, under a Colombo Plan fellowship. He worked at the National Physical Laboratory, New Delhi, India, from 1955 to 1956. Later, he was a research associate at the Harvard College Observatory for one year. At present, Mr. Swarup is doing research work at Stanford University, Stanford, Calif.



G. SWARUP

Anthony Richard Thompson was born in Yorkshire, England. In 1949, he was awarded a State Scholarship to Manchester University, where he received the B.Sc. (Honours) degree in physics, in 1952. From 1952 through 1956, he worked in radio astronomy at Jodrell Bank Experimental Station of the University of Manchester, and in 1956 he received the Ph.D. degree. For nearly two years, Dr. Thompson also worked with E.M.I. Electronics, Ltd., Feltham, Middlesex, on missile guidance and telemetry problems. He is now a research associate of Harvard College Observatory and is at the Harvard Radio Astronomy Station, Fort Davis, Texas.



A. R. THOMPSON

He is a member of the Institute of Physics.

❖

James H. Trexler (S'41-A'44) was born in Missoula, Mont., on May 18, 1918. He attended the Engineering School at Southern Methodist University, Dallas, Tex., from 1936 to 1941. While in school, he did extensive work on the characteristics of meteor spherics. From 1940 to 1942, he was associated with Radio Station WRR in Dallas, Tex. In 1942, he joined the staff of the Naval Research Laboratory



J. H. TREXLER

working in the field of direction finding. His work at the Laboratory since 1946 has been concerned with the directional characteristics of low-level modes of wave propagation. Mr. Trexler is a member of RESA.

Atsushi Tsuchiya was born in Kanazawa, Japan on June 11, 1928. He received the undergraduate degree of Bachelor of Science in astronomy from the University of Tokyo, Tokyo, Japan in 1953.



A. TSUCHIYA

Following his graduation, Mr. Tsuchiya joined the staff of Tokyo Astronomical Observatory, where, for the past four years, he has been engaged in studies in the field of radio astronomy.

Mr. Tsuchiya is a member of the Astronomical Society of Japan.



Harry W. Wells (M'36-SM'43-F'53) was born in Washington, D. C. on January 13, 1907. He received the B.S.E.E. degree in 1928 and the E.E. degree in 1937, both from the University of Maryland, College Park, Md. From 1928-1931, he was engaged in radio engineering activities with the Westinghouse Electric and Manufacturing Co., the All-American Expedition to Borneo, and Heintz and Kaufman, San Francisco, Calif. In 1932, he completed pilot training with

the Air Force and served on active duty as Communications Officer, Langley Field, Va.

Since 1932, Mr. Wells has been a member of the technical and scientific staff of the Carnegie Institution of Washington. He is Chairman of the Upper Atmospheric Section which has conducted pioneering research in problems of the upper atmosphere, the ionosphere, radio wave propagation, and communications.



H. W. WELLS

More recently, he and his associates have pioneered in the study of ionospheric "winds" or traveling disturbances and have initiated a program of research in radio astronomy for studies of radio frequency radiations from the sun and certain "radio" stars.

He has been affiliated with several committees of the Research and Development Board and served to 1953 as Chairman of the Sub-Panel on Propagation, Electronics Committee. In 1947, he received the Award for Scientific Achievement in the Engineering Sciences conferred by the Washington Academy of Sciences. Mr. Wells is Chairman of the USA National Committee of URSI and a member of the Washington Academy

of Sciences, the American Geophysical Union, and the Philosophical Society of Washington.



J. P. Wild was born in Sheffield, Yorkshire, England in 1923. He received the B.A. degree in mathematics and physics at the University of Cambridge in 1943, and received the M.A. degree in 1946. From 1943 to 1947, he was a ship's radar officer in the British Navy.



J. P. WILD

In 1947, Mr. Wild settled in Australia and joined the staff of the CSIRO Radiophysics Laboratory in Sydney. Since 1948, he has been engaged in research in radio astronomy, with the exception of a 15-month period in Europe and the United States during 1954-1955.



Benjamin S. Yaplee, for a photograph and biography please see p. 1027 of the July, 1957, issue of PROCEEDINGS.



# IRE News and Radio Notes

## Calendar of Coming Events and Authors' Deadlines\*

1958

- Nat'l Symp. on Reliability & Quality Control, Statler Hotel, Wash., D. C., Jan. 6-8
- Symp. on Artificial Heart, Lung & Kidney Machines, Rockefeller Med. Elec. Center, New York City, Jan. 15
- Scintillation Counter Cymp., Shoreham Hotel, Wash., D. C., Jan 27-28
- Aviation Day, New York City, Jan. 29
- Cleveland Elec. Conf., Masonic Audit., Cleveland, Ohio, Feb. 14-15
- Transistor-Solid State Circuits Conf., Phil., Pa., Feb. 20-21
- Nuclear Eng. and Science Congress, Palmer House, Chicago, Ill., Mar. 17-21
- IRE Nat'l Convention, N. Y. Coliseum and Waldorf-Astoria Hotel, New York City, Mar. 24-27 (DL\*: Nov. 1, G. L. Haller, IRE Headquarters, New York City)
- Instruments & Regulators Conf., Univ. of Del., Newark, Del., March 31-Apr. 2
- Conf. on Automatic Optimization, Univ. of Del., Apr. 2-4
- Symp. on Electronic Waveguides, Eng. Soc. Bldg., New York City, Apr. 8-10
- SW Regional Conf. & Show, Mun. Audit., San Antonio, Tex., Apr. 10-12
- Conf. on Automatic Techniques, Statler Hotel, Detroit, Mich., Apr. 14-16
- British Radio & Elec. Components Show, Grosvenor House and Park Lane House, London, Eng., Apr. 14-17
- Elec. Components Symp., Ambassador Hotel, Los Angeles, Calif., Apr. 22-24 (DL\*: Nov. 15, E. E. Brewer, Convair, Pomona, Calif.)
- Semiconductor Symposium of Electrochemical Society, Statler Hotel, New York City, Apr. 30-May 1
- Seventh Region Conf. & Show, Sacramento, Calif., Apr. 30-May 2
- PGMTT Symp., Stanford Univ., Stanford, Calif., May 5-7 (DL\*: Jan. 15, K. Tomiyasu, G. E. Microwave Lab., 601 California Ave., Palo Alto, Calif.)
- Western Joint Computer Conf., Ambassador Hotel, Los Angeles, Calif., May 6-8 (DL\*: Jan. 15, Tech. Program, Chairman, P. O. Box 213, Claremont, Calif.)
- Nat'l Aero. & Nav. Elec. Conf., Dayton, Ohio, May 12-14
- IEE Convention on Microwave Values Savoy Place, London, England, May, 10-23
- \*DL=Deadline for submitting abstracts.

(Continued on page 375)

## BIBLIOGRAPHICAL BULLETIN ON COMPUTERS AVAILABLE

Iota Services, Ltd. has announced publication of a monthly annotated bibliographical bulletin covering all material published in Great Britain, the United States, and in other countries in the field of computers. The bulletin may be subscribed to for £6.6s per year from Iota Services, Ltd., 38 Farrington St., London E.C.4, England.

## IRE ELECTS OFFICERS FOR 1958

Donald G. Fink (A'35-SM'45-F'47), Director of Research of the Philco Corporation, Editor of the IRE for the past two years, has been named president of the Institute of Radio Engineers for 1958. Mr. Fink succeeds John T. Henderson (A'28-SM'47-F'51), Principal Research Officer of the National Research Council, Ottawa, Canada, as head of the 64,000-member society.

Carl-Eric Granqvist (A'46-F'55), Director of Svenska Aktiebolaget Gasaccumulator, Stockholm-Lidingo, Sweden will succeed Yasujiro Niwa (A'53-F'54), President of Tokyo Electrical Engineering College, Tokyo, Japan as IRE Vice-President.

Elected as directors for the 1958-1960 term are G. S. Brown (SM'53-F'55), Professor and Head of the Department of Electrical Engineering, Massachusetts Institute of Technology, Cambridge, Mass. and W. H. Doherty (A'29-M'36-SM'43-F'44), Assistant to the President of Bell Telephone Laboratories, Inc., New York, N. Y.

Regional Directors elected for 1958-1959 are as follows: Region 1—R. L. McFarlan (SM'51), Consultant, Chestnut Hill, Mass.; Region 5—E. H. Schulz (A'38-SM'46), Assistant Director of the Armour Research Foundation, Chicago, Ill.; Region 7—G. A. Fowler (A'48-SM'48), Vice-President of Research, Sandia Corporation, Albuquerque, N. M.

Because one of the nominees for the Region 3 directorship moved out of that region, a new election will be held in the near future for a Region 3 Director.

The 1958 IRE Vice-President was born on March 2, 1910 in Ljungby, Sweden. He has the Master of Art degree in electrical engineering from the Royal University of Technology in Stockholm.

Mr. Granqvist holds over twenty-five patents in the field of radio air navigation systems and devices. He has written several textbooks on radio and has also written descriptive booklets on the AGA talking beacon and the AGA vhf direction finder.

As Chief Engineer of Svenska Aktiebolaget Gasaccumulator, Stockholm-Lidingo, Sweden, he was in charge of design, research and development in the Electronic Laboratory of that company. His present title is Director of the Electronic Laboratory.

Mr. Granqvist also belongs to the Swedish society, Svenska Teknologforeningen. He has served as adviser on the Swedish Electric Committee and member of Standard Committee NK 50, too.

## MARS RADIO RELEASES PROGRAM

The Air Force MARS Eastern Technical Net which broadcasts over the air every Sunday afternoon at 2 p.m. (EST) on 3295, 7540, and 7635 kc announces the following programs for January and February: Jan. 5—"N-1 and J-4 Compass Systems," Bernard Lippner; Jan. 12—"Printed Circuits in Military and Civilian Electronics," R. L. Swiggert; Jan. 19—"Applications of Printed Circuits," Allan Kingsbury; Jan. 26—"Maintenance and Repair of Printed Circuits," Lynn Gunsaulus; Feb. 2—"Satellite Tracking with the Mini-Track," Matthew Lebenbaum; Feb. 9—"Antenna Symposium," Bruce Woodward; Feb. 16—"Antenna Symposium," Warren Offutt.

## IRE ANNOUNCES FURTHER AWARDS

The IRE Board of Directors has announced that the 1958 W. R. G. Baker Award will be given to Messrs. R. L. Kyhl and H. F. Webster of the Research Laboratory, General Electric Co., Schenectady, N. Y. for their paper entitled "Breakup of Hollow Cylindrical Electron Beams," which appeared in the October, 1956 issue of IRE TRANSACTIONS on Electron Devices. The award is given annually to the author(s) of the best paper published in the TRANSACTIONS of the IRE Professional Groups.

Arthur Karp (A'54) of Bell Telephone Labs., Inc., Holmdel, N. J., will be the recipient of the 1958 Browder J. Thompson Memorial Prize Award for his paper entitled "Backward-Wave Oscillator Experiments at 100 to 200 Kilomegacycles," which appeared in the April, 1957 issue of PROCEEDINGS OF THE IRE. The Thompson Award is given annually to an author under thirty years of age for a paper recently published by the IRE which constitutes the best combination of technical contribution and presentation of the subject.

Both awards will be presented at the annual banquet on March 26, 1958 at the Waldorf-Astoria Hotel in New York City during the 1958 IRE National Convention.

Seventy-five radio engineers and scientists from the United States and other countries have been named Fellows of the Institute of Radio Engineers. The grade of Fellow is the highest membership grade offered by the IRE and is bestowed only by invitation on those who have made outstanding contributions to radio engineering or allied fields. Photographs of the 1958 IRE Fellows will appear in the April issue of the PROCEEDINGS.

Presentation of the awards will be made by IRE Sections all over the world wherever the recipients reside. Recognition of the awards will be made by the IRE President at the annual banquet on March 26, 1958.

The recipients of the Fellow award, which takes effect January 1, 1958, include one from Brazil, one from Canada, and three from England. They are, respectively, Helio Costas, R. H. Tanner, J. A. Smale, F. H. Wells, and A. F. Wilkins.

## IRE NATIONAL CONVENTION SET FOR MARCH 24-27 AT NEW YORK

The 1958 IRE National Convention will be held at the Waldorf-Astoria Hotel and New York Coliseum in New York City, March 24 through 27.

More than 55,000 engineers and scientists from 40 countries are expected to attend. The 1957 convention drew 53,811.

A comprehensive program of 275 papers, covering the most recent developments in the fields of all 27 IRE Professional Groups, will be presented in 55 sessions at the Waldorf-Astoria and the Coliseum. The high point of the program will be two special symposia on "Electronics in Space" and "Electronic Systems in Industry," to be held Tuesday evening, March 25. Full program details will be announced in the March issue of the PROCEEDINGS OF THE IRE.

The Radio Engineering Show, which will occupy all four floors of the Coliseum, has been expanded to accommodate approximately 850 exhibitors. Approximately \$12,000,000 worth of the latest electronic equipment will be on display, much of it for the first time.

The convention will get under way with the Annual Meeting of the IRE on Monday morning, March 24. Dr. Ernst Weber, acting president of the Polytechnic Institute of Brooklyn, will be guest speaker.

The social events will include a "get-together" cocktail party Monday evening and the annual IRE banquet Wednesday evening, both in the Grand Ballroom of the Waldorf. The banquet will feature a speaker of national prominence and the presentation of the IRE annual awards for 1958. The toastmaster will be G. L. Haller, Gen. Elec. Co. Newly-elected IRE Fellows will also be honored. The spokesman for the new Fellows will be P. E. Haggerty, Texas Instruments. An entertaining program of tours, fashion shows and matinees has also been arranged for the wives of visitors.

All registration will take place on arrival either at the Waldorf or at the Coliseum. Registration fees are \$1.00 for each IRE member, \$3.00 for each non-member. Payment of the fee enables attendance at all sessions and exhibits.

## TWO SECTIONS CHANGE NAMES

On November 20, the IRE Board of Directors approved the change in status of the Berkshire Subsection to full Section, which will be known henceforth as the Western Massachusetts Section. At the same meeting, the Connecticut Valley Section changed its name to the Connecticut Section.

## PG AND SECTION CHANGES MADE

The IRE Executive Committee, at its meeting of December 11, approved the establishment of the Los Angeles Chapter of the Professional Group on Communications Systems.

At the same meeting, the Executive Committee approved the abolition of the Hampton Roads Subsection, and the formation of the Burlington Subsection of the Cedar Rapids Section.

## E. W. ENGSTROM WINS MEDAL

E. W. Engstrom (A'25-M'38-F'40),

Senior Executive Vice-President of RCA, was named recently as recipient of the Industrial Research Institute Medal for 1958.

The medal has been awarded annually since 1945 to honor "outstanding accomplishment in leadership in or management of industrial research which contributes broadly to the development of industry or the public welfare."

Dr. Engstrom, who joined RCA in 1930, has been Senior Executive Vice-President of the corporation since October, 1955. As director of RCA's television research during the 1930's, he was responsible for the development and construction of equipment and for the planning and coordination which led to the development of television. Continuing in charge of research during the 1940's, he was primarily responsible for the organization, growth and activities of RCA Laboratories, which was established as a separate division of RCA in 1942 at Princeton, N. J. At present, he is responsible for the research and development for the entire corporation.

## SWIRECO PLANS CONFERENCE ON INT'L GEOPHYSICAL YEAR

The St. Anthony Hotel and the Municipal Auditorium of San Antonio, Texas, will be the scene of the 1958 Southwestern IRE Conference and Electronic Show, April 10-12. Ten technical sessions will be conducted plus a student paper contest. The current interest in the International Geophysical Year will be the conference theme. Other highlights include a party at the "Pearl Corral," and an evening of entertainment at San Antonio's "La Villita." In addition, there will be 125 exhibit booths for electronic equipment and component manufacturers to show their product.

Proceedings of this conference will be published for the first time in the ten-year history of the SWIRECO.

## ASME AUTOMATIC OPTIMIZATION CONFERENCE SET FOR APRIL 2-4

The Wilmington, Delaware section of the American Society of Mechanical Engineers is sponsoring a conference on automatic optimization at the University of Delaware April 2-4. The IRE, AIEE, ISA and AIChE, who have professional groups analogous to the Instruments and Regulators division of ASME, will also participate in the conference.

Four technical sessions and a panel discussion are on the conference schedule, and conference registrants may choose to visit one of these during the afternoon of April 2: Tidewater Oil's new Delaware City refinery, the electro-mechanical department of the Mechanical Development Laboratory at E. I. du Pont de Nemours, Chrysler-Plymouth assembly plant, or the Delaware Power and Light Generating Station.

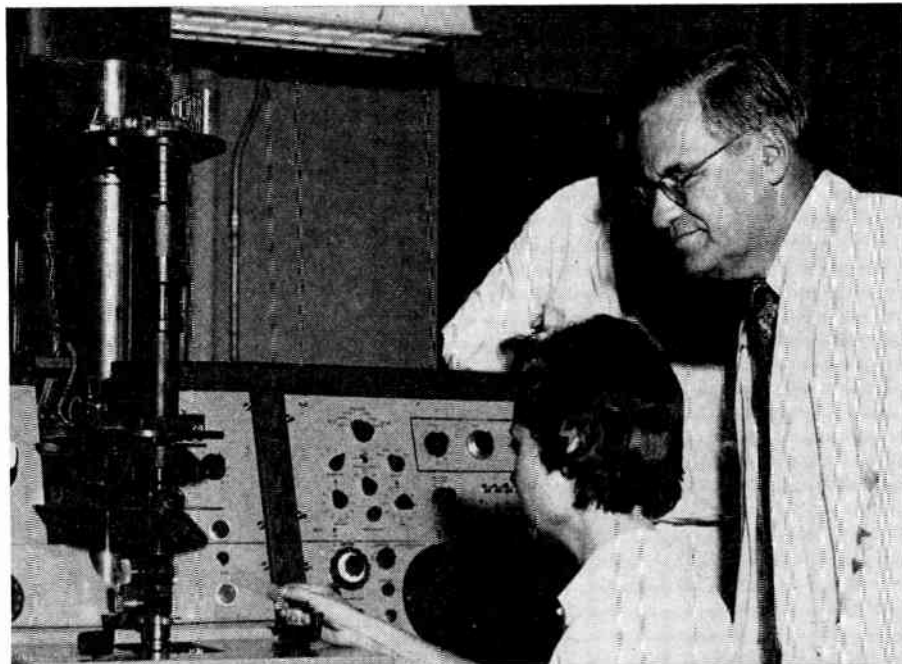
The University of Delaware will provide rooms and six meals at a total cost per registrant of \$30. Persons planning to attend the conference should request registration blanks from L. Bertrand, Instrument Dept., Engineering Service Div., Louviers Bldg., E. I. du Pont de Nemours, Newark, Del.

## Calendar of Coming Events and Authors' Deadlines\*

Continued

- PGPT Symp., Hotel New Yorker, New York City, June 5-6
  - PGMIL Convention, Sheraton-Park Hotel, Wash., D. C., June 16-18
  - Spec. Tech. Conf. on Nonlinear Mag. and Mag. Amplifiers, Los Angeles, Calif., Aug. 6-8
  - Elec. Radio & Standards Conf., Univ. of Colo., Boulder, Colo., Aug. 13-15
  - WESCON, Ambassador Hotel and Pan-Pacific Audit., Los Angeles, Calif., Aug. 19-22
  - Indus. Elec. Conf., Detroit, Mich., Sept. 24-25
  - Nat'l Electronics Conf., Chicago, Ill., Oct. 13-15
  - IRE Canadian Convention, Toronto, Can., Oct. 15-17
  - PGCS Symp. on Aero. Communications, Utica, N. Y., Oct. 20-22
  - Nat'l Simulation Conf., Dallas, Tex., Oct. 23-25
  - EIA-IRE Radio Fall Meeting, Sheraton Hotel, Rochester, N. Y., Oct. 27-29
  - East Coast Aero. & Nav. Elec. Conf., Lord Baltimore Hotel and 7th Regiment Armory, Baltimore, Md., Oct. 27-29
  - PGED Meeting, Shoreham Hotel, Washington, D. C., Oct. 30-Nov. 1
  - PGVC Annual Mtg., Chicago, Ill., Nov. 6-8
  - Atlanta Section Conference, Atlanta-Biltmore Hotel, Atlanta, Ga., Nov. 17-19
  - Elect. Computer Exhibition, Olympia, London, Eng., Nov. 29-Dec. 4
  - Eastern Joint Computer Conf., Bellevue-Stratford Hotel, Philadelphia, Pa., Dec. 3-5
- 1959
- IRE Nat'l Convention, New York City, Mar. 23-26
  - SW Regional Conf., Dallas, Tex., Apr. 16-18
  - Nat'l Aero. & Nav. Elec. Conf., Dayton, Ohio, May 11-13
  - WESCON, San Francisco, Calif., Aug. 18-21
  - Nat'l Electronics Conf., Chicago, Ill., Oct. 12-14
  - East Coast Aero. & Nav. Conf., Baltimore, Md., Oct. 26-28
  - PGED Meeting, Shoreham Hotel, Washington, D. C., Oct. 29-31
  - Radio Fall Meeting, Syracuse, N. Y., Nov. 9-11

\* DL = Deadline for submitting abstracts.



The Cytoanalyzer, a machine designed to detect cancer of the uterus, screens slides almost as fast as they are inserted. Douglas Sprunt, head of the Univ. of Tenn. Institute of Pathology, discusses it with a technician.

#### PIB PLANS SYMPOSIUM ON WAVEGUIDES APRIL 8-10

The Microwave Research Institute of the Polytechnic Institute of Brooklyn plans to hold the eighth in its series of annual international symposia at the auditorium of the Engineering Societies Building, 33 W. 39 St., New York City, Apr. 8-10. This symposium will deal with the interaction of electromagnetic fields and electron or plasma beams in general waveguide regions.

The symposium will have the cooperation of the IRE Professional Groups on Electron Devices, and Microwave Theory & Techniques.

Topics tentatively slated for discussion at this symposium are: fundamental progress reports, mode theories, noise theories, linear and nonlinear theories of space charge waves in open and closed systems, and plasma waves.

#### ETA KAPPA NU PAYS TRIBUTE TO TWO YOUNG IRE MEMBERS

Eta Kappa Nu, national electrical engineering honor society, recently announced that R. P. Crago (A'50-M'54) of Kingston, N. Y., has been named the Outstanding Young Electrical Engineer of 1957. W. R. Beam (A'50-M'55) of Hamilton Square, N. J. received an Honorable Mention award. The 1957 award is the twenty-second in the series which began in 1936. Formal presentation of the awards will be made at a banquet, February 3, during the AIEE Winter General Meeting.

Eligible for the award is any man who on May 1 of each year has been graduated not more than ten years previously from a regular course in electrical engineering from an American college or university and who is not more than 35 years of age. Selection is made on the basis of the candidate's record of achievement in his chosen work; in his service in behalf of his community,

state or nation; in his cultural or esthetic development; and for his professional activities.

Eta Kappa Nu, the sponsor of the annual award, is the national electrical engineering honor society founded at the University of Illinois in 1904. The organization has more than 28,000 members, 71 college and twelve alumni chapters in the principal cities of the United States.

The 1957 Outstanding Young Electrical Engineer has just turned 30 years of age. Recently he was promoted to Director of Engineering, Military Products Div., International Business Machines Corp. Immediately prior to this advancement, he was general manager of the Kingston Military Products Center of the corporation. A graduate of the Carnegie Institute of Technology in 1948 and the recipient of the M.S.E.E. degree from California Institute of Technology in 1949, Mr. Crago has had a meteoric rise in the IBM organization. Upon joining this company in August, 1949 as a technical engineer in the Poughkeepsie laboratory, he was promoted to project engineer in late 1951 and less than two years later advanced to Manager of Engineering Design. He was subsequently assigned complete research and development responsibility for Project High, a vital air-warning computer system the company is producing for the Air Force. He was elevated to general manager in April, 1956. His duties there included the responsibility for engineering, manufacturing, finance, field engineering, and personnel, an autonomous division of 3500 individuals.

Dr. W. R. Beam, at the age of 29, is the manager of Microwave Advanced Development, Tube Div., RCA, at Princeton, N. J. He has made significant contributions in connection with the reduction of fluctuation noise in traveling wave tubes. Educated at the University of Maryland, Dr. Beam received the B.S.E.E. degree in 1947, the M.S. degree in 1950 and the Ph.D. degree in 1953.

#### W. TOLLES WINS RECOGNITION FOR WORK ON CYTOANALYZER

The New York Academy of Science has announced the award of "Fellow" to W. E. Tolles (M'46-SM'56) for his work in the field of biophysics. This award to Walter Tolles is the only fellowship given by the Academy this year for work in the field of medical electronics.

Election to Fellowship in the Academy is a signal, distinguished honor, conferred upon a limited number of members, who, in the estimation of the Council, have done outstanding work toward the advancement of science.

Walter Tolles, a member of the PGME administrative committee, is Head of the Department of Medical and Biological Physics of Airborne Instruments Laboratory, Mineola, N. Y. His department has made contributions to the development of the Cytoanalyzer. This is an electronic instrument which detects cancer in the shed cells of the body.

The Cytoanalyzer is presently under evaluation at the University of Tennessee, Cancer Research Laboratory, at Memphis, Tenn. The equipment has been designed to detect cancer of the uterus by microscopical scanning slides bearing specimen smears.

#### RUSSIAN JOURNALS AVAILABLE

Three Russian journals are now made available in English translations through a grant to the Massachusetts Institute of Technology by the National Science Foundation. They are *Radiotekhnika i Elektronika*, *Radiotekhnika*, and *Elektrosviaz*. M.I.T. has subcontracted the translations and printing of these journals to the Pergamon Institute, a non-profit corporation.

The first issues of *Radiotekhnika* and *Elektrosviaz* to appear in translation will be the No. 7 issues of July, 1957. The first issue of *Radiotekhnika i Elektronika* available in translation will be the No. 1 issue of January, 1957.

Subscription prices for libraries are as follows: *Radiotekhnika i Elektronika*, \$45.00 per year; *Radiotekhnika* and *Elektrosviaz*, \$30.00 each per year. There is a 50 per cent reduction in these prices for individuals. Subscription orders should be addressed to Pergamon Press, Inc., 122 E. 57 St., N. Y. 22, N. Y.

#### IEE PLANS TO HOLD CONVENTION

The Institution of Electrical Engineers is planning a convention on radio aids to aeronautical and marine navigation for March 27-28, 1958, at the Institution, Savoy Place, London, England. The following subjects will be covered: ground, air and shipborne radar; harbor and airfield approach aids; hyperbolic and distance bearing navigational aids; and Doppler and inertia navigation.

The convention is open to members and non-members alike. Those wishing to attend, or requiring copies of the papers only, whether Institution members or not, are required to register with W. K. Brasher, Secretary of the Institution.

Copies of as many of the papers as possible will be available in advance and the complete proceedings of the convention will be published subsequently in a supplement to Part B of the PROCEEDINGS of the Institution.

## OBITUARY

John C. Jensen (M'19-SM'43-F'56)(L), a consulting engineer in Lincoln, Neb., died recently. He had been active in IRE activities. In 1925 he was a member of the Membership and Sections committees, and vice-chairman of the Omaha-Lincoln Section in 1954. He was an IRE representative to the American Association for the Advancement of Science from 1930 to 1956, the ASA Subcommittee on General Terms from 1949 to 1951, and the ASA Sectional Committee (C42) on Definition of Electrical Terms this year until his death.

Dr. Jensen received his B.S. degree in 1909 from Nebraska Wesleyan University, his A.M. degree in 1916 and Ph.D. degree in 1939 from the University of Nebraska. He had been teacher and head of the department of physics at Nebraska Wesleyan for fifty years.

He became a fellow of the American Physical Society in 1935, and held the presidency of the Nebraska Academy of Sciences in 1914 and 1922.

## TECHNICAL COMMITTEE NOTES

The following Technical Committees held meetings this past month:

- October 16—Nuclear Techniques Committee, G. A. Morton, Chairman, National Bureau of Standards, Washington, D. C.
- October 22—Video Techniques Committee, S. Doba, Jr., Chairman, IRE Headquarters.
- October 25—Facsimile Committee, D. Frezzolini, Chairman, Times Building, New York City.

- October 29—Audio Techniques Committee, I. Kerney, Chairman, IRE Headquarters.
- November 6—Antennas and Waveguides Committee, G. A. Deschamps, Chairman, IRE Headquarters.
- November 8—Circuits Committee, W. A. Lynch, Chairman, IRE Headquarters.
- November 12—Feedback Control Systems Committee, J. E. Ward, Chairman, M.I.T., Cambridge, Mass.
- November 14—Standards Committee, M. W. Baldwin, Jr., Chairman, IRE Headquarters.
- November 15—Electron Tubes Committee, G. A. Espersen, Chairman, IRE Headquarters.

## Books

## Solid State Physics by A. J. Dekker

Published (1957) by Prentice-Hall Inc., 70 Fifth Ave., N. Y. 11, N. Y. 523 pages+8 appendix pages +8 index pages+xiv pages. Illus. 9½×6½. \$9.00.

This book is intended as an introductory account of solid state physics for students of engineering, physics, chemistry, and metallurgy. It presupposes an elementary knowledge of atomic physics and some acquaintance with quantum mechanics on the part of the reader. The book appears well-suited for a senior undergraduate or someone beginning a graduate course, or for self-study by a scientist in industry. The only other introductory textbook on solid state physics published in English which is on a par with Professor Dekker's book in breadth of coverage, clarity, and up-to-date treatment is C. Kittel's *Introduction to Solid State Physics*, second edition, 1956. [For a review of the latter, see F. Herman, *PROC. IRE*, vol. 45, p. 250; February, 1957.]

The scope of Prof. Dekker's book is best indicated by a listing of the chapter headings: 1. The Crystalline State; 2. The Specific Heat of Solids and Lattice Vibrations; 3. Some Properties of Metallic Lattices; 4. Some Properties of Simple Alloys; 5. Lattice Energy of Ionic Crystals; 6. Dielectric and Optical Properties of Insulators; 7. Ionic Conductivity and Diffusion; 8. Ferroelectrics; 9. Free Electron Theory of Metals; 10. The Band Theory of Solids; 11. The Conductivity of Metals; 12. The Electron Distribution in Insulators and Semiconductors; 13. Nonpolar Semiconductors; 14. Rectifiers and Transistors; 15. Electronic Properties of Alkali Halides; 16. Luminescence; 17. Secondary Electron Emission; 18. Diamagnetism and Paramagnetism; 19. Ferromagnetism, Antiferromagnetism, and Ferrimagnetism; and 20. Magnetic Relaxation and Resonance Phenomena.

The author, who is a professor of electrical engineering at the University of Minnesota, has taught this course to students having widely differing backgrounds and interests, and has used this experience as a guide to the choice of material and presentation. In this book, he ranges over the entire field of solid state physics, focusing attention on the highlights of the major branches of the subject. The only important branch which is conspicuous by its absence is superconductivity. With the exception of the last three chapters, where the treatment is somewhat sketchy, the author is eminently successful in capturing the essence of each topic, and in expressing it in a succinct and interesting manner.

While the student can hope to become familiar with the essentials of solid state physics through a careful reading of this book, he can hardly expect to attain a mastery of the subject by this alone. But of course Dekker's book is intended as an introduction to the subject, and no more. To achieve an understanding of solid state physics, it is necessary to go far beyond this book, and explore the advanced texts and the original literature. The interested reader is greatly aided in this quest by the copious references contained in the book.

The pedagogical value of the book is further enhanced by the inclusion of problem sets at the end of each chapter. For the most part, the problems are well chosen, and they provide a fair test of the reader's grasp of the preceding material.

The book as a whole is well-organized and clearly written. The author's wide knowledge and obvious enthusiasm show up to good advantage in nearly every chapter. Prof. Dekker is at his best in the chapter on secondary electron emission, a topic which receives only passing mention in most

elementary books on solid state physics. Since the author has made important contributions to this topic, it is only natural that he should treat it in more detail than is customary. A better treatment of secondary electron emission is hard to find.

In summary, we feel that this book is a welcome addition to the pedagogical literature on solid state physics. As such, it is highly recommended to the beginning student.

FRANK HERMAN  
RCA Labs.  
Princeton, N. J.

## The Science of Engineering Materials, ed. by J. E. Goldman

Published (1957) by John Wiley & Sons, Inc., 440 Fourth Ave., N. Y. 16, N. Y. 510 pages+18 index pages+xv pages. Illus. 9½×6½. \$12.00.

This text is a compilation of papers presented at a conference of engineering and physics teachers held at Carnegie Institute of Technology, June 21-25, 1954. The purpose of the conference was to discuss recent technical developments in solid-state science and to explore ways of including these in engineering curricula.

The book contains 18 papers grouped into 6 categories: I, The Structure of Matter—four papers; II, Metals and Alloys—six papers; III, Surfaces—one paper; IV, Magnetism and Magnetic Properties—two papers; V, Semiconductors and Dielectrics—two papers; VI, Non-Crystalline Materials—three papers.

The seventeen authors drawn from universities and industrial laboratories are all recognized authorities in their respective fields. In general, the authors have attempted to discuss the scope, present state of knowledge, theoretical limitations, *i.e.*,

qualitative vs quantitative interpretation of observations and trends in the various subjects presented.

The disciplines employed in the discussions embrace inorganic, organic, and physical chemistry, physics, metallurgy and ceramics as well as some engineering. The scope of subject matter is truly impressive.

The first five parts of this text cover subjects which are generally recognized as belonging to solid-state physics and physical metallurgy. The last part including the physics and chemistry of cement, the molecular structure and mechanical behavior of high polymers, and the physics of glass is a bold extension of the field.

The book is not intended nor is it suitable for use as a classroom text.

The editor and authors have done an excellent job of preparing the material in such a way that the book may be read without a feeling of excessive repetition on the one hand or choppyness on the other as so often happens in compilations of this kind.

It is the feeling of this reviewer that the authors have achieved their objective in surveying a field which must be integrated into engineering curricula as soon as possible. It is recommended to research engineers and engineering faculties as an excellent survey.

L. T. DEVORE  
Stewart-Warner Electronics  
Chicago 51, Ill.

#### Acoustical Engineering by H. F. Olson

Published (1957) by D. Van Nostrand Co., Inc., 257 Fourth Ave., N. Y. 10, N. Y. 703 pages+13 index pages+xix pages. Illus. 9½×6½. \$13.50.

This textbook is a true encyclopedia of applied acoustics embracing practically every phase of the art. The fundamental

problems are treated rather fully and where space prevents extended analysis, references are made to original sources. Those who have previous texts by the same author on similar subjects will do well to supplement them or replace them with this much-expanded volume.

The general approach follows that of Dr. Olson's previous works including excellent illustrations with equivalent circuit diagrams for visualization of performance of acoustical devices by electrically trained people. The EFP (voltage-force-pressure) system of analogies is used throughout the text.

The first five chapters cover the theory of applied acoustics. They deal with sound wave equations, radiation from points, lines and surfaces, mechanical vibrating systems and dynamical analogies. As in previous texts, the writer adheres to the cgs system of units.

Chapters VI and VII deal with cone and horn loudspeakers and enclosures, respectively. A multitude of cone and enclosure configurations are described. Efficiency, distortion, power handling capacity, transient response, and design parameters are well covered. Chapter VIII is a very complete chapter on microphones written with the detail which reflects the important contributions made by the author to this subject. Chapter IX describes miscellaneous transducers—telephone receivers, phonograph recording and reproduction devices, vibration pickups, sound power telephones, electrical megaphones, magnetic recording and reproduction, hearing aid devices, etc. Here we find considerable abbreviation in many areas which is no doubt due to a desire to keep the text within manageable dimensions.

Chapter X is devoted to acoustical measurements of electrical and acoustical devices, microphones, loudspeakers, telephone receivers, phonograph pickups, of acoustical and mechanical impedance, measurement of noise, reverberation time, etc.

Chapter XI develops the principles of architectural acoustics including a description of various types of sound absorbing materials and structures, treatment of studios and theatres, and the principle of sound collection in broadcasting and recording. Chapter XII covers well the principles of hearing, speech and music, and Chapter XIII deals with sound reproduction systems.

A novel addition is found in the form of Chapter XIV on "means for the communication of information." This chapter contains a brief but exhaustive listing of the many possible ways of communicating information, from the printing press invented 400 years ago to some of conceivable systems not yet developed, such as "foreign speech analyzer—domestic speech synthesizer," *i.e.* an instantaneous automatic language translator. Whether such a machine could ever duplicate economically the excellent human translators currently at work at the U.N. is a subject on which we can only speculate. Nevertheless, the advanced thinking exhibited by this chapter will be found to be greatly stimulating.

Chapters XV and XVI treat the subjects of underwater sound and ultrasonics. Their relative brevity is consistent with the rather specialized nature of the subjects, and those who wish to pursue these subjects further will find them well annotated with references to the work of others.

B. B. BAUER  
CBS Laboratories  
New York 22, N. Y.

## Professional Groups†

**Aeronautical & Navigational Electronics**—Joseph General, 6019 Highgate Dr., Baltimore 15, Md.

**Antennas & Propagation**—J. I. Bohnert, Code 5200, Naval Research Lab., Washington 25, D. C.

**Audio**—Dr. H. F. Olson, RCA Labs., Princeton, N. J.

**Automatic Control**—E. M. Grabbe, Ramo-Wooldrige Corp., Box 45067, Airport Station, Los Angeles 45, Calif.

**Broadcast & Television Receivers**—L. R. Fink, General Electric Co., X-Ray Dept., Milwaukee, Wis.

**Broadcast Transmission Systems**—C. H. Owen, 7 W. 66th St., N. Y. 23, N. Y.

**Circuit Theory**—W. H. Huggins, 2813 St. Paul St., Baltimore 18, Md.

**Communications Systems**—J. W. Worthington, Jr., Dawn Dr., Mounted Route, Rome, N. Y.

**Component Parts**—R. M. Soria, American Phenolic Corp., 1830 S. 54 Ave., Chicago 50, Ill.

† Names listed are Group Chairmen.

**Education**—J. D. Ryder, Dept. of Elec. Eng., Mich. State Univ., E. Lansing, Mich.

**Electron Devices**—T. M. Liimatainen, 5415 Connecticut Ave., N.W., Washington, D. C.

**Electronic Computers**—Werner Buchholz, IBM Engineering Lab., Poughkeepsie, N. Y.

**Engineering Management**—C. R. Burrows, Ford Instrument Co., 31-10 Thomson Ave., Long Island City 1, N. Y.

**Engineering Writing and Speech**—D. J. McNamara, Sperry Gyroscope Co., Great Neck, L. I., N. Y.

**Industrial Electronics**—W. R. Thurston, General Radio Co., 285 Massachusetts Ave., Cambridge 39, Mass.

**Information Theory**—W. B. Davenport, Jr., Lincoln Lab., M.I.T., Cambridge, Mass.

**Instrumentation**—F. C. Smith, Jr., Southwestern Industrial Electronics Co., 2831 Post Oak Rd., Houston 19, Tex.

**Medical Electronics**—L. B. Lusted, M.D., Clinical Center, National Institute of

Health, Bethesda 14, Md.

**Microwave Theory and Techniques**—W. L. Pritchard, Raytheon Mfg. Co., Newton, Mass.

**Military Electronics**—W. E. Cleaves, 3807 Fenchurch Rd., Baltimore 18, Md.

**Nuclear Science**—J. N. Grace, Westinghouse Atomic Power Div., Pittsburgh 34, Pa.

**Production Techniques**—E. R. Gamson, Autonetics, 395-91, 12214 Lakewood Blvd., Downey, Calif.

**Radio Interference Reduction**—H. R. Schwenk, Sperry Gyroscope Co., Great Neck, L. I., N. Y.

**Reliability and Quality Control**—Victor Wouk, Beta Electric Corp., 333 E. 103rd St., New York 29, N. Y.

**Telemetry and Remote Control**—C. H. Doersam, Jr., 24 Winthrop Rd., Port Washington, L. I., N. Y.

**Ultrasonics Engineering**—C. M. Harris, 425 Riverside Dr., New York, N. Y.

**Vehicular Communications**—C. M. Heiden, General Electric Co., Syracuse, N. Y.

# Sections\*

- Akron (4)**—H. F. Lanier, 2220—27th St., Cuyahoga Falls, Ohio; Charles Morrill, 2248—16th St., Cuyahoga Falls, Ohio.
- Alamogordo-Holloman (6)**—V. J. Lynch, 1105 Maple Dr., Alamogordo, N. Mex.; Thomas W. Cielinski, 1311—16 St., Alamogordo, N. M.
- Albuquerque-Los Alamos (7)**—B. L. Basore, 2405 Parsifal, N.E., Albuquerque, N. Mex.; John McLay, 3369—48 Loop, Sandia Base, Albuquerque, N. Mex.
- Atlanta (3)**—W. B. Miller, 1369 Holly Lane, N.E., Atlanta 6, Ga.; W. H. White, 1454 S. Gordon St., S.W., Atlanta 10, Ga.
- Baltimore (3)**—M. R. Briggs, Westinghouse Elec. Corp., Box 746, Baltimore 3, Md.; B. Wolfe, 5628 Stonington Ave., Baltimore 7, Md.
- Bay of Quinte (8)**—W. D. Ryan, Cavalry House, Royal Military College, Kingston, Ont., Canada; R. Williamson, R.R. 3, Belleville, Ont., Canada.
- Beaumont-Port Arthur (6)**—F. M. Crum, Dept. of E. E., Lamar State College of Tech., Beaumont, Texas; H. K. Smith, 270 Canterbury Lane, Beaumont, Tex.
- Binghamton (1)**—Robert Nash, 12 Alice St., M.R. 97, Binghamton, N. Y.; Bruce Lockhart, R.D. 3, Binghamton, N. Y.
- Boston (1)**—C. J. Lahanas, 275 Massachusetts Ave., General Radio Co., Cambridge 39, Mass.; (secretary to be elected).
- Buenos Aires**—J. M. Onativia, Bustamante 1865, Buenos Aires, Argentina; L. F. Rocha, Caseros 3321, D.T.O. B., Buenos Aires, Argentina.
- Buffalo-Niagara (1)**—W. S. Holmes, Cornell Aeronautical Labs., 4455 Genesee St., Buffalo 21, N. Y.; R. B. Odden, 573 Allenhurst Rd., Buffalo, N. Y.
- Cedar Rapids (5)**—J. L. Dalton, 2900 E. Ave., N.E., Cedar Rapids, Iowa; S. M. Morrison, 2034 Fourth Ave., S.E., Cedar Rapids, Iowa.
- Central Florida (3)**—G. F. Anderson, Dynatronics, Inc., 717 W. Amelia Ave., Orlando, Fla.; J. W. Downs, 1020 Highland Ave., Eau Gallie, Fla.
- Central Pennsylvania (4)**—W. J. Leiss, 1173 S. Atherton St., State College, Pa.; P. J. Freed, Haller, Raymond & Brown, State College, Pa.
- Chicago (5)**—D. G. Haines, 751 Parkside Ave., Elmhurst, Ill.; S. F. Bushman, 1166 Oakwood Ave., Des Plaines, Ill.
- China Lake (7)**—C. F. Freeman, 100-B Halsey St., China Lake, Calif.; P. K. S. Kim, 200-A Byrnes St., China Lake, Calif.
- Cincinnati (4)**—A. B. Ashman, 225 E. Fourth St., Cincinnati 2, Ohio; R. Nathan, 1841 Bluefield Place, Cincinnati 37, Ohio.
- Cleveland (4)**—W. G. Piwonka, 3121 Huntington Rd., Cleveland 20, Ohio; J. S. Hill, Smith Electronics, Inc., 4900 Euclid Ave., Cleveland 3, Ohio.
- Columbus (4)**—R. L. Cosgriff, 2200 Homestead Dr., Columbus, Ohio; G. J. Falkenbach, Battelle Institute, 505 King Ave., Columbus 1, Ohio.
- Connecticut (1)**—H. M. Lucal, Box U-37, Univ. of Conn., Storrs, Conn.; A. E. Perrins, 951 Sperry Rd., Cheshire, Conn.
- Dallas (6)**—Frank Seay, Collins Radio Co., 1930 Hi-Line Dr., Dallas, Tex.; T. B. Moseley, 6114 Northwood Rd., Dallas 25, Tex.
- Dayton (4)**—N. A. Nelson, 201 Castle Dr., Kettering 9, Ohio; D. G. Clute, 2132 Meriline Ave., Dayton 10, Ohio.
- Denver (6)**—R. S. Kirby, 455 Hawthorne Ave., Boulder, Colorado; W. G. Worcester, 748—10 St., Boulder, Colorado.
- Detroit (4)**—E. C. Johnson, 4417 Crooks Rd., Royal Oak, Mich.; G. E. Ryan, 5296 Devonshire Rd., Detroit 24, Mich.
- Egypt**—H. M. Mahmoud, Faculty of Engineering, Fouad I University, Giza, Cairo, Egypt; El Garhi l El Kashlan, Egyptian Broadcasting, 4, Shari Sherifein, Cairo, Egypt.
- Elmira-Corning (1)**—R. G. Larson, 220 Lynhurst Ave., Windsor Gardens, Horseheads, N. Y.; D. F. Aldrich, 1030 Hoffman St., Elmira, N. Y.
- El Paso (6)**—J. Crosson, 1100 Honeysuckle Drive, El Paso, Tex.; H. Markowitz, 1132 Texas St., El Paso, Tex.
- Emporium (4)**—H. S. Hench, Jr., Sylvan Heights, Emporium, Pa.; H. J. Fromell, Sylvania Elec. Prod. Inc., Emporium, Pa.
- Evansville-Owensboro (5)**—A. K. Mieg, 904 Kelsey Ave., Evansville, Ind.; M. Casler, Evansville College, Evansville, Ind.
- Florida West Coast (3)**—L. J. Link, 3216 Ninth St., North, St. Petersburg, Fla.; R. Murphy, 12112 N. Edison Ave., Tampa 4, Fla.
- Fort Huachuca (7)**—J. K. Oliver, Box 656, Ft. Huachuca, Ariz.; W. C. Shelton, Box 2919, Fort Huachuca, Ariz.
- Fort Wayne (5)**—G. E. Collins, 3101 Lillie St., Fort Wayne, Ind.; H. D. Grosvenor, 1332 Maple Ave., Fort Wayne 6, Ind.
- Fort Worth (6)**—C. W. Macune, 3132 Forest Park Blvd., Fort Worth, Tex.; G. H. Robertson, 5749 Tracyne Drive, Fort Worth 14, Tex.
- Hamilton (8)**—C. N. Chapman, 40 Dundas St., Waterdown, Ont., Canada; C. J. Smith, Gilbert Ave., Dancaster Courts, Sub. Serv. 2, Ancaster, Ont., Canada.
- Hawaii (7)**—Vaughn Kelly, 99-1215 Aiea Hgts. Dr., Aiea, Hawaii; D. L. Grubb, 236 Paiko Dr., Honolulu, Hawaii.
- Houston (6)**—M. A. Arthur, Humble Oil & Refining Co., P.O. Box 2180, Houston 1, Tex.; C. G. Turner, Communications Engineering Co., P.O. Box 12325, Houston 17, Tex.
- Huntsville (3)**—W. O. Frost, P.O. Box 694, Huntsville, Ala.; J. E. Douma, 804 Carmelian, S.E., Huntsville, Ala.
- Indianapolis (5)**—N. G. Drilling, 3002 Ashland Ave., Indianapolis 26, Ind.; R. B. Flint, 4038 Evelyn St., Indianapolis 24, Ind.
- Israel**—E. H. Frei, Weizman Inst. of Science, Rehovoth, Isarel; Moshe Tkatch, Kyriat Motzkin POB 1, Israel.
- Ithaca (1)**—W. E. Gordon, Phillips Hall, Cornell Univ., Ithaca, N. Y.; C. E. Ingalls, 106 Sheldon Rd., Ithaca, N. Y.
- Kansas City (6)**—P. C. Constant, Jr., 3014 E. Meyer Blvd., Kansas City 30, Mo.; N. E. Vilander, 2509 W. 83rd St., Kansas City 15, Mo.
- Little Rock (6)**—J. D. Reid, 2210 Summit, Little Rock, Ark.; J. P. McRae, Route 1, Box 27, Scott, Ark.
- London (8)**—J. C. Warder, 513 Princess Ave., London, Ont., Canada; J. D. B. Moore, 27 McClary Ave., London, Ont., Canada.
- Long Island (2)**—E. G. Fubini, Airborne Instrument Labs., 160 Old Country Rd., Mineola, L. I., N. Y.; E. K. Stodola, 118 Stanton St., Northport, N. Y.
- Los Angeles (7)**—J. K. Gosland, 318 E. Calaveras St., Altadena, Calif.; R. G. Kuck, 854 Bank St., So. Pasadena, Calif.
- Louisville (5)**—M. C. Probst, 5067 Poplar Level Rd., Louisville, Ky.; W. J. Ryan, 207 E. Broadway, Louisville 1, Ky.
- Lubbock (6)**—E. W. Jenkins, Jr., Shell Oil Co., Admin. Dept., Box 1509, Midland, Tex.; J. J. Criswell, 511 50th St., Lubbock, Tex.
- Miami (3)**—W. H. Epperson, 5845 S.W. 108 St., Miami 43, Fla.; R. S. Rich, 7513 S.W. 54 Ct., S. Miami, Fla.
- Milwaukee (5)**—J. E. Jacobs, 6230 Hale Park Dr., Hales Corners, Wis.; F. J. Lofy, Milwaukee School of Engrg., 1025 N. Milwaukee St., Milwaukee 2, Wisc.
- Montreal (8)**—R. E. Penton, 6695 Fielding Ave., Apt. 29, Montreal, Que., Can.; R. Lumsden, 1680 Lepine St., St. Laurent, Montreal 9, Quebec, Canada.
- Newfoundland (8)**—J. B. Austin, Jr., Hq. 1805th AACs Wing, APO 862, c/o PM, New York, N. Y.; J. A. Willis, Canadian Marconi Co., Ltd., Pinetree-NEAC Depot, Pepperrill AFB, St. John's Newfoundland, Canada.
- New Orleans (6)**—M. F. Chapin, 8116 Hampson St., New Orleans, La.; G. A. Hero, 1102 Lowerline St., New Orleans 18, La.
- New York (2)**—J. S. Smith, 3717 Clarendon Rd., Brooklyn, N. Y.; Joseph Reed, 52 Hillcrest Ave., New Rochelle, N. Y.
- Newfoundland (8)**—J. B. Austin, Jr., Hq. 1805th AACs Wing, APO 862, c/o PM, New York, N. Y.; J. A. Willis, Canadian Marconi Co., Ltd., Pinetree-NEAC Depot, Pepperrill AFB, St. John's Newfoundland, Canada.
- New Orleans (6)**—M. F. Chapin, 8116 Hampson St., New Orleans, La.; G. A. Hero, 1102 Lowerline St., New Orleans 18, La.
- New York (2)**—J. S. Smith, 3717 Clarendon Rd., Brooklyn, N. Y.; Joseph Reed, 52 Hillcrest Ave., New Rochelle, N. Y.
- North Carolina (3)**—H. H. Arnold, 548 S. Westview Dr., Winston-Salem, N. C.; C. A. Norwood, 830 Gales Ave., Winston-Salem, N. C.
- Northern Alberta (8)**—D. L. MacDonald, 10330—84 Ave., Edmonton, Alta., Can.; Frank Hollingsworth, 9619—85th St., Edmonton, Alberta, Canada.
- Northern New Jersey (2)**—T. N. Anderson, 1539 Deer Path, Mountainside, N. J.; G. D. Hulst, 73 Mt. Prospect Ave., Verona, N. J.
- Northwest Florida (3)**—G. C. Fleming, 579 E. Gardner Dr., Fort Walton Beach, Fla.; W. F. Kirilin, 67 Laurie Dr., Fort Walton Beach, Fla.
- Oklahoma City (6)**—Nicholas Battenburg, 2004 N.W. 30th St., Oklahoma City 6, Okla.; E. W. Foster, 5905 N.W. 42 St., Oklahoma City 12, Okla.
- Omaha-Lincoln (5)**—J. S. Petrik, c/o KETV, 27 & Douglas Sts., Omaha, Neb.; H. W. Becker, 1214 N. 34 St., Omaha 3, Neb.
- Ottawa (8)**—L. H. Doherty, 227 Barclay Rd., Ottawa 2, Ont., Canada; R. S. Thain,

\* Numerals in parentheses following section designate region number. First name designates Chairman, second name, Secretary.

- 54 Rossland Ave., Box 474, City View, Ont., Canada.
- Philadelphia (3)**—Nels Johnson, Philco Corp., 4700 Wissahickon Ave., Philadelphia 44, Pa.; W. A. Howard, WRCV, 1619 Walnut St., Philadelphia 4, Pa.
- Phoenix (7)**—G. L. McClanathan, 509 E. San Juan Cove, Phoenix, Ariz.; E. S. Shepard, 5716 N. 19 St., Phoenix, Ariz.
- Pittsburgh (4)**—J. B. Woodford, Jr., Box 369, Carnegie Tech. P.O., Pittsburgh 13, Pa.; A. E. Anderson, 1124 Olympic Hts. Dr., Pittsburgh 35, Pa.
- Portland (7)**—D. C. Strain, 7325 S.W. 35 Ave., Portland 19, Ore.; W. E. Marsh, 6110 S.W. Brugger St., Portland 19, Ore.
- Princeton (2)**—L. L. Burns, Jr., RCA Labs., Princeton, N. J.; Sylvan Fich, College of Eng., Rutgers Univ., New Brunswick, N. J.
- Regina (8)**—J. A. Funk, 138 Leopold Crescent, Regina, Saskatchewan, Canada; E. C. Odling, 1121 Minto St., Regina, Saskatchewan, Canada.
- Rio de Janeiro, Brazil**—M. P. De Britto Pereira, Caixa Postal 562, Rio de Janeiro, Brazil; J. A. Hertz, Caixa Postal 97 Lapa, Rio de Janeiro, Brazil.
- Rochester (1)**—B. L. McArdle, Box 54, Brighton Station, Rochester 10, N. Y.; L. D. Smith, 27 Landing Park, Rochester, N. Y.
- Rome-Utica (1)**—Edward R. Orear, Ch., 36 Herthum Rd., Harts Hill Heights, Whitesboro, N. Y.; Robert A. Zachary, Jr., Sec., 11 Arbor Drive, New Hartford, N. Y.
- Sacramento (7)**—R. A. Poucher, Jr., 3021 Mountain View Ave., Sacramento 21, Cal.; X. W. Godfrey, 3220 Fulton Ave., Sacramento 21, Cal.
- St. Louis (6)**—C. E. Mosley, 8622 St. Charles Rock Rd., Overland 14, Mo.; R. D. Rodenroth, 7701 Delmont, Afton 23, Mo.
- Salt Lake City (7)**—J. S. Hooper, 1936 Hubbard Ave., Salt Lake City 5, Utah; A. L. Gunderson, 3906 Parkview Dr., Salt Lake City 17, Utah.
- San Antonio (6)**—F. A. Brogan, 433 Brees Blvd., San Antonio 9, Tex.; W. L. Donaldson, 129 El Cerrito, San Antonio, Tex.
- San Diego (7)**—E. J. Moore, 3601 Eighth St., San Diego 3, Calif.; R. J. Cary, Jr., 4561 Normandie Place, La Mesa, Calif.
- San Francisco (7)**—Meyer Leifer, Electronic Defense Lab., Box 205, Mountain View, Calif.; V. B. Corey, 385 Gravatt Dr., Berkeley 5, Calif.
- Schenectady (1)**—A. E. Rankin, 833 Whitney Dr., Schenectady, N. Y.; Sec.-Treas. to be appointed later.
- Seattle (7)**—R. H. Hoglelund, 1825 E. Lynn St., Seattle 2, Wash.; L. C. Perkins, Box 307, Des Moines, Wash.
- Shreveport (6)**—H. H. Moreland, Hq. 2nd Air Force, Barksdale AFB, La.; L. Hurley, 2736 Rosemont, Shreveport, La.
- South Bend-Mishawaka (5)**—R. D. Ewing, 3755 Terry Lane, Mishawaka, Ind.; H. E. Harry, Bendix Prod. Div.-Missiles, 400 S. Beiger St., Mishawaka, Ind.
- Southern Alberta (8)**—W. K. Allan, 2025 29th Ave., S.W., Calgary, Alta., Canada; R. W. H. Lamb, Radio Station CFCN, 12th Ave. and Sixth St., E., Calgary, Alberta, Canada.
- Syracuse (1)**—J. B. Russell, Salt Spring Rd., Fayetteville, N.Y.; R. N. Lothes, General Electric Co., Bldg. 3—Industrial Park, Syracuse, N. Y.
- Tokyo**—Yasujiro Niwa, Tokyo Elec. Engineering College, 2-2 Kanda-Nishikicho, Chiyoda-Ku, Tokyo, Japan; Fumio Minozuma, 16 Ohara-Machi, Meguro-Ku, Tokyo, Japan.
- Toledo (4)**—H. L. Neuert, 3534 Woodmont Rd., Toledo 13, Ohio; K. P. Herrick, 2516 Fulton St., Toledo 10, Ohio.
- Toronto (8)**—H. W. Jackson, 352 Laird Dr., Toronto 17, Ont., Canada; R. J. A. Turner, 66 Gage Ave., Scarborough, Ont., Canada.
- Tucson (7)**—P. E. Russell, Elec. Engrg. Dept., Univ. of Ariz., Tucson, Ariz.; C. L. Becker, 4411 E. Sixth St., Tucson, Ariz.
- Tulsa (6)**—R. L. Atchison, 415 E. 14 Pl., Tulsa 20, Okla.; B. H. Keller, 1412 S. Winston, Tulsa 12, Okla.
- Twin Cities (5)**—E. W. Harding, 5325 Colfax Ave., S., Minneapolis, Minn.; S. W. Schulz, 3132 Fourth St., S.E., Minneapolis 14, Minn.
- Vancouver (8)**—R. A. Marsh, 3873 W. 23 Ave., Vancouver, B. C., Canada; T. G. Lynch, 739 Edgewood Rd., North Vancouver, B. C., Canada.
- Virginia (3)**—F. E. Brooks, Box 277, Colonial Ave., Colonial Beach, Va.; E. S. Busby, Jr., 1608 'B' St., Portsmouth, Va.
- Washington (3)**—A. H. Schooley, 3940 First St., S.W., Washington 24, D. C.; J. E. Durkovic, 10316 Colesville Rd., Silver Spring, Md.
- Western Massachusetts (1)**—R. P. Sheehan, Ballou Lane, Williamstown, Mass.; A. K. Hooks, Sprague Elec. Co., N. Adams, Mass.
- Wichita (6)**—W. K. Klatt, 2625 Garland, Wichita 4, Kan.; A. T. Murphy, Univ. of Wichita, Dept. of Elec. Engrg., Wichita 14, Kan.
- Williamsport (4)**—(No chairman at present); W. H. Bresee, 1666 Oak Ridge Pl., Williamsport, Pa.
- Winnipeg (8)**—C. J. Hopper, 332 Bronx Ave., Winnipeg 5, Man., Canada; T. J. White, Dept. of E.E., University of Manitoba, Winnipeg 9, Man., Can.

## Subsections

- Buenaventura (7)**—M. H. Fields, 430 Rodrick St., Oxnard, Calif.; D. J. Heron, 1171 Brunswick Lane, Ventura, Calif.
- Charleston (3)**—A. Jonas, 105 Lancaster St., N. Charleston, S. C.; F. A. Smith, Route 4, Melrose Box 572, Charleston, S. C.
- East Bay (7)**—C. W. Park, 6035 Chaboly Terr., Oakland 18, Calif.; Robert Rector, 1425 Edith St., Berkeley, Calif.
- Eastern North Carolina (3)**—H. Hulick, Station WPTF, Insurance Bldg., Raleigh, N.C.; M. C. Todd, Wendell, N.C.
- Erie (1)**—J. D. Heibel, 310 W. Grandview, Erie, Pa.; D. H. Smith, 3025 State St., Erie, Pa.
- Gainesville (3)**—W. E. Lear, Dept. of Elec. Eng., Univ. of Fla., Gainesville, Fla. (Chairman)
- Kitchener-Waterloo (8)**—Jules Kadish, Raytheon Canada, Ltd., 61 Laurel St., Waterloo, Ont., Canada; G. C. Field, 48 Harber Ave., Kitchener, Ont., Canada.
- Lancaster (3)**—W. T. Dyall, 1415 Hillcrest Rd., Lancaster, Pa.; P. W. Kaseman, 405 S. School Lane, Lancaster, Pa.
- Las Cruces-White Sands Proving Grounds (6)**—H. W. Haas, Box 236, State College, N.M.; M. Goldin, 1921 Calle de Suneos, Las Cruces, N. M.
- Lehigh Valley (3)**—F. W. Smith, E.E. Dept., Lafayette College, Alumni Hall of Engrg., Easton, Pa.; L. G. McCracken, Jr., 1774 W. Union Blvd., Bethlehem, Pa.
- Memphis (3)**—R. N. Clark, Box 227, Memphis State Coll., Memphis, Tenn. (Chmn)
- Mid-Hudson (2)**—Altman Lampe, Cramer Rd., R.D. 3, Poughkeepsie, N. Y.; M. R. Marshall, 208 Smith St., Poughkeepsie, N. Y.
- Monmouth (2)**—Edward Massell, Box 433, Locust, N. J.; Harrison Rowe, Box 107, Red Bank, N. J.
- Nashville (3)**—W. W. Stifler, Jr., Aladdin Electronics, Nashville 2, Tenn.; P. E. Dicker, Dept. of Elec. Engrg., Vanderbilt Univ., Nashville 5, Tenn.
- New Hampshire (1)**—M. R. Richmond, 55 Raymond St., Nashua, N. H.; R. O. Goodwin, 86 Broad St., Nashua, N. H.
- Northern Vermont (1)**—Charles Horvath, 15 Iby St., S. Burlington, Vt.; D. M. Wheatley, 14 Patrick St., S. Burlington, Vt.
- Orange Belt (7)**—R. E. Beekman, 113 N. Lillie Ave., Fullerton, Calif.; R. W. Thorpe, 303 S. Louise Ave., Azusa, Calif.
- Palo Alto (7)**—Wayne Abraham, 611 Hansen Way, c/o Varian Associates, Palo Alto, Calif.; W. E. Ayer, 150 Erica Way, Menlo Park, Calif.
- Panama City (3)**—C. B. Koesy, 1815 Moates Ave., St. Andrew Station, Panama City, Fla.; M. H. Naeseth, 1107 Buena Vista Blvd., Panama City, Fla.
- Pasadena (7)**—J. L. Stewart, Assoc. Prof. of Elec. Engrg., Calif. Inst. of Tech., Pasadena, Calif.; J. E. Ranks, 1270 Leonard Ave., Pasadena 8, Calif.
- Quebec (8)**—R. F. Chinnick, 500 La Visitation, Ste. Foye, Quebec City, Que., Can.; P. DuBerger, 1267 Villars Ave., Sillery, Que., Canada.
- Richland (7)**—R. E. Connally, 515 Cottonwood Dr., Richland, Wash.; R. R. Cone, 611 Thayer, Richland, Wash.
- San Fernando (7)**—J. J. Guarrera, 17160 Gresham Ave., Northridge, Calif.; C. C. Olsesfsky, 8100 Aldea Ave., Van Nuys, Calif.
- Santa Barbara (7)**—Walter Hausz, 4520 Via Vistosa, Santa Barbara, Calif.; C. P. Hedges, 316 Coleman Ave., Santa Barbara, Calif.
- USAFIT (4)**—Lt. Cdr. E. M. Lipsey, 46 Spinning Rd., Dayton 3, Ohio; sec.-treas. to be appointed later.
- Westchester County (2)**—D. S. Kellogg, 9 Bradley Farms, Chappaqua, N. Y.; M. J. Lichtenstein, 52 Sprain Valley Rd., Scarsdale, N. Y.
- Western North Carolina (3)**—J. G. Carey, 1429 Lilac Rd., Charlotte, N. C.; R. W. Ramsey, Sr., 614 Clement Ave., Charlotte 4, N. C.

# Abstracts of IRE Transactions

The following issues of "Transactions" have recently been published, and are now available from the Institute of Radio Engineers, Inc., 1 East 79th Street, New York 21, N. Y. at the following prices. The contents of each issue and, where available, abstracts of technical papers are given below.

Sponsoring Group	Publication	Group Members	IRE Members	Non-Members*
Broadcast & TV Receivers	Vol. BTR-3, No. 2	\$1.40	\$2.10	\$4.20
Component Parts	Vol. CP-4, No. 3	1.15	1.70	3.45
Information Theory	Vol. IT-3, No. 3	2.20	3.30	6.00
Reliability & Quality Control	PGRQC-12	.90	1.35	2.70

\* Public libraries and colleges may purchase copies at IRE Member rates.

## Broadcast & TV Receivers

### VOL. BTR-3, No. 2, OCTOBER, 1957

#### The Traveling-Wave VHF Television Transmitting Antenna—M. S. Siukola (p. 49)

A new simple and rugged television antenna has been developed for vhf high channels. The antenna utilizes pairs of slot radiators cut longitudinally in a vertical pipe. In each pair the slots are fed in opposite phase, and the pairs are displaced one-quarter wavelength from each other along the pole. Every other pair is in one vertical plane and the remaining pairs in another perpendicular to this. The slots are fed with a traveling wave within the pole.

The excellent characteristics, most of them inherent in the principle, derive from the unique combination of supporting structure, transmission line, and radiators. The horizontal pattern is formed on a turnstile principle from excellent patterns of single slot pairs even at large pole diameters. The smooth vertical pattern which helps to achieve uniform field strength within the service area is based on exponentially decaying traveling-wave feed. This is especially important in high-gain applications. Proper electrical characteristics of simple slot radiators maintain constant wavelength instead of constant velocity in the transmission line for frequencies in the channel. This assures proper bandwidth. Low-input vswr is due to the traveling-wave nature of the feed. The construction of the antenna is particularly suitable for handling high power. Simplicity of the antenna and low wind load result in economy of both the antenna and the supporting structure.

#### Practical Aspects of TV Tuner Design—C. D. Nestlerode (p. 59)

This paper discusses some of the tv tuner design problems experienced by the author during the product design of tuners used in DuMont Telesets. The subjects discussed are: oscillator radiation, spurious responses, provision for uhf reception, and a typical vhf wafer switch tuner design.

After taking normal precautions of shielding and circuit isolation, the problem of minimizing oscillator radiation reduces to practical aspects of shaft grounding, dress of tuner leads, and interchassis connection points.

The rejection of spurious responses involves the proper choice of tuned circuits and coupling means. All types of direct coupling used in place of mutual coupling have high-pass or low-pass characteristics which reduce the attenuation of frequencies outside the pass

band. It is shown that the combination of variable tuned circuits with low-pass characteristics and a fixed tuned high-pass IF rejection filter can achieve adequate attenuation of spurious responses.

The problems which arise from use of the tuner as an IF preamplifier for uhf reception are discussed and the mechanics of a typical vhf tuner and uhf tuner drive system are described.

#### A Constant Input-Impedance RF Amplifier for VHF Television Receivers—H. B. Yin and H. M. Wasson (p. 65)

Most conventional television tuners exhibit undesirable variations of input impedance at different frequencies within the pass bands and with varying bias voltages applied to the rf amplifier tube. An analysis of the input characteristics of such tuners and commercial television antenna systems, including transmission lines, shows the formation of selective mismatch under certain conditions which may form "holes" within the pass band of any television channel. Such holes degrade the picture quality, particularly for color reception when a deep hole falls upon the color subcarrier. One solution to this problem is presented in this paper, using a constant input-impedance rf amplifier which consists of two stages of grounded-grid triodes in cascade with age voltage being applied to the grid of the second stage. Other performance characteristics of this amplifier, such as noise factor, gain, overloading capability, cross modulation, etc., as compared to those of a conventional cascade rf amplifier, also are described.

#### Color TV Recording on Black and White Lenticular Film—J. M. Brumbaugh, E. D. Goodale and R. D. Kells (p. 71)

In order to present a feature tv program during the favored hours in both the eastern and western parts of the U.S., some form of three-hour "storage" is necessary. Production costs and performer fatigue preclude repeating the live show. For about eight years, monochrome shows have been recorded on film for this purpose, and for later rebroadcast and record purposes.

Several systems have been under study for similar storage of color programs. The first to achieve commercial usage is that described herein, which is based on a refinement of Eastman's early "Kodacolor" process, marketed around 1930. The medium is a "black and white" photographic emulsion, requiring only normal processing, on an embossed 35-mm film base. Tiny horizontal cylindrical lenses are moulded on the base surface, opposite the emulsion. R, G, and B "separation images"

(each consisting of ultraviolet light only) are focused, in registry, in the base. The light for each separation image comes from the lens at different approach angles, so that the R, G, and B information in the composite image lies in separate emulsion strips behind each "lenticule" or cylindrical lens. Color information is recovered through essentially inverse optics. The electronic and optical systems are described in the paper. The over-all system has received commercial acceptance. It provides reasonable cost, adequate safety-factor in processing time, and reproductibility as a 16-mm color print.

#### Transistor Design for Picture IF Stages—R. J. Turner and P. Hermann (p. 76)

In addition to the conventional problems of sensitivity, bandwidth, and transient response, the transistor poses several new problems in television IF design due to its power gain mechanism. In particular, the resistive and capacitive components of output impedance dictate the matched power gain can be obtained only at or below matched bandwidth, and definite limits are thereby imposed on the loaded Q of each stage. Data are presented for high-frequency graded base transistors and high-frequency tetrode transistors. The over-all performance of a five-stage video IF is discussed in terms of: 1) single stage data, 2) stability requirements, 3) method of achieving agc, 4) agc and overload characteristics, 5) pole pattern, gain, and transient response, and 6) noise figure.

#### Color Signal Distortions in Envelope Type of Second Detectors—B. D. Loughlin (p. 81)

When an NTSC color signal transmission is detected by an envelope type of second detector, several distortion components can be produced. In saturated color areas the detected luminance signal may be lower than the intended level, and additionally a 920-kc color-sound beatnote may result.

This paper reviews the characteristics of envelope detectors which produce these color signal distortions and discusses the expected magnitude of these distortions. Some of the methods currently used to reduce these distortions to a tolerable level also are reviewed. Further, several detector system arrangements are described in which these distortions can be cancelled or eliminated.

#### A New Approach to Horizontal Deflection Tube Testing—G. M. Lankard (p. 94)

Static methods of testing horizontal deflection tubes have become inadequate and are being replaced by more significant methods of dynamic testing. This paper presents the problems encountered in arriving at a suitable dynamic test. It suggests a desirable test method to drive the horizontal deflection tube with a square-wave signal, thus permitting the measurement of such parameters as peak currents, Ib-to-Ic2 ratio, and the voltage at the knee of the plate characteristic.

#### Transistorized Television Vertical Deflection System—W. F. Palmer and G. Schiess (p. 98)

Currently available power transistors are capable of driving the deflection coils of large screen television sets without impedance transformation. Direct-coupled, single-ended deflection amplifiers, and problems and their solutions relative to decentering due to dc yoke current components, are discussed.

Sawtooth generators using transistor multivibrators and blocking oscillators have been studied. Various methods of coupling sawtooth generators to the output stage are shown.

Design of vertical deflection section of a 21-inch television receiver employing transistors is discussed with practical circuits being given.

Transistor requirements of these circuits are also reviewed.

1957 Awards of the PGBTR (p. 106)

## Component Parts

VOL. CP-4, No. 3, SEPTEMBER, 1957

Information for Authors (p. 71)

Professional Group on Component Parts Administrative Committee for 1957-1958 (p. 72)

Dielectric Films in Aluminum and Tantalum Electrolytic and Solid Tantalum Capacitors—John Burnham (p. 73)

The characteristics of electrolytic capacitors are determined primarily by the nature of the dielectric oxide film. The nature of this film and the factors which influence its physical and chemical characteristics are discussed.

Electron photomicrographs of the electrolytic oxide film on aluminum, as well as X-ray diffraction and direct electrical measurements of the dry oxide film, reveal that it is crystalline  $\gamma\text{-Al}_2\text{O}_3$ . The characteristics of electrolytic  $\text{Ta}_2\text{O}_5$  films on tantalum are compared with those on aluminum, and the factors that make tantalum capacitors more reliable are indicated.

Transformer Design for Zero Phase Shift—N. R. Grossner (p. 82)

A design method for obtaining minimum phase shift between output and input of a transformer is described. The method is applicable to precision reference transformers employed in analog computers and servo loops where minimum quadrature voltages are mandatory.

A rigorous analysis of the equivalent circuit of the transformer demonstrates that the transformer can be treated as a combination lead and lag network to yield zero phase shift. This is done by making the ratio of primary resistance to primary shunt reactance equal to the quotient of total leakage reactance and load resistance. The procedure consists of 1) designing for theoretical zero phase shift, 2) manual adjustment of the air gap in the magnetic circuit, and 3) precision trimming of the load resistance. Very small shifts of the order of 16 to 50 seconds are obtainable. Optimum techniques for stabilization of phase shift in the presence of frequency, voltage, and temperature variations are also discussed.

Modern Batteries—W. J. Hamer (p. 86)

This article gives an outline of the electric batteries in use today. Included are discussions of primary, secondary, and reserve batteries with a section on batteries as component parts. Also included are discussions of special types of primary batteries, namely, solid-electrolyte batteries, waxy-electrolyte batteries, ion exchange batteries, and nuclear cells.

Bounds for Thermistor Compensation of Resistance and Conductance—A. B. Soble (p. 96)

This paper shows how to compensate the exponential relation between thermistor resistance and temperature: 1) by means of two constant resistances, so that the compensated resistance becomes an S curve winding around an oblique straight line; and 2) by means of three constant resistances, so that the compensated conductance becomes such an S curve.

Formulas are given for the constant resistances so that the errors of the S curve approximations to the oblique lines do not exceed preassigned tolerances.

The first type of compensation is used to compensate a component whose resistance increases linearly with temperature, so that the resistance of the compensated component remains constant within a preassigned tolerance

throughout a preassigned temperature range of operation.

The second type of compensation is applicable to temperature measurement.

Contributors (p. 102)

## Information Theory

VOL. IT-3, No. 3, SEPTEMBER, 1957

Brockway McMillan (p. 172)

Where Do We Stand?—Brockway McMillan (p. 173)

Detection of Fluctuating Pulsed Signals in the Presence of Noise—Peter Swerling (p. 175)

This paper treats the detection of pulsed signals in the presence of receiver noise for the case of randomly fluctuating signal strength. The system considered consists of a predetection stage, a square law envelope detector, and a linear postdetection integrator. The main problem is the calculation of the probability density function of the output of the postdetection integrator. The analysis is carried out for a large family of probability density functions of the signal fluctuations and for very general types of correlation properties of the signal fluctuations. The effects of nonuniform beam shape and of nonuniform weighting of pulses by the postdetection integrator are also taken into account. The function which is actually evaluated is the Laplace transform of the probability density function of the integrator output. In many of the cases treated, the resulting Laplace transform has an inverse of known form. In such cases the evaluation of the probability density function would require the computation of a finite number of constants; in practice this would usually require the use of computing machinery, but would be perfectly feasible with presently available computing machinery.

Fixed Memory Least Squares Filters Using Recursion Methods—Marvin Blum (p. 178)

Given a set of equally spaced measurements, it is possible to curve fit a "least squares" polynomial to the  $N$  observed data points and obtain estimates of the past, present, or future values of the data or its derivatives by appropriate manipulations of the curve fit.

This curve fitting can be accomplished by a linear weighting of the observed data over an interval  $(n-1)T$ . If the data is measured in real time such that a new data point is observed each  $T$  seconds, then the desired output (for example, the smooth or predicted value of the data) can be obtained by sliding these fixed number of weights such that the same weight always multiplies the data which is at a fixed lag with respect to the most recent data. Since these weights are zero for lags greater than  $n$ , they may be described as a fix-finite memory linear digital filter.

In calculating the desired output for each new sample one requires a machine which can store  $n$  coefficients,  $n$  data points and performs  $n$  multiplications and  $n-1$  additions in at least  $T$  seconds. The coefficients do not change but the multiplications and additions must be performed each  $T$  seconds as a new data point is measured.

For large values of  $n$ , and small  $T$ , this may put a severe requirement on the real time solutions of the computer. This paper presents an alternate technique using recursion formulas to obtaining the same results as the  $n$  point weighting equation. The method has the advantage of requiring considerably less storage, multiplications and additions when  $n \gg 1$  and the degree of the curve fitting polynomial ( $K$ ) is small.

Locally Stationary Random Processes—R. A. Silverman (p. 182)

A new kind of random process, the locally stationary random process, is defined, which includes the stationary random process as a special case. Numerous examples of locally stationary random processes are exhibited. By the generalized spectral density  $\Psi(\omega, \omega')$  of a random process is meant the two-dimensional Fourier transform of the covariance of the process; as is well known, in the case of stationary processes,  $\Psi(\omega, \omega')$  reduces to a positive mass distribution on the line  $\omega = \omega'$  in the  $\omega, \omega'$  plane, a fact which is the gist of the familiar Wiener-Khinchine relations. In the case of locally stationary random processes, a relation is found between the covariance and the spectral density which constitutes a natural generalization of the Wiener-Khinchine relations.

The Solution of a Homogeneous Wiener-Hopf Integral Equation Occurring in the Expansion of Second-Order Stationary Random Functions—D. C. Youla (p. 187)

In many of the applications of probability theory to problems of estimation and detection of random functions an eigenvalue integral equation of the type

$$\phi(x) = \lambda \int_0^T K(x-y)\phi(y)dy, \quad 0 \leq x \leq T,$$

is encountered where  $K(x)$  represents the covariance function of a continuous stationary second-order process possessing an absolutely continuous spectral density.

In this paper an explicit operational solution is given for the eigenvalues and eigenfunctions in the special but practical case when the Fourier transform of  $K(x)$  is a rational function of  $\omega^2$ , *i.e.*,

$$K(x) \doteq G(s^2) = \frac{N(s^2)}{D(s^2)}, \quad s = i\omega,$$

in which  $N(s^2)$  and  $D(s^2)$  are polynomials in  $s^2$ .

It is easy to show by elementary methods that the solutions are of the form

$$\phi(x) = \sum_r C_r e^{-\alpha_r x} \cos(\beta_r x + \gamma_r),$$

the constants  $C_r$ ,  $\alpha_r$ ,  $\beta_r$ , and  $\gamma_r$  being linked together by the integral equation. It is precisely the labor involved in their determination that in practice often causes the problem to assume awesome proportions. By means of the results given herein, this labor is diminished to the irreducible minimum—the solving of a transcendental equation.

The Correlation Function of Smoothly Limited Gaussian Noise—R. F. Baum (p. 193)

The correlation function of "smoothly" limited Gaussian noise is calculated and compared with the correlation function of "extremely" clipped Gaussian noise. The limiting function is assumed to have the shape of the error integral curve. The output spectrum is calculated for the case of noise passed through an RC filter.

On the Role of Dynamic Programming in Statistical Communication Theory—R. Bellman and R. Kalaba (p. 197)

In this paper we wish to show that the fundamental problem of determining the utility of a communication channel in conveying information can be interpreted as a problem within the framework of multistage decision processes of stochastic type, and as such may be treated by means of the theory of dynamic programming.

We shall begin by formulating some aspects of the general problem in terms of multistage decision processes, with brief descriptions of stochastic allocation processes and learning processes. Following this, as a simple example of the applicability of the techniques of dynamic programming, we shall discuss in detail a

problem posed recently by Kelly. In this paper, it is shown by Kelly that under certain conditions, the rate of transmission, as defined by Shannon, can be obtained from a certain multistage decision process with an economic criterion. Here we shall complete Kelly's analysis in some essential points, using functional equation techniques, and considerably extend his results.

**Complex Processes for Envelopes of Normal Noise**—Richard Arens (p. 204)

The paper presents a brief exposition of the technique of complex normal random variables as utilized in the study of the envelopes of Gaussian noise processes. The central concept is the pre-envelope  $z(t)$  of a real normal process. The pre-envelope  $z(t)$  of a real function  $x(t)$  is a complex function whose real part is  $x(t)$  and whose absolute value is the envelope, in the sense of high-frequency theory, of  $x(t)$ . The joint probability density for  $z(t)$ ,  $z'(t)$  is found and used to get the threshold crossing rate. Consideration of nonstationary processes is included.

**Correspondence** (p. 208)

**Contributors** (p. 208)

## Reliability & Quality Control

PGRQC-12, NOVEMBER, 1957

**A Redundancy Analog**—A. C. Block  
**The Reliability Qualification of Electronic Equipment**—D. W. Pertschuk  
**Passive Components for Submarine Telephone Cable Repeaters**—M. C. Wooley  
**Statistical Aspects of Reliability in Systems Development**—J. S. Youtcheff

A system reliability program is an operational procedure for obtaining the over-all reliability objectives in the development of a system. The reliability program must be closely integrated with the system developmental activities to assure that the over-all program objectives are fully obtained within the required time scale. The analytical objectives of the system reliability program are twofold. First, the specified system reliability requirements must be apportioned to the subsystems and components to assure adequate equipment design. Second, as component and

subsystem design data are made available throughout the development program, this information must be utilized in predicting the system reliability. In predicting system reliability, it is necessary to determine both the component reliability relationships and the individual component failure probabilities. Several statistical methods for determining component reliability are presented; however, the exact methodology must be tailored to the specific system and development program. System reliability can be predicted by utilizing component reliability data together with an adequate analysis of component and subsystem reliability relationships.

**A Sequential Test for Comparing Component Reliabilities**—C. F. Stevens

A statistical technique is presented by means of which the reliabilities of two types of component (or equipment) may be compared, and a decision made in favor of one type or the other. The technique differs from those previously devised for this purpose in that the assumptions on which it is based are less restrictive and thus more likely to be satisfied in practice.



# Abstracts and References

Compiled by the Radio Research Organization of the Department of Scientific and Industrial Research, London, England, and Published by Arrangement with that Department and the *Electronic and Radio Engineer*, incorporating *Wireless Engineer*, London, England

NOTE: The Institute of Radio Engineers does not have available copies of the publications mentioned in these pages, nor does it have reprints of the articles abstracted. Correspondence regarding these articles and requests for their procurement should be addressed to the individual publications, not to the IRE.

Acoustics and Audio Frequencies.....	386
Antennas and Transmission Lines.....	386
Automatic Computers.....	387
Circuits and Circuit Elements.....	387
General Physics.....	389
Geophysical and Extraterrestrial Phenomena.....	390
Location and Aids to Navigation.....	391
Materials and Subsidiary Techniques..	391
Mathematics.....	394
Measurements and Test Gear.....	394
Other Applications of Radio and Electronics.....	395
Propagation of Waves.....	396
Reception.....	396
Stations and Communication Systems..	396
Subsidiary Apparatus.....	397
Television and Phototelegraphy.....	397
Transmission.....	397
Tubes and Thermionics.....	398
Miscellaneous.....	400

The number in heavy type at the upper left of each Abstract is its Universal Decimal Classification number and is not to be confused with the Decimal Classification used by the United States National Bureau of Standards. The number in heavy type at the top right is the serial number of the Abstract. DC numbers marked with a dagger (†) must be regarded as provisional.

## ACOUSTICS AND AUDIO FREQUENCIES

534.121.1 **3721**

The Calculation of the Resonance Frequencies of Radially Oscillating Circular Disks and Rings—E. Tränkle. (*Frequenz*, vol. 11, pp. 142-145; May, 1957.)

534.2-14 **3722**

Sound Diffraction at a Thin Bounded Elastic Cylindrical Shell—L. M. Lyamshev. (*C.R. Acad. Sci. U.R.S.S.*, vol. 115, pp. 271-273; July 11, 1957. In Russian.) Brief mathematical analysis. See also 309 of 1956.

534.24 **3723**

Reflection of Plane Waves of Sound from a Sinusoidal Surface—H. S. Heaps. (*J. Appl. Phys.*, vol. 28, pp. 815-818; July, 1957.) The amplitudes of the reflected plane, undamped waves are calculated for the least mean square value of the surface pressure. Good agreement is obtained with the values measured by LaCasce and Tainarkin (1938 of 1956).

534.76 **3724**

Experimental Investigations of Monaural Acoustic Localization—A. Manfredi, L. Fiori-Ratti, and S. Criò. (*Ricerca Sci.*, vol. 27, pp. 1155-1160; April, 1957.) Test results indicate the existence in the human ear of a faculty of auditory perspective, particularly for noises of short duration and high harmonic content.

621.395.61 **3725**

On the Phasing of Microphones—B. B. Bauer. (*IRE TRANS.*, vol. AU-4, pp. 155-161; November-December, 1956. Abstract, *PROC. IRE*, vol. 45, pp. 571-572; April, 1957.)

621.395.623.7 **3726**

Loudspeakers in Parallel—J. Moir. (*Wire-*

*less World*, vol. 63, pp. 479-481; October, 1957.) No increase in source size is obtained but advantages exist including lower distortion and increased efficiency.

621.395.623.742:621.375.2.029.3 **3727**

Amplifiers with Directly Coupled Loudspeakers—J. Rodrigues de Miranda. (*Tijdschr. ned. Radiogenoot*, vol. 22, pp. 15-27; January, 1957.) Description of an electrodynamic loudspeaker with 800- $\Omega$  speech coil wound with wire of 40- $\mu$  diameter. A response essentially flat between 20 c and 100 kc is obtained using a preamplifier and a single-ended push-pull amplifier without output transformer. Circuit and characteristics are shown.

621.395.625.3 **3728**

On the Resolving Power in the Process of Magnetic Recording—S. Duinker. (*Tijdschr. ned. Radiogenoot*, vol. 22, pp. 29-48; January, 1957. In English.) Universal field curves are derived for various distances from a recording head of two semi-infinite pole pieces of infinite permeability, and lines of equal field strength are obtained for the resultant field. The recording process is analyzed for the case of a pulse superimposed on a steady dc, with and without ac bias. Resolution, defined in terms of a limiting wavelength, depends on the shape of the field curve and depth of magnetization; with ac bias the relative strength of the biasing field and the critical field strength for the tape are also important. Without ac bias resolution of the order of the gap length is obtainable; with bias a much shorter wavelength can be recorded.

621.395.625.3:621.397.5 **3729**

Video Tape Recorder uses Revolving Heads—Snyder. (See 4018.)

## ANTENNAS AND TRANSMISSION LINES

621.372.2 **3730**

A Graphical Approach to the Study of Irregularities in Transmission Lines—W. T. Blackband. (*Proc. IEE*, Pt. C, vol. 104, pp. 433-438; September, 1957.)

621.372.2 **3731**

Resonance in Two Coupled Sections of a Line with Low Losses—N. S. Kochanov. (*Radiotekhnika, Moscow*, vol. 11, pp. 60-62; July, 1956.) Brief mathematical analysis.

621.372.2:621.372.8 **3732**

A New Type of Surface Waveguide with Bandpass Properties—D. Marcuse. (*Arch. elekt. Übertragung*, vol. 11, pp. 146-148; April, 1957.) An axially stacked waveguide is described which consists of thin circular metal

disks alternating with disks of dielectric material. Transmission of surface waves only takes place in certain frequency bands. Some transmission constants are calculated.

621.372.2:621.372.8 **3733**

Double-Slab Arbitrary-Polarization Surface-Wave Structure—R. E. Plummer and R. C. Hansen. (*Proc. IEE*, Pt. C, vol. 104, pp. 465-471; September, 1957.) An analysis of the double-layer dielectric slab on a perfectly conducting surface. Conditions permitting the propagation of a wave of arbitrary polarization are derived.

621.372.8 **3734**

A Note on the Excitation of Surface Waves—A. L. Cullen. (*Proc. IEE*, Pt. C, vol. 104, pp. 472-474; September, 1957.) An extension of results on the launching efficiency obtained in a previous paper (22 of 1055.)

621.372.2.011.2 **3735**

The Characteristic Impedance of a Slotted Coaxial Line—R. E. Collin. *IRE TRANS.*, vol. MTT-4, pp. 4-8; January, 1956. Abstract, *PROC. IRE*, vol. 44, p. 581; April, 1956.)

621.372.8 **3736**

Waveguide Characteristics—A. E. Karbowiak. (*Electronic Radio Eng.*, vol. 34, pp. 379-287; October, 1957.) Application of the surface impedance approach to the analysis of wave propagation in parallel-plane, rectangular, and circular waveguides leads to a general expression for the propagation coefficient, which holds above and below as well as at the cutoff frequency. Numerical examples are given.

621.372.8 **3737**

Analysis of Some Types of Septate Waveguides—R. G. Mirimanov and G. I. Zhileiko. (*Radiotekhnika i Elektronika*, vol. 2, pp. 172-183; February, 1957.) Six types of waveguides are considered and their main characteristics tabulated.

621.372.8 **3738**

Propagation of Transients in Waveguides—A. E. Karbowiak. (*Proc. IEE*, Pt. C, vol. 104, pp. 339-348; September, 1957.) Basic theory is developed and applied to the propagation of a unit-step-modulated carrier and of pulses. Formulas and graphs are outlined and numerical examples given.

621.372.8 **3739**

Mode Separation at the  $\pi$ -Mode in a Dielectric-Loaded Waveguide Cavity—G. B. Walker and N. D. West. (*Proc. IEE*, Pt. C, vol. 104, pp. 381-387; September, 1957.) A

finite group velocity at the  $\pi$ -mode frequency can be obtained in a waveguide loaded with solid dielectric disks which are reflectionless at the required frequency. Central holes required in the disks to permit passage of an electron beam set up evanescent and the propagating modes but operation is still possible in the  $\pi$  mode.

621.372.8 3740

**A Contribution to the Design of Multi-element Directional Couplers**—J. W. Crompton. (*Proc. IEE*, Pt. C, vol. 104, pp. 398-402; September, 1957.) Analysis of a cascaded set of 2-element couplers emphasizes physical principles and enables the coupling factors and dimensional tolerances of elements to be easily calculated.

621.372.8 3741

**Calculation of Symmetrical Junctions in Waveguides of Circular Section for Waves of the  $H_{0n}$ -Type**—Yu. N. Kazantsev. (*Radiotekhnika i Elektronika*, vol. 2, pp. 150-156; February, 1957.) The reflection coefficient is derived for several forms of dielectric insert and also for a conical metal coupling between two circular waveguides. The dielectric load is calculated which has a small reflection coefficient for the  $H_{01}$  mode.

621.372.8 3742

**Waveguide Power Dividers**—T. G. Hame. (*Electronic Eng.*, vol. 29, pp. 368-373; August, 1957.) New forms of T and Y junctions incorporating wide-band matching wedges or mitres.

621.372.8:538.6 3743

**Gyromagnetic Excitation of a Waveguide**—V. V. Nikol'ski. (*Radiotekhnika i Elektronika*, vol. 2, pp. 157-161; February, 1957.) The formula for the gyromagnetic excitation of a waveguide is generalized for any direction of a constant magnetic field. The use of ferrite slabs or rods magnetized in different planes in rectangular or cylindrical waveguides or in coaxial lines is described.

621.372.8:621.318.134 3744

**Broad-Band Ferrite Microwave Isolator**—P. H. Vartanian, J. L. Melchor, and W. P. Ayres. (*IRE TRANS.*, vol. MTT-4, pp. 8-13; January, 1956. Abstract, *Proc. IRE*, vol. 44, p. 581; April, 1956.)

621.372.8:621.318.134:621.372.5 3745

**The Gyrator**—Roddam. (See 3769.)

621.396.67.029.62:621.3.012.12 3746

**Distortion of a Polar Diagram due to Interposition of Wooden Screen in the Vicinity of a V.H.F. Radiator**—H. R. B. Seetharam and M. N. Gadre. (*J. Inst. Telecommun. Eng., India*, vol. 3, pp. 140-156; March, 1957.) A theoretical and experimental study for different forms, coatings, and humidity.

621.396.677.75 3747

**A Method of Estimating the Power Radiated Directly at the Feed of a Dielectric-Rod Aerial**—R. H. Clarke. (*Proc. IEE*, Pt. B, vol. 104, pp. 511-514; September, 1957.) The method is based on a simple transmission-line analog. As an example the radiation system at  $\text{cm } \lambda$  of a waveguide-fed rod of rectangular cross section is found.

621.396.677.8 3748

**A Method of Raising the Efficiency of Simple Wide-Band Aerials**—S. I. Nadenenko. (*Radiotekhnika, Moscow*, vol. 11, pp. 25-30; August, 1956.) The efficiency of the symmetrical dipole is increased by a plane reflector consisting of conductors parallel to the dipole and supported by the same masts.

621.396.677.8:523.16 3749

**New Radio Telescope**—(*Wireless World*, vol. 63, pp. 477-478; October, 1957.) A brief description of the aperture synthesis technique to be used with the antenna system of the radio astronomy observatory at Cambridge, England.

621.396.677.833:523.16 3750

**The Jodrell Bank Radio Telescope**—Lovell. (See 3847.)

621.396.677.85 3751

**Recent Research on Microwave Optical Systems**—N. Carrara, L. Ronchi, M. Schaffner, and G. Toraldo di Francia. (*Alta Frequenza*, vol. 26, pp. 116-158; April/June, 1957.) Survey of work carried out between 1953 and 1955 at the "Center for Studies in Microwave Physics" in Florence. Some lenses of configuration type are described, including the "Toraldito" lens which is suitable for the rapid scanning of large angles. Methods of aberration correction and the development of microwave lens systems analogous to thick optical lenses are discussed.

#### AUTOMATIC COMPUTERS

681.142 3752

**Progress in Automatic Computers, 1956**—A. Walther and W. Hoffman. (*Z. Ver. Dtsch. Ing.*, vol. 99, pp. 731-737; June 1, 1957.) Brief survey with 198 references.

681.142 3753

**The Design of the Ferranti Pegasus Computer: Part 1**—T. G. H. Brauholtz. (*Electronic Eng.*, vol. 29, pp. 358-363; August, 1957.) A record of some of the considerations from which the design was developed.

681.142 3754

**The Random-Access Memory Accounting Machine**—(*IBM J. Res. Devel.*, vol. 1, pp. 62-71, 72-75; January, 1957.)

**Part 1—System Organization of the IBM 305**—M. L. Lesser and J. W. Haanstra.

**Part 2—The Magnetic-Disk, Random-Access Memory**—T. Noyes and W. E. Dickinson.

681.142 3755

**Machine for Solving Polynomial Equations of Higher Degrees**—G. C. Brack. (*Elektron. Rundschau*, vol. 11, pp. 183-187; June, 1957.)

The method applies to equations with complex coefficients of theoretically any degree. The apparatus described is compact and can be used for solving equations of the fifth degree; solutions are indicated on a tube voltmeter and cro. Operation is illustrated by examples.

681.142 3756

**High-Speed Analogue-to-Digital Converters**—G. J. Herring and D. Lamb. (*J. Brit. IRE*, vol. 17, pp. 407-420; August, 1957.) A summary of general principles in the conversion of voltages from analog computers into digital form, for subsequent processing, and detailed circuits of one such converter. 100-kc pulses are controlled by gates operated by the input voltages in a servo-type circuit.

681.142 3757

**Two New Comparison Instructions for a Three-Address Electronic Digital Computer**—L. Dadda. (*Ricerca Sci.*, vol. 27, pp. 1125-1132; April, 1957.) Description of a programming system based on a particular criterion for comparing binary numbers.

681.142 3758

**A Control Circuit for Magnetic-Drum Storage Systems in Electronic Computers**—L. Dadda. (*Ricerca Sci.*, vol. 27, pp. 1482-

1488; May, 1957.) The circuit described is used for checking binary number read-out for a particular storage system.

681.142 3759

**Digital Compensation for Control and Simulation**—J. Tou. (*Proc. IRE*, vol. 45, pp. 1243-1248; September, 1957.) A technique is described for improving the performance of digital feedback control systems and operational digital simulators by making use of the computer to perform information programming or data processing.

681.142:621-5 3760

**Integration of Computers with Factory Processes**—A. H. Copper. (*J. Brit. IRE*, vol. 17, pp. 431-440; August, 1957.)

681.142:621.3.049.75 3761

**A Three-Dimensional Printed Back Panel**—E. R. Wyma. (*IBM J. Res. Devel.*, vol. 1, pp. 32-38; January, 1957.) Description of a new design for interconnections of printed-circuit packages in the IBM 608 transistorized computer.

681.142:621.375.3 3762

**Magnetic Computer has High Speed**—T. H. Bonn. (*Electronics*, vol. 30, pp. 156-160; August 1, 1957.) Details are given of the magnetic-amplifier circuits and various types of core material.

#### CIRCUITS AND CIRCUIT ELEMENTS

621.3.049.75 3763

**Calculation of Stray Capacitances in Printed Circuit Assemblies of Radio Equipment**—L. M. Kononovich. (*Radiotekhnika, Moscow*, vol. 11, pp. 64-70; August, 1956.) The derivation of design formulas is based on a conformal transformation of printed conductors of various configurations into a coaxial long line.

621.316.82:621.314.63 3764

**Some Characteristics of Metallic Varistors**—G. W. Holbrook and A. L. Dulmage. (*Electronic Eng.*, vol. 29, pp. 386-392; August, 1957.) An attempt is made to provide an equivalent circuit which is applicable to all values of voltages within the rated limits, leading to an expression for describing the performance of the rectifier used as a variable resistor.

621.319.4 3765

**A New Theorem in Electrostatics with Applications to Calculable Standards of Capacitance**—D. G. Lampard. (*Proc. IEE*, Pt. C, vol. 104, pp. 271-280; September, 1957.)

621.372.412 3766

**Standard Hyper-Q Quartz Crystal (100-kc/s GT-Cut)**—Y. Hiruta. (*J. Radio Res. Labs., Japan*, vol. 4, pp. 127-129; April, 1957.) A brief description with photographs and graphical data.

621.372.44 3767

**Transient Response of Two-Terminal Networks**—O. P. D. Cutteridge. (*Proc. IEE*, Pt. C, vol. 104, pp. 234-239; September, 1957.)

621.372.5 3768

**Impedance Transformations by Extension of the Isometric Circle Method to the Three-Dimensional Hyperbolic Space**—E. F. Bolinder. (*J. Math. Phys.*, vol. 36, pp. 49-61; April, 1957.) The analysis or synthesis of a lossy quadrupole from three measurements and the cascading of lossy networks are considered.

621.372.5:621.372.8:621.318.134 3769

**The Gyrator**—T. Roddam. (*Wireless World*, vol. 63, pp. 423-426, 497-500; October, 1957.)

- Nonreciprocity in certain electrical networks is discussed and compared with that in the mechanical gyroscope. A description is given of the classical physics background of the Faraday rotation in a nonreciprocal, microwave device, using a ferrite in an applied magnetic field.
- 621.372.5.029.6 3770  
**General Active, Passive and Nonreciprocal Quadripoles**—G. W. Epprecht. (*Tech. Mitt. Schweiz. Telegr.-Teleph. Verw.*, vol. 35, pp. 169–193; May 1, 1957.) An introduction to quadripole theory with particular reference to microwave applications.
- 621.372.512 3771  
**An All-Pass Network**—W. P. Wilson. (*Electronic Radio Eng.*, vol. 34, pp. 391–394; October, 1957.) A study of transient response in terms of a finite series of Laguerre functions.
- 621.372.512 3772  
**The Characteristics of All-Pass Sections**—W. Taeger. (*Frequenz*, vol. 11, pp. 145–153; May, 1957.) Parallel-T and bridge networks with and without losses are discussed.
- 621.372.54 3773  
**Design Data for Symmetrical Darlington Filters**—J. K. Skwirzynski and J. Zdunek. (*Proc. IEE*, Pt. C, vol. 104, pp. 366–380; September, 1957.) Practical design data are given in graphical form for symmetrical, equally terminated filters consisting of reactances only. Underlying theory is explained with practical hints for alignment of the network.
- 621.372.54 3774  
**Analysis and Synthesis of Transitional Butterworth-Thomson Filters and Band-Pass Amplifiers**—Y. Peless and T. Murakami. (*RCA Rev.*, vol. 18, pp. 60–94; March, 1957.) A new class of filters, designated transitional Butterworth-Thomson (TBT), is described. These have more favorable transient characteristics than either the Butterworth- or Thomson-type filters.
- 621.372.54:519.241.1 3775  
**The Probability Distribution for the Filtered Output of a Multiplier whose Inputs are Correlated, Stationary, Gaussian Time Series**—D. C. Lampard. (*IRE TRANS.* vol. IT-2, pp. 4–11; March, 1956. Abstract, *PROC. IRE*, vol. 44, pp. 955–956; July, 1956.)
- 621.372.54.029.64 3776  
**An Improved Design Procedure for the Multisection Generalized Microwave Filter**—R. Levy. (*Proc. IEE*, Pt. C, vol. 104, pp. 423–432; September, 1957.) An exact treatment of the  $Q$  factor of a direct-coupled filter. Design formulas are given for the bandwidth, pass-band tolerance, and the attenuation in the rejection band for both quarter-wave-coupled and direct-coupled generalized filters.
- 621.372.54.029.64:621.372.8 3777  
**Microwave Filters utilizing the Cut-Off Effect**—P. A. Rizzi. (*IRE TRANS.*, vol. MTT-4, pp. 36–40. January, 1956. Abstract, *PROC. IRE*, vol. 44, p. 581; April, 1956.)
- 621.373.076 3778  
**Posicast Control of Damped Oscillatory Systems**—O. J. M. Smith. (*PROC. IRE*, vol. 45, pp. 1249–1255; September, 1957.) A method of producing dead-beat response in a lightly damped oscillatory feedback system. It consists in exciting several transient oscillations with magnitudes and phases so adjusted that the resultant of the transient oscillation vectors is zero.
- 621.373.4 3779  
**External Influences on an Oscillator**—S. I. Evtyanov. (*Radiotekhnika, Moscow*, vol. 11, pp. 3–12; June, 1956.) A mathematical analysis of the operation of an oscillator subjected to external influences. Both synchronous and asynchronous conditions of operation are considered.
- 621.373.4.029.63 3780  
**Energy Relations in an U.H.F. Valve Oscillator**—L. N. Kolesov. (*Radiotekhnika, Moscow*, vol. 11, pp. 27–42; June, 1956.) The main energy relationships for an uhf triode oscillator are derived; the effects of electron inertia and of the parameters of the oscillatory system are taken into account.
- 621.373.4.072.9 3781  
**Synchronization of Oscillators by Periodically Interrupted Waves**—D. W. Fraser. (*PROC. IRE*, vol. 45, pp. 1256–1268; September, 1957.) The principles, methods, circuit applications, and the theoretical basis of synchronization are discussed. It is demonstrated theoretically and experimentally that the average frequency of the oscillator can be synchronized to the fundamental component or to any sideband of the interrupted signal.
- 621.373.42 3782  
**Uni-control Wide-Range Oscillator**—S. N. Das. (*Electronic Radio Engr.*, vol. 34, pp. 365–368; October, 1957.) A single tank circuit between grid and anode of a triode uses a combination of a variable LC circuit and a variable short-circuited transmission line to give a frequency range of about 23:1 (e.g., 25–580 mc.). Transition from LC mode to transmission-line mode of operation is smooth.
- 621.373.42 3783  
**Synchronization of a Sinusoidal Valve Oscillator by a Subharmonic Signal**—T. A. Gallit and I. I. Minakova. (*Radiotekhnika, Moscow*, vol. 11, pp. 50–56; July, 1956.) Synchronization is considered for the case in which the frequency of the external signal is close to one of the subharmonics of the oscillator. Various operating conditions of the oscillator are investigated.
- 621.373.42:621.316.729 3784  
**Nonstationary Processes in Self-Oscillating Systems with Strong Excitation by Radio Pulses**—E. S. Voronin and I. I. Rogatnev. (*Radiotekhnika i Elektronika*, vol. 2, pp. 144–149; February, 1957.) The conditions for synchronization of a self-oscillating system are investigated.
- 621.373.421 3785  
**Synchronized Systems with Time Delay in the Loop**—Z. J. Jelonek and C. I. Cowan. (*Proc. IEE*, Pt. C, vol. 104, pp. 388–397; September, 1957.) Filters in the feedback loop of synchronized oscillators can be represented under certain conditions by time delay networks. Stability and pulling effect are investigated.
- 621.373.421:621.376.32 3786  
**Further Studies on Asymmetrical Three-Phase Oscillator for Very Wide Frequency Deviation**—P. Kundu. (*Indian J. Phys.*, vol. 31, pp. 83–98; February, 1957.) The circuit described earlier (1650 of 1956) is modified so that the loop gain of the oscillator is less dependent on the frequency-selective elements. Performance is improved.
- 621.373.43+621.317.755 3787  
**High-Power Pulse Generators**—H. G. Bruijning. (*Tijdschr. ned. Radiogenoot*, vol. 22, pp. 1–14; January, 1957. In English.) Description of 1) the development of a thyatron-controlled generator delivering 0.01- $\mu$ sec 200-kw pulses with repetition rate 2000/sec for a short-pulse radar system; 2) a cro with a bandwidth of 400 mc based on a design described by Janssen (1434 of 1951), but using a thyatron to generate the sampling pulse.
- 621.373.431.1:621.318.57 3788  
**Polyphase Multivibrator**—Ya. E. Belen'ki and A. N. Svenson. (*Radiotekhnika, Moscow*, vol. 11, pp. 39–45; July, 1956.) A circuit is described which requires half the number of tubes and components of existing circuits.
- 621.373.44 3789  
**The Build-Up of Oscillations in an Oscillator Operating in the Decimetre Wavelength Range**—N. F. Alekseev. (*Radiotekhnika, Moscow*, vol. 11, pp. 52–63; August, 1956.) A method is described for decreasing the average delay of the leading edge of a pulse and for reducing the "spread" of the delays. Experiments were carried out to determine the initial amplitudes of self-oscillation and free (damped) oscillation and also the preoscillatory noise. Pulses down to 0.1  $\mu$ sec can be generated even if an input pulse of moderate slope is used.
- 621.373.52:621.314.7 3790  
**Stable Transistor Oscillator**—E. Keonjian. (*IRE TRANS.*, vol. CT-3, pp. 38–44; March, 1956. Abstract, *PROC. IRE*, vol. 44, p. 953; July, 1956.)
- 621.373.52:621.373.431.1 3791  
**Two-Terminal Analysis and Synthesis of Junction-Transistor Multivibrators**—J. J. Suran and F. A. Reibert. (*IRE TRANS.*, vol. CT-3, pp. 26–38; March, 1956. Abstract, *PROC. IRE*, vol. 44, pp. 952–953; July, 1956.)
- 621.373.52:621.373.431.1 3792  
**The Astable Multivibrator using Junction Transistors**—V. Cimagalli. (*Alla Frequenza*, vol. 26, pp. 159–184; April/June, 1957.) The behavior of a transistor multivibrator is analyzed on the basis of transistor theory by taking account of various transistor characteristics including the effect of minority-carrier storage, and close agreement with experimental results is found. A three-transistor square-wave generator is described, which produces a waveform of 1.35-v peak-to-peak amplitude and 0.13- $\mu$ sec rise time.
- 621.374.3 3793  
**Millimicrosecond Time-to-Pulse-Height Converter using an R. F. Vernier**—R. L. Chase and W. A. Higinbotham. (*Rev. Sci. Instr.*, vol. 28, pp. 448–451; June, 1957.) Timing is accomplished by reference to the phase of a high-frequency (20-mc) clock. This is indicated by the phase of a low-frequency (200 kc) beat note produced between the clock signal and one generated by the event to be timed.
- 621.374.3 3794  
**The Construction of a Device for Comparing Code Pulses, with Protection against False Operation, and an Investigation into the Operation of such a Device**—B. V. Rybakov. (*Radiotekhnika, Moscow*, vol. 11, pp. 26–38; July, 1956.) A description is given of a device incorporating a new anticoincidence circuit which prevents false operation caused by varying delays in the application and clearance of the pulses to be registered. The operation of the circuit is discussed in detail.
- 621.375:621.385.029.6:621.396.822 3795  
**The Minimum Noise Figure of Unmatched Amplifiers**—Pözl. (See 4065.)
- 621.375.026+621.373.1]:538.632 3796  
**The Hall Generator as Power Amplifier and Oscillator**—F. Kuhrt. (*Elektrotech. Z., Edn A*, vol. 78, pp. 342–344; May 11, 1957.) Brief description of the construction and operation of the Hall-effect "multiplier" and its use as an oscillator. See also 3939 below.

- 621.375.123 3797  
**Degenerative RC-Coupled Amplifiers without Overshoot**—K. Fränz. (*Archiv. elekt. Übertragung*, vol. 11, pp. 159-162; April, 1957.) Conditions are derived for obtaining freedom from overshoot in multistage RC-coupled amplifiers with negative feedback.
- 621.375.13.029.4 3798  
**Positive Current Feedback in L.F. Amplifiers**—G. Ya. Gurovich. (*Radiotekhnika, Moscow*, vol. 11, pp. 58-62; June, 1956.) Certain types of distortion can be compensated without lowering the amplification factor of the stage.
- 621.375.2.018.75 3799  
**A Linear-Logarithmic Amplifier for Ultra-Short Pulses**—H. Kihn and W. E. Barnette. (*RCA Rev.*, vol. 18, pp. 95-135; March, 1957.) The development is described of a five-stage amplifier having an over-all bandwidth of 180 mc, centered on 180 mc and a total dynamic range of 67 db.
- 621.375.2.024:681.142 3800  
**Drift-Corrected D.C. Amplifier**—M. H. McFadden. (*Electronic Radio Eng.*, vol. 34, pp. 358-364; October, 1957.) The need for drift correction is explained and a continuously drift-corrected amplifier suitable for use in either a repetitive or real-time computer, is described.
- 621.375.2.029.4 3801  
**A Low-Frequency Amplifier with Fractional-Ohm Input Impedance**—K. Landecker. (*J. Electronics Control*, vol. 3, pp. 218-224; August, 1957.) The low-impedance dc source is connected in series with a two-button carbon microphone which is excited at 10 kc by a sound wave of constant amplitude. The interrupted ("chopped") current is fed via a 2500/1 transformer into an amplifier tuned to 10 kc. Linear amplification is obtained from a fraction of a volt down to thermal noise voltages.
- 621.375.2.029.4 3802  
**The Consonant Amplifier-Limiter**—D. B. Daniel. (*Radio ü Telev. News*, vol. 57, pp. 49-51; March, 1957.) Circuit details and performance characteristics for an af limiting device with fast response but without the distortion occurring in conventional "clipper" circuits.
- 621.375.2.029.4 3803  
**A 3-Channel Amplifier**—K. W. Betsh. (*Radio ü Telev. News*, vol. 57, pp. 65-68; March, 1957.) This high-fidelity output amplifier incorporates variable electronic crossovers provision for es loudspeakers.
- 621.375.2.133 3804  
**A 7- to 30-Mc/s Preselector**—E. L. Campbell. (*QST*, vol. 41, pp. 16-18; February, 1957.) The design of a regenerative preamplifier, which increases the over-all gain and selectivity of existing equipment, is described.
- 621.375.232.3.029.3 3805  
**Triode Cathode-Followers: a Graphical Analysis for Audio Frequencies**—T. J. Schultz. (*IRE TRANS.*, vol. AU-4, pp. 42-45; March/April, 1956. Abstract, *PROC. IRE*, vol. 44, pt. 1, p. 830; June, 1956.)
- 621.375.3:621.3.042.001.4 3806  
**Core Tester Simplifies Ferro-amplifier Design**—R. W. Roberts and C. C. Horstman. (*Electronics*, vol. 30, pp. 150-153; August 1, 1957.) A method of testing cores of magnetic material is described; the results are applied in normalized design equations for magnetic amplifiers.
- 621.375.4:621.3.087.6:616 3807  
**Transistor Amplifier for Medical Recording**—D. W. R. McKinley and R. S. Richards. (*Electronics*, vol. 30, p. 161-163; August 1, 1957.) "Pen-recorder amplifier provides transformerless system for recording 3-cps heart signals. Modification of feedback circuit gives audio amplifier with up to 5-w output flat within 0.2 db from 20 cps to 20 kc."
- 621.375.4:621.314.7 3808  
**An N-Stage Series Transistor Circuit**—K. H. Beck. (*IRE TRANS.*, vol. CT-3, pp. 44-51; March, 1956. Abstract, *PROC. IRE*, vol. 44, p. 953; July, 1956.)
- 621.375.4+621.314.7|012.8 3809  
**Electric-Network Representation of Transistors—a Survey**—Pritchard. (See 4047.)
- 621.375.4.024 3810  
**A Transistor D.C. Chopper Amplifier**—P. L. Burton. (*Electronic Eng.*, vol. 29, pp. 393-397; August, 1957.) Junction transistors are used as a switch, linear ac amplifier and synchronous rectifier to raise a thermocouple output of 50 mv to about 3 v for telemetering purposes. Printed circuits are used, and the instrument is encapsulated to the size of a 2-inch cube.
- 621.375.4.029.45 3811  
**Distortion due to the Mismatch of Transistors in Push-Pull Audio-Frequency Amplifiers**—K. W. Gurnett and R. A. Hilbourne. (*Proc. IEE*, Pt. C, vol. 104, pp. 411-422; September, 1957.) An analysis of the transistor parameter variations which give rise to even-harmonic distortion. To minimize the latter, some matching of transistor characteristics is necessary; simple matching techniques are described.
- 621.375.432.9 3812  
**The Emitter-Coupled Differential Amplifier**—D. W. Slaughter. (*IRE TRANS.*, vol. CT-3, pp. 51-53; March, 1956. Abstract, *PROC. IRE*, vol. 44, p. 953; July, 1957.)
- 621.375.9.029.64:538.569.4 3813  
**Superregenerative Masers**—P. F. Chester and D. I. Bolef. (*PROC. IRE*, vol. 45, pp. 1287-1289; September, 1957.) The characteristics of a two-level maser amplifier operated both intermittently and superregeneratively are compared. The sensitivity of gain to changes in operating conditions is shown for the cases of continuous regeneration and superregeneration.
- 621.375.9.029.64:538.569.4 3814  
**Maximum Efficiency of the Solid-State Maser**—H. Heffner. (*PROC. IRE*, vol. 45, p. 1289; September, 1957.) The efficiency of a three-state maser of the type proposed by Bloembergen (1062 of 1957) is estimated for operation at saturation.
- 621.376.223 3815  
**The Behaviour of Modulator Circuits with Complex and, in particular, Selective Terminations**—J. Gensel. (*Frequenz*, vol. 11, pp. 153-159 and 175-185; May and June, 1957.) A quasilinear equivalent circuit is derived by means of which the linear and nonlinear distortion of modulators working into filters can be determined. The circuit parameters are tabulated for modulators of the ring, Cowan and series types. See also 2457 of 1955 (Tucker).
- 621.376.32:621.318.134 3816  
**Ferrites for F.M.**—T. W. G. Calvert. (*Wireless World*, vol. 63, pp. 505-507; October, 1957.) Circuits utilizing the change in permeability of a ferrite under an applied magnetic field are described. Changes in inductance of about 1 per cent are obtained from a control current passed through a winding on the core; a 50 per cent change is possible with an external magnetic field. The upper limit in frequency is about 15 mc.
- 621.396.822 3817  
**Experimental Investigation into the Law of the Peak Distribution of Fluctuations with respect to their Duration**—V. I. Tikhonov. (*Radiotekhnika, Moscow*, vol. 11, pp. 31-35; August, 1956.) Experimental methods are described for determining the density distribution of probability of electrical fluctuations at various levels. From the experimental results obtained a table is compiled which gives the total number of points, recurring at a given level and in a given range, for various lengths of peaks and intervals in a noise waveform.
- 621.396.822:016 3818  
**A Bibliography on Noise**—P. L. Chessin. (*IRE TRANS.*, vol. IT-1, pp. 15-31; September, 1955.) A comprehensive bibliography of material published up to 1954. An index of authors and a list of publishers is included. Entries are arranged under the following headings: 1) source works (textbooks); 2) internal noise sources; 3) external noise; 4) noise generation and measurements; 5) impulsive-type noise; 6) modulation and noise; 7) radar applications; 8) noise, communication, and filtering; 9) statistical theory.

## GENERAL PHYSICS

530.145.61 3819

**Extension of WKB Equation**—C. E. Hecht and J. E. Mayer. (*Phys. Rev.*, vol. 106, pp. 1156-1160; June 15, 1957.) The WKB form for the classical region is used to obtain a simple form for the argument  $z(x)$  which makes the solutions valid through the turning point and into the nonclassical region.

535.13 3820

**On a Class of Solutions of Maxwell's Electromagnetic Equations**—G. E. Hudson and D. H. Potts. (*Commun. pure appl. Math.*, vol. 9, pp. 33-43; February, 1956.)

536.2.01:621.3.09 3821

**The Solution of a Thermal Conduction Problems by means of an Analogy**—H. Schlitt. (*Arch. Elektrotech.*, vol. 43, pp. 51-58; January 12, 1957.) An exact solution of the problem is found by using a system of equations analogous to that of the quadruple equations for a finite homogeneous transmission line.

537.12:551.510.53 3822

**Low-Energy Elastic Scattering of Electrons by Oxygen and Nitrogen**—P. Hammerling, W. W. Shine, and B. Kivel. (*J. Appl. Phys.*, vol. 28, pp. 760-764; July, 1957.) The electron-atom interaction potential is formed from 1) the Hartree potential, 2) an exchange term, and 3) a polarization term. The calculated scattering cross sections agree closely with experimental results.

537.222:621.385 3823

**Electric Field of a Charged Spot Produced by an Electron Beam on the Surface of a Dielectric: Part 1**—V. Ya. Upatov. (*Radiotekhnika i Elektronika*, vol. 2, pp. 193-203; February, 1957.) The case of a uniformly charged spot, and that of a spot with Gaussian distribution of the surface charge are discussed.

537.226 3824

**Theory of Dipole Orientation Process in the Dielectric based on the Concept of a Viscoelastic Model: Parts 1 and 2**—S. Sharan. (*J. Inst. Telecommun. Eng.*, vol. 3, pp. 3-11 and 123-129; December, 1956 and March, 1957.)

537.311.31 3825

**Distribution Function for the Classic Electron Gas**—S. V. Tyablikov and V. V. Tolma-

- chev. (*C.R. Acad. Sci. U.R.S.S.*, vol. 114, pp. 1210-1213; June 21, 1957. In Russian.) Brief mathematical analysis.
- 537.311.33:538.632 3826  
**Classification of First-Order Semiconduction Effects through Use of Electrochemical Potentials**—J. A. Swanson. (*IBM J. Res. Devel.*, vol. 1, pp. 39-43; January, 1957.) The use of the electrochemical potentials simplifies the treatment of conduction effects when only small carrier concentration deviations are involved. Poisson's equation can be ignored in the first-order treatment of steady-state effects. Applications to Hall effect and probe potentials are considered.
- 537.311.62 3827  
**Skin Effect in Thin Films and Wires**—B. M. Bolotovskii. (*Zh. Eksp. Teor. Fiz.*, vol. 32, pp. 559-565; March, 1957.) Kinetic theory is used to derive skin-effect equations. An approximate method is given for obtaining the impedance of thin films or wires.
- 537.525.029.6 3828  
**Determination of the Coefficient of Diffusion and Frequency of Ionization in Microwave Discharges**—M. P. Madan, E. I. Gordon, S. J. Buchsbaum, and S. C. Brown. (*Phys. Rev.*, vol. 106, pp. 839-843; June 1, 1957.) The parameters are derived from measurement of the rate of growth of the electron density in a microwave cavity, in which an electric field larger than that necessary for breakdown, is applied.
- 537.533.7 3829  
**Radiation from a Point Charge Moving along the Boundary between Two Media**—V. A. Pafomov. (*Zh. Eksp. Teor. Fiz.*, vol. 32, p. 610; March, 1957.) Expressions are derived for an electron moving along the boundary between two dielectrics.
- 537.56 3830  
**Statistical Mechanical Theory of Transport Phenomena in a Fully Ionized Gas**—W. E. Brittin. (*Phys. Rev.*, vol. 106, pp. 843-847; June 1, 1957.) Nonequilibrium statistical mechanics is applied to a system of charged particles interacting via the electromagnetic field. The particles and field are treated statistically both from the classical and quantum-statistical standpoints.
- 537.56:538.6 3831  
**Oscillations of a Cylindrical Plasma**—T. H. Stix. (*Phys. Rev.*, vol. 106, pp. 1146-1150; June 15, 1957.) A mathematical analysis with physical interpretation of natural modes of oscillation in a longitudinal magnetic field. Hydromagnetic waves and cyclotron-frequency resonance occur in two limiting cases.
- 538.3 3832  
**The Analogue of Kelvin's Theorem in Hydromagnetics**—J. De. (*Naturwiss.*, vol. 44, p. 256; April, 1957. In English.)
- 538.566:535.31 3833  
**Reflection and Refraction of Electromagnetic Waves at Plane Interfaces**—W. E. Williams. (*J. Math. Phys.*, vol. 36, pp. 26-35; April, 1957.) The general problem of an arbitrary em wave incident on a dielectric slab between two different dielectrics is considered.
- 538.566:535.42 3834  
**The Diffraction of an Electromagnetic Wave by a Large Aperture**—R. F. Millar. (*Proc. IEE*, Pt. C, vol. 104, pp. 240-250; September, 1957.) An approximate expression is obtained for the difference from unity of the transmission coefficient for plane waves at normal incidence of a large aperture of rather general form in a plane perfectly conducting screen.
- Details are given for an elliptical aperture. See also 2425 of 1957.
- 537.566:535.43]+534.26 3835  
**High-Frequency Scattering of Electromagnetic Waves**—D. S. Jones. (*Proc. Roy. Soc. A*, vol. 240, pp. 206-213; May 21, 1957.) "The assumption that the illuminated region and the penumbra of a body scatter independently at high frequencies is used to obtain scattering coefficients for perfectly reflecting convex bodies in plane electromagnetic and sound waves. The formulas involve only the scattering coefficients of the circular cylinder and the geometry of the shadow boundary. One general result is that the electromagnetic scattering coefficient of a solid of revolution, when the direction of propagation of the incident wave is along the axis of revolution, is the average of the sound-hard and sound-soft scattering coefficients." See also 3010 of 1957.
- 538.566:537.56 3836  
**Growing Electromagnetic Waves**—V. A. Bailey. (*Phys. Rev.*, vol. 106, p. 1356; June 15, 1957.) A criticism of Piddington's paper (2030 of 1956), noting that his conclusions are based on a criterion contrary to Einstein's principle of special relativity (see, e.g., 105 of 1952).
- 538.569.4:621.375.9.029.64 3837  
**Superregenerative Masers**—Chester and Bolef. (See 3813.)
- 538.569.4:621.375.9.029.64 3838  
**Maximum Efficiency of the Solid-State Maser**—H. Heffner. (See 3814.)
- 538.569.4.029.5 3839  
**Paramagnetic Resonance Detection along the Polarizing Field Direction**—G. Whitfield and A. G. Redfield. (*Phys. Rev.*, vol. 106, pp. 918-920; June 1, 1957.) Report of measurements on diphenyl picryl hydrazyl.
- 538.569.4.029.5:537.56 3840  
**Ion Cyclotron Resonance**—R. F. Saxe. (*Nature, London*, vol. 180, pp. 87-88; July 13, 1957.) Absorption detected in a low-pressure hydrogen discharge in radial electric and varying magnetic fields is thought to correspond to the cyclotron resonance of atomic ions.
- 538.569.4.029.6 3841  
**Microwave Absorption in Ethyl Chloride**—Krishnaji and G. P. Srivastava. (*Phys. Rev.*, vol. 106, pp. 1186-1190; June 15, 1957.) Variation with pressure is determined at 7392 and 8780 mc, and the results are interpreted theoretically. The absorption is equivalent to a nonresonant Debye type, due to a zero-frequency (*Q*-branch) line.
- 538.569.4.029.6 3842  
**A Solid-State Paramagnetic-Resonance Spectrometer**—P. M. Llewellyn. (*J. Sci. Instr.*, vol. 34, pp. 236-239; June, 1957.) A simple and sensitive instrument for use in the frequency range 9-10 kmc at temperatures down to 14°K.
- 538.569.4.029.6:535.343 3843  
**A "Free Space" Absorption Cell for Microwave Spectroscopy**—C. C. Costain. (*Can. J. Phys.*, vol. 35, pp. 241-247; March, 1957.) "The absorption cell consists simply of a pyrex tube with a polystyrene lens and microwave horn at each end to couple to the standard microwave components. The lenses also serve as the vacuum windows. The attenuation at 8.5-mm wavelength is 3.4 db for a 250-cm cell. Since there are no metal surfaces, this type of cell is very suitable for the investigation of reactive molecules."
- 538.63.001.57 3844  
**A Mechanical Model for Demonstrating Gyromagnetic Phenomena**—R. Pottel. (*Tech. Mitt. schweiz. Telegr.-Teleph. Verw.*, vol. 35, pp. 193-196; May 1, 1957.) The model described consists of an electrically driven gyroscope suitably suspended to simulate various magnetic effects.
- GEOPHYSICAL AND EXTRATERRESTRIAL PHENOMENA**
- 523.16 3845  
**German Radio Observatory Stockert**—T. Pederzani. (*Elect. Eng., N. Y.*, vol. 76, pp. 196-200; March, 1957.) See also 1738 of 1957.
- 523.16:621.396.677.8 3846  
**New Radio Telescope**—(See 3749.)
- 523.16:621.396.677.833 3847  
**The Jodrell Bank Radio Telescope**—A. C. B. Lovell. (*Nature, London*, vol. 180, pp. 60-62; July 13, 1957.) The telescope is essentially a paraboloidal steel bowl 250 feet in diameter with the focus in the aperture plane built so that it can be directed towards any part of the sky. Details of the specification are given.
- 523.16:621.396.822 3848  
**Cosmic Radio-Noise Intensities below 10 Mc/s**—Correction to 3126 of 1957: for W/cm<sup>2</sup>, please read W/m<sup>2</sup>.
- 523.16:621.396.822 3849  
**Some Interesting Variations of Background Noise Observed at a Frequency of 17.6 Mc/s**—W. N. Abbott. (*J. Atmos. Terr. Phys.*, vol. 11, no. 1, pp. 72-74; 1957. In French.) Cosmic noise signals at 17.6 mc are found to be weaker 1-3 hours after sunset than one hour before sunset with a reversal of the effect nearer the critical frequency. The effect may be due to the ionosphere.
- 523.5:621.396.96 3850  
**Radar Echoes from Overdense Meteor Trails under Conditions of Severe Diffusion**—G. S. Hawkins. (*Proc. IRE*, vol. 45, pp. 1290-1291; September, 1957.) Formulas for the echo power and scattering cross section are developed. A nomogram is given for computing the radar cross section of diffuse trails. See also 3717 of 1956.
- 523.53 3851  
**The Time Distribution of Meteors**—K. R. R. Bowden and J. G. Davies. (*J. Atmos. Terr. Phys.*, vol. 11, no. 1, pp. 62-66; 1957.) Analysis of records of transient echoes at 36 mc and 72 mc shows no evidence to support previous suggestions that the meteors producing the echoes enter the atmosphere in groups or that many of the echoes are in fact due to cloud discharges.
- 523.75:621.396.11 3852  
**On the Disturbances of Radio Propagation along the North Polar Route**—Hakura. (See 3986.)
- 550.385:523.75 3853  
**Magnetic Activity following a Solar Flare**—R. A. Watson. (*J. Atmos. Terr. Phys.*, vol. 11, no. 1, pp. 59-61; 1957.) "Evidence is examined which suggests that either there is no increase of magnetic activity due to a solar flare or that the increase is a very rare event."
- 550.385:523.78 3854  
**The Fine Structure of the Geomagnetic Solar Eclipse Effect**—H. Volland. (*J. Atmos. Terr. Phys.*, vol. 11, no. 1, pp. 1-13; 1957. In German.) The extension of the theory of the solar-eclipse effect in the geomagnetic field by the introduction of empirical functions, and a de-

tailed discussion of the induction in the earth's interior and other influences makes possible a quantitative interpretation of the effect. As a result of the height dependence of the location of the shadow center height for the effective center of the current-carrying layer can be decided. A method of determining the direction of the  $S_q$  current during an eclipse is mentioned.

550.389.2 3855

**The International Geophysical Year—**(*Radio, Moscow*, no. 5, pp. 20-21; May, 1957.) Outline of the world-wide program involving 5000 scientists. Some special equipment to be used by the U.S.S.R. is mentioned, such as panoramic ionospheric recording equipment and a statistical analyzer for noise and interference. The earth satellite is also discussed.

550.389.2 3856

**The International Geophysical Year—**M. Nicolet. (*Nature, London*, vol. 180, pp. 7-10; July 6, 1957.) Outline of activities of the stations participating in the IGY program. Tables give the number of stations, their location, and their function.

550.389.2 3857

**Amateur Radio and the I.G.Y.—**R. L. Smith-Rose. (*RSGB Bull.*, vol. 32, pp. 396-397; March, 1957.) Suitable projects for radio amateurs in different countries are suggested and the procedure for participation is outlined.

550.389.2 3858

**N.B.S. Participation in the International Geophysical Year—**(*Tech. News Bull. Nat. Bur. Stand.*, vol. 41, pp. 136-140; September, 1957.) The greatest part of the Bureau's efforts will be concerned with the ionosphere, including the phenomena of sporadic E and of forward scatter. In addition there are programs of work on radio noise, whistlers, the "dawn chorus," and airglow. The Bureau is responsible for the World Warning Agency (3128 of 1957). During the IGY 12 stations will be directly operated by the Bureau and 25 operated in close association with it.

550.389.2 3859

**In the Arctic and Antarctic—**(*Radio, Moscow*, no. 5, pp. 12-13; May, 1957.) Five short notes on Russian observation posts including the Antarctic base of Mirny, where solar radiation, and ionospheric, and atmospheric disturbances will be investigated during the IGY. Radio wave propagation and the aurora will also be studied.

550.389.2:629.19 3860

**Artificial Earth Satellites—**V. Vakhnin. (*Radio, Moscow*, no. 6, pp. 14-17; June, 1957.) Information for radio amateurs taking part in the IGY program. General data regarding the orbit of the U.S.S.R. satellite are given, its functions are outlined and the problem of signal reception from it is discussed.

550.389.2:629.19 3861

**Observations of Radio Signals from an Artificial Earth Satellite and their Scientific Significance—**A. Kazantsev. (*Radio, Moscow*, no. 6, pp. 17-19; June, 1957.) A U.S.S.R. satellite launched during the IGY will be equipped with two 1-w transmitters operating at 20 and 40 mc, respectively, alternately transmitting pulse signals of 0.05-0.7-second duration from above the F layer.

550.389.2:629.19 3862

**The Observation of Signals from Artificial Earth Satellites—**(*Radio, Moscow*, no. 7, pp. 17-25; July, 1957.) Basic transmitter data of U.S.A. and U.S.S.R. satellites (see also 3861 above) are summarized. The following two papers outline methods and describe equipment for use by amateurs in locating the satel-

lites, and a further paper deals with the proposed U.S.A. satellite.

**U.S.W. Receiver—**O. Rzhiga and A. Shakhovskoi (pp. 17-20).

**Radiolocation Unit—**V. Dubrovin (pp. 21-23.)

550.389.2:629.19 3863

**The Observation of Signals from Artificial Earth Satellites—**(*Radio, Moscow*, no. 8, pp. 17-20; August, 1957.)

**Method of Observation—**O. Rzhiga and A. Shakhovskoi (pp. 17-19.)

**Work done with the Direction-Finding Equipment—**V. Dubrovin (pp. 19-20.)

Methods are outlined for the observation and recording of signals from a satellite and for determining the instant of its passage overhead. A brief description is given of receiving equipment and reference is made to its experimental use with an airborne transmitter, illustrating the change in the received signal when the aircraft passes overhead. See also 3862 above.

551.510.535 3864

**Tabulation of the Vertical Group Velocities of Ordinary Ionospheric Echoes—**W. Becker. (*Arch. elekt. Übertragung*, vol. 11, pp. 166-172; April, 1957.) Expanded tables of group refractive index for the ordinary ray including values to 4 decimal places given by Shinn (*The Physics of the Ionosphere*, pp. 402-406; 1955) and 6-figure values calculated by the author covering an extended range of gyromagnetic frequencies.

551.510.535 3865

**Measurement of the Gyro Frequency in the F Region—**G. R. Ellis. (*J. Atmos. Terr. Phys.*, vol. 11, no. 1, pp. 54-58; 1957.) The gyro frequency at 378 km is calculated using triple splitting of  $f_oF_2$ . The results are 10 per cent higher than would be expected using an extrapolated ground-level value.

551.510.535:523.75 3866

**The Influence of Solar Flares on the Ionospheric E Layer—**J. Taubenheim. (*J. Atmos. Terr. Phys.*, vol. 11, no. 1, pp. 14-22; 1957. In German.) Solar-flare effects in the E layer are examined quantitatively for selected days. It is concluded that the observed variation in electron density is controlled by the slow decrease of excess radiation rather than by recombination.

551.510.535:523.78 3867

**Investigation of Discrete Sources of Radiation from Solar Eclipse Observations—**N. Mitra. (*Indian J. Phys.*, vol. 31, pp. 69-82; February, 1957.) Ionospheric observations during the partial solar eclipse (89.5 per cent) of July 20, 1944, have been critically examined in order to determine whether the reduction of ion density of the E layer with the progress of the eclipse follows Chapman's theory of layer formation based on a homogeneous distribution of radiation across the solar disk.

551.510.535:621.396.11 3868

**Oblique Ray Paths in the Ionosphere—**Haselgrove. (See 3990.)

551.510.535:621.396.11 3869

**Application of the Generalized Magneto-ionic Theory to the Propagation of Radio Waves at the Magnetic-Dip Poles of the Earth—**Bai. (See 3989.)

551.510.535:621.396.812.3 3870

**An Experimental Verification of Diffraction Microscopy, using Radio Waves—**G. L. Rogers. (*J. Atmos. Terr. Phys.*, vol. 11, no. 1, pp. 51-53; 1957.) An aircraft was flown over a Mitra spaced antenna system and the fading pattern analyzed. See also 2749 of 1957.

551.594.5 3871

**H $\alpha$  Emissions during Aurorae over West-Central Canada—**R. Montalbetti and A. V. Jones. (*J. Atmos. Terr. Phys.*, vol. 11, no. 1, pp. 43-50; 1957.) H $\alpha$  emission in auroras does not support Martyn's theory of a diurnal variation of the sign of auroral particles. It does show that with increasing magnetic disturbance, the southern fringe of strong emission moves southward. H $\alpha$  emission, unlike some nitrogen bands, can be completely missing from strong auroras.

551.594.6:621.396.11 3872

**Heavy-Ion Effects in Audio-Frequency Radio Propagation—**Hines. (See 3991.)

## LOCATION AND AIDS TO NAVIGATION

621.396.96:621.395.625.3 3873

**The Fundamentals of the Storing of Radar Displays on Magnetic Tape—**W. H. Schönfeld and H. Gillmann. (*Elektron. Rundschau*, vol. 11, pp. 165-167; June, 1957.) Outline of experimental recording system for use with bandwidth compression equipment such as described by Groll, *et al.* (3874 below).

621.396.96:621.395.625.3:621.397.2 3874

**Frequency Compression Equipment for Long-Distance Transmission and Magnetic Tape Recording of Radar Displays—**H. Groll, K. Dinter, and K. Lange. (*Elektron. Rundschau*, vol. 11, pp. 155-157; May, 1957.) Brief description of equipment for bandwidth compression using methods discussed in 3744 of 1956 (Meinke and Groll).

621.396.96:681.14 3875

**"Nearest Approach" Calculator—**A. L. P. Milwright. (*Wireless World*, vol. 63, pp. 475-476; October, 1957.) A simple device for obtaining directly, from observations on a true-motion marine radar, the closest approach between two ships which continue on their observed courses.

621.396.96.029.64 3876

**The Calculation of the Effective Reflection Area of a Surface Target in the Centimetre Wavelength Range—**G. I. Perov. (*Radio-tekhnika, Moscow*, vol. 11, pp. 57-59; July, 1956.) Errors are discussed which arise in the derivation of formulas for the effective reflection area when the earth's surface is irradiated by pulses and for the directivity factor of an aircraft antenna.

621.396.967:621.317.3 3877

**Test Set for 3-cm Radar Equipment—**J. Verstraten. (*Philips Telecommun. Rev.*, vol. 17, pp. 123-130; April, 1957.) Measurements can be made of transmitter frequency and pulse length, forward and reflected antenna power, receiver noise figure, and other equipment parameters for all frequencies from 8.5 to 9.6 kmc.

621.396.968:621.376.239:621.396.822 3878

**An Analysis of Signal Detection and Location by Digital Methods—**G. P. Dinneen and I. S. Reed. (*IRE TRANS.*, vol. IT-2, pp. 29-38. March, 1956. Abstract, *Proc. IRE*, vol. 44, p. 956; July, 1956.)

## MATERIALS AND SUBSIDIARY TECHNIQUES

535.215:537.311.33 3879

**Influence of the External Potential and Other Factors on the Capacitor Photo-response of Semiconductors—**V. E. Kozhevnikov and V. E. Lashkarev. (*Radio-tekhnika i Elektronika*, vol. 2, pp. 260-268; March, 1957.) Several semiconductors including  $MnCl_2$ ,  $PbI_2$ ,  $CdS$ , with dielectric layers of mica, cellophane-

mica, or cellophane were investigated by means of the capacitor method. The polarity of photocurrent carriers and the spectral distribution of photosensitivity were recorded.

535.215:537.311.33 3880

**The Influence of Molecular Absorption and the External Electrical Field on the Photoconductivity of Semi-conductors**—V. I. Lyashenko and O. V. Snitko. (*Radiotekhnika i Elektronika*, vol. 2, pp. 269-277; March, 1957.) The method and results of an experimental investigation on the photoconductivity of  $\text{Cu}_2\text{O}$  and molybdenum sulphide are discussed.

535.215:546.23:539.23 3881

**Transit-Time Measurements of Charge Carriers in Amorphous Selenium Films**—W. E. Spear. (*Proc. Phys. Soc.*, vol. 70, pp. 669-675; July 1, 1957.) Measured effective carrier mobilities at room temperature are between 4.7 and  $5.5 \times 10^{-3} \text{ cm}^2/\text{v}$  for electrons and about 0.15  $\text{cm}^2/\text{v}$  for holes. The temperature dependence of the mobilities indicates trapping levels which for electrons are 0.25 eV and for holes are 0.16 eV below the conduction band.

535.215:546.482.21 3882

**Thermal and Electrolytic Activation of Photoconductivity in CdS Crystals**—J. Woods. (*J. Electronics Control*, vol. 3, pp. 225-235; August, 1957.) Two processes whereby the photoconductivity of CdS crystals increases on heating are described. The previously reported activation of CdS by dielectric breakdown (1114 of 1957) is explained in terms of these thermal effects.

535.215:546.482.21 3883

**The Form of Spectral Distribution of Photoconductivity in Single Crystals of CdS**—V. E. Lashkarev, E. A. Sal'kov, G. A. Fedorus, and M. K. Sheinkman. (*C.R. Acad. Sci. U.R.S.S.*, vol. 114, pp. 1203-1205; June 21, 1957. In Russian.) Carrier mobility was found to be independent of  $\lambda$  in the experimental range 4500-5500 Å. The causes of the drop in photocurrent were investigated. Results are shown in graphical form.

535.215:546.492.151 3884

**Photoelectric and Optical Properties of  $\text{HgI}_2$** —D. V. Chepur. (*Radiotekhnika i Elektronika*, vol. 2, pp. 278-286; March, 1957.) The lifetime of photo-current carriers for specimens illuminated by light of differing wavelengths, their quantum efficiency as dependent on temperature, and the optical properties of  $\text{HgI}_2$  are discussed.

535.215:546.57.131 3885

**Inertia of the Internal Photo-effect in Silver Chloride**—K. K. Demidov. (*Radiotekhnika i Elektronika*, vol. 2, pp. 350-351; March, 1957.) The carrier lifetime in specimen of AgCl under monochromatic light of  $\lambda = 400$  to 500  $\mu\mu$  is decreased by additional illumination at  $\lambda = 600$  to 900  $\mu\mu$ .

535.215:546.817.221 3886

**Onset of Photo-e.m.f. in Layers of Lead Sulphide**—R. Ya. Berlaga, M.A. Rumsh, and L. P. Strakhov. (*Radiotekhnika i Elektronika*, vol. 2, pp. 287-290; March, 1957.) Electron diffraction patterns and the microscopic examination of vapor-deposited layers of PbS show the existence of needle-shaped protuberances. The relation of needle orientation to photoelectric characteristics is examined.

535.215:546.817.231 3887

**The Effect of Oxygen on an Evaporated PbSe Layer**—R. H. Jones. (*Proc. Phys. Soc.*, vol. 70, pp. 704-708; July 1, 1957.) An investigation of the mechanism by which oxygen produces photoconductive sensitivity.

535.37 3888

**Luminescence of Silver Bromoiodide Crystals**—F. Moser and F. Urbach. (*Phys. Rev.*, vol. 106, pp. 852-858; June 1, 1957.) Low-temperature measurements are reported. Trapping has been investigated by a study of the slow build-up of fluorescence under weak excitation.

535.371:546.321.31 3889

**Colour Centres in Crystals of KCl, and KCl with Ag Added**—N. G. Politov. (*Radiotekhnika i Elektronika*, vol. 2, pp. 291-295; March, 1957.) The absorption spectrum of single crystals is examined. The spectrum changes after irradiation with ultraviolet and X rays are also considered.

535.376:546.281.26 3890

**Structure and Characteristics of Silicon Carbide Light-Emitting Junctions**—L. Patrick. (*J. Appl. Phys.*, vol. 28, pp. 765-776; July, 1957.) Junctions, where the leakage at the periphery and through "blue spots" has been reduced to a minimum, are found to have a  $p-n^*-n$  structure. A theory of the forward characteristic of the  $p-n^*-n$  junction is given which explains the characteristics observed and their dependence upon temperature. The results of experiments on crystal growing and an explanation of the growth of light-emitting junctions are given.

535.376:546.472.21 3891

**Temperature Dependence of Electroluminescence**—C. H. Haake. (*J. Electrochem. Soc.*, vol. 104, pp. 291-298; May, 1957.) Measurements were made over wide ranges of temperature and frequency on a number of powdered single-band ZnS phosphors containing Cu, Cu-Pb,  $\text{O}_2$ , and Cl impurities. From the temperature dependence of photoluminescence a thermal extinction factor was derived, which when introduced in the electroluminescence brightness values, led to an ideal electroluminescence brightness unaffected by thermal quenching. In general this ideal brightness was found to increase or tend to saturation with increasing temperature, but did not decrease.

537.226/.227:546.431.824-31 3892

**Microstructure of Barium Titanate Ceramics**—R. C. DeVries and J. E. Burke. (*J. Amer. Ceram. Soc.*, vol. 40, pp. 200-206; June 1, 1957.) Using polishing and etching techniques, structural changes due to the application of a dc field can be seen.

537.226/.227:546.431.824-31 3893

**Domain Orientation in Barium Titanate Single Crystals**—D. P. Cameron. (*IBM J. Res. Devel.*, vol. 1, pp. 2-7; January, 1957.)

537.226/.227:546.431.824-31:537.311.33 3894

**Electrical Properties of  $\text{BaTiO}_3$  containing Samarium**—G. G. Harman. (*Phys. Rev.*, vol. 106, pp. 1358-1359; June 15, 1957.) Unusual resistivity variations were associated with crystallographic transitions. From 0 to 120°C, the resistivity was independent of temperature; from 120 to 250°C, it rose rapidly. Below 0°C, semiconducting properties were found.

537.227 3895

**Dielectric Constant and Conductivity of Guanidine Aluminium Sulphate during Switching**—M. Prutton. (*Proc. Phys. Soc.*, vol. 70, pp. 702-703; July 1, 1957.)

537.228.1 3896

**Anisotropy in Polarized Barium Titanate Ceramics**—M. Marutake and T. Ikeda. (*J. Phys. Soc. Japan*, vol. 12, pp. 233-240; March, 1957.)

537.311.32:546.212-16 3897

**The Electrical Conductivity of Ice**—R. S.

Bradley. (*Trans. Faraday Soc.*, vol. 53, pt 5, pp. 687-691; May, 1957.) "The dc electrical conductivity  $\kappa$  of ice has been determined at 0 to -25°C, and is given by  $\kappa = 23.4 \exp(-12300/RT) \text{ ohm}^{-1}\text{cm}^{-1}$ . The results are discussed in terms of proton migration and semiconductor theory.

537.311.33 3898

**An Analysis of Diffusion in Semiconductors**—S. Zaromb. (*IBM J. Res. Devel.*, vol. 1, pp. 57-61; January, 1957.) It is shown that the usual Fick's laws may not apply to the diffusion of impurities in semiconductors. Appreciable covalent compound formation is likely to occur between some substitutional donors and acceptors, leading to a marked dependence of diffusion coefficients on concentration, and to interaction between donor and acceptor diffusion effects.

537.311.33 3899

**Carrier Generation and Recombination in P-N Junctions and P-N Junction Characteristics**—C. T. Sah, R. N. Noyce, and W. Shockley. (*Proc. IRE*, vol. 45, pp. 1228-1243; September, 1957.) For certain  $p-n$  junctions the measured current/voltage characteristics deviate from the ideal case of the diffusion model. It is shown that the current due to generation and recombination of carriers from generation-recombination centers in the space-charge region of a  $p-n$  junction accounts for the observed characteristics. The relative importance of the diffusion current outside the space-charge layer and the recombination current inside the space-charge layer also explains the increase of the emitter efficiency of Si transistors with emitter current.

537.311.33 3900

**Determination of Optical Constants and Carrier Effective Mass of Semiconductors**—W. G. Spitzer and H. Y. Fan. (*Phys. Rev.*, vol. 106, pp. 882-890; June 1, 1957.) By means of reflectivity and absorption measurements in the region 5-35  $\mu$ , the effect of free carriers on the optical constants has been determined for  $n$ - and  $p$ -type Ge, Si, and InSb, and for  $n$ -type InAs.

537.311.33 3901

**Experimental Determination of Injected Carrier Recombination Rates at Dislocations in Semiconductors**—J. P. McKelvey. (*Phys. Rev.*, vol. 106, pp. 910-917; June 1, 1957.) The recombination probabilities associated with lineage boundaries in Ge have been determined by measuring the ratio of injected-carrier concentration on either side of such a boundary. The capture cross sections for a single dislocation correspond to circular recombination areas of diameter 1.15 Å for holes in  $n$ -type Ge and 2.8 Å for electrons in  $p$ -type Ge.

537.311.33 3902

**An Empirical Regularity of Energy Gap in Semiconductors**—T. Miyauchi. (*J. Phys. Soc. Japan*, vol. 12, p. 308; March, 1957.) An empirical linear relation exists for several groups of compounds between the energy gap and  $r_1/r_2$  where  $r_1$  is half the nearest neighbor distance and  $r_2$  is an average of the positive ionic radius.

537.311.33 3903

**Prediction of Semiconductor Surface Response to Ambients by Use of Lewis Acid-Base Theory**—C. G. Peattie and J. R. Macdonald. (*Proc. IRE*, vol. 45, p. 1292; September, 1957.) In this treatment a  $p$ -type surface is considered a Lewis acid (electron-pair acceptor) and an  $n$ -type surface a Lewis base (electron-pair donor).

537.311.33:546.28 3904

**Growth of Silicon Crystals by a Vapour-**

**Phase Pyrolytic Deposition Method**—R. C. Sangster, E. F. Maverick, and M. L. Crouch. (*J. Electrochem. Soc.*, vol. 104, pp. 317–319; May, 1957.) Si crystals are grown by the reaction of gaseous  $\text{SiBr}_4$  with  $\text{H}_2$  at the surfaces of hot Si seed filaments.

537.311.33:546.28 3905

**Some Observations of the Effects of Oxygen on the Minority-Carrier Lifetime and Optical Absorption of Silicon Crystals Pulled in Vacuo**—G. W. Green, C. A. Hogarth, and F. A. Johnson. (*J. Electronics Control*, vol. 3, pp. 171–182; August, 1957.) Discusses the technique of growing single crystals by pulling from a melt in vacuo. For such crystals the carrier lifetime decreases radially from the center. This decrease is attributed to the smaller amount of oxygen impurity near the surface, as shown by optical absorption measurements. In a vacuum oxygen is evaporated from the surface and removed by pumping.

537.311.33:546.28 3906

**Diffusion of Oxygen in Silicon**—R. A. Logan and A. J. Peters. (*J. Appl. Phys.*, vol. 28, pp. 819–820; July, 1957.) The diffused layer is revealed by etching, or by heating at  $450^\circ\text{C}$  the resultant  $n$  layer being demarcated by staining in HF, by the thermal probe technique, or by gold displacement plating.

537.311.33:546.28 3907

**Retrograde Solubility of Aluminium in Silicon**—D. Navon and V. Cherynshev. (*J. Appl. Phys.*, vol. 28, pp. 823–824; July, 1957.) The solubility near the eutectic temperature and the diffusion constants as measured by Al diffusion from an Al-Si are examined.

537.311.33:546.28:535.215 3908

**Analysis of the Photoconductance in Silicon**—L. J. van der Pauw. (*Philips Res. Rep.*, vol. 12, pp. 364–376; August, 1957.) A general expression is derived in terms of bulk and surface properties for the change in the voltage drop across a semiconductor sample due to illumination. The experimental determination of these properties from the low-frequency phase shift between the voltage change and a sinusoidally modulated light signal is illustrated, and results of measurements on  $n$ - and  $p$ -type Si at room temperature are discussed.

537.311.33:546.28:539.164.9 3909

**A Transformation of  $p$ -Si into  $n$ -Si by X Rays**—F. Frey and F. Oberhauser. (*Naturwiss.*, vol. 44, pp. 256–257; April, 1957.) Brief report of experimental results obtained with a single-crystal specimen.

537.311.33:546.28:669.046.54/.55 3910

**Contribution to the Floating-Zone Refining of Silicon**—E. Buehler. (*Rev. Sci. Instr.*, vol. 28, pp. 453–460; June, 1957.)

537.311.33:546.289 3911

**Thermoelectric Power and Resistivity of Solid and Liquid Germanium in the Vicinity of its Melting Point**—C. A. Domenicali. (*J. Appl. Phys.*, vol. 28, pp. 749–753; July, 1957.) The absolute thermoelectric power  $Q$  of high-purity Ge is approximately linear in  $1/T$  for  $400^\circ\text{C} < T < 937^\circ\text{C}$ . For liquid Ge  $Q$  is nearly zero and independent of temperature. The thermoelectric power of liquid relative to solid Ge is  $+70\mu\text{V}/^\circ\text{C}$ .

537.311.33:546.289 3912

**The  $L_{\beta_1}$  and  $L_{\beta_2}$  Lines in the Spectrum of Germanium**—G. P. Borovikova and M. I. Krosunski. (*C. R. Acad. Sci. U.R.S.S.*, vol. 114, pp. 1192–1194; June 21, 1957. In Russian.) Report of investigations on single-crystal high-purity Ge.

537.311.33:546.289 3913

**Depth of Surface Damage due to Abrasion**

on Germanium—B. A. Irving, T. M. Buck, and F. S. McKim. (*J. Electrochem. Soc.*, vol. 104, pp. 396–397; June, 1957.) Comment on 1957 of July and authors' reply.

537.311.33:546.289:535.215:538.63 3914

**Experiments on the Photomagnetolectric Effect in Germanium**—T. M. Buck and F. S. McKim. (*Phys. Rev.*, vol. 106, pp. 904–909; June 1, 1957.) Measurements of the PME short-circuit current and relative increase in conductance have been made over a wide range of light intensity. Results are in accord with the theory of van Roosbroeck (2780 of 1956.)

537.311.33:546.682.86:669.046.54/.55 3915

**The Role of Evaporation in Zone Refining Indium Antimonide**—K. F. Hulme and J. B. Mullin. (*J. Electronics Control*, vol. 3, pp. 160–170; August, 1957.) "Experiments on the refining of InSb are described; they include work with material heavily doped with Zn, Cd, Te, and As. Several lines of evidence show that the important acceptor impurities Zn and Cd are volatile from molten InSb. The removal of acceptors by volatilization under appropriate experimental conditions, followed by zone refining, can yield material with less than  $10^{14}$  excess donors per  $\text{cm}^3$ ."

537.311.33:546.817.221 3916

**Interstitial Diffusion of Copper in PbS Single Crystals**—J. Bloem and F. A. Kröger. (*Philips Res. Rep.*, vol. 12, pp. 281–302; August, 1957.) Report and discussion of results of an experimental investigation showing that at temperatures between  $100^\circ$  and  $500^\circ\text{C}$  Cu can diffuse rapidly into PbS via interstitial sites, causing  $n$ -type conductivity.

537.311.33:546.817.221 3917

**Interstitial Diffusion of Nickel in PbS Single Crystals**—J. Bloem and F. A. Kröger. (*Philips Res. Rep.*, vol. 12, pp. 303–308; August, 1957.) "Under reducing conditions, nickel may penetrate into PbS crystals at temperatures  $T < 500^\circ\text{C}$  at which the self-diffusion in PbS is negligible; it diminishes  $p$ -type conductivity and may cause  $n$ -type conductivity with donors of a depth  $E \approx 0.03$  ev. The diffusion probably takes place via the interlattice with a diffusion constant  $D_{\text{Ni}} = 17.8 \exp(-22000/RT) \text{ cm}^2 \text{ sec}^{-1}$ . Under sulphurizing conditions ( $\text{H}_2\text{S}$ ) the nickel can be drawn out of the crystal again and the original conductivity restored."

537.311.33:546.817.241 3918

**On Electrical Resistivity and Hall Coefficient of PbTe Crystals**—K. Shogenji and S. Uchiyama. (*J. Phys. Soc. Japan*, vol. 12, pp. 252–258; March, 1957.) Results of measurements on PbTe crystals give the intrinsic energy gap as 0.3 ev, and electron/hole mobility ratio as 2.5 with a  $T^{-5/2}$  law for hole mobility.

537.311.33:621.3.082.52 3919

**Pulsed Light tests Minority-Carrier Life**—H. L. Armstrong. (*Electronics*, vol. 30, p. 145; August 1, 1957.) "Xenon discharge tube is rapidly pulsed to illuminate semiconductor material creating hole-electron pairs. Voltage drop across material is observed on oscilloscope to determine minority-carrier lifetime."

537.311.33:621.314.63 3920

**Experimental Investigation of the Transient Behavior of Gold-Germanium Surface Barriers**—O. Curtis, Jr, and B. R. Gossick. (*IRE TRANS. VOL. ED-3*, pp. 163–167; October, 1956.) Abstract, *PROC. IRE*, vol. 45, p. 254; February, 1957.)

537.311.33:621.314.632:621.357.6 3921

**A Quantitative Theory of the Electroformation of Metal/Germanium Point Contacts**—

A. C. Sim. (*J. Electronics Control*, vol. 3, pp. 139–159; August, 1957.) The characteristics of Ge point contacts are improved by electroforming, in which local heating and melting are induced by a current pulse. A quantitative calculation supports the empirical findings that a high-impedance source for the current pulse is desirable and that the pulse length should be greater than 20 m for reproducible results. The improvement obtained with initial microsecond pulses of up to 20 A is discussed and studied theoretically.

537.311.4:621.3.066.6 3922

**A Survey of Contact Resistance Theory for Nominally Clean Surfaces**—W. B. Ittner, III, and P. J. Magill. (*IBM J. Res. Devel.*, vol. 1, pp. 44–48; January, 1957.)

537.533:546.482.21 3923

**Investigations of "Cold" Electron Emission from Cadmium Sulphide Single Crystals**—R. Rompe. (*Radiotekhnika i Elektronika*, vol. 2, pp. 219–221; February, 1957.) Experiments carried out at  $10^{-6}$ -mm Hg pressure showed that electron emission from CdS crystals for 7 kv between anode and cathode produced a current of  $10^{-7}$ a, and for 12.5 kv this increased to  $10^{-3}$ a.

538.22:546.3-1-711-47-26 3924

**New Type of Magnetic Transition in  $\text{Mn}_3\text{ZnC}$** —B. N. Brockhouse and H. P. Myers. (*Can. J. Phys.*, vol. 35, pp. 313–323; March, 1957.) "X-ray and neutron diffraction measurements are reported which demonstrate that at  $231^\circ\text{K}$  there is a second order transition below which ordering of the manganese ions occurs, resulting in a tetragonal distortion of the normally cubic lattice and a complex magnetic structure. One possible magnetic structure is discussed. Above the transition the alloy is apparently a normal ferromagnetic substance."

538.221:538.569.4:539.23 3925

**Stress in Evaporated Ferromagnetic Films**—J. R. MacDonald. (*Phys. Rev.*, vol. 106, pp. 890–892; June 1, 1957.) Ferromagnetic resonance and oscillation-magnetometer measurements on a thin evaporated nickel film annealed in a magnetic field are described. The magnetic annealing produced a preferred magnetic axis in the plane of the film.

538.221:538.632:539.23 3926

**Hall Effect and Ferromagnetism of Very Thin Nickel Films**—R. Coren and H. J. Juretschke. (*J. Appl. Phys.*, vol. 28, pp. 806–809; July, 1957.) The extraordinary Hall constant for films less than 100 Å thick, at room temperatures, is much greater than for bulk nickel.

538.221:621.318.122 3927

**Supermendur, a New Rectangular-Loop Magnetic Material**—H. L. B. Gould and D. H. Wenny. (*Elect. Eng., N. Y.*, vol. 76, pp. 208–211; March, 1957.) Characteristics are given of a Va-Fe-Co alloy which should be particularly useful for power applications. See also 2835 of 1957.

538.221:[621.318.124+621.318.134 3928

**Certain Properties of Ferrites**—J. K. Galt. (*Bell Lab. Rec.*, vol. 35, pp. 126–130; April, 1957.) Basic description of the chemical structure and magnetic behavior of ferrites. The loss mechanisms acting in ferromagnetic materials are outlined.

538.221:621.318.124 3929

**Temperature Dependence of Spontaneous Magnetization in Co-Zn Ferrites at Low Temperatures**—N. M. Reinov and M. F. Stel'makh. (*Radiotekhnika i Elektronika*, vol. 2, pp. 342–344; March 1957.) Experimental results of magnetic saturation of Co-Zn ferrites in

the temperature range from the Curie point to 1.3°K are shown. No abnormal decrease in the magnetic saturation with the lowering of temperature was observed.

538.221:621.318.134 3930  
**Theory of the Spontaneous Magnetization of Ferrites**—E. I. Kondorski, A. S. Pakhomov, and T. Shiklosh. (*Radiotekhnika i Elektronika*, vol. 2, pp. 334–341; March, 1957.) Mathematical analysis of the magnetization of ferromagnetic semiconductors at temperatures near 0°K.

538.221:621.318.134 3931  
**Cation Distribution and Magnetic Moment of Manganese Ferrite**—F. W. Harrison, W. P. Osmond, and R. W. Teale. (*Phys. Rev.*, vol. 106, p. 865; June 1, 1957.)

538.221:621.318.134 3932  
**Molecular Field Fluctuation Effects in Mixed Nickel-Zinc Ferrites**—D. M. Grimes, S. Legvold, and E. F. Westrum. (*Phys. Rev.*, vol. 106, pp. 866–867; June 1, 1957.) The thermal variations of the magnetic moment and heat capacity of some mixed Ni-Zn ferrites are discussed. Experimental data on the magnetic moments are shown.

538.221:621.318.134:534.13 3933  
**Acoustic Relaxations in Ferrite Single Crystals**—D. F. Gibbons. (*J. Appl. Phys.*, vol. 28, pp. 810–814; July, 1957.) A stress-induced relaxation near 40°K, with an activation energy of  $0.03 \pm 0.004$  eV per electron jump, is common to all ferrites with divalent and trivalent ferrous ions on the octahedral sites. In Mn ferrite the activation energy of about 0.3 eV per electron jump depends upon the composition and homogeneity. In Mn and Mn-Zn ferrites a transformation occurs below 14°K; the transition temperature depends upon the composition.

538.221:621.318.134:537.322 3934  
**Thermoelectric Properties of Ferrites in the Range Close to Curie Temperature**—S. A. Varchenya and Ya. G. Dorfman. (*Radiotekhnika i Elektronika*, vol. 2, pp. 345–347; March, 1957.) Ni-Zn ferrites with specific resistance  $10^6$ – $10^7$   $\Omega$  cm were examined. The Peltier and Thomson effects showed similar magnetic anomalies as found in ferromagnetic metals.

538.221:621.318.134:538.569.4 3935  
**Effects of Ceramic Parameters on Microwave Properties of Nickel Ferrite**—S. L. Blum, J. E. Zneimer, and H. Zlotnick. (*J. Amer. Ceram. Soc.*, vol. 40, pp. 143–139; May 1, 1957.) A simple apparatus is described for measuring the magnetic loss as a function of magnetic field for ferrites at a frequency of 10 kmc. Tests on Ni Fe<sub>2</sub>O<sub>4</sub> showed 1) it is possible to vary the width of the ferromagnetic resonance curve by adjusting the porosity of the ferrite; 2) the dc resistivity decreases with an increase in peak firing temperature. The range of resistivities possible in this material is  $10$ – $10^9$   $\Omega$  cm.

538.221:621.318.134:538.569.4 3936  
**Physical and Electrical Properties of a Nickel Ferrite as Affected by Compositional Changes**—S. L. Blum and J. E. Zneimer. (*J. Amer. Ceram. Soc.*, vol. 40, pp. 208–211; June 1, 1957.) Experiments at 10 kmc on Ni<sub>1- $\alpha$</sub> Co <sub>$\alpha$</sub> Fe<sub>2</sub>O<sub>4</sub>, where  $\alpha$  varies from zero to 0.05, show that the ferromagnetic resonance curve may be narrowed by suitable Co addition.

538.245 3937  
**Influence of Foreign Ions on the Critical Field Strength of an Antiferromagnetic**—K. F. Niessen. (*Philips Res. Rep.*, vol. 12, pp. 355–363; August, 1957.) See also 2843 of 1957.

538.245:621.396.822 3938  
**Frequency Spectrum of the Barkhausen Noise**—G. Biorci and D. Pescetti. (*J. Appl. Phys.*, vol. 28, pp. 777–780; July, 1957.) Measurements of iron, nickel, and ferrocube show the spectral density to be constant up to 1 kc and then to decrease rapidly. Agreement with theory is obtained if the single noise pulse is exponential with a time constant of  $10^{-4}$  sec.

538.632:537.311.33 3939  
**The Hall Generator as a Quadripole**—F. Kuhr and W. Hartel. (*Arch. Elektrotech.*, vol. 43, pp. 1–15; January 12, 1957.) The quadripole representation of a Hall-effect device is analyzed, in particular, the dependence of the characteristic impedance on the magnetic field and external circuit conditions. Three types of matching conditions are defined: 1) for achieving linearity, 2) for maximum power output, and 3) for maximum efficiency. The efficiency is calculated for the quadripole equations and evaluated, with the other characteristics, for a given InAs Hall element.

548.0:53 3940  
**Electrical, Optical and Elastic Properties of Diamond Type Crystals: Part 1**—V. S. Mashkevich and K. B. Tolpygo. (*Zh. Eksp. Teor. Fiz.*, vol. 32, pp. 520–525; March, 1957.) The energy contained in a homopolar crystal is represented as a function of displacements and dipole movements of the atoms.

549.514.51 3941  
**Electrical Conductivity of Fused Quartz**—J. Cohen. (*J. Appl. Phys.*, vol. 28, pp. 795–800; July, 1957.) Measurements made in vacuo at temperatures between 600–1400°C show that one specimen obeyed Ohm's law while another did not. The variation in behavior is attributed to differences in the impurity contents.

549.514.51:534.133 3942  
**On the Angle between Wave Front and Displacement of Plane Acoustic Waves in Quartz**—B. van der Veen. (*Philips Res. Rep.*, vol. 12, pp. 273–280; August, 1957.) Development of the theory of piezoelectric vibrations for nonrectangular X-cut crystals free from unwanted flexural modes of vibration.

621.315.61:537.529 3943  
**Statistical Delay of Electrical Breakdown of Solid Dielectrics**—E. A. Konorova. (*Zh. Eksp. Teor. Fiz.*, vol. 32, pp. 603–604; March, 1957.) Tests were made to determine the delay of electrical breakdown of samples of mica 2–10  $\mu$  and glass 3–10  $\mu$  thick. The duration of the voltage application to obtain punctures varied from  $10^{-2}$  to  $5 \times 10^{-8}$  sec. Results are shown graphically.

621.319.4-762 3944  
**Tropicalization—Results of Experiments on Sealing Capacitors**—C. V. Ganapathy, R. Krishnan, and T. V. Ramamurti. (*J. Inst. Telecommun. Eng., India*, vol. 3, pp. 116–122; March, 1957.)

537.311.33 3945  
**Report of the Meeting on Semiconductors held by the Physical Society, in collaboration with British Thomson-Houston Ltd., Rugby, in April 1956.** [Book Review]—Publishers: The Physical Society, London, 153 pp., 20s; 1957. (*Nature, London*, vol. 180, pp. 25–26; July 6, 1957.) The text of 22 of the 23 papers read is given.

#### MATHEMATICS

517:518.2 3946  
**Laguerre Functions: Tables and Properties**—J. W. Head and S. P. Wilson. (*Proc. IEE*,

Pt. C, vol. 104, p. 543; September, 1957.) Discussion on 518 of 1957.

517.512 3947  
**Table of the Fresnel Integral to Six Decimal Places** [Book Review]—T. Pearcey. Publishers: Cambridge University Press, 63 pp., 12s. 6d; 1956; (*Nature, London*, vol. 180, p. 6; July 6, 1957.)

#### MEASUREMENTS AND TEST GEAR

53.082 3948  
**Instrument Transducers**—J. Thomson. (*J. Sci. Instr.*, vol. 34, pp. 217–221; June, 1957.) A survey of available means for converting energy from one form to another, and their application to automatic manufacturing processes.

621.3.018.41(083.74)+529.786]:538.569.4 3949  
**Frequency Shift in Ammonia Absorption due to Self-Broadening**—K. Matsuura, Sugiura, and G. M. Hatoyama. (*J. Phys. Soc. Japan*, vol. 12, p. 314; March, 1957.) Note on a shift in resonance frequency of the ammonia line with pressure near 23870 mc. See also 2858 of 1957.

621.314.7.001.4 3950  
**Measuring Parameters of Junction Transistors**—R. W. Hendrick, Jr. (*Electronics*, vol. 30, pp. 174–176; August 1, 1957.) The instrument measures dynamic ground-emitter characteristics of *p-n-p* or *n-p-n* transistors at any static collector current from 0.15 to 14 ma.

621.314.7.012:621.317.755 3951  
**Investigation of Transistor Characteristics by means of a Cathode-Ray Curve Tracer**—A. M. Bonch-Bruевич and U. B. Soltamov. (*Radiotekhnika i Elektronika*, vol. 2, pp. 311–316; March, 1957.) Description of circuits with photographs of characteristics displayed on the cr tube screen.

621.317.18:621.373.421.1 3952  
**Simple Grid-Dip Oscillator**—R. Ireland and V. Penfold. (*Short Wave Mag.*, vol. 15, pp. 16–18; March, 1957.) Constructional details of a unit covering a wide frequency range.

621.317.3.029.64:621.396.822 3953  
**Improved Microwave Noise Measurements using Ferrites**—C. H. Mayer. (IRE TRANS., vol. MTT-4, pp. 24–28; January, 1956. Abstract, Proc. IRE, vol. 44, p. 581; April, 1956.)

621.317.32 3954  
**Method of Measurement of Potential Distribution on the Surface of a Dielectric**—V. Ya. Upatov. (*Radiotekhnika i Elektronika*, vol. 2, pp. 184–192; February, 1957.) A pulse method for measuring the potential distribution on a nonuniformly charged dielectric is described. A fine graticule placed on the surface of the dielectric is scanned by an electron beam to produce positive or negative pulses according to the charge present. The experimental circuits and some results are given.

621.317.321:537.311.33 3955  
**New Modification of the Capacitance Method of Measuring Potential Difference and its Application to the Study of Contact Potentials of Semiconductors**—B. F. Bogolyubov. (*Radiotekhnika i Elektronika*, vol. 2, pp. 323–327; March, 1957.) The effect of illumination and pressure on the potential difference in metallic Se contacts is investigated. For a pressure  $P \leq 5 \times 10^{-1}$  mm Hg this contact potential does not depend on illumination and remains approximately constant, but for  $P \geq 2 \times 10^{-5}$  mm Hg the contact potential varies linearly with weak illumination. Results for seven samples are tabulated.

- 621.317.328 3956  
A New Type of V.H.F. Field Intensity Meter using a Loop Antenna—H. Koseki. (*J. Radio Res. Labs., Japan*, vol. 4, pp. 123-125; April, 1957.) Calibration is achieved by feeding a comparison voltage, which can be measured, through a coupling circuit to the loop and the receiver. Errors of  $\pm 1$  db over the range 15-100 mc are quoted.
- 621.317.33:621.3.035.4 3957  
A New Device for Conductivity Measurement by Means of Radio Frequency Currents and Nonimmersed Electrodes—G. Barbi. (*Ricerca Sci.*, vol. 27, pp. 1438-1447; May, 1957.) Description of apparatus for measuring the conductivity of electrolytic solutions using a frequency of about 9 mc.
- 621.317.33.029.6:621.317.755 3958  
An Automatic Smith-Diagram Display Unit for Use at Low Power Levels—H. V. Shurmer. (*Proc. IEE*, Pt. B, vol. 104, pp. 507-510; September, 1957.) The method, by which a Smith diagram is directly displayed on a cr tube, may be applied to microwave transmission systems generally.
- 621.317.335.3.029.63/.64:538.569.2.047 3959  
The Determination of Dielectric Constants particularly of Biological Substances in the Range of Decimetre and Centimetre Waves—B. Rajewsky and A. Redhardt. (*Arch. elektr. Übertragung*, vol. 11, pp. 163-166; April, 1957.) A resonance method of measurement such as that used by Schwan and Kamli (813 of 1954) is discussed and formulas are derived facilitating the evaluation of results.
- 621.317.335.3.029.64 3960  
A Method of Determining the Dipole Moment and Relaxation Time from Microwave Measurements—K. V. G. Krishna. (*Trans. Faraday Soc.*, vol. 53, pt. 6, pp. 767-770; June, 1957.) The method is applied to dilute solutions of polar substances in nonpolar solvents and is based on measuring the dielectric constant and loss as a function of concentration.
- 621.317.336 3961  
The Accuracy of Impedance Measurements by means of Long Lines—R. M. Dombregov. (*Radiotekhnika, Moscow*, vol. 11, pp. 66-70; June, 1956.) A formula for correcting the errors due to line losses is derived and a number of curves for facilitating calculations are plotted. The accuracy so obtained is estimated.
- 621.317.34 3962  
Self-Calibrating Method of Measuring Insertion Ratio—(*Tech. News Bull. Nat. Bur. Stand.*, vol. 41, pp. 132-133; September, 1957.) Description of a null method for the determination of phase angle and insertion loss of a network. The circuit illustrated has three parallel legs connected between a rf generator and a monitor. Two of the legs contain piston attenuators, one in series with a phase shifter. The third leg contains the unknown network in series with a second phase shifter which is used for self-calibration.
- 621.317.34.029.64:621.372.5:621.396.822 3963  
Measurements on Noisy Fourpoles at Microwave Frequencies—M. T. Vlaardingerbroeck, K. S. Knol, and P. A. H. Hart. (*Philips Res. Rep.*, vol. 12, pp. 323-332; August, 1957.) A new method of measuring the characteristic noise quantities of noisy linear fourpoles is described. Applied to microwave frequencies this method is very simple when the fourpole is matched to the characteristic impedance of the waveguide, which can always be achieved. The method is applied to a microwave triode amplifier.
- 621.317.342:621.396.65 3964  
Sensitive Group Delay Meters—R. Magnusson. (*Ericsson Tech.*, vol. 13, no. 1, pp. 109-142; 1957.) The requirements of an instrument for measuring the group delay of wide-band radio-link IF amplifiers are stated. A critical survey of existing methods of measuring group delay is given and a delay meter of very high sensitivity is described.
- 621.317.361.029.64:538.569.4 3965  
A Frequency Comparator using Electron and Proton Resonance in a Common Magnetic Field—O. Nourse. (*Nature, London*, vol. 180, p. 192; July 27, 1957.) An outline of a method of measuring microwave frequencies using electron and proton paramagnetic resonances in a common magnetic field. With the ratio of the two resonance frequencies  $\approx 658.5$  the lower frequency can be determined accurately by conventional methods.
- 621.317.382.029.64:621.3.089.6 3966  
Measurements of Efficiency of Bolometer and Thermistor Mounts by Impedance Methods—J. A. Lane. (*Proc. IEE*, Pt. B, vol. 104, pp. 485-486; September, 1957.) The method of calibrating milliwattmeters for microwave frequencies by measuring impedances is compared with the method of calibrating them against standard equipment. The impedance method may be satisfactory for bolometers but is unsatisfactory at present for thermistors.
- 621.317.733.011.22:621.314.58:621.375.13 3967  
An Inductronic Double Bridge—J. H. Miller. (*Elect. Eng., N. Y.*, vol. 76, pp. 300-302; April, 1957.) Low resistances can be measured with accuracy, speed, and simplicity of operation using a system of two "inductronic" dc amplifiers based on a principle applied in the induction galvanometer described by Gilbert (3666 of 1953).
- 621.317.733.3:621.3.011.21 3968  
A Precision Dual Bridge for the Standardization of Admittance at Very High Frequencies—D. Woods. (*Proc. IEE*, Pt. C, vol. 104, pp. 506-521; September, 1957.) A detailed description of a twin-T dual bridge for use in the band 3-300 mc. The inaccuracy in either component of a complex admittance is 0.2 per cent or less at 200 mc. The calibration is based on a range of coaxial susceptance standards whose parameters are calculated from measurements of length and time.
- 621.317.755+621.373.43 3969  
High-Power Pulse Generators—Bruijning. (See 3787.)
- 621.317.755 3970  
A Cathode-Ray-Tube Oscilloscope for Use in Millimicrosecond Pulse Techniques—J. W. Armitage, G. Gaskin, and K. Phillips. (*Electronic Eng.*, vol. 29, pp. 364-367; August, 1957.) The time base employs a thyratron trigger and a hard-tube sweep circuit with a continuously variable sweep speed from 3  $\mu$ sec down to 15  $\mu$ sec with a scan of approximately 2 kv. A cr tube with side-arm connections is used. Full design details are given.
- 621.317.784.029.64 3971  
An Instrument for the Absolute Measurement of Low-Level Microwave Power in the 3-cm Band—A. L. Cullen and H. A. French. (*Proc. IEE*, Pt. C, vol. 104, pp. 456-464; September, 1957.) The instrument consists of a thin metallic rod suspended inside a rectangular  $H_{011}$  cavity. The oscillating system receives periodic impulses from the interaction between the em field and the rod, the source being switched on and off periodically. The estimated error in the range 5-100 mw or more is not greater than  $\pm 2$  per cent.
- 621.317.79:537.56 3972  
An R.F. Probe Technique for the Measurement of Plasma Electron Concentrations in the Presence of Negative Ions—T. H. Y. Yeung and J. Sayers. (*Proc. Phys. Soc.*, vol. 70, pp. 663-668; July 1, 1957.)
- 621.317.794 3973  
An Evaporated Gold Bolometer—E. Archbold. (*J. Sci. Instr.*, vol. 34, pp. 240-242; June, 1957.) Description of an infrared detector with a sensitivity of 1.5 v/w, minimum detectable energy is  $3.6 \times 10^{-16}$ w, measured at 10 c.
- 621.317.794:537.311.33 3974  
Some Problems in the Application of Semiconductor Bolometers—A. M. Bonch-Bruевич and Ya. A. Imas. (*Radiotekhnika i Elektronika*, vol. 2, pp. 317-322; March, 1957.) The instrument described is used for the investigation of fast transients. By means of a compensating RC circuit various time constants are obtained. Such a compensating circuit reduces the threshold sensitivity of the device to a lesser extent than the lowering of bolometer inertia by an increase of its heat radiation.
- 621.317.794:621.396.822 3975  
The Theoretical Sensitivity of the Dicke Radiometer—L. D. Strom. (*Proc. IRE*, vol. 45, pp. 1291-1292; September, 1957.) A new analysis of the Dicke circuit (475 of 1947) has been made which shows that the sensitivity is independent of the detector characteristics.
- 621.317.794.029.64 3976  
The Measurement of Thermal and Similar Radiations at Millimetre Wavelengths—G. R. Nicoll. (*Proc. IEE*, Pt. B, vol. 104, pp. 519-527; September, 1957.) "The measurement of thermal and similar noise radiations at millimetre wavelengths is discussed. It is shown how this type of measurement is applied to radiation from gas discharges, flames, and crystal diodes, and how it is used in certain studies of the atmosphere. Two types of measuring instruments are compared."
- OTHER APPLICATIONS OF RADIO AND ELECTRONICS
- 534-8 3977  
Cleaning by Ultrasonics—L. Atherton. (*Brit. Commun. Electronics*, vol. 4, pp. 138-144; March, 1957.) Small engineering components are suspended in a tank of cleaning solvent in which ultrasonic vibrations are induced by a BaTiO<sub>3</sub> transducer operating at 1 mc.
- 621-57:537.288.4 3978  
Development of the Electrostatic Clutch—C. J. Fitch. (*IBM J. Res. Devel.*, vol. 1, pp. 2-7; January, 1957.) See also 3253 of 1957.
- 621.365.5 3979  
Electronic Heating and Automation—M. T. Elvy. (*J. Brit. IRE*, vol. 17, pp. 443-462; August, 1957.) A survey of principles of induction and dielectric heating and their application to some industrial processes.
- 621.384.6 3980  
Electron Model Fixed-Field Alternating-Gradient Accelerator—F. T. Cole, R. O. Haxby, L. W. Jones, C. H. Pruett, and K. M. Terwilliger. (*Rev. Sci. Instr.*, vol. 28, pp. 403-420; June, 1957.) Detailed description of the design, construction, and performance of a radial-sector model accelerating electrons from 25 to 400 kev.
- 621.384.611 3981  
New Possibilities of Increasing the Efficiency of Accelerators of Charged Particles—E. M. Moroz. (*C. R. Acad. Sci. U.R.S.S.*, vol. 115,

pp. 78-79; July 1, 1957. In Russian.) An improved magnet system is briefly described which consists of three or more sectors producing a uniform magnetic field. See also 3503 of 1956.

621.384.622.2 3982

**The Possibility of Focusing in a Linear Accelerator by means of a Travelling Wave**—V. S. Tkalich. (*Zh. Eksp. Teor. Fiz.*, vol. 32, pp. 625-626; March, 1957.) Theoretical investigation of the simultaneous radial and phase stability of heavy particles obtained by means of the focusing effect of a traveling wave.

621.387.424 3983

**Geiger-Müller Counter Tubes**—J. Sharpe. (*Brit. Commun. Electronics*, vol. 4, pp. 150-157; March, 1957.) Includes a table of representative British types.

621.398:621.3.087.9 3984

**Automatic Data Plotter for F.M./F.M. Telemetry**—H. B. Riblet. (*Electronics*, vol. 30, pp. 182-187; August 1, 1957.) Apparatus for plotting results derived linearly or nonlinearly from telemetry data with any scale factor.

### PROPAGATION OF WAVES

621.396.11 3985

**Wave Propagation over an Irregular Terrain: Part 1**—K. Furutsu. (*J. Radio Res. Labs., Japan*, vol. 4, pp. 135-153; April, 1957.) A mathematical treatment of a model earth in which there are simultaneous discontinuities in the electrical properties and the radius of the earth's surface.

621.396.11:523.75 3986

**On the Disturbances of Radio Propagation along the North Polar Route**—Y. Hakura. (*J. Radio Res. Labs., Japan*, vol. 4, pp. 101-110; April, 1957.) An analysis of disturbances on the WWV-Hiraiso route. Storms are divided into two main types, sudden commencement and M region, but each of these may be recurrent or nonrecurrent. The four types are discussed in terms of solar activity.

621.396.11:538.566 3897

**Fundamental Radio Scatter Propagation Theory**—E. C. S. Megaw. (*Proc. IEE*, Pt. C, vol. 104, pp. 441-455; September, 1957.) A detailed theoretical treatment of scatter propagation beyond the horizon. The spectral density of refractive index fluctuation is derived from the universal equilibrium theory of turbulence, and the results are applied to the problem of fluctuations in the free-space paths for both light and radio waves. The predictions are compared with experiment, and the variation of the intensity of refractive index fluctuations with height is derived. The detailed treatment of radio scatter propagation includes a full analysis of the influence of the geometry of the scattering volume on the received field strength. The form of the scattering cross section implied in the results is compatible with those obtained in alternative treatments based on idealized models. Twenty-nine references.

621.396.11:551.510.53 3988

**The Role of Stratospheric Scattering in Radio Communication**—H. G. Booker and W. E. Gordon. (*Proc. IRE*, vol. 45, pp. 1223-1227; September, 1957.) The mixing-in-gradient hypothesis is applied to the stratosphere and the power scattered to a receiver is calculated. The characteristics of this means of propagation relative to its role in communications are discussed and comparisons are made between observations and theoretical predictions.

621.396.11:551.510.535 3989

**Application of the Generalized Magneto-ionic Theory to the Propagation of Radio Waves**

**at the Magnetic-Dip Poles of the Earth**—C. L. Bai. (*J. Atmos. Terr. Phys.*, vol. 11, no. 1, pp. 31-35; 1957.) Booker's magneto-ionic theory is used to evaluate the reflection levels, at the dip poles, of the ordinary and extraordinary rays at various angles of incidence and for frequencies above and below the gyro frequency.

621.396.11:551.510.535 3990

**Oblique Ray Paths in the Ionosphere**—J. Haselgrove. (*Proc. Phys. Soc.*, vol. 70, pp. 653-662; July 1, 1957.) Ray paths are calculated using an electronic digital computer for propagation in the magnetic meridian plane of the ordinary ray over a flat earth with a parabolic ionosphere. The computed range and equivalent path for various angles of incidence are compared with those given by simple no-field theory.

621.396.11:551.594.6 3991

**Heavy-Ion Effects in Audio-Frequency Radio Propagation**—C. O. Hines. (*J. Atmos. Terr. Phys.*, vol. 11, no. 1, pp. 36-42; 1957.) Propagation of whistlers may be due to ions as well as electrons, whereas the previous theory includes only electrons. The effect is to allow propagation in all directions and to introduce transverse modes with the dispersion in the opposite sense to that for the longitudinal ones.

621.396.11.029.6 3992

**Calculation of the Field Strength in Shadow and Half-Shadow Regions in the Case of Ultra-Short Waves Travelling along a Smooth Spherical Surface of the Earth**—A. I. Kalinin. (*Radiotekhnika, Moscow*, vol. 11, pp. 43-49; June, 1956.) An approximation method is described and its limits of validity are established.

621.396.11.029.62 3993

**Results of Experiments on V.H.F. Overland Propagation beyond the Radio Horizon**—S. Niwa, S. Watanabe, H. Saito, T. Sasaki, Y. Fujii and N. Minowa. (*J. Radio Res. Labs., Japan*, vol. 4, pp. 111-122; April, 1957.) Frequencies near 150 mc were used over a 123-km path in Japan from March to August, 1956. The results are presented in statistical and graphical form.

621.396.812.029.6 3994

**Meteorological Influences on the Hourly Median Field Strength of Ultra Short Waves in the Diffraction Region**—K. Tao. (*J. Radio Res. Labs., Japan*, vol. 4, pp. 155-254; April, 1957.) Statistics of the vertical gradient of atmospheric refractive index over Japan are presented and their effect on vhf propagation discussed. Observed seasonal variations in field strength are correlated with abnormal distributions of refractive index, and reflections from elevated discontinuities are shown to cause high field strength at night. Some eighty references.

### RECEPTION

621.396.621:621.396.666 3995

**Theoretical Investigations of some Diversity Methods**—E. Henze. (*Arch. elekt. Übertragung*, vol. 11, pp. 183-194; May, 1957.) General equations are derived for the characteristics of signals received by means of various antenna and receiver diversity methods. Statistically correlated and uncorrelated signals are considered, and the effect of noise is taken into account.

621.396.621:621.396.822 3996

**The Efficiency of Diversity Reception in the Presence of Interference from Radio Stations Operating at Adjacent Frequencies**—V. M. Rozov. (*Radiotekhnika, Moscow*, vol. 11, pp. 14-25; July, 1956.) The average percentage distortion of telegraph signals when diversity on two antennas is used is compared with the corresponding figure for ordinary reception.

The analysis is carried out for a long-range short-wave radio link.

621.396.621.029.62:621.372.632 3997

**Design Considerations of 50-Mc/s Converters**—D. F. Hadlock. (*QST*, vol. 41, pp. 17-20; March, 1957.) The minimizing of cross modulation and overloading of the first stage from adjacent-channel interference is discussed in relation to the over-all noise figure. A circuit design is presented.

621.396.621.57:621.314.7 3998

**Transistor Superregenerative Detection**—W. F. Chow. (*IRE TRANS.*, vol. CT-3, pp. 58-61; March, 1956. Abstract, *Proc. IRE*, vol. 44, p. 953; July, 1956.)

621.396.82 3999

**Minimum Signal-to-Interference Ratio Required for Broadcasting**—S. C. Mazumdar, G. V. Padhye, and W. V. B. Ramalingam. (*J. Inst. Telecommun. Eng., India*, vol. 3, pp. 110-115; March, 1957.) A determination from listening tests (750 recordings and 12000 opinions) of the protection required for a speech-modulated broadcast signal against interference from speech, music, and cw morse.

### STATIONS AND COMMUNICATION SYSTEMS

621.376:621.396.4 4000

**Single-Sideband Modulation by means of Phase-Shift Systems**—B. B. Shtein. (*Radiotekhnika, Moscow*, vol. 11, pp. 13-26; June, 1956.) The separation of a sideband by means of three-phase modulation is considered. Experiments show that the second sideband can be suppressed by more than 40 db.

621.376.322:621.3.018.78 4001

**Discriminator Distortion in Frequency-Modulation Systems**—R. G. Medhurst and H. D. Hyamson. (*Proc. IEE*, Pt. C, vol. 104, pp. 357-365; September, 1957.) Theory given earlier [2503 of 1954 (Medhurst)] is extended to cover discriminator networks whose characteristics exhibit small departures from ideal forms. Single-tone and noise-band modulations are treated. Two numerical examples are given.

621.376.56:621.396.8 4002

**Some Optimal Signals for Time Measurement**—H. Sherman. (*TRANS. IRE*, vol. IT-2, pp. 24-28; March, 1956. Abstract, *Proc. IRE*, vol. 44, p. 956; July, 1956.) Discussion of the optimum code for determination of the phase of a signal in the presence of Gaussian noise.

621.39 4003

**Communications and the Future**—G. Radley. (*J. Electronics Control*, vol. 3, pp. 211-217; August, 1957.) A survey of current developments with consideration of economic factors. The introduction of electronic exchanges and nation-wide dialing for the telephone service, and links for data transmission are discussed.

621.39.001.11:016 4004

**A Bibliography of Information Theory (Communication Theory-Cybernetics)**—F. L. Stumpers. (*IRE TRANS.*, vol. IT-1, pp. 31-47; September, 1955.) Supplement to previous list (see 1566 of 1954).

621.396.41:621.376.3:621.396.813 4005

**Intermodulation Distortion due to Fading in Frequency-Modulation Frequency-Division Multiplex Trunk Radio Systems**—R. G. Medhurst and M. Hodgkinson. (*Proc. IEE*, Pt. C, vol. 104, pp. 475-480; September, 1957.) A theoretical study, with numerical results, of the dependence of distortion level on the characteristics of the echoes responsible for the fade. See also 1867 of 1956 (Medhurst and Small).

621.396.41.029.6:621.396.822 4006  
**Noise Considerations on Toll Telephone Microwave Radio Systems**—T. A. Comebellick and M. E. Ferguson. (*Elect. Eng., N. Y.*, vol. 76, pp. 314-317; April, 1957.) Performance of microwave radio equipment is analyzed to determine whether it will conform to over-all noise requirements of the telephone network.

621.396.65.029.64 4007  
**Crosstalk Measurements between Antennae on the Johannesburg-Pretoria Microwave Radio System**—D. Davidson and B. P. Mackenzie. (*Trans. S. Afr. Inst. elec. Eng.*, vol. 48, pt. 3, pp. 93-111, discussion, pp. 111-119; March, 1957.) Detailed report of an investigation of excessive crosstalk occurring in a two-frequency system operating in the 4-kmc band. Measurement methods including heterodyne and sweep techniques are described, and the effectiveness of antenna screening and cross polarization in eliminating reflection effects is discussed.

621.396.933 4008  
**Second Annual Symposium on Aeronautical Communications**—J. W. Worthington, Jr. (*IRE TRANS.*, vol. CS-5, pp. 3-130; March, 1957.) The text is given of 17 papers presented at a symposium held at Utica, New York, in October, 1956. Abstracts of most of these papers are given in *PROC. IRE*, vol. 45, pp. 895-896; June, 1957.

#### SUBSIDIARY APPARATUS

621.316.722.078.3 4009  
**A Voltage Stabilizer Principle**—C. Billington and E. Chakanovskis. (*Electronic Eng.*, vol. 29, pp. 374-376; August, 1957.) Positive feedback eliminates the need for an auxiliary negative supply in controlling the output down to zero volts with a series-tube stabilizer arrangement.

621.316.722.078.3 4010  
**A Discussion of Series Valves for Small D. C. Voltage Stabilizers**—C. Billington. (*Electronic Eng.*, vol. 29, pp. 377-379; August, 1957.) "A graphical method of assessing the performance of a series tube is presented. On this basis fifteen tube types are compared, and some tubes not normally used in this application are shown to have unsuspected advantages."

621.316.722.1 4011  
**Stabilization of A.C. Supplies**—O. E. Dzierzynski. (*Wireless World*, vol. 63, pp. 491-496; October, 1957.) A comprehensive, comparative review of methods of voltage control with practical examples of a number of circuits and techniques.

621.316.79:621.365.41 4012  
**Simple Constant-Temperature Oven and Control System**—G. R. Gunther-Mohr and S. Triebwasser. (*IBM J. Res. Devel.*, vol. 1, pp. 84-89; January, 1957.) A thermocouple-monitored system consisting of an oven, a stable reference source and a chopper-amplifier controller unit is described. A stable and uniform temperature,  $\pm 0.1^\circ\text{C}$  from  $200^\circ$  to  $1050^\circ\text{C}$  is maintained in a cylindrical region 5 cm in diameter and 12 cm long.

621.316.925 4013  
**An H. T. Overload Cut-Out Circuit**—J. D. Ralphs. (*Electronic Eng.*, vol. 29, pp. 398-400; August, 1957.) Description of a circuit designed in conjunction with a stabilized hv supply for laboratory work.

#### TELEVISION AND PHOTOTELEGRAPHY

621.397.26:621.396.82 4014  
**Freedom from Interference and the Effi-**

ciency of Radio Phototelegraphy Systems in the Presence of Fluctuation—Type Interference—A. G. Zyuko. (*Radiotekhnika, Moscow*, vol. 11, pp. 14-24; August, 1956.) Four different types of modulation system are compared.

621.397.3:654.171 4015  
**Statistical Methods of Phototelegraphy Transmission**—R. R. Vasil'ev. (*Radiotekhnika i Elektronika*, vol. 2, pp. 136-143; February, 1957.) Two methods of scanning are described whereby the speed of phototelegraphic transmission can be increased. In one, signals are transmitted in binary form, in the other an image is reproduced on a cr tube and photographed.

621.397.33 4016  
**A Variable-Velocity Scanner for Magnetic Deflection of a Scanning Spot**—M. P. Beddoes. (*Proc. IEE*, Pt. C vol. 104, pp. 481-488; September, 1957.) A description of a magnetic scanner with negative feedback. Satisfactory operation is obtained for repetitive scanning rates up to  $10^4$ /sec with a maximum displacement error of no more than 0.2 per cent.

621.397.5:535.623 4017  
**Subjective Colour for Television?**—C. E. M. Hansel. (*Wireless World*, vol. 63, pp. 508-509; October, 1957.) An explanation of color impressions observed on monochrome television in terms of the "Helmholtz top" experiment.

621.397.5:621.395.625.3 4018  
**Video Tape Recorder uses Revolving Heads**—R. H. Snyder. (*Electronics*, vol. 30, pp. 138-144; August 1, 1957.) Low tape speed and extended high-frequency response are achieved by revolving four magnetic recording heads transversely across the tape, which moves only fast enough to prevent overlapping. For another system of rotating pick-up heads, see 2952 of 1956 (Springer).

621.397.5:718.5 4019  
**A 16-mm Television Recording Channel**—M. E. Pemberton. (*Marconi Rev.*, vol. 20, pp. 4-22 and 39-50, 1st and 2nd quarters; 1957.) Details are given of a system operating at 625/405 lines with 50 fields/s or at 525 lines with 60 fields/s. In Part 1 the over-all channel and the recording monitor are described; Part 2 deals with the fast pull-down camera and driving unit, the flywheel-synchronizing panel and the power supplies.

621.397.6 4020  
**Television Links for an Outside Broadcast from a Vessel on Lake Geneva**—F. Grandchamp. (*Tech. Mitt. schweiz. Telegr.-Teleph. Verw.*, vol. 35, pp. 243-248; June 1, 1957. In French.)

621.397.6:535.623 4021  
**Sync Generator for Dot-Interlace TV**—F. T. Thompson. (*Electronics*, vol. 30, p. 170-173; August 1, 1957.) "Accurately phased horizontal and vertical synchronization pulses are obtained by sampling pulses from frequency-divided chains to obtain output corresponding in phase to half-cycle of high-frequency signal. Though design is for 14.7-kc line and 60-cps field frequencies, with 2.47-mc reference frequency, technique is directly applicable to NTSC color systems."

621.397.6:621.396.73 4022  
**An Improved "Roving Eye"**—T. Worswick and G. W. H. Larkby. (*B.B.C. Eng. Div. Monographs*, no. 12, pp. 5-18; April, 1957.) Details are given of a television camera vehicle which can transmit pictures and sound while moving or stationary. Two cameras and associated equipment, power supplies, radio-link apparatus, and antennas are included in a com-

plete self-contained unit particularly suitable for short outside broadcasts.

621.397.611 4023  
**Motion Minimizes Image-Orthicon Burn-In**—J. T. Wilner. (*Electronics*, vol. 30, pp. 180-181; August 1, 1957.) The image orthicon tends to retain a previous camera shot. This effect can be greatly reduced by oscillating slowly the lens board of the television camera.

621.397.611 4024  
**Television Camera with Storage Tube having a Curved Characteristic**—W. Dillenburger. (*Elektron. Rundschau*, vol. 11, pp. 143-146 and 174-178; May and June, 1957.) The design and operation of such a camera system are discussed with particular reference to the vidicon tube.

621.397.611.2:621.317.351 4025  
**Contribution to the Technique of Measurements on Television-Camera Pre-amplifiers**—W. Dillenburger. (*Frequenz*, vol. 11, pp. 137-142; May, 1957. Correction, *ibid.*, vol. 11, p. 191; June, 1957.) Methods for obtaining the frequency characteristics of the preamplifier without removing the camera tube are outlined.

621.397.8 4026  
**The Reception of Crystal Palace Transmissions in Australia**—N. Burton. (*RSGB Bull.* vol. 32, pp. 401-402; March, 1957.)

621.397.8 4027  
**Measurement of Service Area for Television Broadcasting**—(*Tech. News Bull. Nat. Bur. Stand.*, vol. 41, pp. 113-115; August, 1957.) Currently field-strength contours are determined using recorders in moving road vehicles. It is not always possible to use a 30-foot antenna height with such vehicles and extrapolated measurements made with lower antennas are not reliable. Sample measurements at fixed locations are now considered to be more satisfactory.

621.397.8:535.623 4028  
**Level Clamping and some Interference Effects in Colour Television Transmission Systems**—W. Dillenburger. (*Arch. elekt. Übertragung*, vol. 11, pp. 195-213; May, 1957.) Equipment is described which was developed for investigating the effects of level variations, carrier interference, and detuning on picture quality in the 3-channel and NTSC systems. Results are discussed and are illustrated by color photographs.

621.397.813:778.5 4029  
**The Evaluation of Picture Quality in Television**—N. R. Phelp. (*Marconi Rev.*, vol. 20, pp. 23-32, 1st quarter; 1957.) The technique described in 1127 of 1952 (Jesty and Phelp) is applied to assess the performance of a television recording channel.

621.397.828 4030  
**Problems in Metropolitan TV Reception**—S. Holzman. (*Radio u Telev. News*, vol. 57, pp. 38-39; March, 1957.) Suitable remedies for multipath signals and interference are suggested.

#### TRANSMISSION

621.396.61 4031  
**Single-Sideband Exciter**—J. Headland. (*Short Wave Mag.*, vol. 15, pp. 8-15; March, 1957.) Practical details of design and construction of a filter-type SSB unit based on a 93-kc crystal oscillator.

621.396.61 4032  
**A 3-Band 90-Watt Transmitter**—C. C. Tiemeyer. (*QST*, vol. 41, pp. 35-37; March,

1957.) The transmitter operates in the 160-, 80-, and 40-m bands.

621.396.61:621.396.662 4033  
**High-Power Transmitter Tuning Devices—The Mechanical and Electrical Problems**—V. O. Stokes. (*Brit. Commun. Electronics*, vol. 4, pp. 158–162; March, 1957.) Transmitters operating in the 4–27.5-mc band are considered. Tuning and coupling systems used in a 30-kw communication transmitter and a 100-kw broadcasting transmitter are detailed.

#### TUBES AND THERMIONICS

621.314:537.312.8:538.63 4034  
**The Gaussistor, a Solid-State Electronic Valve**—M. Green. (IRE TRANS., vol. ED-3, pp. 133–141; July, 1956. Abstract, PROC. IRE, vol. 44, p. 1642; November, 1956.)

621.314.63:621.316.82 4035  
**Some Characteristics of Metallic Varistors**—Holbrook and Dulmage. (See 3764.)

621.314.632:537.311.33:621.372.632 4036  
**Theory and Operation of Crystal Diodes as Mixers**—G. C. Messenger and C. T. McCoy. (PROC. IRE., vol. 45, pp. 1269–1283; September, 1957.) The electrical parameters of a crystal diode are quantitatively related to its fundamental physical properties and the effects of these parameters on conversion loss at uhf and microwave frequencies are discussed. A figure of merit by which semiconductor materials may be compared for their mixer sensitivity is suggested and it is shown that *n*-type Ge is a better mixer material than *p*-type Si. The relation between conversion loss and noise temperature, and receiver noise are discussed. The application of the theory to the design of mixers is demonstrated.

621.314.632:546.289 4037  
**Investigation of the Input Impedance, and the Experimental Checking of the Equivalent Circuit of Germanium Detectors in the Frequency Range 1–10 Mc/s**—N. E. Skvortsova. (*Radiotekhnika i Elektronika*, vol. 2, pp. 296–310; March, 1957.)

621.314.7+621.314.63 4038  
**A Developmental Intrinsic-Barrier Transistor**—R. M. Warner, Jr. and W. C. Hittinger. (IRE TRANS., vol. ED-3, pp. 157–160; July, 1956. Abstract, PROC. IRE, vol. 44, p. 1642; November, 1956.) See also 2133 of 1955 (Hittinger, et al.).

621.314.7 4039  
**A New Higher-Ambient Transistor**—J. J. Bowe. (IRE TRANS., vol. ED-3, pp. 121–123; July, 1956. Abstract, PROC. IRE, vol. 44, p. 1642; November, 1956.)

621.314.7 4040  
**Design, Construction and High-Frequency Performance of Drift Transistors**—A. L. Kestenbaum and N. H. Ditrick. (*RCA Rev.*, vol. 18, pp. 12–23; March, 1957.) The electrical characteristics of developmental drift transistors are related to their physical structure, which is described.

621.314.7 4141  
**Transistor Characteristics at Very Low Temperatures**—S. Uda. (*J. Inst. Telecommun. Eng., India*, vol. 3, pp. 97–109; March, 1957.) A comparison of terminal dc characteristic curves of common-base *p-n-p* junction transistors measured at liquid helium, liquid air, and room temperatures. Gain is decreased at the lowest temperatures.

621.314.7 4042  
**Effect of Nonlinear Collector Capacitance on Collector-Current Rise Time**—T. R. Bash-

kow. (IRE TRANS., vol. ED-3, pp. 167–172; October, 1956. Abstract, PROC. IRE, vol. 45, p. 254; February, 1957.)

621.314.7:546.289 4043  
**Application Aspects of the Germanium Diffused-Base Transistor**—D. E. Thomas and G. C. Dacey. (IRE TRANS., vol. CT-3, pp. 22–25; March, 1956. Abstract, PROC. IRE, vol. 44, p. 952; July, 1956.)

621.314.7:621.318.57 4044  
**Solution of a Transistor Transient Response Problem**—J. R. Macdonald. (IRE TRANS., vol. CT-3, pp. 54–57; March, 1956. Abstract, PROC. IRE, vol. 44, p. 953; July, 1956.) See also 885 of 1955 (Moll).

621.314.7.001.4 4045  
**Measuring Parameters of Junction Transistors**—Hendrick, Jr. (See 3950.)

621.314.7.012:621.317.755 4046  
**Investigation of Transistor Characteristics by means of a Cathode-Ray Curve Tracer**—Bonch-Bruevich and Soltamov. (See 3951.)

621.314.7+621.375.4].012.8 4047  
**Electric-Network Representation of Transistors—a Survey**—R. L. Pritchard. (IRE TRANS., vol. CT-3, pp. 5–21. March, 1956. Abstract, PROC. IRE, vol. 44, p. 952; July, 1956.)

621.383 4048  
**Photoelectric Cells**—J. D. McGee. (*Proc. IEE*, Pt. B, vol. 104, pp. 467–484; September, 1957.) A review of progress. Topics discussed include the theory of the external and internal photoelectric effects, methods of manufacture and measurement, the characteristics of typical photoelectric cells, and photoconductive and photovoltaic cells.

621.385.029.6 4049  
**Application of the Potential Analogue in Multicavity Klystron Design and Operation**—S. V. Yadavalli. (PROC. IRE vol. 45, pp. 1286–1287; September 1957.) Using space-charge wave theory, relations are developed which allow the output/input voltage ratio of a multicavity klystron with arbitrary parameters to be written down. Expressions for the power gain under broadband conditions are given.

621.385.029.6 4050  
**Description of Operating Characteristics of the Platinotron—a New Microwave Tube Device**—W. C. Brown. (PROC. IRE, vol. 45, pp. 1209–1222; September, 1957.) The platinotron is structurally similar to a magnetron. The electron beam is re-entrant and originates from a cathode coaxial to the rf circuit, but, unlike the magnetron, the rf circuit is not re-entrant and its characteristic impedance is matched at both ends to two external connections over the frequency range of interest. In operation the device acts as an efficient broad-band saturated amplifier when the signal is passed through it in one direction and as a passive network in the other direction. The platinotron may be used as an oscillator of high frequency stability. Details are given of its operation as an amplifier at frequencies in the region of 1300 mc (“ampliftron” operation).

621.385.029.6 4051  
**Platinotron increases Search Radar Range**—W. C. Brown. (*Electronics*, vol. 30, pp. 164–168; August 1, 1957.) The platinotron is a crossed-field microwave tube whose operating frequency is determined externally. It may be used as a wide-band amplifier or as an oscillator; the tube described gives a peak power of 2 mw at frequencies near 1300 mc.

621.385.029.6 4052  
**Positive Ion Oscillations in Long Electron Beams**—T. G. Mihan. (IRE TRANS., vol. ED-3, pp. 117–121; July, 1956. Abstract, PROC. IRE, vol. 44, pp. 1641–1642; November, 1956.)

621.385.029.6 4053  
**Space-Charge Waves for a Finite Magnetic Field at the Cathode of a Cylindrical Electron Stream**—R. Liebscher. (*Arch. elekt. Übertragung* vol. 11, pp. 214–221; May, 1957.) The plasma wavelength is calculated under the assumption of a finite magnetic focusing field at the cathode.

621.385.029.6 4054  
**Space-Charge Limitation on the Focus of Electron Beams**—J. W. Schwartz. (*RCA Rev.*, vol. 18, pp. 3–11; March, 1957.) The motion of electrons within a homocentric uniform-density beam in the presence of space-charge forces is examined. A universal curve for the smallest spot size at the target is obtained. At high beam currents this differs significantly from available curves for the beam cross section at the point of zero radial velocity.

621.385.029.6 4055  
**Effect of Space Charge on the Interaction of an Electron Stream and a Travelling Electromagnetic Wave**—V. N. Shevchik and V. S. Stal'makhov. (*Radiotekhnika i Elektronika*, vol. 2, pp. 230–236; February, 1957.) The conditions necessary for establishing backward-wave oscillation are given. Analytical results are compared with experimental data and formulas of other authors.

621.385.029.6 4056  
**The Cascade Bunching of Electrons Applied to the Analysis of the Interaction of Electron Stream and Travelling Magnetic Wave**—V. N. Shevchik and Yu. D. Zharkov. (*Radiotekhnika i Elektronika*, vol. 2, pp. 237–243; February, 1957.) Expressions are derived for the active and reactive components of electron power. The effect of the interaction of non-synchronous space harmonics on power is examined and results are used for determining the starting conditions for backward-wave oscillators.

621.385.029.6 4057  
**The Reciprocity of the Coupling in Travelling-Wave Valves**—F. Paschke. (*Arch. elekt. Übertragung*, vol. 11, pp. 137–145; April, 1957.) The law of reciprocity is proved which states that to obtain a coupled wave and amplification the field of the undisturbed circuit wave must be present at the beam and the field of the undisturbed space-charge wave must be present at the slow-wave structure. For low-noise operation the amplifier should have a large beam diameter, low beam velocity, and a large coupling impedance. For an ideal travelling-wave tube the maximum gain per beam wavelength obtainable is shown to be  $37.5 (\omega_{p0}/\omega)^{2/3}$  db, where  $\omega_{p0}/\omega$  is the ratio of plasma frequency to signal frequency.

621.385.029.6 4058  
**Investigation of Noise Characteristics of Traveling-Wave Valves**—A. S. Tager. (*Radiotekhnika i Elektronika*, vol. 2, pp. 222–229; February, 1957.) The results of experiments made with tubes having a movable electron gun are discussed with reference to theoretical investigations.

621.385.029.6 4059  
**Modified Contrawound Helix Circuits for High-Power Travelling-Wave Tubes**—C. K. Birdsall and T. E. Everhart. (IRE TRANS., vol. ED-3, pp. 190–204; October, 1956. Abstract, PROC. IRE, vol. 45, p. 254; February, 1957.) See also 1825 or 1955 (Chodorow and Chu).

- 621.385.029.6:537.533 4060  
**Break-Up of Hollow Cylindrical Electron Beams**—R. L. Kylh and H. F. Webster. (IRE TRANS., vol. ED-3, pp. 172-183; October, 1956.) Abstract, PROC. IRE, vol. 45, p. 254; February, 1957.) For earlier report, see *J. Appl. Phys.*, vol. 26, pp. 1386-1387; November, 1955. (Webster).
- 621.385.029.6:537.533 4061  
**Instability of Hollow Beams**—J. R. Pierce. (IRE TRANS., vol. ED-3, pp. 183-189; October, 1956. Abstract, PROC. IRE, vol. 45, p. 254; February, 1957.) See also 4060 above.
- 621.385.029.6:537.54 4062  
**On the Interaction between Microwave Fields and Electrons, with Special Reference to the Strophotron**—B. Agdur. (*Ericsson Tech.* vol. 13, no. 1, pp. 3-108; 1957.) "The interaction between a microwave field and electrons is investigated theoretically in a system where the electrons oscillate in an electrostatic field and a superimposed microwave field both of which are nonlinear. The operating characteristics of such a system are deduced from the theory. The theoretical results are applied to the strophotron oscillator and the measurements performed are in satisfactory agreement with the theory. Of special interest is the fact that both theory and experiments show that it is possible to combine high efficiency with good electronic tuning properties of the tube." See also 3398 of 1954 (Arvén and Romell).
- 621.385.029.6:621.318.2 4063  
**The Design of Periodic Permanent Magnets for Focusing of Electron Beams**—F. Sterzer and W. W. Siekanowicz. (*RCA Rev.*, vol. 18, pp. 39-59; March, 1957.) An extension to the theory of Chang (1202 and 2793 of 1955).
- 621.385.029.6:621.372.2 4064  
**The Interpretation of Homogeneous Delay Systems**—A. I. Shtyrov. (*Radiotekhnika i Elektronika*, vol. 2, pp. 244-251; February, 1957.) The propagation of slow electronic waves in periodic structures of filter type based on internal reflection is compared with propagation in a rectangular comb-type delay structure formed by an anisotropic dielectric.
- 621.385.029.6:621.375:621.396.822 4065  
**The Minimum Noise Figure of Unmatched Amplifiers**—H. Pözl. (*Arch. elekt. Übertragung*, vol. 11, pp. 177-181; April, 1957.) The work of Haus and Robinson (3442 of 1955) is generalized to apply to amplifiers, particularly microwave beam amplifiers, under any conditions of matching. The representation of an amplifier by a scattering matrix is discussed.
- 621.385.029.6:621.396.662 4066  
**Tuning of Interdigital Magnetrons by Coaxial Lines**—A. Singh. (*J. Electronics Control*, vol. 3, pp. 183-193; August, 1957.) The interdigital magnetron, especially the inverted form with the cathode outside the anode, is shown to be especially suitable for tuning by a coaxial line since it has only one cavity. Tuning ranges of 2:1 are calculated and confirmed by cold measurements. Suggested modifications should give wider ranges.
- 621.385.029.6:621.398.822 4067  
**Validity of Traveling-Wave Tube Noise Theory**—R. C. Knechtli and W. R. Beam. (*RCA Rev.*, vol. 18, pp. 24-38; March, 1957.) Experimental results are presented which are substantially in agreement with the first-order theory of noise based on a single space-charge wave. Zero correlation was found between beam-current and electron velocity fluctuations at the potential minimum in front of the cathode.
- 621.385.029.64:621.373.4.018.75 4068  
**Technique of Pulsing Low-Power Reflex Klystrons**—J. I. Davis. (IRE TRANS., vol. MTT-4, pp. 40-47; January, 1956. Abstract, PROC. IRE vol. 44, p. 581; April, 1956.)
- 621.385.032.21 4069  
**Modern Thermionic Cathodes**—R. W. Fane. (*Wireless World*, vol. 63, pp. 488-490; October, 1957.) A review of the main types and their relative merits. Possible future developments in the microwave field are described for all ordinary low-current applications the oxide cathode is still preferred.
- 621.385.032.21:537.568 4070  
**Study of a Method for Reducing the Auto-electronic Cathode Bombardment by the Ions of Residual Gases**—M. I. Elinson, V. A. Gor'kov, and G. F. Vasil'ev. (*Radiotekhnika i Elektronika*, vol. 2, pp. 204-218; February, 1957.)
- 621.385.032.213.2 4071  
**The Relationship between Cathode Emission, Cathode Resistance and Mutual Conductance in Receiving Valves**—M. F. Holmes. (*Proc. IEE*, Pt. C, vol. 104, pp. 251-264; September, 1957.) Techniques available for the measurement of cathode emission and resistance in a normal tube are considered. Reasonable quantitative relations between the parameters are examined and compared with experimental life-test records.
- 621.385.032.216 4072  
**The Conductivity of Oxide Cathodes: Part 1—Potential Distribution**—G. H. Metson. (*Proc. IEE*, Pt. C, vol. 104, pp. 316-322; September, 1957.) For various operating conditions found in common receiving tubes, experiments show that in a well-activated cathode the potential gradient is constant across the oxide matrix but may increase towards the outer surface as deactivation occurs.
- 621.385.032.216 4073  
**The Conductivity of Oxide Cathodes: Part 2—Influence of Ion Movements on Matrix Resistance**—G. H. Metson. (*Proc. IEE* Pt. C, vol. 104, pp. 496-505; September, 1957.) A discussion of the influence of residual gas ions and oxygen matrix on the matrix resistance. For Part 1 see 4072 above.
- 621.385.032.216 4074  
**Lifetime of Oxide Cathodes**—W. Dahlke. (*Telefunken Ztg.*, vol. 30, pp. 55-61. March, 1957. English summary, p. 75.) The results of investigations on versions of the hf pentode Type EF80 are analyzed. Five different core-metal alloys were tested with underheated, overheated, or normally heated filaments and under various load conditions. The corresponding tube characteristics are plotted against hours of operation. The relation of cathode life expectancy to heater voltage is shown for one of the core materials. Above and below the optimum operating temperature cathode poisoning reduces the emission. Results of tests on the uhf triodes Type 2C39A and Type 2C40 are also given.
- 621.385.1.032.29 4075  
**Growth of Anode-to-Grid Capacitance in Low-Voltage Receiving Valves**—F. H. Reynolds, C. G. Johnson, and M. W. Rogers. (*Proc. IEE*, Pt. B, vol. 104, pp. 487-492; September, 1957.) "The capacitance between the anode and the control grid of a certain type of receiving pentode has been found to increase with life, the rate of growth being dependent on the operating conditions of the tube and on the material and processing schedule of the anode. It is shown that the phenomenon is due to the transfer of impurity carbon from the anode to the mica insulators."
- 621.385.2:537.525.92 4076  
**The Space-Charge-Limited Flow of Charged Particles in Planar, Cylindrical and Spherical Diodes at Relativistic Velocities**—E. W. V. Acton. (*J. Electronics Control*, vol. 3, pp. 203-210; August, 1957.) The Langmuir and Child equations are extended to the case of relativistic velocities and the solutions are valid for any value of accelerating voltage.
- 621.385.3 4077  
**Perturbation Analysis of Stationary Dense Electron Flow and a Space-Charge-Limited Triode**—G. A. Stuart and B. Meltzer. (*J. Electronics Control*, vol. 3, pp. 51-62; July, 1957.) The perturbation method is used to deduce the electron flow in planar, cylindrical, and spherical triodes from the rectilinear flow in diodes of the same shape. The analysis is restricted to a range of positive grid voltages.
- 621.385.3 4078  
**On the Amplification Factor of the Triode**—E. B. Moullin. (*Proc. IEE*, Pt. C, vol. 104, pp. 538-541; September, 1957.) Discussion on 2649 of 1957.
- 621.385.3(09) 4079  
**Birth of the Electron-Tube Amplifier**—F. B. Llewellyn. (*Radio & Telev. News*, vol. 57, pp. 43-45; March, 1957.) Historical review of the early work of Lee de Forest and his contemporaries.
- 621.385.3.029.64 4080  
**Microwave Triode Oscillators**—C. L. Andrews. (*Rev. Sci. Instr.*, vol. 28, pp. 443-447; June, 1957.) Disk-seal triodes have been scaled down to give oscillators for frequencies of 4-6 kmc. The upper frequency limit is imposed by the internal circuit and not by the electronics of the tube.
- 621.385.5.011.2 4081  
**The Internal Resistance of a Radio-Frequency Pentode**—J. L. H. Jonker and Z. van Gelder. (*Philips Res. Rep.*, vol. 12, pp. 141-175; April, 1957.) Detailed analysis of the distribution of current between screen grid and anode taking account of the reflection of electrons by the suppressor grid and by the anode, and the extra space charge due to these electrons. To obtain a high value of internal resistance  $R_i$  the reflection coefficient of the suppressor grid must be small, but the effective potential must be kept low. Measurements made on conventional rf pentodes and on specially constructed tubes are reported. Calculated values of  $R_i$  are about 40 per cent above measured values. See also 265 and 3179 of 1951 (Jonker).
- 621.385.832 4082  
**The Heating of Fluorescent Screens Bombarded by Electrons**—G. D. Archard and P. A. Einstein. (*Brit. J. Appl. Phys.*, vol. 8, pp. 232-236; June, 1957.) The temperature rise is calculated for various forms of bombardment, and fair agreement is found with experimental results. Application to practical cr tubes is considered.
- 621.385.832:535.371.07 4083  
**The Movement of the Second Crossover Potential of Insulators**—A. B. McFarlane. (*Brit. J. Appl. Phys.*, vol. 8, pp. 248-252; June, 1957.) By suitable treatment of the luminescent screen of a cr tube, e.g., by setting it in a strong silicate solution or by applying a layer of magnesium oxide smoke to the bombarded surface, the second cross-over potential can be made to follow closely the applied anode voltage. This allows the application of almost unlimited voltages with a consequent gain in luminance and performance.

621.385.832:621.396.662 4084  
**Problems of Comparative Tuning Indication**—G. Linckelmann. (*Telefunken Ztg*, vol. 30, pp. 62-69; March, 1957. English summary, p. 75.) Various methods of comparing two signal voltages by means of "magic eye"-type indicators are discussed. Details are given of the indicator tube Type EMM 801 which has a single cathode. For an application of this tube, see 1455 of 1957 (Troost).

621.387:621.3.032.12:546.293 4085  
**Influence of Argon Content on the Characteristics of Glow-Discharge Tubes**—F. A. Benson and E. F. F. Gillespie. (*Proc. IEE*, Pt. B, vol. 104, pp. 498-506; September, 1957.) A discussion on specially manufactured neon-filled and helium-filled tubes having argon contents from zero to 2.5 per cent. Thirty-five references.

#### MISCELLANEOUS

061.6:621.396 4086  
**The New Radio Research Station, Ditton Park, Slough**—R. L. Smith-Rose. (*Nature*, London, vol. 180, pp. 163-166; July 27, 1957.)

A summary of the program of research and of its part in an international range of activities. See also 3461 of 1955.

389.6(43) 4087  
**50 Years of the A.E.F. [Committee for Units and Symbols]**—E. Flegler. (*Elektrotech. Z., Edn A*, vol. 8, pp. 273-295; April 11, 1957.) This issue contains nine papers dealing with the history, achievements, and tasks of the committee.

621.3.03:356/359 4088  
**Component Developments**—G. W. A. Dunimer. (*Wireless World*, vol. 63, pp. 482-485; October, 1957.) Trends in design and testing of electronic components used by the Armed Services.

621.3.049.75 4089  
**Components for Printed Circuits**—L. W. D. Sharp. (*Brit. Commun. Electronics*, vol. 4, pp. 202-207; April, 1957.) The design features of the various types of component and the methods of insertion and of fixing to wiring boards are tabulated and discussed. Recent mechanical improvements are described and future trends outlined.

621.3.049.75 4090  
**Recent Advances in Automatic Assembly**—L. H. Gipps, and K. M. McKee. (*J. Brit. IRE*, vol. 17, pp. 501-511; September, 1957.) Recent and probable future development of machines for preparing electronic components and inserting them automatically into printed wiring boards are considered. The design of components and the processing of printed wiring boards is discussed in relation to the requirements of automatic assembly.

621.317+681.142]:061.3 4091  
**IRE Instrumentation Conference and Exhibit**—(IRE TRANS. vol. PGI-5, pp. 1-224; June, 1956.) Text of 32 papers read at the Conference in Atlanta, Georgia, November, 28-30, 1955, under the headings: recording and data utilization, data-handling systems, processing techniques, analog-to-digital conversion, and transducers. (For abstracts of papers, see PROC. IRE, vol. 44, pp. 1210-1213; September, 1956.)

621.37/.39(091) 4092  
**A History of some Foundations of Modern Radio-Electronic Technology**—J. H. Hammond, Jr, and E. S. Purington. (PROC. IRE, vol. 45, pp. 1191-1208; September, 1957.)

